NATIONAL AERONAUTICS AND SPACE ADMINISTRATION

Technical Report No. 32-740

Mariner Mars 1964 Project Report: Mission and Spacecraft Development

Volume I. From Project Inception Through Midcourse Maneuver

JET PROPULSION LABORATORY
CALIFORNIA INSTITUTE OF TECHNOLOGY
PASADENA, CALIFORNIA

March 1, 1965

Copyright © 1966
Jet Propulsion Laboratory
California Institute of Technology

Prepared Under Contract No. NAS 7-100
National Aeronautics & Space Administration

PREFACE

On November 28, 1964, *Mariner IV* was successfully launched on a trajectory that would take it within 150,000 miles of Mars. On December 5, 1964, the spacecraft performed a successful midcourse maneuver, altering its flight path so that it would pass within 6118 miles of the planet. The flight took approximately 7½ months, during which time a great deal of scientific information was gathered concerning the near-Earth environment and interplanetary space. On July 14, 1965, *Mariner IV* photographed the surface of Mars, and telemetered to Earth the most advanced scientific and technical data regarding the planet yet recorded.

This volume, the first of a series of volumes that comprise the *Mariner* Mars 1964 Project Report, describes the formation and organization of the project, and traces its development up through the time of the midcourse maneuver. The bulk of this volume describes the development of the spacecraft itself, including design concepts and changes, fabrication and procurement history, and flight performance for the early portion of flight.

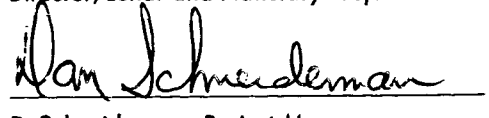
The *Mariner* Mars 1964 mission required the use of a great many new techniques in designing, building, and operating unmanned spacecraft. The success of *Mariner IV* has made these techniques significant, particularly in the light of future space programs. It is hoped that the operations and results documented in this volume will be useful reference to those planning future space missions.



W. H. Pickering, *Director*
Jet Propulsion Laboratory



J. N. James, *Acting Assistant Laboratory Director, Lunar and Planetary Projects*



D. Schneiderman, *Project Manager*
Mariner Mars 1964

ELEMENTS OF THE *MARINER* MARS 1964 PROJECT REPORT

The *Mariner* Mars 1964 Project Report consists of the following volumes:

Mariner Mars 1964 Project Report, Mission and Spacecraft Development, Volume I: From Project Inception Through Midcourse Maneuver (TR 32-740, Vol. I)

Mariner Mars 1964 Project Report, Mission and Spacecraft Development, Volume II: Appendixes (TR 32-740, Vol. II)

Mariner Mars 1964 Project Report, Mission Operations (TR 32-881)

Mariner Mars 1964 Project Report, Spacecraft Performance and Analysis (TR 32-882)

Mariner Mars 1964 Project Report, Scientific Experiments (TR 32-883)

Mariner Mars 1964 Project Report, Television Experiment, Part I: Investigators' Report (TR 32-884, Part I)

Mariner Mars 1964 Project Report, Television Experiment, Part II: Picture Element Matrices (TR 32-884, Part II)

Tracking and Data Acquisition Support for *Mariner* Mars 1964, Volume II: Cruise to Post-Encounter Phase (TM 33-239, Vol. II)

CONTENTS

I. Introduction 1

II. Project History 4
A. Background 4
B. *Mariner* Mars 1964 Proposals 7
C. *Mariner* Mars 1964 Chronology 9

III. Project Organization and Management 14
A. Management Structure 14
1. National Aeronautics and Space Administration 14
2. Jet Propulsion Laboratory 14
3. Lewis Research Center 14
4. Goddard Space Flight Center 14
5. U.S. Air Force Space Systems Division 14
6. Industrial Management 25
7. Permanent Project-wide Bodies 25
8. JPL Staffing at Cape Kennedy 26
B. Intra-project Arrangements 26
1. Authorizations 26
2. Interfaces 28
3. Communications 28
C. JPL Planning and Implementation 28
1. Project Policy and Requirements Document 28
2. Weekly Project Meetings 30
3. Documentation 31
4. Change Control 31
5. Problem/Failure Reports 34
6. Reviews 34
7. P-list 35
8. Pocket Guide 35
D. Schedules and Progress Monitoring 35
1. Schedule Packages 35
2. Flow Plans 36
3. Biweekly Reports 36
4. Special Reports 36

IV. Launch Vehicle System 37
A. Background 37
B. Development of Interface Hardware 40
1. The Shroud System 40

CONTENTS (Cont'd)

2. Over-the-nose Shroud System Design, Development, and Qualification 40
3. Over-the-nose Fiberglass Shroud System Failure Investigation 45
4. All-metal Shroud Fabrication and Qualification 46
5. Shroud System Performance 46
6. Interface Instrumentation and *Agena* Telemetry 47

C. Conversion and Activation of Launch Complexes 48
1. Launch Complex Conversion 48
2. RF Links 49
3. Launch Complex Validations 50

D. Launch Vehicle 50
1. *Atlas* Vehicle 51
2. *Agena D* Vehicle 53
3. Payload Capability 55
4. Flight Performance 57

E. Launch Operations Summary 58
1. Prelaunch Operations 58
2. Countdown and Summary of Launch-on-time Experience 63
3. Launch and Hold Criteria 65
4. Documentation 65

V. Spacecraft System 68

A. General Description 68
1. Power 68
2. Telecommunications 68
3. Attitude Control 76
4. Central Computer and Sequencer 76
5. Propulsion 76
6. Pyrotechnics 77
7. Temperature Control 77
8. Structure 77
9. Science 77

B. Spacecraft Mechanical Configuration 78
1. The Octagon 78
2. Propulsion System 78
3. Attitude Control Gas System 81
4. Solar Pressure Vane System 81
5. Solar Panels 81
6. Attitude Reference Sensors 81
7. Antennas 82
8. Science 82

CONTENTS (Cont'd)

9. Temperature Control 83
10. Adapter Interface 83
C. System Reliability Considerations 83
D. Alternate Modes of Operation 86
E. Spacecraft Weight Control 87

VI. Spacecraft Subsystems: Structure 93
A. Octagon Structure 94
1. Design Description 94
2. Detailed Design 97
3. Material Selection 97
4. Forging Process 98
5. Piece-part Fabrication 98
6. Final Inspection and Assembly 98
7. Special Handling Equipment 99
B. Superstructure 100
1. Function 100
2. Description 100
3. Fabrication 100
C. Solar Panel Structure 102
1. Description 102
2. Design Evolution 102
3. Fabrication 104
4. Testing 105
D. Solar Panel Transporter 107
E. Boost Dampers 107
1. Functional Description 108
2. Design Evolution 109
3. Fabrication 110
4. Testing 111
F. Solar Panel Actuation System and Solar Panel Cruise Dampers 113
1. Functional Description 113
2. Design Evolution 114
3. Fabrication 120
4. Testing 121
G. Science Platform and Actuator 123
1. Functional Description 123
2. Design Implementation 124
3. Design Evolution 129
4. Test Experience 130
H. Structural Design, Analysis, and Testing 131
1. Design Loads and Criteria 131

CONTENTS (Cont'd)

2. Design Approach and Development Plan 131
3. Structural Design and Development 132
4. Composite Analysis 136

VII. Spacecraft Subsystems: Radio 138
A. General Description 138
B. Functional Description 138
1. Reception 138
2. Transmission 142
C. Procurement 144
D. Antenna Subsystem 145
1. Design Evolution of the Low-gain Antenna 146
2. Design Evolution of the High-gain Antenna 148
3. Special Tests 151
4. High-gain Antenna Mechanical Development 152
5. Low-gain Antenna Mechanical Development 157
6. Antenna RF Transmission Lines 159
7. Structural–electrical Interactions of the Low- and High-gain Antenna Design 161
8. Antenna Procurement 161

VIII. Spacecraft Subsystems: Command 162
A. Functional Description 162
1. Command Detector 163
2. Command Decoder 165
3. Command Telemetry 166
B. Physical Description 167
C. Design Evolution 167
D. Procurement and Fabrication 168
E. Test Experience 169

IX. Spacecraft Subsystems: Power 170
A. System Mechanization 170
B. Power Source 170
C. Energy Storage 170
D. Power Regulation 172
E. Direct Current to Alternating Current Inversion 173
F. Power Frequency Synchronization 173
G. Power Distribution 173
H. Battery Charging 173
I. Engineering Telemetry 175
J. Solar Panel Standard Cell Transducers 175
K. Detail Design 176

CONTENTS (Cont'd)

L. Design Evolution 176
1. Subsystem 176
2. Conversion Equipment 178
3. Battery 179
M. Procurement and Fabrication 180
1. Subsystem Conversion Equipment 180
2. Battery 182
3. Solar Panels 182

X. Spacecraft Subsystems: Central Computer and Sequencer 184
A. Functional Description 184
B. Physical Description 190
C. Procurement 190
D. Design and Reliability Effort 191
1. JPL Pre-contract Effort 191
2. JPL/STL Effort 193
3. JPL Post-contract Design 194
E. Fabrication 194
F. Environmental and Postenvironmental Subsystem Tests . . . 195
1. Flight-acceptance Tests 195
2. Type-approval Tests 195
3. Special Tests 196
G. CC&S Performance in Spacecraft System Tests 197

XI. Spacecraft Subsystems: Data Encoder 198
A. Input System 200
1. Commutator 200
2. Sequencer 200
3. Commutator Programmer 200
4. Mode Changing 202
5. Analog Signal Conditioning 203
6. Temperature Measurements 203
7. Digital Signal Conditioning 206
8. Command Detector Monitor 206
9. Event Timer 206
10. Low-speed Deck Position Indicator 207
B. Basic System 207
1. Rate Selector 207
2. Pseudonoise Generator 207
3. Analog-to-digital Converter 208
4. Transfer Register and Data Selector 208

CONTENTS (Cont'd)

5. Biphase Modulator–Mixer 210
6. Power Supply 211
C. Physical Description 211
D. Design Evolution 212
E. Procurement 212
F. Fabrication 212
G. Test Experience 213
H. System Performance 213

XII. Spacecraft Subsystems: Attitude Control 214
A. Purpose and Description 214
1. Acquisition and Cruise Functions 214
2. Maneuver Functions 217
3. *Mariner* Mars 1964 Cruise Attitude Control Subsystem Definition 219
B. System Design Considerations 221
1. Pitch and Yaw Acquisition and Cruise 221
2. Roll Acquisition and Cruise 224
3. Attitude Control Gas Requirement 227
C. Celestial Sensors 229
1. Canopus Sensor 229
2. Sun Shutter 246
3. Sun Sensors 249
4. Sun Gate 252
5. Earth Detector 252
D. Other Attitude Control Subsystems 255
1. Gas Actuator System 255
2. Solar Pressure Vanes 261
3. Jet Vane Actuators 264
4. Gyro Control Assembly 265
E. Flight Performance of the *Mariner IV* Attitude Control Subsystem 267
1. Initial Sun Acquisition 267
2. Star Acquisition 268
3. Solar Vane Acquisition 269
4. First Midcourse Maneuver Sequence 270
5. Second Midcourse Maneuver Sequence 271
6. Autopilot Performance 271
7. Cruise Performance 271

XIII. Spacecraft Subsystems: Propulsion 273
A. Subsystem Description 273

CONTENTS (Cont'd)

B. Spacecraft Weight and CG Determination, and PIPS Positioning 276
1. Propulsion System Alignment 276
2. Weight and CG Measurement 277
3. Method of Vernier Adjustment 280
4. Measurement and Alignment Results 280
C. Performance Capability 282
D. Development and Testing Program 283
1. Component Level Testing 284
2. System Level Testing 287

XIV. Spacecraft Subsystems: Pyrotechnics 291
A. Firing Units 291
1. Design Considerations 291
2. Development and Testing 292
3. Pyrotechnic Monitor Console 294
4. Field Test Kit 294
B. Pyrotechnic Arming Switch 295
1. Description 295
2. Tests 296
C. Separation-initiated Timer 296
1. Functional Description 296
2. Design Implementation 296
3. Installation and Arming 297
4. Test Experience 298

XV. Spacecraft Subsystems: Video Storage 299
A. Subsystem Requirements 299
B. Functional Description 300
1. Technical Characteristics 300
2. Launch Mode 300
3. Record Mode 301
4. Reproduce Mode 303
5. Temperature and Pressure Monitoring 306
C. Physical Description 306
D. Development History 308
E. Procurement 309
F. Fabrication 310
G. Test Experience 310

XVI. Spacecraft Subsystems: Temperature Control 312
A. Temperature Control Subsystem Design 312
1. Requirements 312

CONTENTS (Cont'd)

2. Design Evolution 312
3. Test Experience 313
B. Thermal Shields 314
1. Description 314
2. General Requirements 314
3. Thermal Shield Design 315
4. TCM Testing 317
5. PTM Testing 319
6. Flight Spacecraft Simulator Tests 319
C. Louvers 321
1. Functional Description 321
2. Design Implementation 321
3. Test Experience 323
D. Surface Finishes and Materials 324
1. Surface Selection Criteria 324
2. Applications 324
E. Absorptivity Standard 326
1. Background 326
2. Design Constraints 327
3. Detail Design Description 327
4. Early Flight Results 329

XVII. Spacecraft Subsystems: Electronic Packaging and Cabling 330
A. Packaging Design 330
B. Subassembly Development 330
C. Electronic Assembly and Chassis Development 330
D. Electronic Equipment Integration 335
E. Packaging Techniques 336
1. Planar Packaging 336
2. Hybrid Packaging 336
3. Welded NRT DAS Packaging 336
4. Receiver and Exciter Packaging 338
5. Other Packaging Techniques 338
F. Science Instrument Packaging 339
G. TV Camera Packaging Development 340
1. Tube Failure Investigation 340
2. Tube Environment and Mounting Investigation 340
3. Test Fixtures and Test Methods 341
H. Electronic Equipment Handling, Storing, and Shipping . . . 342
I. Spacecraft Cabling 342
1. Design Concept 342

CONTENTS (Cont'd)

2. Materials 344
3. Fabrication 345
4. Test 346

XVIII. Spacecraft Subsystems: Science 348
A. General Description 348
B. Cosmic Ray Telescope 353
1. Experimental Objectives 353
2. Description 354
3. Design Evolution 356
4. Fabrication 356
5. Test Experience 357
C. Cosmic Dust Detector 358
1. Experimental Objectives 358
2. Description 358
3. Procurement 359
4. Fabrication 359
5. Test Experience 360
D. Trapped Radiation Detector 360
1. Experimental Objectives 360
2. Description 360
3. Procurement 361
4. Fabrication 361
5. Test Experience 361
E. Ionization Chamber 362
1. Experimental Objectives 362
2. Description 363
3. Design Evolution 365
4. Procurement 365
5. Fabrication 365
6. Test Experience 365
F. Solar Plasma Probe 365
1. Experimental Objectives 365
2. Description 366
3. Procurement 369
4. Fabrication 369
5. Test Experience 369
G. Helium Magnetometer 369
1. Experimental Objectives 369
2. Description 370
3. Design Evolution 371
4. Procurement 373
5. Fabrication 373
6. Test Experience 373
H. Television Subsystem 374
1. Experimental Objectives 374

CONTENTS (Cont'd)

2. Description 374
3. Design Evolution 376
4. Procurement 379
5. Fabrication 381
6. Test Experience 381

I. Planetary Scan Subsystem 384
1. Description 384
2. Design Evolution 386
3. Procurement 387
4. Fabrication 387
5. Test Experience 387

J. Data Automation Subsystem 388
1. Functional Description of the Real-time DAS 388
2. Functional Description of NRT DAS 392
3. Physical Description 394
4. Design Evolution 394
5. Procurement 396
6. Fabrication 397
7. Test Experience 400

K. Narrow Angle Mars Gate 401
1. Design Evolution 401
2. Test Experience 403
3. Flight Experience 405

XIX. Spacecraft Operational Support Equipment 406
A. System Management Tools 406
B. Facilities 407
1. JPL Facilities 407
2. AFETR Facilities 407

C. System Test Complex 408
1. Basic Capabilities 409
2. Functional Description 410
3. Electrical Characteristics 411
4. Calibration Program 411
5. Radio Subsystem OSE 411
6. Flight Command Subsystem OSE 412
7. Ground Command Subsystem OSE 415
8. Power Subsystem OSE 417
9. Central Computer and Sequencer OSE 421
10. Data Encoder Subsystem OSE 424
11. Attitude Control Subsystem OSE 425
12. Pyrotechnic Subsystem OSE 429

CONTENTS (Cont'd)

13. Video Storage Subsystem OSE 430
14. Science Subsystem OSE 430
15. Computer Data System 432
16. Telemetry Teletype Encoder 433
17. Central Timing System 435
18. Central Recorder 435
19. Ground Telemetry Subsystem 437
20. Telemetry Processing Subsystem OSE 439
D. Launch Complex Equipment 439
1. Launch Support Power OSE 440
2. LCE Electrical System 443
3. Delivery and Evaluation 443
4. Special Equipment 443
5. Problems and Limitations 443
E. Mechanical Support Equipment 444
1. Ground Handling Equipment 444
2. Magnetometer Mapping Fixture 447

XX. Environmental and Life Tests 449
A. System-level Environmental Tests 452
1. System-level TA Testing 452
2. System-level FA Testing 461
B. Subsystem Environmental Tests 465
1. Subsystem TA Environmental Testing 467
2. Subsystem FA Environmental Testing 468
3. Magnetics 469
4. Life Testing 471
5. Miscellaneous Subsystem Environmental Tests 472
6. Analysis of Subsystem Environmental Tests 475
C. Miscellaneous Qualification and Developmental Testing . . . 477
1. Spacecraft Structural Tests 477
2. STM Testing 482
3. TCM Testing 485
4. DTM Testing 488
5. XTM Testing 491
6. Launch Vehicle Interface Tests 493
7. Other Developmental/Qualification Testing 494
D. Special Problems 502
1. Canopus Sensor 503
2. Vidicon Camera 503
3. LMSC Instrumentation System 504
4. Summary 504

CONTENTS (Cont'd)

XXI. System Tests 505
A. PTM System Testing 505
1. Test Description 505
2. Test Chronology 506
B. Flight Spacecraft System Testing 514
1. Test Description 514
2. *Mariner III* Test Chronology 516
3. *Mariner IV* Test Chronology 521
4. MC-4 Test Chronology 523

XXII. Quality Assurance and Reliability 525
A. The Quality Assurance Program 525
1. Organization 525
2. Systems and Procedures 526
3. Parts Screening Program 527
4. In-process Inspection 527
5. Spacecraft Equipment Certification at SAF 529
6. Spacecraft Shipment to Cape Kennedy 530
B. The Reliability Program 531
1. Reliability Audit 531
2. Problem/Failure Reporting 531
3. Environmental Testing 531
4. Reliability Prediction and Failure Mode Analysis 531
5. Design Review 533
6. Parts Screening 533
7. Failure Analyses 534
8. Postlaunch Reliability Analysis 534

XXIII. Space Flight Operations System 535
A. Organization 535
1. SFO System Design 535
2. Technical Analysis Groups 536
3. Data Processing 538
B. Computer Programs 539
C. SFO System Checkout 539
1. Spacecraft Operational Compatibility Tests 539
2. Operational Tests 544
D. *Mariner* Mars 1964 Mission Summary 545
1. *Mariner III* Summary 545
2. *Mariner IV* Summary 549

XXIV. Systems Analysis and Mission Planning 552
A. Mission Planning 552

CONTENTS (Cont'd)

1. Studies of Impact Probability 552
2. Launch Constraints Analysis 555
3. Range Safety Waiver Request 558
4. Model of Mission-success Probability 558
5. Tracking and Performance Panel Activities 562
6. Operations Optimization 562
7. Mission Analysis of *Mariner III* 563

B. Trajectory Design 563
1. History and Analysis 563
2. Mission Targeting 569
3. *Mariner IV* Biasing 569
4. Flight Results 569

C. Guidance Analysis 575
1. Preflight Analysis and Characteristics of *Mariner* Mars Guidance 575
2. Midcourse Maneuver Operations Program 578
3. Flight Results 581

D. Orbit Determination 584
1. Orbit Determination Methods and Tools 584
2. Accuracy Requirements and Preflight Studies 586
3. Computer Program Development 588
4. Real-time Space Flight Operations 588

XXV. Tracking and Data Acquisition System 591

A. Tracking and Data Acquisition Requirements 591
1. Development and Classification of Requirements 592
2. Launch Vehicle Tracking Requirements Placed on AFETR 592
3. *Agena* Booster Tracking Requirements Placed on GSFC 592
4. Mission Requirements for Tracking Placed on AFETR 592
5. Mission Requirements for Tracking Placed on the DSN 592
6. Telemetry Coverage Requirements 595

B. Support and Facilities 596
1. AFETR Support 596
2. GSFC Support 596
3. DSN Support 600

C. Operational Readiness Testing 613
1. Phase I: Facility Internal Tests 613
2. Phase II: Spacecraft–operations Compatibility Tests . . . 614
3. Phase III: Operational Tests 614

CONTENTS (Cont'd)

D. Tracking Operations 614
1. *Mariner III* Tracking Summary 614
2. *Mariner III* T&DA Support Summary 616
3. *Mariner IV* Tracking Summary 616
4. *Mariner IV* T&DA Support Summary 619
E. Performance Evaluation Summary 620
1. *Mariner III* T&DA Performance Evaluation 620
2. *Mariner IV* T&DA Performance Evaluation 623

XXVI. Problems and Recommendations 628
A. Launch Vehicle System 628
B. Spacecraft System 629
1. Octagon Structure 629
2. Spacecraft Superstructure 629
3. Boost Dampers 630
4. Solar Panel Deployment System and Solar Panel Cruise Dampers 631
5. Science Platform 632
6. Solar Panel Structure 633
C. Radio Subsystem 633
1. Green Corrosion 633
2. Capacitor Problems 633
3. Varactor Diode 633
4. Uniformity of Modules 634
5. RF Filter 634
6. Load Isolator 634
7. Receiver and Exciter Power Supplies 634
8. Power Amplifier and Power Supply 634
9. Ranging Channel 634
10. Antennas 635
11. General Recommendations 635
D. Power Subsystem 636
1. Power Regulators 636
2. Power Synchronizer 636
3. Battery Charger 636
4. Output Transformer 636
5. Battery 636
6. Flight Converter Fabrication 636
E. CC&S Subsystem 637
F. Data Encoder Subsystem 637
G. Attitude Control Subsystem 638
1. Gyro Control Assembly 638

CONTENTS (Cont'd)

2. Solar Pressure Vanes 639
3. Canopus Sensor 639
4. Earth Detector 639
5. Sun Gate and Sun Sensors 639
6. Sun Shutter 639

H. Propulsion Subsystem 640

I. Pyrotechnic Subsystem 640
1. Pyrotechnic Firing Units 640
2. Pyrotechnic Arming Switch 640
3. Separation-initiated Timer 641

J. Video Storage Subsystem 641
1. Electronic Design Changes 641
2. Mechanical Design Changes 642

K. Temperature Control Subsystem 644
1. Thermal Shields 644
2. Louvers 644
3. Finishes and Materials 644

L. Spacecraft Harnessing 646

M. Science Subsystem 646
1. Cosmic Ray Telescope 646
2. Cosmic Dust Detector 647
3. Trapped Radiation Detector 647
4. Ionization Chamber 647
5. Solar Plasma Probe 648
6. Helium Magnetometer 648
7. Television Subsystem 648
8. Planetary Scan Subsystem 649
9. Narrow Angle Mars Gate 649
10. Data Automation Subsystem 650

N. Operational Support Equipment 651
1. Radio OSE 651
2. Video Storage Subsystem OSE 652
3. Ground Handling Equipment 652

O. Environmental Tests 652
1. Dynamic Environments 653
2. Thermal–vacuum Environments 656
3. Magnetics 656
4. Other Problems, Overtests, and Anomalies 656
5. Recommendations 656

Abbreviation List 665

References 668

TABLES

1. *Mariner II* science experiments 7
2. *Mariner* Mars 1964 chronology 10
3. Interface documentation 28
4. Approved engineering change request records 34
5. New features of *Mariner* Mars 1964 launch vehicle and interface . . . 38
6. Summary of key project milestones for the Launch Vehicle System . . . 39
7. *Agena* telemetric measurements of the spacecraft environment . . . 48
8. Launch complex conversion equipment provided by JPL 49
9. Payload performance improvement items implemented for *Mariner* Mars 1964 55
10. Launch vehicle flight event times 57
11. A calendar of major activities at AFETR 59
12. *Atlas* 289D (*Mariner III*) prelaunch problems and field modifications . . 60
13. *Agena* 6931 (*Mariner III*) prelaunch problems and field modifications . 61
14. *Atlas* 288D (*Mariner IV*) prelaunch problems and field modifications . . 62
15. *Agena* 6932 (*Mariner IV*) prelaunch problems and field modifications 63
16. Telemetry channel assignment 71
17. Description of ground commands 75
18. Summary of system redundancy 85
19. Operational flexibility 90
20. Comparative JPL solar panel systems 103
21. Secondary structure vibration test response 133
22. Vibration testing results for flight antenna configuration 133
23. Comparison of analytical and STM modal testing results 137
24. Radio subsystem characteristics 139
25. Low-gain antenna electrical characteristics 148
26. High-gain antenna electrical characteristics 149
27. Power subsystem command capability 174
28. Power subsystem telemetry measurements 175
29. Time between telemetry data samples 175

TABLES (Cont'd)

30. Conversion equipment: component parts status 176
31. Power subsystem reliability 178
32. *Mariner* Mars 1964 CC&S flight sequence 187
33. Detailed CC&S flight sequence explanation 189
34. Environmental and postenvironmental test times 195
35. MC-TA environmental tests 196
36. Attitude control subsystem sequence of operation 222
37. Parametric summary 228
38. Gas Weights for 200-day mission 229
39. Canopus sensor functional requirements imposed by the attitude control subsystem 230
40. Summary of image dissector tube development for *Mariner* Mars star sensor 233
41. Roll error signal 234
42. Diffuse reflectance characteristics of various spacecraft surface finishes 239
43. Light levels required for 0.04 × Canopus 239
44. Statistical test results on a group of 24 primary pairs of Sun sensors . . 251
45. Response time vs light level 254
46. Conductance vs light level 254
47. Thrust-valve specifications 259
48. Weight, CG, and motor alignment of *Mariner* Mars 1964 spacecraft . . 281
49. Nominal performance summary 282
50. Propulsion system weight breakdown 282
51. Summary of vibration testing on a typical *Mariner* Mars spacecraft propulsion system 288
52. Firing ½-amp squibs with midcourse breadboard at reduced energy and −10°C 292
53. Firing 1-w squibs with midcourse prototype 292
54. Firing ½-amp squibs with prototype at reduced energy 293
55. Video storage subsystem technical characteristics 300
56. Mechanical characteristics of VSS electronic subassemblies 308
57. *Mariner* Mars 1964 science instruments and ancillaries 348
58. *Mariner* Mars 1964 principal investigators 350
59. Trapped Radiation Detector counting rates 361

TABLES (Cont'd)

60. Description of Solar Plasma Probe electronics modules 366
61. Plasma Probe voltage sampling format 368
62. *Mariner* Mars 1964 DAS real-time format details 391
63. Specific NAMG requirements 401
64. Power subsystem OSE major assemblies 418
65. System-level environmental test problems and innovations 449
66. Assembly-level vibration vs thermal–vacuum performance 450
67. System-level environmental test requirements 453
68. Vibration test levels 453
69. Roll axis sine-wave inputs 455
70. RF simulation levels and test margins 460
71. EMI receiver equipment sensitivity and requirements 461
72. MC-2 vibration test run schedule 462
73. Comparison of spacecraft FA noise test levels 463
74. Assembly-level environmental test requirements 466
75. Subsystem environmental test summary 466
76. Classification of subsystem environmental test problems or failures . . 467
77. FA environmental test recapitulation 468
78. Magnetics evaluation of *Mariner* Mars 1964 hardware 470
79. *Mariner* Mars 1964 life tests 472
80. Failures encountered during life tests 474
81. Spacecraft separation test conditions and results 492
82. Supplementary objectives of PTM system testing 506
83. PTM test objectives and acceptance criteria 507
84. Flight spacecraft test objectives and acceptance criteria 515
85. Comparative system test schedules, *Mariner III* and *Mariner IV* . . . 520
86. Major operations performed under the quality assurance program . . 525
87. Distribution of electronic and electromagnetic parts throughout the *Mariner* Mars spacecraft subsystems 534
88. SFO computer program description 540
89. Selected aiming points 569
90. Orbit used for determination of the *Mariner IV* midcourse maneuver . . 574
91. *Mariner IV* postmidcourse orbit 574

TABLES (Cont'd)

92. Trajectory characteristics at encounter 574
93. Trajectory characteristics and 1σ dispersions due to injection errors . . 577
94. Aiming zone values 580
95. Terminal conditions 583
96. Maneuver parameters 583
97. Three-limit cycle positions 584
98. T&DA support facilities: *Mariner* Mars 1964 near-Earth trajectory phase 591
99. Launch vehicle tracking coverage required of AFETR (LeRC requirements) 593
100. Launch vehicle tracking coverage required of AFETR (JPL requirements) 594
101. JPL requirements for *Mariner* Mars 1964 spacecraft tracking coverage by the DSN 594
102. DSIF tracking data accuracy 595
103. AFETR launch vehicle telemetry coverage (LeRC requirements) 595
104. AFETR spacecraft telemetry coverage (JPL requirements) 595
105. AFETR instrumentation summary for *Mariner* Mars 1964 598
106. DSIF characteristics and capabilities for *Mariner* Mars 1964 602
107. Operational frequency assignments during flight 602
108. Compatible telecommunications modes 603
109. Ground modes 603
110. Acquisition and prediction information for DSIF stations 603
111. Data logging and processing capabilities 610
112. Operational modes of the data processing subsystem 612
113. Summary of *Mariner III* radar tracking coverage 617
114. Summary of *Mariner III* telemetry coverage 617
115. DSIF station tracking periods through December 1, 1964 618
116. DSIF station tracking periods for anticipated midcourse maneuver . . 618
117. DSIF station tracking periods for midcourse maneuver attempt 618
118. Spacecraft commands for midcourse maneuver 619
119. Summary of *Mariner IV* radar coverage 619
120. Summary of *Mariner IV* telemetry coverage 620
121. Summary of problems encountered during environmental tests . . . 653

TABLES (Cont'd)

122. Environmental test equipment or facility malfunction due to operator error and procedural or inspection inadequacy 657
123. Environmental test equipment or facility damage 658
124. Other problems and malfunctions 659

FIGURES

1. Liftoff of *Mariner IV* from Launch Complex 12 at Cape Kennedy 2
2. *Mariner II* spacecraft, showing some of the science and engineering equipment 6
3. *Mariner* Mars 1964 master schedule as of October 28, 1964 8
4. NASA organization 15
5. Organization of NASA Office of Space Science and Application 16
6. JPL organization 17
7. Spacecraft System management organization 18
8. SFO System management organization 19
9. DSIF System management organization 19
10. *Mariner* Mars 1964 system assignments 20
11. *Mariner* Mars 1964 Project organization 20
12. Lewis Research Center organization 21
13. *Agena* project organization 22
14. John F. Kennedy Space Center organization 23
15. Goddard Space Flight Center organization 24
16. Lockheed Missile and Space Company, Space Programs Division organization 25
17. *Mariner* Mars 1964 operations organization 27
18. Project/system interfaces 29
19. Project matrix organization 30
20. Number of engineering change requests initiated per month 32
21. Accumulated engineering change request profile 33
22. *Mariner* Mars 1964 launch vehicle configuration 50
23. Exploded view of *Mariner* Mars 1964 launch vehicle 51

FIGURES (Cont'd)

24. *Agena D* basic configuration 53
25. History of spacecraft weight and launch vehicle payload capability 56
26. JPL launch-on-time experience 64
27. *Mariner* Mars 1964 spacecraft 69
28. Functional diagram, data encoder commutator 70
29. Flight spacecraft mechanical configuration 79
30. Sequence flow diagram, launch to Sun acquisition 88
31. Sequence flow diagram, roll acquisition 89
32. Spacecraft weight history 92
33. Octagon structure longeron 95
34. Electronic chassis mounting surfaces 95
35. Octagon structure lower ring 96
36. Octagon structure 97
37. Octagon structure final inspection 99
38. Electronic chassis removal fixture 100
39. Superstructure 101
40. Superstructure ring in welding fixture 101
41. Solar panel dynamic modal survey 104
42. Solar panel preliminary acoustical test setup 106
43. Solar panel shroud impact test setup 106
44. Low-frequency longitudinal vibration test setup 106
45. Solar panel deployment test setup 107
46. Solar panel transporter 107
47. Solar panel damper configuration 108
48. Low-gain antenna damper configuration 109
49. Low-gain antenna short damper assembly 110
50. Solar panel boost damper 110
51. Low-gain antenna dampers 111
52. Shipping container, solar panel boost damper 112
53. Damper spring testing fixture 112
54. Solar panel boost damper test machine 113
55. Damper test console 114

FIGURES (Cont'd)

56. Solar panel boost damper rms force vs peak velocity 114
57. Cruise damper installation 115
58. Torsion bar solar panel actuator 115
59. Central solar panel retarder 116
60. Deployment spring installation 117
61. Solar panel open switch and flight cruise damper installation 118
62. Mark I solar panel cruise damper 118
63. Mark I solar panel cruise damper and latch assembly 119
64. Mark II cruise damper, section view 120
65. Mark II cruise damper latch 120
66. Mark II cruise damper components 121
67. Damper filling apparatus 121
68. Solar panels before deployment test 122
69. Damper spring rate test setup 123
70. Cutaway view of science platform 124
71. Platform installed with turret shield 125
72. Scan actuator with cover removed 126
73. Scan actuator clutch assembly 127
74. Science cover assembly 127
75. TV light array assembly 128
76. Cover latch and lanyard assembly 129
77. PIPS structural design 134
78. PIPS structural component idealization 135
79. Forced response analysis structural idealization for solar panels . . . 136
80. Radio subsystem 139
81. Complete radio subsystem assembly 140
82. Radio subsystem functional block diagram 141
83. Transponder phase multiplication 142
84. Typical radio subsystem module 144
85. *Mariner IV* antennas mounted on spacecraft 145
86. *Mariner IV* low-gain antenna and high-gain antenna 146
87. Low-gain antenna aperture 147
88. Low-gain antenna damped support struts 147

FIGURES (Cont'd)

89. Low-gain antenna feed 148
90. High-gain antenna feed 149
91. High-gain antenna radiation pattern through sector minor axis . . . 150
92. High-gain antenna radiation pattern through sector major axis . . . 150
93. High-gain antenna thermal–vibration test 151
94. High-gain antenna temperature control test in 25-ft space simulator . . 151
95. High- and low-gain antenna pattern tests using the developmental test model 152
96. Low-gain antenna pattern, 0 to 180 deg constant clock angle cut, 2298 Mc 153
97. Digital antenna pattern recording of low-gain antenna mounted on flight-type spacecraft 154
98. High-gain antenna support truss 156
99. Low-gain antenna shipping and storing rack 158
100. Command subsystem functional block diagram 162
101. Command word format 163
102. Command detector functional block diagram 164
103. Command decoder functional block diagram 166
104. Typical command subsystem welded cordwood module 167
105. Command subsystem assembly 167
106. Power subsystem functional block diagram 171
107. Solar panel nominal curves: power vs voltage 172
108. Worst-case battery drain vs time 172
109. Three-phase 400-cps waveforms (with resistive loads) 173
110. Power subsystem development flow diagram 177
111. Power subsystem typical Bay I module 178
112. Power regulator assembly, Bay VIII 178
113. CC&S functional block diagram 184
114. Assembled CC&S subsystem 190
115. Typical subassembly 191
116. Contractor clean room 194
117. Data encoder functional block diagram 199
118. Commutator programmer 201
119. Mode programmer 202

FIGURES (Cont'd)

120. Digital word programmer 203
121. Temperature measurement method 204
122. Typical event counter and input conditioning stage 205
123. Command detector monitor 205
124. Event timer 206
125. Pseudonoise generator 207
126. Analog-to-digital converter 209
127. Transfer register and data selector 210
128. Biphase modulator–mixer 211
129. *Mariner* Mars 1964 data encoder 212
130. Data encoder subchassis 212
131. Spacecraft coordinate system 214
132. Sun sensors 215
133. Derived rate damping in the phase plane 216
134. Midcourse motor and jet vane orientation 218
135. Attitude control subsystem functional block diagram 220
136. Acquisition time vs derived-rate limiting 223
137. Roll acquisition block diagram 224
138. Acquisition signal for various objects 225
139. Behavior without error phase logic for a very bright object 226
140. Behavior with roll error signal polarity detection inhibit logic for a very bright object 227
141. Earth cone and clock angles vs days from injection 229
142. Canopus cone angle and Canopus sensor field of view vs time 231
143. Electrostatic image dissector tube 231
144. Canopus sensor waveforms 232
145. Fourier coefficients of modulated photocathode current expressed as a fraction of unmodulated or dc photocathode current 232
146. Rugged electron multiplier 234
147. Canopus sensor block diagram 234
148. Canopus sensor outputs vs star roll error position 235
149. Programmed changes in Canopus sensor field of view 236
150. Canopus sensor 237

FIGURES (Cont'd)

151. Canopus sensor optical system 237
152. Stray light from solar panel as seen by Canopus sensor 238
153. Intensity of stray light to cause apparent 1/25 × Canopus star intensity vs stray light angle 240
154. Roll error signal and intensity signal characteristics of Canopus sensor for Earth 241
155. Performance of Canopus sensor on Earth for the celestial geometry existing during initial roll search 241
156. Cone–clock coordinate picture at start of first roll search 242
157. Field of view of 360-deg roll search in ecliptic coordinates at start of first roll search 243
158. Predicted and actual Canopus sensor output voltage vs clock angle at time of first roll search 244
159. Example of sensor field of view and corresponding brightness measurements taken during roll search 245
160. Sun shutter electronics circuitry 247
161. Sun shutter assembly 248
162. Light intensity vs roll angle 248
163. Light intensity vs cone angle 249
164. Square root Sun sensor system characteristics 249
165. Detector mechanical arrangement (single axis) 250
166. Sun sensors, electrical diagram 250
167. Cadmium sulfide photoconductive cell characteristics 251
168. Square root Sun sensors 251
169. Sun gate assembly 252
170. Sun gate characteristics 253
171. Earth detector outputs vs cone and clock angle for a 0.05 ft-cd Earth . . 253
172. Earth detector outputs vs light intensity 253
173. Earth detector normalized sensitivity curve vs wavelength 254
174. Earth detector circuit diagram 254
175. Earth detector assembly 254
176. Predicted and actual Earth detector output voltages 255
177. Gas actuator system assembly on support fixture 256
178. Gas actuator system assembly mounted on handling fixture 256
179. High-pressure system 257

FIGURES (Cont'd)

180. Fill manifold assembly 257
181. Gas actuator system high-pressure section 257
182. Jet valve with solar vane control 257
183. Pressure vessel after burst test 258
184. Four-valve assembly 259
185. Flight nozzles 259
186. Leak test console 261
187. Solar vane and hardware mounted to back side of solar panel . . . 262
188. Functional schematics of attitude control subsystem 262
189. Functional schematics of vane control 262
190. Gyro control assembly 266
191. Postinjection propulsion system schematic 274
192. Postinjection propulsion system 275
193. One-sigma velocity increment percent error vs velocity increment . . . 276
194. Midcourse motor installation 277
195. Midcourse motor substructure 277
196. Test setup for spacecraft plane of Bay II CG determination 278
197. Test fixture for spacecraft plane of Bay II CG determination 278
198. Test setup for CG determination normal to plane of Bay II 279
199. Test setup for PIPS CG determination in plane of Bay II 279
200. Test setup for PIPS CG determination normal to plane of Bay II 279
201. Thrust degradation as a function of time 283
202. Engine tail-off impulse vs engine burn time 284
203. Propulsion system pneumatic regulator 285
204. Oxidizer explosive valve 286
205. Test setup for modal test of propulsion system 287
206. Typical event-channel and power-supply schematic diagram 291
207. Pyrotechnic firing unit 293
208. Pyrotechnic monitor console 294
209. Pyrotechnic subsystem field test kit 295
210. Pyrotechnic arming switch 295
211. Separation-initiated timer assembly 297
212. SIT with recocking tool engaged 297

FIGURES (Cont'd)

213. Tape transport subassembly with drive motors, heads, and playback preamplifiers 299
214. Launch mode functional block diagram 301
215. Record signal waveforms of video storage subsystem 301
216. Encounter sequence timing 302
217. Picture sequence timing 302
218. Record mode functional block diagram 303
219. Reproduce mode signal waveforms 304
220. Basic peak detection scheme 304
221. Reproduce mode functional block diagram 305
222. Expected temperature profile of mounting case 306
223. Expected pressure drop in mounting case 306
224. Subchassis 16A2, showing playback amplifier, peak detector, code converter, and phase comparator 307
225. Subchassis 16A3, showing voltage-controlled oscillator and playback-motor drive circuits 307
226. Subchassis 16A4, showing power supply and record command circuits 307
227. Subchassis 16A5, showing launch-mode circuitry, control circuits, and record signal circuits 307
228. Solar simulator illumination of TCM 313
229. TCM during space-simulator test 313
230. MC-2 thermal test configuration 314
231. (a) Blanket pattern installed on TCM (top) 315
231. (b) Blanket pattern installed on TCM (bottom) 316
232. Upper thermal and retarder shields (TCM) 316
233. Retarder shield 317
234. Lower shield 317
235. Case shields 317
236. Improved blanket shielding 318
237. Louvers and metal case shield 319
238. Lower shield (platform turret) 320
239. Turret labyrinth seal 321
240. Thermal–vacuum cleaning of upper thermal shield 321

FIGURES (Cont'd)

241. Assembly view of *Mariner* Mars 1964 louvers 322
242. Louvers installed on spacecraft 323
243. Absorptivity standard 328
244. Typical absorptivity standard sensor circuit 328
245. Sensor signal vs temperature 329
246. Predicted temperature history of ideal flat plate samples 329
247. Subsystem electronic packaging 331
248. Spacecraft electronic packaging viewed toward Sun 333
249. Typical *Mariner* Mars 1964 subassembly 334
250. Prototype assembly in block vibration test fixture 335
251. *Mariner* Mars 1964 assembly chassis 335
252. Typical power inverter packaging 336
253. Hybrid packaging of the TV encoder 336
254. Typical welded NRT DAS module 337
255. Typical welded sticks 337
256. NRT DAS subassembly 338
257. Subassembly sectional view 338
258. Typical RF packaging 339
259. Command subassembly 339
260. Soldered-cordwood packaging in the Cosmic Ray Telescope 339
261. Television camera section view 340
262. Comparison of tube mounts tested on hard fixture 341
263. Television special test fixture 341
264. Spacecraft Z-axis responses on TV tube 341
265. Television tube soft mount 342
266. Subassembly handling and storage container 343
267. Assembly shipping container 344
268. Bay IV data encoder and command harness 344
269. Upper and lower ring harnesses 344
270. Fabrication fixture, Bay IV data encoder and command harness . . . 345
271. Upper ring harness fabrication fixture and completed upper ring harness 345
272. Lower ring harness fabrication fixture and adjustable support stand . . 346

FIGURES (Cont'd)

273. *Mariner* Mars 1964 science subsystem functional block diagram . . . 351
274. Science subsystem real-time data format . . . 353
275. *Mariner* Mars 1964 Cosmic Ray Telescope . . . 354
276. Cosmic Ray Telescope . . . 354
277. Cosmic Ray Telescope, cutaway view . . . 355
278. Cosmic Ray Telescope functional block diagram . . . 355
279. *Mariner* Mars 1964 Cosmic Dust Detector . . . 358
280. Cosmic Dust Detector functional block diagram . . . 359
281. *Mariner* Mars 1964 Trapped Radiation Detector . . . 361
282. Trapped Radiation Detector functional block diagram . . . 362
283. *Mariner* Mars 1964 Ionization Chamber . . . 363
284. Typical Ionization Chamber circuit board . . . 363
285. Ionization Chamber functional block diagram . . . 364
286. *Mariner* Mars 1964 Solar Plasma Probe . . . 366
287. Solar Plasma Probe functional block diagram . . . 367
288. Solar Plasma Probe sensor, top and sectioned view . . . 368
289. Individual collector response . . . 368
290. Helium Magnetometer sensor and electronics modules . . . 370
291. Helium Magnetometer sensor schematic . . . 371
292. Helium Magnetometer functional block diagram . . . 372
293. Helium Magnetometer sensor mechanical structure . . . 373
294. Beryllium cassegrain mirrored telescope . . . 374
295. Television subsystem functional block diagram . . . 375
296. Electrostatic vidicon mechanical construction . . . 377
297. Vidicon tube mechanical mounting, soft mount . . . 378
298. *Mariner* Mars 1964 planetary scan subsystem . . . 384
299. Planetary scan subsystem functional block diagram . . . 386
300. Data automation system subassemblies . . . 388
301. Real-time DAS functional block diagram . . . 389
302. Real-time DAS word format . . . 390
303. NRT DAS functional block diagram . . . 393
304. NRT DAS word format . . . 395
305. Real-time logic assembly tree . . . 397

FIGURES (Cont'd)

306. Assembled data automation system envelope 397
307. DAS logic stick 397
308. One side of a DAS logic tray 398
309. Data automation system prototype buffer 399
310. Assembled and welded non-real-time data automation system . . . 400
311. Typical trajectory encounter geometry 402
312. Nominal encounter geometry 402
313. Narrow angle Mars gate 403
314. Exploded view of narrow angle Mars gate 403
315. Electronics module 404
316. Interior of electronics module 404
317. Photosensitive cell in header 404
318. System test complex 409
319. System test complex configuration at SAF 410
320. Radio subsystem OSE 412
321. Radio subsystem OSE functional block diagram 413
322. Flight command subsystem OSE functional block diagram 414
323. Flight command subsystem OSE interfaces during spacecraft testing . . 415
324. Ground command subsystem OSE 416
325. Power subsystem OSE 418
326. Power subsystem OSE functional block diagram 419
327. Central computer and sequencer OSE 421
328. CC&S simulator 422
329. CC&S spacecraft substitution box 423
330. Data encoder OSE 423
331. Data encoder OSE functional block diagram 424
332. Attitude control OSE system test set 425
333. Attitude control OSE system test set functional block diagram 426
334. Gas-valve monitor system for use at atmospheric pressure 427
335. Gas-valve monitor for vacuum-chamber testing 427
336. Field test kit 429
337. Video storage subsystem OSE 430
338. Science OSE 431

FIGURES (Cont'd)

339. Computer data system block diagram 433
340. Typical line printer telemetry data 434
341. Univac 1218 computer and associated control console and magnetic tape units 435
342. Data input system 435
343. Computer data system real-time program flow chart 436
344. Central recorder assembly 437
345. Ground telemetry subsystem assembly 438
346. OSE configuration at Hangar AO and ESF 440
347. OSE configuration at launch complex 440
348. Launch support power OSE functional block diagram 441
349. Typical ac signal conditioning channel block diagram 442
350. Universal support ring and hoisting equipment 445
351. Spacecraft attitude on positioner 446
352. Spacecraft mounted on transport trailer for shipment 446
353. Magnetometer mapping fixture 447
354. PTM subjected to lateral vibration testing 454
355. TA and FA random noise spectra 454
356. PTM torsion test setup before installation of spacecraft adapter . . . 454
357. PTM swept torsional spectrum 454
358. Typical input spectrum, PTM roll axis noise test 455
359. Typical response spectra, spacecraft flight transducer to PTM roll axis noise test 455
360. Spectra ratio, response of spacecraft flight transducer to PTM roll axis noise spectrum 455
361. Type approval shock table input 456
362. Shock spectrum of type approval transient 456
363. Typical shock spectrum, X-direction accelerometer, PTM V-band firing 457
364. Acoustic noise spectrum 458
365. Test setup, MC-4 FA vibration test, Z axis 462
366. Space-simulator system test, solar intensity history 464
367. Comparison of simulated launch pressure profiles to maximum simulated pumpdown capability and to *Mariner* Mars 1964 launch pressures 465

FIGURES (Cont'd)

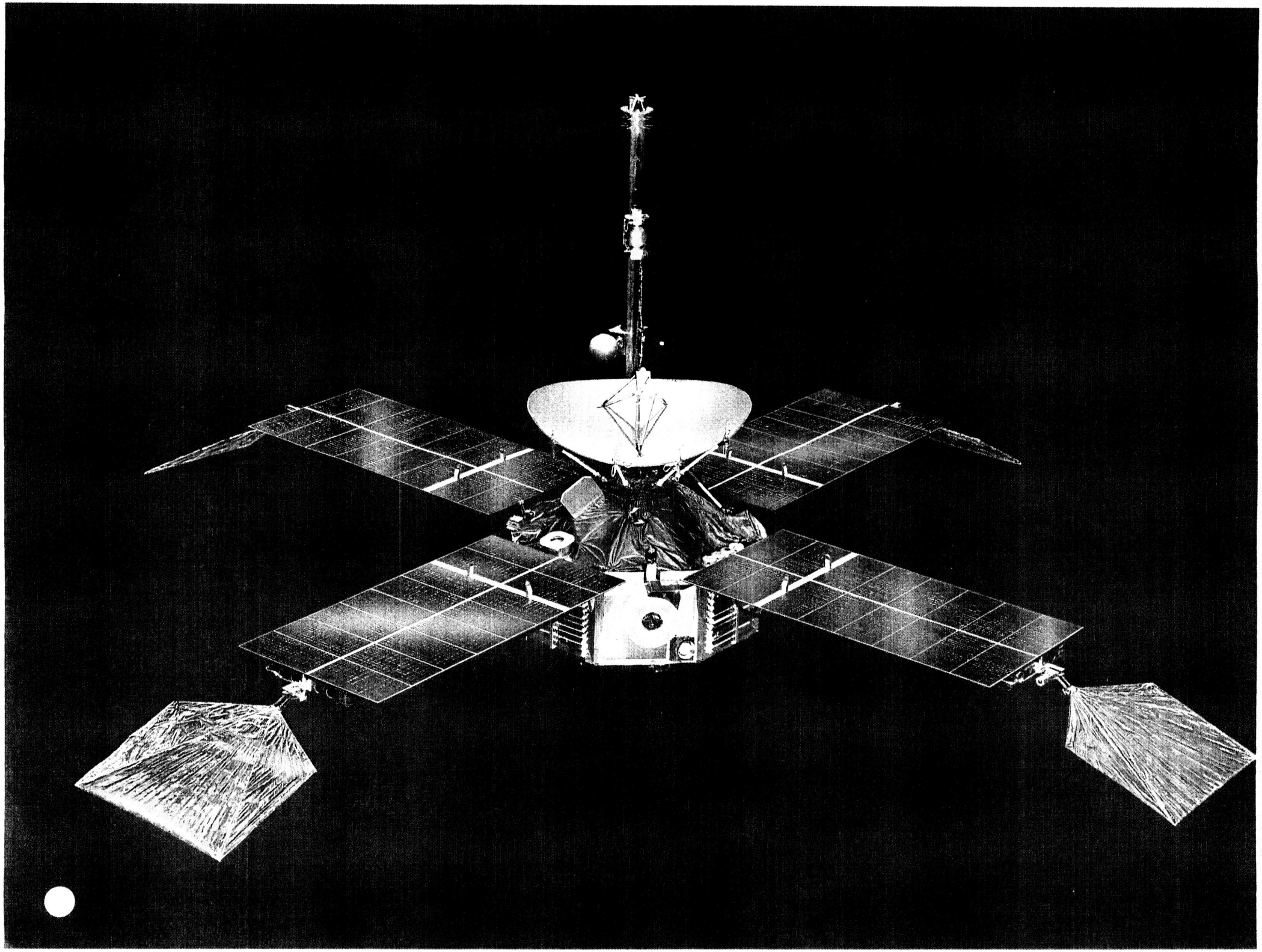
368. Test setup and response curves of vidicon-tube support-material evaluation test 476
369. Developmental spaceframe schedule 478
370. Static test setup 479
371. Overall STM vibration test setup 480
372. High-gain antenna structural response 480
373. PIPS total vector response as a function of tank pressure 481
374. Modal survey test setup 482
375. Solar panel deployment test setup, solar panels undeployed 485
376. Spacecraft setup for stray light reflectance test 487
377. Simulated midcourse interaction test blast diffuser 489
378. DTM mounted to antenna range tower 490
379. XTM separation test model configuration 491
380. Three-bay electronics chassis vibration fixture 495
381. Preliminary matchmate test setup 496
382. High-gain antenna and Canopus sensor temperature control test . . . 497
383. High-gain antenna thermal–vibration test 498
384. Thermal shield material outgassing test setup 499
385. Thermal shield blanket outgassing test setup 499
386. Boost environment spacecraft cavity pressure decay curves 500
387. Ballooned lower thermal blanket 500
388. Solar panel space-simulator test setup 501
389. Low-gain antenna extreme temperature test setup 501
390. Spacecraft in position for magnetic mapping test 510
391. Spacecraft preparation for space-simulator testing 510
392. Quality assurance organization 526
393. *Mariner* Mars 1964 parts screening program 528
394. Typical quality assurance flow plan 529
395. Typical flow of assemblies and subassemblies through SAF 530
396. Typical problem/failure report 532
397. Problem/failure quantity breakdown 533
398. Space flight operations documentation plan 535
399. Space flight operations prelaunch planning and design organization . . 536

FIGURES (Cont'd)

400. SFO operational organization 537
401. Space flight operations organization for *Mariner* Mars 1964 538
402. SFO System communications network 541
403. SFO System test schedule 542
404. Model for computing the probability of planetary impact 553
405. Preliminary summary launch constraints for *Mariner* Mars 1964 . . . 556
406. AFETR and DSIF station view periods for Group I launch period . . . 559
407. Class I tracking and telemetry coverage for Group I launch period . . 560
408. *Mariner* Mars 1964 launch constraints 561
409. Time of flight vs launch date 564
410. Earth–Mars communication distance vs launch date 565
411. Geocentric injection energy C_{3E} vs launch date 567
412. Arrival date vs launch date 568
413. Aiming point and constraint regions for Type I launch and July 15, 1965 arrival 570
414. Ascent trajectory profile 571
415. Sequence of events to Canopus acquisition 572
416. Earth track of *Mariner IV* trajectory 573
417. *Mariner IV* aiming zone and constraint region 575
418. *Mariner IV* trajectory 576
419. Earth–probe distance vs time from launch 576
420. Sun–probe distance vs time from launch 576
421. Earth cone angle vs time from launch 576
422. Type I capability ellipses at 5 days from injection 577
423. Critical coordinate system 577
424. Typical maneuver regions I, II, and III for Type I launch and July 15, 1965 arrival 579
425. Midcourse maneuver constraints 580
426. *Mariner* Mars midcourse maneuver operations program functional block diagram 580
427. Decision program logic diagram 582
428. Midcourse maneuver performance time vs magnitude 583
429. Definition of B·T, B·R system 586
430. Tracking facilities supporting *Mariner* Mars 1964 at Cape Kennedy . . 597

FIGURES (Cont'd)

431. Network communications configuration 601
432. *Mariner* Mars 1964 typical deep space station (S-band) 604
433. Mariner Mars 1964 typical deep space station (L- to S-band conversion) 604
434. Goldstone Venus station, DSIF-13 (100-kw transmitter) 605
435. Communication lines (DSN) 607
436. Data flow from AFETR and DSIF stations to the SFOF 608
437. Complete data flow within the SFOF 609
438. Complete data flow from the SFOF 610
439. Typical user area equipment 611
440. Telemetry processing subsystem 611
441. Single- and dual-thread TPS processing modes 611
442. IBM 7094 processing control scheme 613
443. Science cover honeycomb insert failure 632
444. Science cover skin delamination 632
445. Power system output transformer connections 636
446. *Mariner* Mars PTM (line spectrum) 654
447. *Mariner* Mars PTM (test No. 27) 654
448. Comparison of computed shock spectra 655



I. INTRODUCTION

The purpose of the *Mariner* Mars 1964 Project is to perform the National Aeronautics and Space Administration missions to Mars during the fourth-quarter launch opportunity in 1964. This project replaces the intended *Mariner B* Project launches originally scheduled for the 1964 opportunity, which had to be postponed because of continuing *Centaur* launch vehicle schedule slippages.

The primary objective of the *Mariner* Mars 1964 Project is to conduct close-up (flyby) scientific observations of the planet Mars during the 1964–1965 opportunity and to transmit the results of these observations back to Earth. The planetary observations should, to the greatest practical extent, provide maximum information about Mars. Television, cosmic dust, and a reasonable complement of fields and particles experiments are carried aboard the spacecraft. In addition, an Earth occultation experiment will be performed to obtain data relating to the scale height and pressure of the atmosphere of Mars.

A secondary objective is to provide experience and knowledge about the performance of the basic engineering equipment of an attitude-stabilized flyby spacecraft during a long duration space flight farther away from the Sun than the Earth. An additional secondary objective is to perform certain field and/or particle measurements in interplanetary space and in the vicinity of Mars.

The *Atlas D/Agena D* launch vehicle used in this project had a capability of injecting a separated spacecraft weight of at least 570 lb into a Mars transfer orbit. It was planned to conduct two launchings of the *Mariner* Mars 1964 mission from two separate launch pads. All activities were planned to exploit the limited launch period to the maximum extent. To accomplish this, spacecraft and launch vehicles were processed in parallel, so that, following the launch of the first spacecraft, the second vehicle could be launched without delay no sooner than 2 days after the first launch.

Some unique features, challenging technical unknowns and operational "firsts" associated with the *Mariner* Mars 1964 Project (and contributing to the riskiness of the mission), can be summarized as:

1. Extended flight time: between 230 and 260 days depending upon the trajectory (the 6000-hr lifetime requisite is about twice previous accomplishments)

2. Brief (18 to 28 day) launch period
3. Use of numerous modifications in *Atlas D* and *Agena D* to improve performance
4. *Agena D* two-burn mission using unproven propellant containment restart system
5. New shroud and ejection system
6. New spacecraft–*Agena* separation system
7. Use of the star Canopus for roll-axis attitude stabilization
8. Use of an S-band communication system and extreme (134 million mile) communication distances (2½ times prior records)
9. Provision for dual (restartable) trajectory-correction propulsion system
10. Mission requiring 9 months of successful spacecraft operation to achieve mission success
11. Use of magnetic tape for storage of flight data and replay after planetary encounter
12. Transit beyond Earth's orbit, with decreasing temperatures and radiant energy input to solar panels resulting from increasing Sun distances
13. Increased complexity evidenced by about 138,000 component parts compared to 54,000 on *Mariner II*
14. Use of the spacecraft–Deep Space Network coherent RF loop for direct measurement of a planetary environment

In contrast to the *Mariner* Venus 1962 Project, development lead time permitted (and the mission reliability demands made necessary) full use of both subsystem type approval and proof test model spacecraft validation testing concepts. Planning also provided for three complete sets of fully flight-qualified spacecraft plus a complement of critical spare assemblies. In order to qualify this hardware, the equivalent of three sets of checkout, test, and handling equipment was furnished to support testing and launch operations. As much as possible, the basic launch vehicle and spacecraft configuration extended and exploited the techniques proven on the earlier mission to Venus and on the *Ranger* flights. However, because of unique and more stringent requirements of the mission, numerous departures from previous design techniques had to be made. A considerably more rigorous parts-screening and quality-assurance activity was imposed. Backup designs were carried in several critical areas. Other protective steps were also taken to

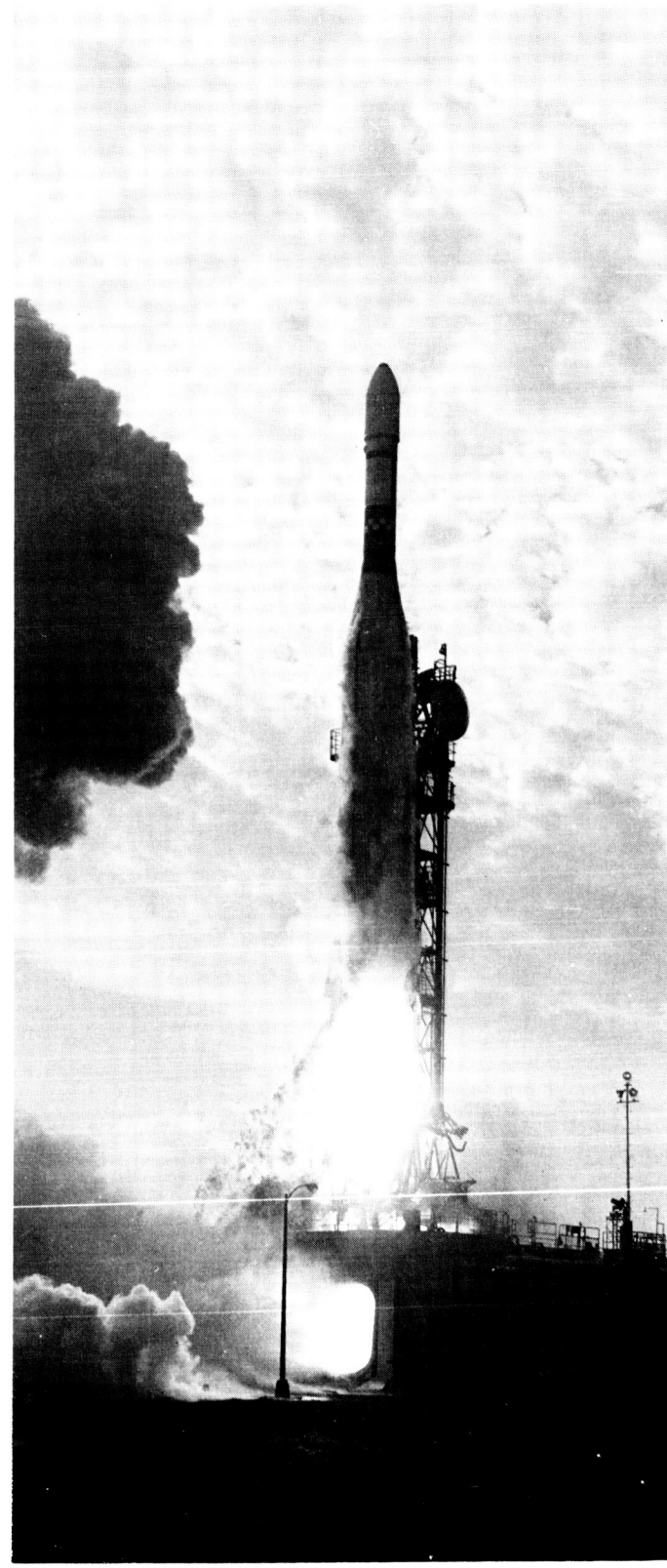


Fig. 1. Liftoff of *Mariner IV* from Launch Complex 12 at Cape Kennedy

preclude catastrophic accidents or natural phenomena from causing the effort to abort before launch could be attempted. All such actions were geared to enhance the probability of success.

The first *Mariner* spacecraft (MC-2) was launched toward Mars on November 5, 1964. The shroud failed to separate from the spacecraft (precluding, among other things, solar panel deployment) and the battery power was depleted 8 hr 43 min after launch. As quickly as an investigation had pinpointed the trouble with reasonable certainty, an all out effort was begun on the design, fabrication, and testing of a new, all-metal shroud.

The second spacecraft (MC-3) was successfully launched on November 28, 1964 from Cape Kennedy on a Mars encounter orbit about the Sun (Fig. 1). Since launch, the spacecraft and mission have assumed the title *Mariner IV* in accordance with NASA policy governing such flights.

As the initial trajectory would have carried the spacecraft about 155,000 miles ahead of the upper leading edge of Mars (beyond useful range), a trajectory correction maneuver was attempted 6 days after launch. This attempt was aborted, however, when the spacecraft roll orientation was disturbed during the critical sequence. The maneuver was successfully accomplished the next day (December 5, 1964) using slightly modified timing. As a consequence, the spacecraft will pass well within the preferred aiming zone.

The PTM (MC-1) has been assigned to support flight anomaly investigations at Pasadena. The backup flight-ready spacecraft (MC-4), selected spare assemblies, and two sets of operational support equipment have been placed in temporary bonded storage at Cape Kennedy. This equipment has been thoroughly checked out and is being protected and preserved, awaiting final disposition.

Mariner IV continues into cruise with the data from all subsystems indicating normal operation. Three CC&S cyclic pulses have been observed as anticipated.

As of midcourse maneuver, system performance has been within tolerance and the spacecraft has functioned as intended during this period. Other volumes of the project report will present flight activities and mission results to the conclusion of the *Mariner* Mars 1964 Project.

II. PROJECT HISTORY

A. Background

The *Mariner* Mars 1964 Project developed from the commitment of the Jet Propulsion Laboratory to the unmanned exploration of space for the National Aeronautics and Space Administration. Following the *Vega* program in 1959 and the *Mariner A*, *Mariner B*, and *Mariner* Venus 1962 Projects, *Mariner* Mars was activated in November 1962, in order to take advantage of the 1964 Mars launch opportunities, despite delays in the development of advanced second-stage vehicles.

The *Mariner A* spacecraft was in the 1250-lb class, and was designed to make scientific investigations in interplanetary space and in the vicinity of Venus during the 1962 and subsequent launch opportunities. The *Mariner B* spacecraft was also in the 1250-lb class and was designed to make scientific investigations in interplanetary space and in the vicinity of Venus and Mars during the 1964 and subsequent launch opportunities. Because of funding limitations, no Mars missions were scheduled in 1962. Both *Mariner A* and *B* spacecraft were to be launched by a vehicle consisting of a modified *Atlas D* first stage and a *Centaur* liquid-hydrogen/liquid-oxygen, high-energy second stage.

The *Centaur* vehicle, under development by General Dynamics/Convair, had two gimbal-mounted engines, each capable of generating 15,000 lb of thrust. Ten small hydrogen peroxide monopropellant engines were provided for attitude control, consolidation of main propellants, and final velocity correction.

The *Mariner A* configuration was originally scheduled to fly the NASA planetary missions to Venus in the summer of 1962 as a developmental spacecraft on originally designated *Atlas/Centaur 7* and *8*. However, slippages in the *Centaur* schedule began to compromise the Venus launches and the missions were forced into a rescheduling. In the summer of 1961, Space Technology Laboratories proposed an *Able M* solid-stage, spinning rocket to be launched by an *Atlas/Agena* vehicle to Mars in 1962, with a dual capability to Venus in 1962 as a backup to *Centaur* slippages. This proposal was considered but not approved by NASA.

By the second week of August 1961, it was generally recognized that the *Centaur* would not be available for the 1962 Venus launch period. Consequently, in mid-August, discussions with NASA explored the possibility of using lightweight, attitude-stabilized spacecraft for the Venus missions, since it was considered most important that the United States launch probes to the planets in 1962 if at all possible. It was also believed by both NASA and JPL that the inclusion of a midcourse guidance capability and the scheduling of two launches within the 1962 period should be accomplished if at all possible.

On August 28, 1961, in a letter to NASA Headquarters, JPL proposed the feasibility of a 1962 Venus mission, based on an *Atlas/Agena* launch vehicle and the use of a hybrid spacecraft combining features of the *Ranger 3* and *Mariner A* designs. The spacecraft for *Mariner* Venus 1962 was proposed to carry 25 lb of instruments (later increased to 40 lb). Only one launch could be guaranteed, but two were possible within the July–September 1962 period if the *Agena* weight could be reduced. The project would not require significant changes in the *Ranger* schedule, but would necessitate the transfer of certain launch vehicles.

In addition to the activation of a *Mariner* Venus 1962 Project, JPL proceeded with the design and development of the *Mariner B* spacecraft, scheduled for launch by *Atlas/Centaur* with dual Mars–Venus capability in 1964 and beyond. Simultaneous with the implementation of the *Mariner* Venus 1962 program and the shift of emphasis in *Mariner B*, the *Mariner A* Project was cancelled, the *Mariner* Venus 1962 Project was activated, and the dual planet capability for the *Centaur*-based *Mariner B* in 1964 was established by NASA authorization.

With the new *Mariner* Venus 1962 Project approved, an all-out effort was begun to design, develop, procure, assemble, test, and launch two separate spacecraft within an 11-month period. In addition, a significant launch vehicle effort involving design modifications and manufacturing changes was undertaken. The many associated efforts encompassing trajectory work, preparation for launch and flight operations, design and fabrication of special ground support equipment and handling fixtures, and implementation of AFETR support were pursued on a "crash" basis.

The *Mariner* Venus 1962 Project was undertaken with the objective of performing meaningful scientific experiments in interplanetary space and in the vicinity of Venus in 1962, with primary emphasis on experiments

relating to the surface and atmosphere of the planet. The program would also enable the Laboratory to recoup part of the investment in time and money already expended for the cancelled *Mariner A* Project.

It was determined that the total spacecraft weight would be about 460 lb, rather than the 1050 to 1250 lb originally planned for *Mariner A* and *Mariner B*. In order to meet the launch schedule, tested flight assemblies and instruments would have to be available in the assembly building at Pasadena on January 15, 1962. When possible, the estimated 40 lb of instruments would have to be procurable essentially in flight configuration, without benefit of breadboard and engineering-model phases of development. Except for the infrared radiometer, all instruments would have to be adaptations of *Ranger* or *Mariner A* designs.

The flight worthiness of the assembled spacecraft was confirmed during an elaborate series of tests conducted at Pasadena. By the end of May 1962, the equipment was ready to ship to Cape Kennedy for final launch preparations. On July 22, 1962, *Mariner 1* was launched but was destroyed by Range Safety at about L + 292 sec because of an erroneous *Atlas* yaw–lift maneuver. Elimination of a faulty character in the booster guidence equation enabled the second spacecraft to be successful. At about that time, preliminary design studies, based upon using the *Atlas/Agena* launch vehicle for the 1964 Mars opportunity, were formally inaugurated at JPL and other NASA centers. This step was taken because it became evident that a *Mariner B* mission, based on the more ambitious *Centaur*, would not be possible due to unavailability of the *Centaur* and other resource limitations. However, it was considered important to the national space effort to conduct meaningful scientific explorations of Mars during the once-every-11-year period of the quiet Sun.

The Mars mission and spacecraft configuration studies continued through the launch of *Mariner II* on August 27, 1962. In addition, guidelines were established for a *Mariner* mission to Venus during the 1964 opportunity, a proposal that was essentially a repeat, with minor revisions, of the *Mariner II* concepts and objectives.

The *Mariner II* spacecraft (Fig. 2) carried six scientific experiments, was identical to *Mariner 1*, and had the same mission: to fly by the planet Venus, performing two scientific experiments (close-range infrared and microwave measurements), and to communicate this information over an interplanetary distance of 36 million miles back to Earth. Four scientific experiments were performed during the flight and in the vicinity of Venus to collect and transmit information on interplanetary phenomena.

The flight time for *Mariner II* was approximately 109 days. The overall flight distance was approximately 180 million miles. *Mariner* passed closer to Venus than any previous Earth-launched spacecraft and was within the desired miss distance.

The *Mariner II* design was a variation of the hexagonal concept used for the JPL *Ranger* series. The hexagonal framework base housed a liquid-fuel rocket motor for trajectory correction, and six modules containing the attitude control subsystem, electronic circuitry for the scientific experiments, power supply, battery and charger, data encoder and command subsystems, digital computer and sequencer, and radio transmitter and receiver. Sun sensors and attitude control jets were mounted on the exterior of the base hexagon.

A tubular superstructure extended upward from the base hexagon, the science experiments were attached to this framework. An omnidirectional antenna was mounted at the peak of the superstructure. A parabolic, high-gain antenna was hinge-mounted below the base hexagon. Also hinged to the base hexagon, two solar panels folded up alongside the spacecraft during the launch, parking orbit, and injection phases, and were unfolded like butterfly wings for the cruise and encounter phases. A command antenna for receiving transmissions from Earth was mounted on one of the panels.

The *Mariner II* science payload is presented in Table 1. The two planetary experiments were designed to operate for a period of 30 min and at distances ranging from approximately 10,200 to 49,200 miles as *Mariner* approached Venus. These radiometers obtained information about the planet's surface temperature distribution and atmospheric thermal energy.

The other experiments made scientific measurements during cruise, through interplanetary space, and in the near vicinity of Venus. The experiments were: a magnetometer; charged-particle detectors, including an ionization chamber and several Geiger–Müller counters; a cosmic dust detector; and a solar plasma detector.

Experiencing some equipment performance degradation, *Mariner II* passed its closest approach (21,648 miles)

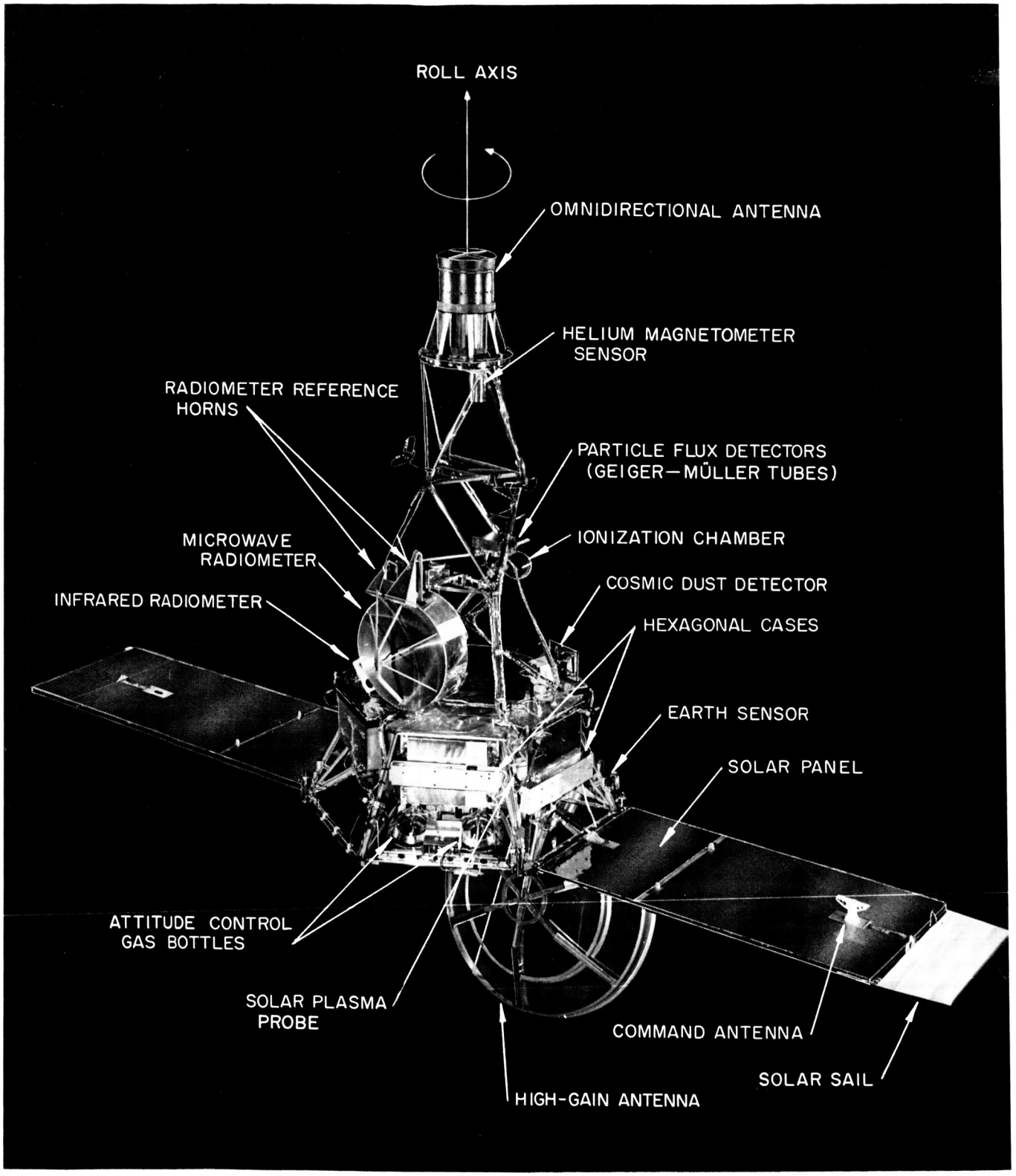


Fig. 2. *Mariner II* spacecraft, showing some of the science and engineering equipment

Table 1. *Mariner II* science experiments

Experiments	Purpose	Weight, lb	Power, w
Microwave radiometer 13.5 and 19 mm	To determine the temperature of the planet surface and details concerning its atmosphere	23.85	6.0
Infrared radiometer 8.4 and 10.4 μ	To determine any fine structure of the cloud layer	2.60	1.6
Magnetometer above 5.0 γ	To measure changes in the planetary and interplanetary magnetic fields	4.66	6.0
Ion chamber and particle flux detector Protons $>$1, 10, 20 Mev Electrons $>$ 0.4, 0.5 and 1 Mev	To measure charged-particle intensity and distribution in interplanetary space and in the vicinity of the planet Venus	2.78	0.4
Cosmic dust detector above 1.3×10^{-10} gm	To measure the density and direction of cosmic dust	1.85	0.1
Solar plasma spectrometer 240 to 8400 ev	To measure the intensity of low-energy protons from the Sun	4.77	1.0
	Total	40.51	15.1

to Venus on December 10, 1962, at about 20:00:00 GMT. Earlier in the day, the tracking station at Goldstone had transmitted a command that had started the radiometer scanning. The scan crossed the planetary disk three times. A total of eighteen data readings were obtained: five points from the sunlit side, five from the dark side, and eight across the terminator. From these readings, it was possible to confirm some theories that existed concerning the nature of Venus and to eliminate others. Comprehensive discussion of flight results as well as other information relating to the *Mariner II* mission can be found in Ref. 1 through 19.

Radio signals from the *Mariner II* spacecraft were heard for the last time by the Deep Space Instrumentation Facility station in Johannesburg, South Africa, at the conclusion of its acquisition period at 07:00:00 GMT on January 3, 1963. At that time, after 129 days of continuous operation, the spacecraft was 53.9 million miles from Earth, was 5.6 million miles beyond Venus, had traveled 223.7 million miles since launch, and had returned over 90 million bits of telemetry data.

This essentially concluded the *Mariner II* mission, except that data examination and analysis has continued over an extended period of time and results are being reported as rapidly as valid conclusions can be published.

B. Mariner Mars 1964 Proposals

The *Mariner* mission to Mars rested firmly on the foundation of technological experience accumulated on the *Mariner* Venus 1962 mission. Many design features of *Mariner* Mars were continuations and extensions of those applied on *Mariner II*, and many of the key personnel (technical, scientific, and managerial) stepped directly into the *Mariner* Mars effort upon concluding their contribution to the *Mariner* Venus Project. This continuity was considered significant.

When the *Mariner* Venus 1962 mission was formally terminated, the earlier proposals for a launch repeat in 1964 to Venus were also officially abandoned primarily due to competition for budget and manpower allocations. It was clear that another Venus fly-by and a Mars fly-by attempt could not both be sustained in 1964. However, the complete success of the *Mariner II* had made it possible for NASA to reorient its program of planetary exploration; NASA announced that, instead of repeating the Venus mission in 1964, it would concentrate on other projects such as the Mars mission for 1964, and subsequent opportunities, and on later Venus missions with more advanced spacecraft.

The feasibility of a Mars spacecraft injected by an inventory *Atlas/Agena* booster had been under intensive study by several NASA centers since before the *Mariner II* launch. The proposals resulting from these studies were presented to NASA Headquarters and exchanged among the centers. Critiques of the various proposals were also forwarded to Headquarters. While the science payload was, to a certain extent, unestablished, official go-ahead for the JPL proposal was received early in November 1962, almost exactly 2 years prior to the first launch possibility. Simultaneously, the *Mariner B* was reduced to a low-level effort. By that time, the *Mariner* Mars 1964 preliminary design had been completed, and design reviews and policy planning were

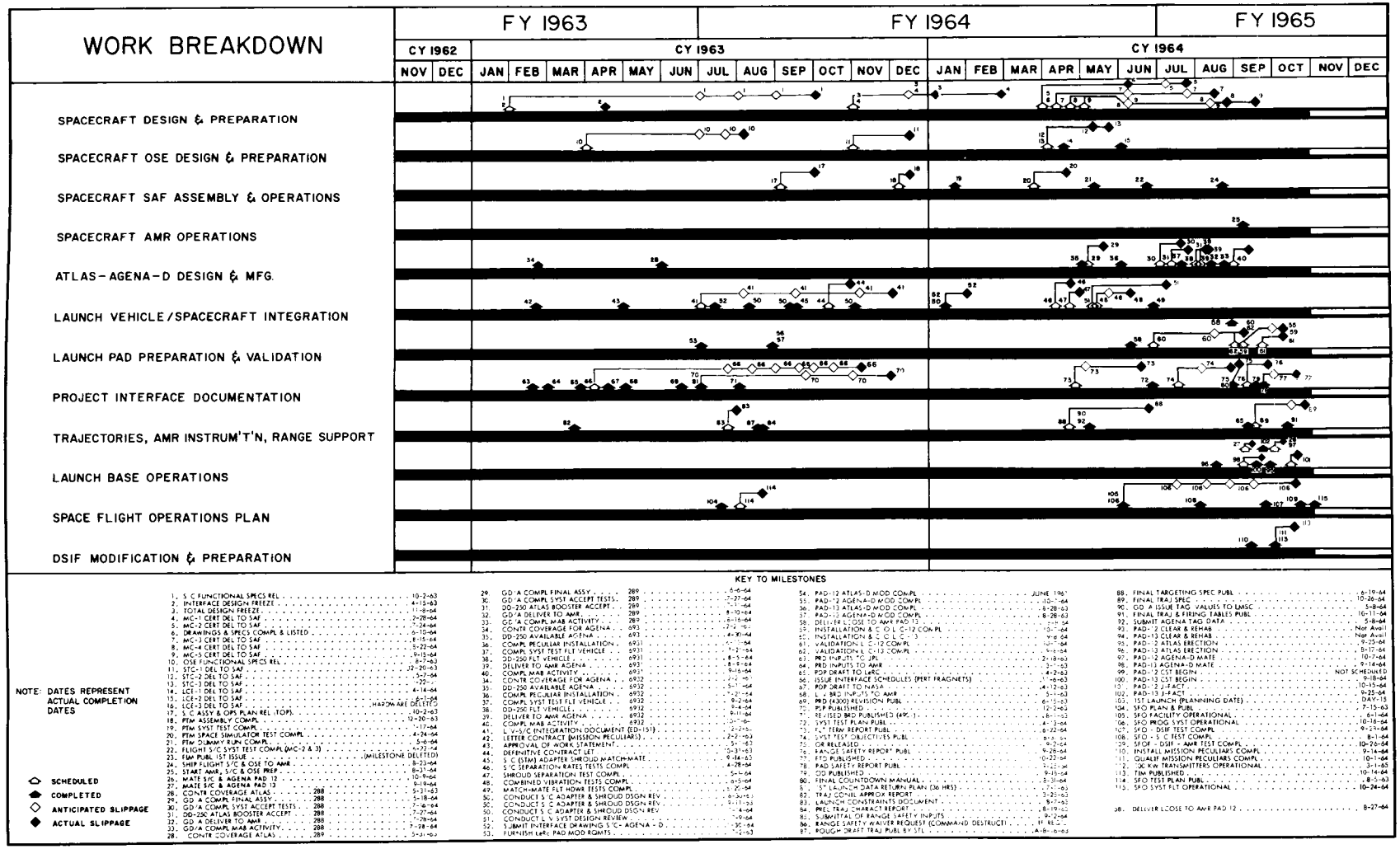


Fig. 3. *Mariner* Mars 1964 master schedule as of October 28, 1964

proceeding. Other studies had shown the necessity for up-rating the *Atlas D/Agena D* launch vehicle payload capability by approximately 100 lb. Final designation of key project systems and personnel was made after the *Mariner* Venus 1962 mission was terminated, and the project evolved as described in the following paragraphs.

C. Mariner Mars 1964 Chronology

Shortly after the formal project go-ahead was given, a master schedule (work breakdown) was established. From that vantage point, at the onset of the project, a total of 131 milestones were selected and their phasing determined across the 2 year span to launch. Inherently, these events were meant to describe the manner in which the project was to be accomplished. Similarly, they were intended to guide the evolution of subsidiary planning and deadlines for governing documentation (see Section III).

Figure 3 indicates the milestone relationships as they were originally chosen, and also compares actual completion of milestones to estimated completion dates. Of the 131 events chosen initially, 123 were eventually needed and did occur. Neglecting the criticality of some of these events, aggregate schedule attainment can be summarized as: 55% were accomplished on time, and the remainder slipped an average of 1.96 months. To this slippage the spacecraft contributed an average delay of 3.94 months, while the spacecraft and OSE combination averaged a slippage of 2.96 months. This record, together with the activities tabulated in Table 2, comprise the key elements of project history.

Beyond this chronicle of planned activities, other events also influenced the project to a significant extent. Some of these events are important because they added uncertainty, increased risk, or initiated particularly serious deviations from established plans. The impact of these unexpected events precipitated major decisions and often forced a reversion to contingency provisions implicit in the original plans. In total, these unusual activities resulted in changes to cost, schedule, and/or mission success probabilities in varying combinations and amounts.

Table 2. *Mariner* Mars 1964 chronology

Week beginning	Year	Event
May 14	1962	Question of *Atlas/Agena*-launched Mars mission first raised due to potential *Centaur* slippage.
May 21		NASA Headquarters Office of Space Science and Applications studied effects on budget to determine if *Atlas/Agena* Mars mission would be pursued.
June 4		Study begun of what spacecraft configuration could be used to fly on an *Atlas/Agena*. *Mariner* Venus 1962 equipment shipped to Cape Kennedy for final launch preparations.
June 11		JPL Systems Division proposals reviewed by Project Office.
June 18		Guidelines established for more detailed *Atlas/Agena* mission studies.
June 25		GSFC study of a Mars mission based on an *Atlas/Agena* with an *Able* M kick stage in process.
July 16		Preliminary design effort formally initiated on *Atlas/Agena* spacecraft identified as *Mariner* M. *Mariner* Venus 1962 launch aborted.
August 6		Copies of JPL *Atlas/Agena* Mars mission study sent to MSFC and LMSC for study of launch vehicle requirements.
August 13		Possibility studied of simplifying midcourse maneuver by less conventional spacecraft configuration.
August 27		JPL reviewed GSFC proposal for Mars mission. *Mariner* M proposal presented at NASA Headquarters. *Mariner II* launch successful, enroute to Venus. Policy guideline document distributed to JPL divisions with requirements for a *Mariner* Venus mission in 1964.
September 10		Possibility of partial solar pressure attitude stabilization system studied.
September 17		Position toward maintaining Mars as an "ecological preserve," and its effect on spacecraft design reviewed.
October 1		*Mariner* M design reviewed by JPL Systems Division and *Mariner* Venus 1962 personnel. *Mariner* Venus 1964 design review begun.
October 14		Word received, but not official go-ahead, that NASA Headquarters had decided on JPL *Mariner* M.
October 29	1962	Preliminary *Mariner* M design completed. *Mariner* Venus 1964 design review completed.
November 5		Official go-ahead received from NASA Headquarters. Project renamed *Mariner* Mars 1964.
November 19		Preliminary Project Policy and Requirements document reviewed.
December 10		*Mariner II* encounter with Venus.
December 17		Questions raised as to whether *Mariner* Venus 1964 would be cancelled.
December 31		Contact with *Mariner II* spacecraft lost. *Mariner* Venus 1964 project cancelled.
January 7	1963	*Mariner* Mars 1964 Project Manager assigned. First contact made with LeRC, prospective Launch Vehicle System subcontractor.
January 14		Effect of including a test shot in *Mariner* Mars 1964 schedule studied. Spacecraft functional specifications released.
January 21		*Atlas/Agena* launch vehicle reviewed with MSFC, LeRC, LMSC, and Air Force Space Systems Division.
January 28		First rewrite of the Project Policy and Requirements document completed. *Mariner B* experimenters briefed on *Mariner* Mars 1964 status. *Atlas/Agena* responsibility officially transferred from MSFC to LeRC.
February 4		Test shot dropped in favor of three launch attempts.
February 11		Preliminary version of Launch Vehicle/Spacecraft Integration specification sent to LeRC and LMSC.
February 18		Project Policy and Requirements document, representing a large increase in QA requirements, released.
February 25		Detailed schedule completed.
March 11		New experiment package for *Mariner* Mars proposed by NASA Headquarters.
March 18		Study with justification for a three-shot mission sent to NASA Headquarters. First "official" launch vehicle performance estimates received from LeRC/LMSC.

Table 2. (Cont'd)

Week beginning	Year	Event
March 25	1963	Direction received from NASA Headquarters to change the science payload. Spacecraft design review in process.
April 1		Project Development Plan sent to LeRC for review. First launch vehicle/spacecraft interface meeting held. NASA Headquarters informed of project approach to handling changed science payload. Infrared radiometer dropped because radio propagation could not be accommodated.
April 8		First meeting with Project Manager and System Manager held at LMSC, and use of a design goal of $C_3 = 10.2$ km^2/sec^2 for 570-lb spacecraft agreed upon. Comments from LeRC on Project Development Plan received and integration begun.
April 15		Science instrument interface specifications mailed to experimenters.
April 22		Meeting regarding feasibility of combined system tests held at Cape Kennedy.
April 29		Impact of dot component DAS, an unproven design, realized for first time.
May 6		Decision made to use dot component DAS. The 10-w cavity amplifier tube appeared to be a potential problem.
May 13		First version of the SFOF/DSIF/Spacecraft Interface Document reviewed.
May 20		Final Project Development Plan sent to LeRC for signature.
May 27		Scope of project reduced because of budget considerations; launch, one spare spacecraft, and related OSE deleted.
June 3		NASA Headquarters agreed to science payload outlined by JPL in early April.
June 10		First of the biweekly project status reports sent to NASA Headquarters.
June 17		DSIF requested to review feasibility of supporting last half of *Mariner* Mars 1964 mission flight with 100-kw transmitter.
June 24		Last of design evaluation tests on *Mariner* Venus 1962 spare spacecraft completed.
July 1		Dot component DAS reported to be behind schedule.
July 8	1963	Final Project Development Plan sent to NASA Headquarters. Television system test conducted using breadboard equipment. First issue of Space Flight Operations Plan and launch constraints document reviewed.
July 15		Spacecraft weight reported to be as high as 592 lb. New Space Flight Operations Plan reviewed and comments submitted.
July 22		Combined system tests planning meeting held at LeRC. Potential late deliveries of PTM hardware to SAF indicated.
July 29		Continued signs of late deliveries of PTM hardware appeared due to budget problems and increased QA and documentation requirements.
August 5		Project Manager and Launch Vehicle System Manager met to discuss launch vehicle/spacecraft interface problems. Project estimated to be running 6 to 8 weeks behind schedule.
August 12		NASA Headquarters quarterly review of project conducted. Clamshell shroud failed to open in test.
August 19		Preliminary plan for a *Mariner* Mars 1966 mission developed.
August 26		Revised version of Launch Vehicle/Spacecraft Integration Document reviewed by LeRC.
September 2		Clamshell shroud testing stopped until review could be made. Late SAF delivery predicted for many PTM items.
September 9		Potential problem of tape binding in tape recorder reported.
September 16		System of biweekly listing of delinquent critical areas established.
September 23		Clamshell nose fairing separation test conducted at Rye Canyon. Contamination and shock observed as possible serious problem for spacecraft.
September 30		Lifetime of 10-w cavity RF amplifier tube indicated as potential problem. Need to initiate a full-development over-the-nose shroud became evident.
October 7		Project Development Plan Revision 1 sent to NASA Headquarters.
October 14		TCM in 25-ft space simulator. High-Rel parts procurement predicted to delay delivery of flight hardware to SAF.

Table 2. (Cont'd)

Week beginning	Year	Event
October 21	1963	Project requirements for documentation reduced.
October 28		Many PTM items delivered late to SAF. Shroud design study in process.
November 4		Reports from *Ranger* indicated that coating of terminals in electronic subchassis may have caused diode cracking.
November 11		NASA Headquarters quarterly review of project equipment shipped to Langley Air Force Base for SMIT test.
November 18		Over-the-nose shroud selected for use on *Mariner* Mars spacecraft.
November 25		SMIT tests started.
December 2		PTM deliveries still not complete.
December 9		First five SMIT tests indicated possible attitude control stability problems; next four tests successful after modification to reduce gas flow.
December 16		PTM power turned on. Launch vehicle/spacecraft interface schedules signed off by LeRC/LMSC/JPL.
December 23		Interim report of spacecraft arrival time at Mars indicated that encounter could be planned for over Goldstone.
December 30		SAF computer data system delivered.
January 6	1964	Blanket freeze imposed on entire spacecraft design. Meeting on conversion schedule for LC 13 held.
January 13		First system test on PTM completed. Final shroud design review. First acoustic test performed using DTM.
January 20		Launch Vehicle/Spacecraft Integration schedules published. Goldstone Duplicate Standard receiver ordered for spacecraft STC equipment.
January 27		Canopus sensor photomultiplier tube failed TA vibration test and required redesign.
February 3		Spacecraft life test plan completed. Familiarization lecture presented to LMSC launch vehicle personnel by Project Manager.
February 10		PTM updated with engineering change requests. Revision 2 of Project Development Plan sent to NASA Headquarters. Familiarization lecture presented to GD/C launch vehicle personnel by Project Manager.
February 17	1964	Late flight equipment delivery to SAF predicted. Concern over the status of the 10-w RF amplifier tube developed.
February 24		NASA Headquarters quarterly review, and science experimenter's meeting held. Question raised about soldering technique on connectors.
March 2		Magnetic mapping of PTM begun. Test of PTM started in 25-ft space simulator. DAS dot diode failed in thermal–vacuum testing.
March 9		Possible occultation experiment studied. DTM shipped to LMSC for combined vibration tests. Television tube failed to pass TA vibration level testing.
March 16		Launch vehicle design reviewed at LMSC; potential problem in *Agena* restart seen. PTM completed space-simulator test. Copies of Test and Operation Plan requested by NASA Headquarters.
March 23		First flight hardware delivered to SAF.
March 30		PTM completed vibration test with very few problems. Spacecraft separation tests started.
April 6		Trouble appeared in low output power and life expectancy of 10-w RF amplifier. TWT backup system initiated. Workshop meeting on spacecraft testing techniques compared several NASA projects.
April 13		Shroud separation tests started.
April 20		First flight spacecraft (MC-2) "power on" tests started. DAS dot resistors showed a tendency to change resistance value.
April 27		Review of DAS units showed that none of the existing units was flightworthy and all had to be rebuilt.
May 4		Occultation experiment proposal sent to NASA Headquarters. Decision made to fabricate flight welded cordwood construction NRT DAS and modified RT DAS.
May 11		PTM used in SMIT tests in JPL 25-ft space simulator.
May 18		Use of project P-list (see Section III) begun. NASA Headquarters quarterly review held. Late shipment of MC-3 and MC-4 to Cape Kennedy delayed LC 12 launch day to November 18. System tests started on MC-2.

Table 2. (Cont'd)

Week beginning	Year	Event
May 25	1964	"Glitch" experienced by PTM in 25-ft space simulator isolated to faulty ultraviolet experiment.
June 1		MC-3 system tests performed.
June 8		Canopus sensor passed TA test. Decision made to use hybrid 10-w amplifier system in flight.
June 15		Occultation experiment approved. Ultraviolet experiment removed from spacecraft flight complement. Shroud RF leakage began to be a problem.
June 22		"Free mode" test performed without cables and with use of solar power. Canopus sensor failed on retest of TA levels. Trouble experienced in SFOF program.
June 29		Over 300 open problem/failure reports discovered.
July 6		Final launch vehicle design reviewed. Television shutter bearing design found unsatisfactory.
July 13		MC-2 tested in 25-ft space simulator. Addendum to Project Development Plan issued.
July 20		Canopus sensor high-voltage power supply transformer replaced. Satisfactory television coverage appeared possible with Type II trajectory.
July 27		*Atlas* 288 delivered to Cape Kennedy. Transistors in power subsystem found incorrectly mounted reworked.
August 3		*Agena* 6931 shipped to Cape Kennedy. Mission Operations Plan issued for the first time.
August 10		Revision 1 of Space Flight Operations Plan published. Computer programs found inadequate during first FPAC test in SFOF.
August 17		MC-2 shipped to Cape Kennedy. Earliest launch days established for LC 13 and LC 12.
August 24		Hurricane Cleo closed down all operations for one day. Success of Solar Plasma Probe became questionable because of arcing or corona.
August 31	1964	Inadvertent pressure rise recorded in 25-ft space simulator during MC-4 test.
September 7		Hurricane Dora resulted in removal of launch vehicle from LC 13. All *Surveyor* programming work in SFOF dropped in readiness for launch operation support.
September 14		MC-3 shipped to Cape Kennedy. *Atlas* damaged during reassembly of launch vehicle on LC 13. President Johnson visited *Mariner* operations at Cape Kennedy.
September 21		MC-4 shipped to Cape Kennedy. Launch constraints document published.
September 28		Combined system tests completed. Flightworthy Canopus sensors shipped to Cape Kennedy.
October 5		All major systems held at Cape Kennedy reviewed by Project Office. Flight solar panels degaussed.
October 12		All preflight tests completed, MC-2 ready for final assembly to launch vehicle.
October 19		Final SFOF integration test. MC-3 ready for flight.
October 26		Revision 2 of Space Flight Operations Plan distributed. Final Standard Trajectories published. Power converter problem experienced on *Agena*.
November 2		MC-2 launched on November 5; shroud did not separate from spacecraft; spacecraft kept alive for 8 hr and 43 min by battery power. Test shroud failed in simulated launch thermal–vacuum test, giving a clue to the failure mechanism on the MC-2 launch.
November 9		Removal of *Agena* retro-rockets and command destruct system to extend launch window. Work begun by LMSC on a metal shroud.
November 16		MC-3 final system test rerun.
November 23		LMSC metal shroud selected for flight. MC-3 *(Mariner IV)* launch successful.
November 30		*Mariner IV* performed successful midcourse maneuver on December 5.

III. PROJECT ORGANIZATION AND MANAGEMENT

A. Management Structure

1. National Aeronautics and Space Administration

The responsibility for the *Mariner* Mars 1964 Project at the National Aeronautics and Space Administration Headquarters was vested in the office of the Director of Lunar and Planetary Programs, under the overall cognizance and direction of the Office of Space Science and Applications. Figures 4 and 5 show the NASA organization of these offices.

2. Jet Propulsion Laboratory

Under the master contract between NASA and the California Institute of Technology, JPL was assigned project management authority and responsibility for the *Mariner* Mars 1964 Project, and was also assigned the system management authority and responsibility for: (1) the Spacecraft System, (2) the Deep Space Instrumentation Facility System, and (3) the Space Flight Operations System. Figure 6 shows the organization of the Jet Propulsion Laboratory; Fig. 7, 8, and 9 present the system management organizations. A summary of system management assignments derived for the project is given in Fig. 10, and the associated organizational arrangement is shown in Fig. 11.

3. Lewis Research Center

Responsibility for the overall management and conduct of the launch vehicle portion of the *Mariner* Mars 1964 Project was delegated to Lewis Research Center. This assignment included administrative and technical cognizance and control over the Launch Vehicle System procurement, booster launch and flight operations, and the delivery and analysis of flight performance and tracking information up to the time of spacecraft injection. Figure 12 presents the LeRC organization.

a. Launch Vehicle System responsibility. Upon receipt (early in 1963) of the launch vehicle assignment, formerly held by the George C. Marshall Space Flight Center, the Director of LeRC established as his principal agent the *Agena* Project Office (Fig. 13), whose chief became the Launch Vehicle System Manager. A detached plant representative branch office in Sunnyvale, California, also reported to the *Agena* Project Office. The *Agena* Project Office had the responsibility of ensuring proper vehicle support to several NASA projects that use the *Agena* and *Atlas* vehicles, including the *Mariner* Mars 1964 Project. Accordingly, this office entered into agreements with Air Force representatives for procurement of *Atlas D* and *Agena D* stages, and coordinated the adaptation and use of these stages. Their responsibilities included: transfers of funds, procurement, modification, aerospace ground equipment, planning and implementation of launch-to-injection tracking and instrumentation, and certification of performance and reliability analysis. Design, development, and delivery of a qualified launch-vehicle-to-spacecraft adapter, protective shroud, and separation system were also a part of the launch vehicle responsibility. This effort entailed spacecraft compatibility considerations, logistics, facilities, and supporting ground equipment for the various phases of manufacturing, testing, and launch preparations.

b. Launch support activities. The performance of launch operations for NASA was under the supervision of the John F. Kennedy Space Center organization. Operational support requirements and objectives specified by the mission, the spacecraft, and the launch vehicle were levied and coordinated through the NASA Test Support Office at the Patrick Air Force Base to engage the capabilities and commit the local and worldwide complex of AFETR. Similarly, safety and technical limitations were imposed by AFETR policy or by the availability of facilities. Figure 14 shows the John F. Kennedy Space Center organization.

4. Goddard Space Flight Center

Under the technical cognizance of LeRC, the actual conduct of launch operations was directed by the Goddard Launch Operations organization of GSFC, also shown in Fig. 14. In addition, the communications division of GSFC provided the national and overseas data transmission line network support during the space flight testing and operations phases of the project. The GSFC organization is shown in Fig. 15. The data transmission services were supervised by the NASA Tracking and Data Acquisition Office.

5. U.S. Air Force Space System Divisions

Essentially, the Air Force Space Systems Division (and their designees) acted as agents for LeRC in procurement, logistics, and management support of the launch vehicle. The operational, administrative, and technical support to obtain and deliver the basic *Atlas/Agena* was

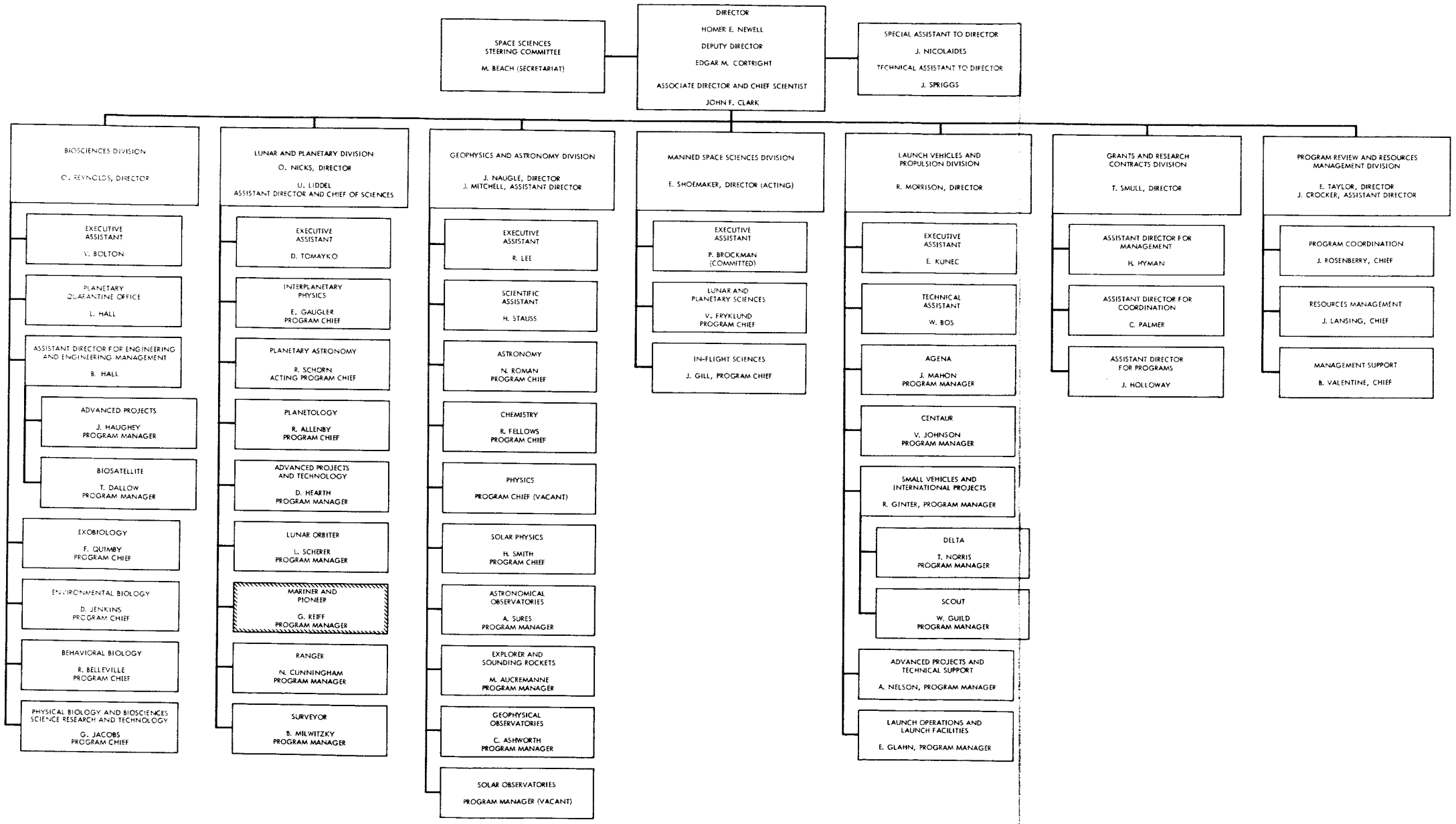


Fig. 5. Organization of NASA Office of Space Science and Application

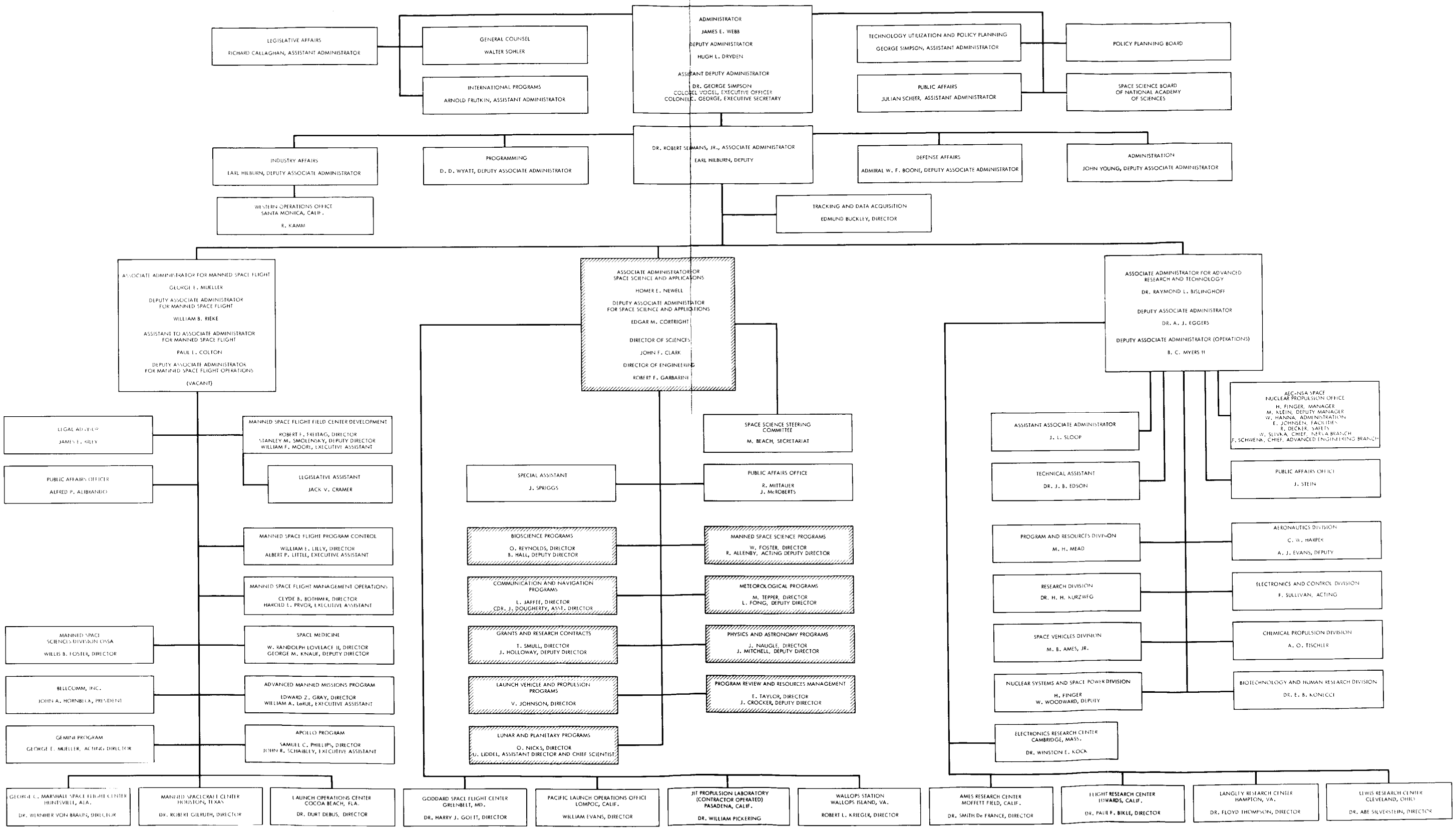


Fig. 4. NASA organization

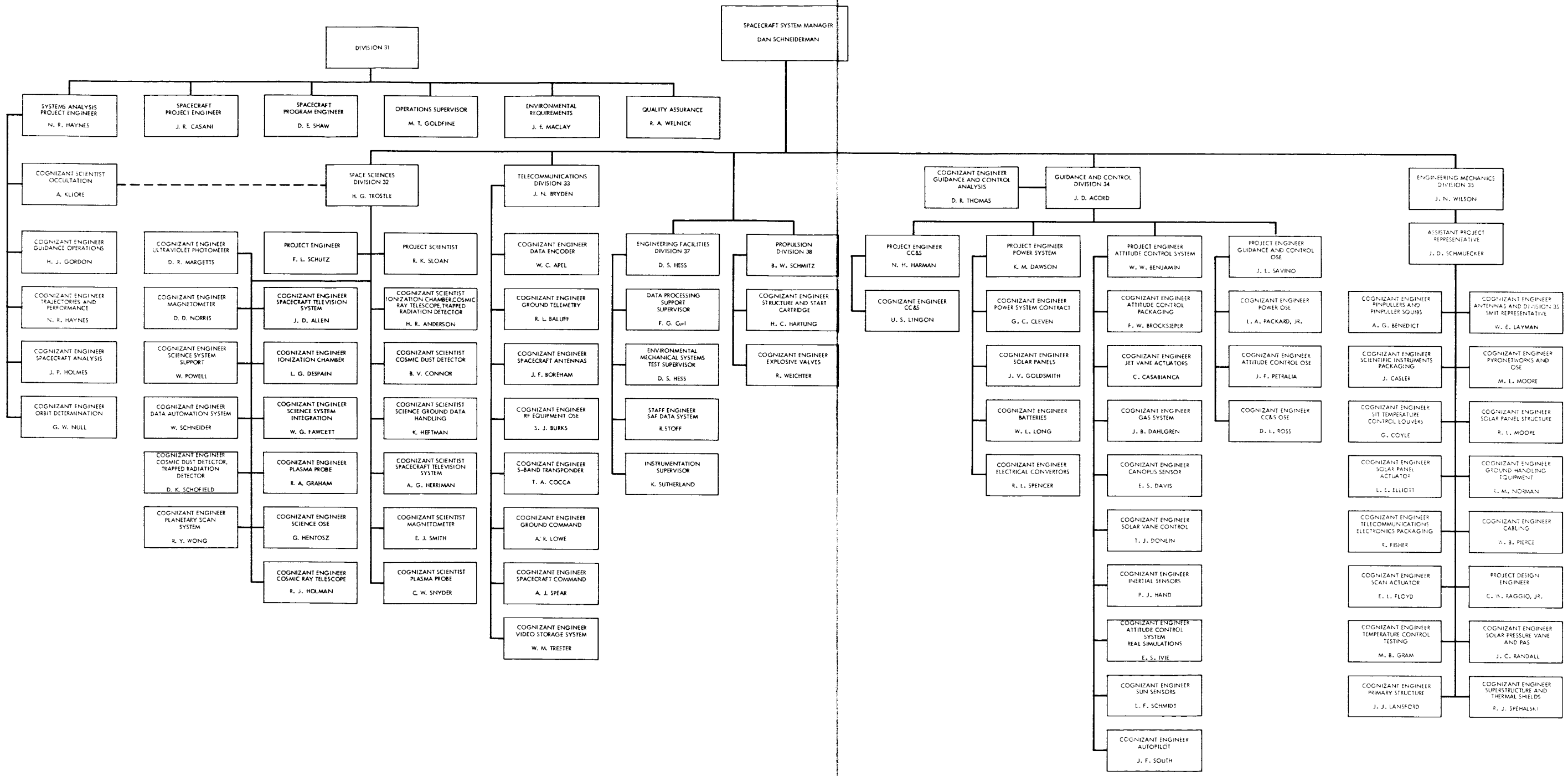


Fig. 7. Spacecraft System management organization

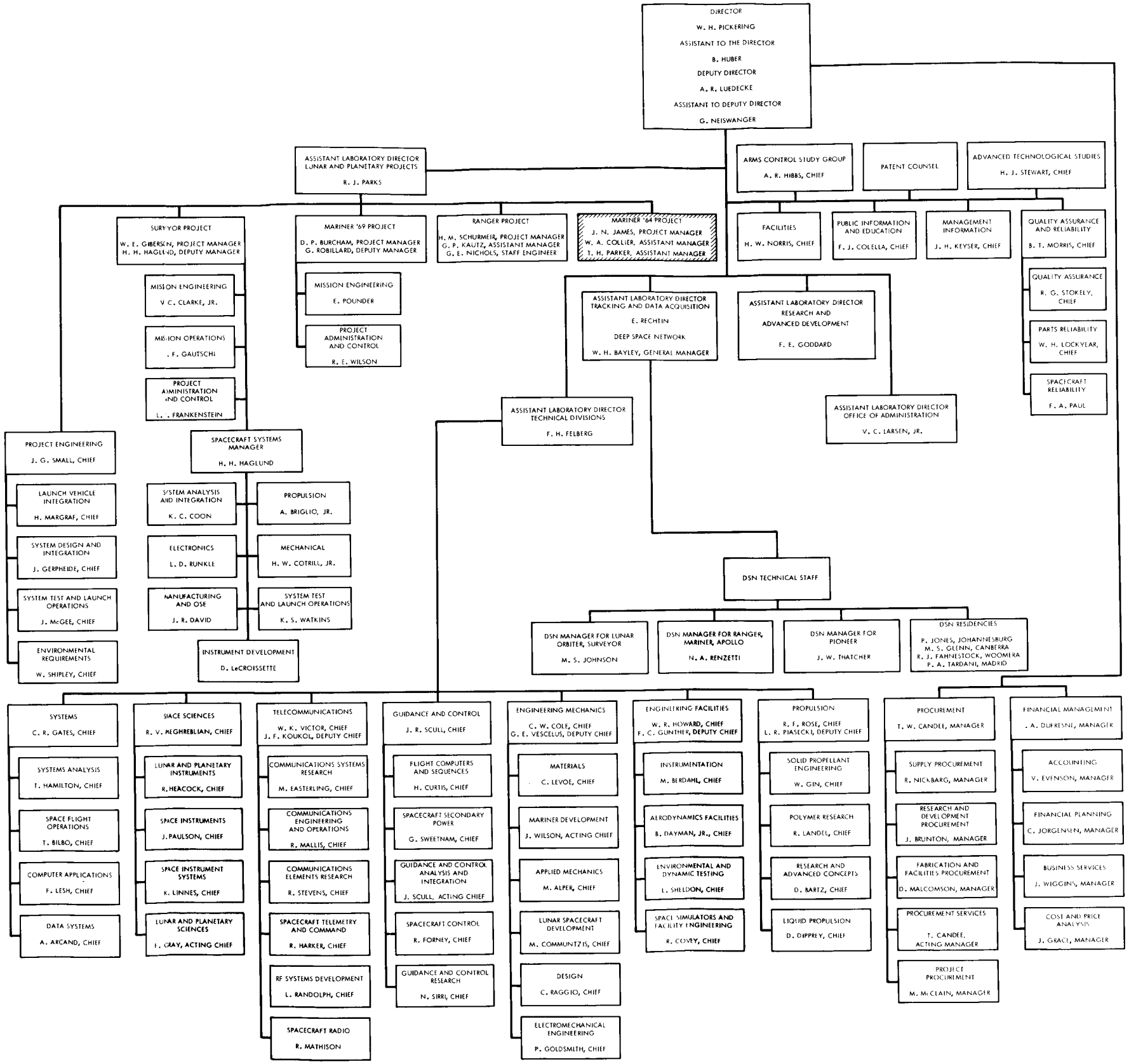


Fig. 6. JPL organization

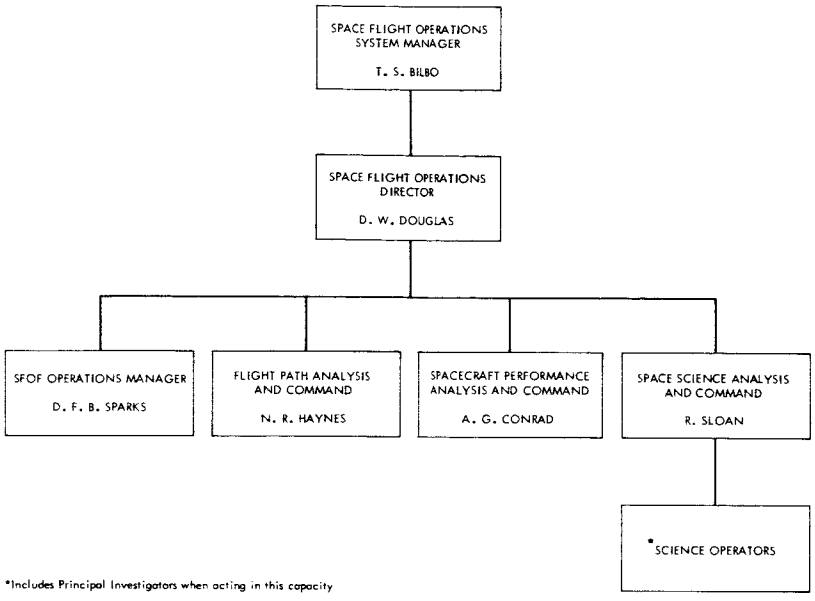
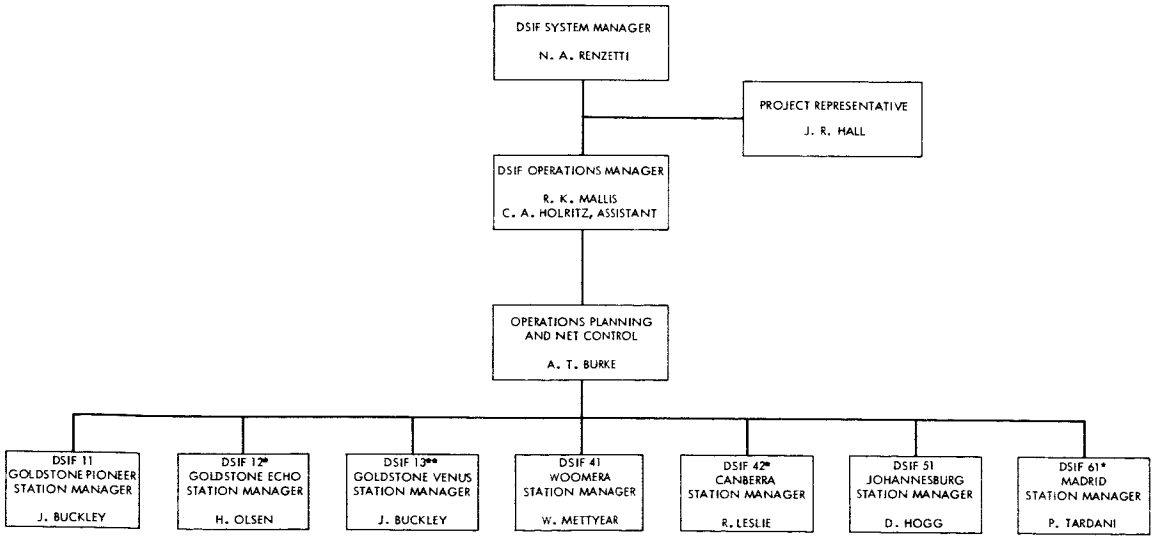


Fig. 8. SFO System management organization



*Not primary stations, may be committed during cruise mode.

**Committed 3-1/2 months prior to encounter.

Fig. 9. DSIF System management organization

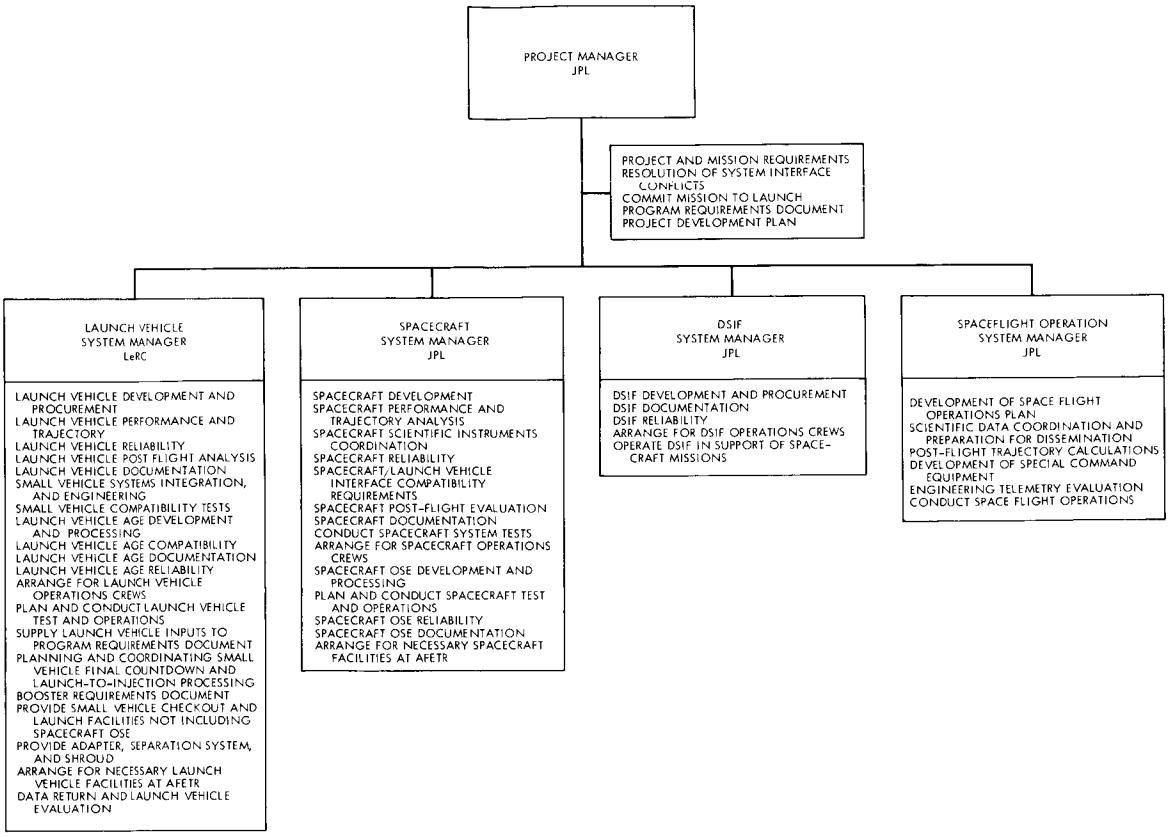


Fig. 10. *Mariner* Mars 1964 system assignments

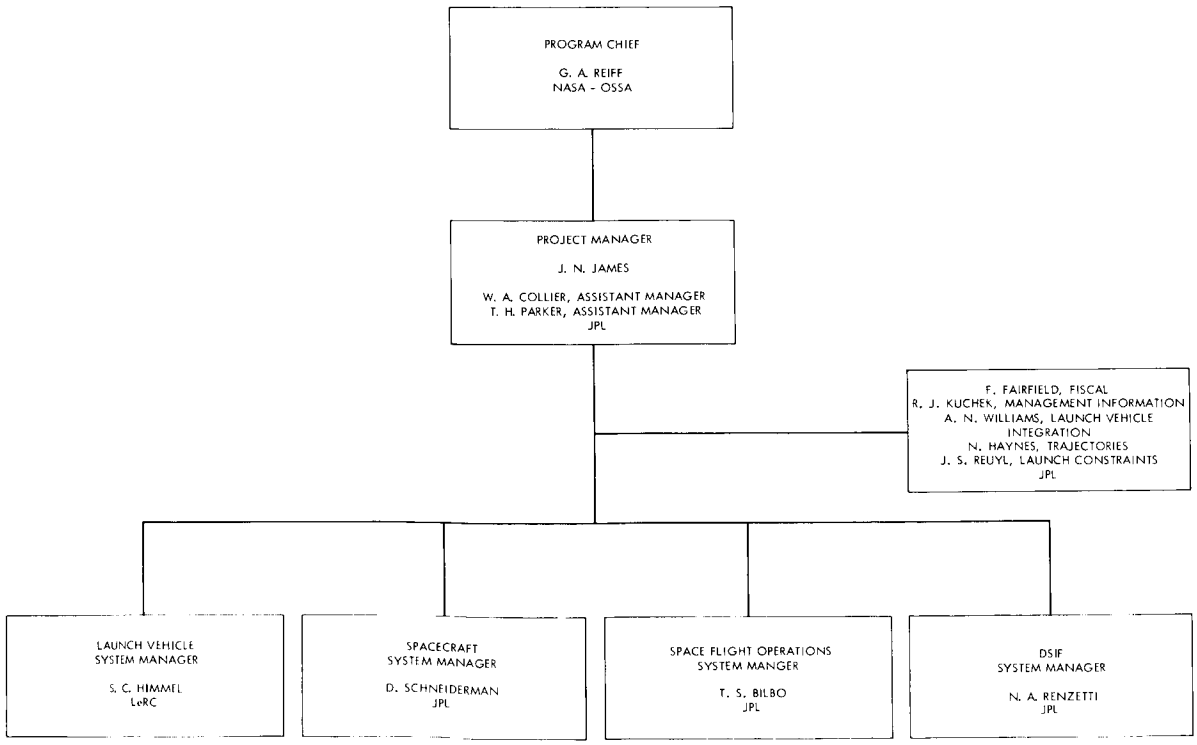


Fig. 11. *Mariner* Mars 1964 Project organization

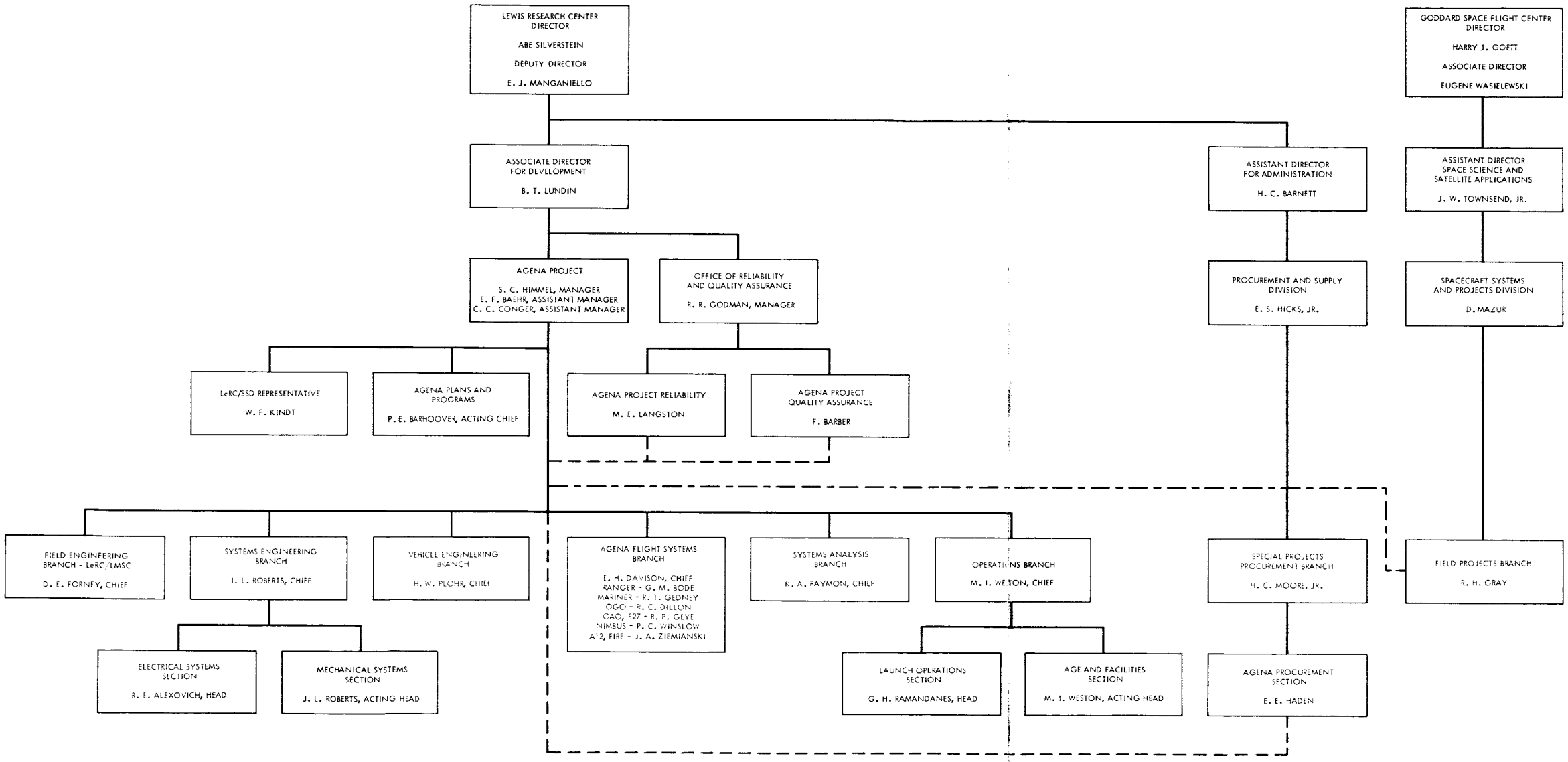


Fig. 13. *Agena* project organization

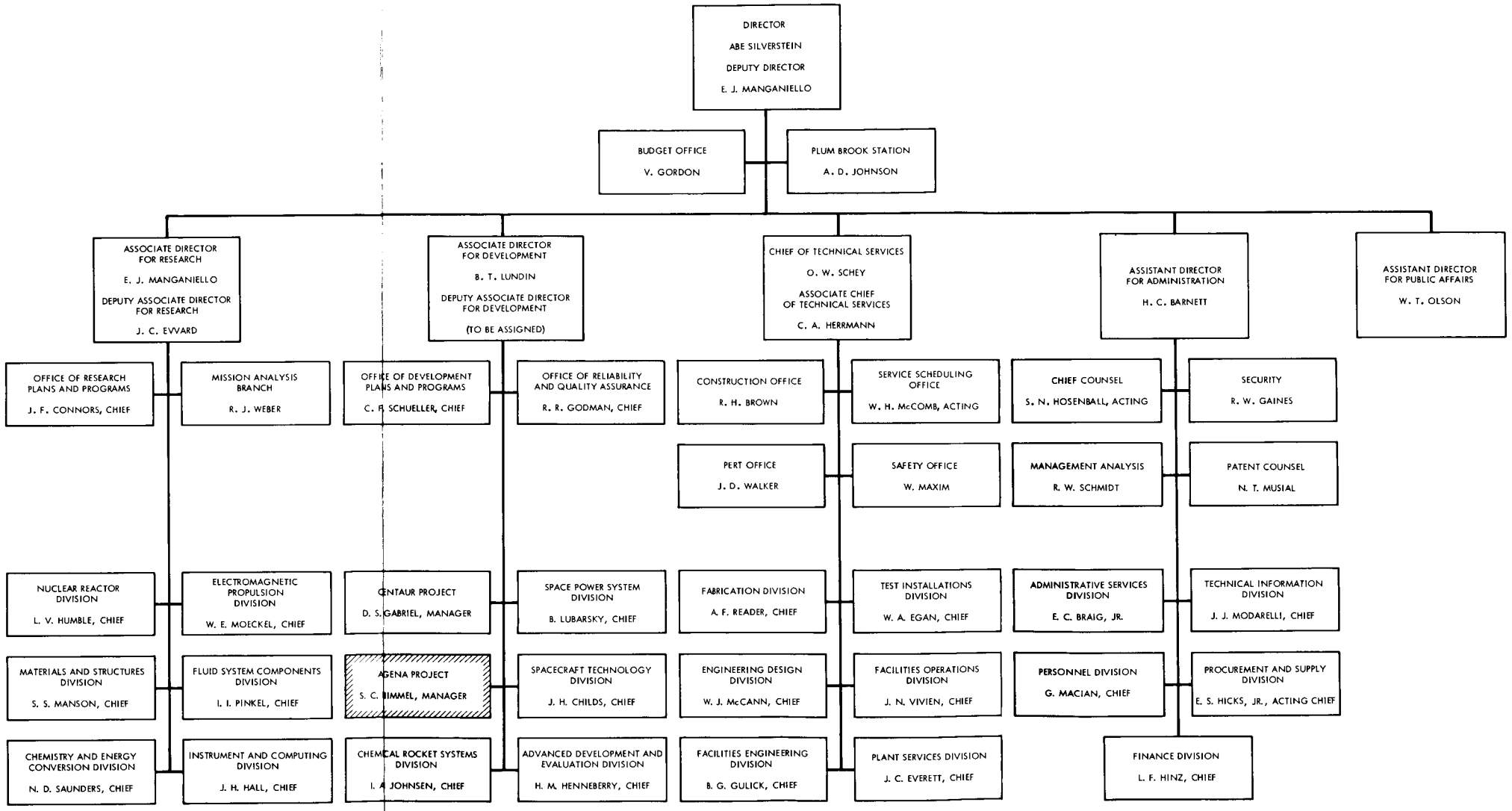


Fig. 12. Lewis Research Center organization

21-1

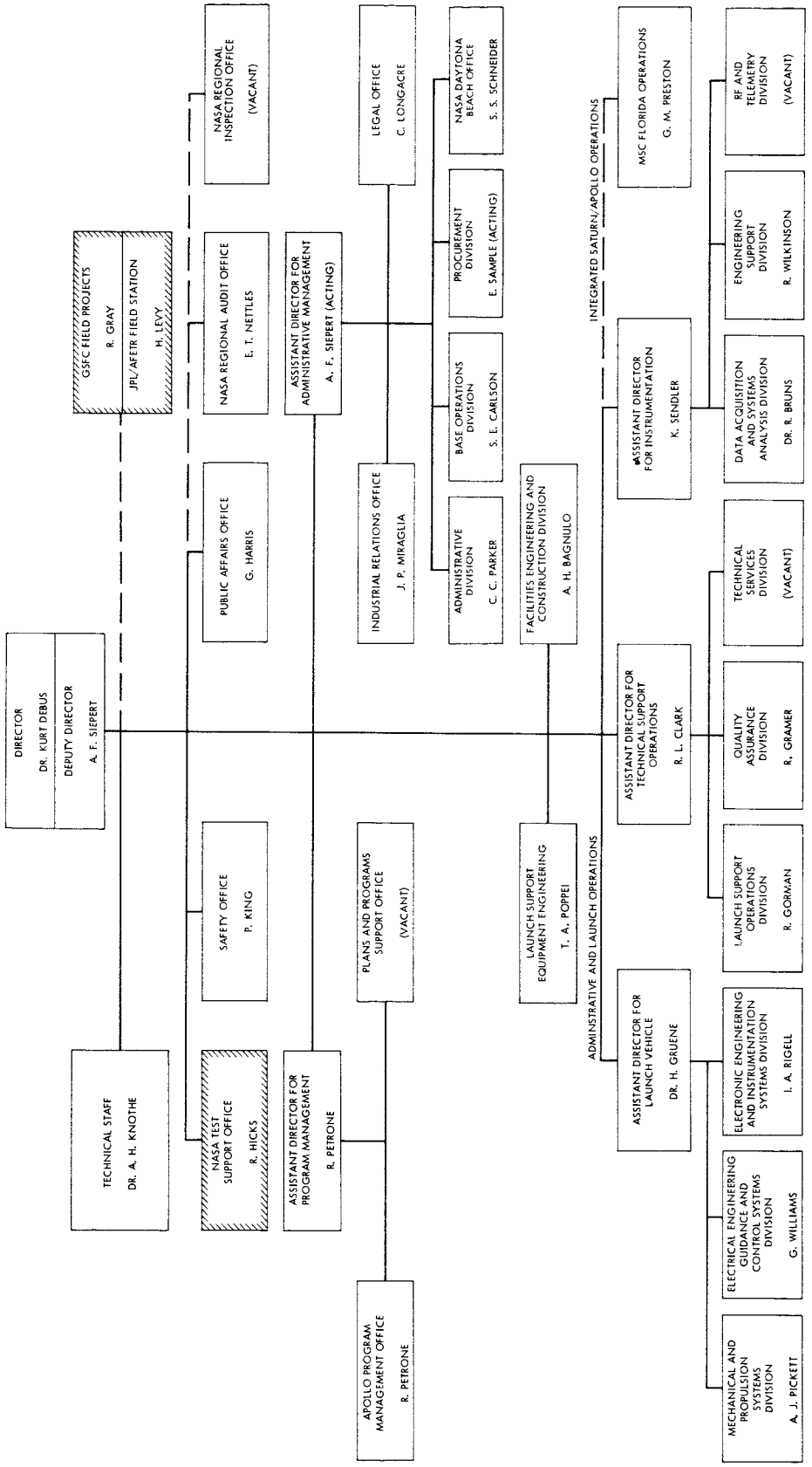


Fig. 14. John F. Kennedy Space Center organization

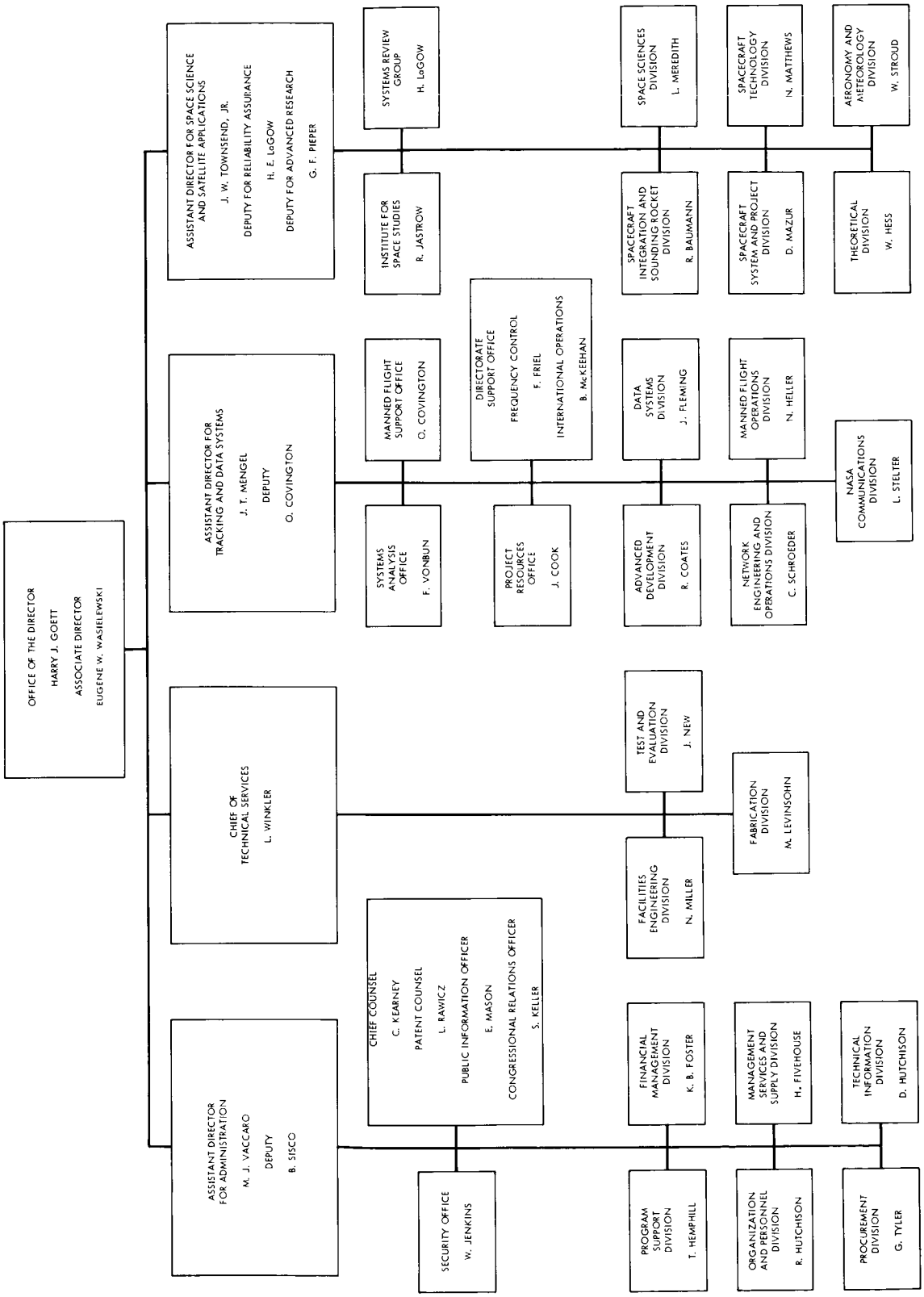


Fig. 15. Goddard Space Flight Center organization

provided in accordance with usual Air Force procedures. The Air Force monitored and concurred with the conversion of the basic *Atlas/Agena* launch vehicle necessary to accomplish NASA mission objectives.

6. Industrial Management

The incorporation of *Mariner* mission-peculiar equipment in the *Agena D* and the adaptation of conventional *Agena D* military hardware were performed by the Medium Space Vehicle Programs Office of Lockheed Missiles and Space Company under the cognizance of the company's Space Programs Division (Fig. 16). This organization was effectively under contract to LeRC to discharge all launch vehicle responsibilities, except for the procurement of the basic *Agena D* vehicles. The Medium Space Vehicle Programs Office interfaced with General Dynamics/Convair, producer of the *Atlas D*, and with Space Technology Laboratories, the launch vehicle trajectory and flight performance analysis contractor. The local LeRC Plant Representative Office was located adjacent to the Medium Space Vehicle Programs Office, which facilitated monitoring of LMSC status and permitted coordination of interface activities between JPL, LeRC, and other agencies involved. Design, qualification, and delivery of the shroud system was also performed by the Medium Space Vehicle Programs Office.

7. Permanent Project-wide Bodies

In order to use the relationships and experience developed on earlier *Ranger* and *Mariner* missions, existing advisory panels were used for *Mariner* Mars 1964, which provided technical advice to the Project Office and

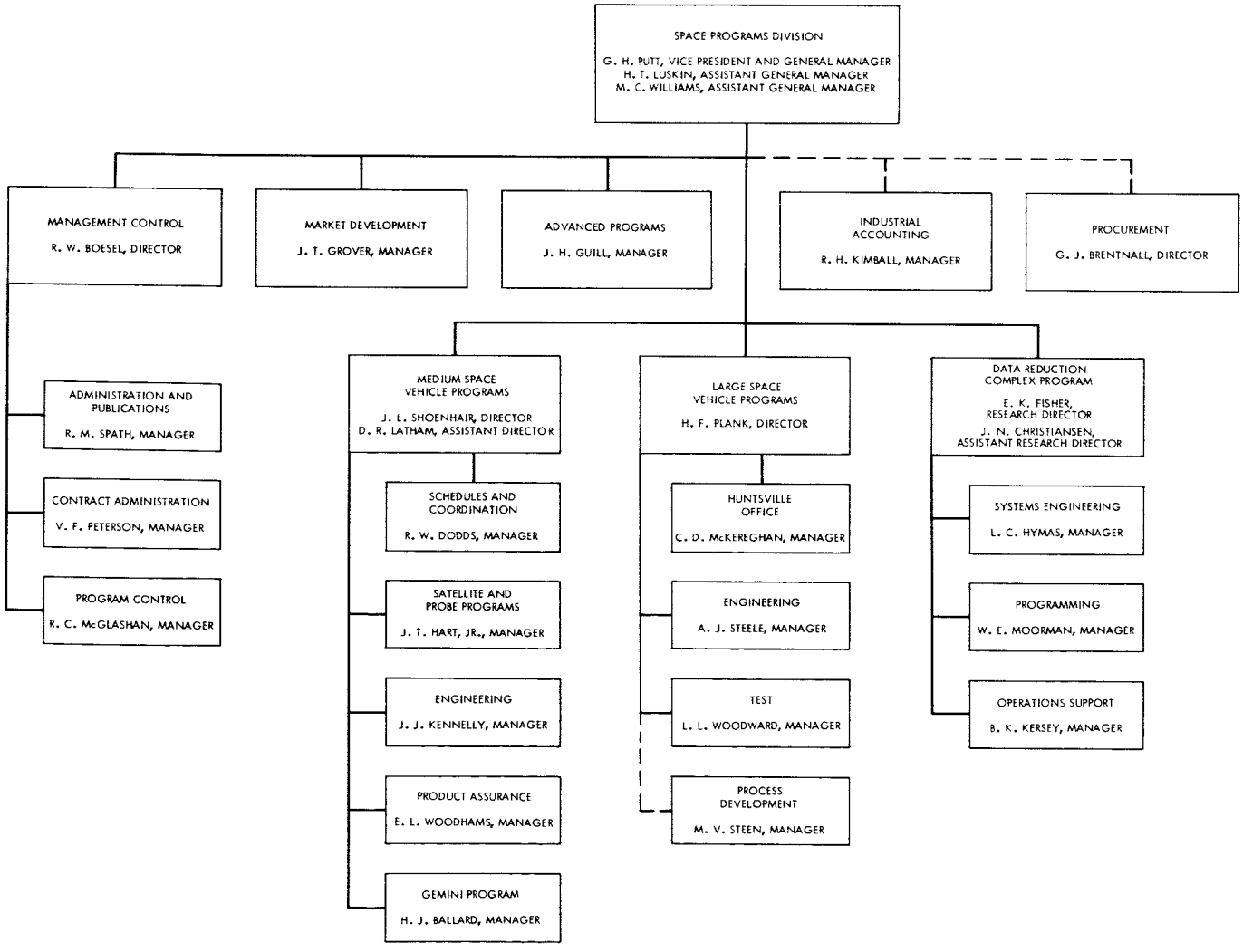


Fig. 16. Lockheed Missile and Space Company, Space Programs Division organization

systems managers. These panels, however, exercised no technical direction over JPL, LeRC, or their contractors.

a. Performance control, trajectories, guidance and control, and flight dynamics panel. This panel continually monitored, compiled, evaluated, and coordinated data relating to performance, trajectories, guidance and control, and flight dynamics as they interacted with the launch vehicle, the shroud, and the spacecraft.

b. Tracking, communication, inflight measurements and telemetry panel. This group continually monitored, compiled, evaluated, and coordinated data relating to tracking, communications, inflight measurements, and telemetry as these items interacted with the launch vehicle, the shroud, and the spacecraft.

c. Launch operations working group. This group acted as the prime mechanism for coordinating flight preparations at Cape Kennedy. Members participated in launch vehicle, spacecraft, support facilities, and range readiness meetings.

d. Launch vehicle integration group. This group, representing working levels of LeRC, LMSC, and JPL, was concerned with resolving incompatibilities between the launch vehicle, the shroud, and the spacecraft. The group proposed resolutions to interface problems and suggested acceptability criteria.

8. JPL Staffing at Cape Kennedy

Due to the unique critical character of the field and launch operations phase and to the need for extremely accurate and timely communications between the field operations and JPL Pasadena during this phase, a special JPL manning plan was devised to support Cape Kennedy activities. The prime ground rule was to have enough background information and the proper number of people with the correct kinds of equipment and experience available on the spot to investigate and recommend action or to make good decisions quickly. The basis for the staffing plan, diagramed in Fig. 17, was:

1. An optimum balance of engineering and management capability in support of launch operations was maintained between Cape Kennedy and Pasadena, where the TA subsystems, PTM, parts stock, environmental test laboratories, procurement means, and other non-operational resources remained.
2. No repairs, except replacement at the assembly level, were planned for the subsystems at Cape Kennedy. As a general rule, emergency rework or retrofit was performed at JPL or at the facility of the contractor who originally fabricated the unit. In the latter case, quality control surveillance was at least as thorough as that used for the original fabrication.
3. No equipment was assembled to, or removed from, the spacecraft and tested or handled as a subsystem, other than those exceptions specifically approved by the Spacecraft Systems Manager.
4. Each Cape Kennedy division representative was a full-time member of the AFETR team and exercised both administrative and technical control over the members of his division comprising his staff. The divisional people assigned to spacecraft checkout teams were under the control of the Spacecraft Operations Manager rather than the division representative. The Cape Kennedy division representative provided liaison with his counterpart at Pasadena.

Travel of extra personnel to the field was closely controlled by the JPL Project Office. The designated reporting channels and lines of authority and responsibility crossed and superseded those of the formal JPL organization, and were applicable for the duration of an individual's residence at the launch base.

B. Intra-project Arrangements

In addition to the organizational framework discussed above, certain functions were expressly established and defined in the top authorization and control documents. When approved by the responsible individuals, these publications constituted the set of agreements to perform or commit the services and support of the various organizations involved. In many instances, the exact method and procedure to be followed was also described so that delegated authority could be appropriately exercised.

1. Authorizations

The NASA Headquarters approval for the *Mariner* Mars 1964 Project was established in the Project Approval Document. On the basis of the mission objectives and other information contained in this publication, and in conjunction with the NASA Management Instruction 4-1-1 (which outlines how the resources and diverse talents of the NASA centers are to be marshalled on a project), JPL prepared the Project Development Plan. Primarily, the Project Development Plan developed the System Management function and responsibility assignments. In addition, it also summarized the mission or project objectives, justification, technical plan, quality and reliability considerations, procurement management, resource needs, operations plan, reports, and the charters

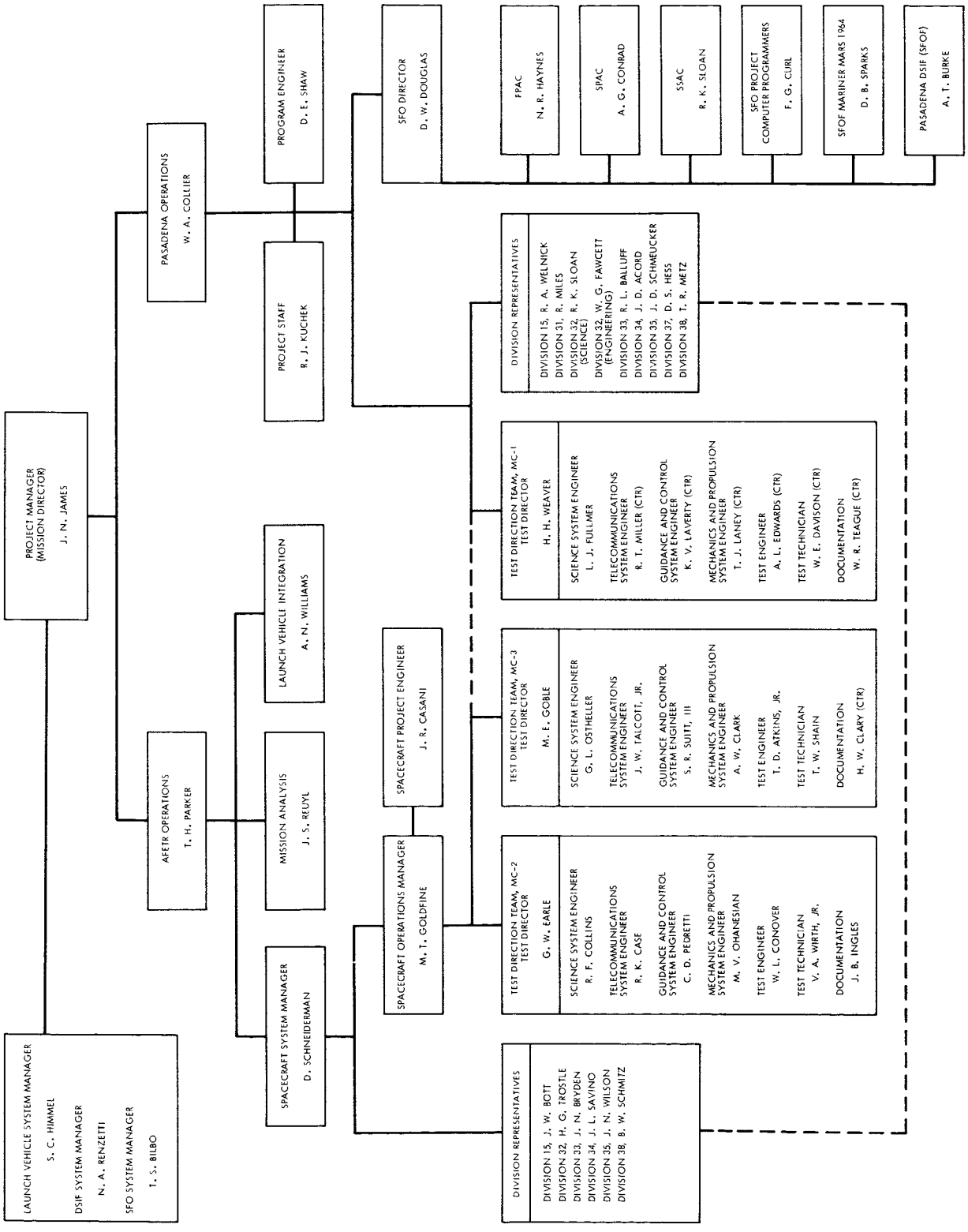


Fig. 17. *Mariner* Mars 1964 operations organization

or operating relationships. The master schedule milestones and due dates were also contained in the Project Development Plan. The management assignment agreements proved extremely important in handling the spacecraft/launch vehicle/AFETR interface and planning, because the Launch Vehicle System and AFETR resources were significant responsibilities not under the direct control of JPL management or project authority. The *Mariner* Mars 1964 Project Development Plan was amended three times; the last addendum was made to include the occultation experiment and to revise the science instrument payload. This compact was signed by all managers and agents contributing to or committing resources to the project.

2. Interfaces

Beyond the agreements reached and described in the Project Development Plan, a set of documents was developed that expanded upon the requirements and restraints prevailing between the various subsystems. The chief documents of this kind are listed in Table 3.

The relationships existing between the systems are diagramed in Fig. 18. As far as possible, interfaces were administratively and technically designed to provide the simplest interchange (and thus produce a minimum number of errors) across the boundary lines.

3. Communications

Because of the diversity of participation and the necessity for close control and coordination of activities to meet a brief launch opportunity, measures were undertaken to promote better understanding of the mission. Its challenges, such as meeting each schedule milestone, had to be brought to the attention of everyone possible who could, by his actions, influence the success or failure of the effort. In order to assist in the resolution of problems, keep the channels of communication open, and inform and unite the different organizations toward achieving the objectives of the *Mariner* Mars 1964 Project, numerous personal contacts were made. Launch vehicle contractors, spacecraft contractors, DSIF tracking stations, and AFETR personnel were contacted as much as possible and given briefings on the mission.

C. JPL Planning and Implementation

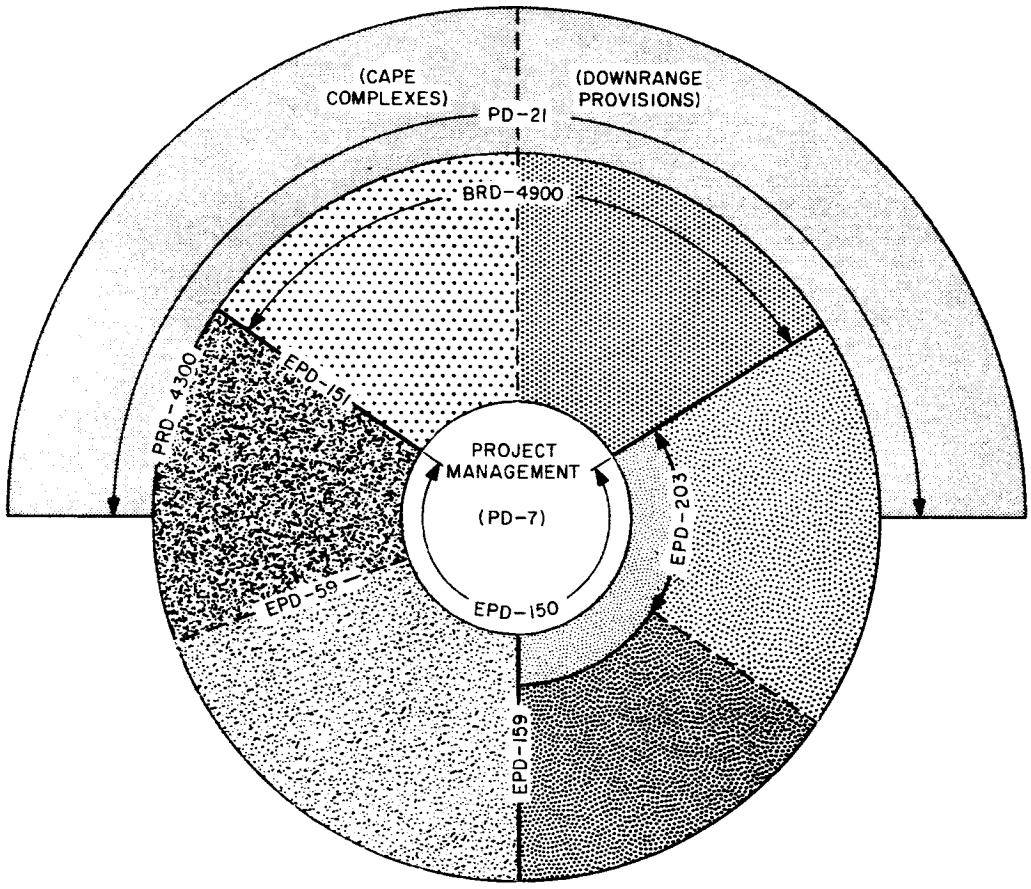
In addition to the project management responsibility for the *Mariner* mission, JPL was also responsible for: (1) the design, fabrication, and testing of the spacecraft and its associated ground support equipment; (2) the space flight operations of the spacecraft from injection to planetary encounter; and (3) the Deep Space Instrumentation Facility tracking operations. To implement these responsibilities, certain techniques were developed by the Project Office.

1. Project Policy and Requirements Document

The Project Policy and Requirements document (Appendix A) established the operational procedures for the project within JPL by stating mission objectives, system requirements, and milestones, and by providing an overall guideline schedule. The document bears a similarity to the Project Development Plan in that it represents the compact between the JPL Project Office

Table 3. Interface documentation

Document No.	Subject	Cognizant agent	Type of interface	Interface areas
EPD-59	Science instruments requirements	JPL	Technical	Spacecraft/science instruments
EPD-150	Policy and requirements document	JPL	Management	Project/technical division
EPD-151	Spacecraft/launch vehicle integration	JPL	Technical	Spacecraft/launch vehicle
EPD-159	Spacecraft/SFO/DSIF interface	JPL	Technical	Spacecraft/SFO/DSIF
EPD-203	SFOF capabilities	JPL	Facilities	Project/SFOF
PD-21	Mission operations plan	JPL	Operations	All systems/launch operations
PD-23	Launch constraints planning	JPL	Operations	Project/launch operations
BRD-4900	Booster requirements document	LeRC	Technical and operations	Launch vehicle/AFETR
PRD-4300	Program requirements document	AFETR	Technical and operations	Mariner Mars mission/AFETR



AIR FORCE EASTERN TEST RANGE

ATLAS } LAUNCH VEHICLE SYSTEM

AGENA }

MARINER MARS SPACECRAFT } SPACECRAFT SYSTEM

SCIENCE INSTRUMENTS }

SPACE FLIGHT OPERATIONS SYSTEM

DSIF } DEEP SPACE NETWORK SYSTEM

SFOF }

Fig. 18. Project/system interfaces

and the JPL line management for execution of the project. Together with the budget guidelines issued periodically, this document became the keystone for conduct of in-house project activities. In many cases, the JPL technical divisions engaged subcontractors to perform services in line with the responsibilities defined in the document. Among the basic innovations and extensions to the similar document used for *Mariner II* were the following additional requirements:

1. Parts screening
2. Problem/failure report system
3. In-process inspection
4. Comprehensive documentation
5. Rigorous status monitoring

The policy and requirements document complemented the Project Development Plan by expanding the system management concepts into a matrix organization (Fig. 19) and presenting a compatible project master schedule.

To coordinate (at the peak) 1100 individuals working on the project at JPL, Project Representatives were designated for each JPL technical division. Of all the personnel in each division, the Project Representative was the one authority familiar with overall aspects of the project, He policed the interfaces, monitored the progress, aided in the exchange of information and, in general, was the catalyst for the project in his parent division.

Wide dissemination and continued reconfirmation of basic policies and requirements tended to ensure that the entire "team" was moving toward established goals and that progress could be defined by suitable measuring points. Only two revisions were needed to the original policy and requirements document: one made the initial space flight operations requirements more explicit, and the other reduced documentation requisites when serious slippages on that account seemed imminent.

2. Weekly Project Meetings

Regular meetings were held with the JPL system managers and the Project Representatives indicated in Fig. 19. At these meetings, each representative reported upon what he considered to be the most serious problems

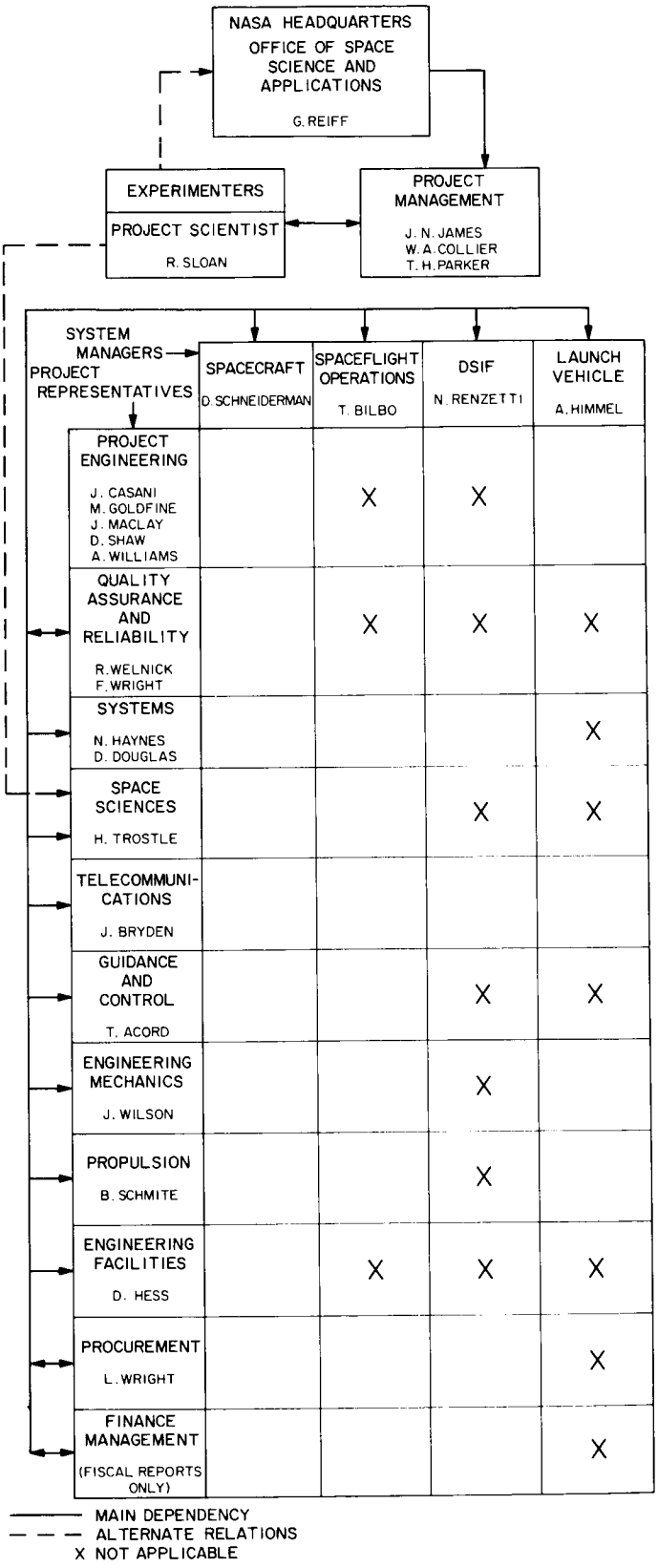


Fig. 19. Project matrix organization

facing his particular area. From these reports, assignments for the action to be taken were made and carried in the weekly minutes until the action was completed. The minutes were published and distributed rapidly to all interested personnel at JPL.

In the JPL matrix organization, the Project Representative's parent technical division was involved in activities other than *Mariner*, and the Project Representative held influence over only those resources committed to the *Mariner* project by the division manager. Recognizing the limited authority of the Project Representatives, the Project Office, in cooperation with other projects, participated in an "overlay" series of monthly meetings with the division managers (the controllers of all manpower resources) to inform them of the project's progress, to receive reports of their division's contribution to the project, and to solicit their advice regarding the project. The ultimate objective was to keep division managers properly informed so that they would be better prepared to bring manpower to bear when a serious problem occurred.

Although there was a certain amount of redundancy in this system, it is believed that these meetings, by occasionally drawing the division managers into project affairs, resulted in a more rapid and effective commitment of talent to the crises that did arise. As a matter of interest, five outstanding examples of such crises can be noted:

1. The inability of the early spacecraft Canopus sensor photomultiplier tubes to pass the launch vibration environment
2. The deterioration of the spacecraft DAS pellet resistors under high temperature test
3. The inability of the original TV camera vidicon tube to survive unexpectedly severe vibration environment on the cantilevered scan platform
4. The slow degradation of the spacecraft S-band power amplifier triode over hundreds of hours of operation
5. The rupture of the fiberglass shroud during the *Mariner III* launch

Each of these crises were "firsts" in that these devices were being flown for the first time on any mission. Examples (2) and (4) were recognized and solved in the Spring of 1964 by the division managers grouping together special task forces of considerable size and ability. Appropriate techniques were applied both within and outside JPL for the resolution of the other problems.

3. Documentation

In addition to the control and interface publications evolved to identify management and technical factors, the Project Policy and Requirements document also designated a series of overriding Laboratory-wide specifications that applied to JPL systems and responsibilities, and that could be revised only with prior concurrence of the Project Office.[1] Essentially, these specifications defined the process quality level desired.

The policy and requirements document also called for the preparation of other major classes of internal documentation and reports at times appropriate to the status of design or hardware evolution. A summary of this literature applicable to the *Mariner* Mars 1964 Project is contained in Appendix B, and one form of the drawing tabulation is given in Appendix C. Both of these lists were compiled and issued periodically throughout the lifetime of the project.

4. Change Control

Following the precedent established with the *Mariner* Venus 1962 Project, a sequential "freeze" was imposed on the design of the *Mariner* Mars 1964 spacecraft. Basically, it was necessary to phase the "lock up" of the spacecraft design in a discrete sequence without inhibiting necessary design action. The problem of when and how to freeze the design was complicated by the natural tendency of the hardware-producing divisions to set the cut-off date as late as possible, preferring other areas to freeze as early as possible. The main significance of the early freezes, since they concerned functional characteristics, was the fact that design decisions and trade-offs had been made. A tardy freeze date implied that certain functional definitions were not solidified and that hardware delivery would probably slip. This forecast was uncomfortably accurate.

If an item was frozen, it simply meant that changes were discouraged, although such changes might be made if an engineering change request was reviewed and approved by the Spacecraft System management. Appeals could be made to project management if the change were not approved by Spacecraft System management.

[1]Mariner C Project Policy and Requirements, Engineering Planning Document No. 150, Jet Propulsion Laboratory, Pasadena, California, February 25, 1963.

Throughout the project, however, there was no instance in which the Spacecraft System Manager's decision was reversed.

In order to effect control, a freeze list was inaugurated on March 11, 1963, which included all released functional specifications. This gave the cognizant division engineers freedom to change the internal designs as long as the functional specifications were not violated. Additions to the freeze list were made periodically and distributed broadly; the final version (Appendix D) was released December 3, 1963.

Other controlling documents, such as the spacecraft envelope control drawings and circuit interface drawings, were progressively placed on the freeze list. In general, interfaces were resolved and controlled as rapidly as possible until January 1964, the time of delivery of the PTM equipment for assembly; at that time, a total spacecraft freeze was imposed. After that date, it was felt that any change would have a significant impact on the rest of the system. Recognizing the need to resolve spacecraft/OSE incompatibility on the ground equipment side of the interface, total OSE freeze was deferred until May 1964. Only changes regarded as mandatory for mission success were subsequently permitted. Such changes were still numerous, as shown in Fig. 20 and 21. Some of the delay in closing out the engineering change requests was attributable to processing time, especially when key individuals were occupied with launch operations. The total engineering change request listing is contained in Appendix E.

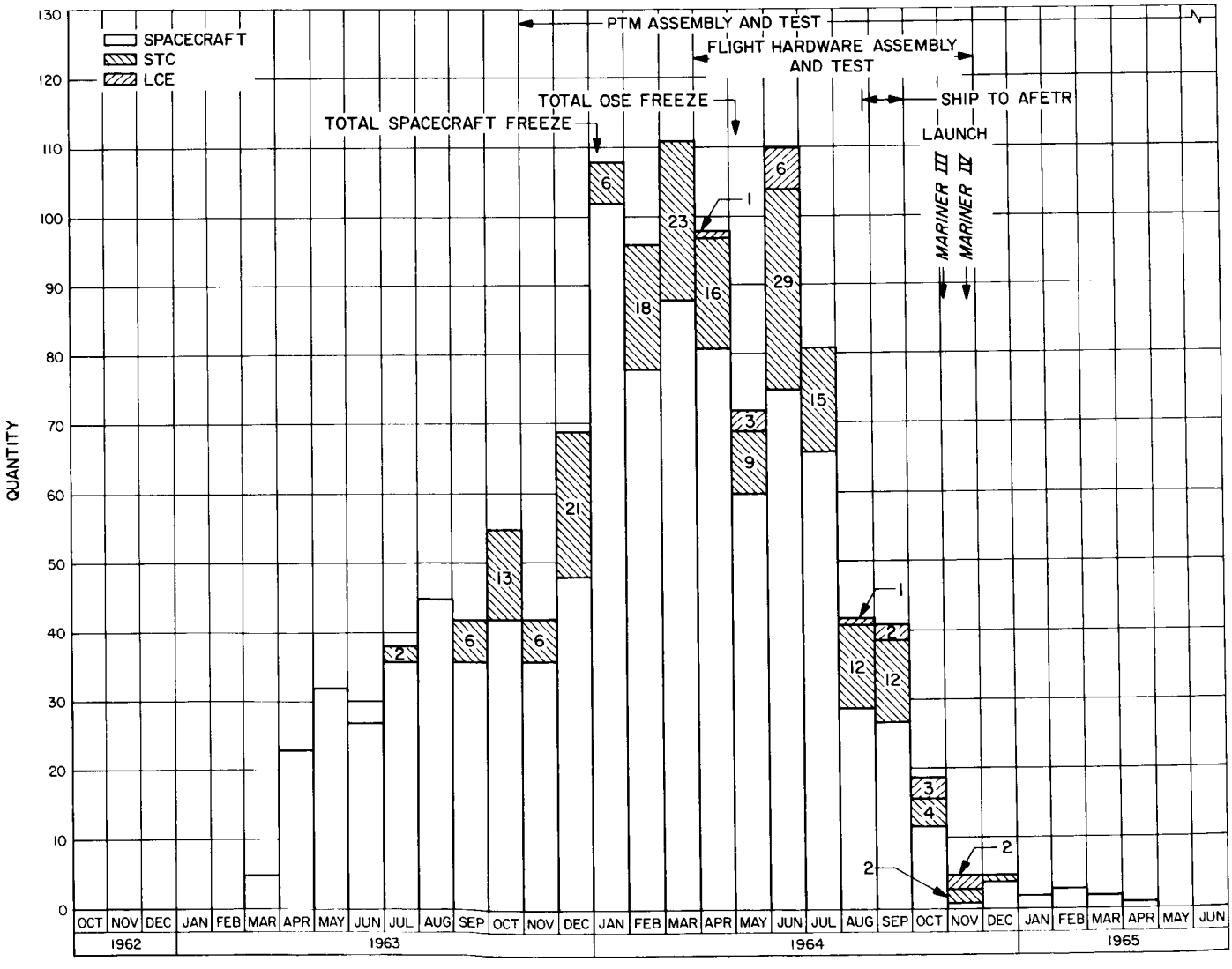


Fig. 20. Number of engineering change requests initiated per month

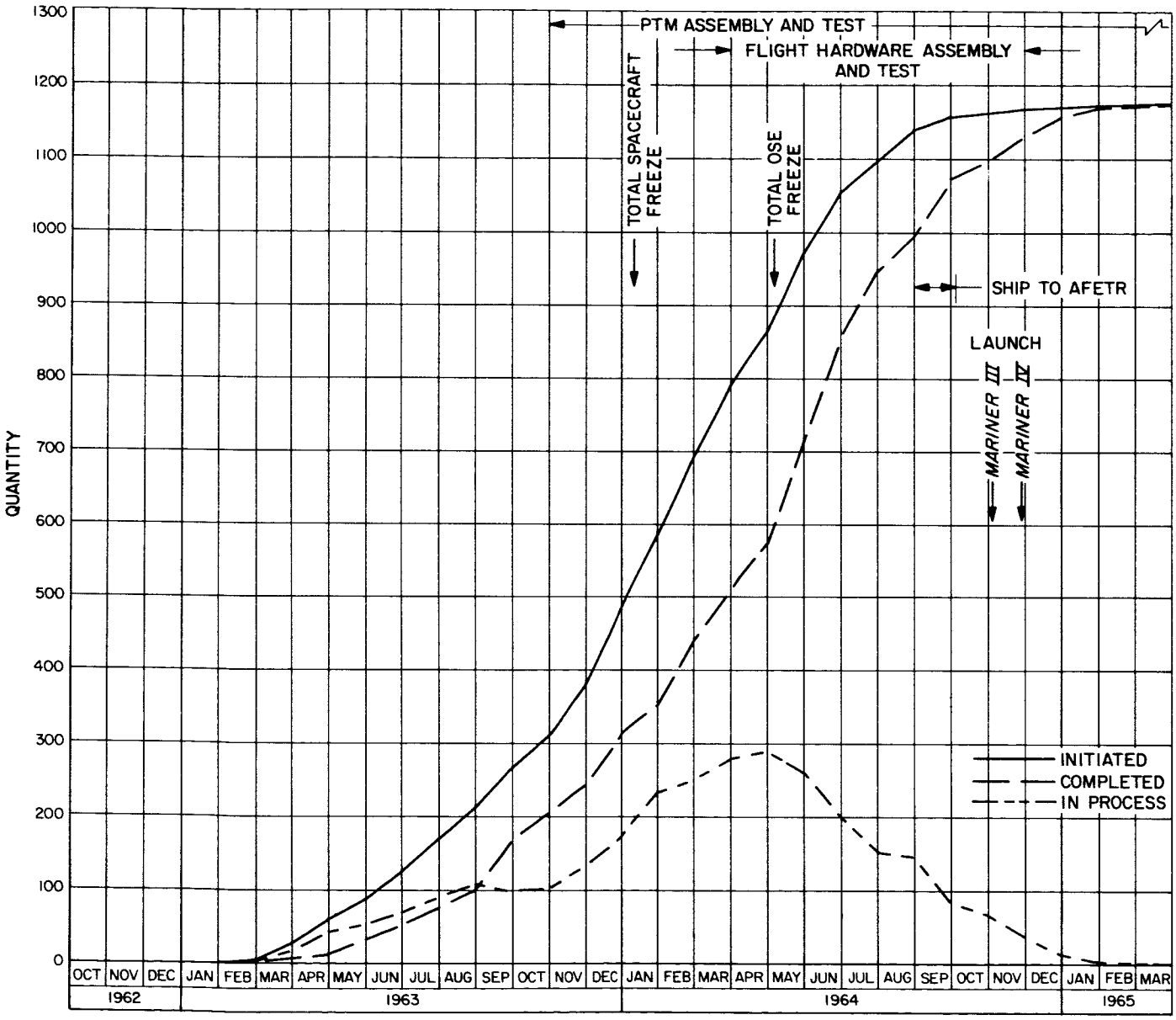


Fig. 21. Accumulated engineering change request profile

A numerical list of engineering change requests is provided in Table 4, in which it can be seen that the more proven or conventional subsystems, such as the command subsystem, the CC&S, and the data encoder, had relatively few changes in view of their complexity. In contrast, such interface areas as the system level design and spacecraft wiring, and the more experimental subsystems such as radio and attitude control, experienced more numerous revisions. Also, the comparatively late definition of the science hardware caused these units, in most cases, to have relatively fewer changes.

Table 4. Approved engineering change request records

Item	Spacecraft	OSE	Total
Miscellaneous	—	—	15
System level	155	2	157
Radio	69	14	83
Command	19	9	28
Power	79	20	99
CC&S	32	8	40
Data encoder	38	4	42
Attitude control	127	22	149
Pyrotechnics	27	8	35
Wiring and cabling	105	39	144
PIPS	14	—	14
Thermal control	30	—	30
Tape recorder	51	6	57
DAS	32	35	67
Cosmic Ray Telescope	13	1	14
Cosmic Dust Detector	10	—	10
Trapped Radiation Detector	9	1	10
Ionization Chamber	13	—	13
Solar Plasma Probe	45	—	45
Helium Magnetometer	17	—	17
Planetary scan platform	29	—	29
UV photometer[a]	18	—	18
Television	32	—	32
Computer data system	—	5	5
Telemetry processing	—	2	2
Central timing	—	3	3
GCS	—	10	10
Central recorder	—	4	4
Ground telemetry	—	20	20
Total	946	213	1174

[a]Not included in totals.

Another way of evaluating the data in Table 4 is to consider the number of serious basic design changes imposed. While many of the 1174 total changes were for routine improvements or to keep complete records, several significant design revisions also occurred; these involved either an extensive change, a potentially major hardware delivery perturbation, or some other threat to mission success. These major changes can be enumerated as follows:

1. Deletion of the infrared spectrometer and resulting adjustment of the science payload in April 1963
2. Incorporation of a hybrid radio subsystem design in the spring of 1964
3. Addition of the CC&S relay electrical latch module
4. Removal of the ultraviolet photometer experiment
5. Revision of the magnetometer power supply to preclude interference effects
6. Continual redefinition of the gas system plumbing hardware and its routing
7. Replacement of the Canopus sensor high-voltage transformer

5. Problem/Failure Reports

Complementing the design freeze and change control system was the incorporation of a rigorous problem/failure reporting system, which was also a strong tool. Problem/failure reports had to be written on any anomaly whatsoever associated with the spacecraft, beginning with the testing of the first modules that would ultimately be used in TA, PTM, or flight spacecraft. Preparation of these reports, which were to be written as soon as possible after the observance of improper operation, continued into the space flight phase. The results of this system are discussed in Section XXII. An estimated 1070 of these reports were written after freeze and resulted in design modifications through engineering change requests.

6. Reviews

Quarterly reviews of the project status were held by NASA, and, on these occasions, the Project Office was

exposed to careful scrutiny in all areas. The burden of this and many other reviews fell heavily upon the matrix organization.

In addition, a detailed spacecraft subsystem review was held in the spring of 1963. In the summer of 1964, a series of pre-shipping acceptance reviews were held on each prototype spacecraft. A series of launch readiness reviews at JPL and Cape Kennedy determined equipment flightworthiness based upon test qualification and problem/failure report experience. In addition to these "motivational" briefings, numerous reviews were also held regarding launch vehicle performance and preparation. Beyond these formal project examinations, the cognizant areas were given continuous internal critical analysis and careful study. Quality Assurance personnel performed similar efforts. When crucial problems were uncovered, they continued to receive Spacecraft System and project management attention until satisfactorily resolved.

7. P-list

Following the precedent formed on the *Mariner* Venus Project, a P-list was established to focus attention upon and keep cognizant individuals informed of all problems that were considered to be jeopardizing the mission. By agreement with the technical divisions, once a problem was serious enough to be placed on the list, the most effective people available were to be assigned to its solution. In order to preserve its emphasis, the list was not issued until about 4 months before spacecraft delivery to Cape Kennedy.

The list duplicated a problem/failure report in some instances, but it was broader in scope; and, when issued rapidly and used judiciously, it was an effective tool. Essentially, it focused attention upon those problems most in need of resolution. The composite P-list summary (Appendix F), shows that the average response time to resolve a problem was 27.8 days, the maximum response time was 134 days, and the minimum time was 1 day.

8. Pocket Guide

One small but effective informal technique to disseminate information of broad interest was the distribution of a pocket-size notebook to matrix and management personnel. As informative data were obtained, they were reduced and distributed to book holders. While this information was never considered flawless (and there was never a concerted effort to keep it up to date), it did provide material for quick reference and enabled personnel to become quickly oriented to many aspects of the project. At various times, schedules, reference numbers, command, telemetry channel, and telephone lists were included, as well as graphic presentation of such data as launch window and launch configuration. The "little black book" is expected to be further enhanced with flight information as particulars become available.

D. Schedules and Progress Monitoring

1. Schedule Packages

The progress of the events listed in the master schedule (Fig. 3) was reported regularly to NASA Headquarters. These same milestones were also listed in the Project Development Plan (together with the signature concurrence of the system managers), and from them a series of more detailed schedules was generated. One prime set of schedules involved the launch vehicle and AFETR responsibilities of LeRC. Similarly, the Project Policy and Requirements document also contained a basic schedule with a few carefully defined line items compatible with the Project Development Plan. In addition, the Policy and Requirements document called for the preparation of a comprehensive set of schedules by the JPL personnel cognizant of each activity. Accordingly, the second prime set of schedules also included one set of charts, which was a condensation of the launch vehicle interface planning and status as described in the first prime set of schedules. All of these schedules, presented in Appendix G, formed the basic progress reporting structure. The total schedule package, kept internally compatible and deriving its major end dates from the master schedule, served as a reliable source for the regular project status report to NASA Headquarters. Major schedule revisions were made several times during the life of the project (the schedules were updated about eight times).

It was the policy of the Project Office to accept the schedules as being, at all times, dynamic in nature and, therefore, subject to change with prior concurrence of the Project Office. Unilateral revision of project milestones was prohibited. Accordingly, it was also Project Office policy to insist that all phases of the project be scheduled with the best available information, and to use the schedules as a measurement of planning efficiency.

With each schedule slippage, certain sacrifices were made and greater risks taken. In effect, acknowledgment of a delay meant that some desired aspect of the project

was abandoned, which reduced confidence in the ability to achieve the mission objectives. When problems occurred that threatened the possibility of meeting the immutable launch period, the project grudgingly fell back to the next most favorable course of action available at the time.

From time to time, selected areas also provided special or expanded schedules to assist planning and communications regarding those aspects of the project. An example is the SFO test schedule issued in conjunction with the Space Flight Operations Plan.

2. Flow Plans

To control the interval between the time that the system was defined and the time that flight-qualified assemblies were delivered to SAF, a third set of schedules was prepared. These schedules were more detailed, but intentionally not so extensive as to require handling by a computer. They were also constrained to conform to the prime and secondary sets of schedules. They pertained exclusively to the development of the spacecraft; they resembled PERT in format and intent and were called flow charts. A separate flow chart was assigned for preparation and reporting for each item on the equipment list, which had to be prepared by the Spacecraft System Manager as early as possible after the system design. The equipment list enumerated the spacecraft assemblies in the configurations in which they were to be carried as spares, tested environmentally, and delivered to SAF. Since an assembly would typically involve modules from more than one technical division, it was necessary to assign its flow chart to one Project Representative, with the Project Representatives from the other divisions supplying inputs.

A number of standard milestones applicable to all equipment is defined by the Policy and Requirements document for use on the flow charts. Emphasis was given to accurate notation of the relationships between events, and to the hardware or information exchange deadlines across the divisional interfaces.

Examples of the flow charts are given in Appendix G. The diversity of the format was of considerably less concern than the accuracy of the information given and the ability of the organizations to meet or better their agreed deadlines.

3. Biweekly Reports

The Project Representatives were required to submit reports biweekly on their progress as compared to their own flow charts. With each 2-week cycle, new completions were noted or new estimates of completion were given on the single sheet that continually recirculated between the Project Representatives and the staff charged with compiling the results. To facilitate compilation of a composite report and to enable the conditions to be categorized by each division, subsystem, Spacecraft System, hardware document, due date, slip time, or test progress, a manual-sort card system was used (Appendix G). While this work could obviously have been performed with automatic data processing machines, the key-sort cards could be manipulated manually without the inherent delays or priority problems involved with computer time availability. The delinquent flow chart events were tabulated biweekly and reports were submitted to project management, division management, and Project Representatives. These lists of delays were also worked into graphs, the curves of which were considered more informative as trend indications than as absolute measurements. The combination of the "overdue bill" and trend graph enabled division management both to sense improvement or degradation and to pinpoint the troublesome areas. Special adjustments and additional curves were made when especially difficult or serious problems occurred; a total of about 1100 flow chart events were monitored throughout the life of the project.

4. Special Reports

During various stages of the project, special working report formats and techniques were evolved to focus attention on existing or expected problems. Special charts were made that showed the estimates and actual accomplishment of hardware delivery to SAF (Appendix G). From these charts, test operations personnel could plan their day-to-day activities. Essentially, each special chart was derived from flow chart inputs. The special charts show repetitious slips that clearly indicate the inability to predict delivery. This SAF delivery milestone was treated as important and inviolate as the launch date itself. On that basis, schedule information prepared from weekly SAF delivery certification reports was included in a report to JPL management.

Another form for presenting this information was derived from a merging of flow chart reports and QA status logs from SAF (Appendix G). These matrixes indicate the system-level test exposure obtained by the various subsystems on a given spacecraft. While these charts were used primarily to decide the choice of equipment for flight, they also show the extent to which subsystems were exchanged among spacecraft during the Pasadena and Cape Kennedy qualification testing.

IV. LAUNCH VEHICLE SYSTEM

A. Background

The nominal minimum *vis viva* energy (C_3) required of the launch vehicle for the 1964 Mars launch period was 10.2 km²/sec². To attain this energy at the point of spacecraft separation and for a target spacecraft weight of 570 lb, the launch vehicle had to have a payload capability of about 100 lb more than could be delivered by the *Atlas D/Agena B* used as the *Mariner II* booster. Preliminary studies showed that a modified *Atlas D* and an improved *Agena D* could satisfy mission requirements.

The *Ranger* shroud, although adequate for the *Mariner* Venus 1962 mission, was too small to accommodate a spacecraft for a Mars mission. A new shroud design was clearly required. A fiberglass shroud design concept, originally called UNIPAC, had been generated by NASA prior to the inception of the *Mariner* Mars 1964 Project. The objective of UNIPAC was to standardize shrouds for NASA *Agena* programs to the maximum feasible degree. In the UNIPAC shroud concept, separation was accomplished by using pyrotechnics to sever the shroud longitudinally and internal jets to open the severed halves at the nose. The clamshell design failed to meet development schedules and was replaced by an over-the-nose design. Significant features among the detailed design requirements were total encapsulation of the spacecraft, the incorporation of a spacecraft umbilical connector in the side of the shroud, and a test requirement for matchmate tests of spacecraft and interface hardware (both test and flight) before shipment to the launch site.

The *Mariner* Mars 1964 mission imposed several new requirements on operations at Cape Kennedy compared to the *Mariner* Venus 1962 mission. For the *Mariner* Venus mission, two launch vehicles were committed but only one pad. For the *Mariner* Mars 1964 mission, two launch pads and two vehicle systems were required in order to obtain an acceptable launch probability of success. The dual pad requirement reduced the hazards to the mission from catastrophic damage to the pad either by missions immediately preceding the *Mariner* Mars mission or by the first spacecraft launched. Dual pad availability was also important because the nominal launch period was only about 28 days, compared to the nominal length of about 50 days for the *Mariner II* mission. Two pads would permit the immediate shift of launch operations to the second pad if the vehicle on the first pad encountered problems or was launched. (In the one-pad case, about 21 days would normally be required to refurbish the pad and erect the second launch vehicle.)

One of the two pads (LC 12) had to be modified to accommodate checkout of the *Agena D*. Both pads (LC 12 and 13) required modifications in support of mission-peculiar hardware and of the spacecraft. The extreme communications distance of the Mars mission imposed severe requirements for on-pad checkout of the spacecraft telecommunications system both in the blockhouse and in Hangar AO.

A firm requirement was established for return of telemetry and launch vehicle tracking data from downrange stations within a nominal time of 36 hr. The value of the data return plan was dramatized by the failure of the shroud on *Mariner III* and the rapid assessment of the failure mode. Expedited return of the downrange data was a large factor in gaining the time for the analyses and the redesign and test efforts required to obtain a satisfactory shroud for the launch of *Mariner IV*.

In an early definition of the *Mariner* Mars 1964 mission, a test flight was proposed that would have required a third launch vehicle. This proposal was unattainable because of resource limitations and, to compensate for the deletion, an "early" combined systems test of a spacecraft, a launch vehicle, and a launch complex was established as a firm requirement to verify overall compatibility and protect the launch window.

The most fundamental constraint on the mission was the launch period. The launch vehicle, the spacecraft, and the launch complex had to be in flight-ready condition at the opening of this period, which was established, for initial planning purposes, at a nominal 44 days. Activities of JPL, LMSC, GD/C, and AFETR had to be scheduled to be compatible with the ephemeris of Mars.

Significant new features were used for the *Mariner* Mars 1964 mission involving the launch vehicle and its interface with the spacecraft. These new features are listed in Table 5 together with the extent of flightworthiness proof. A summary of key project milestones is presented in Table 6.

The objective of spacecraft/launch vehicle integration activities was to ensure that the spacecraft and the launch vehicle were compatible with each other, and

Table 5. New features of *Mariner* Mars 1964 launch vehicle and interface

Item	New feature
Atlas	Guidance shock mounts.[a] Lubrication of oil tank temperature probe to obtain a more precise "hold" limitation.[a] MA-5 engines (used on standard *Atlas* at higher rated thrust). Derated vernier engines (used on standard *Atlas*). Lightweight telemetry (used on *Mercury*, standard *Atlas*, *Ranger*, *Nike-Zeus*). Titanium helium bottle (used on *EGO* and *Centaur*). Booster steering (used on *EGO* and Air Force missions). Optimized pitch program (used on *EGO*).
Agena	*Agena D* SS-01B model. Maximum of four SS-01B flights prior to *Mariner* Mars 1964, none requiring restart. Dual burn and short coast with containment feature of Additional Basic Capability program.[a] Propellant isolation valves added for two-burn mission with containment feature.[a] Positive continuous ullage system added to ensure satisfactory engine restart.[a] Type XII inverter (three flights not *Agena* prime prior to *Mariner* Mars 1964). Model 2C horizon sensor (two piggy-back flights scheduled ahead of *Mariner* Mars 1964). Thermal insulation panels removed from aft equipment rack.[a] Modified Type V telemetry transmitter.[a] 45-sec restart timer interval instead of 30 sec.[a] Extended *Agena* coast period prior to retro-maneuver.[a] First NASA mission with *Agena D* (any model). Hercules rocket for *Agena* retro-maneuver (removed for *Mariner IV*).
Interface hardware	Fiberglass honeycomb over-the-nose shroud with close clearances (replaced with all-metal shroud for *Mariner IV*).[a] Spacecraft umbilical connection through shroud.[a] V-bands for shroud and spacecraft attachment and separation.[a] New lightweight adapter—diaphragm assembly.[a] Simultaneous backup commands for *Atlas* separation, shroud separation, and firing of *Atlas* retro-rockets.[a] New launch-to-injection instrumentation on *Agena* and interface hardware.[a] New inflight electrical disconnect, SIT, and PAS.[a]
Interface organizations	Incentive contract between LeRC and LMSC based on cost incentives. Separation of *Agena D* and NASA missions engineering. New LeRC/NASA Launch Vehicle Systems Manager. Guidance procured by LeRC instead of Air Force.
Procedures	Dual pad capability. Combined systems test at Cape Kennedy. 36-hr data return. Cold cloud weather constraint on *Agena*.

[a]First time for any mission

Table 5. (Cont'd)

Item	New feature
Launch complexes	Helium pressurization used for LOX fill on LC 13.
	Increased capability for *Agena D* checkout on-pad, removing requirement to demate *Agena* after J-FACT.
	Very tight ground-wind constraint (21 mph) with shroud cooling blanket on.
	Calibrated S-band signal from spacecraft returned to Hangar AO.

Table 6. Summary of key project milestones for the Launch Vehicle System

Category	Event	Date
Contract	Letter contract go-ahead	2-21-63
	Work statement approval	5-1-63
	Definitive contract effective	10-31-63
Launch Vehicle System reviews	Preliminary design review	11-7-63
	Intermediate design review	3-17-64
	Final Launch Vehicle System review	7-9-64
NASA Headquarters reviews	Review of *Mariner* and *Ranger* program plans	1-23-63
	NASA project review	11-14-63 7-23-64 10-7-64
	36-hr data return meeting	11-7-64
	Mariner Mars 1964 status meeting	11-11-64
	Mariner IV launch readiness meeting	11-25-64
Shroud events	Fiberglass shroud failure mode verified by JPL	11-8-64
	Flight metal shroud completed and delivered by LMSC to Cape Kennedy	11-22-64
	Qualification testing of the second metal shroud completed by LMSC	11-26-64
	All fabrication, assembly and test of pyrotechnic shroud cancelled by LMSC under LeRC direction, and design, fabrication, assembly, and tests of the over-the-nose (flight and test) shrouds started.	12-15-64
Validation of launch complexes	LC 13 validated	9-8-64
	LC 12 validated	10-8-64
Booster on stand	*Atlas* 289D erected on LC 13	8-17-64
	Atlas 289D re-erected on LC 13	9-14-64
	Atlas 288D erected on LC 12	9-28-64
Vehicle on stand	*Agena* 6931 on LC 13	9-15-64
	Agena 6932 on LC 12	10-6-64
Spacecraft on stand	*Mariner III* on LC 13	9-18-64
	Mariner IV on LC 12	10-9-64
B-FACT on LC 12 and 13	Preliminary B-FACT on LC 13	9-24-64
	Preliminary B-FACT on LC 12	10-13-64
	Final B-FACT on LC 13	10-26-64
	Final B-FACT on LC 12	10-30-64
J-FACT on LC 12 and 13	Preliminary J-FACT on LC 13	9-25-64
	Preliminary J-FACT on LC 12	10-15-64
	Final J-FACT on LC 13	10-29-64
	Intermediate J-FACT on LC 12	11-18-64
	Final J-FACT on LC 12	11-23-64
Launch dates	*Mariner III* launched from Cape Kennedy	11-5-64
	Mariner IV launched from Cape Kennedy	11-28-64

that project requirements in this interface were met. On a functional basis, the scope included compatibility of design and adequacy of tests of interface hardware; requirements for mission-peculiar pad modifications and spacecraft OSE; requirements for prelaunch tests of mission-peculiar ground and flight equipment; surveillance of launch vehicle performance and related launch vehicle modifications; and scheduling of all interface activities critical to mission success.

B. Development of Interface Hardware

1. The Shroud System

The spacecraft shroud system is that portion of the launch vehicle forward of the *Agena D* forward equipment rack. The shroud system consists of:

1. The spacecraft/*Agena D* attachment structure, called the spacecraft adapter, which includes the shroud-to-*Agena D* attachment structure or transition section
2. The aerodynamic nose fairing or shroud that covers and protects the spacecraft during prelaunch checkout and the ascent phase of flight
3. A diaphragm that closes the aft end of the spacecraft adapter at the *Agena D* forward equipment rack interface (the diaphragm was required to complete the total encapsulation of the spacecraft by the shroud system in order to ensure cleanliness and controlled humidity)
4. An RF coupler and parasitic antenna that couples the output from the spacecraft omnidirectional antenna for transmission through the RF opaque shroud
5. An electrical connector between the spacecraft and *Agena D* that disconnects at spacecraft separation
6. Environmental measurement instrumentation and spacecraft and shroud separation monitoring instrumentation
7. Spacecraft adapter V-band assembly for separating the spacecraft from the *Agena*
8. Shroud adapter V-band assembly for jettisoning the shroud
9. Shroud ejection spring system
10. Spacecraft/*Agena D* ejection spring system

The four large rectangular solar panels of the *Mariner* Mars could not be canted as efficiently inboard as the trapezoidal panels of the *Mariner* Venus and *Ranger* spacecraft were. Also, the high-gain antenna was located at the top of the spacecraft, thereby simplifying the spacecraft/launch vehicle interface. For these reasons, the nose fairing of the *Mariner* Venus or *Ranger* configuration could not be used, and a new shroud design was required.

Some of the initial design approaches studied were: (1) shroud RF opacity that, if required, could be obtained by an all-metal shroud or by lining a fiberglass honeycomb shell with aluminum foil; (2) provision of RF antenna couplers for monitoring of the spacecraft radio system on-pad and during vehicle ascent until shroud ejection, if an RF opaque shroud were used; (3) an electrical umbilical disconnect for direct access to the spacecraft; (4) payload temperature control on-pad and during ascent; (5) sterilization of the surfaces of the spacecraft that would be exposed to sterilizing gases introduced into the shroud cavity.

The shroud system designs permitted total encapsulation of the spacecraft in a contamination-free environment prior to being moved to the launch complex for mating with the launch vehicle. One of the designs was a clamshell configuration based on the UNIPAC shroud. The other was an over-the-nose ejection configuration using a modified UNIPAC shroud.

The clamshell configuration was selected as the primary design, and the over-the-nose design was delegated as the alternate. Unsuccessful explosive separation tests of the clamshell shroud in October 1963, however, resulted in the conclusion that an explosive separation system could not be developed with confidence in the time remaining until launch. It was suggested that further development of the clamshell shroud be constrained to the use of a mechanical means of inflight separation, using a minimum of explosive devices.

In November 1963, LMSC made a recommendation (with which LeRC concurred) to establish the over-the-nose shroud system as the primary shroud for the *Mariner* Mars 1964 mission, and to continue the clamshell shroud development effort as a backup for the over-the-nose shroud.

2. Over-the-nose Shroud System Design, Development, and Qualification

a. Design and testing. Eleven months remained before launch and 6 months remained before all three flight

shrouds and adapters were required at JPL for mechanical and electrical mating with the flight spacecraft. To meet this schedule, flight shrouds had to be fabricated almost simultaneously with the test shrouds. Fortunately, the over-the-nose shroud used many of the clamshell shroud components, such as the fiberglass-honeycomb shroud halves, the magnesium transition section, the umbilical door, the RF coupler system, and the nose dome. Many of the materials and qualification tests performed on the clamshell shroud honeycomb structure were considered still valid for the over-the-nose shroud design. Also, many of the studies and analyses generated for the clamshell shroud were directly applicable to the new configuration.

Changes were required on the spacecraft to accommodate the new shroud design. One significant spacecraft change was the addition of skid rails to the solar panels to prevent catastrophic damage to the spacecraft in the event the shroud impacted the spacecraft during ejection.

The over-the-nose shroud was identical to the clamshell shroud with the following exceptions:

1. Elimination of pyrotechnic segmentation system
2. Addition of one-piece fiberglass and magnesium section connected to the beryllium nose dome
3. Addition of spring cartridge assemblies for shroud ejection
4. Modification of lower shroud ring for a V-band clamp configuration
5. Modification of spacecraft adapter structure to add a ring with a shroud mating V-band clamp configuration and shroud separation spring push-off surface
6. Addition of shroud-to-adapter V-band and explosive bolts and associated harnesses
7. Addition of aerodynamic fairings to the shroud body to protect the shroud ejection-spring cartridges and V-band clamp

The first test shroud was subjected to the following tests at JPL in conjunction with the spacecraft:

1. Spacecraft acoustic test
2. RF calibrations and RF interference tests
3. Purging test
4. V-band pyrotechnic firing test for measuring shock loading imparted to the spacecraft
5. High-voltage static-discharge tests
6. Static structural tests during spacecraft qualification testing
7. Vibration testing during spacecraft development and qualification testing

The principal shroud qualification tests performed by LMSC were:

1. Collapse pressure
2. Static structural
3. RF leakage
4. Static–thermal
5. Acoustic

All required qualification testing was satisfactorily completed except for shroud RF leakage and purging gas leakage. Both RF and gas leakage requirements were eventually relaxed when it was concluded that they could not be reliably met in time for the launch.

b. V-band. A V-band consisting of two semicircular halves was used to attach the shroud to the adapter section. Each band segment was fitted with bathtub fittings at each end and with shoes approximately 4 in. long that were clipped to the bands, leaving an approximately 1¼-in. space between shoes. The shoes contained V-grooves for mating with the V-foot profile of the shroud and adapter interface rings. Two explosive bolts were used to tension the band around the shroud and adapter mating joint.

Ejection of the V-band assembly was accomplished by firing the explosive squibs, which fractured the V-band bolts at a prenotched diameter. The stored energy in the V-band (tension equal to approximately 6500 lb) was thereby released causing the bands to rapidly contract, straighten, and move away from the shroud and adapter.

Ultimate load tests in the installed position were performed by LMSC to verify the load-carrying capability of the band, shoes, and bathtub fittings. Band tension was established through analysis, and the capability of the adapter and shroud for resisting V-band loading was established through analysis and testing. No difficulties in the band were experienced throughout the entire testing program. A long-term tension test was also performed to qualify the V-band for up to 30 days on-pad without retensioning.

c. Explosive bolts. The explosive bolts were threaded right- and left-handed on opposite ends. Spherical seat washers were used for optimum nut-bearing surface area and torquing characteristics. Each bolt had a dual bridge wire squib in each end. The explosive bolts had previously been qualified and flown on a satellite program. No difficulties were experienced throughout the *Mariner* Mars program.

d. Strain gauges. Separate strain gauges were used for monitoring V-band tension during the installation and checkout period and during flight. The installation strain gauges were mounted at three positions on each band segment. Strain-gauge calibration was performed on a special jig and hydraulic loading machine. During band tensioning, strain-gauge readings were made at approximately 500-lb increments until the launch-criteria tension load of 6500 lb was reached.

The flight strain gauges were a semiconductor type. One strain gauge was mounted on each band segment. Calibration of the flight gauges was accomplished by using the installation strain-gauge data. Flight strain-gauge tension was telemetered from the *Agena D*. Flight data were erratic and the validity of the data received was uncertain. Readings wandered during pad operations, and in two cases dropped out during both *Mariner* flights. This was unfortunate since valid failure analysis data were badly needed to resolve the *Mariner III* failure.

e. Electrical harness assemblies. Two electrical harness assemblies were used to carry the wires from each of the two explosive bolts and flight strain gauges. The wires ran from the explosive bolt squibs and strain gauges to pull-away connectors mounted on the adapter below each bolt assembly. Special brackets were provided to guide the connectors for a straight pull away from the adapter connector halves.

f. Shroud ejection system. Shroud ejection was accomplished by four ejection spring assemblies mounted in the shroud lower end. Each assembly consisted of two tension springs connected to two rods riding in linear ball-bearing guides. The two rods were firmly attached to each other, and ejection would occur even if one of the two springs failed. The springs were matched for spring rate and free length, and were assembled in pairs for optimum balance between assemblies. Rod alignment and length were adjustable. The ejection springs accelerated the shroud to a separation velocity of approximately 92 in./sec. An extensive series of separation tests verified the ability of the spring assemblies to eject the shroud without collision with the spacecraft.

g. RF transmission. For monitoring the spacecraft radio during the launch phase of flight until shroud ejection, the shroud contained a coupler (located over the omnidirectional antenna) joined by a coaxial cable to a parasitic slot antenna mounted flush with the aerodynamic contour of the shroud. The shroud coupler and parasitic antenna requirements were deleted for *Mariner IV*, however, to expedite the delivery of the all-metal shroud.

For ground checkout and calibration purposes, three spacecraft RF links were provided:

1. Low-gain antenna link: omnidirectional antenna signals were transmitted by the shroud parasitic slot antenna directly to Hangar AO when the service tower was removed, and by means of a portable external coupler bolted on the outside of the shroud when the service tower was in place.
2. High-gain antenna link: the output of a probe on the high-gain antenna was carried by a coaxial cable out through the spacecraft umbilical cable.
3. Precision link: the output of a precision directional coupler, located between the spacecraft transmitter and omnidirectional antenna, was carried by a second coaxial cable out through the spacecraft umbilical cable.

h. RF interface hardware. Radio-frequency interface hardware, such as precision couplers, shroud slot antennas, RF cables, and connectors were given comprehensive acceptance tests. These tests consisted of bench measurements of VSWR, insertion loss, and impedance.

Several RF problems were encountered late in the program and special tests were initiated to resolve them. Included among these special tests were: shroud RF leakage, shroud external coupler nonrepeatability and leakage, catenary cable pin drift, excessive VSWR and insertion-loss variations, and contamination of the umbilical connector with potting resin. The shroud leakage problem was severe. The external coupler repeatability problem was found by tests to be a mechanical installation problem that was solved by the use of guide-pins. Coupler leakage was eliminated by stiffening the flange and increasing the number of attachment screws. Testing of the catenary cable with its RF connectors indicated the need for refabricating the connector to provide satisfactory VSWR and insertion loss. The

umbilical connector mechanism was made inoperative by the intrusion of potting resin. The connectors were salvaged successfully by contracting for the delicate rework of the several contaminated ground-half connectors.

i. Shroud system cleaning. Metallic, silastic, and miscellaneous dirt particles were observed on the adapter during matchmate, and were subsequently removed with a vacuum cleaner. Upon removal of the shroud after completion of the matchmate tests, additional contamination was seen on the spacecraft and adapter. Evidently the particles had been dislodged from crevices in the shroud during handling. As a result, LMSC developed a more comprehensive cleaning procedure for the shroud system that included acoustic cleaning in a chamber using an air horn as the noise source.

During the spacecraft adapter mating operations at Cape Kennedy, additional silastic (used for corrosion protection of the V-band) and dirt particles and a chalky residue were noticed on the adapter. As a consequence, LMSC removed the silastic, rubbed the chalky areas with alcohol, and revacuumed the adapter. Normal clean room attire (including gloves) was worn by all personnel in the Explosive Safe Facility. By adhering to spacecraft cleanliness techniques, confidence was established that the shroud, adapter, and spacecraft were as clean as possible at the time encapsulation was accomplished.

j. Sealing and purging. A dry-nitrogen purging system was used to maintain a positive shroud-cavity pressure to preclude moisture and dirt from entering crevices during launch complex operations. Purge fittings were located near the nose of the shroud and at the adapter for connection of the purge system. It was necessary to remove the purge system when the service tower was removed at about L − 130 min. Consequently, there was at least a 3-hr period prior to launch when no purging was provided. Tests during J-FACT and simulated launch had shown a negligible increase in humidity during comparable periods of suspended purging.

The shroud was sealed with vinyl tape at the areas found to leak after encapsulation. The umbilical connector had a soft collar that sealed the shroud umbilical opening when the cable was installed. The final acceptance criteria specified that, at 60 standard ft^3/min of nitrogen flow, the shroud-cavity pressure should be at least 2 in. H_2O. All shroud systems were adequately sealed prior to final transfer from the ESF clean room area.

k. Venting. A shroud-cavity pressure relief and vent valve was provided in the diaphragm. It was an acceleration- and pressure-sensitive check valve that was inoperative until after liftoff. This allowed one-way venting of the shroud cavity. No difficulties with the valve were encountered during any adapter or shroud system qualification testing.

l. Adapter. The basic adapter structure was comprised of two semimonocoque 0.060-in. magnesium conical sections. One conical section converged from the common base ring to the mounting plane of the spacecraft. The other conical section diverged from the common base ring to the shroud mounting ring. The diameter at the common base was 60.0 in., the same as the *Agena D* forward equipment rack.

The program redirection to use the over-the-nose shroud required no drastic changes in the adapter design; however, it did require an extension of the divergent adapter conical section to mate with the shroud at a station farther forward and with a mounting ring of greater diameter.

A diaphragm of thin magnesium sheet was attached circumferentially to the adapter base ring for sealing the lower end of the adapter. A spherical depression was formed in the center portion of the diaphragm to allow clearance for the spacecraft science package. The center portion of the diaphragm was riveted to the outer annular flat section at a ring that was also secured to the *Agena* forward equipment rack by means of supporting posts and clamps. This means of support prevented "drum-head" effects. Electrical connectors were provided through the diaphragm to carry the spacecraft composite telemetry modulation, adapter instrumentation, and pyrotechnic circuits to the *Agena D*.

The adapter base ring was a solid, precision machined ring to which were riveted the conical sections that supported the spacecraft and shroud. The diaphragm was also riveted to this base ring. The adapter was attached to the *Agena D* forward equipment rack by means of 48 bolts through the base ring. The lower surface of the base ring was scraped for a minimum of 80% contact with the *Agena D* mating surface, a maximum gap width of 0.006 in., and a maximum gap length of 4.00 in. Peel-type shims were also placed between the adapter lower ring and the *Agena D* mating ring at a step-machined surface to ensure uniform clamping and to achieve spacecraft/*Agena D* longitudinal axis parallelism. Four indexing pins were located around the inner

circumferential diameter for proper spacecraft/launch vehicle orientation.

The over-the-nose shroud configuration adapter was subjected to the following tests at JPL:

1. Spacecraft modal survey
2. Spacecraft low-frequency, high-frequency, and torsional vibration
3. Spacecraft acoustical
4. Spacecraft EMI
5. Purging
6. High-voltage discharge
7. Spacecraft RF and antenna-pattern
8. V-band release effects on spacecraft
9. Flight-type matchmate
10. Spacecraft flight-acceptance vibration

Except for equipment mounted on the adapter, no problems or difficulties were encountered with the basic adapter structures.

The only reported developmental difficulties encountered during the adapter development program were:

1. Dimensional control of the shroud, spacecraft, and *Agena D* attachment surfaces. Application of special techniques, tooling, and procedures during fabrication, handling, installation, and shipment corrected the deficiencies.
2. Contamination resulting from fabrication, handling, protection, and storage. Special acoustical cleaning, handling, shipping and pre-spacecraft-mating cleaning procedures reduced contamination to acceptable limits.

m. Spacecraft attachment and V-band. The spacecraft/adapter interface consisted of eight mounting pads attached to the inner adapter conical section. Eight mating pads on the spacecraft (with shear lips projecting below the separation plane at the inner diameter) indexed the spacecraft with the adapter and carried the transverse shear loads during launch. The mounting pads of both the spacecraft and adapter were profiled on the outer diameter surfaces to accommodate a V-band. Extensions to the adapter mounting pads were provided at either side of the spacecraft pads to permit mounting of an eccentrically drilled, five-sided washer that was used to carry torsional and transverse shear loads. The shear washers were set for a 0.002- to 0.008-in. gap with the spacecraft foot. Screws clamped the washers to the pad extensions.

The V-band retention system consisted of several nylon lanyard and spring sections attached between clips on the adapter and corresponding clips on the V-band shoes and explosive-bolt assemblies. During early separation development testing, the lanyards failed because of the V-band retraction impulse. Grommets were added to the clips and the size of the lanyards was changed to eliminate this problem.

The retract springs were redesigned after it was discovered (from slow motion films of the band during separation) that the band was hitting the spacecraft. With the addition of retract springs and lanyards to the explosive-bolt assemblies, it was demonstrated after some 35 spacecraft separation tests that the V-band when released would consistently retract into the area between the shroud and the spacecraft adapter sections without impacting the spacecraft.

The V-band was subjected to a series of separate development tests, including long-term fatigue tests. The tension load for flight was ultimately established at 2500 $\pm$ 50 lb. Other tests performed on the V-band were static tests, V-band firing tests, and V-band post-release trajectory evaluations.

n. V-band separation. Two squibs were located in each bolt assembly, and two bridgewires were used in each bolt. One squib could release a bolt as well as detonate the other squib in the assembly. In addition, either of the two explosive-bolt release assemblies would reliably release the band as demonstrated during qualification testing. Therefore, the pyrotechnic system was considered highly redundant and reliable.

o. Spacecraft separation system. The spacecraft separation system consisted of four equally spaced spring mechanisms mounted on the adapter that acted against four mating pads on the spacecraft through hemispherical bearing plates. Each spring mechanism could be separately aligned, adjusted for preload, and adjusted for stroke. Springs with uniform precision length were selectively chosen to ensure that all springs would have uniform spring-rate characteristics. Linear ball-bearing bushings were used to provide uniform low-friction spring guidance during the separation stroke. The end of the guide bearing on the spacecraft was spherical to

provide point contact and precision force transfer locations for minimizing tip-off at, and for optimum control of, spacecraft separation.

The spacecraft separation-initiated timer required an adjustable pad on the adapter to bear against until separation occurred. The SIT pad was a horizontal screw with a large head ground for the SIT plunger bearing surface. The screw was mounted in a fixed bracket bolted to the transition section.

The spacecraft pyrotechnic arming switch, activated at spacecraft separation, rested against a flat horizontal pad on the adapter. The pad had only a vertical adjustment.

The separation spring assemblies were qualified as part of the adapter assembly. A long series of spacecraft separation tests was required to complete the qualification of the system. In the flight of *Mariner IV*, the separation spring assemblies separated the spacecraft as designed. Tip-off rates were well below 1 deg/sec, and the separation velocity was approximately 2 ft/sec.

p. Inflight electrical disconnect. The inflight electrical disconnect design provided for internal springs, which were used to counterbalance pin drag forces at separation; consequently, spacecraft separation perturbations from the inflight disconnect were very small. The male half, mounted on the adapter, included a phenolic plate used as the spring pushoff force transfer surface, and also provided a high dielectric surface after separation that maintained proper pin spacing at all times.

q. Combined vibration test. The spacecraft/shroud/adapter combined vibration test dynamically qualified the shroud and adapter. A test spacecraft, dynamically similar to flight spacecraft, was used to confirm the following: structural integrity of the adapter and shroud, dynamic clearance envelope with the spacecraft, shroud and spacecraft V-band dynamic structural capability, and continuity and low noise of the inflight disconnect fitting during vibration. Upon completion of the vibration testing, the V-bands were released to verify their integrity. The system performed as designed.

r. Static discharge tests. As a result of *Ranger* flight anomalies and observations of films of the *Ranger* launches, static discharge tests were performed on the *Mariner* spacecraft to evaluate spacecraft vulnerability. A Van de Graff generator was used to build up an electrical charge on the shroud system encapsulating the PTM spacecraft. The entire assembly was mounted on an *Agena* forward equipment rack. The test was considered inconclusive for *Mariner*; no effect on the spacecraft was observed. The electrostatic charging phenomenon and its effect on spacecraft is not completely understood, and it is recommended that follow-on programs pursue additional testing and analysis. It has been requested of NASA Headquarters that tests and inflight measurements be made by the launch vehicle centers.

s. Preliminary matchmate test. The PTM spacecraft, identical in all respects to the flight spacecraft, was used to perform a preliminary but formal matchmate with the test shroud that was supposed to represent the flight shrouds in all respects. The primary intentions were to: (1) mate the spacecraft using preliminary flight mating procedures, (2) provide flight operations personnel with experience in mating the hardware, (3) evaluate aerospace ground equipment tools and handling equipment, and (4) establish any deficiencies or design changes that might be required to ensure flight-hardware compatibility. The test proved to be very valuable, particularly to the personnel responsible for Cape Kennedy operations. It is believed that the cost was inconsequential compared to the training gained by all personnel.

t. Flight matchmate test. Approximately 1 month after the preliminary matchmate test, LMSC shipped the partially completed flight shroud systems to JPL for matchmate tests with the MC-2 and MC-3 flight spacecraft. The following matchmates were accomplished:

1. MC-2 spacecraft to 6931 shroud system
2. MC-3 spacecraft to 6932 shroud system
3. MC-2 spacecraft to 6931A shroud system
4. MC-3 spacecraft to 6931A shroud system

One of the purposes of the matchmating activity, besides verification of flight hardware and aerospace ground equipment compatibility was the demonstration that flight hardware and aerospace ground equipment were in a flight-ready status.

3. Over-the-nose Fiberglass Shroud System Failure Investigation

The failure of *Mariner III* on November 5, 1964, was immediately investigated. Telemetry data indicated that the spacecraft solar panels failed to deploy and that the spacecraft failed to acquire the Sun. Launch vehicle data

indicated *Agena D* fuel depletion shutdown, and tracking data indicated insufficient injection velocity. Additional analysis of the data revealed that the shroud failed to be ejected clear of the spacecraft.

a. JPL investigation activity. The day after the *Mariner III* launch, the possibility was suggested of a shroud structural failure due to skin separation from the fiberglass honeycomb core. Immediate action was taken to subject a test shroud to a combined thermal–vacuum test. The launch-profile pressure decay was simulated; however, due to limited availability of heating lamps, the shroud skin temperature could not be brought near the expected flight levels. Nevertheless, the shroud skin delaminated and further evaluation indicated that the flight failure mode probably was similar. An extensive series of materials tests was performed on undamaged portions of the test shroud and on new samples provided by the vendor.

b. LeRC/LMSC investigation activity. As soon as tests of the shroud established the *Mariner III* probable failure mode, LMSC removed flight-quality fiberglass honeycomb pyrotechnically separated shroud halves from storage for use in further evaluation tests. Since JPL had the only readily available vacuum chamber with flight-profile vacuum and temperature-simulation capability, LMSC forwarded several shroud halves to JPL for testing under LMSC direction.

The chamber was modified by JPL to provide improved launch-profile heating capability. An extensive 24-hr/day test program was implemented. One of the shroud halves was perforated to vent the honeycomb structure and was subjected to an acoustic noise test in addition to the simulated launch-profile pressure–temperature tests.

4. All-metal Shroud Fabrication and Qualification

a. LMSC all-metal shroud. Efforts were directed toward the development of an all-metal shroud when postflight investigation revealed the *Mariner III* probable failure mode to be fiberglass skin separation. An LeRC/LMSC/JPL task team was formed to design and qualify an all-metal shroud. The fiberglass structure was replaced by a magnesium section with an inner thermal liner. The first replacement shroud was completed and delivered to Cape Kennedy within 17 days of the original failure.

A second all-metal shroud was built by LMSC and subjected to static structural tests and separation tests under thermal loading to qualify the design for flight. The final test was satisfactorily completed November 26. Upon notification of satisfactory completion of the static structural test, November 27 was established as the first launch attempt for *Mariner IV*.

b. JPL all-metal shroud. As a "last-ditch" backup, an analytical study and design effort for an all-metal shroud for the *Mariner IV* launch was also undertaken by JPL. The beryllium nose dome, ogive section, ejection spring assemblies, thermal liner, and lower shroud ring from the previously damaged test shroud were used. An aluminum body and internal thermal liner were fabricated, and the assembly was completed by November 25, some 20 days after the first launch. Qualification testing, including shroud separation tests using a specially-constructed test fixture, was also conducted during that period to ensure that the shroud would be flightworthy.

5. Shroud System Performance

The flight performance of the fiberglass shroud was unsatisfactory as developed for the *Mariner III* mission. The metal shroud produced under forced draft conditions for *Mariner IV*, however, was successful in meeting primary mission requirements. The metal shroud did not contain an RF coupler, and thus fell short of meeting requirements for checkout and monitoring of the spacecraft RF system (through the omnidirectional antenna, over an air link, both on-pad and in flight).

The flight performance of *Mariner IV* demonstrated that the shroud and adapter system was mechanically and electrically compatible with the spacecraft and the launch vehicle. The metal shroud successfully ejected over the spacecraft without striking it, and did not subsequently collide with the spacecraft/*Agena* combination. Shroud and spacecraft V-bands separated properly without impacting the flight vehicle. At spacecraft separation, the electrical disconnect fitting functioned properly, as did the separation initiated timer and pyrotechnic arming switch. The separation springs ejected the spacecraft without excessive tumbling motion.

The *Mariner III* launch brought to light a structural weakness in the shroud, which the interface hardware qualification and acceptance test program or quality assurance techniques were not capable of uncovering. The weakness (skin separation from the core) was of such a nature that it could have been detected only by tests under combined environments (temperature, vacuum, and time). Such tests were not performed on the shroud system until after the failure of the *Mariner III* shroud.

The weakness of the shroud was also related to shroud quality control, in that skin separation was most readily induced at points of local bonding defects. Local defects could easily be inflicted inadvertently on the shroud during handling, test, and checkout operations. No adequately reliable method was available for inspecting the fiberglass sandwich. Even the crude coin-tapping inspection method was not used for inspection of the flight shrouds after assembly of the shroud halves into a single structure. Sensitivity to combined environmental conditions and to the fabrication process was later found to be characteristic of fiberglass sandwich structures. The two principal advantages that were put forth in favor of the fiberglass UNIPAC shroud when the initial choice was made were never to be realized on the *Mariner* program. These advantages were:

1. Weight savings
2. Universal shroud system

At the conclusion of the *Mariner IV* metal shroud effort, it was estimated that an all-metal shroud could have been built that would have been no heavier than the over-the-nose fiberglass shroud. Fiberglass weight increases were necessary because of such phenomena as resin weight increase and core thickness increase. The effect of shroud weight difference on payload is only about 10% of the actual weight because it is jettisoned during ascent. Therefore, even the original estimated advantage of using fiberglass would have been relatively small.

Difficulties in maintaining development schedules for *Mariner* over-the-nose shroud and interface hardware prevented the continued development of the UNIPAC design; serious difficulty had been encountered with the flexible linear-shaped-charge separation joint. It was necessary to redirect the effort toward an over-the-nose mechanical separation system, which had the greatest chance of successful qualification and delivery within the rigid *Mariner* schedule. Following the launch of *Mariner III*, it was necessary to further redirect the program to an all-metal shroud. Thus, a universal shroud was never achieved.

The universality of the UNIPAC concept and the apparent weight efficiency of fiberglass construction were understandably appealing in the early phases of the program. However, in retrospect, it is clear that metal should have been selected because it would have been more compatible with the limitations of the *Mariner* development and test schedule as well as with available inspection techniques and quality control capability.

6. Interface Instrumentation and *Agena* Telemetry

a. Instrumentation. The instrumentation requirements for spacecraft environmental measurements were:

1. Three low-frequency accelerometers and two high-frequency accelerometers. One high-frequency accelerometer was for axial vibration measurement on the spacecraft, and the others, mounted close to the spacecraft mating surface on the adapter, were for measuring tangential, axial, and radial vibration.
2. A microphone mounted on the adapter for recording the acoustical environment in the shroud cavity. The shroud microphone was subsequently deleted in favor of a vibrometer because tests revealed that the low-frequency response of the microphone and its amplifier extended below 1 cps, causing the microphone to respond to changes in the static pressure inside the shroud cavity.
3. Three spacecraft separation monitoring potentiometers for linear and tip-off rate measurement.
4. Spacecraft V-band tension monitoring flight gauges. These gauges were the semiconductor type bonded to two of the six turnbuckles. The change to a semiconductor strain gauge occurred late in the program and it was not fully qualified for flight. The gauges used to monitor V-band tension during installation were the conventional strain-gauge type. Calibration problems with the semiconductor gauges left doubts as to the ability to verify band tension in flight.
5. Shroud V-band tension monitoring flight strain gauges. These gauges were similar to the ones mounted on the spacecraft V-band.
6. A pressure transducer mounted on the adapter to provide shroud cavity pressure data.
7. Two shroud separation monitoring microswitches mounted on the adapter. No problems were experienced with these devices.
8. A thermistor located at the adapter diaphragm.
9. A thermistor attached to the spacecraft umbilical to monitor shroud-cavity temperature until liftoff and umbilical release. Special on-pad cooling tests were used to correlate critical spacecraft component temperatures with shroud-cavity temperature as measured by the umbilical thermistor.

All of the interface instrumentation, except the spacecraft high-frequency vibrometer and the umbilical thermistor for measuring shroud-cavity temperature, was mounted on the adapter. An electrical harness was mounted in the adapter with cable clips to carry the instrumentation and V-band explosive-bolt squib cables. The harness was wrapped with aluminum foil and rewrapped with glass tape for thermal control and prevention of contamination. Terminal boards for connections to the V-band strain gauges and for the mounting of balancing resistors were also located in the adapter. The terminal boards were not protected from short circuiting that might have occurred at the time the *Mariner III* shroud failed.

b.* Agena *telemetry. The *Agena* telemetry subsystem continuously transmitted, at a subcarrier center frequency of 98 kc, the spacecraft composite modulation from launch to spacecraft separation. The spacecraft telemetry signals comprised the audio spectrum between 20 cps and 2.4 kc. The data encoder/*Agena* telemetry interface was a two-wire interface, one wire of which was *Agena* telemetry ground. The data encoder output was transformer-isolated and varied 5 v peak-to-peak. The measurements of interest to the spacecraft environment are given in Table 7.

Table 7. *Agena* telemetric measurements of the spacecraft environment

Agena channel No.	Function
3	Shroud V-band tension
4	Shroud V-band tension
5	Spacecraft V-band tension
6	Spacecraft V-band tension
8	Spacecraft separation potentiometer
9	Spacecraft separation potentiometer
11	Spacecraft separation potentiometer
10	Adapter accelerometer (radial)
12	Adapter accelerometer (tangential)
13	Adapter accelerometer (tangential)
17	Spacecraft vibrometer (axial)
18	Adapter vibrometer
F	Spacecraft telemetry (composite)
15–33	Shroud cavity pressure
15–38	Shroud separation microswitches
16–18	Adapter diaphragm temperature

Telemetry channels 8, 9, and 11 were time-shared. From launch until just prior to shroud separation, these channels were used to monitor the accelerations, in orthogonal axes, of the *Agena* inertial guidance package. When switched, they measured the analog output of the three spacecraft separation potentiometers.

Channel 15 was a commutated telemetry channel that sampled 60 *Agena* functions. Two of the 60 functions (numbers 33 and 38) were of concern to the performance of the shroud system. Measurement 15-33 was the shroud-cavity pressure. This transducer was a twisted tube connected to a variable reluctance pickup. Measurement 15-38 recorded the discrete event of shroud separation from the adapter.

C. Conversion and Activation of Launch Complexes

1. Launch Complex Conversion

Mission planning called for two launches during the 1964 Mars opportunity. Due to the short launch period compared to the turnaround time for one pad, two launch complexes, LC 12 and LC 13, were assigned to support the mission. Launch complex 12 is a NASA pad and LC 13 is an Air Force pad.

A conversion plan was defined and implemented to enable conversion of the two complexes to the configuration required for *Mariner*. This plan included the modification of LC 12 from the *Agena B* configuration to *Agena D* and subsequently back to *Agena B*.

The schedule for conversion of LC 13 had to be coordinated with the Air Force so that modifications to the complex could be made when there was no Air Force vehicle on the stand. However, some installation activity was permitted on a noninterference basis.

Modifications and additions to the blockhouse, the service tower, and the umbilical tower were required. Pad conversion schedules, activation manuals, and conversion plans were coordinated between all the participating agencies (LMSC, GD/C, JPL, AFSC/SSD, LeRC). The conversion plan provided a description of the equipment and tasks required for conversion of AFETR Launch Complexes 12 and 13 to the *Mariner* Mars 1964 configuration. A list of the mission-peculiar equipment is presented in Table 8.

Table 8. Launch complex conversion equipment provided by JPL

Area	Location	Equipment	Area	Location	Equipment
Launch stand	Launch pad building	400-cps generators	Launch complex cabling	From pot head in transfer room to JPL J-box on umbilical tower	Video pairs
		400-cps remote control panel		From long-line cables to J-box in launch pad building (LC 13 only)	Terminal adapter cables
		60-cps remote control panel		From long-line cables to J-box in launch operations building	Terminal adapter cables
		Spacecraft power control console (J-box and line amplifiers)		JPL test coordinator's console to GD/C terminal board	Final-stage vehicle (spacecraft) ready signal switch cable
Service tower (gantry)	Service tower	6-ft S-band antenna		From filter/regulator to receptacle on umbilical tower (LC 13 only)	60-cps cable
	Service tower	JPL portable gaseous N_2 control unit		From receptacle to umbilical tower J-box (LC 13 only)	400-cps cable
Umbilical tower	Umbilical tower	10-ft antenna, S-band filter regulator, 60-cps power		From receptacle to JPL launch pad console (LC 13 only)	400-cps cable
	Umbilical tower	J-box			
Launch operations building	Launch operations building	Monitor and control console (includes J-box and circuit breakers)			
		Final-stage vehicle (spacecraft) ready signal switch			
		Test coordinator's console			

2. RF Links

Two-way S-band transmission was required, while on-pad, between the JPL launch checkout station (Hangar AO) and each of three points within the spacecraft: the low-gain antenna, the high-gain antenna, and the precision calibrated coupler. For this purpose, an antenna was mounted on the service tower and another on the umbilical tower. Both antennas pointed toward an antenna on Hangar AO, which contained the spacecraft systems test complex.

Prelaunch checkout equipment was designed to enable RF system checkout and precise calibration in the presence of an RF opaque spacecraft shroud (leakage down 40 db). Late in the shroud development program, RF testing disclosed that the shroud provided only about 12 db of RF isolation. This high leakage level would have prevented reliable checkout and precise calibration of the RF links unless compensating changes were made to the RF monitoring system on-pad. Several unsuccessful attempts were made to reduce shroud leakage to a tolerable level by applying silver paint to the inner surface of the shroud and RF mesh gasketing and aluminum foil to suspected leaky joints and interfaces. It was found that a major redesign of the shroud would be required to improve its RF leakage characteristic to a tolerable level.

Because no time remained for such redesigning, the decision was made to change the ground checkout links to provide low-loss, hard-line cables from the spacecraft to the monitoring racks in the blockhouse. This provided a method for calibration, monitoring, and checkout that was independent of shroud leakage, but only with respect to high gain and precision links; no hard-line connection to the low-gain antenna was feasible once the service tower was rolled back.

The major redesign activity required to accommodate the hard line consisted of: (1) low-loss cable procurement; (2) design of cable troughs and trays from the base

of the umbilical tower to the blockhouse; (3) redesign of the installation and logic of the directional couplers and RF switches on the umbilical tower; (4) selection, installation, and test of a 10-ft parabolic antenna to replace the 6-ft parabolic antenna originally installed near the top of the umbilical tower; (5) installation of a standard rack in the blockhouse at the JPL console location to house the RF monitoring and calibration equipment; and (6) preparation of a procedure for checkout and acceptance testing of the RF system at the completion of the installation.

3. Launch Complex Validations

The validation of the launch complexes included verification that the installed equipment as specified for *Mariner* was in accordance with approved drawings and/or specifications. The purpose of facility validation was to verify compatibility between mission-peculiar launch control or launch support subsystems located in the blockhouse, the service tower, the umbilical tower, and equipment in locations remote from the launch pad. Among the remote sites affected were Hangars AO and AE. The mission operations center and spacecraft system test complex were in Hangar AO. The launch vehicle control center was in Hangar AE. *Agena* telemetry for *Mariner IV* was patched into Hangar AO from Hangar AE.

Validation of the facility included the following checks on LC 12 and LC13:

1. Launcher functional and restrictive procedure checks
2. Launch alignment checks
3. Launcher rotation
4. Launcher rise off switch adjustment
5. Booster on-stand capability
6. Facility checkout vehicle fit checks (includes spacecraft shroud with flight half umbilical disconnect)
7. Umbilical release checks, including *Agena D* flight checkout vehicle
8. Blanket retract test (facility checkout vehicle)
9. Vehicle function generator electrical checks
10. Vehicle on-stand capability checks
11. Spacecraft simulator checks
12. Spacecraft mechanical checks and gaseous nitrogen purge
13. Spacecraft on-stand capability checks

D. Launch Vehicle

The *Mariner* Mars launch vehicles consisted of two stages: the first stage was a mission-oriented improved *Atlas D*, and the second stage was an improved *Agena D* modified to meet the requirements of the mission. The shroud and adapter structure protected the spacecraft from the external environment during the portion of the ascent trajectory within Earth's sensible atmosphere. The *Agena D* launch vehicle is shown in the launch configuration in Fig. 22, and an exploded view is shown in Fig. 23.

The serial numbers of the vehicles launched are:

	Spacecraft serial No.	*Atlas* booster	*Agena D*	Launch complex
Mariner III	MC-2	289D	6931	13
Mariner IV	MC-3	288D	6932	12

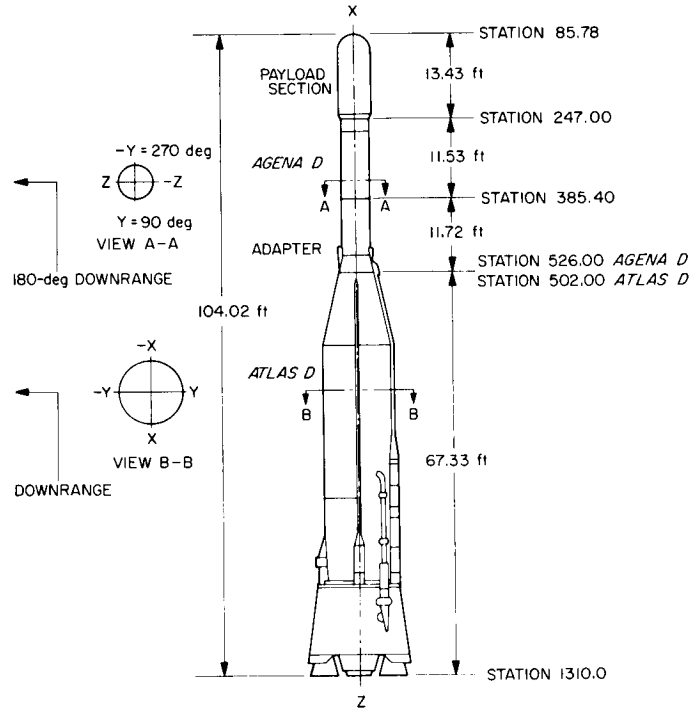


Fig. 22. *Mariner* Mars 1964 launch vehicle configuration

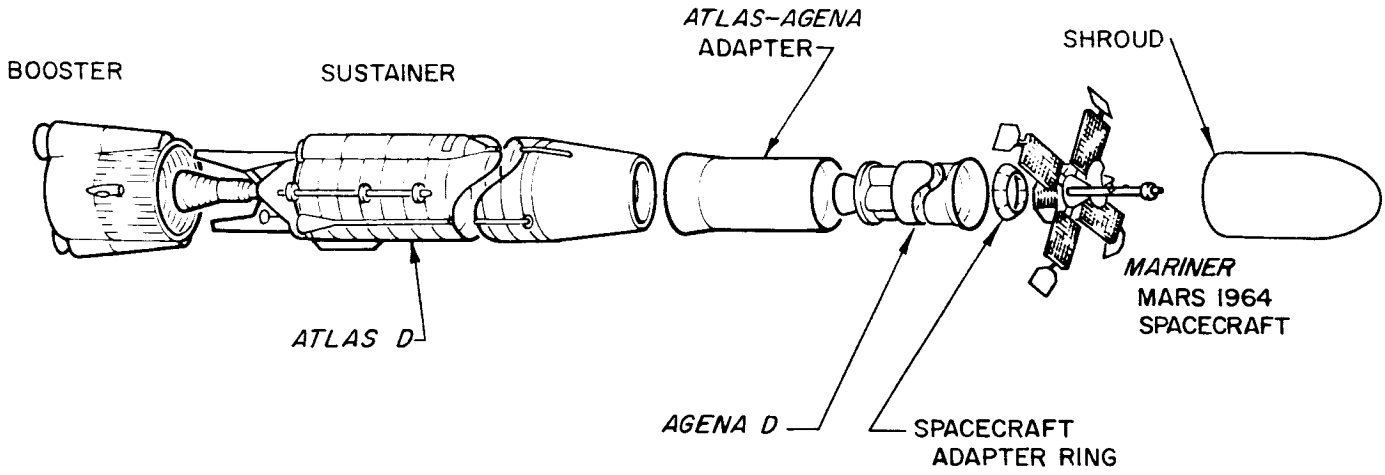


Fig. 23. Exploded view of *Mariner* Mars 1964 launch vehicle

1. *Atlas* Vehicle

The one-and-a-half-stage *Atlas* provided the required thrust to place the *Agena*/spacecraft combination on the required ascent trajectory.

a. Airframe. The *Atlas* airframe consisted of a cylindrical stainless-steel structure into which all other subsystems were integrated. The airframe consisted of: (1) the main propellant tank section; (2) the aft booster section; and (3) the forward interstage adapter section. When assembled, the *Atlas* airframe was approximately 67 ft in length and 10 ft in diameter.

b. Propulsion. The *Atlas* propulsion system used for the mission was the MA-5 liquid-propellant rocket engine system, with RP-1 and liquid oxygen as propellants. This engine system was developed for the *Atlas* standard Launch Vehicle System (SLV-3); however, the engine system thrust was derated from the standard *Atlas* value to the nominal *Atlas D* value for the Mars spacecraft. The overall nominal thrust rating of the *Mariner* MA-5 engine system at liftoff was 367,340 lb. The MA-5 cluster rocket engine consisted of three subassemblies: one booster engine system (two thrust chambers, optimized for low-altitude performance), one sustainer engine (one thrust chamber optimized for high-altitude performance), and two vernier engines (one thrust chamber each for attitude control and velocity trim). The vernier engines were derated from a thrust of 1000 to 670 lb in order to increase the payload capability. Other improvements in the *Mariner* Mars *Atlas* propulsion system over the *Mariner II Atlas* propulsion system were a redesigned boost turbopump gear case, a redesigned sustainer engine lubrication oil system, hypergolic starting on all engines, and many more minor improvements.

c. Electrical system. Primary power for the *Atlas* subsystems was supplied by a remotely activated 28-v silver-zinc battery. The battery package was to be a newly developed, individual, manually activated, 28-v battery used to supply power to the *Atlas* telemetry system. However, the new battery failed to pass the qualification tests so the previously used, remotely activated battery was reused. Secondary power was supplied by a 400-cps, three-phase inverter. The 28-vdc power was converted to 115/125 vac as required for the flight-control system and the guidance system. A magnetic amplifier regulator controlled the voltage and frequency to within a range of +1.5%. A changeover switch was provided for switching both ac and dc power from external to internal power through related power-distribution cables and harnesses to the appropriate guidance and autopilot canisters.

d. Hydraulic system. The *Atlas* launch vehicle contained two independent hydraulic systems that supplied the operating pressure required to position the engine thrust chambers for directional and roll control of the vehicle. The booster hydraulic system furnished hydraulic pressure for booster engine gimbaling prior to staging. It consisted of a variable displacement pump, a reservoir, two accumulators, four booster-engine actuators and associated valves and plumbing.

The sustainer vernier system provided hydraulic pressure for sustainer and vernier engine gimbaling and for operating propellant utilization valves and gas generator valves. This system was comprised of a variable displacement pump, a reservoir, an accumulator, two sustainer-engine actuators, four vernier-engine actuators, a pressure manifold, a return manifold, a head suppression valve, a

propellant utilization valve, a gas generator blade valve, and associated valves and plumbing.

e. Pneumatic system. The standard type pneumatic system—consisting of helium storage bottles, pressure regulators, and LOX boiloff valve—had the following primary functions: (1) maintaining adequate pressurization of the main propellant tanks, hydraulic reservoirs, and engine lubrication oil tanks; (2) providing pressure for various engine control functions; (3) providing inflight repressurization of various propellant tanks; and (4) providing activation pressure for booster separation systems.

f. Guidance system. The Mod III G missile-borne guidance set consisted of a rate beacon, a pulse beacon, a decoder, antennas, and associated equipment. The rate beacon received CW signals from the ground-rate measuring equipment and transmitted a return signal for extracting range-rate and lateral-rate information. The pulse beacon received signals from the X-band position tracking radar and generated a beacon return pulse that was transmitted to the tracking radar for range, azimuth, and elevation tracking. The decoder received command messages from the ground system through the pulse beacon; these messages were subsequently decoded and discrete commands or guidance steering corrections relayed to the flight control system. The *Atlas* boosters used newly designed vibration-isolation mounts for the guidance canisters to reduce their vibration environment. This mounting system required flexible wave guides to carry the RF signals between the canisters and the rigid pod-mounted antennas.

g. Flight control system. This system consisted of a flight programmer, an autopilot, and ten gimbaled thrust-chamber actuator assemblies. The system stabilized and steered the vehicle along the desired trajectory by controlling the orientation of the engine thrust vectors. Pitch steering commands are normally generated by the flight programmer from launch until booster staging, and by a combination of the flight programmer and guidance system from staging until the end of *Atlas* sustainer-powered flight. However, in order to permit early correction of booster dispersions from the nominal ascent trajectory, the capability to steer the vehicle by use of the guidance system prior to booster staging was implemented. Booster steering was enabled from 100 to 110 sec after liftoff with a $\pm 1.5\ \sigma$ deadband about the nominal trajectory and a steering rate of 0.28 deg/sec. Booster steering occurred on the *Mariner III* ascent, but the small trajectory dispersion did not require it during the *Mariner IV* flight.

h. Propellant utilization system. The propellant utilization system was comprised of two modified mercury manometer assemblies that sensed the fuel-tank and oxidizer-tank head pressures, an electronic computer comparator, a hydraulically actuated sustainer engine fuel-control valve, manometer sensing lines, and an electrical harness. The propellant utilization system maintained a desired balance in the propellant mass remaining in each tank as it was expended. Thus, the proper mixture ratio was maintained by minimizing the imbalance of residual propellants at sustainer engine cutoff.

i. Range safety command system. The airborne Range safety command subsystem was a modified Mark II, consisting of a destructor and a destructor control unit. The destructor control unit consisted of two antenna pairs, an antenna ring coupler, two receiver-decoder units, an arming device, a power and signal control unit, a battery pack, and a single destructor unit. Commands were transmitted by coded tone modulation of a carrier wave. These coded signals were decoded and used to energize relays and supply 28 v to the destruct and/or engine-cutoff control circuits. Redundancy was provided by the two antenna pairs and the two receiver-decoder units.

j. Telemetry system. The telemetry system monitored and telemetered *Atlas* functional conditions prior to launch through *Atlas/Agena* separation. The system consisted of a lightweight telemetry package, a battery package, an antenna system, transducers, and associated wiring.

The telemetry package was a 17 channel system consisting of 12 subcarrier channels and five noncommutated channels, transmitted on a carrier frequency of 229.9 Mc at a power level of 7 to 11 w. The package contained an RF transmitter, a frequency-multiplexing network, subcarrier oscillators, commutators, and an inflight calibration unit.

The antenna system was composed of two matched-slot radiator antennas mounted on the forward ends of the two *Atlas* equipment pods. Power to each of the antennas was divided equally by a T-coupler.

The transmitter used in previous NASA *Atlas* flights was not used on the *Mariner* Mars vehicles because the NASA/LeRC requirements for the data from that system were deleted. This change decreased the *Atlas* sustainer weight by 52.5 lb.

2. *Agena D* Vehicle

An improved *Agena D* SS-01B provided the dual-burn capability and attitude control required to place the spacecraft on the predetermined geocentric transfer orbit. The SS-01B basic vehicle differed from the SS-01A model by the following major improvements:

1. Addition of propellant sumps and containment screens
2. Use of beryllium doors and skins on forward section
3. Use of beryllium horizon seeker blow-off fairings
4. Use of a pyrotechnic-operated helium valve
5. Elimination of an electrical power control unit

These improvements were incorporated by the Air Force prior to transfer of the vehicle to NASA. The *Agena D* configuration is illustrated in Fig. 24.

a. Airframe. The *Agena D* airframe was a cylindrical structure approximately 5 ft in diameter and 20.6 ft long. The length of the vehicle is measured from the aft end of the engine nozzle to the forward section of the forward equipment rack. The vehicle spaceframe consisted of four major sections: the forward section, the tank section, the aft section, and the booster-adapter section. The forward section carried guidance, flight-control electronics, telemetry, command, tracking, electrical power, and propellant-pressurization equipment. The telemetry, guidance, and electrical power components were module-mounted for simplified checkout and interchangeability. The tank section stored the fuel and oxidizer necessary for operation of the main rocket engine and also provided the supporting structure between the forward and aft vehicle sections. The aft section provided for structural support and attachment of the rocket engine assembly, pneumatic attitude control thrust valves, nitrogen storage spheres; and it contained provisions for alignment with the booster adapter. Ready

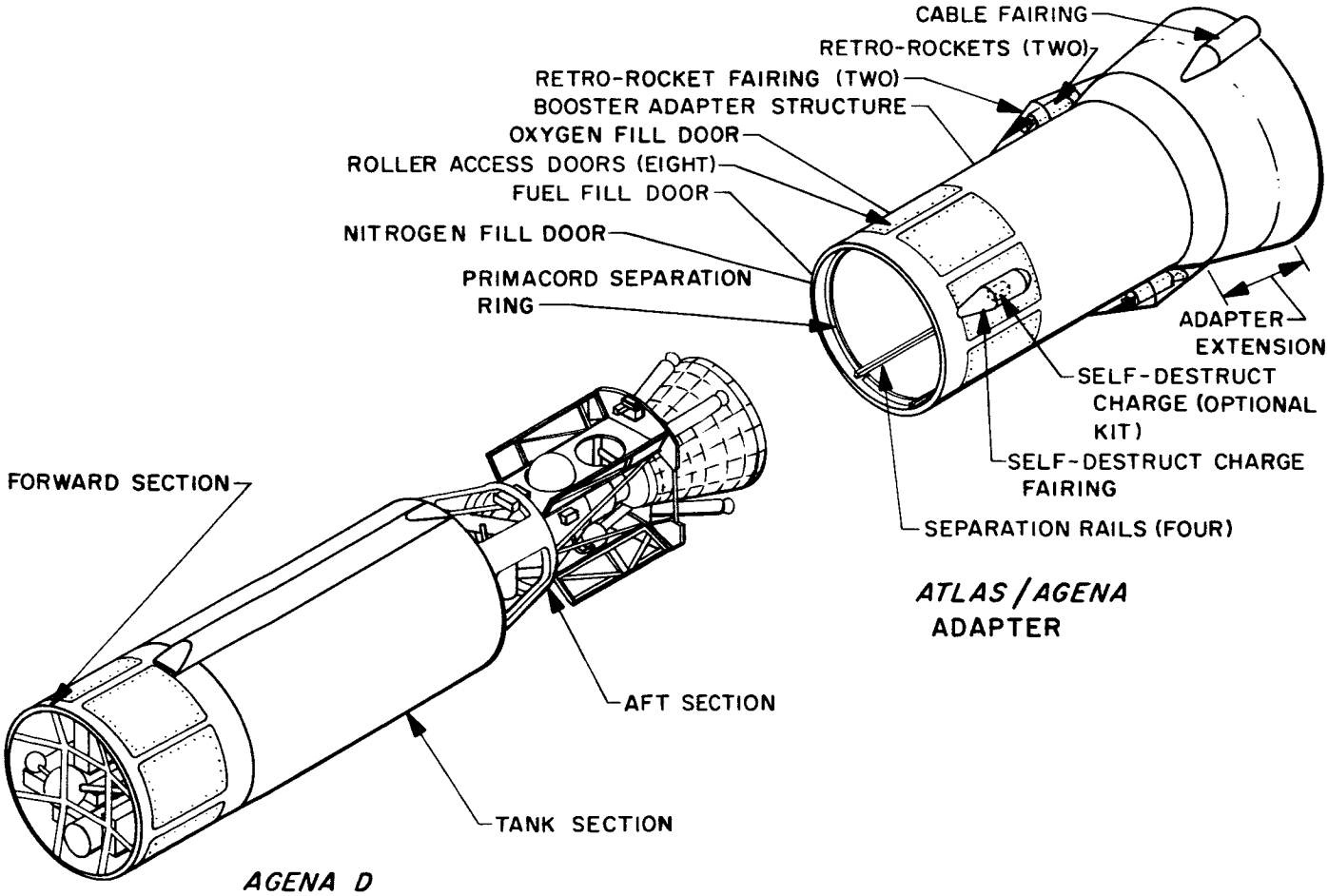


Fig. 24. *Agena D* basic configuration

access to all parts of the engine, plumbing, and wiring was made possible by the aft section open-frame design. The booster adapter section was the interconnecting structure between the *Agena D* and the *Atlas*. This section also housed the two retro-rockets used for separation of the *Atlas* from the *Agena*.

b. Propulsion. The propulsion system was composed of an engine with dual restart capability and a propellant and pressurization subsystem. The engine was designed for a nominal thrust duration of 240 sec with an overall thrust rating of 16,000 lb (vacuum). Propellants used for engine operation were unsymmetrical dimethylhydrazine as the fuel and inhibited red fuming nitric acid as the oxidizer. Propellant tanks were pressurized with helium to ensure proper propellant pump operation. The propellant and pressurization system maintained the desired pressures in the propellant tanks and at the engine turbopump inlet, and provided for passage of propellants between these units. This system consisted of a helium supply sphere, control valves and couplings, propellant isolation valves, and associated propellant lines and bellows. At the aft end of the SS-01B propellant tanks, sumps were provided to position the propellant at the inlets to the fuel and oxidizer pumps. The sump contained a fine mesh screen that permitted flow of propellants into the sump during the *Agena* first burn and inhibited a return flow during the coast phase. This new feature of the *Agena D* system was developed for the purpose of eliminating the heavier ullage rockets previously used.

Because a flight demonstration of the engine restart capability could not be obtained prior to launch, a positive continuous ullage control system was added. This system, activated just after first burn termination, consisted of a small nozzle using bleed high-pressure attitude control gas to provide a small positive thrust to overcome drag during the parking orbit coast phase. This thrust provided assurance that the propellants would be maintained at the bottom of the tanks and that bubble formation would be minimized in the sump.

c. Electrical system. The electrical system supplied power to the *Agena* systems. Two primary batteries supplied 22 to 29.25 vdc (through the main power transfer switch) to the pyrotechnics, the telemetry and C-band tracking beacon, the guidance module, the 400-cps inverter, and the dc-to-dc converter. The 400-cps inverter supplied 115-v, 400-cps single-phase and three-phase power to the inertial reference package, the velocity meter, the horizon meter, the timer, and the flight-control electronics. The dc-to-dc converter supplied plus and minus 28.3 vdc.

d. Guidance and control system. The primary function of the guidance and control system was to: (1) maintain the *Agena* at the proper attitude at all times; (2) provide switch closures at the proper times to accomplish the desired ascent sequence of events; and (3) provide the propulsion shutdown signal after the desired velocity to be gained had been achieved. The major components of the system were the inertial reference package, the horizon sensor, the flight-control electronics unit, the hydraulic attitude control system, the pneumatic attitude control system, the velocity meter, and two electromechanical timers. The inertial reference was provided by the inertial reference package; the Earth reference for the inertial reference package was supplied by the horizon sensor. The inertial reference package controlled the attitude of the *Agena* by applying attitude error signals to the flight-control system, which, in turn, applied torques to the *Agena*. The inertial reference package received inputs from the motion of the vehicle and from the horizon sensor, the geocentric rate circuit, and the command programmer. Thus, although the reference package provided an inertial reference, this reference was up-dated whenever the package received an input from any of the four previously mentioned sources.

Error signals from the reference package were applied to the flight-control electronics unit, in which they were processed and applied to the hydraulic attitude control system and the pneumatic attitude control system. Two hydraulic actuators gimbaled the engine, providing thrust-vector control; six nitrogen gas attitude control jets were provided to torque the vehicle.

The velocity meter used a pulse-generating accelerometer and a pulse counter to provide an engine shutdown signal when the desired velocity to be gained had been achieved. The standard sequence timer consisted of a synchronous motor, 12 dual-counter assemblies, and 72 switches. Switch closures at 24 discrete times provided the programming for the ascent sequence of events and the engine start. At the end of the parking-orbit period, the restart timer restarted the standard sequence timer, which then sequenced the remaining *Agena* events. The guidance junction box and flight-control junction box provided the interconnects required by the guidance and control system.

e. Communications and control. The communications system monitored and measured, via electrical signals, functional and environmental conditions of the *Agena* and the spacecraft during the ascent phase to spacecraft injection, and during the *Agena* retro-maneuver. The system which transmitted these measurements was composed of a Type V 17 channel FM/FM telemetry system with turbine speed on the modulation bus. Major components of this system were a VHF 10-w transmitter (RF amplified), voltage-controlled oscillators, RF switch, programmer, dc-to-dc converter, signal conditioners, and commutators. A transponder in the C-band range was used to assist ground-radar tracking by the AFETR stations.

f. Command destruct system. On *Mariner III*, the command destruct system provided a ground-controlled destruct capability from liftoff through *Agena* first-burn cutoff + 15 sec. The system consisted of two antennas and receivers, an RF coupler, a secondary battery power supply, a destruct initiator, and a destruct charge.

On *Mariner IV*, the *Agena* flight-termination system was comprised of two secondary batteries, a destruct initiator, premature separation switches, and necessary electrical circuitry. It would use the antenna and receivers of the *Atlas* LV-3A to receive and relay the destruct signal in case of a command to destruct. In addition, if the *Atlas* LV-3A and *Agena* separated prior to the programmed time, the destruct charge would have been detonated automatically.

3. Payload Capability

Launch vehicle payload capability was of critical concern to the *Mariner* Mars mission because the design goal for spacecraft weight (570 lb) was about 100 lb greater than initial *Atlas/Agena* vehicle capability for an injection energy (C_3) of 10.2 km²/sec² at the onset of the program. Hardware and software improvement programs were implemented to obtain the required increase in capability. Table 9 lists the significant improvements that were implemented. Figure 25 presents the chronology of spacecraft weight and vehicle payload capability from early 1963 until launching. For the *Mariner* Mars 1964 mission, one unit of C_3 energy km²/sec² was equivalent to approximately 33 lb of payload.

Initially, the mission was programmed to use the standard *Atlas* SLV-3; however, GD/C was directed to switch to the *Atlas D* LV-3A in April 1963, when it had become apparent that the standard *Atlas* schedule could not support the mission. At the time the change was made, the standard *Atlas* capability was estimated to be about 20 lb greater than a nominal *Atlas D*. It was possible to make the improvements listed in Table 9 on the *Mariner Atlas D* so that the vehicle had about 60 lb greater capability than a nominal *Atlas D*, and about 40 lb greater capability than a standard *Atlas*. It would

Table 9. Payload performance improvement items implemented for *Mariner* Mars 1964

Category	Item	Payload improvement, lb actual gain	Remarks
Atlas	Derated verniers	20	
	Lightweight telepack	9	
	Optimized pitch program	25	
	Mod III G guidance equations	12	
	Booster steering	5	
	Lightweight titanium helium bottles	2	
Agena	Additional basic capability changes:		
	Propellant containment and scavenging	47.2	Includes use of positive continuous ullage control (−5 lb)
	Beryllium skins and doors	19.8	
	Pyrotechnic operated helium valve	2.2	
	Positive continuous ullage elimination	4.5	
	Type XIIA inverter	8	Incorporated in basic *Agena* SS-01B
	Lightweight C-band beacon	6	
	Unitized J-box	—	Incorporated in basic *Agena* SS-01B
	Hercules retro-rocket[a]	3	Replaced Aerojet rocket
Emergency items	Retro-rocket removal	19	On *Mariner IV* only
	Command destruct replaced by self-destruct system	24	On *Mariner IV* only

[a]Eliminated on *Mariner IV* in favor of trajectory bias.

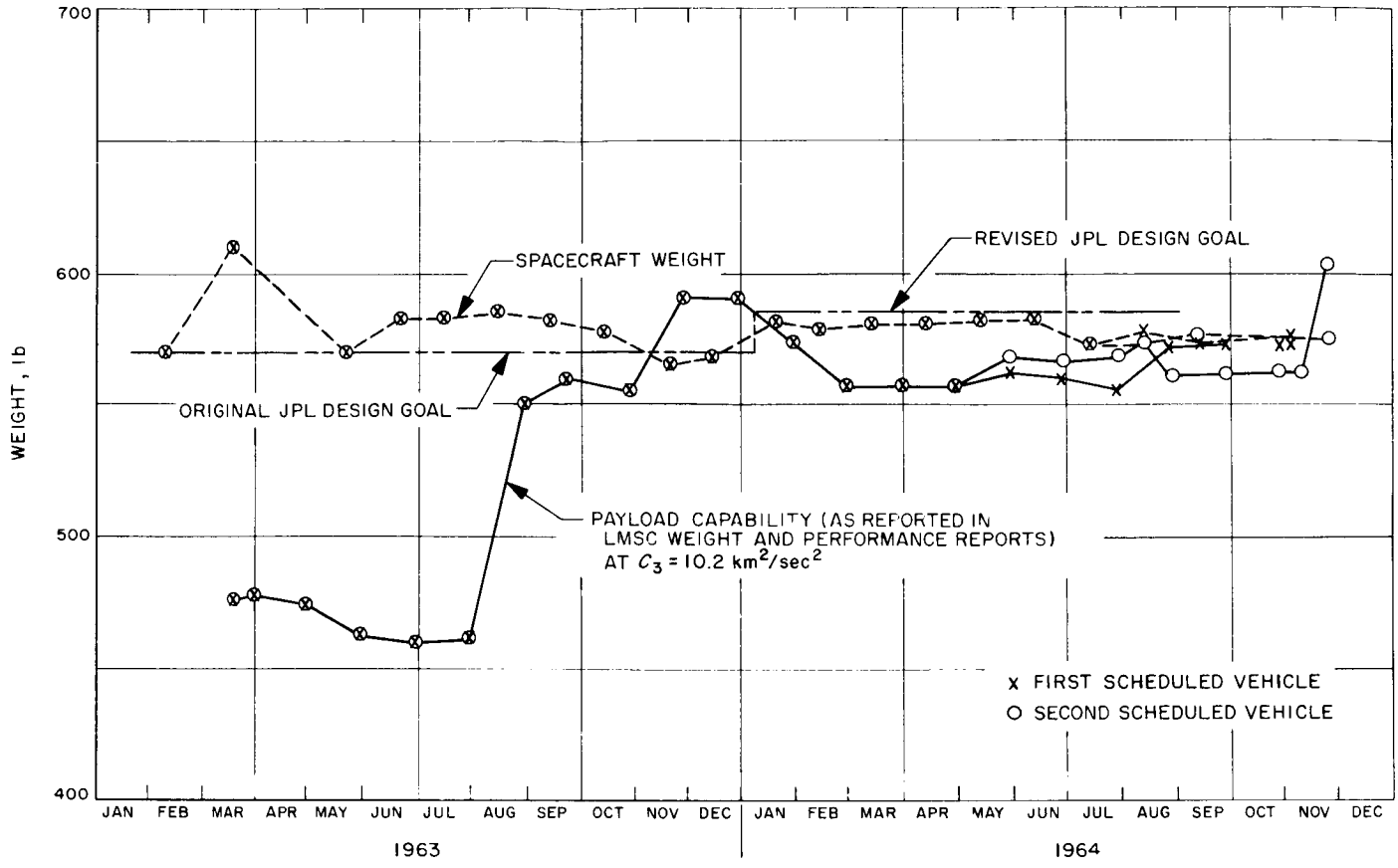


Fig. 25. History of spacecraft weight and launch vehicle payload capability

not have been possible to achieve the same gains on the standard *Atlas*, since its design was already frozen.

The principal gain achieved by using the *Atlas* MA-5 engine was the derating of the vernier engines from 1000-lb to 670-lb thrust. This reduced the propellant consumed by the vernier engines, thus making more propellant available for the main engines to deliver higher effective specific impulse.

The optimized pitch program provided a flatter, more efficient *Atlas* ascent trajectory consistent with the aerodynamic loads and heating constraints.

The Mod III G guidance equations made a significant payload gain possible by determining more efficient *Atlas* sustainer steering commands. These commands attempted to correct the vehicle trajectory only enough to arrive at the proper aiming point. With the original guidance equations, larger steering commands were generated, which attempted to return the vehicle as rapidly as possible to the nominal flight path. The payload gain originally thought to be possible by use of booster steering was considerably reduced because of implementation of the more efficient Mod III G guidance equations. Booster steering was implemented, therefore, primarily for reliability purposes and to ensure better guidance antenna look angles.

The *Agena* Additional Basic Capability improvements were a block of changes incorporated on the basic *Agena D* vehicles delivered off the Air Force assembly line. The most important change from the performance capability standpoint was the propellant tank and sump redesign that: (1) reduced unavailable residuals by providing improved scavenging, and (2) provided containment of sufficient propellant within the tank sumps to eliminate the need for ullage rockets. Because the containment feature could not be flight-qualified for a two-burn mission prior to launch, the positive continuous ullage control system was required on the *Mariner* vehicle to ensure the second *Agena* start.

The first launch vehicle delivered to Cape Kennedy (*Atlas* 288D and *Agena* 6931) was originally scheduled for erection on LC 13, which was the only launch complex available early enough to support a launch on the first two days of the launch period. However, when vehicle tag values became available in June 1964, *Atlas* 289D was substituted on LC 13 because that vehicle had about 10 lb (equivalent to 0.3 km²/sec²) greater capability than 288D. The additional capability available from 289D was required to ensure 3 σ propellant reserves on the first day of the launch period.

In June 1964, GD/C reported that nitrogen dilution of the LOX on LC 13 would reduce performance of the vehicle launched from that pad by the equivalent of as much as 10 lb of payload. Nitrogen dilution of LOX on LC 13 was due to the use of a nitrogen pressure LOX transfer system on that launch complex. (A mechanical pump transfer system was used on LC 12.) Nitrogen dilution would increase with each LOX transfer, and the 10-lb payload penalty was based on the dilution that might be expected after several transfers. To avoid a payload penalty on LC 13, helium was substituted for nitrogen as the pressurization gas, which eliminated the LOX dilution problem. The final performance capability of the first vehicle (*Atlas* 289D/*Agena* 6931/MC-2 on LC 13) prior to launch was 572 lb at a C_3 of 10.2 km²/sec², which was equivalent to an energy of 10.11 km²/sec² for the actual MC-2 spacecraft weight of 575 lb.

After the launch and failure of *Mariner III*, emergency measures were taken to offset the additional weight and drag of the new all-metal shroud and to extend the available launch period for the second launch. The *Agena* retro-rocket was removed and the *Agena* command destruct was replaced with a self-destruct system. Substitution of the self-destruct system provided a significant increase in capability because the self-destruct system was separated with the *Atlas* sustainer stage (about 10:1 payload trade-off), whereas the command destruct would have been carried to injection (1:1 payload trade-off).

The net effect of these improvements, together with the all-metal shroud, was a 40-lb gain in payload capability, which was equivalent to 1.225 km²/sec². The final performance capability of the second vehicle (*Atlas* 288D/*Agena* 6932/MC-3 on LC 12) at launch was 702 lb at a C_3 of 10.2 km²/sec², which was equivalent to an energy of 11.0 km²/sec² for the actual MC-3 spacecraft weight of 575 lb.

4. Flight Performance

Table 10 presents the major *Atlas/Agena* sequence of events. No changes in the nominal sequence of events were made after *Mariner III* launch, except for the events related to the *Agena* destruct and retro systems. Actual event times and several nominal times are given for both launches.

Table 10. Launch vehicle flight event times

Mark event number	Event	Time, sec		
		Nominal	Actual (from liftoff)	
			Mariner III	*Mariner IV*
	Liftoff	L + 0	0	0
I	*Atlas* booster engine cutoff	L + 133.5	133.43	134.00
II	*Atlas* booster engine separation	L + 136.6		
III	*Atlas* sustainer engine cutoff	L + 299.9	302.25	299.00
IV	*Atlas* vernier engine cutoff	L + 219.8	320.21	317.50
V	Shroud ejection	L + 322	322.40	
VI	*Atlas/Agena* separation	L + 324.5	324.60	321.74
	Initiate *Agena* −120 deg/min pitch rate	L + 355		
	Transfer to −3.21 deg/min pitch rate	L + 359		
VII	*Agena* first-burn ignition	L + 379	373.48	371.37
VIII	*Agena* first-burn cutoff	L + 525.3	521.98	517.25
IX	*Agena* second-burn ignition	L + 1740.3 to L + 2924.4	1919.98	2450.80
X	*Agena* second-burn cutoff (injection)	Mark IX + 97	2016.01	2546.60
XI & XII	*Agena*/spacecraft separation	Mark IX + 258	2178.08	2708.80
	Agena yaw maneuver start	Mark IX + 261	2180.96	No yaw maneuver required
	Agena yaw maneuver completion	Mark IX + 321		
XIII	*Agena* retro-rocket completion	Mark XI + 600	2778.0	—

a. Mariner III. The launch vehicle injected the spacecraft with a velocity insufficient (by 836 ft/sec) to achieve the required Mars flyby trajectory. In all other respects, preliminary analysis indicates launch vehicle performance was satisfactory.

All *Atlas* flight objectives were met. At L + 103.1 sec, a transient disturbance was registered by all *Agena* acceleration and strain transducers, interface instrumentation, and *Atlas* rate gyros. *Agena* events occurred nominally, except that first-burn shutdown was initiated later than nominal, and second-burn shutdown occurred earlier than nominal due to oxidizer depletion. During both burns, combustion-chamber pressure and specific impulse were slightly higher than nominal, resulting in higher-than-predicted engine performance. Computations run by LMSC show that the added weight of an unseparated shroud would have caused approximately the additional increments of burn time that occurred. Although the two shroud separation microswitches indicated separation (only 0.060 in. of travel required to actuate) at the proper time, all other evidence supports the theory that the shroud did not, in fact, eject clear of the spacecraft.

Booster pitch steering was enabled between 100 and 110 sec in flight. Beginning at L + 108.7 sec, pitchdown commands of 13% (0.27 deg/sec) magnitude and ½-sec duration each were generated during four of the subsequent six computer cycles. This resulted in a total pitchdown command of 0.534 deg. The last of the four commands was initiated at approximately 111 sec, which was consistent with the Mod III computing system program.

b. Mariner IV. The launch vehicle injected *Mariner IV* well within the midcourse correction capability of the spacecraft to achieve the desired heliocentric trajectory. Preliminary analysis indicated that all *Atlas* systems performed satisfactorily and that all *Atlas* objectives were met. Booster steering was enabled between 100 and 110 sec in flight; however, no booster steering commands were sent because the vehicle remained within 1.5 σ of the programmed trajectory.

Analysis of *Agena* data confirmed satisfactory vehicle operation and that all *Agena* objectives were met. The oxidizer-pump lip-seal pressure measurement indicated an erratic decay during first burn from approximately 15 psia to 1.5 psia over a 10-sec period. It later went up to 4 psia and, at second-burn ignition, to 9 psia. Following shutdown, it stabilized at 1.5 psia.

E. Launch Operations Summary

1. Prelaunch Operations

A calendar of launch vehicle prelaunch events commencing with arrival of the launch vehicles at Cape Kennedy is presented in Table 11.

a. MC-2/6931 shroud system. Upon completion of the combined systems test, the encapsulated spacecraft was returned to the clean room in Hangar AO and demated. Rework and retrofit of the 6931 shroud system was initiated immediately to prepare it for flight. Among the more important details requiring correction were:

1. Replacement of the beryllium nose dome that had a smudged surface
2. Rework of the umbilical door and its seal
3. Installation of accelerometers on the adapter
4. Rewrapping of the electrical harness with glass tape
5. Replacement of the spacecraft V-band retention springs
6. Realignment of the shroud V-band electrical disconnect guide brackets
7. Replacement of the vent valve with a preset and calibrated assembly

Rework, retrofit, and cleaning were completed on November 3, 1964 when encapsulation was accomplished in the JPL Explosive Safe Facility. The assembly was then moved to LC 13 and mated to *Agena* 6931.

b. MC-3/6932 shroud system. The mating of MC-3 with the *Agena* 6932 adapter was scheduled for approximately 3 weeks after the MC-2/*Agena* 6931 matchmating. The main difficulty experienced was in reworking the umbilical door for proper sealing and repeatable locking.

Upon completion of adapter mating with MC-3, the encapsulated spacecraft was moved to LC 12 and mated to the *Agena* 6932/*Atlas* 288D for J-FACT and simulated launch. After successful completion of these tests, the encapsulated MC-3 spacecraft was returned to the ESF. Final cleaning and miscellaneous retrofit on the 6932 adapter and shroud was performed, including the installation of V-band pyrotechnics. The spacecraft was readied for launch and reencapsulated in the ESF. Final umbilical door closure checks were made and the assembly was moved to LC 13 for remating to the 6932/288D

Table 11. A calendar of major activities at Cape Kennedy

Event	Date, 1964	
	Mariner III	*Mariner IV*
Agena arrived at Cape Kennedy	August 9	September 12[a]
Atlas arrived at Cape Kennedy	August 10	July 28
Atlas erected on-pad	August 17	September 28
Spacecraft arrived at Cape Kennedy	August 28	September 14
Shroud/adapter system arrived at Cape Kennedy	August 31	September 16[b]
Atlas returned to Hangar J; *Agena* moved to Hangar AM	September 8[a]	Not applicable
Agena returned to Hangar AE	September 10	Not applicable
Atlas reerected on pad	September 15	Not applicable
Agena mated to *Atlas*	September 15	October 7
Agena and booster adapter demated and returned to Hangar AE	September 16[c]	Not applicable
Spacecraft mated to adapter at Hangar AO	September 16	September 28
Shroud mated to adapter at Hangar AO	September 17	September 29
Atlas booster and sustainer sections demated and remated on-pad	September 17[c]	Not applicable
Booster adapter and *Agena* remated to *Atlas*	September 18	Not applicable
Spacecraft mated to *Agena*	September 18–19	October 9
First B-FACT	September 24	October 13[d]
First J-FACT	September 25	October 15[d]
Simulated launch	September 28	Not applicable
Spacecraft demated	September 29–30	October 14

Event	Date, 1964	
	Mariner III	*Mariner IV*
Agena demated, returned to Hangar AE	September 30	October 16
Spacecraft moved to ESF	October 1	October 27
Spacecraft returned to Hangar AO	October 6	Not applicable
Spacecraft moved to ESF again	October 21	Not applicable
Atlas propellants tanked	October 21	October 19–20
Spacecraft mated to adapter at ESF	October 23	October 28
Agena remated	October 24	October 28
Second B-FACT	October 26	October 30
Shroud mated to spacecraft and adapter at ESF	October 26	October 30
Spacecraft remated to *Agena*	October 27	October 31
Spacecraft demated	Not applicable	November 6
Agena demated for revalidation at Hangar AE	Not applicable	November 7
Agena remated	Not applicable	November 15
Second J-FACT	October 29	November 18[b]
Atlas/*Agena* temporary separation for urgent action survey	Not applicable	November 19
Metal shroud arrived at Cape Kennedy	Not applicable	November 22
Third J-FACT	Not applicable	November 23[d]
Spacecraft remated	Not applicable	November 24
Simulated launch	November 2	Not applicable
Launch	November 5	November 28

[a]4 days late due to Hurricane Dora.

[b]Shroud arrived September 16, 1964, without adapter.

[c]For repair of *Atlas* damage caused by stretch-mechanism failure.

[d]Spacecraft not included in test.

launch vehicle combination. The plan to have both spacecraft/launch vehicle systems ready simultaneously for launch operations was accomplished.

c. MC-3 all-metal shroud system. The all-metal shroud, which had been fabricated on a "crash" basis, was flown to Cape Kennedy on November 22. The shroud was taken to the ESF for unpacking, inspection, and the installation of handling gear.

Early the following morning, a matchmate attempt was made. The MC-3 spacecraft had been mated to the original 6932 adapter and had not been removed since the last mate. The strain gauges on the spacecraft V-band showed no loss of tension during this period of time. Because the mating surface of the new shroud had been scraped to fit the 6931A adapter, it was anticipated that poor seating on the adapter would result. A thin coat of bluing was applied to the shroud mating ring, and the

shroud was lowered over the spacecraft and adapter. An inspection after the mate disclosed that 95% of the mating surface made contact, and all gaps were less than 4 in. long.

Before the final spacecraft mate, a final check of the shroud spring alignment and stroke was made by placing the shroud on blocks on a level table with springs extended. This measurement was accomplished during the

Table 12. *Atlas* 289 D *(Mariner III)* prelaunch problems and field modifications

Category	Problems and modifications
Airframe	Stretch-sling failure causing damage to booster separation ring
Flight control	Autopilot servo amplifiers replaced to change from 50- to 45-deg vernier yaw bias
	False indication of excessive yaw displacement gyro drift
	Ten autopilot connectors rejected due to poor workmanship
	Anomaly in yaw signal amplifier monitoring circuit indicating nonlinearity during yaw steering
Hydraulics	Sustainer and vernier engine actuators changed
	Internal pressure switches changed on booster and sustainer systems
Pneumatics	Contaminated fuel tank pressure regulator replaced
	Damaged fuel pressurization Y-duct spanner nut replaced
	Leaking fuel relief valve replaced
	Failed pad cooling unit compressor replaced
	Failed booster bottle pressure control switch replaced
Electrical	Main missile battery aft mounting holes required elongation
	Main missile battery harness required rerouting to allow battery installation
	Defective staging disconnect replaced
Propulsion	Fuel start tank vent check valve replaced
	Fuel and LOX elbow orifices to vernier engines changed
	Sustainer LOX regulator replaced due to out-of-dimensional tolerance
	Two sustainer hydraulic control packages replaced because null point too high
Propellant utilization	Valve protractor required realignment
	Valve mechanical stop required resetting
	Loose protractor cotter key required tightening with subsequent shaft realignment
	Error demodulator output voltage required resetting
	One can plug with pins having solder voids replaced
Range safety command	Command receiver with varying AGC replaced
Telemetry	Noisy hydraulic accumulator transducer replaced
	Oscillating LOX pump inlet transducer replaced
	Partly shorted pitch transducer replaced
	Engine position transducers required recalibration
	Transponder RF input/AGC measurement deleted because Azusa system not used
Guidance	Two defective "ground-test-only" pulse beacon canisters replaced
	Flight rate beacon replaced with modified beacon having improved reliability
	Canister harness required rerouting for new mounting brackets
Azusa	Azusa system removed for mission at direction of LeRC
Land line instrumentation	Cross-connected plugs required reinstallation
	Defective airborne disconnect plug replaced
	Two intermittent pins bypassed with substitute pins
	No replacement available for defective LOX storage tank level transducer
	Time did not permit replacement of two damaged bending strain transducers
Propellant loading	Both control pressure regulators unstable and had history of poor reliability
Propellant-level control	Failed LOX 95% level indicator-light relay replaced
Complex	One umbilical solenoid with excessive lead length rejected
	Three relays failed within 3 weeks. Problem investigated because of common use of relay in launch complex circuits
	Service tower firex stub-up relief valve broken off during launch

early morning hours of November 24, and was followed by final encapsulation of the spacecraft.

A shroud leak test was conducted with the umbilical door taped shut. Water pressure of 2.3 in. was maintained at a flow rate of 2 ft^3/min. However, a significant drop in pressure was detected when the umbilical door was untaped. Some difficulty had been encountered previously in trying to get the door to shut properly. It was suspected that the door was off-center and not sealing tightly around all edges. The door was readjusted and it appeared to close and lock satisfactorily; however, another pressure check revealed a leak, which was caused by a gap in the shroud skirt below the umbilical door. When this gap was taped over, the leak rate was acceptable.

The encapsulated assembly was moved to LC 13 on November 24 for mating with the launch vehicle. On November 27, during the countdown of the first launch attempt, it was noticed that the shroud V-band explosive-bolt wiring harness was protruding beyond the shroud aerodynamic skirt protective area. Contoured pieces of cork were epoxy-bonded to the shroud skirt to increase the protection of the explosive bolts from aerodynamic heating. Vinyl tape, used for pressure sealing other areas of the shroud, was placed over the cork to improve airflow characteristics.

d. Prelaunch vehicle problems. The more significant *Mariner III* and *Mariner IV Atlas* and *Agena* prelaunch problems and field modifications are listed in Tables 12 through 15.

Table 13. *Agena 6931 (Mariner III)* prelaunch problems and field modifications

Category	Problems and modifications
Airframe	Corroded ground contacts and surface areas of booster adapter and extension cleaned and treated.
	0.010-in. gouge in booster adapter due to *Atlas* stretch-sling failure burnished and painted.
	Mislocated access hole in GD/C debris shield reworked.
	Sticking horizon sensor pinpuller replaced.
Propulsion	Fuel vent quick disconnect with scored mating surface replaced.
	Gas generator oxidizer filter assembly with damaged flare surface replaced.
	Leaking helium pressure transducer adapter fitting with scratched flare replaced, and missing O-ring installed.
	Deformed flange of turbine manifold starter inlet port replaced. Metal chips found in inlet throat removed prior to reinstallation.
	Scored-gimbal actuation bolt replaced.
	Fuel valve replaced with unit of improved design.
	Positive continuous ullage control kit installed and tested. Orifice not seated due to improperly machined cap and resulting damage to holder—unit repaired.
	Seal fitted to leaking positive continuous ullage control holder assembly at line connection.
Electrical	Command destruct kit wiring harness replaced with modified harness.
	Four holes in power distribution J-box sealed with tape per specification.
	Two short harnesses replaced.
	Shorted Type IX dc-to-dc converter power supply replaced.
	Aft safe/arm J-box with two defective relays replaced. All similar type relays in vehicle tested and found to function satisfactorily.
Guidance and flight control	Flight control J-box removed for guidance deadband modification, reinstalled and revalidation-tested.
	Secondary sequence timer replaced by direction from spacecraft.
	Primary sequence timer removed to reset time for operation of oxidizer propellant isolation valve; spare timer temporarily installed.
	Defective guidance module velocity-meter accelerometer and electronics package replaced.
	Velocity-meter counter replaced because of anomalous readout. Counter later found not to be at fault.
Communications	Telemetry transmitter with low output replaced.
	Improper spacers under telemetry connector replaced to correct channel calibration shift problem.
	Switch and calibrate unit removed for modification (additional diode required).
	Faulty beacon transponder replaced.
	Faulty commutator switch motor replaced.

Table 14. *Atlas* 288 D *(Mariner IV)* prelaunch problems and field modifications

Category	Problems and modifications	Category	Problems and modifications
Airframe	Booster and sustainer boots replaced by modified boots; modified boots required addition of safety wire to meet specification. Second modification also required.	Propulsion	Compressor with uneven performance replaced.
			Booster fuel staging valve replaced.
			Fuel start-tank vent check valve replaced.
Flight control	Three autopilot harness plugs replaced after X-ray survey.		Vernier LOX and fuel-orifice elbows changed.
	Sustainer and vernier actuator servos replaced.		Sustainer LOX bootstrap check valve and line with leaky joint replaced.
	Programmer replaced after faulty operation in propellant utilization test.		Booster gas-generator fuel-supply line with leaky flexible hose section replaced.
	Second programmer replaced after malfunction in B-FACT.		Drifting ISS regulator output pressure readjusted.
	Autopilot with nonlinear roll integrator output replaced.	Range safety command	Receiver with fluctuating AGC level replaced.
	All autopilots including spares returned to vendor for rework.	Telemetry	Erratic transducer replaced.
			Detached LOX start-tank transducer reinstalled.
	Gyro group with random blinking spinning light replaced.	Guidance	Waveguide assembly with pitted exterior replaced.
	Gyro group having no spinning indication in laboratory test rejected.		Second waveguide assembly with pitted exterior replaced.
	Gyro group having intermittent spinning light in laboratory test rejected.		Rate beacon replaced with unit having power-supply modifications.
			Pulse beacon with noisy signal return replaced.
Hydraulics	Sustainer and vernier actuators replaced.	Propellant loading	Leaking airborne LOX fill and drain replaced.
	Internal hydraulic-pressure switches changed.		Maladjusted fuel fill- and drain-valve position-indicating microswitch corrected.
	Failed hydraulic-pressure unit first-stage low-pressure pump replaced.		
Pneumatics	Contamination in fuel-ullage test tank caused by duct-clamp failure removed.		Corroded fuel-pump plug repaired. Circuit modification should prevent repetition of this problem.

Table 15. *Agena* 6932 *(Mariner IV)* prelaunch problems and field modifications

Category	Problems and modifications
Airframe	Cable interfering with horizon-sensor door heated and bent to fit.
	Harness with damaged connector replaced.
	Broken umbilical door spring replaced.
	Interfering bolt filed to fit.
	Corrosion of tank section due to moisture from cooling blanket removed.
Propulsion	Conax valve filter assembly with scratched seal surface replaced.
	Pyrotechnic helium control valve with leaking line connection replaced.
	Incorrectly machined orifice holder nozzle replaced.
	Leaky nitrogen supply tube assembly replaced.
	Second leaky nitrogen supply tube assembly repaired by installing flare savers.
	Oxidizer pressure switch with faulty test-indicator light replaced.
	Second oxidizer pressure switch failed to close and replaced.
	Line with leak at combustion-chamber pressure-switch fitting junction replaced.
	Leaky valve replaced.
	Agena retro-rocket removed at NASA direction.
Electrical	Converter (dc-to-dc) with no power output indicated replaced.
	Second and third dc-to-dc converters replaced but problem later located in test equipment with interchanged fuses.
	Three-phase inverter, which was subjected to excessive voltage, replaced.
Guidance and flight control	Five guidance harnesses with bent pins replaced.
	Two small loose pieces of thermal sleeving removed from guidance J-box.
	Velocity-meter counter replaced by modified unit.
Communications	Faulty harness reworked.
	Telemetry transmitter exhibiting dropout during J-FACT replaced.

2. Countdown and Summary of Launch-on-time Experience

The countdown interruptions experienced on *Mariner III* and *Mariner IV* are shown in Fig. 26 in which they can be compared with earlier *Mariner* countdown experiences. Figure 26 also presents the total number of days in the launch periods of each mission, launch attempts per launch, and total window penetration prior to launch.

The problems that resulted in countdown holds or cancellations are explained below and are keyed to Fig. 26 by item number.

a. Mariner III. The *Mariner III*/*Atlas* 289D/*Agena D* 6931 vehicle was launched from AFETR Launch Complex 13 on the second day of the launch period, November 5, 1964, at 19:22:04.92 GMT.

The first launch attempt ① was originally scheduled for November 4, 1964; however, on November 3, it was rescheduled for November 5 to permit a series of tests on the newly replaced *Agena* safe/arm relays in the aft J-box. The launch countdown was initiated at L − 405 min on November 5, and proceeded normally with the following holds.

At L − 275 min ②, a hold was called because of the loss of industrial power at the launch complex, which was caused by a bird flying into a power transformer at L − 306 min. Power was restored 2 min after the hold was called; however, the hold was continued for a total duration of 31 min to permit the *Atlas* to return to the proper countdown configuration.

At L − 60 min ③, the first planned hold was called, which was originally scheduled to last 60 min. The hold was reduced to 29 min to meet launch-window requirements and, due to clock adjustment during the hold, finally resulted in an actual duration of 28 min.

At L − 7 min ④, the second planned hold was called, which was originally scheduled for 10 min, but was extended to 37 min to evaluate a reported malfunction in the antenna drive servomechanism at the DSIF station in Woomera, Australia.

At L − 2 min ⑤, a brief hold of approximately 1 min was called because LOX topping had not been completed. Also, Antigua radar station 91.18 was reported intermittent. The countdown was recycled to L − 7 min

and the hold maintained to retop LOX. Additional time was required to recycle the spacecraft and for AFETR evaluation of the *Agena* beacon readout for the new launch plan. The total hold time was 11 min.

At L − 2 min ⑥, a hold was called on the second cycle because of the Antigua radar station problem noted earlier. The countdown was recycled again to L − 7 min and held for problem evaluation. The radar problem was cleared but AFETR requested 5 min to reorient for a required launch-plan change. Antigua station 91.18 then lost power supply and the requirement for station 91.18 radar was deleted. The total hold time was 11 min.

At L − 3½ min ⑦, a momentary hold of 1 min was called on the third cycle to verify LOX topping status. At that time, Antigua station 91.18 was reported operative again. After this hold, the count proceeded without incident through liftoff.

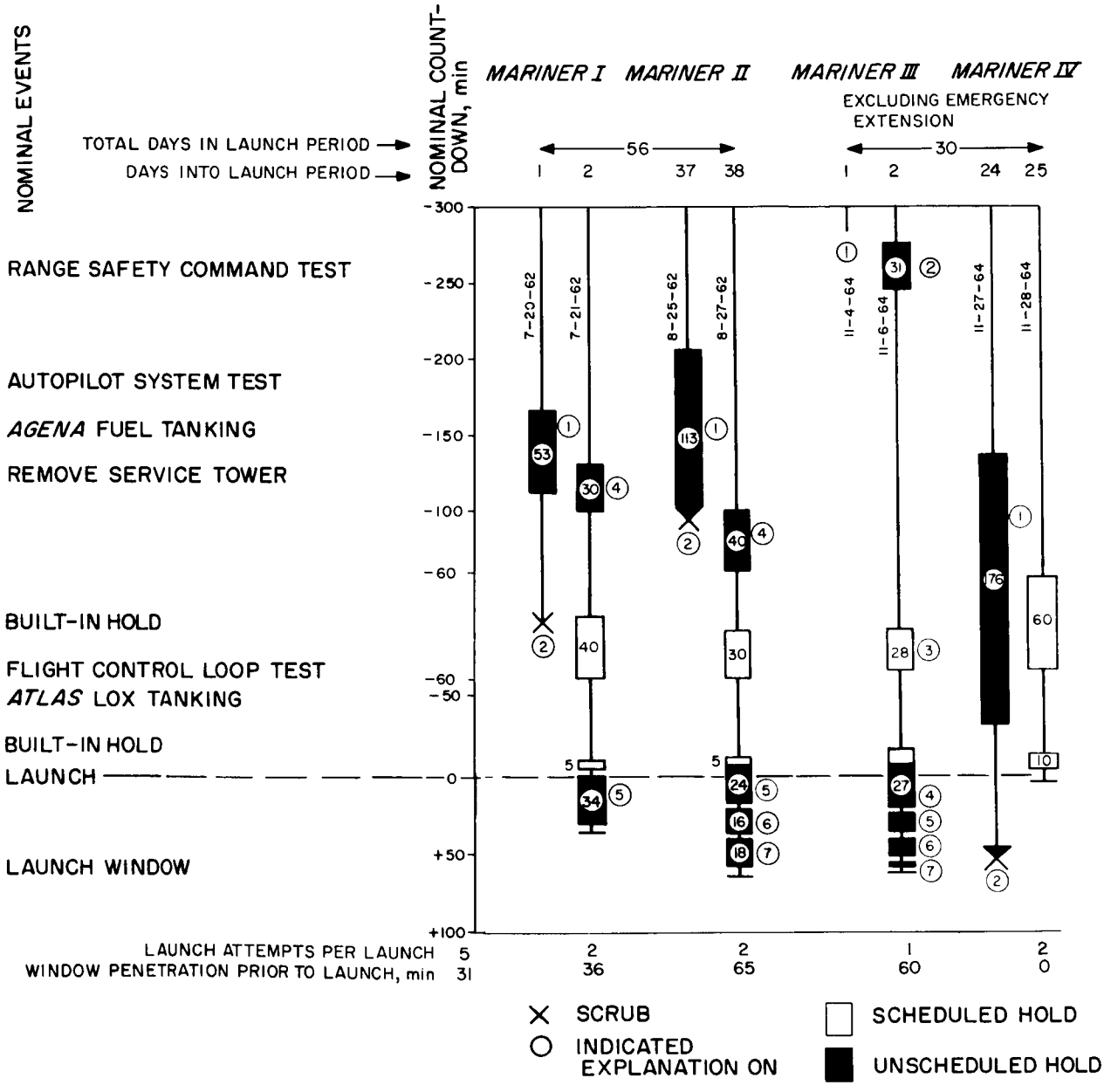


Fig. 26. JPL launch-on-time experience

b. Mariner IV. The *Mariner IV/Atlas* 288D/*Agena D* 6932 vehicle was launched November 28, 1964, at 14:22:01.3 GMT from AFETR Launch Complex 12 on the second of two launch attempts. The launch proceeded on schedule through liftoff with no significant problems encountered. The first launch attempt was conducted on November 27 with the following holds.

At L − 135 min ①, a hold of 176 min was called to evaluate an apparent problem due to the pyrotechnic harness on the shroud protruding out into the air stream. The count was resumed when analysis of the problem indicated that the condition was not detrimental.

At L − 60 min ②, a hold was called to analyze a spacecraft communications subsystem anomaly. The launch attempt was scrubbed after a 6-min hold, since insufficient time remained in the window to evaluate the anomaly. The countdown was later continued to L − 30 min as a simulated launch exercise.

3. Launch and Hold Criteria

a. Shroud-cavity temperature. Prelaunch control of the shroud-cavity ambient temperature between 40 and 65°F was a requirement to ensure that critical spacecraft temperatures would not exceed design limits in flight prior to Sun acquisition. Shroud-cavity ambient temperature was monitored before launch by means of a thermistor located inside the umbilical door and one on the spacecraft umbilical cable connector. Because tests had indicated that the ground cooling system was marginal for maintaining the shroud-cavity temperature below the 65°F limitation on hot days, the spacecraft temperature limitations were reassessed in order to determine a maximum temperature launch and hold criteria. The most critical spacecraft component was the Canopus sensor. The criterion finally established was a maximum Canopus sensor temperature of 90°F prior to launch. Canopus sensor temperature was also monitored and normally ran about 10°F above the ambient cavity temperature as measured by the thermistor attached to the umbilical connector.

b. Ground-wind constraint. The use of the shroud cooling blanket imposed a tighter ground-wind constraint on the launch vehicle. The wind restriction determined by GD/C for the vehicle with cooling blanket installed and service tower removed was between 20 and 23 mph depending on wind direction. Without the cooling blanket installed, the wind restriction could be relaxed to between 32 and 35 mph. A plan was adopted at Cape Kennedy to help relieve the tight wind restriction as follows:

Weather conditions (Predicted at launch)

Wind, mph	*Temperature,* °F	*Plan*
< 21	All values	Normal count with blanket retract at L − 0
≥ 21	≤ 70	Blanket removal at L − 175 min
≥ 21	> 70	Scrub the launch

Actual wind and temperature conditions were such that all countdowns conducted with intent to launch were carried out with blanket retract at L − 0.

c. Shroud and spacecraft V-band tension. Launch and hold criteria for shroud and spacecraft V-band tension were:

	Maximum, lb	*Minimum,* lb
Spacecraft	2700	2300
Shroud	7000	6000

These limits were for the tension readings monitored by land line in the blockhouse.

On *Mariner III*, one of the two shroud V-band strain gauges indicated gradual decay in tension over a period of several days. By the day before launch, it had dropped below the 6000-lb limit. Tapping of the V-band with a mallet to overcome friction and to equalize tension over the band length, as was done during V-band installation, did not indicate a defective or partially relaxed band. Therefore, it was concluded that the low gauge was in error and launch operations were resumed a few hours later that night. On *Mariner IV*, all V-band strain gauges remained within limits prior to liftoff. As noted earlier, all flight V-band gauges were of the new semiconductor type.

4. Documentation

The documents most directly applicable to the conduct of the prelaunch and launch operations are described below. They emanated from the Project Development Plan that delineated the manner and extent to which the contributing NASA agencies were involved. The Project Development Plan authorized the mission and was the

governing document in terms of mission objectives and the resources to be committed to the *Mariner* program. It included estimates of manpower and funding costs, the spacecraft technical development plan, quality assurance provisions, the management plan, procurement arrangements, handling of data, and a delineation of the areas of responsibility existing among the several NASA agencies involved.

a. Mission Operations Plan. The Mission Operations Plan provided management-type guidelines pertaining to the *Mariner* launch operations at Cape Kennedy, and established project policy in areas not covered in other documentation. The Mission Operations Plan was considered as the controlling document in the event of conflict with other *Mariner* project publications. It provided information concerning the *Mariner* launches; the structure and relationships of management; the functional integration of facilities as organized in support of the launch operations; a launch plan; launch and hold criteria; and a description of combined tests and launch-complex communication assignments.

b. Master Launch Countdown. This document provided integrated step-by-step instructions for all launch-complex and Cape Kennedy activities required to launch the *Atlas* booster, *Agena* second stage, and *Mariner* spacecraft, and included pad securing/abort procedures for the *Atlas*. *Agena* and spacecraft abort procedures were included in internal documents of LMSC and JPL. Supplementary to the Master Launch Countdown, each participating agency also used its own detailed launch procedures for internal operations. All appropriate countdowns were employed and verified in the combined system test on LC 13, and in B-FACT, J-FACT, and simulated launch tests.

c. Launch Test Directive. This document covered mandatory preflight vehicle procedures, launch requirements, and vehicle configuration, and listed nominal inflight event times during the preinjection period. Telemetry channel assignments for the launch vehicle and the spacecraft were also included.

d. Launch Constraints Planning document. This document described the policy, design, and resources that constrained the launch period and the launch window. The document examined constraints in the areas of range safety, the launch vehicle, the spacecraft, and its near-Earth trajectories. It described tracking and telemetry requirements from launch through launch plus 3 hr, and the resources needed to meet these requirements. During the launch period, supplements to this document were issued daily, as required, which defined the precise launch plan for the following day.

e. Test and Operations Plan. The Test and Operations Plan described test and operations plans for the *Mariner* spacecraft, including spacecraft launch and hold criteria.

f. Pad Safety Report. This document provided information on pyrotechnics, propellant, and pressurization systems associated with the *Agena D* stage and the *Mariner* spacecraft.

g. Booster Requirements Document. The Booster Requirements Document defined the support requirements of the *Atlas/Agena* launch vehicle. It treated only the standard *Atlas/Agena* configuration and reflected the support requirements that were independent of the payload or of the mission.

h. Program Requirements document. This document defined the requirements imposed on AFETR for supporting the *Mariner* Mars 1964 launches. It included information on the mission, tracking and telemetry requirements, meteorological service requirements, support instrumentation, materials and services, transportation logistics, aircraft and ships required, data processing, and launch facilities. The document was prepared by the NASA *Agena* Mission Office using inputs from LeRC, JPL, STL, LMSC and GD/C.

i. Program Support Plan. The Program Support Plan indicated the AFETR capability and readiness to comply with the requirements listed in the Program Requirements document.

j. Operations Requirements. These documents defined the AFETR support required for each test to be conducted during launch and prelaunch operations.

k. Operations Directives. The Operations Directives were the official AFETR publications that mobilized the resources of AFETR. Each Operations Directive supported the AFETR user's operations requirements for a specific test or a series of tests of an overall program. The Operations Directives constituted the official reply to the Operations Requirements and established a base for scheduling tests and committing AFETR support.

l. Project interface schedules. Because the launch period is fixed for planet encounter missions, scheduling of project milestones played a particularly important part in the *Mariner* Mars 1964 program. The JPL schedule

document for project milestones was entitled *Spacecraft/ Launch Vehicle Integration Plan.* Milestones taken from the *Mariner* Project Development Plan were given special emphasis. The document was broken down into five parts: (1) Spacecraft/launch vehicle interface hardware activities, (2) Launch criteria, (3) Spacecraft OSE and launch complex modification, (4) AFETR operations, and (5) *Atlas/Agena* milestones.

A running plot showing the number of scheduled events compared to the number of events accomplished was incorporated in the front of each issue. The revision cycle was originally set at 2 weeks, but that frequency could not be maintained. Revised pages were issued as rapidly as they could be prepared, checked, and reproduced for issue to all participating governmental and industrial organizations.

V. SPACECRAFT SYSTEM

A. General Description

Figure 27 shows the *Mariner* Mars 1964 spacecraft and illustrates some of the significant aspects of the configuration. The spacecraft is fully attitude-stabilized, using the Sun and Canopus as reference objects. A two-way communications system provides telemetry to the Earth, command capability to the spacecraft, and angle tracking, doppler, and ranging data for orbit determination.

The spacecraft has a propulsion system capable of executing two trajectory correction maneuvers. Error computation for midcourse correction is based upon Earth angular measurements, two-way doppler frequency shift, and range, with measurements of one-way doppler as a backup. Nominally, the spacecraft needs to perform only one midcourse correction, which is based upon a determination of the orbit from ground tracking data. A backup capability of performing a second midcourse maneuver is available. The total 1 σ rms target error due to maneuver execution errors and to orbit uncertainty does not exceed 7000 km.

1. Power

Power during the launch-to-solar-acquisition phase and during maneuvers is provided by a battery. While the spacecraft is solar-oriented, power is derived from photovoltaic cells.

In order to ensure maximum reliability, the power subsystem is designed to require no battery power after initial solar acquisition except during maneuvers. The battery is maintained in a state of full charge, and is available during the encounter phase as an emergency backup source in the event that a degradation of the solar panels occurs. The battery also provides power for reacquisition in the event of a noncatastrophic loss of attitude control.

The photovoltaic cells are arranged on four erectable panels having a combined total area of 70 ft^2. The panels are folded in the launch configuration. Power from the photovoltaic cells and/or the battery is converted and distributed to users as 2.4-kc square-wave power. A smaller amount of 400-cps power is used for special purposes.

2. Telecommunications

The telecommunications system (1) determines the angular position, the doppler frequency shift, and the range of the spacecraft for orbit determination; (2) uses commands from Earth for controlling spacecraft operation; and (3) telemeters engineering and scientific information from the spacecraft.

The spacecraft telecommunications system consists of:

1. Radio—receiver; transmitters (RF exciters and power amplifiers); antennas
2. Command
3. Telemetry—data encoder; video storage subsystem

The radio subsystem is involved with tracking, command, and telemetry. It must:

1. Receive the RF signal transmitted to the spacecraft from the DSIF
2. Coherently translate the frequency and phase of the received RF signal by a fixed ratio
3. Demodulate the received RF signal and send a composite command signal to the spacecraft command subsystem
4. Demodulate the range code transmitted to the spacecraft from the DSIF
5. Modulate the transmitter signal with the demodulated ranging signal
6. Modulate the transmitter with a composite telemetry signal
7. Transmit the modulated RF signal to the stations of the DSIF

The antennas consist of a high-gain fixed elliptical parabolic section antenna and a low-gain antenna that provides essentially uniform coverage in the forward hemisphere of the spacecraft.

The low-gain antenna is the primary antenna for the Earth-to-spacecraft link. Communication during the first half of the flight is maintained through this antenna using the 10-kw DSIF transmitters. The 100-kw transmitter at Goldstone is required to support the second half of the flight unless the receiver is switched to the high-gain antenna. Switchover to the high-gain antenna, and back to the low-gain antenna if desired, may be effected by ground command. If the receiver is on the high-gain antenna and the gyros are turned on, the receiver will immediately be switched to the low-gain

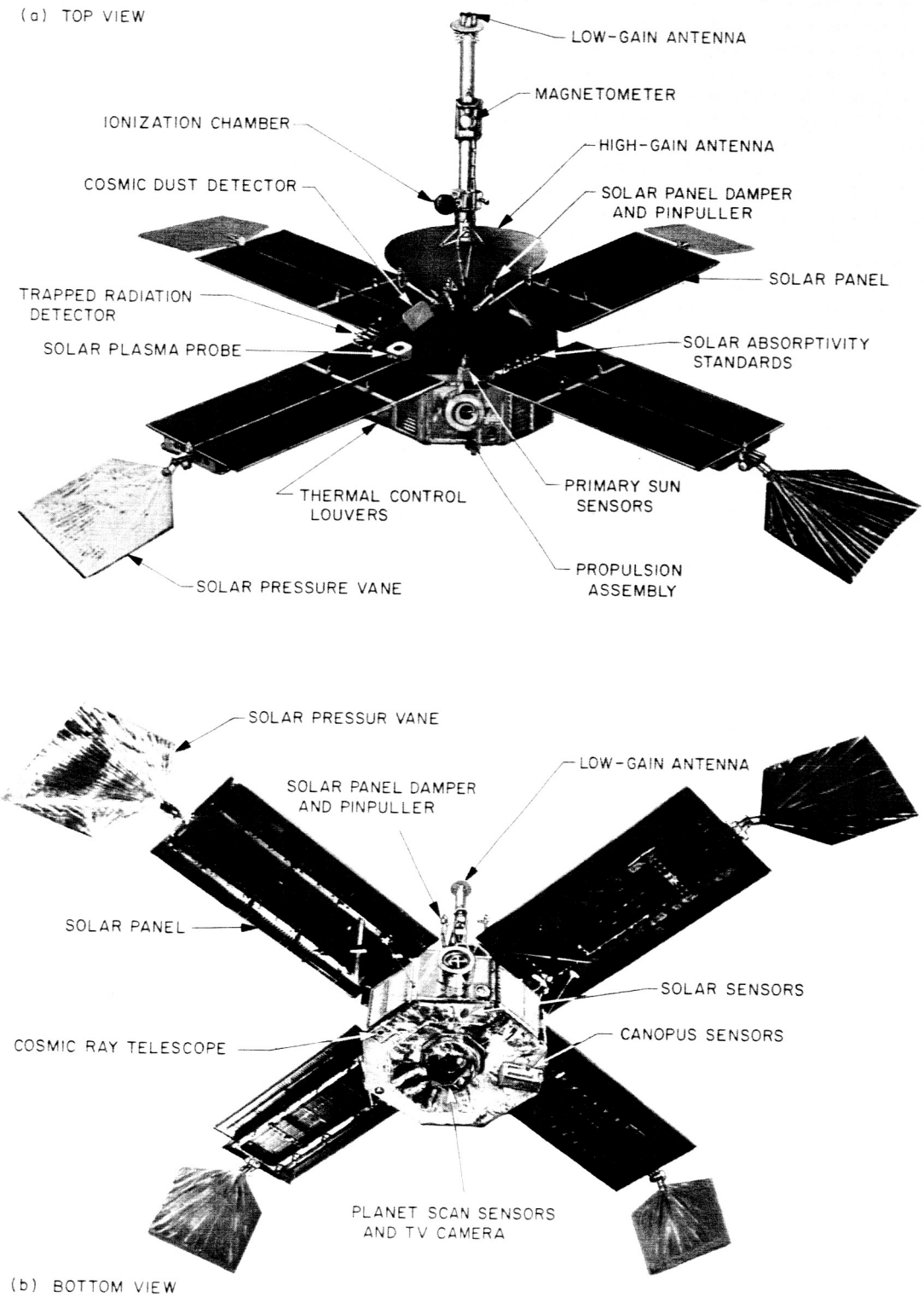


Fig. 27. *Mariner* Mars 1964 spacecraft

antenna. Onboard backup logic automatically cycles the receiver between the high- and low-gain antennas every 66⅔ hr if the receiver loses the Earth signal and does not regain it for two successive occurrences of the 66⅔-hr cyclic pulse.

The transmitting subsystem contains two redundant RF power amplifiers and two redundant RF exciters usable in any of the possible combinations. A transmitter made up of one RF power amplifier and one RF exciter operates coherently with the receiving subsystem, and the redundant equipment is, to the maximum extent possible, independent of the receiving subsystem and the operating transmitter equipment. Selection of the RF amplifiers and of the RF exciters is by onboard logic with ground command backup.

The output from the transmitting subsystem can be connected to either the high-gain antenna or the low-gain antenna. Switchover occurs on command from the CC&S with ground command backup. Transmission via the high-gain antenna is required for approximately the second half of the mission.

Spacecraft performance and scientific data, both digital and analog, are transmitted in a continuous stream of telemetry information, in the form of binary bits. The bits effect binary modulation of a subcarrier, which phase-modulates the main RF carrier. To form the stream of information (composite telemetry signal), various analog engineering data are sequentially sampled (multiplexed). The multiplexed data are converted to binary form and multiplexed with binary scientific data. There are four data modes:

1. Mode 1 is used during maneuvers. In this mode, only engineering data are sampled. Mode 1 may also be used to increase the engineering data sampling during cruise to aid in failure analysis if required.
2. Mode 2 is used during the launch phase, initial acquisition, and cruise. Blocks of engineering data 140 bits long are alternated with blocks of science data 280 bits long.
3. Mode 3 is used during the encounter phase while the TV and planetary scan subsystems are viewing the planet. In this mode, only science data are sampled.
4. Mode 4 is used to play back the stored science data from the tape machine. Following the transmission of each complete picture, approximately 2 hr of real-time Mode 1 engineering data are transmitted.

The data modes are differentiated by the specific data format in each mode without considering the bit rate. Data transmission is in digital form at bit rates of either 8⅓ or 33⅓ bps. Selection of the bit rates is by command from CC&S with ground-command backup.

The telemetry subsystem accommodates 100 commutated measurements including synchronization, framing, and subcommutation requirements. Selection of the data modes is by ground command or onboard logic, depending on the sequence of inflight events. A list of the telemetry channel assignments is given in Table 16. Figure 28 shows the functional arrangement of the data encoder commutator.

The command subsystem has a capacity for 29 direct commands and 1 quantitative command. The command bit rate is 1.0 bps. The ground-transmitted signal may be modulated by command data to control various spacecraft functions. The spacecraft receiver demodulates the composite received signal and routes the command subcarriers to the command subsystem. The command subsystem detects the command binary wave train, decodes the information content of this wave train, and

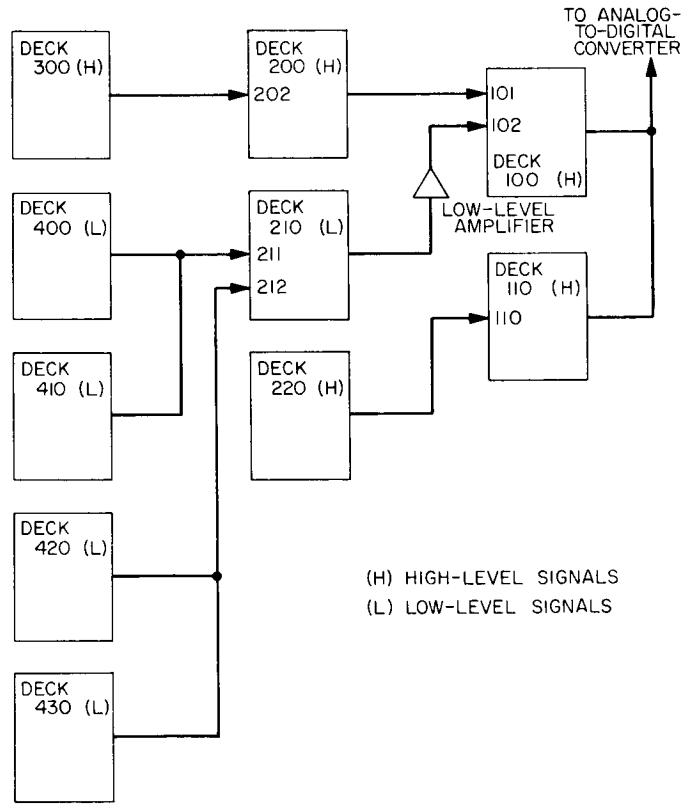


Fig. 28. Functional diagram, data encoder commutator

Table 16. Telemetry channel assignment

Channel	Measurement	Measured range		Accuracy %	Time between samples			
					Data Mode 1		Data Mode 2	
		Parameter	Voltage		33⅓ bps	8⅓ bps	33⅓ bps	8⅓ bps
100	Synchronization	"1111111"	Digital	3	4.20	16.8	12.6	50.4 (<1 min)
101	Deck 200	—	0 to 3 vdc					
102	Deck 210	—						
103	Receiver AGC (coarse)	−90 to −150 dbm						
104	Command detector monitor	$-3.4 < \Delta 2f_n < +3.4$ cps	Digital	—				
105	Pitch gyro/fine Sun sensor	±20 mrad/sec ±15 mrad	±1.5 vdc	3				
106	Yaw gyro/fine Sun sensor	±20 mrad/sec ±15 mrad						
107	Roll gyro/Earth position detector	±20 mrad/sec 0 to 0.1 ft-cd						
108	Canopus intensity	0.2 to 10 times Canopus	0 to 3 vdc					
109	PS&L output voltage	23 to 53 v						
110	Deck 220	—						
111	Receiver SPE	±600 cps	±1.5 vdc					
112	Pitch position	±20°F						
113	Yaw position	±20°F						
114	Roll position/roll search	±26 mrad						
115	Event counter No. 1 Pyrotechnic amperes Gyros on Solar panel 4A1 open Event counter No. 2 CC&S events Solar panel 4A3 open	—	Digital	—				
116	Event counter No. 3 Pyrotechnic arm Pyrotechnic amperes Solar panel 4A5 open End-of-tape loop Event counter No. 4 Command events Sun acquisition Solar panel 4A7 open Scan platform unlatched	—		—				
117	Thrust chamber pressure	0 to 300 psia	0 to +3 vdc	3				
118	Propulsion N_2 tank pressure	0 to 4000 psia						
119	Propellant tank pressure	0 to 500 psia						

Table 16. (Cont'd)

Channel	Measurement	Measured range		Accuracy %	Time between samples			
		Parameter	Voltage		Data Mode 1		Data Mode 2	
					33⅓ bps	8⅓ bps	33⅓ bps	8⅓ bps
200	Synchronization	"1111111"	Digital	—	42.0	168.0	126.0	504.0 (8⅖ min)
201	Low deck position	0 to 19	Digital	—				
202	Deck 300	—	0 to 3 vdc	3				
203	Dual booster/regulator input current	0 to 10 amp						
204	PS&L current to commutator converter	0 to 5 amp						
205	Main booster/regulator output current	0 to 5 amp						
206	Battery voltage	23 to 40 v						
207	2.4-kc inverter output voltage	40 to 60 v						
208	Attitude control X/−Y gas pressure	0 to 4000 psia						
209	Attitude control −X/Y gas pressure	0 to 4000 psia						
210	Receiver local oscillator drive	0 to 3 mw	0 to 100 mv					
211	Deck 400 and 410	—		5				
212	Deck 420 and 430	—		5				
213	High-gain antenna drive	0 to 14 w		3				
214	Low-gain antenna drive	0 to 14 w						
215	Receiver AGC (fine)	−118 to −142 dbm						
216	Battery charge current	0 to 1 amp	0 to 3 vdc					
217	Propellant temperature	25 to 150°F	500 to 600 Ω	5				
218	Attitude control X/−Y gas temperature							
219	Attitude control −X/Y gas temperature							
220	CC&S timing of events	—	Digital					
221	Maneuver booster/regulator output current	0 to 5 amp	0 to 3 vdc	3				
222	Solar panel 4A1 current							
223	Solar panel 4A5 current							
224	Solar panel 4A3 current							
225	Solar panel 4A7 current							
226	Battery current drain	0 to 10 amp						
227	2.4-kc inverter output current	0 to 2.5 amp						
228	Oxidizer pressure	0 to 500 psia						
229	Exciter power output	0 to 0.6 w						
300	Cathode/helix current	0 to 135 ma 0 to 16 ma			420.0	1680.0	1260.0	5040.0 (1 hr, 28 min)

Table 16. (Cont'd)

Channel	Measurement	Measured range		Accuracy %	Time between samples			
		Parameter	Voltage		Data Mode 1		Data Mode 2	
					33⅓ bps	8⅓ bps	33⅓ bps	8⅓ bps
301	Exciter voltage No. 1	0 to −25 vdc	±1.5 vdc	3	420.0	1680.0	1260.0	5040.0 (1 hr, 28 min)
302	Exciter voltage No. 2	0 to −15 vdc	↓	↓	↓	↓	↓	↓
303	Canopus sensor cone angle	47 to 105°	↓	↓	↓	↓	↓	↓
304	Recorder pressure	0 to 40 psia	0 to 3 v	↓	↓	↓	↓	↓
305	Solar vane position + X	15 to 55°F	↓	↓	↓	↓	↓	↓
306	Solar vane position − X	↓	↓	↓	↓	↓	↓	↓
307	Solar vane position + Y	↓	↓	↓	↓	↓	↓	↓
308	Solar vane position − Y	↓	↓	↓	↓	↓	↓	↓
309	CC&S 28-v monitor	0 to 56 v	↓	↓	↓	↓	↓	↓
400	Synchronization	"1111111"	Digital	↓	840.0	3360.0	2520.0	10,080.0 (2 hr, 48 min)
401	Bay I temperature	25 to 150°F	500 to 600 Ω	5	↓	↓	↓	↓
402	Bay III temperature	25 to 150°F	↓	↓	↓	↓	↓	↓
403	Spare	—	↓	↓	↓	↓	↓	↓
404	Bay V temperature	25 to 150°F	↓	↓	↓	↓	↓	↓
405	Bay VI temperature	25 to 150°F	↓	↓	↓	↓	↓	↓
406	Bay VII louver position indication	500 to 600 Ω	↓	↓	↓	↓	↓	↓
407	Power regulator assembly temperature	25 to 175°F	↓	↓	↓	↓	↓	↓
408	Propulsion N_2 tank temperature	25 to 150°F	↓	↓	↓	↓	↓	↓
409	Solar panel 4A1 front temperature	−40 to +160°F	↓	↓	↓	↓	↓	↓
410	Canopus sensor temperature	−50 to +150°F	↓	↓	↓	↓	↓	↓
411	Scan actuator temperature	25 to 200°F	↓	↓	↓	↓	↓	↓
412	Absorptivity standard temperature No. 1	0 to 140°F	↓	↓	↓	↓	↓	↓
413	Absorptivity standard temperature No. 2	130 to 275°F	↓	↓	↓	↓	↓	↓
414	Science cover and science cover identification	500 to 600 Ω	↓	↓	↓	↓	↓	↓
415	Standard cell current	0 to 100 ma	0 to 100 mv	↓	↓	↓	↓	↓
416	Radiation resistant cell current	0 to 100 ma	↓	↓	↓	↓	↓	↓
417	Standard cell voltage	0 to 1 v	↓	↓	↓	↓	↓	↓
418	TV temperature	−60 to 150°F	500 to 600 Ω	↓	↓	↓	↓	↓
419	Ionization Chamber temperature	−20 to 200°F	↓	↓	↓	↓	↓	↓
420	Temperature reference	—	↓	↓	↓	↓	↓	↓
421	Bay II temperature	25 to 150°F	↓	↓	↓	↓	↓	↓

Table 16. (Cont'd)

Channel	Measurement	Measured range		Accuracy %	Time between samples			
					Data Mode 1		Data Mode 2	
		Parameter	Voltage		33⅓ bps	8⅓ bps	33⅓ bps	8⅓ bps
422	Bay III louver position indication	500 to 600 Ω	500 to 600 Ω	5	840.0	3360.0	2520.0	10,080.0 (2 hr, 48 min)
423	Bay IV temperature	25 to 150°F						
424	Crystal oscillator temperature	25 to 150°F						
425	Bay I louver position indication	500 to 600 Ω						
426	Bay VII temperature	25 to 150°F						
427	Spare	—						
428	Battery temperature	25 to 150°F						
429	Solar panel 4A5 front temperature	−40 to 160°F						
430	Lower ring temperature above Canopus sensor	25 to 150°F						
431	Upper ring temperature under Sun sensor	25 to 150°F						
432	Absorptivity standard temperature No. 3	130 to 275°F						
433	Absorptivity standard temperature No. 4	75 to 275°F						
434	Upper thermal shield temperature	70 to 300°F						
435	Lower thermal shield temperature	−300 to 0°F						
436	Recorder temperature	25 to 150°F						
437	Scan platform inertial thermal subsystem temperature	−50 to 150°F						
438	Trapped Radiation Detector temperature	25 to 150°F						
439	Magnetometer temperature	−75 to 150°F						

issues the necessary command signals to the appropriate spacecraft subsystems. A description of the DC and QC commands available is given in Table 17.

The video-storage subsystem has a 5.24×10^6-bit storage capacity. It receives data at a bit rate of 10,700 bps from the DAS, and reads out synchronously with the telemetry subsystem at a bit rate of 8⅓ bps. The video storage subsystem stores on magnetic tape the bit information produced by the television scan, and plays back the information through the telemetry subsystem several days after planetary encounter.

The ranging subsystem is capable of measuring the Earth–spacecraft range unambiguously to a distance of 10^6 km. The ground-transmitted signal may be modulated by a long binary wave train known as the range code. This range code is retransmitted as modulation on the spacecraft signal. The range code is received at the ground station, and shifted in time relative to the original signal by the round-trip radio propagation time. Ground measurement of this time shift provides a measurement of spacecraft range.

The frequency of the signal received by the spacecraft is less than the ground-transmitted frequency due to the doppler effect, since the spacecraft is receding from the ground antenna. Similarly, the ground-received signal is lower in frequency than the spacecraft-transmitted signal. Ground measurement of this two-way doppler shift provides a measurement of spacecraft radial velocity.

Table 17. Description of ground commands

Command	Description
DC-1	Transfers the data encoder to Data Mode 1 operation (all engineering words) as soon as the transfer is acceptable to the data encoder transfer logic.
DC-2	Transfers the data encoder to Data Mode 2 operation (20 engineering words, 40 science words) as soon as the transfer is acceptable to the data encoder transfer logic. Applies 2.4-kc power to the cruise science instruments.
DC-3	Transfers the data encoder to Data Mode 3 operation (all science words) as soon as the transfer is acceptable to the data encoder transfer logic.
DC-4	Transfers the data encoder to Data Mode 4/1 operation (TV picture data or engineering data) as soon as the transfer is acceptable to the data encoder transfer logic. If TV picture data are available from the tape recorder, TV data are telemetered; if no TV data are present, as between TV pictures, then engineering data are telemetered. Removes 2.4-kc power from the cruise science instruments.
DC-5	Transfers the data encoder from one of its two bit rates (8⅓ and 33⅓ bps) to the other. Causes a change from either one of these bit rates to the other.
DC-6	Transfers the data encoder from one of its two ADC pseudonoise generators to the other (A and B). Causes a change from either one of these to the other.
DC-7	Changes radio power amplifiers. The radio subsystem has an A (TWT) and a B (cavity) power amplifier.
DC-8	Changes radio exciters. The radio subsystem has an A and a B exciter.
DC-9	Turns the spacecraft radio ranging receiver on or off.
DC-10	Causes the radio subsystem circulator switches to be conditioned so that the spacecraft transmits via the high-gain antenna and receives via the low-gain antenna.
DC-11	Causes the radio subsystem circulator switches to be conditioned so that the spacecraft transmits and receives via the high-gain antenna.
DC-12	Causes the radio subsystem circulator switches to be conditioned so that the spacecraft transmits and receives via the low-gain antenna.
DC-13	Removes the attitude control excitation power from the CC&S control lines so that the attitude control functions that are controlled by the CC&S are disabled. Also prevents the pyrotechnic control circuitry from firing the motor start and stop squibs.
DC-14	Reverses the state of all the relays acted upon by a DC-13 command; therefore, it resets the DC-13 command and reverts the attitude control and pyrotechnic subsystems back to CC&S control.
DC-15	Causes the Canopus sensor roll error signal to be applied to the roll gas-jet electronics at all times, regardless of whether or not the roll acquisition logic is satisfied. Also prevents the roll search signal from being applied to the roll channel and roll acquisition logic violations from turning on the gyros.
DC-16	Initiates a narrow angle acquisition signal and thereby conditions the DAS logic to begin the TV picture-taking sequence and to transfer the data encoder to Data Mode 3.
DC-17	Causes a step change in the Canopus sensor cone angle by changing the voltage on the deflection plates of the Canopus sensor's image dissector.
DC-18	Turns on the gyros (in the inertial mode) and the Canopus sensor Sun shutter, and turns off the Canopus sensor. Also turns on the turn command generator and conditions the attitude control circuitry for commanded roll turns. Succeeding commands cause +2.25-deg roll turns.
DC-19	Serves as the reset for DC-15, DC-18 and DC-20 commands.
DC-20	Turns off the Canopus sensor, turns on the Canopus sensor Sun shutter, and inhibits the roll acquisition logic from turning on the gyros.
DC-21	Simulates a Canopus-acquisition logic violation, turns on the gyros, and applies a negative roll search signal to the roll gas-jet electronics, thereby causing the spacecraft to roll and search in the negative direction to acquire a new target. Also causes the spacecraft to roll and turn −2.25 deg, if preceded by a DC-18 command.
DC-22	Changes video storage tape tracks by applying power to a record head and by gating the output of the playback amplifiers.
DC-23	Sets relays in the pyrotechnic subsystem so that the CC&S commands M-6 and M-7 are routed to the squibs allotted to the second motor burn.
DC-24	Removes 400-cps single-phase power from the scan platform drive motor.
DC-25	Causes 2.4-kc power to be applied to encounter science loads and the video storage subsystem, and to the cruise science loads if 2.4-kc power to cruise science is off. At the same time, it applies 52 vdc from the booster regulator to the 400-cps single-phase inverter, which in turn supplies power to the scan-subsystem drive motor and the video storage subsystem record motor. It also enables the battery charger boost mode and causes the pyrotechnic subsystem to energize the solenoid that releases the scan platform cover.

Table 17. (Cont'd)

Command	Description		Command	Description
DC-26	Removes 2.4-kc power from all of the science loads (video storage 2.4-kc power remains on) and removes 52-vdc power from the 400-cps single-phase inverter. It also enables the battery charger boost mode.		QC1-1	Sets the pitch turn polarity and preloads the CC&S pitch shift register so that, at a counting rate of 1 pps, the register will fill in the required time interval for the attitude control subsystem to pitch turn the spacecraft the amount required for a given midcourse maneuver.
DC-27	Starts the maneuver sequence by issuing CC&S command M-1 (turn on the gyros), by applying power to the CC&S maneuver clock, and by removing the maneuver clamp and a flip-flop reset signal from the CC&S maneuver circuitry.		QC1-2	Sets the roll turn polarity and preloads the CC&S roll shift register so that, at a counting rate of 1 pps, the register will fill in the required time interval for the attitude control subsystem to roll turn the spacecraft the amount required for a given midcourse maneuver.
DC-28	Removes 2.4-kc power from the video storage subsystem and enables the charge mode of the battery charger.		QC1-3	Preloads the CC&S velocity shift register so that, at a counting rate of 20 pps, the register will fill in the time interval necessary for the midcourse motor to burn in order that the spacecraft can obtain the required velocity change for a given midcourse maneuver.
DC-29	Sets relays in the pyrotechnic subsystem so that the CC&S commands M-6 and M-7 are routed to the squibs allotted to the first motor burn.			

3. Attitude Control

The attitude control subsystem functions in three distinct but related modes:

1. *Acquisition and cruise mode.* In this mode, the attitude control subsystem is capable of acquiring and maintaining three-axis stabilization (using the Sun and Canopus as reference objects) to a nominal accuracy of ± 0.5 deg with respect to each axis. Reacquisition, in the event of loss of acquisition for any noncatastrophic reason, is automatic.
2. *Maneuver mode.* In this mode, the attitude control subsystem, in response to commands from the CC&S, is capable of pointing the propulsion-subsystem thrust axis to any desired new orientation with a 1 σ accuracy of ± 0.5 deg from the nominal reference attitude and with a drift rate of less than 0.5 deg/hr. This stability is maintained during motor burn by use of an autopilot jet-vane actuation system.
3. *Inertial roll mode.* In this mode, similar to the acquisition and cruise mode with respect to the pitch and yaw axes, the attitude control subsystem accepts an inertial position error signal in the roll channel, rather than in the Canopus sensor position error. In this mode, also, roll turn increment commands may be accomplished by ground command.

4. Central Computer and Sequencer

The CC&S provides the following timing, sequencing, and control of the spacecraft subsystems:

1. A 38.4-kc basic timing waveform for the power subsystem
2. A timing pulse every 66⅔ hr for the radio subsystem
3. Initiation of timed events and sequences during flight for various subsystems

5. Propulsion

The propulsion subsystem has a nominal vacuum thrust capability of 50 lb. The tankage is sized for a maximum velocity increment of 80 m/sec to a 600-lb spacecraft. Velocity increments as small as 0.2 m/sec (to a 600-lb spacecraft) are possible.

The propulsion subsystem is capable of two starts. The ignition and thrust termination signals are generated by the pyrotechnic subsystem upon command from the CC&S. Jet vanes capable of deflecting the midcourse motor jet stream provide thrust vector control through ± 5 deg.

6. Pyrotechnics

The spacecraft design employs a number of squib-actuated devices such as solar panel latches, scan platform latches, propulsion system valves, and a solenoid-actuated instrument cover. The pyrotechnic subsystem accepts commands from the appropriate sources and provides the energy necessary to fire the proper squibs and to activate the solenoid. The subsystem is armed at spacecraft separation so that an inadvertent or spurious command prior to that time cannot cause a premature squib firing.

7. Temperature Control

The four major variables affecting temperature of spacecraft components are incident solar radiation, electrical power expenditure, thermal transfer between components, and thermal radiation from the spacecraft into space. The temperature control subsystem is comprised of all devices and treatments employed to maintain temperatures within specified bounds.

The principal active temperature control devices are six variable-emittance louver assemblies mounted on six of the electronic assemblies. Passive devices include removable multilayer blankets shielding the top and bottom of the spacecraft octagon, polished aluminum shields on electronic assemblies, and numerous other shields covering spacecraft exterior surfaces. Surface treatments having particular thermal properties are also used extensively on spacecraft components.

8. Structure

The spacecraft primary structure is the octagonal electronic compartment. Seven compartment bays support electronic assemblies and the eighth bay supports the postinjection propulsion system.

Principal structures attaching to the primary structures are:

1. Six electronic assembly chassis, each containing a number of modular electronic subchassis. One assembly attaches to each of six bays.
2. The electronic assembly chassis containing the spacecraft battery and a portion of the power subsystem electronics.
3. The postinjection propulsion system motor support.
4. Four solar panels supporting solar cells furnishing spacecraft power.
5. The high-gain antenna support.
6. The low-gain antenna support.
7. The ring harness trough.
8. The scanning platform supporting planet-oriented science.
9. Supports for scientific instruments and engineering devices.
10. The spacecraft adapter, the transitional structure placed between the *Agena* stage and the spacecraft primary octagonal structure.

9. Science

The science payload consists of equipment implementing each of seven science experiments, and additional equipment to control and support the science equipment.

a. Science experiment equipment. The television equipment provides for topographic reconnaissance of part of the surface of Mars. It is comprised of a Cassegrain telescope, vidicon tube, and associated electronics.

The Helium Magnetometer equipment is designed to measure magnetic field strength in three orthogonal axes. It consists of a sensor containing a plasma of helium atoms, and associated electronics that contain servo amplifiers driving coils surrounding the plasma.

The Ionization Chamber and particle flux detector detect and measure the omnidirectional flux of corpuscular radiation in space and in the vicinity of Mars. Ionization produced by this flux is also measured. Equipment components are: an ionization chamber containing argon gas, a Geiger–Müller counter, and associated electronics.

The Cosmic Dust Detector makes direct measurements of dust particle momentum and mass distribution, particularly in regions encountered having unusually high numbers of such particles. Penetration detectors, acoustic detectors, and associated electronics comprise the cosmic dust equipment.

A Cosmic Ray Telescope, consisting of three gold silicon solid-state detectors and an electronic logic section, measures certain charged particles approaching the instrument within a conical acceptance zone.

Such magnetically trapped particles as exist in the vicinity of Mars are measured for distribution, energy and identity by the Trapped Radiation Detector, which consists of three Geiger–Müller detectors, a silicon surface-barrier detector, and electronic discriminators and amplifiers.

The Solar Plasma Probe (by means of a collector cup, high-voltage power supply, and output circuitry) measures the density, velocities, temperatures, and direction of movement of low-energy protons streaming outward from the Sun.

b. Control and support equipment. The science data automation subsystem accepts data presented in diverse formats and rates from the experimental equipment and converts the data to a form suitable for transmission from the spacecraft to Earth, controlling, sequencing, sampling, buffering, and encoding as necessary in the performance of its task. The output of the television equipment is converted to a form suitable for the video storage subsystem magnetic tape recorder.

A planetary scan platform is provided for the television camera. It has the ability to find and hold the correct camera attitude as the spacecraft passes by the planet. The scan platform first scans back and forth about the spacecraft roll axis and, when Mars enters the scan optical sensor field of view, ceases scan and tracks Mars in the same lateral direction.

A narrow angle Mars gate detects the sufficient advance of Mars, relative to the spacecraft, inhibiting further tracking by the scan platform. Thus, locked in position, the television equipment begins the sequence of pictures to be stored and then transmitted back to Earth.

B. Spacecraft Mechanical Configuration

The primary objective of the spacecraft configuration was to minimize nonelectronic weight within a total spacecraft weight of 570 lb. This was accomplished by (1) structurally integrating the electronic packaging design into the basic spacecraft structure, (2) minimizing the number of articulated or deployed elements, and (3) attaching the spacecraft to the *Agena* in a direct manner. Layouts of various sizes and shapes were made of the spacecraft main electronic compartments. These schemes ranged from cylindrical shapes, with subchassis attached directly to the exterior of the cylinder, to more complex shapes, with the subchassis clustered in electronic assemblies, which were mounted as units to the primary structure. During preliminary design, a wide range of configurations was considered that culminated in three basically different shapes: cruciform, square, and octagon. The octagon was chosen primarily because it represented a minimum departure from existing JPL technology yet ensured minimum mechanical weight.

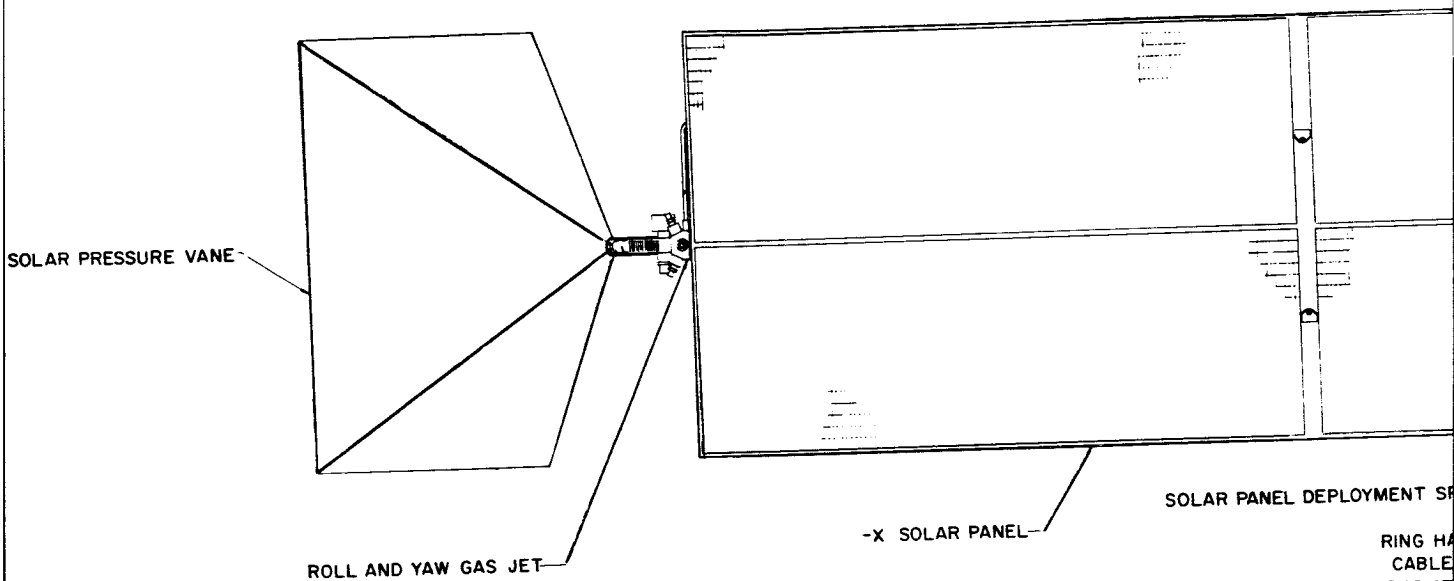
Once the octagon was chosen, it was decided to investigate further whether the electronic subchassis should be stacked vertically, as in *Ranger* and *Mariner* Venus, or in two horizontal rows, with case interconnections along the horizontal center line of each case. Differences between the advantages and disadvantages of these two approaches were small and, in some cases, debatable. The vertical module arrangement was chosen because it presented a simpler structural interface (ease of assembly and maintenance of alignment) and appeared easier to cable. This choice was in keeping with the philosophy of making a minimum change from *Mariner* Venus or from existing JPL technology. The final flight spacecraft mechanical configuration is shown in Fig. 29.

1. The Octagon

The spacecraft primary electronic compartment consists of an octagonal structure approximately 18 in. high and 54.5 in. across the points. Seven bays contain spacecraft electronics. Six of these bays are standard chassis containing standard 6 × 6-in. subchassis as well as some special subchassis. The seventh bay houses the battery on its inboard mounting plane and the power regulator assembly on the outboard mounting surface. Each electronic assembly is secured to the basic structure by screws on the inboard and outboard mounting surfaces as well as through both the top and bottom rings. In this way, the electronic packaging structure carries part of the basic structure loads. The eighth bay of the octagon structure contains the midcourse propulsion system.

2. Propulsion System

The propulsion system is mounted in a bay between solar panels to minimize exhaust impingement on the panels during motor firing. This unit is attached to the inboard plane of the bay, with the thrust axis approximately normal to the spacecraft roll axis (Z axis). The propulsion system mounting/adapting structure was machined after the spacecraft CG was determined so that the thrust axis would be pointed through the CG with a minimum error.



NOTE: UPPER AND PROPULSION SYSTEM THERMAL SHIELDS, HIGH-GAIN ANTENNA AND SUPPORT TRUSS, COAXIAL CABLE, +Y AND -Y SOLAR PRESSURE VANES AND ACTUATORS REMOVED FOR CLARITY

CW CLOCKWISE
CCW COUNTERCLOCKWISE
ACQ ACQUISITION

-X SOLAR

EARTH DE
SQUARE-ROOT S
SENSOR (PRIMA

SOLAR PANEL DEPLOYMENT SP

RING HA
CABLE
TRAPPED RADIAT

+Y

CASE HARNESS SUPPOR

RF

EARTH DETECTOR

SQUARE-ROOT SUN SENSOR (PI

LOW-GAIN ANTENNA

ION CHAMBE

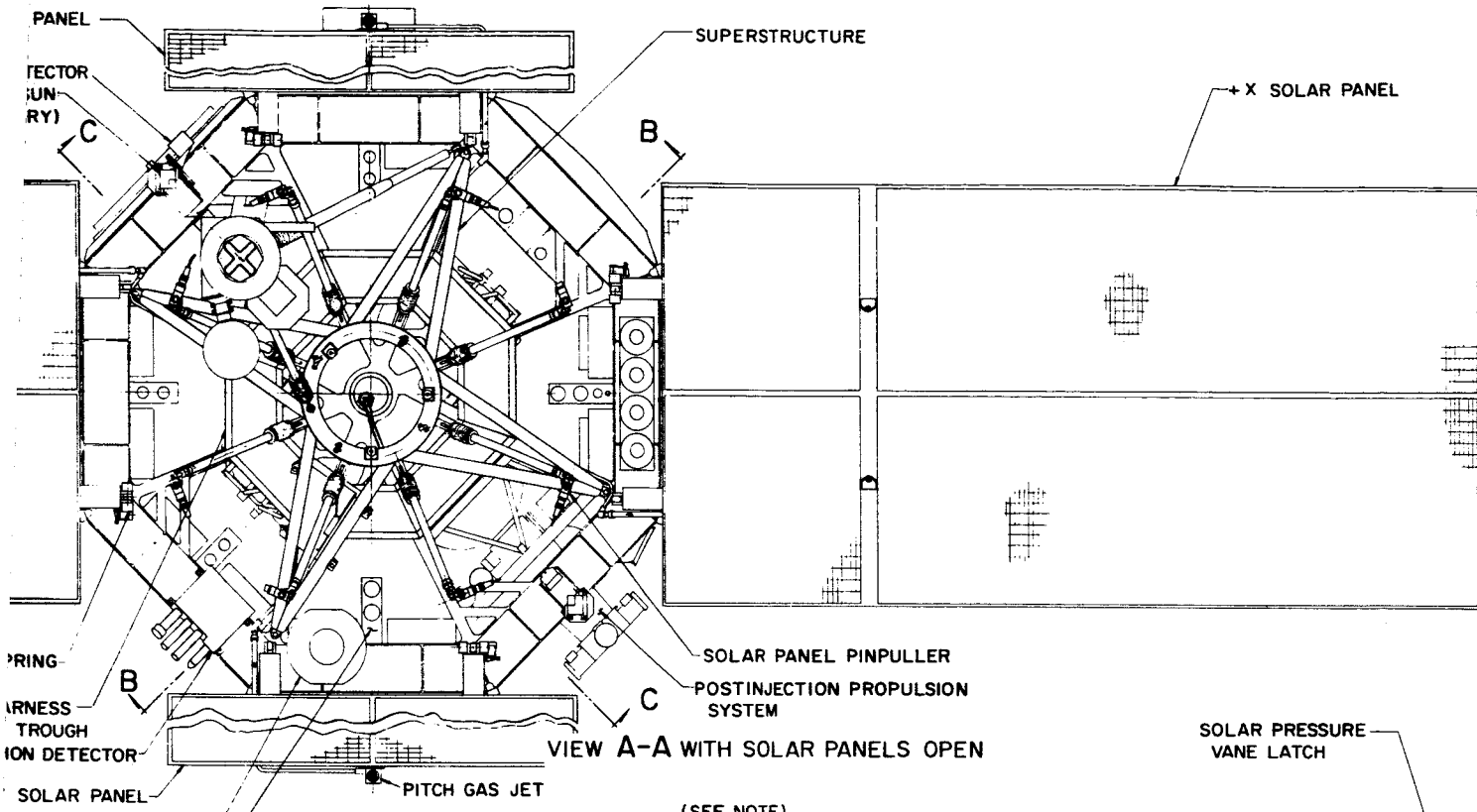
BA

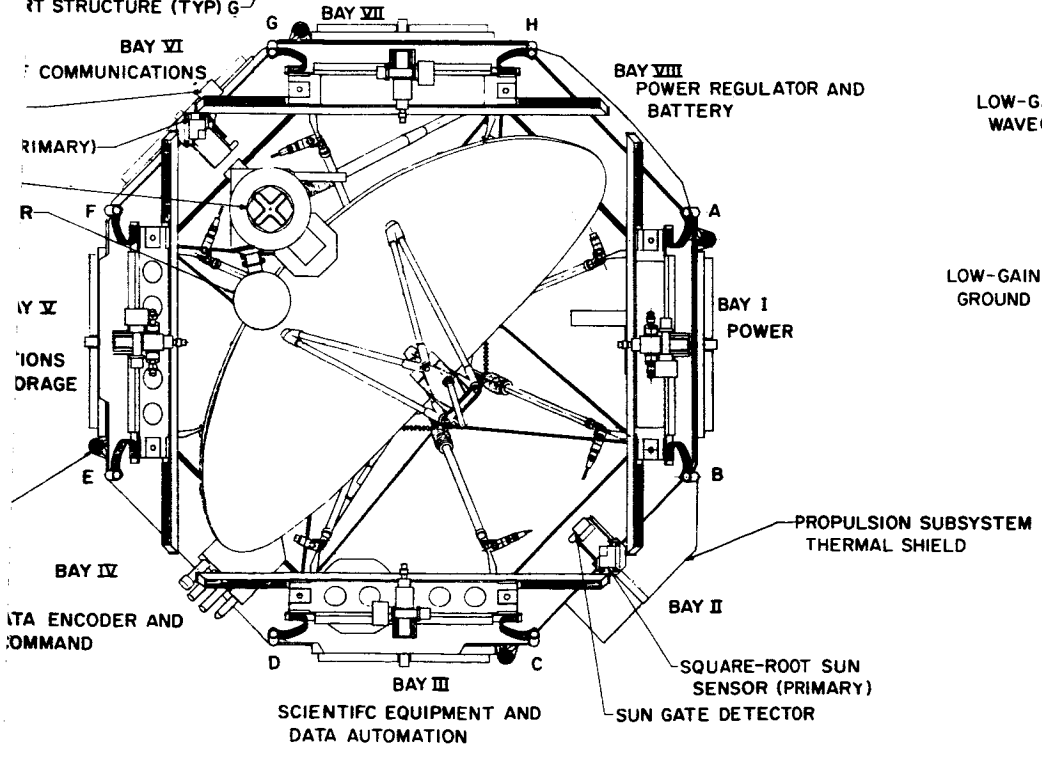
RF COMMUNICAT
AND VIDEO ST

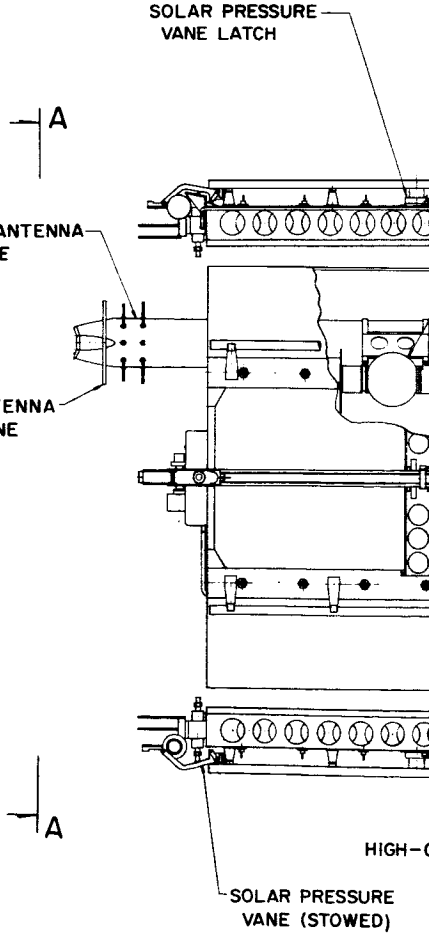
SOLAR PANEL OPEN
DAMPER (CRUISE)

DA
C

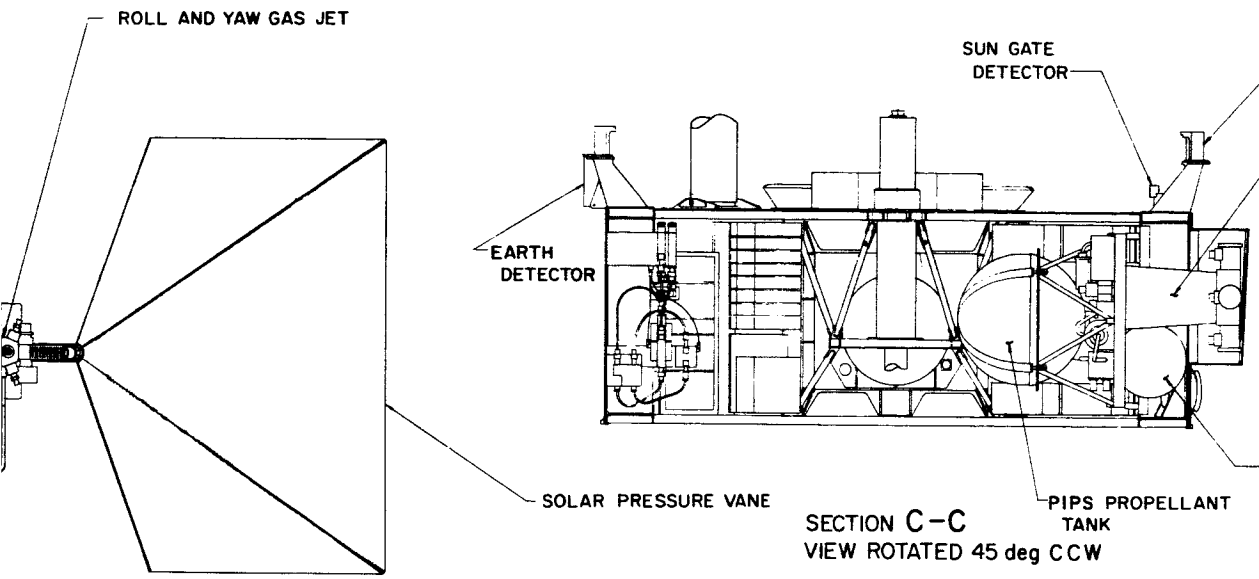
79-1


PANEL
SUPERSTRUCTURE
+X SOLAR PANEL
C
B
B
C
SOLAR PANEL PINPULLER
POSTINJECTION PROPULSION SYSTEM
PITCH GAS JET
SOLAR PANEL
PLASMA PROBE
ATTITUDE CONTROL AND C C & S
VIEW A-A WITH SOLAR PANELS OPEN
(SEE NOTE)

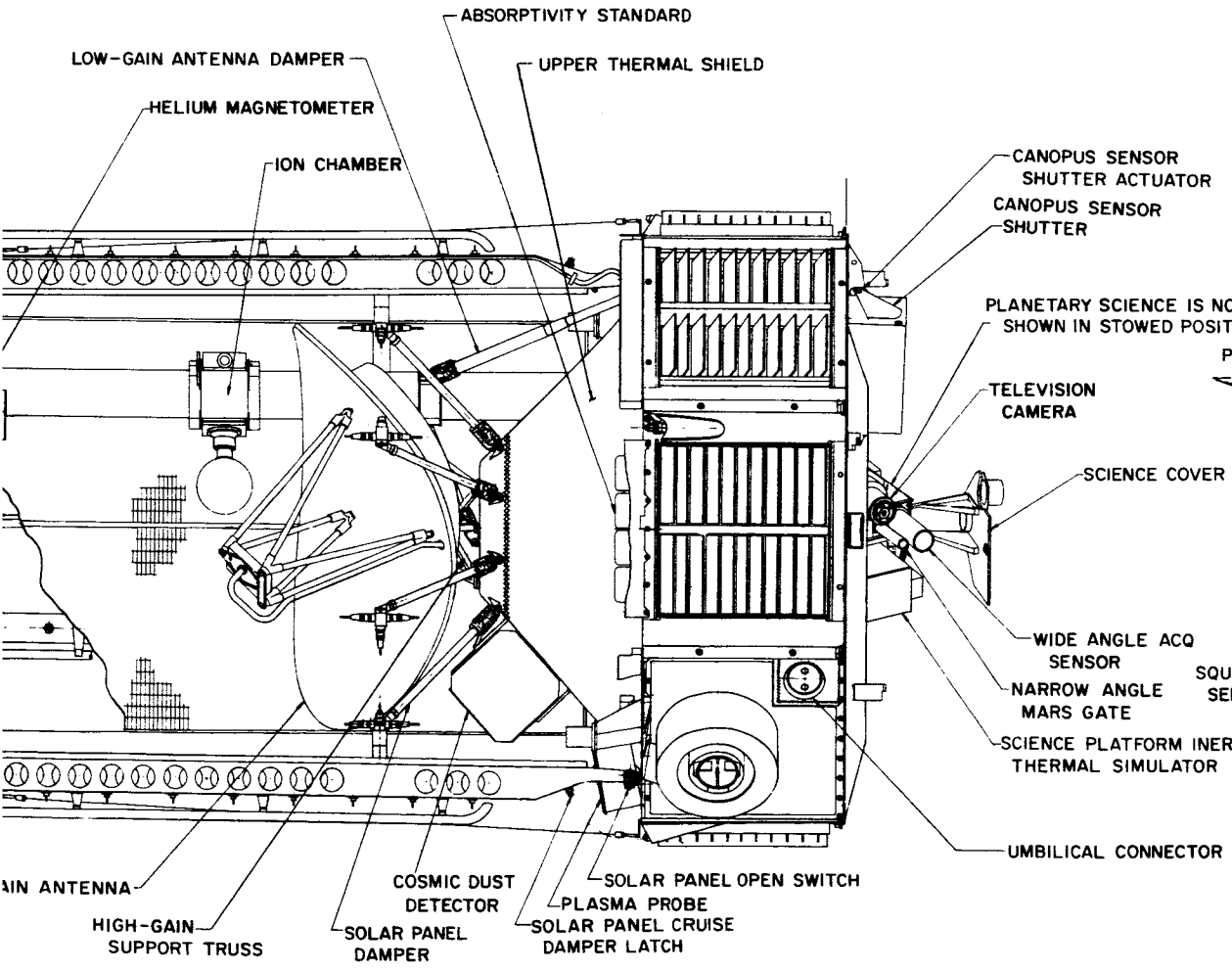

BAY VII
G
H
BAY VI
COMMUNICATIONS
BAY VIII
POWER REGULATOR AND BATTERY
F
A
BAY I
POWER
E
B
BAY IV
BAY II
D
C
BAY III
SCIENTIFC EQUIPMENT AND DATA AUTOMATION
PROPULSION SUBSYSTEM THERMAL SHIELD
SQUARE-ROOT SUN SENSOR (PRIMARY)
SUN GATE DETECTOR


SOLAR PRESSURE VANE LATCH
A
LOW-GAIN ANTENNA WAVEGUIDE
LOW-GAIN ANTENNA GROUND PLANE
A
SOLAR PRESSURE VANE (STOWED)

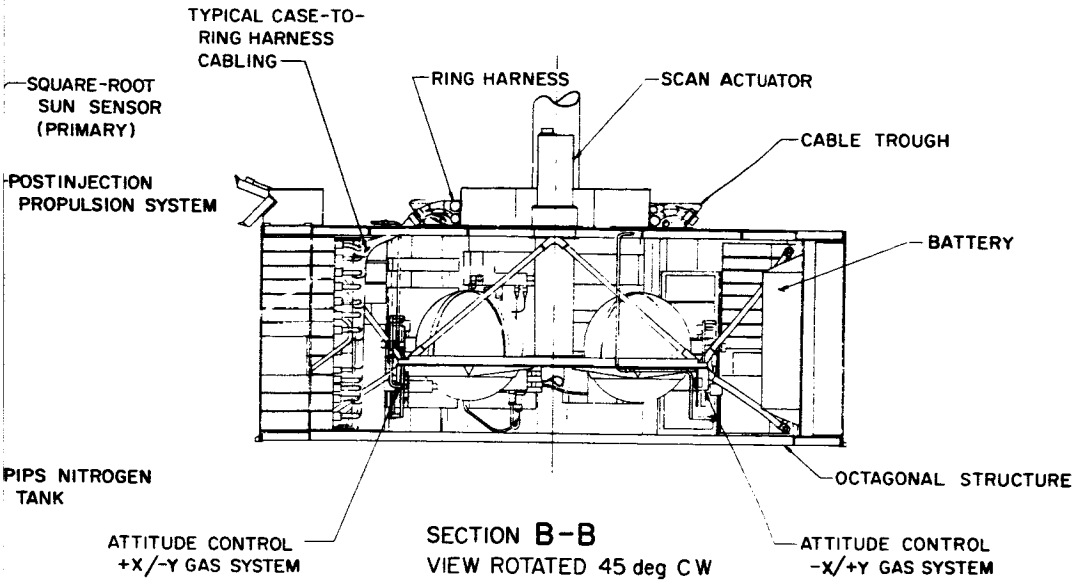
79-2



SECTION C-C
VIEW ROTATED 45 deg CCW



80-1



SECTION B-B
VIEW ROTATED 45 deg CW

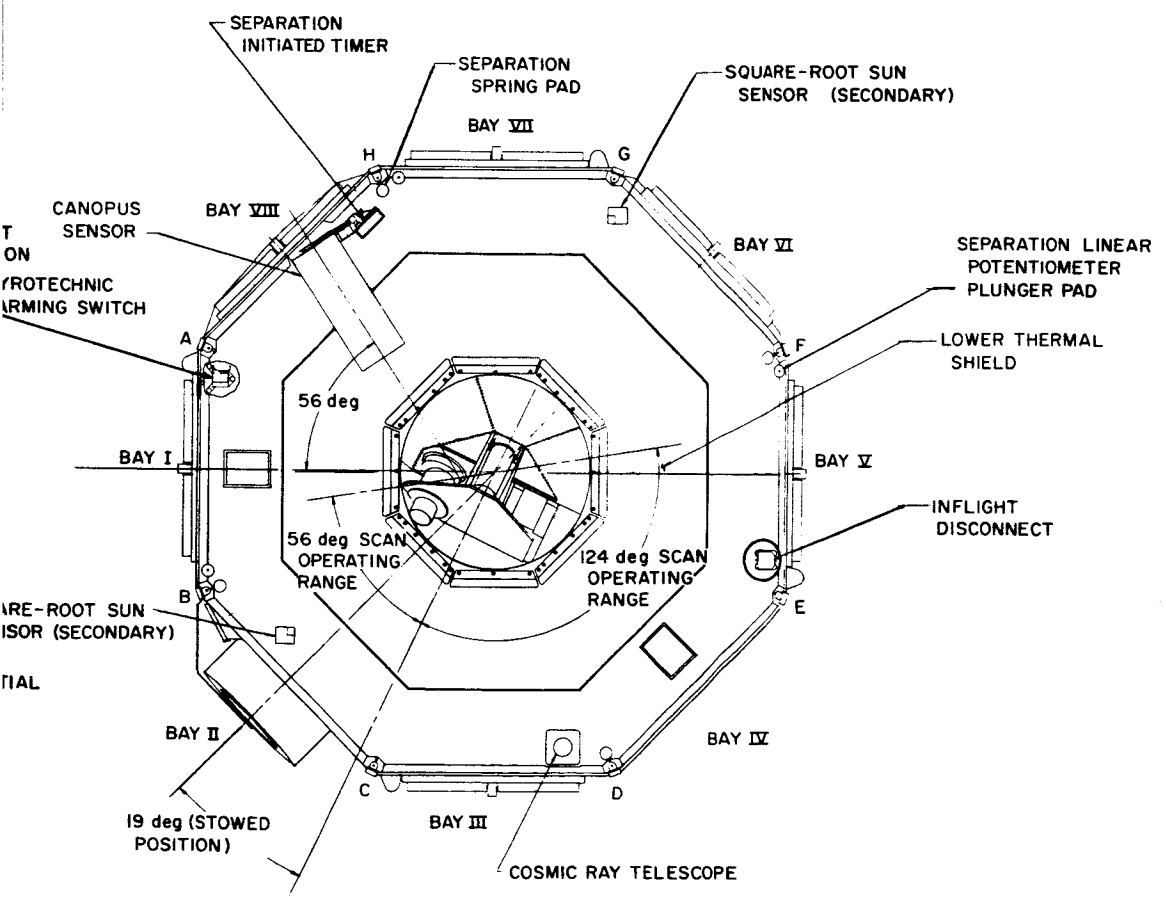


Fig. 29. Flight spacecraft mechanical configuration

80-2

3. Attitude Control Gas System

The attitude control gas system is located on a secondary structure internal to the octagon. Since the gas system dissipates very little electrical power and requires relatively close control of temperature, enclosing it in the temperature-controlled volume slaves its temperature to that of the octagon.

The attitude control gas system consists of two half systems, either of which is sufficient for controlling the spacecraft should the other fail. Each half system is mechanically interchangeable with the other. A half system consists of a spherical storage pressure vessel 9 in. in diameter and containing 2.50 lb of nitrogen. The storage vessel is mounted on an equipment plate that also holds the regulator, plumbing, and other gas-system equipment. From the equipment plate, low-pressure plumbing is routed through the spacecraft internal structure to an X-axis and a Y-axis solar panel. The plumbing is then routed through a length of flexible tubing across the solar panel hinge line, along a solar panel spar, to a manifold and jets at the center of each solar panel tip. Each X-axis manifold has four jets to give positive and negative yaw and roll control, and each Y-axis manifold has two jets for pitch control. The roll jets are canted at a 21-deg angle to the plane of the panel end beam to minimize jet exhaust impingement on the beam surface. The gas jets are located at the solar panel tips to maximize the reaction force moment.

4. Solar Pressure Vane System

The solar pressure vane auxiliary attitude control subsystem is also located at the tip of the solar panels. Each assembly is attached to a gas-jet manifold. During the boost portion of flight, the vane was folded, stowed, and latched along the back of the solar panel. After spacecraft separation and after the solar panels were unlatched, the vane latch was released by a lanyard attached to the top of the octagon. Springs then erected the vane to a 35-deg angle to the plane of the panel and deployed the vane to provide 7 ft^2 of reflecting surface. The inboard vane edge is tapered away from the end of the panel to avoid impingement due to gas-jet exhaust. Once erected and deployed, the vanes are driven by an actuator linked electrically to the gas-jet system. A bimetallic strip in series with the electrical actuator senses a thermal input from sunlight to provide damping to the spacecraft motion through the vanes.

5. Solar Panels

The primary source of spacecraft power is derived from photovoltaic cells mounted on panels that are normal to the Sun's rays during the cruise portion of flight. Due to spacecraft power requirements, a solar panel area of 70 ft^2 was required. This area was provided by four rectangular panels. A rectangular shape was chosen because it could be used efficiently for mounting rectangular-shaped solar cells. The four panels were attached to the top of the octagon at Bays I, III, V, and VII. Each panel was 71.4 × 35.5 in. and was mechanically and electrically interchangeable with any other panel. Each panel was attached to the octagon at two points through a clevis, close tolerance bolt, monoball joint. During boost, the panels were folded to a near-vertical position above the spacecraft to comply with shroud clearance requirements. The panel tips were inclined inboard 0.6 in. beyond the vertical to allow adequate shroud clearance during both boost and shroud jettison.

During flight, at a fixed time after separation of the spacecraft from the *Agena*, the panels were separated from their damper supports by means of pyrotechnically actuated pinpullers located at the interface of the damper and the solar panel bracket. The panels were then deployed approximately 90 deg to a plane normal to the Sun's rays after Sun stabilization. Panel deployment was accomplished by torsion-spring actuators located at the hinge point on one spar on each panel. Upon reaching the deployed position, the panels engaged a latch between the cruise damper located on the front of the panel bay and the base of the panel spar. The cruise damper functioned as a positive latch to locate the panel and absorb its deployment energy and to isolate panel vibrations from the guidance autopilot during firing of the midcourse propulsion subsystem.

6. Attitude Reference Sensors

Once the solar panels were fully deployed, an essentially unrestricted field of view was provided for the Sun sensors located atop pedestals on Bays II and VI. These sensors provided error signals to the attitude control subsystem, thereby permitting the spacecraft to find and lock onto the Sun. The primary Sun sensors are mounted on pedestals to provide minimum interference with their fields of view from the high-gain antenna, the solar panel dampers, the pinpullers and cabling, the solar panels, and the brackets. Since the Sun sensors are most sensitive in their zenith direction, the panel

dampers, pinpullers, and wiring, located above the sensors, are kept toward the spacecraft center line and beyond the sensor view. However, the solar panel support brackets protrude slightly into their view after panel deployment.

The remainder of the Sun sensor subsystem consists of secondary sensors on the bottom of the spacecraft and a Sun gate mounted on the Bay II pedestal. The secondary Sun sensors are located to provide a hemispherical view on the aft end of the spacecraft, and, in conjunction with the primaries, allow 4 π sterad coverage. The Sun gate is a narrow angle ($\pm$3 deg half-angle cone) Sun sensor that informs the attitude control logic when the Sun is within its field of view (acquired), and automatically initiates a reacquisition sequence should the Sun pass from its view. The Sun gate is mounted near the Bay II Sun sensor for ease of alignment and to minimize cable complexity.

The remainder of the attitude reference subsystem consists of a Canopus star sensor mounted at the base of Bay VIII and an Earth detector mounted on the side of the Bay VI Sun sensor pedestal. The star sensor identifies the star Canopus and uses it as a spacecraft roll reference. The Earth detector is used to confirm that the star sensor has found Canopus. Early in flight, when the sensor is locked on Canopus, the Earth detector senses light from Earth. The Canopus sensor is located at the bottom of the spacecraft to minimize Sun illumination on it. It is mounted under Bay VIII to provide an optimum field of view between the panels near the attitude control electronic assembly on Case VII.

7. Antennas

The radio-antenna subsystem is comprised of a low-gain antenna and a high-gain antenna. The low-gain antenna is a 4-in. diameter, thin-wall aluminum tube mounted on top of the spacecraft and aligned parallel to the roll axis. The tube performs both as a waveguide and an antenna support structure. The top of the tube is crimped in a cruciform shape and holds a 7-in. diameter ground plane to control the antenna pattern The antenna radiates directly from the cruciform aperture. The tube is attached at its base to the top of the octagon and supported at approximately ¼ its length by two damped struts positioned approximately 90 deg to one another. One damper runs from the antenna to a corner of the octagon; the other runs from the antenna to the top ring on the superstructure. The dampers used here are similar to those used for solar panel support and were used for the same reasons; that is, to reduce dynamic loading and to, thereby, minimize weight. The low-gain antenna was designed to be 88 in. long, so that in the boost configuration it would be 1 ft above the tips of the stowed solar panels and thereby present an acceptable antenna pattern. It is located as near the spacecraft roll axis as practical to enhance roll symmetry for the antenna pattern.

The high-gain antenna is a parabolically contoured dish elliptical in plan form with a 46-in. major diameter and a 21-in. minor diameter. The dish is attached through a support truss to the spacecraft superstructure at three points. The support truss holds the antenna at a fixed 38-deg angle to the spacecraft roll axis. The superstructure mounting-hole pattern fixes the antenna at a 259-deg angle, measured in the spacecraft X–Y plane, from the optical axis of the Canopus sensor. In this way, the antenna is fixed to point at Earth when the spacecraft arrives at Mars. The elliptical antenna configuration shapes the beam to provide communications significantly before and after the Earth passes over the point of maximum antenna gain. The high-gain antenna support configuration nests the dish among the panels, dampers, and other components to allow adequate clearance with a minimum of structural weight.

8. Science

The spacecraft science subsystem consists of cruise phase science experiments mounted about the spacecraft, and planet science mounted on a scan platform at the bottom center of the spacecraft. These experiments are located to satisfy their field-of-view requirements without significantly compromising other spacecraft subsystems. The Magnetometer is located near the top of the low-gain antenna waveguide to separate it from the main mass of the spacecraft but far enough from the antenna top to prevent interference with the antenna pattern. The Ionization Chamber experiment is located on the waveguide to provide maximum field of view, since it is spherically sensitive, but without significantly affecting the high-gain antenna pattern or Magnetometer measurements. The remainder of the cruise instruments are located to satisfy their individual requirements.

The planet science experiments originally consisted of a television and an infrared spectrometer experiment. The IR device was later exchanged for an ultraviolet photometer, which was ultimately replaced by an inertial thermal simulator. The final planet package consisted of the TV, the simulator, and two planet sensors(a wide angle acquisition sensor for finding the planet and a narrow angle Mars gate to initiate the data-recording

sequence). These instruments are mounted on the scan platform at a 120-deg angle to the spacecraft −Z axis to optimize visual lighting conditions at the planet. The platform is driven by a scan actuator mounted on the top of the octagon through a tube running along the center of the spacecraft to the platform. The actuator is capable of scanning the platform through a 180-deg roll angle.

9. Temperature Control

The temperature control subsystem covers the entire spacecraft. The configuration is shaped to minimize thermal problems by providing: (1) a primary electronic compartment shielded from the Sun, (2) primary radiating surfaces to which louvers could be attached to handle power fluctuations (enclosing temperature-critical items within the electronic compartment where possible), and (3) a relatively thermally clean exterior (i.e., a minimum of protrusions and reentrant corners). Temperature control is accomplished by passive means (coatings and shields) where feasible, with louvers provided on six bays to handle internal power fluctuations as well as analytical and test uncertainties. Flexible thermal shield blankets cover the top and bottom of the spacecraft, and rigid aluminum shields cover the remaining sides of the octagon structure not housing louvers.

10. Adapter Interface

The spacecraft attached to the *Agena* through a conical transition section (adapter) mounted on the top of the *Agena* forward equipment rack. The spacecraft mated with the adapter through feet at the eight corners of the octagon, and it was secured by shoes that mated the adapter and the spacecraft feet in a V-shaped groove. The eight shoes were secured by a V-band running around the eight corners with sufficient tension to provide a radial force and keep the spacecraft and adapter mated. The V-band was separated in flight by two explosive devices at opposite sides of the vehicle. (Either device would have been adequate to free the V-band and thereby remove the shoes and allow separation.) The spacecraft was then ejected by four springs located at alternate corners of the spacecraft in the adapter.

C. *System Reliability Considerations*

The mission objectives imposed very severe requirements on the *Mariner* Mars 1964 spacecraft design. Energy requirements dictated that the weight be minimal, yet the mission duration of 220 to 275 days to encounter and the 150 million mile communication distance necessitated high performance and extreme reliability. A design philosophy had to be developed that would allow the optimization of all three design parameters: weight (and therefore trajectory capability), performance, and reliability. The difficult parameters (weight and performance) were relatively inflexible, and the problem became one of providing extreme reliability without a corresponding cost in weight and performance.

The most straightforward method of increasing reliability was to institute a particularly rigid program of quality assurance. This type of reliability increase was attained by (1) designing adequate performance margins, (2) instituting parts qualification and selection programs, (3) carrying out extensive inspection procedures at both the parts manufacture and subsystem assembly levels, and (4) submitting the assembled flight items to well designed prototype and flight qualification testing.

Examination of the mission objectives clearly indicated that although the quality-assurance type of reliability increase was certainly necessary, it would not be sufficient. For example, if the spacecraft had 30,000 electrical components, each with a mean time between failures of 100 million hours, the probability that at least one component failure would occur by the end of 6000 hr of operation was 0.84. The spacecraft design had to enable proper operation in spite of failures as well as without them. The failure of a critical component could not only result in the loss of a single function, but could also induce such nonstandard operating conditions that other components would be overstressed and failures would propagate throughout the system.

Under these constraints, the only practical way to provide the required system reliability was through the use of redundancy, either by paralleling two or more physically identical systems or by paralleling two or more functionally identical but physically different systems. Block redundancy, the paralleling of two identical units, would protect against loss of function as the result of random failures. If one unit failed, the other would continue to operate independently. If the failure was causal, however (such as a design failure or an overstress due to some external perturbation), both units would be likely to experience the same failure. Functional redundancy, the paralleling of physically different but functionally identical subsystems, offered greater protection against causal failures, but also, in many cases, could be designed into the system at relatively low cost in terms of weight, volume, power, and complexity. The prime

objective in using functional redundancy was to provide at least two separate and independent paths by which a critical operation could be performed. This type of redundancy, for example, is found in the deployment scheme for the protective cover on the scan and television optics. The primary path for deployment of the cover involves operating a solenoid to unlatch the cover, then allowing the spring-loaded cover to drop. As a secondary path, a lanyard is connected to the cover so that motion of the scan platform will unlatch the cover. The primary path, then, depends upon the correct operation of the pyrotechnic control assemblies and the solenoid, while the secondary path depends upon structural integrity and proper operation of the scan platform actuator. The paths are separate and independent, with the result that no noncatastrophic failure can be postulated that will fail both paths, short of two failures in the cover itself.

It would have been possible to include a redundant CC&S in the spacecraft design, but any advantages would have been outweighed by the bulk of the redundant unit, the complexity of an onboard failure detection network, and the operational inflexibility of such a system. A much simpler and more direct method of increasing the reliability of onboard switching functions was to increase the capability of the already existing command subsystem to provide backup command capability. Again, a set of separate and independent paths was provided for critical functions. (The value of this approach was well proven during the encounter of the planet Venus by *Mariner II*.)

Certain types of subsystems, however, lent themselves better to block redundancy than to any other technique. Subsystems whose design was well understood and tested, and whose probable failure modes involved component failures and/or perturbations almost entirely random in nature were prime candidates for block redundancy. Thus, two completely independent nitrogen gas systems were used for attitude stabilization. Provided that the flight equipment was well enough controlled during manufacture, assembly, and testing to preclude any severe weaknesses or manufacturing flaws, two probable failure modes would be (1) loss of gas pressure due to randomly occurring meteoroid punctures, and (2) loss of pressure and function due to randomly occurring stuck gas valves. In the former case, the redundant half gas system would continue to operate independently. Appropriate sizing of the quantity of gas carried would allow normal attitude stabilization for the balance of the mission. In the latter case, the redundancy of gas valves between the two half systems would permit normal operation if a valve failed closed; if it failed open there would be two opposing valves to counteract it: one in its own half system and one in the redundant half system. If the gas load were sized properly, then, after all of the gas in the failed half system was expended, enough would remain in the redundant half system to allow the completion of the mission.

Block redundancy is used in a number of other areas in the spacecraft. Two pyrotechnic control assemblies are used in parallel, each operating its own pyrotechnic devices or, at least, separate burn wires in the same device. The pyrotechnic half systems operate simultaneously and independently, and each is sufficient for all pyrotechnic functions through the end of midcourse maneuver.

In a number of areas in which simultaneous operation of redundant units is not permissible, time-sharing redundant elements are used, and are switched on and off line either by onboard failure-sensing devices or by ground command. Two RF power amplifiers are used in the radio subsystem. The power output from the on-line amplifier is continuously monitored in a control unit on the spacecraft. Should the power output become degraded, the next 66⅔-hr cyclic pulses issued by the CC&S would cause the control unit to switch the degraded power amplifier and its associated power supply off line and switch on the redundant amplifier and power supply. Switching may also be accomplished by ground command (an example of the integrated use of block and functional redundancy to produce the highest possible system reliability). This method is also used with the radio subsystem's dual RF exciters.

The spacecraft power subsystem uses redundancy techniques in two areas at the system level: power boosting and regulation, and timing. The spacecraft has two separate power booster/regulators, one primarily for fixed loads and the other for varying and intermittent loads. This permits the fixed-load (main) booster to be sized for peak efficiency during the power-critical period at encounter. Efficiency is not of prime consideration for the intermittent (maneuver) booster, since its duty cycle is extremely low and, normally, it will not operate for extended periods near encounter. Therefore, it was sized to have the capability of assuming all of the spacecraft loads in the event of a main booster failure. A failure detection circuit, which senses an overvoltage or undervoltage condition, operates the switching network that removes the main booster and inserts the maneuver

booster. A redundant timing system is also provided for the frequency control of the 2.4-kc and 400-cps power. Primary timing is derived from the CC&S; should this path fail, there is a backup oscillator in the power subsystem capable of assuming the timing function. A second backup is provided through the design of the inverters, which have a natural frequency approximately equal to the nominal clock frequency, so that near-normal operation may be maintained in the absence of any external synchronization.

Finally, two units are provided in the data encoder for the conversion of analog data to a digital format and for the generation of the pseudonoise code. Switching between units is accomplished by ground command.

In many cases, the gain in system reliability appears small compared with the costs imposed upon the system. This is not true, however, if the function is so critical that a small degradation, let alone a catastrophic failure, is sufficient to impair the opportunity for any attainment of the mission objectives, as would be the case with the communications transponder. At the very minimum, a downlink RF signal must be maintained that is sufficiently above threshold to be stable. Attitude stabilization is critical because proper pointing of the directional antenna is dependent upon the correct orientation of the spacecraft in all three axes. Communications from the spacecraft may be lost if a degradation occurs in the power subsystem's capability to regulate voltage or control frequency. Such a degradation can be translated

Table 18. Summary of system redundancy

Item	Type of redundancy	Description	Item	Type of redundancy	Description
RF power amplifiers	Block	Two complete power amplifiers plus associated power supplies switchable either by internal logic or by ground command. Only one operates at any time.	Power frequency control	Block	Primary control is a 38.4-kc synchronization signal from the CC&S. In the absence of this signal, synchronization is derived from an oscillator internal to power, or the inverters will free-run at approximately 2.4 kc.
RF exciters	Block	Two identical exciters switchable either by internal logic or by ground command. Only one operates at any time.	Analog to digital converter and pseudonoise code generator	Block	Two identical units switchable by ground command. Only one operating at any time.
Pyrotechnics assemblies	Block	Two identical half systems, both on line continuously after separation.	Cruise science control relay	Functional	Either separation or ground command DC-2 controls the primary cruise science power supply relay. A secondary relay is driven by CC&S MT-7 or ground command DC-25 to ensure cruise science on during encounter.
PAS	Block	Two separation-activated switches: pyrotechnic arming switch, and separation initiated timer. Either one can power both pyrotechnic half systems.	Science cover drop	Functional	Primary control is solenoid-actuated via the pyrotechnic assembly. The backup system is a lanyard.
Attitude control gas system	Block	Two half systems and pressure bottles. Both operate continuously after attitude control turn-on.	End of TV record sequence	Functional	Primary control is second end-of-tape signal. Secondary control is inhibition of *start record* commands after 11 non-real-time science frames.
Power booster regulator	Block	Failure sensing circuit that detects over/under voltage condition at main booster output. Switches maneuver booster on and main booster off.	Spacecraft cruise and encounter events	Functional	CC&S events are primary. Backup control is via ground command.
			Midcourse trajectory correction	Block	Duplicate pyrotechnic actuated valves provide the capability for two midcourse maneuvers.

directly into an inability of the Canopus sensor to provide control about the roll axis.

A brief summary of items to which system redundancy was applied is presented in Table 18. The items listed are those for which two or more redundant units of hardware were included in the design using either the block or functional approach to system redundancy. In each case, either of the redundant items can be used to perform a nominal mission.

D. Alternate Modes of Operation

Apart from the general spacecraft reliability considerations are a number of problems involving (1) degraded operation, given failures or abnormal environments; (2) operational flexibility; and (3) design and operational procedures for time-critical functions. The approach to these problems was to create or exploit some alternate mode of spacecraft operation. Generally, for each function considered, one or more alternates have been available with a minimum of design perturbation required. Alternate modes of operation permit the spacecraft to continue operating, even with failures or abnormal environments, and if the modes can be selected by ground command, operational flexibility is afforded. The alternate mode approach has also proved especially valuable in the treatment of time-critical functions.

The phases of the mission that lent themselves best to an alternate mode design approach were the spacecraft/*Agena* separation and the initial Sun acquisition. These phases covered the period in which the spacecraft had to make the transition from the ascent configuration to cruise configuration. During the ascent, two environmental factors (the high vibrational loadings and the passage through the critical pressure region) imposed severe constraints on the spacecraft configuration. As a result, spacecraft structures were clamped to prevent damage, no high-voltage circuits were to operate, no power was to be applied to the pyrotechnics subsystem, magnetic latching relays were to be either electrically held or designed to reset at power application, and the video-storage tape drive was to run to prevent possible tape spillage. All of these conditions had to attain a normal cruise state between separation and initial star acquisition. Since separation from the *Agena* was a positive action mandatory for proper functioning of the spacecraft, most of the events that had to take place after injection were initiated by separation, that is, by the removal of electrical shorts across the *Agena* separation connector; or by the activation of spring-loaded pressure switches located at the separation interface. The CC&S relay hold function, the tape-drive power, and the "RF power up" and "cruise science on" commands were all mechanized with shorting plugs across the separation connector. In each case, power was supplied through the separation connector to operate circuitry that held its user in the launch state. Upon removal of this power, the user reverted to its normal cruise state. Of course, failure of the separation connector or associated cabling was possible; short circuits could occur internal to the spacecraft, for example. In such a case, it was necessary to find some alternate means to return the user subsystems to a cruise state.

The maneuver booster power supply is normally turned off for all but a few periods during the mission, one of which is the launch phase. By supplying power from the maneuver booster to hold the user subsystems in the launch condition, a secondary method of initiating cruise mode was established. In two of the cases (drive to the tape recorder and cruise science on) the secondary method was a true functional redundancy, since neither of these conditions was affected by maneuver booster operation after it was once turned off. The "cruise science on" command was not affected because the command is unidirectional; i.e., although cruise science would be turned on every time the maneuver booster cycled (in the event of a separation connector failure), there was no means of turning cruise science off by the same path. For the drive to the tape recorder, the circuit can remove itself from operation once it has functioned. In the other two cases—RF power up and the relay hold circuit—this secondary method was an alternate operating mode in which the spacecraft was capable of somewhat degraded performance. The RF power would stay high when the maneuver booster was on if the short circuit was to spacecraft ground—the only degradation being an additional 1 w of power drawn from the maneuver booster. If the short was across the separation connector, however, RF power would cycle up and down as the maneuver booster turned on and off. As a result, telemetry would be lost each time the gyros were turned on in this mode. However, the RF radiated power returns to normal each time the gyros are turned off again. In the case of the CC&S relay hold circuit, all of the relays are reset each time the gyros come on, and none of them can be set until the gyros go off again. The primary degradation to spacecraft performance that results from this scheme is the loss of any capability to perform a trajectory correction.

A number of other examples of alternate operating modes exist, principally at the subsystem rather than at the system level. Foremost among these is the attitude control subsystem, in which a variety of stabilization modes are available either as automatic backups or upon ground command.

Figures 30 and 31 show some of the automatic backup functions on board the spacecraft, the alternate modes of operation available, and the command decisions and command sequences required for each.

Table 19 summarizes the major operational switching points associated with either the functional redundancy or alternate mode design approach. In general, the functions included are limited to those for which an option may be exercised by the flight operations personnel during the mission. Insofar as possible, the options have been listed in order of descending desirability and/or probability of use.

E. Spacecraft Weight Control

A weight control program was put into effect so that all rigid-body mass parameters and consistent weight data would be provided from one official source. The general philosophy during the course of the program was to produce the lightest practicable spacecraft. A weight goal of 570 lb was established, with no contingency allowances. No "padding" was included in any weight figure.

The weight control function included:

1. Derivation, both computationally and experimentally, of rigid-body mass parameters characterized by weight, CG, moments of inertia, and products of inertia
2. Acquisition and compilation of data required for weight distributions in accordance with stipulated requirements for structural and dynamic analysis.
3. Maintenance of records of current weight status reflecting improved knowledge of design and development progress
4. Preparation of periodic weight status reports
5. Acquisition of actual weights, CG, and centroidal moments of inertia for system components or subsystems
6. Generation and maintenance of records of actual weight data paralleling those for calculated or estimated weight data
7. Analysis of weight status and presentation of relevant design recommendations

Accumulation of data relative to spacecraft weight, CG, moments of inertia, and products of inertia began concurrently with preliminary design. The best estimates of weight and configuration were obtained, and were then reviewed and modified for consistency with the design goal. A justification allowance weight was allocated as a weight margin to cover expected discrepancies between the sum of the weights of the individual spacecraft subassemblies and the total weight of the assembled spacecraft. The revised estimates were reviewed to ensure the inclusion of weight for mounting hardware, wiring, and related structures.

Actual weights of spacecraft hardware were initially obtained as the prototypes were constructed and weighed. Discrepancies between the actual weight and the estimated or calculated weight were investigated and resolved. As the flight hardware was completed, the actual weights were obtained, and any discrepancies encountered were reconciled. A careful account of attachment hardware weight utilization was maintained to prevent double entry errors from occurring. Spacecraft assemblies were weighed, and CG and moments of inertia were experimentally determined. Each spacecraft was reweighed at Cape Kennedy just prior to launch.

The weight control program provided weight reports in a variety of formats, using sequencing codes for subsystem, assembly, design responsibility, effectivity, and actual, calculated, and estimated weights. Each report total was further subdivided into actual weight, calculated weight, and estimated weight. When modifications were made, the corrections were key-punched on cards, which were then used to modify the magnetic tape upon which the data was stored.

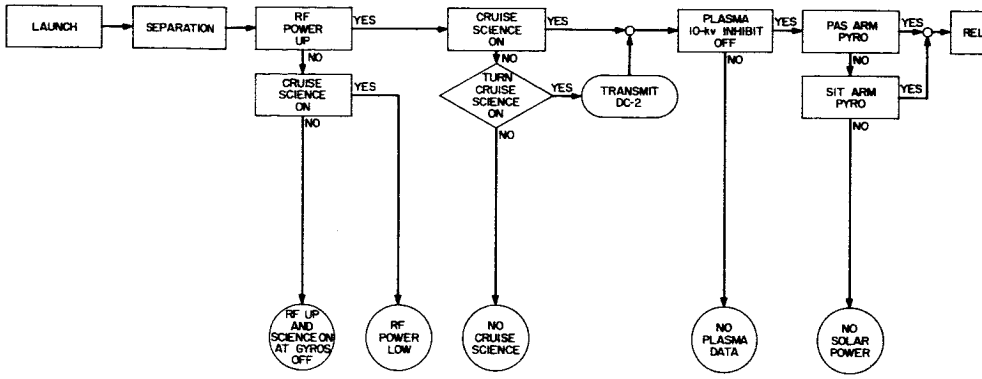
Each spacecraft was carried in the program as a separate entity, and actual weight variations between serial-numbered components assigned to specific spacecraft were reflected in the current weight report.

In addition to monitoring current weights, another computer program was used that provided moments of inertia, products of inertia, CG, and inverse J-matrix as a function of current weight changes. The program also provided true-length distances from each component to the Magnetometer sensor.

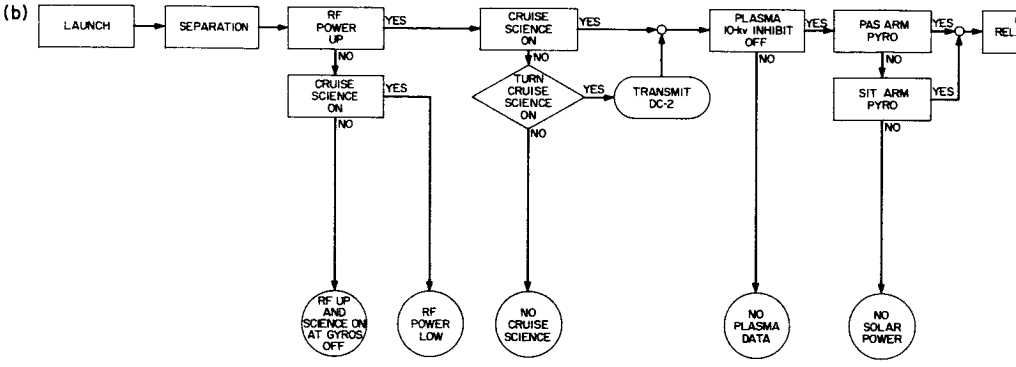
Table 19. Operational flexibility

Function	Design approach/remarks	Options
Cruise science on	Functionally redundant with an alternate mode of operation at encounter	Power switched on at separation when holding current removed from power subsystem relay. DC-2, which also switches encoder to Data Mode 2. Alternate power route activated at turn-on of encounter science (DC-25 or CC&S MT-7). Prior to separation, primary mode may be exercised by turning off gyros.
RF power up	Alternate mode	Removal of separation connector releases holding circuit. Turn-off of gyros releases holding circuit. Power up/down will cycle with gyros.
VSS launch mode off	Alternate mode	Removal of separation connector activates count one end of tape and stop logic. Gyro turn-off removes tape drive power.
CC&S relay hold off	Alternate mode	Removal of separation connector interrupts holding current. Gyros off turns off holding current. Relays will reset if gyros are turned on again.
Solar panel deployment	Functionally redundant	Separation initiated timer CC&S L-1 event.
Attitude control on	Functionally redundant. Turns on Sun sensors and switching amplifiers	Pyrotechnic arming switch. CC&S L-2 event. DC-13, which also turns on Canopus sensor and sets maneuver inhibit logic.
Canopus sensor on	Functionally redundant	CC&S L-3, which also turns on solar vane electronics. DC-13, which also turns on attitude control and sets maneuver inhibit logic.
Switch data rates	Functionally redundant	CC&S MT-6 switches to 8⅓ bps. DC-5 switches bit rates (toggle).
Canopus cone-angle update	Functionally redundant	CC&S MT-1, MT-2, MT-3, and MT-4. DC-17.
Antenna switching	Functionally redundant plus alternate mode. The initial state of the system determines the reaction to any switching input	CC&S MT-5 switches to transmit via high-gain antenna and enables CY-1 logic. DC-10 switches to transmit via high-gain antenna and to receive via low-gain antenna. DC-11 switches to transmit and receive via high-gain antenna. DC-12 switches to transmit and receive via low-gain antenna. Gyros on switches to receive via low-gain antenna. Two consecutive CY-1 cyclics with receiver out of lock will switch receiver to other antenna. Each subsequent consecutive CY-1 with receiver out of lock will switch receiver.
Roll control	Alternate mode	Normally initiated at L-3 or DC-13. Canopus sensor on with brightness gates in effect. This mode may be restored after use of an alternate by DC-19. DC-15. Canopus sensor on, brightness gates removed from circuit. Canopus sensor will track any detectable light source. Gyros disabled. DC-18. Inertial roll control. Canopus sensor off, gyros on. Pitch and yaw gyros in rate mode, Sun sensors unaffected. DC-20. No roll control. Canopus sensor off, gyros off. Rate mode, prior to Sun gate only. Gyros on in rate mode. Magnetometer calibrate roll mode; subsequent to Sun gate, prior to L-3/DC-13 only.

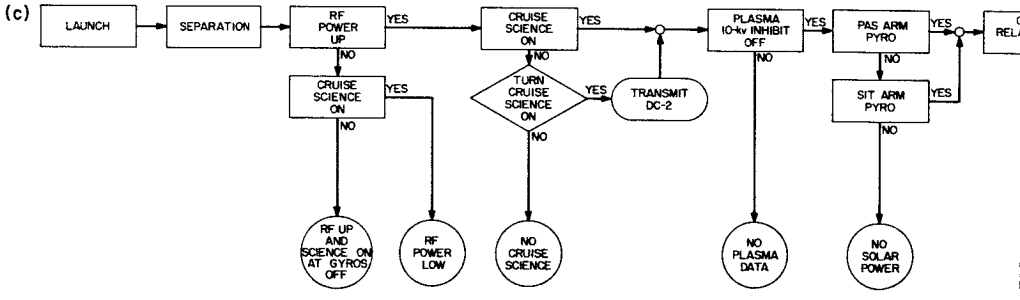
(a)


LAUNCH
SEPARATION
RF POWER UP
YES
NO
CRUISE SCIENCE ON
YES
NO
PLASMA 10-kv INHIBIT OFF
YES
NO
PAS ARM PYRO
YES
NO
REL
CRUISE SCIENCE ON
YES
NO
TURN CRUISE SCIENCE ON
YES
NO
TRANSMIT DC-2
SIT ARM PYRO
YES
NO
RF UP AND SCIENCE ON AT GYROS OFF
RF POWER LOW
NO CRUISE SCIENCE
NO PLASMA DATA
NO SOLAR POWER

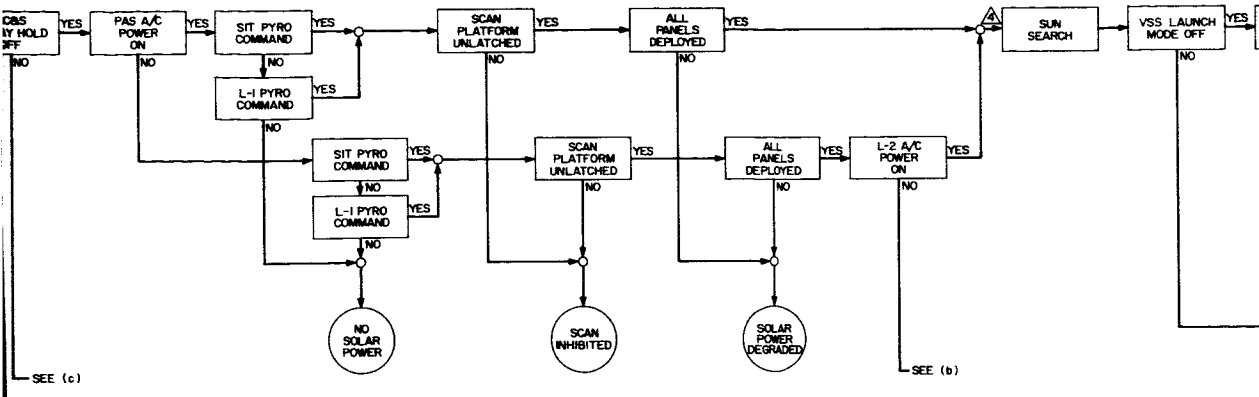
(b)

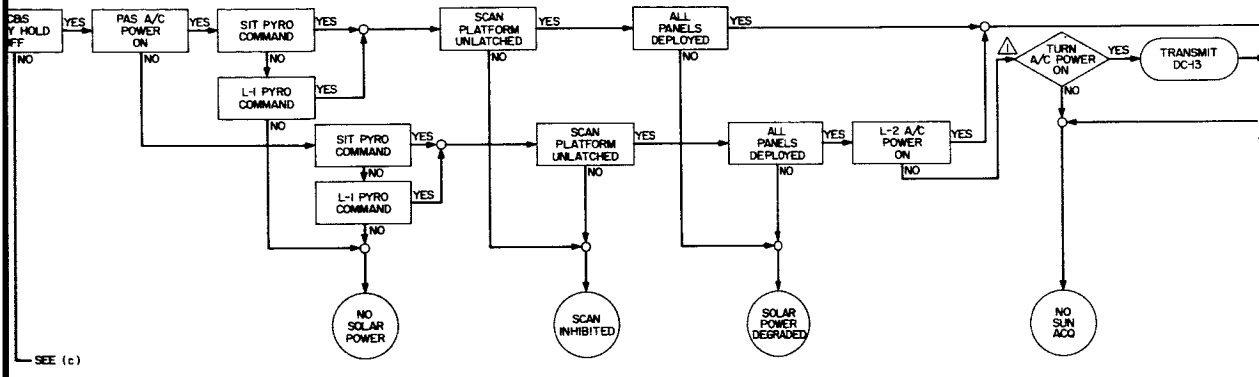

LAUNCH
SEPARATION
RF POWER UP
YES
NO
CRUISE SCIENCE ON
YES
NO
PLASMA 10-kv INHIBIT OFF
YES
NO
PAS ARM PYRO
YES
NO
REL
CRUISE SCIENCE ON
YES
NO
TURN CRUISE SCIENCE ON
YES
NO
TRANSMIT DC-2
SIT ARM PYRO
YES
NO
RF UP AND SCIENCE ON AT GYROS OFF
RF POWER LOW
NO CRUISE SCIENCE
NO PLASMA DATA
NO SOLAR POWER

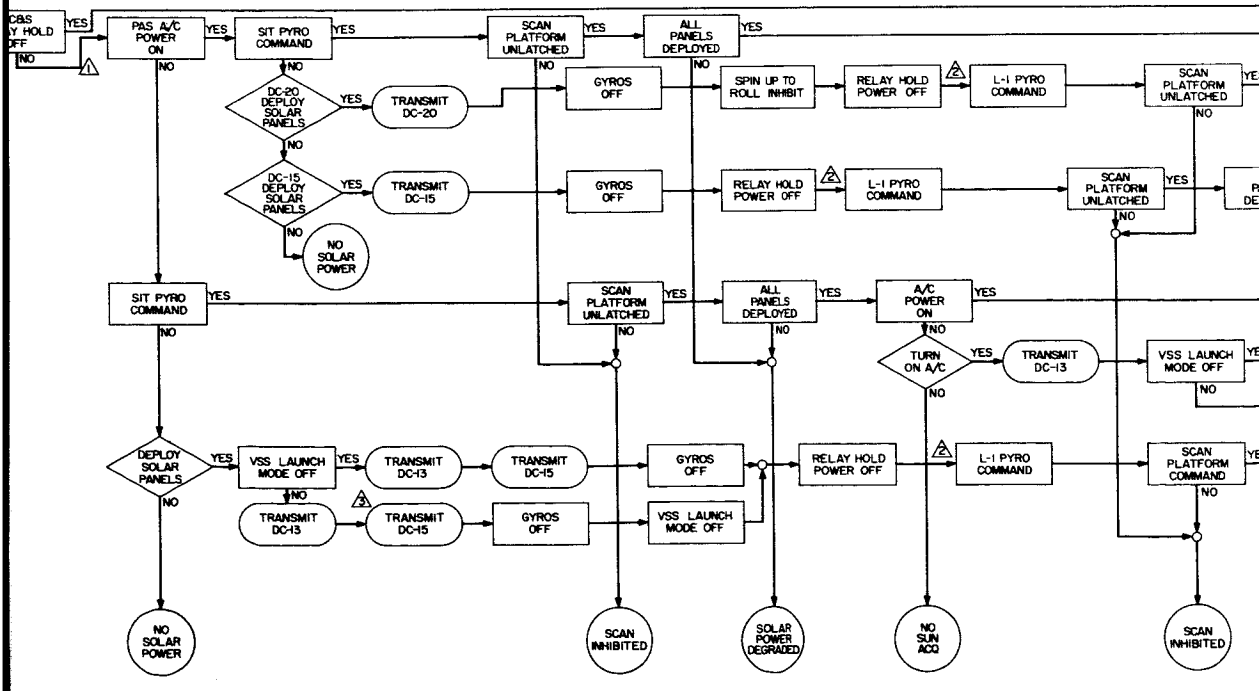
(c)

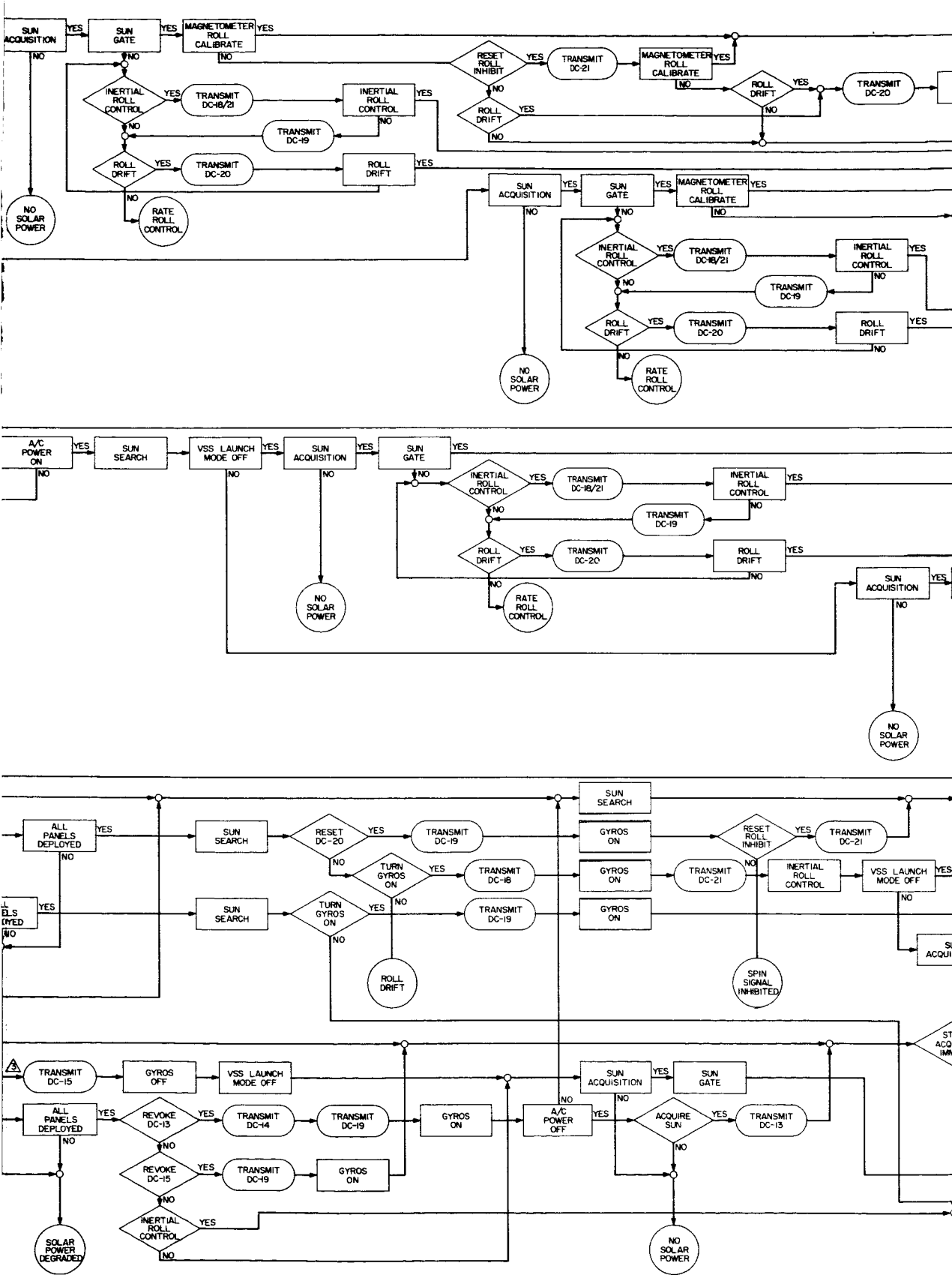

LAUNCH
SEPARATION
RF POWER UP
YES
NO
CRUISE SCIENCE ON
YES
NO
PLASMA 10-kv INHIBIT OFF
YES
NO
PAS ARM PYRO
YES
NO
CRUISE SCIENCE ON
YES
NO
TURN CRUISE SCIENCE ON
YES
NO
TRANSMIT DC-2
SIT ARM PYRO
YES
NO
RF UP AND SCIENCE ON AT GYROS OFF
RF POWER LOW
NO CRUISE SCIENCE
NO PLASMA DATA
NO SOLAR POWER

89-1

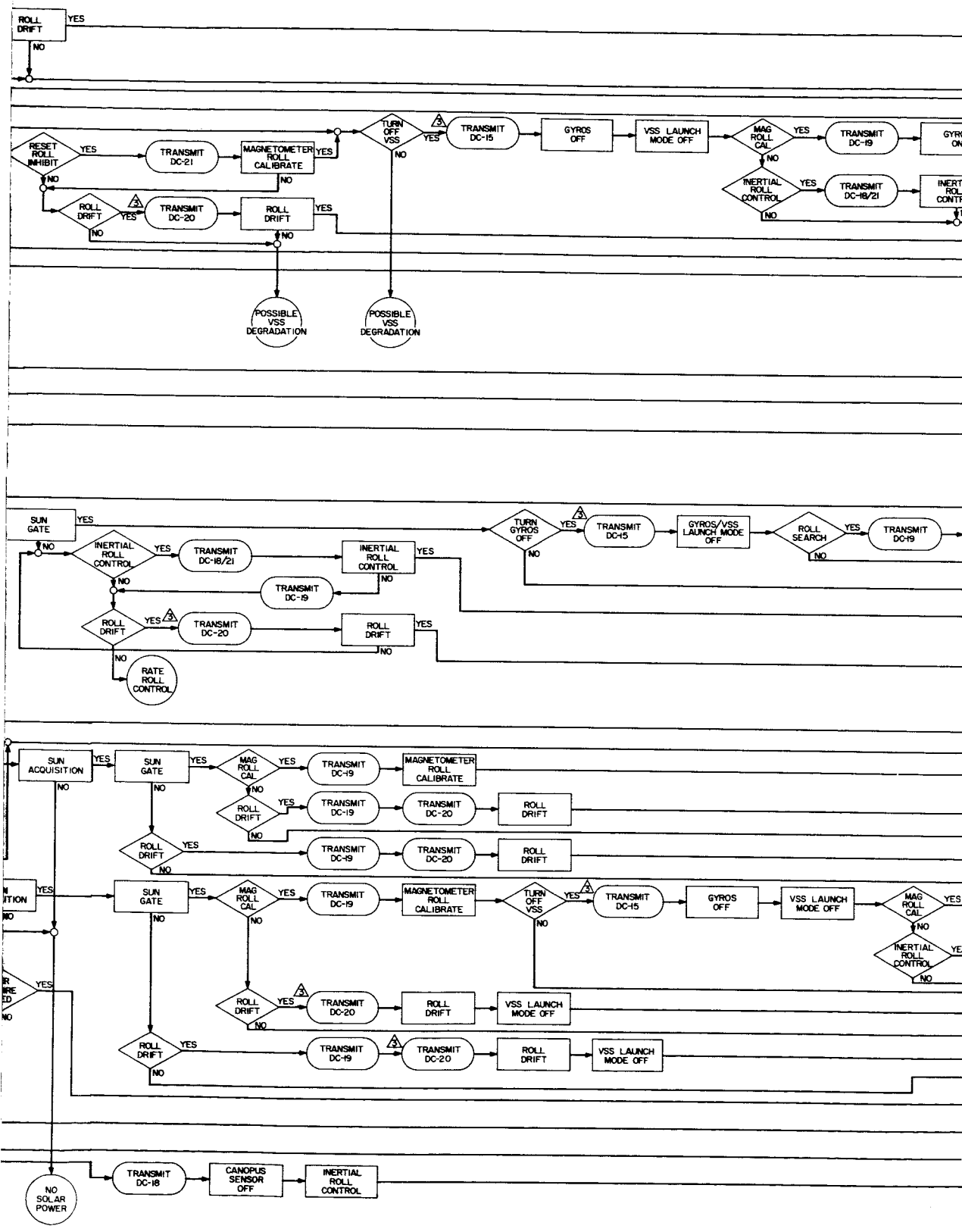

C&S HOLD OFF
YES
NO
PAS A/C POWER ON
SIT PYRO COMMAND
L-1 PYRO COMMAND
SCAN PLATFORM UNLATCHED
ALL PANELS DEPLOYED
SUN SEARCH
VSS LAUNCH MODE OFF
L-2 A/C POWER ON
NO SOLAR POWER
SCAN INHIBITED
SOLAR POWER DEGRADED
SEE (b)
SEE (c)


C&S HOLD OFF
YES
NO
PAS A/C POWER ON
SIT PYRO COMMAND
L-1 PYRO COMMAND
SCAN PLATFORM UNLATCHED
ALL PANELS DEPLOYED
TURN A/C POWER ON
TRANSMIT DC-13
L-2 A/C POWER ON
NO SOLAR POWER
SCAN INHIBITED
SOLAR POWER DEGRADED
NO SUN ACQ
SEE (c)


C&S HOLD OFF
YES
NO
PAS A/C POWER ON
SIT PYRO COMMAND
SCAN PLATFORM UNLATCHED
ALL PANELS DEPLOYED
DC-20 DEPLOY SOLAR PANELS
TRANSMIT DC-20
DC-15 DEPLOY SOLAR PANELS
TRANSMIT DC-15
NO SOLAR POWER
GYROS OFF
SPIN UP TO ROLL INHIBIT
RELAY HOLD POWER OFF
L-1 PYRO COMMAND
A/C POWER ON
TURN ON A/C
TRANSMIT DC-13
VSS LAUNCH MODE OFF
DEPLOY SOLAR PANELS
TRANSMIT DC-15
SCAN PLATFORM COMMAND
NO SUN ACQ
SCAN INHIBITED
SOLAR POWER DEGRADED


SUN ACQUISITION
YES
NO
SUN GATE
MAGNETOMETER ROLL CALIBRATE
INERTIAL ROLL CONTROL
TRANSMIT DC-16/21
TRANSMIT DC-19
ROLL DRIFT
TRANSMIT DC-20
RESET ROLL INHIBIT
TRANSMIT DC-21
NO SOLAR POWER
RATE ROLL CONTROL
A/C POWER ON
SUN SEARCH
VSS LAUNCH MODE OFF
ALL PANELS DEPLOYED
RESET DC-20
TURN GYROS ON
TRANSMIT DC-18
GYROS ON
SPIN SIGNAL INHIBITED
TRANSMIT DC-15
GYROS OFF
REVOKE DC-13
TRANSMIT DC-14
REVOKE DC-15
A/C POWER OFF
ACQUIRE SUN
SOLAR POWER DEGRADED

89.3


ROLL DRIFT
YES
NO
RESET ROLL INHIBIT
TRANSMIT DC-21
MAGNETOMETER ROLL CALIBRATE
ROLL DRIFT
TRANSMIT DC-20
TURN OFF VSS
TRANSMIT DC-15
GYROS OFF
VSS LAUNCH MODE OFF
MAG ROLL CAL
TRANSMIT DC-19
INERTIAL ROLL CONTROL
TRANSMIT DC-18/21
POSSIBLE VSS DEGRADATION
POSSIBLE VSS DEGRADATION
SUN GATE
INERTIAL ROLL CONTROL
TRANSMIT DC-18/21
TRANSMIT DC-19
ROLL DRIFT
TRANSMIT DC-20
RATE ROLL CONTROL
TURN GYROS OFF
TRANSMIT DC-15
GYROS/VSS LAUNCH MODE OFF
ROLL SEARCH
TRANSMIT DC-19
SUN ACQUISITION
SUN GATE
MAG ROLL CAL
TRANSMIT DC-19
MAGNETOMETER ROLL CALIBRATE
ROLL DRIFT
TRANSMIT DC-20
TURN OFF VSS
TRANSMIT DC-15
GYROS OFF
VSS LAUNCH MODE OFF
INERTIAL ROLL CONTROL
TRANSMIT DC-18
CANOPUS SENSOR OFF
NO SOLAR POWER

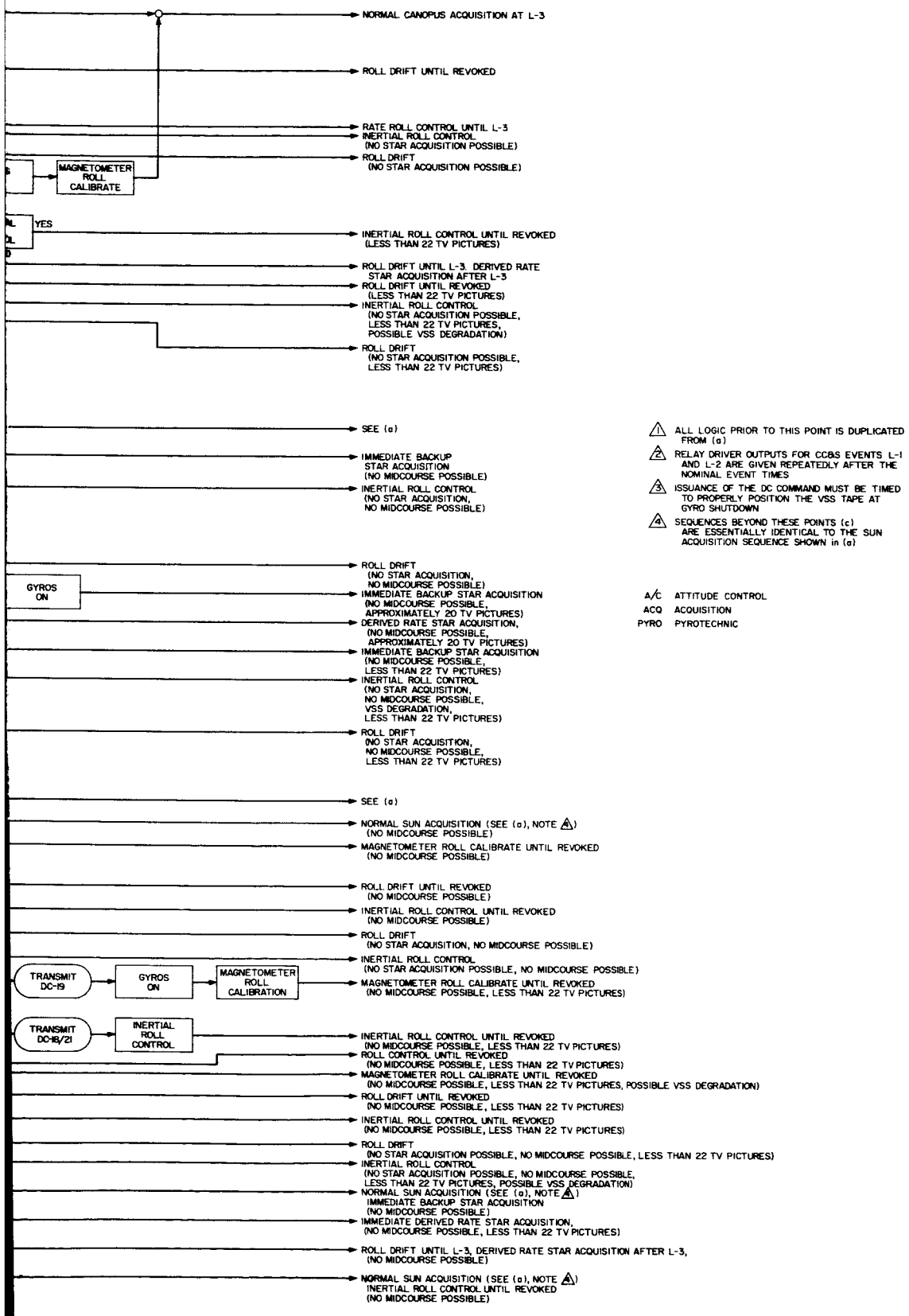


Fig. 30. Sequence flow diagram, launch to Sun acquisition

89-5

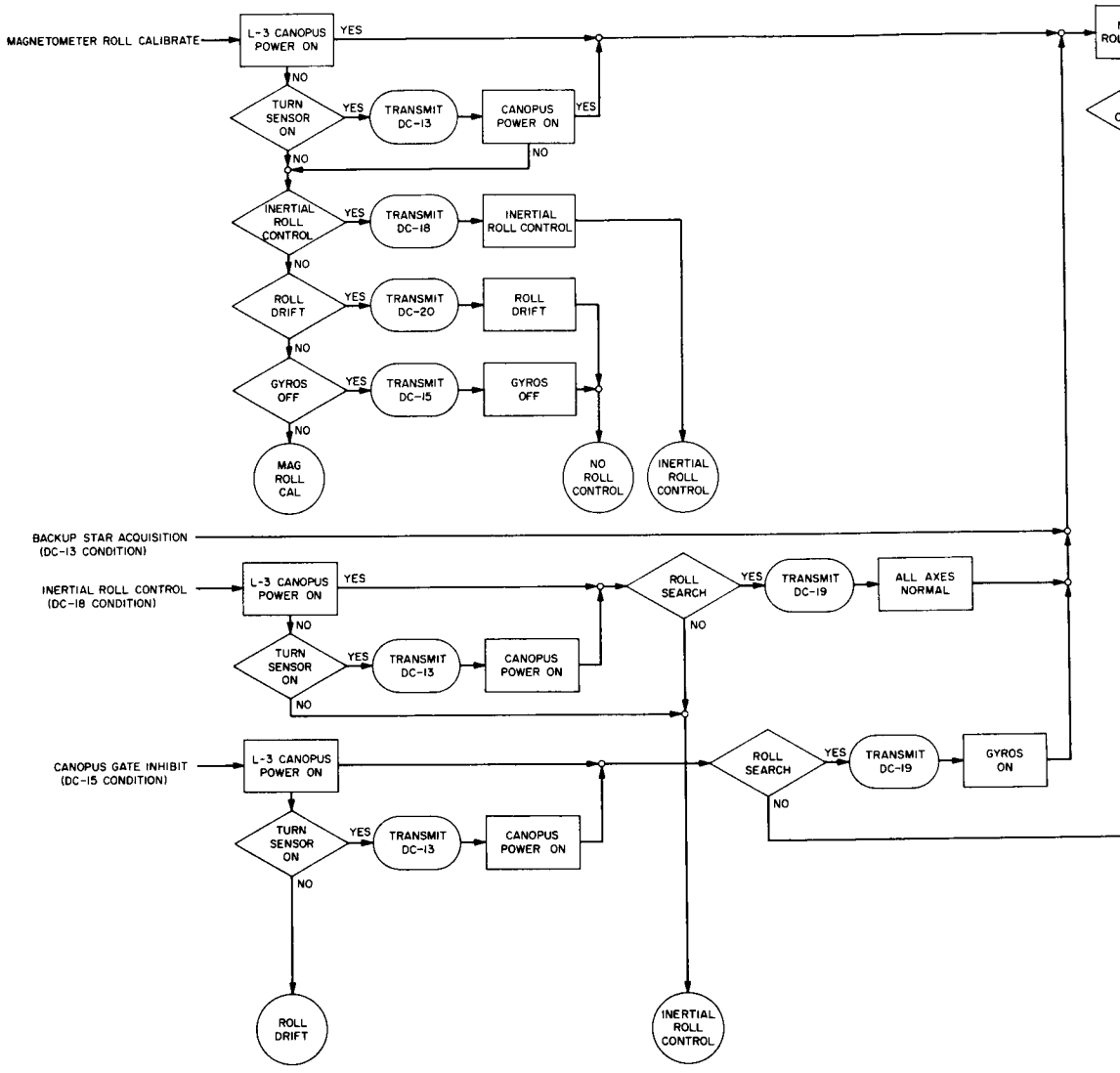
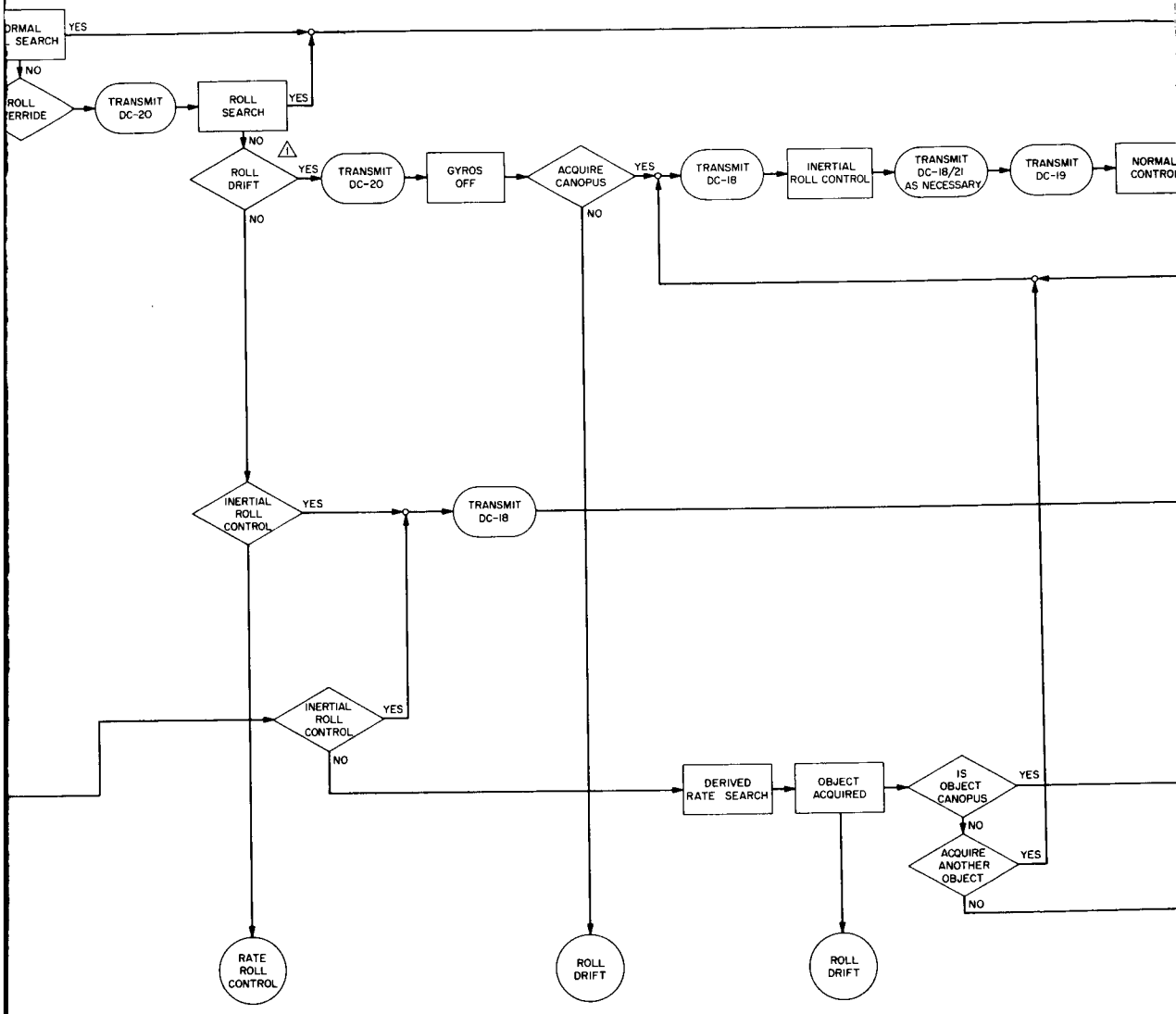
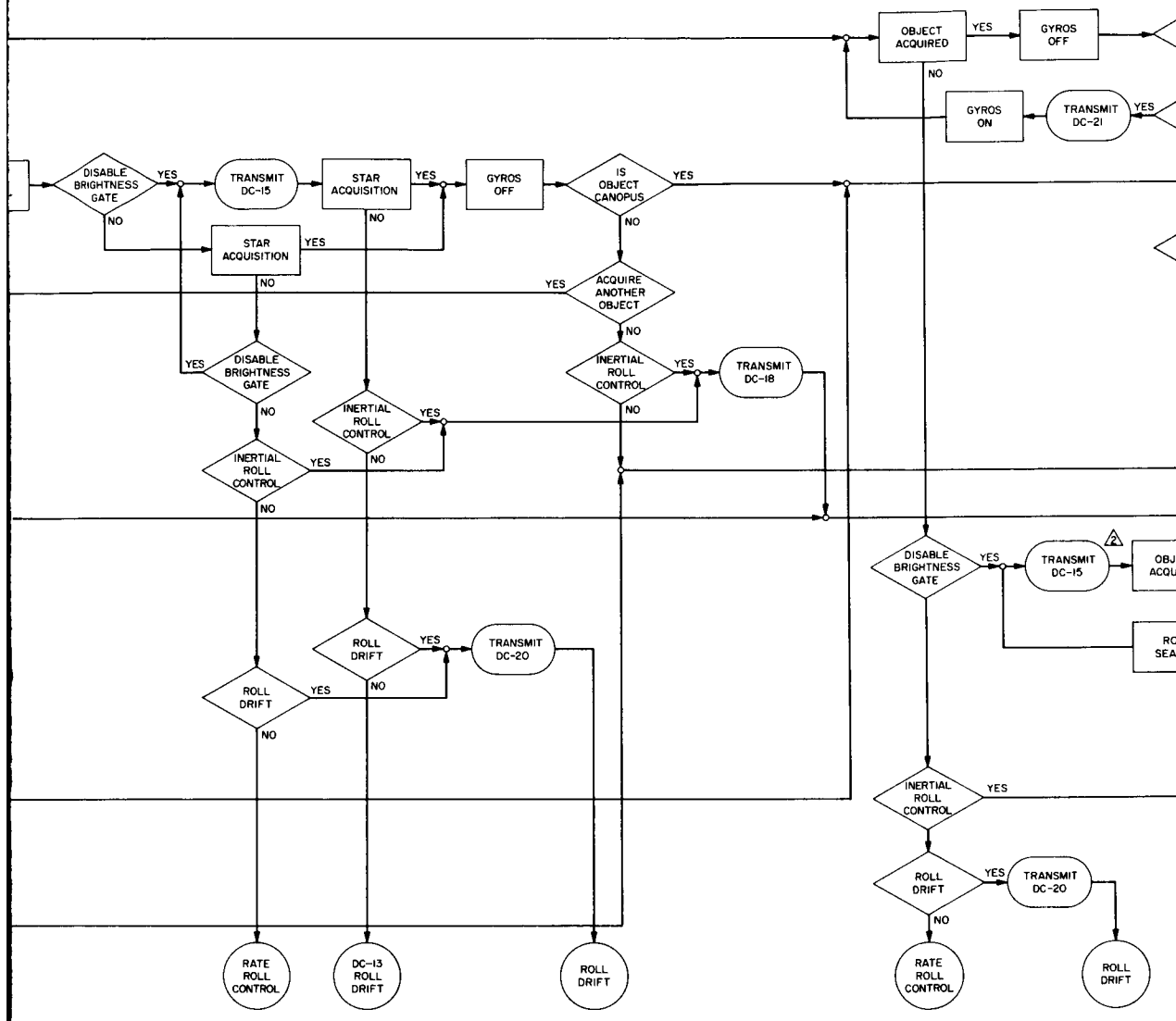


Fig. 31. Sequence flow diagram, roll acquisition


ORMAL SEARCH
YES
NO
ROLL ERRIDE
TRANSMIT DC-20
ROLL SEARCH
YES
NO
ROLL DRIFT
YES
TRANSMIT DC-20
GYROS OFF
ACQUIRE CANOPUS
YES
NO
TRANSMIT DC-18
INERTIAL ROLL CONTROL
TRANSMIT DC-18/21 AS NECESSARY
TRANSMIT DC-19
NORMAL CONTRO
INERTIAL ROLL CONTROL
YES
TRANSMIT DC-18
INERTIAL ROLL CONTROL
YES
NO
DERIVED RATE SEARCH
OBJECT ACQUIRED
IS OBJECT CANOPUS
YES
NO
ACQUIRE ANOTHER OBJECT
YES
NO
RATE ROLL CONTROL
ROLL DRIFT
ROLL DRIFT


OBJECT ACQUIRED
YES
GYROS OFF
NO
GYROS ON
TRANSMIT DC-21
YES
DISABLE BRIGHTNESS GATE
YES
TRANSMIT DC-15
STAR ACQUISITION
YES
GYROS OFF
IS OBJECT CANOPUS
YES
NO
STAR ACQUISITION
YES
NO
YES
ACQUIRE ANOTHER OBJECT
NO
YES
DISABLE BRIGHTNESS GATE
INERTIAL ROLL CONTROL
YES
TRANSMIT DC-18
NO
INERTIAL ROLL CONTROL
YES
NO
INERTIAL ROLL CONTROL
YES
NO
DISABLE BRIGHTNESS GATE
YES
TRANSMIT DC-15
2
ROLL DRIFT
YES
TRANSMIT DC-20
NO
ROLL DRIFT
YES
NO
INERTIAL ROLL CONTROL
YES
ROLL DRIFT
YES
TRANSMIT DC-20
NO
RATE ROLL CONTROL
DC-13 ROLL DRIFT
ROLL DRIFT
RATE ROLL CONTROL
ROLL DRIFT

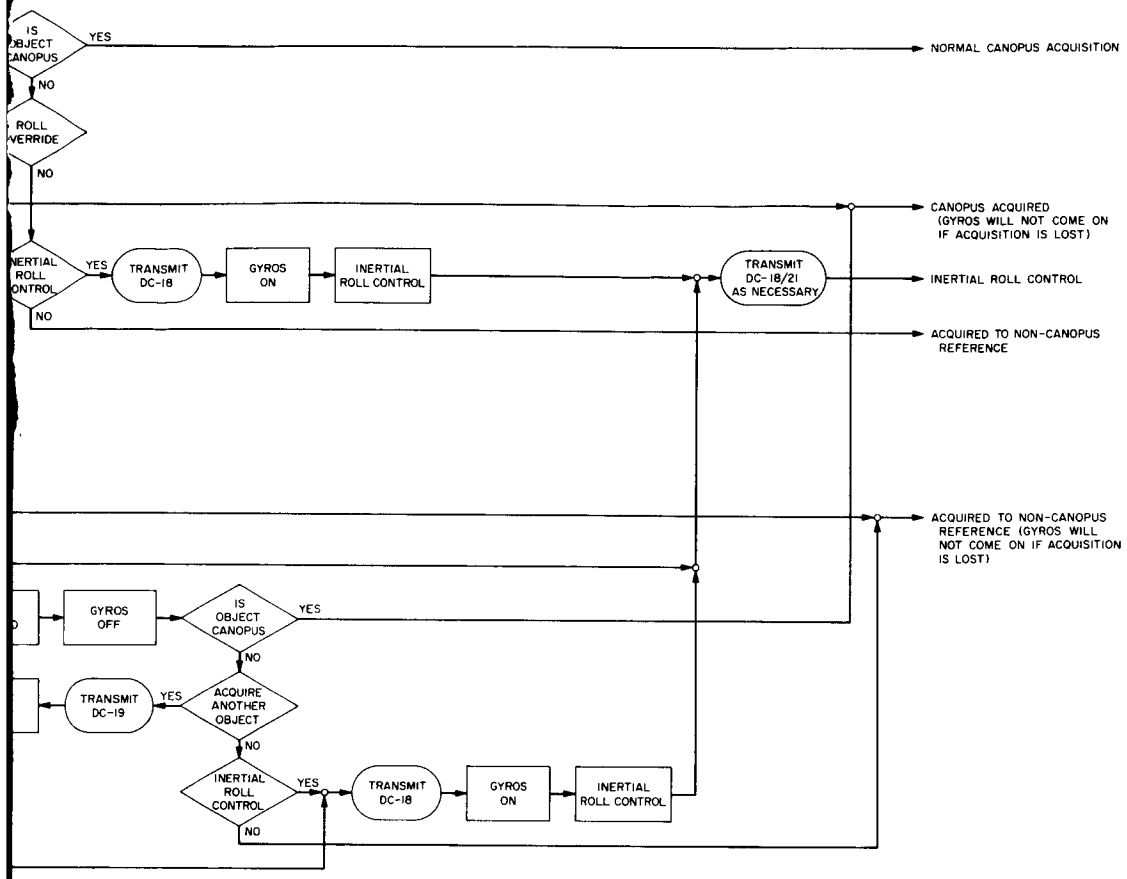

IS OBJECT CANOPUS
YES
NO
NORMAL CANOPUS ACQUISITION
ROLL VERRIDE
NO
CANOPUS ACQUIRED (GYROS WILL NOT COME ON IF ACQUISITION IS LOST)
NERTIAL ROLL ONTROL
YES
TRANSMIT DC-18
GYROS ON
INERTIAL ROLL CONTROL
TRANSMIT DC-18/21 AS NECESSARY
INERTIAL ROLL CONTROL
NO
ACQUIRED TO NON-CANOPUS REFERENCE
ACQUIRED TO NON-CANOPUS REFERENCE (GYROS WILL NOT COME ON IF ACQUISITION IS LOST)
GYROS OFF
IS OBJECT CANOPUS
YES
NO
TRANSMIT DC-19
YES
ACQUIRE ANOTHER OBJECT
NO
INERTIAL ROLL CONTROL
YES
TRANSMIT DC-18
GYROS ON
INERTIAL ROLL CONTROL
NO

Table 19. (Cont'd)

Function	Design approach/remarks	Options	Function	Design approach/remarks	Options
Roll control	Alternate mode	Normal search. Initiated by L-3 or DC-13. Until initial acquisition only. Acquisition override, DC-21. Results in normal search.	Data mode switching to Data Mode 3	Functionally redundant	Wide angle acquisition. Narrow angle acquisition or TV planet-in-view if wide angle acquisition has not occurred. DC-3.
Data mode switching to Data Mode 1	Functionally redundant for midcourse phase	DC-27 switches to Data Mode 1, and starts midcourse sequence. DC-1.	Data mode switching to Data Mode 4	Functionally redundant. If there are no data present on the VSS tape, data are automatically formatted to Data Mode 1	CC&S MT-9. Tape playback and Data Mode 4. DC-4. Tape playback and Data Mode 4.
Data mode switching to Data Mode 2	Functionally redundant	Reset of MT-1 relay during midcourse. Also initiates reacquisition. DC-2, which also turns on cruise science. DC-25, which also turns on encounter science. VSS second end of tape or end of NRT DAS frame No. 11, whichever comes first. MT-7.	Encounter science on	Functionally redundant	CC&S MT-7. DC-25.
			Encounter science off	Functionally redundant	CC&S MT-8. DC-26.
			VSS tape track change	Functionally redundant	Internal logic triggered by end-of-tape signal. DC-22.

The input for the program consisted of component weight, centroid coordinates $\bar{x}$, $\bar{y}$, and $\bar{z}$, local moments of inertia, and local products of inertia for each component. The coordinates were obtained by analysis of existing drawings; the local moments and products of inertia of each component were computed manually using existing drawings. The spacecraft moments of inertia were determined experimentally.

Monthly reports presented the current weight, CG, moments of inertia, products of inertia, and inverse J-matrix for each of three phases of the trajectory, namely: launch, before midcourse maneuver, and after midcourse maneuver. The weight was subdivided into actual and calculated weights by percentage, and a complete explanation of weight changes was included in each report. Pointing information for the PIPS was also supplied in the form of lateral offset distance and rotation angle. The variation of spacecraft total weight as a function of time is shown in Fig. 32.

The MC-3 spacecraft was weighed in at 574.27 lb, but, prior to launch, the weight increased to 574.74 lb because of component replacements. The final weight report differed from the measured value by 5.06 lb, or slightly less than 0.9%. Presumably, part of this difference was installation hardware not accounted for.

The MC-3 spacecraft CG was experimentally determined to be X = 0.698 in., Y = −0.023 in., and Z = −12.293 in. The corresponding calculated values were X = 0.65 in., Y = −0.02 in., and Z = −12.20 in. The difference between the calculated values and the measured values amounted to X = 0.048 in., Y = 0.003 in., and Z = 0.093 in. The MC-2 spacecraft CG was experimentally determined to be X = 0.784 in., Y = 0.104 in., and Z = −12.302 in.

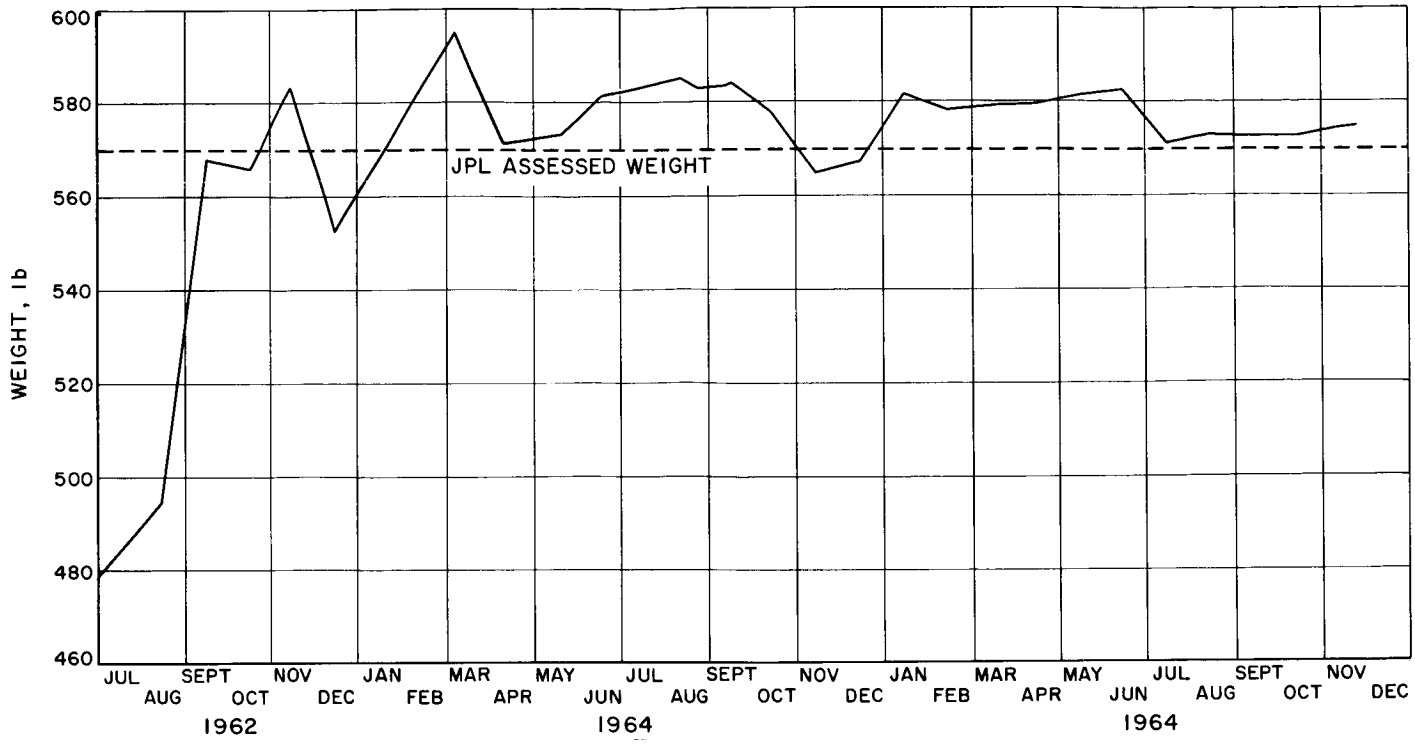


Fig. 32. Spacecraft weight history

VI. SPACECRAFT SUBSYSTEMS: STRUCTURE

The spacecraft structural design was influenced by ten considerations.

The structure had to be designed and built in an unusually short time. To meet the tight schedule, the structure was designed to be fabricated with relative ease using existing assembly techniques.

The structural components had to be lightweight and yet strong and rigid enough to enable all spacecraft components to survive the boost and postinjection propulsion environments.

The view angle constraints imposed by the solar panels, attitude control sensors, antennas, and science instruments had to be achieved by efficient structural design.

The temperature control design criteria had to be met. These criteria consisted of thermally isolating the main portion of the spacecraft from the changing solar heat inputs, and enclosing this hardware within an envelope that could be easily temperature-controlled.

Realistic mechanical alignments between the reference surfaces and the critical components had to be provided and maintained.

The number and complexity of the deployment and articulation operations had to be minimized without compromising the mission objectives.

It had to be possible to break the structure down into discrete elements, which could be designed and fabricated separately, and which, when assembled as a complete unit, would provide an integrated lightweight structure.

The structure had to be flexible enough to accommodate late changes and revisions in hardware design without major redesign.

The design had to be compatible with the ground-handling considerations. The system testing and operations had to be conducted with minimum spacecraft disassembly; access had to be provided for these operations without disassembling the major electronic elements from the spacecraft.

The final spacecraft assembly and button-up operations just prior to launch had to be made in a fast, straightforward, and simple manner.

The *Mariner* spacecraft structure is composed of the following components:

1. The basic octagon structure, which houses the electronic equipment, the cabling, the PIPS and the attitude control gas vessels and regulators. To the octagon structure are mounted miscellaneous science instruments, the attitude control sensors, the side and lower thermal shields, and all other exterior protrusions. The base of the octagon structure provides the spacecraft structural portion of the launch vehicle interface.
2. The superstructure supports the fixed high-gain antenna and the Cosmic Dust Detector instrument, and mounts the solar panel boost and low-gain antenna support dampers. It also supports the upper thermal shield.
3. The four identical solar panel structures support the 70 ft^2 of solar cells. The attitude control gas jets and solar pressure vanes are attached to the ends of the solar panels.
4. The boost dampers restrain and align the low-gain antenna and the four undeployed solar panels. The vibration inputs to these elements are reduced by the boost dampers. Pyrotechnic pinpullers on the ends of the eight solar panel boost dampers release the panels upon command.
5. The panel deployment area includes: clock-type power springs to rotate each panel 90 deg to its deployed position; the necessary instrumentation to signal that the panels have been deployed; and the cruise dampers, which restrain the panels at their deployed position and align and retard them from further movement after deployment. (The cruise dampers also minimize the panel inertial excursions during the midcourse maneuver.)
6. The science platform is mounted to the central portion of the octagon structure and provides the mounting for the planet-oriented science instruments and sensors. The scan actuator is capable of rotating the science platform instruments to the proper pointing position to obtain scientific information at Mars encounter. A cover is provided to

protect the delicate instruments from sunlight and cosmic dust.

Because the structure is highly integrated, most of the structural analysis, development, and qualification tests were made on the complete spacecraft structure. Qualification tests were performed using a complete flight spacecraft frame containing mass mockups of all electronic and propulsion equipment. Although problems were encountered during the design and test phases, the adequacy of the spacecraft structural design was confirmed by these tests.

A. Octagon Structure

The octagon structure is the core of the *Mariner* Mars 1964 spacecraft. It structurally supports all of the spacecraft components and houses the booster-mounting interface. The final structural configuration evolved from a series of design studies in which various basic structural shapes were investigated. The octagon shape, with the electronic packaging integrated into the structural design, was selected because it has the following inherent attributes:

1. The structure can tie the spacecraft elements together with adequate strength and rigidity, and with minimal weight (30 lb).
2. The *Ranger* and *Mariner* Venus 1962 subassembly profiles can be efficiently packaged in the electronic chassis, which are integrated into the structure.
3. During the design stage, additional space can be provided for electronics growth by increasing the height of the octagon structure.
4. The total spacecraft temperature control approach can be satisfactorily implemented.
5. The solar panels can be easily attached to the basic load-carrying structure.
6. The planet-oriented science instruments can be located in a desirable position.

The structure was fabricated of large machined magnesium forgings. Critical-tolerance surfaces were machined on these parts prior to final assembly to minimize assembly time and weight. The achievement of a minimum-weight structural design tended to compromise the operational aspects of the total design. Special fixtures were required to handle the electronic assemblies; the spacecraft had to be mounted to a special support structure; and special shear panels had to be installed in the structure whenever components were removed. The structure was very delicate and had to be treated as such.

The selection of a structure that was fabricated from large machined components and was structurally dependent on other components created operational areas of concern. Constant attention to these potential problem areas resulted in a lightweight functional design. Eight octagon structures were fabricated—four for structural, thermal, and booster interface tests, and four for flight.

1. Design Description

a. Primary structure. The primary portion of the basic octagon structure is composed of two octagonal rings, each approximately ¾ in. thick and 55 in. in diameter. Longerons 16½ in. high (Fig. 33) are mounted at the octagon corners and separate the two rings. Electronic chassis, approximately 4 in. deep, are mounted in the rectangular openings formed by the rings and longerons (Fig. 34). The chassis in six bays consist of a flat, shear-web outer surface and three web members normal to the chassis shear web. These members support the inboard portion of two vertical rows of electronic subassemblies by their mounting ears. The center web member, a box section, also provides the structural support for the cable harness.

The periphery of the chassis shear web is bolted to the exterior surfaces of the longerons and the upper and lower rings. The interior of the chassis is bolted to the octagon structure at four points. The center web member is bolted to the top and bottom rings, and each of the two outer webs are mated to the inboard surfaces of the longerons by shear pins and bolts.

The seventh bay houses a portion of the power conversion equipment and the battery. The power conversion equipment chassis is bolted to the outside surface of the octagon structure in the same way as the chassis shear web. The battery is mounted to the inner vertical face of the longeron and to the center of the upper- and lower-ring webs in the same manner as the inboard portion of the chassis.

The eighth bay houses the postinjection propulsion system. The PIPS is attached to the structure by fittings located in the corners of the bay. A 0.030-in.-thick shear web is bolted to the exterior face of the opening. The shear web contains two openings: one for the umbilical connector, and a second for the protruding motor nozzle and jet-vane actuators. The second opening is covered

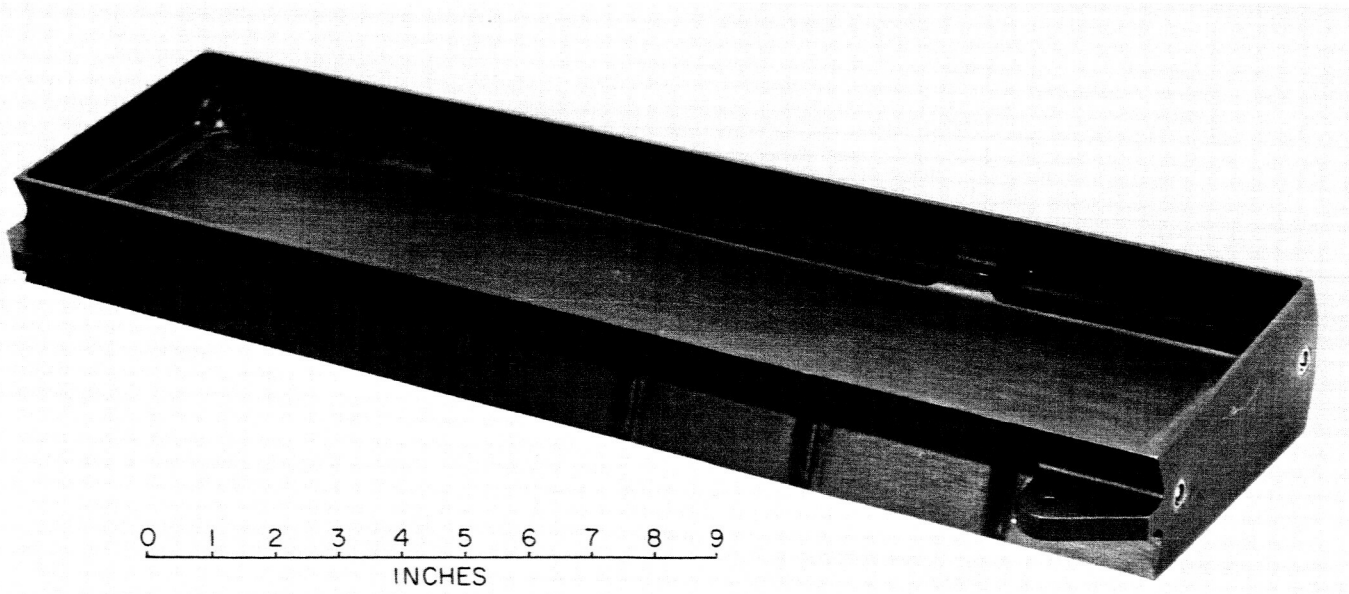


Fig. 33. Octagon structure longeron

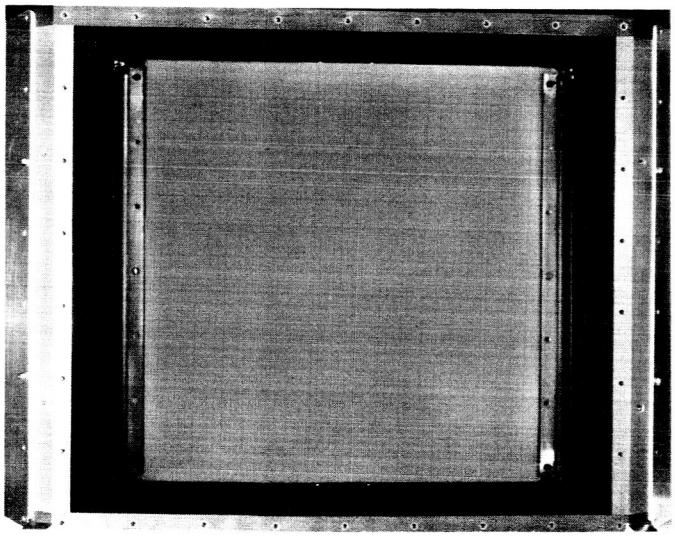


Fig. 34. Electronic chassis mounting surfaces

with a cylindrical can-type structure, which acts as a thermal shield and reduces the chances of the delicate motor and jet vane actuator parts being hit.

The lower ring (Fig. 35) provides mounting surfaces for many components. The secondary sensors and Canopus sensor are bolted to mounting and indexing surfaces that were machined on the lower ring. Mounting holes and surfaces are also provided for the Canopus sensor Sun shutter, the pyrotechnic arming switch, and the separation-initiated timer. Brackets mounted to the lower ring support the inflight electrical connector, and provide the necessary bearing surfaces for spacecraft ejection springs and separation-velocity linear potentiometers mounted on the *Agena* adapter.

The spacecraft was attached to the *Agena* adapter at the eight exterior corners of the lower ring. It was restrained by a V-band that clamped eight 1-in.-wide feet so that they would bear on a corresponding surface on the adapter. The compressive force of the tensioned V-band, reacting on the upper foot surface, reacted the axial loads and eliminated the possibility of the spacecraft chattering during vibration. Radial loads were reacted by a 0.185-in. shear lip on the lower ring, which bore against a corresponding surface on the adapter. Torsional loads between the spacecraft and the adapter were reacted by (1) the friction forces between the spacecraft and the adapter mounting surfaces, and (2) shear washers and bolts inserted on either side of the eight feet.

The spacecraft mounting surface was machined to be coplanar within 0.005 in. The radial tolerances between the shear lips were held to 0.010 in. Because the adapter radial-spring constant is much lower than that of the spacecraft, the adapter was deformed during the V-band tensioning operation until the mounting surface was seated and the two shear lip surfaces came in contact.

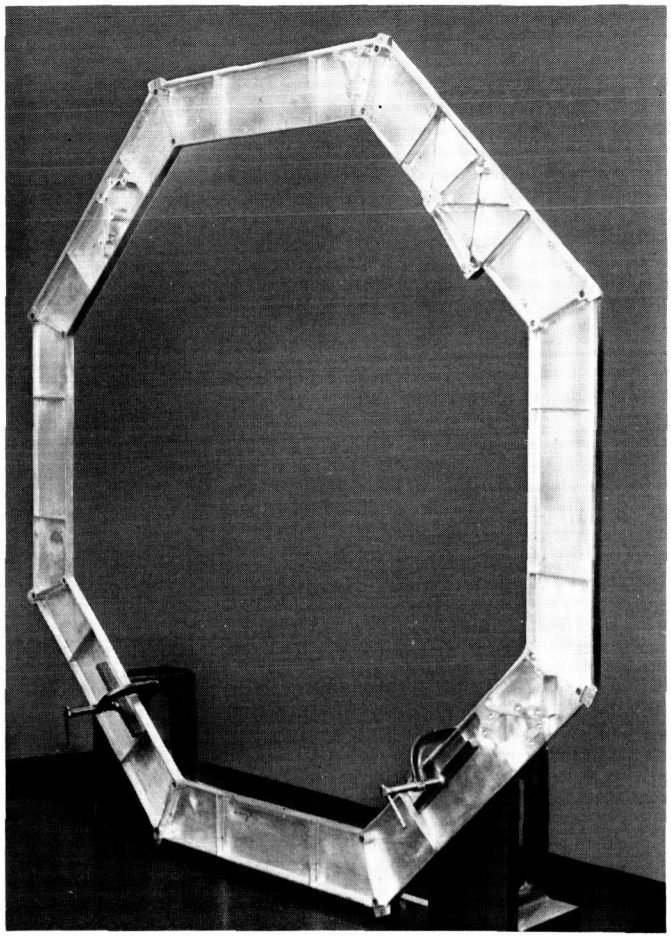


Fig. 35. Octagon structure lower ring

During assembly, test operations, and shipment, the spacecraft was attached in a similar manner to a support structure called a universal ring (U-ring). However, because the U-ring structure was stiff, the spacecraft structure was forced to deform to the highly controlled U-ring dimensions.

The upper and lower rings are attached to the longerons by means of four bolts at each longeron—two through the bottom ring, and two through the top ring. The rings are also riveted to the longerons for additional strength.

Because the electronic packaging techniques were integral with the structural design, temporary shear panels had to be attached to the exterior of the bays to prevent the structure from tending to parallelogram. These shear panels were installed whenever the electronic assemblies were removed.

The top ring contains mounting and indexing surfaces for the Sun-sensor pedestals and brackets for mounting the Trapped Radiation Detector, the Solar Plasma Probe, and the absorptivity standard. The solar panels are mounted to rod-end monoballs at each of the inner corners of the top ring. These rod ends also attach the longerons to the upper ring. The superstructure is mounted at four corners of the inboard portion of the upper ring. The peripheral structure of the top ring is basically identical to the lower ring, except for the feet on the lower ring.

b. Secondary structure. The top ring contains eight T-section spokes that extended radially inboard to a central hub. This spoke arrangement is the upper part of what is called the secondary structure. This structure is stiffened torsionally in three ways:

1. The spokes are offset at the center from the center hub, to react the torsional loads in tension and compression rather than by bending.

2. The circular-cable trough structure is bolted to each of the spokes, which increases the ring torsional rigidity and achieves some stiffening of the T-sections.

3. A channel to support the base of the low-gain antenna extends from an area near the outboard edge of the top ring to an adjacent spoke in the area immediately outboard of the cable trough.

In addition to the spoke structure of the top ring, the secondary structure consists of a central tube, which is mounted inside the upper-ring central hub, Fig. 36 (a), and an H-frame structure, Fig. 36 (b), through the center of which the lower end of the central torque tube is mounted. The central torque tube contains bearings on each end that support the science platform structure. The science platform structure was restrained during the boost environment by a pyrotechnic pinpuller that is mounted on the base of the H-frame structure. The dual attitude control system gas bottle and regulator support plates are mounted to the H-frame. Each gas bottle is mounted on an equipment plate; this plate is bolted to the open part of the H-frame on three sides. The fourth side of the plate is composed of a flange that provides the necessary stiffness for and mounts the regulator. With the attitude control gas system installed, the H-frame became a rectangular shear web with the central torque tube running through the center.

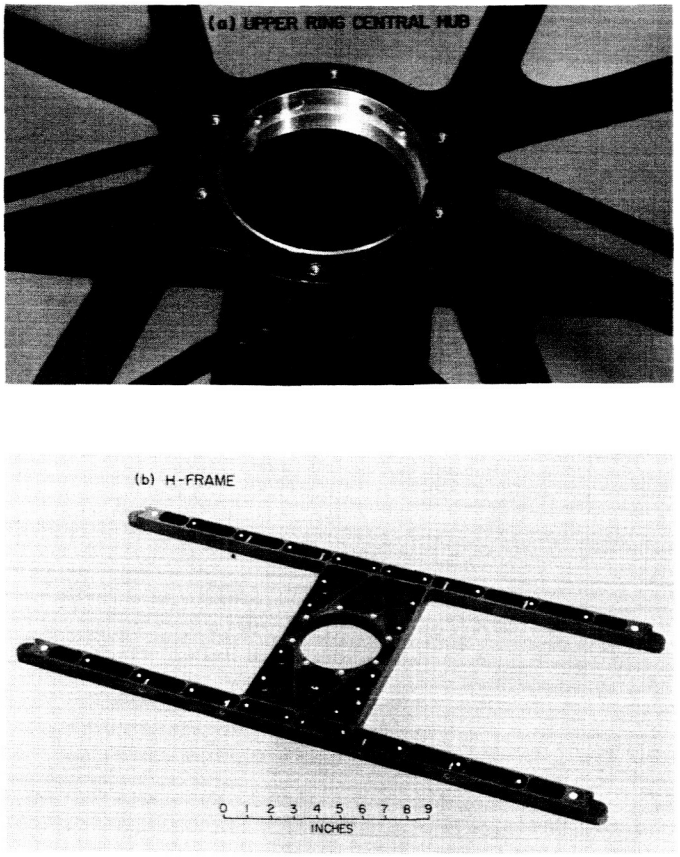


Fig. 36. Octagon structure

Twelve truss tubes are included to attach the corners of the H-frame structure to the top ring and to the primary structure. Four stiffening tubes, running from a corner of the H-frame assembly to the area of the upper-ring hub, react the H-frame transverse loads into the top-ring structure. These tubes can be only ½ in. in diameter, since they miss the attitude control gas vessels by only ⅛ in. Each of the four corners of the H-frame structure is attached in a wishbone fashion to the top and bottom of the primary structure longerons by two ⅝-in. diameter swaged tubes. These tubes provide transverse restraint for the secondary structure.

2. Detailed Design

During the early phases of the design effort, preliminary layouts were used to fabricate a full-size mockup. This mockup allowed the design to be seen in three dimensions, and enabled gross geometric incompatibilities and detail fabrication and assembly problems to be brought to light. During the detailed design, three areas were under constant scrutiny:

1. Detailed parts were designed to be readily fabricated. The machined rings, for example, were designed to be machined by standard profile techniques with a minimum of setups. The need for undercutting during machining was eliminated whenever possible.
2. The structure was designed to be fabricated with a minimum of assembly tooling and machining. Wherever possible, the final surfaces were held dimensionally on the detailed parts. The most critical tolerance was that specified for the flatness of the upper and lower rings: 0.010 in. in 54 in. The dimensional relationships between the rings and the longerons were held to ensure that they would mate when assembled, and that the electronic chassis would readily mount to the spacecraft. Mechanical alignment tolerances between critical surfaces were held on the piece parts to minimize the final assembly time and any hazardous machining operations required on the assembled structure.
3. Weight was reduced wherever possible. Minimum-gauge materials were specified on the drawings, and machined parts were designed to minimize the material remaining around attach points. For example, machined bosses were radiused rather than left square. This effort saved about 4% of the basic structural weight. Additional weight was saved because excess material was not required for machining operations after final assembly.

3. Material Selection

The material selected for the top and bottom rings, longerons, and H-frame was forged magnesium. It was selected over aluminum, steel, and other magnesium materials because it has the following attributes:

1. Nonmagnetism
2. Larger allowable tolerance for given allowable weight variations
3. Less weight for the same size fillet radii
4. Less weight required for superficial, nonstructural bosses
5. Ease of machining
6. Ductility
7. Grain flow
8. Strength
9. Dimensional stability

The other structural members were designed to be fabricated of aluminum: 6061-T6 was selected for all tubes, and 2024-T4 was used for the tube fittings.

4. Forging Process

After the material had been selected and the design had proceeded to the point at which the forging-billet requirements had been established, several vendors were requested to bid on forging the magnesium with the following minimum guaranteed properties:

$S_{\text{compressive yield}} = 20 \times 10^3$ psi, short transverse

$S_{\text{tensile yield}} = 26 \times 10^3$ psi, radial or longitudinal
$= 19 \times 10^3$ psi, circumferential or long transverse

$S_{\text{tensile ultimate}} = 42 \times 10^3$ psi, radial or longitudinal
$= 37 \times 10^3$ psi, circumferential or long transverse

Only one vendor was willing to produce all forgings with the required guarantee of physical properties; the parts were forged from cast ingots of ZK-60A. They were tested for physical properties and chemical composition before the forging process began.

A 50,000-ton forging press was used for the large pancake ring forgings, and smaller presses were used for the longeron and H-frame forgings. A closed-dye forging was made for forging the large billets because of the ultimate material strengths required. To obtain the necessary properties, the billets had to undergo large amounts of metal working.

The materials were forged at a temperature of approximately 675°F, had a minimum of 10% cold-working, and were solution heat-treated at 300 ± 10°F for 24 hr.

After forging operations, the billets were chemically acid-etched to inspect for cracks and to preserve them during ultrasonic inspection. The billets were ultrasonically inspected to Mil-Std-271, Class A, and were guaranteed to Class B. After ultrasonic inspection, pieces were removed from each forging and tested by the forging vendor.

After arrival at JPL, the billets were Blanchard-ground on two large parallel surfaces, stress-relieved for 4 hr at 300°F, and subjected to ultrasonic- and fluorescent-penetrant inspections.

During that period, the detail design of the spacecraft octagon structure was still in process. Some design changes were prohibited because of the dimensional restrictions imposed by the overall forging dimensions from which the octagon piece-parts were to be machined.

5. Piece-part Fabrication

The aluminum piece-parts were fabricated by standard techniques. The most complex portion of the piece-part fabrication was that associated with machining the magnesium forgings. The upper ring, lower ring, and H-frame were designed so that most of the machining could be accomplished with straight-plunge milling and simple lathe operations. The large upper and lower rings presented a problem in clamping and handling because of their flexibility and thin web sections. The longerons were not as straightforward in their design, but they did not present any unique fabrication problems. Extensive tooling was used to minimize scrappage and to ensure that the final parts would pass inspection.

Two vendors were selected to machine the first rings because the schedule dictated that good parts had to be machined in a short time. The choice of two vendors increased the chances of receiving good parts early. The vendor that produced acceptable parts on schedule at the lowest cost was given the contract for machining the remaining parts. After rough machining, the first parts were subjected to a stress-relieving operation at 300°F for 1 hr, and were fluorescent-penetrant inspected for cracks. Later, the parts were stress-relieved for 4 hr. After the final machining, the parts were again penetrant and dimensionally inspected. The magnesium parts were given a Dow 7 treatment to protect against corrosion and to provide a base for paint that would be applied later over much of the structure. In the areas of the final structure that were not painted, the Dow 7 treatment provided the proper temperature control surface properties.

6. Final Inspection and Assembly

The octagon was built in the JPL sheet metal shop and was assembled on the spacecraft-handling U-ring. The lower ring was mounted to the U-ring and restrained by the U-ring shoes. The eight longerons, which were machined in matched sets of eight to obtain a constant overall height, were bolted to the bottom ring with two close-tolerance bolts. The top ring was then bolted on

top of each longeron by a solar panel rod end and a close-tolerance bolt. After the top ring had been rotationally aligned to the lower ring, the rings were riveted to the longerons.

The center torque tube was then placed in the center hub of the top ring and aligned to the base reference plane, the spacecraft structure/U-ring mounting surface. The H-frame was mounted to the center tube and aligned parallel to the base reference plane and rotationally to one of the bay surfaces. The center tube was then riveted to the top ring and to the H-frame. With the H-frame in place, the twelve tubes and fittings, which restrained the H-frame, were located, and pilot holes were drilled. The four tube fittings that attached to the longerons were placed inside the swaged tubes and were riveted with aluminum rivets. The other eight fittings were placed over the tubes and attached with blind rivets. These fittings were designed to present a flat exterior surface for the rivet-driving gun to bear against. This feature reduced the possibility of the rivet being driven off center and coming loose. Miscellaneous brackets and pads were bolted, riveted, or bonded in place to the top and bottom rings.

Matched drill jigs were used to drill close-tolerance holes for the electronic chassis, the battery, the midcourse motor bay shear web, and the attitude control gas bottle equipment plates. These items were mounted with female fasteners called press nuts, which were used in lieu of nut plates. They had the advantage of being rapidly and easily installed; they were nonmagnetic; they were capped to prevent thread chips from falling out during the many hardware-installation and removal operations; and they presented steel side walls to the male fastener. This latter feature eliminated the possibility of the bolt threads tapping the softer magnesium material causing chips or loading up the screw threads, which happens when nut plates are placed on the backside of a mounting surface. The press nuts also had the advantage of being replaceable; they could be drilled out and replaced with another press nut that could be bonded to the magnesium parent material.

Titanium bolts were used to assemble the structure and to mount all the spacecraft structural components. The use of titanium saved about 3 lb of spacecraft weight. It was found that the softer titanium screws galled when they were threaded into deformed-thread locking nuts. These nuts had been deformed to provide the proper locking torque with hardened steel screws. New nuts that were less deformed, but that still provided the necessary locking torque, were procured for use with the titanium screws.

After the octagon structure was assembled, it was moved to the paint shop where the temperature control paints were applied and the Dow 7 surfaces touched up with Dow 17.

The structure was thoroughly inspected after assembly with the ground-handling shear webs in place (Fig. 37). All drawing tolerances were met and the critical alignments were recorded for future reference. The only additional machining that was required was the four close-tolerance bolt holes for mounting the PIPS substructure.

7. Special Handling Equipment

The spacecraft structural design complicated the ground-handling operations. As stated previously, shear webs had to be bolted over the outside of the bays to keep the structure from tending to parallelogram when the electronic chassis were removed.

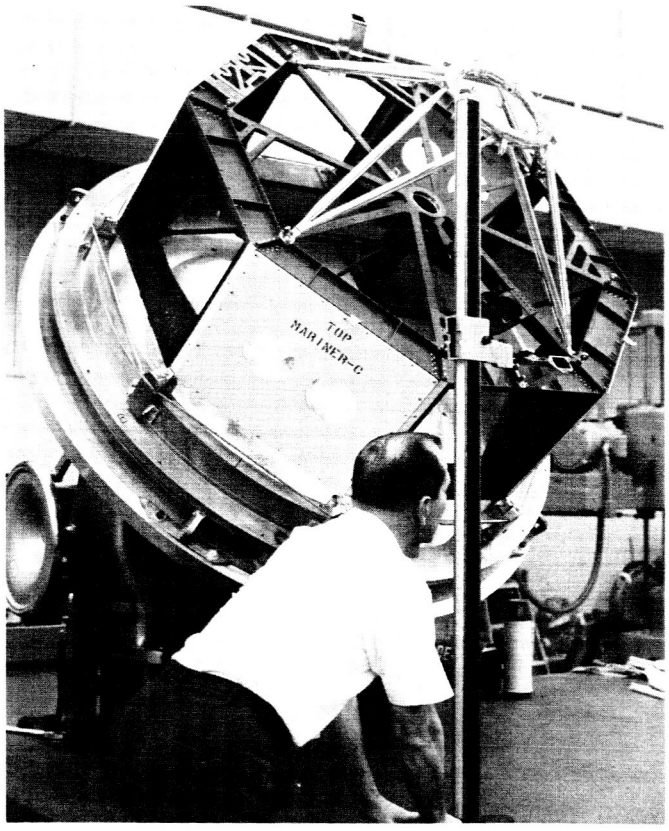


Fig. 37. Octagon structure final inspection

During all the handling and shipping operations, the spacecraft was mated to the U-ring. The U-ring was exceptionally stiff in order to restrain the spacecraft structure. When the spacecraft was moved, the lifting sling had to be attached to the U-ring. In the few cases when the spacecraft was lifted from the U-ring, the hoisting cables were attached to lifting straps bolted to the outboard edge of the longerons. These pickup points were used when the spacecraft was lifted to be mated to the LMSC adapter for vibration tests, matchmate tests, or flight mating operations. The only times that the spacecraft was not on the U-ring or on the LMSC adapter was during the space-simulator tests, during the spacecraft weight and CG operations, and during the SMIT tests.

The electronic assemblies that were installed in the octagon structure weighed 40 to 50 lb. Because the chassis were flush with the octagon structure, a special handling frame (Fig. 38) was required to support the assemblies when they were inserted in the octagon.

This handling frame consisted of a hinge support that was hard-mounted to the octagon longerons. It also contained a double-hinge arrangement that allowed the chassis to be inserted straight into the octagon opening. When the chassis was removed from the octagon, the chassis handling frame could be lifted out of the hard-mounted half of the hinge, and the electronic chassis carried to a work bench or installed in the chassis handling frame.

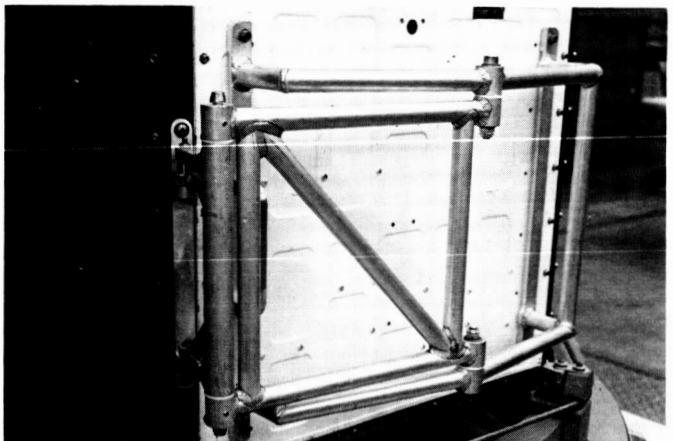


Fig. 38. Electronic chassis removal fixture

B. Superstructure

1. Function

In order to support the equipment required above the top of the octagon structure, an additional structure, the superstructure, was needed. This superstructure supported: the high-gain antenna; the solar panels through their boost dampers; one low-gain antenna damper; the Cosmic Dust Detector; the upper thermal shield; and a central retarder and cables for controlling the opening speed of the solar panels. Of these, the last was not required because of a late change in the design; however, the superstructure was built to accommodate it.

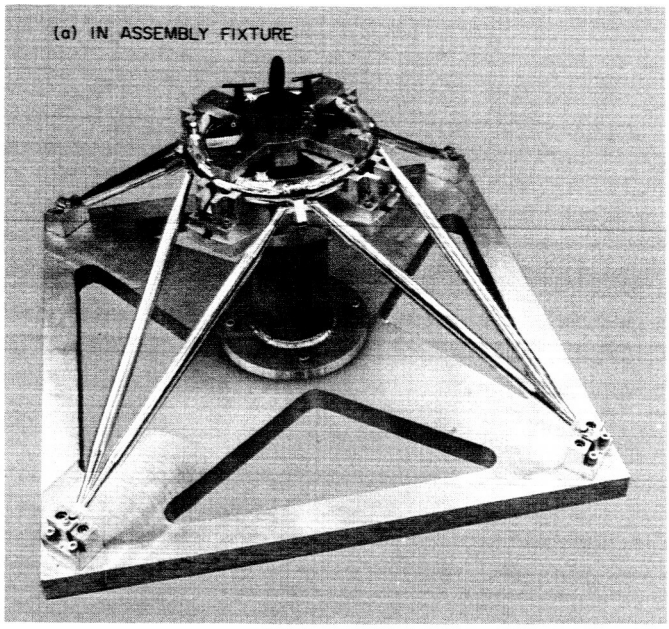
2. Description

The superstructure is shown in its assembly fixture in Fig. 39 (a) and attached to the octagon in Fig. 39 (b). It is an eight-membered, welded, aluminum truss with a formed top ring for mounting the antenna, and four feet at the base for attaching to the octagon structure.

3. Fabrication

The truss ring was formed from 1⅝ outside diameter by ⅛-in. wall tubing, bent to a nominal 5.36-in. radius in half rings. The ring halves were then machined and welded to form a complete ring. Four types of ring fittings were machined to be welded to the ring for the next assembly. They consisted of high-gain antenna support pads, solar panel damper clevis fittings, solar panel damper clevis and truss tube fittings, and a low-gain antenna damper fitting. All fittings were machined from 6061-T6 aluminum, and were then annealed prior to welding. Each fitting was made with sufficient extra material to allow for machining to required dimensions after welding.

The ring weldment and fittings were tack-welded in a fixture (Fig. 40) in a heated environment (hot plate and photo flood lights), then removed from the fixture and finish-welded in the heated environment. After welding, all welds were radiographically and fluorescent-penetrant inspected. If unacceptable defects were present, they were removed by grinding and, subsequently, reinspected radiographically to ensure removal of the defect. Once the defects were removed, the part was rewelded and reinspected. This cycle was reiterated until the part was free of rejectable defects (cracks, chain porosity, sharp porosity, inclusions, nonfusion, and poor penetration) or was scrapped. After heat-treating, the radiographic and dye penetrant inspection was performed again. If the part was still acceptable, it was continued through its processing. If defects were noted,



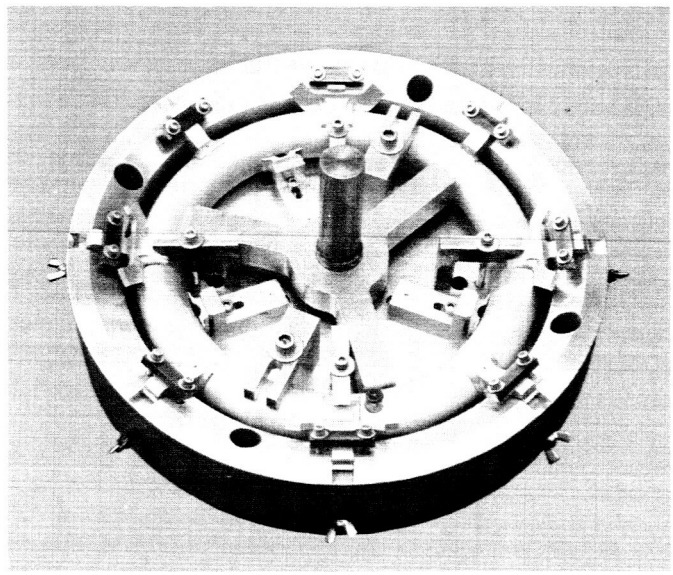


Fig. 40. Superstructure ring in welding fixture

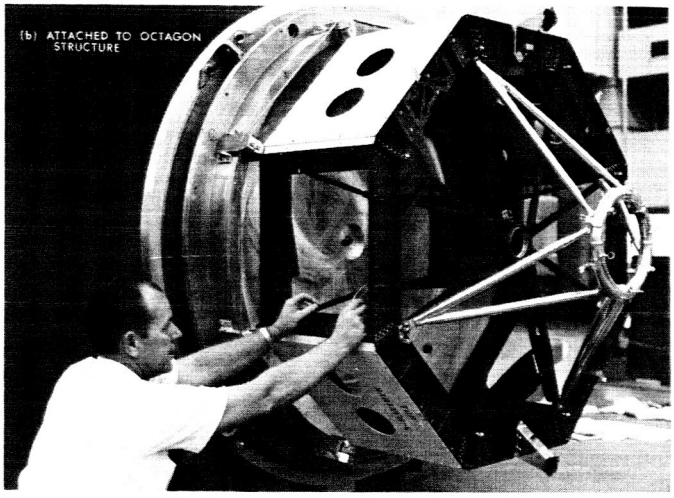


Fig. 39. Superstructure

the process described above was reiterated. After heat treating, the truss-ring weldment was chemically milled to reduce the tube wall thickness from 0.058 in. to 0.040 (+0.005/−0.000) in. This process removed approximately 1 lb from the ring and left sufficient material to be structurally adequate. The part was then machined, inspected, and polished to prepare it for the next assembly.

The truss strut tubes were formed from 1 in. in diameter by 0.035-in. wall aluminum tubing (6061-0). The ends of the tubes were swaged to 0.590 in. to minimize the size required for the end fittings. After swaging and treating to the 6061-T6 condition, the inside diameter of the swaged ends was honed to remove inclusions and imperfections due to the forming process. The tube ends were then fluorescent-penetrant inspected and machined. After the tubes were polished and inspected, they were ready for final assembly.

Final assembly welding took place in the welding fixture shown in Fig. 40 (a). The truss-ring weldment, eight strut tubes, and four feet were tack-welded together in the fixture and then finish-welded in the free state. The welds were then radiographically and fluorescent-penetrant inspected. If rework was required, it was performed in the same manner as that described for the truss-ring weldment. When all welds were acceptable, the assembly was replaced in the welding fixture and stress-relieved. After stress-relieving, the assembly was placed in another fixture, similar to that used for welding, and machined to final dimensions. Following final machining, brackets were riveted on, press nuts were installed, polished surfaces were touched up, and the assembly was inspected.

The *Mariner* Mars spacecraft superstructure performs a complicated structural function. Because of this function, it lends itself to a welded design that presents some fabrication problems. Due to the tight schedule, these problems were more binding than they would have been under more leisurely circumstances. Not enough time was available to develop optimum solutions or redesigns. However, all parts were delivered on schedule, did the job, and were lightweight (3.1 lb).

C. Solar Panel Structure

1. Description

The solar panel structure for the *Mariner* Mars 1964 spacecraft consists of a rectangular corrugated plate, or substrate, supported by a pair of parallel longitudinal beams, or spars. The corrugated plate is constructed of a flat skin reinforced with 0.5-in.-deep symmetric lateral corrugations. The photovoltaic solar cells are bonded with a silicone rubber adhesive to the flat side of the corrugated plate. Dimensions of the panel, 71.4 × 35.5 in., were selected to allow use of a modular cell arrangement throughout, thus optimizing solar cell packing density and minimizing cabling and wiring weights. In order to minimize total weight, modularized substrate structural schemes were avoided, since these systems generally involve increased weight associated with redundant structure, additional fasteners, and overlapping splice joints.

At the inboard edge of the panel, the parallel box-section spars terminate in clevis hinge fittings. These hinge fittings connect to matching rod-end bearings on the spacecraft bus. A second pair of spacecraft-to-panel attachments is provided at approximately the third point of the spar by a pair of damped spring struts. Thus, the panel structural scheme may be described as a damped, elastically supported cantilever system. To minimize the mechanical transmission of vibratory energy from the spars to the delicate corrugated substrate, the longitudinal spars are located at approximately the nodes of the free–free lateral substrate. This decouples spar and substrate dynamic responses. Intercostals, diagonal cross braces, and an outboard end beam were provided and installed between the spars to give torsional rigidity to the structure as well as to provide mounting surfaces for certain ancillary hardware items (i.e., attitude control plumbing, gas jets and solar pressure vane assemblies). When the aerodynamic shroud separation scheme changed from a clamshell to an over-the-nose separation (in late 1963), a pair of elastically supported guide rails was installed on the already fabricated solar panel flight hardware. These rails were provided to protect the solar panels from possible impact and damage by the shroud as it was ejected from the launch vehicle.

2. Design Evolution

a. Configuration and preliminary design. Configuration development of the solar panels was closely coupled with the configuration development of the primary spacecraft. This resulted from the large panel area requirement for the *Mariner* Mars 1964 spacecraft. A Sun-oriented, planar solar array of rectangular planform was selected for maximum gross solar panel efficiency and simplified cabling. An early structural concept of this array consisted of doubly articulating (folding) rectangular pairs of panels latched together above the center of the spacecraft in an A-frame fashion. This concept was rejected because it failed to allow sufficient room for packaging the spacecraft antenna systems.

The next configuration considered was the four-panel system adopted for use on the final spacecraft. For the launch phase, a number of latching concepts were developed around the basic four-panel arrangement. Among these were: the tip-corner latch concepts with and without damping elements; the cross-tied concept with spring-back tie rods diagonally across the undeployed outboard panel tips; the intermediate damper-support strut concept; and the intermediate damper-support strut concept with preloaded tip bumpers. The intermediate damper-support concept was selected from these candidate schemes for the following reasons:

1. Enough experience and knowledge existed concerning the response of intermediate damper-supported panel systems from *Mariner II* and *Ranger* to make it feasible.
2. Intermediate damper supports were considered to be more effective in attenuating a broad range of resonant conditions, whereas tip dampers were considered to be effective in attenuating only the lowest resonances of the panel.
3. Tip dampers would have required the location of excessive quantities of hardware at the panel tips (dampers, pyrotechnic devices, additional structure, and additional end fittings).
4. The synergetic response characteristics of the damped tip-latched panel structure could not be determined analytically without inordinate analytical effort. This was in contrast to the rather straightforward, but nonetheless lengthy, analytical task for a single panel on intermediate damper supports.

b. Design constraints. One of the most critical constraints upon configuration selection and detail design was a stringent weight limitation. This weight limitation dictated a radical departure from past solar panel structural designs. The highly reliable panel structures of the *Ranger* and *Mariner* Venus 1962 programs had to be abandoned in favor of a new structure of approximately half the weight per surface area (Ref. 20).

The initial design met and surpassed the minimum goals of 0.50 lb/ft^2; however, as the program evolved, the weight of the panels grew somewhat. A comparison of solar-oriented planar structural weights for all past JPL space programs is shown in Table 20, which does not include the weights of attitude control devices installed upon the panels.

Table 20. Comparative JPL solar panel systems

Program	Total area ft^2	Panel area ft^2	Structural weight per ft^2
Mariner A	39.4	19.7	1.10
Mariner B[a]	94.0	23	1.08
Mariner II	24.4	12.2	1.15
Ranger VII, VIII, IX	24.4	12.2	1.2
Mariner III, IV	70.4	17.6	0.58

[a]Fold-out panels only, fixed panels not included.

The rectangular shape of the four panels per spacecraft led to a rather restrictive limitation upon dynamic motion at the outboard tip of the panels. This limitation was equally critical with respect to the shroud and to the adjacent panels. One of the primary reasons for selecting and using damped support struts for these panels was to attenuate dynamic excursions minimizing the required dynamic envelope. The secondary objective was to reduce induced dynamic loads. Because of the lack of inertial symmetry in equipment installed on the panels, torsional vibration modes and torsional stiffnesses became as important to the dynamic envelope problem as the flexural stiffness properties of the panel.

c. Design and fabrication contract. A subcontractor was selected to perform detailed design and fabrication of the 32 solar panel assemblies required for the *Mariner* Mars 1964 program. Severe scheduling limitations were forced upon the subcontractor by the long lead time nature of the total photovoltaic power system fabrication and qualification effort.

d. Substrate selection. The restrictive weight limitation caused rejection of many potential structural schemes. Two competitive sections were finally considered: a honeycomb of low-density core, and a corrugated sheet. The corrugated sheet was selected over the low-density honeycomb primarily for thermal reasons. Conductive paths from front-surface absorption to back-surface heat rejection were far superior with the corrugated sheet concept. Also, the open-backed corrugated sheet allowed good working access when repair for modification work—such as addition of grommets, cabling fasteners, inserts, clips, rerouting cables, or straightening shear webs—became necessary. A third feature is that visual inspection and quality control of workmanship and/or damage was feasible with the open-backed corrugated sheet and was not possible with a honeycomb sandwich construction.

To satisfy the weight constraints and stiffness requirements of the design specification, the contractor developed 0.5-in. thick corrugation of aluminum alloy having a facing skin thickness of 0.005 to 0.0055 in., and a corrugation thickness of 0.0035 to 0.0040 in. The crowns and troughs of the corrugations were 0.3 in. in width, and the overall corrugation had a pitch of 0.9 in. Approximately half of the material in the inclined webs of the corrugations was removed by circular flanged lightening hole perforations.

e. Structural attachments. Previous contractor-fabricated corrugated solar panel structures used by JPL incorporated spot-welding as the primary skin-to-corrugation attachment. With the extremely light-gauge material selected for the *Mariner* Mars 1964 panels, spot-welding became a questionable technique. Early in design, sample segments of the proposed spot-welded substrate construction were subjected to a type-approval acoustic environment. These samples failed to survive and spot-welding was therefore abandoned in favor of an all-bonded substrate construction. In all instances, the spot-welded construction failed in the heat-affected region of the parent sheet material around the spot-weld nugget. Sample segments of the all-bonded substrate construction were subjected to the same acoustic environment and showed no apparent degradation.

Attachment of the substrate to the spars posed several problems. It was recognized that the differences in substrate and spar dimensional tolerances would be sufficient to induce crippling stresses and facing skin ripples in the substrate if it were "pulled" into intimate contact with the spar. An additional problem was the absence of sufficient structural material in the lightweight substrate section to permit discrete mechanical attachments—e.g., rivets and screws. For these reasons, it was decided to bond the corrugated sheet to the parallel spars with a thick "leveling course" of epoxy bonding material. This provided continuous attachment of each corrugation cap over the full width of the spar

flange, and, at the same time, provided a noncritical region for the correction of accumulated fabrication tolerances. Considerable thought was given to the method of transferring corrugation shear forces in the region of the spar. One approach considered effective (followed on *Mariner B*) was filling the corrugation trough with a bonded shear core material; however, since it was costly and heavy, it was rejected. A rather marginal approach was selected that allowed the shear to be carried completely by the perforated and flanged inclined substrate webs.

f. Prototype panel tests. The first hardware item delivered to JPL was used for the development and perfection of quality assurance inspection techniques, for preliminary structural dynamic tests, and for mechanical component compatibility or matchmate checks. These tests demonstrated that the ultrasonic bond inspection immersion procedure was incompatible with the magnesium spar hinge fittings and the several different aluminum alloys used for intercostal details and miscellaneous fasteners. The problem involved the corrosive nature of the wetting agent used in the ultrasonic tank fluid. Sensitive materials were changed to less reactive aluminum alloys. Dynamic modal surveys of the prototype panel (Fig. 41) demonstrated that the torsional stiffness of the spars was significantly different than estimated. This led to a design reevaluation of the panel and the addition of a torsion X-brace. As was pointed out above, this torsional stiffness requirement was critical to the satisfaction of the dynamic envelope constraint.

g. Power system effects. To simplify and minimize cabling, it has been the practice on recent JPL flight programs to mount Zener diode units on the back side of the solar array, thus allowing the array structure to act as a heat-dissipating radiator for the zener diode elements of the power system. In the *Ranger*-type structure a sizable I-section member was used to provide the required thermal mass. To minimize weight on the *Mariner* Mars 1964 panel, the spars were modified in such a way as to provide adequate conductive paths to the radiating elements of the panel. Slight weight increases resulted because of spar flange material thickness increases from 0.024 to 0.032 in. This was the first example of structural design progressing to the point at which it no longer sized the component weight or thickness. The temperature control conduction path criteria controlled the skin gauge.

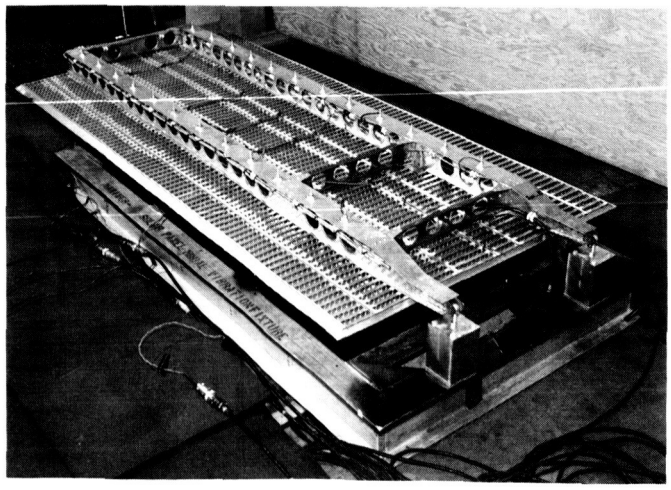


Fig. 41. Solar panel dynamic modal survey

h. Temperature control and dielectric coatings. Radiation of excess thermal energy from the rear of the corrugated substrate was enhanced by the use of a coating of black thermal control material. Since the heat radiation requirement of the 1964 Mars mission was less severe than the 1962 Venus requirement, no attempt was made to completely cover the inner corrugated surfaces with the thermal coating. This had the dual benefit of reducing weight and simplifying fabrication procedures. In the last stages of qualification testing, it was discovered that the diffused reflective characteristics of the satin-finish coating produced undesirable illumination within the field of view of the critically important Canopus star sensor. This problem was corrected on the flight panels by painting them with a glossy finish material of essentially the same type.

An 0.003-in. clear epoxy dielectric coating was applied to the flat front surface of the panel to isolate the solar cell system electrically from the metallic substrate. This dielectric demonstrated excellent resistance to concentrated pressures and heat, as might be applied by a soldering iron.

3. Fabrication

a. Frame assembly. Typical sheet-metal construction techniques were used on all except the machined aluminum-alloy hinge fittings and the damper support fittings. All flanged components at spars, intercostals, and beams were of 0.018-in. material and formed to desired configuration using hydroform stamping techniques. The component sheet parts were aligned in jigs and tack-riveted together at important locations. Removed from the jig fixtures, the tacked members were completely spot-welded. Returned to assembly jigs, the completed spars, beams, and intercostals were aligned

and then interconnected with rivets to form the composite frame assembly. All fasteners and inserts were installed in the completed frame while in the assembly jig. This phase of fabrication was free of major problems.

b. Substrate. Fabrication of the substrate and its attachment to the spar frame assembly constituted the major problems in the fabrication process. The initial difficulty was to obtain sufficient quantities of 0.0035- and 0.0050-in. material that did not contain ripples without requiring a separate and costly mill run. Other problems were: preparing the surfaces for bonding, properly laying all adhesive prior to bonding the substrate to corrugations, and controlling adhesive weight.

c. Bonding. The bonding operations of attaching the corrugated sheet stock to the skin and then to the spar frame assembly were the most sensitive and precarious phases of panel assembly. Careful preparation of each faying surface was tailored to the specific material and all previous fabrication processes. Once prepared, these surfaces were protected with specially selected adhesive tape. All handling prior to the actual bonding step took place with this protective tape in position. The actual bonding operations took place in an environmentally controlled "white-smock" bonding room.

d. Installation of doublers. During preliminary STM vehicle vibration tests, gross dynamic-buckling failures of the solar panel substrate took place. Investigation of these failures led to the fact that much of the corrugated substrate material was only about half as thick as it should have been. The reason for this may still be argued; however, it appears that the most likely causes were: (1) poor inspection technique applied at the wrong point in the process; (2) lack of engineering control over shop procedures in chemical milling and surface-etching processes. This problem was discovered too late to allow a redesign of the panel substrate, but, since the failures were of a buckling nature rather than of a strength nature, it was concluded that the addition of bonded doublers to the corrugated flange sections would suffice.

e. Installation of shroud bumper rails. The bumper rails were simple aluminum tubular rails supported on curved fiberglass springs. The tubular rails and springs were sized to withstand an impact from the *Agena* shroud and to minimize deflections so that no damage to the vital solar power system would result. The fiberglass springs were located on the spars where space existed, and mounted in such a way as to minimize shading of the zener diodes. Because of the rather uneven spacing of springs, spring stiffness constants were tailored to the individual location to provide a uniformly varying spring rate as required by the shroud impact design criteria.

4. Testing

a. Developmental testing. Developmental tests included substrate buckling and fatigue tests, a preliminary acoustic test, and vibration tests.

Substrate buckling and fatigue tests. A series of tests was conducted on sample substrates to determine the fatigue properties and the static and dynamic buckling characteristics (including fixity coefficients) of the critical unsupported substrate back corrugation flats.

Panel preliminary acoustic test. This test, conducted on the prototype panel, verified the adequacy of the all-bonded panel to survive the qualification acoustic environment. Figure 42 shows the panel in the acoustic facility.

Developmental vibration tests. Two tests were performed at assumed vibratory input levels. In the first test, the panel was supported on dampers, and in the second test the panel was hard-mounted using no dampers. The purpose of these tests was to check out the two qualification test configurations for the solar panel system. For the low-frequency high-input domain, damped supports were required for panel survival. For the high-frequency complex wave domain, dampers were eliminated for test simplicity. During the low-frequency tests, elastic buckling of certain corrugations carrying accelerometers was observed. It was found that use of even the lightest-weight accelerometers increased the inertial loads significantly. For all subsequent tests throughout the Mars 1964 program, no accelerometers were mounted on the substrate corrugations.

b. Qualification testing. The qualification tests consisted of a thermal and static-load test, a TA acoustic test, a shroud impact test, a low-frequency vibration test, and solar panel deployment tests.

Thermal and static load test. This test verified the adequacy of the panel to withstand the specified thermal and static design loads and was performed as an element of the panel design and fabrication contract (Ref. 21). The thermal–vacuum cycling tests were performed in the GD/C facility, whereas the static tests were performed in the GD/C engineering test lab.

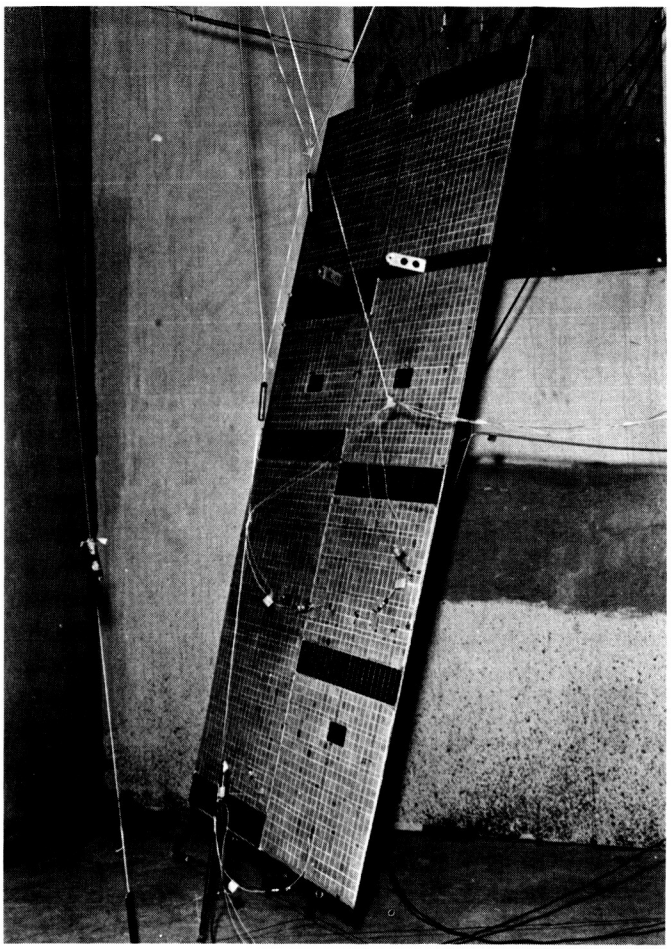


Fig. 42. Solar panel preliminary acoustical test setup

Type-approval acoustic test. This test was essentially a repeat of the previously described developmental test using a different facility. Superior spectral characteristics were attained using Ling air modulating transducers.

Shroud impact test. This test qualified the bumper rail system by subjecting a single solar panel and a pair of adjacent panels to various impacts of a pendulous mass simulating the inertial effects of the shroud. Figure 43 illustrates the test setup and pendulous mass for the two-panel phase of this test.

Low-frequency vibration test. Formal qualification of the panel damper system consisted of a low-frequency (5 to 150 cps) sinusoidal vibration test. The purpose of this test was to determine the ability of the panel to survive *Mariner* vibration environment without degradation. A second purpose of the test was to determine the frequency response characteristics of the solar panels as

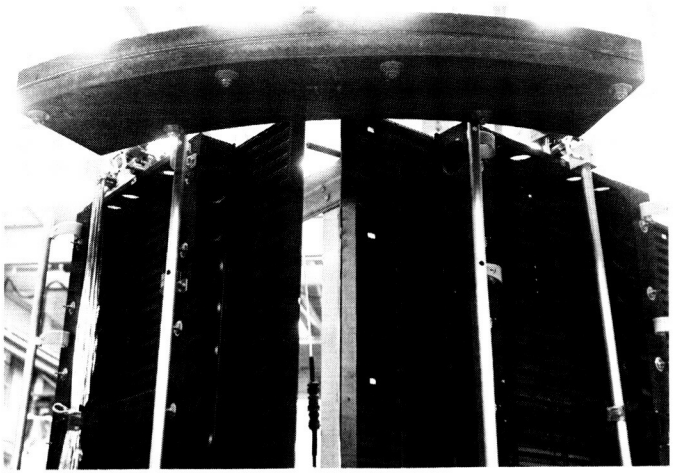


Fig. 43. Solar panel shroud impact test setup

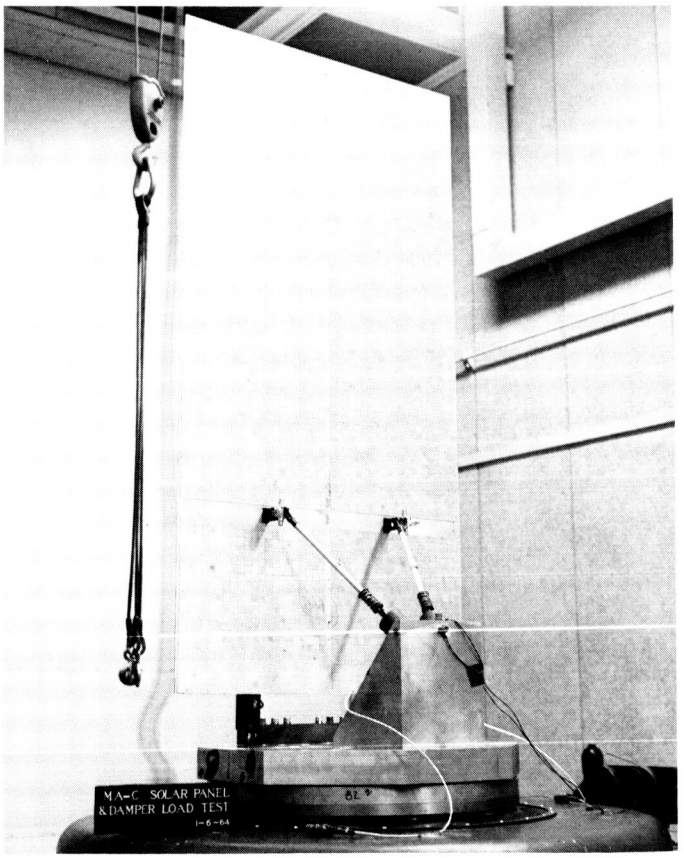


Fig. 44. Low-frequency longitudinal vibration test setup

supported upon discrete dampers in the spacecraft configuration. The input levels to the test were rather carefully developed from preliminary STM test data to envelop panel responses for the most critical spacecraft test conditions. The results of the test were satisfying;

the panel successfully passed the qualification sequence and demonstrated structural adequacy for flight purposes (Ref. 21). Figure 44 shows the setup for the low-frequency longitudinal vibration test.

Solar panel deployment tests. A complete series of tests was conducted to simulate a range of spacecraft and booster failure modes that might have affected deployment performance and hardware integrity. The tests revealed no probable failure modes or potential degradation of the hardware. Figure 45 shows a typical deployment test setup on the PTM spacecraft.

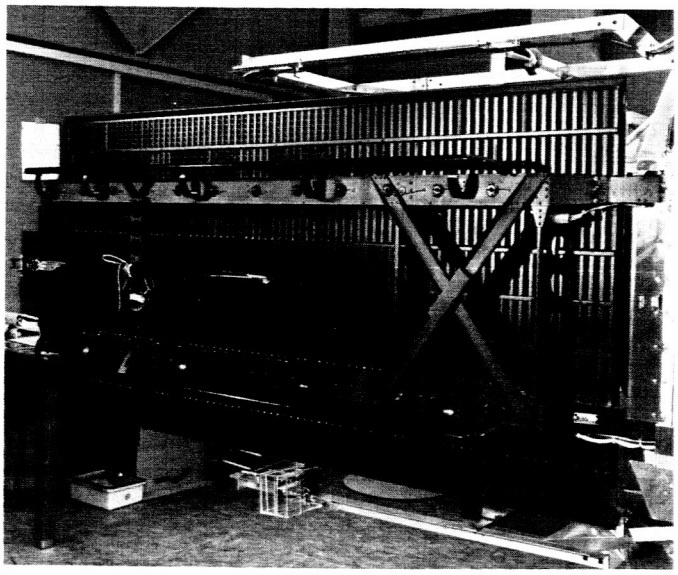


Fig. 45. Solar panel deployment test setup

D. Solar Panel Transporter

The spacecraft solar panels were shipped in special four-wheeled transport trailers (Fig. 46), which could be towed by standard vehicles, that were used for transporting the solar panels about the Laboratory, to and from vendors, to the special solar panel test site, and to Cape Kennedy.

The transport trailer enclosures were fabricated of a sandwich aluminum structure. The core material was foam-in-place polyurethane. The trailer featured a full-width rear door for easy access to the panels. Four solar panels in their handling frames could be moved inside the enclosure on special support racks; these racks supported the panels during transport and storage, and enabled exterior unloading of the panels.

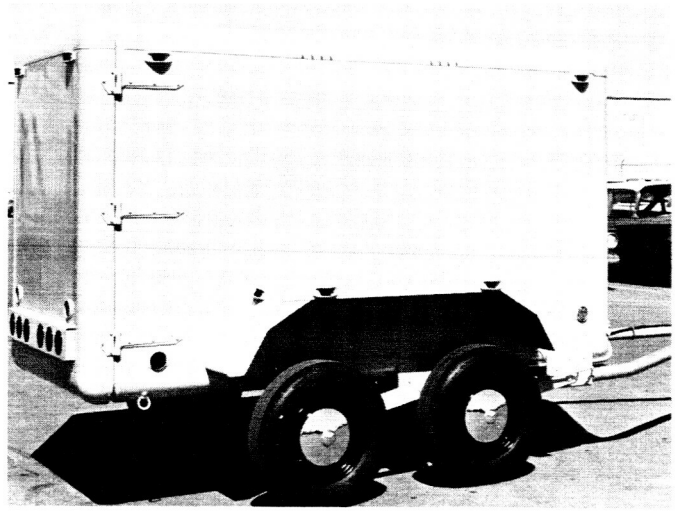


Fig. 46. Solar panel transporter

The trailers were designed to meet the temperature and humidity portions of the environmental specifications for a typical spacecraft component shipping container. The vibratory design philosophy consisted of developing a trailer and suspension system that would isolate the panels from all significant structural road shocks. To accomplish this, the enclosure was mounted on a special tandem suspension system with a nonlinear deflection curve. This suspension system along with low pressure tires eliminated the possibility of the enclosure from "bottoming out" during high transportation impacts.

Because of the particular function and character of the solar panel transporter shipping container, a special dynamic qualification test was conducted. An instrumented type-approval celled solar panel was mounted in a trailer and driven across country. The route included a number of specific road and driving conditions. It was concluded from the panel electrical performance after the test and from test vibration data that the transport trailer, when under extreme road and/or driving conditions, effectively isolated the solar panels from the transportation environment.

E. Boost Dampers

During the development of the *Mariner* Mars spacecraft, it became clear that the solar panel weight would be excessive if *Mariner* Venus 1962 type panels were used. Because of their location on the spacecraft, it appeared that the Mars panels would have to withstand more vibration than the *Mariner* Venus 1962 panels; yet, because the *Mariner* Mars 1964 needed more panel area

per spacecraft pound, heavy panel construction led to an unbearable penalty in overall spacecraft weight. These "facts of life" resulted in the use of an unconventional damped-strut support system for the panels, which protected the panels from vibration and allowed a very significant reduction in their weight.

The prototype panel was built on a very low budget out of thin-gauge aluminum honeycomb construction. Each damper was composed of two concentric tubes and a 2-mil annulus filled with hydrocarbon grease. By using this test hardware, design feasibility was verified in time to affect the flight spacecraft.

Concurrent with the development of the solar panel damped support system, another use of a heavily damped structure was investigated. In this case, not only weight but also space limitations required a very tall, slender structure for the low-gain antenna support. This structure was 7 ft tall and 4 in. in diameter. Supported by conventional techniques, it would have developed tip excursions in excess of 10 in. during spacecraft vibration qualification, and would have induced excessive loads into the spacecraft upper structure. A damped support system was proposed for the control of this slender structure, and subsequent testing indicated that the damped support system would reduce the structure's loads and excursions by a factor of more than 20. The tests were conducted on a thin-walled aluminum tube supported by concentric tube dampers described previously. A variation-of-damping-coefficient test series revealed that the structure's resonant behavior was highly insensitive to variations in damping.

From the tests described above, it was concluded that the use of damped structures would result in large savings of structural weight, and would allow the use of a desirable, lightweight, slender, low-gain antenna support structure.

1. Functional Description

a. Solar panel boost dampers. The solar panel boost dampers positioned the solar panel during ground operations and during the boost phase of the mission, and they reduced the dynamic environment as seen by the solar panel. Shortly after the spacecraft was separated from the boost vehicle, the panels were deployed by releasing one end of each of two dampers from the panel. Once the panels were deployed, the dampers served no further useful function. The solar panel, damper, and superstructure geometry are shown in Fig. 47, which illustrates two sets of development solar panels and dampers undergoing a simulated shroud-impact test.

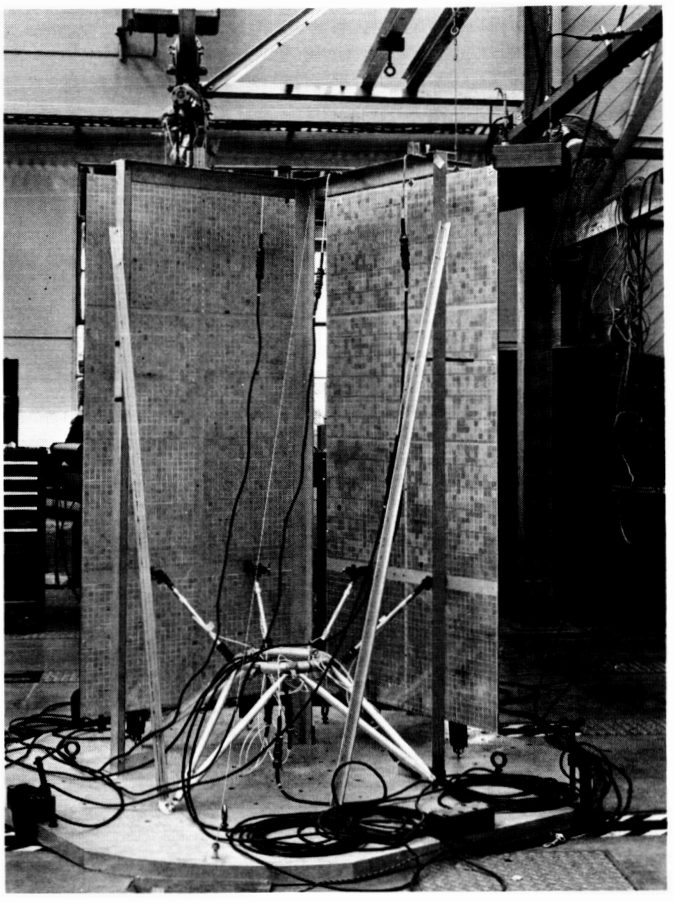


Fig. 47. Solar panel damper configuration

The damper, which consists of two spring-centered concentric tubes with the annulus filled with a silicone fluid, is attached to the superstructure at one end with an adjustable monoball rod end, and is attached to the solar panel by means of a pyrotechnic pinpuller. The adjustable rod end is used to provide solar panel alignment adjustment. The damping constant for these dampers is a nominal 15 lb/in./sec, a value chosen on the basis of test and analysis of the solar panel structure. The nominal spring rate of the damper is 185 lb/in., a value determined by the static side-load criteria and the dynamic envelope of the spacecraft. Due to the mounting geometry of the dampers, both a right-hand and a left-hand damper are provided for each solar panel; the only difference between the two is in the pinpuller mounting bracket at the upper end of the damper.

b. Low-gain antenna dampers. The low-gain antenna dampers position the low-gain antenna at all times, and

reduced the dynamic environment as seen by the low-gain antenna during the boost phase. The low-gain antenna and associated damper geometry are shown in Fig. 48, which illustrates the TA antenna unit undergoing a shock test while being supported by two development dampers. The short antenna damper is attached to a clevis on the superstructure ring, and the long antenna damper is attached to a bracket that is fastened to the bus structure at one of the solar panel hinge rod ends.

As is the case with the solar panel dampers, the low-gain antenna dampers consist of two spring-centered concentric tubes with the annulus filled with a silicone fluid. Due to the mounting geometry, the short and long dampers have different damping and spring constants; however, the damping-force and spring-force components of the two dampers, in a plane perpendicular to the antenna, are equal.

The nominal damping rate of the short damper is 5.5 lb/in./sec, and the nominal spring rate is 160 lb/in. The nominal damping rate for the long damper is 11 lb/in./sec, and the nominal spring rate is 320 lb/in. The two dampers are attached to the antenna in such a way that their center lines intersect. This prevents additional bending and torsional loads from being developed.

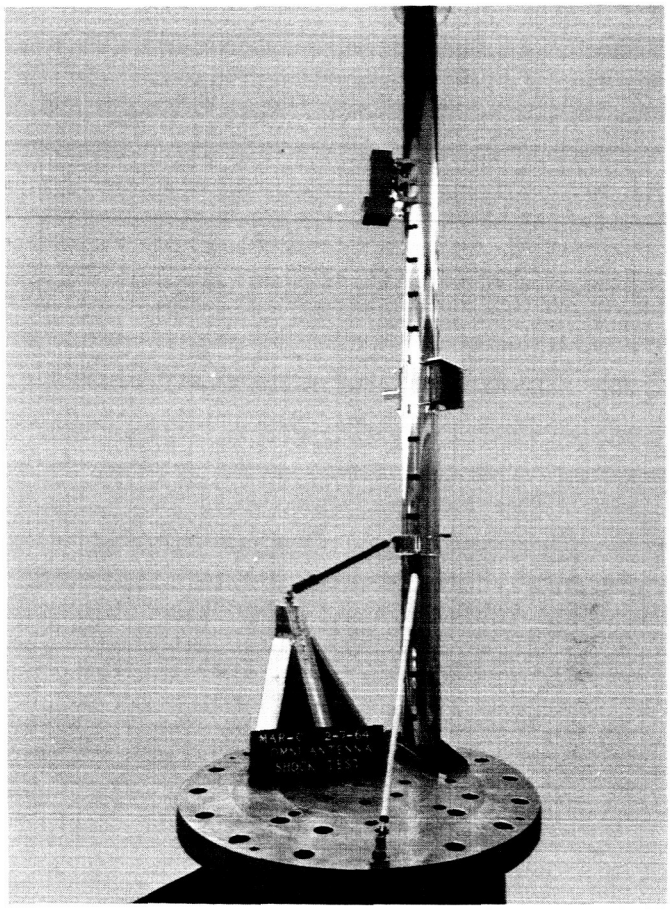


Fig. 48. Low-gain antenna damper configuration

2. Design Evolution

Since the solar panel boost dampers and the low-gain antenna dampers differ only in envelope constraints, the following discussion, while referring specifically to the solar panel boost dampers, also applies to the low-gain antenna dampers. In arriving at a final damper design, a large number of constraints were considered. Among these were: functional requirements, envelope constraints, weight limitations, strength and stiffness requirements, thermal constraints, and material constraints.

a. Functional design. The first problem that had to be solved in the damper design was selection of the damping fluid. In selecting a fluid, a trade-off had to be made between the shear-rate effects of a fluid and the temperature effects. Typical hydrocarbon oils and greases showed decreasing viscosity changes on the order of 10 or 20 over reasonable temperature operating limits, while typical silicone fluids (methyl-polysiloxanes) showed decreases on the order of 2 over the same temperature limits. The damped-structure feasibility tests demonstrated that changes in damping on the order of 2 could be tolerated without noticeable effects. On this basis, primarily, a silicone fluid was selected for the dampers. Additional considerations in selecting this fluid were its excellent high-temperature stability and its very low vapor pressure.

To obtain the desired damping rates, a highly viscous fluid was required. A fluid with a nominal kinematic viscosity of 500,000 cs was selected.

The damper is nonlinear in behavior; in fact, the damping force will be proportional to the square root of the velocity. For the solar panel boost dampers, the following dimensions were selected

$$D = 0.567 \text{ in.}$$

$$L = 9.36 \text{ in.}$$

$$\Delta = 0.005 \text{ in.}$$

A velocity of 10 in./sec yielded a damping coefficient of 16.6 lb-sec/in., which was close to the nominal rate of 15 lb-sec/in. that was specified early in the program.

The annular clearance was a very sensitive parameter in the problem, indicating that close tolerance control on this dimension was warranted. If the annular clearance changed from 0.005 to 0.006 in., then the damping coefficient at 10 in./sec changed from 16.6 to 15.2 lb-sec/in., and a decrease of the annular clearance to 0.004 in. resulted in a damping coefficient at 10 in./sec of 13.2 lb-sec/in. The damping coefficient was

$$c = 46.0\,V^{-0.51}$$

which, at 10 in./sec, is 14.4 lb-sec/in.

b. Detail design. The materials used in the design of the dampers were all common spacecraft materials. The damper tubes were an anodic hard-coated aluminum alloy. The damper spring was fabricated from beryllium copper spring stock, and the damper spring plugs were fabricated from magnesium alloy. The various tube end fittings were also fabricated from the same magnesium alloy. The fluid sealing devices were a combination of O-rings and teflon slipper seals. The various components were assembled with a common two-part heat-cured epoxy.

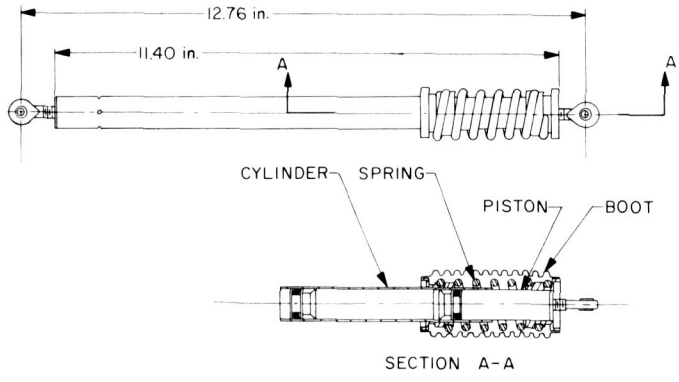


Fig. 49. Low-gain antenna short damper assembly

A mylar boot was bonded over the spring assemblies on each end of the dampers to prevent potential outgassing of the damping fluid in case the sealing device leaked. The internal volume of the damper was vented through a hole, which was directed away from any part of the spacecraft, to prevent a buildup of internal pressure during the boost phase of the launch that would tend to cause seepage of the damping fluid past the seals. With the exception of the short low-gain antenna damper, which was always in the shade of the high-gain antenna, the dampers were painted with temperature control paint to ensure their cool temperature. This also had the effect of maintaining a low vapor pressure in the damping fluid.

Figure 49 is a schematic drawing of the short low-gain antenna damper. Figures 50 and 51 show the completed flight-type dampers. It should be noted in Fig. 51 (b) that over half of the length of the damper is merely a tube to provide the required length to the damper. This tube was fabricated from unidirectional-filament epoxy fiberglass cloth, which provides a lightweight structure and a very low heat conduction path into the spacecraft bus.

3. Fabrication

All damper piece-parts were fabricated by local vendors on firm fixed-price contracts. Upon receipt from the vendor, the parts underwent all the necessary inspection procedures to ensure compliance with the applicable specifications. Accepted parts were placed in bonded stores pending assembly operations, and rejects were returned to the vendor. The actual assembly of the damper was performed by JPL technicians under close monitoring of the JPL cognizant engineer and JPL Quality Assurance personnel.

The first steps in the assembly operations were to put together the piston subassembly, the cylinder subassembly, and the spring subassembly. The spring subassembly

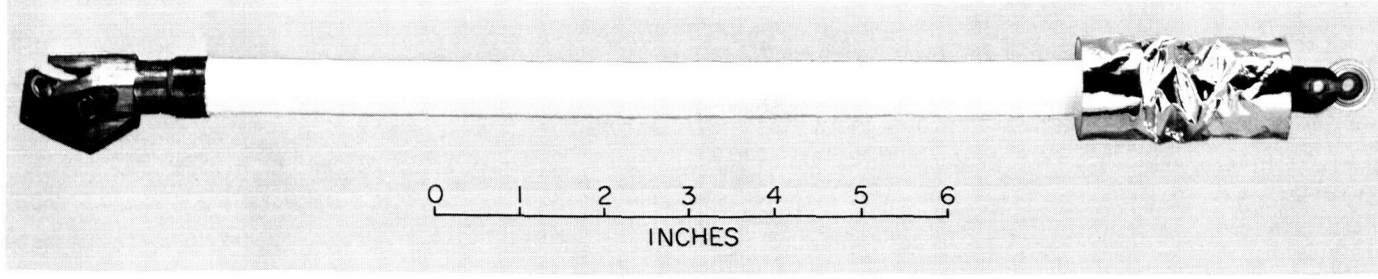


Fig. 50. Solar panel boost damper

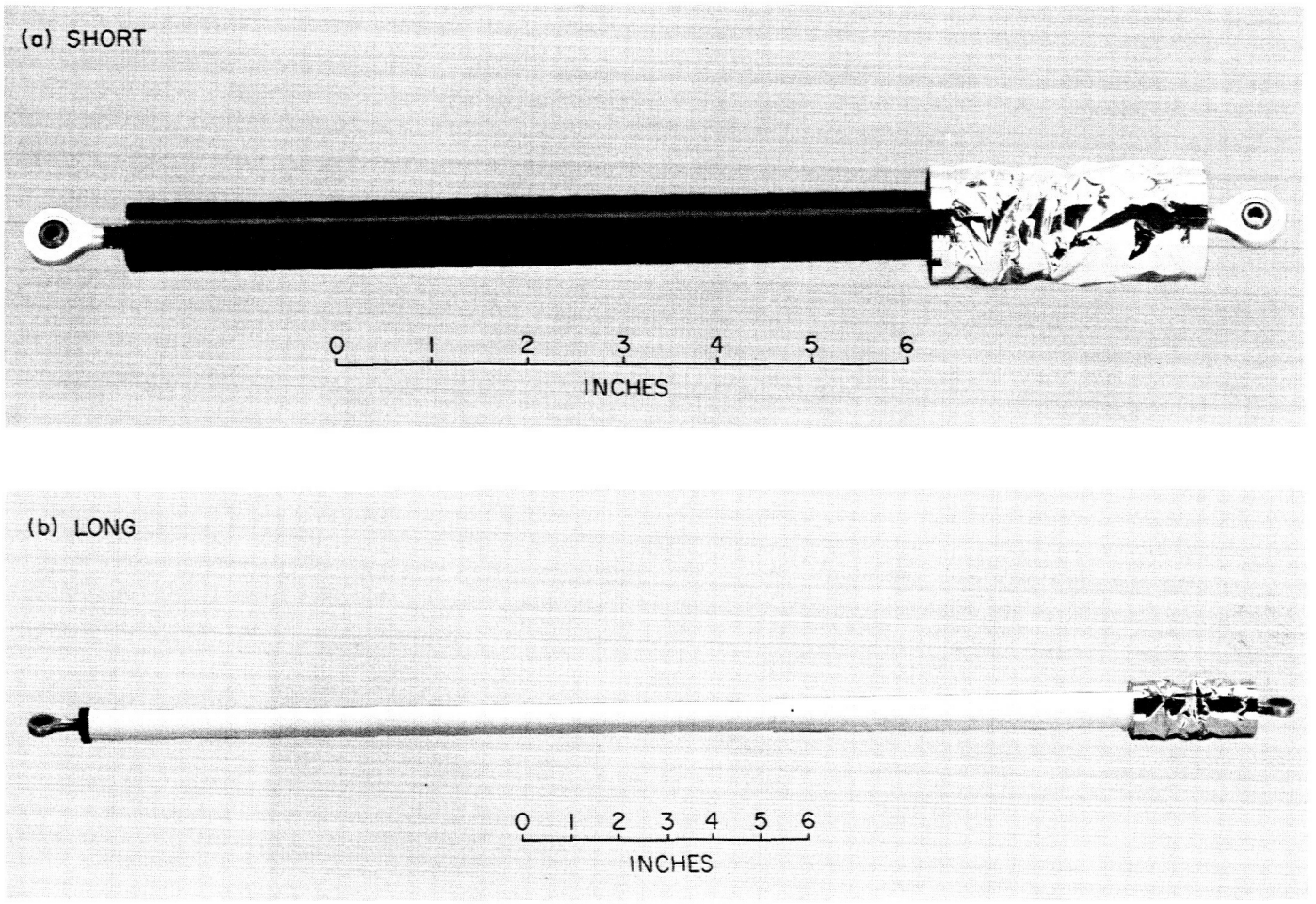


Fig. 51. Low-gain antenna dampers

was assembled by screwing the two spring plugs into the spring until the proper spring rate was achieved. The next step was to fill the damper with the damping fluid. At the completion of the filling operation, the damper was tested for proper damping properties. If the test showed that the damper was not filled properly, the damper was pulled apart, cleaned, refilled, and retested.

The final assembly operation consisted of bonding the spring assembly on the damper, applying the temperature control paint where required, and installing the mylar boot over the spring assembly. After final cleaning operations, the dampers were packed in shipping containers (Fig. 52) pending final testing operations.

4. Testing

a. General testing. The testing program for the boost dampers consisted of both functional and environmental testing. Functional testing was performed during the assembly operations to ensure a properly assembled damper. This phase was followed by environmental testing, which was also followed by a complete set of functional tests prior to SAF delivery. In addition to the functional testing described in this section, numerous functional tests involving the boost dampers were performed in various phases of development and qualification testing of the spacecraft; these were the STM vibration test series, the PTM vibration test series, the solar panel vibration tests, and the low-gain antenna vibration tests.

b. Functional testing. The functional testing of the boost dampers consisted of measuring the spring rate and the damping rate for the damper. The spring rate measurement was performed on the spring (1) as received from the vendor, (2) at the subassembly level with the spring plugs installed, and (3) on the completed damper after environmental testing. Figure 53 shows a

spring subassembly mounted in the damper spring rate tester. This device consisted of a load cell, a means for deflecting the spring, and a dial indicator for measuring the deflection of the spring. With minor adjustments, this device was used for all the spring-rate tests indicated.



Fig. 52. Shipping container, solar panel boost damper

A contract was made to develop a damper test machine to JPL specifications. This machine was to consist of a variable speed, variable displacement, scotch-yoke drive capable of a frequency range of 0 to 70 cps, and a displacement range, depending on the particular frequency, of ± 0.025 to $+0.250$ in. Figure 54 illustrates a solar panel boost damper mounted in the test machine developed. Figure 55 shows the test and control console used with the tester during the damper test program.

The test and control console provided a programmed speed control signal to the test machine that, in conjunction with the preset displacement of the test machine, provided a programmed sinusoidal velocity to the damper. The sinusoidal force signal was passed through an rms converter to obtain a dc signal to drive an *xy* plotter. The resulting plot obtained from this test setup was the rms damping force vs peak sinusoidal velocity. The test console also contained an oscilloscope for waveform monitoring and a phase meter to determine the phase angle of the damping force relative to a velocity or displacement signal. Figure 56 shows a characteristic damping curve for the solar panel boost dampers. The curves for the low-gain antenna dampers are of the same shape but of different amplitude.

c. Environmental testing. The damper TA environmental testing consisted of vibration testing, shock testing, centrifuge testing, thermal–shock testing, and thermal–vacuum testing. No problems were encountered in the TA test program.

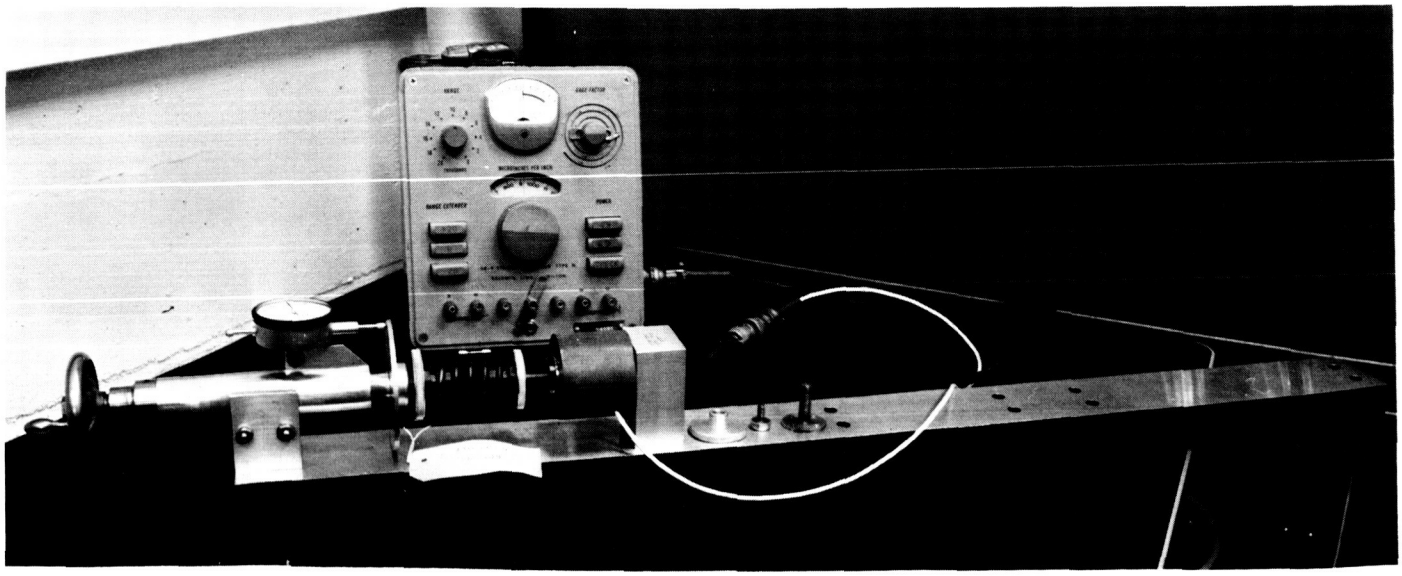


Fig. 53. Damper spring testing fixture

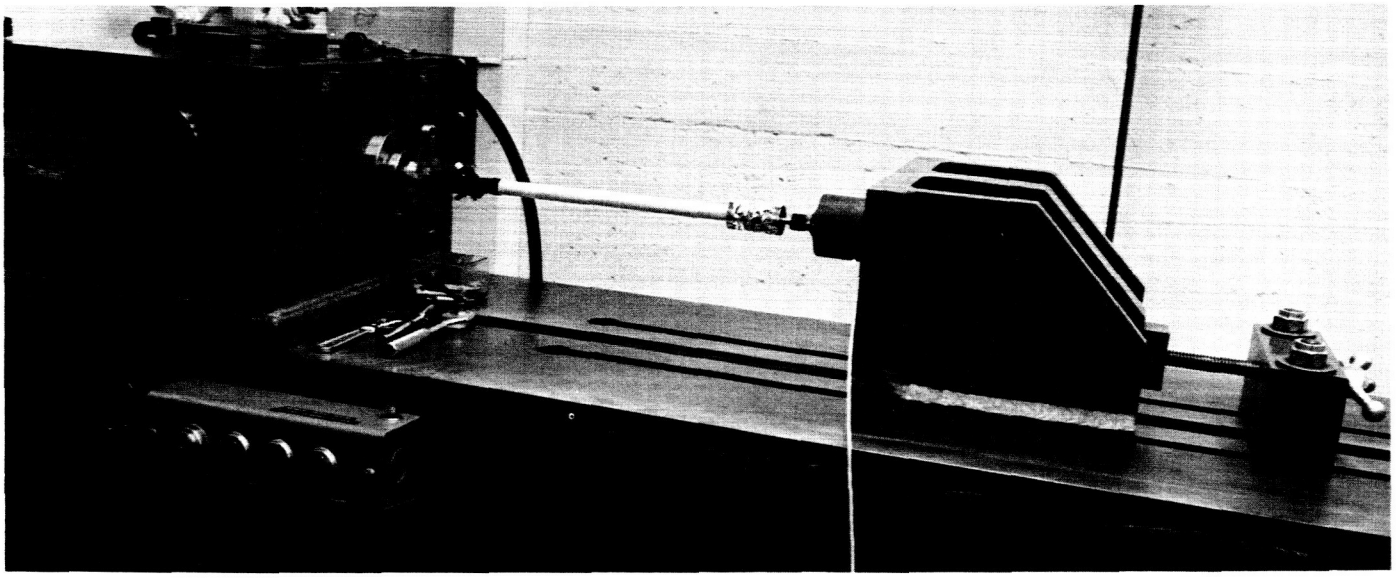


Fig. 54. Solar panel boost damper test machine

The FA environmental testing consisted of vibration and thermal–vacuum testing. Late in the development program, several solar panel boost dampers were found to have damping curves slightly out of tolerance after environmental testing. Investigation showed that this change was a result of the thermal–vacuum tests. Although the mechanism of the change was not definitely established, it may have been due to the outgassing of a low volatility constituent of the silicone fluid, albeit none was ever detected. Since the dampers had no functional requirements to provide damping after long vacuum soaks, the flight dampers were exempted from the thermal–vacuum test cycle.

F. Solar Panel Actuation System and Solar Panel Cruise Dampers

The solar panels on *Mariner* were stowed in a vertical position during launch and were deployed approximately 90 deg after booster separation in order to expose large areas of solar cells to sunlight. The panels were held in their stowed position by two boost dampers per panel. One end of the boost dampers was attached to the spacecraft superstructure and the other end was attached at a point about one-fourth of the way up the panel.

An explosive-squib pinpuller formed the interface between the boost dampers and the solar panels. After spacecraft separation from the *Agena*, these pinpullers were actuated, allowing the panels to deploy to their cruise position. Once the panels were at the cruise position, an additional requirement was imposed by the midcourse motor subsystem. To reduce panel flapping during midcourse motor burn, panel cruise dampers were required. Latches were also required to maintain contact between the panel and the cruise damper during the vibration phase of the midcourse maneuver. To move the panels from the stowed to the cruise position, a solar panel actuation system evolved as a result of various experiments and developmental tests.

1. Functional Description

a. Solar panel deployment system. The solar panel deployment system was used to move the solar panels through an arc of approximately 90 deg from the latched to the deployed position. This was to be done at a controlled angular velocity unless analysis and testing showed it to be unnecessary. Switches were actuated by each panel to indicate, via telemetry, that each panel had deployed. The switches were installed so that they closed momentarily to prevent blocking the data encoder registers from subsequent events.

b. Cruise dampers. The cruise dampers served three distinct functions during the flight: (1) they arrested the deployment motion of the solar panels; (2) they positioned the panels throughout the flight; and (3) they provided a specified dynamic coupling between the spacecraft bus and the solar panels.

The first function required that the kinetic energy of the moving solar panel be removed in such a way

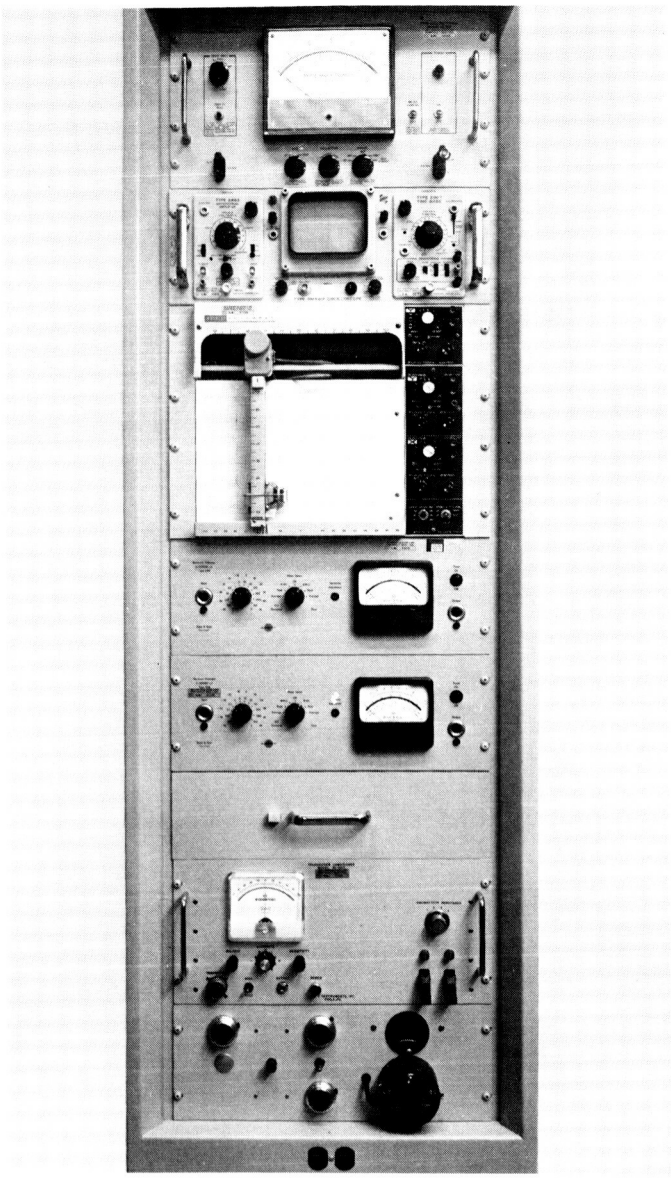


Fig. 55. Damper test console

that stresses in the panel and octagon structure be held at safe levels. It should be noted here that the kinetic energy in the moving panel is just the change in potential energy in the deploy spring, except for the very small amount lost to coulomb and hysteritic damping present in the hinges, cabling, and attitude gas tubing. The second requirement (positioning the panels during cruise) was that the panel position be adjustable over a range of −0.2 to +1.2 deg from the base reference plane. The third requirement was that the rigid body mode of the bus panel system be between 0.5 and 5.0 cps with all four panels matched within 10%, and, further, that the damping ratio in this mode be between 0.15 and 0.7 with any two panels matched within 0.1.

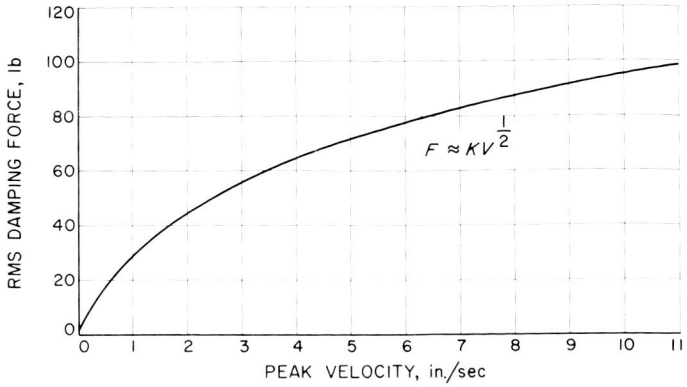


Fig. 56. Solar panel boost damper rms force vs peak velocity

The damper and latch system, which evolved as a result of the above functional requirements together with other spacecraft requirements, was a small hydraulic "dash-pot" mounted to the upper right-hand corner of each of the odd-numbered electronic cases. A mating latch was mounted on the right-hand spar of each corresponding solar panel, as shown in Fig. 57.

2. Design Evolution

a. Solar panel deployment methods. The technique of solar panel deployment for the *Ranger* and *Mariner* Venus 1962 spacecraft was a hydraulically damped linear actuator. The entire unit was self-contained, with a compression spring supplying the force to a push rod. The damping was accomplished by pushing silicone fluid through an adjustable orifice; the orifice size determined the panel deployment times. The units were similar to a conventional automotive shock absorber in both appearance and size.

At the outset of the program, there was much concern over this type of linear actuator. It was feared that the silicone fluid would leak out of the actuator during the long space flight (8+ months), contaminating the spacecraft temperature control surfaces and the optical instruments. The linear motion of such an actuator was hard to seal from the start, and the effect of long exposure to space environment on the seals was not known. A program was started to design and develop a solar panel actuator that would reduce the probability of contaminating the spacecraft with oils or other foreign materials.

Torsion-bar actuator. The first design concept considered was a torsion-bar actuator (Fig. 58), which used a beryllium copper torsion bar to supply the deployment

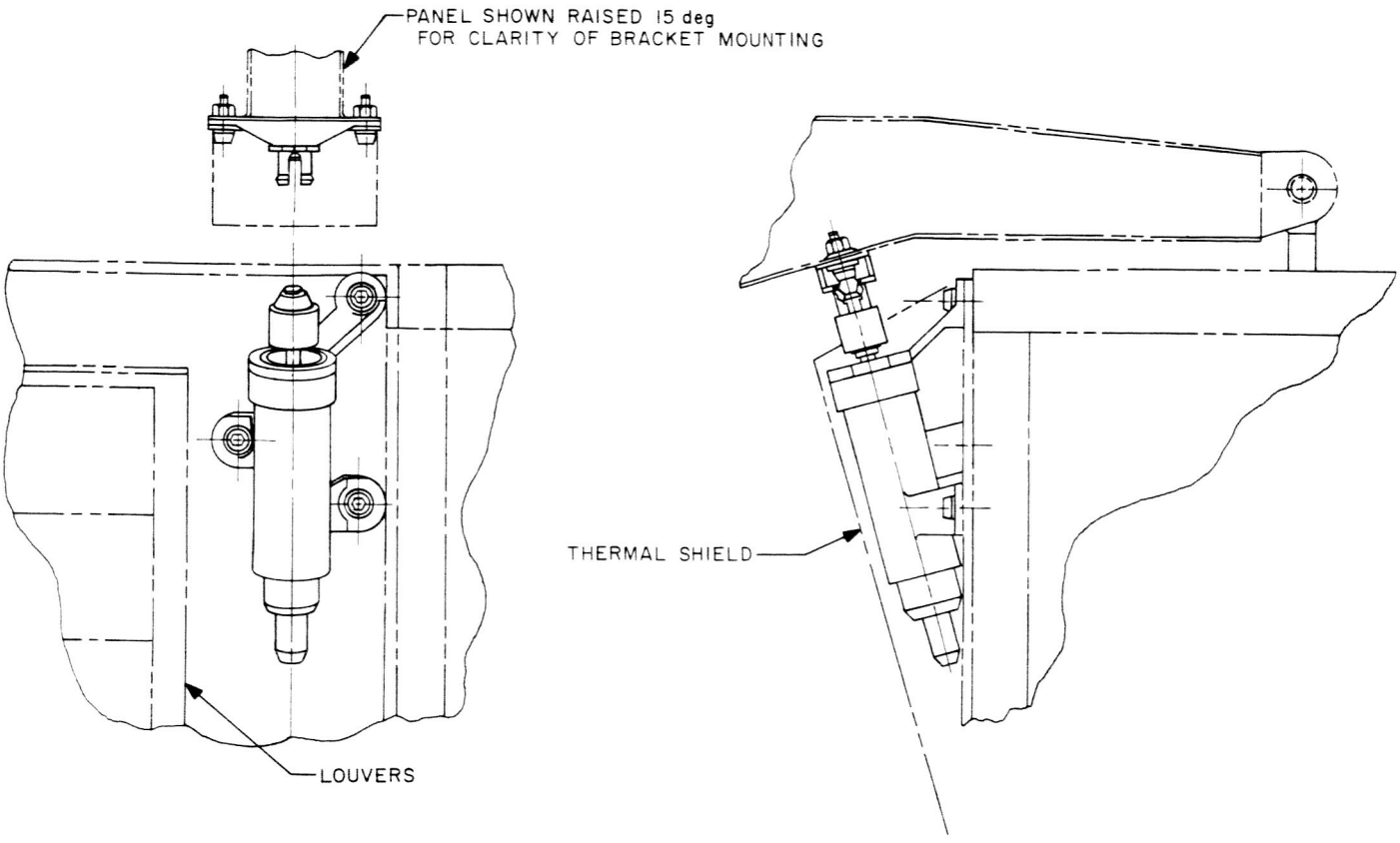


Fig. 57. Cruise damper installation

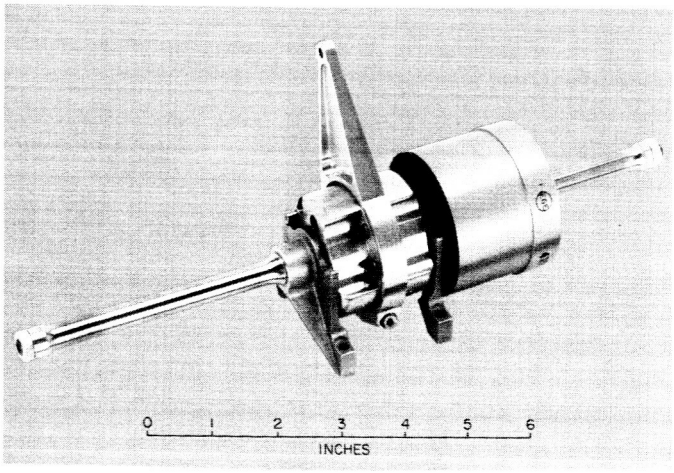


Fig. 58. Torsion bar solar panel actuator

torque and a centrifugal friction brake to retard the motion and maintain the panel deployment at a constant angular rate. The torsion bar was 11 in. long and 0.187 in. in diameter. One end of the bar was attached to the solar panel and the other end was attached to the spacecraft bus. A step-up planetary gear box and a centrifugal friction brake (similar to the technique used in telephone dials to control the dial angular velocity when released) were oriented parallel to the torsion bar, with one end anchored to the spacecraft bus and the other to the solar panel. When the panels were first released, the panel angular velocity was low and the friction brake had no effect. As the panel rate increased, however, this velocity was multiplied through the planetary gear stage. The excess centrifugal force then caused friction pads in the brake to contact a lining. Thus, the panel deployment velocity was held constant by the friction damping.

Central retarder. Because weight was an important factor, another design was sought that would accomplish the solar panel deployment, but with a lighter weight mechanism than the 4.5 lb allocated for the torsion-bar actuators. It was theorized that the panels could be individually actuated with torsion bars or other devices, and that all panels could be retarded by

one central retarder. Such a system had several advantages; one included the increase in overall reliability by the reduction of the number of separate subsystems and components.

A design finally evolved that used two negator leaf springs at each panel hinge and a central hydraulic retarder (Fig. 59) mounted on the superstructure under the high-gain antenna. A cable was attached from each of the four panels to the retarder. The retarder was designed to allow the four panels to open simultaneously in approximately 45 sec. The retarder assembly was a hydraulic vane torque motor that developed resistance to motion by forcing fluid from one side of the vane to the other through a tapered orifice. The tapered orifice had an adjustable needle valve to vary panel opening times. A check valve was included to allow quick return during checkout operations.

A clock spring was connected between the retarder vane and the case to provide a torque to rewind the retarder during checkout operations, and to keep the cables to the panels taut during the boost portion of flight.

To overcome the contaminating effect of leaking hydraulic fluid, it was first decided to use alcohol as the working fluid. During development phases, however, it was found that the low viscosity of alcohol required extremely close fits and tolerances in the retarder, and the alcohol was discarded in favor of silicone oil. Larger clearances would reduce the probability of the retarder binding or seizing. (The total weight of this new system was estimated to be 3.5 lb, or a savings of 1.0 lb over the torsion-bar actuator.) In addition, the rotary seal is much more reliable than the linear seal that was used on the *Ranger* and *Mariner* Venus 1962 actuators.

At first, the panel deployment was to be accomplished by the use of two negator leaf springs on each panel. Two springs were used for redundancy; one spring provided sufficient torque (12.5 in.-lb) to deploy the panel if the other spring should become inoperative. The leaf springs worked over a 1.250-in.-diameter segment

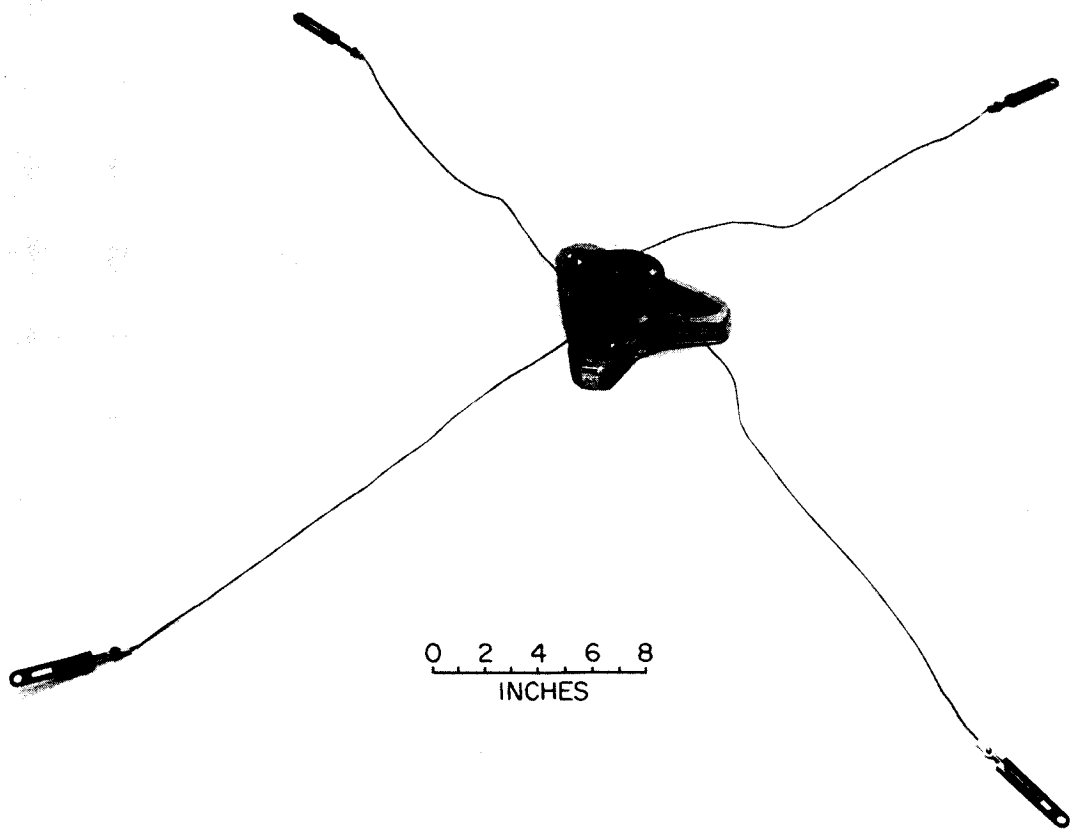


Fig. 59. Central solar panel retarder

of a drum attached to the bus in the solar panel hinge area. The other end of the leaf springs worked over a 0.250-in-diameter roller cantilevered on one side and attached to the solar panel spar. Several problems were uncovered with the leaf spring configuration when the prototypes were built and assembled. Several parts were overstressed, which resulted in excessive deformation.

A later design used two clock springs per panel, one on each side of the panel spar. The outside of the clock springs was anchored to the bus, and the inside of the springs worked on an arbor that was pinned to the solar panel spar and worked over the panel hinge bolt (Fig. 60). The springs were made of Elgiloy to meet the magnetic requirements.

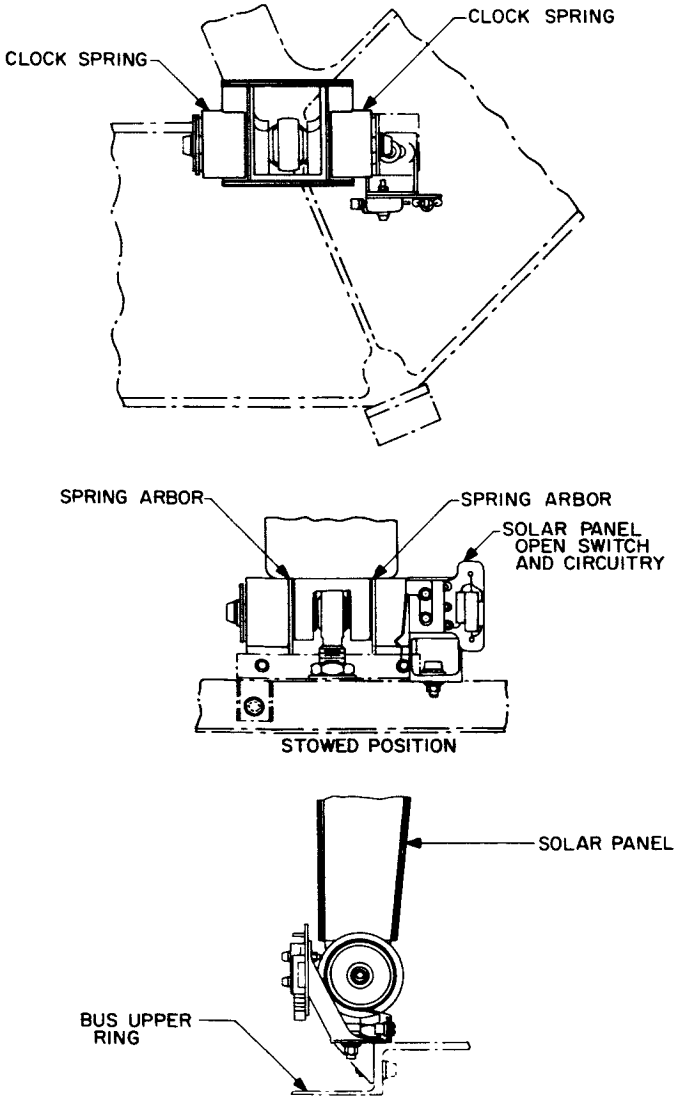


Fig. 60. Deployment spring installation

A complete series of panel deployment tests (described below) indicated the following problems with the design:

1. The retarder rewind spring was too strong at the end of the panel stroke
2. The panel deployment springs were too weak at the end of the panel stroke

A program was then begun to solve these problems. A spring-loaded ball detent was designed to hold the retarder in the cocked position. The detent travel was limited, and the striker plate was sloped so that no force was absorbed in sliding the ball over a plate once sufficient force was applied to release the detent. Vibration tests were performed to make certain that the whipping cables would not generate a force high enough to release the retarder detent and allow the retarder to unwind.

The panel deployment torque was also increased from the nominal 25.0 to 40.0 in.-lb. This increase was accomplished by the addition of two more clock springs per panel, which resulted in four springs per panel. Although 30.0 in.-lb was deemed sufficient to do the job, an additional clock spring was installed for redundancy. The changes to the retarder and to the panel deployment springs were shown to be sufficient.

Free-fall (unretarded) systems. As a backup effort to the central retarder panel deployment system, a second design approach was considered that saved weight and increased the system reliability. The retarder was removed from the spacecraft, which allowed the panels to free-fall to their deployed positions. The actuation system had to be modified slightly for the free-fall panel system. The spring output torque was 25.0 in.-lb nominal for two springs, and was increased to 40.0 in. -lb with four springs to offset the retarder torques. For the free-fall system, however, it was necessary to reduce the torques to less than 20.0 in.-lb to prevent excess panel energy when the panel fully deployed. The original two-clock-spring configuration was revived for this design; the only modification required was to wind the springs only one turn instead of two turns. The torques obtained were 18.0 in.-lb at the panel stowed position and 15.0 in.-lb at the panel deployed position. With only one spring operating, the torques would be half of the above values. The effect of the free-fall system on the cruise dampers will be discussed later. The free-fall system was not selected initially because of the uncertainty that the delicate solar panel structure and cells would survive a free-fall deployment.

Solar panel open switch. The mechanization of the solar panel open switch was basically the same for all the panel deployment schemes considered. A microswitch was used with a beryllium copper leaf-spring actuator. The spring and actuator were mounted on the panel deployment spring bracket. The switch actuator spring was positioned so that the edge of the panel spar first closed the circuit at a panel position of 30 deg from the deployed position. At about 15 deg from the deployed position, the edge of the panel passed by the leaf spring, allowing the microswitch to reopen (Fig. 61). In a failure-mode analysis, it was determined that a failure of the switch circuit to reopen was fairly significant. A closed circuit, as stated before, would block the data encoder register from recording any subsequent events. As a backup for the mechanical reopening of the switch, it was decided to place an RC parallel network in series with the microswitch. In the event the switch failed to reopen, the capacitor would charge at a rate determined by the time constant. When charged, the capacitor would then act as an open circuit, allowing future events to be recorded on that data encoder channel.

b. Solar panel cruise dampers. The functional requirements of the cruise damper that have already been given were for the cruise damper "as flown." Until the free-fall concept was implemented, the cruise damper had no requirement to arrest the panel motion, so that the original requirements were only to position the panel and provide a specified dynamic coupling between the panel and the bus. However, the requirements for a specified dynamic coupling, which are due to autopilot requirements, were originally much more severe than the requirements to which the final dampers were designed. Figure 62 shows the Mark I damper originally designed for the *Mariner* Mars 1964 spacecraft. The task to be accomplished was to provide four dampers (when mounted on a spacecraft with the spacecraft in *any position* with respect to the Sun) with damping, as specified, and matched to within 5%[2]. Consideration of these requirements together with some simple analyses was enough to demonstrate that temperature excursions must be held to the minimum possible, and that there must be some type of temperature-compensated damping. Analysis indicated that it would be possible to keep the temperature of the damper to within a 30°F temperature range by slaving the damper temperature to the bus temperature and by proper shielding. To minimize the effect of this temperature range on the damping properties, the piston was made of nylon and the cylinder was made of magnesium. The effect obtained by using these two different materials was that as the temperature rose, the annular gap between the cylinder and the piston would decrease in a manner that could be used to compensate for the decreasing damping-fluid viscosity. Upon consideration of temperature-viscosity relationships for many fluids, it was clear that perfect compensation was not practical. The requirement that the damping fluids have a very low vapor pressure (to reduce the chance of contamination of the spacecraft) and a small viscosity change with temperature led to the selection of a silicone fluid for the damping medium. A silicone fluid was chosen after a series of tests; the viscosity of this fluid was 1000 cs.

[2]The requirements for the midcourse maneuver are that the spacecraft be able to point the motor in any direction; and since there is no *a priori* information on the maneuver, all possible maneuvers in design must be assumed.

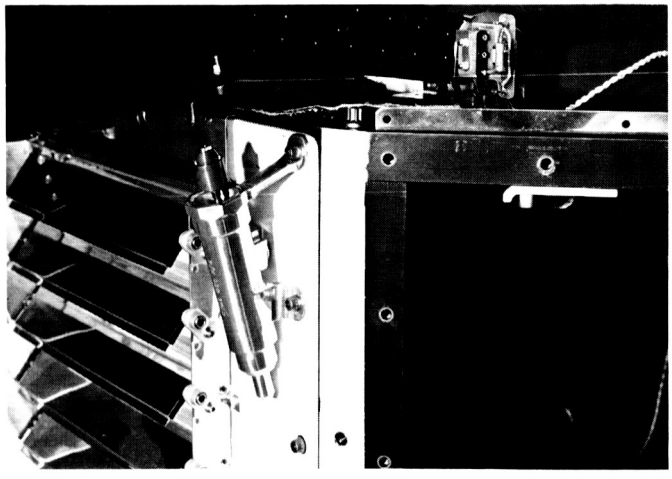


Fig. 61. Solar panel open switch and flight cruise damper installation

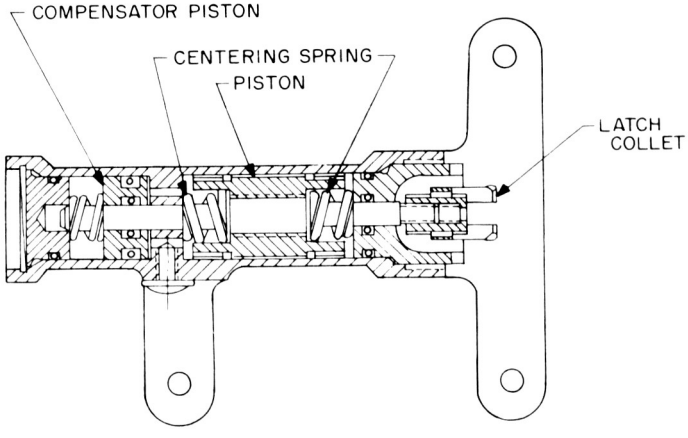


Fig. 62. Mark I solar panel cruise damper

The piston centering springs were of conventional compression-spring design and were fabricated from a commercial nonmagnetic spring alloy. The damper shaft was fabricated from a titanium alloy. The selection of the titanium alloy resulted from a requirement for a high-strength, nonmagnetic, lightweight metal with low heat conduction properties (to prevent heat flow from the back side of the solar panel through the damper). The O-rings used as seals were fabricated from a material that had proved to be a very satisfactory seal for spacecraft use. The top and bottom caps and the compensation piston were fabricated from aluminum alloy. For temperature-control purposes, the magnesium damper body was gold-plated and polished. As a precaution against potential rubbing between the titanium shaft and the aluminum top cap, the shaft was coated with a baked-on dry lubricant.

In order to provide damping to the panel in the deployed position, it was desirable that the panel latch to the damper as it opened. The nominal requirements for a latch of this type were that it need a very small engaging force, a relatively high retraction force, no backlash, and ease of operation during ground operations.

After investigating a large number of possible latch types, a collet-type latch was designed. This consisted of a beryllium copper collet that was mounted on the end of the damper shaft and that accepted a probe from the deployed solar panel. As soon as the collet accepted the probe, a sleeve on the probe dropped over the collet to lock the latch. The most difficult obstacle to surmount in this particular design was the fact that two mating parts did not engage along a tangent to the panel deploy arc, resulting in a transverse component of motion during the engaging operation. Due to the constraints of the spacecraft envelope existing at that time, there was nothing that could be done to eliminate this problem except to carefully adjust the latch on the spacecraft. The damper and latch assembly (Fig. 63) weighed 0.15 lb, which was within the original weight allocation for this device.

With the decision to proceed with a free-fall panel deployment system, it became imperative to redesign the cruise damper system (Mark II). Because this decision was made very late in the program, only the most necessary changes could be incorporated. The mandatory change was to provide sufficient stroke (i.e., energy dissipation) to the damper so that it would not bottom-out, thus preventing shock loads from being transmitted into the bus or the solar panel. The biggest question that had

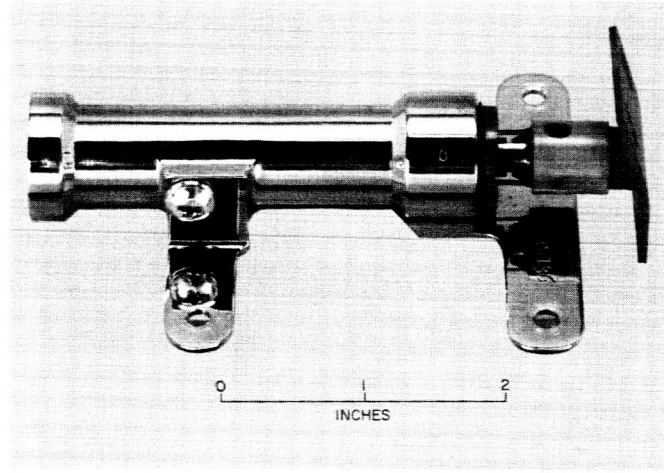


Fig. 63. Mark I solar panel cruise damper and latch assembly

to be answered was whether or not the damping requirements were compatible with the retardation requirements for panel deployment.

The maximum stroke of the damper was limited by interface constraints between the solar panel and the bus. The spring rate of the damper springs was determined by the panel frequency requirements. With these parameters defined, or at least bounded, an analysis of the panel deploy dynamics was performed and the system requirements were found to be reasonably compatible. To implement the system, it was necessary to ask for a change in the panel damping requirements from a damping ratio of 0.6 to 1.0 matched to 5%, to a ratio of 0.15 to 0.70 matched to within 0.1. An analysis of the panel-to-damper latching sequence indicated that the small transverse component of motion during the latching operation, which occurred in the previous design, would be intolerable in a damper design having a longer stroke. To remove the transverse latching motion component, it proved necessary to tip the damper about 16 deg with respect to the mounting surface, so that the latch engagement sequence would take place along the tangent to the panel deploy arc.

The requirement to tip the damper with respect to the bus forced a relocation of the compensating piston from the bottom of the damper to the top. Figure 64 illustrates the mechanization of the compensation piston. If there had been room to leave it located at the bottom, a very stiff spring would have been required to prevent it from moving in the same direction as the damping piston, which moved downward during the retardation phase. It should be observed that in the Mark I design

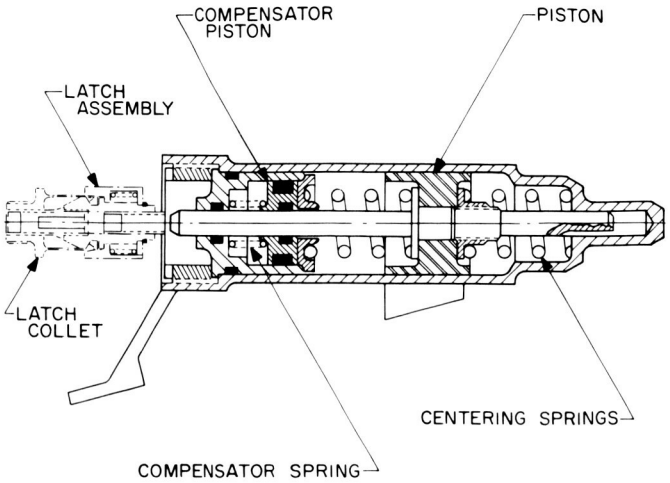


Fig. 64. Mark II cruise damper, section view

the compensator functioned only as a thermal-expansion compensator, but in the Mark II design it also functioned as a volume compensator for the piston-rod motion.

As a result of the increased function placed on the Mark II cruise damper, the weight allocation was increased to 0.25 lb per unit, and the units as flown weighed 0.22 lb. The weight increase is attributed to the increase in piston stroke from ± 0.016 to ± 0.186 in., the larger centering springs, and the fact that the body of the damper was fabricated from aluminum instead of magnesium. Figure 65 (a) shows the Mark II latch just before the mating operation; the latch after completion of the mating operation may be seen in Fig. 65 (b).

3. Fabrication

a. Solar panel deployment system. The solar panel deployment system consisted mainly of piece-parts fabricated by vendors. Before assembly onto the spacecraft, each part was dimensionally checked and visually inspected by JPL Quality Assurance personnel. One item that did have minor fabrication problems was the clock springs. The springs were made from material 0.025 in. thick. As originally specified, the material was to have been 70% cold-reduced prior to forming. This value of cold-reduction and subsequent heat treatment led to an ultimate tensile strength of 295,000 psi. It was found, however, that the 0.125-in. bend radii specified was too small, and material fracture occurred during formation. The cold-reduction was changed to 50%, resulting in a lower ultimate tensile strength of 230,000 psi, and the parts were formed to the original dimensions. The safety margin was still sufficiently large that no problems were encountered.

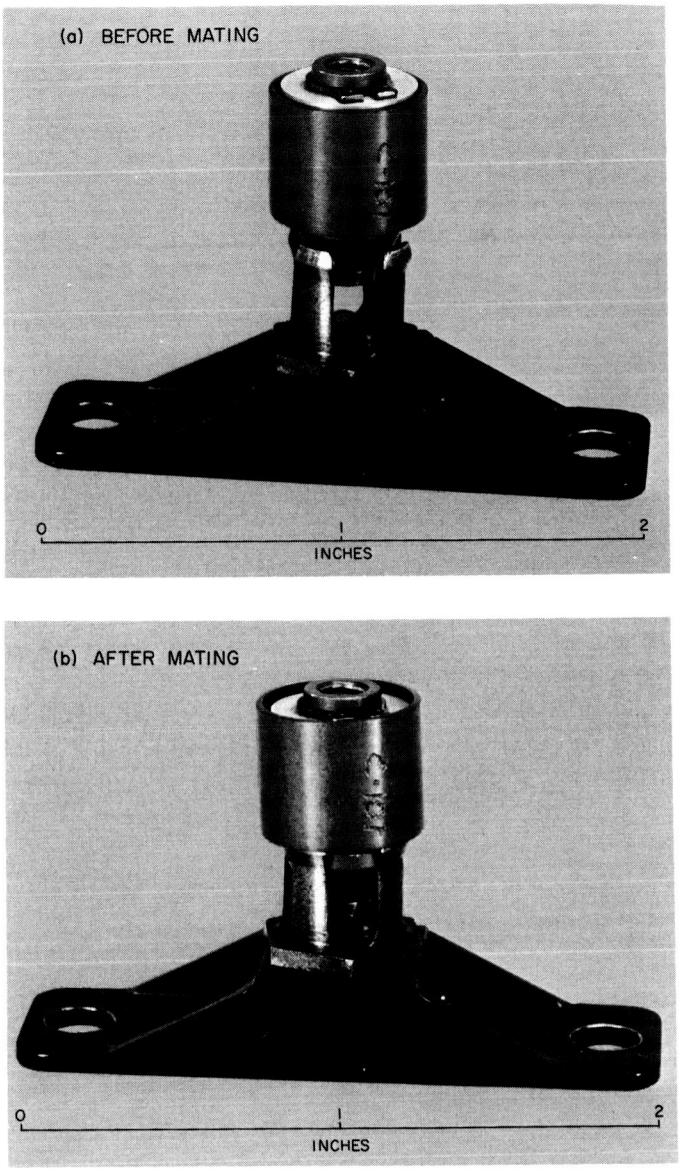


Fig. 65. Mark II cruise damper latch

b. Cruise dampers. Mechanical inspection of the piece-parts was provided by JPL Quality Assurance personnel after the vendors delivered the parts. Following acceptance of the part by the cognizant JPL engineer and QA engineer, the parts were placed in bonded stores pending final assembly and testing. All of the parts of the Mark II damper are shown in Fig. 66. The actual assembly of the dampers and latches was performed by JPL technicians under the supervision of JPL Quality Assurance personnel. The filling process was done in a vacuum environment to preclude the entry of air bubbles in the complete damper. The presence of a very small bubble

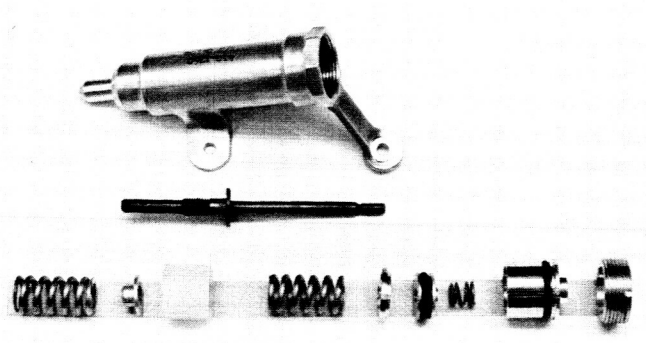


Fig. 66. Mark II cruise damper components

would have been sufficient to change the damper properties by an amount that is easily detectable in routine performance testing. Figure 67 shows two prototype dampers mounted in the filling apparatus after the vacuum bell jar was removed.

4. Testing

a. Solar panel deployment system. The first tests to be performed on a complete solar panel deployment system involved the centrally retarded system. The STM spacecraft was held by a low-level positioner, with the spacecraft X axis vertical. Panels were mounted on Bays III and VII, and a weight and pulley system was used to simulate the torque of the Bay I and V deployment springs. (Figure 68 shows the Bay VII setup.) The weight and pulley system was designed to give a decreasing torque as the panel moved toward the deployed position in order to provide simulation of the deployment-spring torque curve. In addition, the weights hit limits before the two panels fully deployed. This left the two panels to pull against the retarder, a condition that was very likely to occur in flight; i.e., the probability of all panels latching simultaneously was low.

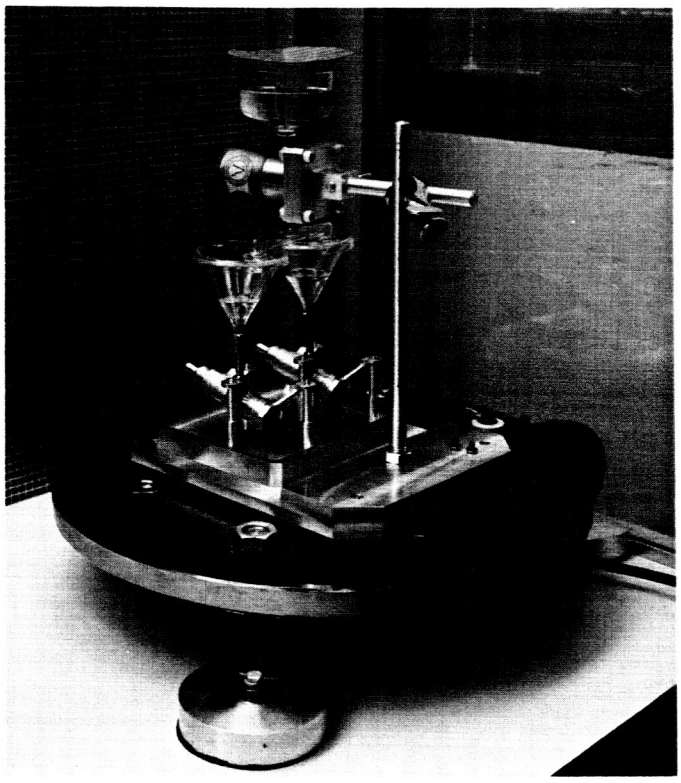


Fig. 67. Damper filling apparatus

The retarder used in this test was a reworked unit that was flight-like except for the metering needle and rewind-spring adjustment. When it was found that the ability of the panel deployment springs to counteract the retarder rewind spring was marginal, the rewind-spring preload was decreased by unwinding the spring 180 deg. The solar panels were equipped with dummy cells and gas-jet mass mockups, but no cabling or plumbing. The complete vane systems were installed on both panels, except that strings were substituted for the mylar vane covering to reduce air drag as the vanes deployed. The solar panels and the weights were released with a flight-type pyrotechnic subsystem as a check on that subsystem.

A second series of tests was conducted using the STM in the same manner as in the previous test. This same series of tests was also made on the centrally retarded system but included the modifications required as a result of the first tests (e.g., four clock springs, detent in the retarder). Only one panel was installed (Bay III) and connected to the retarder. The weight and pulley system was not used, so the one set of panel springs had to deploy the panel as well as the retarder from the stowed to the deployed position. Although this was more than the springs were supposed to do, it was felt to be a worthwhile but conservative test. The retarder was set for a nominal 20-sec panel opening time with all panel springs operating at 40 in.-lb. The spring torque was then set at 30 in.-lb to provide a worst-case test. The one panel was hand-released and all subsystems performed as designed. The panel spring torque was sufficient to release the retarder ball detent, to deploy the panel, and to latch the panel at the end of the stroke. Deployment times were consistently 145 to 150 sec, which was considered normal for only one panel.

In the third series of panel deployment tests, the STM was again used but the panels were deployed unretarded. With a torque of 25 in.-lb per panel, the panel

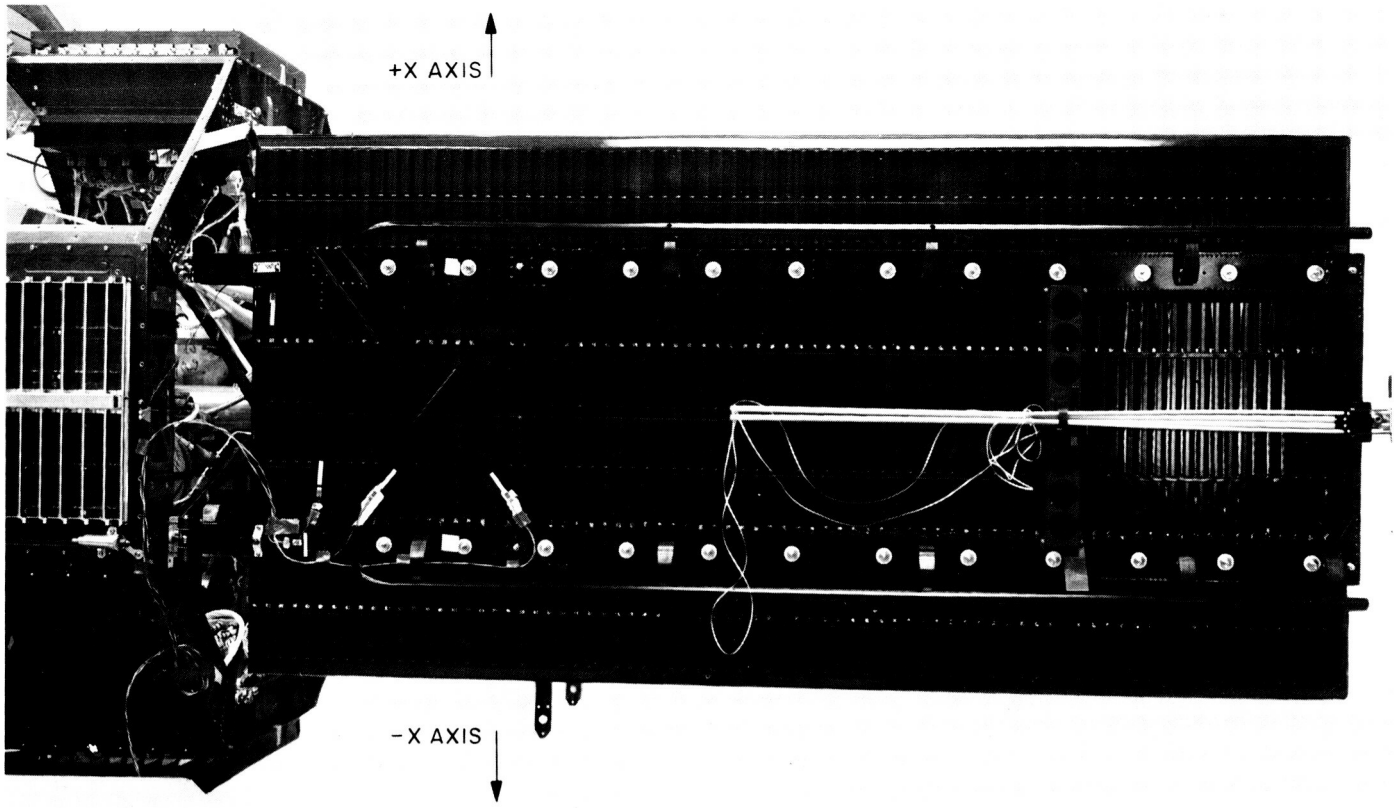


Fig. 68. Solar panels before deployment test

deployment time was approximately 5½ sec. The impact of the panel on the cruise damper caused the damper to bottom, but no visual evidence of yielding was noted either in the panel or in the cruise damper. The cruise-damper latch failed to latch the panel the first time, but latched the panel after the first bounce. This characteristic was later traced to faulty adjustment of the latch-engaging parts. Therefore, it appeared that this approach had a high probability of working if the cruise dampers were redesigned to serve as panel catchers as well as flapping-mode dampers.

A fourth series of tests was performed to verify the analysis of the unretarded panel deployment system. A solar panel was mounted to a rigid test stand with the hinge axis vertical. A Mark II cruise damper was used. Compensation for gravity and air-drag effects was accomplished by tilting the hinge axis 0.29 deg and by biasing the spring torques so that opening times in air compared with nominal opening times in a vacuum. In these tests, the panel was instrumented at critical points with strain gauges and/or accelerometers. Large spacecraft tip-off rates were simulated by increasing or decreasing the panel deployment spring torque. These tests verified that the free-fall panel deployment system could be committed to flight.

b. Cruise dampers. The tests to which the cruise dampers were subjected were functional and environmental. The functional testing included tests performed on the damper itself and, also, tests in which the damper was installed on the spacecraft. The environmental tests were operational system tests and will not be discussed here.

The functional tests included a spring-rate check, which was used to verify that the spring rate of the completed damper was within specified limits. Figure 69 shows a completed damper mounted on the spring-rate check fixture. This fixture was also used to verify that the completed damper was capable of traveling over its specified stroke.

The damping-rate and the arrest-rate tests were performed on a pendulum test fixture. The pendulum was designed to have the same moment of inertia as a flight solar panel. The damping rate was determined by

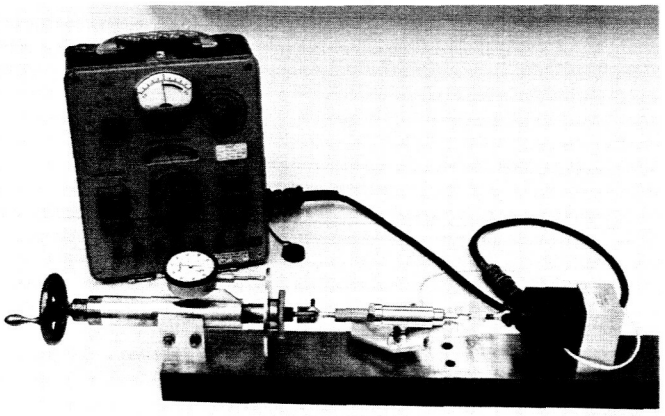


Fig. 69. Damper spring rate test setup

mounting the damper and latch on the test fixture, displacing the pendulum a distance equal to the worst-case panel displacement, and then releasing the pendulum to obtain the damping decrement curve, which was recorded on a plotter. The arrest-rate capability of the damper was demonstrated by displacing the pendulum a distance corresponding to the energy level of the panel deployment springs, and then releasing the pendulum to swing against the damper. It should be noted that one latch assembly was used on this test fixture for all 26 dampers tested (about 300 simulated worst-case panel deployments), and that this latch was still operational at the end of the test program.

The functional testing of the latch consisted of two mechanical tests to determine the latch-engaging and latch-retraction forces. These two tests were carried out on simple, deadweight testing fixtures.

The cruise damper environmental testing consisted of thermal–vacuum and high-frequency complex-wave testing for the FA tests. For type-approval testing, the TA damper was also subjected to shock, centrifuge, and transportation environmental testing. Each damper and latch assembly was checked by the magnetometer mapping facility prior to SAF delivery, to be sure that the magnetic-field specification requirements had been met.

G. *Science Platform and Actuator*

1. Functional Description

The objective of the science platform subsystem was to provide a gimbaled support structure for the planet-oriented science instruments capable of satisfying the pointing requirements of these experiments. In addition to the basic pointing-direction requirements, the platform subsystem had to satisfy other basic considerations such as structural and thermal compatibility, alignment accuracies, and Spacecraft System interaction requirements. To establish design ground rules, the following basic functional definitions were generated.

a. Payload definition. The planetary science and acquisition sensors consisted of a television subsystem, an ultraviolet photometer, a wide angle Mars seeker, and a narrow angle Mars sensor. The total weight of the platform-mounted sensors was 11.5 lb. All sensors were to be mounted to provide parallel optical axes. The integrated package was to be located so that it would provide an unobstructed field of view of the planet near the region of closest approach. The thermal environment had to be compatible with operating temperature extremes of -20 and $+40$°C.

b. Platform definition. To provide the necessary field of view and to be compatible with the basic bus structural requirements, the science package was mounted at the bottom of the central cavity of the basic octagon. The pointing direction was chosen to be 120 deg from the Sun direction, with the scan axis parallel to the spacecraft Z axis. Scan freedom was defined as a 180-deg motion about the scan axis centered in the predicted nominal direction of Mars. This amount of scan amplitude was felt to be easily attainable without compromise, and to more than satisfy the coverage required for a 3 σ trajectory dispersion.

Platform alignment criteria were established to be compatible with reasonable manufacturing tolerances and yet not to compromise the instruments' pointing-direction accuracy. The ability to remove and replace subassemblies without realignment of the assembly was also considered. Distributing the tolerances among the various subsystems yielded a platform-to-bus alignment of $\pm$ 1 deg, with a maximum error between science mounting planes of 0.1 deg. Mounting plane tolerance included any stand-offs required for electrical or thermal isolation.

c. Actuator definition. Since the actuator requirements were similar to those for the *Mariner II* radiometer actuator, an attempt was made to use as much of this design as was applicable. In general, the motor and much of the gear train could be used, resulting in a power input requirement defined as 26 v 400 cps single phase, with a maximum power of 4 w. The output shaft characteristics were established as a single speed of 0.5 deg/sec, with an output-torque slip clutch limited to 40 in.-lb.

The choice of output torque was based on tests of the *Mariner II* actuator capabilities and appeared to be more than sufficient for the application.

d. Science cover definition. In addition to the basic requirements for providing structural support and articulation, a deployable cover was integrated into the platform structure. The function of this cover was (1) to provide protection for the sensor optics from stray sunlight and micrometeorite damage during cruise, and (2) to provide a light-source array, powered from the ground umbilical, to check proper operation of the science and acquisition sensors during system and on-pad tests. Actuation of the cover deployment mechanism was provided by the pyrotechnic subsystem, and was sequenced to occur at the beginning of the encounter phase.

2. Design Implementation

a. Science platform. Restrictions on the required field of view and scan freedom limited the selection of possible structural configurations to that of a cantilevered tube mounted in bearings to provide scan motion. A machined, two-piece aluminum instrument mount was riveted to the overhung portion of the tube, and scan motion was introduced through a splined drive link located on the inboard end. The relative location of the scan actuator and drive link was based on considerations of cable harness routing to the science instruments. The assembled configuration in cutaway view is shown in Fig. 70.

Cable flexure across the scan joint was accomplished by securing the cable on the bus structure to the actuator end of the support tube and to the instrument platform at the opposite end. The cable was then twisted over the full length of the support tube (15 in.), which provided low torque and reasonable resistance to abrasion. To enhance the low torque characteristics of the cable routing, it was specified that teflon insulation be used on all conductors, and that harness fabrication be done with no twist imparted to the bundle. Twisted pairs were allowed in cases in which signal noise could be an overriding consideration.

To support the boost-environment loads, the scan tube was sized at an outside diameter of 3.00 in. with 0.060-in. walls, thereby giving a first-mode bending frequency of approximately 80 cps. Torsion loads were supported through a single pinpuller latch located immediately below the lower bearing mounted to the H-frame structure. A check on the effect of latch stiffness and tube size on torsional frequency modes demonstrated a first-mode torsional resonance of 150 cps. The resulting input

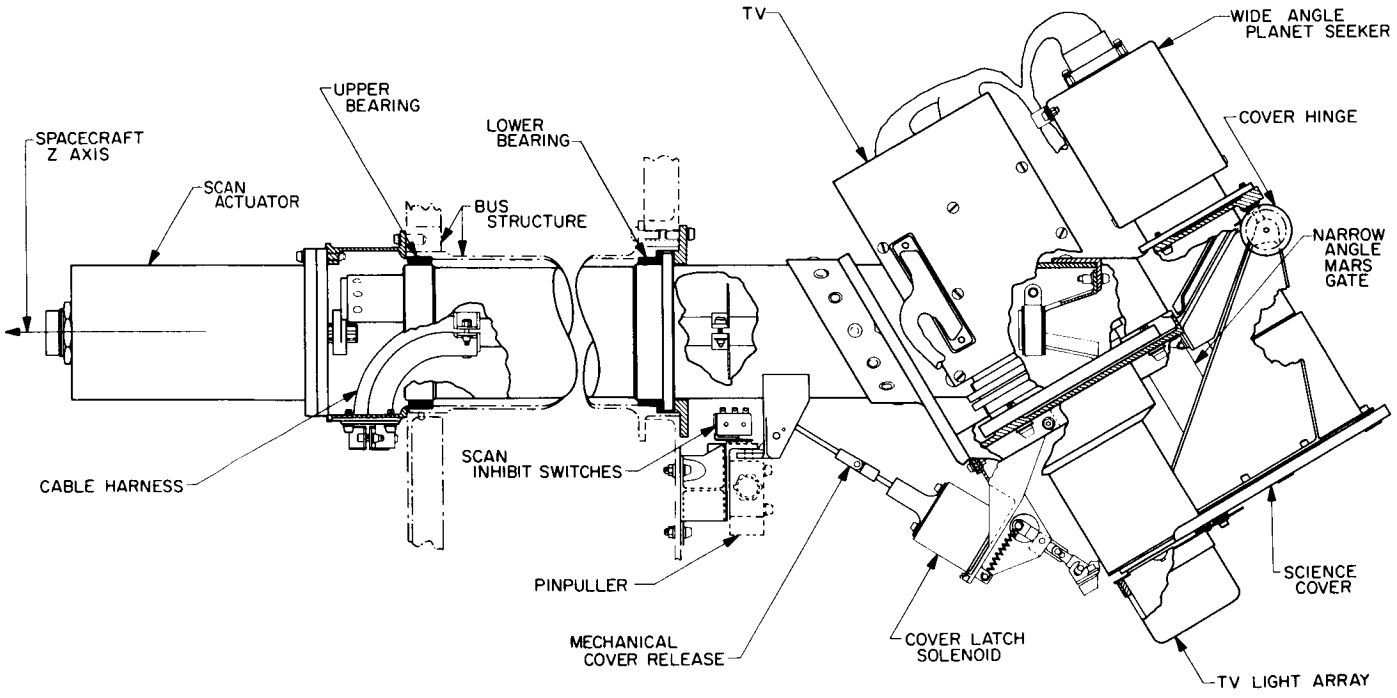


Fig. 70. Cutaway view of science platform

to the science instruments was considered to be sufficiently below the first critical frequency of the instruments to avoid any problems.

To provide the critical alignment between instruments, the platform structure was designed as a one-piece machining, with all bulkhead mounting planes parallel. Each instrument attach point was a raised boss that, after final assembly and stress relieving, could be faced off to the required 0.1-deg mounting plane tolerance. Where electrical insulation was required at the interface, 0.003-in.-thick mica washers were found to exhibit enough uniformity and lack of compressibility that alignment was not affected.

The bearings selected for use on the scan platform were of the sleeve-liner type, with the liner material a teflon-filled asbestos. The notable characteristics of this material are good dimensional stability, low coefficient of friction, and high compression strength. The compression strength is on the order of 20,000 psi, and the mode of bearing failure is of plastic deformation rather than delamination or spalling, which could cause shaft seizure. Diametral bearing clearance was established as 0.002 in., and was based on anticipated temperature gradients across the joint and consideration for the resulting nonlinear response of the system to vibration input. Axial loads were removed through the flanged lower bearing, and an end play of 0.0005 to 0.0015 in. was set during assembly by the use of peelable shims.

As eventually defined, the temperature requirements of the platform-mounted instruments were somewhat compatible, allowing them to be handled as a uniform temperature assembly. Since the required environment was much the same as the basic spacecraft, the attempt was made to thermally couple the science platform to the much larger thermal mass of the bus. As a result of the poor conduction path through the scan bearings, radiation transfer had to be relied upon almost entirely. As a first attempt, the 1-ft length of scan tube through the center of the bus was black-anodized, as was the support structure on the bus. All external surfaces on the science instruments and science platform were polished or gold-plated to reduce heat loss. The resultant temperature balance of the instruments appeared somewhat marginal, so it was decided to enclose the entire package in an insulated turret shell that rotated with the platform. With the science packages painted black and open directly to the interior of the bus, radiation transfer was greatly improved. The resultant configuration as assembled on a flight spacecraft is shown in Fig. 71.

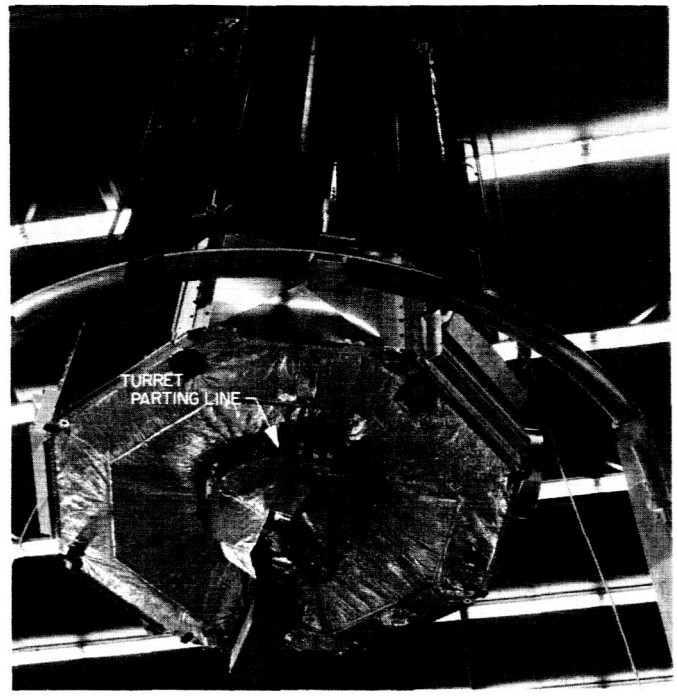


Fig. 71. Platform installed with turret shield

The platform could be installed with or without the science instruments attached. The installation sequence consisted of inserting the platform tube through the lower bearing while feeding the complete harness assembly ahead of it. The platform was then aligned and fixed in place by installing the split-cap bearing. Engaging the pinpuller latch automatically positioned the platform rotationally, thus allowing installation of the prealigned actuator. Instruments, science cover, and thermal shields could then be attached whenever systems checkout was required.

b. Scan actuator. The early concept of the science planetary scan subsystem consisted of an integral science-instrument support platform and a scan actuator. This configuration would have made it possible to remove the scan platform and actuator as a unit. As the requirements became better defined, it was obvious that the amount of cabling required for the science instruments could not be controlled by a service loop at the base of the spacecraft. A scheme of routing the cables down the scan platform axis tube was devised; this scheme required that the scan actuator be separated from the scan platform and be relocated on top of the primary structure.

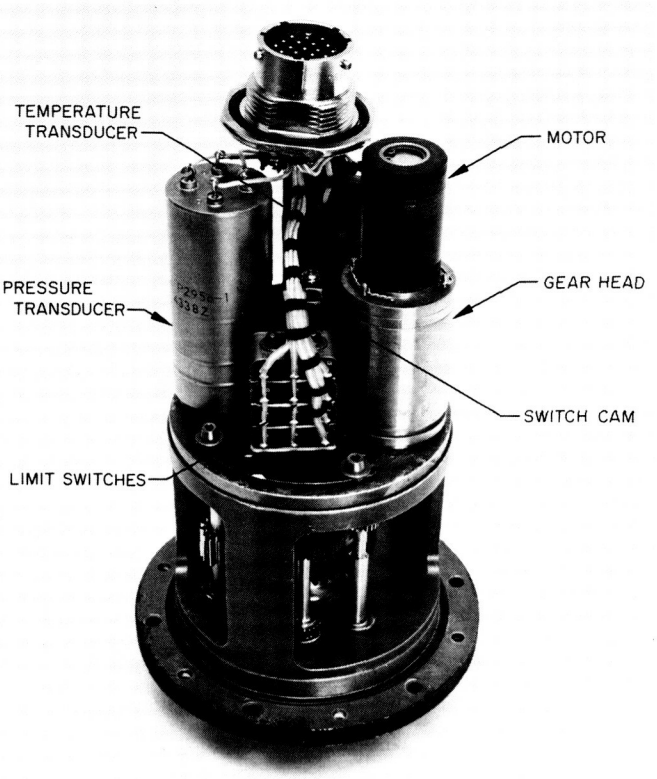


Fig. 72. Scan actuator with cover removed

The scan actuator (Fig. 72) consists primarily of a 400-cps, 26-v, 8000-rpm synchronous motor and reduction gearing to give an output speed of 0.5 deg/sec. The first stage of reduction (980:1) is achieved in a gearhead attached to the motor. An additional 980:1 reduction is achieved external to the motor gearhead, using a magnesium housing and standard gearing techniques.

The scan angle required of the actuator is ± 90 deg from a center position. A set of cam-operated microswitches pulses the scan logic system at each limit, thus reversing the direction of the scan. At each limit there are two microswitches: the first closes at the ± 90-deg limit, and the second acts as a backup and closes a few degrees beyond the 90-deg limit. The switches used are hermetically sealed units capable of operating in a vacuum. The cam that operates the switches is an integral part of the output shaft and, thus, is not affected by backlash errors in the reduction gearing.

An angular position indication is provided by coupling a potentiometer to the output shaft through a stage of antibacklash gearing. The potentiometer is capable of reading over 345 deg of rotation. In order to use the full rotation of the potentiometer for 180 deg of output shaft rotation, a 1.8:1 stage of step-up gearing is provided.

To provide engineering pressure and temperature information, transducers were installed internal to the scan actuator. The pressure transducer was provided to indicate the effectiveness of actuator pressure seals. The actuator assembly was pressurized to 2 atm with dry air to eliminate the possibility of cold-welding compatible materials. Air was used because of its oxygen content, which replaces the oxide coating on components as it is removed by operation wear. The temperature transducer was provided to monitor the internal actuator temperature during the flight cruise mode and to monitor the temperature rise during motor operation.

A torque capability of 100 in.-lb at the actuator output was possible from this motor and gear reduction; however, for operational reasons, a clutch was included in the final reduction stage and limited the torque to 40 in.-lb. The clutch design is somewhat unique in that it is cam-operated and is not solely dependent upon the breakaway and running friction coefficients of the clutch surfaces. As a result, the breakaway and running torques are nearly identical.

The clutch plates are conical, and the outer plate is the gear-driven element (Fig. 73). When the clutch is slipping, the outer plate is free to rotate about the output shaft. The inner plate is spring-loaded against the outer plate and transmits the torque from the outer driven plate to the shaft through the cam. The cam in this application consists of three ⅛-in. balls caged in detents. When there is no torque being applied by the scan actuator, the balls are free in their detents. As torque is applied, the detent flange on the output shaft attempts to rotate with respect to the inner clutch plate, thus transmitting the torque through the balls. When the resistive torque reaches 40 in.-lb, the balls attempt to cam out of the detents, compressing the springs loading the inner clutch plate, and, thus, separating the clutch plates and disrupting the drive train.

The bearings used in the actuator, with the exception of the output shaft bushing, are phenolic separator Class 7 ball bearings. Each bearing and separator was vacuum-impregnated with silicone oil. A torque trace of each bearing was required from the vendor to ensure 100% inspection. To prevent "Brinelling" during vibration, the lower end of the output shaft was supported in a teflon compound bushing rather than on a ball bearing.

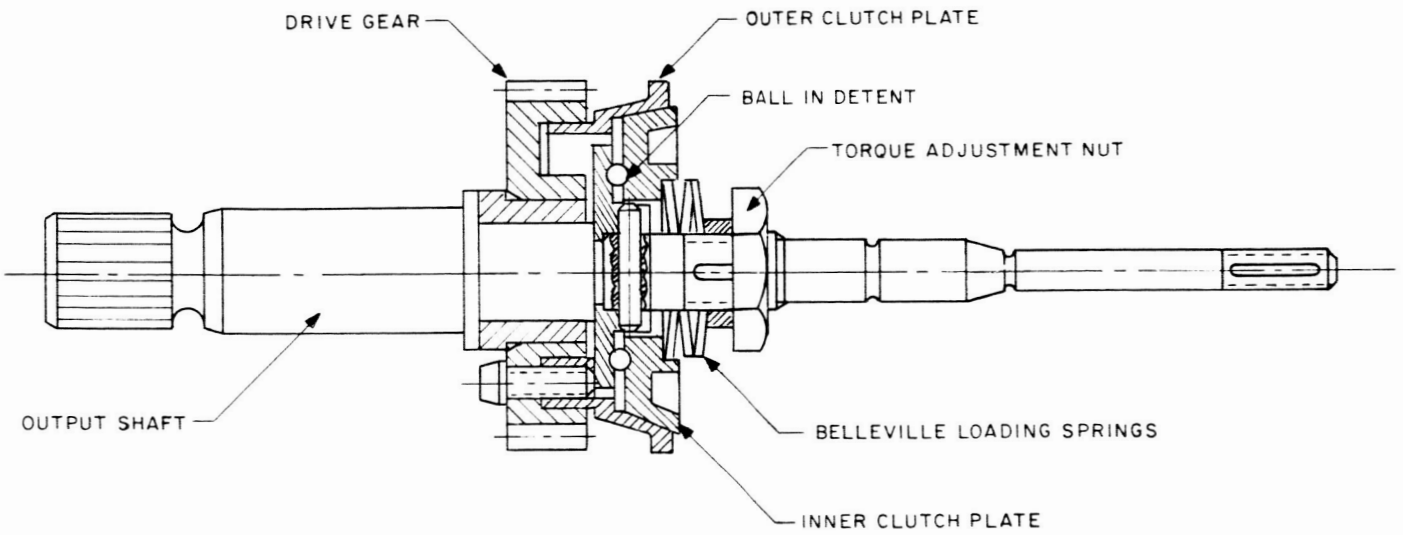


Fig. 73. Scan actuator clutch assembly

The output shaft was pressure-sealed by two viton quadrings spaced 0.050 in. apart. When coated with silicone oil, the quadrings, with the void between them filled with oil, provided a labyrinth-type seal. The gear housing cover was sealed with viton O-rings around the electrical connector and housing separation plane. A glass-header type electrical connector was used to prevent leakage.

c. Science cover. At the time the science cover requirement was established, detail design was greatly hampered because of the lack of definition of the instrument configurations. A platform mounting interface was agreed upon, but the details of the optics for the TV and wide angle sensor had only been narrowed down to four possible combinations. Therefore, if a cover were to be designed to meet the hardware delivery schedule, the choice had to be made to either (1) proceed with the design of four separate cover assemblies, optimizing each one to that particular combination of instruments, or (2) provide a basic cover mounting plate sized to handle the envelope of configurations and to vary only the attachments required for each instrument. The second approach was the one selected. Although the final assembly was not the most ideal, the design approach turned out to be fortuitous in that the wide angle seeker selected did not satisfy the original interfaces and the resultant effect on the cover design was limited to a revision in the one attachment. The cover, as eventually assembled, is shown in Fig. 74.

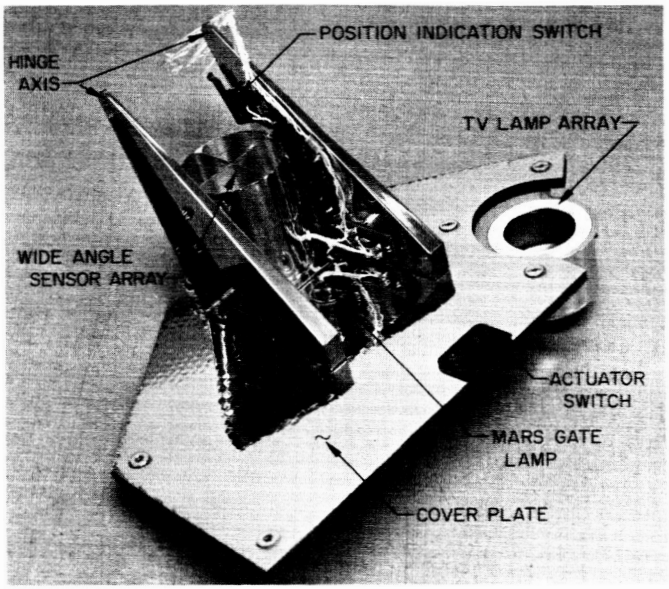


Fig. 74. Science cover assembly

The requirements for the cover plate were that it be lightweight, that it provide low heat loss, and, most important, that its bending be of such stiffness that boost loads would not be amplified through the cover into the optics assemblies. A honeycomb structure inherently satisfied these criteria, and a bonded-aluminum honeycomb sandwich was selected. It should be mentioned, however, that the number of threaded fittings necessary for this configuration tended to degrade the weight/stiffness ratio considerably, with the resultant structural efficiency being only slightly superior to more standard fabrication techniques. The materials used consisted of a 3/16-in. hexagonal honeycomb core made

of 0.0007-in.-thick aluminum alloy. The cover sheets were 0.004-in. aluminum alloy bonded to the core with an adhesive and cured in temperature cycles up to 350°F. Another adhesive was used as fill in insert locations and around the edge of the plate.

The hinge bearings chosen were a stock item, threaded shank monoball bearings, with a material substitution of corrosion-resistant steel for magnetic considerations. The monoball liner consists of a teflon-fiberglass weave of the type successfully used on the *Mariner II* spacecraft in a similar application. A bearing run-in procedure was used to ensure low friction with 3 in.-oz. maximum breakaway torque being reasonably achieved. Alignment of the cover hinge axis was easily accomplished by threading the two monoballs in unequal turns, as required, during assembly.

Clock springs of 0.016-in. nonmagnetic spring material were used to provide the cover opening force. Molybdenum disulfide dry lubrication was deposited on the spring material to guarantee a resistance to cold-welding when the spring was preloaded. Since inflight actuation was 0 g, the spring preload needed only to overcome bearing friction and cable resistance. However, ground testability requirements gave a considerable margin to this value, resulting in a specified spring torque of 24 in.-oz per spring in the latched position. Such a large torque thus allowed each spring the capability of reliably operating the cover in the event that a spring failure should occur.

With the highly over-powered opening springs, full cover deployment in 0 g could occur in less than 1 sec; thus, it was necessary to provide a semielastic end-of-travel stop. Flat beryllium copper springs were used to stop the cover; the energy was sufficiently dissipated in sliding contact between the hinge and the spring during rebound.

In general, the individual lens-cover housings consist of a 0.020-in.-thick double-walled aluminum shell such as the TV cover assembly shown in Fig. 75. Double-filament bulbs are mounted in teflon inserts, and blocking diodes and terminal boards are mounted on the back side of the inner shell. An outer shell was used to protect the optics from outgassed deposits originating from the adhesives and conformal coatings. In the case of the TV cup, a bumper was attached to provide the required stray light shielding; it was flexible enough not to transmit vibration loads from the cover to the optics assembly. The housing used for the wide angle planet sensor was similar, with the exceptions of the location of the

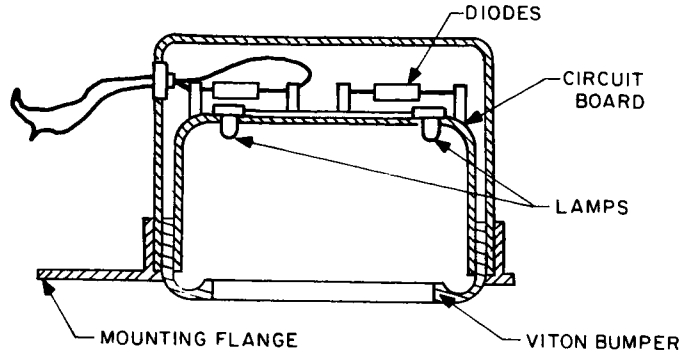


Fig. 75. TV light array assembly

lamp and the use of quadrant baffles to sequence the areas illuminated.

To complete the science cover assembly, the individual lens covers were attached to the cover plate and the "pigtail" wiring routed to a terminal board on the hinge leg. A plug-in harness to the platform was attached at the same terminal board with a service loop across the hinge axis. A three-wire system through the umbilical supplied the cover lights with power. Light sequencing was accomplished by reversing the polarity of the dc source to various wire pairs in conjunction with the cover-mounted blocking diodes.

The importance of actuation reliability to the success of the mission required that the cover latch and actuator be as foolproof as possible. To this end, large performance margins were used in all components. The latch itself consisted of a simple over-center linkage powered by dual dry-film coated stainless springs. Link pivots were dry-film coated stainless shafts in aluminum housings; side clearance was adjusted by teflon washers. The springs, when in the on-center position, generated approximately 13 lbf, with the required over-center motion set to trigger at 2 lb.

The primary latch actuator was chosen, after some consideration for the use of pyrotechnics, to be a tractive magnet, push-type solenoid. The simple solenoid appeared to satisfy the performance crietria, was compatible with the capacitor discharge power supply, and, most important, could use a much simplified reliability test program as compared to a single-shot pyrotechnic device. To be compatible with the power input available, the minimum performance of the solenoid would necessarily be 2 lbf at the start of a 0.090-in. stroke when subjected to a capacitor discharge of 4000 μf at 26 v. Therefore, to allow a performance margin, the minimum

acceptance criterion was established as 3 lb minimum force at 20 v. As finally tested, the solenoid was capable of 3.8 lbf at 20 v and 5.8 lbf at the rated 26 v capacitor charge voltage, or approximately three times the required latch actuation force. Total solenoid weight was set at 4.5 oz, with a maximum allowable armature weight of 0.25 oz limited by the dynamic force to unlatch during vibration. Intuitive concern for the magnetic properties of a solenoid was relieved by the closed-field design, which resulted in a measured 6 γ at 1 ft, thus satisfying the flight equipment specification.

If the solenoid failed to work, an independent mechanical backup was provided. The mechanism chosen consisted of a spring-loaded lanyard plunger that would be automatically tripped when the scan platform rotated. The spring was sized to account for the possibility of the primary failure being a hangup of the solenoid armature. The resultant configuration (Fig. 76) thus allowed nearly complete redundancy and performance margins capable of accounting for any reasonably conceived failure modes.

3. Design Evolution

a. Revisions in functional requirements. A more drastic revision to the scan platform occurred when the decision was made to eliminate the infrared spectrometer, weighing some 20 lb, and to substitute in its place the ultraviolet photometer, weighing approximately 6.5 lb; this cut the total platform-mounted payload weight in half. Although this redefinition required the platform to be completely redesigned, the resulting configuration was less complex. As an example, the use of a cantilevered support would not have been possible with the infrared spectrometer payload weight, since not only would the support tube size have been unreasonable but also the bus structure could not have supported such bending moments. The configuration, therefore, required a bearing support below the instruments, which was to be hinged out of the way (following boost) to provide scan motion clearance.

Following the final selection of instruments, the scan platform was subjected to numerous revisions as a result

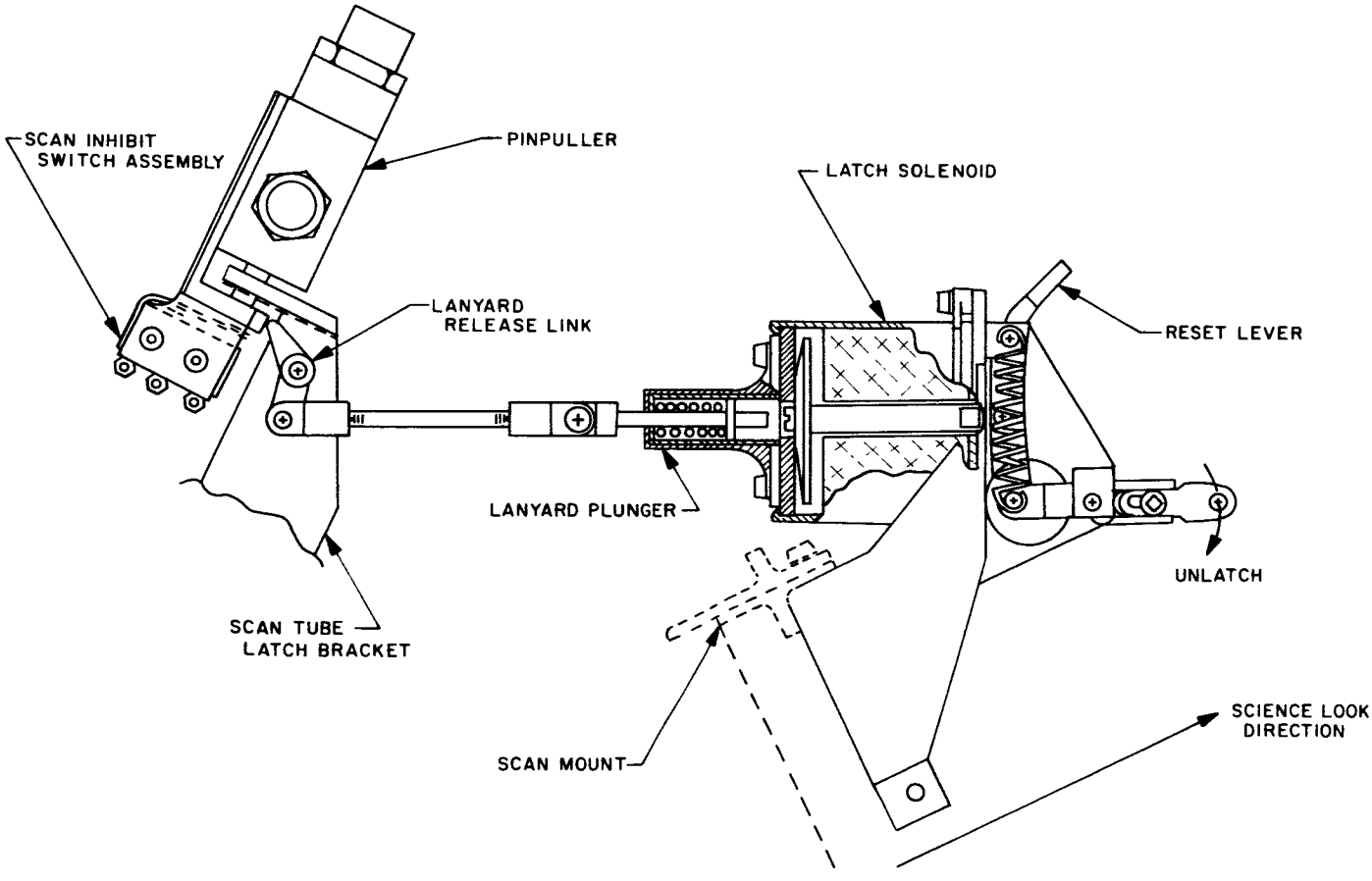


Fig. 76. Cover latch and lanyard assembly

of redefinition in the trajectory approach geometry. Although the effect did not cause a complete redesign, scan amplitude and stow position were changed three times in order to locate the instruments in the nominal look direction of the planet, while it was stowed, in the event of a scan subsystem malfunction. The trajectory eventually selected forced this failure-mode requirement to be violated, since the resulting latch position could not be accommodated without a loss in schedule.

A late requirement was the request for a scan motor interlock switch that would inhibit scan power to the actuator when the platform release latch was engaged. The mechanization consisted of merely attaching two hermetically sealed microswitches in parallel, with the leaf-spring actuator follower resting against the end of the pinpuller latch pin. When the pinpuller was actuated, the spring follower was released, allowing redundant switch closures to the actuator power supply.

b. Telemetry requirements. As the flight sequence became better established and the telemetry channel availability became better known, analysis of failure modes in the planetary science sequence indicated that proper evaluation of status was necessary if an alternate operational mode were to be used. In particular, information as to whether the platform latch was disengaged properly had to be known prior to the midcourse maneuver, since such a failure in the assembly's ability to scan would bias the choice of aiming points. As mentioned previously, it was necessary to disregard the requirement of having the nominal trajectory compatible with the stow position in favor of the scientific value of an Earth-occultation trajectory. If a scan latch failure had occurred, the knowledge could have affected the decision of what maneuver to attempt.

To provide the necessary latch indication, a third microswitch was added to the scan inhibit switch assembly. This switch was wired to a data encoder register so that an event count would be recorded when the latch pin was retracted. Suitable capacitor and blocking-diode circuitry was added to the switch assembly to make it compatible with the data encoder input.

Information regarding the status of the science cover was important to several inflight decisions. The first failure mode to be considered was the possibility of inadvertent deployment during boost. If such a failure occurred the midcourse correction would have to be performed using a maneuver that would not allow incident or direct sunlight on the science optics. Since data encoder event telemetry could not be properly interpreted during boost, this failure mode implied the use of a regularly sampled telemetry channel.

A second failure mode requiring cover position information would occur at planet encounter, at which time it would become necessary to identify proper actuation during the normal flight sequence. Backup command would be available, which would recycle the deployment sequence, but the decision to use it had to be based on flight data supplied by a regularly sampled telemetry channel.

To mechanize the telemetry indication, a hermetically sealed microswitch, which was located so that it would actuate with the cover in the deployed position, was mounted on one leg of the science cover. Ballast resistors were attached across the normally open and normally closed terminals so that an approximate 20 Ω step in the 500 to 600 Ω telemetry input would occur when actuated. This scheme thus allowed the telemetry channel to be used for normal telemetry information, with the cover indication a known offset in the data.

In addition to the normal science data analysis telemetry, such as output shaft position, the actuator was equipped with temperature and pressure transducers to allow diagnosis of the actuator itself. Actual operating temperature and the ability of the case pressure seals to maintain an internal pressure were considered valuable engineering knowledge. The importance of such information became apparent at the beginning of the design phase when it was realized that, although much of the mechanization was based on the successful *Mariner II* actuator, no flight data were available to extrapolate the adequacy of long-term vacuum storage.

4. Test Experience

a. Actuator tests. Environmental testing was performed in accordance with JPL specifications, with only one unit failing to pass the requirements. This unit failed to maintain pressure following the test sequence; however, the failure was found to be porosity of the gear housing and was not attributable to the tests performed on the unit.

A special test was conducted to determine the deterioration rate of the actuator clutch. The actuator was operated for 24 hr, and the initial output torque recorded at 40 in.-lb. At the end of the 24-hr period, the torque had decreased to approximately 38 in.-lb, which was considered to be reasonable.

A life test was conducted on the scan actuator by driving a science platform while it was subjected to a vacuum of 10^{-6} mm Hg. In the event the actuator loses pressure during flight, the life test was conducted with the pressure plug removed. Since the vacuum chamber cannot reach the low pressures of the space environment, the actuator was heated to 160°F to speed up lubricant evaporation. The actuator was operated for 14 hr each day for 80 days. The position potentiometer output voltage was constantly recorded to indicate actuator speed changes or erratic operation. No malfunctions were noted during the test.

b. Science cover and latch tests. Qualification of the latch and cover assembly prior to spacecraft delivery consisted of a series of environmental and performance tests. Briefly, these tests were conducted as follows: (1) the solenoid was cycled in a vacuum at various temperature extremes, assembled to the latch, recycled, then assembled to a cover and repeatedly unlatched in a vacuum, using both actuator and lanyard backup; (2) the assembly was subjected to the general environmental specification consisting of humidity storage, shock, static acceleration, low-frequency vibration, and high-frequency complex wave vibration; (3) the performance tests discussed above were repeated for the completed assembly.

Performance of the assembly during the initial qualification tests was hampered by the fabrication problem with the honeycomb plate. The lack of proper insert bonding was exhibited during the first high-frequency complex-wave vibration when the inserts came loose, allowing eventual destruction of the cover hinges and latch fittings. Following the incorporation of properly fabricated hardware, qualification proceeded with no failures noted in any developmental or flight-hardware test.

c. Integrated platform and cover assembly tests. The qualification program for this assembly consisted of a series of structures to test thermal compatibility, interface compatibility, static- and dynamic-load verification, separation, operation, and other system-oriented functions. Complete assemblies were delivered to each developmental spacecraft and performance was monitored to determine their acceptance during each phase. For the purpose of evaluation, the major areas of concern during the developmental program were structural integrity and thermal compatibility. Operational performance was verified during systems tests on the PTM and flight spacecraft.

Complete system tests were conducted with the platform, actuator, science instruments, and science cover installed on the flight spacecraft. Simulated flight sequences were performed to determine if the basic design goals were achieved; namely, that the actuator was operating properly, using the flight instruments, and was providing proper scan motion; and that the science cover and latch assembly were capable of performing their proper functions of (1) actuation using flight pyrotechnic power supplies, and (2) instrument calibration using the cover lamp array. As a result of this test program, several minor incompatibilities were uncovered that were quickly resolved, which allowed complete acceptance of the subsystem.

H. Structural Design, Analysis, and Testing

The *Mariner* Mars 1964 spacecraft frame development drew heavily on previous Laboratory programs; this led to the evolution of the integrated primary structure/electronic packaging approach.

1. Design Loads and Criteria

The structural design criteria were evolved from those used on previous programs. The load-condition portion of the criteria consist of several combinations of equivalent static and vibratory loads. The structurally significant vibratory loads are specified as sinusoidal inputs, implying a steady-state sinusoid or a very slow-frequency sweep. Compatibility of this type of vibratory specification with the more transient nature of the flight vibration loads is provided, to some extent, by the inclusion of suppression levels based on the resultant loads produced at the spacecraft separation plane. However, the stiff box-like nature of the primary structure leads to vibration modes of various spacecraft elements with little participation by the primary structure. This minimized the effect of suppression, since "beam" loads were not developed.

2. Design Approach and Development Plan

The goal of minimum structural weight, together with maximum reliability, was pursued throughout the program. The most apparent target for structural weight saving was the solar-power structural system. Solar panel structures similar to those used on previous spacecraft would have weighed about 100 lb. The *Mariner* Mars 1964 design used only half this weight.

The design approach provided for the early developmental testing of a composite spacecraft structure. The

first step was to estimate the equivalent static loads for the component based on past experience. The initial structural design of the component was then determined for these loads, and the stiffness characteristics of this structure were determined.

The first composite analysis, performed using an idealization for each part, demonstrated the same elastic behavior as the initially designed structure for the significant modes. This composite analysis indicated potential deleterious coupling and provided the basis for the determination of stiffness requirements for the component structures. Stiffness requirements were also dictated by deflection limitations.

Modifications to the initial component structural design were made as a result of these stiffness requirements, and another composite analysis was performed using new idealizations. This analysis provided a better estimate of component loads from which another component structural design was proposed. This iterative cycling occurred a number of times as the design progressed.

An early structural test model provided a test basis for improving the analytical mode. A modal survey performed on the STM provided a high confidence in the lightly damped, linear portions of the analytical model prior to qualification-level testing. The analytical portion of the approach provided early design information and enhanced the ultimate test results both by establishing a better basis for test planning and by providing a vehicle for extending previous analytical and test results to a potentially modified structure.

This combination of analysis and testing was the basis of the structural development plan. In practice, the steps described for this approach were complicated by design changes and by the time lags in the various component development schedules. The late development of the modal combination analysis computer program also required the use of less sophisticated analytical techniques than originally planned. However, the success of the general plan recommends it for use in other spacecraft development programs.

3. Structural Design and Development

a. Primary structure. The primary structure is located between two concentric octagonal cylinders. The structure consists of an upper and a lower ring connected by eight webbed longerons and the electronic-packaging chassis located within this structure. The packaging outer shear plates performed the triple purpose of:

1. Supporting the electronics equipment
2. Stiffening the structure torsionally and axially
3. Providing conduction paths for temperature control

The integrated packaging approach was the most significant aspect of the basic structure design. Also, it resulted in a very rigid structure for supporting the other spacecraft elements. The spacecraft loads were carried through the primary structure to the booster adapter. The load carrying points also formed the spacecraft portion of the separation joint.

The high structural rigidity minimized dynamic coupling between the basic structure modes and those of other spacecraft structural elements. Coupling still occurred between some elements (e.g., between the midcourse propulsion unit and the secondary structure science platform), but the minimization of coupling was an extremely desirable design goal.

b. Secondary structure. The secondary structure, located internal to the octagon structure, supported the science platform, the upper ring harness, and the attitude control gas bottles. The structural design and development of the secondary structure was a function of various stiffness and strength criteria. In an effort to design the structure so that primary vibration modes of major components would not couple, it was desirable that: (1) the science platform have a fundamental frequency greater than 50 cps, (2) the overall torsion and bending modes be less than 70 cps (first torsion of launch vehicle configuration) and greater than 30 cps (solar panel vibration region), and (3) the midcourse motor and secondary structure not couple dynamically.

A hard-mounted, three-dimensional, pin-jointed analysis was performed using the stiffness matrix structural analysis computer program. This program, known as STIFF-EIG (Ref. 22), is the one from which the modal and response characteristics of the secondary structure for both static and dynamic loads were determined. This analysis was coordinated with the overall composite analysis to satisfy the above criteria and to predict the dynamic loads. Developmental STM modal and vibration exciter testing was performed, from which the response of the secondary structure was determined. Agreement between these results and analytical predictions was considered good (Table 21), in light of the

Table 21. Secondary structure vibration test response

Mode description	Analytic frequency, cps	Test frequency, cps
Torsion of secondary structure	57.0	59.7
Planetary science platform bending	48.7	48.3

nonlinearity in the structure due to tolerances in the science platform bearings.

c. High-gain antenna and superstructure. The high-gain antenna is mounted to the top of the superstructure, which bolts to the top of the primary structure. The superstructure also supports the solar panel boost dampers and part of the low-gain antenna.

Strength and stiffness requirements determined the high-gain antenna and superstructure structural design criteria. It was required that the lower controlling modes of the two structures should not couple and thereby induce high loads into the high-gain antenna. Because the solar panel boost dampers were connected to the top of the superstructure, realistic input loads other than upper limits were not obtainable from the composite analysis as performed with STIFF-EIG. However, a dynamic analysis was made on the two-structure combination, with the effect of the solar panels and omnidirectional antenna considered as point masses. Based on past experience, a conservative assumption was made for a maximum peak acceleration of 100 g (high-gain antenna feed) for the lowest six modes. With this assumption, member loads, frequencies, and corresponding mode shapes were calculated. From the analyses, it was noted that, because of structural geometry, the fundamental frequencies of the two structures overlapped and adequate modal separation was achieved only after much member-area juggling.

Because of a late design definition, the superstructure ring contained some complex load paths. The solar panel, low-gain antenna, and high-gain antenna loads, which should have passed directly from member to member, were ultimately required to take eccentric paths through the ring, resulting in an adequate but heavier structure. Also, the structure was more flexible than desired.

The design procedure for the high-gain antenna dish was primarily an experimental approach. Subsequent to an initial study period during which the general configuration was fixed, two honeycomb antenna dishes were fabricated—one of a fiberglass skin core construction and the other of all aluminum. The object was to determine experimentally which construction was best and what modifications should be made, if any. Design decisions were based on the relative response to hard-mounted vibration-exciter sinusoidal testing. The aluminum dish was selected as the best structural configuration. A symmetric four-point support system appeared far superior to the existing three-point support system. However, schedule limitations precluded any major change to the antenna structure.

Experimental investigations on the flight antenna configuration were conducted. A prototype antenna dish and support structure were modal-tested to determine dynamic response, natural frequencies, mode shapes, and equivalent viscous damping ratios. Although unique problems existed during the test (for example, how to take accelerometer readings in all three orthogonal directions on an ultra-lightweight structure and account for the moving accelerometer mass), the biggest problem was determining how to attach the modal vibration exciters to the lightweight honeycomb dish. Rubber suction cups were used for the modal testing, since no better method of attachment had yet been developed.

The modal analysis results are considered good, as can be seen in Table 22, which shows the agreement between the frequencies of the three basic vibration modes obtained by hard-mounted vibration-exciter and modal-survey testing.

A hard-mounted high-gain antenna dish and support structure were subsequently qualified as components after successfully passing a sinusoidal vibration test along the spacecraft Z axis and along the dish major axis at a level of 3 g rms. However, during the STM type-approval tests, wrinkles appeared in the underside skin

Table 22. Vibration testing results for flight antenna configuration

Test No.	Description of mode	Modal analysis frequency result cps	Frequency of vibration-exciter testing, cps
1	Rocking of antenna truss at minor dish axis	64.02	64.0
2	First bending of dish at minor dish axis	97.39	101.0
3	Twisting of dish at major dish axis	140.50	140.0

adjacent to the elliptical support beam tips. Thin doublers were bonded to the back side of the reflector to stiffen the skin locally in the wrinkled region. The antenna subsequently passed all type-approval tests.

d. Postinjection propulsion system. The major load-carrying components of the PIPS consisted of the fuel tank and its support structure, the thrust plate, and the combustion chamber (Fig. 77). The spherical titanium fuel tank was supported about its girth by a tapered ring that used a spring-loaded metal strap to maintain a preload between the tank and the ring. The aluminum tank support ring was connected to the thrust plate by means of a thin-walled aluminum tube truss. The PIPS thrust plate was structurally mounted to the spacecraft by the PIPS support structure.

The thrust plate was fabricated from two plates (which were spaced apart by thin structural sections) that were machined into one plate. The machined plate and a flat plate were dip-brazed to form one closed member. The combustion chamber was bolted directly to the thrust plate, and the nitrogen tank was preloaded against the thrust plate by spring-loaded metal straps.

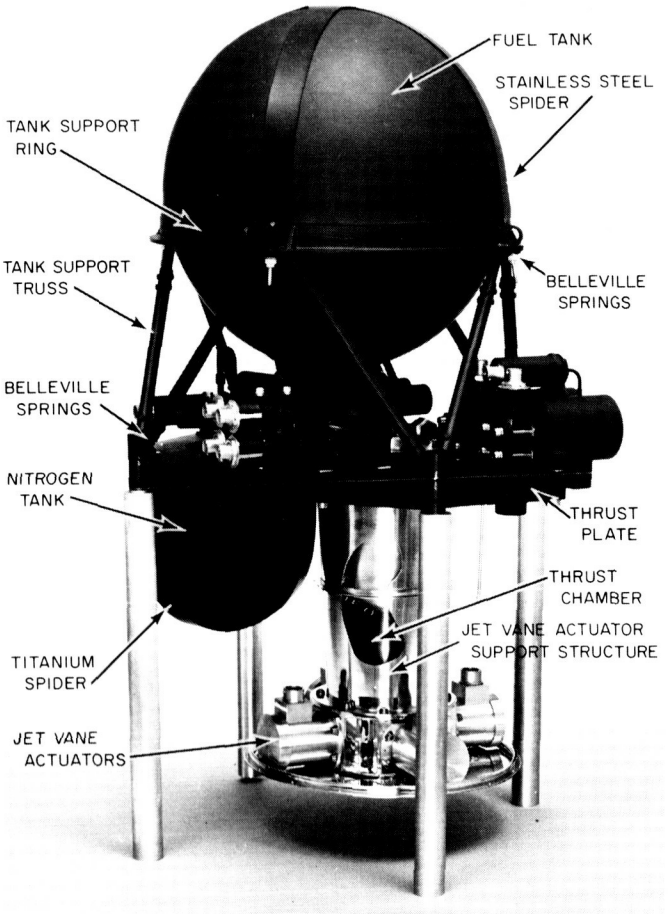


Fig. 77. PIPS structural design

The structural design philosophy of the postinjection propulsion system was dependent on both strength and stiffness requirements. The most critical dynamic loading of the basic structure, induced by the elastic response of the spacecraft/PIPS combination, was obtained from the spacecraft composite analysis. This consisted of an acceleration acting at the CG of the PIPS fuel tank, perpendicular to the thrust axis of the motor. To avoid dynamic coupling with other spacecraft structures, the PIPS was designed to have a hard-mounted fundamental response frequency of 70 cps. This separated the PIPS response from predicted response frequencies of other major components sufficiently to eliminate dynamic coupling. Dynamic deflection of the PIPS fuel tank parallel to the thrust axis of the motor was restricted to 0.100 in. maximum to avoid interference with the spacecraft secondary structure.

After the PIPS preliminary structural geometry was determined, a detailed analysis of the structure was performed with the aid of the stiffness matrix structural analysis computer program. The structural idealization used (for a three-dimensional rigid-jointed structure subjected to support excitation) is illustrated in Fig 78. The tubular cross section of the members in the tank support truss and of the PIPS mounting frame, along with the equivalent discrete members idealized from the thrust plate, made the PIPS well suited for the type of analysis used.

Postinjection propulsion system dynamic-qualification vibration testing and structural developmental testing was begun with a test series using the STM hard-mounted on a vibration fixture.

The PIPS was subjected, along its thrust axis and along two other orthogonal axes, to a programmed sequence of (1) band-limited Gaussian noise and (2) combined noise and sinusoidal vibration. The harmonic sweep was such that the time rate of change of frequency increased directly with frequency. Only one pure noise test was conducted, and two sweeps up and down the frequency range were conducted for a total of 10 min. The acceleration test levels and their results were as follows:

1. White Gaussian noise, PSD of 0.20 g^2/cps from 30(to 1000 cps, with a 6 db/octave roll-off from 100(

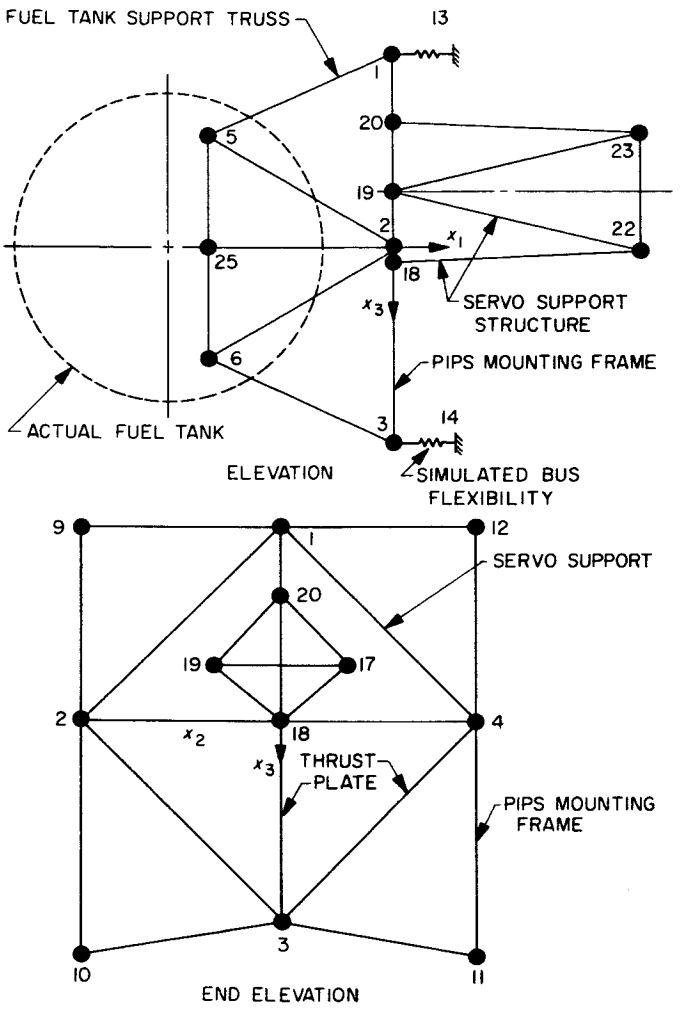


Fig. 78. PIPS structural component idealization

to 2000 cps, a 3 db/octave roll-off from 300 to 20 cps, and a 24 db/octave roll-off below 30 and above 2000 cps for 3 min

2. A 2.5 g rms sinusoid between 20 and 100 cps
3. White Gaussian noise, PSD of 0.010 g^2/cps, band-limited between 100 and 2000 cps, plus a 2.5 g rms sinusoid superimposed on the noise between 100 and 450 cps
4. White Gaussian noise, PSD of 0.010 g^2/cps, band-limited between 100 and 2000 cps, plus an 8 g rms sinusoid superimposed on the noise between 450 and 2000 cps

The STM PIPS was complete with bladdered fuel tank and its support structure, nitrogen, thrust chamber, thrust plate, and support frame. Preliminary test results showed that dynamic amplification from the PIPS support frame to the CG of the fuel tank was a function of fuel tank pressure. This amplification increased from 2 for zero tank pressure to 12 for a full tank pressure of 400 psi.

Final vibration qualification testing was done on the complete STM vehicle at full fuel tank pressure in the most critical axis of excitation for the PIPS (i.e., along the spacecraft roll axis). Propellant tank test pressures were 150, 300, and 400 psi; the maximum dynamic response of the PIPS occurred at a maximum flight pressure of 400 psi. The highly nonlinear behavior of the PIPS was caused by the fluid sloshing in the bladdered fuel tank. Response information for the PIPS propellant tank during the most critical Z axis low-frequency test showed that an input excitation at 108 cps excited the fundamental slosh frequency at 54 cps.

e. Solar panel structure. One of the most critical constraints on configuration selection and detail design of the solar panel structure was a stringent weight limitation. This weight limitation dictated a radical departure from past solar panel structural designs. The highly reliable panel structures of the *Ranger* and *Mariner* Venus 1962 programs were abandoned in favor of a new structure of approximately half the weight per surface area. As might be expected, this step function reduction in structural weight required a considerable development program to demonstrate appropriate reliability for flight purposes.

A damped system of support was selected to attenuate dynamic motion and loads and to allow necessary reductions in structural weight.

In launch configuration, the panels were oriented approximately parallel to the longitudinal axis of the launch vehicle; consequently, the steady-state boost accelerations were of little consequence to panel design. The controlling design load proved to be lateral booster vibration. Response computations for the damper-supported panel system were originally performed on the IBM 1620 digital computer. Subsequent refined response analyses were carried out on the IBM 7094 digital computer. These response analyses resulted in a set of magnification factors that were translated into the equivalent design static load elements of a design specification. This design specification stated basic static criteria of 5 g for spar design and 20 g for substrate design. The design load for the substrate is now considered to be low, because of the relatively ineffective participation of the damper supports in the attenuation of transverse substrate responses.

Detailed static stress analysis was performed by the solar panel contractor and documented in a formal stress report (Ref. 23). Dynamic normal mode and response analyses of the panel were also performed. In general, the dynamic response analyses used consolidated parameter systems of from 37 to 90 nodes per panel. It was found that a grid system of 44 nodes, with 3 deg of freedom per node, adequately represented the first five normal modes of the system. This idealization is shown in Fig. 79. The digital computation problem of determining panel dynamic responses to a periodic forcing function was by no means trivial. The damper supports of the panel required the use of a complex orthogonality condition, with corresponding complex modal vectors and complex response amplitudes (Ref. 24 and 25). Because of this formidable task, a parallel analog computer response solution was undertaken. Both digital and analog approaches eventually yielded comparable results.

A set of preliminary tests was conducted to build early confidence in the adequacy of the panel design.

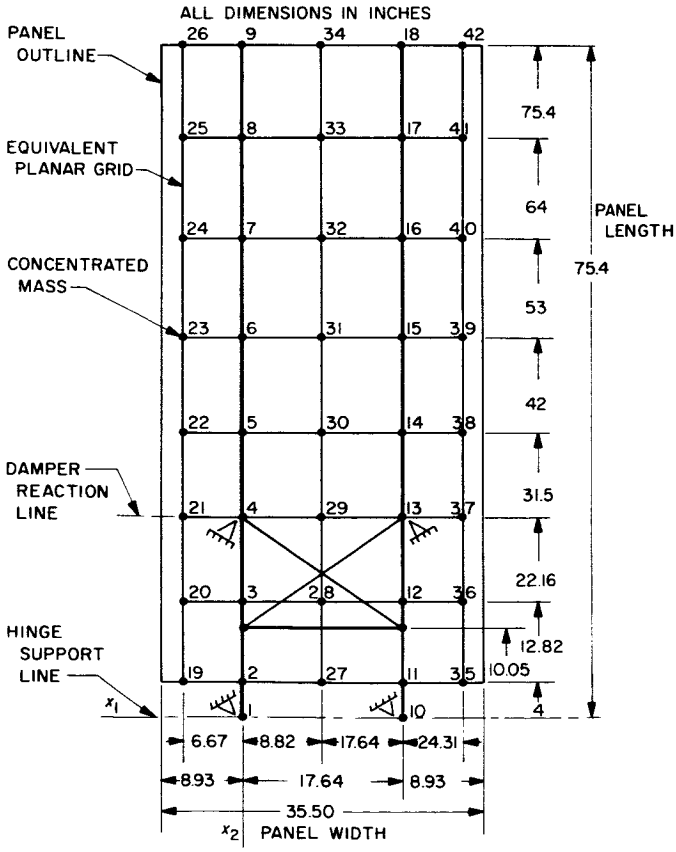


Fig. 79. Forced response analysis structural idealization for solar panels

1. *Panel static test.* This test verified the adequacy of the panel to withstand the specified static design loads, and was performed as a part of the panel design and fabrication contract (Ref. 26).
2. *Panel acoustic test.* This test verified the adequacy of the all-bonded panel to survive the qualification acoustic environment.
3. *Preliminary vibration tests.* Two tests were performed at assumed vibratory input levels. In one test the panel was supported on dampers and in the other test the panel was hard-mounted using no dampers.
4. *Substrate buckling and fatigue tests.* A series of tests was conducted to determine the fatigue properties and the static and dynamic buckling characteristics (including fixity coefficients) of the critical unsupported substrate back corrugation flats. These tests verified the nature of the conservative assumptions used for design.

Formal qualification of the panel damper system consisted of a low-frequency (5 to 150 cps) sinusoidal vibration test. The purpose of this test was to determine the ability of the panel to survive the *Mariner* vibration environment without degradation. A second purpose of the test was to determine the frequency response characteristics of the solar panels, as supported upon discrete dampers in the spacecraft launch configuration. The input levels to this test were carefully developed from preliminary STM test data to envelop panel responses for the most critical spacecraft test conditions.

The results of this test were satisfying, and the panel successfully passed the qualification sequence and demonstrated structural adequacy for flight purposes. Subsequent tests to failure vividly illustrated the lack of excessive (unnecessary) margins of safety. At 112% of ultimate vibratory load, functionally noncritical cracks developed in the substrate corrugations.

4. Composite Analysis

An overall spacecraft structure composite analysis was performed to determine the modal and response characteristics of the composite structure for static and dynamic loads. These results were used for the prediction of loading conditions and dynamic coupling for major substructures.

a. General description of analysis methods. The fundamental tool used to perform the composite analysis

was the modal combination computer program developed for the 7094 IBM computer. Unfortunately, this program was not working early enough to employ it during design, and the task was accomplished using the stiffness matrix structural analysis computer program (STIFF-EIG) with a sacrifice in accuracy and versatility.

b. Analysis Plan and Idealization (STIFF-EIG). Realizing the size limitation of the stiffness matrix structural analysis, the composite structure was idealized as a three-dimensional pin-jointed structure. Symmetry was assumed around a vertical plane through the midcourse motor axis. To emphasize various major structural components, the spacecraft was idealized with and without the effect of solar panels and adapter. The most useful idealization considered the stiffness and mass effect of the adapter with the masses of the solar panels and omnidirectional antenna at their support points. Although detailed structural idealization of the major structural components was lost by using STIFF-EIG, the general effect of each component on the overall structure was retained in the analysis.

c. STIFF-EIG vs modal testing results. Agreement between analytical and STM modal testing results was considered good. A brief comparison of the results for the major spacecraft modes is summarized in Table 23.

Table 23. Comparison of analytical and STM modal testing results

Mode description	Test results	
	Modal cps	Analytical cps
Science platform vibrating in X-axis direction coupled with midcourse motor	48.3	48.75
Midcourse motor vibrating in Z-axis direction coupled with science platform	48.2	44.32
High-gain antenna minor axis rocking	38.3	39.43
Science platform and secondary structure vibrating in Z-axis direction	92.3	93.80

The problem of science platform and midcourse motor dynamic coupling was eliminated when a stiffer midcourse motor frame was used.

d. Analysis plane and idealization (modal combination program). In using the modal combination program for the composite analysis, individual STIFF-EIG analyses of the various structural components were tied together into a large overall response solution of the composite structure. The detail of the structural idealization for each component was retained, and the amount of individual damping (large and small) in each component was considered.

VII. SPACECRAFT SUBSYSTEMS: RADIO

A. General Description

The *Mariner IV* radio is an S-band system designed to provide reliable communications for a distance of more than 150 million miles and survive in space for a minimum of 9 months under environmental conditions found from launch through Mars encounter.

The radio package consists of a phase-coherent transponder using a transmitter configuration designed for maximum reliability of spacecraft-transmitted signals through the independent use of redundant exciters and power amplifiers. The transponder has the capability of (1) receiving Earth-transmitted commands and transmitting verifications of such commands, (2) transmitting scientific data gathered during the flight to and past the planet, (3) transmitting information regarding the progress and behavior of the spacecraft during its flight, and (4) using a turnaround ranging system to detect a wideband pseudonoise code that has been modulated on the received signal and to remodulate it on the transmitted carrier.

The S-band transponder was developed from the basic L-band transponder used on the *Mariner* Venus 1962 and *Ranger* spacecraft. Development of the S-band system provided improvements in the following areas:

1. The design of the two signal amplifiers preceding the AGC detector was improved to obtain stages that do not saturate under noise conditions at threshold. The threshold noise level is 23.5 db above the signal level, the signal level being held nearly constant over the dynamic range by the AGC system. The stages were designed to provide constant signal gain with noise levels 5.5 db above the rms threshold noise voltages.
2. Phase distortion of the detected command signal was reduced by a change in the type and bandwidth of the crystal filter in the second IF amplifier. The bandwidth was increased to extend the linear phase characteristics across the modulation spectrum, and the crystal-filter design was changed to reduce the slope of the phase change across the bandpass.
3. The receiver noise figure was reduced with the design of a mixer using cartridge-type mixer diodes in lieu of the miniature diodes and low-noise transistors in the preamplifier.
4. Improved circuitry in the multiplier chains reduced the level of coherent sidebands. This eliminated the problem of interference from sidebands in the local oscillator reference signal.
5. Phase control of the signal and reference to the ranging detector over the temperature and dynamic range was accomplished at 9.5 Mc.
6. The output power level of the solid-state stages was increased from 10 to 500 mw. In the *Mariner IV* application, this eliminated one of the power-tube amplifiers, thereby increasing the system reliability.
7. A reduction in weight was accomplished primarily by two changes. First, module chassis were reduced in thickness from 1/8 to 1/16 in. Second, all non-RF stages were packaged using the welded-cordwood-module technique. With this technique it was possible to reduce the number of modules in the system from 15 to 13. The combined reduction in weight resulting from both these changes was approximately 4.0 lb.

The assembly of the radio subsystem is contained in two cases that are mounted to the octagonal structure of the spacecraft. Case V, which houses the transponder receiver and its power supply, is shown in Fig. 80(a). Case VI houses the transmitting portion of the transponder (including the TWT power amplifier and triode cavity amplifier with their associated power supplies), two band-rejection filters, one four-port circulator switch, one five-port circulator switch, two directional couplers, and a control unit switching logic. Case VI is shown in Fig. 80(b). The modules are interconnected by shielded two-conductor cable and RF coaxial cable. All circuitry, except the triode cavity amplifier and TWT amplifier, is solid state. The complete radio subsystem assembly is shown in Fig. 81.

Reception of Earth-transmitted signals or transmission of spacecraft signals is through either a low-gain omnidirectional antenna or a high-gain directional antenna. A block diagram of the radio subsystem is shown in Fig. 82. The parameters are listed in Table 24.

B. Functional Description

1. Reception

The received signal is amplified by a double-conversion, superheterodyne, automatic phase-tracking receiver.

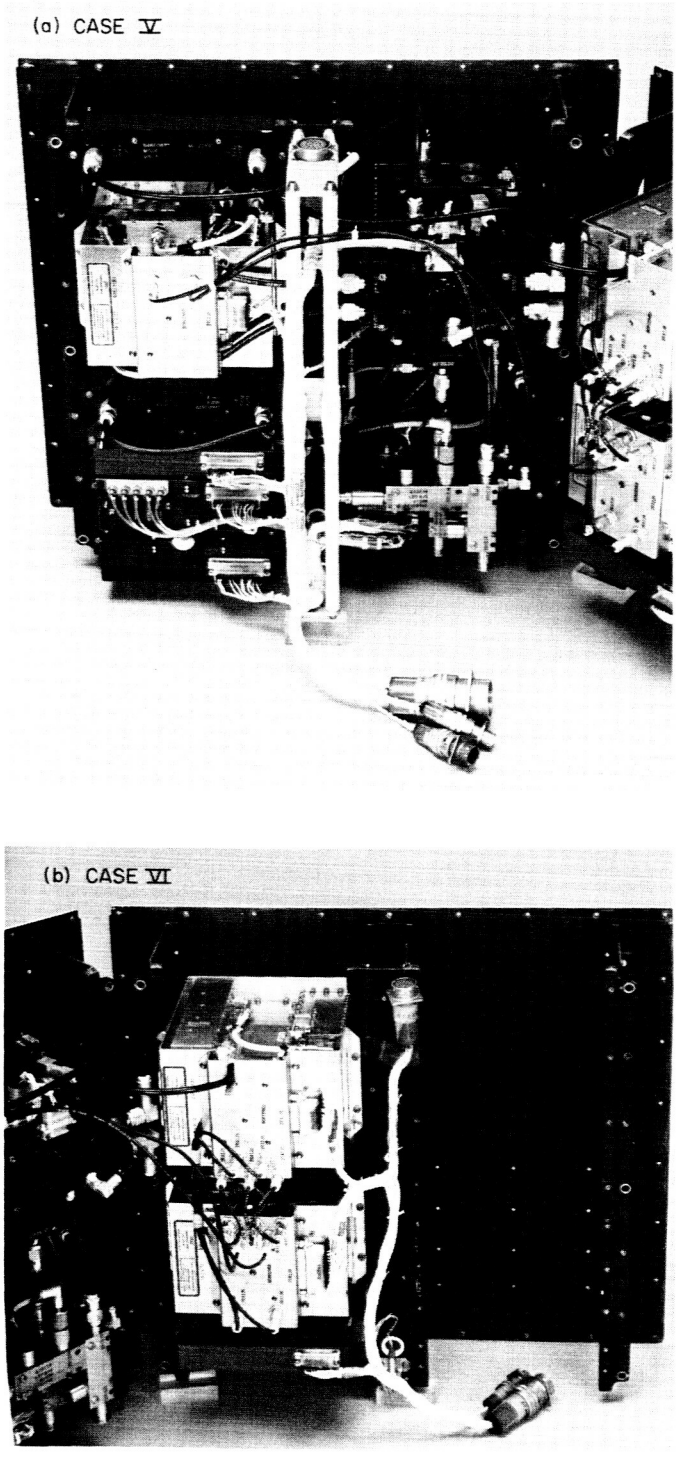


Fig. 80. Radio subsystem

a. Automatic phase tracking loop. Phase coherence is accomplished by an automatic phase tracking loop that is closed around the entire receiver by way of the first local oscillator. The system multiplication is constructed as shown in Fig. 83. The receiver multiplication equals 110.5 (or 0.5 + 3 − 1 + 108), the transmitter multiplication equals 120, and the ratio between the received and transmitted frequencies is 110.5/120 or 221/240. It can be seen from the diagram that all of the local oscillator and detector reference signals are derived by frequency multiplication from the receiver VCO. The loop parameters have been selected by minimizing the total mean square phase error over the receiver dynamic range of input signal-to-noise conditions.

Table 24. Radio subsystem characteristics

Characteristic	Numerical value
Receiver	
Frequency	2116 Mc
Noise temperature (maximum) including preselector	3370°K
Threshold carrier level	−150 dbm
Dynamic range to threshold	−70 dbm
Maximum receiver gain	193 db
Direct current input power	5.5 w
APC loop, threshold design values	
Loop noise bandwidth	20 cps
Suppression factor	0.058
Detector gain	20 v/rad
VCO gain	120 cps/v
Phase gain	110.5
Predetection bandwidth	4.5 Kc
AGC loop, design values	
Noise bandwidth	0.5 cps
Receiver gain control	16 db/v
Detector gain	0.1 v/db
Amplifier gain	15 v/v
Ranging channel	
Overall bandwidth at video output	1.8 Mc
Ranging modulation index	0.45 rad
Transmitter	
Frequency	2295 Mc
Power output	
Exciter	+27 dbm
TWT amplifier	+40 dbm
Cavity	+38 dbm
Phase modulation range	0 to 1.5 rad
Phase modulation bandwidth (3 db)	1.8 Mc
Input power	
Exciter	8.0 w
TWT amplifier	45.5 w
Cavity	23.3 w
Power supply	
Efficiency (exciter)	72%
Efficiency (power amplifier)	80%
Total system weight (less chassis and cable harness)	35 lb

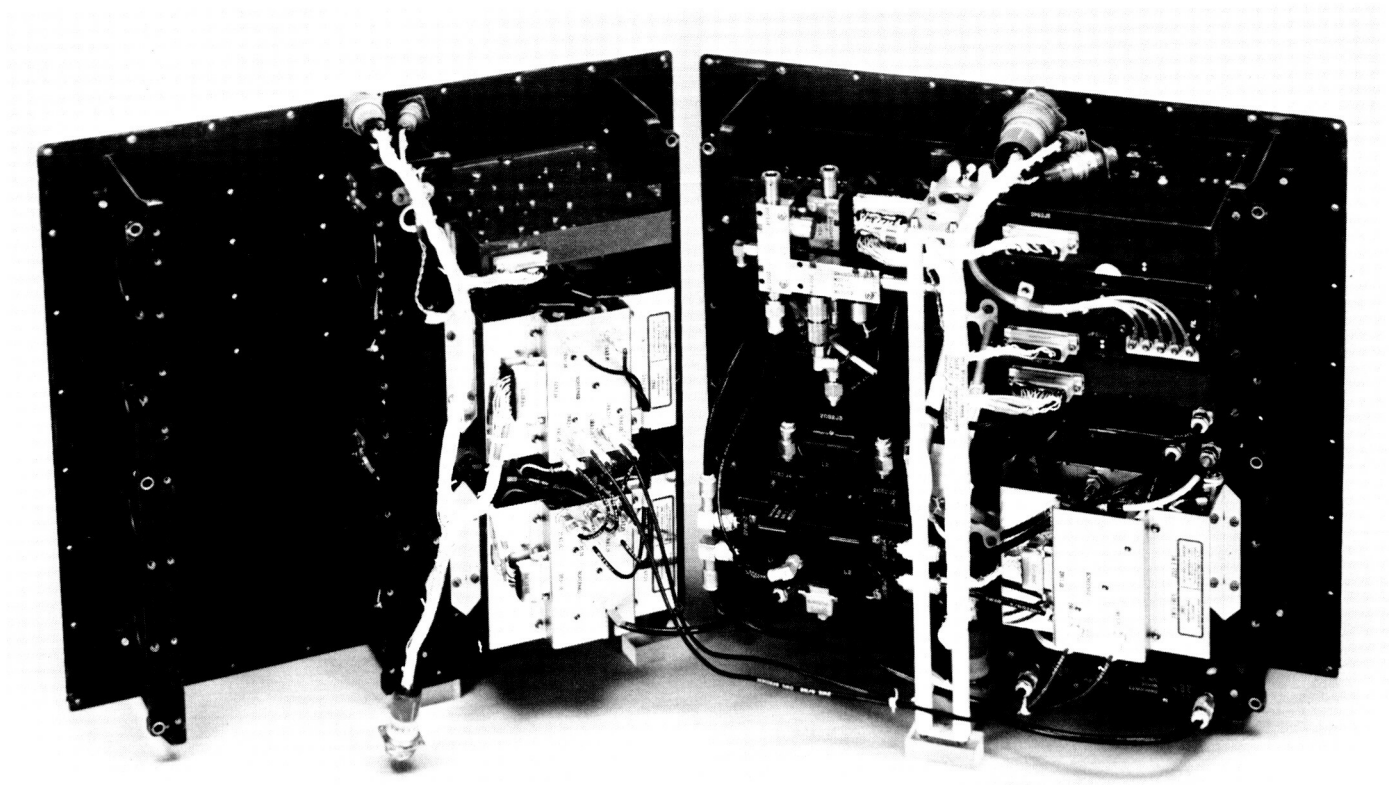


Fig. 81. Complete radio subsystem assembly

b. Receiver response. The receiving section of the transponder is designed with a predetection noise bandwidth of 4.5 kc and a loop noise bandwidth ($2B_1$) of 20 cps. A bandpass limiter placed ahead of the loop phase detector holds constant the total signal-plus-noise voltage into the loop, making the loop noise bandwidth dependent upon the signal-to-noise ratio in accordance with the limiter suppression effect. The loop noise bandwidth of 20 cps is obtained with a suppression factor of 0.0588. When the suppression factor becomes unity, as is the case for input signal-to-noise ratios greater than 20 db, the loop noise bandwidth approaches 233 cps as a limit. It is important to note here that, in effect, this bandwidth change makes it possible to track comparatively large signal variations that are apt to appear during the launch and near-orbit phases of the mission.

c. Modulation response. Phase modulation is extracted from the phase tracking loop as the untracked output of the loop phase detector. Thus, if the receiver response is H, the modulation response is $1 - H$. The high-frequency characteristics of the measured response are restricted by the predetection bandwidth and remain essentially constant, while the low-frequency characteristics are affected by the loop-noise bandwidth variation as a function of signal level.

d. Receiver threshold. The threshold signal level, under which the transponder maintains reliable phase coherence between the input and output signal, is defined to be that level at which the loop rms phase error is equal to 1 rad. This level corresponds to unity signal-to-noise ratio in the phase-controlled loop. The nominal signal level at which it occurs is found from the loop noise bandwidth and the receiver noise figure. For the *Mariner* transponder, this figure is typically −150 dbm.

e. Signal amplifications. A total forward gain of about 193 db was designed into the receiver to ensure limiting at the phase detector under threshold conditions, and to provide for the effects of aging, temperature, radiation, and detuning. This amount of gain is sufficient to maintain the limiter output at 15 dbm and a level of −22 dbm ± 1 db into the amplitude detector. The gain is provided by a 47.8-Mc preamplifier nominally set at 46 db (including first mixer loss), a gain-controlled 47.8-Mc IF amplifier with a controllable range

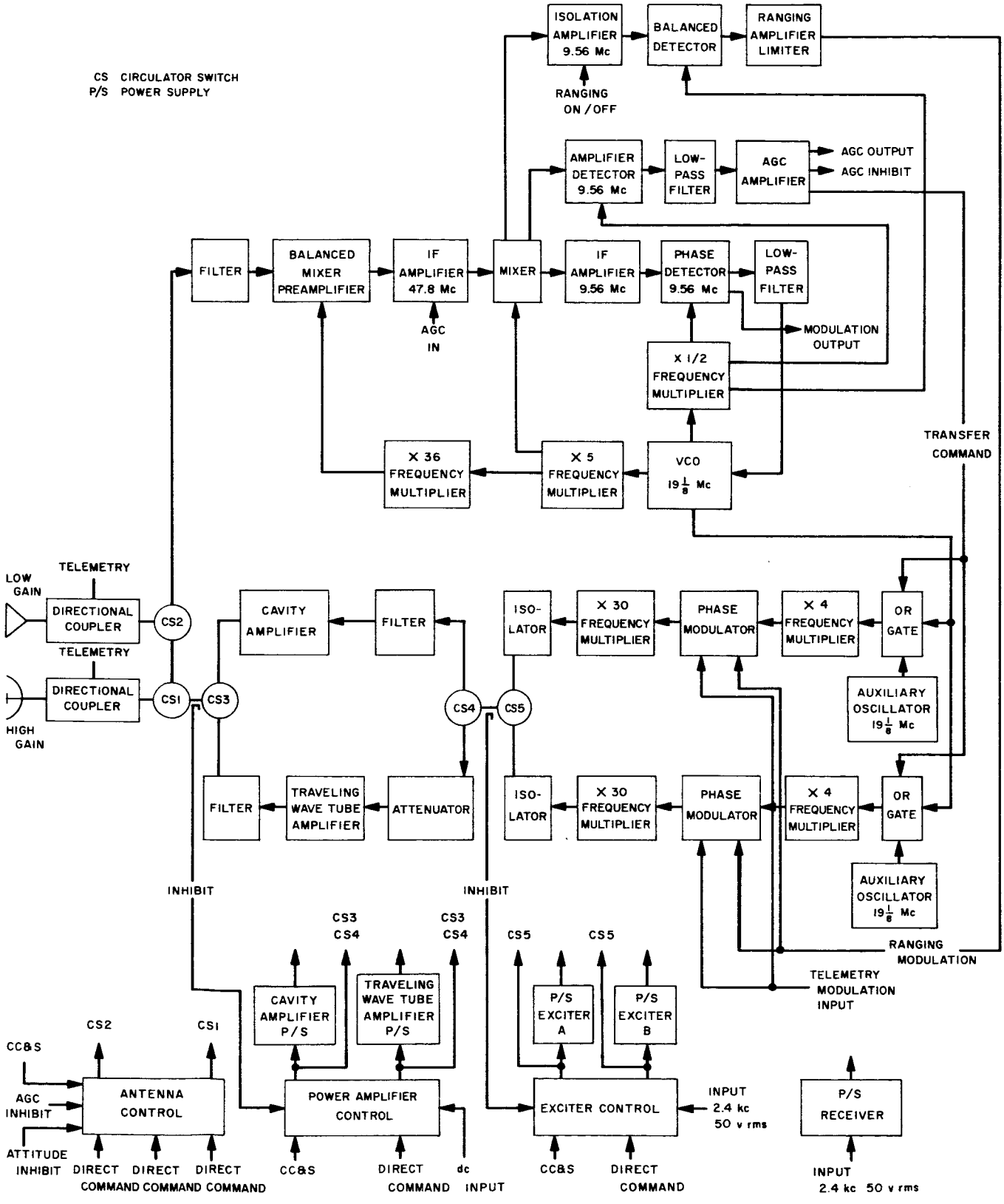


Fig. 82. Radio subsystem functional block diagram

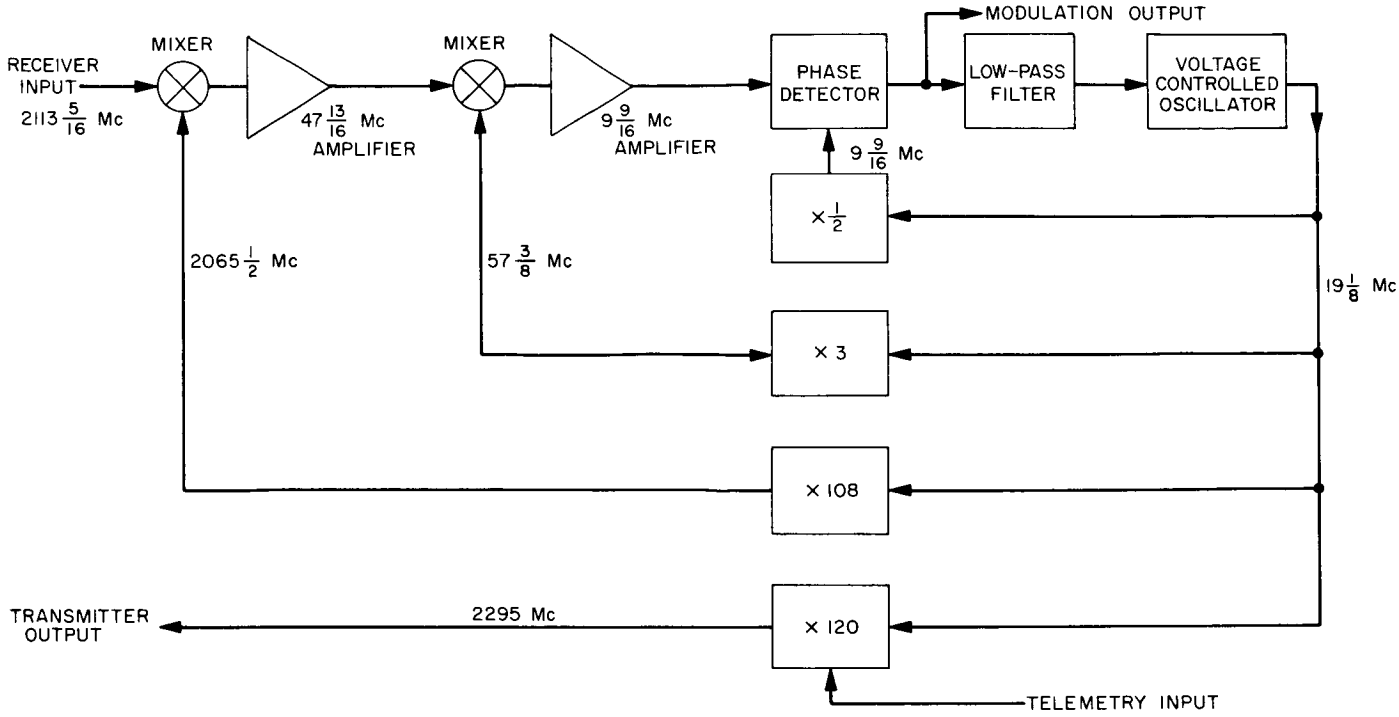


Fig. 83. Transponder phase multiplication

from −51 db to +52 db, and a 9.56-Mc IF amplifier nominally fixed at a gain of 95 db.

f. Automatic gain control system. Coherent automatic gain control is applied to the 47.8-Mc IF amplifiers. By means of a synchronous amplitude detector and AGC filter, the gain of the receiver is controlled only by the amplitude of the received signal. In this way, the system provides an accurate analog of the receiver input signal strength. The AGC loop is designed to have a noise bandwidth of 0.85 to 0.33 cps over the range of input signal levels from −70 to −150 dbm.

g. Turnaround ranging channel. The ranging loop was designed to detect the 498-kc ranging information transmitted on the uplink carrier, to amplify and detect the information, and to retransmit it as phase modulation on the downlink carrier (Ref. 27). There are two modules that are common to the ranging loop: these are the 9.56-Mc isolation amplifier and balanced phase detector, and the wide-band limiting amplifier. The ranging channel is turned on or off by direct (ground) command.

h. Receiver power supply. A single power supply furnishes −15 and +15 v regulated power to the transponder receiver. The power supply operates from the spacecraft 50-v-rms, 2.4-kc source, delivering regulated power at an efficiency of 72% or better.

2. Transmission

The transmitted signal is derived from either the voltage-controlled crystal oscillator or a fixed-frequency crystal oscillator (auxiliary oscillator). The VCO-derived signal is used when the receiver APC loop is in lock with the Earth-transmitted signal, and thereby provides a transmitted signal that is phase-coherent with the received signal but translated in frequency by the constant 221/240 ratio between the received and transmitted frequencies. During periods that the transponder is not in two-way lock, the receiver noise is prevented from modulating the transmitted carrier by automatically switching the VCO output off and energizing the auxiliary oscillator to excite the transmitter. Mode transfer is controlled by the receiver AGC signal.

a. Modulator. The modulating signal is applied after the first multiplier stage X4 in the transmitter. Modulation is accomplished by varying the tuning of a parallel resonant circuit containing voltage variable capacitors. The instantaneous reactance of the circuit is controlled by the instantaneous value of the modulating signal. The modulated RF is multiplied by a factor of 30 to provide the transponder transmitter phase-modulated output.

b. Redundant transmitters. Two exciters and two RF power amplifiers make up the transmitting portion of the transponder. Either exciter, when energized, drives the TWT and/or the triode cavity amplifier. Only one amplifier and one exciter are operating at any given time. A band-reject filter is used to prevent undesirable products of the transmitted signal appearing at the receiver frequency from interfering with the receiver. One filter is located at the output of the TWT amplifier. The other is located at the input of the triode cavity amplifier. These locations shorten the RF path from the cavity amplifier output to the antenna, without significantly degrading system filtering effectiveness and increasing the available margin in cavity RF power output. Switching of the primary power applied to the power supplies determines which combination of exciter power amplifier is used. A simple resistive network parallels the exciter inputs.

The RF switches select exciter output, power amplifier input and output, and the antenna to be used. The RF switches are controlled by the control-unit output voltage.

Exciters. The two exciters are of identical design; each provides a minimum of 500 mw of RF power when energized. The design is solid state; it uses the latest varactor-multiplier techniques to obtain maximum reliability and efficiency. Included as part of the exciter is a phase modulator capable of accepting ranging and telemetry modulation signal inputs simultaneously. An isolator at the output of each exciter prevents variations in load VSWR from detuning the final stage.

Power amplifiers. Either a triode coaxial cavity amplifier or a traveling wave tube amplifier is used for the power-amplifier stage. The triode cavity amplifier has a low- and a high-power mode. At launch, the triode plate voltage was 110 vdc. At vehicle separation, an interlock raised the voltage during the initial portions of the flight and eliminated the possibility of voltage breakdown through the critical pressure zone. The RF power output at reduced plate voltage is nominally 1 w; the RF power output at high plate voltage is nominally 7 w. The efficiency is typically 30%.

The TWT amplifier is one of a class of microwave tubes known as linear-beam amplifiers in which the electron gun is designed to optimize thermal characteristics and the RF structure is designed to optimize gain and efficiency (Ref. 28). The RF power output is nominally 10 w; the efficiency is typically 22%.

Power supplies. Separate power supplies furnish regulated power of -15 and -25 v to the exciters. The power supplies are packaged as a single unit and operate from the common 50-v-rms, 2.4-kc input that is switched to either supply by a relay located in the control unit. The TWT amplifier power supply and triode cavity amplifier power supply are integral units individually packaged; both operate directly off the spacecraft solar panel power supplied on a common line that is switched to either supply by a relay located in the control unit. The major functions of the power supplies are input-voltage regulation, rectification, and filtering. The dc-to-ac conversion is required only of the power-amplifier power supplies. All power supplies are solid state and deliver regulated power at an efficiency of 72% or better.

RF switches. The type of switches used are voltage-operated circulators. These switches offer a matched-load impedance and a means of changing the RF path while maintaining a low insertion loss in the path. The application of a positive or negative drive voltage from the control unit causes the RF signal to circulate in a clockwise or counterclockwise direction from the input terminal. The next terminal in the direction of circulation becomes the output terminal. The terminal opposite to the direction of circulation becomes isolated. In this manner, the required switching is obtained with the necessary isolation, minimum insertion loss, and maximum reliability.

Control unit. The control unit contains solid-state switches, relay switches, logic circuits, and telemetry conditioning circuits, and provides the output voltages applied to the RF switches. The unit accepts signals from the command, attitude control, and CC&S subsystems, and conditions the exciter and antenna drive levels for the data encoder telemetry channels.

The antenna control circuit switches two external loads and accepts signals from seven sources. The circuit switches high-gain and low-gain antennas by changing the polarity of circulator switches to direct RF signal paths to and from the selected antenna. The antenna control circuit accepts four command inputs, a cyclic input, an attitude control input, and an acquisition signal input. The command inputs switch the external loads when they are accepted in a compatible combination with the state of the control unit output. The cyclic-signal input, a grounded or open circuit, operates the solid-state switches in the receiver–antenna switch circuit when the inhibit signal is not present. This inhibit signal

appears and remains on the circuit whenever the acquisition signal is −4.5 v, or less negative. When the acquisition signal is −5.5 v, or more negative, the cyclic signal does not actuate the solid-state switch but removes the circuit inhibit state. Subsequent application of the cyclic signal then operates the solid-state switch. This circuit uses the cyclic input only for actuating the solid-state switch. The attitude control input switches the drive to the receiver low-gain antenna state whenever the Canopus sensor loses lock, but it does not interfere with subsequent command inputs.

The power-amplifier control circuit switches two external loads and accepts signals from four sources. The circuit applies dc voltage to one or the other of the redundant power-amplifier power supplies, and simultaneously reverses the polarity of circulator switches to direct the amplifier input and output. The control circuit accepts a command input signal, a cyclic signal, a low-level dc input, and a high-level dc input. The switching function is activated by the cyclic input in the event the low-level dc input, monitored at the amplifier output, drops below 600 mv. The switching function is also activated by the command signal regardless of the dc level monitored. The cyclic input does not actuate switching if dc input is 700 mv or more.

The exciter control circuit also switches two external loads and accepts signals from four sources. The circuit applies a 2.4-kc square wave to one or the other of the redundant exciter power supplies, and simultaneously reverses the polarity of circulator switches to direct the exciter output. This circuit also accepts a command input signal, a cyclic input signal, a dc voltage signal ranging between 0 and 1.5 v, and a 2.4-kc square wave signal. The circuit-switching function is activated by the cyclic signal input in the event the dc input, monitored at the exciter output, drops below 600 mv. The switching function is also activated by the command signal, regardless of the dc level monitored. The cyclic input does not activate switching if the dc input is 700 mv or more.

The control unit accepts four power monitor signals, five command signals, a 2.4-kc square wave input, a high-level dc input, a cyclic signal input, an acquisition signal, and two mode transfer signals. The five command signals, the cyclic signal, and the mode transfer signals provide a ground or open circuit to the switching circuits.

The 2.4-kc square wave, applied to a transformer rectifier, provides a B+ switching voltage that is applied through the contacts of a relay switch or a solid-state switch to a terminal of each of the circulator switches. The 2.4-kc square wave is also used to energize the power supplies to the exciters through contacts of a relay switch. The dc input, controlled by a relay switch, is applied to energize the power supplies of the power amplifiers. The acquisition signal voltage is −1 to −9 v. This signal controls a bistable flip-flop, which provides an inhibit function to the solid-state switch. The inhibit appears and remains when the acquisition voltage is −4.5 v, or less negative. If the acquisition voltage is −5.5 v or more negative, application of the cyclic input will not actuate the solid-state switches but will remove the inhibit function. A subsequent application of the cyclic signal will actuate the solid-state switch.

C. Procurement

At the start of procurement, contractors and JPL established a flow chart showing each step of fabrication and inspection points. Route cards, inspection plans, and check lists were prepared in conjunction with the flow chart. Workmanship standards were reviewed and acceptance criteria were established.

Serialization of all parts was accomplished by means of a detailed screening specification prepared by the contractor, which required that the test data be recorded and maintained for documentation purposes by incoming inspection. For equipment such as the transponder, the serial number of the part was recorded along with the

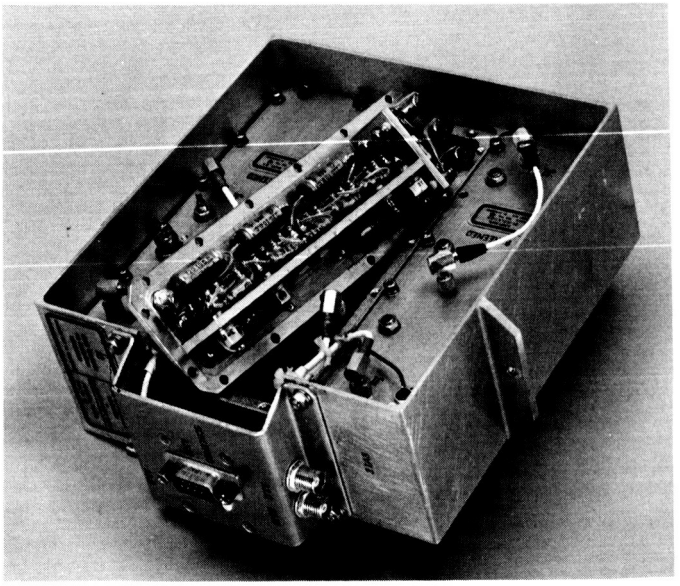


Fig. 84. Typical radio subsystem module

serial number of the module or system. In the event of a part failure, the test data, lot information, and date the part was received were thus traceable.

If a failure occurred during either module or system testing, JPL was notified within 24 hr as to the type of failure and the recommended action taken. Parts requiring analysis were submitted to reliability and component specialists for analysis and recommended corrective action. After the failure was corrected, the affected item was reinspected and retested to verify that the corrective action solved the problem.

Figure 84 shows a typical module of the radio subsystem.

D. Antenna Subsystem

At the inception of the *Mariner* Mars design, it was clear that the solutions to the spacecraft antenna problems could not be patterned after the previous planetary probe, *Mariner II*, or its lunar counterpart, *Ranger*, for several reasons. First, the look angles to Earth from a Mars-bound spacecraft are entirely different from those of Venus and the Moon, plus the fact that the Earth–Mars range at encounter would be more than three times that to Venus and more than 50 times that to the Moon. Second, it would be the first use by JPL of the S-band frequency (*Ranger* and *Mariner II* used 840- to 960-Mc frequencies). Third, weight was critical and, hence, only 15 lb was allotted for the entire antenna system, whereas *Ranger* used 30 lb and *Mariner II* used 41 lb.

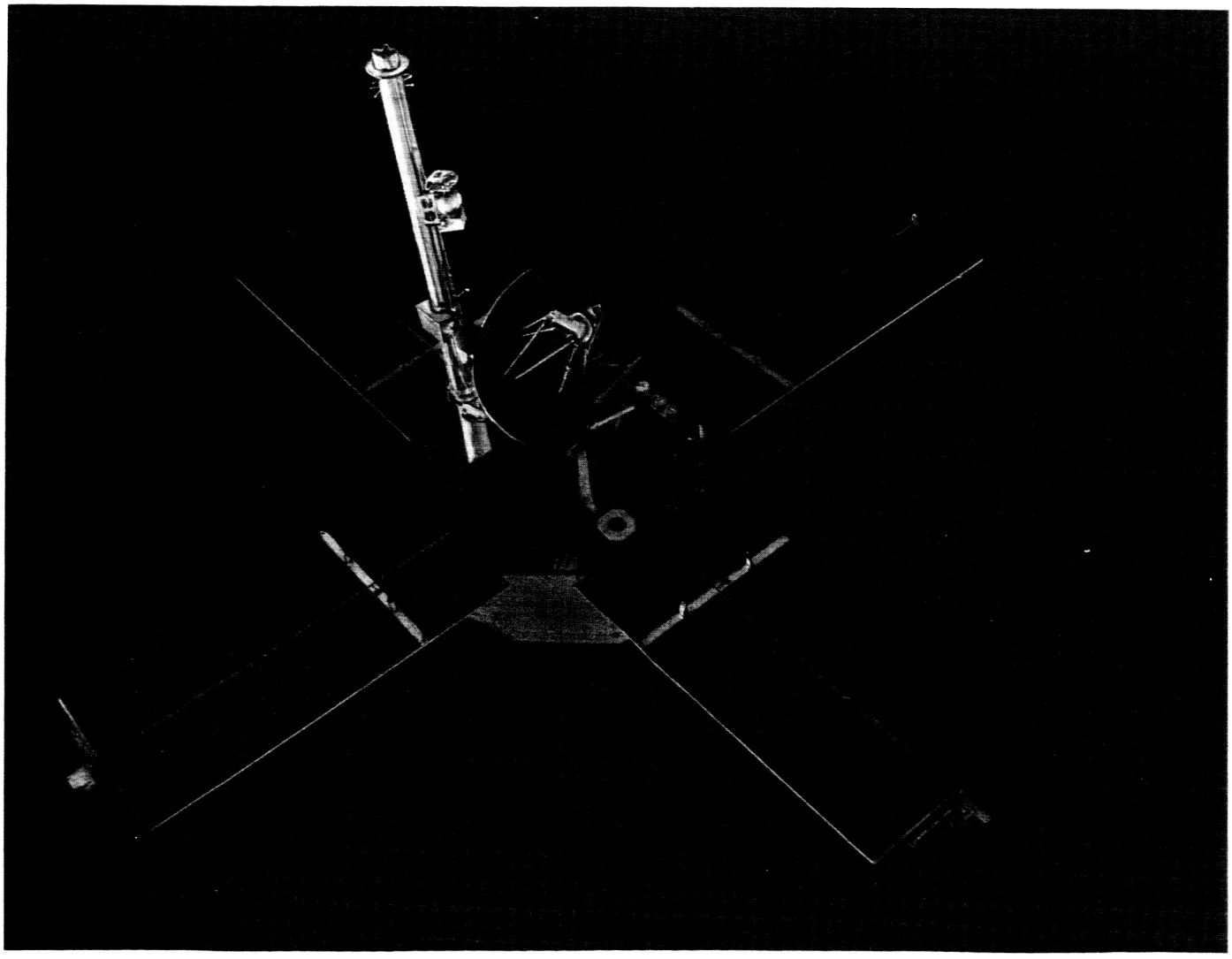


Fig. 85. *Mariner IV* antennas mounted on spacecraft

The spacecraft antenna system includes the low-gain antenna, the high-gain antenna, and both of their transmission lines. The antennas may be seen mounted on a flight spacecraft in Fig. 85.

The functions of the low-gain antenna, shown in Fig. 86(a), are to receive commands from Earth during the entire flight, and to transmit flight telemetry to Earth during the first half of the mission when the spacecraft is near Earth and the look angles to Earth vary widely. The low-gain antenna must also be able to receive commands and transmit telemetry to and from Earth during midcourse maneuvers.

The high-gain antenna, seen in Fig. 86(b), a 46 × 21-in. elliptical paraboloidal sector with a peak 23-db gain, is mounted on the spacecraft in a fixed position so that the look angles to Earth during the last half of the flight will fall within the main lobe of the antenna. The antenna's primary function is to transmit telemetry to Earth during the last half of the transfer orbit and for 20 days after planetary encounter during the video playback period.

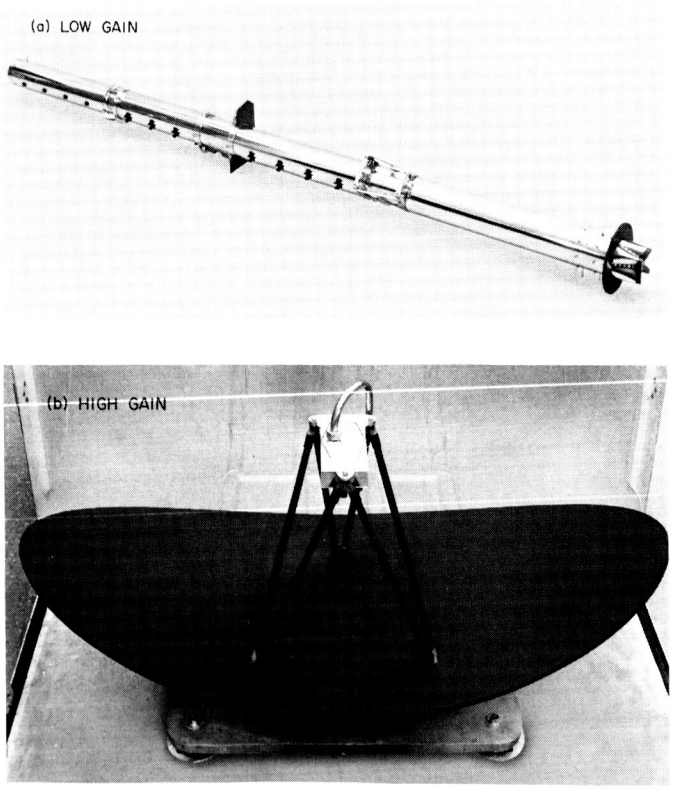


Fig. 86. *Mariner IV* low-gain and high-gain antennas

The function of the transmission lines is to transfer RF energy between the radio subsystem and the antenna in the most efficient manner.

1. Design Evolution of the Low-gain Antenna

One of the most fundamental considerations in the design of the low-gain antenna was the transfer orbit characteristics and, hence, the look angles to Earth and to the Sun from an inertially oriented spacecraft. The spacecraft roll axis would always be pointed toward the Sun. This fixed the reference source (the Sun) for two axes (pitch and yaw) and allowed the solar array to be deployed symmetrically about the roll axis. It also allowed the direction of Earth, relative to the Sun-oriented spacecraft roll axis, to be determined for any particular mission or trajectory. This angle is defined as the Earth–probe–Sun angle.

The third axis of freedom (the roll axis) is also fixed to a reference. However, the omnidirectional or low-gain antenna is mounted on the spacecraft with its axis of symmetry colinear with or parallel to the roll axis, and, hence, it is independent of the roll axis reference. One of the prime reasons for this orientation of the low-gain antenna is that, in the event the third axis reference is lost or not acquired, the command communications capability to the spacecraft can be guaranteed regardless of the third axis orientation. Of course, the communications distance (the distance beyond which telemetry to Earth is no longer possible) depends primarily upon spacecraft transmitted power and antenna gain.

The Earth–probe–Sun angles for the *Ranger* program were constrained, for various reasons, to be between 40 and 140 deg. The low-gain antenna used to implement this requirement was a disk-cone linearly polarized antenna. This antenna radiated a toroidal pattern with nulls along both ends of the roll axis. It was necessary to mount the antenna sufficiently far above the bus and solar array (1) to gain a clear view of all required look angles and (2) to reduce the interference ripple caused by the reflection off of the spacecraft structure.

The Earth–probe–Sun angles for *Mariner II* were in the rear hemisphere (away from the Sun) of the spacecraft, except during a short period when the spacecraft was close to Earth. Due to the limited design time for that program, a *Ranger* low-gain antenna was used for near-Earth telemetry, and a turnstile–dipole combination was used on either side of one of the solar panels for command reception. The rear-looking turnstile was fed

at a 6-db-higher level than the dipole that was used for near-Earth fill-in.

Since the trajectory to Mars goes outside the Earth's orbit, the Earth–probe–Sun angles are primarily in the forward hemisphere of the spacecraft. There were some trajectories in the early part of the launch window that created Earth–probe–Sun angles near Earth up to 130 deg from the Sun line. This look-angle geometry indicated that a simple, circularly polarized antenna such as a turnstile, spiral, or crossed slot could be used. The basic pattern of these antennas is a cardioid of revolution, with the maximum along the axis of symmetry. Beam shaping can be controlled with the use of ground plane location, size, and shape.

A major problem was the placement of the radiating aperture sufficiently far above the plane of the solar array to (1) enable good look-angle geometry, (2) be above the tips of the solar panels when folded, and (3) avoid energy reflecting off of the solar array. Another major engineering design hurdle was the requirement that the antenna and its support structure be very lightweight in order to avoid shifting the spacecraft center of gravity upward beyond the midcourse motor's pointing adjustment range and to keep the total spacecraft weight low.

The design concept satisfying these requirements was a low-gain antenna formed as the termination of a tall cylindrical waveguide. The waveguide acts as both the mechanical support structure for and the electrical transmission line to the low-gain antenna. The 7-ft tall, 4-in.-diameter tubular waveguide, shown in Fig. 86(b), was too weak a structure when supported in a conventional manner to withstand the vibration levels of the spacecraft boost environment; however, it did fulfill the requirements of not occluding the high-gain antenna or the fields of view of the science instruments, and it did place the low-gain antenna high enough above the spacecraft near the spacecraft center line.

The waveguide was made of 0.025-in. wall thickness, 4-in.-diameter tubing, with the antenna aperture (a crossed slot) section formed into the end of the tube as a four-section crimp. The remainder of the basic radiating structure was a 7-in.-diameter by ¼-in.-thick aluminum honeycomb ground plane bonded to the tube ¼ λ behind the cross-slot aperture (Fig. 87).

The resulting total weight of 2.7 lb for antenna and support structure (contrasted with an estimated 12 lb for an unusable conventional design approach) satisfied the requirement for lightweight construction, and left

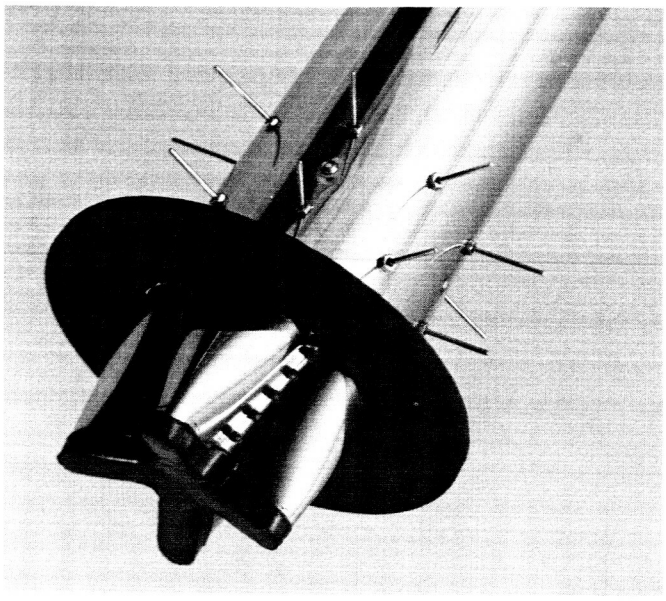


Fig. 87. Low-gain antenna aperture

only the problem of how to make the structure survive during boost vibration. This structural vibration problem was solved by supporting the waveguide tube with two damped struts (Fig. 88) whose damping coefficients

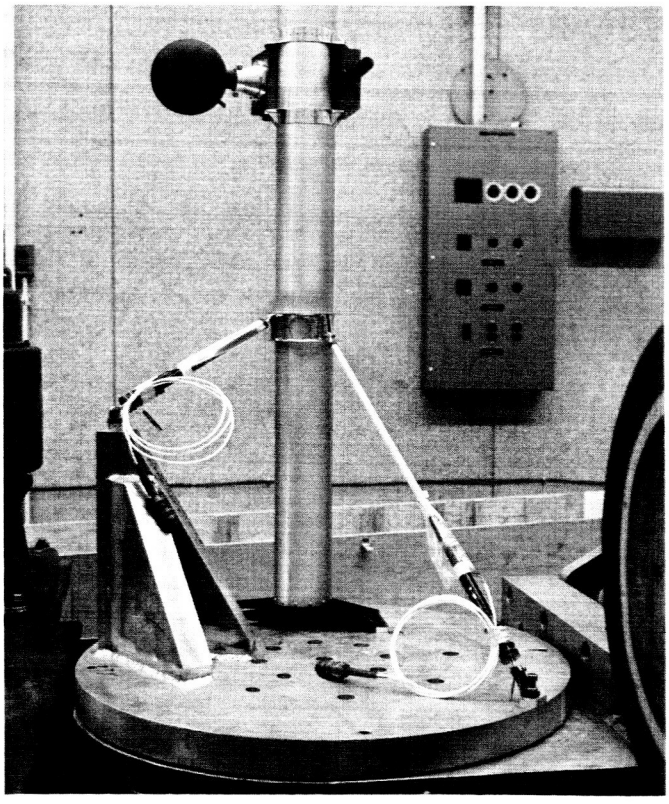


Fig. 88. Low-gain antenna damped support struts

were sized to strongly couple the first few bending modes of the waveguide tube. The application of damped structural control to the waveguide structure was so successful that vibrational stresses in the tube's primary bending mode were reduced by a factor greater than 20, and secondary resonances were similarly reduced below the level of structural significance.

The feed or mode launcher located at the base of the waveguide is a constant-pitch conical spiral wire conductor supported on a fiberglass cone (Fig. 89). The function of the feed is to convert the RF energy from the coaxial TE_M mode into the circularly polarized TE_{11} waveguide mode. The conical feature of the feed produces broadband characteristics in both impedance and ellipticity. The free-space match of the feed is less than 1.3:1 from 2 to 4 Gc, and the ellipticity is less than 1 db from 2050 to 2350 Mc.

Upon assembly of the flight waveguides to the mode launchers, it was discovered that variations in mechanical tolerances of the tube roundness and crimp geometry produced unacceptably high pattern ellipticity and VSWR. The solution to this problem was to use two irises (circular disks each with a large hole in the center) in the waveguide near the aperture. The iris nearest the aperture was used to produce the desired ellipticity, and the other one was used to obtain the desired match.

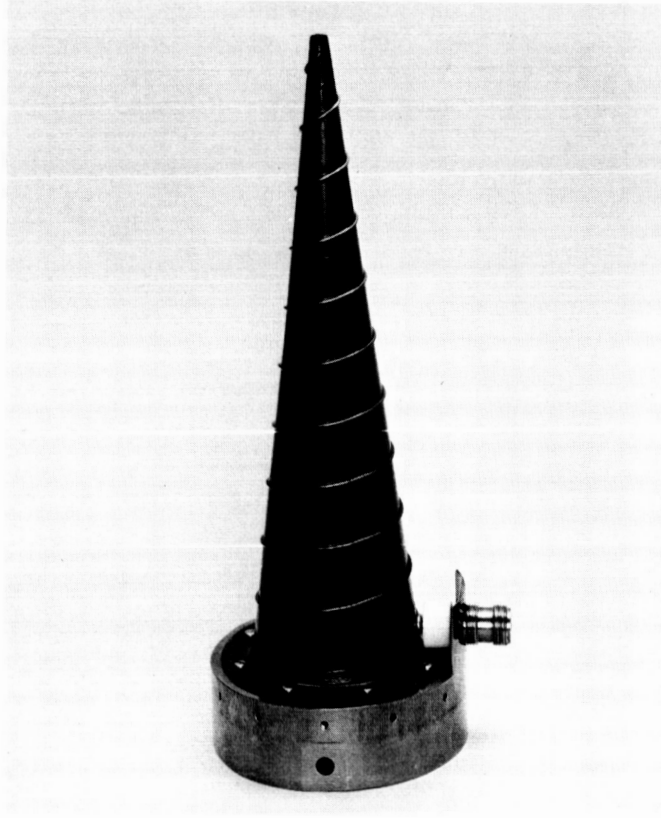


Fig. 89. Low-gain antenna feed

The final electrical parameters of the low-gain antenna are listed in Table 25.

Table 25. Low-gain antenna electrical characteristics

Parameter	Value at 2116 Mc	Value at 2298 Mc
Peak gain (relative to circular isotropic)	6.4 db	5.4 db
Ellipticity on axis	4.3 db	2.1 db
VSWR	1.4:1	1.3:1
Polarization	Right-hand circular	

2. Design Evolution of the High-gain Antenna

Since the primary function of the high-gain antenna is to guarantee transmission of the planetary science data back to Earth, the choice of the size and type of antenna and its location on the spacecraft was almost immediately limited. Since the data return had to be guaranteed, reliability of operation had to be a paramount consideration; and since the look-angle variations during the period from encounter to encounter plus 20 days were limited to a few degrees in cone angle and a fraction of a degree in clock angle, it was decided to fix the antenna on the spacecraft without articulation or deployment.

The only place available for locating a high-gain antenna of any practical size with an unobstructed view of Earth during the encounter phase was on top of the spacecraft superstructure, which was constructed primarily to support the folded solar panels during the launch phase of the mission. To this support truss were attached eight struts (dampers) extending radially upward to the solar panels, two struts to each panel; these struts formed a conical obstruction that the mounted high-gain antenna had to clear. The solar panels were also a limiting factor to the size of the antenna.

As a result, the largest circularly symmetric antenna (a parabolic antenna selected on the basis of its higher gain-to-weight ratio) that could occupy the available space was 40 in. in diameter. However, if such an antenna had been used, a period of telemetry blackout would have resulted during the middle of the mission

when the spacecraft was beyond the range of the low-gain antenna and before the look angles to Earth entered the region of the main lobe of the high-gain antenna. This was highly undesirable, and the only conventional solutions to the problem were (1) to use a third fill-in medium-gain antenna, (2) to articulate the high-gain antenna (even by a single step), or (3) to reduce the gain of the high-gain antenna until the main lobe broadened sufficiently to eliminate the blackout. All of these solutions had their undesirable aspects in either added complexity or reduced performance.

The solution used on *Mariner IV*, shown in Fig. 86(b), represents the best compromise design. If an elliptical sector of a parabolic antenna were used in the available space, the major axis could be as long as 46 in. and, for an approximate 2:1 aspect ratio, would reduce the peak gain by only 1.8 db. The prime advantage of the sector is that, in the plane of the minor axis, the beamwidth is the same as a symmetrical antenna of the minor axis dimension but at a 3-db-higher level.

The dimensions and shape of the reflector were not finalized until a thorough parameter study had been performed on the feed system. Weight and size were of primary importance in the feed design considerations. Weight was important because the feed and antenna support structures had to be sized to hold the feed about 16 in. in front of the parabolic reflector vertex. Size was important since the feed of a relatively small reflector at S-band presents a blockage factor that can seriously reduce efficiency.

A small antenna feed that was under development for the *Mariner B* program appeared to be an ideal choice. The three outstanding features were its small box-shaped ground plane (approximately 0.6 λ square), its low ellipticity over the entire main lobe (less than 1 db), and its low back-radiation (typically -20 to -25 db). Two of these cupped turnstile antennas were arrayed together to produce the proper illumination for the elliptically shaped reflector (Fig. 90).

It was decided to use element spacing and box dimensions that could illuminate a sector with the highest aspect ratio obtainable with two elements, since this would produce the broadest beamwidth in the plane of the Earth track (look angles to Earth during the trajectory) and, hence, reduce the "grey-out" problem to a minimum. Grey-out occurs when the nominal communications margin is positive but less than the sum of the negative system tolerances.

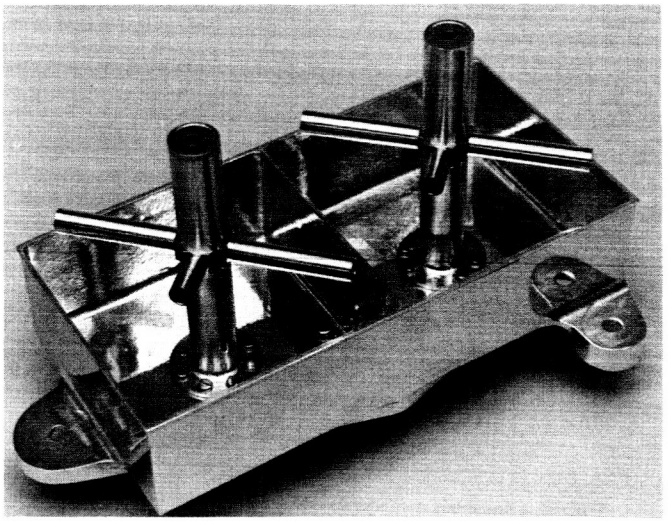


Fig. 90. High-gain antenna feed

In order to feed the two turnstile elements in phase and with equal amplitude, a strip-line power splitter and matching circuit was built into the back of the dual-box ground plane. Matching this circuit to the typically narrow-band turnstile elements at both 2298 and 2116 Mc turned into a major problem area during preliminary design. The VSWR at 2298 Mc was 1.2:1, while at 2116 Mc it was 4.0:1 with a simple T-junction. However, the problem was eventually solved by extending the length of the strip-line from the common T to the elements to include $\frac{1}{4}$ λ transformers, and by using matching stubs.

The final results of the design effort produced an antenna with the nominal characteristics given in Table 26.

The high-gain antenna radiation patterns in the planes of the minor and major axes are shown in Fig. 91 and 92.

Table 26. High-gain antenna electrical characteristics

Parameter	Value at 2116 Mc	Value at 2298 Mc
Peak gain (relative to circular isotropic)	21.8 db	23.3 db
Ellipticity on axis	6.5 db	0.6 db
VSWR	1.22:1	1.14:1
Polarization	Right-hand circular	

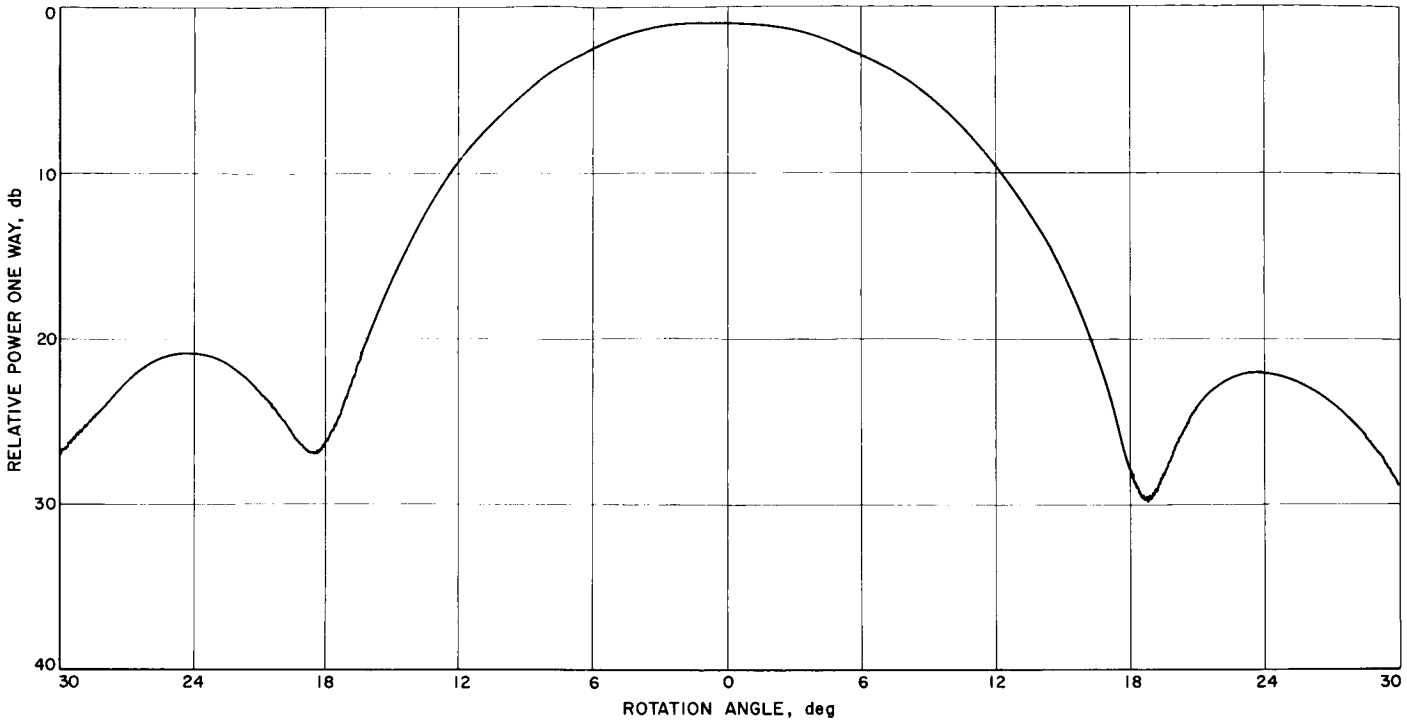


Fig. 91. High-gain antenna radiation pattern through sector minor axis

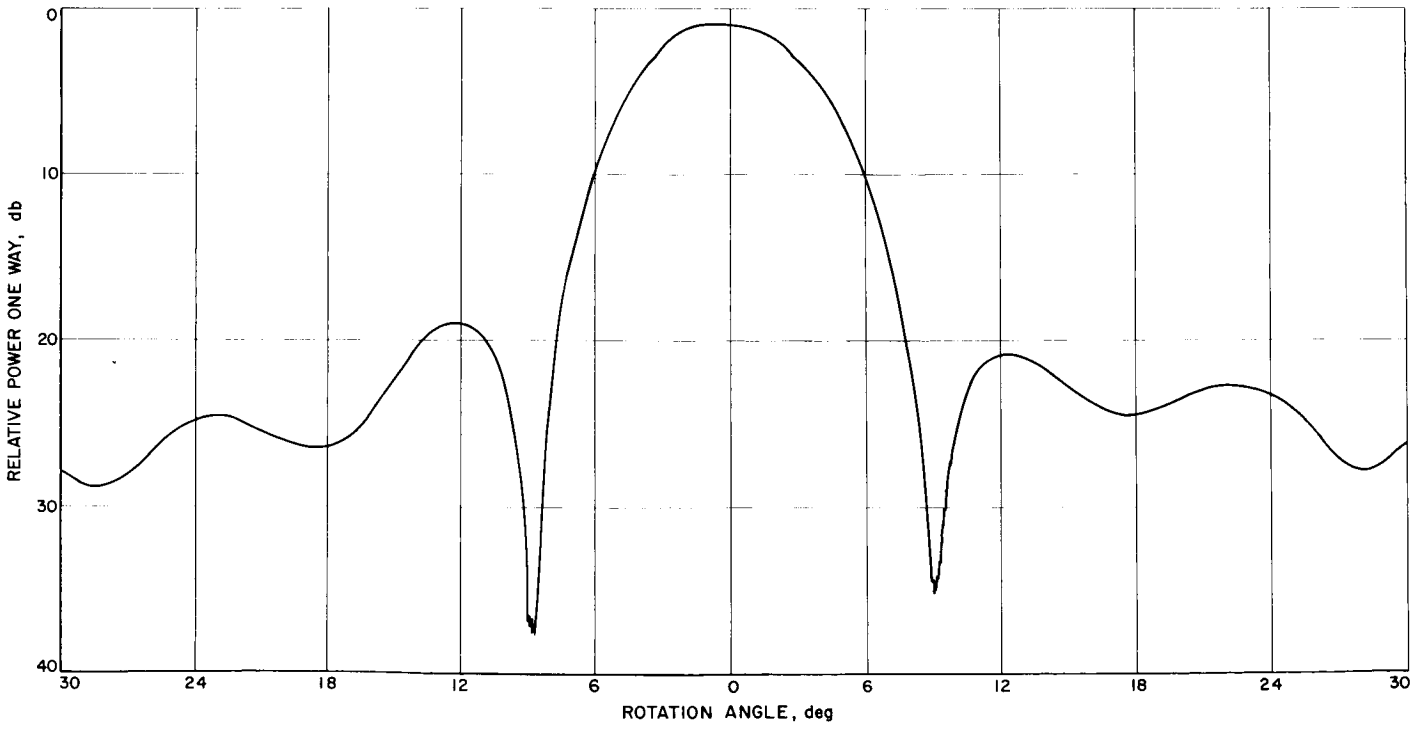


Fig. 92. High-gain antenna radiation pattern through sector major axis

3. Special Tests

a. High-gain antenna thermal–vibration test. During analysis of the *Mariner* boost environment at the high-gain antenna, it was discovered that considerable aerodynamic heating of the antenna reflector would occur during the *Agena* burns. This heating led to some structural weakening of the bonded reflector and presented the possibility that the vibration levels experienced during *Agena* burns might significantly weaken the antenna. A combined thermal–vibration antenna test was performed to verify that this condition would not degrade the antenna structure (Fig. 93). A bank of heat lamps provided the required 220°F temperature, and a special magnetic tape was tailored to provide a vibration environment equivalent to the *Agena* burn. The vibration testing simulated transient impulses by the input of exponentially decaying sinusoids and also by the input of rapidly frequency-swept sinusoids. These two types of inputs were analytically tailored to produce the same structural response of the antenna, and the results of the two types of tests were compared to determine the similarity between the results and the analytical predictions.

The results revealed only moderate agreement between the antenna's structural response to the swept sine and the decaying sine transient, although the antenna easily passed both tests. It was concluded that further refinement of the transient testing technique was needed to achieve accurate transient waveforms in the test laboratory.

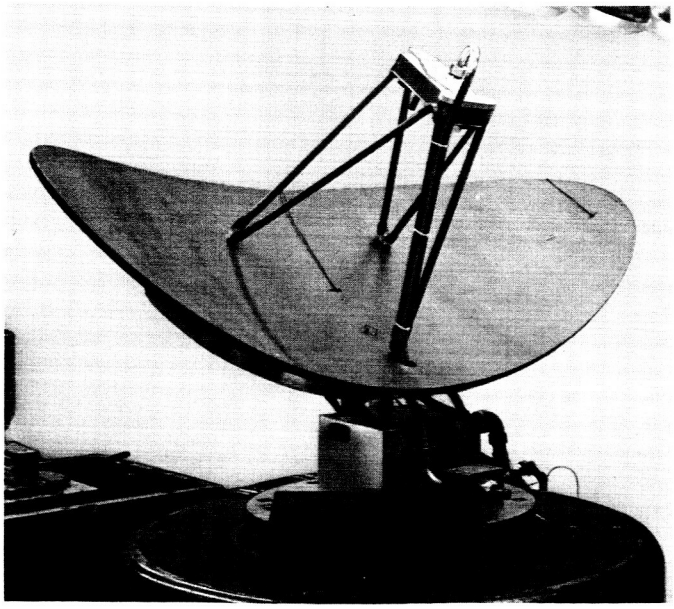


Fig. 93. High-gain antenna thermal–vibration test

b. High-gain antenna temperature control design verification test. This high-gain antenna test was intended to reveal any focusing of sunlight on the feed that could result in the feed overheating. An octagonal frame, simulating the spacecraft, was fitted with heaters so that its temperature could be controlled to match expected spacecraft temperatures. The high-gain antenna assembly was mounted to the top of the frame, along with a multiple-layer mylar heat shield, which simulated the antenna–spacecraft thermal interface. The entire apparatus was suspended in the 25-ft solar simulator in a position that simulated the worst-case antenna heating configuration. Figure 94 shows the test apparatus in the simulator.

The high-gain antenna feed did not exceed 70°F in the test. This was well below its maximum allowable temperature of 150°F. The test showed that there would not be any significant sunlight focusing on the feed, and therefore no special provisions or maneuver orientation restrictions were required.

c. High- and low-gain antenna pattern tests (mockup). Antenna pattern tests were conducted to confirm the

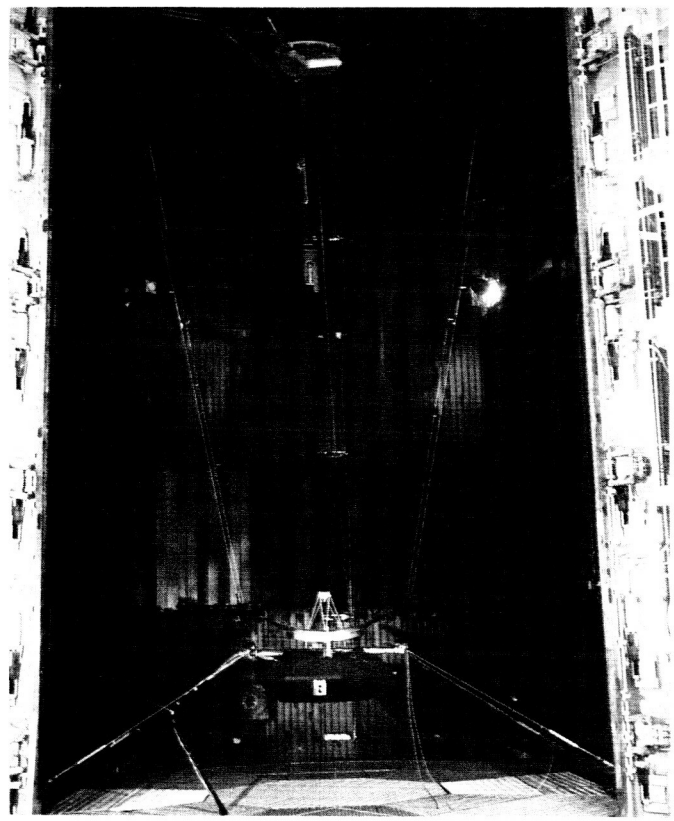


Fig. 94. High-gain antenna temperature control test in 25-ft space simulator

adequacy of the spacecraft high- and low-gain antenna RF patterns. These patterns had to be known for different spacecraft configurations and attitudes.

The initial tests were performed using a full scale aluminum spacecraft mockup, which duplicated the exterior spacecraft envelope to within ±½ in. The mockup included accurate antenna mounting dimensions and simulated all RF reflective surfaces. Structurally, the mockup had to withstand winds up to 40 mph and generally rougher handling than a flight spacecraft.

The test range consists of a 22-ft-high fiberglass tower on which the mockup spacecraft was mounted with the roll axis parallel to the ground. A shelter approximately 100 yards from the tower houses the controls for rotating the tower and instrumentation recording equipment. A 10-ft diameter dish antenna is situated 3300 ft away from the tower; the antenna was used to illuminate the spacecraft with RF energy.

The spacecraft high-gain antenna was aimed at the remote dish by a theodolite, which, in turn, indexed the tower for repositioning.

The spacecraft was rotated in clock and azimuth angles while illuminated by the remote dish. A digital antenna-pattern recorder continuously recorded on magnetic tape the signal levels at different spacecraft orientations.

Satisfactory preliminary antenna pattern information was recorded from this test. However, further testing on a flight-type antenna system was required. Later tests verified that a more representative spacecraft geometry was required for determining final pattern profiles.

d. Developmental test model pattern tests. The developmental test model spacecraft was used for final pattern tests. The sequence of operation was much the same as for the mockup vehicle pattern tests, except for the spacecraft handling operation. The preparation of the spacecraft included removing all internal components for weight reduction, and adding simulated solar vanes, science experiments, and temperature control louvers. The use of flight-type solar panels dictated that wind load calculations heavily influence the design of the spaceframe support structure and mounting technique (Fig. 95). Alignment of the spacecraft to the remote antenna was aided by the use of a telescopic sight that was mounted directly to the spacecraft. To safeguard the vehicle and to obtain more accurate data, a wind velocity meter was installed, after which the spacecraft was reoriented to a more favorable position in high winds.

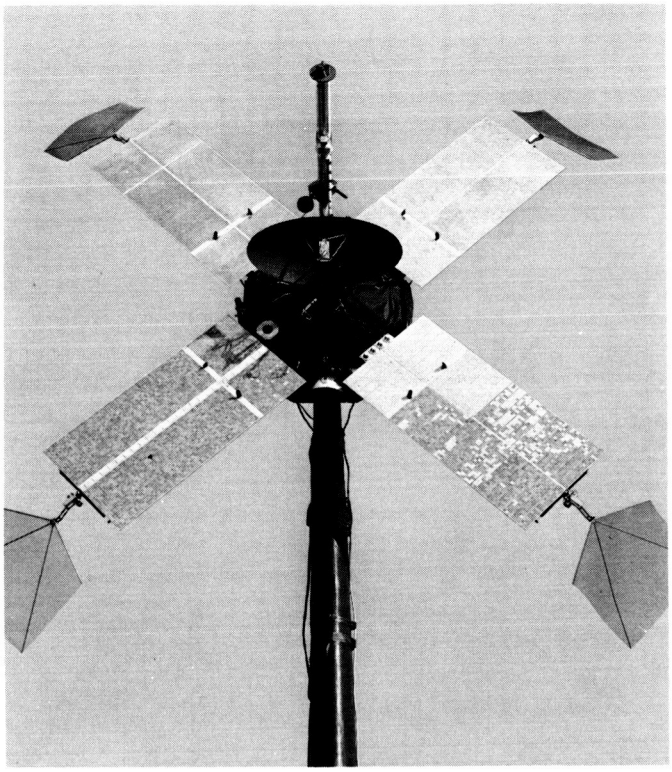


Fig. 95. High- and low-gain antenna pattern tests using the developmental test model

Figures 96 and 97 compare the effect of the spacecraft on the low-gain antenna radiation pattern. Figure 96 is a right- and left-hand circularly polarized pattern of the antenna itself. Figure 97 is a right-hand circular-polarization pattern in the same plane of the antenna but mounted on the spacecraft. The higher-frequency ripple superimposed on the nominal pattern is caused by reflections off of the spacecraft structure from 0 to 110 deg and a combination of reflections and diffraction from 110 to 180 deg.

4. High-gain Antenna Mechanical Development

a. High-gain antenna reflector development. The *Mariner* Mars high-gain antenna reflector, unlike the *Mariner* Venus 1962 and *Ranger* reflectors, was required to be self-supporting during the vibration and acceleration of rocket launch. The auxiliary reflector support structure used for the *Mariner* Venus 1962 and *Ranger* antennas could not be used because the *Mariner* Mars antenna had to be located on top of, rather than underneath, the spacecraft. Without auxiliary supports, a

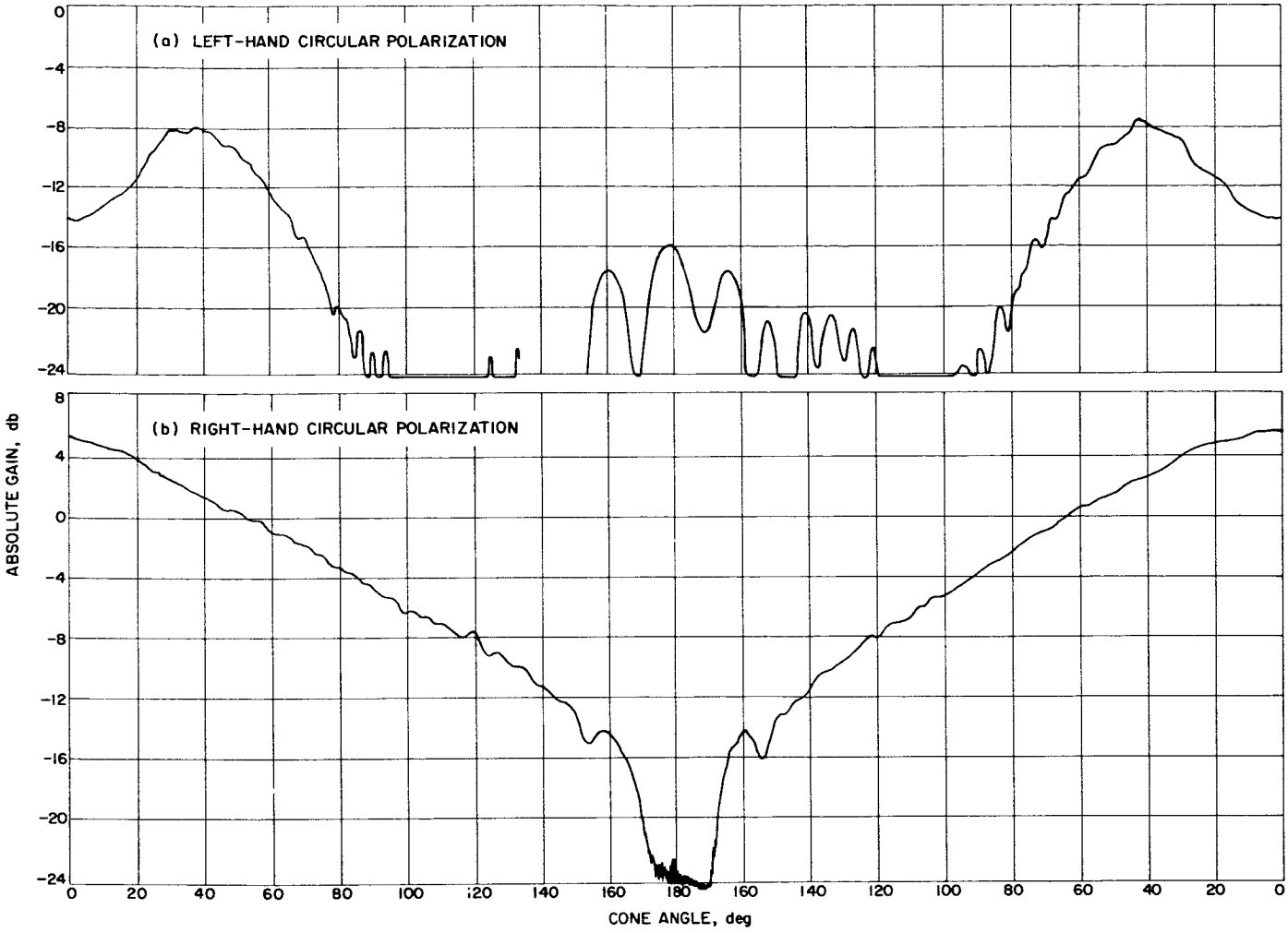


Fig. 96. Low-gain antenna pattern, 0 to 180 deg constant clock angle cut, 2298 Mc

Mariner Venus 1962/*Ranger* type of reflector structure would have had to be greatly strengthened in order to survive the boost environment, which would have resulted in a prohibitive weight.

The development of new antenna reflector design concepts had been underway in the *Mariner B* project for approximately a year prior to the start of the *Mariner* Mars project, and three approaches were showing promise of success. These approaches were: (1) explosion-forming and chemically milling an aluminum parabolic reflector, then fabricating a support structure to strengthen the basic shell and attaching that structure to the shell's back side; (2) hot-molding a fiberglass honeycomb core to a parabolic shape, then laying up thin fiberglass face skins on that core; and (3) machining an aluminum honeycomb core to a parabolic shape, then vacuum-drawing aluminum-foil face skins and bonding them to the core. All three approaches could be made to work, although each offered some advantages and some significant problems. The main drawback of the explosion-formed reflector was its low stiffness-to-weight ratio and, hence, its high total weight for a given application. The *Mariner* weight limitations made this predictable and conservative approach seem an undesirable one to pursue.

The fiberglass honeycomb reflector offered the high stiffness-to-weight ratio of a honeycomb sandwich construction combined with the ease of fabrication inherent in fiberglass laminate lay-ups. The actual construction of this reflector, however, revealed some difficult problems. A combination of weight control difficulties, poor structural performance, and conductive coating problems

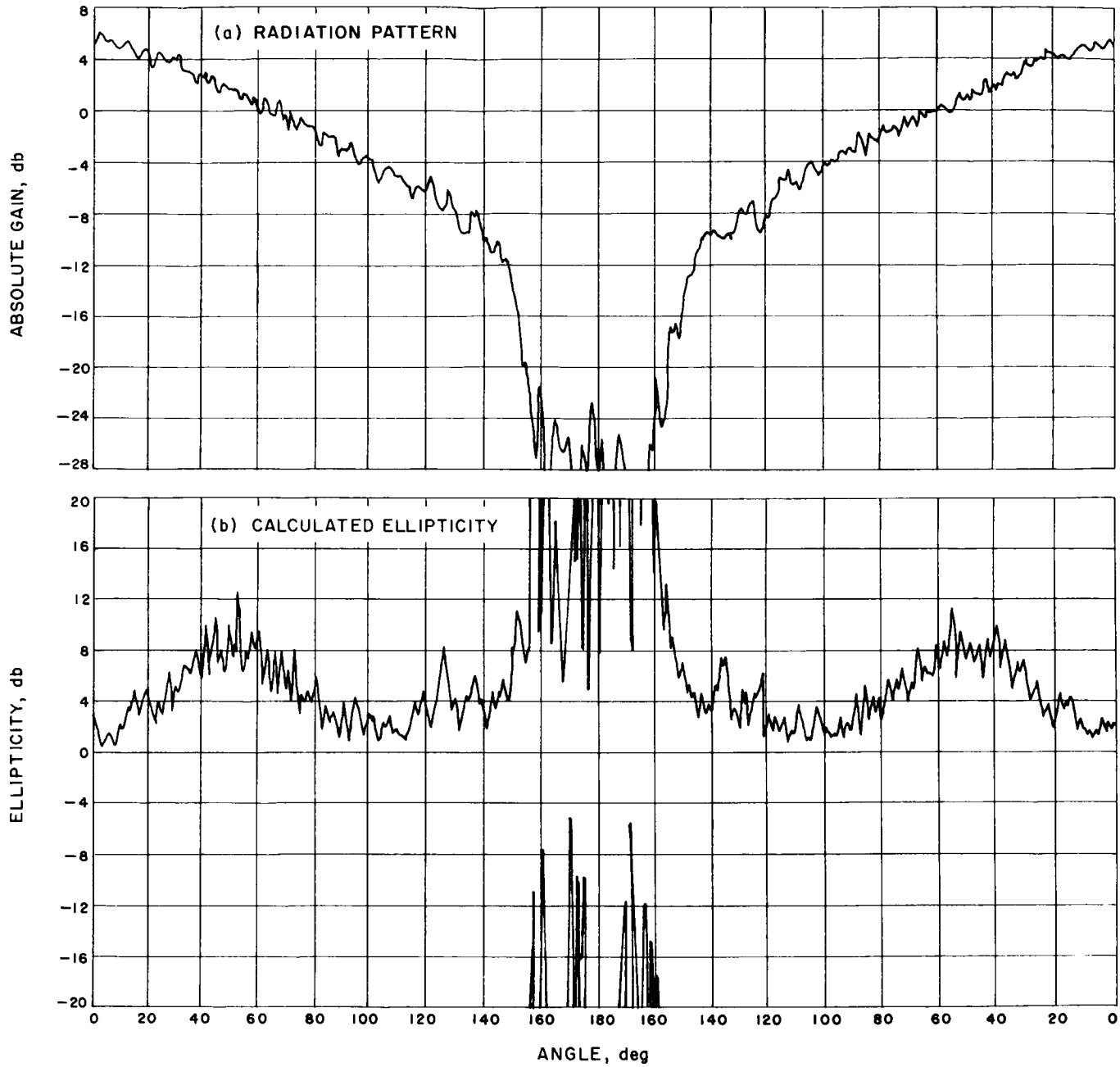


Fig. 97. Digital antenna pattern recording of low-gain antenna mounted on flight-type spacecraft

made the fiberglass honeycomb reflector an undesirable choice for the high-gain antenna design and, consequently it was eliminated from further consideration.

b. Aluminum honeycomb reflector. The aluminum honeycomb reflector offered the potential of a higher stiffness-to-weight ratio (lower weight) than any other material and/or construction technique. However, attainment of this full potential was hampered by the difficult fabrication problems associated with forming and bonding aluminum foils into a reliable structure. Nevertheless, it was decided that the *Mariner* reflector design would use aluminum honeycomb construction.

Three major fabrication problems were considered in formulating the *Mariner* high-gain antenna reflector. These were: (1) the difficulty of forming the foil face skins without rupturing them; (2) the expense, production time, and accuracy problems involved in machining the reflector's honeycomb core from a massive block of

aluminum honeycomb; and (3) the problem of reducing adhesive weight and, at the same time, ensuring structurally reliable bonds between face skins and core.

The face skin drawing problem was solved by using very soft aluminum and by being exceptionally careful to select foil with no mill roller marks or imperfections. Because the use of soft aluminum did not weaken the reflector structure, the failure mode of very lightweight honeycomb sandwich construction is a buckling of the face skins, a phenomenon dependent on the elastic modulus of the face skins and not on their yield strength.

The core machining problem was minimized by designing the reflector as a thin shell supported by a honeycomb back beam structure. The thin reflector was then formed to a parabolic shape from a ½-in.-thick sheet of honeycomb (rather than being machined from a monolithic block). The amount of machining required to produce a back beam structure from a block of honeycomb core was small compared to the amount required to produce a complete reflector shell. The "thin shell plus back beam" reflector design made it possible to produce a lighter-weight structure than would have been possible with a deep section shell, since stiffness from the back beam could be strategically placed in areas of maximum stress with a minimum of dead weight being carried in the reflector structure.

The high adhesive weight problem, which was very serious in the fiberglass reflector fabrication, remained a problem in the fabrication of foil-gauge aluminum honeycomb structures. The problem was that when enough adhesive was used to form large reliable fillets and to bridge crevices between core and face skins, that adhesive layer then became a significant part of the structure's weight.

The obvious approach to reducing adhesive weight was the use of a very thin adhesive film in the face-skin bonding operation. No commercial structural adhesive was available in the weight desired; however, some investigation revealed that a thin film (1 mil) adhesive, originally designed for bonding copper foil to fiberglass circuit boards, was available. This adhesive had not previously been used in honeycomb structural bonding, but it did have good wetting properties, fairly good peel strength, and was commercially available on short notice. Laboratory testing on small samples of honeycomb indicated good sandwich strength (200 psi flatwise tension) and acceptable peeling behavior.

An alternate approach to reducing adhesive weight was using liquid adhesive (rather than the partially precured films) and roller-coating it onto the honeycomb core cell edges just before applying the face skins. The many drawbacks of the roller-coating technique, however, led to the selection of thin film bonding as the only acceptable lightweight bonding technique.

There was some concern about the thin-film-bonded structure's sensitivity to the tolerance variations encountered from piece to piece. Of special concern was the possibility of unevenly cut honeycomb failing to meet the face skins with a tight enough fitting join line. If this occurred, crevices would exist at the joint that the sparsely used adhesive could not fill, and the structural strength of the sandwich would be greatly reduced. To ensure that no such crevices would exist during bonding, the sandwich structure was bonded with a vacuum bag over the reflector's back skin and with a soft surface between the reflector's front skin and the parabolic mandrel. Such an arrangement pressed the 4-mil face skins against the honeycomb core hard enough to stretch the face skin material into dimples over each cell. This ensured that the perimeter of each cell was a tight join line ready for bonding. The slight dimpling of the reflector face skins did not reduce the stiffness of the reflector as measured by natural resonant frequency of the structure, and did not degrade its radio reflector characteristics.

The dimpling technique worked very well in the production of thin-skin reflector shells with a resulting successful production of ten reflectors and no rejects. Unfortunately, this technique was not applicable to bonding of the heavier 16-mil skins used on the reflector's back stiffening beam. A test back beam was bonded using the lightweight 1-mil film adhesive and 16-mil skins, but significant areas of the face skins failed to bond properly to the core; the skins were too stiff to follow slight variations in the core height. Fortunately, the total area of the beam skin bonds was only 154 in.^{2} as compared to the reflector face skin's bond area of 1620 in.^{2}, so it seemed reasonable to switch to a heavier adhesive for this small area rather than try to develop lightweight bonding techniques for thick face skins. The final result of reflector fabrication was a 46 × 21.2-in. elliptical sector of an 8-in.-deep parabola with a weight of 1.73 lb, a fundamental resonant frequency of 120 cps, and a maximum variation from the desired parabolic surface of 0.040 in. or approximately 0.007 λ at S-band frequencies. This accuracy is almost an order of magnitude greater than was necessary for good reflector performance; thus, frequencies of radio transmission an

order of magnitude higher could be accommodated with no improvement in reflector accuracy required.

c. Antenna support truss. The geometry of the transfer orbit from Earth to Mars required the high-gain antenna to be mounted on top of the spacecraft and to be pointed down 38 deg from the vertical. This pointing angle required the use of a rather awkward support truss (Fig. 98), consisting of a conventional three-point to three-point trusswork skewed so that the top plane of the truss was at a 38-deg angle to the bottom plane. With a little juggling of dimensions, it was possible to place six of the nine truss members in a single plane. These six members and their associated joints were then simplified to a single plate hogged-out into a network of magnesium channel sections, and the remaining three members were created by the conventional application of aluminum tubes with riveted magnesium end fittings. This truss could have been made stiffer and would have been easier to mate with the spacecraft superstructure had it been a four-point to four-point mount rather than a three-point to three-point mount. However, adjustability of the antenna pointing angle in the field (by shimming the truss) was considered an important design requisite. Had the truss been mounted at four points, it would have been difficult to make adjustments and even more difficult to prevent development of residual stresses due to such adjustments. Furthermore, the three-legged truss minimized the possibility of internal thermal stresses developing due to thermal gradients in the truss.

A major decision in the design of the antenna support truss was the choice between closing the top of the truss with three conventional truss members and closing the truss with the honeycomb reflector shell. The conventional truss member closure offered the advantages of easy analysis and member sizing, but had the distinct disadvantage of creating a redundant structure parallel to the reflector. It was decided to use the conventional closure, and the thermal stresses inherent in the redundant truss structure were minimized by thermally clamping the reflector and back truss. The truss tubes and joints were polished to minimize heat loss. The attach points to the dish were large area attachments that maximized heat transfer from the reflector to the truss. Severe thermal testing of the reflector and back truss was conducted during spacecraft system tests, with the reflector making transient thermal excursions from +200 to −40°F in 15 min. No structural problems occurred during these tests. Further thermal tests of steady-state conditions indicated that reflector tip deflections of less than 0.025 in. would occur as the reflector temperature

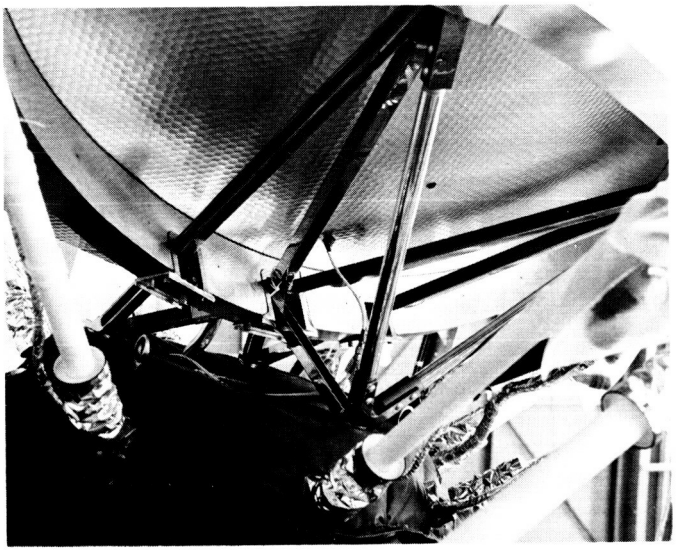


Fig. 98. High-gain antenna support truss

ranged from 200°F in the near-Earth conditions to 50°F in the near-Mars conditions. These small excursions were entirely acceptable, and the attempts at thermal clamping of the truss and reflector were deemed successful.

d. Feed support truss. The feed support truss was required to hold the feed of the high-gain antenna above the reflector and to be adjustable so that the feed could be translated parallel and perpendicular to the reflector plane during assembly. Also, it was desirable that the feed have the capability of being rocked, with respect to the support truss, to allow accurate pointing of the feed toward the center of the reflector. These adjustments were accomplished by shimming between the reflector and truss for feed translations, and shimming between the feed and the truss for feed rotations (rocking). In addition to providing support and allowing adjustment, the feed support truss was required to be nonconductive and as transparent to S-band radiation as practical, and to maintain accurate feed alignment over the expected range of temperatures between Earth and Mars. The nonconductivity requirement led to the use of unidirectional fiberglass tubing and plastic end fittings in the feed truss construction.

Attaching unidirectional fiberglass tubes to truss end fittings posed a new problem in fabrication. The use of rivets was ruled out by the extremely low bearing strength of fiberglass in the direction of load (a rivet would just slide along between the fiber stringers under load). The only reasonable solution for the end fitting

attachment was to use bonded joints, and even this posed a problem in quality control. In order to make the bond joints inspectable, the truss end fittings were machined from clear plastic and were designed so that the fittings slipped over the tubes rather than inside them. The fittings were drilled with adhesive injection holes and adhesive was syringed into the holes; coverage of the adhesive was observed through the clear tube fittings. This technique yielded consistent 85 to 90% bond areas and presented no significant problems.

The fittings themselves were machined from a high-strength lexan plastic (10,000 psi ultimate) with good toughness, fairly good dimensional stability, and a density about half that of aluminum. The use of plastic rather than aluminum end fittings, and the use of unidirectional rather than commercial grade fiberglass tubes led to the development of a feed support truss with half the weight of a more conventionally designed one. At the same time, this lightweight truss was much more resistant to vibrational and shock overloads than a conventional truss would have been. The truss design concept was so successful that it would be wise to consider its application to future spacecraft designs.

e. High-gain antenna feed design. The high-gain antenna feed is composed of two turnstile antennas (feed tubes supporting crossed dipoles) mounted in a rectangular box, which faces down toward the reflector vertex. The main support tube and crossed dipole tubes of each turnstile were machined as one piece from high-temper aluminum alloy. These machinings were cheaper, lighter, stronger, and more accurately made than the equivalent fabricated oven-brazed assemblies used on *Mariner* Venus 1962 and *Ranger*. The *Mariner* Mars machined turnstile assemblies were superior in every way to the former brazed assemblies. The final feed assembling was accomplished by simply bolting the turnstiles, feed box, electrical connector, and electrical distribution printed circuit together into one assembly. The reflector was installed on the antenna support truss and shimmed into proper alignment. The feed, feed coax, and feed support truss were then mated to the reflector and shimmed into alignment. A final inspection verified reflector and feed alignment, and the antenna was delivered to the antenna range for pattern checks.

f. Special properties of foil-gauge aluminum honeycomb structure. Because of the fragile nature of the high-gain reflector, considerable concern was expressed about its repairability and the likelihood of irreparable damage occurring during routine handling. To help prevent handling damage the reflector was edged with a rigid foam filler that could withstand minor knocks and squeezes.

Both times that antenna reflectors were damaged, it was the result of a heavy blow to the edge of the reflector. These blows caused the honeycomb core to collapse laterally and shear the face-skin bonds. The unsupported face skins then lifted from the core surface and folded back with no severe wrinkling or tearing. The damage looked much worse than it was and, in fact, was easily repaired, since no tearing or crumpling of the honeycomb cell walls or of the face skins had occurred. To repair the damage, the face skins were folded back from the core, the core was pulled back into an expanded condition using right angled forceps, and the face skins were coated with adhesive, clamped into position against the core, and allowed to cure. This repair sequence was performed in less than an hour without removing the antenna from the spacecraft and without significantly delaying other spacecraft operations that were in process.

g. Special testing of foil-gauge aluminum honeycomb structure. The temperature sensitivity of a bonded structure and the thin gauge of the aluminum foils used in the structure led to two special tests unique to the antenna reflector. These tests were deemed necessary for the proper qualification of the reflector for spacecraft application.

One test was an acoustical environment test in which 145 db of white noise was played upon the reflector face. There was some concern that high-amplitude flutter would be induced in the aluminum foils, and that the flutter would either rupture the cells or weaken the bonds within the sandwich. However, no problems were encountered in the test.

The second test that became necessary was a low-level vibration test described in paragraph 3a.

5. Low-gain Antenna Mechanical Development

a. Fabrication. Once it was established that the waveguide-fed low-gain antenna was electrically and mechanically feasible, it became necessary to develop manufacturing methods that would produce dimensionally accurate waveguides and terminations from large diameter thin-walled aluminum tubing. Some typical waveguide tube dimensional requirements were: (1) a tube roundness within 0.003 of the tube diameter (an electrical constraint), (2) a tube wall thickness equaling 0.006 of the tube diameter (a weight consideration), and

(3) formation of a four-pointed crimp at the tube end, transitioning in one tube diameter from the round waveguide section to an accurate, crossed-slot aperture (an electrical constraint). In addition to severe dimensional constraints, it was required that the waveguide be made of highly tempered aluminum in order to prevent the tubing from getting out-of-round during normal handling. The use of high yield strength aluminum in the forming operations caused problems in manufacturing: primarily, spring-back, the possibility of brittle fracture during severe forming, and dimensional control difficulties. The tubing was specially drawn into 7½-ft by 0.025-in. wall sections from relatively thick-walled short sections of tubing stock; and, in a multiple draw operation, it was accurately sized to the required diameter and roundness tolerances. A secondary forming operation used an adjustable inside mandrel, and an exterior clamping die created the crossed-slot (cruciform) aperture that formed the radiating element. The tube was then hung by one end in a heat-treat oven and artificially aged. Each of the manufacturing steps significantly influenced the tube roundness, straightness, and cruciform dimensions to such an extent that only selected tubes could be used as flight antennas; the remainder of the tubes were used for structural test models and antenna performance sensitivity tests.

Further complications in tube production developed when the need for two additional specifications was brought to light. One of these required that the interior of the tubes be gold-plated to ensure that no skin corrosion was present to inhibit radio propagation within the waveguide. The second specification was that the tube's exterior be polished to a mirror-bright finish in order to properly control the temperature of the waveguide and scientific instruments attached to the waveguide.

An evaluation of tube-surface corrosion rates and of surface corrosion effects on RF propagation was conducted. The results of this corrosion evaluation were that no significant propagation effects would occur on a buffed aluminum surface in an air-conditioned environment within a one to two year period. As a result of the corrosion testing program, the gold-plating program was dropped and the tube interiors were given a corrosion-inhibiting finish buff after heat treatment.

The temperature control requirement that waveguide exterior surfaces be polished mirror-bright led to an unexpected production problem. Polishing the waveguide tube surface created high local temperatures and pressures where the buffing wheel contacted the aluminum, and the buffing created unbalanced surface stresses that induced bowing in the tube. On test waveguides the finish buffing induced bends as large as ⅜ in., even though the tubes were water-cooled from the inside and the buffing was done by a very experienced and competent workman. Tube warping during final polish proved to be such a problem that compromise techniques were seriously considered. It was finally concluded that a lightly buffed hazy-mirror finish provided very nearly the same temperature effect as a heavily buffed bright-mirror finish, but without the production problems of high surface stresses and bowed tubes. A hazy-mirror finish was successfully used on the flight waveguides.

b. Detailed design. Some problems were encountered in the process of designing the low-gain antenna, its mounting hardware, and the attach bracketry for the waveguide-mounted science experiments. For instance, the process of choosing waveguide tube wall thickness was not based on the usual structural criteria of the strength required to withstand spacecraft boost environment. It became necessary to choose a wall thickness based on the nebulous criterion of minimum gauge for successful tube production, minimum gauge for ease of handling, and minimum gauge for achieving acceptable waveguide roundness. Although it was the most nebulous, it was the criterion of handling that actually sized the waveguide thickness.

During flight spacecraft assembly and operations, the assembly technicians were given special instruction on antenna handling, and a special shipping and storing rack (Fig. 99) was used with the result that no flight



Fig. 99. Low-gain antenna shipping and storing rack

waveguide tubes were damaged at any time during the program.

The dimensional variations of the waveguide termination cruciform and the variations in waveguide roundness from tube to tube did cause some serious difficulty in early phases of the low-gain antenna development program. It was never well established whether the antenna performance variations were due primarily to waveguide out-of-roundness or to cruciform tolerance variations. Both tolerance problems were solved, however, with a technique of antenna tuning using internally mounted iris plates. This made the antenna performance less sensitive to the tolerance variations that were produced during manufacture.

In addition to the problems associated with thin gauge waveguide tubing, another set of problems was presented by an electrical requirement that no items such as rivets, screws, bolts, or nuts could be allowed on the inner surface of the waveguide tube. The result was the extensive use of bonding in the attachment of bracketry to the waveguide tube. The bracketry was made in the form of close-fit hoops that slid over the waveguide tube and then were bonded in place. The bonding was accomplished by injecting adhesive through vent holes in the bracketry with a syringe. This technique proved to produce bonding over 50 to 80% of the joint area as opposed to less than 20% of the area when the parts were precoated with adhesive and slipped together. The bracket hoops were made quite wide, with typical joint safety factors running well over a factor of 10. Such conservative joint design alleviated concern over bonded joint failure, and, because of the lack of load concentration, the flight bracketry designs came out lighter than they would have if they had been designed for riveting. No failures of bracket bond joints occurred during any phase of the test and flight programs; in fact, an ultimate load test of the most suspect bracket resulted in a bracket failure at five times the design load with still no failure in its bonded joint. An interesting advantage of the bonded bracketry was discovered when magnetometer scientists asked that one bracket be electrically insulated from the waveguide tube. This was accomplished by simply bonding a thin layer of fiberglass inside the bracket hoop, then bonding the hoop with fiberglass to the waveguide tube.

6. Antenna RF Transmission Lines

The *Mariner* Mars antenna transmission lines consist of two coaxial cables running from the top of the communications bay on the spacecraft bus to the low- and high-gain antenna feed input connectors. The transmission lines were required to be extremely light weight, to be low loss, and to be routed between terminals by the shortest possible route. Previous spacecraft cables consisted of the RG series of flexible cables, which are quite heavy because they use a solid dielectric between center and outer conductors of the coaxial cable. For the *Mariner* Mars high-gain antenna, it was decided to use semiflexible solid outer conductor coaxial cables. With the solid outer conductor construction, the coaxial cable dielectric could be made hollow, allowing the same diameter semiflexible cable but with less weight and transmission loss than an equivalent RG cable. The long (5-ft) cable run to the high-gain antenna made this lightweight low-loss cable very desirable.

In contrast to the high-gain antenna, the low-gain antenna feed connector was located very near the communications bay. The short cable run that was required and the fact that the low-gain antenna could move under loading, stipulated that a short piece of flexible cable be used for the low-gain antenna transmission line. To minimize weight and provide the required flexibility, RG-142A/U cable with gold-plated aluminum type N connectors was used. Because of the low RF power level (10 w), the air dielectric section of the mated type N connector was not susceptible to multipacting-type RF breakdown, and the design was the same as the original cables used on *Ranger*. A temperature control outer covering was not required on the cable because the unit was completely within the spacecraft thermal shielding.

In addition to the normal electrical impedance and insertion loss measurements, the production units were checked for pin depth and concentricity, and X-rays of the attached connectors were made to ensure proper assembly. As a sidelight, it was discovered that the flexible cable center conductor was copper-jacketed steel; however, the small amount of ferrous material was located far enough away from the spacecraft Helium Magnetometer not to affect its operation.

Early in the design phase it was decided to use ½-in.-diameter high-temperature cable, with a hollow silver-plated aluminum center conductor, to run from the communications bay to a point below the rear of the high-gain antenna reflector where a reducer coupling would be located to meet ⅜-in. cable coming from the antenna feed. The reducer coupling would be used to connect the different sized cables together and to provide a cable disconnect to facilitate mating the high-gain antenna to the spacecraft. One-half inch cable was

selected for use below the reflector to minimize loss, and 3/8-in. cable was selected for use above the reflector to minimize shadow loss and distortion of the high-gain pattern.

The cable design layout had to be accomplished by descriptive geometry from prototype structural drawings of the spacecraft since no mockups were available. To simplify tooling and layout, all bend radii of the cable assembly were to be the same. Tests of cable VSWR versus bend radii showed that a bend factor of 3 (i.e., minimum bend radius equal to three times the cable diameter) could be used. A bend factor of 10 is normally recommended; however, by careful tooling design, the tendency for the outer conductor to collapse and the inner conductor to move off center was avoided.

Further investigation of the design indicated that by removing the connector at the high-gain feed and using 1/2-in. chemically milled cable for the complete run, the reducer would decrease in weight and complexity to a simple union, and the overall insertion loss of the cable could be reduced with hardly any weight change over the first design. It was also determined that the 1/2-in. cable did not cause any significant antenna performance changes due to the increased size.

Eliminating the feed connector required the development of a new series of adapters and terminations along with slotted line transitions for testing purposes. The weight saving turned out to be somewhat marginal, while the increase in complexity in testing was rather large. However, since no transitions or adapters to various sections were required for flight, the electrical performance was improved over the standard adapter–connector–connector–adapter RF fitting arrangement. The disconnect union below the high-gain reflector was designed originally to provide separation by reversing the process of attaching the union to the cable. The one-piece union was attached to the cable by a tapered, toothed split ring driven by a jam nut against a mating taper in the union body. The split ring was constricted, so that its teeth dug into the rather soft aluminum of the cable outer conductor. It was felt that this operation could be successfully accomplished a dozen or more times before the cable would be prejudiced toward separating at the tooth marks. However, later vibration testing showed that the unsecured jam nuts that drove the split rings could be loosened during vibration, and it was decided to secure the assembly with epoxy. Hence, a split union had to be designed to effect separation of the antenna from the spacecraft. The final design was a male and female tapered flanged version of the original one-piece union secured with two internally tapered semicircular rings. The rings had ears for being mated with nylock screws. The tolerances on the union parts were adjusted three times, and, even then, selectivity was finally required to allow proper mating of the many small critical parts.

To accommodate the chemical milling, the cable had to be specially run at the factory to prevent any scratches and to select lengths that did not have pits or dents in the cable, since chemical milling would simply reproduce the imperfections in the thinner-walled finished product. Two runs were rejected before a final satisfactory run was obtained and, unfortunately, by that time the development schedule had to eliminate chemical milling because there was not enough time remaining.

Special hand-polished bending blocks were fabricated to bend the cable, and extreme care was exercised to avoid scratching the surface of the soft aluminum. The entire bending run had to be committed at the same time, since there was insufficient lead time to bend one cable, cut it to length, assemble connectors, and test on a mockup. It was felt that minor length differences could be taken care of by simply hand-tightening or increasing some of the many bends in the cable. Minor angular discrepancies could also be corrected in the same way. As it turned out, the upper cables were 1/2 in. too short and a bend in the lower cable was misoriented by about 45 deg.

After bending, the cables were cut to length on a milling machine; cable contamination caused by chips entering the space between the inner and outer conductors was prevented by blowing filtered shop air through the free end of the cable. After cutting, the upper cable was mirror-polished for thermal control.

To allow a short lower cable run, it was decided to use a right-angle connector on the cable end at the communications bay. A special gold-plated aluminum connector with a brazed miter joint and weighing less than 1 oz was fabricated. Extensive vibration and shock testing, with X-rays taken both before and after each test, was required to verify the mechanical adequacy of the design.

The cables could not be rigidly fastened to the spacecraft's tubular superstructure, so special viton spacers were fabricated to mate between the cable and the spacecraft. The cable and structure were then tied together with dacron lacing cord, with the viton spacer bonded between the two pieces.

The upper cable was permanently attached to the high-gain antenna and remained there to limit the amount of assembly required around the easily crushed honeycomb reflector.

The semiflexible cable became semirigid after all the bends were put in, and the cable run stiffened the high-gain feed support assembly. It was necessary, in fact, to ensure perfect cable alignment to the feed support structure before final assembly in order to keep the cable from pulling the feed out of alignment. The cable ends were masked so that, during the chemical milling process, full wall thickness could be retained for connector attachment. The cables had to be bent before they were chemically milled, because full wall thickness was required to prevent collapsing during bending. One-half inch cable with a final wall thickness of 0.015 to 0.020 in. caused no problems even in bend areas.

7. Structural–electrical Interactions of the Low- and High-gain Antenna Design

During the design phases of the low- and high-gain antennas, it was important that the constraints of and the alternative approaches to each problem be well understood by both the mechanical and the electrical engineers guiding the design. For instance, an electrical requirement that the waveguide interior be gold-plated resulted in a mechanical problem in holding tube tolerances and in developing plating techniques. These problems disappeared after subsequent discussions, and a short test program revealed that buffing the interior was easier and satisfied the electrical conductivity requirements. Conversely, when the electrical engineer had difficulty obtaining ready-made parabolic spinnings of correct contour for initial high-gain antenna development tests, the mechanical engineer was able to have such spinnings made in time to meet development schedules. Close coordination of the electrical and mechanical trade-offs between weight, dimensional accuracy, antenna pattern variations, and antenna positioning was imperative to the successful development and production of these high-performance lightweight antennas. Because a straightforward development would have nearly doubled the lead time required for delivery of a flight antenna, an approach was used that involved analytical rough estimation of the antenna configuration. This approach was followed by parallel efforts of analytical configuration refinement and a gross test program using a range of antenna geometries that would hopefully cover the elusive optimum case. About midway through the analytical refinement and testing program, an educated guess was made at the exact configurations of the antennas, and detailed flight hardware design was begun on the assumption that this guess would be unerringly correct. In the case of the low-gain antenna, the electrical predictions were enough in error that significant retrofits had to be made to the flight antennas in order to give them the proper radiation pattern. It was only because of the mechanical simplicity of these retrofits that very serious schedule slips were not incurred. In the case of the high-gain antenna, the configuration prediction involved choosing an optimum parabolic contour, an optimum feed position with respect to that contour, and an optimum feed size for the optimum contour. The possibility was always present that tests would prove the design unacceptable and that the delivery schedule would abruptly slip as a new design was begun. A combination of good luck and sound engineering judgment led to a test verification that the original flight antenna design would meet all of the antenna efficiency and pattern requirements of the mission. The 11-month delivery time was achieved by a process that involved 3-month forecasts of development test results and development testing that proceeded smoothly to the predicted conclusions with very little back-tracking or study of blind-alley approaches. Had the antenna development testing turned up any serious technical problems, it might well have taken an additional 2 months to establish the proper antenna geometry, and an additional 5 months to deliver the flight antennas.

8. Antenna Procurement

In general, both the high-gain and the low-gain antennas were made up of a main part (the parabolic reflector, the waveguide tube), a series of detailed parts (truss members, end fittings, attachment brackets), and an electrical feed; all of these various parts were purchased from outside contractors. Inspection and final assembly of the detailed parts were performed at JPL, allowing close surveillance of piece-part deliveries and the application of emergency procurement methods whenever a slow piece-part delivery threatened to hold up final assembly of an antenna.

The production of the antenna feeds was performed by a subcontractor under the guidance of JPL; however, all other parts were produced for JPL by specialty machine shops and fabrication shops. The aluminum honeycomb reflector was sufficiently expensive and complicated that it received considerable special attention during its manufacture; in fact, several reflector design changes were made at the suggestion of the fabricator that resulted in a stronger, lighter, and more reliable finished structure.

VIII. SPACECRAFT SUBSYSTEMS: COMMAND

A. Functional Description

A functional block diagram of the command subsystem is shown in Fig. 100. Upon transmission of the appropriate command signal from the ground, the command subsystem aboard the spacecraft executes either of two types of commands. For a direct command, the subsystem generates a momentary switch closure or closures in other spacecraft subsystem circuits. For a quantitative command, the subsystem directs a sequence of binary digits (bits) representing midcourse maneuver information to the spacecraft CC&S subsystem. The command subsystem is comprised of the command detector, decoder, and transformer–rectifier. The command detector receives the command signal from the spacecraft radio subsystem. The signal contains the command word information bits, which biphase-modulate a sinusoidal subcarrier. The subcarrier is added to a synchronizing signal containing a pseudonoise code. The synchronizing signal provides the phase reference signal used to phase-demodulate the command word subcarrier. The detector processes and acquires phase coherence (locks up) with the command synchronization signal, which establishes bit synchronization and the phase reference signal. By multiplying the command word information subcarrier by the phase reference signal and applying the resulting output to a matched filter, the detector recovers the command word bits. The matched filter minimizes the bit error rate as a function of signal-to-noise ratio.

The command decoder receives the command word bits, determines the command word transmitted, and issues the proper output to the spacecraft subsystem or subsystems using the command word.

The detector also establishes a detector lock signal that inhibits the decoder command word decoding function when the signal indicates that the detector is out of lock with the command signal. The detector and decoder provide the spacecraft telemetry subsystem with signals that are converted into telemetry information concerning the functional operation of the command subsystem. The transformer–rectifier unit converts the spacecraft ac voltage into the ac and dc voltages required by the command subsystem. A standard description of the *Mariner* command word format is given in Fig. 101.

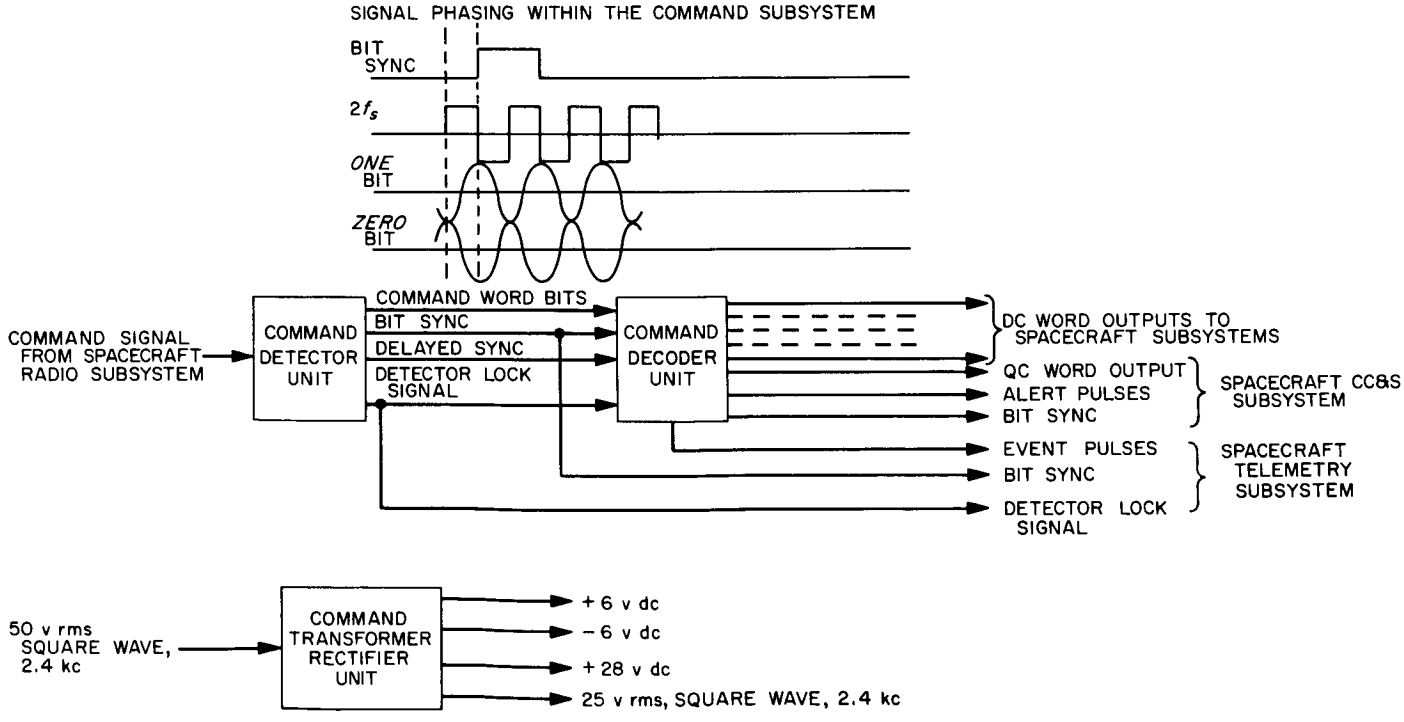


Fig. 100. Command subsystem functional block diagram

DIRECT COMMAND FORMAT

COMMAND BIT NO.	1	2	3	4	5	6	7	8	9	10	11	12	13	14	15	16	17	18	19	20	21	22	23	24	25	26
COMMAND BIT IDENTIFICATION	COM-MAND DECODER START			COMMAND ADDRESS						ADDRESS PARITY See Note 1		BITS 12–26 HAVE NO SIGNIFICANCE IN DC'S. IN QC'S THEY FORM PART OF THE CC&S COMMAND. REFER TO QUANTITATIVE COMMAND FORMAT														
COMMAND BIT VALUE	1	1	0	VARIABLE								*ZERO* FOR DC'S; VARIABLE FOR QC'S														

QUANTITATIVE COMMAND FORMAT

COMMAND BIT NO.		1	2	3	4	5	6	7	8	9	10	11	12	13	14	15	16	17	18	19	20	21	22	23	24	25	26
CC&S COMMAND BIT NO.										1	2	3	4	5	6	7	8	9	10	11	12	13	14	15	16	17	18
CC&S COMMAND BIT IDENTIFICATION										CC&S ADDRESS					See Note 3	TIME VALUE See Note 5											See Note 4
										See Note 2			Register Selector															
QC COM-MAND BIT VALUES	PITCH TURN	1	1	0	0	1	1	0	0	0	1	1	1	0	ODD PARITY	VARIABLE											POLARITY
	ROLL TURN	1	1	0	0	1	1	0	0	0	0	0	0	1		VARIABLE											
	MOTOR BURN	1	1	0	0	1	1	0	0	0	1	0	1	1		VARIABLE											

NOTES:

1. COMMAND BITS 10 AND 11 ARE ADJUSTED TO ENSURE AGAINST SINGLE BIT ERRORS CAUSING AN INCORRECT COMMAND WORD OUTPUT.
2. COMMAND BITS 9 THROUGH 11 (CC&S COMMAND BITS 1 THROUGH 3) ARE NOT USED QUANTITATIVELY BY CC&S BUT ARE USED TO REMAIN COMPATIBLE WITH PREVIOUSLY DESIGNED HARDWARE (*MARINER* VENUS 1962).
3. COMMAND BIT 14 (CC&S COMMAND BIT 6) IS ADJUSTED IN QC'S TO GIVE AN ODD NUMBER OF ONE BITS IN COMMAND BITS 9 THROUGH 26 (CC&S BITS 1 THROUGH 18).
4. COMMAND BIT 26 (CC&S COMMAND BIT 18) MUST BE A ONE TO PRODUCE A CLOCKWISE (POSITIVE) SPACECRAFT ROTATION ABOUT THE SPECIFIED SPACECRAFT AXIS. A ZERO IN THIS BIT POSITION WILL RESULT IN A COUNTERCLOCKWISE (NEGATIVE) SPACECRAFT ROTATION ABOUT THE SPECIFIED SPACECRAFT AXIS. POLARITY BIT FOR MOTOR BURN COMMAND IS ALWAYS ONE.
5. COMMAND BITS 15 THROUGH 25 (CC&S COMMAND BITS 7 THROUGH 17) ARE A PSEUDO-BINARY CODE REPRESENTATION OF THE TURN OR MOTOR BURN DURATION.

Fig. 101. Command word format

The command signal output from the transponder consists of the following signals linearly added:

1. The command word information subcarrier consists of a biphase-modulated, sinusoidal signal. The command word information signal equals V sin $(2\pi 2f_s t \pm \pi/2)$, which equals $\pm V \cos (2\pi 2f_s t)$, where $+\pi/2$ corresponds to a binary zero and $-\pi/2$ corresponds to a binary one. The polarity of the signal remains constant over each bit time.
2. A synchronizing information signal consists of a pseudonoise coded sequence modulo two added to a square wave signal at a frequency of $2f_s$.

The two signals are added to form the command signal to give $P_s/P_c = 2$, where P_s represents the synchronization-signal power, and P_c represents the command word information-subcarrier power. This power ratio minimizes the bit-error probability as a function of signal-to-noise ratio.

1. Command Detector

A functional diagram of the command detector is presented in Fig. 102. The detector performs three main functions:

1. Demodulation of the biphase-modulated sinusoidal subcarrier, which is accomplished by the detector command word channel
2. Establishment of a phase reference signal for use in demodulating the sinusoidal subcarrier, and establishment of bit synchronization, which is accomplished by the command synchronization channel

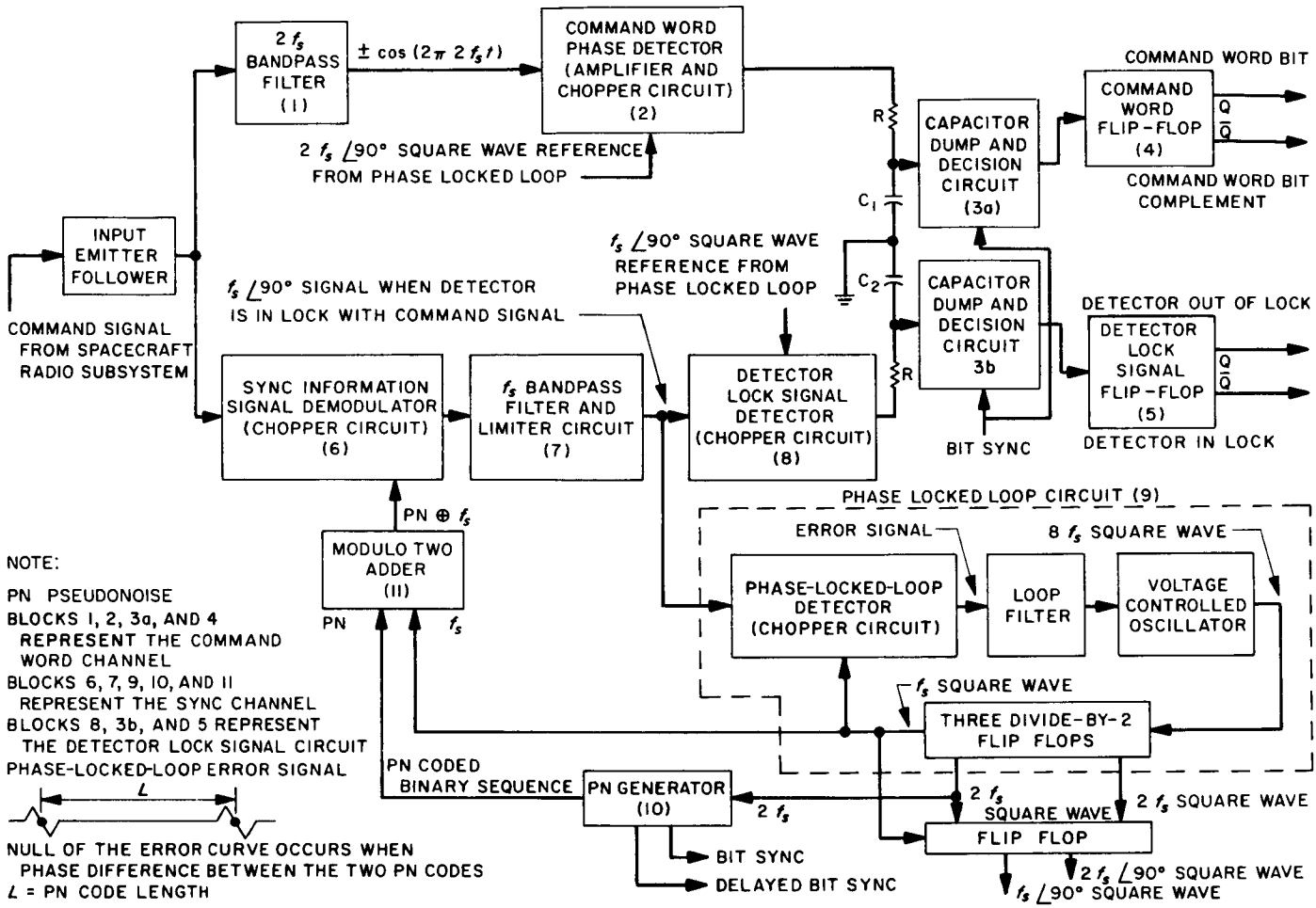


Fig. 102. Command detector functional block diagram

3. Establishment of the detector lock signal, which indicates whether or not the detector is in lock with the command signal, and which is accomplished by the detector lock circuit

a. Detector command word channel. The detector command word channel selects the command word information signal (biphase-modulated sinusoidal subcarrier) from the command signal with a 2 f_s bandpass filter (Fig. 102). The filter has a 3-db bandwidth of 40 cps, and an insertion loss of 8 ± 0.8 db, and introduces less than a 4-deg phase shift. The subcarrier is phase-coherently-demodulated through multiplication of the subcarrier by a phase reference signal from the detector synchronization channel and through filtering of the multiplied signals by a matched RC filter that effectively integrates the signal. The charge C_1 accumulated on the capacitor (Fig. 102) during integration is dumped by the dump circuit at bit synchronization time, and applied to a decision circuit where the polarity of the charge is determined; a positive charge represents a recovered binary digit one; a negative charge recovered represents a binary digit zero. The decision circuit triggers the command word flip-flop to the state representing the command word binary digit. The recovered command word bits are directed to the command decoder for processing and decoding.

b. Detector synchronization channel. The detector synchronization channel selects the synchronization information from the command signal through the multiplication of the command signal by PN + f_s at the synchronization information signal demodulator, where PN represents the pseudonoise code binary sequence generated by the detector pseudonoise generator, and f_s represents a square wave signal from the phase-locked loop circuit. The synchronization information obtained at the output of the f_s bandpass filter is cos ($2\pi f_s t$)

whenever the detector has acquired phase coherence with the command signal. When the detector is not in lock, the output is random. The cos $(2\pi f_s t)$ synchronization signal passed through a limiter (Block 7, Fig. 102) is used to develop an error signal to drive the phase-locked-loop VCO through multiplication of the signal by a reference square wave at the phase-locked-loop phase detector. The error signal is effectively the cross-correlation of the command synchronization signal PN + 2 f_s with the PN signal of the detector. The phase-locked-loop circuit is a second order closed-loop servo system whose VCO is made to track the phase and frequency of the command signal 2 f_s frequency when the recovered synchronization signal out of the f_s bandpass filter is cos $(2\pi f_s t)$. When the synchronization signal is random (detector not in lock), the 2 f_s frequencies of the detector phase-locked loop and the command signal are offset slightly to cause a rate of change in the relative phase difference between the two PN signals. This eventually results in a zero phase difference (approximately 6 min), the recovered synchronization signal of cos $(2\pi f_s t)$, and detector lock-up with the command signal. The synchronization channel f_s filter has a 3-db bandwidth of 40 cps, an insertion loss of 8 $\pm$ 0.8 db, and introduces less than a 2-deg phase shift. The synchronization channel phase-locked loop has a threshold loop noise bandwidth of 2 cps and a damping ratio of 0.707. The synchronization generator pseudonoise generator is driven at a 2 f_s rate. Bit synchronization pulses emanate from the pseudonoise generator every complete cycle of the pseudonoise code sequencer. The time between bit synchronization pulses (1 sec) is the pulse width of the command bits.

c. Detector lock signal circuit. The limited synchronization signal from the f_s bandpass filter is also multiplied by a reference square wave at f_s frequency (with 90-deg phase shift) at the detector lock signal detector. The output of the detector lock signal detector is then applied to a matched RC filter and a decision circuit in the command word channel. When the synchronization signal output of the f_s bandpass filter is cos $(2\pi f_s t)$ (detector in lock), the charge accumulated on the capacitor C_2 (Fig. 102) during integration time is negative. When the charge is dumped at bit synchronization time and applied to the decision circuit, the decision circuit measures the negative voltage (associated with the negative charge) added to a positive threshold bias voltage. If the algebraic sum of the voltages is negative, the decision circuit will then trigger the detector lock signal flip-flop to the state indicating that the detector is in lock with the command signal. When the algebraic sum of the voltages is positive, the decision circuit triggers the detector lock signal flip-flop to the state indicating that the detector is out of lock. The positive bias is inserted into the circuit to ensure that an out-of-lock indication occurs when the output of the f_s filter is random and the matched filter integrates to zero.

2. Command Decoder

A functional block diagram of the command decoder is presented in Fig. 103. The decoder provides two main functions:

1. Command word processing and decoding, which is accomplished by the decoder logic functions
2. Command word output execution, which is accomplished by the decoder isolation switches

a. Decoder inhibit circuit. When the detector lock signal indicates that the detector is in lock, the decoder inhibit circuit permits command word processing and decoding. Should the detector lock signal indicate that the detector is out of lock at some time before or during the processing of the command word, the inhibit circuit immediately inhibits decoder functioning and allows no further word processing until the decoder receives 26 consecutive *zero* bits from the command detector after the detector lock signal indicates that the detector is in lock once again.

b. Decoder function. When the command word/decoder start bits are recognized by the decoder timing circuit, a flip-flop counter begins a binary counting sequence to provide timing signals. In the meantime, the command word bits are being shifted into the decoder address storage flip-flops. At the proper binary count (occurring when the address bits fill the address storage flip-flops), the timing circuit issues the matrix interrogation signal that allows the proper NAND gate in the decoder matrix to open. This particular NAND gate is set to open a short time before the matrix interrogation signal by the outputs of the decoder address flip-flops containing the command address bits. The NAND gate is kept open by the matrix interrogation signal for 100 msec. In the case of a DC word, the proper DC word isolation switch or switches are closed. In case of a QC word, the QC word output flip-flop stops alert pulses and allows the 9 through 26 command word bits to be issued to the spacecraft CC&S subsystem. Bit-synchronization pulses, coincident with the command word bits, are issued to the CC&S during the QC word output readout. All outputs to the CC&S are issued through isolation switches.

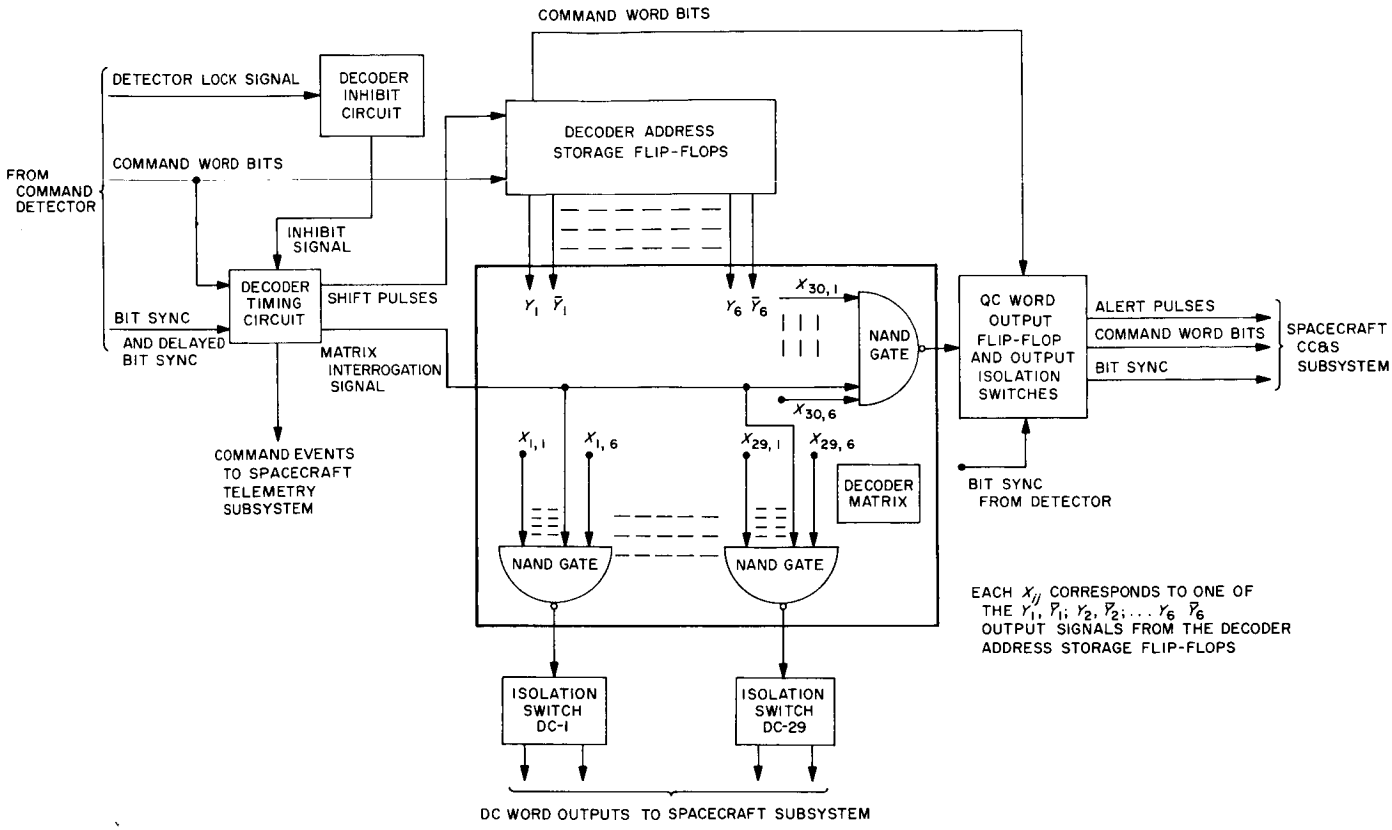


Fig. 103. Command decoder functional block diagram

At another particular count of the timing-circuit binary counter (occurring when the twenty-sixth bit of the command word has been issued through the first address storage flip-flop), the timing circuit resets all decoder logic functions to the passive state, rendering them once again capable of recognizing the command word/decoder start bits and processing the ensuing command word.

3. Command Telemetry

Three command signals are directed to the spacecraft telemetry subsystem to be telemetered to Earth. The signals time-share the telemetry transmission channel and are sampled at a rate determined by the telemetry mode.

Detector bit synchronization pulses are sent to the telemetry subsystem to be conditioned into information concerning the detector VCO frequency. Between telemetry-data sample times, reference pulses at the spacecraft 2.4-kc frequency are counted in an interval between two consecutive bit synchronization pulses. The number counted is indirectly proportional to the pseudo-noise bit rate and thus the VCO frequency. Therefore, an average of the VCO frequency (over an approximate 1-sec interval) is telemetered each telemetry-data sample time. The VCO frequency data are required to determine the proper ground command signal frequency that will minimize command-lock acquisition time.

The detector lock signal is directed to the telemetry subsystem to be converted into one bit of information regarding the detector lock condition. If the lock signal indicates "out of lock" for at least 1 sec in the interval between telemetry sampling times, the detector lock telemetry data will be at the binary state indicating out of lock at the next sampling time. If no out-of-lock indications occur, the binary state indicating in lock will result. The detector lock data indicate when the command subsystem is capable of detecting and processing the command signal.

Command event pulses are telemetered approximately 10 sec after the command decoder has recognized the decoder start bits of a command word. The event pulse indicates normal decoding timing function upon reception of the start bits. It is also normally coincident with a command address recognition and a DC command

execution by the decoder. In the case of a QC command, a second event pulse will be telemetered immediately after the last QC bit is directed to the CC&S subsystem.

B. Physical Description

The subsystem components were constructed in welded cordwood modules. A typical module is shown in Fig. 104 prior to encapsulation with epoxy resin. The modules are soldered to circuit boards as shown in Fig. 105. One circuit board with 16 modules and one with 14 modules, as shown in this figure, are glued together and bolted in a 6 × 6 × 1.1-in. frame. The subsystem consists of seven frames of approximately 2300 solid-state electronic components. The weight of the subsystem, less the wiring harness and case, is approximately 9.5 lb. The power consumed is less than 3.50 w.

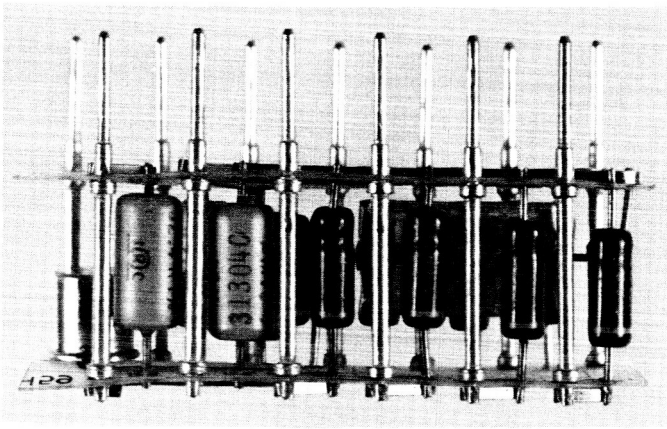


Fig. 104. Typical command subsystem welded cordwood module

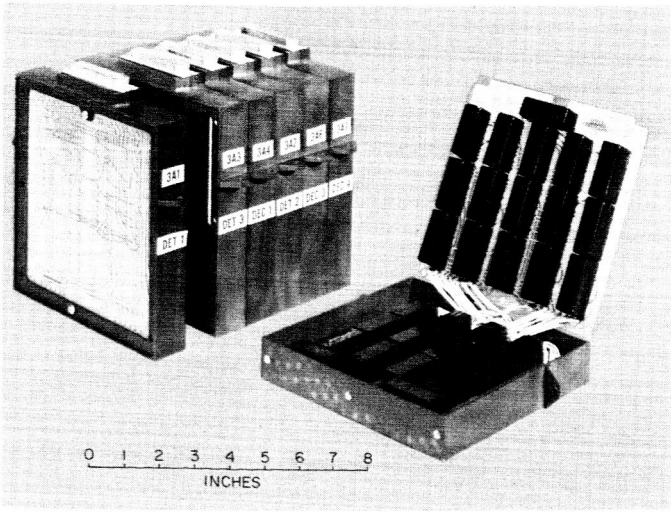


Fig. 105. Command subsystem assembly

C. Design Evolution

The *Mariner* Mars 1964 command subsystem design is basically that of the *Mariner* Venus subsystem, except for an increase in DC commands from 12 to 29 and the modifications described in the following paragraphs.

For the *Mariner* Venus command subsystem, a binary one, generated inadvertently and transmitted to the subsystem, could begin the command decoder operation. This did not necessarily generate an incorrect command execution but caused command event pulses to be telemetered, which could be confusing. Moreover, although the *Mariner* Venus addresses were coded to detect single bit errors, a single bit error in the zero bits preceding the command word bits could conceivably cause an incorrect command output. For the *Mariner* Mars 1964 word subsystem, the decoder only begins functioning with the reception of bit 110, thus making spurious decoder operation more unlikely. The command word format (Fig. 101) is also arranged so that no single bit error anywhere before or in the command word bits can cause an incorrect command word execution.

The command word information signal has been shifted 90 deg with respect to the phase of the pseudo-noise clock signal at a 2 f_s frequency. This was done to eliminate an interference of the command word information signal upon the synchronization signal. This interference results in a distorted phase-locked loop error curve and consequently in problems in locking up the detector.

In order to obtain a sharply defined square wave reference signal in the detector at 2 f_s ∠90 deg to detect the command word information signal, the detector VCO frequency was changed from 4 to 8 f_s. This change allows generation of the phase reference signal with ordinary command logic circuits.

The command packaging is basically that used in *Mariner* Venus. However, one "sandwich" is contained in a frame as opposed to two per frame in the *Mariner* Venus subsystem. The reasons for the change were (1) to make both sides of a sandwich easily accessible for inspection, and (2) to reduce handling and disturbance of sections of the subsystem not affected by modification or repair being accomplished on other sections. However, the first reason was partially invalidated when a

web had to be placed across the frame to give greater package rigidity.

Initially, the command modules were to be soldered cordwood modules as in the *Mariner* Venus command subsystem. However, it was determined that solder joints inside the modules could be raised to the melting point when soldering the modules to the "mother boards" during subsystem assembly. Since the joints inside the module could not be inspected for correct soldering once they had been potted, the possible degradation of the module construction during mother-board assembly was thought to be a serious problem. To alleviate this situation, a complete modification of the module manufacturing technique was incorporated and the modules were redesigned for welded cordwood construction. A typical command welded module is shown in Fig. 104.

All welded module layouts and the required weld schedules were checked and approved before incorporation into the module manufacturing program. Similarly, the actual module manufacturing was closely monitored and controlled by strict welding specifications. As a result, very few problems were encountered during module manufacture.

In addition to the occurrence of an event pulse at command-decoder/command recognition time, it was deemed desirable to have an event issued at the end of a QC command transmission. Thus, two command events are telemetered for a QC command.

The circuitry required to condition the appropriate command signals for telemetering the detector 2 f_s frequency to Earth was removed from the command subsystem and logically placed in the flight telemetry subsystem.

Initially, sufficient weight was allotted to the command subsystem to allow for redundant command detectors, transformer–rectifiers, and decoder program control units. However, this redundancy had to be abandoned from the design because of weight allotment.

All of these modifications to the *Mariner* Venus design were made prior to fabrication of the subsystems. The following two modifications were introduced after delivery of the PTM subsystem.

1. Initial procurements of voltage-controlled oscillators for the *Mariner* Mars 1964 program had proved unsatisfactory both in the manufacturing techniques used and in the resulting electrical performance. As a consequence, the prime subcontractor for the command subsystem was requested to develop a VCO that would employ only JPL preferred components and that would be packaged in a module construction meeting high quality control standards. As the result of an extensive 3-month VCO design program, a VCO circuit was completed that incorporated a field effect transistor as the input buffer stage and a conventional multivibrator as the oscillator stage. Voltage regulation for transistor bias was accomplished with Zener diodes. One dc supply voltage (28 vdc) was required to operate the VCO. The new VCO modules were manufactured in time to be incorporated into the type-approval subsystem and all flight subsystems. The PTM subsystem was retrofitted at a convenient time in the PTM spacecraft test program.
2. A web across the command frame was required to increase frame rigidity. Since the new frames were compatible with the old frames, retrofitting the subsystems was easily accomplished.

D. Procurement and Fabrication

With the exception of a few component types, the greatest majority of components used in the command subsystem were JPL preferred parts. All components were procured, screened, and tested according to procurement specifications generated for each component type.

A manufacturing flow chart was generated listing the necessary manufacturing, quality control, and test steps to be taken in the construction of the flight subsystems. In addition, PERT charts, which indicated the necessary goals to be accomplished throughout the program, for the flight and ground equipment were established. Required completion dates were also included on the charts. The significant fabrication problems are described below.

It was determined that the soldering of the modules to the circuit boards could cause enough heat flow into the modules to melt the solder joints in the modules. Since the modules were encapsulated and the module solder joints were not available for reinspection, this was thought to be a serious problem. As a solution, it was decided to construct welded cordwood modules instead of soldered modules. This meant completely new module layout designs and weld schedules for the various weld joints required. The module layouts to be redesigned were constrained to the same pin layout so that new circuit board layouts were not required. The contractor

exhibited an extremely reliable and well controlled welded module construction technique.

The construction of the three flight subsystems was accomplished on time and under a well controlled manufacturing program. However, during final manufacturer testing of the MC-2 flight subsystem, a failure of the decoder logic occurred very briefly during temperature tests. The failure could not be repeated and therefore could not be traced and definitely pinpointed. Suspected modules were replaced and the system was thoroughly tested over the temperature range. The failure did not reoccur at the contractor's. However, the same failure occurred during initial JPL bench testing. Fortunately, the failure condition remained long enough to trace it to a definite logic area in the decoder. The logic circuit boards concerned with the failure were completely disassembled, and all modules directly involved were replaced. The newly constructed logic boards were then placed in the MC-4 subsystem and thoroughly tested. No further problems were experienced during subsequent testing with any subsystem. In the final analysis, it was decided that contamination of the circuit board was the cause of the failure, although no fault with the circuit board was ever detected.

E. Test Experience

Before being shipped to SAF or submitted to life tests, each command subsystem underwent the following tests:

1. Initial subsystem tests at the manufacturer's prior to shipment to JPL
2. Initial performance tests prior to vibration test
3. Vibration test
4. Performance test prior to thermal–vacuum test
5. Thermal–vacuum test
6. Final performance test after thermal–vacuum test

The subsystem tests, item (1), included testing performance over the temperature range and statistical testing, which checked command bit errors and the out-of-lock indication rate as a function of signal-to-noise ratio.

The performance tests prior to vibration and before and after thermal–vacuum tests, item (2), consisted of a detailed observation and recording of all the subsystem logic and analog parameters at maximum, minimum, and nominal temperatures. The data were recorded on special test sheets included in the particular environmental specification for that subsystem. The test sheets were arranged to facilitate comparison of a particular parameter value over the temperature range before and after the vibration and thermal–vacuum tests. Parameter value trends or degradation occurring throughout the tests were thus recorded and could be easily discerned.

The PTM subsystem successfully experienced an interface compatibility test with interfacing subsystems that were available. In order to obtain as much statistical data as possible on the performance of the subsystem as a function of signal-to-noise ratio, bit error tests on the subsystems were run between active testing and during the long thermal–vacuum tests. After all tests for each subsystem were accomplished, the test data were analyzed and a decision was made as to whether the subsystem passed the environmental and performance tests.

Except for one test anomaly, subsystem testing was highly successful. The problem was encountered in the environmental lab during thermal–vacuum tests. During these tests, an occasional incorrect command was detected by the test-console monitoring circuitry. After an investigation of the situation, it was decided that noise induced into the cabling was triggering the test-console circuitry. To prove this conjecture, 10 MΩ resistors (similar to the open impedance of the switches) were substituted for the flight command output switches in the test. The command OSE still continued to report an occasional incorrect switch closure. Since this was impossible with resistors in the circuit, it was decided that the indications must have been due to noise.

Although this proved that noise induced into the cables could erroneously trigger the test-console circuitry, it did not prove that the noise was not also closing the command output switches. Noise induced switch closures were found to be possible during initial PTM spacecraft system tests. Spacecraft noise induced into the command/radio interface lines could cause very fast command transient switch closures. Because the radio input circuitry is very sensitive, the radio responded to the command switch closures. All other command users required much more of an energy input than could be developed by the noise switch closure. No other interface problems were experienced. The noise induced into the radio lines was effectively filtered by placing a capacitor across the command output switch.

No further problems or failures were experienced with any command subsystem in test at JPL or at Cape Kennedy.

IX. SPACECRAFT SUBSYSTEMS: POWER

A. System Mechanization

The *Mariner* Mars 1964 spacecraft power subsystem performs two major spacecraft functions:

1. It generates standard voltages for distribution to spacecraft users
2. It controls the turning-on and turning-off of various loads

To carry out these functions, a system was designed with a power source of four photovolatic solar panels containing a combined active area of 70 ft^2, a 1200-w-hr silver zinc battery to provide power during periods of non-Sun orientation, dc regulating devices, 2.4-kc inverters, 400-cps inverters, battery charging, load switching, and frequency control devices.

The power subsystem electronics are located in two of the spacecraft's eight bays. Bay VIII contains the power regulators, the power switch and logic, and the majority of the telemetry circuits. Bay I contains the inverters, the battery charger, the power synchronizer, and the power distribution assembly, as well as two pyrotechnic subassemblies that are not part of the power subsystem. The battery is located on the inboard side of Bay VIII and directly adjacent to Bay I. The solar panels are attached to the spacecraft bus at the top of Bays I, III, V and VII. Figure 106 shows the functional block diagram of the power subsystem.

B. Power Source

The main source of spacecraft power is from four photovoltaic solar panels with a combined active area of 70 ft^2. Each panel consists of four electrically isolated sections containing 1764 p on n silicon solar cells. Electrically, each section is made up of 21 parallel sections of 84 cells in series. These sections are connected to the unregulated power bus through blocking diodes that prevent reverse current flow in the event of a short in any one section. This ensures that one short in the solar panel cell matrix would reduce the power capability by, at most, 1/16.

The solar panels were sized to carry all loads from postmaneuver to after Mars encounter. This significantly increased the theoretical probability of performing the encounter sequence successfully, since it removed the battery (which is used to supply power whenever the solar panels are not Sun-oriented) as a series element in the reliability calculations after the midcourse maneuver.

Due to the fact that launch trajectories allow the spacecraft to spend some time in the Earth's shadow, and because of *Mariner's* large solar panel power capability near Earth, limiting of the panel output voltage was required immediately after exit from the Earth's shadow. Solar panel temperatures as low as $-80°$C were expected, which could lead to voltages as high as 68 v if no limiting were provided. Although regulation equipment could have been designed to handle the high-voltage peak, it could only have been done by allowing a substantial decrease in regulator efficiency and a reduction in component derating factors. To remedy the problem, the voltage output of each section was limited to 50 v by a string of six 50-w Zener diodes.

Figure 107 shows the nominal, steady-state temperature, solar panel power vs voltage plots (minus diodes) for near Earth, 100 days after launch, and Mars encounter environments. Also shown is the worst-case power demand at Mars.

During the early design phase when the exact flight solar panel output power, the exact power system loads, and the exact conversion-equipment efficiencies were not known, the anticipated nominal panel power was reduced by a factor of 20.5% to obtain an available-power number that could be used in the design. This 20.5% factor was broken down as follows:

1. 5% for operation off of the solar panel maximum power point
2. 7% for solar panel design and test tolerances
3. 8.5% for efficiency and load uncertainties

The substantial power margins shown in Fig. 107 were primarily due to increased solar-cell efficiency resulting from better control (less cell degradation) during the panel fabrication than initially predicted.

C. Energy Storage

During periods of non-Sun orientation, spacecraft power is obtained from a silver zinc 18-cell secondary battery. The battery had a capacity of 1200 w-hr at launch, and is capable of withstanding a continuous float charge. The battery interfaces with the unregulated bus

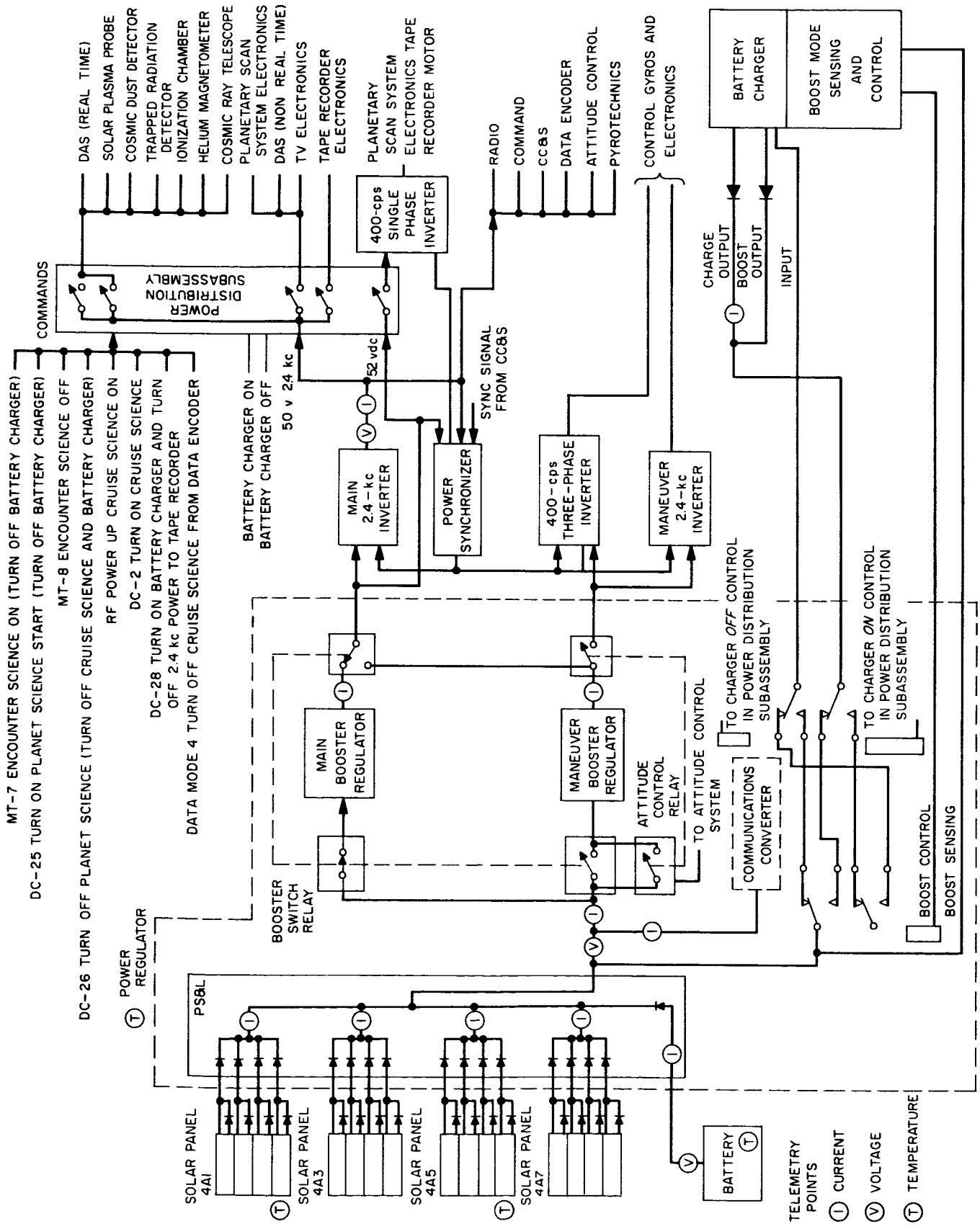


Fig. 106. Power subsystem functional block diagram

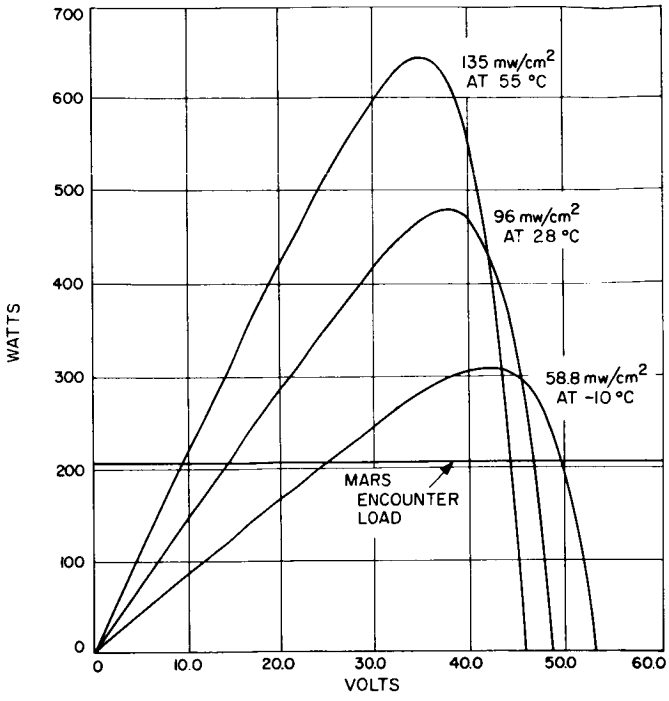


Fig. 107. Solar panel nominal curves: power vs voltage

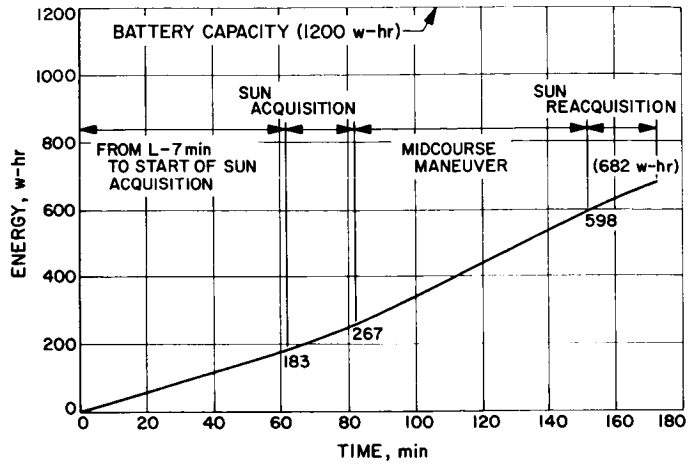


Fig. 108. Worst-case battery drain vs time

through a blocking diode in such a way that it is disconnected from the bus whenever the solar panel voltage exceeds that of the battery.

Normally, the battery is used to supply power from 7 min before launch until solar panel Sun acquisition. From Sun acquisition until the midcourse maneuver, 2 to 10 days, the battery is partially recharged using the flight charger. Following the maneuver, the battery is fully recharged and the charger turned off, after which it is a redundant energy source and not normally expected to be used again. For increased reliability, the battery capacity was chosen so that both the launch and maneuver phases could be completed without battery recharging. Figure 108 shows that for the longest possible launch and maneuver periods, a total of 682 w-hr would be removed from the battery. Designed in this manner, the battery charger was removed as a series element in the reliability calculations.

D. Power Regulation

The voltage regulating elements of the power subsystem consist of two booster regulators, each capable of operating at power levels up to 150 w. The regulators accept power from the unregulated bus at voltages ranging from 25 vdc (the lowest battery voltage) to 50 vdc (the highest solar panel voltage), and add sufficient voltage to bring the outputs up to 52 vdc ± 1%. The main booster regulator is on throughout the entire flight, supplying power to all spacecraft loads except the communications converter, which accepts unregulated power directly from the battery or solar panels.

The maneuver booster regulator is used to power a large part of the attitude control subsystem, and is on during the launch and midcourse maneuver phases. (Turn-on of the maneuver booster regulator is normally controlled by the attitude control subsystem.) The main reason for using the two regulators is the increased reliability they provide. If a failure occurs in the main regulator that allows its output to leave a 47-to 59-v range for a period of 2 to 3 sec, onboard logic will sense a failure, start the maneuver regulator, and permanently transfer all spacecraft loads to this unit. In order to protect the power users from a failure that would allow the regulator to go full *on* (resulting in a 68-v output for 2 to 3 sec), overvoltage protection limits the voltage to 60 vdc. All spacecraft areas can stand this 16% overvoltage for 3 sec.

Choice of the booster-type regulator, as opposed to the "down-regulating" switched regulator, was based primarily on reliability considerations. Even if both regulators should fail, a diode shunt path exists around the regulators that will allow the inverters to run directly from the solar panels. Solar panel output voltage varies from about 43 v near Earth to 50 v at Mars. Thus, a failure of both regulators near Mars would mean a dc output to the inverters of approximately 48 vdc (two diode drops exist between the panels and the dc output) instead of 52 vdc. Tests have shown that even at this reduced output voltage the mission could be completed.

E. Direct Current to Alternating Current Inversion

The main power for spacecraft users is a 100-v peak-to-peak 2.4-kc square wave obtained from a dc to ac inverter. Users take this power and, by using transformer–rectifier combinations, obtain the needed dc voltages for their equipment. This method of distributing energy has proved superior to dc distribution on *Mariner* Mars for two reasons:

1. User voltage requirements vary greatly especially with the science instruments, many of which require over 1 kv. Moving these high voltages around the spacecraft in cables is difficult.

2. Greater design flexibility is obtained since users can change voltage requirements late in a program without affecting the power subsystem or requiring changes in the spacecraft cabling.

Under normal conditions, the main inverter receives dc power from the main regulator. An identical inverter receives dc power from the maneuver booster regulator and supplies 100 v peak-to-peak 2.4-kc voltage to the attitude control subsystem. Also running from the maneuver regulator is a 28-v-rms, 400-cps, three-phase inverter that delivers step square wave power to the gyro spin motors. Figure 109 shows the three-phase waveform. Using this waveform in preference to a sine wave saved approximately 1 lb in inverter weight and had no adverse effect on gyro operation. A 400-cps, single-phase square wave inverter, supplying nominal outputs of 56 v peak-to-peak to the science scan platform and 65 v peak-to-peak to the VSS, operates from the main regulator. This inverter is to be off except at Mars encounter.

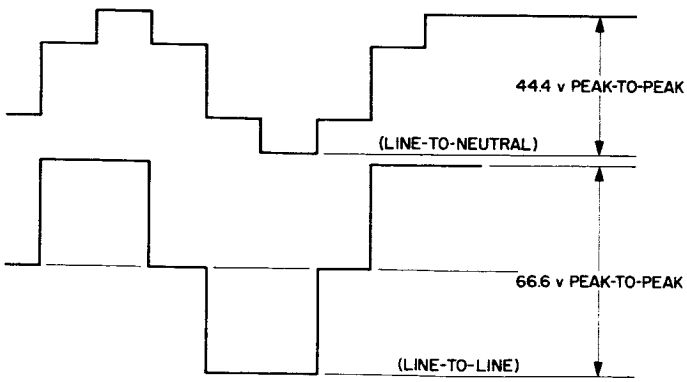


Fig. 109. Three-phase 400-cps waveforms (with resistive loads)

F. Power Frequency Synchronization

The power synchronizer unit provides a synchronizing signal or a frequency-stable driving voltage for all power subsystem inverters. A 38.4-kc signal received from the CC&S is counted down to provide both 2.4-kc single-phase and 400-cps single-phase and three-phase signals. In the 2.4-kc and 400-cps single-phase inverters, these signals are used to frequency-synchronize the units and obtain 0.01% stability. The 400-cps three-phase inverter is actually a power amplifier driven from the power synchronizer with an accuracy of 0.01%. If the CC&S fails to produce the 38.4-kc signal, or if a CC&S failure should result in a signal frequency of twice 38.4 kc, a 38.4-kc oscillator (internal to the power synchronizer) starts, automatically disconnects the CC&S input, and picks up as the frequency source. While running on its internal oscillator, the frequency of the power subsystem is controlled to $\pm$ 2%. If the internal oscillator or the synchronizer countdown chain should fail, the 2.4-kc and 400-cps single-phase inverters will free-run within 5% of the desired frequency. All spacecraft systems can operate satisfactorily at frequencies in this worst case at $\pm$ 5% frequency range.

G. Power Distribution

Some spacecraft systems always receive power whenever the power subsystem is operating; others are turned on and off during various parts of the mission by onboard logic or direct radio command. The actual switching of these loads is done by the power system in the power distribution assembly. This unit accepts commands from other spacecraft systems and translates the commands into relay closures. Since loads are switched in units (e.g., cruise science experiments and encounter science experiments), central control of the switching, as opposed to individual user switching, proved highly successful. Table 27 shows the power subsystem command flexibility.

In order to prevent random switching of loads, considerable care was taken in the design of the distribution electronics to make them insensitive to noise and transients. Also, all inputs into the assembly, which came from various spacecraft systems, were isolated to prevent interaction in a failure mode.

H. Battery Charging

After solar panel Sun acquisition, the battery is recharged using the flight battery charger. The charger takes power from the unregulated bus and delivers a current-limited voltage regulated charge to the battery.

Table 27. Power subsystem command capability

Control input	Source	Type of signal	Required action by power subsystem
1. Encounter start[a]	MT-7	Isolated circuit closure (permanent)	Connect planet science to primary 2.4 kc Connect cruise science to primary 2.4 kc Turn on 400-cps, single-phase supply Connect tape machine to primary 2.4 kc Turn off battery charger
2. Encounter start[b]	DC-25	Isolated circuit closure (pulse > 100 msec)	Same as No. 1
3. Encounter terminate	MT-8	Isolated circuit closure (permanent)	Disconnect planetary science 2.4-kc power source Disconnect redundant cruise science 2.4-kc power source Turn off 400-cps, single-phase supply
4. All science battery charger off[c]	DC-26	Isolated circuit closure (pulse > 100 msec)	Same as No. 3 Same as No. 3 Same as No. 3 Disconnect main cruise science 2.4-kc power source Turn off battery charger
5. Transmitter power up, cruise science on	Spacecraft separation connector	Series interruptions on one isolated circuit	Connect cruise science to primary 2.4-kc power source Provide RF power-up signal by opening normally closed relay contact (irreversible in flight)
6. Cruise science on	DC-2	Isolated circuit closure (pulse > 100 msec)	Connect cruise science to primary 2.4-kc power source
7. Battery charger on	DC-28	Isolated circuit closure (pulse > 100 msec)	Turn on battery charger Turn off tape electronics
8. Change to Data Mode 4	Data encoder	Isolated circuit closure	Disconnect cruise science from primary 2.4-kc power source

[a]Redundant connection.

[b]Backup for No. 1.

[c]Backup for No. 3.

After the battery is fully charged, the capability exists to turn off the charger by direct radio command to prolong battery life. If it is necessary to use the battery again as a result of losing Sun acquisition, a radio command capability exists for reapplying the charger.

In addition to its battery charging function, the charger can also be used to remove the solar panel/battery combination from an unnecessary battery sharing mode. Such a mode can be entered if a power transient instantaneously exceeds the maximum power capability of the solar panels. If this should happen during the latter part of the mission when the battery charger is turned off, onboard logic would sense the condition, shift the charger into a current-limited constant voltage mode of high capacity, connect the input of the charger to the battery and the output to the unregulated power bus, and boost the system out of sharing. When sharing ceases, the logic would return the unit to its normal off position. Boosting is inhibited during periods when battery sharing should normally occur (i.e., launch and midcourse maneuver). If unnecessary battery sharing occurs near Earth when the charger is charging the battery in a normal manner (a very unlikely occurrence due to the large power capability of the solar panels in this region), onboard logic would sense the sharing condition, stop the battery charging operation, and await a ground command. A direct radio command can then be sent to start

the boost mode. This implies, obviously, that the functions of battery charging and boosting are mutually exclusive since they are performed using the same electronics.

I. Engineering Telemetry

Figure 106 shows the location of 18 of the 22 power subsystem telemetry points. Not included are the three solar panel standard cell transducers and the Bay I (all electronics except the two dc regulators and the battery) temperature transducers. Table 28 lists all 22 telemetry points. Measurements were taken at different sample rates depending on the location in the sampling sequence and the spacecraft data mode. Table 29 shows the rates of transmission of the engineering data. With the exception of the solar panel standard cell transducers, all measurements are self explanatory.

Table 28. Power subsystem telemetry measurements

Channel	Measurement	Range	Deck rate
109	PS&L output voltage	23 to 53 vdc	High
203	Dual booster regulator input current	0 to 10 amp	Medium
204	PS&L current to communication	0 to 5 amp	Medium
205	Main booster regulator output current	0 to 5 amp	Medium
206	Battery voltage	23 to 40 vdc	Medium
207	Main 2.4-kc output voltage	40 to 60 vdc	Medium
216	Battery charge current	0 to 1 amp	Medium
221	Maneuver booster regulator output	0 to 5 amp	Medium
222	Solar panel 4A1 current	0 to 5 amp	Medium
223	Solar panel 4A5 current	0 to 5 amp	Medium
224	Solar panel 4A3 current	0 to 5 amp	Medium
225	Solar panel 4A7 current	0 to 5 amp	Medium
226	Battery drain current	0 to 10 amp	Medium
227	Main 2.4-kc output current	0.5 to 2.5 amp	Medium
401	Bay I temperature	25 to 175°F	Low
407	Bay VIII temperature	25 to 175°F	Low
409	Solar panel 4A1 temperature	−40 to 160°F	Low
415	Standard cell current	0 to 100 ma	Low
416	Radiation resistant cell current	0 to 100 ma	Low
417	Standard cell voltage	0 to 100 mv	Low
428	Battery temperature	25 to 150°F	Low
429	Solar panel 4A5 temperature	−40 to 160°F	Low

Table 29. Time between telemetry data samples

Deck rate	Data Mode 1		Data Mode 2	
	33⅓ bps	8⅓ bps	33⅓ bps	8⅓ bps
High	4.20	16.8	12.6	50.4
Medium	42.0	168	126	504
Low	840	3360	2520	10,080

Selection of the points to be monitored was originally based on the following criteria:

1. The currents flowing into and out of all functional elements should be known.
2. The temperatures of all functional elements should be known.
3. Input and output voltages of all elements should be measured.
4. Sufficient information should be available to verify, using power subsystem loading, proper operation of other spacecraft subsystems.
5. The failure of any one transducer should have a minimum effect on the knowledge about the subsystem.

A sufficient number of telemetry channels were not available to meet all the criteria. In general, since the subsystem was voltage-regulated, currents were considered more indicative of proper performance than voltages. Voltage measurements were limited to the subsystem input and output and the battery. In many cases, placement of the current monitors is such that if a transducer should fail, its monitored parameter can be inferred from the other operating monitors.

J. Solar Panel Standard Cell Transducers

In order to more accurately determine the current voltage characteristics of the solar panels in flight, the outputs of three standard solar cells are telemetered. The open-circuit voltage and short-circuit current of two cells, identical to those used in the solar arrays, form the bases of the predictions. These readings are compared to Earth-based readings, and the open-circuit voltages and short-circuit current of the four-panel combination are determined. These readings, in turn, lead to the determination of solar panel maximum power capability and spacecraft power margins. The third cell is a radiation

insensitive cell; i.e., it is a standard p on n silicon solar cell that has been degraded by radiation to a point at which further radiation has little effect on cell output. By comparing its short-circuit output in flight to the short-circuit output of the other standard cell, it may be possible to determine whether radiation is degrading the solar panels.

K. Detail Design

The process of designing, manufacturing, testing, and providing quality assurance for the subsystem is represented by the flow diagram shown in Fig. 110. After the functional requirements of each power subsystem element had been determined, detailed design was begun. Functional-element reliability (e.g., the process of designing reliable inverters) involves, to a large extent, parts selection and application. The power conversion equipment (excluding solar panels and the battery) contained 913 electrical components, and, in some areas, failures would obviously have led to termination of the mission. In order to minimize the possibility of such failures, parts selection and application were closely controlled, and, whenever possible, component selection was made from the JPL Preferred Parts List. In many cases, JPL high-reliability parts, manufactured to strict Laboratory specifications from raw material to finished product, were used. *All* power subsystem parts were either high-reliability types or were screened by the power subsystem manufacturer to JPL screening specifications. Table 30 shows the percentages of high-reliability, preferred parts, and non-preferred parts (not included on JPL Preferred Parts List) in the power subsystem electronics. Included in the 27.9% non-preferred parts were such things as specially made chokes and transformers that were not commercially available, and, hence, were not on the JPL list.

In applying these high-reliability or screened parts in circuits, the units were severely derated (i.e., power and voltage) by the designer to meet JPL standards. A list was compiled for all power subsystem parts showing the stress rating of the individual units versus the actual stress level in the circuit. The stress ratio of these two numbers was a closely watched item.

Prototype units were manufactured after breadboard testing was completed. This hardware was identical to the flight gear in mechanical layout and electrical characteristics, and served both to debug the manufacturing process and to provide a flight-equivalent test set. Again, this hardware pointed out changes that were required before production of flight hardware. Figure 111 shows a typical Bay I module. Figure 112 shows the power regulator assembly located in Bay VIII.

Table 30. Conversion equipment: component parts status

Unit	High-reliability parts	Preferred parts	Non-preferred parts[a]	Totals
Power regulators assembly	92 (26.4%)	144 (41.4%)	112 (32.2%)	348
Power distribution assembly	90 (52.9%)	31 (18.2%)	49 (28.9%)	170
Power synchronizer	88 (40.2%)	74 (33.8%)	57 (26.0%)	219
Battery charger	24 (27.0%)	44 (49.4%)	21 (23.6%)	89
2.4-kc inverters (2)	8 (20.5%)	24 (61.5%)	7 (18.0%)	39
400-cps, single-phase inverter	2 (9.1%)	18 (81.8%)	2 (9.1%)	22
400-cps, three-phase inverter	1 (3.9%)	18 (69.2%)	7 (26.9%)	26
Total	305 (33.4%)	353 (38.7%)	255 (27.9%)	913
Total high reliability and preferred parts is 658 (72.1%)				

[a]Not on JPL Preferred Parts List.

L. Design Evolution

1. Subsystem

In the initial design phases of the *Mariner* Mars 1964 mission, it was shown that the power subsystem mechanization used on the *Mariner II*, which encountered Venus in December of 1962, would be inadequate for the longer mission to Mars. The calculated reliability of the *Mariner II* power system was 0.72 (Ref. 20). This was based on a mission time of 2600 hr. The calculated probability of success of this system for the 6000-hr Mars mission would be 0.46. To get a higher calculated reliability for the *Mariner* Mars mission, the various functional blocks of the power system were analyzed for their calculated reliability. The booster regulator (with its 76 parts) had a calculated failure rate of 0.016 failures per thousand hours; hence, it was one of the largest contributors to the system unreliability. Because of its critical nature, it was made redundant.

Based on the number of parts, the power synchronizer (with 219 parts) was the most unreliable power subsystem element. All but 12 of its parts could be charged against the 400-cps three-phase inverter, since the 2.4-kc

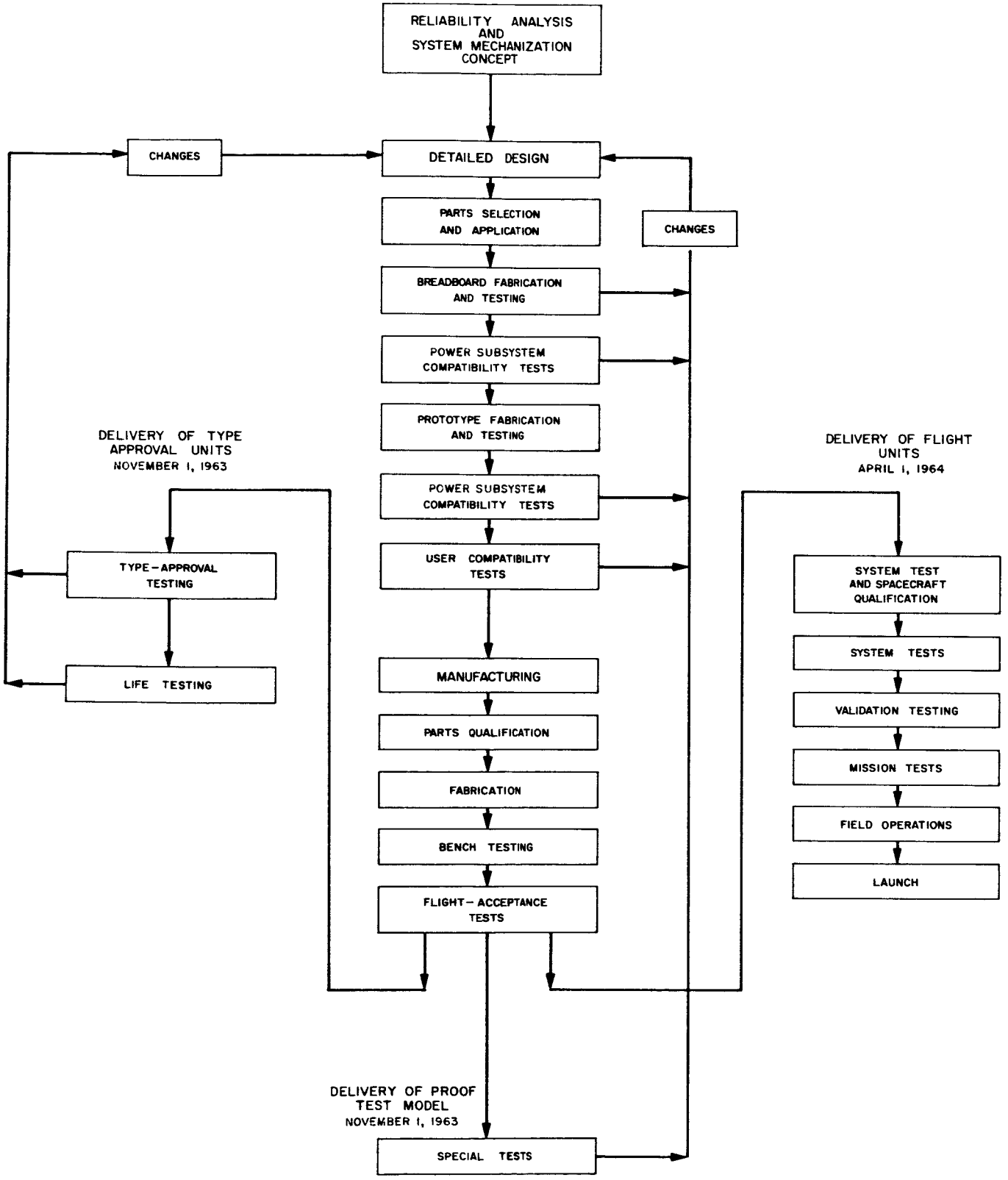


Fig. 110. Power subsystem development flow diagram

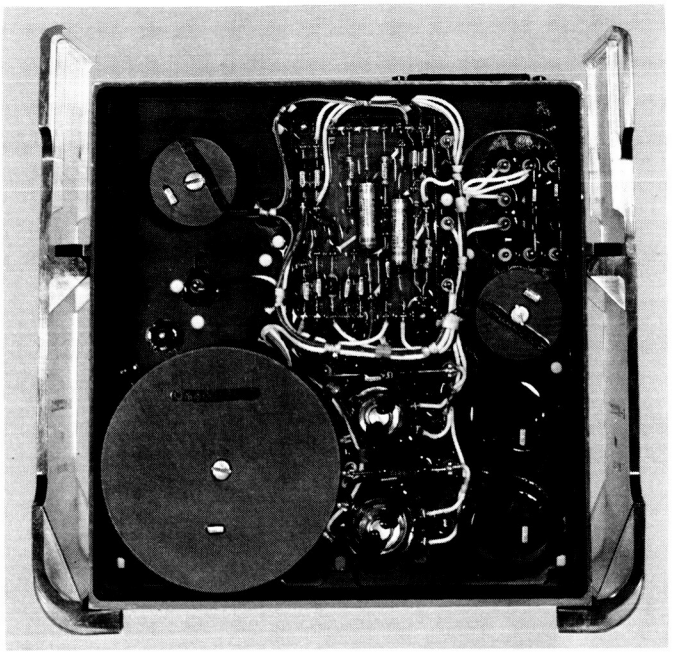


Fig. 111. Power subsystem typical Bay I module

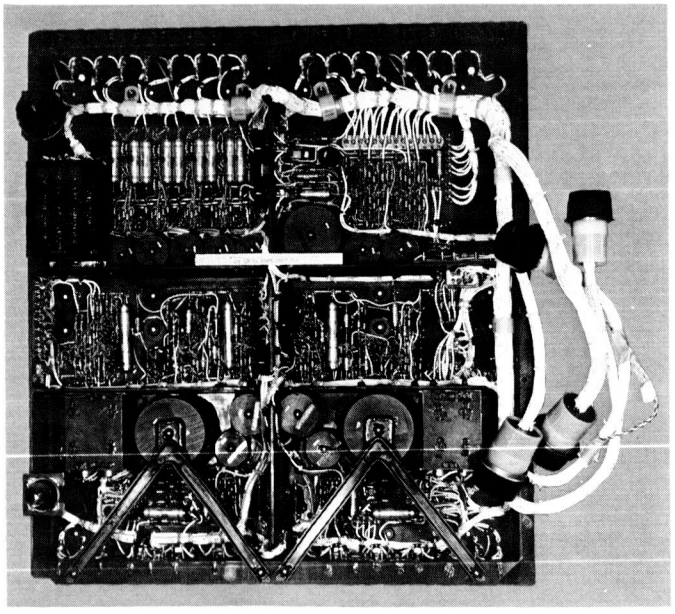


Fig. 112. Power regulator assembly, Bay VIII

inverters had the capability of free-running. Rather than use one leg of the three-phase inverters to drive the tape recorder at encounter, which would have made the mission dependent upon the power synchronizer for the full 6000 hr, a 400-cps single-phase inverter with a free-running capability was used. This made the power subsystem dependent on the synchronizer only through midcourse, which, in a normal mission, should occur within 240 hr of launch.

Another design mechanization that was used solely to increase reliability was the fusing of the noncritical telemetry circuits. One fuse in the power regulator assembly removed the 106 parts associated with telemetry as a source of unreliability.

By using reliability approaches, such as those discussed, together with the criteria for sizing the solar panels and battery, it was possible to raise the reliability of the *Mariner* Mars 1964 power subsystem considerably over that possible with the *Mariner II* subsystem. The power subsystem reliability, as computed for several points along the mission profile, is shown in Table 31. Again, the *Mariner II* estimated reliability was 0.72. Thus, the estimated probability of success for the *Mariner* Mars power subsystem was about equal to that of the *Mariner II* subsystem. It is significant, however, that the estimated reliability achieved with the *Mariner* Mars 1964 system was based on a greater parts count and almost two-and-a-half times the mission lifetime.

Table 31. Power subsystem reliability

Event	Time, hr	Estimated reliability
First maneuver	44	0.99
Second maneuver	288	0.96
↓	750	0.95
	2600	0.87
	4500	0.79
Encounter	6000	0.72
End playback	6213	0.71

Between the time the power subsystem mechanization was finalized and the flight hardware was delivered, several design changes were made. Some of these resulted from changing spacecraft requirements; others were incorporated to increase the performance margins and reliability of the power subsystem.

2. Conversion Equipment

In the early stages of the spacecraft design, it was determined that the 400-cps single-phase inverter loads could use square wave power instead of the originally

planned sine wave power. This resulted in the removal of approximately 1 lb in sine wave filters from the 400-cps single-phase inverter, and, also, in increased unit reliability with no decrease in spacecraft performance.

Also early in the program, it was found that the tape recorder would have to run during the launch phase. Since it was not possible to alter the mechanization of the power subsystem to run the 400-cps, single-phase inverter at launch without completely redesigning the power distribution assembly, tests were conducted with the tape recorder motor running from one phase of the 400-cps, three-phase gyro inverter. These tests were successful, and the subsystem was mechanized to have the tape recorder run from this source during the launch.

Several areas were reviewed and changed as a result of PTM testing:

1. The booster regulators were modified to: decrease transient response time, remove a low-frequency ripple of 100 to 200 mv amplitude, remove a turn-on voltage overshoot, and increase the regulators' phase and gain margins.

2. The input inductor in the main 2.4-kc inverter was removed to decrease the unit's output impedance.

3. Modifications were made to the 400-cps, single-phase inverter frequency-synchronization circuitry to provide greater margins at low input voltage. Also, the inductance–capacitance input filter was removed from the unit to reduce a transient at encounter science turn-on.

4. Noise filtering was added to the command input lines of the power distribution assembly, and circuit modifications were incorporated to guarantee that the latching relays in the unit would not change states at spacecraft power turn-on and turn-off.

During bench testing of the flight hardware, it was discovered that the relays used to switch booster regulators in a failure mode and to turn-on the maneuver regulator were being subjected to high-surge currents at relay closure. This was due primarily to charging of large downstream filter capacitors. A resistor diode network was added to precharge these capacitors and a resistance–capacitance network was placed across the relay contacts to prevent arcing when the relays opened. No further relay problems were observed.

Rather late in the PTM testing, several other changes were incorporated:

1. Three 50-w, 20-v, Zener diodes in series on the output of the main regulator were added. In the event of a booster regulator failure that would have allowed the unit to go full on, these diodes would have limited the output voltage to 60 v until the switch to the maneuver regulator occurred.

2. As a result of system tests, the capability of turning off 2.4-kc power to the tape-recorder electronics was added to the DC-28 "battery-charger-on" command.

3. The CC&S failure-sensing logic, located in the power synchronizer, was made sensitive to twice the normal 38.4-kc CC&S signal.

4. To improve design margins, the boost-mode output power of the battery charger was increased by several circuit changes.

5. The RF "power-up" and "cruise-science-on" logic was mechanized so that the events would occur at maneuver regulator shut-off if they did not take place at spacecraft/*Agena* separation.

3. Battery

The *Mariner* Mars 1964 battery design evolved directly from the *Mariner II* battery. The more important differences were: cell orientation, plate thickness, and the additional wrap of cellophane.

While cell orientation is not important in the zero gravity of space, it was important during the many hours and days of spacecraft testing. Oriented cells proved to have a cycle life of over 20 cycles when kept upright. This was reduced to about 5 cycles before failure when cells were inverted or placed on their side.

Increased plate thickness provides greater specific capacity (w-hr/lb), but it reduces total plate area and maximum load current for a given amount of silver. The additional wrap of cellophane reduced the rate of self-discharge loss by about 50% and extended cell life appreciably.

Float-charge capability was provided. This was accomplished by using excess ZnO in the negative plate and a minimum amount of electrolyte. Due to unusual voltage characteristics of the silver zinc battery while charging, using a sensing circuit to turn off the battery charger at the correct time would have been quite complicated.

With float-charge capability, the complicated circuit was not needed, and total reliance on battery charger turn-off was eliminated.

M. Procurement and Fabrication

1. Subsystem Conversion Equipment

a. Procurement. The initial plan for the *Mariner* Mars power subsystem was to have the entire subsystem procurement, including operations support, under one contract. The concept of contracting the entire system, rather than specific tasks, was employed in an attempt to best use the limited JPL personnel resources. It was intended that one technical representative would provide the primary go-between with the contractor. The technical representative, while responsible for the overall technical conduct of the contract, was not responsible for the design of the specific components of the power subsystem. When a solution to a design problem was required, the JPL cognizant engineer for the subsystem component in question was called in to provide the solution. This enabled the JPL cognizant engineers to spend nearly full time on technical problems rather than having to deal with the administrative problems associated with procurement.

The contract for the system-concept type of contracting contained the following tasks for the solar panel subsystem:

Task I: The contractor would provide two engineers to be in residence for 7 months at JPL to assist in solar panel electrical design.

Task II: The contractor would fabricate, assemble and test the following: 21 batteries; two type-approval solar panels and 10 flight solar panels (the contractor was furnished panel substrates); and six sets of electrical converters.

Task III: The contractor would provide two operations support teams, each consisting of one engineer and one technician.

The contractor was to obtain assembled batteries on a directed procurement from a subcontractor previously selected by JPL; the contractor was only to perform flight acceptance testing prior to delivery to JPL. The other equipment in Task II was to be fabricated and assembled by the contractor using government-furnished equipment and commercial component parts.

The overall *Mariner* Mars 1964 program was executed on a tight schedule, and stringent time constraints were imposed on all subsystem procurements. In the power subsystem, this caused a necessary overlap of the design, development, fabrication, and test phases of the solar panels and the electrical converters. This resulted in many design changes being required as a result of fabrication difficulties, bench-testing deficiencies, and spacecraft incompatibilities.

It became necessary to partially terminate the entire Task III portion of field support and replace it with a separate labor-hour contract with the same contractor. This reduction in an overly large scope of work resulted in ease of administration and cost accounting.

b. Fabrication. The fabrication of the power subsystem conversion equipment was done at a contractor's facility. A contractor was chosen who had the facilities and capability to perform the fabrication and testing to JPL standards. The equipment was fabricated in a dust-free, pressurized clean room, access to which was restricted to the necessary minimum of personnel. Everyone entering the clean room was required to wear a cap and gown; in addition, those who actually handled the flight equipment being built wore gloves.

The design of the conversion equipment was the responsibility of JPL but the fabrication methods were merely approved by JPL. The manufacturing, planning, and scheduling was completed and approved before any fabrication of flight units began. The manufacturing planners used the JPL drawings to plan the steps of the fabrication procedure. These step-by-step procedures were then used by the fabrication personnel, since the JPL drawings were not available to them. The planning consisted of first separating the fabrication of a subassembly into some number of discrete subtasks. Each of these subtasks was then separated into individual steps, which were itemized in proper sequence on a shop order. This shop order referenced, where applicable, parts lists, visual aids, and JPL or contractor process specifications. The parts lists and visual aids were part of the planning. The parts lists included all the components and materials needed for each specific step on a particular shop order. The serial number assigned to individual components in screening was recorded along with its type, value, size, and circuit symbol. The visual aids were an elaborate method of graphically illustrating such things as component location, mounting methods, wire routing, and termination points.

In addition to the contractor's manufacturing planning, JPL had a contractual requirement for a fabrication flow plan. A fabrication flow plan was generated for each subassembly by separating the fabrication procedure into subtasks. These subtasks were the same ones used as a basis for the shop orders mentioned earlier. As the shop orders became detailed, the details were included on the flow plans. This allowed a check on the development of the planning, and provided a necessary cohesiveness to the overall planning effort.

The flow plans included no schedule data. Schedules were made by using simplified flow plans and relating time to particular operations in order to determine the time spans needed for fabrication of the various units. By this method, the contractor was able to arrive at the date on which he had to begin fabrication in order to meet his contractual delivery requirements.

The contractor's QA organization wrote inspection procedures for each step. These procedures listed the specific items of work that had just been completed and how they should be inspected. The JPL drawings were used by the contractor's QA inspectors on the steps that required a visual aid. The JPL source inspectors performed a redundant inspection of some of the contractor inspections where it was felt that a double inspection would ensure flight quality units.

The individually fabricated units were electrically bench-tested as the last step of the manufacturing process. The bench testing consisted of a resistance and continuity test and an electrical bench test prior to the application of conformal coating, and an identical electrical test subsequent to conformal coating of the unit. The conformal coating was a thin layer of a polyurethane base material applied over the circuit boards and other components that acted as an electrical insulator and a seal to prevent corrosion and contamination. The test procedures were written by the contractor but were based on JPL detail specifications. The contractor's QA inspectors performed a continuous surveillance on all bench testing.

A log book was maintained for each unit by the contractor's QA organization. This log book contained the shop orders, the parts lists, JPL inspection reports, material review board actions, all test data, all JPL QA records for components or materials used, and any contractor-generated documents or records that applied to a specific unit. These log books were approved by the JPL QA engineer for proper content prior to the delivery of a unit to JPL. Since only six units each of eight types were built, a more flexible manufacturing planning system should have been used, which would have greatly alleviated many of the problems that were encountered.

c. Testing. All environmental testing on the power conversion equipment was done on a case level. The power conversion gear included the power regulator, Bay VIII (which is one large unit), and Bay I (which contains the power distribution, power synchronizer, battery charger, and inverter modules).

Six complete sets of power conversion equipment went through the flight acceptance tests. For the most part, FA testing was uneventful, demonstrating only that the equipment was adequate for that environment. However, one failure of the power regulator occurred in FA tests, which led to a design change: at high temperature, the high leakage in one transistor did not allow the booster failure circuitry to reset. The addition of a bleed-off resistor eliminated the problem for all transistors within specification at all temperatures.

Type-approval testing exposed several conditions that required design changes. For cases containing only electronic circuitry (such as the two power cases), the most important tests for type approval were complex-wave vibration and vacuum temperature. All other tests appeared to be of no difficulty and were passed with ease.

The first TA complex-wave vibration test led to several design changes. The heavy motor-driven switch, used to transfer from external to internal power, was badly damaged. One mounting flange was broken, the other flange was cracked. The case for this switch was magnesium. Fortunately, an investigation into mu-metal for the case of the switch was already under way to reduce the switch's excessive magnetic field. The mu-metal-cased switch was much stronger, and, when installed in the TA Bay VIII, easily passed vibration tests.

During the same vibration test, the potting fillet around the base of the booster-regulator power transformers had broken loose. The transformers did not break loose. Braces were added to eliminate the distortion of the chassis under vibration that caused the broken fillets. With the braces and a switch to a mu-metal case, Bay VIII passed the TA complex-wave vibration test.

After 6 days of high temperature during the TA thermal–vacuum test, a transistor in the battery charger failed. Subsequent investigation showed that a capacitor

was discharged through the transistor when the boost mode circuitry was reset. This, together with the TA high-temperature environment, led to the failure. Discharging the capacitor in a different fashion alleviated the problem. After this modification, the circuitry performed to specification during a complete TA test.

It is felt that the experience gained in the type-approval testing assisted in the elimination of questionable areas that did not show up in the FA testing. Flight-acceptance testing demonstrated that the modules were capable of withstanding the actual flight conditions.

2. Battery

a. Procurement. Procurement was conducted in two phases: development and production. Battery development was obtained on a cost-plus-fixed-fee contract; requests for programming were sent to ten companies. Six proposals were received and evaluated. The work included design of the Mark VI battery, including special tooling and a quality control plan. A mockup battery and four test batteries were delivered on this contract.

Production quantities (21 batteries) were procured by the power subsystem contractor. Because the type of battery specified deteriorates with time, flight batteries and spares were ordered for delivery as close to flight time as practicable.

b. Testing. Type-approval tests were conducted at JPL. Three batteries passed the required environmental tests as well as electrical tests designed to simulate worst-case operational conditions.

Flight-acceptance tests were conducted by the power subsystem contractor at his battery laboratory and environmental test facility. Two minor problems developed during the testing program: battery weight, and voltage stability during vibration. The vendor could not consistently keep weight below the desired maximum 33.3 lb; weights were as high as 33.5 lb. During environmental vibration testing, the maximum prescribed voltage variation was 0.010 v; momentary variations as high as 0.025 v were obtained on most batteries. It was decided that these problems did not appreciably affect battery mission capability. Specifications were relaxed to 33.6-lb maximum weight and 0.040-v maximum voltage variation during vibration testing.

All batteries used for spacecraft system tests performed well. Only one failure occurred. On the seventh discharge of battery No. 1, the voltage of one cell dropped to zero. No specific cause of failure could be found. Subsequent system test batteries were limited to 5 cycles to protect the spacecraft from possible battery failure.

3. Solar Panels

The solar panels are made up of 7056, 1 × 2-cm p on n boron-diffused silicon solar cells bonded to an aluminum substrate. There are four separate electrical sections on every panel, each isolated from the other by a dielectric coating. The solar cells are electrically interconnected in each section into a series parallel matrix of 84 cells in a series, and 21 cells in parallel by kovar bus bars. The output of each of the 16 electrical sections, or panels, is then paralleled in the power switch and logic section of the conversion subsystem. Each electrical section is also shunt-regulated by a series string of six 50-w, 8.2-v Zener diodes that are heat-sinked to the relatively heavy spar assemblies used to support and stiffen the solar cell substrate. Electrical connections from solar cells to the PS&L subsystem is accomplished through redundant 20-gauge, teflon-wrapped, copper wire and a Bendix JC00A18-32 connector.

Thermal control and low-energy radiation-damage protection of the silicon solar cells was obtained through the use of 6-mil microsheet cover glasses, which had been coated with an interference-type filter designed to reflect solar energy below wavelengths of 415 μ. The weight of a complete solar panel (e.g., cells, diodes, substrate) was approximately 18.7 lb, and the panel area for mounting the solar cells constituted a surface 71.5 in. long by 35.5 in. wide. The solar panels were also used to support the attitude control jets and the solar pressure vanes; however, neither of these two systems will be discussed in this section. The substrate of the spacecraft was lightweight and fragile and the design and techniques of assembling such items as the solar cell matrixes, harnessing, and Zener diodes had to be oriented to work with this component. The surface skin of the panel was only 5 mils thick backed by a corrugated stiffener of approximately 3 mils. An accident as simple as a pencil dropping from a worker's pocket onto the panel could have penetrated its surface and seriously damaged it. Because of this fragility, the design of the complete solar panel assembly evolved around techniques to minimize handling and proximity to the substrate. A dielectric coating made of an epoxy lacquer was sprayed on the substrate in a 3-mil coating rather than the bonding of fiberglass used to insulate the cells from the substrate on the *Ranger* Block III panels.

A solar cell module configuration was developed to minimize the soldering and assembly time on the solar panels. The submodules were fabricated so that all solar cells were soldered to their bus bars, and a thermal control filter was bonded to the cell surfaces before assembling to the panels. A system of heavy-gauge circuit boards was developed to provide interconnecting points for the cells and the panel wiring, and a teflon-grommeted feedthrough approach was used to eliminate the requirement for supporting insulating stand-offs in the aluminum skin of the substrate. This modulization approach of cells, substrate, and wiring proved to have some further benefits.

Solar cell modules that had been completely soldered and filtered before being assembled to the panel were easier to test electrically, to match, and to put into series strings. Such modules also improved the power-producing capability of the solar panel. The independence of the substrate and wiring also permitted greater freedom in assembly.

The most significant change from the initial prototype panel to the TA and flight hardware was the development of an automatic assembly technique and the change of bus bar material from copper to kovar. The prototype panel was fabricated using hand-soldering techniques. During the fabrication period, an experimental submodule manufacturing program was initiated to investigate the potential of using tunnel-oven soldering, or inductance soldering to fuse the bus bars to the solar cells. The results of this program indicated that a significant increase in power output of the average submodule could be obtained over the submodules produced (to that time) by the hand-soldering technique. It also appeared that, through the tunnel-oven process, greater production rates, smaller attrition rates, and lower fabrication costs could be attained. One apparent disadvantage of this type of assembly was that it was not known what the effects of the launch–space environment would have on submodules assembled by tunnel-oven soldering. The bus bars are fused to the solar cells when both are at a temperature of approximately 380°F. It was also not known what the effect might be of the resulting thermal stress, which would be built into submodules thus fabricated, because of the very large difference in thermal expansion characteristics of copper and the silicon solar cells. A thermal shock program was initiated to evaluate the characteristics of tunnel-oven fabricated copper submodules compared to similarly fabricated submodules using bus bars made from kovar. Kovar is a material with coefficient-of-expansion characteristics similar to silicon, and is used by some solar array fabricators for bus bar purposes. The test results indicated a definite superiority of the kovar submodules. The kovar modules could be fabricated to produce the same electrical output as copper but would survive shock rates as great as those that could be generated by a liquid nitrogen/boiling water dip test. The copper submodules would literally snap apart when subjected to this high shock rate. The relatively light weight of the solar panel made thermal shock rates in excess of 28°C/min possible, and it was felt important that if kovar could be qualified for the solar array, a definitely superior panel with a significant increase in power reliability could be developed. To evaluate the effects of kovar on the magnetic characteristics of a solar panel, a full-sized prototype panel (configuration of the mission panel design fabricated with submodules), assembled via tunnel-oven soldering techniques and using kovar bus bars, was produced. The magnetic characteristics along with the electrical and mechanical characteristics of the kovar panels were checked before and after TA environmental and vibration testing of the panel. The results of the tests indicated that the magnetic influence of the kovar at one magnetometer distance from the panels would be negligible.

The general electrical and mechanical characteristics of the panel appeared to be good after completion of this testing program, and production began on kovar configuration panels. It was later discovered, after all flight panels were fabricated, that the data-reduction technique involved in performing the original magnetic test was in error, and that there could have been a significant magnetic field created by the kovar after the panels were vibration-tested on a table that had a strong external magnetic field around it. Tests of all flight panels indicated the presence of a magnetic field, and a program was initiated at JPL to degauss the panels. A program is continuing to further evaluate the magnetic characteristics of the panels after launch, vibration, and a long term exposure to the space environment. Preliminary results indicate that a degaussed panel would not be remagnetized due to launch and launch–space environment.

A total of ten flight-cell solar panels was manufactured for the mission. The electrical characteristics of the panel, as a result of the improved materials and techniques used in the fabrication, resulted in the production of a close uniformity of the performance characteristics of each panel. No detectable degradation of the panel as a result of the environmental qualification program was noted, and approximately 25% greater power-producing capability than that specified in the original detail specification of the solar panels was obtained.

X. SPACECRAFT SUBSYSTEMS: CENTRAL COMPUTER AND SEQUENCER

The CC&S subsystem represents a second generation evolution of the *Mariner* Venus 1962 CC&S subsystem. The initial requirements for this evolution were:

1. Functionally the *Mariner* Mars 1964 CC&S was to have been the *Mariner* Venus 1962 CC&S with less than 10% modification. One new subassembly (making a new total of 9) was to provide additional cruise commands primarily for the star sensor.
2. The *Mariner* Venus 1962 CC&S drawing package was to be used with only those modifications necessary to incorporate new requirements.
3. The quality of electronic components was to be upgraded to include only JPL Hi-Rel components and components covered by JPL screening specifications.
4. Circuit designs were to be analytically studied for worst-case margins. Resultant circuit modifications compatible with the schedule and packaging layouts were to be incorporated.
5. Magnetic circuitry was to be prepackaged and pretested prior to subassembly installation.
6. A major subcontractor, under JPL supervision, was to accomplish the above requirements.

A. Functional Description

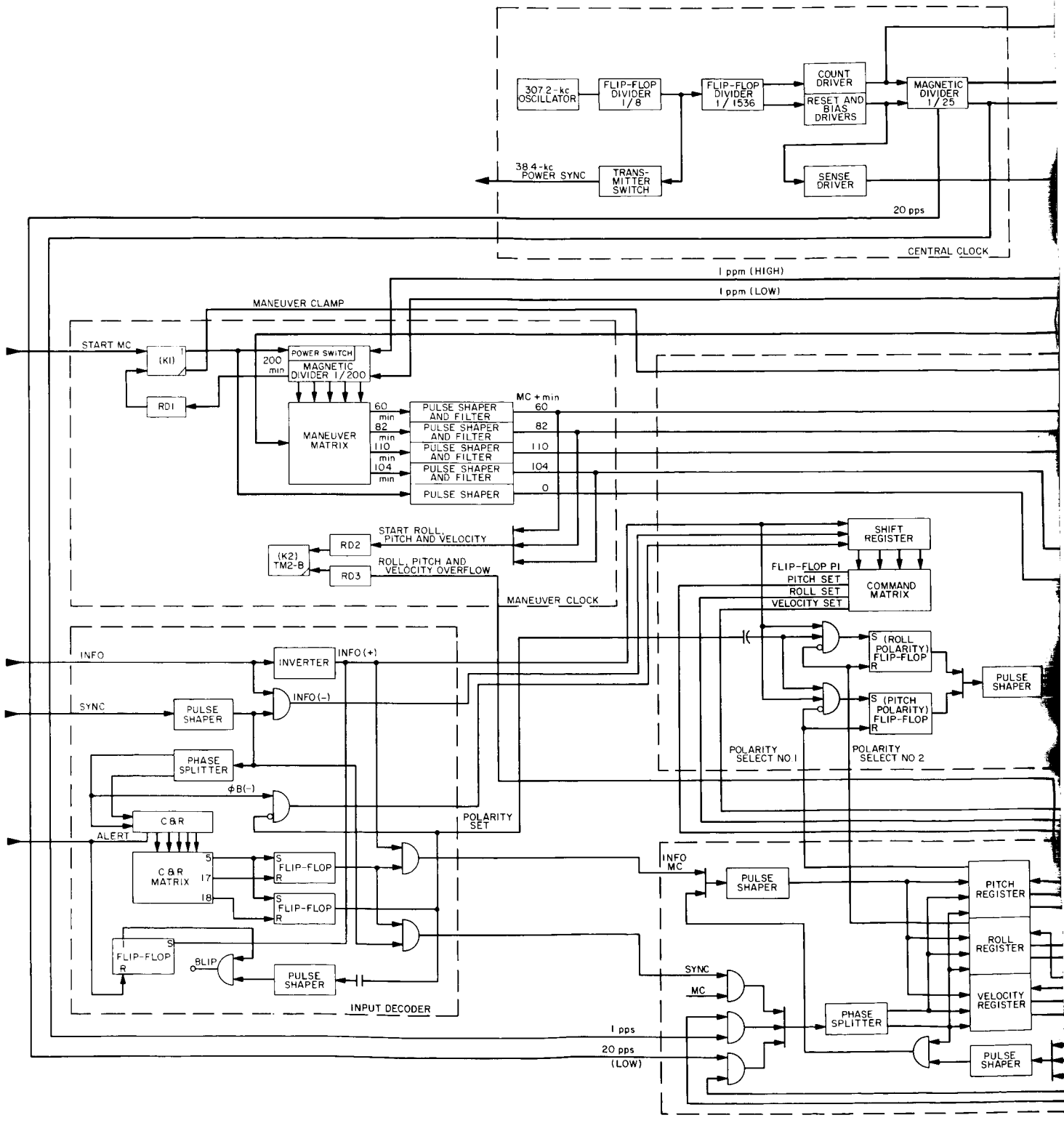
The *Mariner* Mars 1964 central computer and sequencer is responsible for spacecraft time-sequenced events (excluding the science experiment sequence). In performing this function, the CC&S must keep track of spacecraft time after launch, and execute commands at predetermined times during the mission. Figure 113 is a functional block diagram of the CC&S subsystem. Briefly, the CC&S:

1. Provides a 38.4-kc synchronization frequency used as a spacecraft time reference
2. Provides commands, shortly after injection, to extend solar panels and turn on attitude control power
3. Provides decoding and duration storage capability for the three midcourse maneuver parameters: pitch and roll position, and velocity correction
4. Provides sequenced commands to the attitude control subsystem for spacecraft positioning, and start and stop commands to the pyrotechnic control unit for motor burn during the midcourse maneuver
5. Provides on-pad adjustment capability of the planetary encounter start and stop commands normally sent to the science subsystem in the vicinity of the planet
6. Provides commands at predetermined times prior to and after encounter start to change the Canopus cone angle, data rate, and transponder operation modes (master timer sequence)
7. Provides a continuous 66⅔-hr periodic command to the radio subsystem for backup switching of redundant elements

The 38.4-kc synchronous signal is a square wave obtained by frequency division from the central 307.2-kc oscillator in the CC&S. This oscillator is crystal-controlled with a frequency stability of ±0.01% over the temperature range of −10 to +85°C. The 38.4-kc signal is used by the power subsystem as a stable frequency synchronization for the spacecraft primary 2.4-kc ac power.

Further frequency division of the crystal-oscillator-derived frequency yields frequencies of 25 pps, 20 pps, 1 pps, 1 ppm, one pulse every 3⅓ hr, and one pulse every 66⅔ hr. The 25-pps signal is used to sample the magnetic counter matrix outputs. The 20-pps signal is used to time the motor burn. The 1-pps signal is used as the time reference during countdown of the pitch and roll midcourse maneuver turns. The 1-ppm signal served as the basic count frequency for the launch events (solar panel extension at L + 53 min and attitude control power on at L + 57 min). The 1-ppm signal was also used as the basic count input to the midcourse counter during the midcourse maneuver to provide pitch, roll, and velocity-correction start commands at 60, 82, and 104 min after the start of midcourse. Five 3⅓-hr pulses are counted to obtain the command to enable the passive control system. The 3⅓-hr pulses are also used as the basic input to the pulse counter associated with the master timer and encounter commands. The 66⅔-hr cyclic command is used by the radio subsystem to sense the Earth lock of the transmitter and receiver.

In addition to the basic 3⅓-hr input, the encounter pulse counter could also be advanced by update pulses from the CC&S/OSE blockhouse panel prior to launch.


307.2-kc OSCILLATOR
FLIP-FLOP DIVIDER 1/8
FLIP-FLOP DIVIDER 1/1536
COUNT DRIVER
RESET AND BIAS DRIVERS
MAGNETIC DIVIDER 1/25
38.4-kc POWER SYNC
TRANS-MITTER SWITCH
SENSE DRIVER
20 pps
CENTRAL CLOCK
1 ppm (HIGH)
1 ppm (LOW)
MANEUVER CLAMP
START MC
(K1)
RD1
POWER SWITCH
200 min
MAGNETIC DIVIDER 1/200
MANEUVER MATRIX
60 min
82 min
110 min
104 min
PULSE SHAPER AND FILTER
PULSE SHAPER AND FILTER
PULSE SHAPER AND FILTER
PULSE SHAPER AND FILTER
PULSE SHAPER
MC + min
60
82
110
104
0
START ROLL, PITCH AND VELOCITY
(K2) TM2-B
RD2
RD3
ROLL, PITCH AND VELOCITY OVERFLOW
MANEUVER CLOCK
SHIFT REGISTER
FLIP-FLOP P1
PITCH SET
ROLL SET
VELOCITY SET
COMMAND MATRIX
INFO
INVERTER
INFO (+)
INFO (-)
SYNC
PULSE SHAPER
PHASE SPLITTER
ϕB(-)
C&R
ALERT
C&R MATRIX
5
17
18
S FLIP-FLOP R
S FLIP-FLOP R
S FLIP-FLOP R
BLIP
PULSE SHAPER
INPUT DECODER
POLARITY SET
S (ROLL POLARITY) FLIP-FLOP R
S (PITCH POLARITY) FLIP-FLOP R
PULSE SHAPER
POLARITY SELECT NO 1
POLARITY SELECT NO 2
INFO MC
PULSE SHAPER
PITCH REGISTER
ROLL REGISTER
VELOCITY REGISTER
SYNC
MC
PHASE SPLITTER
PULSE SHAPER
1 pps
20 pps (LOW)

185-1

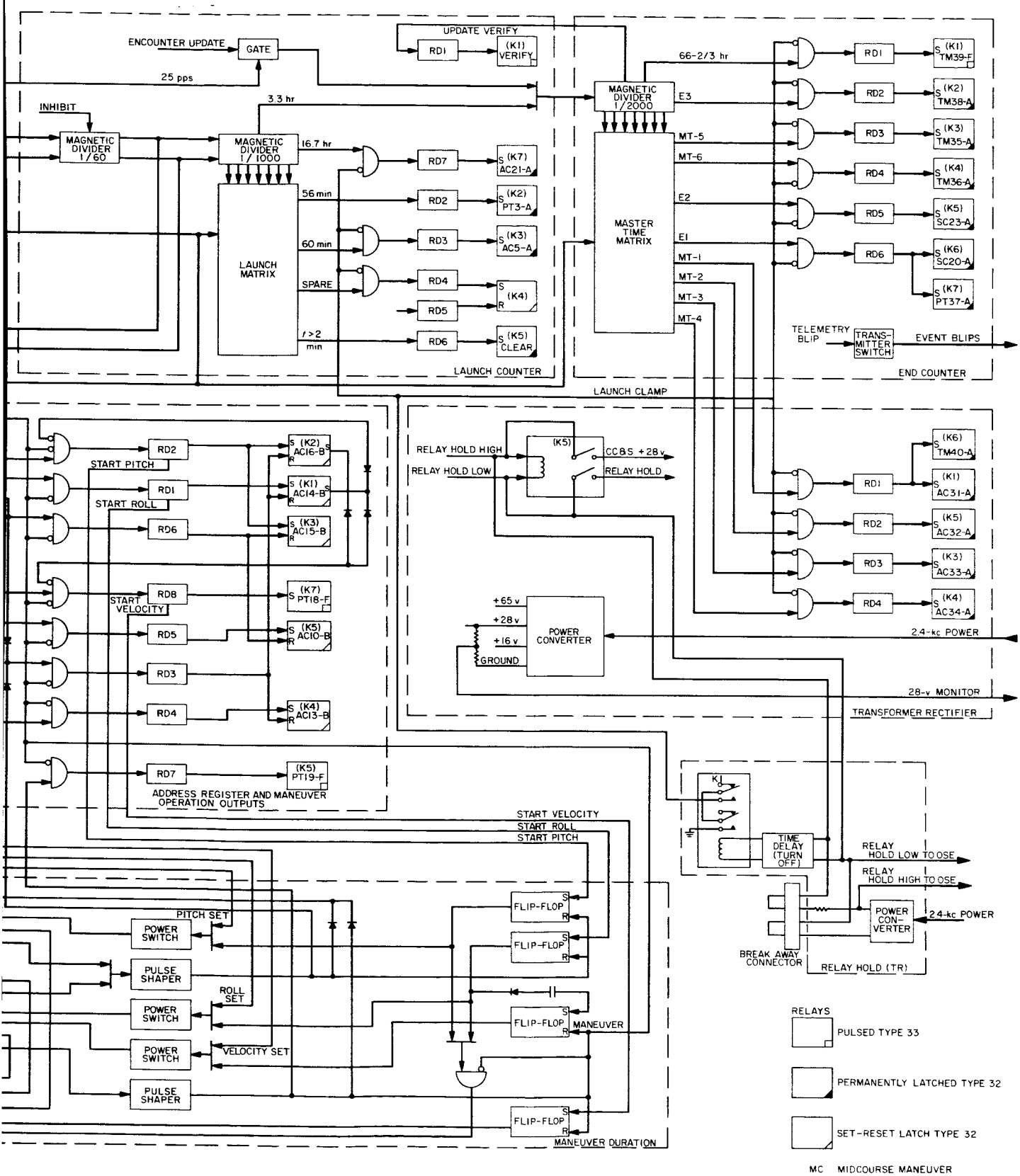


Fig. 113. CC&S functional block diagram

These update pulses are necessary to adjust the time after launch at which the encounter start command is given. With this blockhouse signal, the encounter start command could be adjusted to occur at any 3⅓-hr increment between L + 3⅓ hr and L + 277 days. The encounter stop command is actuated a fixed 13⅓ hr after encounter start.

Since all commands are referenced to launch or a short time before, the CC&S had to be inhibited until the proper time was reached in the countdown. The CC&S is normally inhibited before spacecraft power is turned on, and is released at L − 3 min. The inhibit was located at the 1-pps point in the counter chain, and, thus, prevented all frequencies or repetition rates beyond 1 pps from functioning.

In addition to the blockhouse inhibit and update functions described above, there was also a clear command to enable the CC&S counters to be cleared to zero before the inhibit was released. The relay hold function, which was initiated prior to spacecraft power on, commanded all relays to the reset position and held them there until it was released. This prevented any command relay from being actuated erroneously on the launch pad prior to launch. If any relay was not in the reset condition, the relay position indicator (RELAYS) lamp would have glowed red. In addition to this prelaunch protection, a spacecraft/*Agena D* separation connector inhibited all CC&S relay actuators until spacecraft separation.

After the inhibit was released at L − 3 min, the CC&S began counting and, 2 min later, sent a "clear release" command to the blockhouse to extinguish the lamp on the panel. At the time the inhibit was released, a counter in the blockhouse was started at the rate of 1 pps. When the clear indicator extinguished, the count was stopped and the time read by the counter was noted. The counter read 000119 + 0, − 1 sec, which provided a cursory check of the CC&S's ability to count correctly.

All CC&S commands, with the exception of the 38.4-kc synchronization signal and the event blip output, are relay contact closures that either apply or remove user power from the signal lines between the CC&S and the other spacecraft subsystems. Each command relay, upon actuation, generates an event blip that is sent to the telemetry subsystem for subsequent transmission to Earth. The 38.4-kc synchronization signal and the event blip output are transformer-coupled to the user.

The CC&S flight sequence is shown in Table 32. The commands used by the CC&S are L-1 through L-3, M-1 through M-7, MT-1 through MT-9, and CY-1. Table 33 gives a detailed explanation of these commands in terms of the flight sequence shown in Table 32.

Table 32. *Mariner* Mars 1964 CC&S flight sequence

Sequence	Reference No.	Time	Command designation	Relay	Function
	1	L − 3 min	—	—	Release CC&S inhibit
	2	L − 1 min	—	Clear relay	Indication of CC&S clock operation
Launch	3	L = 0	—	—	Liftoff
	4	L + 53 min	L-1 (set)	PT3-A (set)	Extend solar panels
	5	L + 57 min	L-2 (set)	AC5-A (set)	Energize attitude control electronics
	6	L + 16⅔ hr	L-3 (set)	AC21-A (set)	Energize Canopus sensor and deploy solar vanes
	7	M − 90 min (nominal)	—	—	Transmission of quantitative commands
	8	M = 0	M-1 (set)	AC10-B (set)	Gyros on
Midcourse			M-2 (set)	AC15-B (set)	Spacecraft on inertial control
	9	M + 60 min	M-3 (set)	AC13-B (set)	Pitch turn polarity (set if turn is positive)
			M-4 (set)	AC16-B (set)	Pitch turn start
			—	TM2-B (set)	Maneuver timer start

Table 32. (Cont'd)

Sequence	Reference No.	Time	Command designation	Relay	Function
Midcourse (Cont'd)	10	M + 60 min (plus duration of pitch turn)	M-3 (reset)	AC13-B (reset)	Polarity relay reset
			M-4 (reset)	AC16-B (reset)	Pitch turn stop
			—	TM2-B (reset)	Maneuver timer stop
	11	M + 82 min	M-3 (set)	AC13-B (set)	Roll turn polarity (set if turn is positive)
			M-5 (set)	AC14-B (set)	Roll turn start
			—	TM2-B (set)	Maneuver timer start
	12	M + 82 min (plus duration of roll turn)	M-3 (reset)	AC13-B (reset)	Polarity relay reset
			M-5 (reset)	AC14-B (reset)	Roll turn stop
			—	TM2-B (reset)	Maneuver timer stop
	13	M + 104 min	M-6 (pulsed)	PT18-F (pulsed)	Ignite midcourse motor
			—	TM2-B (set)	Maneuver timer start
	14	M + 104 min (plus duration of motor burn)	M-7 (pulsed)	PT19-F (pulsed)	Shut off midcourse motor
			—	TM2-B (reset)	Maneuver timer stop
	15	M + 110 min	M-1 (reset)	AC10-B (reset)	Gyros off
			M-2 (reset)	AC15-B (reset)	Spacecraft off inertial control (reacquire Sun and Canopus)
	16	M + 199 min	—	—	CC&S maneuver counter off
Cruise	17	E − 192 days	MT-6 (set)	TM36-A (set)	Switch to 8⅓ bps data rate
	18	E − 137 days	MT-1 (set)	AC31-A (set)	Canopus sensor cone angle update No. 1
	19	E − 131 days	MT-5 (set)	TM35-A (set)	Switch to high-gain antenna
	20	E − 103 days	MT-2 (set)	AC32-A (set)	Canopus sensor cone angle update No. 2
	21	E − 68 days	MT-3 (set)	AC33-A (set)	Canopus sensor cone angle update No. 3
	22	E − 30 days	MT-4 (set)	AC34-A (set)	Canopus sensor cone angle update No. 4
	23	E − 6⅔ hr	MT-7 (set)	SC20-A (set)	Encounter science on (or all science on)
				PT37-A (set)	Deploy science platform cover
Encounter	24	E + 6⅔ hr	MT-8 (set)	SC23-A (set)	Encounter science off (or all science off)
	25	E + 13⅓ hr	MT-9 (set)	TM38-A (set)	Start data playback
All phases	26	Every 66⅔ hr	CY-1 (pulsed)	TM39-F (pulsed)	Emergency radio switching command

Table 33. Detailed CC&S flight sequence explanation

Reference No.	Function
1	Release of CC&S inhibit, at L minus 3 min, starts the CC&S clock counting normally.
2	Clear relay indication, at L minus 2 min, indicates that the CC&S clock is counting normally in the launch counter subassembly.
3	Liftoff occurs 3 min after release of CC&S inhibit.
4	The L-1 command, at L plus 53 min, commands the pyrotechnic subsystem to blow the solar panel squibs and allow the panels to assume a normal cruise position (extended).
5	The L-2 command, at L plus 57 min, energizes the attitude control electronics and starts the Sun-acquisition sequence.
6	The L-3 command, at L plus 16⅔ hr, energizes the Canopus sensor, and starts the Canopus acquisition sequence. This command also deploys the solar vanes.
7	The QC1-1, QC1-2, and QC1-3 commands, at M − 90 min, are sent to the spacecraft and stored in the CC&S. These commands describe the duration and polarity of the pitch and roll turns, and the duration of the motor burn.
8	The M-1 command is coincident with the maneuver start command at M = 0. The M-1 command turns on the spacecraft gyros for a 1-hr warmup period prior to starting the first turn. The command also switches the data encoder to Data Mode 1.
9	The M-2, M-3, and M-4 set commands and TM2-B relay set all occur at M plus 60 min. The M-2 command inhibits the Sun and Earth acquisition, puts the spacecraft on inertial control, and energizes the autopilot. The M-3 command regulates the polarity of the turn (set if positive, reset if negative). The M-4 command starts the pitch turn by energizing the appropriate attitude control pitch gas jet. The TM2-B relay in the CC&S energizes a shift register used for timing the turn. The register starts shifting at a rate of about 2½ pps when the turn starts, and stops shifting at the end of the turn. The duration of the turn is then calculated by observing initial and final states of the shift register.
10	The pitch turn is terminated by the resetting of M-3, M-4, and relay TM2-B (overflow of the pitch shift register). M-3 resets the polarity relay, M-4 stops the turn, and relay TM2-B shuts off the maneuver timing register. The duration of the turn is determined from the QC1-1 quantitative command (Reference No. 7).
11	The M-3 and M-5 set commands and TM2-B relay set all occur at M plus 82 min. The M-3 command regulates the polarity of the turn; M-5 starts the roll turn; and relay TM2-B starts the timing register.
12	The roll turn is terminated by the resetting of M-3, M-5, and relay TM2-B. The duration of the roll turn is determined from the QC1-2 command.
13	The M-6 command and TM2-B relay set occur at M plus 104 min. The M-6 command is in the form of a momentary relay closure (pulse-type relay), and goes to the pyrotechnic subsystem. Squibs associated with the mechanics of motor ignition are energized, and the midcourse motor is fired. The TM2-B relay starts the timing register.
14	The midcourse motor is shut off by the M-7 set command (pulsed relay) and the resetting of TM2-B relay. A squib firing assembly is used in mechanizing the motor shutoff. The duration of the motor burn is determined from the QC1-3 command.
15	The M-1 and M-2 reset commands occur at M plus 110 min. The M-1 command turns the gyros off, and the M-2 takes the spacecraft off inertial control, turns off the autopilot, and initiates the Sun- and Canopus-reacquisition sequences.
16	At M plus 199 min, the CC&S maneuver counter overflows and shuts itself off.
17	The MT-6 command, at E minus 192 days, switches the data encoder from a bit rate of 33⅓ to 8⅓ bps.
18	The MT-1 command, at E minus 137 days, is the first update of the Canopus star sensor cone angle. The angle is changed by 4.6 deg to compensate for the changing Canopus–probe–Sun angle and the resulting pointing of the high-gain antenna (the angle changes as the spacecraft-to-Earth range increases).
19	The MT-5 command, at E minus 131 days, switches the spacecraft transmitter from the omnidirectional antenna to the high-gain antenna.
20	The MT-2 command, at E minus 103 days, is the second 4.6-deg Canopus sensor cone angle update.
21	The MT-3 command, at E minus 68 days, is the third 4.6-deg Canopus sensor cone angle update.
22	The MT-4 command, at E minus 30 days, is the fourth 4.6-deg Canopus sensor cone angle update.
23	The MT-7 command, at E minus 6⅔ hr, turns on all science instruments. (Normally the cruise science would already be on, so the command would just turn on the encounter science.) The MT-7 command also blows off the protective cover placed over the science platform and encounter experiment optics (using squib firing assemblies), and turns off the battery charger.

Table 33. (Cont'd)

Reference No.	Function		Reference No.	Function
24	The MT-8 command, at E plus 6⅔ hr, turns off encounter science and disconnects the redundant cruise science on command.		26	The CY-1 command is a pulse-type relay closure that is commanded every 66⅔ hr during the flight. The command is used to automatically switch the radio subsystem from one antenna to the other in case of a loss of lock with the DSIF stations for two successive CY-1 cyclics. An automatic switch to a second transmitter is also caused by the cyclic in case of a spacecraft transmitter failure.
25	The MT-9 command, at E plus 13⅓ hr, starts the tape playback of TV pictures, turns cruise science off, and switches the data encoder to Data Mode 4.			

B. Physical Description

The CC&S was packaged in eight 6 × 6 × 1-in., and one 6 × 2.5 × 1⅜-in. subchassis. The total weight of the subsystem was approximately 14 lb. Terminal encapsulation added approximately 0.02 to 0.04 lb to the weight listed for each subassembly. Figure 114 shows an assembled CC&S subsystem; both sides of a typical subassembly are shown in Fig. 115(a) and (b).

The CC&S subsystem consumed approximately 11 w of 2.4-kc power during the prelaunch and boost phases of the flight. The power consumption dropped to approximately 5.5 w after spacecraft separation due to the relay hold function (provided by the relay hold transformer–rectifier unit) being turned off at that time.

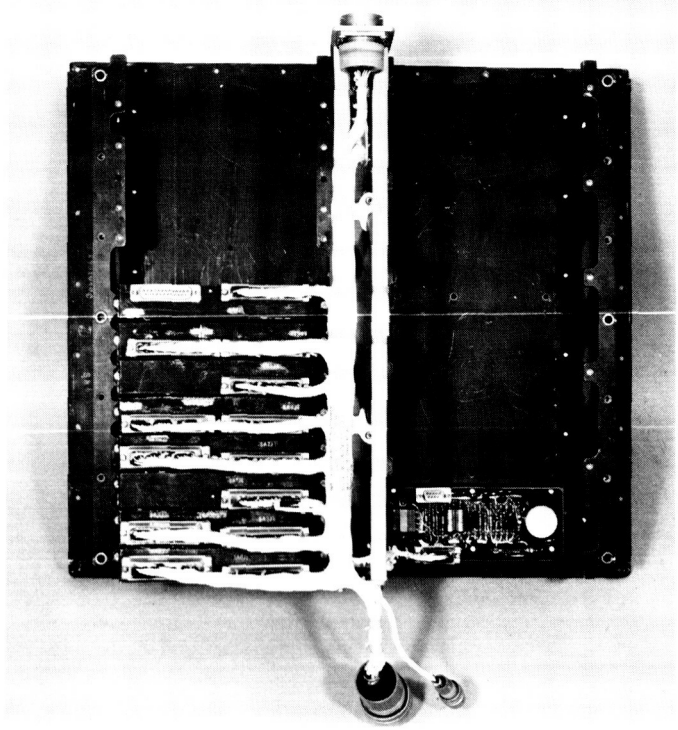


Fig. 114. Assembled CC&S subsystem

C. Procurement

Five major companies were requested to submit bids on the CC&S effort. The contractor effort on the CC&S was briefly:

1. Design review and reliability study (9 engineer man-months)
2. Design of one new subassembly (drawings and breadboard)
3. Fabrication and verification testing of one flight prototype CC&S
4. Fabrication and testing of seven flight CC&S (one CC&S to be type-approval tested)

Issuance of the CC&S contract was delayed until January 1963. During this delay, many of the proposal restraints were violated and/or made obsolete. As a result, the definitive contract was not signed until August 1963.

As the CC&S contract progressed, changes within the change-of-scope clause of the contract were introduced by JPL engineering change instruction forms. These change instructions directed the contractor to make changes in such areas as component values, manufacturing processes, and controlling specifications. The difficulties associated with the fabrication and test of magnetic submodules led to the following additional contract modifications: (1) the vendor was to subcontract the fabrication and test of magnetic counter submodules to another vendor in accordance with JPL-furnished fabrication and test

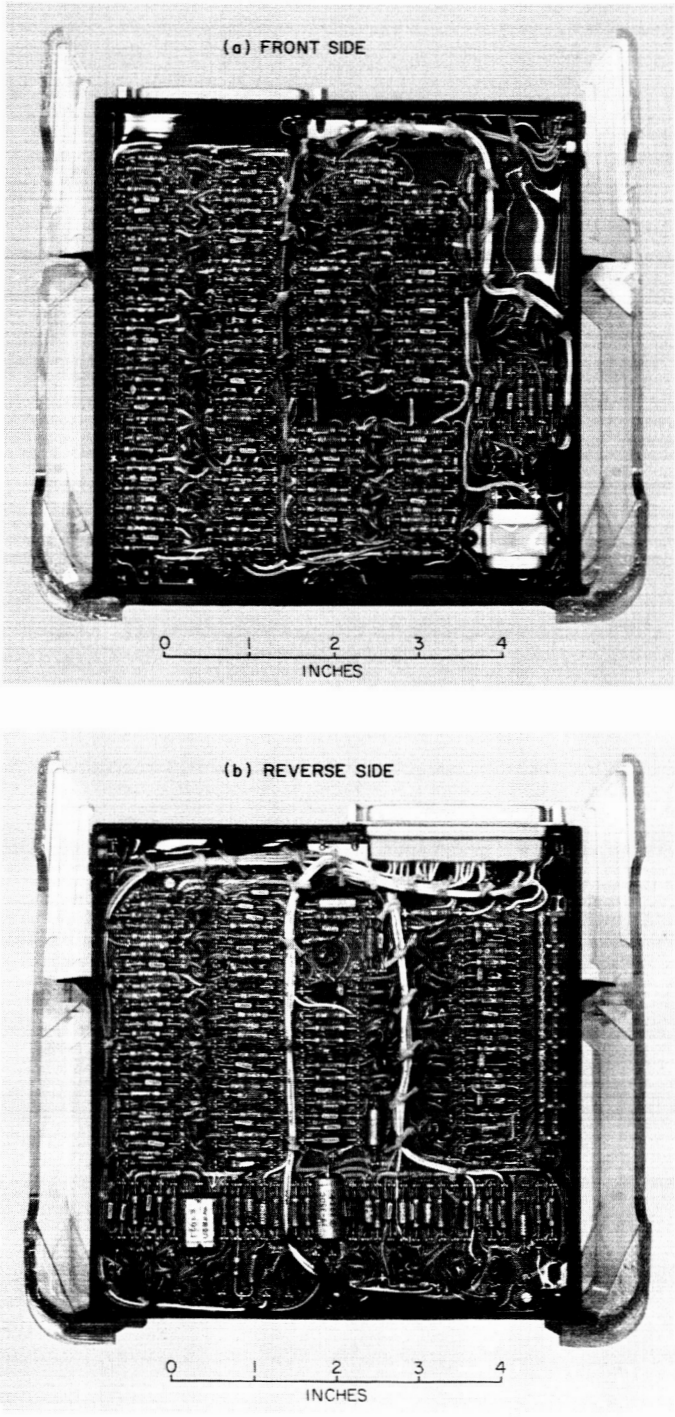


Fig. 115. Typical subassembly

documentation; (2) the magnetic shift register submodules were to be furnished by JPL, who, in turn, would obtain it from another source. The reason for handling each of these procurements differently was that the documentation for the magnetic counter procurement was previously developed under an advanced design contract to the vendor, while the magnetic shift register procurements required considerable design and development effort.

After completion of the contractor effort, two major program requirements were imposed on the CC&S. One required a new CC&S subassembly, the relay hold transformer–rectifier, to supply continuous relay latching current during the spacecraft boost environment, and the other required encapsulation of all terminals and coating of all component part leads. These tasks, deemed necessary as a result of *Ranger* flight experiences, were accomplished at JPL.

D. Design and Reliability Effort

1. JPL Pre-contract Effort

a. Mission-required changes. The CC&S design effort was begun in October 1962, when a duplicate of the *Mariner II* CC&S drawing package was reproduced and entitled *Mariner* Mars 1964. These drawings were updated to meet project-required changes prior to the release of the manufacturing contract to STL. The changes made were:

1. The trajectory required that the launch events occur at times other than those specified for *Mariner II*. These times were easily changed by altering the diode pattern in the launch matrix.
2. Change in the attitude control subsystem demanded modification of the maneuver timing matrix. Alteration of the diode pattern in the maneuver timing matrix satisfied the requirements.
3. The placement of the midcourse motor in one of the side bays of the spacecraft required a reversal in the order of the roll and pitch turns. This was accomplished by renaming the appropriate shift registers and interchanging their output connections.
4. The experience obtained from previous flights indicated that direct timing of the midcourse motor burn period could be used instead of an accelerometer to determine velocity correction. A 20-pps count was derived from the clock chain and used in place of the accelerometer input pulses. A 102-sec maximum midcourse motor burn duration was obtained by this method.
5. The increased flight time (approximately 220 days) and the new guidance system, using the Sun and Canopus for fixed reference points, required additional events and at times that were not previously

available from the CC&S. A new module (master timer) was tentatively assigned to perform the required task. The addition of the ninth module was dropped after it was determined that the events required could be timed with reference to encounter instead of to launch. The end counter was also referenced to encounter and, thus, both counters were merged. The space required to incorporate readout capability and a diode matrix into the end counter was obtained by the removal of the *Mariner II* CC&S Earth-acquisition counter, which was no longer necessary. The additional event times also required six more relay drivers and associated relays to provide interfaces with the desired subsystems. The relays and their drivers, which provided interfaces for the midcourse maneuver, were all shifted into the address register and maneuver duration output module. This shift, and the placement of some relays and drivers in the transformer–rectifier, provided ample circuitry for the execution of the events.

6. Changes in the interface requirements of the 38.4-kc power synchronizing signal and the telemetry blip event indicator signal demanded changes to the circuits providing these isolated outputs.

7. All components that did not have Hi-Rel or JPL screening specification were replaced by parts that did. This modification was straightforward and required very little circuit change for incorporation.

b. Enhancement changes. Improvements in both system performance and reliability were also introduced into the CC&S prior to letting the fabrication contract. The changes made were:

1. Parity checking circuitry was added in the input decoder module to perform single (or odd) bit error detection on maneuver timing information. Odd parity was used to ensure that information was being received; if no information (no *ones*) was received, no parity check signal would be generated.

2. Logic circuitry was added to inhibit the command for the start of midcourse motor burn if either the roll or pitch commands were not completed within the maximum time allotted for the turns. This circuitry also inhibited a restart of pitch while the roll turn was in progress. Logic was added to ensure that if the roll and pitch relays were both set at the same time, the attitude control subsystem would only see the pitch command.

3. The desire to have precise information on maneuver turns and motor-burn periods prompted the inclusion of the maneuver timer relay. The relay is set at the start of any turn or motor firing and is reset upon completion of the event. The relay gates clock pulses to a counter in the data encoder. The contents of this counter are read out to give the precise duration of the event.

4. The maneuver duration magnetics were purchased under separate contract for inclusion in the maneuver duration subassembly. This magnetic package was prepotted and tested to 20% voltage margins at type-approval temperature levels. The basic shift register core was also changed to a 100-mil (from an 80-mil) core to provide a better signal-to-noise ratio.

5. A separate contract was also initiated for the manufacture, test, and encapsulation of the magnetic counters. These prepackaged magnetic counters were tested to 20% voltage margins at the type-approval temperature levels. This concept improved the electrical performance of the counters and considerably simplified subassembly fabrication.

6. The method used for readout of the magnetic counters was changed. Pulse priming of the readout transfluxors was incorporated to increase the signal-to-noise ratio of the counter outputs. This method increased the amplitude and pulse width of the signals used in the launch, maneuver, and end counter matrixes and, thus, provided greater assurances of satisfactory operation. The pulse priming method necessitated the incorporation of a bias driver but also allowed the removal of the 5-v bias supply. A reduction of overall system power was also achieved.

7. The count, reset, and sense drivers for the magnetic counters were also redesigned. The redesigned circuits provided outputs less sensitive to temperature and component parameter drift than the previous drivers.

8. The addition of another ferrite core in the maneuver-matrix magnetic filters reduced the output noise by a factor of 5 and, thus, favorably increased the signal-to-noise ratio.

9. In an effort to reduce the power drain and the noise on the 28-v supply, logic was added to inhibit any further activation of the relay drivers controlling launch events one and two (Table 32) after the first overflow of the launch counter.

10. Subassembly circuit boards were cleaned up by reworking mechanical dimensions and removing nonessential printed wiring.

Approximately 8% change in component count was incurred in the modification of the *Mariner* Venus CC&S to the basic *Mariner* Mars 1964 configuration.

2. JPL/STL Effort

A design review study was included in the basic fabrication contract to provide direct engineering support for the CC&S. This study was divided into three main areas: (1) a circuit analysis and design support team was established to aid in the evaluation and redesign of the circuitry used in the CC&S; (2) a materials, processes, and packaging review was performed to improve the mechanical assembly and to provide engineering support for the fabrication facility; (3) a reliability assessment was made of the CC&S to provide a measure of the probability of success for the CC&S flight.

a. Circuit analysis and design review. The circuit analysis and design review was directed toward improving the operating margins of the CC&S. A complete set of component parameters and list of specific tasks were given to the contractor. The areas that were considered by JPL to be the weakest were listed and their priority indicated. The ground rules placed on the contractor were:

1. All circuits should be checked for 20% operating voltage margin at type-approval temperature levels.
2. JPL-supplied component parameters and derating factors should be used.
3. A reasonable worst-case circuit design and analysis should be performed. The worst-case design limitations were that the tracking of power supplies be maintained in determining load and input requirements, and that the tracking of component worst-case parameters with temperature be followed.
4. Circuit redesign should cause minimum change in circuit board layout.
5. Only JPL-screened or Hi-Rel components could be used in any circuit redesign.
6. The existing power supply voltages were to be used exclusively (no new voltages could be added).
7. Areas outlined by JPL were to be analyzed before any emphasis was placed on other areas of the CC&S.
8. All recommended changes must be submitted to JPL in time to be incorporated into the first prototype system. All change orders were to be initiated by JPL and incorporated at JPL's discretion.

Approximately 15% of the components within the CC&S were changed as a result of the design review. The main areas modified were:

1. Flip-flops in the clock chain
2. Crystal oscillator buffer circuit
3. Magnetic filters in the maneuver clock
4. Flip-flop trigger level gates
5. Relay driver input circuitry
6. Sense amplifiers in the maneuver duration subassembly
7. A new power transformer design

b. Materials, processes, and packaging review. The materials, processes, and packaging review accomplished the following specific tasks:

1. Investigation of the advisability of replacing Eccofoam with a conformal coating of Solithane 113
2. Investigation of the properties of Sylgard 182 and their relation to ferrite cores
3. Exploration of the methods of improving back-side printed circuit board connections
4. Examination of the layouts and recommendation of changes to correct discrepancies and deficiencies in inaccurate tolerances, improper component lead lengths, unnecessary lead bending, inadequate electrical insulation
5. Review of various bonding techniques and materials used in the design
6. Review of circuit board layouts and recommendation of changes that would substantially reduce the number of back-side printed circuit connections

Changes due to the materials and processes review included:

1. Solithane 113 conformal coating replacing Eccofoam
2. Some 600 designer hours being added to the contract to modify printed circuit boards to eliminate back-side printed wiring wherever possible
3. Many results of the encapsulant and soldering studies being transmitted to the manufacturing areas

c. Reliability effort. A measure of the reliability of the CC&S was the task of the reliability review. This probability-of-success figure was to be generated from *Minuteman* failure-rate data for the components used in the subsystem. Two assessments were to be computed. The first would give the probability of survival of the entire subsystem for a 220-day mission with midcourse correction only necessary during the first 7 days. The second assessment would consider a 250-day mission and would give the probability of success for each event.

3. JPL Post-contract Design

Due to uncertainties in performance of relays in the launch vibration and shock environment, a design change was authorized for relays to be held in reset position during the launch-to-spacecraft separation interval. To accomplish this task, it was necessary to design a new power subassembly to be incorporated into the CC&S (relay hold transformer–rectifier). Since this effort was begun in March 1964 with CC&S flight deliveries due in April, it was necessary to design, fabricate, and test the new subassembly at JPL. This effort required generating complete fabrication documentation and the fabrication and test of one breadboard, two prototype, and six flight subassemblies. The effort was conducted so that testing and integration of these new units with the contractor-fabricated CC&S did not delay CC&S schedules.

E. Fabrication

Fabrication of the CC&S took place in the contractor's clean-room facilities (Fig. 116), which consisted of a sealed-off portion of a building, with the temperature, dust, and humidity controlled. White coats, smocks, and gloves were required for all personnel.



Fig. 116. Contractor clean room

Fabrication techniques used by the contractor complied with the basic JPL requirements, although the *Mariner* Mars 1964 CC&S packaging was nearly identical to that of the *Mariner* Venus. Hence, certain areas such as documentation standards, packaging density, and some fabrication requirements, such as harnessing and component lead lengths, could not always comply. The major problem areas encountered by the contractor were:

1. In the circuit board fabrication, problems with pad lifting, board warpage, delamination, and terminal solderability were never fully solved. Large amounts of scrappage and rework were necessary to meet JPL standards.

2. Due to extreme packaging density and the requirements to fillet all components to the circuit boards with Solithane 113, problems associated with component placement caused undesirable amounts of rework, and/or led to excessive uses of Solithane in many cases.

3. Also due to extreme packaging density, subassembly harnessing often required excessive use of Stycast 1095 to bridge harness runs over components and terminals to avoid potential teflon cold-flow conditions.

Magnetic counter submodules were fabricated under subcontract to the major contractor and in accordance with JPL specifications. Major problem areas encountered were:

1. Evacuation of bubbles from the Sylgard 182 potting compound, which encapsulated the magnetic cores within their plastic holders, required solution of difficult process control problems.

2. Rotation of terminals mounted in the plastic holders, due to handling of external leads, caused the size 40 magnetic wire from the cores to break at the terminal. Special handling procedures and the bonding down of external leads was necessary to control this problem.

Shift register submodules were fabricated by a third supplier under JPL contract. The major fabrication problem developed from the manner in which ferrite cores and diodes were mounted on the circuit board. Adequate core–diode separation was not ensured in the early fabrication techniques. After encapsulation of the submodules in Solithane 113, temperature-induced contractions within the Solithane forced the core against the diode

and resulted in broken cores and eventual electrical failure. Fabrication techniques were modified to ensure core–diode separation. As an added safety factor, the amount of Solithane encapsulant was also reduced to the minimum necessary.

F. Environmental and Postenvironmental Subsystem Tests

1. Flight-acceptance Tests

Each flight subsystem was required to pass flight-acceptance tests that consisted of special vibration and thermal–vacuum sequences. These environmental tests were intended to simulate, on a small scale, the actual environments expected in flight. The vibration sequence consisted of sinusoidal and white-noise sequences at various acceleration levels (maximum 9 *g*). The thermal–vacuum sequence consisted of environments between 32°F (2 hr) and 131°F (40 hr) at a pressure of 10^{-4} mm Hg or less. These tests were performed using the automatic OSE sequence that was used for previous subsystem tests. After each subsystem passed the flight-acceptance tests, it was retested under the voltage and temperature margins previously tested to, in order to verify that no performance degradation had occurred as a result of the environmental tests.

Table 34 lists the environmental and post-environmental test times for each flight subsystem, and also for the type-approval subsystem for comparison. Those subsystems that had test times appreciably above the average are discussed below.

a. MC-01 subsystem. The MC-01 prototype subsystem had extra test time associated with each test performed. This was due primarily to the fact that on this subsystem the environmental and postenvironmental testing was performed by personnel unfamiliar with JPL flight-acceptance test requirements.

The only subsystem problems that occurred during these tests were a reoccurrence of the velocity register problem at low voltage/low temperature, and a test-set problem that was easily rectified. These problems occurred during the postenvironmental voltage/temperature margin tests.

b. MC-02 subsystem. The MC-02 subsystem had extra test time associated with the thermal–vacuum test due to the following problems: (1) The *Agena* clamp circuitry in the OSE malfunctioned so that the clamp function could not be released, (2) The CC&S subsystem was adversely affected by other equipment in the area. Specifically, extra counts were being introduced through the "master-timer speedup" interface (which was subsequently eliminated because of its noise susceptibility), and midcourse commands occurred at nonstandard times, presumably also because of noise.

2. Type-approval Tests

In addition to flight-acceptance tests, one flight equivalent subsystem (MC-TA) was required to pass a special set of type-approval tests that were designed to test the subsystem under extreme environmental conditions. These tests were intended to simulate worst-case flight environments.

Table 35 lists each test and the operation time associated with it. Most of the tests were routine and were accomplished without incident. The acceleration test required extra test time due to problems encountered with the slip rings on the acceleration fixture. There were no CC&S problems during the actual test, however.

Table 34. Environmental and postenvironmental test times

Subsystem test	Test times, hr								
	MC-01	MC-TA	MC-02	MC-03	MC-04	MC-05	Total	Overall average	Flight average
Environmental	91	55.7	169.0	54.3	59.7	58.8	488.1	81.5	85.5
Vibration	15	5.5	5.0	4.6	5.0	9.0	44.1	7.4	5.9
Thermal–vacuum	76	50.2	164.0	49.7	54.7	49.8	444.0	74.1	79.6
Postenvironmental	48	22.9	22.0	22.3	21.7	23.3	160.2	26.7	22.3
Total environmental and postenvironmental	139	78.6	191.0	76.6	81.4	82.1	648.3	108.2	107.8

Table 35. MC-TA environmental tests

Test	Time, hr
Flight-acceptance	
Vibration	5.5
Thermal–vacuum	50.2
Total	55.7
Type-approval	
Low frequency vibration	5.8
Complex wave vibration	6.0
Shock	5.6
Bench handling	1.2
Acceleration	27.8
Explosive atmosphere	2.3
Humidity	5.2
RF interference	15.0
Thermal–vacuum	301.7
Magnetic-field mapping	1.5
Total	372.1
Postenvironmental	22.9
Total test time	450.7

The CC&S subsystem experienced problems during the humidity test. The humidity chamber was designed to introduce moisture into the chamber atmosphere by way of a steam inlet. The initial temperature of the steam was much higher than the subsystem, and water condensed on parts, terminals, and circuit boards. This water appeared to contain a residue that lowered the electrical impedance between terminals or leads considerably. As a result of this phenomenon, an event blip tantalum capacitor in the 5A6 unit was shorted out, and its event blip was not received during the test. The capacitor was replaced, but later analysis on the part showed that it had not failed and that the short, or near short, was most probably caused by moisture between one lead and the case. After replacing the capacitor, the subsystem was returned to the humidity chamber and the tests were rerun. A malfunction occurred again, this time in the 5A7 unit. It became obvious, at that point, that the humidity test could not be performed satisfactorily. The subsystem was cleaned and the remainder of the type-approval tests were performed. It was noted during cleaning that the condensate in some instances contained a solid substance. Efforts to identify this substance were not successful. Terminals and leads were not fully coated at that time, which could have contributed to the problem. As a result, all flight subassembly terminals and leads were fully coated as a project requirement. As a final note, other subsystems had similar problems and the humidity test was waived as a type approval requirement.

After all the type approval tests were completed, the MC-TA subsystem was retested under the voltage and temperature margins previously tested to. Since no decrease in margins as a result of the environmental tests was apparent, the subsystem was released for life test.

3. Special Tests

a. Capacitor leakage test. Each subassembly that contained capacitive-coupled relay drivers had test points that were located to allow measurement of the leakage current of the coupling capacitor and of the output transistor of each relay driver. Since the output transistor (planar) normally had much lower leakage current than the capacitor (tantalum), the leakage current measured was essentially that of the capacitor. A common failure mode of a tantalum capacitor is excess leakage current, which can be detected by periodic measurement. Any suspect capacitor can thus be replaced. This special capacitor leakage test was performed periodically during the prelaunch test phase of each CC&S subsystem.

b. 2.4-kc power dropout test. A special test was performed to observe the effect of power (2.4-kc) transients and momentary dropouts on the CC&S subsystem. Two levels of power dropout were used: −40% and −100%. No problems were observed with the CC&S subsystem with the −40% voltage test. The test was run at 75 and 132°F, and with various time durations. One problem did occur with the −100% voltage test. Whenever the transient was commanded after the midcourse start signal was issued, the shift register power on flip-flops in the 5A5 unit were observed to change state, which resulted in power being applied to all three shift registers simultaneously. The condition of having two or more registers on at the same time caused all information previously stored in those registers to be destroyed. This problem was prevented during non-midcourse times by the midcourse clamp function. A simple solution for this problem was not found, and due to the late date at which these tests were performed, no corrective action was taken. It should be noted that power dropouts of this magnitude were not expected during normal spacecraft operation. If transients of this magnitude had occurred, they would have been detectable, and the

midcourse maneuver would presumably have been aborted and restarted.

c. 2.4-kc high-voltage test. A special test was performed on the engineering prototype (MC-EP) subsystem to verify CC&S operation with the 2.4-kc input greater than 50 v rms (nominal). The 16- and 28-vdc sources in the CC&S are Zener-regulated and, therefore, no problem was expected with the circuitry that would use these source voltages. However, the 65-vdc source is not Zener-regulated and the test was performed primarily to check the circuitry that would use this voltage. The 2.4-kc input voltage was raised from 50 to 70 v rms with a corresponding increase of the 65-vdc source to 86 vdc. The CC&S functioned satisfactorily at the increased voltage.

G. CC&S Performance in Spacecraft System Tests

The CC&S subassembly MC-01 was included in the PTM spacecraft and operated for 1300 hr during the spacecraft system tests. The following problems occurred in the CC&S subsystem during these tests:

1. The CC&S master timer picked up spurious counts
2. The CC&S 10-kc inhibit did not hold
3. Fuses blew in the CC&S 5A9 subassembly
4. Spurious reset of output event relays occurred

The master-timer problem of picking up spurious counts had occurred before delivery of the CC&S for spacecraft tests. This problem resulted from noise being integrated and inserted as counts by the master-timer speedup interface circuitry. Prior to SAF delivery, the input impedance of this interface was decreased as much as feasible, which resulted in the elimination of the problem between CC&S and CC&S OSE. This fix, however, did not hold in the spacecraft tests because of longer interface cable runs and a considerably noisier environment. The interface circuitry was again reviewed and the interface was modified to achieve additional noise filtering. This fix was satisfactory for spacecraft tests at SAF; however, for tests in the space simulator at JPL, the problem occurred again because of longer cable runs and a noisier environment than at SAF. During the same series of space simulator tests, CC&S OSE personnel introduced the idea of using the encounter update interface to accomplish master-timer speedup. This update interface is an umbilical function and was designed to have high noise rejection. The modification was made and the problem was subsequently eliminated.

The problem of the 10-kc inhibit failing first appeared in PTM space-simulator tests. No troubleshooting time was allowed during these tests, so that no opportunity existed to investigate the problem. The suspected cause was poor simulator cabling that, it was felt, had not been adequately checked out prior to spacecraft tests. Nearly 2 months later, the problem recurred in PTM system tests at SAF. A study of the problem was then made, and it was determined that ground noise in the system test complex was causing the problem. The problem was simulated in the CC&S laboratory, and an OSE modification satisfactorily eliminated the problem by introducing a reverse bias to serve as a noise guard.

The new CC&S 5A9 subassembly was integrated into the PTM spacecraft just prior to acoustic tests on the spacecraft. At the conclusion of the acoustic tests, it was found that the protective fuse in the 5A9 unit had blown. Since an unauthorized test box, which caused several problems, was inserted during the acoustic tests, it was believed that the 5A9 unit outputs had been inadvertently shorted, which blew the fuse. However, the fuse was again blown in subsequent space-simulator tests. Due to schedule restrictions, it was necessary to continue PTM tests with an opportunity to investigate the problem delayed until the MC-2 spacecraft was available. At turn-on of the 5A9 subassembly in the MC-2 spacecraft, the fuse was blown again. Further studies revealed that the 2.4-kc maneuver power used by the 5A9 unit had about 20% overshoot at turn-on. This overshoot saturated the 5A9 transformer primary, which had a 12% design margin, and blew the fuse. The 5A9 transformers were replaced and the problem was not repeated.

The spurious reset of relays was first observed in PTM space simulator tests. Access to the CC&S for trouble shooting was not possible; this problem was not pursued on the PTM. The problem next appeared in MC-3 spacecraft tests. Testing revealed that noise between spacecraft ground and OSE chassis ground was triggering reset circuitry in the OSE, which was resetting CC&S relays. Resistance–capacitance filters were added to the OSE sensitive lines and the problem was not repeated.

XI. SPACECRAFT SUBSYSTEMS: DATA ENCODER

The function of the data encoder is to accept spacecraft measurement data in the form of analog voltages and digital information; convert the data into 7-bit nonreturn-to-zero words in serial form; modulate a subcarrier with the binary data; and add synchronization information, which forms a signal to be presented to the radio transmitter.

The data encoder operates at two data rates (8⅓ and 33⅓ bps) and in four data modes. Figure 117 is a functional block diagram of the system.

Two system rates are derived from the 2.4-kc main power frequency. This basic signal is divided down by binary dividers to furnish frequencies termed 4 f_s and 2 f_s, which are the data and synchronization subcarriers, respectively. Two sets of 4 f_s and 2 f_s are selected to provide two system rates. The 2 f_s frequency is used to clock the pseudonoise synchronous-code generator, which generates bit-synchronous and word-synchronous timing pulses for the data encoder.

Ninety analog and digital engineering data plus ten subcommutation and frame synchronization channels are accommodated on the completely solid-state commutator. The switches are arranged in a three-layer subcommutator, as illustrated in Fig. 117, to allow four basic sampling rates. Inputs on decks 100 and 110 are sampled at 1/20, the basic word rate. Inputs on decks 200, 210, and 220 are sampled at 1/200, the basic word rate. Inputs on deck 300 are sampled at 1/2000, the basic word rate. Inputs on decks 400, 410, 420, and 430 are sampled at 1/4000, the basic word rate.

All high-level analog signals are normalized to a 0- to 3-v range. All low-level analog inputs are normalized to a 0- to 100-mv range and then amplified by 30. Digital inputs are handled in the transfer register, the seven-stage storage register, and clocked to the data selector by the programmer.

Event inputs, consisting of switch closures, are sensed and stored in four event registers. The programmer reads out these registers into the data selector.

The programmer uses complementary flip-flop sequencers, synchronized in pairs or groups of three, to provide circuit redundancy without additional circuitry. The programmer outputs consist of time-multiplexed gates that drive the commutator switches, transfer register, and other signal-handling circuits.

Analog input signals from the commutator are routed to a high-impedance, unity-gain isolation amplifier. The analog signals are then converted to 7-bit digital words by a successive approximation technique in the analog-to-digital converter. Four parallel digital data inputs are processed into serial 7-bit binary words and inserted at the appropriate time in the data format. The four sources of data are the analog-to-digital converter, transfer register, science data automation subsystem, and video storage subsystem. The data format is programmed by the mode controls through the commutator programmer. These circuits provide gating signals to the data selector circuit to indicate which data source is to be accepted into the data train. Appropriate gating in the data selector applies the proper output to the steering inputs of a 1-bit buffer synchronizer flip-flop, which ensures precise synchronization of each source of data with the data encoder bit synchronization.

To increase the inherent reliability of the data encoder, a standby analog-to-digital converter and pseudonoise generator is used in the system. In the event of a failure of one of the two circuits, power can be switched by real-time command to the standby circuit.

In the biphase modulator, the 7-bit nonreturn-to-zero data are used to biphase-modulate the 4 f_s data subcarrier. The synchronization channel of the modulator combines the pseudonoise code and 2 f_s clock in EXCLUSIVE OR addition. The data channel is mixed with the synchronizing channel at the proper voltage ratio. This mixed signal is then routed through output isolation amplifiers to the spacecraft transmitter and the OSE.

All digital circuitry in the data encoder was built using a line of standard NAND logic, which was developed for use in the *Mariner B* telecommunications system, and NOR logic. There are two families of logic: the first, or low-speed group, has a 45-kc maximum repetition rate; the second, or high-speed group, has a 2-Mc repetition rate.

Low-speed group (45 kc). The circuits listed below are used to implement logic requirements that do not exceed a 45-kc repetition rate. Their low power requirements

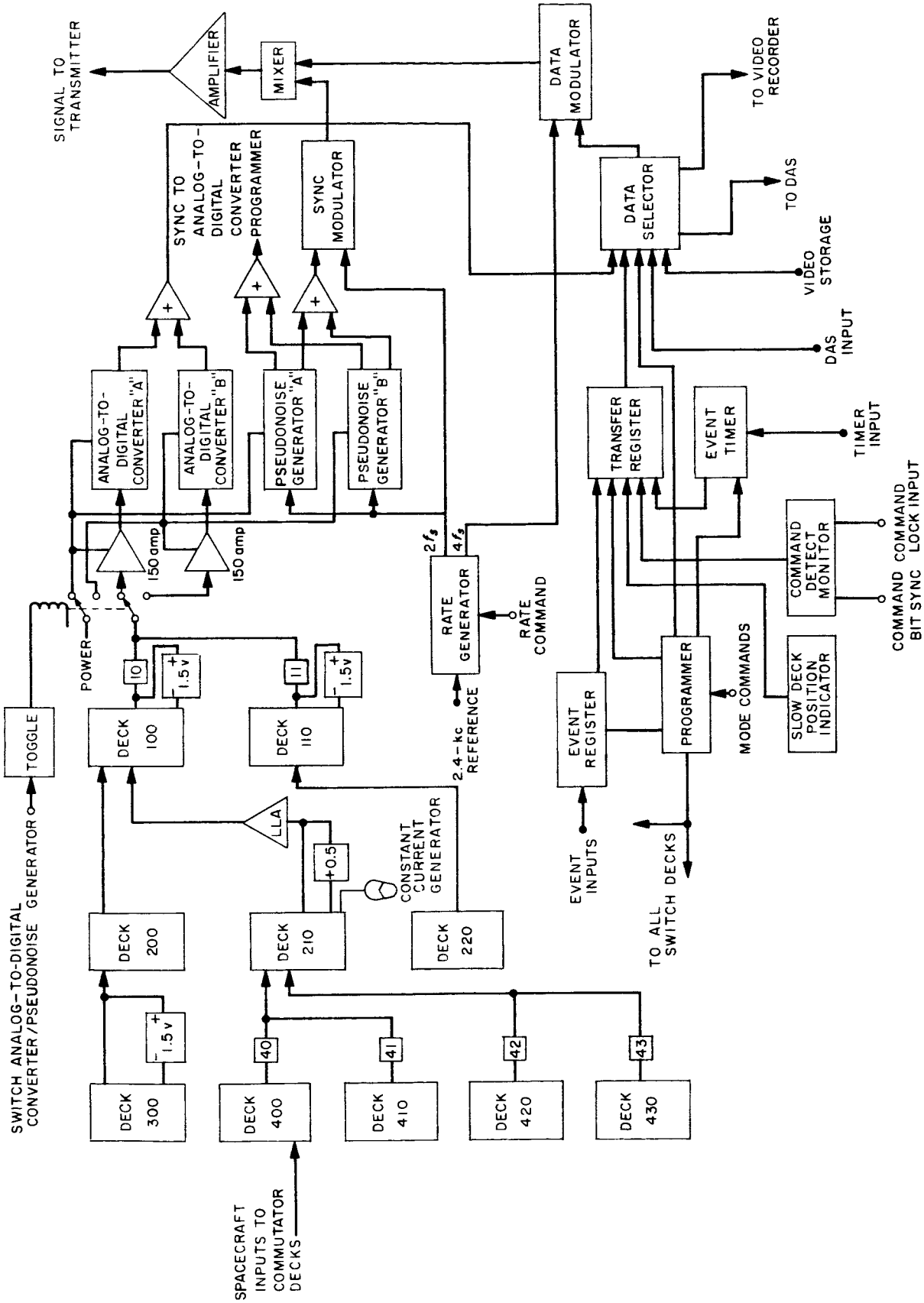


Fig. 117. Data encoder functional block diagram

are more desirable than the 2-Mc logic family, and therefore are used whenever possible. The following circuits are packaged in standard logic modules:

1. 4-input NAND gate and 2-input NAND gate
2. 8-input NAND gate
3. Reset–set flip-flop
4. Universal flip-flop
5. 4-input NOR gate and 2-input NOR gate
6. Noninverting driver

High-speed group (2 Mc). The 2-Mc circuits are used when speed or loading requirements preclude the use of the 45-kc circuits. The following circuits are packaged in standard logic modules:

1. 4-input NAND gate and 2-input NAND gate
2. 8-input NAND gate
3. Reset–set flip-flop (standard)
4. Reset–set flip-flop (universal)
5. Noninverting driver

A. Input System

The input system is the portion of the encoder that receives, routes, and conditions the input data. This system includes the commutator, programmer, and signal conditioning circuits.

The commutator consists of solid-state switches driven by complementary flip-flop shift registers, which are called sequencers. These sequencers, together with the logic circuits, are designated as the commutator programmer.

The signal conditioning circuits convert nonstandard inputs to standard levels or formats required by the basic system. The circuits included in this category are the low-level amplifier, temperature networks, "bucking" supplies, event counters, and digital data input gating.

1. Commutator

Figure 117 shows the ten switch decks that comprise the commutator. Each switch deck has ten positions. The high-speed frame includes decks 100 and 110, which are sampled sequentially. Output switches 10 and 11 are required since the switches in decks 100 and 110 are sequenced in parallel.

The medium-speed frame consists of decks 200, 210, and 220. These decks are channeled into decks 100 and 110 and are stepped once for each complete revolution of the high-speed frame.

The low-speed frame consists of decks 300, 400, 410, 420, and 430. These decks feed into decks 200 and 210 and are stepped once for each cycle of the medium-speed frame. Output switches 40 and 42 are on for one cycle of the low-speed decks. This, in effect, creates two 20-length decks and one 10-length deck in the low-speed frame.

The data encoder provides for four modes of operation, each creating a different data format. These formats are:

Data Mode	*Operation*	*Format*
1	Maneuvers	Decks 100 and 110 are sampled sequentially
2	Launch and cruise	Decks 100 and 110 are sampled sequentially with a 280-bit science DAS read-in occurring after deck 110
3	Encounter	Science DAS read-in only
4	Video playback	Video storage read-in only in the presence of the data present signal from the recorder

2. Sequencer

The sequencer consists of a ten-stage shift register, using complementary flip-flops so that only the "on" stage draws power. The outputs provide a low impedance to ground when the stage is on, which turns the appropriate commutator switch on and provides a logic signal for use in the commutator programmer.

3. Commutator Programmer

The commutator switches are programmed with the logic illustrated in Fig. 118. Word synchronization is used to clock sequencers 100 and 110. These sequencers are synchronized by synchronizer 100, an OR gate driving a monostable flip-flop. If sequencers 100 or 110 lose synchronization, the first to have a *one* in the last stage will provide an output pulse from the synchronizer when that stage is turned off. This output pulse resets both sequencers to stage *zero*. The circuit then functions as

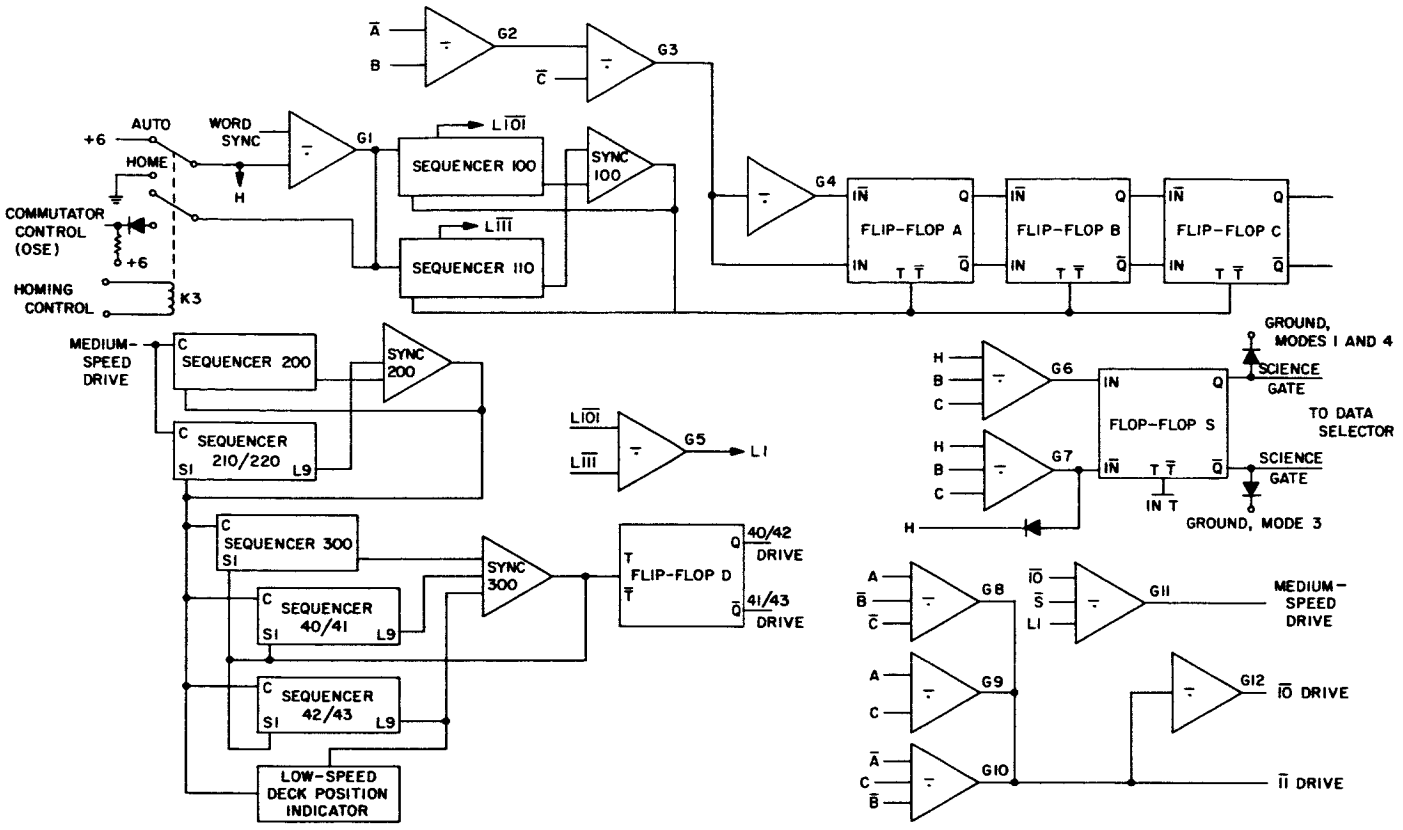


Fig. 118. Commutator programmer

two synchronized ring counters. High-speed programming continues to operate at a full 20- or 60-word length, even though one of the sequencers fails, because of the parallel redundancy.

Flip-flops A, B, and C are connected as a synchronous counter in a 6-count sequence. Synchronizer 100 output, or word synchronization, divided by 10, clocks the counter. Since the counter is stepped once every 10 words, a cycle is completed every 60 words. By decoding the counter, a 60-word format is realized for Data Mode 2 operation. Output switches 10 and 11 are programmed by the decoding provided by gates G8, G9, and G10. This provides an alternate conduction of switches 10 and 11, allowing decks 100 and 110 to be sampled sequentially.

Flip-flop S performs the function of gating science data (DAS) into the encoder during the last 40 words of the high-speed frame (Data Mode 2). The flip-flop is connected as a shift register element, set by the interrogate pulse during the eleventh word of the high-speed frame, and reset by the interrogate pulse during the first word of the frame. (Interrogate pulse is the timing pulse used to clock the shift register element.) This one-word delay is required since the analog-to-digital converter output lags the commutator by one word. The flip-flop also blocks the analog-to-digital converter output from the data selector during the 40-word read-in of DAS data.

In Data Mode 1, the flip-flop is prevented from being set by collector clamping from the mode relay (Fig. 119). This permits the high-speed commutator to cycle in a 20-word frame. Data Mode 2 relays allow G6 and G7 to steer flip-flop S to be set and reset at appropriate times in the high-speed frame. Data Mode 3 is implemented by clamping flip-flop S in the set state, thereby providing continuous science data read-in.

The medium-speed programmer consists of sequencers 200 and 210/220, synchronizer 200, and gate G11. The medium deck clock drive is provided by G11. Timing provides that the medium deck drive occur at position 111 in the high-speed frame. This drive is inhibited during the science data read-in, since two medium deck positions would be skipped if the decks were stepped during the 40-word science read-in. The sequencers are synchronized in the same manner as those in the high-speed frame.

The low-speed sequencers (300, 400/410, and 420/430) are clocked by synchronizer 200 output, allowing the low-speed frame to be stepped once per revolution of the medium-speed frame. Synchronizer 300 duplicates the task of synchronizers 100 and 200 in synchronizing all sequencers. Flip-flop D provides an alternate drive for switches 40/42 and 41/43 to implement the 20-length decks.

The ground equipment is capable of homing the commutator by blocking normal commutator drive and substituting a faster drive signal. The homing relay is a spring-return relay activated by the operational support equipment.

4. Mode Changing

Mode changing (Fig. 119) is accomplished by using three latching relays (K1, K2, and K3). Each mode command activates an isolated pulse switch in the spacecraft. The relay drivers set or reset the relays upon receipt of the mode-change command (schedule in Fig. 119).

MODE RELAY SCHEDULE

MODE	K1	K2	K3
1	R	S	R
2	S	S	R
3	S	R	R
4	R	S	S

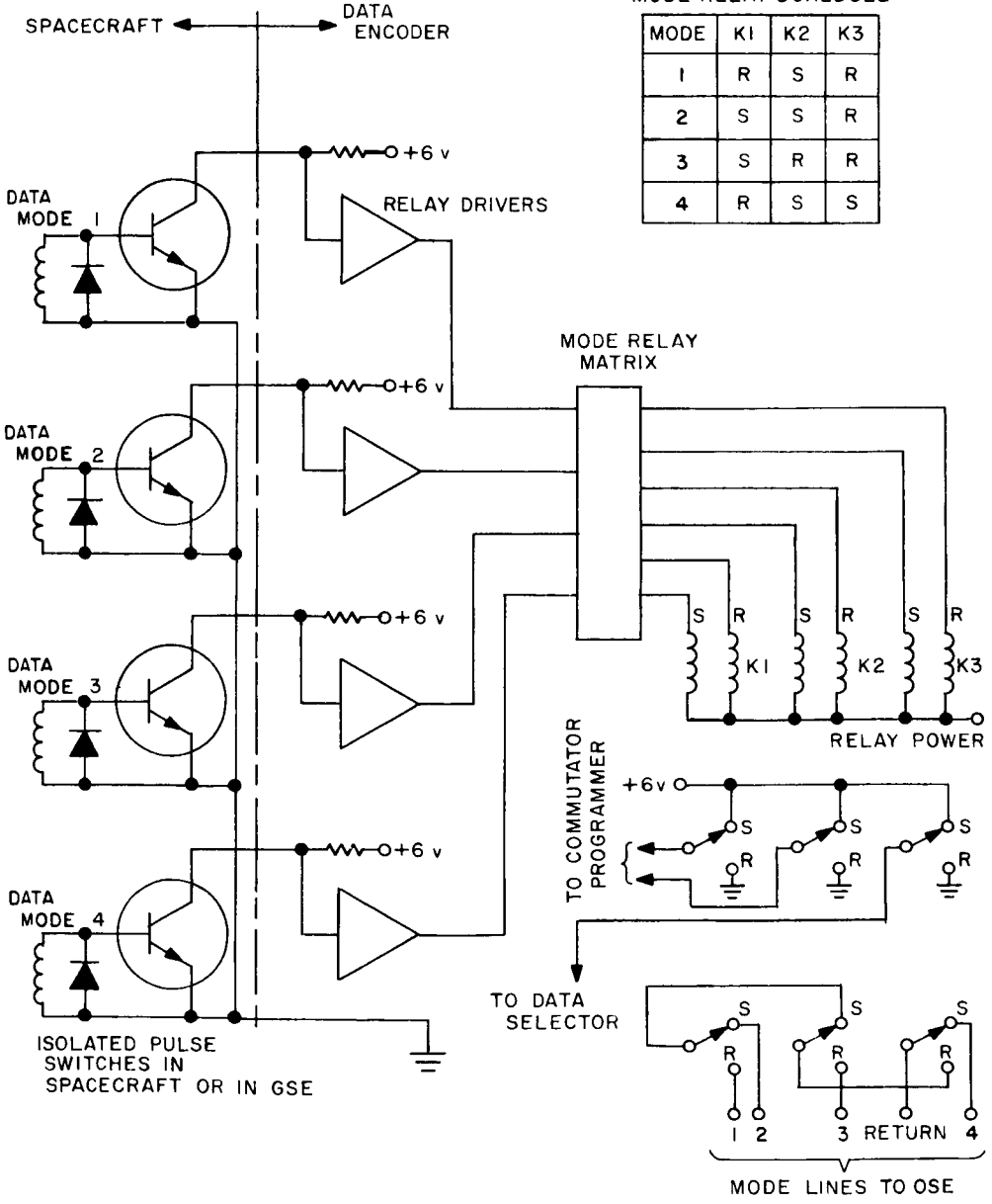


Fig. 119. Mode programmer

The relays control appropriate logic to accomplish the mode change. Hard-line mode indication to the operational support equipment is also provided by these relays.

In addition to the commutator analog inputs, there are several digital signals that must be gated-in at appropriate times during the commutator frame. The programming for these signals is accomplished by logic illustrated in Fig. 120.

The appropriate sequencer logic L outputs are inverted by the NAND gates before being processed by the various coincidence gates. All digital input signals are conditioned to a parallel format. The buffers that contain this information must receive an interrogate pulse when the data is to be transferred into the transfer register. Figure 120 shows gating that creates the interrogate pulses.

The S1 output is used to produce all *ones* in the ADC register for commutator frame synchronization in the data. All other data consisting of all *ones* are prohibited by the logic check performed in the ADC. The three-deck synchronization signals are also sent to the OSE through separate gates.

5. Analog Signal Conditioning

Low-level and temperature-measurement inputs of 0- to 100-mv signals are amplified to 0 to 3 v for input to the analog-to-digital converter. This is accomplished with a chopper-stabilized dc amplifier, with a gain of 30.

The ±1.5-v inputs have to be converted to 0 to 3 v for input to the ADC. This is done by inserting a 1.5-v bucking supply in series with the ±1.5-v signals, thus converting them to 0 to 3 v.

6. Temperature Measurements

Figure 121 illustrates the temperature measurement mechanization. A 1-ma constant-current generator supplies current to each transducer, one at a time, through one pole of the double-pole switches in decks 210, 400,

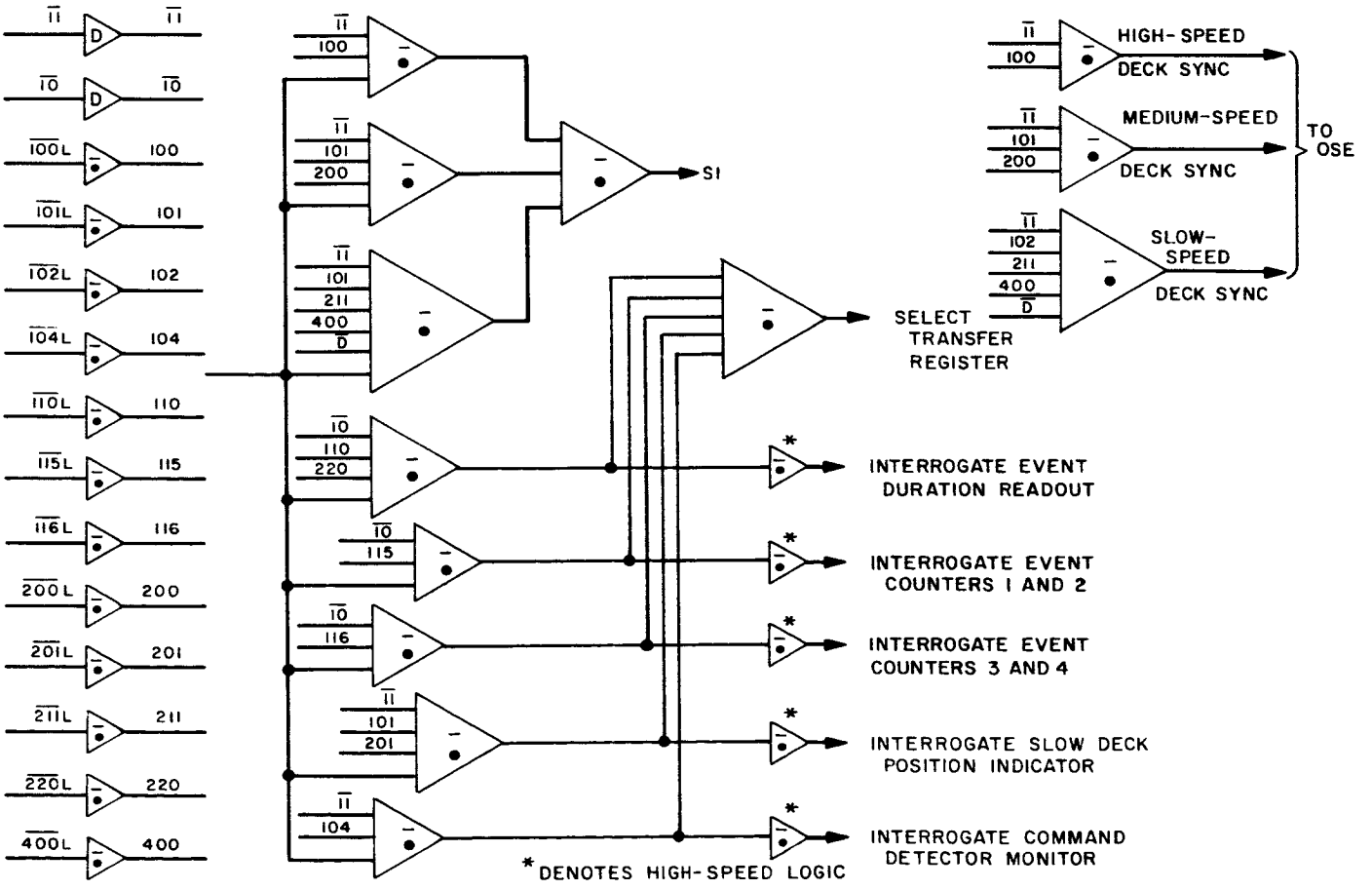


Fig. 120. Digital word programmer

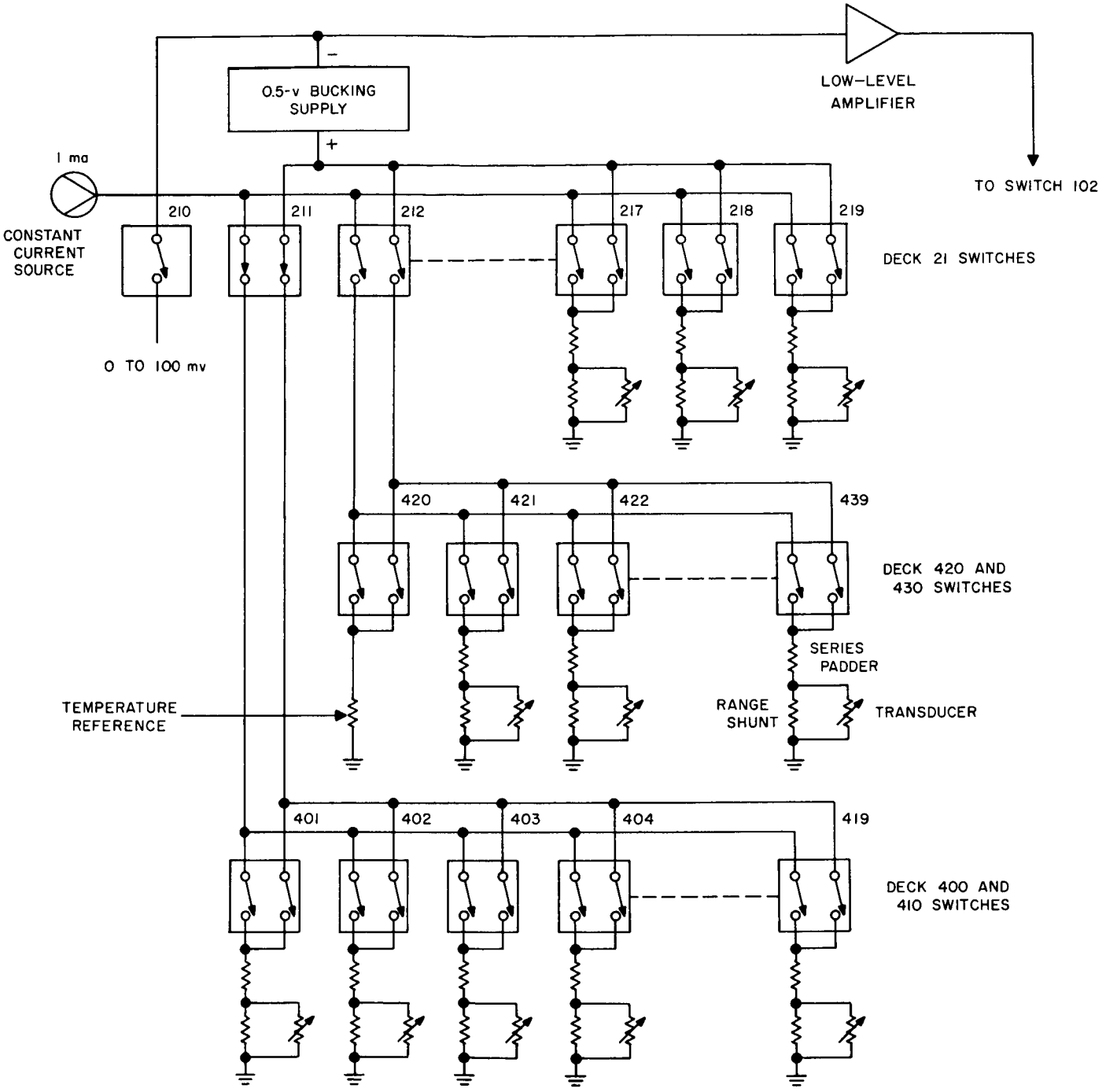


Fig. 121. Temperature measurement method

410, 420, and 430. A parallel resistor shunts the transducer resistance change to a standard 100 Ω change for all ranges. A series resistor is included to transform the total network resistance to 500 Ω at the low-temperature end. The total network resistance at the high-temperature end is 600 Ω. With a constant current of 1 ma applied to the network, the voltage across the network varies from 0.5 to 0.6 v from low-band to high-band temperature. This network voltage is then commutated through the other pole of the double-pole switch and bucked down by a series 0.5-v bucking supply, presenting signals between 0 and 100 mv to the low-level amplifier. This system presents an advantage over the bridge method previously used, in that a transducer

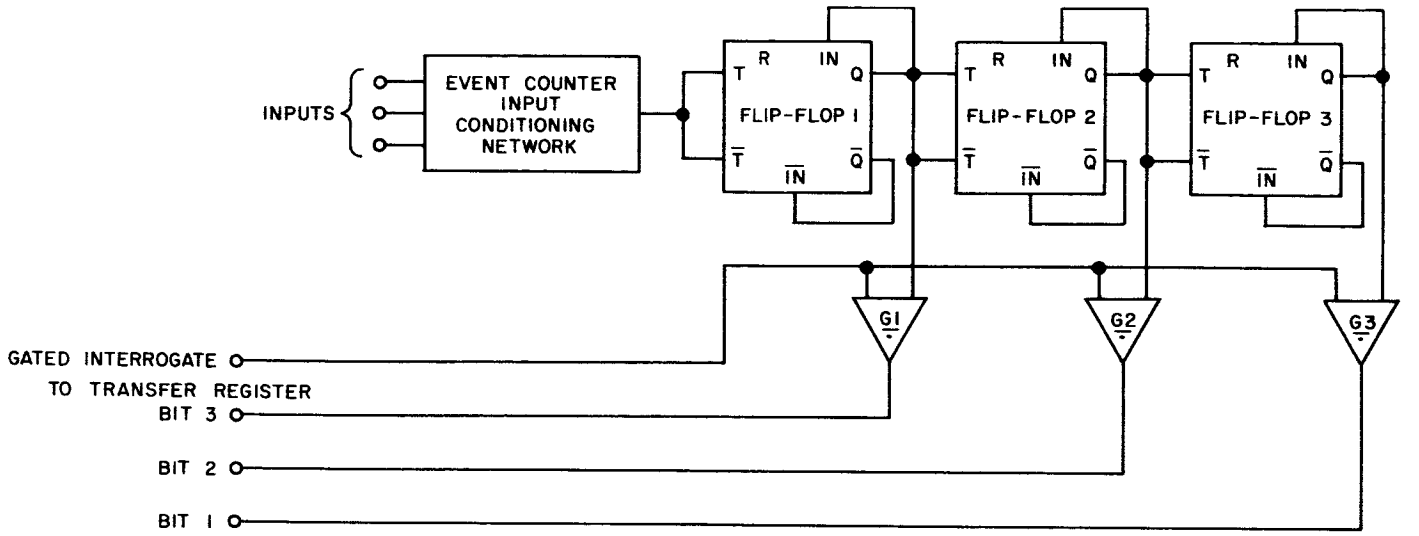


Fig. 122. Typical event counter and input conditioning stage

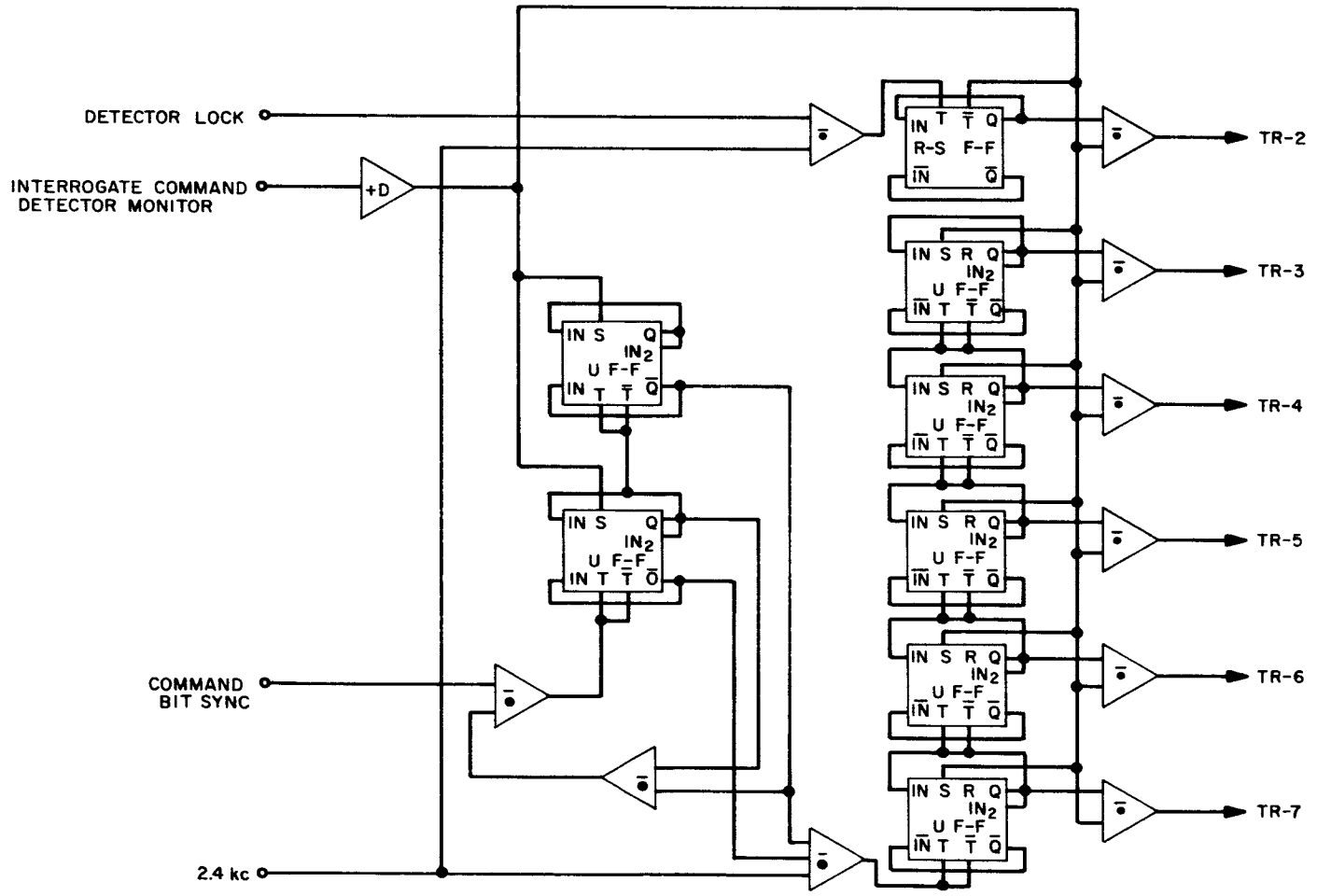


Fig. 123. Command detector monitor

shorted to ground does not upset all of the temperature measurements.

7. Digital Signal Conditioning

Four event counters are provided to count random events from the spacecraft. Each counter (Fig. 122) has an eight-count capacity (three stages). Twelve inputs are isolated pulse switch, relay, and microswitch 4-msec closures. These twelve sources are connected to the encoder so that a closure grounds the input conditioning circuit to provide a count pulse to the counter.

The event counters are read out in two pairs of three-stage counters in successive channels (115 and 116). Each pair creates 6 bits of data and reads into the transfer register by a selected interrogate pulse. The fourth bit is a *zero*, which prevents an all-*ones* word.

8. Command Detector Monitor

The command detector monitor is illustrated in Fig. 123. Command bit synchronization and a detector lock signal are received from the spacecraft command subsystem. A five-stage counter counts the 2.4-kc spacecraft clock signal for one command-bit-synchronous interval, and is reset at the interrogate pulse (word 104) trailing edge. A storage flip-flop is reset by the interrogate pulse trailing edge and, if the detector in-lock signal goes to high-level at any time prior to the following interrogate pulse, it sets the storage flip-flop. Parallel data from six stages are gated into the transfer register.

9. Event Timer

The event timer measures time during the opening of a switch from the CC&S (Fig. 124). Word-synchronization divided by two is used as a reference frequency that is gated into a seven-stage binary counter for the gate duration. This count is stored for commutator readout, which is accomplished by dumping the data in parallel into the transfer register.

An all-*ones* word is prohibited by steering the second counter stage to reset on the succeeding word-synchronization (divided by two) pulse if the most significant digits are *ones*. This eliminates all *zeros*, which results in a 126-count capacity.

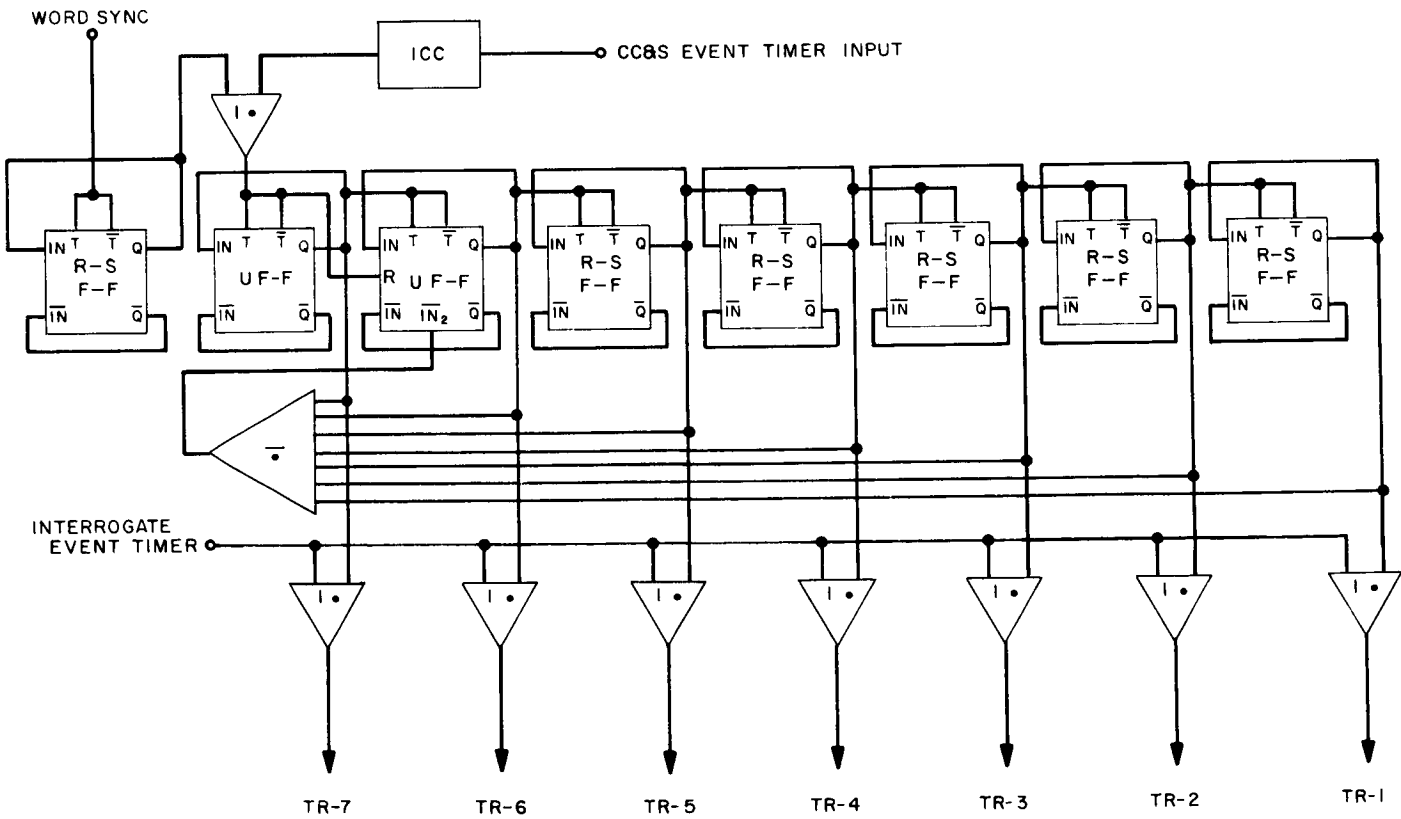


Fig. 124. Event timer

10. Low-speed Deck Position Indicator

The low-speed deck position is read in as a data word on each medium-speed commutator cycle. This low-speed deck position information is generated in a four-stage counter. The counter and low-speed decks are kept in synchronization by a set pulse from the output of synchronizer 300. The counter toggle input is low-speed drive. Flip-flop D in the low-speed programmer provides which of alternate decks 400/420 and 410/430 is in use. Deck position is read out by a selected interrogate pulse on word 201, dumping the 5-bit code into the transfer register. A sixth data bit (in the word) contains a digital indication of which pseudonoise generator–ADC combination is in use.

B. Basic System

The basic system is the portion of the encoder that receives conditioned time-multiplexed analog data from the input system. The system also generates the serial data train, synchronization code, the two subcarriers, and all clock frequencies for the encoder. The major elements of this system are the rate selector, pseudo-noise generator, analog-to-digital converter, biphase modulator–mixer, and the power supply.

1. Rate Selector

The data encoder synchronization circuits frequency is derived from the 2.4-kc square wave primary power. Noise and switching transients suppression on the 2.4-kc signal, which would cause synchronization circuits malfunction, is accomplished with an overdriven transistor limiter circuit. A four-stage binary divider supplies the proper 4 f_s signal for the two required data rates (33⅓ and 8⅓ bps).

2. Pseudonoise Generator

The pseudonoise generator (Fig. 125) is comprised of standard high-speed digital circuit modules. The pseudo-

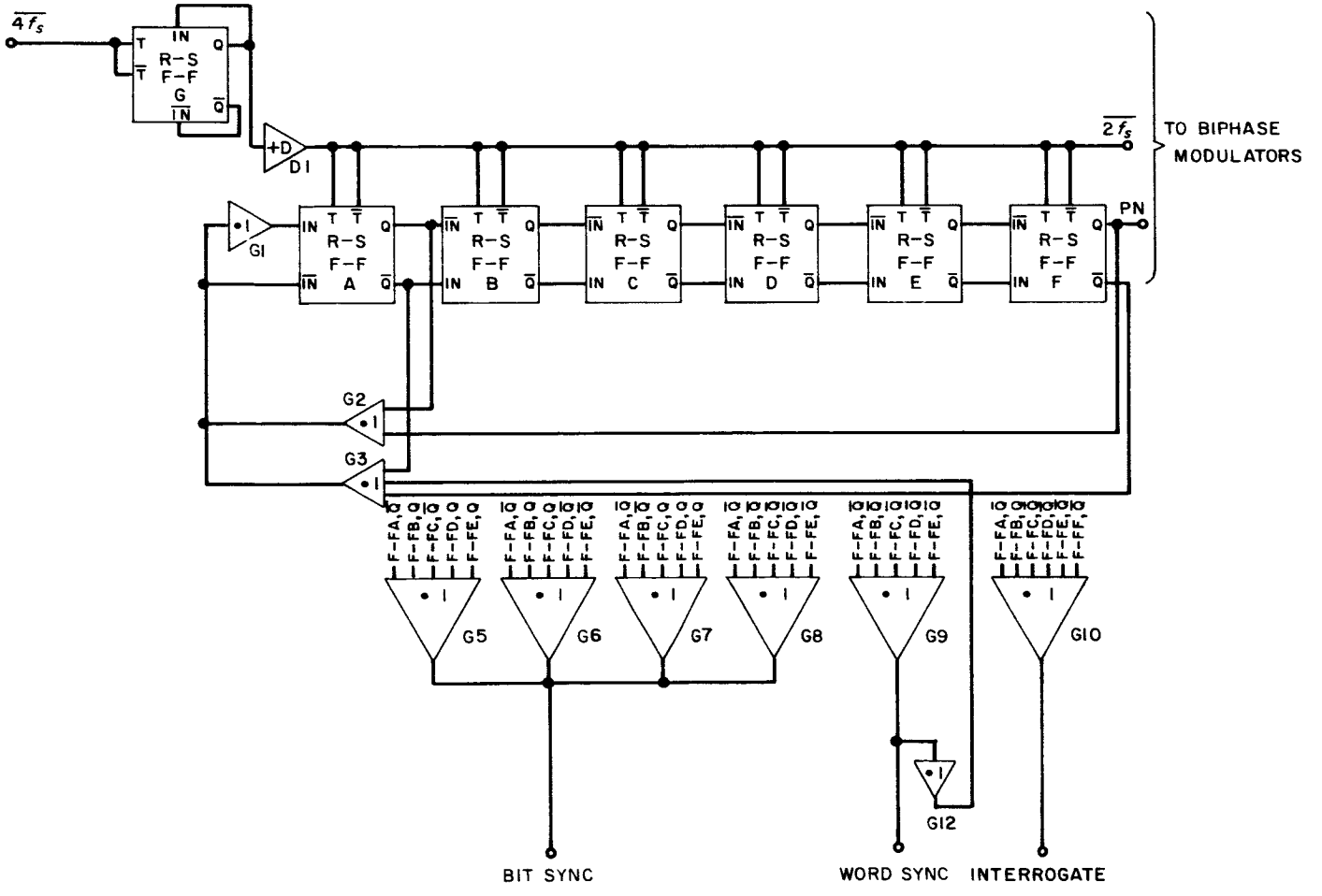


Fig. 125. Pseudonoise generator

noise generator provides system timing pulses and a 63-bit pseudonoise code.

Three synchronization outputs are provided by the pseudonoise generator: data-word synchronization, bit synchronization, and an interrogate pulse. A data-word synchronization pulse occurs at the beginning of the 63-bit pseudonoise code; thus, a word length is 63 bits of the pseudonoise code. A bit-synchronization pulse also occurs at the beginning of the pseudonoise code and every 9 bits of the code thereafter. Therefore, seven bit-synchronization pulses are generated for every data-word synchronization pulse.

An interrogate pulse is generated concurrently with the sixtieth bit of the pseudonoise code, which is just prior to the first bit-synchronization pulse of the following data word. This pulse begins the digitizing cycle of the ADC or interrogates parallel read-in gates for the transfer of digital data to the transfer register.

The pseudonoise code is generated by a six-stage shift register with logic feedback so that the opposing states of the register ends are sensed. Opposite-end states cause the first stage to be set, while a like-end state causes the first stage to be reset. The NAND gates G1, G2, and G3 perform this logic operation so that flip-flop A is steered as

$$\overline{IN} = \overline{AF} + \overline{AF}$$

$$IN = AF + \overline{AF}$$

When power is first applied to the pseudonoise generator and all the flip-flops are reset, a lockup of the register will occur. To prevent that condition, $\overline{WORD}$ is ANDed with $\bar{A}$ and $\bar{F}$ at NAND gate G3. Thus, in the event of all *zeros* in the register, the G3 output steers IN of flip-flop A low, and the next clock pulse will set flip-flop A, eliminating the possibility of lockup.

The logic equation $\overline{BIT}\ \overline{SYNC} = \bar{A}\,B\,\bar{C}\,D\,E + \bar{A}\,B\,C\,\bar{D}\,\bar{E} + \bar{A}\,\bar{B}\,C\,D\,E + \bar{A}\,\bar{B}\,\bar{C}\,\bar{D}\,\bar{E}$ is implemented by NAND gates G5, G6, G7, and G8, which provide inverted system bit synchronization. Gate G9 implements the equation $\overline{WORD}\ \overline{SYNC} = \bar{A}\,\bar{B}\,\bar{C}\,\bar{D}\,\bar{E}\,\bar{F}$ to provide system word synchronization. Gate G10 implements the equation $\overline{INTERROGATE} = \bar{A}\,\bar{B}\,\bar{C}\,\bar{D}\,\bar{E}\,\bar{F}$, to provide interrogate pulses for system operation. The pseudonoise code is obtained at the Q side of flip-flop F.

3. Analog-to-digital Converter

The ADC is of the successive-approximation type as shown in Fig. 126. The ADC is comprised of five basic circuits: the digitizing pulse generator, the decoder, the comparator isolation amplifier, the low-pass filter, and the comparator. The 50-cycle cutoff low-pass filter is used ahead of the comparator to prevent spurious signals that would cause false indications during the ADC digitizing period.

A high-input-impedance unity-gain amplifier is compared with precision binary-weighted trial voltages. These trial voltages are generated in the decoder ladder network, which is supplied from a precision reference supply. The output of the comparator is a positive signal step voltage whenever the amplitude of the trial voltage exceeds the amplitude of the analog voltage to be digitized. The decoder ladder network output voltage is controlled by a series of seven switches that are, in turn, driven by the ADC register flip-flops A through G. The ADC register is sequenced by the digitizing pulse generator at a rate of 6.7 μsec/bit or 47 μsec/word.

4. Transfer Register and Data Selector

The transfer register and data selector are illustrated in Fig. 127.

The transfer register is used to convert parallel digital data from the event counters, event-timer, command detector monitor, and the low-speed deck position indicator into nonreturn-to-zero data. The data sources are sampled by an interrogate pulse at a specified time in the data format. Negative pulses at transfer register inputs TR-1 through TR-7 set the appropriate flip-flops in the register.

The data selector gates transfer data into the output data train, when the commutator is in the proper sequence position for transfer register readout. The commutator position gate steers a control flip-flop, which is set with an interrogate pulse and reset on the following interrogate pulse. When the flip-flop is set, the transfer register data is gated into the output data train, blocking the ADC data gate in the data selector.

When the data selector is at Data Mode 1, the science and video storage data gates are continuously blocked. With the selector at Data Mode 2, the science gate is high during the science readout. This allows the science data to pass through the data selector while the inverted

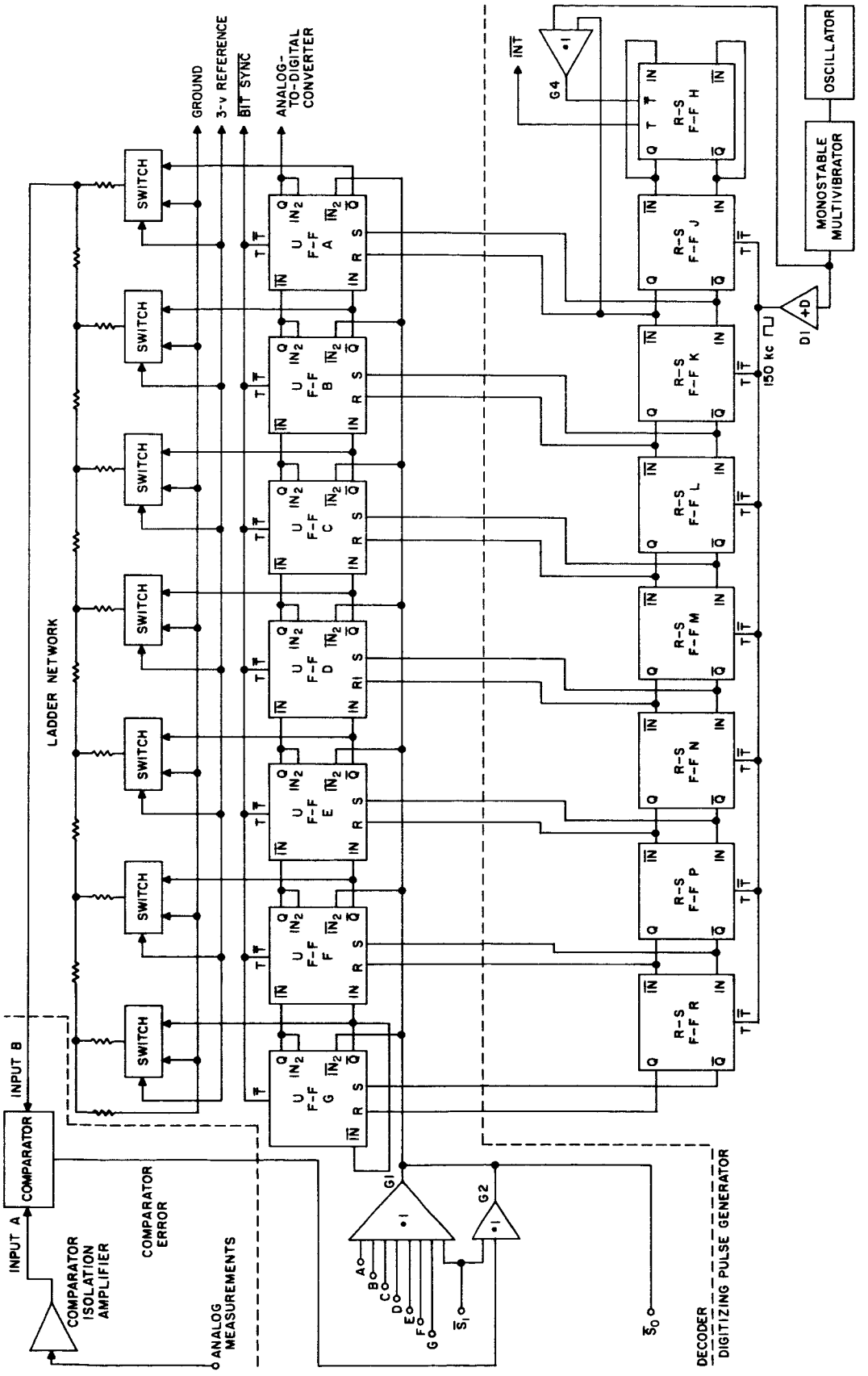


Fig. 126. Analog-to-digital converter

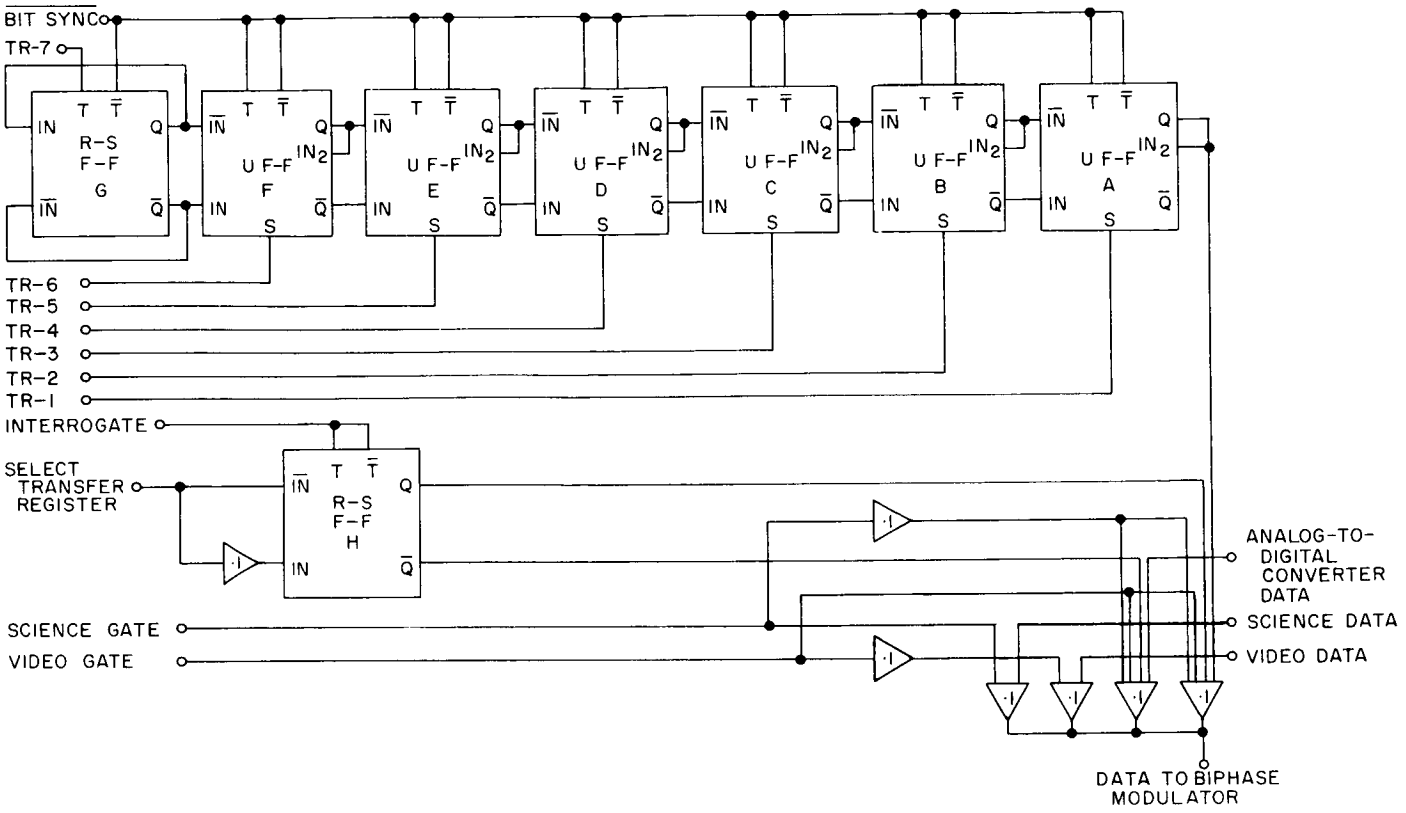


Fig. 127. Transfer register and data selector

science gate blocks the ADC and transfer register data gates. When in Data Mode 3, the science gate is continuously passing science data, exclusively.

Video recorder data, continuously blocked in Data Modes 1, 2, and 3, are enabled in Data Mode 4. This is accomplished by the video gate being held high, passing video recorder data and blocking all other data.

Science and video recorder readout conditions include the supplying of bit synchronization to the respective system and of a gate signal to the subsystem furnishing data.

5. Biphase Modulator–Mixer

A biphase modulator–mixer logic diagram is shown in Fig. 128.

The biphase modulators implement the Modulo 2 logic addition of 4 f_s, and data, and the 2 f_s, and pseudo-noise. Data from the data selector circuit steer the inputs of a 1-bit buffer synchronizer flip-flop to ensure precise synchronization of each source of data to the data encoder, with the data encoder bit and word synchronizations.

The mixer combines the data and synchronizing channels in a 1.79:1 voltage ratio. The combination of the two channels results in a mixed signal with four possible voltage levels: 3.000, 1.925, 1.075, and 0 v, as outlined by the following logic equations

$$v_3 = 3.000\ \text{v} = 4f_s \oplus \text{data} \cdot 2f_s \oplus \text{PN}$$

$$v_2 = 1.925\ \text{v} = 4f_s \oplus \text{data} \cdot \overline{2f_s \oplus \text{PN}}$$

$$v_1 = 1.075\ \text{v} = \overline{4f_s \oplus \text{data}} \cdot 2f_s \oplus \text{PN}$$

$$v_0 = 0 = \overline{4f_s \oplus \text{data}} \cdot \overline{2f_s \oplus \text{PN}}$$

A combination of three inverted transistors and a resistive voltage divider provide the four voltage levels. In the inverted connection, the transistors exhibit very low offset voltages from collector to emitter. Therefore, the output voltage-level drift of the mixer is held to less than $\pm 1.0\%$, peak to peak.

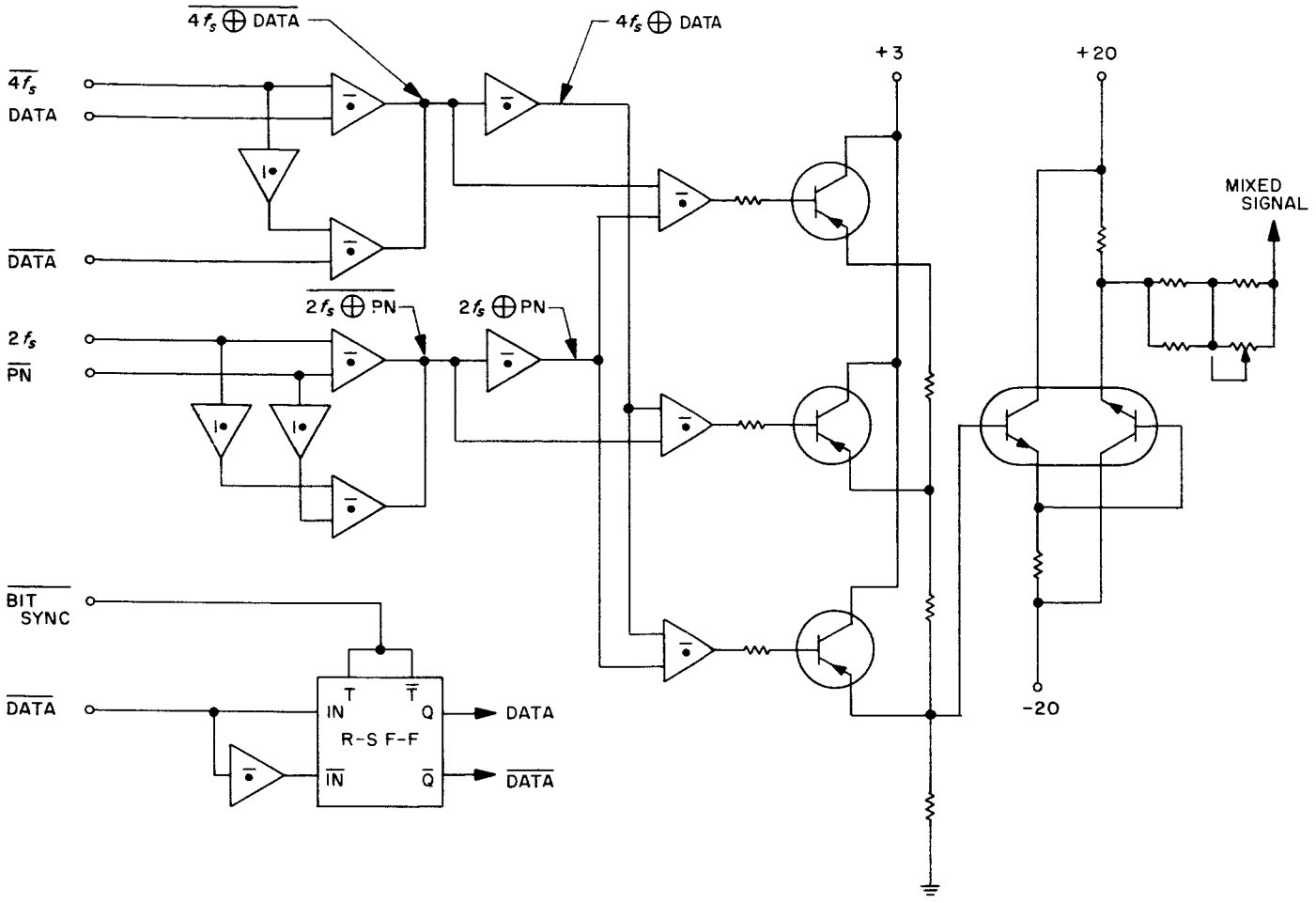


Fig. 128. Biphase modulator–mixer

To prevent loading the mixer voltage divider network, the mixer output is isolated by an emitter-follower circuit. The mixer output is coupled to three output isolation amplifiers. The output amplifier, which routes the mixed signal to the transmitter, is dc-coupled from the mixer to provide the desired output signal voltage deviation of 0 to 2.52 v. The amplifier is a complementary emitter-follower configuration to eliminate voltage level offset. Total voltage variation on the output-mixed signal will be less than ±2.5% of peak-to-peak value. The second amplifier, which routes the mixed signal to the operational support equipment, is a similar complementary emitter-follower. The third amplifier is an ac-coupled, cascaded emitter-follower, transformer output circuit for driving the *Agena D* telemetry transmitter during the launch ascent phase.

6. Power Supply

The primary power provided is a 2.4 kc, 100-v peak-to-peak square wave. The data encoder power supply transforms this ac signal to the following dc voltages and currents:

+20 vdc, regulated ±0.5%, 50-ma load

−20 vdc, regulated ±0.5%, 30-ma load

+6 vdc, unregulated ±0.5%, 500-ma load

−6 vdc, unregulated ±5%, 30-ma load

+3 vdc, regulated ±0.1%, 12-ma load

+1.5 vdc, Zener-stabilized, negligible load, isolated

C. Physical Description

Physically, the data encoder occupies approximately two-thirds of a standard electronics case as shown in Fig. 129. The command subsystem occupies the remainder of the case. The weight of the data encoder, less wiring harness and case, is 22.5 lb.

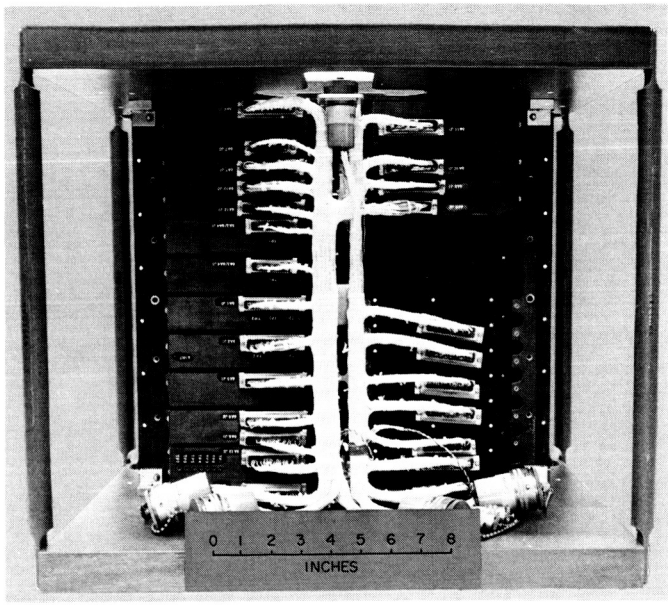


Fig. 129. *Mariner* Mars 1964 data encoder

D. Design Evolution

The *Mariner* Mars 1964 data encoder was e latest in a series of designs that began with the *Mariner A* program. All of these designs were basically of the same type; i.e., time-multiplexed, pulse-code modulation telemetry systems. The *Mariner* Mars 1964 data encoder used refinements of techniques and processes used in the previous programs. The majority of the design was based on the *Mariner B* data encoder.

The design phase of the system included a reliability study of the various techniques considered, so the reliability improvements of one concept over another could be seen more readily. A reliability estimate was then made on the final design, based on known parts failure rates.

A worst-case analysis was performed on all circuits in the data encoder. The analysis consisted of ensuring proper circuit performance over all combinations of voltage and component parameter variations (under both steady-state dc operation and sinusoidal ac operation, where appropriate). Also, as a part of the reliability program, a stress analysis was made of all circuits in the data encoder, which verified that all components were operated well below their maximum voltage and current ratings.

As a result of the worst-case analysis and system design reviews, some redesign was carried out before the design was frozen in May 1963.

E. Procurement

The data encoders and associated ground equipment were procured through a contractor who had had previous experience with similar equipment.

F. Fabrication

The data encoders were fabricated by conventional, reliable techniques. Digital circuits were assembled into encapsulated, soldered cordwood modules. These modules, along with discrete components for all analog circuits, were soldered to printed circuit interconnection boards. The interconnection boards were then bonded into the standard subchassis (Fig. 130).

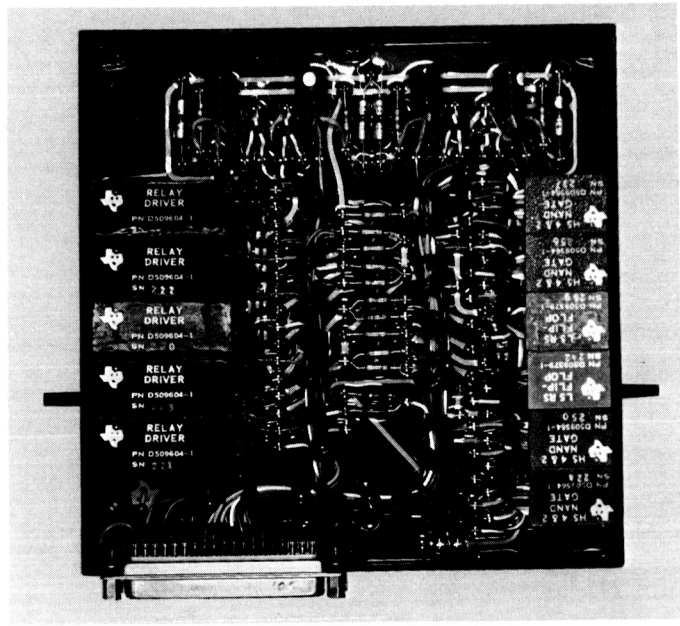


Fig. 130. Data encoder subchassis

All fabrication was accomplished in contractor cleanroom facilities, according to the applicable JPL specifications. Quality control inspection was made at various steps in the manufacturing process by both the contractor and JPL resident inspectors.

Electronics parts were selected from the JPL Preferred Parts List wherever possible; however, other parts had to be used in applications in which the Preferred Parts List did not contain the component with the desired characteristics. When available, parts were purchased under a JPL procurement specification by which the vendor performed the screening. These parts were screened as to proper operating characteristics by the contractor.

The majority of parts were purchased unscreened from the vendor, because of unavailability of procurement specifications. In the case of parts not having a screening specification, one was written by the contractor and approved by JPL. All parts used in the data encoder were screened per an approved specification.

G. Test Experience

The flight model data encoders passed the flight-acceptance tests. Only one problem was encountered during these tests: a loss of commutator synchronization during vibration. Failure analysis revealed a transistor in a clock driver circuit that had an extra lead attached to the base post in the transistor case; this lead, under vibration, was shorting to the case, producing a base-to-collector short. The module was replaced and the test was successfully completed.

The TA model experienced considerable difficulty passing the type-approval tests. The first problem was an oscillation that developed in the constant current supply under vibration and low temperatures. This was cured by adding capacitors between the power lines and the ground. The next problem occurred when an uncased capacitor in a bucking supply developed a partial short during the humidity test. The capacitor was replaced.

During the second complex vibration test, it was noted that the low-level channels exhibited a slight offset. This effect was traced to a pair of ceramic capacitors in the low-level amplifier, which, when vibrated, produced a small voltage due to the piezoelectric effect of the ceramic. This voltage was then amplified by the low-level amplifier, producing the offset. This was not a failure, but was recognized as characteristic of the unit.

Type-approval testing of the unit was terminated after the unit had successfully passed all environmental tests but the humidity test. During the humidity tests, it was observed that water was condensing throughout the data encoder, forming high-resistance paths across components as they were covered with water. It was decided that, because such an environment would never be encountered by the unit, the humidity test would be waived.

H. System Performance

Up to the midcourse maneuver, the *Mariner IV* data encoder performed flawlessly with one exception: the "deck skip" problem, discussed previously, did occur several times (three hours after launch, and again occasionally until December 7, 1964). The L + 3 hr occurrence has not been definitely explained, although all deck skips subsequent to that time have been correlated with high-voltage arcing in the Solar Plasma Probe.

XII. SPACECRAFT SUBSYSTEMS: ATTITUDE CONTROL

A. Purpose and Description

The functions of the attitude control subsystem are related to the several modes of operation of this subsystem. During the acquisition and cruise mode of operation, the function of the subsystem is to establish and maintain three-axis stable orientation of the spacecraft so that the sensitive surface of the solar panels faces the Sun, and the Canopus sensor views the star Canopus. With this orientation established, the fixed-position communications high-gain antenna should point toward the Earth during the latter portion of the flight.

During the midcourse maneuver mode, the attitude control subsystem has to orient the spacecraft so that the thrust vector of the onboard rocket motor is aligned to some predetermined direction in space. It has to maintain this orientation during the motor burn period and then re-establish the cruise orientation.

The spacecraft body axis system is shown in Fig. 131. Positive pitch, yaw, and roll turns are defined.

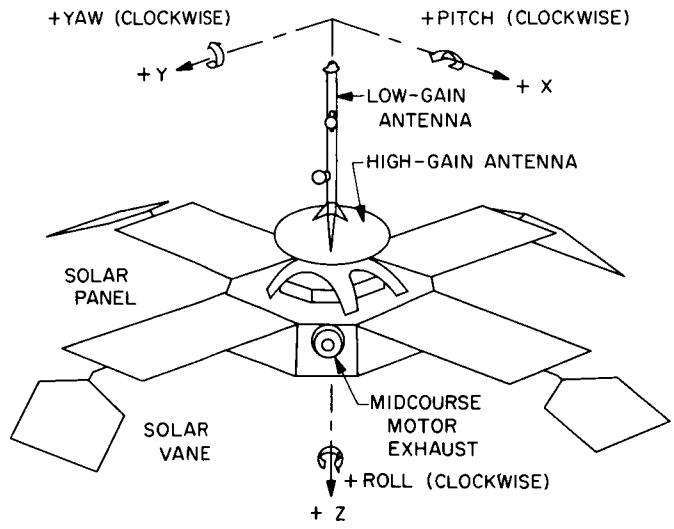


Fig. 131. Spacecraft coordinate system

1. Acquisition and Cruise Functions

After the spacecraft was injected into its heliocentric trajectory, it established the three-axis cruise orientation. This process began when attitude control dc power was switched on. Angular position errors about the pitch and yaw axes were sensed by Sun sensors. Rotation rates about all three axes were sensed by three single-degree-of-freedom gyroscopes. Both rate and position were used as inputs to switching amplifiers, which switched power to gas jet actuators when the sum of the inputs exceeded a certain deadband value. These actuators operated gas jets that released nitrogen, and caused torques on the spacecraft so that the pitch and yaw rate and position errors were reduced to limit cycle values. The roll rate was fixed at a constant spin level that was used to calibrate the science magnetometer at that time.

Roll acquisition began with CC&S command L-3 at L + 997 min. The roll rate was reduced to a search level and power was applied to the Canopus sensor. Roll angular-position error would be sensed when a body with a brightness of from ¼ to 8 times Canopus entered the field of view of the Canopus sensor. Once this illumination was sensed, the roll rate and roll position error were reduced to limit cycle values, and the three-axis cruise orientation was established. The gyros were turned off at that time and rate damping was provided by the derived rate signal fed back around the switching amplifier. The solar vanes, which had been turned on by command L-3, were then able to reduce the unbalancing solar torques, thus reducing the pitch and yaw limit cycle levels.

a. Attitude control cruise power. The cruise power for attitude control is the transformer-isolated 50-v-rms output of the main 2.4-kc inverter. This signal is rectified to provide the ±26 vdc, which is routed to the CC&S for attitude control command switching. The Canopus sensor supplies a 25-vdc signal to the CC&S for Canopus-sensor cone-angle updates.

b. Sun sensors. The cruise and acquisition Sun sensors are the position-sensing elements in the pitch and yaw cruise attitude control loops. Power to the cruise sensors is provided by the ±26-vdc signals, routed through two relays, and a regulator, which reduces the signals to ±16 vdc. The first relay supplies sensor power upon receipt of the attitude control power on command. The second relay turns the sensor power off during a midcourse maneuver. The cruise Sun sensors are oriented so that their null axes point in the direction of the spacecraft negative roll axis.

Power to the acquisition sensors is provided by the ±26-vdc signal, routed through the above two relays, and a third relay, which is controlled by the Sun gate.

(The Sun gate keeps the power to the acquisition sensors on during Sun acquisition.) The acquisition sensors are positioned so that the Sun will always be visible to at least one set of sensors during acquisition. This gives the sensors a 4π sterad (complete sphere) field of view. Power to the acquisition sensor is switched off when the Sun-gate sensor is looking at the Sun.

The Sun sensors consist of a photoresistor mounted beneath a shadow mask. The sensors are connected in pairs so that the output is a dc signal proportional to the angular deviation of the sensor axis from the line of sight to the Sun (Fig. 132). The sensor polarity is such that a positive pitch (or yaw) rotation of the spacecraft from its null position gives a negative voltage.

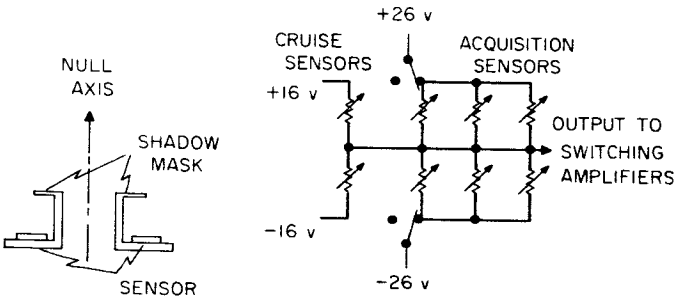


Fig. 132. Sun sensors

c. Sun gate. The Sun gate is used to determine when the spacecraft has acquired the Sun. The Sun-gate sensor is a set of photoresistors masked so that they are sensitive to spacecraft cone angle but insensitive to clock angle. The sensor will turn off the gate signal when the negative roll axis is within approximately 2½ deg of the Sun line.

The Sun-gate signal holds the power to the acquisition Sun sensors on and holds the Canopus sensor power off. When the signal disappears, power is switched from the acquisition Sun sensors to roll–search logic. The gate signal holding the Canopus sensor power off is also removed.

d. Canopus sensor. The Canopus sensor is the position-sensing element in the roll attitude control loop. Power is provided by the 50-v-rms signal from the main 2.4-kc inverter. This power is switched to either the sensor electronics or the Sun shutter. When the electronics are on, the shutter is off. The Sun shutter protects the sensor from the damaging effects of very bright objects when the sensor's electronics are off. The sensor electronics are held off by the Sun-gate signal, CC&S command M-2, DC-18, DC-20, or by CC&S command L-3 before it has occurred.

The position of Canopus is described by its cone angle from the Sun and its clock angle about the spacecraft–Sun line (defined as zero with the clock angle of all other objects measured from Canopus). The sensor has a field of view of approximately 11 deg in cone and 4 deg in clock. The 11-deg field of view in cone is repositioned electronically to follow Canopus through a total excursion of 28 deg. These cone-angle changes are commanded by the end counter of the CC&S and are backed up by DC-17. Each CC&S or DC-17 command will change the cone angle one increment of 4.6 deg cyclically.

e. Roll-search logic. The roll–search logic provides the spin and search signals used in the roll attitude control channel. The ±26-vdc power is provided when this power is switched from the acquisition Sun sensors.

When the Canopus sensor is off, the spin signal is made available to the roll-axis control system. When this negative signal is switched into the roll switching amplifier, the spacecraft establishes a negative roll rate of approximately 3.5 mrad/sec. This is used for calibrating the science magnetometer. When event L-3 occurs (L + 997 min), the spin signal is permanently disabled.

When the Canopus sensor is on, the search signal is made available to the roll switching amplifier. This negative signal establishes a spacecraft roll rate of approximately 2.0 mrad/sec. When an object has been acquired, the search signal still exists but is no longer input to the switching amplifier.

A signal from the roll negative-torque gas jets is fed back to the roll–search logic. If the negative-roll jets stay on for more than approximately 30 sec, the search signal will be inhibited. Thus, if the roll gyro malfunctions and fails to null out the search signal being fed into the switching amplifier, the search signal will be switched off after 30 sec to prevent the spacecraft from spinning up to damaging rates. This inhibit may be reset by the use of DC-21.

f. Canopus gate. The Canopus gate is used to switch the roll-axis control system from the search to the acquire mode. The ±26-vdc power used comes on when the attitude control power goes on at separation. Both the acquire signal and the roll error signal from the Canopus sensor are input to this gate. When the acquire signal is received, and if the roll error signal is negative,

the Canopus gate will switch a relay causing the roll error signal to be input to the roll switching amplifier in place of the search signal. The signal that holds the gyros on is removed by this relay at the same time. A check of the roll error-signal polarity prevents reflections of very bright objects from being acquired that are within the acceptable intensity range but with inverted roll error signals. Acquiring a very bright object with an inverted error signal would cause the spacecraft to go into a high-velocity limit cycle with rapid gas consumption. If the acquire signal goes off, the gate will reset the relay, switching the search signal into the roll switching amplifier and providing a turn-on signal for the gyros.

g. Gyros. Three single-degree-of-freedom gyros provide the rate error signal to the pitch, yaw, and roll attitude control loops. Power for the gyro motors is supplied by the three-phase 400-cps inverter. Power to the amplifiers in the gyro loops is provided from the maneuver 2.4-kc inverter. All gyro power is held on by the gyro switch control, which may be triggered by any of several signals. During launch the switch is held on by attitude control power through CC&S command L-2 and the gyro arming switch. When either of these opens, this power is removed. When the relay controlled by the Canopus gate is in the search mode, a signal is routed to the gyro switch control. In addition, CC&S command M-1 or M-2, or DC-18 will hold the gyros on. The switch control has a 200-sec delay in turning off, allowing part of the roll rate to be damped out when the Canopus sensor acquires a body and switches off the signal to the gyros.

When used during acquisition, all gyros have an output to the switching amplifiers that is proportional to the sensed spacecraft angular rate. For a positive rotation rate, the output to the switching amplifier is a negative dc signal. The gyros are turned off after Canopus has been acquired and are not used during cruise. They are next used during the midcourse maneuver.

h. Switching amplifiers, derived rate, and gas subsystem. The switching amplifiers used the position and rate error signals during acquisition to control gas-valve actuators. Both ac and dc power is provided by the main 2.4-kc inverter. The switching amplifiers begin operation when the attitude control dc power is switched on at separation.

A deadband is provided so that the gas jets will not be on continuously. The amplifiers have a minimum on-time characteristic (20 msec) that controls the size of the nominal limit cycle. The gas-valve actuators open the valves to the gas jets that release nitrogen. The gas system consists of two independent gas supplies and sets of jets. Thus, if one jet should stick open and exhaust the nitrogen supply in one bottle, there will still be enough nitrogen left in the other bottle to perform the necessary attitude control functions.

The configuration of the switching amplifiers and gas jets is such that a positive signal into the switching amplifier, above the deadband level, causes the gas jets, which apply a positive restoring torque to the spacecraft, to open. Thus, if the spacecraft makes a negative rotation from its null position or if a negative rotation rate exists, a positive signal is sent to the switching amplifier, and causes a positive restoring torque.

Since the gyros are switched off after Canopus acquisition, their rate error signal is not available to the switching amplifiers during cruise mode. Rate control is provided by the derived-rate feedback signal around the switching amplifier. The behavior in the phase plane is shown in Fig. 133.

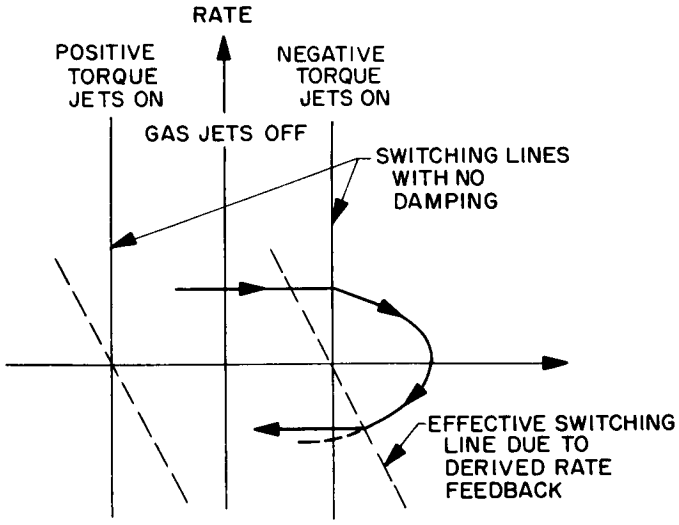


Fig. 133. Derived rate damping in the phase plane

The switching line without derived rate is vertical. When the switching amplifier power switch activates the gas jets, the derived-rate compensation essentially integrates this signal and feeds it back to the input. Due to the sign inversion in the switching amplifier, the feedback signal is opposite in polarity to the position-error input. Therefore, the switching amplifier will turn off sooner with the feedback than it would without it, and will introduce damping into the control loops as shown in the figure.

i. Solar vanes. The *Mariner* Mars 1964 spacecraft is equipped with reflective vanes that adjust to balance the solar torques and reduce the pitch and yaw limit cycle size to within the switching amplifier deadband during cruise. The ±26-vdc power for the adaptive balancing system is turned on by the CC&S L-3 command at L + 997 min.

After the solar vanes are extended, the firing of the gas jets balances the vane positions. The firing of one opposing jet more than the other indicates an external torque imbalance, and the vanes are stepped with each jet firing to counteract this imbalance. This continues until the opposing jets are pulsing with equal frequency, signifying a balanced condition. At some time after a near balance condition is attained by the gas-jet system, the solar vanes provide thermal damping to force the spacecraft to a near null condition within the switching amplifier deadband. The damping is provided by thermal actuators that draw no power. This balanced condition continues as long as no rapid changes in the external torque conditions occur.

j. Earth detector. The Earth detector is used to verify the acquisition of Canopus after the roll search is completed. If Sun and Canopus acquisition are accomplished, the detector will sense reflected sunlight from the Earth during the early parts of the flight. The detector's field of view is 83 deg in cone and 26 deg in clock, which is designed to cover the change in direction from the spacecraft to Earth due to differences in individual trajectories.

The Earth detector consists of a photocell in series with a fixed resistor, both of which have 26 vdc applied across them. The voltage across the fixed resistor changes in relation to the light received by the photocell. This voltage, indicating light flux, is telemetered whenever the gyros are off.

k. Narrow angle Mars gate. The narrow angle Mars gate performs the important function of backing up the TV planet acquisition signal to stop platform scan. It is mounted on the spacecraft to indicate when Mars is in the field of view of the Mars gate sensor near encounter. It is powered by the science DAS, and its signal is used by this subsystem for science switching purposes near encounter.

2. Maneuver Functions

Errors during injection guidance may cause the actual trajectory of the spacecraft to differ from the nominal trajectory. If this difference is large enough, a midcourse maneuver is required to correct the miss distance. *Mariner* Mars 1964 is capable of two midcourse maneuvers.

The function of the attitude control subsystem during the midcourse maneuver mode is to orient the thrust vector of a body-fixed rocket motor to some predetermined direction in space. To do this, the spacecraft has to perform a pitch and roll turn in sequence as controlled by the CC&S. This orientation is maintained during motor burn by controlling the thrust vector to pass through the spacecraft CG with an autopilot. After the maneuver, the spacecraft returns to the cruise orientation.

a. Attitude control maneuver power. The same power sources used in the acquisition mode are used during the midcourse maneuver. The gyro power is switched on by CC&S command M-1. The three-phase 400-cps inverter supplies power for the gyro spin motors. Power for the gyro amplifiers, command current regulator, roll one-shots, and midcourse autopilot is provided by the maneuver 2.4-kc inverter.

Attitude control plus 26-vdc power are provided to the CC&S so that it may be switched back to the attitude control by CC&S commands. The maneuver may be stopped by switching off this power to the CC&S with DC-13.

b. Rate and position of gyros. The gyros warm up for 60 min after the midcourse sequence is begun by CC&S command M-1. The M-2 CC&S command then switches power off to all the Sun sensors and switches capacitors into the feedback loop of all three gyros. These capacitors then integrate the sensed rate to give a position error signal. Thus, the gyros provide rate plus position error signals to the switching amplifiers for the remainder of the maneuver.

The pitch turn begins with the M-4 event, which occurs simultaneously with M-2. The turn is accomplished by switching a constant current from the command current regulator into the gyro torquer. The CC&S polarity relay M-3 selects the proper polarity current. A positive current causes a negative spacecraft turn, and a negative current causes a positive spacecraft turn. When the current is first applied to the torquer, the gyro senses the error signal and applies it to the switching amplifier. The gas jets fire until the resulting spacecraft rate nulls the torquer signal. The spacecraft then continues to turn at this constant rate as long as the

torquer current is applied. After a period of time specified by the stored pitch command, the CC&S switches off this current. Since the torquer signal due to the command current is no longer present to null the sensed rate, the gas jets operate to reduce the pitch rate and position errors to small limit-cycle excursions about the new pitch position.

The roll turn is initiated by CC&S event M-5, and is performed in a manner similar to the pitch turn. Command current, whose polarity is controlled by the CC&S polarity relay M-3, is input to the roll torquer. The new pitch and roll positions are maintained for the remainder of the maneuver.

During the motor burn, which begins with CC&S event M-6, the gyro signals act through the autopilot amplifiers to continuously adjust the jet vane angles within the rocket nozzle. This angle adjustment controls the torques generated by the motor thrust so that spacecraft attitude is maintained during burn. Although the gyro signals are sent to the autopilot during the turns, the autopilot has no effect on the spacecraft attitude until the midcourse motor ignites.

The maneuver sequence is terminated when the CC&S M-1 and M-2 relays are reset. The gyros remain on, however, since the Canopus sensor is off. When M-2 is reset, Sun sensor power is applied again and normal Sun reacquisition begins. The gyros turn off 200 sec after the Canopus sensor acquires an object.

c. Capacitor cycling. Before the capacitors are connected into the gyro loop, they are in an unenergized portion of the gyro circuitry for an extended period of time. In this configuration, they tend to lose dielectric strength, which precludes their proper functioning when connected into the gyro loop. In order to correct this difficulty the capacitors are temporarily connected in series between +35 vdc and −35 vdc and then reconnected in the parallel configuration. This cycling process results in a "reforming" of the capacitors and occurs immediately after gyro turn-on for approximately 12 sec. If DC-18 is used to turn on the gyros, the cycling does not occur. The cycling circuitry is switched out of the loop by CC&S M-2 so that a failure in its circuitry does not affect the maneuver.

d. Roll one-shots. The roll one-shots are emergency circuits controlled by DC-18 and DC-21 commands. If the Canopus sensor fails, the roll position may be controlled by switching the capacitor into the roll gyro feedback loop using DC-18. Vernier control may be obtained by using the roll one-shots. The 2-deg one-shot, triggered by DC-18, will switch a positive command current into the roll gyro torquer for a time equivalent to a 2-deg roll turn. The −2 deg one-shot, triggered by DC-21, will switch a negative command current into the roll gyro torquer for a time equivalent to a −2 deg roll turn. The spacecraft will not perform the −2 deg roll turn unless the capacitor has previously been switched into the gyro loop by DC-18.

e. Autopilot. The midcourse autopilot is used to control the attitude of the spacecraft during midcourse motor burn. This control is accomplished by continuous adjustment of the angular positions of four jet vanes mounted at the downstream end of the midcourse motor nozzle. Since the motor is not mounted along any of the spacecraft body axes, the motion of each jet vane is controlled by a mixture of the signals of the three gyros. Figure 134 shows the orientation of the spacecraft midcourse motor and the jet vanes.

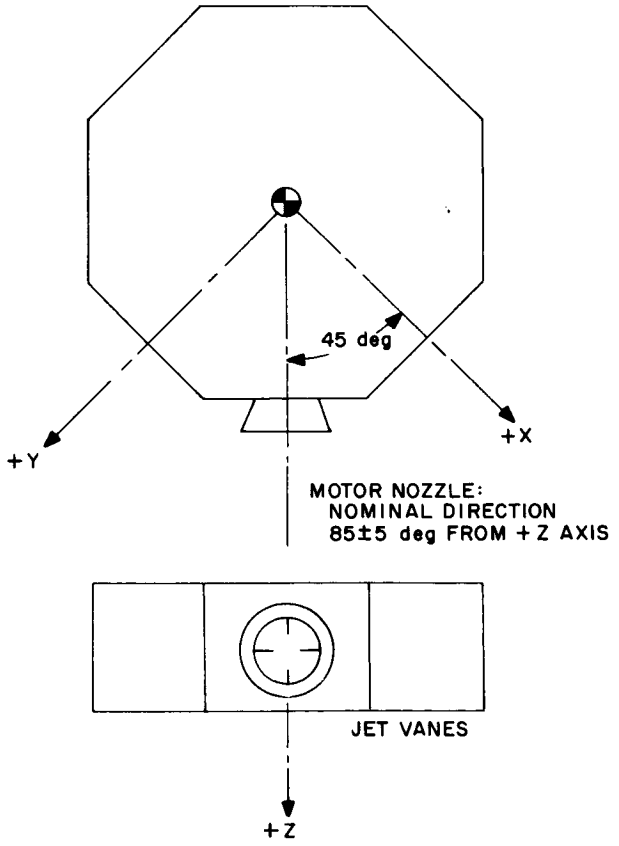


Fig. 134. Midcourse motor and jet vane orientation

Each jet vane has its own separate control system, consisting of an autopilot amplifier, a jet vane actuator and a feedback loop. Power to the autopilot is provided by the maneuver 2.4-kc inverter, and is switched on by the CC&S M-2 event. The three gyro signals and the feedback signal are summed in different ratios at the input to each amplifier. The jet vanes are then adjusted so that the motor thrust vector passes through the spacecraft CG, thus nulling the gyro error signals.

3. *Mariner* Mars 1964 Cruise Attitude Control Subsystem Definition

The functional mechanization of the *Mariner* Mars 1964 attitude control subsystem is shown in Fig. 135. The following discussion describes the functions of the various commands and sequence of operations during the flight.

a. Functions of CC&S commands. The functions of the CC&S commands are:

1. The L-2 command is the main power signal that energizes the attitude control subsystem after *Agena D*/spacecraft separation. Once power is applied to the subsystem, it remains on throughout the balance of the mission. This is a timed command in the CC&S sequence. (Prior to separation, power is applied to the gyros through this relay; hence, the gyros are on from launch.)

2. The M-1 command is issued approximately 1 hr before the midcourse command to permit gyro warmup and temperature stabilization, and remains activated throughout the entire maneuver period. It actuates the gyro control relay and thereby applies gyro loop power.

3. The M-2 command is the inertial mode command signal, which is derived from the CC&S, and is applied throughout the entire maneuver period. As an application of the command, the star sensor and roll–search command are disabled, the pitch and yaw sensor error signals are replaced with the gyro signals, and the autopilot is energized. This command also places the pitch, yaw, and roll gyros in the integrating gyro.

4. The M-3 command sets the polarity of the command to be executed by the M-4 and M-5 commands.

5. The M-4 and M-5 command signals apply torquing current to the gyros during maneuver turning periods, and determine the length of time the command is applied. These command polarities and times are computed on the ground from trajectory observations, are transmitted to the spacecraft, and are stored in the CC&S prior to the execution of the command.

6. The MT-1, MT-2, MT-3, and MT-4 commands are sent during flight to update the Canopus sensor cone angles as a function of the trajectory.

b. Functions of attitude control relays. The functions of the attitude control relays are:

1. The gyro control relay switches power to the gyros, grounds the output of the switching amplifier compensation networks, and controls the three-phase gyro spin motor power inverter. It is actuated by M-1, L-2, and the Canopus acquisition gate through diode logic.

2. The Canopus acquisition gate relay is a latching-type relay that is actuated through diode logic by the roll override ground command and the Canopus gate signal. The gate relay is reset when attitude control power is turned on. The gate channel applies a positive pulse through the inversion amplifier to the gate relay when the Canopus sensor has acquired the star. Upon loss of Canopus acquisition, a negative pulse is applied to the gate relay through the inversion amplifier, which transfers the roll input of the switching amplifier from the Canopus sensor roll error signal to the search command signal. Also, the acquisition gate relay supplies a command signal to turn on the gyros whenever the Canopus sensor does not have star acquisition. The roll override signal is capable of overriding the Canopus acquisition signal in the event that the wrong object is acquired. This command only transfers the acquisition gate relay from the acquired state to the unacquired state.

c. Functions of discrete (ground) commands. The functions of the discrete commands are:

1. The DC-13 command provides the capability of inhibiting all CC&S maneuver commands and permits normal automatic attitude control operation despite any type of CC&S failure.

2. The DC-14 command provides the reset of DC-13 to return the attitude control subsystem to CC&S control.

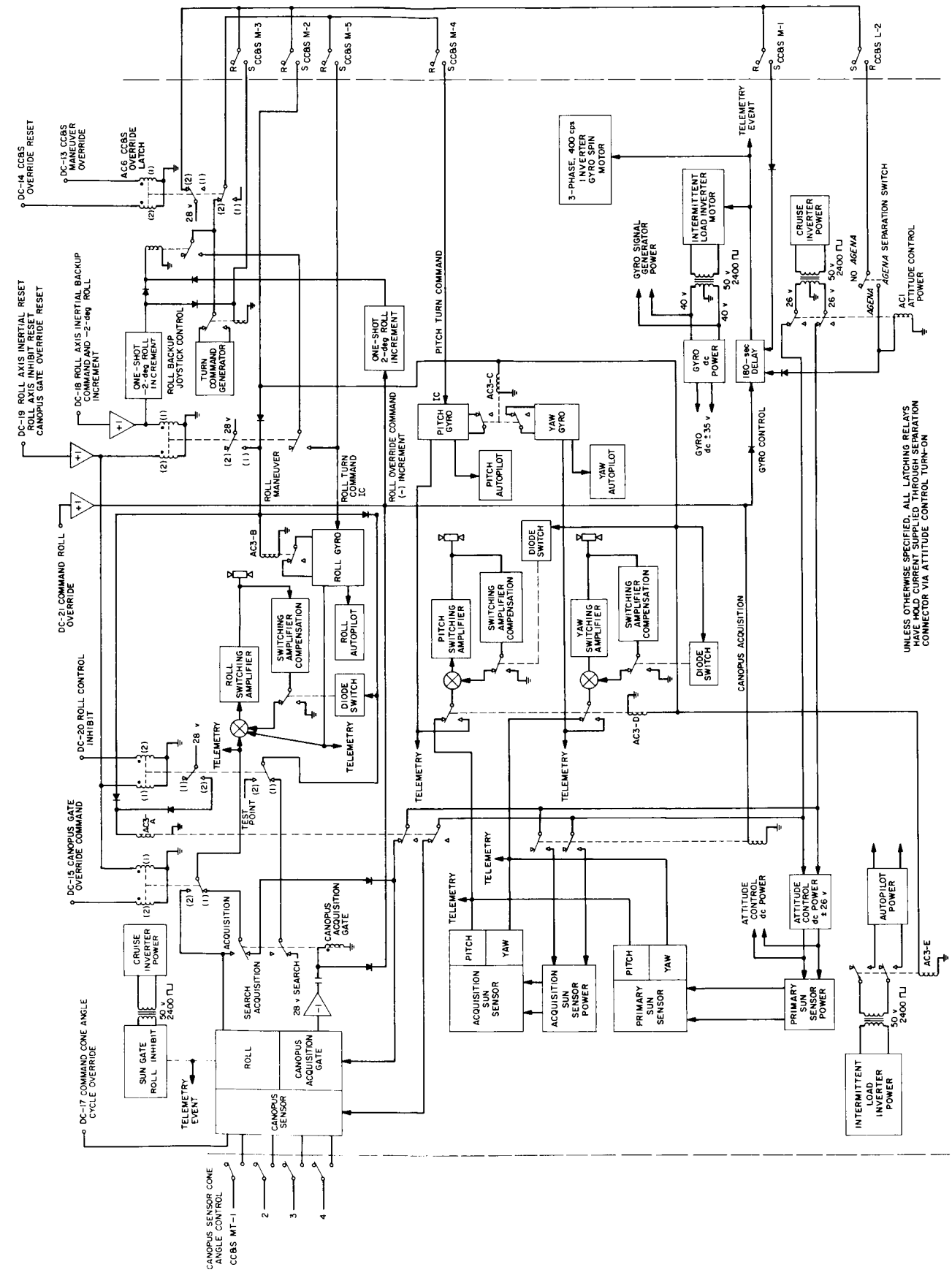


Fig. 135. Attitude control subsystem functional block diagram

3. The DC-18 command places the roll axis under inertial control and commands a negative increment in roll position (if the same command has previously been received). The command turns on the gyros, turns off power to the Canopus sensor, places the roll gyro in the integrating mode, and commands a standard rate turn in the positive direction for a fixed time. This command is also used to provide backup (redundant) roll stabilization in the event of a Canopus sensor malfunction or if other than normal roll position is required at any time.
4. The DC-19 command returns the roll axis to normal automatic optical control. It resets commands DC-17, DC-18, and DC-20.
5. The DC-20 command provides the capability of disabling roll axis control completely. In the event of a Canopus sensor malfunction early in flight, the inertial backup mode could not provide the required operational lifetime; therefore, the command would enable the gyros to be turned off by disabling the Canopus sensor and star gate logic.
6. The DC-21 command provides the roll acquisition override command if DC-18 has not previously been received, or commands a negative roll position increment if DC-18 has been received. In the first case, DC-21 forces the roll axis to reject a previously acquired object and search for a new object. In the latter case (DC-18 previously received), the command provides incremental ground control for the roll axis of the spacecraft (positive increment roll position).
7. The DC-17 command enables the Canopus sensor cone angles to be set during flight in the event of a CC&S malfunction.
8. The DC-15 command is the Canopus sensor brightness gate override. It provides the capability of allowing the Canopus sensor to acquire any celestial object of sufficient brightness to give an output.

d. Sequence of operations. Several sequences of operation take place in the attitude control subsystem. These may be summarized as follows:

1. Initial Sun and Canopus acquisition
2. Midcourse maneuver
3. Reacquisition after midcourse maneuver
4. Reacquisition in case of a noncatastrophic disturbance
5. Roll override
6. Roll inertial backup
7. Canopus gate override command
8. CC&S override command
9. Solar pressure control of Sun-line attitude control.

A detailed description of the sequences is given in Table 36.

B. System Design Considerations

1. Pitch and Yaw Acquisition and Cruise

a. Derived-rate acquisition. Derived-rate compensation for attitude control was very successfully used for cruise operation on the *Mariner II* spacecraft. Nevertheless, gyros were used for acquisition. On the other hand, one of the advantages of derived rate is the fact that it is a passive compensation scheme and does not require actual rate feedback through gyros. Therefore, if derived rate could be used for acquisition as well as for cruise, the control system would be simpler and more dependable. Since derived rate does not use actual rate information, these advantages would be bought at the expense of efficiency; i.e., more gas consumption and longer acquisition time. Consequently, a study was made of acquisition characteristics of a derived-rate system, as especially applied to the pitch and yaw systems on the *Mariner* Mars 1964 spacecraft.

On the basis of this study, it was concluded that derived-rate acquisition on more than one axis at a time would be undesirable. It was decided that it would be necessary to use gyros for rate information during acquisition and to have the gyros switched off after a 200-sec time delay following star acquisition in the roll-axis control system. This was similar to the *Mariner II* system.

b. Final pitch and yaw acquisition system. Once it was determined that it was necessary to use gyros for acquisition, the system was optimized for that configuration.

In order to promote reliability, it was decided to have the derived-rate feedback hard-wired so that it was in the system at all times. The derived rate was then considered to be primarily for cruise operation with only limited capability for acquisition performance in the event of a gyro failure. But since the derived-rate signal is in at all times, it tends to degrade the acquisition performance with rate feedback from the gyros. This is due

Table 36. Attitude control subsystem sequence of operation

Operation	Initial condition	Sequence	Description
Initial Sun and Canopus acquisition	Derived rate feedback is in pitch and yaw and rate feedback from gyro are in roll. (Gyro control is actuated by AC1 at launch.) Sun sensor error signals (AC3-D) are switched in. Star gate acquisition relay is in search position. Secondary Sun sensors (AC4) are switched in.	Sun acquisition Canopus acquisition	L-2 turns on power to the control system. Sun sensors start pitch and yaw acquisition. L-2 remains set throughout flight. Gyros have been on since launch. At the L-2 event, roll—search begins, and the Canopus sensor is activated. Canopus falls into the field of view of the Canopus sensor and activates the star acquisition gate, which switches from the roll—search command to the roll error signal from the Canopus sensor. The star acquisition gate also deactivates the gyro control, which transfers the roll axis system to derived-rate control from gyro control and turns off secondary (acquisition) Sun sensors.
Midcourse maneuver	Sun sensors and Canopus sensor are controlling spacecraft attitude. Control system is in derived-rate mode (pitch, yaw, and roll axes).	Commanded turn	M-1 activates the gyro control 1 hr prior to this sequence, which turns on the gyros and supplies gyro rate feedback for the roll axis. (Replaces derived rate damping.) M-2 switches out Canopus sensor power (AC3-A) and search command power; transfers from optical sensor (AC3-A, AC3-D) to gyro control in the pitch, yaw, and roll gyros in the integrating mode (AC3-B, AC3-C). Event also applies power to the autopilot subsystem (AC3-E) to be used during motor firing. M-3 sets polarity of the turn to be executed in both roll and pitch axes. It is set or reset at the start of both the roll and pitch turns. M-5 switches in the command current to the roll gyro, and the timing of this command determines the magnitude of the roll turn.
Reacquisition after midcourse maneuver	Sun and Canopus sensor are switched out (M-2, AC3-D). Gyros are in integrating mode (AC3-B, AC3-C). Secondary Sun sensors are on (AC4). Gyros remain on due to Canopus acquisition gate signal applied to gyro relay.	Reacquisition	M-1 is opened. M-2 removes inertial hold mode and applies power to the Canopus sensor. Sun and Canopus acquisition proceeds as in Sun and Canopus acquisition sequence.
Reacquisition in case of a non-catastrophic disturbance	Sun sensors and Canopus sensor are controlling system. Control system is in switching amplifier compensation mode.	Following simultaneous loss of pitch, yaw, and roll control	Loss of roll control activates gyro control and turns on gyros through the Canopus acquisition gate. Secondary Sun sensors are activated by the acquisition gate, and roll axis is then under gyro rate damping in place of switching amplifier compensation. Roll search commences. Reacquisition proceeds as in Sun and Canopus acquisition sequences.
Roll override	Sun and Canopus sensors are controlling spacecraft attitude. Canopus sensor has acquired and is tracking the wrong object.	Roll—override command	DC-21 switches the acquisition gate relay to search position, which introduces search command. Gyros are turned on and search continues for a new object. Following acquisition of Canopus, Sun and Canopus acquisition proceeds as in Canopus acquisition sequence.
Roll inertial backup	Sun sensors are controlling pitch and yaw axes' attitude. Roll axis is uncontrolled due to star-sensor malfunction.	Inertial backup	DC-20 is sent to conserve gyro lifetime. DC-18 is initiated. Gyros are turned on and roll gyro is placed in the integrating mode. Spacecraft is under three-axis control and roll axis is controlled for communications by DC-18 and DC-21. Continuous correction for gyro drift and initial orientation is provided by DC-18 and DC-21.

Table 36. (Cont'd)

Operation	Initial condition	Sequence	Description
Canopus gate override	Pitch and yaw axes are controlled. Roll axis is in search mode and cone angle is at proper position. Intensity measurement of Canopus sensor indicates star acquisition; however, no acquisition event is indicated.	Canopus gate override command	DC-15 is sent when spacecraft roll orientation is near correct position. Canopus sensor acquires object and reduces roll rate, and gyros are shut off. Spacecraft is under three-axis control even though Canopus gate circuitry has failed.
CC&S override	CC&S fails to issue a command to attitude control or a malfunction of CC&S commands into the attitude control subsystem.	CC&S override command	Attitude control subsystem malfunction is due to CC&S malfunction. Command is issued and attitude control is removed from CC&S control. Attitude control subsystem is independent of CC&S commands. Canopus cone angles are set by DC-17.
Sun-line attitude control	Sun/Canopus acquisition is complete (cruise mode). Solar sails are erected at solar panel erection.	Solar pressure control	L-3 activates power to solar pressure control system. Solar pressure control system is in the adaptive mode to correct for center of pressure and CG offsets resulting in pitch and yaw torques.

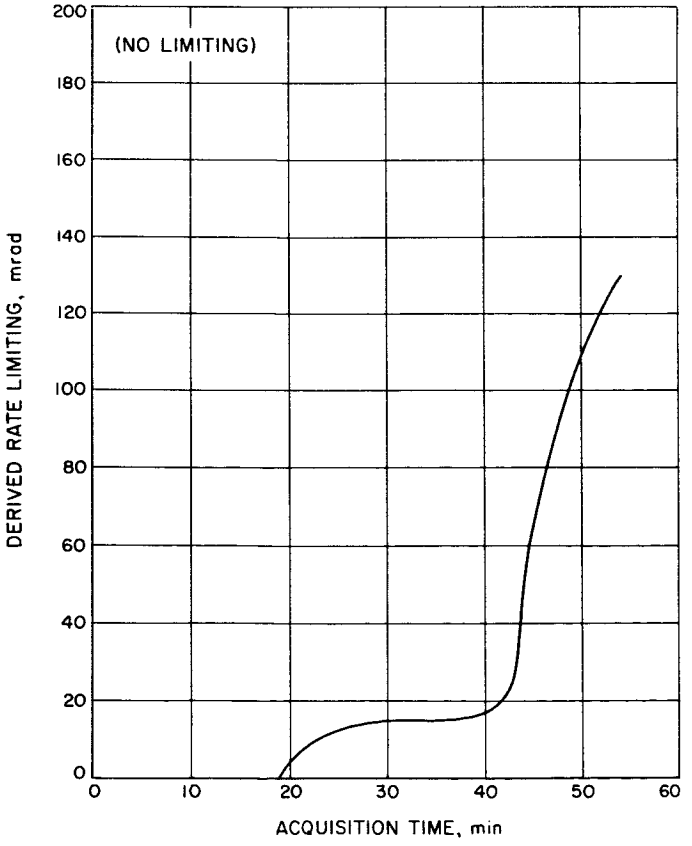


Fig. 136. Acquisition time vs derived-rate limiting

to the fact that the system normally switches on a rate-plus-position signal, but the derived-rate system switches on a position signal only. Therefore, the derived-rate signal is usually "bucking" the gyro rate signal. This effect could have been minimized by limiting the derived-rate output, but, since the minimum derived-rate gain is determined by the cruise requirements, it was necessary to limit the derived-rate signal by clipping at some desired level below which the derived rate would operate in the optimum cruise-mode fashion. An analog computer solution was run of acquisition time as a function of derived-rate limiting and the results are shown in Fig. 136. On the basis of the computer solution, it was decided to limit the derived-rate output to 9.0 mrad by clipping. Under these circumstances, the acquisition system was hardly affected by the presence of the derived-rate network.

The acquisition mode was optimized, with respect to the rate-plus-position feedback, with a rate-to-position gain of 7.0 sec. The limit-cycle mode could be optimized without regard for acquisition due to the derived-rate limiting, and the derived-rate parameters selected were as follows:

1. Unrestricted gain = 160 mrad
2. Limiting = 9.0 mrad

3. Charge time constant = 15 sec
4. Discharge time constant = −120 sec

2. Roll Acquisition and Cruise

The primary angular position reference used for *Mariner* Mars 1964 roll attitude control is the Canopus sensor. The roll-acquisition problem is an example of the general acquisition problem encountered when the position sensor used has a narrow field of view and produces no useful error signal outside the field of view. One solution of the problem is the generation of an artificial position error signal to be used when the star is outside the field of view.

a. Acquisition with reversible commanded search logic. In order to ensure acquisition from reasonable search rates (e.g., 0.2 deg/sec or greater) the reversible commanded search logic is used. If the polarity of the search command signal e_c is reversed at switch point S2, the spacecraft will roll in a direction so that the star is driven back into the field of view. The effect of the reversible commanded search logic is to provide an equivalent saturated position sensor characteristic outside the field of view. The mechanization shown in Fig. 137 uses the fact that the correct search polarity when leaving the field of view is always opposite to the polarity that drove the star into the field of view. The acquisition signal e_q is, therefore, used to change the state of the search polarity flip-flop. The polarity will then be correct when the star leaves the field of view.

A very definite possibility exists of the acquisition of an undesirable object. The roll-override command changes the relay to the search mode and resets the search-polarity flip-flop to a preferred state. Thus, the spacecraft always searches in the same direction until the next object is acquired.

b. Search command problems. Investigations revealed that the nature of the output from the star sensor created logic problems in the reversible commanded search system. The identification and acquisition of Canopus forms the major problem of roll-axis attitude control. The acquisition gate provides a logic signal that discriminates against objects that differ markedly from Canopus in brightness. However, false acquisition signals occur over an off-null angular region for a very bright object because the apparent brightness falls within Canopus brightness range. Extremely bright objects may also cause inverted phase error signals. If this is left uncorrected, the resultant roll motion may be a high-velocity limit cycle with very rapid gas consumption.

To avoid the problems presented by very bright objects causing inverted error signals, logic, in addition to

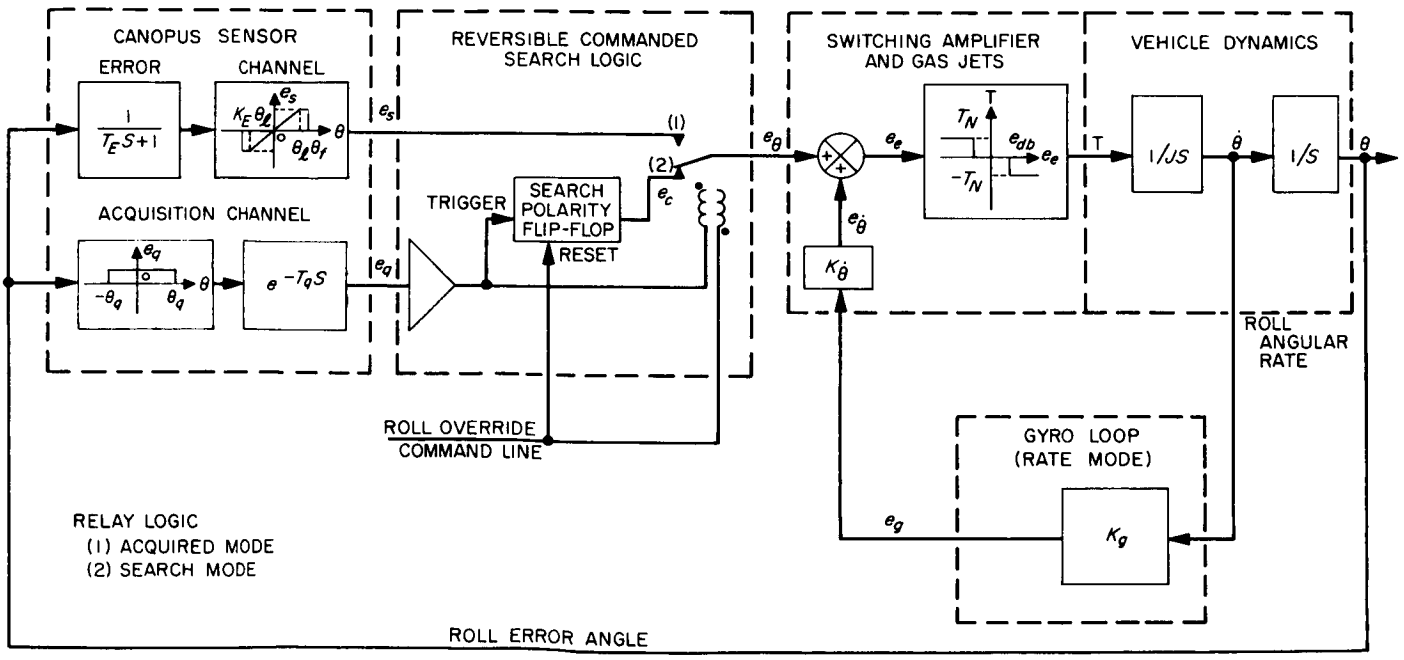


Fig. 137. Roll acquisition block diagram

acquisition signal, is required. The additional logic is based on inhibition of the acquisition signal by a roll-error-signal polarity detection. The mechanization is relatively simple and reliable using unidirectional roll search. Unidirectional roll search has inherent noise rejection properties; i.e., spurious acquisition signals and very narrow field-of-view objects are automatically rejected. Acquisition of Canopus with unidirectional search requires a ± 2 deg minimum field of view for Canopus brightness objects, a requirement feasible with the present Canopus sensor.

c. Roll attitude control subsystem description. The Canopus sensor provides two signals. The roll error signal e_s is proportional to the roll error angle θ over a range of $|\theta| < |\theta_l|$ and is constant for $\theta_l \leq |\theta| < \theta_f$. The acquisition signal is a logic signal that indicates when $|\theta| < \theta_f$. When the acquisition signal is true, the relay is in position (1) and position error information is obtained from the Canopus sensor; i.e., $e_\theta = e_s$. When the acquisition signal is false, the relay selects e_c as the artificial error signal. The voltage e_c causes the spacecraft to roll until the next acquisition. A rate-integrating gyro provides a rate measurement signal that sums with e_θ to form the error signal for the switching amplifier and attitude control gas jets.

d. False objects. The roll control system must have the capability of searching through the entire 2π rad of roll angle, rejecting objects that differ markedly from Canopus brightness. Canopus is identified by comparing brightness measurements of objects encountered during roll search with Canopus brightness. The acquisition signal consists of the upper and lower brightness gates summed in the sensor, and discriminates against objects that are too bright or too dim (Fig. 138). In Fig. 138(a), both gates, and, hence, the acquisition signal, are true in the shaded areas. The false object that is too dim causes no difficulty, as seen in Fig. 138(b). A false object that is too bright, however, qualifies the lower gate and upper gate in the region in which the apparent brightness is in the Canopus brightness range; thus, a false acquisition signal is present, as shown in Fig. 138(c). The situation is complicated by the possibility of inverted-phase roll error signals in the acquisition region. This phenomenon is due to reflections, and arises when extremely bright objects are encountered. The sensor signals for the inverted error signal case are shown in Fig. 139.

If the inverted error signal region is much smaller than the field of view of Canopus, roll motion will continue until the upper gate goes false. For a wider inverted error signal region, the motion will reverse, as in Fig. 139(a), and be driven to the initial acquisition line. Then the system will return to the search mode and the search signal will drive the object back into the field of view causing a limit cycle on the acquisition line. The too-bright, but not inverted, case is illustrated in Fig. 139(b).

Similar reasoning predicts a resultant high-velocity limit cycle that causes very rapid gas consumption because the jets are on almost continuously.

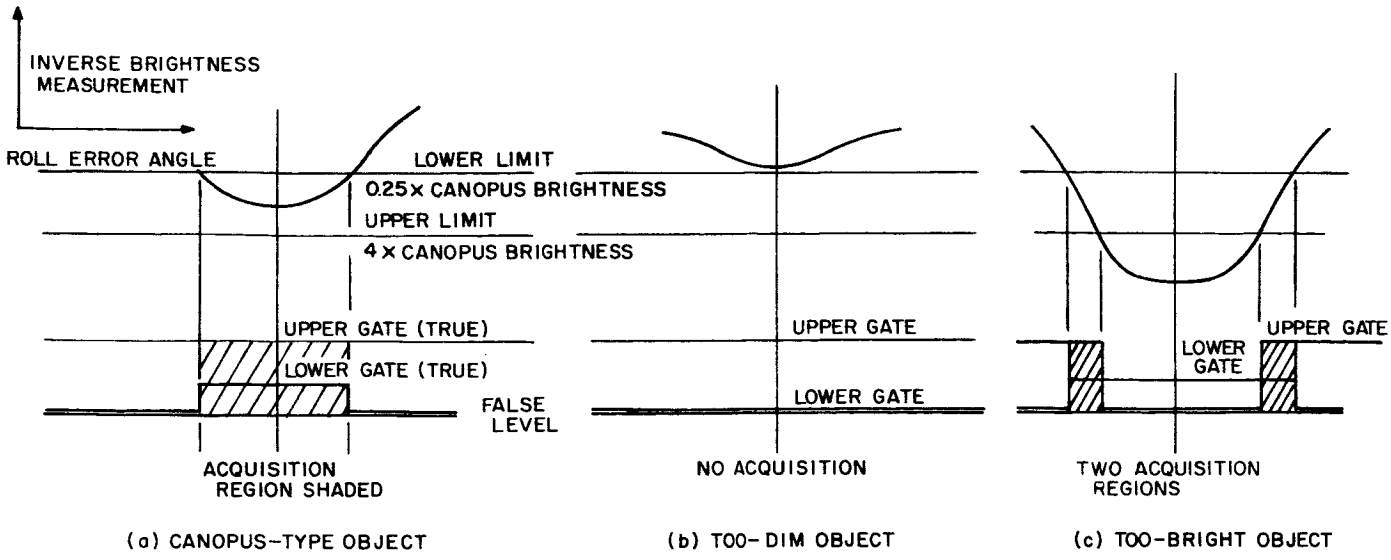
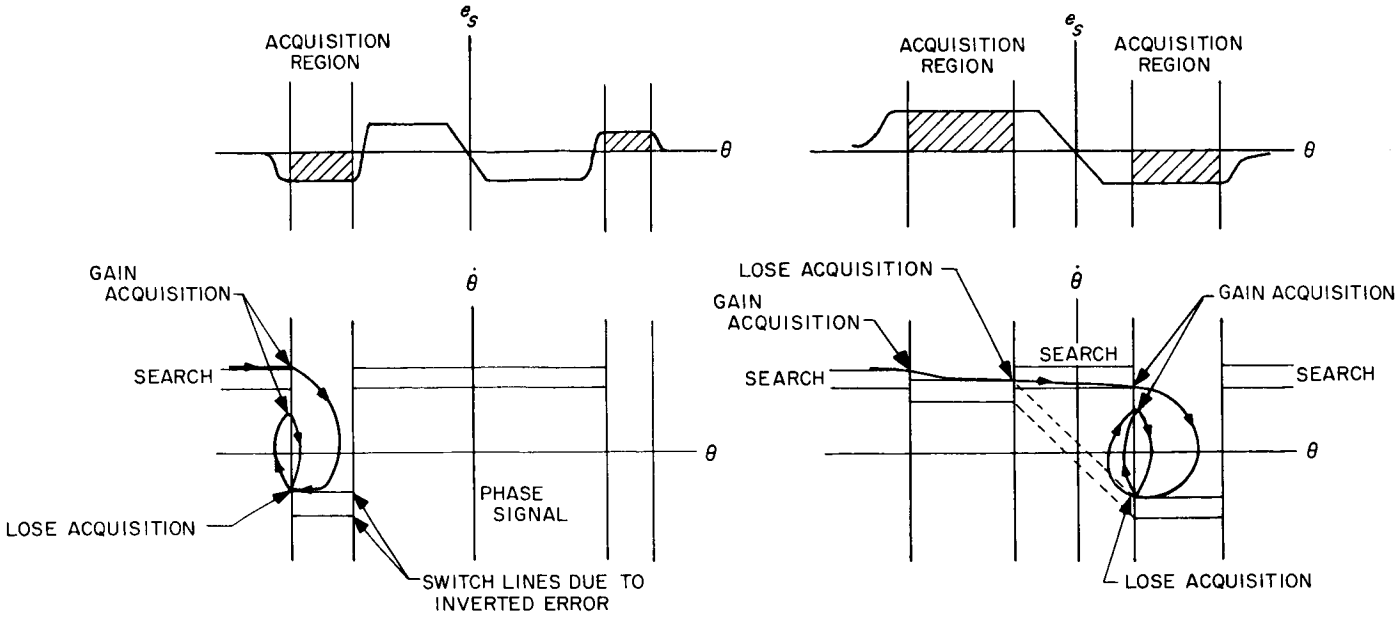


Fig. 138. Acquisition signal for various objects



(a) INVERTED PHASE ROLL ERROR SIGNAL (b) ROLL ERROR SIGNAL NOT INVERTED

Fig. 139. Behavior without error phase logic for a very bright object

e. Mechanization. The logic necessary to handle the too-bright object case is rather simple when unidirectional search is used. The mechanization is based on the fact that the roll error signal of Canopus has the same polarity as the search signal at the instant that the acquisition signal changes from false to true. Therefore, a detection of a wrong polarity error signal is used to inhibit the acquisition signal and prevent the change of state from search to acquired mode. Thus, the roll control loop will never see the inverted phase error signal and will continue to search; this case is illustrated in Fig. 140(a). The case of a too-bright object with proper polarity error signal causes no difficulty because the polarity detection logic will inhibit acquisition in the region where turn-around motion might occur; Fig. 140(b) illustrates this case.

The inhibit circuitry is quite simple; it consists of a transistor, which, when saturated by a proper polarity roll error signal, provides a path to ground when the mode relay is pulsed from search mode to acquired mode. Once in the acquired mode, the transistor is kept saturated by the signal that is present on the other pole of the mode relay. Thus, the loss of acquisition will not be inhibited from changing the mode relay state to search.

The unidirectional search mechanization automatically rejects objects whose brightness measurement is close enough to Canopus' brightness to qualify the lower gate over an angular region much smaller than the Canopus field of view. The deceleration is insufficient to remove the search rate in the angular region of acquisition and search resumes.

f. Roll acquisition without gyros. It was necessary to consider the ability of the roll control system to acquire with gyros in order to investigate how well the system could handle transients without losing acquisition and going into roll search. As a matter of course, this study indicated that the selection of the derived-rate parameters was primarily influenced by the transient reacquisition requirement.

Tests were conducted on a single-axis simulator using actual attitude control electronics and a Canopus sensor. One of the most significant discoveries was the fact that the Canopus-sensor time constant of 350 msec caused a significant degradation in the expected performance. This was due to the fact that the sensor signal lagged the derived-rate feedback so that there was virtually no damping. The problem was solved by increasing the derived-rate gain and decreasing the time constant. In order to improve limit-cycle performance, the discharge time constant was made to be twice the charge time constant. (The longer discharge time constant allows the feedback signal to remain in longer to prevent noise from

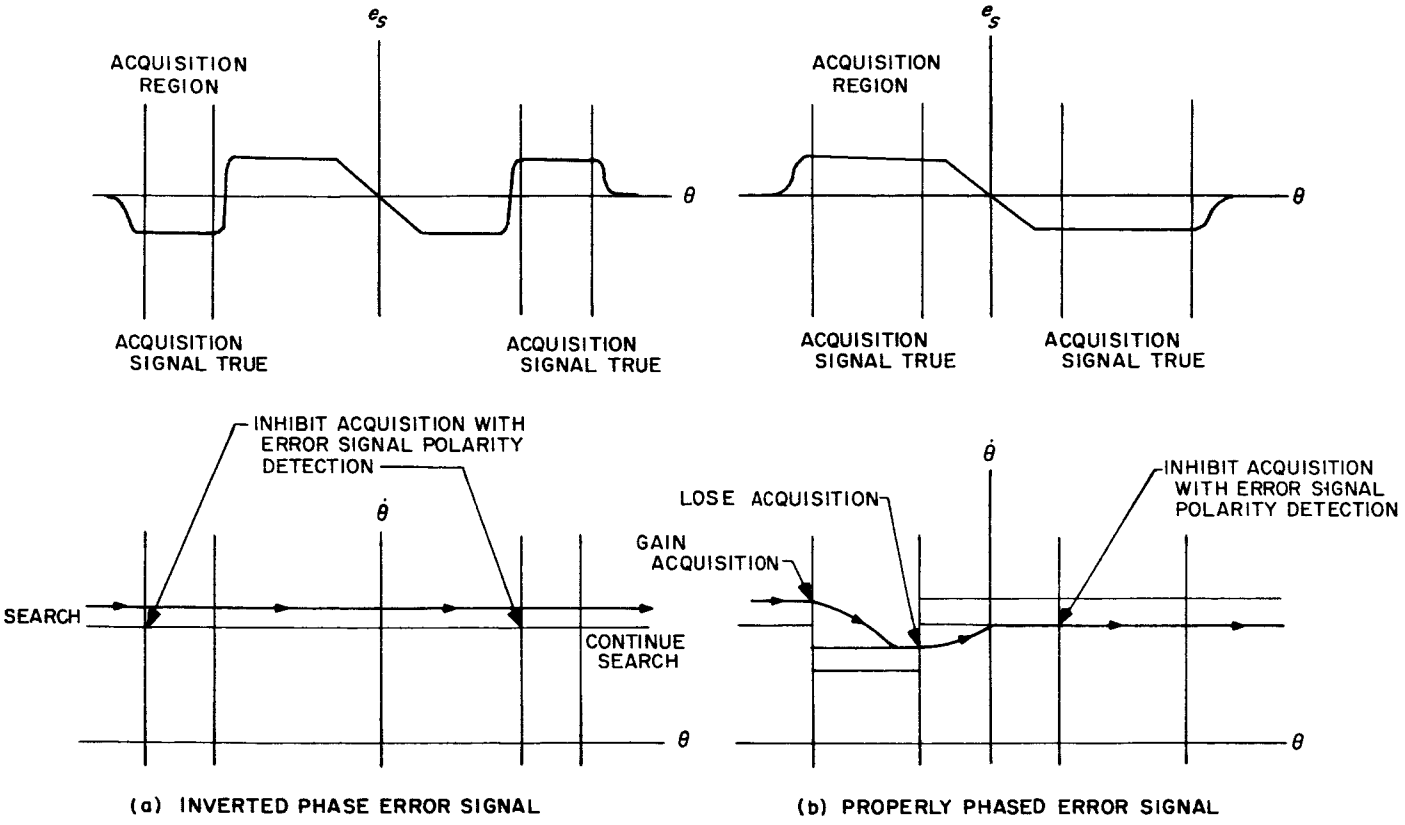


Fig. 140. Behavior with roll error signal polarity detection inhibit logic for a very bright object

causing double pulsing.) The final derived-rate parameters selected were:

1. Maximum (saturated) output = 320 mrad
2. Charge time constant = 9.0 sec
3. Discharge time constant = 18.0 sec
4. Derived-rate limiting = 30 mrad

With these parameters, the simulation with the Canopus sensor indicated that it was possible to acquire an object on derived rate with a rate as high as 4.9 mrad/sec. This capability was enough to handle any known transients.

3. Attitude Control Gas Requirement

The amount of attitude control gas to be stored on the spacecraft depended on the gas consumption during initial acquisition, maneuvers, reacquisitions, and cruise. Gas consumption during cruise required a predication of disturbance torques experienced during cruise. If the solar vane system functioned properly, then unbalanced torque and gas consumption during cruise would be very small. The gas system, however, had to be capable of performing the attitude control function without the aid of the solar vanes and despite any failures of the solar vane system that would produce large unbalance torques. The total gas weight stored was sufficient to accommodate solar vane system failures and redundant half gas system failures.

Gas consumption data during initial acquisition was obtained from computer studies of spacecraft dynamic behavior while the large initial tumbling rates were being removed. Gas consumption during reacquisition after maneuvers and disturbances would be much less than during initial acquisition, because the spacecraft rates to be removed would be much lower than initial spacecraft injection rates.

During midcourse maneuver, the commanded turns would require the spacecraft to accelerate from near-zero angular velocity to the commanded turning rate, and, at the completion of the turn, to decelerate to zero velocity. In general, the gain and removal of the turning rates would occur in both the pitch and the roll axes.

During the midcourse motor firing, the spacecraft attitude would be stabilized by the autopilot, but the attitude control gas jets would remain on.

Gas consumption during cruise would vary as a function of the type of disturbance present. The gas consumption would be dependent on the limit-cycle dimensions. A steady torque disturbance would tend to compress the limit cycle against one side of the deadband. Transient disturbances of non-zero average value would accelerate the spacecraft to much higher angular rates than nominal limit-cycle rates. At the edge of the deadband, these rates would be reduced by multiple pulsing of the gas jets with coasting motion between pulses until turn-around motion was achieved. The average effect of these disturbances would be very small compared to the effect of a steady torque imbalance.

The relative gas consumption was readily converted to gas weight consumed by use of a momentum balance equation. The specific impulse of the gas has a different value for continuous jet firing and for pulsed (pulse width < 0.1 sec) operation. All phases of the mission which incorporated derived-rate increment stabilization fell into the latter category.

Table 37 shows the *Mariner* Mars 1964 attitude control subsystem parameters and resultant gas weight conversions.

The *Mariner* Mars gas system was composed of two separate half systems with separate gas storage bottles so that a valve-open failure would not be catastrophic. The failed open valve would deplete the half system that supplied that valve, and, in addition, would deplete one-third of the gas in the other half system to offset the torque caused by the failed valve. Therefore, three times the estimated gas consumption had to be stored in addition to the predicted leakage per half system.

One of the main sources of unbalanced torques is the failure of a solar vane to erect. A single vane failure mode occurs when one vane fails to erect but the opposite vane adapts properly. The worst case occurs when

Table 37. Parametric summary

Parameter	Symbol	Units	Pitch	Yaw	Roll
Moment of inertia	J	slug-ft^2	60	60	104
Angular acceleration constant	α	mrad/sec^2	0.225	0.225	0.225
Effective moment arm	ℓ	cm	240	240	225
Gas specific impulse (continuous)	I_S	sec	60	60	60
Gas specific impulse (pulsing)	I_S	sec	35	35	35
Limit-cycle deadband	θ_{db}	mrad	8	8	4
Switch amplifier minimum on time	t_m	msec	20	20	20
Total mission time	t_t	days	200	200	200
Gas weight conversion (continuous)	W/t_{on}	lb/sec	3.2×10^{-5}	3.2×10^{-5}	5.5×10^{-5}
Gas weight conversion (pulsing)	W/t_{on}	lb/sec	5.5×10^{-5}	5.5×10^{-5}	9.5×10^{-5}
Unbalance torque conversion	$W/T_{D,\,avg}$	lb/dyne-cm	4.7×10^{-3}	4.7×10^{-3}	4.7×10^{-3}
Gas weight consumed	W	lb			
Initial acquisition			0.055	0.055	0.017
Maneuvers			0.005	0.004	0.009
Reacquisitions			0.030	0.030	0.011

NOTE: Noncruise total = 0.215 lb
Leakage per half system = 0.375 lb
Stored weight for zero cruise disturbance = $0.375 + 3 \times 0.215 = 1.0$ lb

Table 38. Gas weights for a 200-day mission

Mode description	Total average unbalanced torque about all axes dyne-cm	Cruise mode gas weight expended due to unbalanced torque lb	Total stored gas weight necessary to accommodate the mode (includes cruise consumption) lb
All unbalanced torque removed	0	0	1.0
Mariner II unbalanced torque	73	0.34	3 × 0.34 + 1 = 2.1
Expected unbalanced and single axis failure	73 + 26 = 99	0.43	3 × 0.43 + 1 = 2.3
Expected unbalanced and double solar vane failure	73 + 66 = 139	0.65	3 × 0.65 + 1 = 2.95

one vane fails to erect and the opposite vane fails to adapt. Table 38 summarizes the cases likely to be encountered.

In view of the analyses made concerning possible gas consumption, it was recommended that the spacecraft carry a stored gas weight of 6.9 lb. This gas storage calculation actually represented a conservative estimate of the acquisition requirements. Single-axis derived-rate acquisition was assumed, which represented a failure mode of operation since it was planned to use gyros. Due to the spacecraft weight problems that were encountered, it was decided to cut the stored weight to 5.2 lb gas. The use of gas as measured during the *Mariner IV* flight has been well within the storage requirements.

C. Celestial Sensors

1. Canopus Sensor

a. History. Early in 1959 it was realized that three-axis attitude control using the Sun and Earth for angular reference was undesirable for typical Mars missions. Two primary difficulties were apparent. The first difficulty was that Earth would be quite near the Sun, as seen from the spacecraft, for an extended period. This would make it difficult to build a simple and reliable Earth sensor for roll control of the spacecraft. During this period, the dim Earth would be seen near the very intense Sun and on a bright background of solar corona. Any loss of lock would present an extremely difficult reacquisition and identification problem. The second difficulty was that maintenance of accurate roll control would be difficult due to the small Sun–spacecraft–Earth angle. In the limiting case of Sun–spacecraft–Earth angle equal to 0, roll control would be lost. Midcourse corrections in this region would be impossible. Attitude control studies indicated that the object angle of the Sun–spacecraft–roll references should, in fact, be between 45 and 135 deg for good control.

The Sun was considered to be one of the necessary reference objects because it could be identified and tracked easily. Sun orientation was also desirable for such reasons as thermal control and the collection of solar power. Choice of the second (or roll reference) object, however, seemed difficult, and no exceptionally good choice was apparent. Tentative selection of the roll reference object was first made early in 1960.

It was reasoned that if the Sun were used as a primary reference, if most trajectories lay near the ecliptic plane, and if the Sun–probe roll reference object angle must be near 90 deg (for best attitude control), then the roll reference star must lie near the ecliptic North or South Pole. A search for an easily distinguishable star in those regions yielded an obvious choice: the bright star Canopus.

Once the choice of Canopus became known and accepted, further trajectory studies revealed another advantage to the Sun–Canopus reference system. On most of the Earth–Mars trajectories being considered, during the last 110 days before encounter the Earth direction would be relatively constant, as shown in Fig. 141. This property made possible the use of a fixed

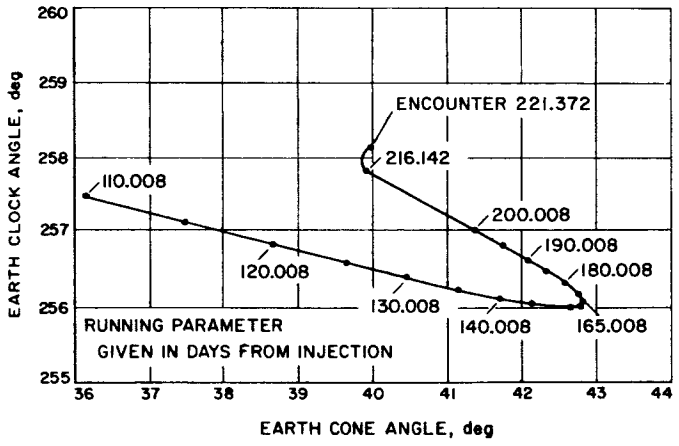


Fig. 141. Earth cone and clock angles vs days from injection

omnidirectional antenna for communication purposes for the near-Earth portion of flight and a fixed directional antenna for the near-Mars portion of flight; thus, the requirement for a movable antenna was eliminated entirely.

Although actual development of the Canopus sensor used on *Mariner IV* did not begin until mid 1962, mechanization studies directed toward development of simple and practical schemes for tracking Canopus were undertaken immediately after Canopus was selected in early 1960. The following general requirements were envisioned:

1. The device had to consume little power, preferably under 5 w.
2. A high probability of successful operation over extremely long periods in space was mandatory. Actual mission flight times were set at between 6000 and 25,000 hr.
3. Since Canopus is not perpendicular to the ecliptic, a certain amount of gimbaling (±15 deg on one axis) was required.
4. To survive launch environment, the device had to be extremely rugged.
5. A weight under 7 lb was desirable.
6. Cruise and midcourse maneuver guidance requirements demanded extremely reliable identification of the star Canopus by either onboard logic or ground-based logic.

At that time, the state of the art for star tracker devices did not match these general requirements. In particular, the modulation and scanning techniques used an assemblage of moving mechanical parts such as spinning reticules, nodding mirrors, cams, and gears. Such techniques would require lubrication, pressurization, high power, and have questionable lifetimes. The image dissector, which could be scanned electronically, was recognized as a potential solution of the total problem.

b. Detailed functional requirements. There were many functional requirements placed on the Canopus sensor. The requirements imposed by the attitude control subsystem are tabulated in Table 39.

A minimum field of view in roll of ±2 deg was required to ensure stopping the spacecraft and acquiring Canopus, considering a partially failed attitude control subsystem. Even though a 0.5-deg 3 σ null error would be responsible for only 1% of the total squared error (1 σ) of the midcourse maneuver, 0.1-deg null accuracy was easily achieved and was made a requirement for convenience in bench checkout.

Table 39. Canopus sensor functional requirements imposed by the attitude control subsystem

Category	Requirement
Linear range	±0.85 deg
Field of view in roll	±2.0 deg minimum
Scale factor	8 v/deg ±20%
Angle noise	2 mrad peak to peak
Time constant	<0.5 sec
Null accuracy	0.1 deg

Figure 142 shows how the Sun–probe–Canopus angle changes during a flight to Mars in 1964. Two modes of updating the sensor cone angle were required. A radio command was incorporated to back up the automatic mode that relies on the CC&S closing relays at preset times. For simplicity in the CC&S, update times were to be preset to a fixed number of days prior to encounter. Preflight uncertainty of inflight Canopus cone angle at each of the fixed update times, the uncertainty of the alignment of the field of view, the signal-to-noise advantages of a minimum field of view, and the simplicity and weight advantages of a minimum number of updates entered into the choice of an 11-deg field of view in cone angle and five discrete positions (as indicated in Fig. 142).

Acquiring Canopus involves performing a stabilized roll search at 0.116 deg/sec until the Canopus sensor senses a star of the proper intensity. Roll control is then transferred to the roll-position error signal produced by the Canopus sensor. A gate and a voltage proportional to intensity are used for the logic signal to perform this transfer.

The high gate is required to protect the photocathode from damage due to the acquisition of Earth. Tests have shown that the cesium-antimony photocathode suffers a permanent 30 to 40% degradation in sensitivity when illuminated with 2000 ft-cd for 10 min (if sensor voltages are on). The equivalent illumination of the photocathode within the image of Earth on the photocathode is about 3000 ft-cd. This is independent of the range to Earth as

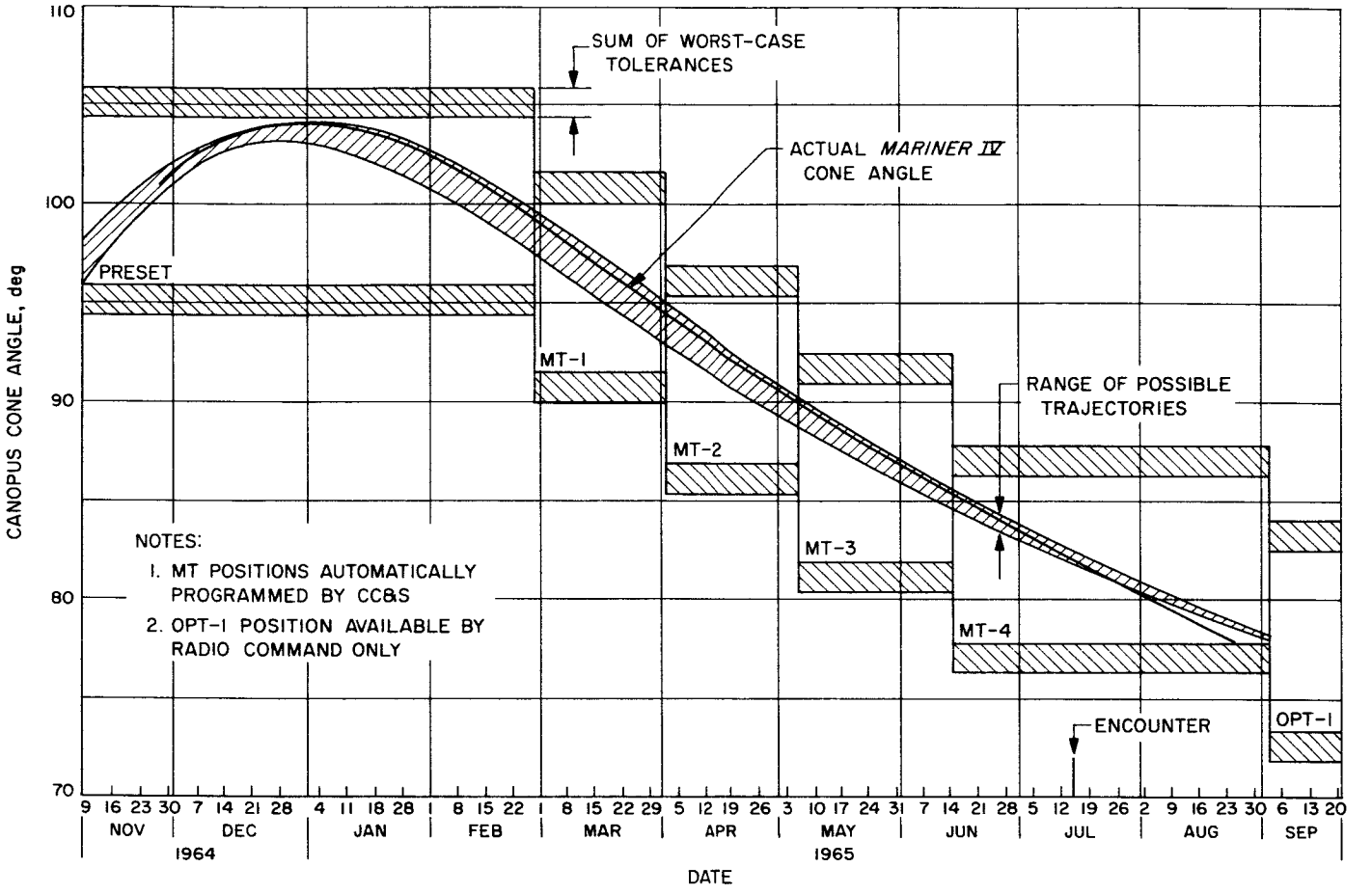


Fig. 142. Canopus cone angle and Canopus sensor field of view vs time

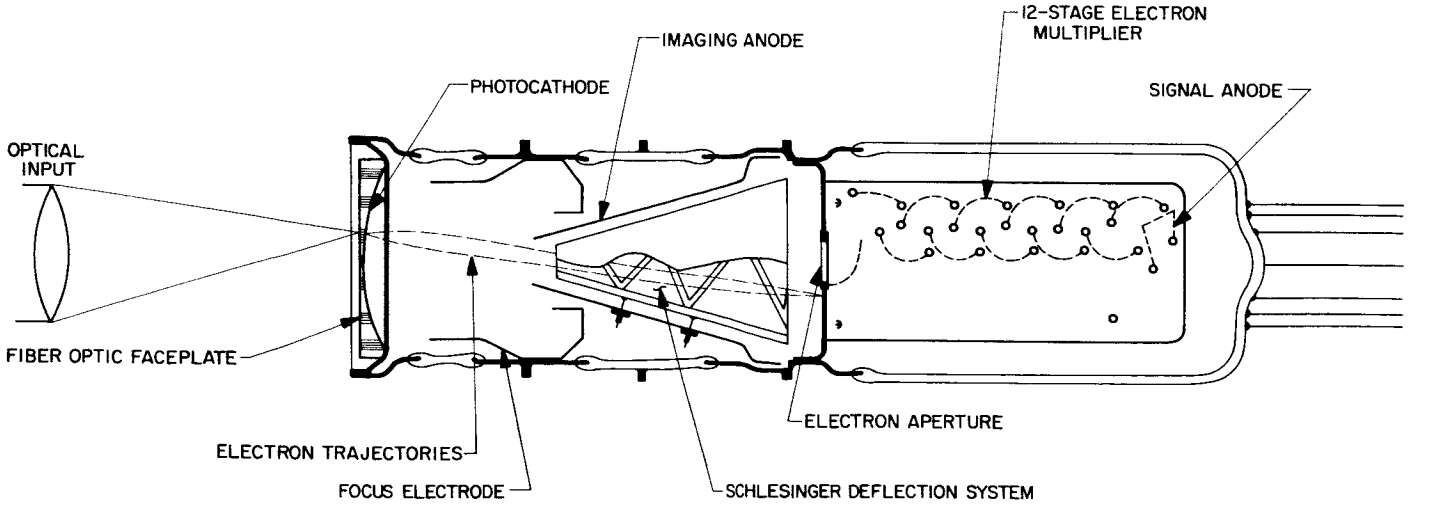


Fig. 143. Electrostatic image dissector tube

long as the angular diameter is greater than the resolution of the lens. Tests on a simulated 3-deg diameter Earth at the roll-search rate of 0.1 deg did not degrade the luminous sensitivity of the cathode. Therefore, protection was not required if the spacecraft was in roll search. The high gate was set at 8 times Canopus to prevent the acquisition of Earth.

The possibility of the Sun being focused on the photocathode during initial acquisition or during a maneuver was also considered. The illumination of the photocathode within the image of the Sun is approximately 2×10^8 ft-cd. Static exposure tests were run to simulate the effect of the image of the Sun moving across the photocathode at the spacecraft maneuver rate (0.1 deg/sec). Since the Sun is 0.5 deg in diameter, a static exposure of 5 sec is equivalent to the dynamic exposure expectable in flight. Pointing a Canopus sensor, with the power off, at the Sun (one-half an Earth solar constant) for 5 sec caused a significant loss in sensitivity. Therefore a fail-safe Sun detector and a mechanical Sun shutter were incorporated to protect the photocathode from potential damage.

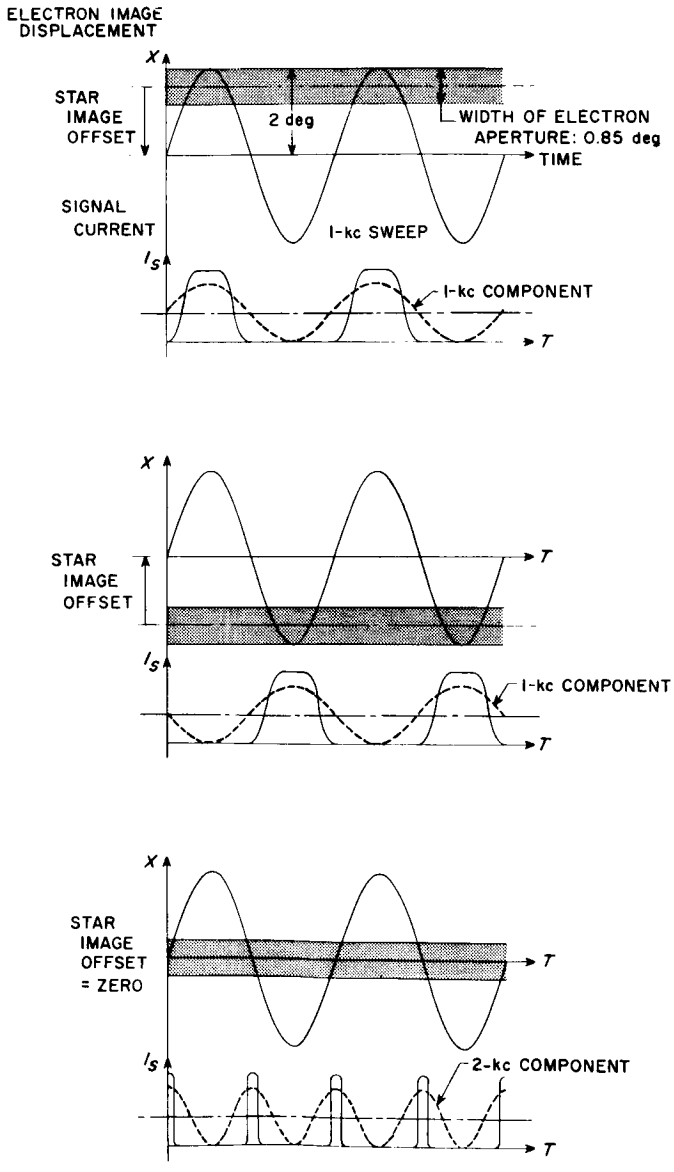


Fig. 144. Canopus sensor waveforms

c. Image dissector. Understanding the electrostatic image dissector is fundamental to understanding the operation of the *Mariner IV* star sensor. The device consists of a cesium antimony photocathode, an electrostatic electron optical image section, an electrostatic deflection yoke, and a conventional electron multiplier, all combined into one vacuum tube. Figure 143 shows a cross section of the image dissector.

The electron aperture in the dissector is 0.160 in. long by 0.012 in. wide. The 0.160-in. axis of the slit is oriented parallel to the cone direction. The 0.012-in. axis is oriented parallel to the roll axis. Projected through the optical system, the aperture has an instantaneous field of view that is 0.85 × 11 deg. This field of view is sinusoidally scanned at 1 kc a total of 4 deg peak-to-peak in the roll-angle direction. Figure 144 illustrates the pulse train that is generated for various roll-angle positions of the star. Roll-position and star-intensity information are contained in these pulse trains. Figure 145 shows the results of a Fourier harmonic analysis of the pulse train. The polarity and magnitude of a star's roll-angle position is contained in the 1-kc component of the

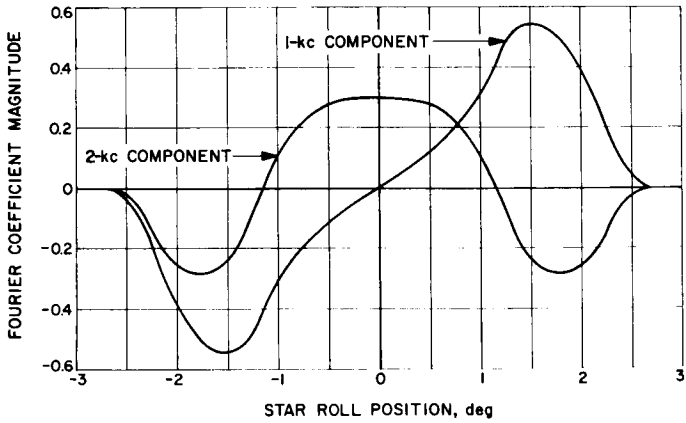


Fig. 145. Fourier coefficients of modulated photocathode current expressed as a fraction of unmodulated or dc photocathode current

pulse train, while the 2-kc component is proportional to the intensity of the star when the star is centered in the field of view.

d. Image dissector development. There were many problems, both electrical and mechanical, connected with the development of the image-dissector tubes. Problems with luminous sensitivity, gain, and deflection-plate alignment of the electron aperture were solved quickly. A serious problem with uniformity of secondary emission of the first dynode was finally solved in the rugged image dissector. The electron aperture in the image dissector was 0.160 in. long by 0.012 in. wide. The secondary emission efficiency depended upon location of the electron image along the long axis of this aperture. Minimum first dynode sensitivity was specified at 70% of the maximum sensitivity. Shrinkage was high with this specification, and the tubes that were delivered early in the program were barely within tolerance. Parameters of the processing procedure and electron optics were studied in connection with the problem. The solution was found in the processing, cleaning, and degreasing techniques used. An improved cleaning technique was incorporated for processing of the silver magnesium dynode buckets with excellent results. Tubes incorporating these dynodes had consistent dynode uniformity in excess of 85%. This processing improvement was incorporated in all the rugged tubes.

To help stabilize operating parameters, tubes were burned-in with about the same photocurrent density as in the star image, with the same anode current, and with the maximum operating voltage on the last two dynodes. The gain of the intermediate stages was adjusted to meet the stated objectives.

Early failures in an engineering model sensor showed that TA vibration could not be passed with the "regular" tube due to failure of the butt welds at the point where the dynode wires passed through the glass stem. Two programs were begun at that time to obtain flightworthy tubes. Table 40 summarizes the features of the three types of tubes that evolved from these two programs. Due to a time limitation, the improved tube program was made the prime plan of attack and the rugged tube program was made the backup. The "T" tube (so-called because of the thick stem wires) was evolved in an effort to improve scheduling after the failure of the improved tube in the special TA test. The stems with the necked leads, which were procured for the rugged-tube program, were used to make the improved tubes. Because of the thick stem wires, these tubes proved to be no better than the improved tubes. The thick stem just transferred the loading to another weld that failed at approximately the same vibration level as the weakest weld in the improved tubes.

Table 40. Summary of image dissector tube development for the *Mariner* Mars star sensor

Feature	Tube			
	Regular	Improved	"T"	Rugged
Tweezer welds	X			
Nickel to kovar butt weld at the stem	X			
Shortened and kinked dynode leads	Some	X	X	X
Quality control		X	X	X
Weld schedules		X	X	X
Welding tabs on concentric parts		X	X	X
Necked kovar stem lead			X	X
Two-part focus electrode				X
Snubbers on the multiplier				X

The rugged-tube program involved an attack on the fundamental engineering problems of high stresses on the internal stem wires and the weldability of the assembly. With the aid of a telescope and synchronous photography, the vibration characteristics of the tubes were studied. The multiplier assembly has fundamental reasonances, with Q's of 9, in the range of 300 to 400 cps. Analysis showed that high stress occurred on the anode and twelfth dynode leads where they passed through the stem and where they attached to the dynode buckets. These leads failed repeatedly. Not only were the leads heavily stressed but also the sizing of the lead materials caused a very unfavorable heat balance in the wire-to-wire spot welds in the leads, resulting in especially weak welds. Figure 146 shows the two major changes incorporated in the rugged design. Snubbers, which constrained the multiplier in the glass envelope, removed the load from the twelfth dynode and anode leads. The necked stem lead provided more weldable-wire combinations while retaining required flexibility in the external leads. The rugged tube proved worthy of its name. Vibration tests were conducted on the rugged electron multiplier. It survived vibration inputs in excess of 30 g rms in the range of 100 to 2000 cps. Using optical monitoring techniques, the structure was examined for renonances in this frequency range and none was detected. The snubbers very effectively supported the electron multiplier,

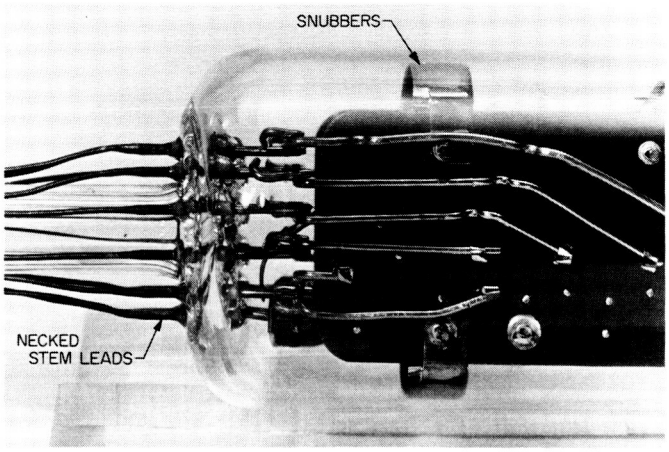


Fig. 146. Rugged electron multiplier

and kinks in each dynode lead, which contacted the photoceramic side plates, effectively damped out individual wire resonances.

A sensor with a rugged tube passed the *Mariner* Mars 1964 TA testing requirements without difficulty. All flight sensors used rugged tubes.

e. Electronics. A block diagram of the sensor is shown in Fig. 147. There are two channels, the roll error channel and the intensity channel. In the roll channel, the magnitude and phase of the pulse-train 1-kc component are detected using a half-wave phase-sensitive synchronous demodulator. The output of the demodulator is filtered to a half-power bandwidth of 0.312 cps.

Table 41 outlines the performance of the roll error channel. The roll error signal is expected to perform within quoted specifications over temperature extremes of 0 to 100°F, supply voltage variations of ±3%, and power-supply frequency variations of ±1%. Degraded performance of the roll error channel can be expected over temperature extremes of −50 to +150°F, supply

Table 41. Roll error signal

Parameter	Value
Scale factor	8 v/deg
Stability of scale factor	±20%
Typical roll error noise	
1 × Canopus	0.015 deg peak to peak
¼ × Canopus	0.025 deg peak to peak
Time constant	0.5 sec
Null stability	±0.125 deg

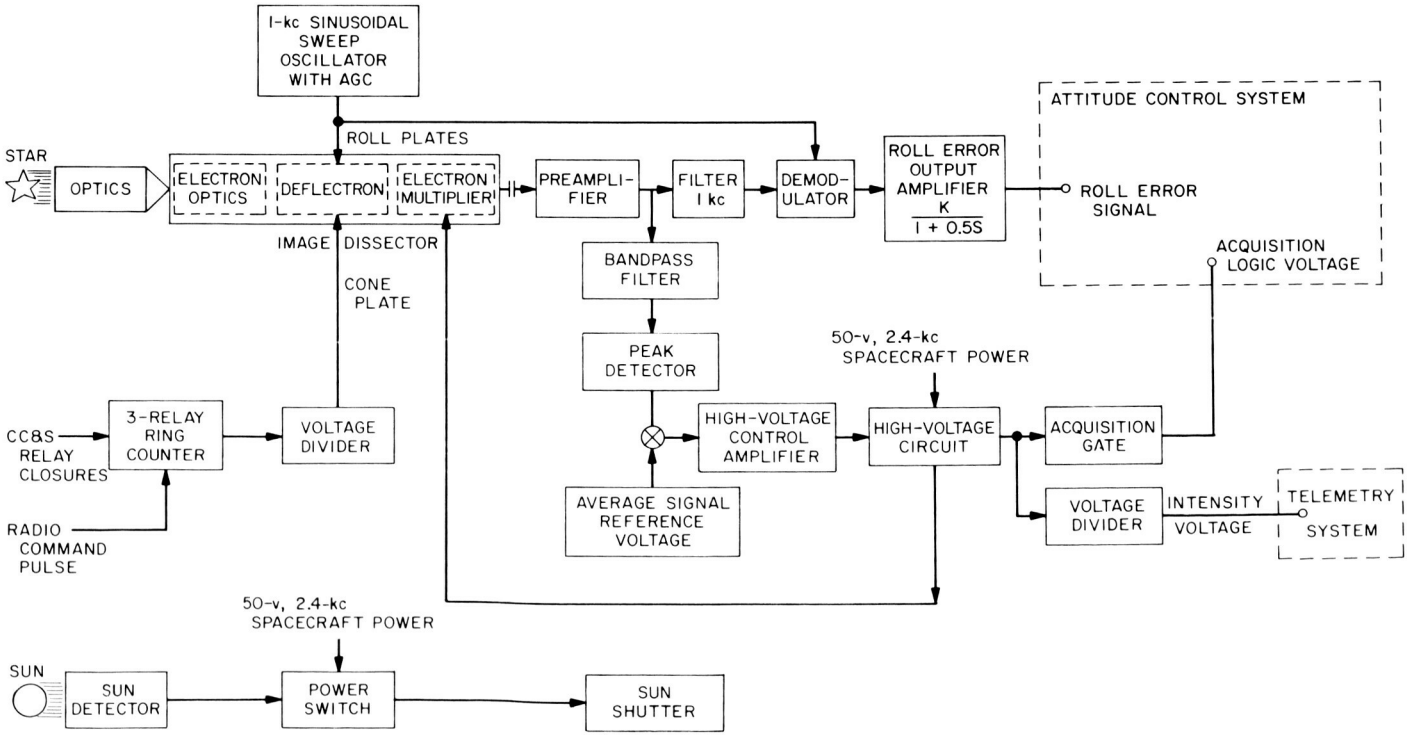


Fig. 147. Canopus sensor block diagram

voltage variations of −10 to +40%, and supply frequency variations of −5 to +2.5%. The null stability includes the effects of supply voltage variation, supply frequency variation, time, star intensity, and cone angle. The null is not affected in any way by signal phase shifts. However, phase shifts that occur prior to the demodulator will reduce the roll error scale factor. The largest single source of null instability is the cone angle update. Null instability with cone angle can be attributed to: (1) deflection nonlinearity in the image dissector, (2) mechanical alignment of the tube to the sensor mounting feet, and (3) the network that compensates for misalignment between the deflection plates and the aperture of the tube.

Roll error scale-factor stability depends upon having a constant amplitude pulse out of the preamplifier. A high voltage AGC loop is used for this purpose in the *Mariner IV* Canopus sensor. The preamplifier output is filtered with a bandpass filter that includes 1 kc and

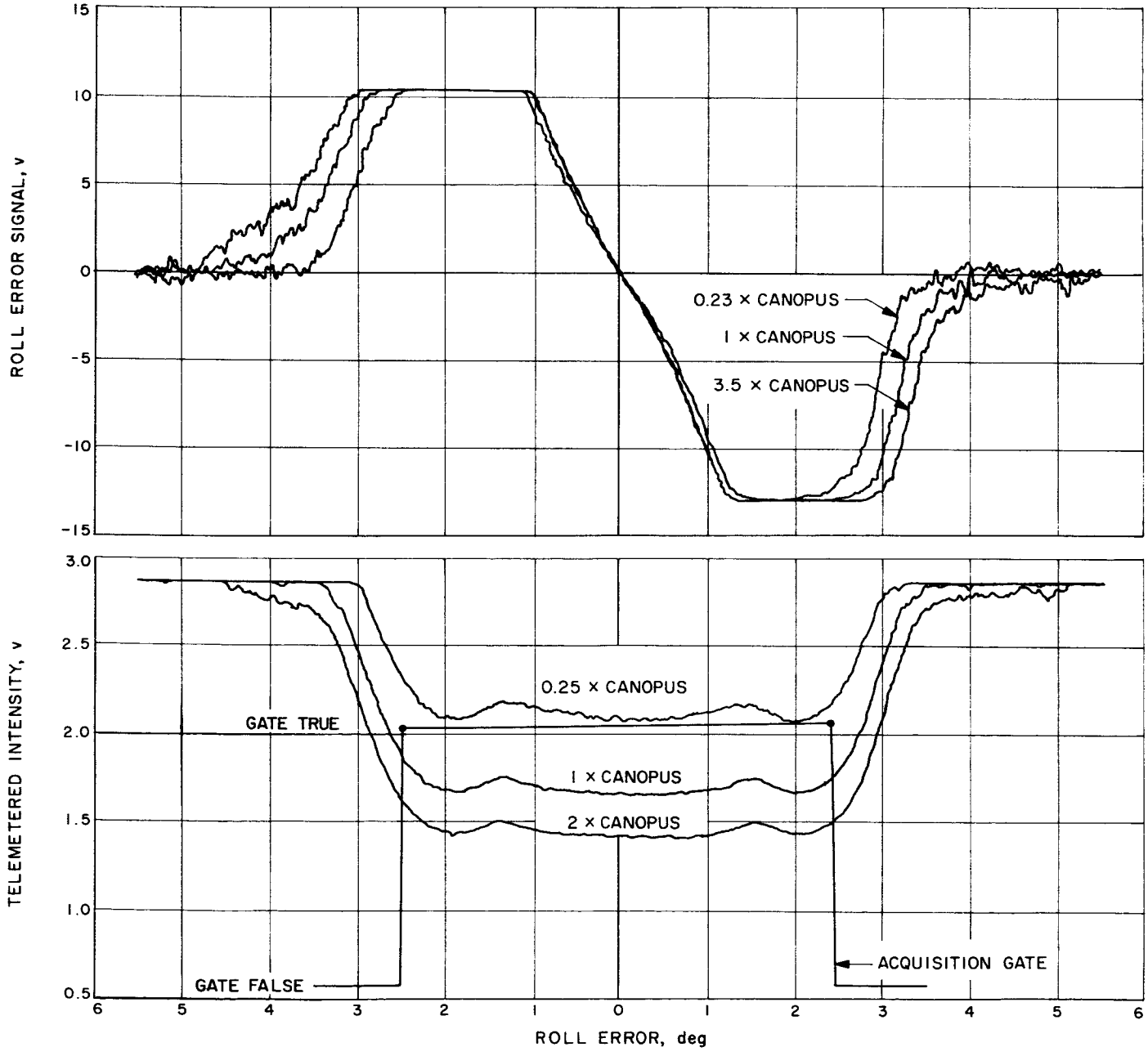


Fig. 148. Canopus sensor outputs vs star roll error position

2 kc. This signal is peak-detected, and is used to adjust the high voltage on the image dissector electron multiplier. By varying the electron-multiplier gain, the high-voltage loop provides a constant output from the preamplifier for a very wide range of star intensities. The high voltage normally operates at about 1000 v when Canopus is in the field of view. The value of the high voltage is the measure of star intensity. A voltage proportional to the high voltage is taken from the high-voltage circuit and used to drive the acquisition gate. This voltage is also telemetered back to Earth for use in star identification. In addition to the ability to handle a large dynamic range of star intensities, the high-voltage AGC loop has other advantages. It automatically protects the electron multiplier from excessive current if a bright object is encountered. Combined with wide acquisition gates, the high-voltage loop will compensate for large degradations in image-dissector sensitivity or gain.

Figure 148 is a representative summary of the three sensor output functions as they vary with the roll position of the star for various star intensities. The noise on these plots is characteristic of sensor noise. The variation in apparent star intensity with roll angle is inherent in the signal processing since the higher harmonics of the signal are filtered out.

Two other functions are contained in the Canopus sensor: a Sun-shutter drive circuit and a power supply for updating the cone angle field of view. The cone angle is updated by preprogrammed relay closures in the CC&S. The CC&S is backed up by a radio command input. The cone-angle generator is a three-relay, eight-bit binary ring counter and a voltage divider. There are five required positions of the cone field of view and three optional positions. The optional positions all overlap the cone angle of Canopus at encounter. The center line of each field of view is shown in Fig. 149. The use of the image dissector made electronic gimbaling possible.

Power is supplied to the Sun-shutter circuit only when power to the Canopus sensor is off. A cadmium sulfide cell is used to detect the presence of the Sun in the field of view of the sensor. Power is supplied to an external Sun shutter when this cell is illuminated with greater than 1000 ft-cd.

There are 265 electronic parts and 24 transistors in the Canopus sensor. The unit weighs 5 lb and consumes only 1.5 w of power. The low power consumption is largely the result of the use of the electrostatic image dissector and series-resonant high-voltage power supplies.

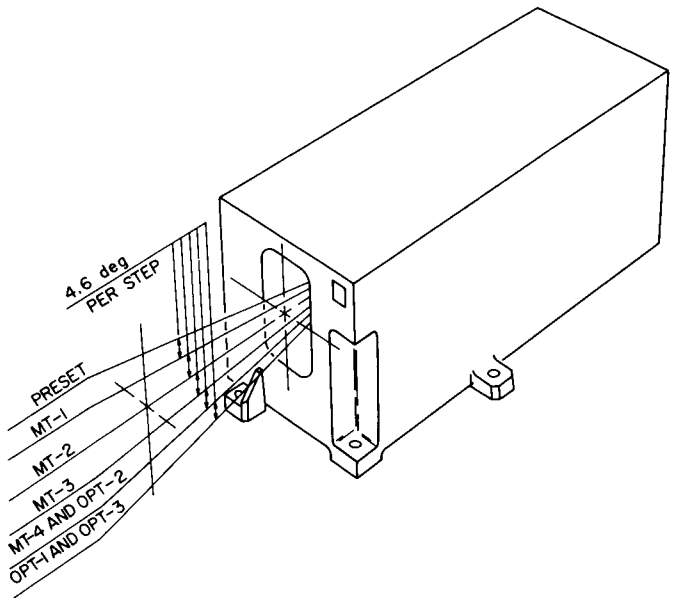


Fig. 149. Programmed changes in Canopus sensor field of view

f. Mechanical design. Mechanical design of the sensor was complicated by the required cantilever mounting. To cope with this condition, it was found desirable to package the electronics well toward the front of the shade to help balance the sensor. Figure 150(a) shows the sensor with all the covers in place. The location of the mounting feet was determined by the spacecraft interface.

The sensor is integrated into a single unit. It houses the shade, the optics, the image dissector, and all the electronics. The image dissector is mounted in O-rings, and constrained axially by a clamp at the front, which prevents changes in the optical focus with temperature and stressing of the image dissector. The optics are mounted in a barrel that is flange-mounted to the chassis of the sensor. Focusing was accomplished by sliding the lens inside the barrel and clamping it into place. Alignment of the optical axis with the electrical null of the image dissector was provided for by means of ample clearance holes on the flange. The baffles and aperture compensator dropped in as a unit. The baffle assembly was fabricated of 0.020-in. stock, and is very lightweight. The sensor is enclosed by four cover plates. Three of the covers serve as dust covers; the fourth is used to seal out light from the optics and image dissector and to give the structure torsional rigidity.

Figure 150(b) shows a completed sensor with the covers removed. The chassis was machined from one

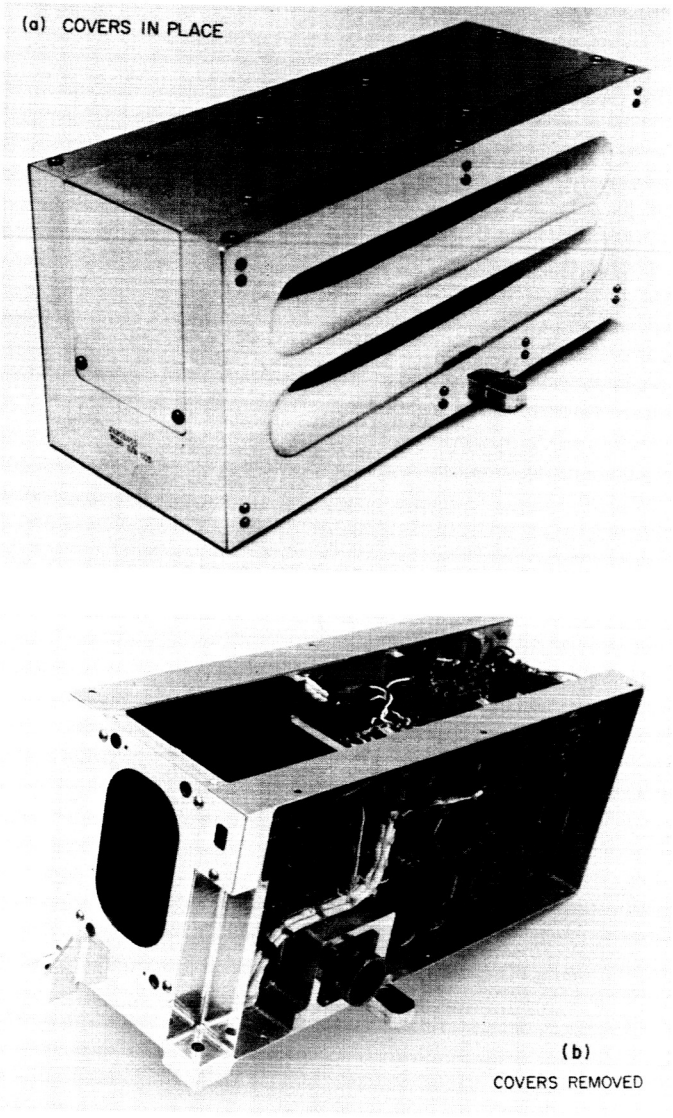


Fig. 150. Canopus sensor

piece of aluminum, with a typical wall thickness of 0.040 in. Considerable care was required to machine the chassis. Structural fraction of the total sensor weight was 38.4%. This included the chassis, the dust covers, and all aluminum parts. Low total weight (5.0 lb) was achieved for a fundamental chassis resonance of 350 cps. Packaging of the electronic circuitry takes advantage of the open mechanical configuration of the sensor. Conventional single-sided, printed circuit boards are arranged around the three sides of the image-dissector tube. The sensor is completely accessible and functional with the dust covers removed. Only one connector is used at the spacecraft interface. A preamplifier is packaged immediately above the image-dissector tube. Shielding was not required on any wires, except the incoming 2.4-kc power cable.

g. Optical design. The optical system of the sensor consists of a shade, a catadioptric lens, and an aperture compensator.

The lens was designed to have uniform image quality in a field of view 4 × 40 deg. It has an 0.8-in. focal length and a geometric speed of f/0.6. However, the effective speed considering the center occultation and the aperture compensator is f/1.0. The lens and aperture compensator are shown in Fig. 151. Without the aperture compensator, the image intensity would fall off to 66% of the on-axis value at 16 deg off axis in cone angle. This aperture modulation is offset by the fingers of the aperture compensator. For a star on axis, the fingers block all rays above and below the secondary reflector. For a star below the axis by 16 deg, the fingers only block rays that are below the secondary reflector. The area of the aperture is equal for a star at 0 deg and at ±16 deg off axis. The secondary variations in aperture area were masked out by variations in cathode sensitivity that were normally about 10%.

Because of the sensor susceptibility to spacecraft stray light and bright objects (like Earth) 10 to 25 deg outside the field of view, considerable effort was expended to minimize the intensity of stray light reaching the image plane. The aluminizing patterns on the catadioptric lens were modified to reduce stray reflections, and an edging technique was developed to minimize the light reflected

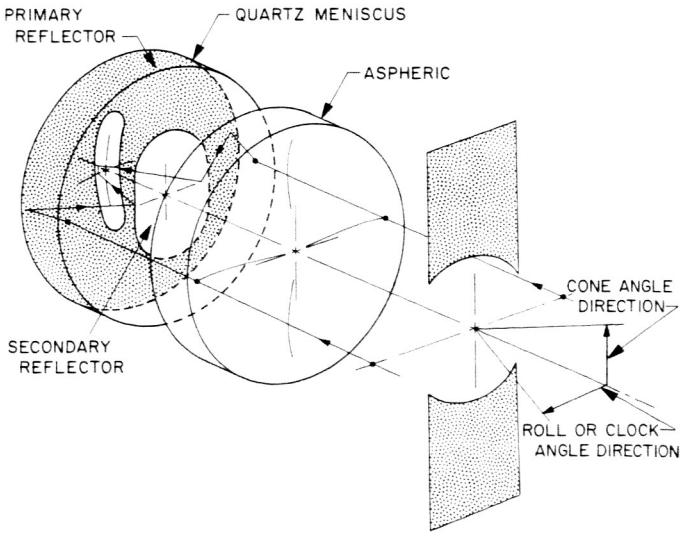


Fig. 151. Canopus sensor optical system

off the edges of the lens. The edges were first polished and then painted with Cat-a-lac black paint. Choice of Cat-a-lac black paint was a compromise between vacuum stability and optical properties. Lenses were fabricated from the highest grades of synthetic quartz and light flint glass. The flight lenses were of image-plane quality with an exceptional polish, and were free of bubbles and other defects. The front element was tested for radiation susceptibility. No degradation was expected due to the Van Allen belts surrounding Earth. Since the geometric speed was f/0.6, centering and mounting were quite critical; however, no problems were encountered.

h. Spacecraft stray light environment. The problem of determining stray-light response of the Canopus sensor was complicated by the configuration of the spacecraft and the availability of test facilities.

Figure 152 illustrates the stray-light environment caused by sunlight reflected from the solar vanes. The photograph was taken with a camera located on the Canopus sensor. Even though the angle between the panel and the edge of the primary field of view of the sensor is 33 deg, the flux into the sensor baffle is over two million times greater than the flux from Canopus. Much of this stray radiation gets scattered into the primary field of view by the optical system. An overall go/no-go test with the complete spacecraft illuminated with one solar constant and with the Canopus sensor looking at a simulated star was studied but found to be impractical. As a compromise, the spacecraft was illuminated in piece-meal fashion by a 27-in. diameter Sun bundle in a special 40-ft hemispherical dark room. The total reflectance in the direction of the Canopus sensor of each hardware item was measured with a visual photometer. The reflectance of sunlight in the spectral-response region of the Canopus sensor was assumed to be the same as in the visual region. Total Canopus sensor illumination due to reflected sunlight was then calculated. Certain modifications were required to bring the stray light down to an acceptable level. These modifications included the addition and modification of light shades used on hardware bathed in sunlight. In addition, the following rules were applied wherever conditions required:

1. Spacecraft hardware had to be kept far away from the optical axis of the star sensor (preferably greater than 90 deg).

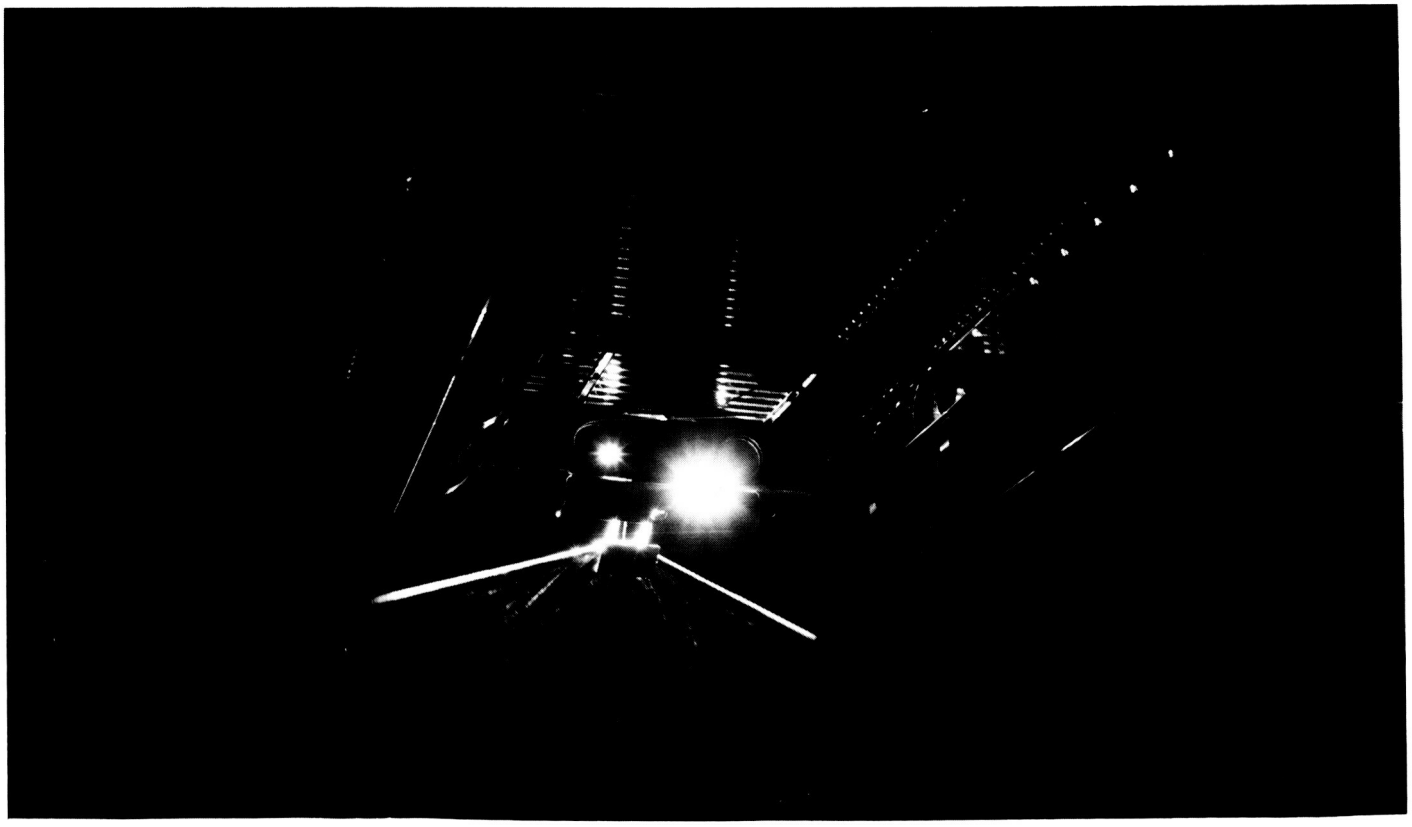


Fig. 152. Stray light from solar panel as seen by Canopus sensor

2. Hardware in the hemisphere visible from the baffles of the sensor had to have a very low diffuse reflectance, and be free from highlighting compound curves.

3. Hardware that had to be within 90 deg of the optical axis of the sensor had to be located toward the Sun, so that the sides visible from the sensor would not be illuminated directly by sunlight.

An investigation of the diffuse reflectance of various spacecraft surface finishes was conducted to determine the most desirable finish. The results are tabulated in Table 42. Laminar X500 gloss black paint was applied liberally to all surfaces within 90 deg of the optical axis of the sensor. For a weight penalty of less than 1.0 lb, the spacecraft stray light was reduced from about 0.5 ft-cd per panel to 0.043 ft-cd per panel.

Table 42. Diffuse reflectance characteristics of various spacecraft surface finishes

Spacecraft finishes							Test laboratory surfaces	
θ_1, deg	θ_2, deg	Gloss X500 %	Flat X500 %	Flat Cat-a-lac black %	Satin X500 %	Black velvet %	Black Carrara glass %	Coffin cloth %
0	30	0.5	6.1	5.3	0.7	2.5	—	—
0	60	0.25	5.1	4.1	0.4	2.7	0.003	—
0	45	—	—	—	—	—	—	0.23

In addition to determining the stray-light environment of the sensor on the spacecraft, it was necessary to determine the sensitivity of the Canopus sensor to stray light and to screen each flight sensor for verification of its ability to perform in the presence of stray light. The sensitivity of a sensor to light from outside the primary field of view is a complex function of the shade, the optics, and the signal processing. In addition, contamination of the lens or baffle could significantly degrade the performance of a sensor in a stray-light environment. A wire 0.005 in. in diameter by 0.100 in. long, placed just inside the edge of front baffle, degraded the sensor sensitivity to stray light by a factor of 4 to 30 depending on the parameter used to judge sensitivity. This test was partly responsible for the promotion of spacecraft and shroud cleanliness as well as sensor cleanliness.

The sensor function that turned out to be the most sensitive to stray light was the star-intensity voltage, which is telemetered to Earth for use in the ground-based real-time map matching. A sensor sensitivity threshold of 0.04 times Canopus was adequate to ensure a good star map. All other sensor functions were less sensitive to stray light. Null shifts, reduction of scale factor, and reduction of the error-signal saturation voltages could all be induced by stray light. However, the light levels required to do these things were several orders of magnitude higher than the light levels required to interfere with the star-intensity roll map.

Each sensor was tested to verify that it had adequate insensitivity to stray light. It was established that the apparent star intensity caused by 0.1 ft-cd of light at 35 deg from the optical axis in roll should be less than 0.04 times Canopus. The light level required by each of the flight sensors for an apparent intensity of 0.04 times Canopus is tabulated in Table 43.

Table 43. Light levels required for 0.04 × Canopus

Spacecraft	Critical light level, ft-cd
Mariner III	0.51
Mariner IV	0.21
Spare	0.23

Figure 153 shows the variation of sensitivity of the Canopus sensor to stray light with roll angle and cone angle. The curve is an average of two flight sensors, and does not indicate the variability in sensitivity that was observed. Variations in stray-light response between sensors as large as an order of magnitude were observed.

i. Earth light. When *Mariner IV* initially acquired Canopus, it was positioned so that Earth could not appear directly within the sensor field of view at any time during roll search. Earth, however, was only 21 deg away from the optical axis of the sensor, and illumination on the spacecraft due to Earth light was over 1 ft-cd. Located only 21 deg from the optical axis, the performance of the sensor was definitely affected. Figure 154 shows the roll error signal and the intensity signal as a function of the roll position of Earth. Initial-acquisition geometry of Earth was simulated for this test. The curve shown represents a test run after *Mariner IV* was launched and explains a discrepancy between the *a priori* star map and the real-time inflight star map.

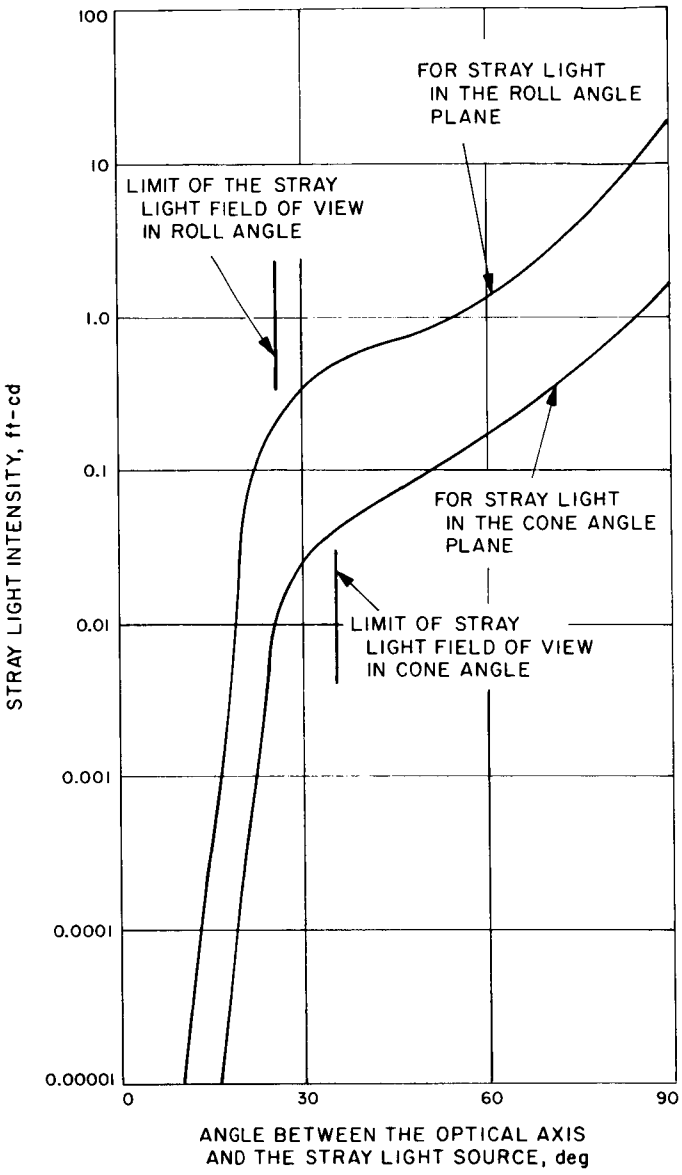


Fig. 153. Intensity of stray light to cause apparent 1/25 × Canopus star intensity vs stray light angle

The Canopus sensor was not tested prior to launch for the precise Earth geometry that existed for the November 28 trajectory. Certain standard tests were run, however, on a simulated Earth early in the prototype phase of the development. These tests showed that it was possible for Earth, the Moon, or Mars to cause the Canopus sensor to deliver error signals of improper phase simultaneously with an acquisition gate signal. This phenomenon occurred while the bright celestial object was still far off axis. Figure 155 shows a plot of the sensor characteristics taken on the *Mariner IV* sensor with the Earth geometry simulated for a launch early in November. Inverted phase error signals occur at ±27 deg from the optical axis and the acquisition gate is true in a large region common to the inverted error signal.

The inverted error signals are caused by reflected light. As a bright object rises toward the optical axis from the right, it first illuminates the side of the baffle and lens to the left of the optical axis. This light from the baffle and lens makes its way directly to the photocathode in which it is modulated and appears as an error signal of improper phase. The angle at which this phenomenon begins to take place corresponds to within 1 deg of the angle at which direct Earth light falls on the front element of the optical system. Reflections off the retainer ring on the front element are suspected to be the cause.

Since this behavior could be expected from any star sensor, and since this performance would seriously confuse the control system, the attitude control subsystem logic was mechanized to handle the inverted error signals. A unidirectional search was employed and the attitude control acquisition logic required both a true Canopus sensor acquisition gate and a −4 v error signal to transfer roll control to the Canopus sensor.

Figure 154 shows that there are two stable nulls and three unstable nulls in the error characteristic of Earth when it is out of the primary field of view in both the roll- and cone-angle directions. During one roll search in the flight of *Mariner IV*, three stable nulls were acquired because the apparent intensity was right for acquisition. This extremely unusual error signal did not cause the spacecraft to behave abnormally.

j. Star acquisition and recognition. The mandatory requirement for positive star identification was solved through development of a map-matching scheme that required no onboard logic other than a brightness measurement and simple magnitude gates. In addition, to provide backup to a possible brightness-channel telemetry failure, omnidirectional-antenna lobe pattern and magnetometer zero crossings were used to estimate roll position during an initial 16-hr magnetometer calibration phase of flight. A very simple photoconductive Earth detector was also added, which would detect Earth if the Canopus sensor was oriented in the direction of Canopus.

This total system provided 100% identification certainty even in the event of one telemetry channel failure

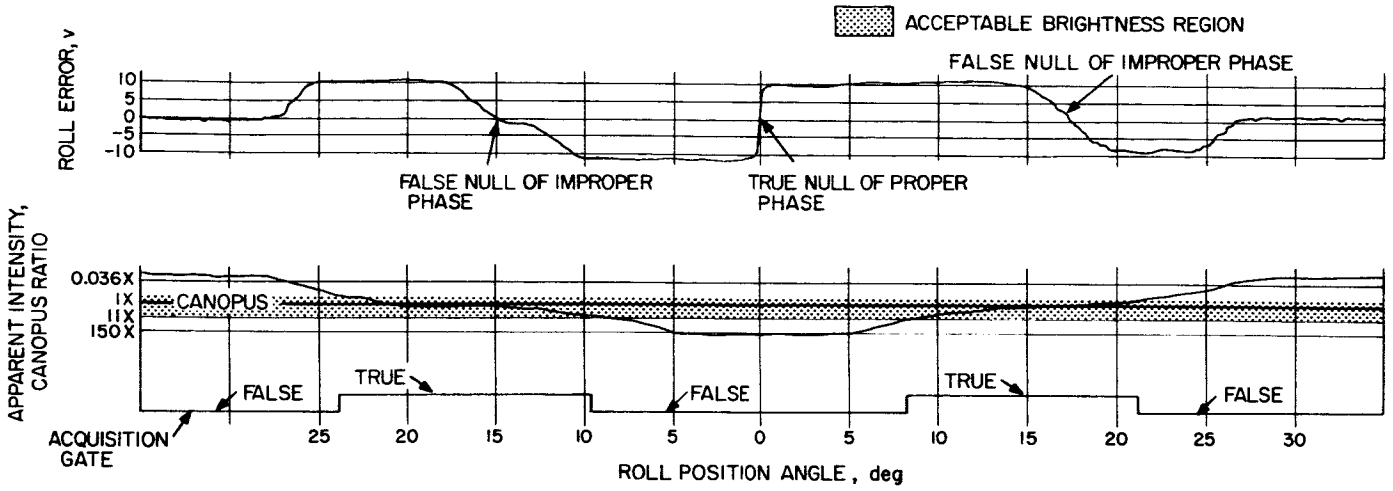


Fig. 154. Roll error signal and intensity signal characteristics of Canopus sensor for Earth

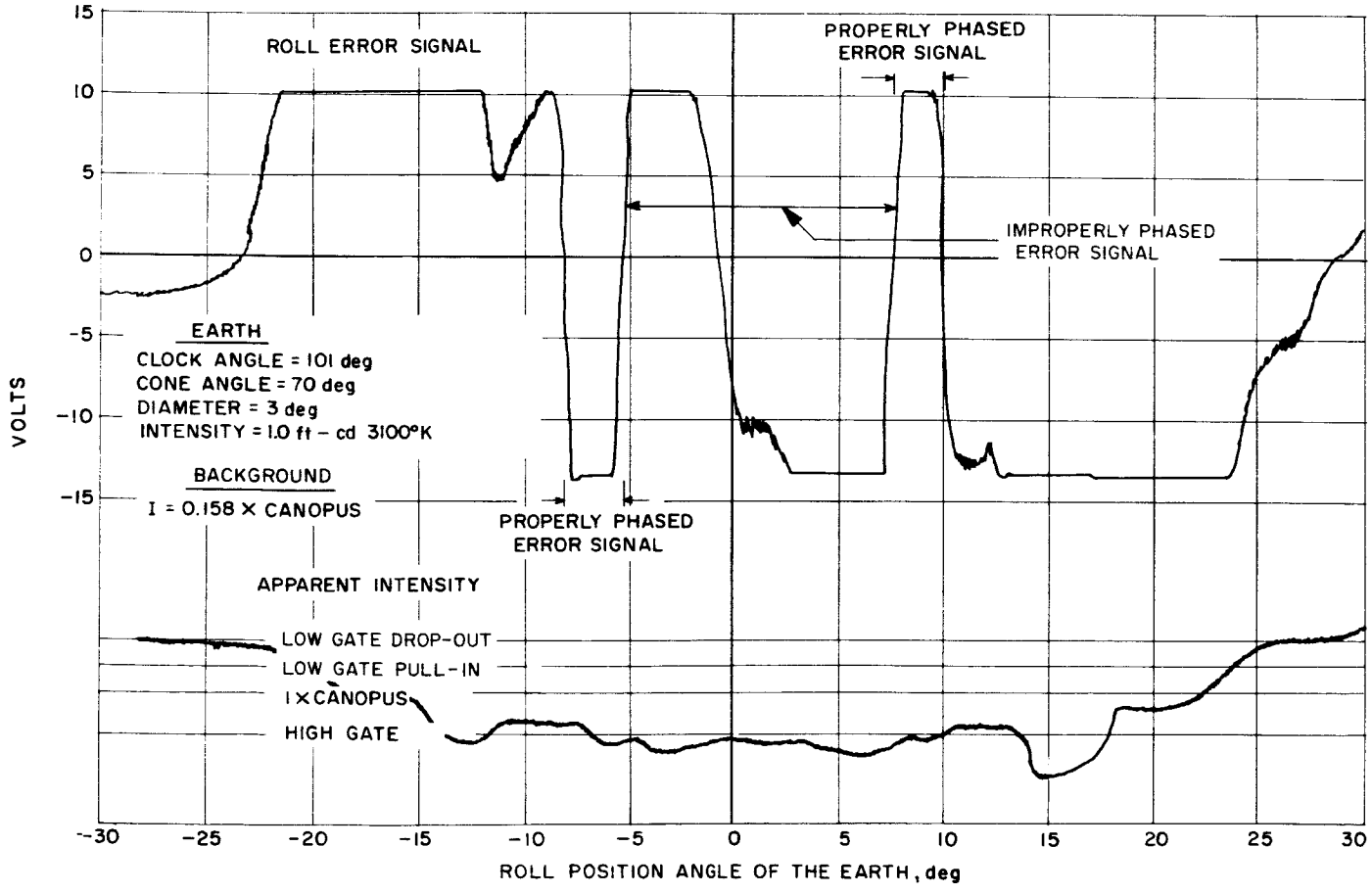


Fig. 155. Performance of Canopus sensor on Earth for the celestial geometry existing during initial roll search

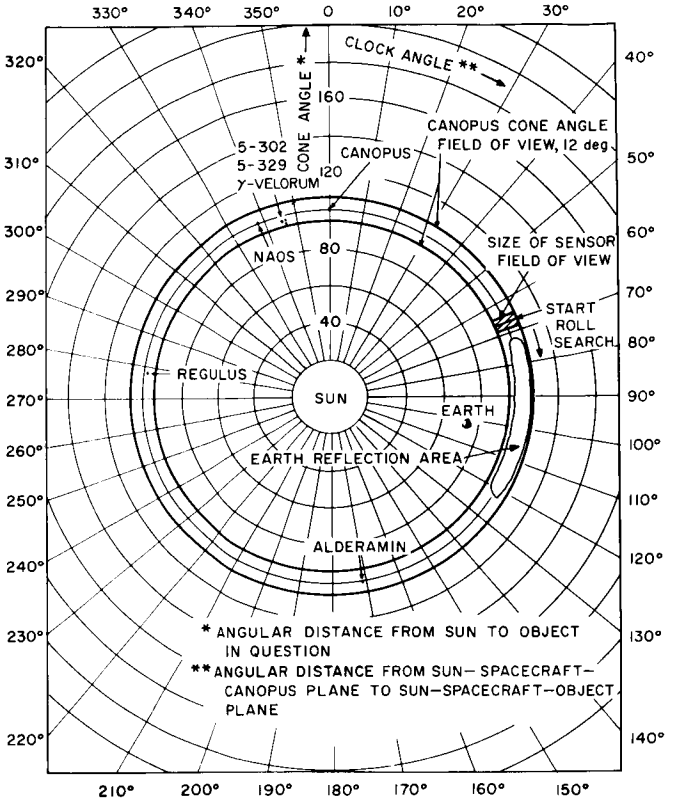


Fig. 156. Cone–clock coordinate picture at start of first roll search

and with all complex logic, computation, and data storage done on the ground. The geometric picture at the start of the first roll search is illustrated in Fig. 156. In ecliptic coordinates, the complete 360-deg roll–search field of view takes the form shown in Fig. 157.

Figure 158 is a plot of the predicted sensor output voltage versus clock angle at the time of first roll search. This was made by constructing a Canopus sensor response model based on laboratory calibration tests. The tests determined sensor response to flat backgrounds, stars of varying brightness, multiple stars, and stars plus flat backgrounds. In addition, it was necessary to determine response to extremely intense objects such as the Moon or Earth. These could appear more than a million times as intense as Canopus. Stray-light effects from such objects were significant even though they were far from the principal field of view. In Fig. 158, the predicted Earth stray-light effect is shown at a clock angle of 102 deg. In flight, this effect proved to be a very important bit of information for roll-angle determination.

The position of *Mariner IV* in the solar system is known by ground tracking and storage of trajectory parameters in a ground-based computer. Since the spacecraft is Sun–line stabilized and the Canopus sensor cone-angle field of view is known, it is possible to predict precisely what celestial objects will pass through or near its field of view as a 360-deg roll search is performed at any given time. A ground-based computer contains stored information on the celestial coordinates and relative Canopus brightness ratio of 423 stars plus background brightness of Zodiacal light and the Milky Way. The computation of the Canopus ratio of each planet is based on its range and phase angle. This information is fed into the calibrated sensor model to determine the estimated total sensor output versus clock (roll) angle as shown in Fig. 158.

Ground real-time identification of the prominent celestial objects passed during roll search was facilitated by isolating and recording the sensor brightness telemetry measurement on a recorder. A special plot of the *a priori* star map was made on a clear plastic sheet using the same scaling as was used on the recorder. As the *Mariner IV* rolled slowly during its search for an object of acceptable brightness, each prominent star could be quickly identified by relating the recorder plot to the plastic overlay plot.

Prior to midcourse maneuver, there were 13 periods of commanded roll search by *Mariner IV*. The perimeter of the sensor field of view at each brightness data sample has been plotted both in galactic coordinates and ecliptic coordinates. Hopefully, this will provide astronomers with valuable new information about the background brightness of Zodiacal light and the Milky Way as seen from outside the Earth's atmosphere. An example of such a plot is shown in Fig. 159.

The identification, or rather decision, of Canopus acquisition was accomplished on the ground and not on board the spacecraft. At first glance, however, it would seem possible to set the onboard logic brightness gates "tight" enough that the spacecraft would lock on only Canopus. Careful consideration showed this to be hazardous and, in fact, impossible. The elimination of planets was not possible for they might, depending on their range and phase angle, appear exactly at the Canopus level. More important considerations, however, were related to the serious consequences of setting the gates too tightly and missing the expected level entirely. This would have required a mandatory gate override command and a subsequent derived-rate acquisition without benefit of gyro rate signals. This was extremely undesirable since (1) the derived-rate acquisition mode was relatively new and not flight-proven, and (2) the

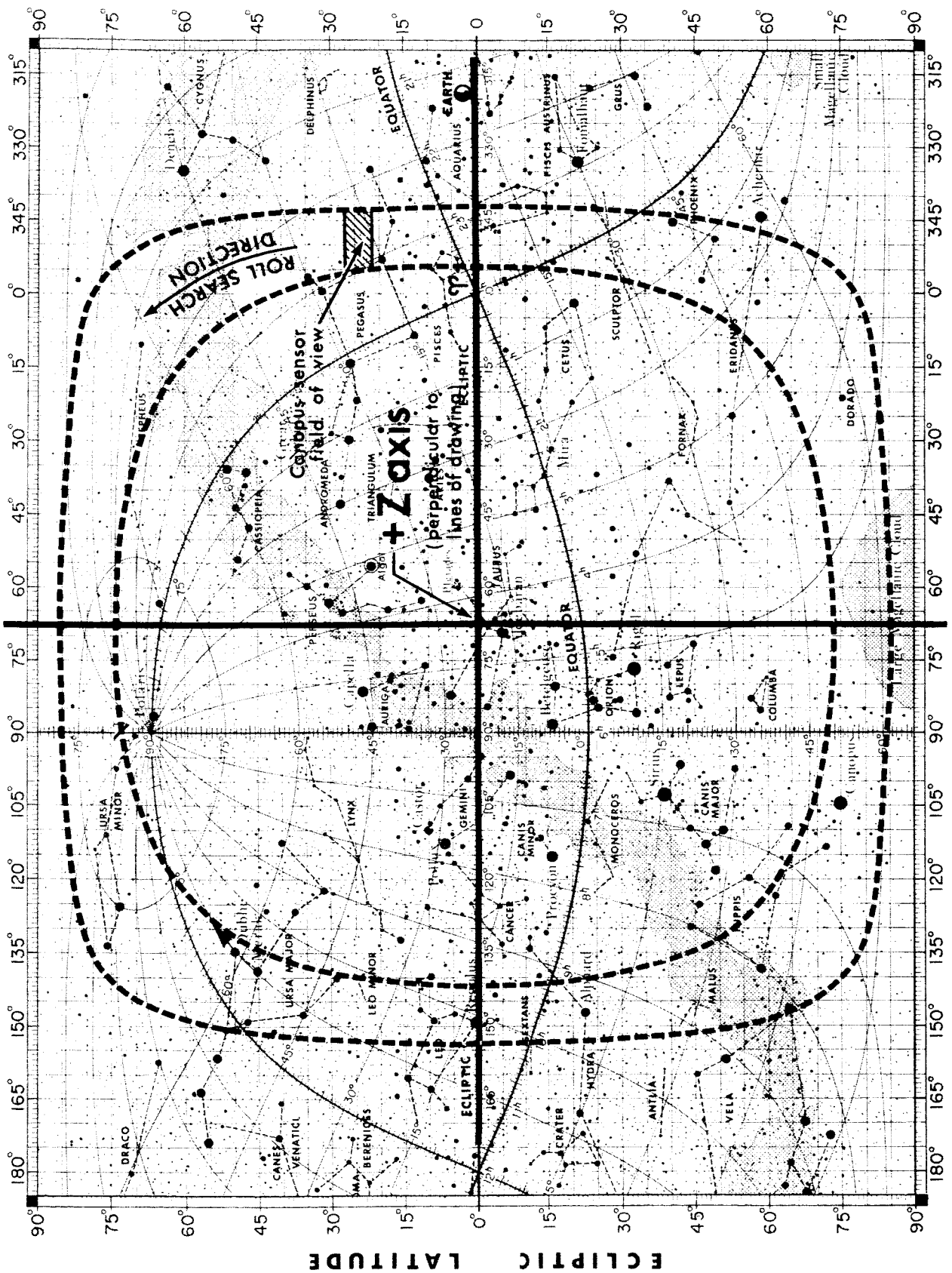


Fig. 157. Field of view of 360-deg roll search in ecliptic coordinates at start of first roll search

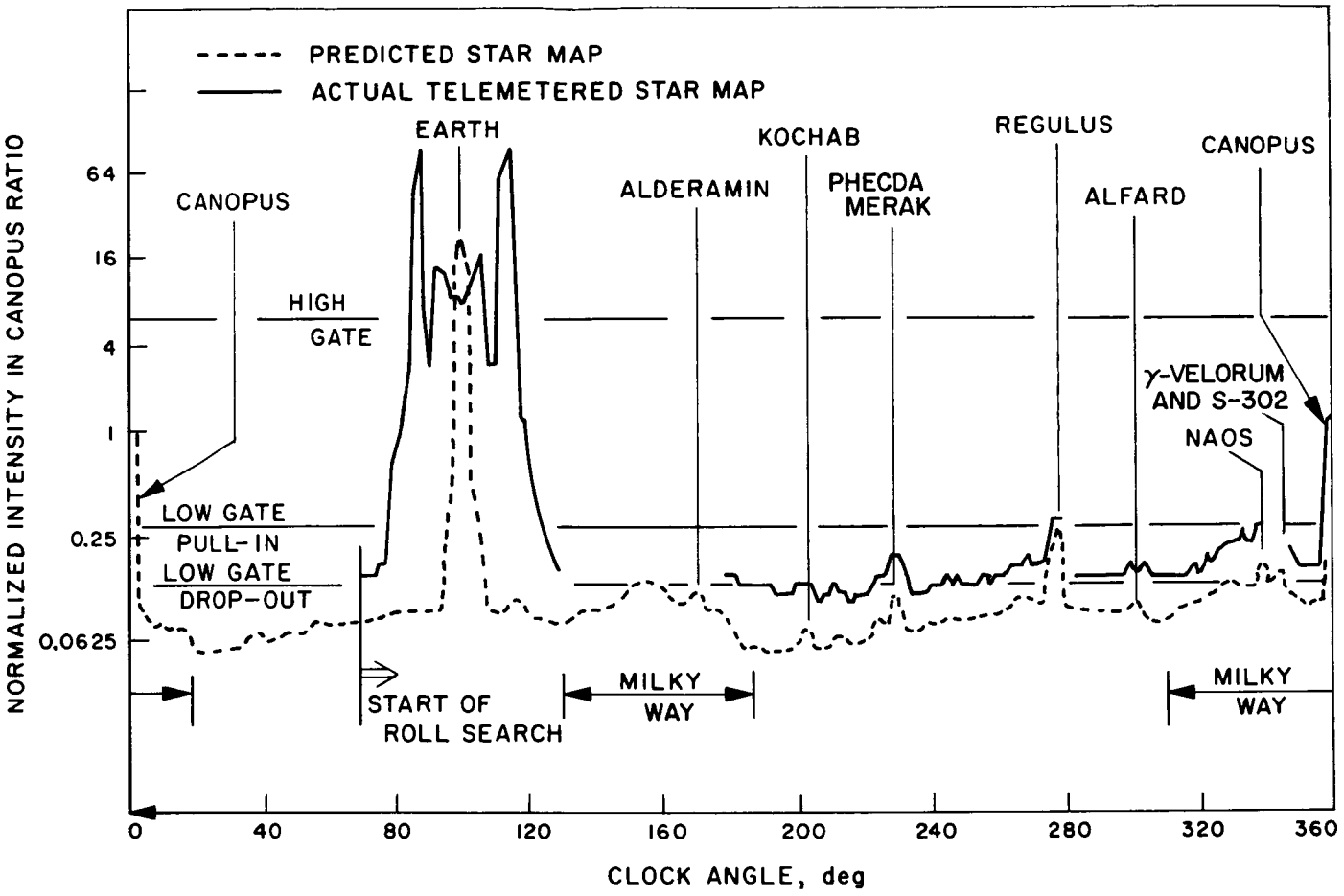


Fig. 158. Predicted and actual Canopus sensor output voltage vs clock angle at time of first roll search

spacecraft, without benefit of any brightness gate logic, would virtually stop on every star it saw. The necessary ground commands to get the spacecraft to proceed to Canopus in such a mode were many and complex. Setting the gates fairly wide and accepting the necessity for the more simple roll override command was decided upon.

k. Flight experience. The *Mariner IV* attitude control subsystem has experienced several disturbances on the roll channel. These disturbances have shown up in different ways, depending on the condition of the spacecraft. The ways in which the spacecraft has been disturbed are: (1) the roll-position signal has changed abruptly, (2) the gyros have turned on, (3) the intensity signal has increased momentarily, and (4) acquisition of Canopus has been lost and the spacecraft has gone into automatic roll search. During the first two weeks of flight, these disturbances occurred at the rate of about one every other day; in fact, the first attempt to perform a midcourse maneuver was aborted when the spacecraft lost lock on Canopus and went into roll search at the beginning of the sequence. Many theories (from cosmic rays to spacecraft electrical transients) were advanced to explain the disturbances. Probabilities were computed and tests were run, but none of the theories was able to produce the frequency and magnitude of the observed disturbances.

Before launch, considerable attention was given to spacecraft cleanliness. It was a well established fact that a lambert, spherical dust particle 0.005 in. in diameter in the field of view of the sensor appeared 8 times Canopus from a distance of 4 ft due to reflected sunlight. However, since solar pressure was calculated to accelerate particles to escape velocity in less than 0.1% of their orbital period about the spacecraft, and since it was expected that any electrical charge picked up by the spacecraft would be identical in polarity to any electrical charge picked up by spacecraft-born dust, loose dust was expected to be accelerated away from the spacecraft leaving the Canopus sensor free from interference. Even so, considerable care was taken to keep the spacecraft

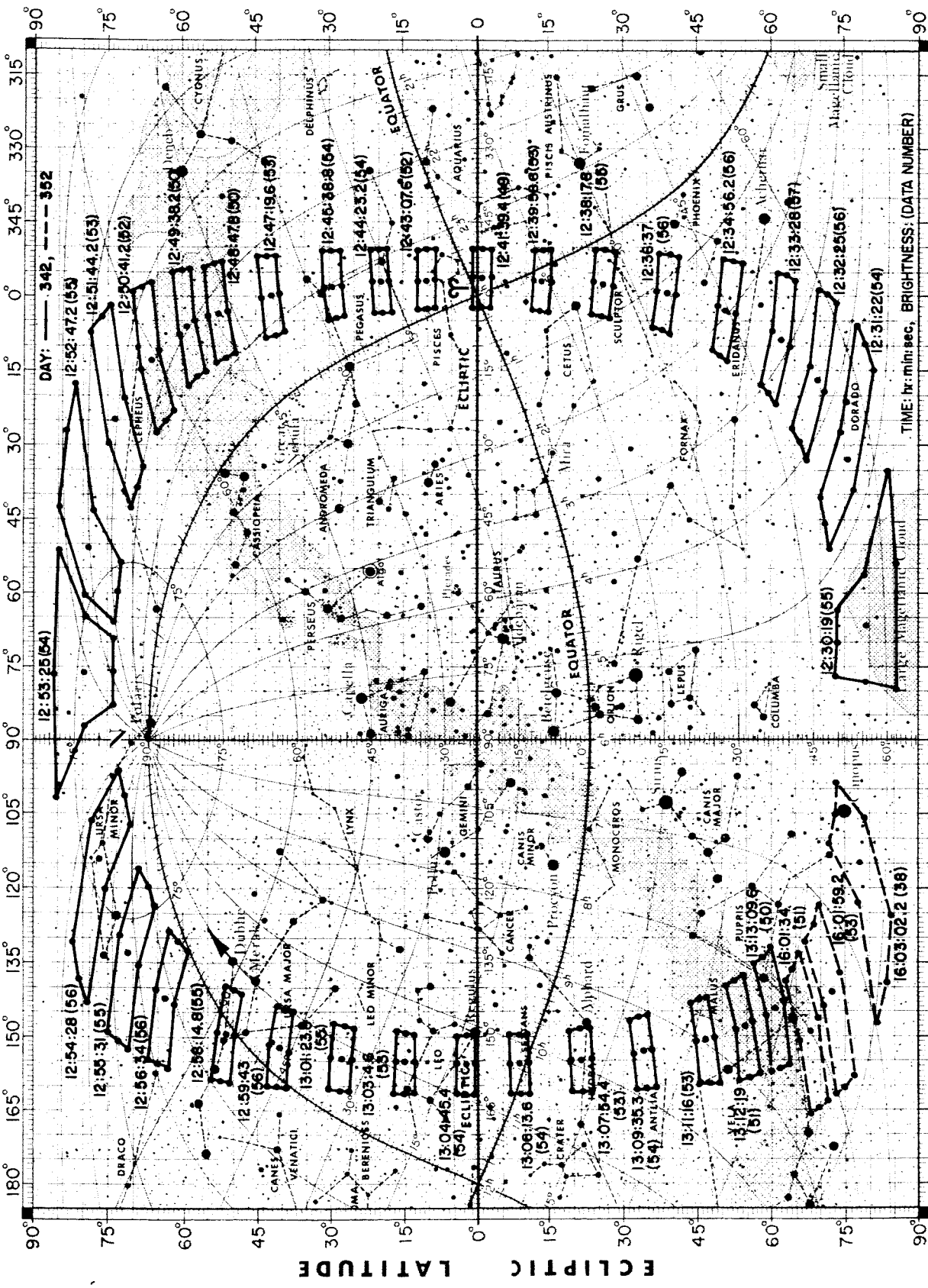


Fig. 159. Example of sensor field of view and corresponding brightness measurements taken during roll search

clean. To explain the roll disturbances, a mechanism was required whereby particles could be continually released from the spacecraft. It was suggested that meteoroid impacts on the spacecraft could release dust particles, and an analysis of this release mechanism was performed. The analysis was based on published estimates of meteoroid fluxes and took into account the geometry of the *Mariner IV* spacecraft and the sensitivity of the Canopus sensor. The principal conclusion reached is described below.

The observed phenomena on *Mariner IV* can be explained by assuming that small (10^{-14} to 10^{-12} g) meteoroids impact the solar panels and vanes and impart a low velocity (10^{-2} to 10 cm/sec) to 3- to 5-mil diameter dust particles that are on the panels. The dust particles are accelerated by solar radiation pressure as soon as they leave the shaded area behind the panels. As a result, most of the particles that are released with very low velocities (10^{-2} to 10^{-1} cm/sec) are accelerated to velocities of 0.2 to 0.5 cm/sec before entering the field of view of the Canopus sensor. Approximately 0.3% of the dust particles released from the two solar panels nearest the Canopus sensor "drift" into the field of view of the sensor and reflect sufficient sunlight into the Canopus sensor to produce the observed effect. The nominal expected frequency of such an event varies from approximately 5 events per day to 1 event every 20 days. The frequencies bracket the observed frequencies on *Mariner IV*. Even if the meteoroid flux estimates used are off by an order of magnitude either way, the observed phenomena are consistent with the proposed mechanism. The event duration predicted lies between 1 and 500 sec, with most of the event durations in the range of 10 to 50 sec.

The dynamic behavior of the spacecraft during each of the first six roll disturbances was simulated using a single-axis dynamic simulation of the spacecraft roll axis and dust particles. There were no flight data that could not be closely simulated using the dust-particle model.

The most troubling result of the dust-particle disturbances was loss of Canopus acquisition and subsequent automatic roll search. In order to initiate a roll search while the spacecraft was locked on Canopus, it was necessary for the Canopus sensor intensity gate to be violated, thus resetting the logic in the attitude control subsystem to the roll–search mode. In order to decrease the probability of losing lock on Canopus, the DC-15 command was sent to the spacecraft while it was locked on Canopus. This command caused the attitude control subsystem to ignore the acquisition gate signal from the Canopus sensor and to rely exclusively on the Canopus sensor error signal for roll attitude control. The command proved to be an effective solution to the problem. Small disturbances continue to occur due to occasional dust particles drifting through the field of view; however, Canopus lock has been solidly maintained since the command was sent.

2. Sun Shutter

a. History and design evolution. During development of the Canopus sensor, it was found that the Sun could burn spots on the image dissector photocathode. An occurrence of this sort during Sun acquisition was possible even though unlikely. To prevent damage of this nature, a Sun shutter mechanism was developed.

A cadmium sulfide photoconductive cell was used to detect the Sun and to provide a logic signal whenever the Sun entered the sensor field of view. This cell was mounted in a cavity in the front face of the Canopus sensor. Light baffles and a field stop were designed to give it a field of view similar to that of the sensor. Consideration was given to enclosing the shutter mechanism within the sensor assembly, but limited space, the schedule, and the desire to keep magnetic fields low near the image-dissector tube made this undesirable.

An external Sun shutter assembly with a modified, commercially available rotary solenoid as the actuator was used. The Sun detector and logic circuitry to provide the 22-v energizing signal to the solenoid was made an integral part of the sensor.

A return spring was furnished in the rotary solenoid; however, an additional spring was designed into the solenoid hub and blade assembly to provide a redundant force for the return stroke. Failure of the blade to return to the deenergized position would have prevented operation of the sensor. The commercial rotary solenoid chosen used metal balls and inclined planes to convert the linear armature motion to rotary motion, which is not good practice for high-vacuum environments.

During research and development on the problem of lubricating the commercial solenoid, nonmetallic balls made from nylon impregnated with molybdenum disulfide were tested. It was found that these balls also required lubrication for proper operation. Teflon lubricating powder was found to be an effective lubricant. To ensure that the teflon powder would not migrate from the areas in which it was needed, a technique was developed to impregnate the outer surface of the

nylon with teflon powder. A very light spray coating of teflon in a phenolic binder was then applied, and baked on to increase the mechanical bond. Environmental and special vacuum life tests verified that this method of lubrication was entirely satisfactory.

The shutter blade, as originally designed, was subject to fatigue failures imposed by the high deceleration at the end of the solenoid stroke. Failures occurred after as few as 500 repetitive cycles under ambient room conditions. The type of material was changed, and the blade shape was changed to provide corner fillets to reduce the local stresses. The redesigned shutter blades were tested to well over 10,000 repetitive cycles without failure.

b. Detailed functional requirements. The Sun detector and associated circuitry to provide the excitation signal to the Sun shutter assembly were housed in the Canopus sensor. The functional requirements for the shutter assembly were:

1. Actuation voltage. Upon application of 16 vdc to the input terminals, the shutter blade had to execute a full stroke (deenergized to energized position).
2. Actuation current. The current required for the actuation voltage was not to exceed 0.22 amp.
3. Return stroke test. With the excitation voltage removed, the shutter had to return completely to the deenergized position.
4. Low voltage test. Upon application of 5-vdc excitation, the shutter had to remain in the deenergized position.

c. Description. The following paragraphs describe the electronics, the mechanical design, and the detector and field of view of the Sun shutter.

Electronics. Figure 160 illustrates the portion of the attitude control circuitry that is related to the Sun shutter. The circuitry shown to the right of connector J1 is housed within the Canopus sensor. The solenoid K1 shown to the left of J1 is the Sun shutter solenoid. Also to the left of J1 is the power relay K2, which is energized by the attitude control logic whenever the spacecraft is

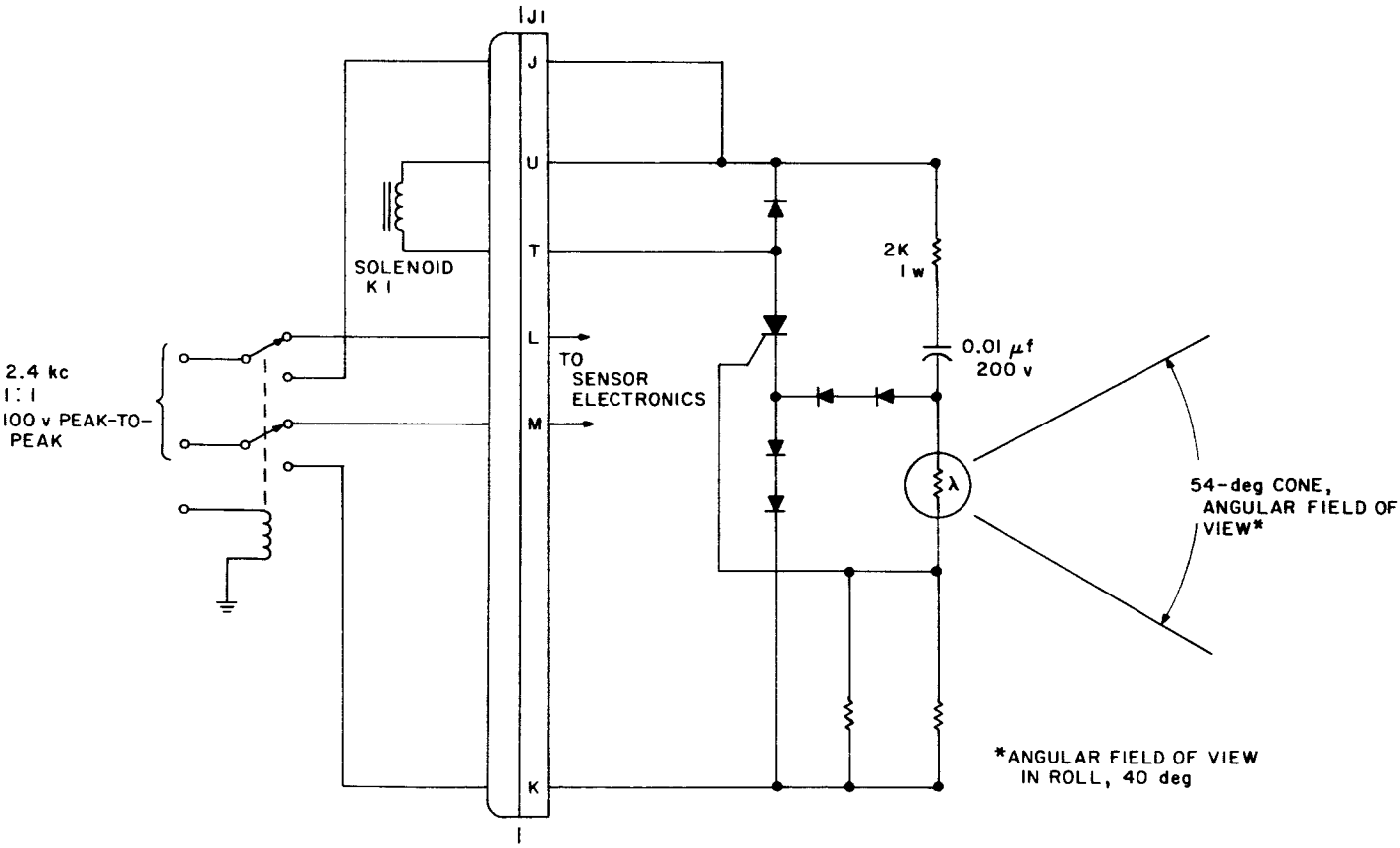


Fig. 160. Sun shutter electronics circuitry

not locked onto the Sun. This arrangement ensures that a false signal cannot operate K1 unless Sun acquisition is lost, and there is a possibility of the Sun coming into the sensor field of view.

Primary power to the circuit is supplied by the spacecraft 2.4-kc square-wave power supply. The shutter closing signal is provided by the cadmium sulfide detector V2, which drives the silicon controlled rectifier CS1. The SCR provides rectification of the 2.4-kc input to provide dc power to the solenoid. Diode CR6 is a suppression diode to prevent voltage surges. Diodes CR2, CR3, CR4, and CR5 are used to temperature-compensate the circuit. Resistors R109, R111, R112, and capacitor C79 form a voltage divider network for the detector V2. The exact value of resistor R112 is selected to set the light-level switching point.

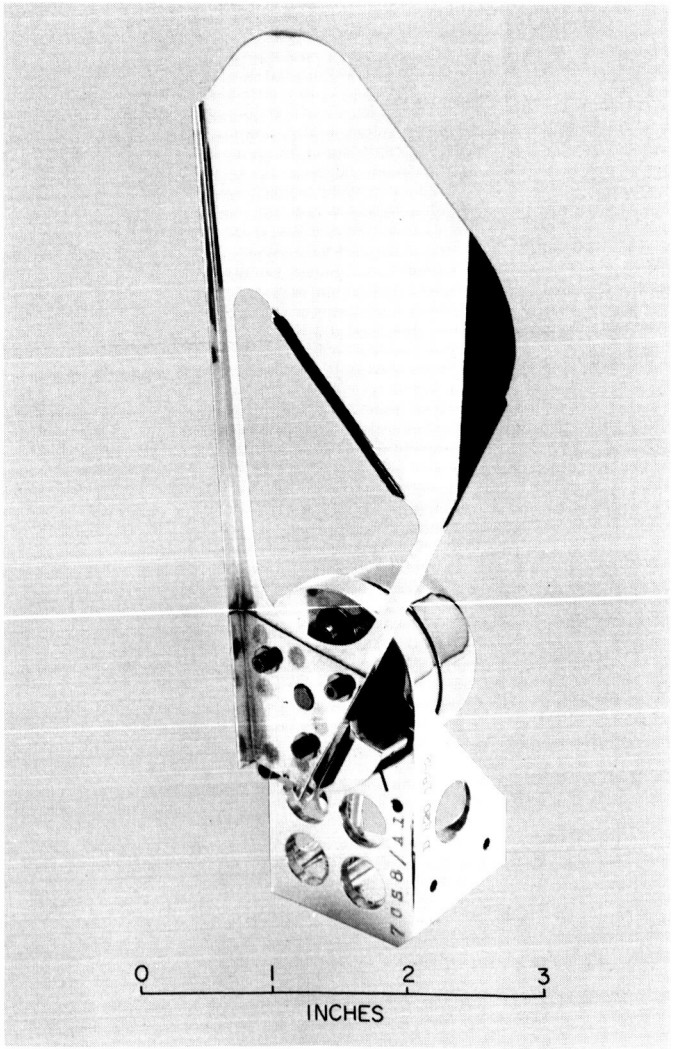


Fig. 161. Sun shutter assembly

Mechanical design. The Sun shutter assembly (Fig. 161) is comprised of a modified commercial solenoid; a hub, solenoid return spring, and shutter blade assembly; and a mounting bracket that attaches to the spacecraft bus. The assembly is positioned so that, when energized, the lightweight shutter blade covers the sensor lens aperture. When deenergized, the shutter completely clears the sensor field of view, preventing any erroneous sensor output signals caused by stray light from the shutter.

Detector and field of view. The cadmium sulfide detector V2 is a Clairex 705L cell, which is the same as that used in the Earth detector.[3]

The approximate field of view of the Sun detector is ±20 deg in roll and ±27 deg in cone. The precise field of view is determined by the intensity and position of the source; this relationship for the roll-angle field of view is shown in Fig. 162. Figure 163 shows this relationship for the cone-angle field of view.

d. Flight experience. The Sun shutter should actuate only if the Canopus sensor is directed approximately

[3]Figure 173 presents a normalized sensitivity curve with respect to wavelength, a chart of response time versus light level, and a chart of conductance versus light level and temperature.

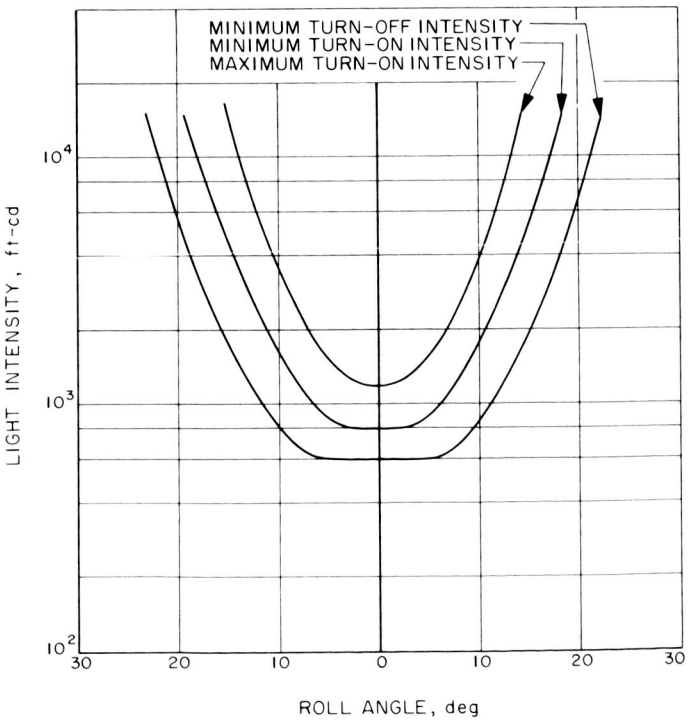


Fig. 162. Light intensity vs roll angle

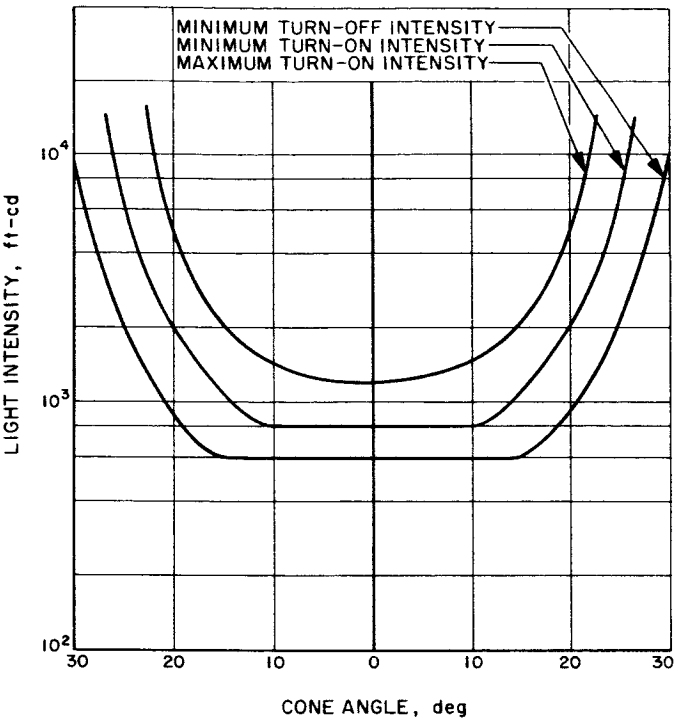


Fig. 163. Light intensity vs cone angle

toward the Sun. This could occur during acquisition or during any spacecraft failure mode in which loss of both Sun and Canopus lock might occur. It was not deemed advisable to incorporate a telemetry channel to determine when the Sun shutter was energized, and none of the existing telemetry channels provide a positive indication of whether it has operated during the flight of *Mariner IV*. It is, of course, known that the shutter has so far remained in the deenergized position, since the sensor would not operate normally if the shutter had entered its field of view.

3. Sun Sensors

a. History and design evolution. The original design requirements of the square root Sun sensors specified an output signal the voltage of which was proportional to the square root of the error angle from null in both the pitch and yaw axes. This is how the name "square root Sun sensors" originated. During the development of the sensors, the signal requirements were changed to provide a greater scale factor near null and signal saturation at approximately 100 deg from null. This modified, single-axis, error signal curve is shown in Fig. 164.

The *Mariner IV* Sun sensors operate on the same basic principle as did the *Ranger* Sun sensors. The actual configuration is very different, however, for two reasons:

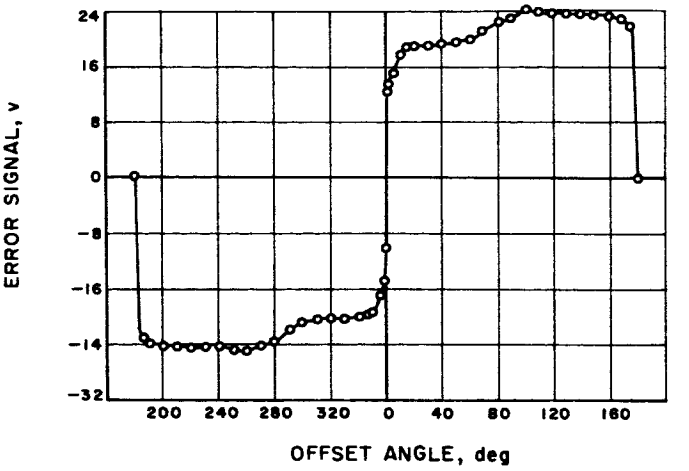


Fig. 164. Square root Sun sensor system characteristics

(1) the difference in the required output signal characteristics, and (2) the accessibility of mounting locations on the spacecraft.

The *Ranger* spacecraft design allowed mounting of acquisition sensors on the solar panel tips and the cruise sensors on the spacecraft bus. This mounting arrangement was ideal to meet the 2π sterad field-of-view requirement with the minimum number of detectors.

During the *Mariner* Mars spacecraft design, it became desirable to mount all Sun sensors on the spacecraft bus to prevent the solar vanes from restricting their field of view, and to avoid added weight on the solar panel tips. In order to prevent shadowing of the detectors by the solar panels or solar vanes, the function of each detector, which looks out from the bus into the plane of the solar panels, was accomplished by two paralleled detectors. One of these detectors was mounted on the sunlit side of the spacecraft bus and the other on the dark side. Each of these detectors was then provided with a field stop to eliminate shadows or reflections from the solar panels as shown in Fig. 165. The total number of detectors required for the two-axis system is 16, compared to 12 for the *Ranger* system.

Excitation voltages of ± 16 and ± 26 vdc are required to achieve the desired output curve shape. The electrical diagram is shown in Fig. 166.

The basic function of the square root Sun sensors is to provide error signals that can be used by the attitude control subsystem to attain Sun acquisition and to maintain Sun lock after acquisition. The basic design techniques used for both the *Ranger* and *Mariner* Mars Sun

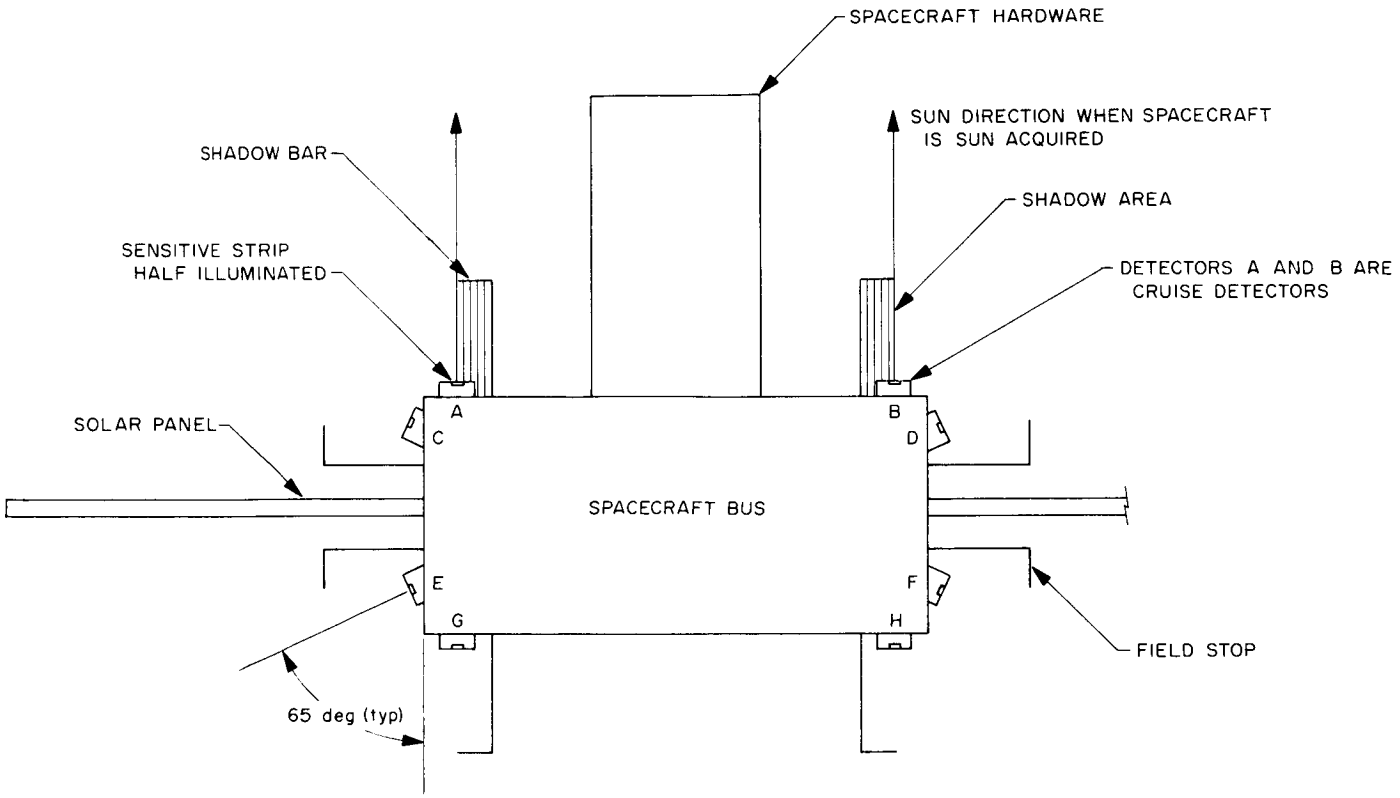


Fig. 165. Detector mechanical arrangement (single axis)

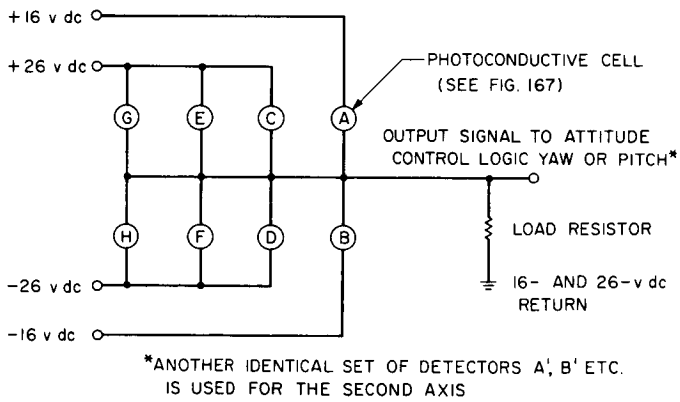


Fig. 166. Sun sensors, electrical diagram

sensors were the same. The statistical results from accuracy tests run on 24 *Ranger* primary sensors were therefore considered to be indicative of both *Ranger* and *Mariner* Mars sensor accuracy. These data are shown in Table 44.

b. Description. The Sun sensor detector used for both *Ranger* and *Mariner* programs was a cadmium sulfide photoconductive cell. Figure 167 illustrates the change in resistance of this detector with light intensity. The curve in the figure was produced by measuring the resistance of four detectors, at various levels of sunlight, using neutral density filters.

The square-root Sun sensor system is comprised of four separate assemblies, each containing four cadmium sulfide detectors. A full set of sensors is shown in Fig. 168. Two identical assemblies are mounted 180 deg apart about the roll axis on the sunlit side of the spacecraft and are called the primary Sun sensor assemblies. One of these assemblies contains the A and C detectors shown in Fig. 165. Also included are A′C′ detectors to produce an output function for the second axis. The other assembly contains the B, B′, D, and D′ detectors. By physically separating the cruise detector pairs A, B, A′, and B′ by the width of the spacecraft (Fig. 165), signal degradation caused by shadowing or reflections from spacecraft components is prevented.

The other two sensor assemblies are mounted on the dark side of the spacecraft bus in the same manner. These are called secondary assemblies; one contains detectors E, E′, G, and G′, and the other contains detectors F, F′, H, and H′. The secondary assemblies differ from the primary assemblies in that they require plus and

Table 44. Statistical test results on a group of 24 primary pairs of Sun sensors

Condition	Null offset		Condition	Scale factor	
	Average value sec of arc	1σ distribution about mean sec of arc		Average change, %	1σ distribution, %
At 70°F	+ 0.72	12	At 70°F	0	—
At 40°F	− 5.0	22	At 40°F	− 1.15	2.9
At 140°F	+ 0.72	28	At 140°F	+ 3.14	1.6
At 160°F	+15.5	31	At 160°F	+10.26	4.8
At 0.7 solar constant	+ 0.72	12	At 0.7 solar constant	0	—
At 0.5 solar constant	+ 2.1	—	At 0.5 solar constant	− 0.74	0.316 (only 6 pairs sampled)
At 0.35 solar constant	− 3.3	15 (only 6 pairs sampled)	At 0.35 solar constant	− 0.76	0.7 (only 6 pairs sampled)
After FA testing	− 2.5	20	After FA testing	0.17	2.16

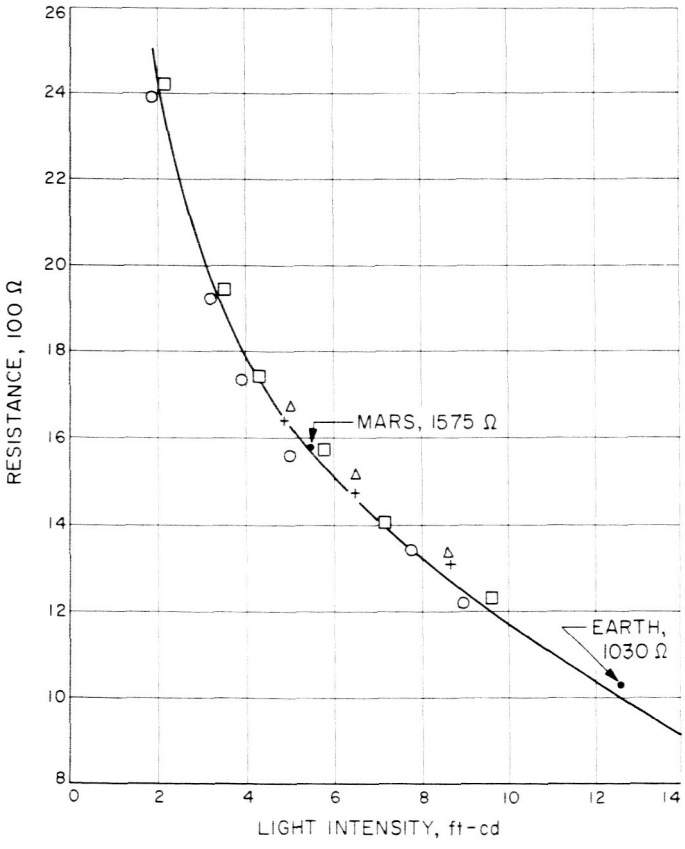


Fig. 167. Cadmium sulfide photoconductive cell characteristics

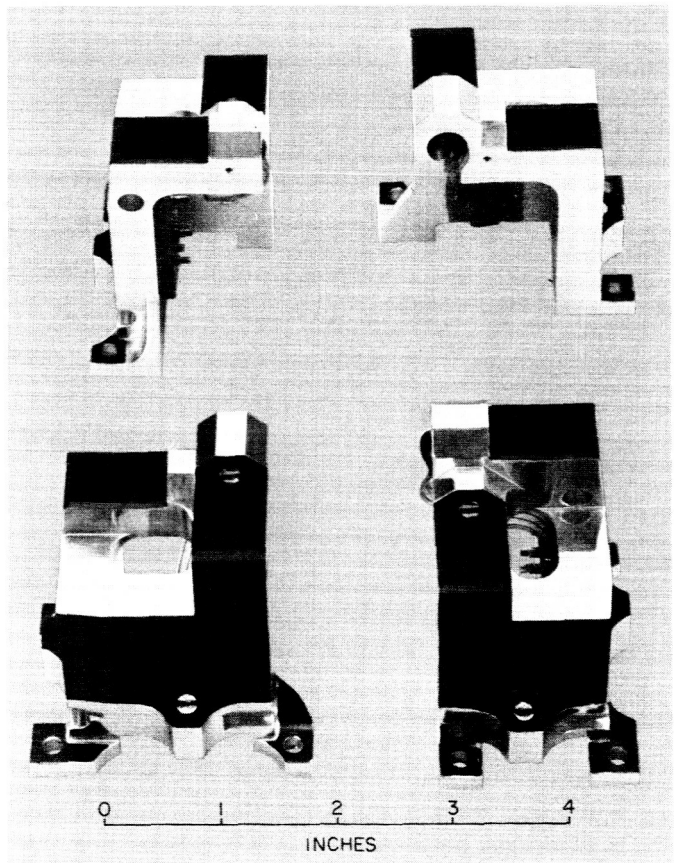


Fig. 168. Square root Sun sensors

minus 26 vdc excitation only, whereas the primary assemblies also require plus and minus 16 vdc as indicated in Fig. 166.

c. Environmental testing. One failure of the square root sensors occurred during the first type approval vibration test. The postenvironmental performance test disclosed an open circuit to one side of an acquisition detector. The wire splice joining the detector lead and the lead from the terminal board had failed open. The splicing technique was changed so that the splices could be totally enclosed and supported by the silicone rubber

potting material that was used to anchor each detector into its housing cavity. The type-approval vibration test was then repeated successfully and no failures of this type were encountered with the flight units.

A second type of failure occurred during the flight-acceptance vibration testing of a secondary flight sensor when an open occurred within a detector. Microscopic inspection indicated that a substandard indium solder joint at the junction of the detector wafer and the lead wire coming in through the glass header of the detector enclosure was responsible. The detector was replaced and the unit was retested successfully.

4. Sun Gate

a. History and design evolution. The *Mariner IV* Sun gate is a design modification of the Sun gate that was flown on the *Mariner II* spacecraft. The *Mariner II* Sun gate consisted of a block-like frame that enclosed two cadmium sulfide detectors, each having a sensitive area 0.050 in. wide by approximately 0.190 in. long. Each detector was housed in a cavity covered by an aperture plate that had an opening approximately the same size as the sensitive area of the detector. The detectors were mounted 90 deg apart about the roll axis. In this manner, sunlight could energize both cells only when the spacecraft was Sun-acquired. The cells were connected in series, and their resistance was used by the attitude control logic to sense Sun acquisition.

The *Mariner IV* Sun gate incorporates design modifications to increase its inherent reliability. Two cadmium sulfide detectors of the same type as those used on *Mariner II* are used. Either one can fail in an open state and the Sun gate will continue to function within acceptable limits. It was estimated that the probability of a detector failing in a shorted state is extremely remote, since the sensitive strip is 0.050 in. wide and is protected from foreign material by a hermetically sealed enclosure.

The basic functional requirements for the Sun gate are to provide to the attitude control subsystem an indication of Sun acquisition.

b. Description. The detectors used in the Sun gate are identical to the ones used in the square root Sun sensors. The Sun gate assembly (Fig. 169) is comprised of a block-like frame that houses two separate cadmium sulfide photocells, associated light baffles and apertures, plus an externally located terminal board. The sensitive area of each cell is restricted to a rectangular area of 0.050 × 0.037 in. by a masking baffle. The field-limiting

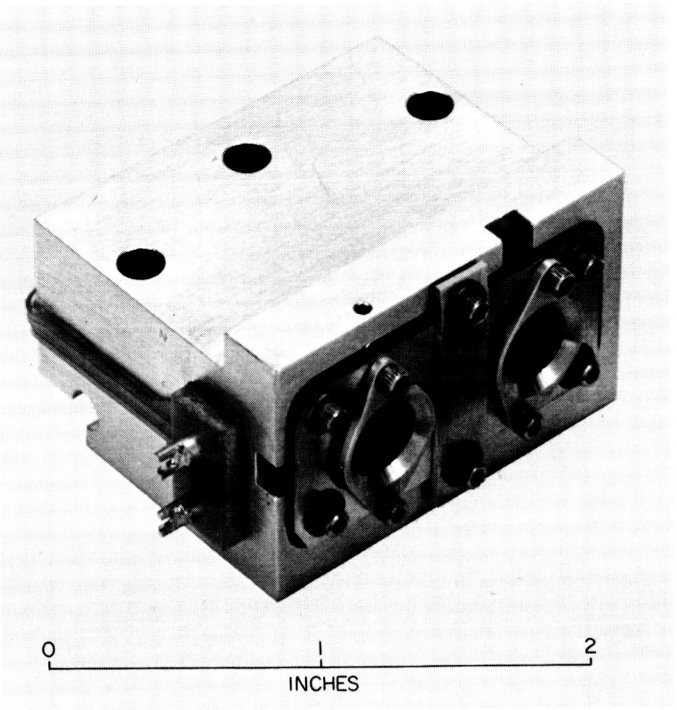


Fig. 169. Sun gate assembly

aperture for each cell is adjustable in two axes for alignment purposes and includes a central opening 0.070 in. in diameter. A stray-light baffle, having a central opening 0.125 in. in diameter, is located approximately half way between the outer field-limiting aperture and the photocell surface.

Restriction of the detector sensitive area was required to achieve the circular field-of-view characteristic (Fig. 170). Each photocell assembly thus provides satisfactory output signals for either yaw, pitch, or combined yaw and pitch errors. The two photodetectors are connected in parallel. If one detector should fail open, the other detector will still provide output characteristics at twice the normal resistance. With the triggering level of the attitude control logic set at 14 kΩ, this would cause the spacecraft to assume a Sun-lock condition at 4-deg angular error from the roll axis. This compares to 5.1 deg if both cells were operating in parallel.

5. Earth Detector

a. Design evolution. The extreme importance of knowing roll attitude prior to midcourse maneuver, even in the event of certain telemetry-channel failures, pointed out the need for including an Earth detector on *Mariner IV*. Studies of the trajectory showed that early in the mission the Earth direction would be relatively constant if

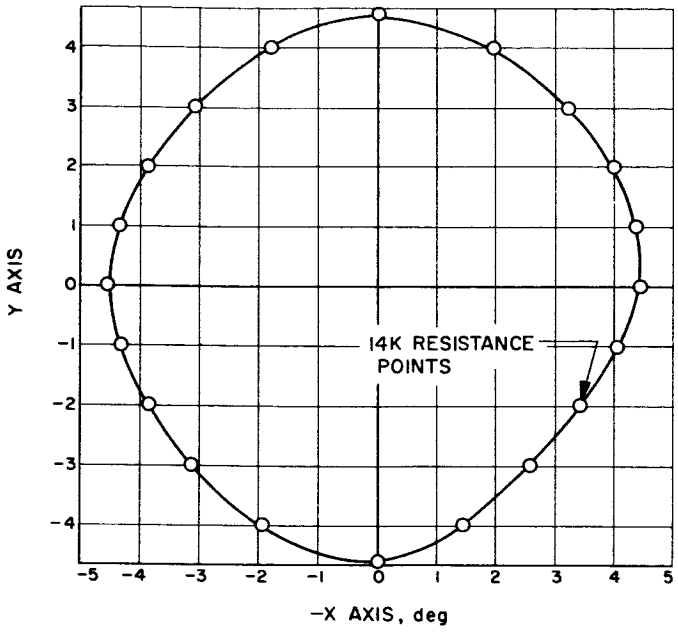


Fig. 170. Sun gate characteristics

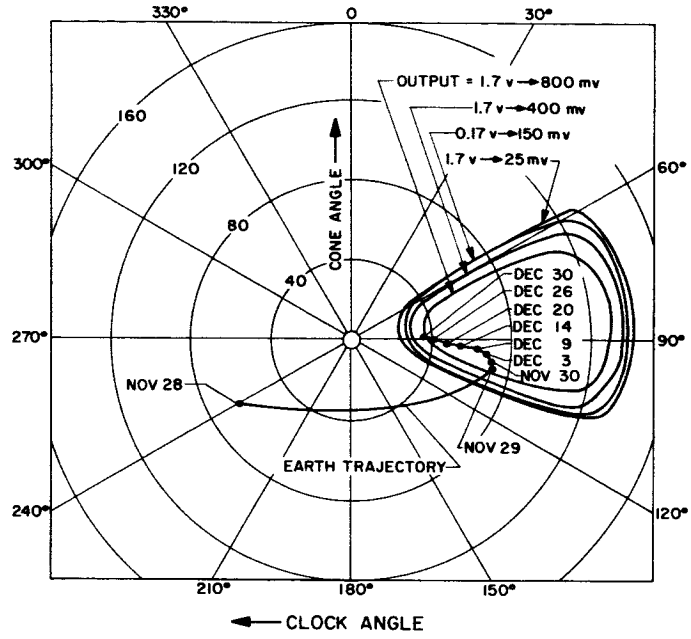


Fig. 171. Earth detector outputs vs cone and clock angle for a 0.05 ft-cd Earth

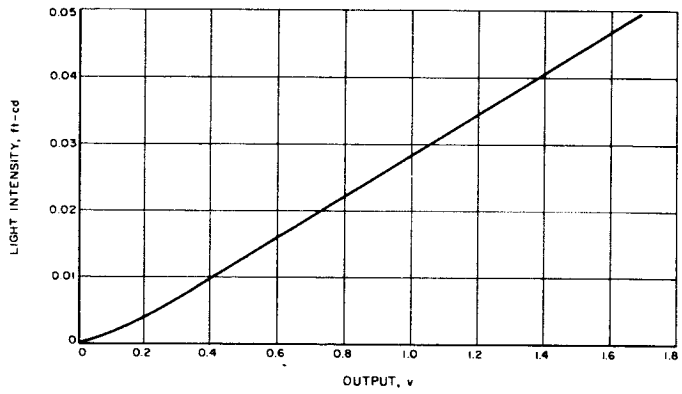


Fig. 172. Earth detector outputs vs light intensity

Canopus were acquired in roll. Since Earth is a large and bright object, it could be detected by a relatively simple device. A photoconductive cadmium sulfide cell with no lens would reliably sense Earth for approximately 20 days. This would provide a backup means of Canopus identification (for most trajectories) during the crucial midcourse maneuver portion of the mission. The functional requirements for the Earth detector were:

1. It had to be sufficiently sensitive to provide meaningful outputs for the first 10 mission days
2. It had to be small in size, in weight, and in power
3. It had to have a field of view large enough to detect Earth regardless of the trajectory
4. It had to have a stray-light field of view small enough to eliminate interference from all illuminated spacecraft parts

b. Description. The Earth detector is a simple and lightweight device (142 grams) made up of a light-sensing element and an arrangement of baffles. The detector is a cadmium sulfide photocell housed in a transistor can. The resistance of the detector changes with variations in light input. Its sensitivity is sufficient to produce a detectable output signal from a light input of 0.001 ft-cd. Figure 171 is a plot of constant Earth-detector output contours versus cone and clock angle for a 0.05 ft-cd Earth. Figure 172 is a plot of light intensity versus output voltage of the Earth detector. Figure 173 indicates the normalized sensitivity curve with respect to wavelength. Table 45 is a chart of the response time to light levels and Table 46 tabulates the variations in conductance at various temperatures of the cell. Figure 174 illustrates the sensing element and its allied circuit components. Figure 175 shows the completed Earth detector with four baffles and the small Sun shield. Located nearest the sensing element is a 0.030 by 0.090 in. rectangular opening that determines the effective detector size. The second baffle defines the primary field of view, which was optimized to be as large as possible in both cone and clock angles without encountering any

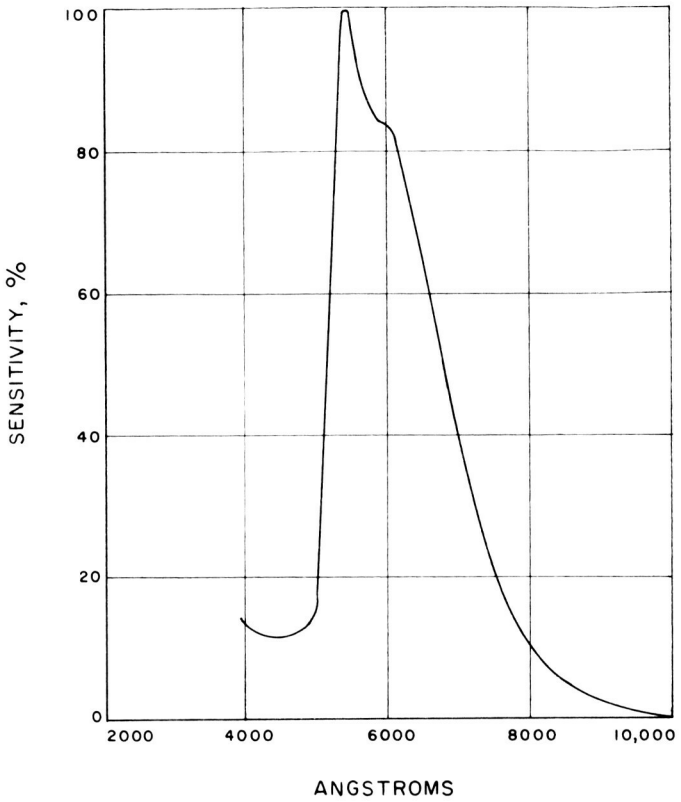


Fig. 173. Earth detector normalized sensitivity curve vs wavelength

Table 45. Response time vs light level

Response time[a]	Light level, ft-cd				
	0.01	0.1	1	10	100
Rise	2.8	0.30	0.07	0.02	0.007
Decay	1.3	0.22	0.06	0.02	0.014

[a]To 1–1/e of final reading.

Table 46. Conductance vs light level

Temperature, °C	Light level, ft-cd				
	0.01	0.1	1	10	100
−25	115	97	93	90	94
0	103	97	95	94	96
25	100	100	100	100	100
50	107	109	114	115	106
75	114	126	131	138	105

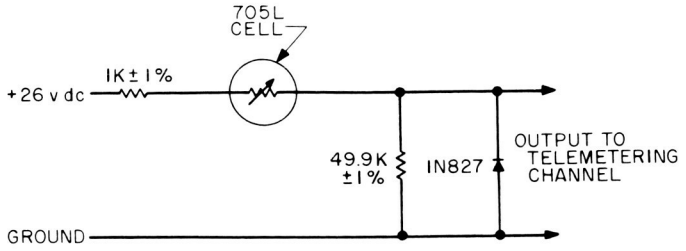
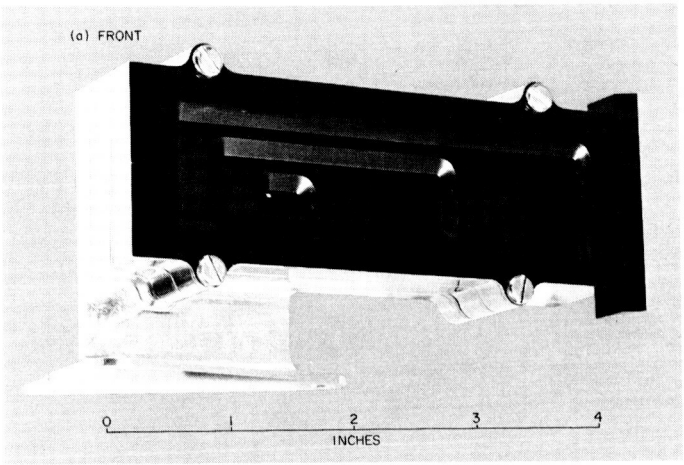


Fig. 174. Earth detector circuit diagram



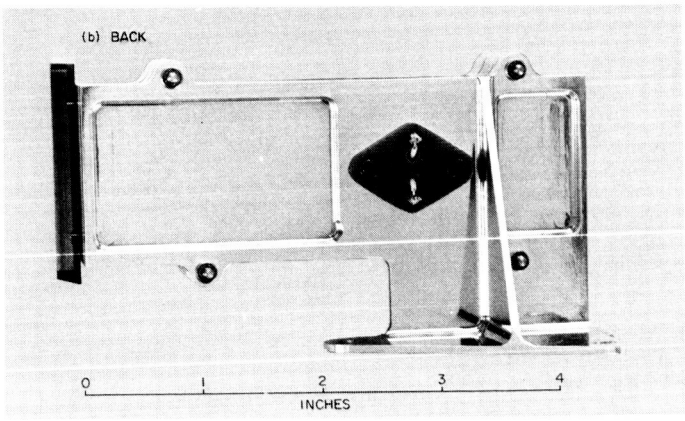


Fig. 175. Earth detector assembly

spacecraft interference. The clock angle field of view is restricted by the solar panels.

Figure 176 is a plot of the predicted and actual Earth detector output voltages versus time, which are well within the design goal for the instrument. No additional telemetry channels were required, since the Earth detector shared the roll gyro channel.

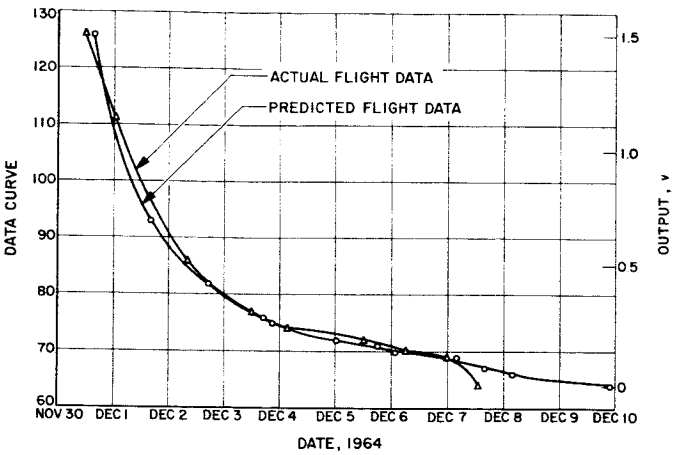


Fig. 176. Predicted and actual Earth detector output voltages

D. Other Attitude Control Subsystems

1. Gas Actuator System

The *Mariner* Mars 1964 gas actuator system, which uses cold gas (nitrogen) as the working fluid, was the culmination of five years of attitude control gas-actuator development. Contamination, the greatest problem inherent in these systems, was controlled by: (1) thrust valves that had the characteristic of zero contamination generation in the sensitive valving areas, (2) ultra-clean heliarc welding techniques for clean-room compatibility, and (3) flexible metal tubing that served as hinge components so that torque arms could be optimized. The system also encompassed a strap-on, contamination-closed unitized design providing ultimate control at the fabrication level.

Redundancy in the gas system was provided by the use of two independent assemblies with sufficient gas capacity to allow for a worst-case failure of one assembly.

a. Description. The system is comprised of two identical assemblies, each assembly having an independent gas supply. Six thrust valves in each assembly are located on the ends of the solar panels to provide the most efficient torquing moment and to increase the stored momentum. Each valve in an assembly has a companion in the other assembly that provides a pure couple.

In the event of a worst-case failure, such as a valve failing to close after the first spacecraft operation, one assembly would be bled down completely. The torque created by the failed valve would be countered by one valve in each assembly, resulting in the ultimate loss to the remaining assembly of one-third of its gas supply. The gas budget used allows for this mode of failure, whereas a gas budget for a non-failure case would have to be three times as big.

In a spacecraft system employing mass expulsion actuators, a tight pressure circuit having low losses due to leakage is paramount. Mission times of 250 days present a challenge to both static and dynamic seal techniques. A choice of hard-seal metal-to-metal thrust valves was made early in the program, although soft-seal technology had made impressive showings. Mechanical fittings, such as the B-nut type, were minimized because of inherent leak and contamination problems. Welding methods were considered for the static seals; it was felt at the time of development that a welding process would provide more ultimate control on contamination than the brazing methods in use at that time.

The permissible leak rate out of the many seals and connections of the *Mariner* Mars gas system was set at 30 cm^3/hr (at standard pressure) per assembly. Quantitative leak tests of the system after assembly reflected leak rates that were almost wholly made up of valve leakage. Each valve was allowed to leak up to 3 cm^3/hr during qualification testing. If each valve was leaking at its maximum allowable rate, the total leakage per assembly would become 18 cm^3/hr, a factor well below the maximum allowed for each assembly. Other seal types used in the system besides welded fittings include: (1) one AN fitting,(having bull-nose terminations connected to B-nut flare fittings) used in each line running to a solar panel to provide backup flexibility in the event of mismatch and as a field separation joint in case of an emergency replacement of a gas-system extremity (i.e., from separation joint to the hardware on the end of the solar panel); (2) a valve-to-manifold seal made with an X-bar seal, which allowed a flange joint in an area in which contamination sensitivity (i.e., the valve) is highest; and (3) a vessel-coupling seal, which is a crush type with a soft metal washer loaded to each side by serrated couplings.

A gas-system assembly is shown mounted on a support fixture in Fig. 177. The base fixture is essentially identical in configuration with a section of the spacecraft bus, and acts as jig tooling during fabrication of the distribution lines. The upper parts of the fixture are mechanical frames that act as solar panel fixtures when the assembly is mounted on the spacecraft bus. As seen in Fig. 178, the frames are deployed as the solar panels would be during flight. Two flexible joints are provided in each leg of plumbing running out to a solar panel.

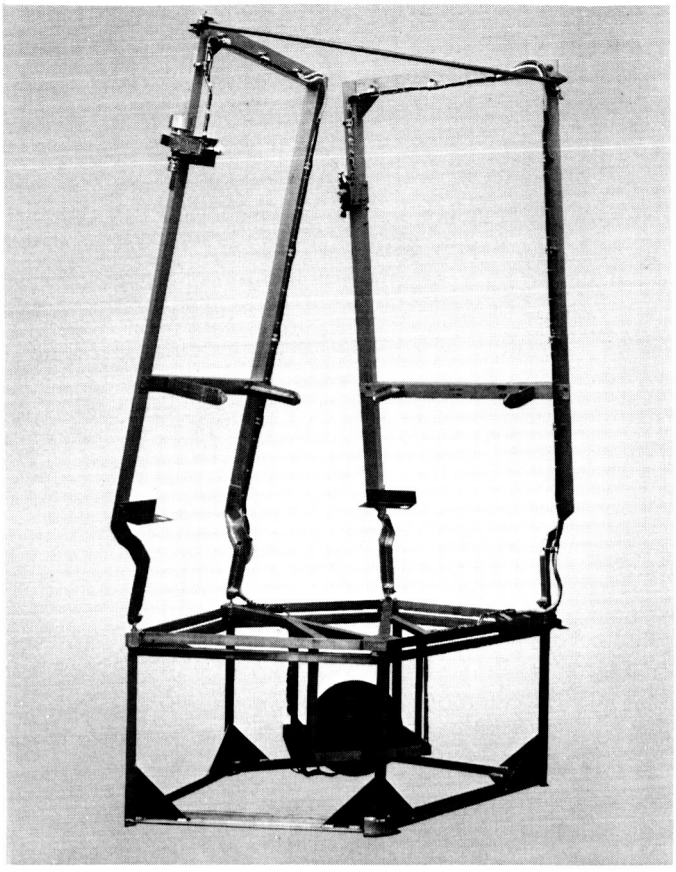


Fig. 177. Gas actuator system assembly on support fixture

One flexible tube acts as a hinge adjacent to the connection (i.e., monoball swivel joint) of the panel to the bus. A second flexible tube is provided, which allows the panel plumbing to be folded back, making the gas assembly shipping container smaller and more compatible with the spacecraft shipping van.

Figure 179 shows a view of the high-pressure section in an intermediate fabrication step. An OSE manifold assembly that was developed at JPL is shown next to the receptacle. This manifold assembly, also called a fill manifold assembly, was one of the most important controls for the gas system during assembly qualification and field testing on the spacecraft. The manifold is shown schematically in Fig. 180.

Gas introduced into the system must pass through the control filter, which has a rating of 0.5 μ absolute. This manifold assembly was installed into the high-pressure assembly in a clean room as though it were a flight component. It remained on the assembly through all preflight operations and it was removed only after the final charging operation of the system prior to flight. Thus, contamination control was retained by means of the OSE manifold through all operations up to launch.

The completed high pressure section of the gas system is shown in Fig. 181 and 182 after the temperature transducers were mounted and the thermal control paint

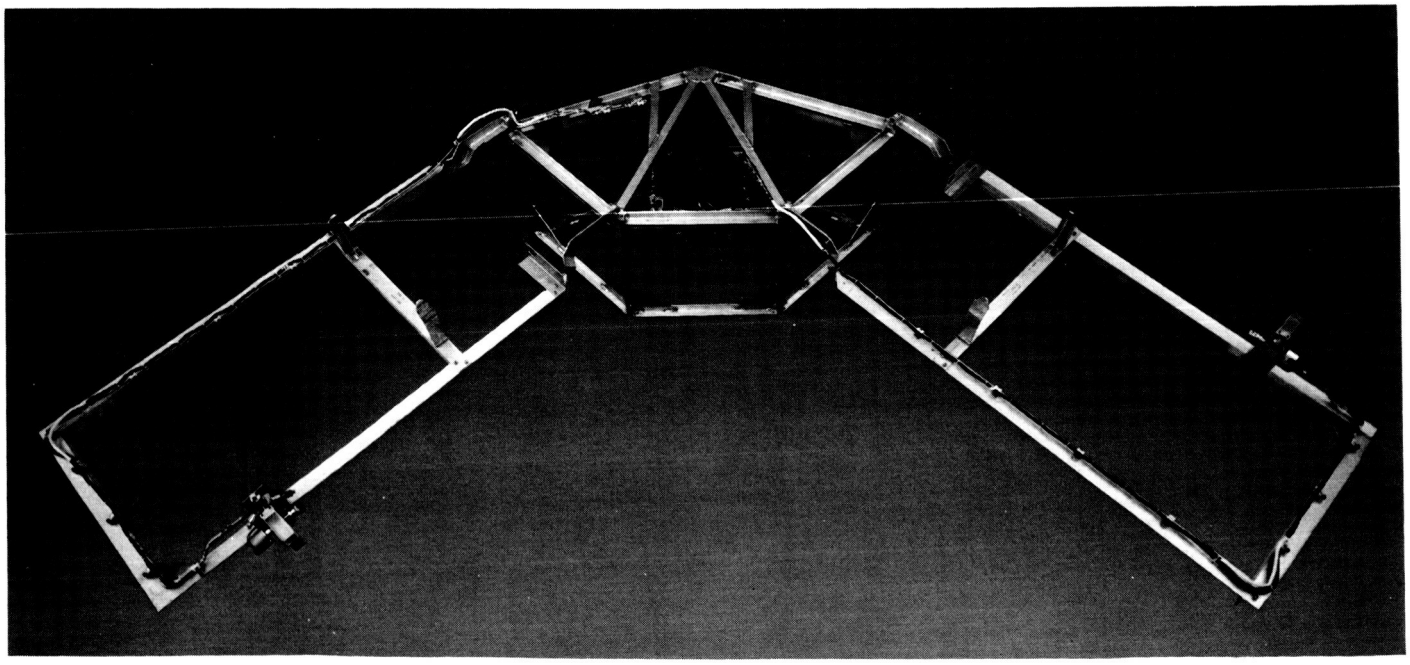


Fig. 178. Gas actuator system assembly mounted on handling fixture

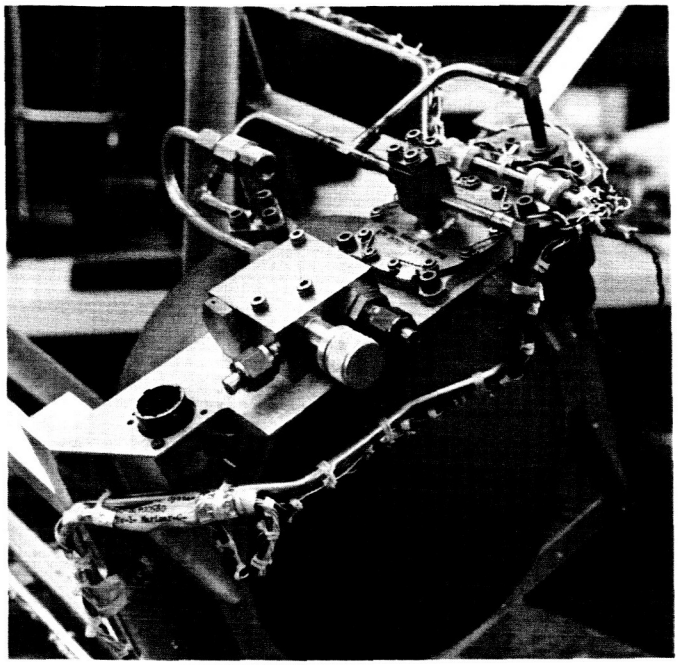


Fig. 179. High-pressure system

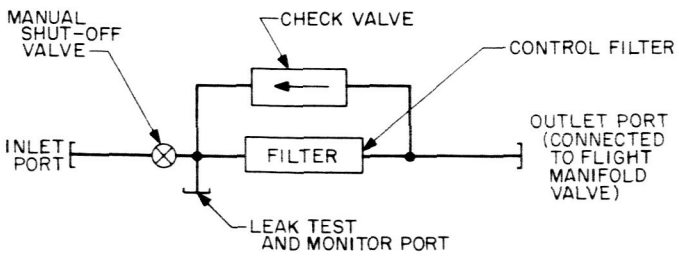


Fig. 180. Fill manifold assembly

added. One transducer serves as the flight temperature pickup and the other is used for OSE monitoring of vessel temperature during pressurization or depressurization operations. The pressure vessel is supported on the equipment plate, the stiffened rectangular structure in Fig. 182, by a spider-like four-legged strap that loads the vessel into a cushioned spherical seat.

The configuration of each gas system assembly made it impractical to test environmentally on an assembly level, and, therefore, it was decided that environmental qualification would be conducted on functional subassembly levels. The functional subassemblies were the high pressure assembly (often called equipment-plate assembly) and the four- and two-port valve assemblies. After FA qualification of the subassemblies, the hardware was returned to the clean room for installation on the support fixture and welding to the low pressure

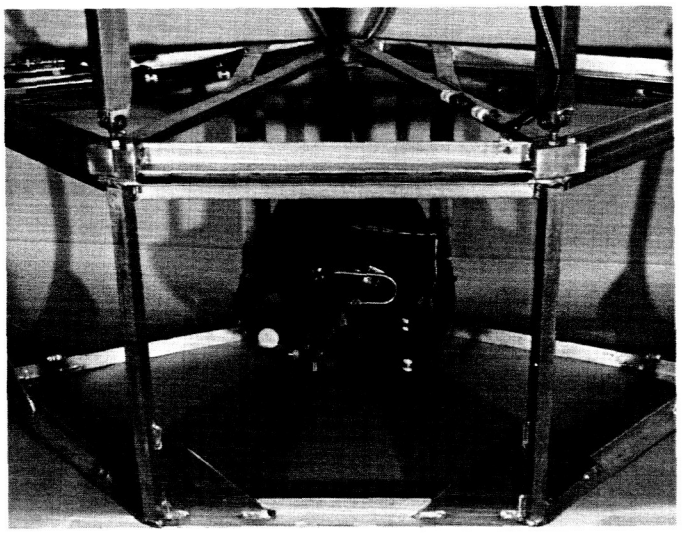


Fig. 181. Gas actuator system high-pressure section

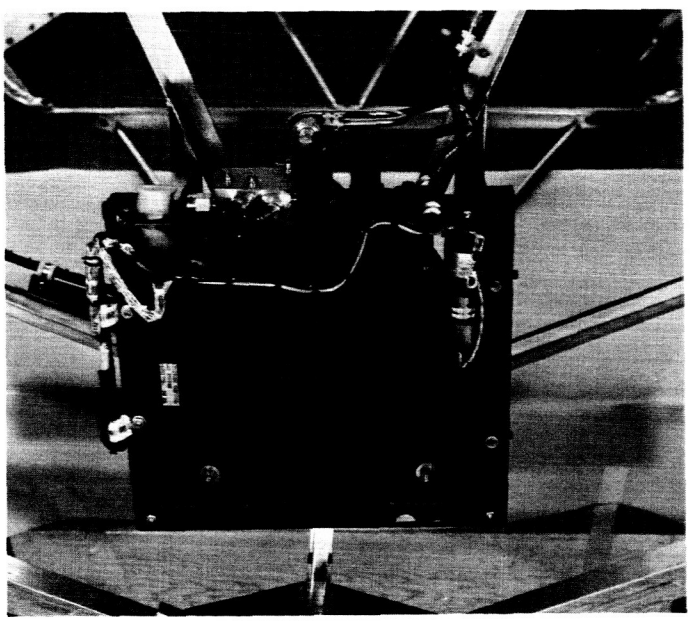


Fig. 182. Jet valve with solar vane control

plumbing. After welding, the assembly was leak-tested using a helium mass spectrometer. Additional tests were performed on the assembly at designated times when thrust-valve and regulator characteristics were monitored. The regulator performance was evaluated by carefully hooking the monitoring equipment to the outlet of one thrust valve that was actuated and held in an open position while a second valve was actuated. This means of testing negated the requirement to open the assembly anywhere between the inlet fill manifold and the valve outlets, thus alleviating a serious contamination control problem and minimizing the number of seals per system.

b. Components. The major components of the attitude control gas actuator system are the pressure vessel, the regulator, the valves, the high pressure circuit, the flexible tube assemblies, and the cable assembly.

Vessel. Preliminary design studies on gas weight requirements indicated a need for 9 lb of nitrogen. This weight was three times the weight required for a worst-case mission without a failure. After several reiterations, the gas budget was approved for a nominal 5 lb, but not until after fabrication had started on vessels based on a 7-lb budget. The outside diameter of the vessel had to be frozen because of interface considerations, leaving the wall thickness as the only parameter that could be changed. The resulting vessel was approximately 10% larger in diameter than an optimum design. Also, the working pressure was changed from 3200 to 2500 psi.

The vessel is of spherical shape, with the hemispheres joined by a uniweld technique. Titanium was selected as the material because of its weldability, its physical and tensile properties, and its toughness. The single terminating boss on the vessel has an entry hole of only 0.156 in. through which the vessel was pressurized, and through which cleaning fluids had to be passed. The small opening was necessitated by the seal design, which was concentric to the hole. Cleaning was effectively accomplished by inserting an entry tube through the hole. Fluids used for ultrasonic cleaning and flushings could be expediently passed in and out of the vessel through the tube.

Type-approval testing of the vessel included proof and burst tests. Three units, chosen at random, were tested to destruction. The first unit was hydrostatically burst on a single pressure cycle. From this result, a bulk yield point was established from volume pressure data. A proof pressure based on 85% of bulk yield was established for the design. The two remaining TA units were subsequently proof-cycled three times before being continued hydrostatically to the burst pressures. A specification to the manufacturer required that the three burst values fall within 4% of one another. Figure 183 shows a vessel after burst testing. Wall-thickness measurements before and after burst are also correlated to toughness and yield properties.

Qualification testing of the remaining units included hydrostatic and cryogenic tests. Each vessel was proof-cycled three times at room temperature, and cryogenically tested at 1.4 times the room-temperature proof

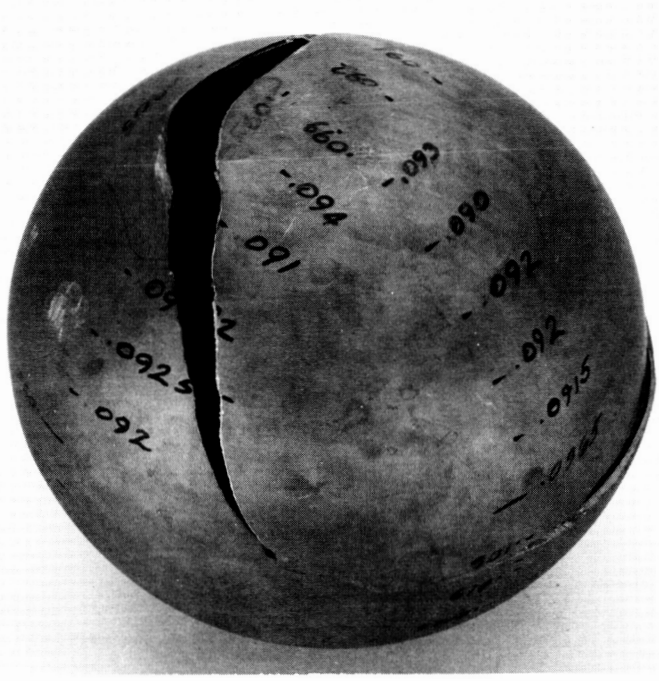


Fig. 183. Pressure vessel after burst test

level with liquid nitrogen. The latter test is considered an extremely effective test by which to establish structural integrity. A microflaw, which can go undetected in radiographic and penetrant inspections, will propagate to destruction at cryogenic temperatures. After component qualification, the vessel received several pneumatic proof tests as part of system qualification.

Regulator. With the exception of the inlet and outlet configuration, the *Mariner* Venus regulator was essentially the same as the *Ranger* regulator. The unit was a single-stage design that regulates to 15 $\pm$ 1.2 psi above ambient pressure over an inlet range of 100 to 3500 psi. In Fig. 179, the *Mariner* Mars regulator is shown adjacent to the fill manifold assembly. The regulator does not contain a relief feature because each of the thrust valves downstream is self-relieving. The control poppet is a 0.062 in. precision tungsten carbide ball that is activated by direct linkage to the sensing diaphragm. The leakage specification is 3 cm^3/hr maximum over the specified life of 250,000 cycles. If a regulator were qualified by the manufacturer (qualification included 20,000 cycles of operation) and later failed to meet this leak specification, the problem was almost inevitably traced back to contamination. Contamination control was vital to successful performance of the regulator and the thrust valves, was deemed critical to ultimate reliability, and was maintained at a maximum particle size of 5 μ metallic and ceramic and 25 μ plastic.

The regulator performance and functional tests included, but were not necessarily limited to, the following: proof pressure, external leakage, internal leakage, flow tests, cycle tests, and filter tests performed to determine possible wear generation. Internal leakage was determined by pressure sensing of a downstream volume. Flow tests were performed over the range of inlet pressures at weight flow rates of 10^{-4} to 2×10^{-3} lb/sec. Before flight, each regulator received a minimum of 50,000 cycles of operation.

Valves. In the prototype thrust-valve unit, a magnetic stainless steel was used for the body and shell to avoid a requirement for plating. Simplicity was the keynote in the design. Other salient features include: (1) a flange mount to eliminate problems associated with threaded connections, (2) moving parts ahead of the ball poppet made of extremely hard materials with almost unbounded cycle life, and (3) a self-relieving feature produced by designing the poppet to open in the direction of gas flow, which also allows a smooth transition in the seat area so that contaminants are less likely to pile up because of discontinuities in the gas stream.

Valve components are mounted on manifolds to form either a four-valve assembly, as shown in Fig. 184, or a two-valve assembly. The figure also shows a solar vane actuator mounted on bosses provided on the manifold. Test nozzles are shown terminating each valve. From the test nozzle, flexible tubing was run to OSE pressure switches for monitoring valve actuations during system tests on the spacecraft. The test nozzles also included a 0.005-in. screen filter to preclude large contaminants from entering the valve outlet.

Some of the performance and functional specifications for the thrust valves are listed in Table 47.

The flight nozzles that are mounted to the outlet side of the valve are shown in Fig. 185. The orifice sizes range from 0.0114 to 0.0147 in., and provide a thrust level of 2.32×10^{-3} and 3.90×10^{-3} lb, respectively, at a valve inlet pressure of 15 psi.

High pressure circuit. The high pressure circuit is made up of the fill manifold assembly, the flight manifold, the pressure transducer, and tubing. The flight manifold, which includes a manual shut-off valve, is

Table 47. Thrust-valve specifications

Item	Specification
Leakage during qualification	3 cm^3/hr maximum
Relief pressure	50 psi maximum
Response time to open	15 msec maximum
Response time to close	5 msec maximum
Operating voltage	25 v
Cycle life	500,000 cycles
Wear (particle size generated during flight qualification of 50,000 cycles)	5 μ maximum

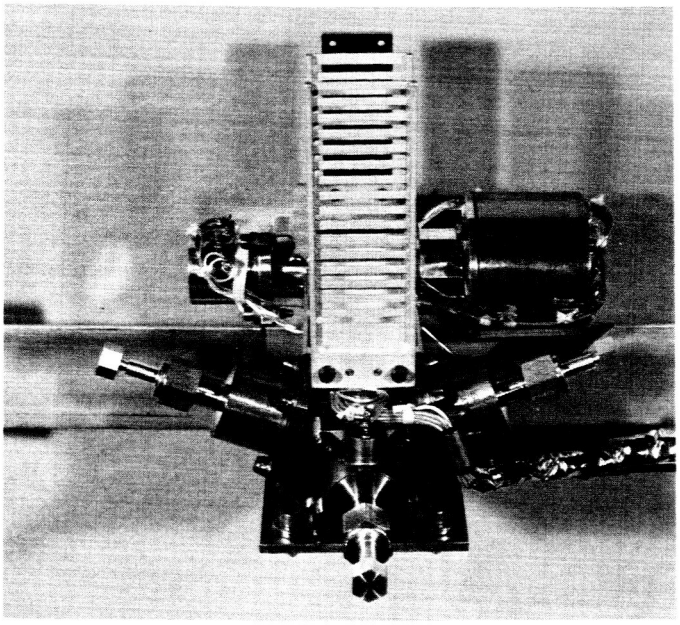


Fig. 184. Four-valve assembly

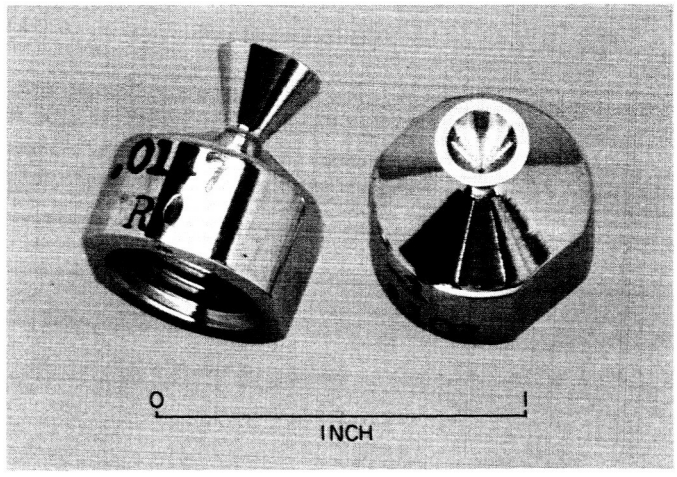


Fig. 185. Flight nozzles

mounted directly to the pressure vessel boss. This circuit was fabricated as a separate subassembly so that the regulator was not exposed unnecessarily to heating during welding. During the testing of the prototype high pressure circuit after assembly to the regulator, it was learned that the regulator would oscillate in a nonstandard mode during normal flow tests. Investigations later exposed the fact that the tubing running from the flight manifold to the regulator was loading the inlet regulator tube, which, in turn, increased the friction loads in the piloting section of the regulator. The oscillations caused by this problem were eliminated by the addition of two bends in the tubing run, which disassociated the regulator from loading effects. The thin-wall stainless tubing used in both the low and high pressure circuits measures 0.246 in. outside diameter and has a wall thickness of 0.016 in. Burst testing of the tubing was performed on samples having sharp bends and typical weld connections. Burst values in excess of 11,000 psi were consistently noted.

Flexible tube assemblies. The flexible tube assemblies were required as pneumatic jumpers in the hinge area of the solar panels and along the solar panel for flexibility. The problem inherent with metal flexible tubing is built-in contamination, which is extremely difficult and often impossible to remove.

The eventual design became a 3/16-in. convolution tube, fully annealed by a bright-anneal process. Before heat-treating, the tubing was thoroughly cleaned, and care was taken to maintain cleanliness throughout the heat-treating process. Cycle tests of the flight design indicated cycle life to be between 1200 and 3000 flexures, each flexure consisting of deploying and erecting the solar panels.

Cable assembly. The gas system assembly cable harness interfaces with an 18-pin connector from the attitude control electronics. Cable, which is exposed to direct sunlight, is wrapped with aluminized mylar tape. The cable running on the dark side of the solar panel was jacketed in black teflon tubing to minimize reflections.

c. Fabrication and process development. Fabrication of the gas actuator system required the development of various techniques and processes in such areas as welding, tube bending, and leak testing. These processes are discussed in the following paragraphs.

Welding development. There were some problems involved in the welding of the stainless-steel tubings for the gas actuating system, in which the tubing wall thickness was only 0.016 in. and the contamination had to be held to particles of less than 5 μ. Because welded tubular assemblies were impossible to clean, the fixtures and tubular lengths had to be cleaned before welding, and maintained clean during and after welding. Such contaminants as weld splatter and oxide layers could not be allowed to enter into the internal portions of the tubing. An extremely fine touch was required on the part of the welder, as was the utmost integrity in reporting any possible blow-throughs during the welding process.

The welding process took place within a super-clean room, and the contamination level in the clean room was monitored at all times throughout the welding process.

Tube bending. The tubular assembly was fabricated outside of the super-clean room, and special jigs and fixtures were constructed to assist in the tube bending and fabricating operation. The tubes were completely filled with a special pitch and were then bent to accuracies within $\pm$0.015 in. The flexible portions of the tube assembly were also sized and cleaned prior to welding and the entire assembly was prefitted and pretested for fit on a fixture duplicating the spacecraft bus and solar panel arrangement in configuration. A complete inspection was then made of all parts to eliminate all sharp edges and burrs prior to precleaning and delivery to the clean room area. The pitch was then melted and allowed to run out, and the tubes were flushed with solvent.

Leak testing. Essentially three different methods of testing for pressure integrity of both the high- and low-pressure tubular assemblies were used. The first was a "snoop" solution that looked for bubbles; the second involved helium and the helium mass spectrometer; and the third was a leak test console. A liquid snoop solution was used in the clean room as a simple inspection tool. Any leakage noted in this manner was immediately corrected by the welding technique. After the assembly was completed, it was delivered to an area serviced by a helium mass spectrometer. A small portion of helium was injected into the high-pressure system, and the valves were exercised to allow the nitrogen and helium mixture to circulate throughout the entire high- and low-pressure tubular systems. A "sniffing" leakage test was then conducted by the helium mass spectrometer.

No leakage above 30 cm^3/hr standard was permitted, including all valve and seal leakages. After the assembly was completed it was too large for a mass-spectrometer leakage test, so the leak test console was used. This system was basically a calibrated high-pressure storage tank

contained in a test console with a differential pressure gauge. The technique was to balance the pressure of the small vessel contained within the console with the test pressure in the gas system. Usually, the gas system was already mounted onto the bus as a part of the overall *Mariner* Mars structure. After temperature stabilization was achieved, any leakage in the gas system would show up as a pressure differential. Figure 186 shows the leak test console.

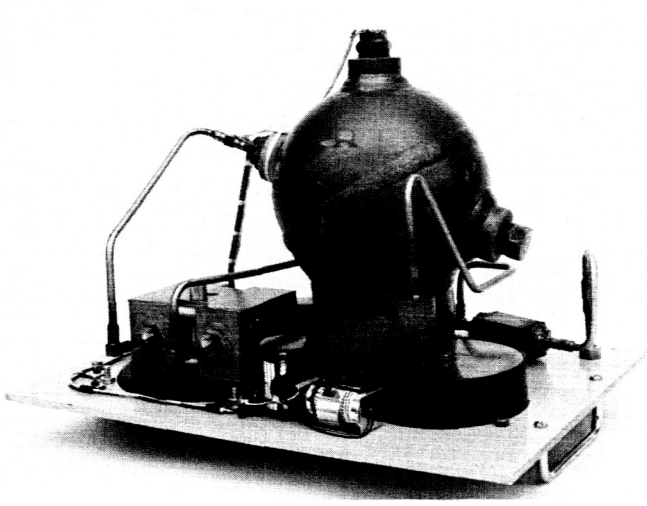


Fig. 186. Leak test console

2. Solar Pressure Vanes

a. Description. The solar pressure vanes are movable control surfaces mounted at the tip of the solar panels. They were added to the spacecraft to conserve gas during the 8-month flight to Mars and to act as a partial backup in the event the gas system should fail. Briefly, the solar vanes accomplish three things:

1. They shift the spacecraft center of solar pressure behind the spacecraft center of mass, which results in a statically stable configuration.
2. They shift the center of solar pressure laterally aligning it directly behind the center of mass in the spacecraft null position.
3. They produce spacecraft oscillation damping by providing a slight force in opposition to the spacecraft velocity.

Function 1 is accomplished when the vane first deploys from behind the solar panel. Function 2 is accomplished by moving the vanes with stepping motors wired to the attitude control gas jets. Jet firings indicate that the direction of the center of pressure should be moved; the motors then step the vanes accordingly. Function 3 is accomplished by sensing the spacecraft attitude with respect to the Sun and moving the vanes through a small angle to damp spacecraft oscillation. Functions 2 and 3 are mechanized by the solar vane actuator.

The structural portions of the solar pressure vane control system are the solar pressure vane, latching mechanism, and vane deployment mechanism. The solar vane is attached to the deployment mechanism, which, in turn, is attached to the solar vane actuator at the end of each solar panel. The solar vanes are stowed against the back of the solar panels during launch and are held in place by the latching mechanism. The latching mechanism consists of an aluminum section to support the vane, a strap to hold the vane, and a spring-loaded pin to hold the loose end of the strap. A lanyard from the spring-loaded pin to the spacecraft bus holds the strap in the latched position. As the solar panels deploy, the lanyard effectively increases in length, releasing the strap allowing the vane to unfold and deploy to its cruise position. Deployment is accomplished by the use of a torsion spring with 11 in.-oz of torque and low-friction pivots.

The vane consists of four aluminum tubes extending outward from a point. The outer tubes are spring-loaded to pull the covering taut; the inner tubes merely "float" to support the covering in the middle sections. The covering is 1-mil aluminized black mylar bonded to the framework. The vane is folded in a manner similar to a fan with radial pleats. Folding of the vane was deemed necessary as the result of a failure mode analysis. If the latching mechanism failed to function, a folded vane would not affect the thermal balance of the panel. Figure 187 shows the solar vane hardware mounted to the back side of the solar panel.

b. Functional description. Figures 188 (a) and (b) show functional schematics that illustrate the operation of the solar pressure vanes. The spacecraft has four solar panels arranged symmetrically perpendicular to the Sun line. At the end of each solar panel is a vane capable of rotating about the end of the panel. The vanes are actuated by thermal actuators; i.e., they produce an angular output proportional to a heat input. A Sun shade is fixed to each solar panel so that if a line perpendicular to the solar panels is not parallel to the Sun line, depending upon the direction to the Sun, more or less of a thermal

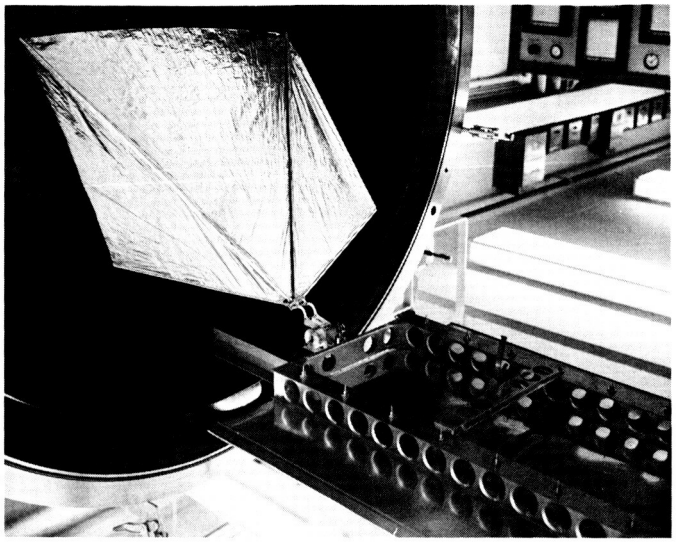


Fig. 187. Solar vane and hardware mounted to back side of solar panel

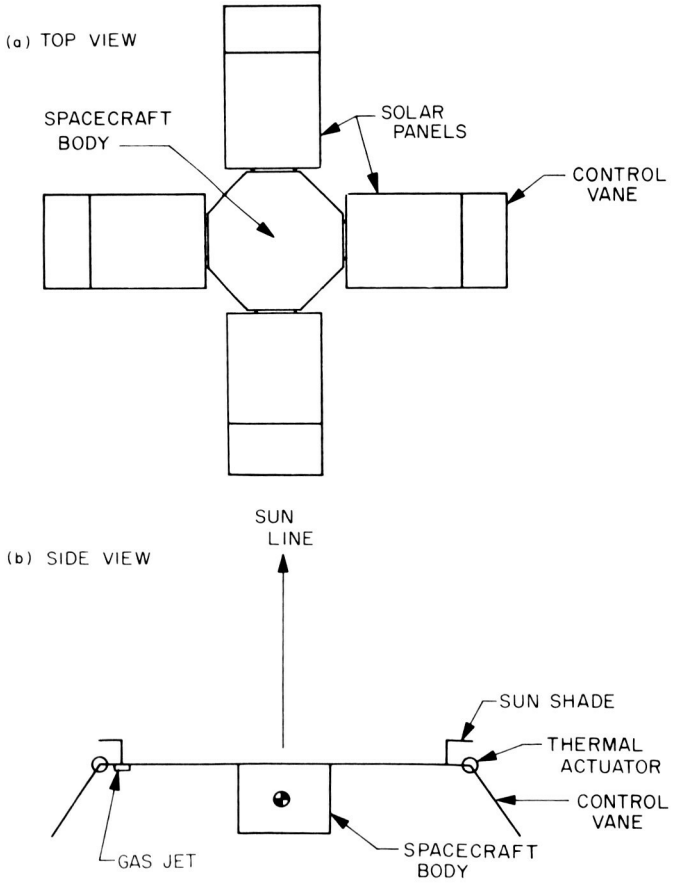


Fig. 188. Functional schematics of attitude control subsystem

actuator is exposed to the Sun. The resulting heat transfer causes an angular rotation of the vanes about the end of the solar panel, which, in turn, causes a change in the solar torques on the spacecraft. These torques are used to control the pitch and yaw axes to maintain Sun-line attitude control.

Figure 189 (a) shows a cross section through the center of the spacecraft, perpendicular to one of the control axes (pitch or yaw). Therefore, the angle θ_s between the Sun line and the line perpendicular to the solar panels is the pitch (or yaw) error. Since the solar panels are in front of the CG of the spacecraft (i.e., toward the Sun), it is apparent that the spacecraft is basically unstable. An angular error θ_s causes an unbalanced torque that tends to increase θ_s. The philosophy of the control system is that in the steady-state situation in Fig. 189 (b), the vanes must produce a stable spacecraft. As shown in Fig. 189 (a), vane angle θ_v is measured from the plane of the solar panels and is positive in a direction away from the Sun line. A certain combination of vane area, vane length, and positive vane angle are required to produce a stable spacecraft.

If the spacecraft is given an impulse, it will oscillate in an undamped mode about the control axis since there is no damping. The vanes are used to provide damping by employing a positive feedback scheme. If the space-

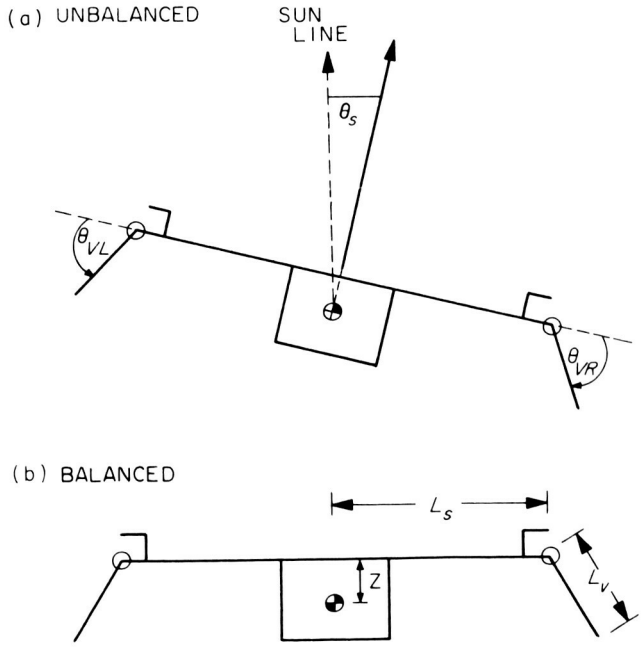


Fig. 189. Functional schematics of vane control

craft is in an oscillatory mode, the Sun shades will differentially expose the thermal actuators to the Sun. These are phased so as to reduce the restoring torque of the spacecraft by rotating the vanes in the proper direction. For the example in Fig. 189 (a), this would involve decreasing θ_{vR} and increasing θ_{vL}. This means that the return angular velocity of the spacecraft will be reduced, thereby providing damping. The open-loop gain of the control system must be less than one in order for the system to be stable.

One very important aspect of the spacecraft is the fact that it is not symmetrical as far as solar torques are concerned. There are differential areas and reflectivities. Consequently, it takes an unsymmetrical vane configuration to produce a stable spacecraft pointing at the Sun. Therefore, it was desirable to have an adaptive mode of operation that would change the vane angles differentially in order to balance and stabilize the spacecraft. When the vanes reach the desired angles, they will be nominal angles about which the vanes will operate to produce control system damping for any other torque disturbances.

The adaptive mode uses a cold-gas mass expulsion system with an optical sensor as the primary acquisition system. This is similar to the *Mariner II* attitude control, which used a switching amplifier to produce a deadband for limit-cycle operation. The output of this switching amplifier is used as input for the adaptive mode of the solar torque control system. Whenever the switching amplifier output indicates that the spacecraft is up against one side of the deadband of the limit cycle, a pulse is sent to an actuator to give the vanes a small step change in direction to make the spacecraft move back to null. Successive switches of the switching amplifier on one side of the deadband then cause the vanes to null out the unbalanced torque that is causing the switching. When there is equal (i.e., alternate) switching on each side of the deadband, the spacecraft is balanced, and the damping provided by the thermal actuators will then eliminate the limit cycling. There is probably a null offset due to the minimum size of the stepping-motor capability, but it is within the deadband of the switching amplifier.

c. Design evolution. It was originally decided to use ¼-mil aluminized mylar reinforced with dacron thread on 2-in. centers. The dacron thread was bonded to the mylar with a special adhesive, and increased the resistance to tear propagation in the event the mylar should be torn either in panel deployment or by meteorites during flight.

Since the vane was thermally isolated from the spacecraft, the expected temperatures of the vane covering were between +250 and −350°F. Although the capabilities of mylar were known, the dacron and adhesive were placed in liquid helium (−452°F) to establish their limitations. The mylar with adhesive and reinforcing thread remained flexible at this temperature and no bad effects were observed.

A special test was performed in the 25-ft simulator to duplicate the high temperatures that might occur during parking orbit conditions. The temperature of the vane on the panel facing the Sun was sufficient (240°F) to soften the adhesive and cause the folded vane to bond together where the dacron thread had been placed. The vane would not unfold after this test. It was decided to eliminate the dacron thread and use a thicker gauge mylar. It was found that 1-mil mylar had about the same resistance to tear as the reinforced ¼-mil material. A vane was covered with 1-mil mylar and retested. In the second test, the mylar itself softened and the same results were noted as before.

At that point, it was decided to cover the vane on the panel pointed at the Sun during parking orbit with 1-mil teflon. In addition, the vane was folded so that the teflon surface rather than the aluminized side faced outward; the high-emissivity surface would reduce the vane temperature. Testing of the vane indicated that it would open properly. For the other three vanes, mylar was retained because of the black back-side requirement imposed by the Canopus sensor. The vanes, however, were folded in the same manner as the teflon vane, with the high-emissivity surface exposed. With this type of folding and with their position on the spacecraft away from the Sun during parking orbit, the maximum temperature expected was 200°F. Tests were again performed and no problems were encountered with the vane opening.

With the change from a clamshell to a one-piece shroud, the solar vane hardware was modified slightly to increase the spacecraft-to-shroud clearance. The deployment and the latching mechanisms were modified to lower the vane approximately 1 in. Deployment tests were then conducted to make certain the vane would clear the solar panel rails as it deployed. Although it cleared, it was marginal and a guide was incorporated between the panel and the rail to prevent jamming.

The electromechanical actuator was designed so that it would require multiple part failures in the control before complete failure of the solar vane control would result. To outwit the cold-welding that occurs in the

hard vacuum of space, the control was designed to have bearings, gears, potentiometer, and switch contacts protected from space vacuum. This was done by using O-rings on all case junctions, closure plates, and output shafts that would be exposed to space vacuum. A low vapor pressure lubricant was used on the gears so that if the O-ring seals did not hold, a long period would be required to evaporate the lubricant.

The electronic driver used with the control is mounted around the step servomotor to reduce interconnecting lead length. The circuit used is a silicon-controlled rectifier ring amplifier. A capacitor discharge into the motor winding is used to step the motor, which allows high energy into the motor when needed and low power drain on a continuous basis. This averaging greatly reduces the continuous power demand upon the spacecraft power source.

The switch assembly, mounted with the potentiometer, limits the travel of the control angular output to 40 deg, so that the television experiment, the wide angle planet sensor, and the star sensor will not be masked by the vane.

The basic design that evolved was simply a bimetal element and shading arrangement. If the bimetal element were partially shaded by a shade fixed to the spacecraft, the amount of light and, thus, the bimetal temperature would change with variations of spacecraft position. Changes in the bimetal temperature cause the bimetal tip to displace through a small angle. Thus, changes in spacecraft position would also change the vane angle through the actuator.

The bimetal equilibrium temperature is determined by the conduction and radiation losses between the bimetal and the spacecraft and also by the reradiation of heat to surrounding space. To reduce the effect of conduction and radiation losses, it was decided to size the bimetal and shades so that these losses would be an order of magnitude less than the light energy coming into the bimetal for the nominal case.

Since the total dynamic range for the thermal actuator was to be approximately 5 deg, multiple shades were selected rather than a single shade. With a single shade, the change in energy to the bimetal element is small for a given angular change unless the shade–bimetal separation is large. The multiple shades allow for large changes in energy input for the same spacecraft angular change, while keeping the bimetal–shade separation small. A change in spacecraft angle of 5 deg with the multiple shades causes bimetal illumination to change from 0 to 50%. Although a change from 0 to 100% illumination would be desirable, it is impossible to achieve since the shade will always result in a partial masking of the bimetal.

d. Fabrication. A template was first made to cut mylar to the exact shape required. Next, frame guides were attached to ¾-in. plywood. The mylar was then positioned on the plywood surface and taped down with masking tape around the edges. The wrinkles in the mylar were worked out by repeatedly going around the edges and pulling the mylar and retaping. With this completed, the framework was placed in the guides and lowered into contact with the mylar.

The folding of the vane was accomplished fairly easily by the use of heavy-paper folding templates. Since the mylar had very little body, templates were made from paper and folded in the configuration desired for the vane. One template was then placed on each side of the vane and the framework collapsed. The paper templates folded at the predetermined points and the mylar followed, since it was sandwiched between the templates. Before the tubes were brought completely together, the templates were slipped out without disturbing the mylar.

e. Testing. The vane hardware was subjected to both TA and FA tests as well as several developmental tests. The type-approval tests consisted of the shipping-container vibration and drop test, the 12-day thermal–vacuum test, and a complete series of vibration and acoustic tests on the STM composite spacecraft. The flight-acceptance tests included a vibration test on the composite flight spacecraft.

3. Jet Vane Actuators

The thrust vector control is an assembly of four jet vane actuators mounted upon a ring. This assembly is placed upon the nozzle exhaust of the midcourse maneuver rocket engine (with the vanes extended into the flame) as the output control of the spacecraft autopilot. This assembly corrects for errors in pitch, yaw, and roll as commanded by the autopilot during the midcourse firing of the rocket engine.

Each jet vane actuator consists of a dc torquer, a potentiometer readout feedback to the autopilot, a sealed case containing the atmosphere, and an output shaft with

the vane mounted. There is no telemetry of the vane position.

The dc torquer is a two-pole permanent magnet rotor with a 200 Ω, single-winding stator. There are no slip rings or flexible leads. The angular operating range of the torquer is ±26 deg about the center position. The torquer exhibits an electrical time constant of 4.25 msec to match it to the remainder of the autopilot.

The potentiometer is an infinite resolution conductive plastic element with a resistance of 20 kΩ. The wiper assembly is mounted on the actuator shaft with a slip ring to carry the wiper signal to the connector. The moment of inertia of the rotor, brush block, and shaft is 8.95 g-cm^2.

The sealed-case housing uses an O-ring seal on the output shaft with a low vapor pressure grease to assist in sealing and to lubricate the O-ring. The sealed case contains sufficient atmosphere to protect the actuator bearings and potentiometer wiper from the effects of space vacuum.

The actuator torque delivered has a slope of 0.0336 in.-oz/ma in both directions. The starting torque to overcome the O-ring seal friction and potentiometer-wiper friction has a maximum of 0.6 in.-oz, which indicates that a current of nearly 18 ma is necessary to start the actuator moving.

4. Gyro Control Assembly

a. Functional description. The purpose of the gyro control assembly is to provide inertial rate and position information to the spacecraft attitude control subsystem. This information is used in damping the spacecraft motion during acquisition or for steering during the midcourse maneuver motor burn period.

Three modes of operation are possible within the gyro control assembly. The first is a conventional rate mode. Rebalance currents to the three gyro torquers are used to develop voltages proportional to spacecraft turning rates. This rate mode is used to damp spacecraft turns during acquisition of the Sun or of Canopus.

In the second mode, the gyro gimbal is torqued by a precision current for a controlled length of time. Motion of the gyro gimbal produces an error signal to a switching amplifier in the attitude control subsystem. Gas is then vented through the appropriate jets causing the spacecraft to follow the gyro gimbal motion. In order to allow a wider range of motion for the gyro input axis, a large integrating capacitor is inserted into the rebalance loop during this mode. This capacitor stores a voltage proportional to the gimbal motion and allows greater gyro input range to be obtained.

The third mode of operation is used to steer the spacecraft during the maneuver. The rebalance loop is the same as mode 2 but the precision command current is removed. Gyro output signals are then fed to the autopilot and jet vane actuators to keep the spacecraft on the correct heading during the motor burn period.

The overall operation of this three-gyro system is the same as that of the *Mariner* Venus and *Ranger* systems with one exception. In order to provide a backup mode of operation in the event of a Canopus sensor failure, the roll axis can be controlled through the radio command system. The radio command will act upon the roll gyro to provide an incremental roll capability.

The roll increment will be either a clockwise 2 deg or a counterclockwise 2 deg depending on which command is transmitted. Upon receipt of an initial roll–override command, the roll gyro only will go to the integrate mode. Subsequent commands will activate one of two 12-sec monostable (one-shot) multivibrators, which will drive a relay in the precision command current generator. Torquing current will then go to the roll gyro producing the same turning action described previously. Another identical one-shot is used in the same manner to generate the opposite sign command current.

b. Physical description. The gyro control assembly consists of three major subassemblies. These units are attached to one another mechanically and are electrically mated and calibrated.

The first unit is the electronic package. It contains all power supplies, rebalance amplifiers, precision command current generator, and other miscellaneous electronics. The unit is of welded-cordwood construction with each of the subsections outlined above packaged into a small, replaceable, welded, encapsulated module.

The 16 encapsulated modules are interconnected by means of a single, three-level, multilayer printed circuit board. Interconnecting straps are welded between nicked riser pins on the multilayer board and similar pins extending from the base of the encapsulated modules.

Three amplifiers are required for the gyro rebalance loops, one for each of the pitch, yaw, and roll gyro loops; all are identical in design and function. These three amplifiers occupy six of the 16 encapsulated modules.

The gyro package contains the three floated-rate integrating gyros. This unit also contains a number of relays, resistors, capacitors, and inductors associated with the gyros.

In the integrating capacitor bank, 12 special tantalum capacitors, each of 1020 μf, are used to store the gyro gimbal motion. These capacitors, plus protective resistors, are encapsulated in this subassembly.

The total weight of the three mated subassemblies is 10.9 lb. Power consumption is on the order of 18 w.

Figure 190 is a photograph of the complete assembly. The small cylindrical object on the top of the central gyro package is a running time meter used to indicate the total number of hours of gyro running time. This is a plug-in unit and is removed prior to final spacecraft installation.

The gyroscope selected for use in this assembly is a miniature, floated-rate integrating type. The original version of the gyro was designed as a platform-stabilizing gyro and was intended to operate at a constant 180°F. Due to the fact that no power is available on the spacecraft to heat the gyro to this temperature, a much lighter flotation fluid is used in the *Mariner* Mars version. This less-viscous fluid permits operation over a range of 85 to 130°F, which is the temperature the gyro assumes due to heat from the spin motor.

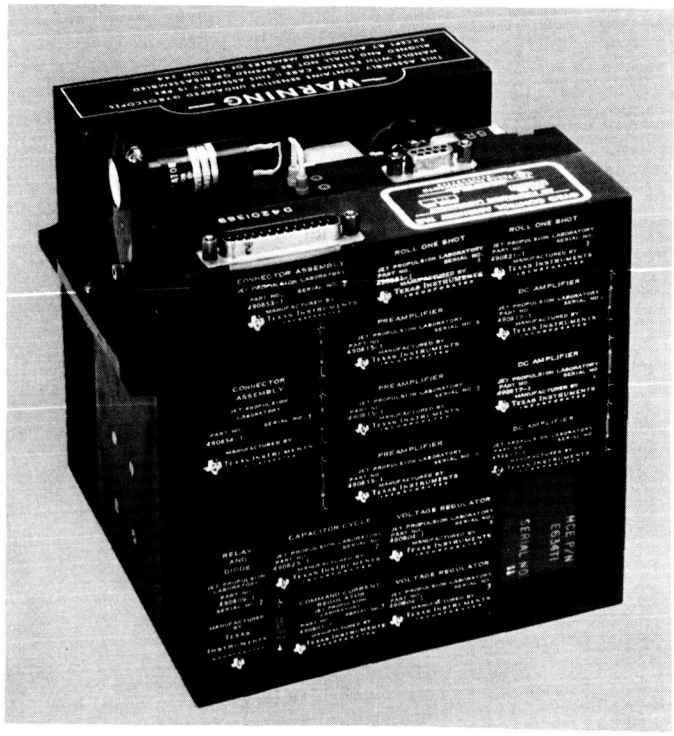


Fig. 190. Gyro control assembly

The gyro in its final form weighs 0.70 lb, requires 3.2 w at 400 cps on the spin motor, and, with the large integrating capacitor used in the system, can store an input angle of 6 deg. Typical magnetic leakage fields were on the order of 2 to 3 γ at 3.5 ft.

c. Design. Welded, encapsulated modular design was used in the *Mariner* Mars gyro electronics subassembly. In all past designs, the gyros were placed in one subassembly and the electronics in another. These subassemblies were then interconnected by means of the regular case harness. In the *Mariner* Mars approach, the packages are tied together by means of through bolts and all interface connections are kept within the assembly. A single external interface connector is brought out to the attitude control subsystem and one small test connector is also provided.

Once the prototype system was designed and built, the only changes introduced were to encapsulate the interface connectors on their back sides in order to reduce wire motion during vibration and to cement the electronic modules to the subchassis to increase their rigidity under conditions of high vibration and shock.

d. Testing. A typical test program on each gyro involved an average of 30 runs of heading test data and 6 runs of tumble-table testing prior to acceptance of the gyro for use in a flight system. Between 50 and 60 hr of motor running time were involved in this preacceptance stage. Four major parameters were determined from these tests. These were torquer scale factor, non-acceleration-sensitive drift rates, spin-axis mass unbalance, and input-axis mass unbalance.

The electronic subassembly was checked by the vendor at several stages of assembly. First, each module was tested prior to encapsulation at 0, 25 and 70°C, and again after encapsulation at the same temperatures. The modules were assembled to the subchassis structure and the procedure repeated again.

The special tantalum integrating capacitors were tested for both leakage and capacity. The bank of four capacitors required for each channel of the system was made up of selected units matched for capacity in such a manner that each half section was within 3% of the other half section. A special semiautomatic leakage tester was designed to increase the accuracy of the leakage-current measurement. Repeated leakage checks were made after assembly of the capacitor bank and a careful watch was kept on trends from that time on.

After all three subassemblies were declared satisfactory on an individual basis, they were brought together and mated, both electrically and mechanically. Testing was then started on an assembly level for the same parameters mentioned before as well as an extended period of commanded turn-rate calibration using a servo table. Due to the fact that no gyro temperature control was permitted on the spacecraft, it was necessary to calibrate the commanded turn rates at four different temperatures around the expected nominal value.

The gyro control assembly was subjected to all environmental tests, such as vibration and thermal–vacuum, while in the same spacecraft case structure as the attitude control subsystem, in order to obtain conditions as similar to actual flight environments as possible. Test data taken before environmental tests were compared with similar data taken after environmental exposure to observe the total effect of the environmental test series.

After successfully passing all the tests, the gyro control assembly was delivered to the spacecraft assembly facility for final visual and mechanical inspection and installed in the spacecraft. Prior to shipment of the spacecraft to Cape Kennedy, the gyro control assembly was removed and sent to the gyro laboratory for a final check. After the final tests, the gyro assembly was hand-carried to Cape Kennedy on commercial aircraft, since it was somewhat susceptible to the prolonged low-frequency vibration and angular rates usually experienced in truck transportation.

A final brief test was performed after arrival at the Cape using identical test equipment in a small inertial sensor laboratory at the Cape spacecraft checkout facility. The gyro control assembly was then installed in the spacecraft for the last time.

As a result of this extensive test program, a number of defects and anomalies were discovered. During TA vibration, several module interconnecting ribbons broke because of an improper module-attaching scheme. This was a true catastrophic failure, but the gyro remained undamaged. (A minor redesign corrected the problem.) The serious condition of gyro contamination was brought to light during the single gyro acceptance test phase. Later, one of the gyros that had been reworked for contamination was found to have developed a short on the pick-off output; this was caused by a small solder ball trapped under a feedthrough terminal. Three cases of anomalous behavior of gyros were found. In one case it was noise on the output, in another it was an inability to pass the cogging test for fixed drifts with one set of electronics while working correctly with another, and in the last case it was a matter of erratic behavior. In each case additional tests of these gyros failed to disclose the cause of the anomaly. The gyros were set aside and used in nonflight spare gyro control assembly subsystems.

Life testing of the TA subsystem showed that the gyros are capable of running throughout the entire mission without significant deterioration.

E. *Flight Performance of the* Mariner IV *Attitude Control Subsystem*

1. Initial Sun Acquisition

When separation of the spacecraft from the second stage occurred, the spacecraft was in the Earth's shadow. In the shadow, there are no Sun-sensor error signals, but the three single-degree-of-freedom gyros about each spacecraft axis sense the tumbling of the spacecraft and turn on the control jets until the rates are reduced to within the deadband of the switching amplifier. This rate deadband is ± 1.27 mrad/sec in pitch and yaw and ± 0.33 mrad/sec in roll. When the spacecraft was first observed in the shadow, the rates were already within the deadband, indicating that the separation rates were very low. The actual time of exit from the Earth's shadow took place at 15:17:35 GMT, but Sun-sensor signals were first noted at 15:15:36 GMT due to the refraction of sunlight through the Earth's atmosphere.

When the spacecraft was completely in the sunlight, the pitch error was seen to be equal to -1.0 deg, and, for all practical purposes, the pitch axis had acquired the Sun. The yaw Sun sensors were saturated and had established a rate determined by this saturation equal to -2.2 mrad/sec (-0.126 deg/sec). The yaw sensors came out of saturation at 15:29:56 GMT at an angle of $+11.5$ deg. This would indicate that, at the start of yaw acquisition, the yaw angle was about $+106$ deg.

A Sun-gate event occurred at 15:30:59 GMT. This indicated that the Sun-gate cone-angle field of view was 2.2 deg, which was within the design tolerance.

The Sun gate initiated the magnetometer calibration spin as required. A search signal was switched into the roll-axis control system, and the spacecraft accelerated to a rate of −3.55 mrad/sec (−0.203 deg/sec), which was the design nominal.

During the magnetometer spin mode, the pitch and yaw errors were observed to limit cycle against one side of the deadband. The pitch axis stayed at +8.7 mrad/edge and yaw at −8.5 mrad/edge. This was as expected and was due to cross-coupling from the cross products of inertia.

2. Star Acquisition

a. Star identification procedure. Before the flight, it was felt that star identification would be a major problem. This was derived from the fact that the only information from the star sensor, other than an error signal, is a brightness measurement and the cone angle of an object within ±5 deg. The absolute calibration of the star sensor for all the stars in the sky is not known and the problem is further complicated by the brightness signal, including the integrated background of stars in the field. But, during the roll–search mode, the sensor makes good relative measurements of the star and background brightness. This information is basic to the star-identification procedure.

A map-matching technique was developed to identify objects seen by the star sensor during the roll–search mode. As an aid to establishing the map-matching technique, other corroborating information was used for initial acquisition. This included (1) a fixed, wide-angle (26 × 83 deg) field-of-view Earth detector to provide an output if Canopus were in the star sensor; (2) magnetometer information obtained during the calibration mode for rate and position information; and (3) low-gain antenna pattern variations to provide rate and position information. The magnetometer and antenna information was very crude and could only be used with a low weighting function on its corroboration.

Fundamental to the matching was an *a priori* telemetry map of sensor brightness output versus clock angle (angle about the Sun line measured from Canopus). A reasonably sophisticated mathematical model of the star sensor and the sky, including the Milky Way, was developed so that with trajectory information an IBM 7094 program printed a map of the expected telemetry output of the brightness channel seen during roll search. This, then, would be matched with an actual telemetry map to identify observed objects.

Initially, an extensive computer program was devised to process the telemetry data to produce the actual telemetry map. This was statistically correlated with the *a priori* map, Earth-detector output, magnetometer data, and low-gain antenna data. Whenever an object was acquired subsequent to a roll search, a calculation was made of the probability that each acquirable object had been acquired. If the object was not Canopus, roll override would institute another roll search, and another computer run was made until Canopus was identified as acquired.

The computerized version of the map matching was necessary because of the lack of knowledge of the sensor response to innumerable objects and the integrated background that would be seen by the sensor. Until the sensor could actually be calibrated in flight, the uncertainties required that the best possible analysis techniques be prepared beforehand.

In addition to the computerized star-identification program, a second map-matching technique was developed and implemented during the flight, which was much simpler but required actual flight experience to prove reliability. A continuous strip chart recorder was employed to plot in real time the star-sensor brightness telemetry. An *a priori* map, derived from the computer program, was transcribed on a transparent overlay to the same scale as the real-time telemetry plot so that they could be instantaneously compared during the roll search. The process turned out to be surprisingly good and became the primary technique for star identification; it was quite accurate and the fastest possible way of identifying objects.

b. First star acquisition. Initial roll acquisition was commanded by the CC&S to take place at 06:59:00 GMT on day 334 (November 29). Just prior to this command (CC&S L-3), the spacecraft was in the magnetometer calibration mode, rolling at a rate of −3.55 mrad/sec (−0.203 deg/sec). At the roll–acquisition command, the search command signal was switched in and the roll rate was reduced to −2.35 mrad/sec (−0.135 deg/sec), which, as would be expected, is the upper edge of the deadband about the nominal search rate. An acquisition occurred at 07:07:47 GMT. At that point, Earth-light reflections on the star sensor optics caused a bright enough

background, along with a spurious error signal, to cause the acquisition logic to discontinue the roll search. Even though there was no acquirable object, a logic acquisition had been effected. The clock angle at that point was about 129 deg.

Even though the logic circuitry was satisfied, there was no real error signal and the roll axis was essentially in a drift mode with the jets firing at random because of background noise. It turned out that the cumulative action was to cause the spacecraft to drift primarily in a direction of increasing clock angle. At some unknown time during the drift, the star Aldermin was acquired at a clock angle of 171 deg after the spacecraft had drifted about 42 deg. Aldermin is about 0.05 times as bright as Canopus, with a bright background, and the error signals were too noisy to determine the time of acquisition.

At 13:12:34 GMT on the day following launch, the spacecraft went into an automatic roll search. The loss of roll acquisition was the first of a series of losses of acquisition that eventually were realized to be caused by minute particles floating by and reflecting light into the sensor. At 13:26:15 GMT, after 13 min and 41 sec of roll search, the star Regulus was acquired at a clock angle of 278 deg. Lock was maintained on Regulus, since Canopus acquisition was not necessary to the mission at that time.

At 09:13:47 GMT on day 335 (November 30), DC-21 (roll override) was initiated and the star Naos was acquired at 09:20:56 GMT at a clock angle of 338 deg. Another DC-21 caused Velorum to be acquired at a clock angle of 343 deg at 10:46:00 GMT. Finally, Canopus was acquired by a DC-21 initiated at 10:57:57 and lock was obtained at 10:59:38 GMT.

3. Solar Vane Acquisition

Since the solar panels are on the side of the bus toward the Sun, a situation exists in which the solar force will try to flip the spacecraft around if the roll axis does not point precisely at the Sun. The solar vanes are mounted on the ends of the solar panels at a nominal angle of 35 deg from the plane of the solar panels, away from the Sun. This puts the center of pressure behind the center of gravity, and if the roll axis does not point at the Sun, there is a restoring torque to bring it back.

On *Mariner IV*, it was seen that, at their initial deployment, the solar vanes were far past their nominal position of 35 deg away from the plane of the solar panels. They were deployed to the following positions:

Vane	*Position*
+X	21 deg
−X	15 deg
+Y	17 deg
−Y	11 deg

The cause for the failure to deploy properly was determined to be due to the fact that the deployment tests conducted before the flight had an unsuspected source of friction that damped the deployment motion. This friction was not present in space.

In spite of the overtravel on the vane deployment, the center of pressure is behind the center of gravity, and there is a net restoring torque of about 1.1 dyne-cm/deg about the pitch axis and 1.7 dyne-cm/deg about the yaw axis.

Stepping motor actuators were employed to move the vanes about their nominal deployment angle to cancel out unbalanced torques on the spacecraft. The vane actuators will step 0.01 deg each time the switching amplifier pulses a jet. If a clockwise jet fires, the vanes move counterclockwise to reduce the torque that caused the clockwise jet to fire. In this manner, the difference in the clockwise and counterclockwise pulses causes the vanes to gradually counterbalance the unbalanced torques.

On *Mariner IV*, even though the vanes were deployed incorrectly and their torque-to-angular motion gain was reduced, the +X and −X vanes, which control the yaw axis, actually did compensate for an unbalanced torque that appeared to be due mainly to the high-gain antenna. However, the +Y and −Y vanes have not been working in the torque-balancing mode. This is undoubtedly due to the fact that they are in a failure mode of electrical lockup. The design of the stepping motors is such that if a valve is fired during the first 30 msec from the time the stepping motors are activated, the actuators will lock up permanently. Since the actuators were turned on coincidently with the start of the roll search, it is very likely that a valve fired during the first 30 msec of actuator turn-on.

One of the first things that became apparent about the disturbance torques on the spacecraft was the fact that they are not constant. The unbalanced torque about the yaw axis was reduced from about 25 dyne-cm to about 5 dyne-cm, but at that level the torques continually varied. In fact, the torques varied by 1 or 2 dyne-cm from one limit cycle to the next. Over longer periods of time (i.e., several days), they would vary as much as 5 to 10 dyne-cm. In the adaptive mode about the yaw axis, the stepping motor actuators have followed these variations and have been seen to reverse direction. It is impossible for the thermal control bimetal actuators to damp out the limit cycle, since this is completely beyond their capability. In fact, it is also very difficult to tell if they are even working. The maximum restoring torque of the spacecraft vane system over the ½-deg limit cycle is 0.85 dyne-cm, and the vane damping torque is 0.30 dyne-cm. Since the disturbance torques will change from one cycle to the next as much as 2.0 dyne-cm, it is very difficult to separate the effect of disturbance torques from that of vane torques.

These varying disturbance torques are obviously not solar torques. In an effort to explain them, three causes have been postulated:

1. Variation in solar wind, which, having different momentum transfer properties than photons, would cause variable torques
2. Outgassing from the spacecraft
3. Normal attitude control valve leakage

Inquiry revealed that the force level of the solar wind is insignificant except for occasional activity separated by many months. The outgassing forces are unknown, but it would not seem, from a qualitative point of view, that they would cause such variable activity.

A calculation was made of the forces due to normal valve leakage, which was measured during tests to be an average of 3.0 cm^3/hr per valve at standard conditions. Assuming that nominal gas laws apply at this condition, the torque was calculated to be 16 dyne-cm per valve. There are four valves per axis (two clockwise and two counterclockwise). It has been observed in testing that the leakage will vary for each valve actuation even though it averages out over a period of time. It seems apparent, then, that the valve leakage can explain the variation in the disturbance torques, especially the changes that occur from one valve actuation to the next.

4. First Midcourse Maneuver Sequence

The start of the midcourse maneuver sequence (initiation of DC-27) took place at 14:35:00 GMT on day 339 (December 4). This command turned on the gyros for warmup 1 hr prior to the start of the commanded turns. At 14:35:47 GMT, the gyros came on and started to spin up. The spin up of the gyros caused a disturbance in the attitude control subsystem, and the pitch, yaw, and roll error signals were driven over to one side of the deadband. The roll channel started limit cycling against the negative side of the deadband with an angular excursion of one data number, which is a resolution of 0.41 mrad. After 49.3 sec of operation (eleven frames of data), a large transient was observed (4.2 sec later), which showed the spacecraft going into automatic roll search that continued until Earth-light reflections caused an acquisition to occur at 14:52:32 GMT at a clock angle of about 90 deg.

The fact that the roll error signal was forced to one side of the deadband by the gyro spinup was a completely expected, normal event. The gyro turn-on was timed to be most favorable in direction and position within the deadband to compensate for spinup reaction. The huge transient in the roll channel and subsequent loss of acquisition was catastrophic to the initiation of the maneuver and caused it to be aborted and postponed for one day. The one sample of roll error of −16.0 mrad is impossible to explain by actual spacecraft motion, because the impulse required would be catastrophic and would have been observed in the pitch and yaw channels and on the roll gyro. It appears that the signal was an electrical transient of some kind.

In view of the experience and analysis in connection with the loss of star acquisition in general, which generated the minute particle theory as the cause of losses of acquisition, it seems that the loss of Canopus at the initiation of midcourse falls into the same category. It is postulated that the time correlation of gyro warmup to subsequent loss of acquisition was due to the gyro starting transient shaking loose particles from the solar panels, and these particles were then driven past the star sensor by solar pressure or by spacecraft static charge. An instantaneous bright flash would cause a high gate violation and a false error signal. Since the resolution of events in this mode is 4.2 sec, it is possible to miss getting a sample of the flash in the brightness channel.

The performance of the spacecraft at initiation of gyro warmup, prior to the start of the second and successful

midcourse sequence, was identical to the first except for the loss of acquisition.

5. Second Midcourse Maneuver Sequence

The start of the second and successful midcourse maneuver sequence took place with the initiation of DC-27 at 14:25:13 GMT on day 340 (December 5). The gyros came on and the gyro spinup caused the roll limit cycle to stay on the negative side of the deadband, as in the first maneuver try. After the gyros were up to speed, the roll limit cycle was normal.

The maneuver consisted of a pitch turn of −39.16 deg and a roll turn of +156.07 deg. The pitch-turn starting transient was seen at 15:26:12 and the stopping transient at 15:28:54 GMT. The start-roll transient was at 15:47:10 and the stopping transient at 16:01:19 GMT. The turns were correct in every respect. The amount of overshoot in the rate plus position measurement seen during the starting and stopping transients was seen to be within the tolerances expected for the given control system acceleration of 0.45 mrad/sec. This is the only good confirmation available of the steady-state operation of the gas jets.

The start of motor burn was at 16:09:10 and motor burn stopped at 16:09:30 GMT. The action of the autopilot during this time is discussed in a separate section.

Sun reacquisition was commanded by the CC&S at 16:15:10 GMT. Since the pitch turn was of such a small magnitude, the Sun reacquisition was quick, taking place at 16:21:07. Again the Sun-gate field of view was seen to be 2.2 deg.

The Sun-gate event started roll search for Canopus and the first star acquired was Velorum at 16:44:36 at a cone angle of 342.8 deg. Roll override was initiated at 16:52:50, and Canopus was acquired at 16:55:00 when regular roll control was established.

6. Autopilot Performance

The midcourse maneuver was initiated at 14:25:13 on day 340 (December 5) with gyro warmup. At 15:25:12, the attitude control subsystem was switched to inertial mode and the commanded turns were started. The turn angles include a vernier adjustment in pitch and roll to compensate for a known CG misalignment error. The action of the autopilot under the known CG misalignment rotates the thrust vector to the proper direction in inertial space.

A vernier adjustment was also made to the motor burn time to compensate for jet vane drag. The compensation was based on the predicted initial conditions to the autopilot from the attitude control subsystem. On the basis of the commanded turn angles, it was expected that solar torques would keep both pitch and yaw angular positions held against the negative side of the attitude control deadband. This initial angular offset causes the autopilot to drive the jet vanes hard-over, which produces 6-lbf drag. The integral of the drag force over the transient period following motor ignition provides the magnitude of the motor burn time correction. The actual position of the spacecraft in the pitch and yaw attitude control deadband was exactly as predicted.

The midcourse rocket was ignited at 16:09:09.6 and burned for 20.4 sec. Four data points on the gyro signals were received during the motor burn period. Although this did not provide enough data for a thorough analysis, three events of significance appear to fit the observed points: (1) the first data point after motor ignition indicates a transient overshoot in pitch and yaw (this would be expected from the known, initial conditions on the autopilot); (2) for the remaining three points during the burn period, pitch and yaw maintained an equal and opposite offset, indicating a CG misalignment angle of approximately 2.2 mrad or 0.064 in.; and (3) a very slow motion in the roll channel may have been a low-amplitude limit cycle due to friction in the jet vane actuators. (This limit cycle is theoretically predictable and has been observed in analog computer simulations, but has not been observed in previous spacecraft because of insufficient data during the midcourse maneuvers.)

The entire midcourse maneuver and the performance of all subsystems was very satisfactory. Tracking data have verified that the *Mariner IV* midcourse was very accurate.

7. Cruise Performance

The most noteworthy observation made during the attitude control cruise portion of the flight was the fact that transients in the roll control system caused the spacecraft to go into the automatic roll–search sequence. In some cases, a brightness transient was associated with the roll error transient. Five of the roll transients were noted in the first ten days of flight.

After lengthy analysis and simulation, it was determined that the most likely and probable cause of the roll transients was that minute, bright particles were

floating by the Canopus sensor and causing brightness transients that exceeded the upper brightness gate limits of the sensor. If the error signal in the sensor was negative, reacquisition would immediately take place; otherwise, the automatic roll search would take place. A flat specular particle of 0.005-in. diameter would give a brightness indication to the upper gate level (8 times Canopus) at a distance of 2500 ft from the sensor. The bright flashes are of short duration and the telemetry resolution is not good enough to sample them very frequently.

An investigation was performed to locate a possible mechanism for the generation of particles. It was discovered that extremely small meteoroids (approximately 10^{-3} grams) impacting the spacecraft could cause the release of dust and lint in frequency of occurrence in the range to explain the observations.

It was recommended that DC-15 be used because it would remove the high gate from the control system logic circuitry. This was done at 17:30:00 on day 352 (December 17). Up to that time the use of DC-15 had been very successful. Many roll transients have been observed, but none has caused a loss of acquisition. There seems to be little danger that a particle will cause the sensor to lose Canopus because the bright flashes from the sensor are of such short duration.

In the limit-cycle operation of the control system, the limit-cycle rates are determined by a minimum rate increment established by a minimum on-time circuit. The design goal for the rate increment was 9.0 μrad/sec. In the pitch and yaw systems, the minimum rate increment turned out to be 18.4 μrad/sec, and 14.0 μrad/sec in roll. The reason for this is still being investigated. It should be noted, however, that the effect on the cruise gas consumption is negligible due to the large reserve available.

The rate of gas consumption being used during the cruise mode is 3.76×10^{-3} lb per day $\pm$ 10%.

XIII. SPACECRAFT SUBSYSTEMS: PROPULSION

In conjunction with the Spacecraft Development Program, JPL developed a two-start 50-lb-thrust monopropellant hydrazine propulsion system for use on the spacecraft as a trajectory correction and maneuver rocket.

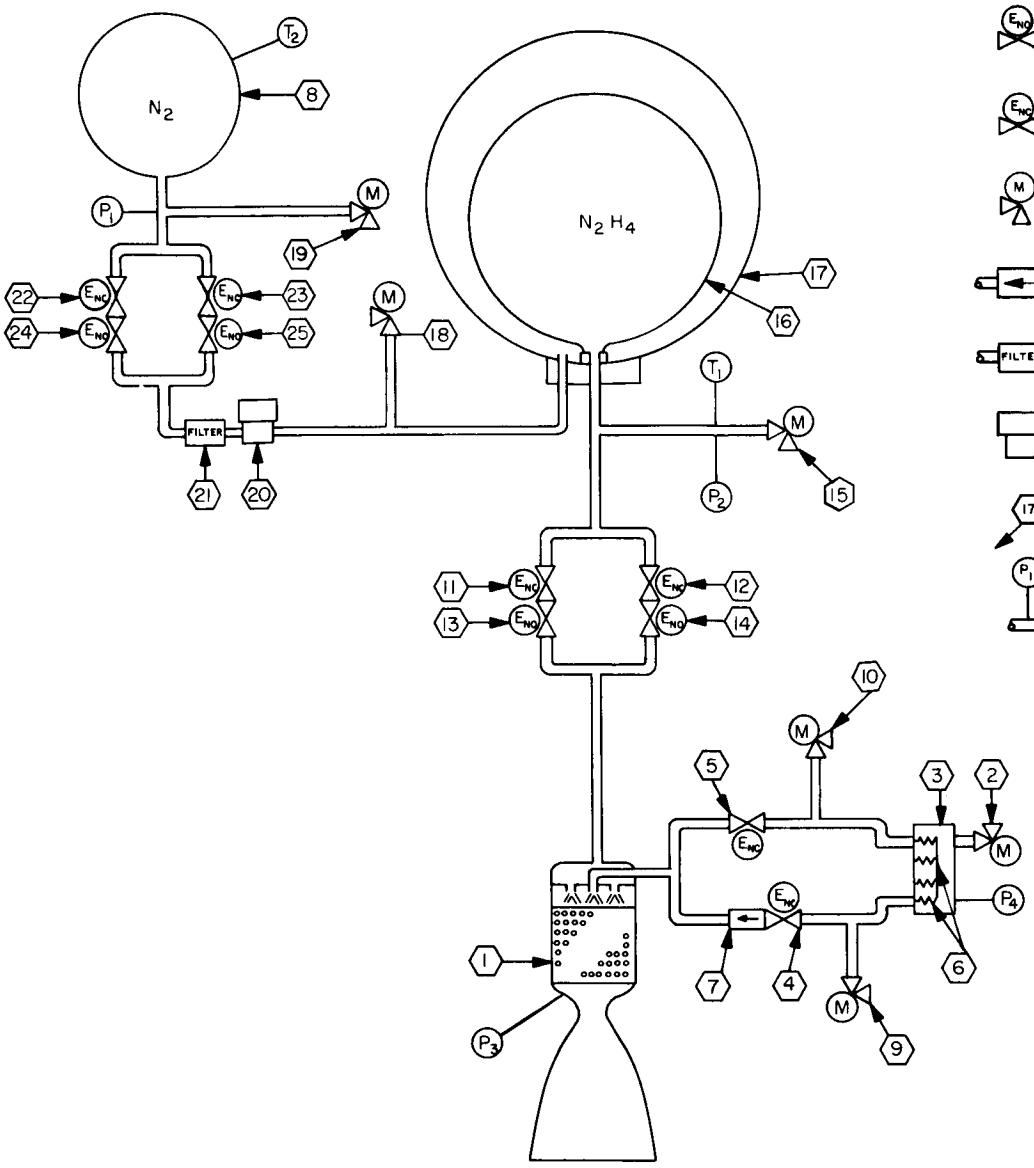
As designed for the *Mariner* Mars 1964 mission, this propulsion system was to remove or reduce the *Atlas/Agena* launch injection dispersion errors so that a Mars flyby with a sufficiently small miss distance could be reasonably assured. Nominally, this function was to be performed during a single spacecraft midcourse maneuver (occurring approximately 4 to 10 days after launch), at which time the spacecraft would be directed to turn to a prescribed position in space and impart a corrective impulse via the postinjection propulsion system. A second propulsion system firing was available to further refine the trajectory. If the second maneuver were not required for spacecraft trajectory correction, it was requested that, mission so allowing, a restart experiment be performed subsequent to planetary encounter and playback of encounter scientific data. The purpose of the experiment was to demonstrate propulsion system long-term space-storage capability, restart capability after prolonged storage in space, and system reliability.

A. Subsystem Description

The propulsion subsystem used a liquid monopropellant anhydrous hydrazine as the propellant, and nominally developed a 50-lb vacuum thrust and 236 lbf-sec/lbm vacuum specific impulse (without jet vanes). It was functionally a regulated-gas, pressure-fed, constant-thrust rocket. Principal system components consisted of a high-pressure gas reservoir, a pneumatic pressure regulator, a propellant tank and propellant bladder, an ignition reservoir, explosive valves for start and shutoff functions, and a rocket engine. The rocket engine contained a quantity of catalyst to accelerate the decomposition of the hydrazine. Four jet vanes were located at the exit plane of the nozzle and were used to provide spacecraft roll, yaw, and pitch control during engine burn. A schematic of the system is shown in Fig. 191, and a flight-type system is shown in Fig. 192.

The design and operational philosophy of the system shown in Fig. 191 was directed toward maximizing system reliability and reproducibility, minimizing preflight handling and spacecraft interactions, minimizing inflight electrical signals and sequencing, and minimizing the number of system components.

The system concept shown in Fig. 191 was predicated on the basis that it satisfy the requirements for long term storage (maximum of 250 days) and multiple-starts (maximum of two) imposed by the mission. In order to better fulfill the long-term storage requirements, pressurization by gaseous nitrogen was used in lieu of gaseous helium, which is more prone to leakage. In a like manner, welded and brazed tubing and fittings were used wherever possible to minimize the number of potential leak sources. Also, metal seals were used (where welding and brazing were impractical) in place of elastomeric seals to alleviate the effects of radiation, hard vacuum, and long-term storage on the critical system seals. Multiple start capability was realized by the inclusion of "ganged" explosive valves with two parallel branches of normally closed (start)/normally open (shutoff) valve groups in the nitrogen and fuel circuits, and two normally closed valves in parallel in the oxidizer circuit. Individual start cartridges (15 cm^3 of N_2O_4 each) were used for each of the two starts; both cartridges were pressurized by a common source. The propulsion system could be fueled, pressurized, and monitored for several weeks prior to placement within the spacecraft and actual launch. The system in the pressurized and fueled condition was safe for personnel to work around over the temperature extreme of 35 to 125°F (burst pressures of the pressure vessels were a factor of 2.2 greater than maximum working pressures at 125°F). No spacecraft umbilicals or hardlines are required to maintain the propulsion system in the "ready" condition. The firing of the postinjection propulsion system was controlled by the CC&S, which received the time, direction, and duration of the midcourse firing through the ground-to-spacecraft communication link. After the spacecraft had assumed the correct firing attitude, the postinjection propulsion system was ignited (at the prescribed time) through an electrical signal that was originated in the CC&S. Inasmuch as the propellant tank was pre-pressurized, the rocket engine ignition could occur concurrently with the release of the high-pressure nitrogen to the regulator without allowing time for the propellant tank pressures to build up to the normal operating level. Thrust termination was controlled by the CC&S via an electrical signal once the specified (commanded) burning time had been realized(as determined by the spacecraft timer).



TWO-WAY VALVE, EXPLOSIVELY OPERATED, NORMALLY OPEN

TWO-WAY VALVE, EXPLOSIVELY OPERATED, NORMALLY CLOSED

ANGLE VALVE, MANUALLY OPERATED

CHECK VALVE

FILTER

PRESET REGULATOR

COMPONENT NUMBERS

INSTRUMENTATION NUMBERS

COMPONENTS

No.	DESCRIPTION
1	ROCKET ENGINE
2	N_2 FILL VALVE, IGNITION CARTRIDGE
3	N_2 RESERVOIR, IGNITION CARTRIDGE
4	OXIDIZER VALVE, START 1
5	OXIDIZER VALVE, START 2
6	OXIDIZER RESERVOIR, IGNITION CARTRIDGE
7	CHECK VALVE
8	NITROGEN TANK
9	OXIDIZER FILL VALVE 1, IGNITION CARTRIDGE
10	OXIDIZER FILL VALVE 2, IGNITION CARTRIDGE
11	PROPELLANT VALVE, START 1
12	PROPELLANT VALVE, START 2
13	PROPELLANT VALVE, SHUTOFF 1
14	PROPELLANT VALVE, SHUTOFF 2
15	FILL VALVE, PROPELLANT
16	PROPELLANT BLADDER
17	PROPELLANT TANK
18	PREPRESSURIZATION VALVE, NITROGEN
19	FILL VALVE, NITROGEN TANK
20	PRESSURE REGULATOR, NITROGEN
21	NITROGEN FILTER
22	NITROGEN VALVE, START 1
23	NITROGEN VALVE, START 2
24	NITROGEN VALVE, SHUTOFF 1
25	NITROGEN VALVE, SHUTOFF 2

INSTRUMENTATION

PRESSURE TRANSDUCERS

- P_1 NITROGEN TANK
- P_2 PROPELLANT TANK
- P_3 THRUST CHAMBER
- P_4 IGNITION CARTRIDGE N_2 RESERVOIR

TEMPERATURE TRANSDUCERS

- T_1 PROPELLANT
- T_2 NITROGEN TANK

NOTE:
EVENT REGISTER DATA (BLIP DATA) ON EXPLOSIVE VALVE START AND SHUTOFF CURRENT

Fig. 191. Postinjection propulsion system schematic

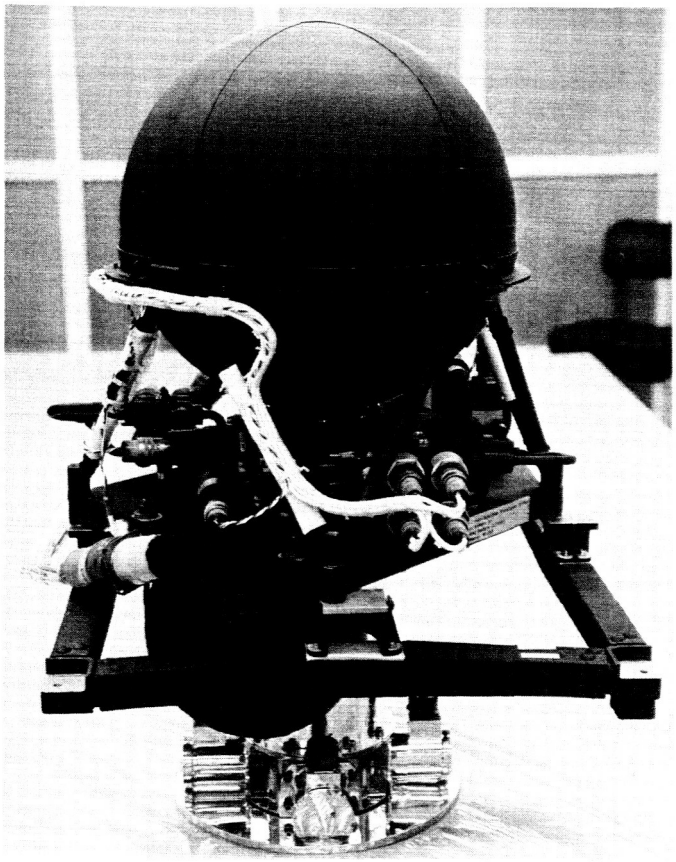


Fig. 192. Postinjection propulsion system

During the rocket engine firing, spacecraft attitude was maintained by the autopilot-controlled jet vane actuators. Referencing Fig. 191, the specific sequence of events for the propulsion system for each engine ignition and shutoff was:

1. At the command signal from the CC&S to ignite the engine, normally closed explosively actuated valves ⟨22⟩[4] or ⟨23⟩[5], ⟨11⟩[4] or ⟨12⟩[5], and ⟨4⟩[4] or ⟨5⟩[5] were activated allowing regulated nitrogen pressurization of the propellant tank, propellant flow to the rocket engine, and injection of a small quantity of nitrogen tetroxide to the rocket engine.
2. Hypergolic ignition ensues, followed by continuous catalytic monopropellant decomposition of the anhydrous hydrazine.
3. At the command signal from the CC&S to terminate rocket thrust, normally open explosively actuated valves ⟨13⟩[6] or ⟨14⟩[7], and ⟨24⟩[6] or ⟨25⟩[7] were activated, terminating propellant flow to the rocket engine and positively isolating the remaining pressure in the nitrogen sphere from the propellant tank.

[4]First start
[5]Second start
[6]First shut-off
[7]Second shut-off

The following design requirements for the postinjection propulsion system were a result of spacecraft physical and operational restraints, *Agena D* injection guidance accuracies, ground and inflight environment conditions, propulsion system characteristics, and the requirements imposed on the spacecraft design characteristics and restraints:

1. The unit had to be capable of imparting to a 600-lb spacecraft a maximum velocity increment of 60 m/sec, for fulfillment of maximum expected midcourse maneuver requirements.
2. The propulsion system had to be capable of delivering a minimum midcourse correction velocity increment of 0.100 m/sec to a 600-lb spacecraft.
3. The propulsion system had to be capable of a total of two ignitions and thrust terminations with a minimum duration of 4 hr between consecutive engine firings.
4. The unit had to ignite and operate in a vacuum environment.
5. The unit had to undergo ignition in a gravitationless environment.
6. The preflight-to-launch ambient temperature range of the propulsion system had to be 35 to 125°F.
7. The propulsion system temperature limits from time of launch up through the termination of the flight had to be 35 to 125°F.
8. The unit had to be capable of vacuum-environment storage in excess of 250 days without causing any deleterious effects on the spacecraft attitude control or performance.
9. The rocket engine nominal steady-state vacuum thrust, with the four jet vanes deflected through 10 deg, had to be no greater than 52.5 lb and no less than 47.5 lb.
10. The vacuum specific impulse upon which propellant load and velocity increment capability were to be determined had to be 232.7 lbf-sec/lbm; this value corresponded, approximately, to the rocket-engine vacuum thrust with all four jets vanes deflected through 10 deg.
11. The propulsion system had to be capable of providing variable total impulse for fulfillment of

velocity increment requirements ranging from 0.1 to 60 m/sec; total impulse control was to be provided by a spacecraft timer that controls the engine burn time. The engine total impulse and velocity increment were to be predictable to approximately the 1 σ accuracies shown in Fig. 193.

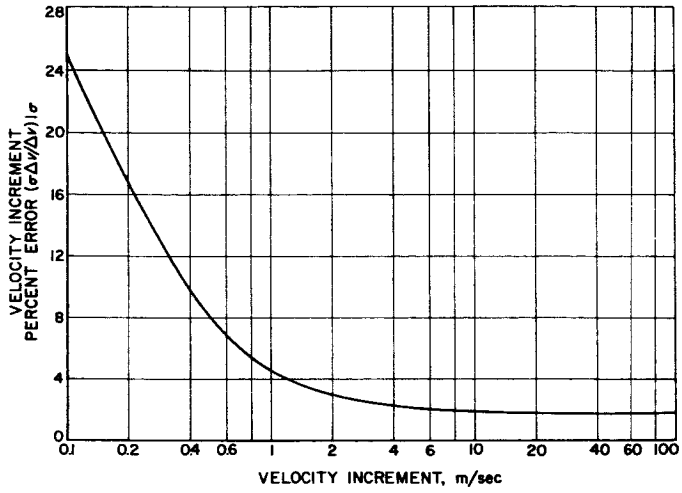


Fig. 193. One-sigma velocity increment percent error vs velocity increment

12. Thrust vector control was to be provided by four jet vanes, each capable of producing approximately 2.4 lb of lift in the fully deflected position. The radial distance from the rocket engine center line to the center of pressure of each jet vane was to be approximately 1.08 in.

13. The propulsion system thrust chamber and nominal thrust vector were to be located normal to the spacecraft roll axis and coincident with the predicted spacecraft center of gravity. To permit adjustment capability of the thrust vector, the propulsion system was to be adjustable within a 1-in.-diameter circle; and, through the use of separate propulsion system–spacecraft mounting structures, the propulsion system and thrust vector were to be capable of being tilted ± 2.0 deg along the spacecraft roll axis.

14. The effective engine thrust vector was to be predictable to within ± 0.2 deg of the geometrical engine center line measured at a plane passing through the throat of the engine.

15. Three simultaneous dual-bridgewire squib firings were required for each engine ignition (total of two ignitions), and two simultaneous dual-bridgewire squib firings were required for each engine thrust termination (total of two thrust terminations). The required minimum time between ignition (start) squib firings and thrust termination (shutoff) squib firings was 50 msec.

16. The propulsion system, in the fueled and pressurized condition, had to be safe for personnel to work around at temperatures up to 125°F.

B. Spacecraft Weight and CG Determination, and PIPS Positioning

The mass of the spacecraft must be accurately known to establish proper injection performance and midcourse propulsion burn times. The CG position must be accurately known so that the midcourse propulsion system thrust vector may be aligned to eliminate offset torques. Alignment of the motor's thrust axis was accomplished by adjusting the position of the motor relative to the spacecraft structure. If known CG shifts occur after final motor positioning, corrections to maneuver turns may be made to account for these shifts. This correction capability by the method of vernier adjustments is discussed below.

1. Propulsion System Alignment

The propulsion system is mounted to the spacecraft by means of a substructure. The functions of the substructure are twofold: (1) to provide sufficient structural support for the motor, and (2) to adjust the thrust axis of the motor so that it passes through the spacecraft's center of gravity. A propulsion system installation schematic is shown in Fig. 194, and Fig. 195 is a detail of the substructure.

The substructure was fabricated of four square aluminum tubes. The four corner joints were made by fittings that also provide the substructure-to-spacecraft mounting surface. This surface is shown by plane B in Fig. 194 and Fig. 195. The holes in the four fittings accept close tolerance fasteners that attach the substructure to four brackets on the spacecraft in the plane of Bay II. Four midcourse motor mounting blocks were mounted on the approximate centers of the square tubes. The tops of these blocks, which measure approximately 1.5 in.^{2}, were machined coplanar after assembly. This plane is shown as plane C in Fig. 194 and 195; the thrust plate of the propulsion system is mounted to it.

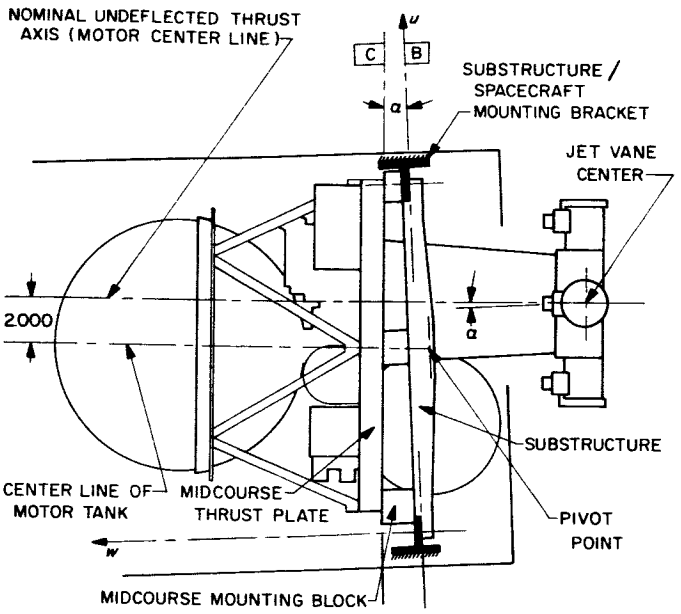


Fig. 194. Midcourse motor installation

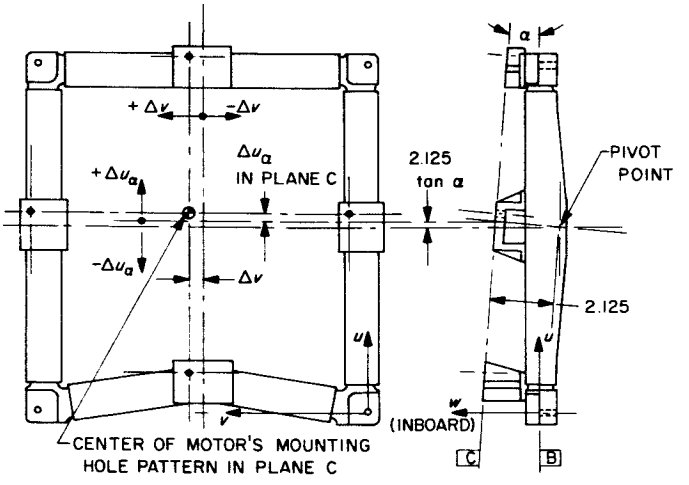


Fig. 195. Midcourse motor substructure

A coordinate system common to both the spacecraft and the propulsion system was chosen for motor alignment and CG measurement. This coordinate system has its origin at the center of propulsion system-to-spacecraft mounting hole in the common mounting surface, plane B. The system is desirable since its use eliminates dimensional tolerance buildups. The coordinate system is shown in Fig. 195, and is labeled *u-v-w*.

After measurement of the center of gravity, three variable dimensions were specified and used in the machining of the substructure's mounting blocks. The three adjustments that could be made to align the motor's thrust axis with the CG were:

1. A rotation of plane C about a defined pivot point so that it would make an angle to plane B of $\alpha = 0$ deg to $\alpha = 4$ deg. (The angle α is illustrated in both figures.)
2. A translation of the motor's mounting hole pattern in plane C by as much as ± 0.500 in. from the center of Bay II, parallel to the spacecraft separation plane, or along the v axis. This translation is shown by Δv in Fig. 195.
3. A translation of the motor's mounting hole pattern in plane C by as much as 0.375 in. up, and 0.25 in. down. This translation is shown by Δu_α in Fig. 195. Downward translation was limited at small angles by dynamic envelope clearance constraints. If $\Delta u_\alpha = 0$, the center line of the fuel tank would pass through the defined pivot point as shown in Fig. 194.

The approximately vertical adjustment (3) is redundant to the rotational adjustment (1) for the majority of CG positions, but was included to allow all motors to be inclined at the same angle on any of the flight spacecraft. This was desirable since each autopilot had to be calibrated for the given angle, and having the angles identical allowed autopilot interchangeability among spacecraft.

After the initial CG measurement at JPL, the substructure's blocks were machined to the determined angle and four mounting holes drilled at the proper translations so that the thrust vector passed through the CG. A second substructure was machined to the same angle but no holes were drilled. After the final CG was measured at AFETR, the second substructure could be drilled and used if the CG shift (due to hardware replacement between the two CG measurements) was of sufficient magnitude. It was undesirable to have to use this spare frame because it would have required hand machining in the field.

2. Weight and CG Measurement

The weight and CG test empirically determined these properties of the spacecraft (less the propulsion unit) and of the propulsion unit itself. A rotation and two translations of the propulsion system, consistent with the adjustment capability of the motor positioning, were then calculated to align the thrust vector with the combined motor/spacecraft center of gravity. With these

adjustments known, the combined weight and CG were calculated. Four setups were necessary to perform the entire test.

a. Spacecraft less propulsion system CG in the plane of Bay II (Setup 1). Two of the three CG coordinates ($\overline{u}_s$ and $\overline{v}_s$) and the weight of the spacecraft were determined by this test. The setup is shown in Fig. 196. Because of geometric constraints, it was impossible to measure reactions directly on the spacecraft; hence, a fixture was required to adapt from the propulsion system mounting brackets of Bay II to the load cells. The fixture was essentially two triangles: one was a right triangle that picked up three of the four mounting brackets, and the other was an equilateral triangle whose apexes located the 500-lb load cells (Fig. 197).

The spacecraft (less the propulsion unit) with the fixture installed was set on the CG stand and reactions were recorded. The solar panels were held open by struts, the length of which was set during cruise damper adjustment. The solar vanes were folded. Reactions were

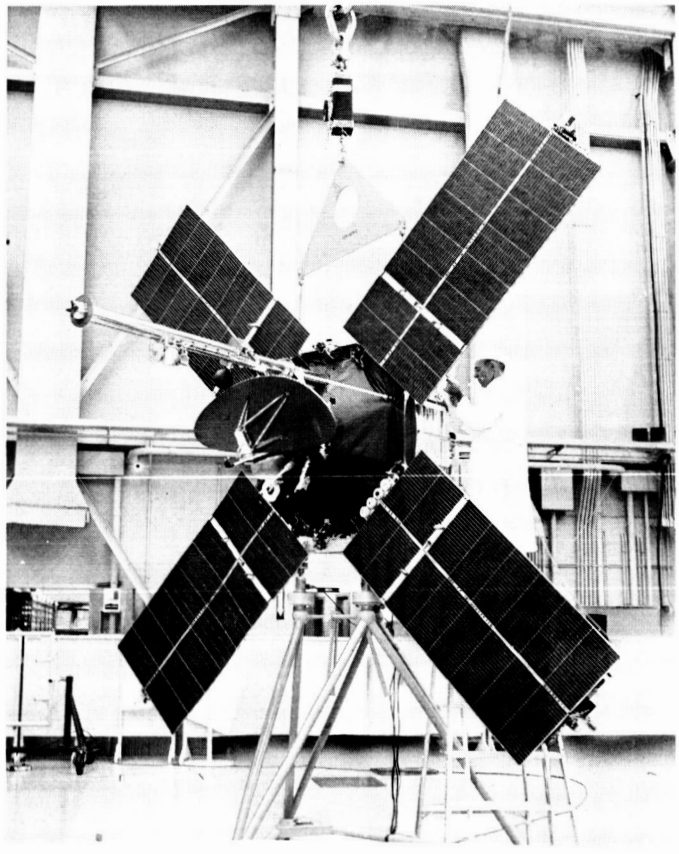


Fig. 196. Test setup for spacecraft plane of Bay II CG determination

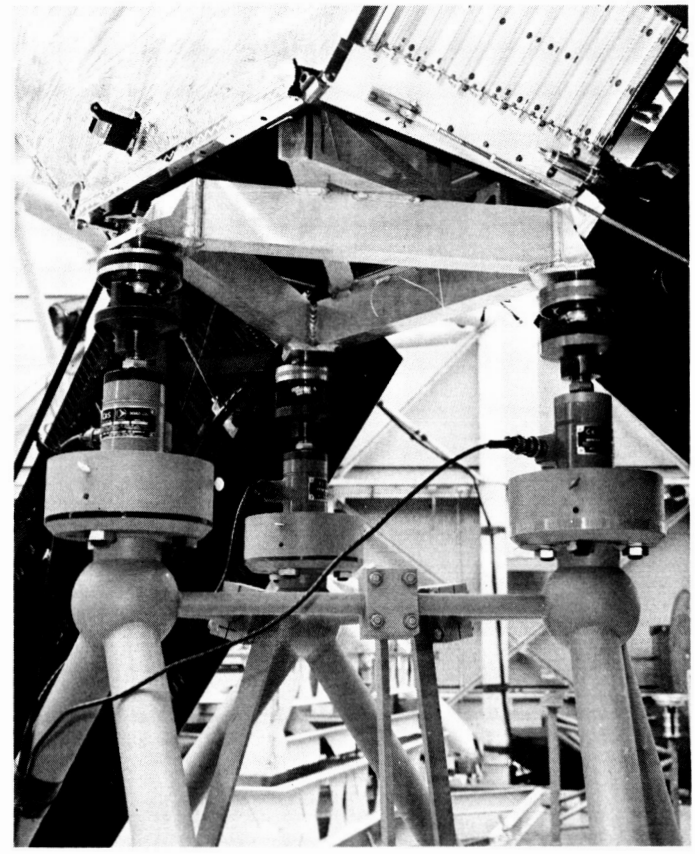


Fig. 197. Test fixture for spacecraft plane of Bay II CG determination

taken again in two additional positions (spacecraft rotated 120 deg) to correct for load-cell and leveling errors. The load cells were floating to ensure axial force only. Their positions were determined by inspected dimensions of the fixture. Using the average of the three force measurements taken at each point and making corrections for the fixture, missing nitrogen gas, solar panel struts, and undeployed solar vanes, the weight and projected position of the CG in the plane of Bay II were determined for the spacecraft less the propulsion unit.

b. Spacecraft less propulsion system CG normal to the plane of Bay II (Setup 2). To obtain the CG position of the spacecraft (less propulsion system) normal to the plane of Bay II ($\overline{w}_s$), the spacecraft was installed on a spacecraft support ring that had been fitted with an adapter that picked up the load cells. This assembly was then set on three 500-lb load cells on the *Mariner II* CG stand (Fig. 198). The solar panels were secured in the open position, and the solar vanes were stowed. Reactions were measured by the load cells at the three points of the fixture in three positions 120 deg apart.

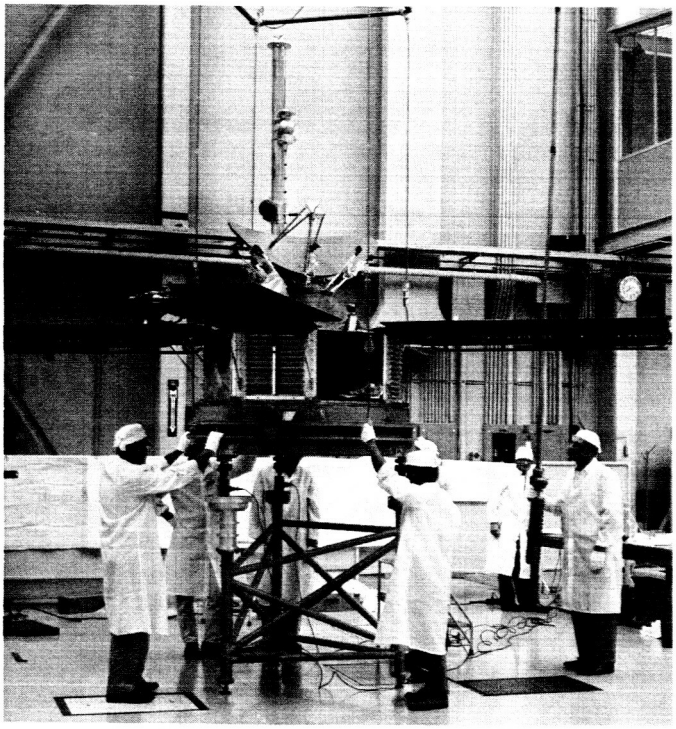


Fig. 198. Test setup for CG determination normal to plane of Bay II

The spacecraft was then rotated 180 deg, with respect to the spacecraft support ring, and the sequence repeated. Reversing the spacecraft on the ring eliminated the ring weight and CG from the spacecraft CG calculations. The eccentricity of the spacecraft CG from the structure's center line was calculated and related back to the plane of Bay II, giving the CG coordinate normal to this plane.

c. Propulsion system CG (Setups 3 and 4). The weight and CG of the propulsion system were measured before fueling. Two setups were required: one for the CG as projected into the plane of Bay II ($\overline{u}_p$ and $\overline{v}_p$), as shown in Fig. 199; and one for the CG normal to the plane of Bay II ($\overline{w}_p$), shown in Fig. 200. The propulsion system was mounted on the midcourse motor weighing fixture. This fixture was set onto the three load cells in two planes at right angles to each other as shown in the figures. The same base stand used for the spacecraft Bay II CG test was used for both of these tests. Reactions were measured with 100-lb load cells, since their accuracy was better than that of the 500-lb cells used in

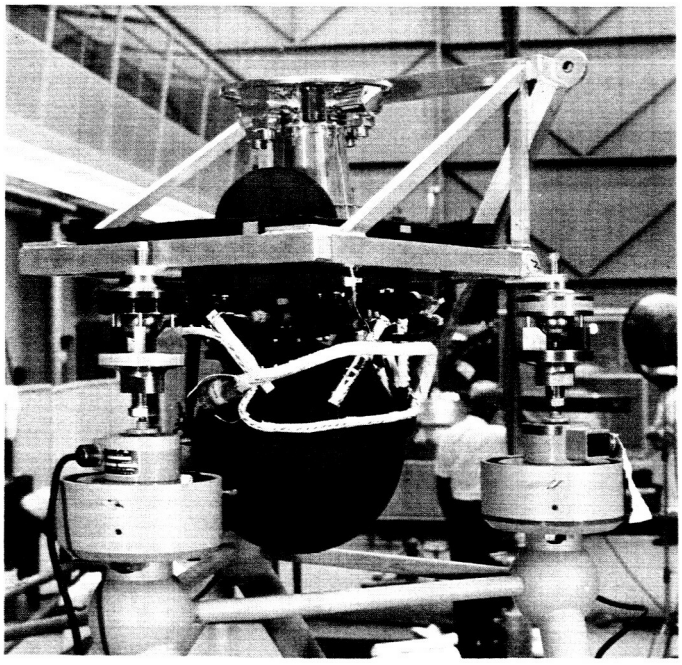


Fig. 199. Test setup for PIPS CG determination in plane of Bay II

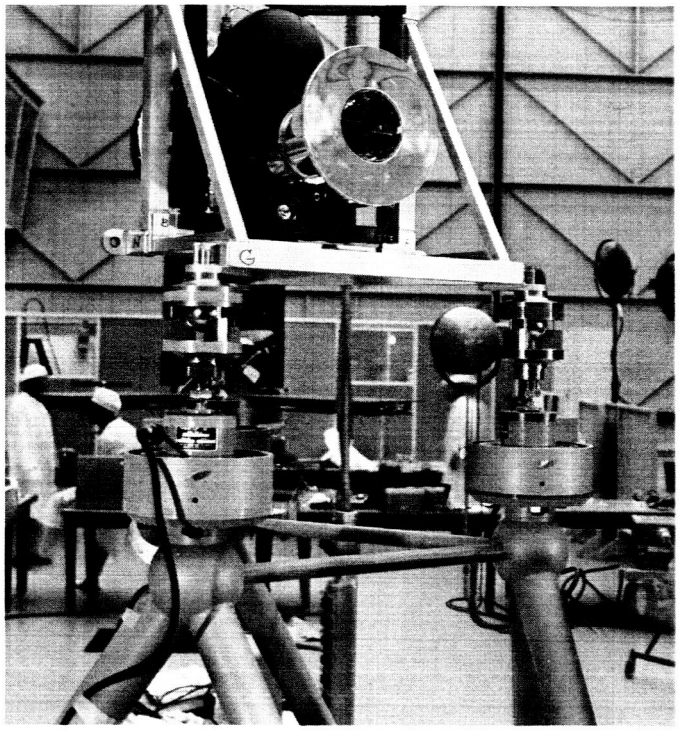


Fig. 200. Test setup for PIPS CG determination normal to plane of Bay II

the spacecraft weight and CG determination. In each setup, three sets of readings were taken at positions 120 deg apart to minimize load-cell and leveling errors. Corrections were made for fixture weight and missing propellant and gas. From the results of the two setups, the PIPS weight and the three coordinates of its CG were obtained.

An error analysis that included load-cell uncertainties, dimensional uncertainties, and uncertainties in the corrections applied for missing and added components showed that the uncertainty in total spacecraft CG position resulted in a maximum 2.5-mrad uncertainty in midcourse pointing accuracy.

3. Method of Vernier Adjustment

For small CG shifts, a method of correction other than repositioning of the motor was available. This method was to perform vernier adjustments on pitch- and roll-maneuver turns to account for all known misalignment of the motor's center line from the center of gravity. Instead of pointing the motor center line in the direction of the desired midcourse velocity increment, the stabilized thrust vector, a line through the jet vane center and the known average CG during motor burn, could be pointed in that direction. The input to the midcourse maneuver program simply defines the thrust vector in spacecraft coordinates so that it includes the known geometrical offsets plus the calculable initial rotations of the spacecraft. Rotations at the initiation of motor burn are caused by initial torques that result from the geometrical offsets before the autopilot and jet vanes have pointed the thrust vector through the CG. The midcourse program, which equivalently gave the magnitude and polarity of the turns, automatically calculated adjusted turns.

The autopilot, which controlled spacecraft attitude during motor burn, had the capability to correct for an offset in excess of 20 mrad. (The angle referred to is the amount the thrust vector must shift to pass through the center of gravity.) To determine vernier adjustment capability, the sum of errors and uncertainties were subtracted from the autopilot's capability. Uncertainties considered were mechanical misalignments in assembly of the propulsion system, concentricity of the undeflected thrust vector with the motor center line, center-of-gravity measurement uncertainties, and unknown CG shifts due to attitude control gas depletion and solar panel mislocation. Subtracting the 4.11 mrad 3σ sum of these uncertainties from the autopilot capability, it was determined that the method of vernier adjustments could be used to correct for offsets up to 15.89 mrad.

Only a portion of the vernier adjustment capability could be allocated to correct for CG shifts due to hardware replacement between initial and final CG measurements. Some of the capability had to be allocated for CG shifts after final CG measurement (which was the final repositioning opportunity). After the final-positioning opportunity, possible shifts from three sources were considered:

1. Hardware replacement after final CG. To reserve vernier adjustment capability for this source of misalignment, a possible but unlikely set of circumstances was arbitrarily selected. These were exchanging two solar panels that differed in weight by ½ lb, and a 3¼ lb addition or removal in electronic cases. These changes would additively shift the CG by 6.84 mrad.
2. Possible failures. Three otherwise noncatastrophic failures were considered: (1) 90% attitude control gas depletion, (2) a solar vane failing to open, and (3) the science cover opening prior to maneuver. These would have caused a resultant maximum CG shift of 2.13 mrad.
3. Midcourse fuel depletion. For a second maneuver, 95% fuel depletion during the first maneuver was assumed. This would have caused a 2.59 mrad CG shift.

Subtracting the sum of possible known misalignments due to the above three sources from the total vernier adjustment capability gave a 4.33 mrad remainder. This amounted to a 0.125-in. shift of the center of gravity at the roll axis, which, then, was the portion of the vernier adjustment capability allocated to account for CG shifts between initial and final CG measurements. If the shift had been greater than ⅛ in. perpendicular to the motor center line, the motor would have been repositioned by machining and installing the spare substructure.

4. Measurement and Alignment Results

The weight and center of gravity of each of the flight spacecraft were measured at JPL. In every case, the CG fell outside the horizontal adjustment capability of the motor positioning, but within the total capability. The motors were positioned, all at the same angle α, with vertical translation to give perfect alignment along the u_a axis and with the maximum 0.500-in. horizontal translation. The weights and CG were again measured at AFETR. In no case was the shift in CG greater than

0.125 in., thus eliminating the need to reposition any motor. Table 48 gives the weight and CG position in conventional spacecraft coordinates and motor alignment parameters after each test for the three spacecraft. It also contains corrected weight, CG position, and alignments at the time of launch of *Mariner III* and *Mariner IV*, and the average CG and alignment during the successful *Mariner IV* midcourse maneuver.

The changes in CG position and alignment between tests at JPL and the Cape were attributed to hardware replacement. Changes between the final measurement and launch were also due to hardware replacement, and were calculated on the basis of QA status log records. For *Mariner* Mars 1964, the actual average CG position at midcourse was calculated from the position at launch. Half the midcourse fuel depletion for the predicted 20-sec burn (a prediction that resulted from a previous nominal calculation) and the abnormally high position of the four solar vanes entered into this computation. The seemingly large 0.030-in. shifts in $\bar{X}$ and $\bar{Y}$ do not appreciably affect the alignment, since the fuel tank lies along the horizontal projection of the thrust axis. The vector summation of the two actual misalignments listed (0.012 in.) corresponds to an angular misalignment of 0.43 mrad. This number is extremely small compared to the 15.89-mrad correction capability using the method of vernier adjustments. The offsets were included in the input to the final maneuver calculation, but their magnitudes were too small to change the pitch and roll turn

Table 48. Weight, CG, and motor alignment of *Mariner* Mars 1964 spacecraft

Property[a]	Direction	MC-2		MC-3		MC-4	
		JPL	Cape Kennedy	JPL	Cape Kennedy	JPL	Cape Kennedy
Measured weight, lb		574.64	574.81	575.62	574.27	575.61	577.16
Measured CG position	$\bar{X}$ $\bar{Y}$ $\bar{Z}$	0.780 0.018 −12.292	0.780 0.091 −12.306	0.718 − 0.025 −12.303	0.691 − 0.020 −12.304	0.717 − 0.001 −12.274	0.790 − 0.071 −12.242
Jet vane position	X_{jv} Y_{jv} Z_{jv}	20.591 19.884 −11.312	20.591 19.884 −11.312	20.592 19.885 −11.321	20.592 19.885 −11.321	20.591 19.884 −11.292	20.591 19.884 −11.292
Motor alignment CG test, in.	Horizontal offset	0.038	0.013	0.024	0.003	0.006	0.107
	Vertical offset	0	0.016	0	0	0	0.032
Corrected weight at launch, lb			575.37		574.74		
Corrected cruise configuration CG at launch	$\bar{X}$ $\bar{Y}$ $\bar{Z}$		0.784 0.104 −12.302		0.698 − 0.023 −12.293		
Corrected motor alignment at launch, in.	Horizontal offset		0.019		0.010		
	Vertical offset		0.012		0.002		
Actual average CG position at midcourse	$\bar{X}$ $\bar{Y}$ $\bar{Z}$				0.668 − 0.052 −12.313		
Actual motor alignment at midcourse, in.	Horizontal offset				0.009		
	Vertical offset				0.008		

[a]Motor tilt $\angle \alpha$ for all three spacecraft listed is 2°0′0″.

times that had been previously calculated in the nominal run.

An examination of the data presented in Table 48 shows that the maximum weight difference between any two spacecraft was less than 3 lb, and the maximum difference in CG positions was less than 0.08 in. If the last test on the spare spacecraft at Cape Kennedy were neglected, the differences would have been approximately half those quoted above. (There was a possible justification for having neglected this last test, since it was terminated before completion by the launch of *Mariner IV*. Many components that should have been weighed and entered into corrections were not included.) In any case, similarity between the vehicles was excellent, which confirmed the consistency of the quality level to which the components were manufactured.

C. Performance Capability

The *Mariner* Mars 1964 postinjection propulsion system developed, nominally, 50 lb of vacuum thrust and a vacuum specific impulse of 236 lbf-sec/lbm (without jet vanes). Table 49 summarizes the major engine performance characteristics of the monopropellant engine and jet vane system. Length restrictions resulted in a nozzle with an expansion ratio of 44:1. However, early in the program before the nozzle expansion ratio was fixed, an engine with an expansion ratio of 103:1 was designed, fabricated, and tested in a near-vacuum environment. This engine delivered a vacuum specific impulse of 243 lbf-sec/lbm and would have resulted in a net payload advantage had the length restriction not been imposed.

Table 50 represents a weight breakdown of the postinjection propulsion system. It should be noted that, as discussed earlier, the propellant and nitrogen tanks were safety-factor vessels (burst pressure at least 2.2 times

Table 49. Nominal performance summary

Engine characteristic	Value
Vacuum specific impulse (without jet vanes)	236.0 lbf-sec/lbm
Vacuum specific impulse (four jet vanes deflected 10 deg)[a]	232.7 lbf-sec/lbm
Vacuum thrust (without jet vanes)	50.71 lbf
Vacuum thrust (four jet vanes deflected 10 deg)	50.00 lbf
Vacuum thrust coefficient[b] (without jet vanes)[c]	1.7500
Characteristic velocity[b]	4340 ft/sec
Propellant flow rate	0.21487 lbm/sec
Throat area (ambient)	0.15 in^2
Stagnation chamber pressure[b]	189.4 psia
Nozzle expansion ratio	44:1
Specific heat ratio	1.38
Maximum thrust vector deflection capability (two jet vanes deflected 25 deg)	±5.0 deg

[a]Jet vane maximum deflection capability equaled 25 deg, but expected maximum steady-state deflection was approximately 10 deg.

[b]Based on actual steady-state hot throat area (1.99% larger than ambient temperature throat area).

[c]Jet vane data in null position were negligible; therefore, null position engine data and engine data without jet vanes were essentially equal.

Table 50. Propulsion system weight breakdown

Item	Weight, lb
Dry unserviced weight	
Propulsion structure assembly	3.87
Engine and catalyst	2.50
Engine insulation	0.10
Propellant tank	2.80
Propellant bladder	1.00
Propellant valve	1.50
Propellant tank pressure transducer	0.27
Propellant tank temperature transducer	0.10
Oxidizer pressure transducer	0.27
Thrust chamber pressure transducer	0.30
Nitrogen tank	1.90
Nitrogen valve	1.00
Nitrogen pressure regulator	1.20
Nitrogen tank pressure transducer	0.27
Nitrogen tank temperature transducer	0.02
Oxidizer start cartridge	2.40
Tubing and fittings	3.20
Thrust-vector control assembly	2.60
Pyrotechnic harness	0.69
Instrumentation harness	0.69
Total dry unserviced weight	26.68
Wet weight	
Propellant	21.50
Oxidizer	0.13
Nitrogen gas	1.00
Squibs	0.62
Total net weight	49.93

maximum working pressure at 125°F), which, when pressurized, were safe for personnel to work around. In addition, the fact that the propulsion system was a relatively small system with system-fixed weights (not affected by propellant load) prevailing should be kept in mind when viewing the system weights in Table 50.

Unlike the *Ranger* and *Mariner II* spacecraft, the *Mariner* Mars 1964 spacecraft used a timer shutoff mechanism for the propulsion system instead of an integrating accelerometer circuit. The inclusion of a timer shutoff mechanism placed stringent total impulse predictability and reproducibility requirements on the post-injection propulsion system. The propulsion system design had to be capable of providing variable total impulse for fulfillment of velocity-increment requirements ranging from 0.1 to 60 m/sec for a 600-lb spacecraft. The total impulse control was provided by the before-mentioned spacecraft timer that controlled the engine burn time. Error analysis indicated that the engine total impulse and velocity increment could be predictable to approximately the 1 σ accuracies (including spacecraft timer errors) depicted in Fig. 193. Subsequent improvements in the propulsion system testing and instrumentation techniques reduced these errors by a factor of 3.

Typically, monopropellant hydrazine rocket engines have a long transient during which the engine is operating at reduced performance while the catalyst bed attains thermal equilibrium. Because of the spacecraft mechanization for engine burn duration (commanded fixed burn time as compared to accelerometer shutoff on previous Laboratory spacecraft), the prediction of the thrust transient was of paramount importance to minimize correction dispersion errors. A thrust degradation factor, which accounted for the reduced engine performance, was experimentally determined through a series of propulsion system tests. This thrust degradation factor is depicted as a function of time in Fig. 201.

In order to properly size the propellant load necessary to provide a specified velocity increment, it was necessary to determine the additional propellant to be carried in order to account for the start transient performance degradation. Reduction of test data for the additional propellant needed to account for the start transient performance degradation resulted in a value of 0.14 lb. Therefore, in order to determine the propellant needed to provide a given spacecraft with a given velocity increment, 0.14 lb was added to the value obtained from the momentum exchange relationship.

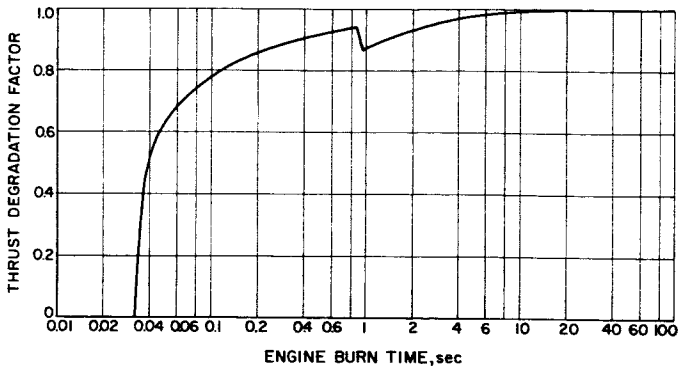


Fig. 201. Thrust degradation as a function of time

The minimum velocity increment capability of the propulsion system was very important since, statistically, an extremely small correction has a finite probability of being required to correct for injection or previous correction dispersion errors. The design goal of the *Mariner* Mars 1964 propulsion system was to be able to supply a minimum velocity increment capability of 0.1 m/sec to a 600-lb spacecraft. For velocity increments of this magnitude, the tail-off impulse from the hold-up propellant in the propellant lines contributes significantly to the total impulse required. Experimental and analytical programs were conducted to define the engine tail-off impulse as a function of engine burn time. The analytical model included the following variables:

1. Gas in the thrust chamber
2. Liquid fuel in the thrust chamber wetting the catalyst, and fuel in the injection spray
3. Injected oxidizer (if engine shutoff occurs during the bipropellant ignition)
4. Oxidizer trapped in the line
5. Fuel trapped in the fuel line and injector manifold
6. Catalyst bed temperature as a function of engine burn time

Engine tests were run for 0.1, 0.3, 1, 5, 10, 30, 60, and 100 sec, during which time tail-off measurements were made. The experimental results agreed very closely with the analytical analysis, which was later tailored to pass through the data; this agreement resulted in the curve of engine tail-off impulse vs time shown in Fig. 202.

D. Development and Testing Program

Initial planning, design approach, and configuration studies of the propulsion system were started in June

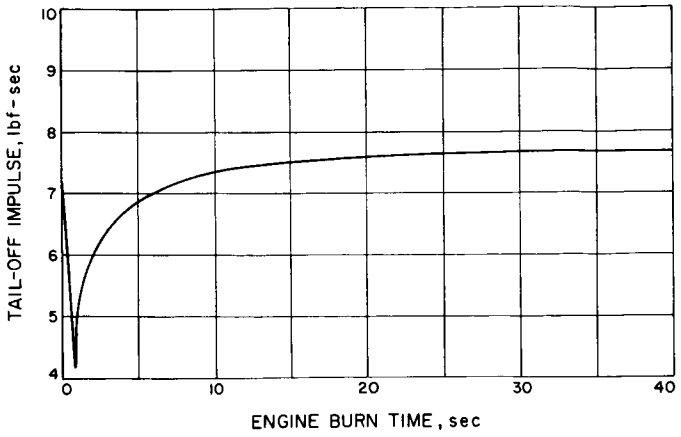


Fig. 202. Engine tail-off impulse vs engine burn time

1962 in conjunction with the initial design studies of the *Mariner* Mars 1964 mission. Several approaches to the two-start, long-term space-storage requirements were considered and preliminary system designs were made of several approaches. In September 1962, a system design (represented in Fig. 191) was selected as the one most satisfying the mission requirements and having a high probability of successful development. The possibility of using a spontaneous catalyst in lieu of an oxidizer (N_2O_4) start slug system was carried along as a possible modification to the design depicted in the figure. Promising results in the development of a catalyst, producing spontaneous decomposition of anhydrous hydrazine at ambient temperatures, had been achieved. In April 1963, it was decided that the catalyst was not developed to a point at which it could be considered for this application and was dropped from further consideration.

Upon completion of the spacecraft preliminary design and finalization of the system schematic, a systematic propulsion system development program was initiated with the goal of delivering the first FA tested propulsion system for incorporation into the *Mariner* Mars 1964 PTM in November 1963.

1. Component Level Testing

a. Rocket engine. The rocket engine used in the propulsion system was essentially identical to that used in the *Ranger* propulsion system. The only modifications were changes in flange attachments to components for packaging purposes, the addition of a chamber pressure tap for inflight telemetry of chamber pressure during engine burn, and the addition of an insulation jacket around the engine chamber wall to preclude radiant heat transfer to the spacecraft during engine burn.

The engine was subjected to type-approval testing consisting of environmental humidity, shock, static acceleration, and boost-phase vibration tests. These tests were followed by two engine firings at nominal chamber pressure, each of 300-sec duration. No anomalies were noted in either of the tests. A second engine was subjected to flight-acceptance tests consisting of an injector performance test and a boost-phase vibration test. Upon completion of these tests, an attempt was made to fire the engine at 1.5 times nominal chamber pressure for 300 sec. A failure of the chamber wall occurred at the end of 71 sec of operating time. This test had previously been passed on the *Ranger* Block III engine, which was essentially identical in design. However, post-test analyses indicated that the insulation jacket that was placed around the engine chamber to preclude heat transfer to the spacecraft during engine firing raised the wall temperature approximately 200°F, which, compounded by the 1.5 times nominal chamber pressure, put the material above its yield point. The chamber wall thickness was subsequently changed from 0.031 to 0.045 in. The engine was then successfully fired twice for 200 sec with each firing at 1.25 times nominal chamber pressure. Two tests were then made, each of 100-sec duration, with the engine installed in an inverted position. The purpose of these tests was to demonstrate that the holdup propellant at engine shutdown would vaporize off without detonating from heat soak back from the catalyst bed. Subsequently, the engine was fired at 1.33, 1.50, and 1.67 times nominal chamber pressure, each for 200 sec. All tests were successfully completed once the thickness was increased, and the engine was considered qualified for flight.

b. Oxidizer start cartridge. The start cartridge used on the propulsion system was similar to that used on the *Ranger* Block III propulsion system; the design was modified to provide a two-start capability. It consisted of two metallic bellows welded into a single housing. Normally closed explosive valves were connected to the outlet of the bellows with a check valve between them to prevent backflow of oxidizer into the other bellows during the second engine firing (Fig. 191). Approximately 15 cm^3 of oxidizer was contained in the internal volume of each bellows. The exterior of the bellows was pressurized with gaseous nitrogen. When the explosive valve was fired, the nitrogen gas compressed the bellows and injected the oxidizer into the engine for ignition.

c. Fuel tank bladder. To eliminate the fuel tank pressure rise noted during the *Mariner II* and *Ranger V* flights, the bladder material was changed. Permeability tests with the new compound indicated no measurable

rates during a 90-hr test period. A compatibility test with the compound was made by immersing a sample of the material in a glass vial of hydrazine at ambient temperature and measuring pressure rise as a function of time. At the end of 6 months of testing, the pressure rise was only 10 psi. In addition, a fuel tank and bladder assembly was filled with hydrazine, pressurized, and stored at ambient conditions with the pressure rise monitored on a daily basis. No pressure rise was noted after 6 months of storage. The results of these compatibility tests indicated that the new bladder material was adequate for the Mars mission.

Type-approval testing on the bladder consisted of initial leak tests followed by 50 cycles of pressure–vacuum cycling on the bladder. The bladder was then used in the TA-1 propulsion system type-approval tests.

d. Pneumatic regulator. The pneumatic regulator for the propulsion system was a JPL design. It was similar to that used on the *Ranger* Block III systems, the main modification being that electron beam welding of the diaphragm was used to ensure better seal characteristics. A cutaway view of the regulator is shown in Fig. 203. The regulator maintained a constant pressure to the fuel tank of the midcourse propulsion system, nominally flowing 0.006 lb/sec gaseous nitrogen. During flow, the supply pressure decayed from 3600 psia to 50 psig above outlet pressure. The regulator had to be capable of shutting off flow and maintaining minimal leakage during this locked-up condition. The regulator was an all-metal, unidirectional-flow, normally open type and operated in the following manner: the variable inlet pressure flowed around the ball and seat into the low pressure outlet chamber; impression of this pressure on the effective diaphragm area resulted in controlled outlet pressure. Displacement during operation was accomplished by flexure of the diaphragm along with the mechanical backup configuration and by predetermined outlet pressure maintained by an equalizing force from the Belleville springs. The structural materials were primarily nonferrous to minimize magnetic characteristics.

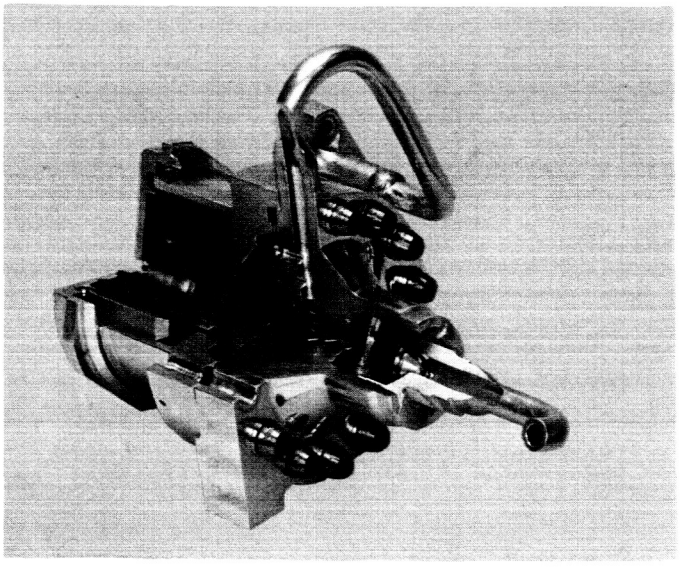


Fig. 203. Propulsion system pneumatic regulator

The type-approval test program consisted of initially undergoing proof, leak, flow, and lock-up tests to ensure proper operation of the regulator prior to proceeding into the environmental testing. The environmental tests consisted of shock, static acceleration, vibration, and temperature tests at 14 and 167°F. During and after the environmental tests, the regulator was functionally operated (approximately 21 times) to ensure its correct operation.

During the early portions of the development program, considerable difficulty was experienced in meeting the internal leakage rate requirement of 4 cm^3/hr with the regulator in the lock-up condition. This problem was traced to contamination of the ball seat area by some particulate material emanating from a mesh filter located at the inlet of the regulator. The filter was redesigned to a labyrinth type and no further difficulty was noted.

e. Explosive valves. Explosively actuated valves were used to accomplish all valving functions on the propulsion system. Because of the criticality of the explosive-valve development, two designs were carried out to ensure that the flight hardware schedule commitments could be met. One design used two of the existing *Ranger* single-start explosive valves in a parallel arrangement with an intermediate manifold. This design, which satisfied the Mars mission two-start requirement, represented a backup to the primary design. However, the existing *Ranger* valve internal seal design only marginally met the long-term space-storage requirements imposed by the Mars mission. In addition, the squib used in the *Ranger* explosive valve was only marginally acceptable. The primary explosive valve design involved an entirely new approach using an all-brazed construction that integrally manifolded two valves together in parallel. This valve–squib combination was manufactured by a vendor. Early in the program, in order to ensure the design adequacy of the valve–squib combination, the vendor was directed to perform a feasibility

test in which the nominal squib charge was to be doubled to demonstrate that the valve and squib would not suffer any damage. The nominal squib charge was then to be halved to demonstrate that the valve would still operate satisfactorily. During both series of tests, the valve operated satisfactorily and all parts remained intact; however, venting of gases past the glass seal on the squib pins was noted on all tests. Gas venting of the squib was considered unsatisfactory because of possible contamination of optical surfaces on the spacecraft. The vendor used a squib that operated on a detonating principle in preference to a gas-generating squib. An analysis of the valve indicated that satisfactory operation would be obtained by a gas-generating squib that developed an initial pressure of approximately 30,000 to 40,000 psia. A gas-generating squib that produced the before-mentioned pressures was procured and evaluated. The evaluation consisted of fabricating four squibs each of nominal one half, one and one third, one and two thirds, and double charge and firing them in the valve–squib combination. Two squibs of each group were fired at 14°F and two were fired at 167°F. During the nominal charge and one half charge tests, normal valve operation was obtained and no venting of the squib gases was evident. In the firing of the one and one third charge squibs, the valve operation was normal but two of the squibs exhibited slight leakage past the pin seal joint. In the firing of the one and two thirds charge test, the valve operation was normal but one squib exhibited a slight gas leakage past the pin seal. During the double-charge test, gas leakage past the pins occurred on all four squibs and, in one case, a pin blew out; and it was felt that the heat generated from the squib firing was great enough to melt the braze joint material. It was decided that these evaluation tests demonstrated that the gas-generating squib was superior to the valve–squib combination. It was also decided that the slight pin leakage at the one and one-third and one-and-two-thirds nominal charge would be eliminated by improvements in the quality control procedures used in brazing the pins into the squib header. On the basis of these tests, the gas-generating squib was selected to be used for valve actuation.

As part of the development program on the explosive valve, it was originally planned to run a formal Bruceton test to determine the minimum squib charge required for valve actuation, and the maximum charge allowable before valve or squib failure. The nominal squib charge was to be chosen on the basis of these data. However, the schedule did not allow for these tests to be performed so a best estimate of the charge was made based on the before-mentioned evaluation of the gas-generating squibs. In place of the Bruceton test, a developmental test program was conducted in which valves with maximum and minimum clearances were purchased along with squibs whose charge was one-half nominal and one-and-two-thirds nominal. The test program was designed so that the effects of under- and over-charge squibs could be evaluated with minimum and maximum clearance valves. (All of these valve–squib combinations were subjected to type-approval testing, which was followed by functional tests of the valves.) In all cases, normal valve operation was obtained indicating that very adequate design margins existed with this valve–squib combination.

Two failures occurred during the type-approval program. A post-operation leak check of the oxidizer valves revealed a failure of the braze joint between the nipple and valve body. A failure of this joint would allow leakage of chamber pressure gases during engine operation. The location of the braze joint failure is shown in Fig. 204. An analysis of the braze joint indicated that it was underdesigned; the program schedule did not allow for its complete redesign. The solution to the failure was to add another serration concentric with and outside of the braze joint. This fix would prevent external leakage

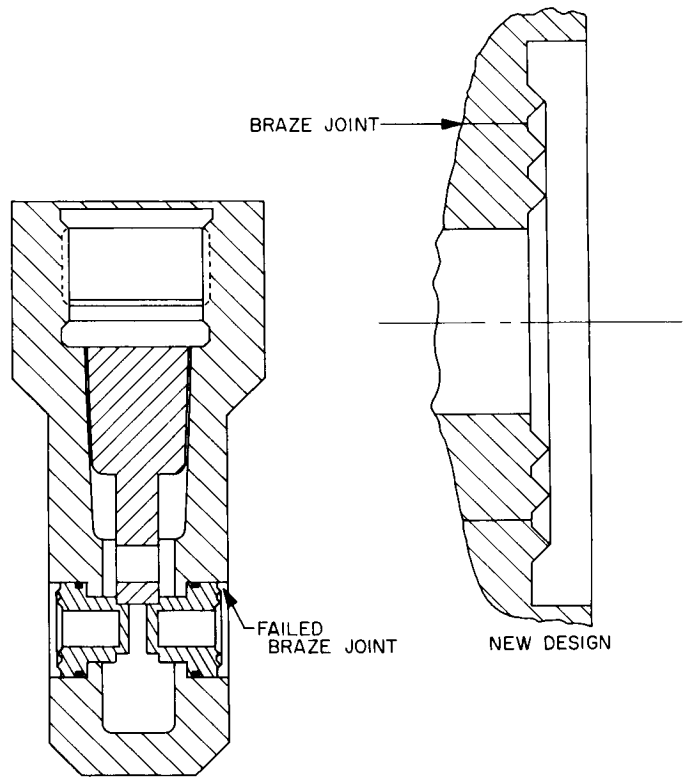


Fig. 204. Oxidizer explosive valve

when the braze joint failed; thereby ensuring that the braze joint failure would in no way compromise the reliability of the valve to function properly. The new seal design was successfully demonstrated as preventing external leakage and the valve was considered to be qualified for flight.

The other failure occurred during the squib portion of the type-approval tests. Two squibs fired when they were subjected to a second static-discharge test of 10 kv from a 300-pf capacitor. (Approximately 100 squibs were subjected to this test). Analysis of the failure revealed that the circuitry used in conducting the test had a resonance condition such that the squib was actually being subjected to twice the desired test voltage. Analysis of the squib insulation indicated that voltages of approximately 20,000 to 25,000 v could puncture the insulation and thus lead to a squib failure. The circuitry used for this test was modified to eliminate the resonance condition and no further problems were encountered.

f. Tankage. The propellant and nitrogen tanks on the propulsion system were made of titanium alloy. The propulsion system design dictated that the minimum burst pressure for each tank be 945 psia and 7265 psia.

Three propellant tanks and three nitrogen tanks were subjected to type-approval testing. Each tank was hydrostatically proof-pressurized to 1.5 times its maximum operating pressure through three cycles with pressure volume measurements being taken. Two of the three nitrogen tanks and two of the three propellant tanks were continuously pressurized on the third cycle to burst at a rate that would best show the pressure effect on the tank. The third propellant and nitrogen tank underwent type-approval testing with the complete TA-1 propulsion system. Upon completion of the system type-approval tests, the tanks were again subjected to three cycles of proof test with the pressure carried to the burst point on the third cycle. The results of the tests indicated that the minimum burst pressure was 972 psia on the fuel tank and 7370 psia on the nitrogen tank.

2. System Level Testing

Two propulsion systems were subjected to type-approval testing. The TA-1 system was assembled from components that had previously passed either type-approval or flight-acceptance tests. This system was then subjected to environmental tests that are detailed in the ensuing paragraphs. The TA-2 system was assembled from components that had previously passed flight-acceptance testing. Complete system firings over the design limits of initial tank pressurization levels were conducted with this system. Upon completion of the TA-2 firings, the system was used in a life test described in detail in the ensuing paragraphs.

a. TA-1 system. Upon completion of the TA-1 propulsion system assembly, the system was subjected to a series of modal tests. A typical test setup for these series of tests is shown in Fig. 205. This series of tests was concerned with the determination of the structural resonant frequencies and the corresponding modes of vibration. Very low vibration levels were fed into the structure at various frequencies until the resonant points were found. Readings taken from accelerometers mounted at various points on the structure were used to define the mode shapes. Very good correlation was noted between the actual test data and the analysis upon which the structural design was based. Upon completion of the modal tests, the TA-1 system was subjected to a series of preliminary vibration tests to determine amplification factors at selected points on the structure. Vibration levels from 0.5 to 2.5 g rms were fed into the system sweeping at frequencies of 50 to 400 cps. During these tests, it was found that the first resonant frequency of the structure

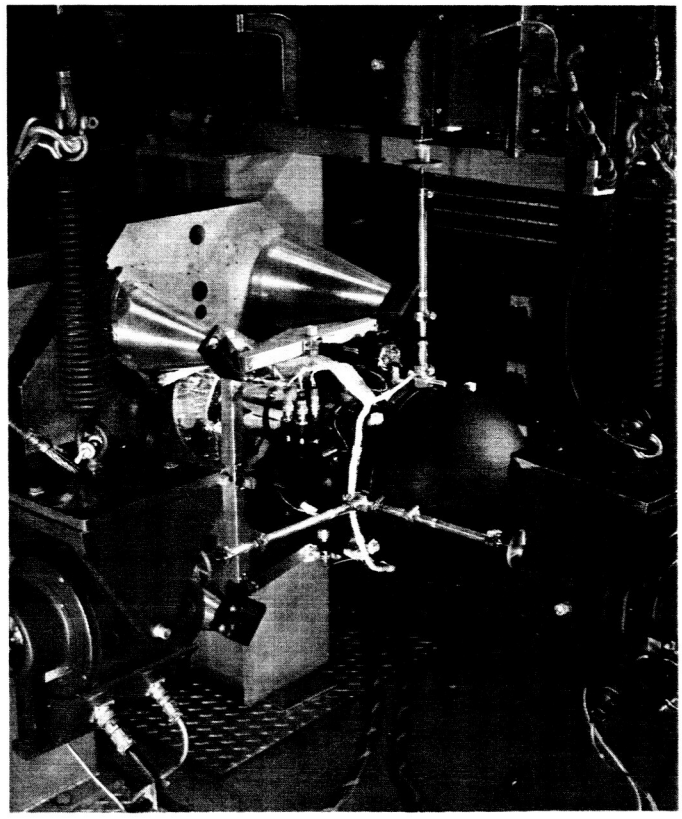


Fig. 205. Test setup for modal test of propulsion system

was approximately 140 cps. At this resonant frequency, an amplification factor of 5 was measured at the CG of the structure. The TA-1 system was subsequently installed in a shipping container and subjected to the transportation and handling, drop, and vibration tests. The system was then subjected to the space-flight shock test and the static acceleration test. After each of these tests, a thorough leak check was performed on the system and no leakage or other system failures were noted.

Upon completion of the static acceleration test, the start cartridge was filled with nitrogen tetroxide, the propellant tank was filled with water to simulate the propellant, and the system tankage was pressurized to the maximum expected flight values. The system was then subjected to the boost-phase vibration test. Before conducting the test, a 1-g input was fed into the propulsion system and a frequency sweep was made from 20 to 2000 cps. During this frequency sweep, very high acceleration levels were noted at the fuel tank attachment point when the structure's resonant point was reached. The amplification factor was a factor of 10 higher than had been noted on the premilinary vibration tests previously conducted. The difference between the tests was that the tankage had not been pressurized during the preliminary vibration tests. Apparently, introducing a gas at high pressure between the propellant tank wall and the propellant expulsion bladder (the bladder contains 21.5 lb of hydrazine) inhibits sloshing of the propellant. Since sloshing contributes to damping because energy is dissipated, inhibiting sloshing resulted in markedly higher amplification factors throughout the propulsion system. At that point, it was felt that the propulsion system could not pass the formal type-approval vibration test if the high amplification factor existed with higher vibration inputs.

To ascertain the quantitative effects of pressurizing the propellant tank and increasing acceleration inputs, a number of tests were made, sweeping from 20 to 150 cps, with tank pressures of 0, 150, 275, and 395 psig and input accelerations from 1 to 5 g rms with a propulsion system similar to TA-1. As expected, the amplification factor went up with pressure and down with increasing input acceleration. The amplification factor at the propellant tank support ring and the propulsion system support structure were typical and are tabulated in Table 51.

The results of the before-mentioned testing and results from the STM spacecraft testing, which indicated that the input levels to the propulsion system were lower than originally thought, suggested that the system could pass the formal type-approval vibration tests. The actual test levels and sequence in which the TA-1 system was tested were as follows:

1. A 2.5 g rms sinusoid from 20 to 100 cps and back to 20 cps
2. White Gaussian noise, PSD of 0.20 g^2/cps from 300 to 1000 cps, with a 6 db/octave roll-off from 1000 to 2000 cps, a 3 db/octave roll-off from 300 to 20 cps, and a 24 db/octave roll-off below 30 and above 2000 cps for 3 min
3. White Gaussian noise, PSD of 0.010 g^2/cps, band-limited between 100 and 2000 cps, and a 2.5 g rms sinusoid superimposed on the noise sweeping from 100 to 450 and back to 100 cps

Table 51. Summary of vibration testing on a typical *Mariner* Mars spacecraft propulsion system

Input acceleration g rms	Propellant tank pressure psig	Resonant frequency cps	Tank ring amplification factor	Substructure amplification factor
Vibration perpendicular to rocket engine thrust axis				
1	0	78	2	6
1	150	78	6	15
1	275	74	8	23
1	395	72	9	26
2	150	74	5	12
2	395	68	6	18
3	150	72	4	10
3	395	64	5	14
4	150	66	4	9
4	395	64	5	18
5	395	64	5	16
Vibration parallel to rocket engine thrust axis				
1	0	118	2	6
1	150	108	10	22
1	275	104	12	30
1	395	102	18	45
2	150	104	8	19
2	395	102	13	32
3	0	104	2	5
3	150	96	8	18
3	395	96	10	23
4	150	92	8	18
4	395	92	8	16
5	395	94	8	9

4. White Gaussian noise, PSD of 0.010 g^2/cps, band-limited between 100 and 2000 cps, and an 8 g rms sinusoid superimposed on the noise sweeping from 450 to 2000 and back to 450 cps

The total time for steps 1, 2 and 3 was 10 min. Sweep through the frequencies was controlled so that time rate of change of frequency increased directly with frequency.

No structural damage was noted during the vibration tests on the TA-1 system. After completion of the vibration tests, the system was subjected to temperature tests and then fired while at temperature. The first test consisted of a 2-hr soak at 40°F followed by an additional 2-hr soak at 167°F. The system was then fired while at 167°F for 60 sec. Nominal system performance was obtained during the test. The system was then soaked at 40°F for 2 hr, after which it was again successfully fired for 30 sec.

b. TA-2 system. The TA-2 propulsion system was built up from components that had previously passed flight-acceptance testing. The testing on this propulsion system consisted of conducting firings at various tank pressures in order to define system start transients and steady-state operation under a variety of starting conditions. For the first test, all tanks were pressurized to their nominal values (propellant tank 304 psia, nitrogen tank 3000 psia, start cartridge 400 psia). The first test was run for 80 sec, and the results were very close to the predicted performance of the system. For the second firing of the system, the initial pressures were those remaining from the previous test at shutdown. The second test was 15 sec long, and nominal performance was obtained. After the second test, the explosive valves were replaced and the system was refilled with propellants. For the third test, the tanks were pressurized to their maximum expected flight values (propellant tank 410 psia, nitrogen tank 3300 psia, start cartridge 445 psia). The third test was 95 sec long and no anomalies were noted. The system was then refueled with propellants and a fourth test at low tank-prepressurization levels (propellant tank 125 psia, nitrogen tank 2800 psia, start cartridge 345 psia) was attempted. The system was shut off after 14 sec of operation when it was observed that the pressure regulator did not regulate until the propellant tank pressure had reached 500 psig. Post-run examination of the regulator indicated that considerable amounts of 25 μ particles had been deposited on the regulator seat area, causing the regulator to malfunction. These particles emanated from the nitrogen explosive valves, located upstream of the pressure regulator, when they were fired. Normally a filter is contained upstream of the regulator and prevents particle contamination of the pressure regulator. However, at the time the pressure regulator was being qualified, it was extremely difficult to get clean filters. In order not to delay system firings, it was decided to build the pressure regulator for the TA-2 system without a filter, since it was felt that the danger from particle contamination of the dirty filters (they could not be cleaned successfully) was as great as contamination from the explosive valves. Another regulator with a good filter was assembled into the TA-2 system and the fourth test of the series was successfully completed. After this test, the third test was repeated with good results.

c. Life test. Upon completion of the TA-2 system tests, the system was torn down and reassembled with new components that also had previously passed flight-acceptance testing. Prior to assembling, the rocket engine and pneumatic regulator were installed in a standard calibration system and subjected to a thrust calibration test in the same manner as that of the flight systems. Two tests, which were 60 sec and 30 sec long, were performed in a high-altitude facility. System total impulse as well as other system operating parameters were measured during the test and supplied data that could be compared to system firings performed during the life test.

Upon completion of system assembly, the system was filled with propellants and pressurized to the nominal flight levels. It was then installed in a storage trailer, the ambient temperature of which was maintained at 125°F for the life test. During the first month of storage, a pressure rise of approximately 1.5 psia per day was noted in the fuel tank, indicating incompatibility between the bladder and hydrazine at that temperature. At the end of 1 month of storage, the system was removed from the trailer, installed in a high-altitude facility, and test-fired for 60 sec. Normal system operation was obtained. The total impulse measured was within 3% of the value obtained during the calibration test previously described. This value was well within the required impulse reproducibility depicted in Fig. 193.

Upon completion of the firing, the unit was reinstalled in the storage trailer at a temperature of approximately 120°F. The same rate of pressure rise in the fuel tank was again noted. At the end of approximately 3½ months' total storage time, the system temperature was lowered to 90°F to determine the change in rate of fuel-tank pressure rise. No pressure rise was noted

during the following 2 weeks, indicating that the pressure-rise rate was very temperature-dependent as was expected. Some other testing had indicated that the rate changed by a factor of 3 for each 10°F change in temperature. The 90°F temperature was still 50% above the expected flight temperature.

At the end of 4 months' storage time, the unit was removed from storage and fired a second time for 30 sec. The total impulse measured was within 0.2% of that obtained during the calibration test of 30 sec. The unit was again installed in the storage trailer at 120°F. For the next 2 months, the fuel tank pressure again continued to rise at 1.5 psia per day. At the end of 6 months' storage time, the system temperature was reduced to 100°F, and was held between 80 and 100°F for an additional 4 months with no fuel-tank pressure rise noted. Throughout the 10 months of storage, the nitrogen tank pressure remained very constant and no measurable leakage was noted.

Two and one-half months after the start of the life test, a drop of approximately 4 psia per day was noted in the start cartridge. This pressure loss indication suggested that either the metal bellows in the start cartridge or the pressure transducer had failed. Subsequent investigation revealed that the braze joint attaching the bourdon tube in the pressure transducer had failed and was allowing pressure to leak into the sealed cavity of the transducer. Thus, as the pressure in the transducer cavity increased, a decrease in pressure across the bourdon tube resulted in the indicated pressure loss. Placement of a visual pressure gauge on the start-cartridge nitrogen reservoir revealed that the pressure in the cartridge was remaining constant. The braze joint had previously been recognized as a problem and had been redesigned. However, when the life test began, the redesigned transducer was not available.

In summary, the life test proved that the system could be stored for prolonged periods of time and fired, and that the system total impulse was repeatable within the required limits. The test indicated that compatibility of the fuel tank bladder and hydrazine can become a problem if the system temperature in flight approaches 120°F. The design adequacy of the seals used in the system was well verified and no leakage, other than the pressure transducer failure, was noted.

XIV. SPACECRAFT SUBSYSTEMS: PYROTECHNICS

A. Firing Units

1. Design Considerations

In the design of the spacecraft pyrotechnic firing units, the following spacecraft functions had to be performed:

1. Pin retraction of eight solar panel latches
2. Pin retraction of one science platform latch
3. First start, midcourse motor
4. First stop, midcourse motor
5. Second start, midcourse motor
6. Second stop, midcourse motor
7. Solenoid release, science cover

In addition, the firing units had to contain switching circuitry which, upon command, would inhibit firing of the midcourse motor, release the inhibit, and transfer the command to fire the motor to either of the two groups of on–off squibs.

The squib initiation circuitry of the *Mariner* Mars 1964 spacecraft pyrotechnic subsystem differs considerably from previous designs, and was first proposed for *Mariner B*. The principle of the circuit consists in storing electrical energy on capacitors and switching this energy upon command to the appropriate squibs by means of semiconductors. The capacitors are trickle-charged from the 2.4-kc bus and are common to as many event channels as available. This requires four capacitor banks to permit redundant propulsion valve actuations with a minimal on–off time. Each semiconductor switch is unique to a single event channel.

The circuit change was considered justified as follows. First, the combination of capacitor storage and semiconductor switch reduced the component count by a factor of ⅔ compared to the battery and relay combination. This was mainly because the components formerly needed to open the circuit after firing a squib were eliminated. The circuit is, in effect, self-quenching. Second, the semiconductor switches were more adequately rated than the miniature relays they replaced. Ground handling problems have caused AFETR to require 1-w no-fire squibs on future spacecraft, which necessitates the switching of considerable power if all related squibs are fired simultaneously. Simultaneous firing further reduces the component count of the initiation circuitry. Third, it was believed that a capacitor would be more reliable than the battery that it replaced for a mission of long duration. It is noted that the main spacecraft battery was given primary consideration for non-Sun orientation or for emergency backup at Mars encounter.

The firing unit was designed and sized to reliably fire 1-amp/1-w midcourse propulsion squibs, which require 0.15 j per squib. The squib vendor was changed, and the squib eventually selected required only 0.03 j (almost identical to the pinpuller squib requirements). In the worst case involving four pinpuller squibs and the smaller capacitor tank, the design provided four times the required energy delivered to each squib.

The pyrotechnic subsystem had the same degree of redundancy as previous subsystems. The system used dual power supplies, dual firing switches, and dual squibs. Where dual squibs were not feasible, devices with dual bridgewires were employed. Command inputs were nonredundant except for the first command (erect solar panels), which used a delayed separation switch as a backup.

The schematic diagram (Fig. 206) shows the elements of a typical event channel and power supply. The crucial circuit elements of the subsystem were considered to be the energy storage capacitors in the power supplies and the power switches. Each capacitor bank consists of two or three tantalum capacitors of approximately 1800 μf each.

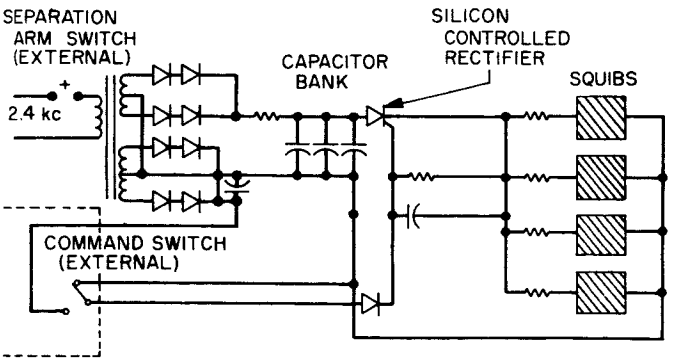


Fig. 206. Typical event-channel and power-supply schematic diagram

2. Development and Testing

Of the three types of capacitors subjected to environmental testing and accelerated life testing, none proved to be entirely satisfactory. As a result, a "crash" product improvement program was instituted by one of the capacitor manufacturers to successfully meet JPL requirements.

Silicon-controlled rectifiers were selected as the most reliable, most compact, and least magnetic device capable of switching the required current. They were chosen for their high current-switching capability and the simplicity with which they can be switched. The type finally chosen was manufactured and tested to the *Minuteman* specifications.

The circuit was breadboarded and live squibs were fired predictably. The breadboard fired more than 2,600,000 simulated squibs on a life-test basis with no component failures, whereupon the test was concluded.

Twenty-three pinpuller squibs were fired to demonstrate the ability of the breadboard circuit to fire such squibs at reduced energy with the circuitry stabilized at −10°C. Four squibs were fired at a time from a 3700 μf capacitor bank. This simulated the portion of the first pyrotechnic event in which four pinpuller squibs would be fired from the smaller capacitor bank. An estimated harness resistance of 0.3 Ω was used. Stored energy was reduced incrementally by reducing the capacitor voltage.

The results of these tests are tabulated in Table 52. In test No. 7, three squib lines were intentionally short-circuited at the squib end to see what affect it would have on the remaining squib: it fired satisfactorily in 1.0 msec. The results of this series of tests demonstrated that the circuit functioned satisfactorily at −10°C and at greatly reduced energy. At 19 v, the capacitor bank had 48% of its nominal energy. Fabrication of a prototype squib-firing unit followed.

Twenty-five 1-w squibs from various vendors were fired with the prototype. The postinjection propulsion valve squib designated was not available at the time of the test, so a test of samples from other vendor types of 1-w squibs was run to get some feel for the operation of squibs of that class with a stored-energy system.

Testing was done with the prototype of the squib initiation circuit under conditions simulating flight conditions as nearly as possible. Three squibs were fired at the appropriate time in the valve channel. Connections were through a shielded harness with a loop resistance of 0.3 Ω. One squib of each group of three was fired into a valve-sized test chamber, and the other two were fired into the open. Oscillograms were made of the current drawn by each squib, from which functioning time was read. The functioning time of the squib is defined (for pyrotechnic control-unit design purposes) as the time from current turn-on to bridgewire burnout. Due to the extremely small sample size of the 1-w squibs (only five squibs of any one type) and the desirability of firing three at a time for realism, all squibs were fired at the nominal capacitor bank voltage of 27.5 v.

The results of these tests are shown in Table 53. Subsequent to the test, it was learned that the valve squib would have initiation characteristics identical to those used in test No. 3. The conclusions from this test were:

1. All squibs fired.
2. The spread in sensitivities produced a spread in functioning times of 4:1.
3. One type of squib consistently had a disconcerting "hang-fire" characteristic.

Table 52. Firing ½-amp squibs with midcourse breadboard at reduced energy and −10°C

Test No.	Capacitor voltage	Number of squibs	Average function time, msec
1	28	4	0.4
2	25	4	0.45
3	22	4	0.55
4	19	4	0.8
5	19	4	0.75
6	28	2	0.3
7	19	1	1.0

Table 53. Firing 1-w squibs with midcourse prototype

Test No.	Functioning time, msec				
	Squib 1	Squib 2	Squib 3	Squib 4	Squib 5
1	0.5	0.4	0.5		
2	0.75	0.7	0.8		
3	0.3	0.3	0.3		
4	1.0	1.2	1.0	1.0	1.0
5	0.8	0.5	0.5	0.6	0.5
6	0.4	0.4	0.4		
7	0.4	0.3	0.35		

4. Examination of the oscillograms indicated that a considerable portion of the capacitor bank's charge remained at the time of bridgewire burnout. For example, in firing the least-sensitive squib of the lot of twenty-five, the voltage across the squib decreased from 10 v at turn-on to 7.5 v at burnout.

Six pinpuller squibs were fired with the prototype at reduced energy. Two squibs were fired at a time, each in a separate pinpuller. The remaining firing unit output lines were loaded with 1.5 Ω resistors, and the typical harness resistance of 0.3 Ω was used.

The pinpuller squibs are much more sensitive than the propulsion squibs (⅜-w no-fire rating), yet they were to be fired from the same size capacitor bank as the propulsion-valve squibs. Thus, the pinpuller squibs did not impose a limiting requirement on the capacitor bank. Therefore, it was considered adequate to test these squibs at a few points of very low energy. The points chosen were 22, 20, and 18 v. The 18-v point represents 43% of the nominal stored charge.

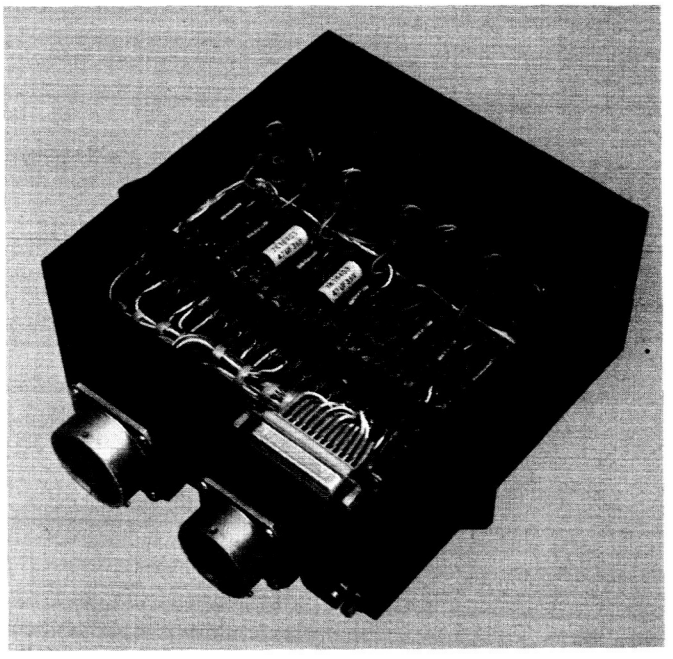
The results of this test are given in Table 54. It is noted that the function time varied smoothly as the current was decreased, and that the dispersion in function times was still quite small even at the low current. The circuit was considered entirely adequate to fire the squib.

Table 54. Firing ½-amp squibs with prototype at reduced energy

Test No.	Capacitor voltage	Functioning time, msec	
		Squib 1	Squib 2
1	22	0.5	0.55
2	20	0.6	0.65
3	18	0.75	0.8

Fourteen pyrotechnic firing units were fabricated to fulfill the needs of the *Mariner* Mars 1964 program. Two views of the units are shown in Fig. 207 (a) and (b).

Except for the first two units fabricated, all components used were subjected to rigid screening tests. Since delivery of screened components was late, the two units were fabricated with unscreened parts to meet project scheduling of the PTM spacecraft. The second pair of units fabricated was subjected to type-approval tests according to JPL specification. All others, including the first two units, were subjected to flight-acceptance tests according to JPL specification.



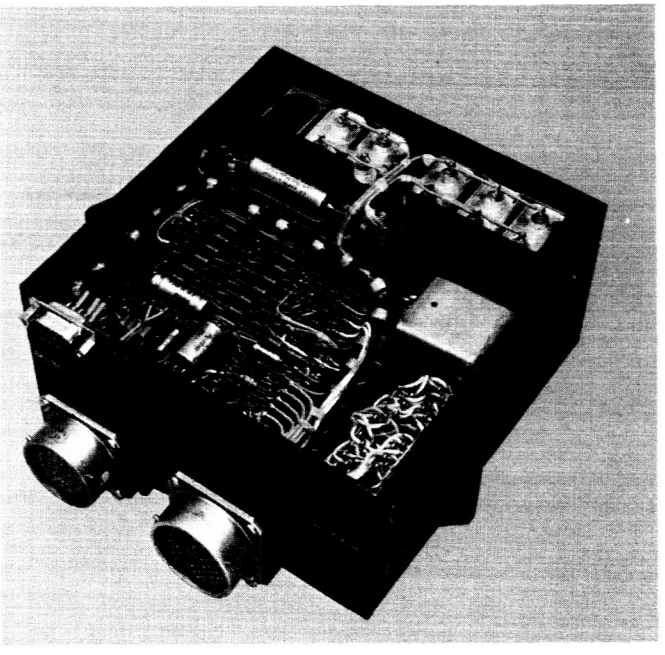


Fig. 207. Pyrotechnic firing unit

In all tests on all units, two catastrophic failures occurred. In both failures the subminiature PIPS inhibit relays were involved. During postfabrication bench electrical checks, an inhibit relay in one unit failed to transfer to either position. Since the relays were not yet potted, the relay was replaced. The other failure occurred during flight-acceptance vibration tests on two units when one of the four inhibit relays failed to actuate

when commanded. The failure was never repeatable in any subsequent tests. Nevertheless, because of the single unexplained failure, the units were considered "non flight" and were assigned for use in the PTM spacecraft.

3. Pyrotechnic Monitor Console

During systems tests, operation of the pyrotechnic subsystems was monitored by means of special monitoring consoles (Fig. 208). When connected with spacecraft direct-access cables, the console provided the following functions:

1. Series test circuitry enabling determination of squib or squib simulator continuity before and after a firing sequence without an inspection of the squibs.

2. Measurement of capacitor bank and command voltages within the pyrotechnic control subassemblies.

3. High-speed, direct-writing oscillograph recording of each squib-firing current pulse as it occurs.

4. Lights indicating the firing of each group of squibs. (This circuitry monitors the squib-firing circuits continuously and provides a latched indication in the event of a premature, or spontaneous, squib firing.)

5. Indicating lamps permitting determination of the position of midcourse inhibit and transfer relays.

6. Elapsed time indicators recording total time power applied to the pyrotechnic control units, secondarily providing a visual indication of arming (power on) of each pyrotechnic control unit.

Through the spacecraft umbilical connector and umbilical junction box, the console provides:

1. Fail-safe indication of the pyrotechnic subsystem disarmed, or "safe," condition

2. Indication of the actuation of any solar panel or scan platform pinpuller

The panel is identical to that used in the blockhouse to monitor the subsystem prior to launch. The console also contains a 2.4-kc power supply that permits operational checkout of the subsystem in the absence of all other subsystems.

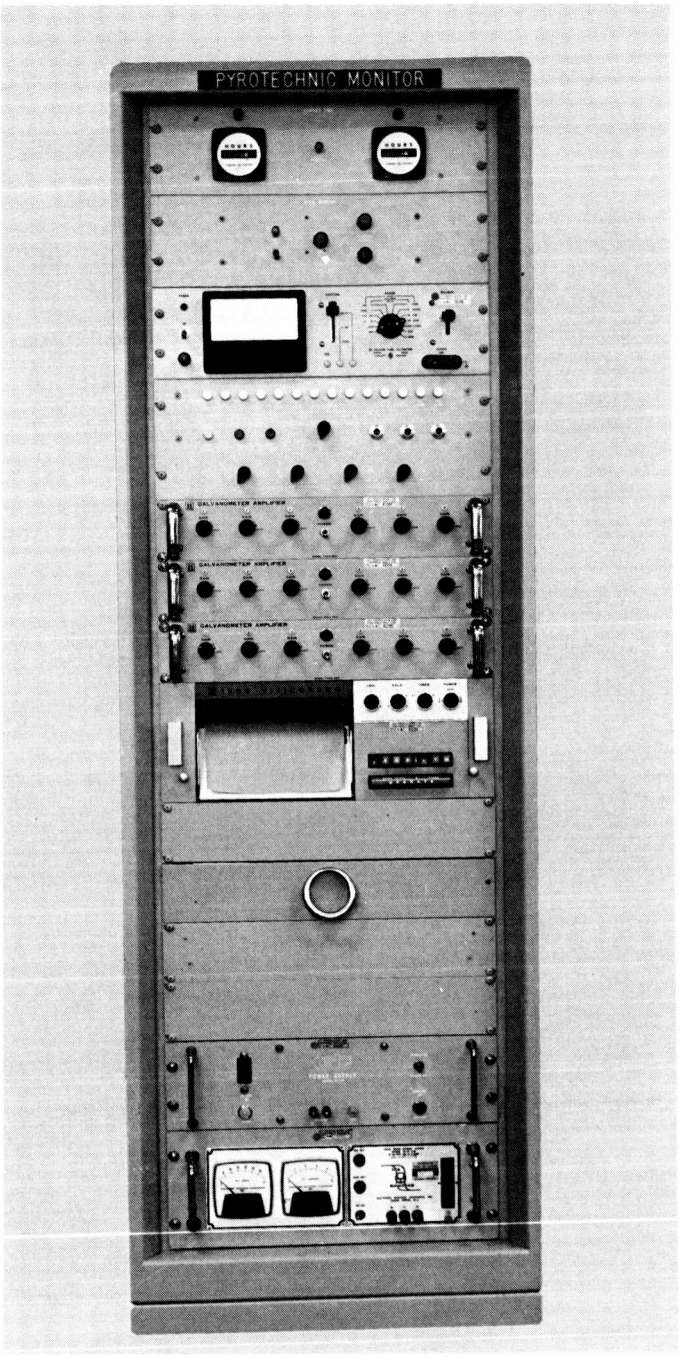


Fig. 208. Pyrotechnic monitor console

4. Field Test Kit

The field test kit (Fig. 209) is a self-powered portable instrument used to determine the condition of the spacecraft pyrotechnic subsystem prior to and after the installation of squibs or squib simulators, and to verify that the subsystem is flight-ready after final spacecraft flight

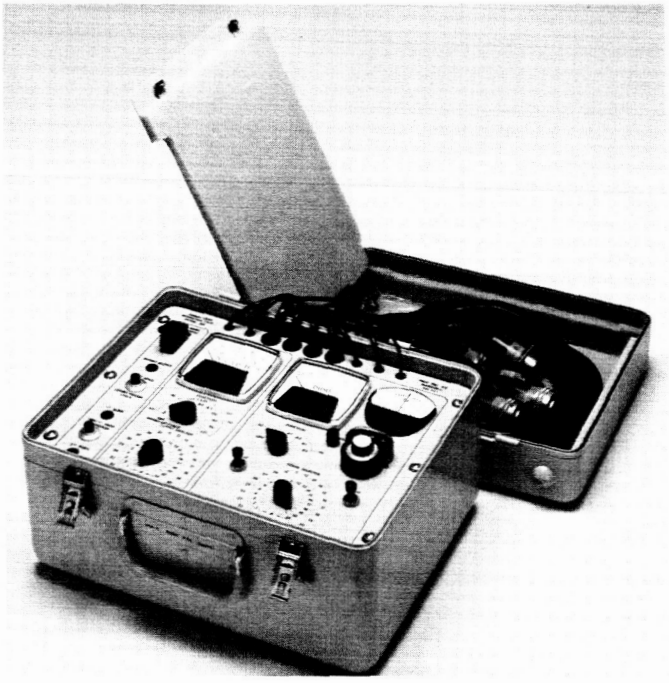


Fig. 209. Pyrotechnic subsystem field test kit

preparation in the AFETR explosive safe facility. The instrument performs the following functions:

1. Determines the voltage charge on capacitor banks within the pyro firing units
2. Discharges capacitor banks if a charge exists
3. Determines that all squib firing lines are continuous and are not shorted or grounded
4. Accurately measures the resistance of each squib and squib firing line
5. Indicates the position of propulsion transfer relays within the pyrotechnic firing units
6. Indicates the position of propulsion inhibit relays within the pyrotechnic firing units
7. Indicates the presence of any potential existing on the output of the pyrotechnic firing units
8. Uses self-test circuitry for battery condition, meter, and indicator integrity

B. Pyrotechnic Arming Switch

1. Description

The pyrotechnic system was unarmed prior to spacecraft separation so that an inadvertent or spurious command prior to separation could not cause a premature squib firing. The system was armed at *Agena D*/spacecraft separation by the pyrotechnic arming switch. Arming was accomplished by supplying 2.4-kc power to the system from the spacecraft main inverter. Auxiliary functions of the PAS were:

1. Arming event indication to the data encoder
2. An *Agena D* isolation amplifier *off* function
3. Prelaunch monitoring of the switch's disarmed state
4. Turn-on of attitude control subsystem

The pyrotechnic arming function was backed up by the separation initiated timer, and the attitude control turn-on was backed up by the CC&S in the event of a PAS failure.

The PAS (Fig. 210) consisted of a bank of four hermetically sealed microswitches actuated by two beryllium-copper leaf springs. The leaf springs rested on a pad on the *Agena D* adapter, holding the microswitches in the open position. At spacecraft separation, the leaf springs were free to move, allowing the switches to close. The switches and leaf springs were mounted in a machined aluminum housing that was bolted to the spacecraft lower ring. The nominal wall thickness for this machined housing was 0.020 in., which contributed to the low PAS

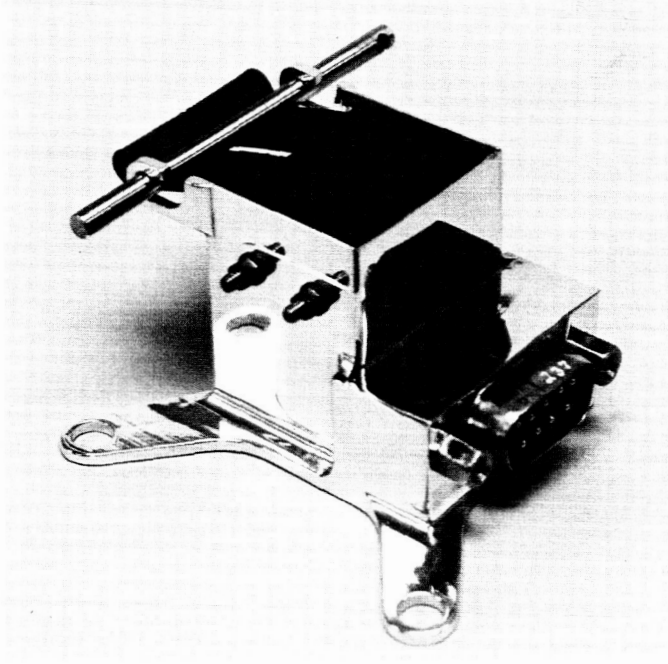


Fig. 210. Pyrotechnic arming switch

weight of 43 g. A nine-pin connector was also incorporated into the housing to provide a convenient breakpoint in the cabling. In addition, an arming pin was included into the design to hold the switches in the disarmed position prior to mating the spacecraft to the adapter. The pin was removed after the spacecraft and *Agena D* adapter were mated.

2. Tests

A typical PAS was subjected to type-approval tests as defined by JPL specification. During the shock and vibration portions of the test, the switches were externally wired in series and monitored with a digital counter to detect contact chatter. A switch staying open for longer than 10 msec would have been cause for rejection. In the thermal–vacuum test, the PAS was actuated by a solenoid every 5 min. The switches were "observed" with a brush recorder to ensure that each switch had closed upon actuation. Approximately 3000 actuations were performed during the 12-day thermal–vacuum test. No failures were noted during any phase of the TA tests.

All flight units were given the flight-acceptance tests per JPL specification. As with the TA tests, the switches were monitored for chatter during the vibration tests and were actuated every 5 min during the 42-hr thermal–vacuum test series of approximately 600 actuations. Although no failures were noted during FA tests, one switch indicated a switch chatter duration of approximately 3 msec in the vibration testing.

C. Separation-initiated Timer

1. Functional Description

The purpose of the separation-initiated timer was to provide two time-delayed switching functions sequenced from spacecraft separation. The two events and their defined tolerances were: (1) arming the pyrotechnic subsystem at 25 sec, ±10 sec, and (2) providing solar panel deployment command at pyrotechnic arming plus 80 sec, ±15 sec. Pyrotechnic arming consisted of a switch closure to the 2.4-kc power supply with a maximum drain of 200 ma. Solar panel deploy command consisted of a 26-vdc pulse to the pyrotechnic SCR circuit with a duration of 20 msec minimum to 1 sec maximum. Deploy command power was supplied externally, and pulse forming was accomplished by capacitors in series.

In addition to the basic timing sequence, two verification switches were added to provide (1) ground checkout of safe condition, and (2) inflight event indication of solar panel deploy signal. Both of these functions consisted of a simple switch closure with external power supplied.

To provide the necessary redundancy in the flight sequence, both pyrotechnic functions were backed up by separate subsystems. Pyrotechnic arming was accomplished at separation by the PAS located at the spacecraft/adapter interface. Solar panel deployment was backed up by a CC&S relay sequenced independently from the SIT.

2. Design Implementation

Initial mechanization mode studies indicated that four main categories of developed devices were available, which would provide the time-delay switching required. The linear dashpotentiometer, in conjunction with hermetically sealed microswitches, was chosen as being the most reliable, having a minimum of parts and providing adequate timing accuracy. Other devices considered were: (1) chemical timers, which presented problems in testing because they are one-shot devices, (2) mechanical timers consisting of a drive spring and escapement mechanism, which were discarded because of their complexity, and (3) electrical timers, which require power-supply integration.

Consideration of the preceding devices led to selection of the spring-driven hydraulic piston as the primary scheme. Previous in-house design, development, and continued reliability work indicated that such a device presented the least start-up problems. Basically, the device shown in Fig. 211 is a scaled-down *Ranger* timer with series redundancy in all sealing elements. The one major departure from the *Ranger* design involves the use of hermetically sealed microswitches in place of rotary wafer switches. Test data from several hundred hermetically sealed microswitches indicated that they have a higher confidence level than the rotary elements of the *Ranger* model, and can be tested and qualified on a large-lot basis. Figure 212 is a view of the final switch-deck configuration.

A review of the possible failure modes of the hydraulic-piston type of timer was an indication of its inherent reliability. Due to its simplicity, the normal modes of failure are loss of fluid or blocking of the capillary tube. The first mode of failure would result in a rapid timing sequence, which would have no effect on the pyrotechnic arm but would cause the solar panel deployment system to not respond because of insufficient charge-up time in the pyrotechnic control subsystem. The inclusion

of series capacitors blocked this circuit, however, and allowed the CC&S backup to perform its redundant function. The second failure mode of slow response would cause timing to be out of tolerance but acceptable. In no case did a failure compromise the operation of the redundant sequence.

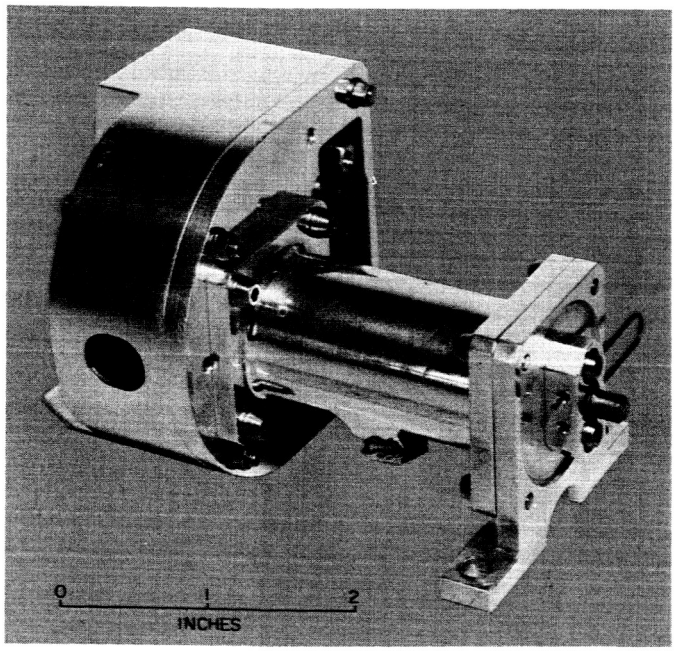


Fig. 211. Separation-initiated timer assembly

To protect the assembly against these failure modes, double O-rings were installed on all static and dynamic seals, and filtered oil was used in conjunction with a large diameter capillary tube.

Silicon oil of approximately 7000-cs viscosity, in conjunction with a capillary metering tube, gave the required 2-min full stroke at room temperature. Where necessary, oil blending was used to calibrate the assembly for proper timing. Oil volume compensation was provided by closed-cell silicone rubber inserts on the low-pressure side of the piston.

3. Installation and Arming

During tests and normal bench handling, the SIT could be actuated by the removal of an arming pin on the timer shaft. Due to the construction of the switch deck, rearming necessitated resetting the switch followers before the timer shaft could be inserted. To eliminate the possibility of damage during this procedure, a special recocking tool was fabricated that would position the switches automatically when it was mated with the timer body.

When installed on the spacecraft, the SIT was located on the lower ring with the plunger oriented parallel to the separation plane and extending radially outward. Proper mating and adjustment of the timer in the limited access of the spacecraft adapter was accomplished through the use of an adjustable pad on the adapter

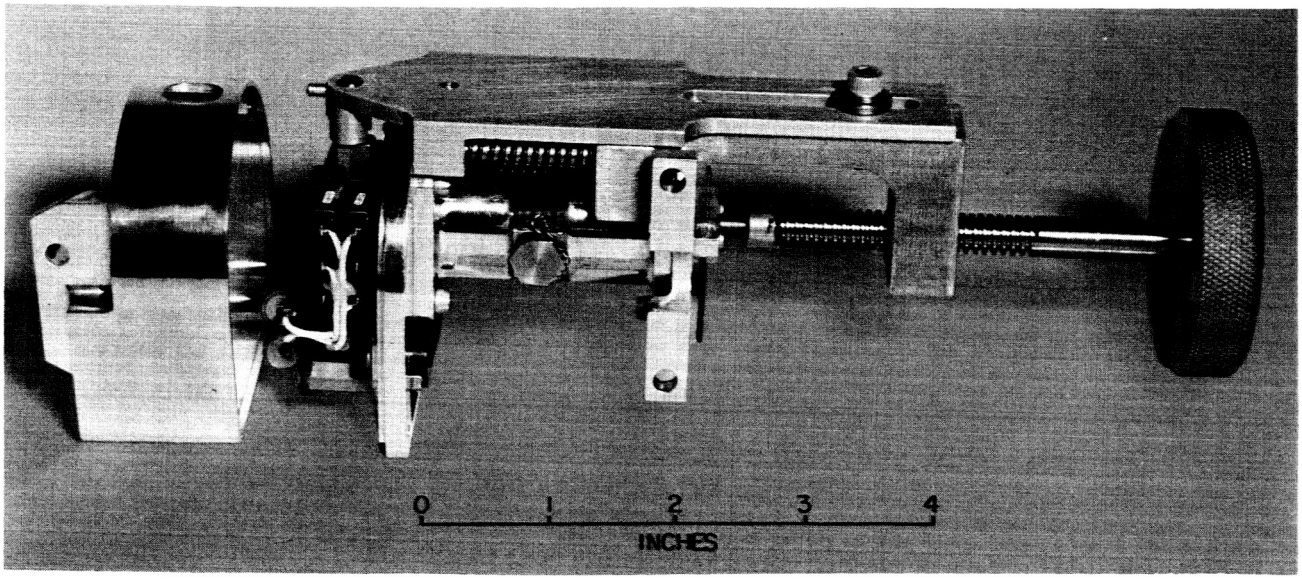


Fig. 212. SIT with recocking tool engaged

side of the interface. After spacecraft matchmate, the pad could be moved forward until pressure was removed from the timer arming pin. This allowed automatic positioning of the timer shaft stroke. When the spacecraft was demated, the pin could be reinserted and the pad moved back. To recock the timer if the shaft were allowed to extend required that the spacecraft be demated to allow access for the recocking tool. Since it was not a requirement to cycle the timer after matchmate, this was not considered a serious drawback.

4. Test Experience

The SIT was subjected, with satisfactory results, to qualification tests and to the flight operations imposed during system tests. The following minor difficulties arose during the developmental program, but none was sufficiently serious to require a design change.

Although silicon oil, which has a low-viscosity index, was used for the timer fluid, initial temperature cycling tests made it apparent that the timing tolerance imposed could not be achieved. Reevaluating the reasons for the specified tolerances indicated that the only critical timing necessary was a minimum of 60 sec between arming and deploy. Therefore, the nominal actuation times were revised to compensate for the temperature dependency and to allow for the worst-case separation in the two functions. No design change was required.

In conjunction with the temperature–timing dependency, tests indicated that the pressure compensation value of the closed-cell silicone insert was marginal. Reasonable compensation was available over most of the temperature range, including the anticipated flight temperatures, but pressure increased sharply near the upper TA limit of 140°F. Operation was not affected, no leakage occurred on any assembly, and all components were well below yield; therefore, it was concluded that no design change was warranted.

During vibration qualification of a flight spare timer, it was noted that switch chatter was present in one switch; inspection of the assembly showed that the switch was adjusted improperly. The switch deck was adjusted, requalified, but held as a spare only. Although switch chatter is considered a cause for rejection, it should be mentioned that in the particular application, such an occurrence would not cause premature actuation due to the time constants involved.

Except for the minor problems mentioned, the remaining malfunctions encountered were a consequence of procedural error during system tests. Improper adjustment of matchmate and improper use of the recocking tool were the major contributors to assembly malfunction resulting occasionally in equipment damage. Double checks on written procedures and operator training sessions were used to eliminate the problem.

XV. SPACECRAFT SUBSYSTEMS: VIDEO STORAGE

A. Subsystem Requirements

By the fall of 1962, the *Mariner* Mars 1964 mission requirements had been sufficiently defined to indicate a definite need for spacecraft onboard data storage of approximately 5×10^6 bits capacity. By that time, the development of a recorder with a capacity of 10^6 bits had been completed; this recorder used one data track on a 300-ft endless loop and was capable of synchronous playback at 8⅓ bps. At the same time, a 10^7 bit recorder was under development, which used three data tracks and one synchronization track on a 700-ft endless loop and was capable of synchronous playback at low tape speeds. A 10^8 bit reel-to-reel recorder was also being developed.

Because of the stringent reliability requirements imposed on the spacecraft design by the 9-month mission, and the short time available for subsystem design and fabrication, it was decided to use a recorder storage system similar to those already developed, as seen in Fig. 213 (a) and (b). After considering the data storage requirements imposed by a *Mariner*-type mission and the relative progress of the 10^6, 10^7, and 10^8 bit development programs, the functional specifications outlined in the following paragraphs were defined for *Mariner* Mars 1964.

The video storage subsystem (or recorder system) records digitized television data during a planetary encounter or flyby, and reproduces these data at a much lower rate following encounter.

The recorder system accepts fully serialized, return-to-zero data from the data automation subsystem at a fixed rate of 10,700 bps, and can store a minimum of 5.24×10^6 bits of video data, which is equivalent to 20 television pictures. It reproduces, for coding by the data encoder, synchronous, fully serialized, nonreturn-to-zero, binary data at a fixed output rate of 8⅓ bps.

Provisions were included for operating the recorder system, in a limited sense, during launch. This mode of

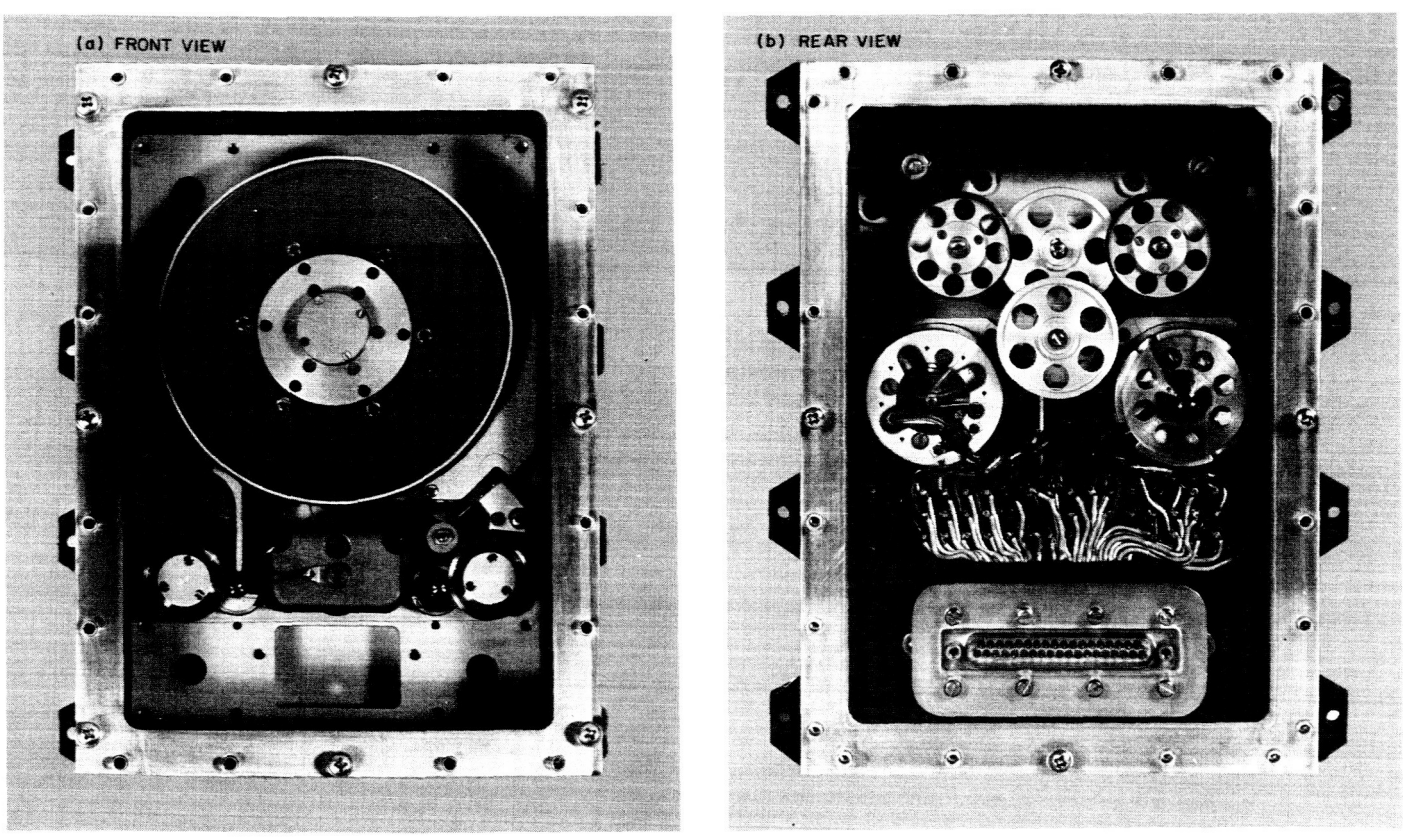


Fig. 213. Tape transport subassembly with drive motors, heads, and playback preamplifiers

operation terminated shortly after separation of the spacecraft from the *Agena*.

The prototype design and fabrication phase was completed in February 1964. At that time, the functional and detailed design described in this section had been completed. Since that time, the system design has remained essentially unchanged.

B. Functional Description

1. Technical Characteristics

The technical characteristics of the video storage subsystem are listed in Table 55.

2. Launch Mode

During the launch phase of the flight, the tape transport (Fig. 213) was operated at record speed to minimize the possibility of tape spillage, although no actual recording took place. The record motor was started shortly before launch, and continued running until after the spacecraft separated from the *Agena D*. After separation, the tape was positioned automatically to the proper point in preparation for planetary encounter.

Table 55. Video storage subsystem technical characteristics

Item	Description
Performance characteristics	Bit capacity of 5.24×10^6 on two tracks of 0.25-in. tape, 330 ft long. Additional capacity is available in the form of wasted tape to allow acceleration and deceleration before and after each recording interval.
Record bit rate	Return-to-zero data 10,700 bps.
Reproduce bit rate	Average 8⅓ bps NRZ data. Synchronization is achieved through the use of a phase-locked-loop tape speed control slaved to a bit-synchronous multiple.
Bit error rate	Less than 1 in 10^4 bits, not counting errors accumulated while establishing lock or due to track change at end of tape.
Record mode tape speed	Average 12.84 in./sec.
Reproduce mode tape speed	Average 0.01 in./sec when the system is phase-locked. Speed will normally drift down to approximately 0.009 in./sec when operating over erased tape as a result of losing lock.
Launch mode tape speed	Average 12.84 in./sec.
Operating temperature range	The recorder system was designed to operate over a temperature range from −10 to +70°C in actual flight. The temperature is expected to remain between 0 and 55°C.

Launch mode control signals applied to the recorder system through the spacecraft umbilical can set or reset the magnetic latching relay, as shown in the launch mode functional diagram (Fig. 214), whether gyro power is applied to the recorder system or not. Indication of relay position is obtained by monitoring the resistance appearing across the two umbilical lines.

If gyro power is applied to the recorder system and the latching relay is set by means of a launch mode *on* signal, the magnetic bias relay will energize and start the record motor. The tape is set in motion whenever the record or playback motors are running; the record motor always overrides the playback motor. In launch mode operation, the record motor drives the tape at the same speed as in record mode (12.84 in./sec), although acceleration to operating speed takes a longer time in launch mode. A pulse is generated for every complete pass of the tape by the auxiliary end-of-tape circuit as an end-of-tape foil (spliced into the endless loop) passes over the end-of-tape sensor contacts.

When the spacecraft separated from the *Agena D*, the end-of-tape pulse was combined in an AND gate with the *Agena* separation signal. The AND result was applied through an OR gate and driver amplifier to the latching relay. This pulse reset the latching relay, which, in turn, deenergized the bias relay, thereby removing power from the record motor and locking out the launch mode circuitry. After the record motor and tape coasted to a stop, the end-of-tape foil was positioned at a point approximately 2.5 ft beyond the record/reproduce head. This was the normal tape position from which to start the encounter record sequence.

In the event that separation from the *Agena* had not been clean and the separation signal had not occurred because of shorted connector pins, the record motor would have continued running until the gyro power had shut down. Subsequent application of gyro power to the recorder system would have automatically reset the latching relay by means of the delayed monopulse generator, thus locking out any further action of the launch mode circuits. Should this relay have been reset, the tape might not be positioned properly for planetary encounter, and recording and picture capacity might be reduced to as low as ten pictures.

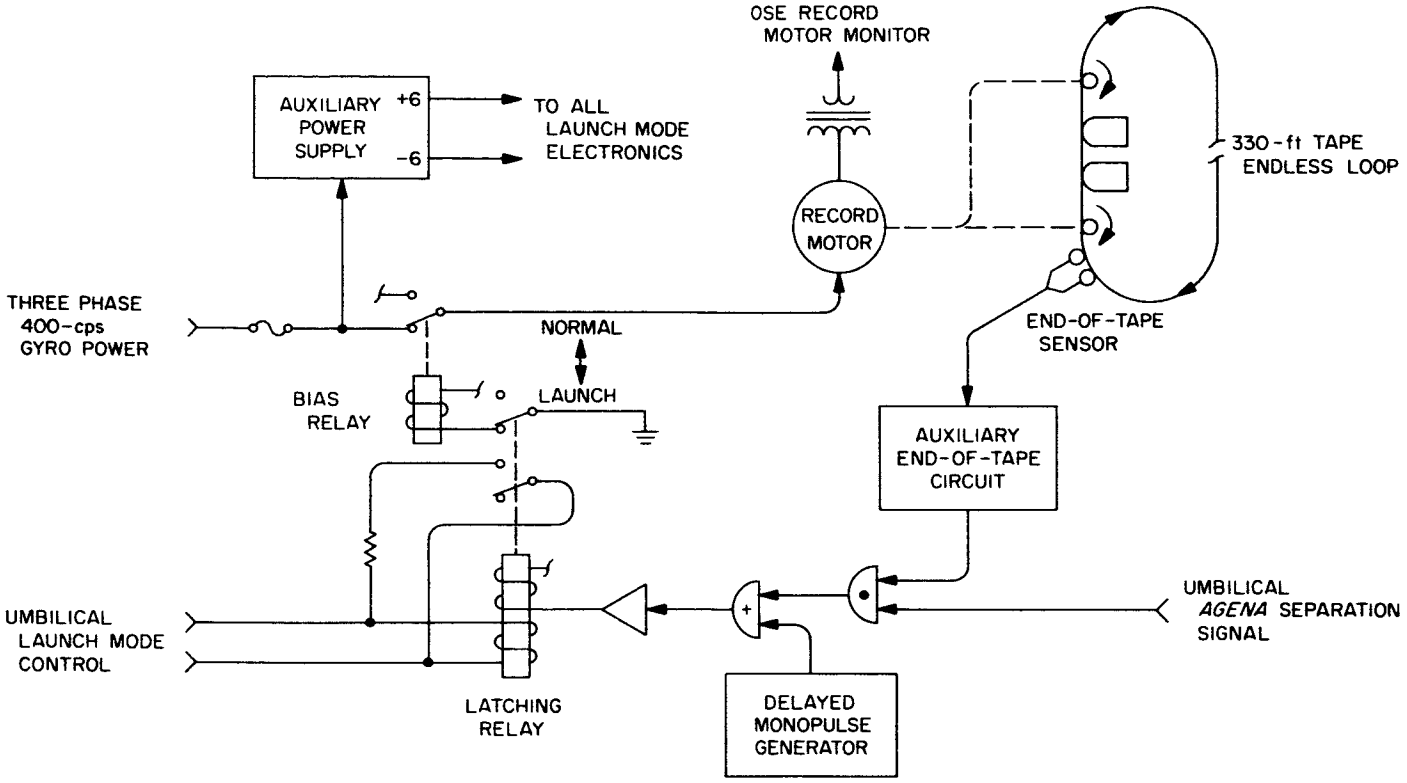


Fig. 214. Launch mode functional block diagram

Telemetric indication of record motor shutdown after spacecraft separation could be obtained by monitoring gyro supply power consumption. To facilitate testing, the signal developed across the record motor was brought out to the OSE interface.

3. Record Mode

Application of 2.4-kc power and single-phase 400-cps power prior to encounter energizes all sections of the recorder system (Fig. 215 through 218), except those associated with the launch mode. Assuming that the tape is positioned properly, the recorder system is ready to record at least 20 picture sequences while making two complete passes of the tape, changing tracks after the first pass and returning to the initial track after the second pass. Response to record commands is inhibited after the end-of-tape foil passes the sensor contacts the second time.

The recorder system uses the frequency-doubled method of encoding the tape. This code was arranged so that there would be at least one flux reversal in each bit cell. In this manner, the clock was contained in the data sequences. As seen in the record signal waveforms

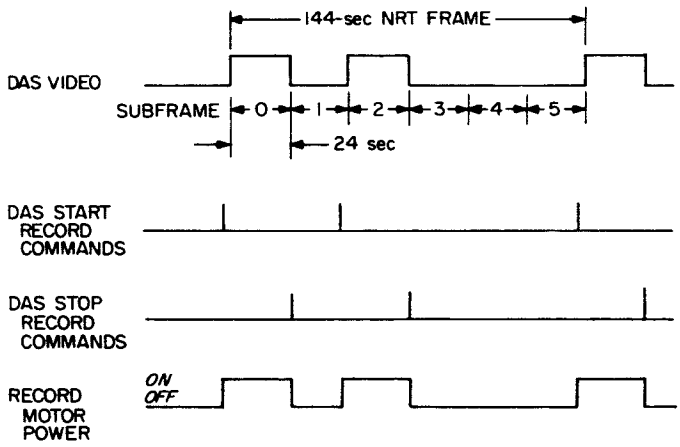


Fig. 215. Record signal waveforms of video storage subsystem

(Fig. 215), a flux reversal always occurs at the boundaries of a bit cell. If the data indicate a logical *one*, a flux reversal occurs also in the center of the bit cell. No reversal in the center of the cell indicates a logical *zero*.

The absence of a playback command signal from the data encoder conditions the system for recording by

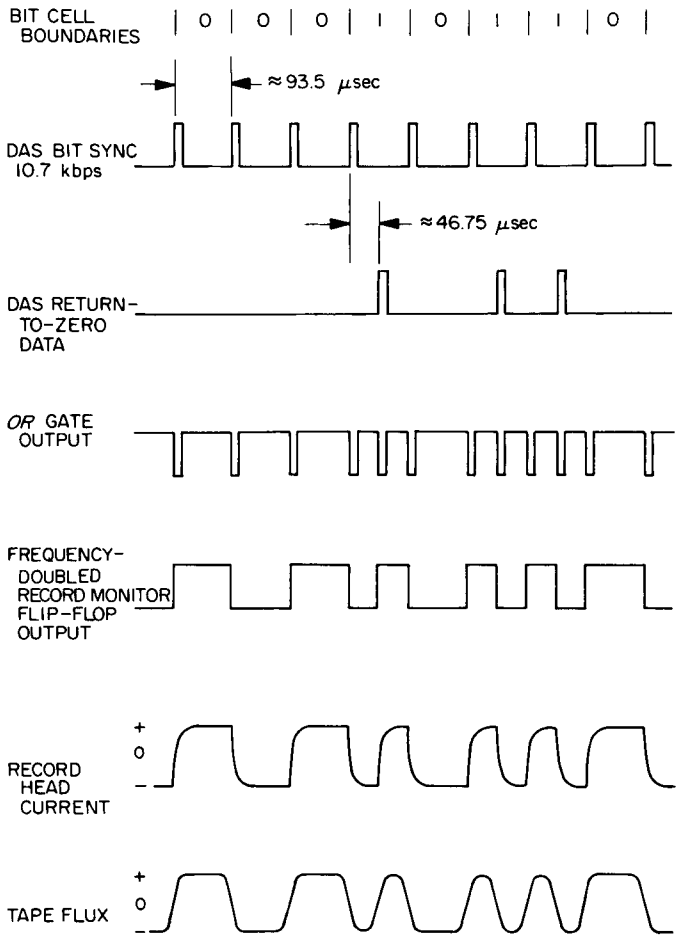


Fig. 216. Encounter sequence timing

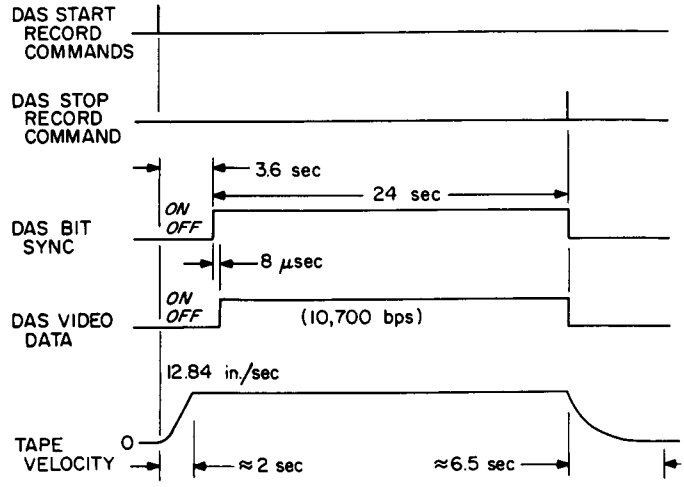


Fig. 217. Picture sequence timing

applying power to the record head drivers, as shown in the record mode functional diagram (Fig. 218). Thus, whenever the recorder system is not operating in the reproduce mode, it is in the record mode and will record or erase the tape. Spot erasure of the tape will occur while the tape is stationary if the playback command signal is removed.

Application of the DAS return-to-zero data pulses and synchronization pulses in the proper phase relationship to an OR gate and flip-flop generates the frequency-doubled code. The signal is fed to the NRZ head drivers, which, together with the record heads, magnetize the tape appropriately. It should be noted that, if data and synchronization pulses are not present, the tape will be biased continuously in one direction or the other, a condition that exists between recorder picture sequences. The NRZ method of recording allows re-recording over old data and/or erasure. Frequency-doubled code signals were monitored by the OSE during testing.

The start–stop–record relay applies power to the record motor whenever it is in the start position. Control pulses from the DAS or OSE can position the relay to either state. The second set of contacts on the relay is used for monitoring purposes through the integrator monitor lines of the spacecraft umbilical interface. (This was done to verify that the relay was in the stop position before launch.) Should the relay be left inadvertently in the start position, the record motor would start running immediately upon application of 400-cps power before encounter. The record motor monitor will be available in the encounter mode as it was in launch-mode operation.

During recording, a pulse is generated for each complete pass of the tape by the end-of-tape circuit as the end-of-tape foil passes over the sensor contacts. This end-of-tape pulse is applied internally to the track-change and count-two sections of the recorder system and externally to the DAS, data encoder, and OSE. In a normal planetary encounter record sequence, the DAS ignores the first end-of-tape pulse and responds to the second if it occurs between the beginning of the nineteenth and the end of the twenty-second picture sequence. The DAS is mechanized to terminate encounter record sequences either upon receipt of the second end-of-tape pulse or at the end of the twenty-second picture if an end-of-tape pulse has not been received. This function is backed up by the count-two-and-stop sections of the recorder. For telemetry purposes, end-of-tape pulses register on an event counter in the data encoder. The end-of-tape signal was brought out to the OSE for test purposes, mainly to index the tape transport to the beginning of the loop.

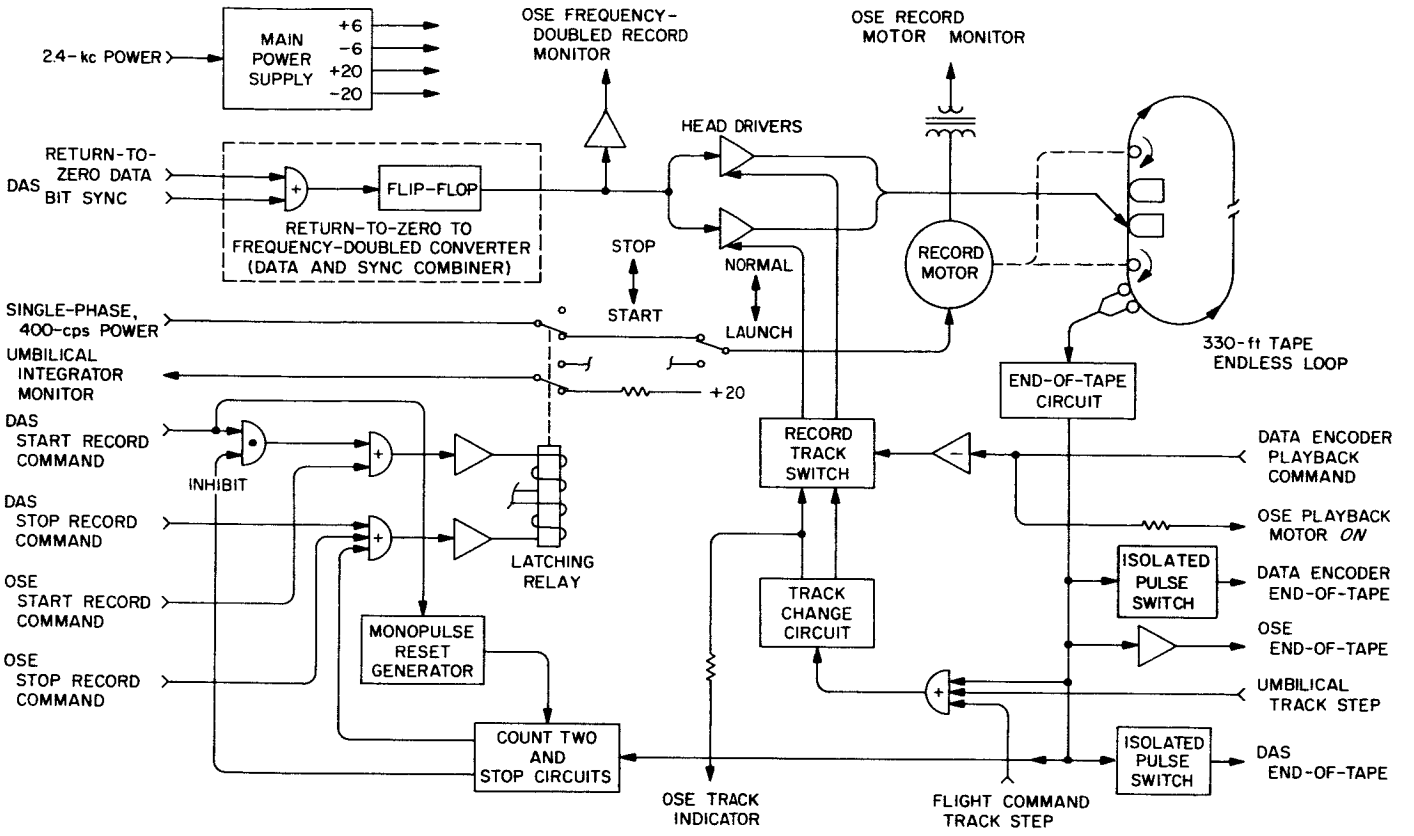


Fig. 218. Record mode functional block diagram

Track changes take place whenever the end-of-tape circuit generates a pulse. The track change circuit incorporates a magnetic latching relay arranged in a bistable flip-flop configuration. Track indication was brought out to the OSE for monitoring purposes. An umbilical track-step command is available as well as a track-step command from the flight command subsystem.

The count-two-and-stop circuits of the recorder system function automatically to issue a stop-record command to the recorder and to inhibit DAS start record commands upon receipt of the second end-of-tape signal. The counter is set to zero by the first DAS start-record command acting through a monopulse reset generator. Further reset of the counter is impossible unless 2.4-kc power is removed from the system. Once two end-of-tape pulses have registered on the counter, it inhibits start-record commands and has no further effect on the system.

Typical picture record sequence timing is delineated in Fig. 217. It should be noted that video data are delayed after a start-record command to allow the tape to reach the proper speed before actually recording. The tape is erased during this delay and also during coast-down after a stop-record command. Approximately 6 ft of tape is re-erased in this manner for each picture sequence. Synchronous pulses (all *zeros*) are applied 8 msec before data so that errors are minimized as the system attains synchronization during the reproduce mode.

Pictures are recorded in two sequence frames (Fig. 216). Sufficient time is allowed for the tape transport to come completely to rest between pictures. Track change will occur normally during the eleventh picture sequence, and storage capacity will be reached during the twenty-second sequence.

4. Reproduce Mode

After planetary encounter, once the data have been recorded, the recorder system will be switched into the reproduce mode (Fig. 219 through 221) by a command from the data encoder. Playback signals will be amplified and operated on in such a manner as to reproduce

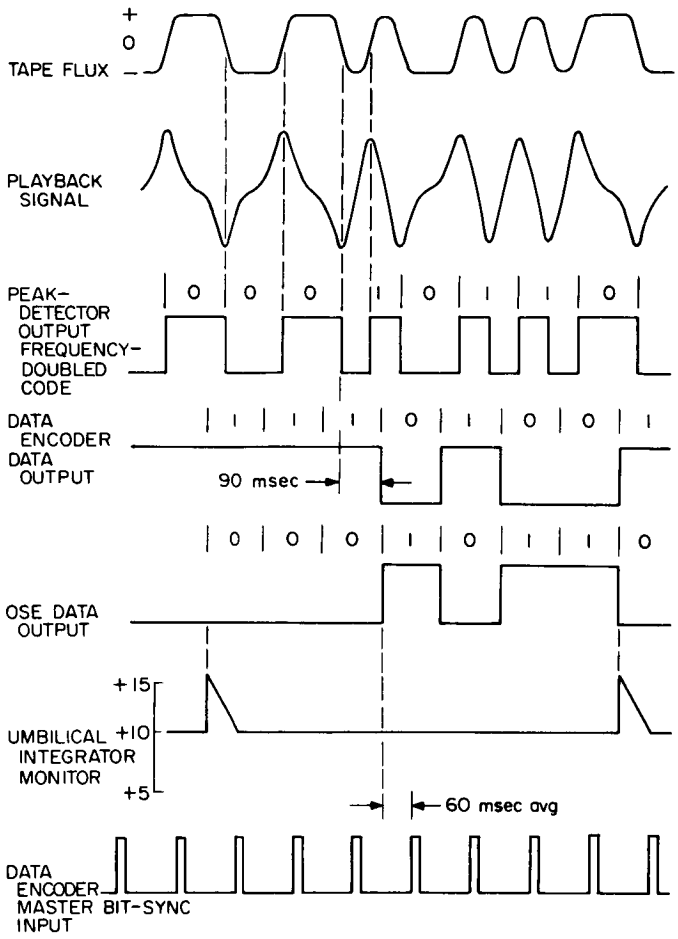


Fig. 219. Reproduce mode signal waveforms

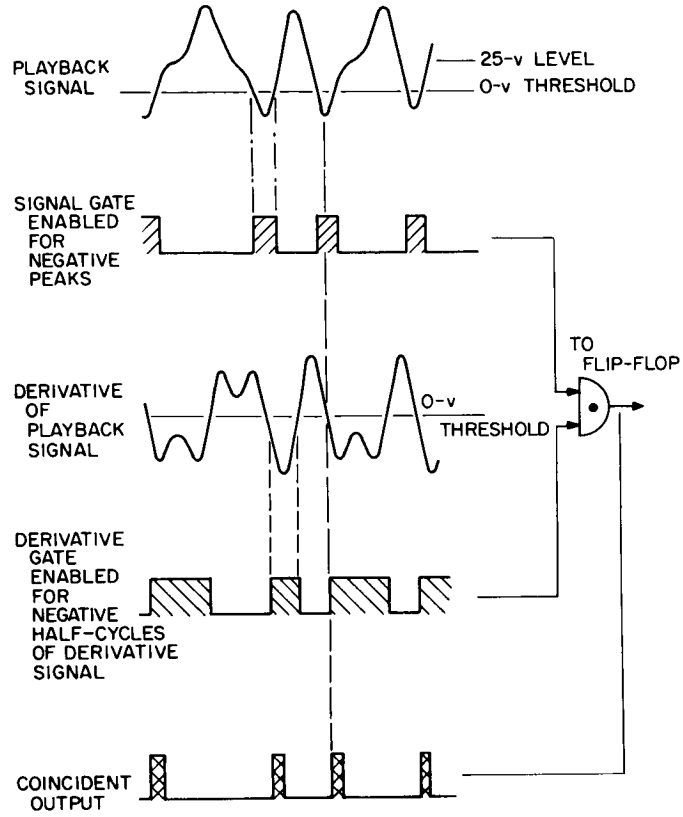


Fig. 220. Basic peak detection scheme

the frequency-doubled code waveform that was recorded. Bit synchronization will be separated from the data and compared in phase with the master bit synchronization from the data encoder. These comparisons will indirectly determine the frequency of the voltage-controlled oscillator that dictates playback tape speed. When the correct speed and phase are achieved, the tape-signal-derived bit synchronization and the master bit synchronization will be in the proper phase relationship for accurate readout of the data. If a stable phase relationship has been established, the recorder system is said to be phase-locked. The reproduce mode may continue indefinitely after encounter, and the system automatically changes tracks once for each pass of the tape. Complete reproduction of a sequence of 20 pictures requires from 8 to 10 days. Because sections of the tape are erased between record sequences, data will not be present at the output of the system for approximately 2 hr between picture data blocks. Provision was made in the recorder system for detecting this condition and for automatically switching the data encoder from Data Mode 4 (data playback) to Data Mode 1 (engineering data).

Passage of the tape over the reproduce head gap produces a signal that is roughly the derivative of the tape flux as indicated in the reproduce-signal waveform diagram (Fig. 219). This signal, with a voltage of 50 μv peak to peak, is amplified by low-noise preamplifiers located in the tape transport subassembly and routed to the playback track switch and main amplifier. Signals from both tracks are applied simultaneously to the playback track switch, which selects one signal at a time. During checkout, the output from the main amplifier was available at the OSE through a special monitor amplifier.

The peak detector reproduces the recorded frequency-doubled waveform. Figure 220 explains the basic operating principle. Peak detection is accomplished by combining the derivative of the playback signal with the selected peaks of the playback signal itself in a coincidence gate that drives one side of a flip-flop. Similar circuitry, using the alternate half cycles, drives the other

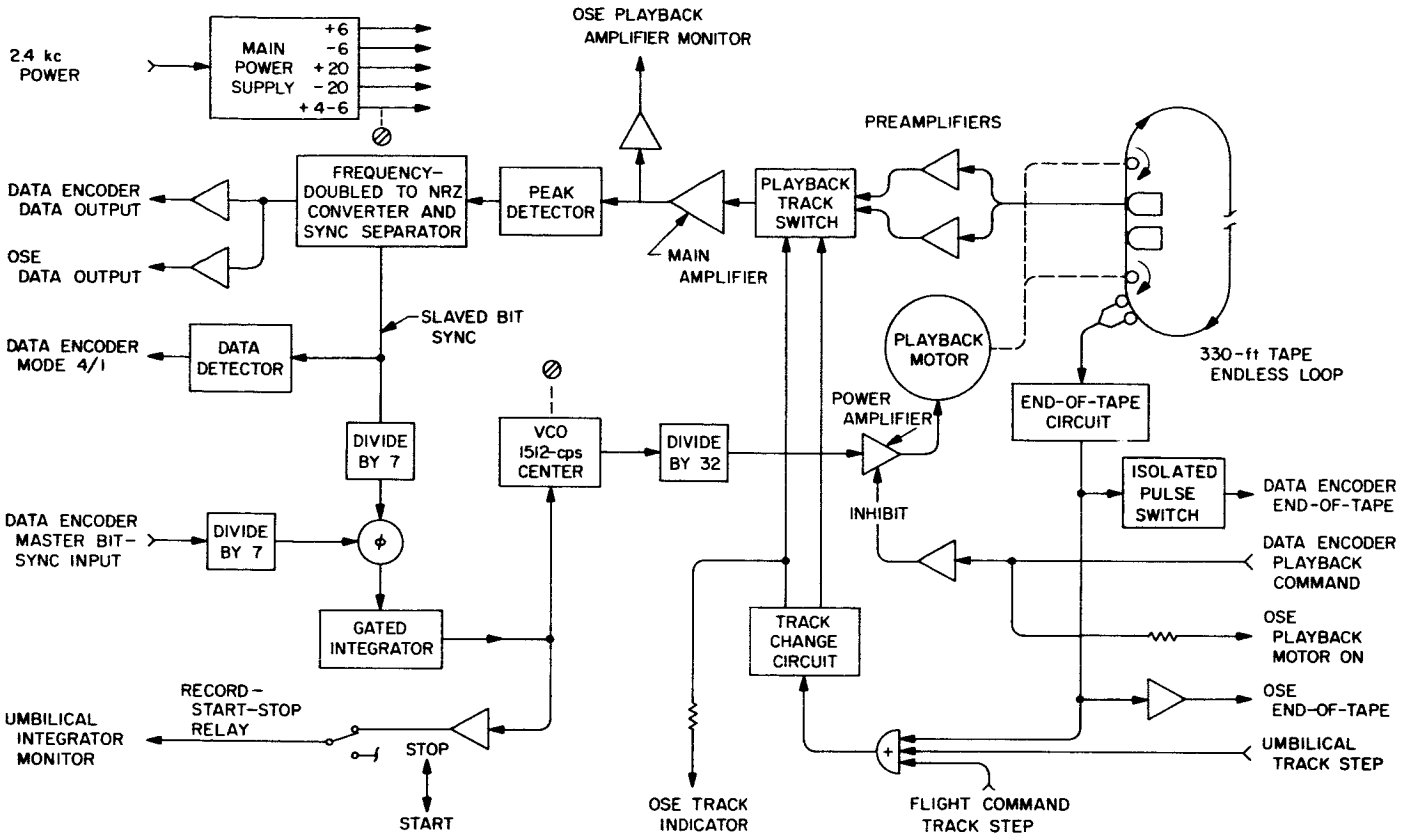


Fig. 221. Reproduce mode functional block diagram

side of the same flip-flop. Push–pull circuitry is used throughout. The playback signal peak amplitude must exceed the threshold level in order to enable the coincidence gate. Output ceases if the peaks do not exceed the threshold setting.

Separation of the bit synchronization from the frequency-doubled code is accomplished in the frequency-doubled/nonreturn-to-zero converter, which contains two one-shots and appropriate logic elements coupled with the flip-flop necessary to convert the code. Data output from the recorder system is fed to the data encoder inverted. Data output is available at the OSE for test purposes.

After separation from the frequency-doubled code, the slaved bit synchronization is divided by seven and applied to a phase comparator along the divided master bit synchronization from the data encoder. By means of the gated integrator circuit, instantaneous phase comparison occurs. As indicated in Fig. 219, the integrator waveform follows a reset, rundown, and hold sequence. The holding level is a direct indication of the instantaneous phase difference between the divided master bit synchronization and the divided slave bit synchronization. During initial lockup of the system, the gated integrator holding voltage level may vary anywhere from 5 to 15 v. Once the lock is established, variations in holding level rarely exceed 2 v peak-to-peak, although a variation of 5 v peak-to-peak can occur without loss of lock. The integrator signal is brought out through a special monitor amplifier and the extra contacts of the start–stop–record relay to the spacecraft umbilical interface. Initial phase lock of the system is accomplished in approximately seven phase comparisons.

The gated integrator directly controls the frequency of a voltage-controlled oscillator whose output is divided and applied by means of a power amplifier to the playback motor. The VCO has a nominal center frequency of 1512 cps, deviating $\pm 8\%$ for a 10-v variation in the gated integrator output. A center-frequency adjustment was provided to compensate for tolerances in the overall recorder system. Because playback-motor drive voltage requirements may vary from one tape transport subassembly to the next, the supply voltage applied to the playback-motor power amplifier could be varied. A playback command from the data encoder enables the

playback-motor power amplifier. Absence of this command signal inhibits the playback-motor power amplifier and, as noted previously, switches the system into the record mode.

Each complete pass of the tape loop generates an end-of-tape pulse as the end-of-tape foil passes over sensor contacts. As in the record mode, the end-of-tape pulse is applied to the track-change circuits and is also fed out to an event counter in the data encoder. In addition, the end-of-tape pulse is brought out to the OSE.

The track-change circuit determines which preamplifier signal is applied to the main amplifier. A track change may be triggered by an end-of-tape pulse, a track-step command from the spacecraft umbilical, or a track-step command from the flight command subsystem.

5. Temperature and Pressure Monitoring

The temperature of the main mounting plate of the transport subassembly is measured by means of a temperature transducer, which is monitored for telemetry purposes by the data encoder. Expected temperatures of the case in which the video storage subsystem was mounted are indicated in Fig. 222. Temperature transducer indications may be expected to lag behind case temperatures considerably because of the inherent thermal isolation of the main mounting plate.

The tape transport (Fig. 213) is a hermetically sealed unit. Verification of proper seal was obtained by telemetering the output of a pressure transducer mounted within the transport case. A gradual pressure loss was expected because of molecular diffusion of the gas through the seal elastomer. The leak rate due to molecular diffusion was directly proportional to temperature and the pressure difference across the seal. Thus, it was difficult to accurately predict pressure changes versus time; however, Fig. 223 depicts an expected worst-case plot.

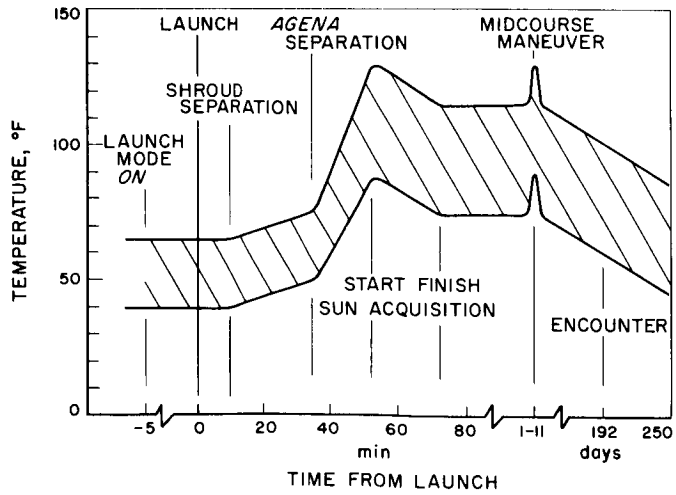


Fig. 222. Expected temperature profile of mounting case

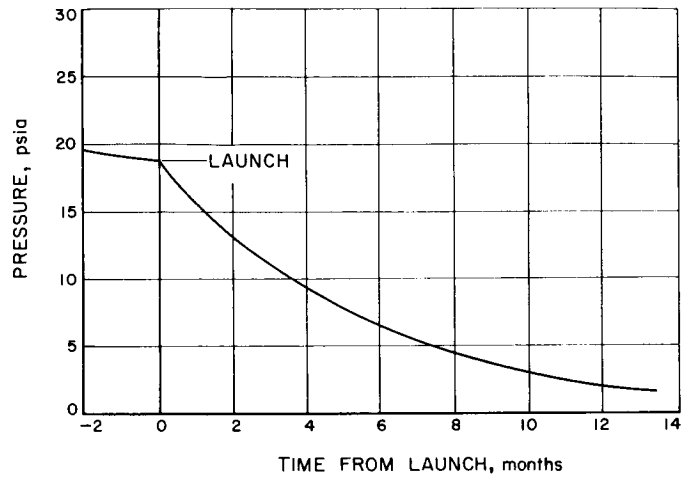


Fig. 223. Expected pressure drop in mounting case

C. Physical Description

The video storage subsystem is packaged in four standard JPL electronic subchassis and in a hermetically sealed unit. These subassemblies, together with the subsystem wiring harness, are mounted in half of Case V in the spacecraft structure.

The tape transport subassembly (Fig. 213) is also a hermetically sealed unit, which contains the basic tape transport mechanism including drive motors, heads, and playback preamplifiers. The purpose of the hermetic seal is to maintain a sufficiently high pressure inside the transport case to prevent evaporation of critical recorder lubricants, which start to evaporate at approximately 0.1 psi. The seal will have maintained a final pressure greater than 3 psi at planet encounter, since the transport internal pressure was 22 psi at the time of launch.

The transport assembly is mounted on vibration isolators within its own housing in order to protect the transport bearings from becoming "brinnelled" during high shock environments. This approach allowed the overall spacecraft structure to maintain its rigidity through the hard-mounting of all subassemblies while

providing protection to the transport bearings. In addition, temperature and pressure transducers were included for telemetry purposes.

The subchassis shown in Fig. 224 houses the major portion of the reproduce electronics, including the main playback amplifier, peak detector section, code converter, phase comparator, and output stages.

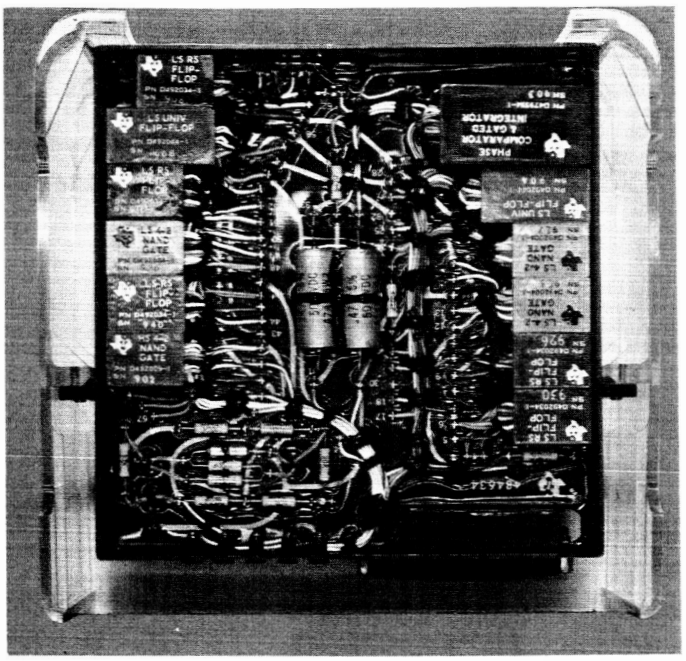


Fig. 224. Subchassis 16A2, showing playback amplifier, peak detector, code converter, and phase comparator

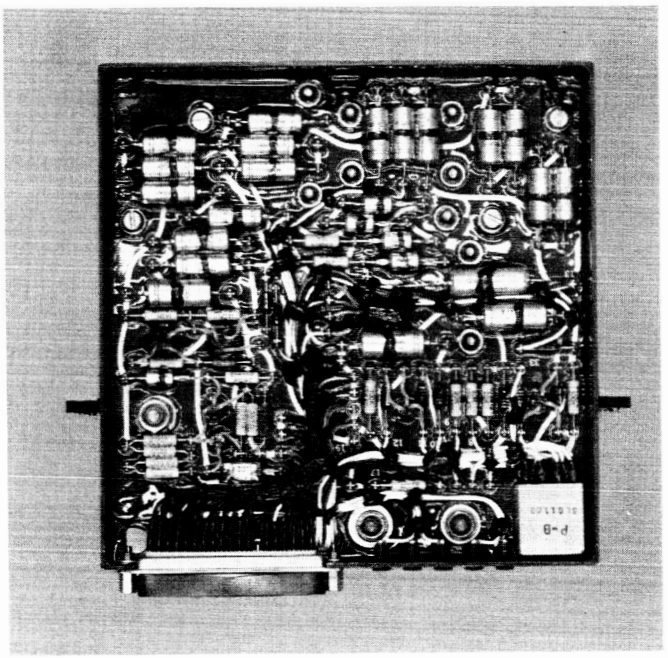


Fig. 226. Subchassis 16A4, showing power supply and record command circuits

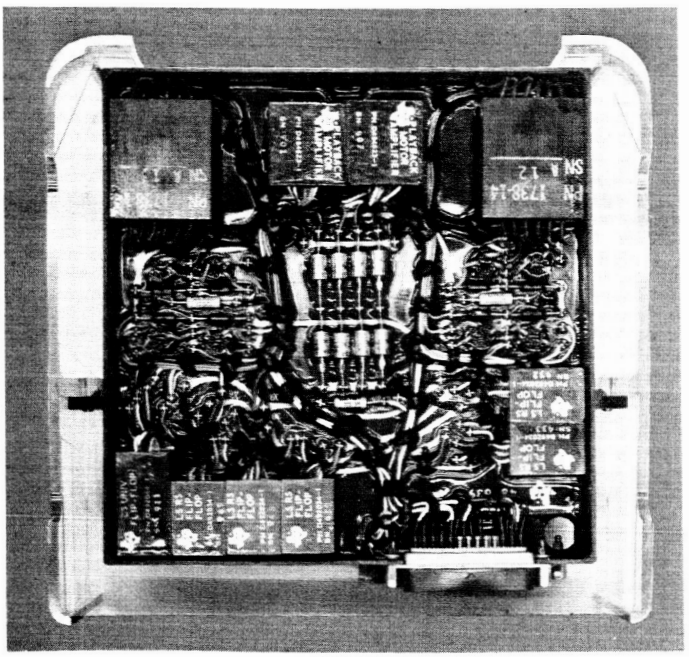


Fig. 225. Subchassis 16A3, showing voltage-controlled oscillator and playback-motor drive circuits

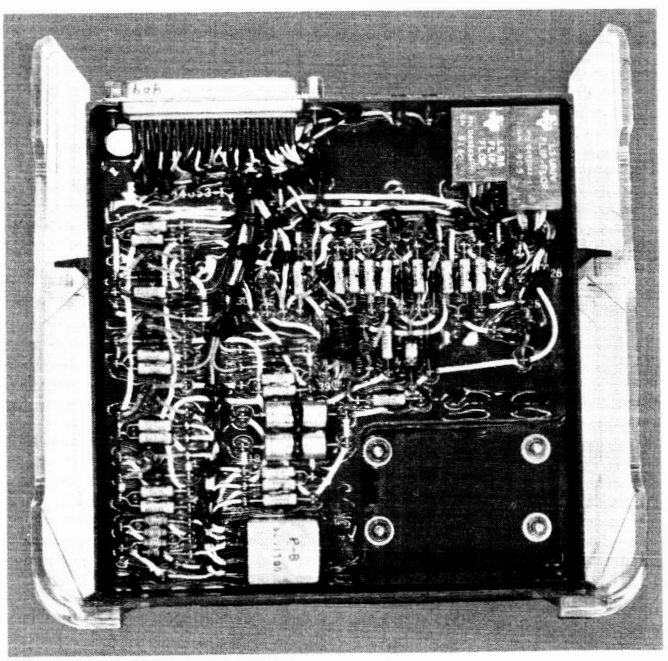


Fig. 227. Subchassis 16A5, showing launch-mode circuitry, control circuits, and record signal circuits

The subchassis shown in Fig. 225 houses the remainder of the reproduce electronics consisting of the voltage-controlled oscillator and playback-motor drive electronics. In addition, most of the record signal electronics and part of the control section are located there.

The subchassis shown in Fig. 226 contains various power supplies that generate voltages for the recorder system from the main spacecraft 2.4-kc power distribution system. This subchassis also contains the record command circuits for controlling the record motor.

The subchassis shown in Fig. 227 houses the launch mode circuitry, control circuits, and the remainder of the record signal electronics.

The mechanical characteristics of these subassemblies are listed in Table 56.

Table 56. Mechanical characteristics of VSS electronic subassemblies

Subchassis	Weight, lb	Volume, in.^{3}
16A1	9.29	226.0
16A2	1.74	59.5
16A3	1.71	59.5
16A4	2.28	76.5
16A5	1.79	59.5
Total	16.81	481.0

The electrical power for the video storage subsystem is derived mainly from the 2.4-kc spacecraft supply. The record motor will require a special 400-cps power source while recording planetary encounter data. The spacecraft gyro power was used during launch mode operation to run the record motor. The 2.4-kc power supply furnished 100-v peak to peak or 50-v-rms square wave. The record mode will require 3 w, and the playback mode will require 4 w. The 400-cps single-phase power supply will furnish 65 v peak to peak or 32.5-v-rms square wave. The record mode will require 4.5 w for operation and 8 w for motor start. The 400-cps three-phase power supply (one phase only will be used) will furnish 66-v peak to peak or 24-v-rms castled wave Launch mode *off* (standby) used 0.2 w, and launch mode *on* used 3.5 w.

D. Development History

In September 1962, JPL issued the first specification relating to the system that ultimately evolved into the *Mariner* Mars 1964 video storage subsystem. It called for an endless-loop tape recorder capable of storing 2×10^6 bits on one data track, operating with serial nonreturn-to-zero input at 13,200 bps, and delivering a fully bit and word synchronous serial nonreturn-to-zero output at 8⅓ bps. A second track was included for recording word synchronous data.

A recorder had been developed for JPL, with a capacity of 10^6 bits. It used one data track on a 300-ft endless loop, and was capable of synchronous playback at 8⅓ bps. At the same time, another recorder was being developed for JPL, with a capacity of 10^7 bits, using three data tracks and one synchronization track on a 700-ft endless loop, which was similarly capable of synchronous playback at low tape speeds.

As the *Mariner* Mars data storage requirements became better understood, it was evident that the specified 2×10^6 bit capacity would probably not be adequate, and that at least a 5×10^6 bit capacity would be required. It was also evident that two data tracks would be needed to keep the tape length within the range of the then current experience. With a packaging density of 400 bits/in. per track and with two tracks, 5×10^6 bits would require 520 ft of tape. If the system were arranged to index from track to track after each tape passage, rather than simply to record alternate data bits on alternate tracks, playback speed would have been around 0.02 in./sec at 8⅓ bps, and record speed would have been near 33 in./sec. At that time, it was also learned that allowance would have to be made for 20 starts and stops in record mode, raising the tape length estimate from 520 ft to between 580 and 600 ft. These parameters indicated a mechanism more similar to the 10^7 bit transport. The weight of this mechanism was considered to be a serious drawback and became the subject of considerable further independent considerations by the designers of the recorder and by JPL.

An alternate scheme was discussed, in which the two synchronous tracks (as required in the two-data track scheme for storing 0.5×10^6 bits discussed above) could be used as two additional data tracks, if the data were recorded in a frequency-doubling code rather than as simple nonreturn to zero. This alternate led to the consideration of a transport operating at 0.02 in./sec and 31.7 in./sec, and having approximately 300 ft of tape.

Estimates made by the designers of the recorder indicated that this new approach could result in a weight savings of up to 5 lb as compared to the larger transport, and JPL requested a proposal on this basis.

The technical proposal made in December 1962 discussed a transport with an endless-tape loop, approximately 300 ft in length, in which four data tracks were to be recorded and played back sequentially. Tape speeds were chosen as 0.02 and 31.7 in./sec corresponding to playback rates of 8⅓ bps and record data rates of 13,200 bps. Packaging density was to have been 417 bits/in. per track. Extra synchronous tracks were eliminated by recording the data in a froquency-doubled code in which a flux reversal occurred at each boundary of each bit cell, and for a *ones* code in the bit-cell center as well. Bit-synchronizing clock signals could have been extracted from this code along with the data during playback. Word synchronization was unnecessary in the system in which the recorder was to operate.

Bit-synchronous playback was to have been achieved by using a phase-locked-loop tape speed control similar to the scheme originally developed in the 10^6 bit system. Tape bit-synchronizing pulses and clock bit-synchronizing pulses were to have been compared in phase at spaced intervals.

The waveform of the playback head output signal that resulted from a crowded frequency-doubling coded recording led to consideration of replacing the more conventional playback-level detecting circuitry with a passive filter arrangement, which would result in proper spacing of signal *zero* crossings rather than signal peaks. This system was believed to be capable of yielding better signal-to-noise characteristics by taking advantage of the frequency components of the playback signal instead of depending merely on its instantaneous amplitude.

Late in January 1963, the *Mariner* DAS/VSS interfaces had been discussed sufficiently to present a final functional interface definition between the two subsystems. As a result of this definition, the capacity requirement increased to 5.24×10^6 bits. Twenty stop–start cycles were expected during recording. It was specified that the waste tape resulting from each stop–start cycle would be equivalent to 1 to 2 hr time in playback.

By February 1963, two major problems existed:

1. Experimental work was lending to the conclusion that the proposed method of detecting the playback signal by taking advantage of pulse crowding effects would not work at the low tape packaging density that had been chosen. Past success of this method at considerably greater packaging densities was probably due to effects secondary to a simple relationship between the gap length and recorded wavelength.
2. The question of whether the transport should be hard-mounted had led to detailed investigation of different mounting schemes providing the required stiffness but allowing for suitable vibration protection.

Other subjects requiring engineering study included the necessity of momentum compensation in the transport and the necessity for exercising the transport during the flight period.

Continuing work on the problem of playback signal detection mentioned above showed that an acceptable signal-to-noise ratio greater than 30 db could be achieved consistently at a tape speed as low as 0.01 in./sec, with packaging density increased proportionally to maintain the specified bit rate. Changing the proposed system accordingly would have resulted either in cutting the tape length in half or in reducing the number of tracks from four to two. The second choice was felt to be the better of the two.

Along with the suggestion to halve the tape speeds and go to two tracks, it was proposed that the transport be supported on vibration isolators within its own housing rather than the entire assembly mounted on isolators. This system would provide JPL with the desired stiffness and still afford adequate protection for the transport. These proposals were accepted by JPL in March 1963.

Even with the increased packaging density, problems still existed with the proposed system for playback signal detection. The system could not provide the needed spectral response because of head rather than tape limitations. Efforts were turned toward developing an improved true peak detector circuit. The new scheme involved correlating the playback signal with its own derivative, and it proved quite successful.

E. Procurement

Under close JPL supervision, four major companies participated in the design of the flight and ground *Mariner* Mars video storage subsystems.

One contractor performed the detailed design of the mechanical and electrical portions of the flight system, with the exception of the electrical power supplies, and developed a high-reliability motor for use in the tape transport. In addition, the same contractor fabricated seven tape transports and one recorder breadboard system minus the power supplies, and supplied two engineers (one at JPL, one at the Cape) to aid in the testing and evaluation of the spacecraft. Another contractor performed a worst-case analysis of the electrical design of the flight system and designed the flight-system power supplies. In addition, the second contractor fabricated one breadboard power supply and seven sets of VSS electronics, and also furnished two field service personnel to aid in the testing and evaluation of the spacecraft. A third contractor performed the detailed design and fabrication of four VSS operational ground support systems. A fourth contractor conducted a mechanical worst-case analysis on the tape transport. Several other contractors participated to a lesser degree by supplying catalog parts (modified to the JPL quality control requirements) or furnished test facilities.

F. Fabrication

The flight VSS were fabricated in strict accordance with JPL quality assurance specifications. To guarantee that all contractors were complying with this specification, JPL resident inspectors were permanently located at the two major contractors' plants, and roving inspectors covered the smaller contractors.

The video storage operational support equipment was built to standard industry requirements. The equipment was inspected for workmanship and safety by JPL inspectors before it was accepted.

G. Test Experience

Seven flight VSS were built and tested. All flight systems were tested under JPL supervision and had to completely pass JPL test specifications before any system was accepted from the subcontractors. Tests on the VSS type-approval unit were conducted at room temperature, 70°C, and −10°C. The remaining six systems were tested at room temperature, 55°C, and 0°C.

During April 1963, JPL began an extensive investigation of whether or not the transport could survive the *Mariner* TA shock test. Equivalent tests had been waived in the previous development efforts. It was felt that the capstan assembly was the most susceptible to damage; hence, a capstan assembly and fixtures were prepared especially for shock testing. The TA shock test was duplicated as nearly as possible on an impact shock-test device. The assembly failed these tests. In each case, the bearings brinnelled as a result of the tests.

The second major technical difficulty was that of tape failure at the TA temperature extremes. Although the tape had operated successfully in earlier developmental units, it failed in this transport at 80°C apparently because of the increase in tape speed over that of the earlier tape transports.

During the last of the formal predelivery tests on the prototype (at 80°C), the tape jammed up on starting. This failure led to a long continuing series of tests and investigations of possible causes and fixes. This failure occurred with two new conditions: (1) a long temperature soak at 80°C with the machine inoperative during the transition from room temperature, and (2) a dry nitrogen–helium atmosphere. Factors that had to be investigated included:

1. Presence of helium
2. Lack of moisture
3. Increased friction
4. Bad hub size
5. Wrong hub material
6. Bad choice of tape lubricant
7. Possibility of critical tape length
8. Improper tape curing
9. Poor tape stiffness
10. Too much imbalance in thermal coefficients of expansion
11. Direction of winding

Some specially made tape was procured from a contractor for evaluation. Although operable throughout the temperature range, the samples shed loose debris at an excessive rate and could not be used. Another tape was provided by the original tape supplier. Even with the new tape, the upper temperature design limit had to be changed from 80 to 70°C. Contractor tests showed the third tape to be adequate at 70°C. Later tests showed that in the range above 70°C there was little actual performance difference between the third tape and the original one. The transport remained limited to an upper extreme of 70°C because of the inability to start at temperatures much above that point with either tape.

Beyond 70°C and up to 80°C, failures to start were somewhat random, although there was a definite link to soak time.

In spite of many bench tests indicating satisfactory life for the end-of-tape sensing mechanism, it was proved to have seriously limited life in the prototype and the flight units. This limitation existed not only because the foil ceased to make good contact with the sensor slip rings, but also because the circuit that was actuated by the contact action responded to the multiple closures induced by dirt buildup on the conductive foil. The problem existed primarily at playback speed, although there was one failure at record speed. Due to an extremely tight flight spacecraft testing schedule, a design change could not be implemented into the system to correct this problem. However, a telemetry track change command was added to the control system to circumvent operational problems that could result from the foil and sensor difficulty in the absence of a new circuit. Transports had previously been vibrated immediately after being mounted in the case. However, the TA vibration took place shortly after an exposure to a temperature shock, and the exposure loosened the fasteners holding the transport in its case and caused failure. An improved method of securing the fasteners was devised and ultimately incorporated in all units.

During the final test phase, a large number of bit errors was noted and attributed to noise sensitivity of the open test setup. More exhaustive tests at JPL (in May 1964) after delivery of the systems, revealed that their bit error rate was excessive. An investigation turned up a design problem in the playback data logic circuitry leading to a tendency to generate errors favoring *ones*. A solution was proposed, but was not adopted because of the approaching launch date.

Because of recurrent problems with tape and the conductive foil, it was established that tape would be replaced after the systems had been subjected to flight-acceptance tests at JPL.

The serial number 5 video storage subsystem was installed in the *Mariner III* spacecraft in June 1964, and the serial number 7 VSS was installed in the *Mariner IV* spacecraft during July 1964. These systems were selected on the basis of their superior performance during subsystem contractor and JPL testing. They functioned as designed between the time they were installed in the spacecraft and the respective spacecraft launch times. Both systems operated perfectly during the launch phases of *Mariner III* and *IV*. The *Mariner IV* VSS was properly positioned for a planetary encounter sequence.

XVI. SPACECRAFT SUBSYSTEMS: TEMPERATURE CONTROL

The temperature control subsystem is comprised of all devices and design features used to maintain temperatures within specified bounds for all spacecraft components. Hardware included: louvers, radiation shields, surface coatings, thermal insulation, and temperature sensors. Design details influenced by the temperature control requirements included component placement, methods of attachment, structural material and configuration when conduction is important, and the surface finish of the structure and components.

A. Temperature Control Subsystem Design

1. Requirements

The magnitude and distribution of solar and electrical heat inputs, together with the thermal characteristics of the spacecraft, determined spacecraft component temperatures. It was not difficult to obtain acceptable spacecraft temperatures in the Sun-oriented condition for a fixed solar intensity. However, short-term variations in solar heat input occurred during launch and midcourse maneuver due to the lack of normal spacecraft Sun orientation, and a long-term decrease occurred enroute to Mars due to increasing solar distance. These variations produced corresponding changes in spacecraft temperatures. A further complication was caused by temporary increases in internal power dissipation in the bus during the time of maximum solar heating (gyros on; midcourse motor firing) and a decrease during minimum solar heating (TV picture playback). Accommodating these changes in heat input within allowable component temperatures was the most significant problem of temperature control.

2. Design Evolution

Salient features of the bus temperature control design requirements are isolation from solar heating, minimum internal resistance to radiative and conductive heat transfer, and variable emittance louvers on most electronic bays. Protection from the variable Sun input is provided by a multiple-layer aluminized mylar upper thermal shield. Localized internal hot spots are prevented by the use of good thermal conduction joints and by the treatment of interior surfaces to produce high emittance. Louvers suppress the temperature excursion caused by unavoidable solar inputs via thermal-shield heat leaks and radiation from the solar panels to the case faces.

External science instruments and appendages are separately and passively controlled by surface property selection and Sun shielding where appropriate. Conductive and/or radiative thermal coupling with the actively controlled bus is used whenever it is possible to minimize both transient and long-term temperature variations.

Care was taken to design around the limitations of the solar simulator in the JPL 25-ft space chamber. The upper thermal shield was faced with black dacron, and thermal grey coatings were used when possible on sunlit surfaces to render spacecraft temperatures insensitive to simulator/Sun-spectrum differences. Sun shades were fabricated and positioned so that the 5-deg decollimation angle of the solar simulator was relatively unimportant to spacecraft temperatures.

The initial temperature control design was based on analysis of the temperature profile between Earth and Mars and of the temperature requirements for the various spacecraft subsystems. Solar dependency for the bus was estimated from *Mariner II* flight data, and resulted in the specification of louvers for Bays I, III, IV, VII, and VIII. Significant changes to the preliminary design were made during TCM testing on the space simulator, which produced an acceptable thermal design. Major changes in bus shielding and appendage painting were made at that time also.

Between the TCM and PTM simulator thermal tests, further modifications were made for a variety of reasons. Analysis of the TCM thermal tests and PTM systems test indicated that the mean bus temperature was somewhat lower than that desired. Thermal design data confirmed that changes had been made to the spacecraft, and weight was critical. For one or more of these reasons, the following changes were made:

1. The Canopus sensor was hard-mounted (conductively coupled) to the bus
2. Planetary scan science was radiatively coupled with the bus by extending the lower thermal shield
3. Louvers were removed from Bays IV and VIII, and were replaced by aluminum shields
4. Louvers replaced the shield on Bay V
5. Bay II motor shield modified

These modifications again produced an acceptable thermal design, as confirmed during the PTM simulator test.

Prior to the testing of the MC-2 spacecraft, a set of louvers was removed from Bay V and placed on Bay VI to accommodate the increased heat dissipation of the TWT RF component. Minor shield changes were also made to optimize flight temperatures. However, temperatures on the Ionization Chamber and the bus were much higher than expected. The Ionization Chamber anomaly was traced to a surface coating problem and corrected. The high bus temperatures stemmed from increased battery charger power dissipation (22-w increment) and a Sun input (at Earth) of from 2.5 to 5 w in Bays I, II, VI, and VII. The latter condition was caused by stray light reflectors, which had been added to these bays. In order to reduce temperatures to levels acceptable for flight, louvers were replaced on Bays V and VIII, and shield modifications were made to drop the average bus temperature. These changes produced the desired effect, but the Bay II Sun sensor was still operating near its upper temperature limit.

A Sun shield was added to the Bay II Sun sensor pedestal after the test to lower the Sun sensor temperature. Space-simulator tests of MC-3 and MC-4 verified the adequacy of the design, and no further modifications were made.

3. Test Experience

Temperature control testing may be divided into three broad categories:

1. Space-simulator testing of the TCM
2. Space-simulator testing of the PTM and flight spacecraft
3. Supplementary and developmental tests

Summaries of the more important thermal tests are given below.

a. Temperature control model. The TCM of the *Mariner* Mars 1964 spacecraft was tested in the JPL 25-ft space simulator during October and November 1963. Figures 228 and 229 show the final test configuration. Ten separate tests, comprising 35 test modes, were conducted. The TCM was positioned in three Sun attitudes: Sun oriented, pitched 90 deg, and pitched 180 deg. Various combinations of solar intensity and internal power dissipation were tested. Modifications necessary to achieve adequate temperature control were made as necessary, and the resulting thermal design was tested in all flight modes.

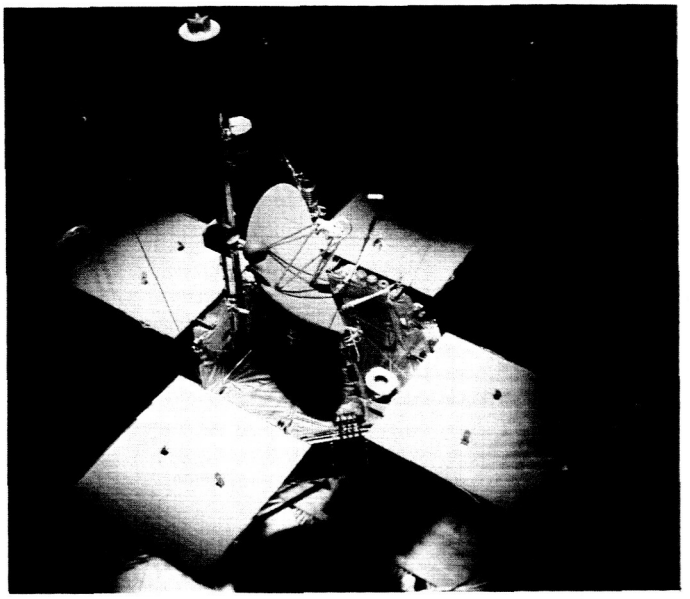


Fig. 228. Solar simulator illumination of TCM

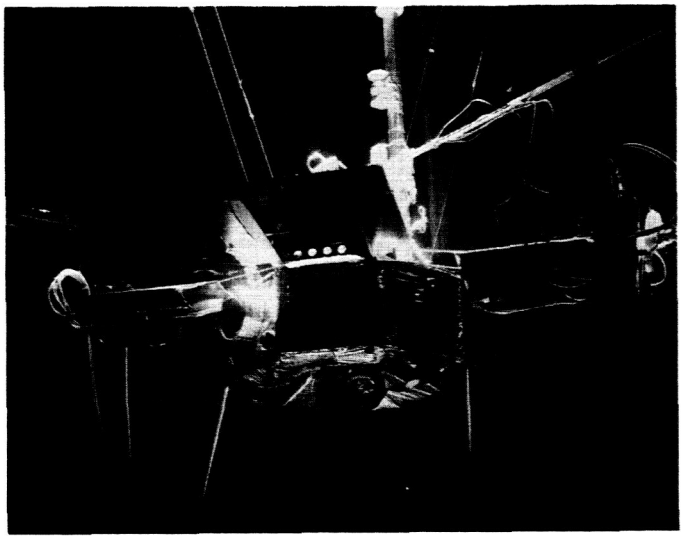


Fig. 229. TCM during space-simulator test

b. Flight-type spacecraft. A temperature control test of the PTM was performed in the 25-ft space simulator in April 1964. All components operated within allowable temperature limits, but minor changes to the bus thermal shield were needed to optimize flight temperatures.

A temperature control test of the MC-2 spacecraft was performed in the space simulator in July 1964. Significant changes to the thermal design were required during the test to reduce the bus temperatures to an acceptable level. Figure 230 shows the spacecraft in the space simulator. A temperature correlation was obtained between a minimum cable test (thermal test) and a normal systems test. The systems-test portion yielded temperatures only a few degrees lower than the thermal test except for units directly affected by sensor hoods (such as Sun sensors and the Canopus sensor).

Temperature control verification tests of MC-3 were carried out in the space simulator during August 1964 and tests of MC-4 during September 1964. Both spacecraft operated within desired temperature ranges. Temperature reproducibility among flight spacecraft was found to be generally good, although variations did exist.

c. Supplementary tests. A preliminary temperature control test of the Canopus sensor and high-gain antenna was performed in June 1963. The test objective was to demonstrate the feasibility of the Canopus sensor thermal design as well as survival capability of the sensor during a worst-case midcourse maneuver. The high-gain antenna test was intended to reveal any focusing of sunlight on the feed that could result in feed burnout. The test results indicated no survival problems for either the sensor or feed. An acceptable flight thermal design was worked out for the sensor.

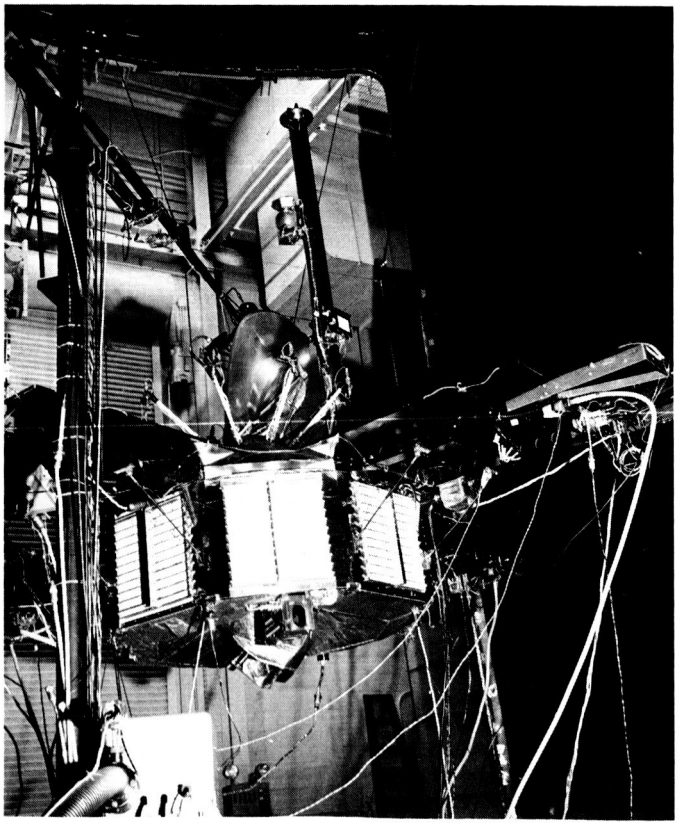


Fig. 230. MC-2 thermal test configuration

Tests were performed in the space simulator during January 1964 to determine thermal characteristics of the solar panel structure, to experimentally obtain appropriate paint patterns for the solar vane actuator and the attitude control jet assemblies, to verify high-temperature survival of the solar vanes, and to obtain absorptivities for various temperature control surfaces in the solar-simulator spectrum. All test objectives were satisfied.

B. Thermal Shields

1. Description

The term thermal shields, as referred to on the *Mariner* Mars 1964, pertains to the removable passive temperature control shielding. The thermal shields consist of multilayer mylar blankets shielding the top and bottom of the spacecraft, and thin-gauge polished aluminum shields on the periphery electronic cases. Not including the attach and support hardware, approximately 30 of these items covered nearly 70% of the spacecraft basic octagon. The complete shielding system weighed about 8 lb, and contained approximately 200 parts.

2. General Requirements

To minimize the effect of the decreasing Sun intensity, the solar dependence of the bus had to be small and known. The upper thermal shield thus had to prevent solar radiation as a changing source of the bus heat input. The peripheral and lower shields, primarily exposed to low-temperature space, had to minimize the spacecraft heat loss to that sink. During midcourse maneuver, all shielding normally shaded had to be capable of withstanding short periods of solar radiation. Although thermal shielding requirements had been considered during preliminary design, detailed shield mounting provisions were not included in the final structure design. When the shields were finally defined, they had to be added with minimum effects on spacecraft weight, structure, components, and configuration envelope. Design of the thermal shields had to be compatible with the environments of fabrication and handling, spacecraft system testing, component accessibility, and final assembly procedures. Structurally, the shields had to survive the launch environment, ground handling, and assembly operations.

3. Thermal Shield Design

To satisfy the thermal and mechanical requirements, a flexible-type multilayer blanket was used on the top and bottom of the spacecraft. The blankets were fabricated from wrinkled aluminized mylar sheets at a density of approximately 140 sheets per inch. The blanket thickness could be varied to achieve an optimum thermal barrier. Little structural support was necessary because of the lightweight and flexible features of the blanket design. The behavior of the shield allowed it to conform in geometrically difficult areas. The task of defining the shield configuration was accomplished by tailoring patterns directly from a spacecraft, as seen in Fig. 231 (a) and (b). These paper patterns were transferred to hard cardboard and then to full size engineering drawings. The full size paper patterns on the spacecraft allowed visual and physical verification of the pattern sizes. The non-blanket-type side shielding was easily defined by conventional engineering drawings. The thermal shields used for the first series of simulator tests are described below.

a. Upper thermal-shield blanket. This blanket had to insulate the octagon from the solar heat input. During flight, the inner surface would remain at a constant near bus average (75°F at Earth mode), while the outer Sun-exposed surface would attain 260°F.

The blanket consisted of 30 layers of vacuum-metallized ¼-mil mylar polyester film. The mylar was coated on one side only with an aluminum layer having a thickness of approximately 3.0 μin. Before assembling the aluminized-mylar sheets into blanket form, they were wrinkled by hand-gathering the film into a small bundle and crushing it. The permanent wrinkles or creases that resulted fractured the aluminized layer into approximately 160 segments per square inch. The purpose of the crinkling was to minimize the number of point contacts between successive layers. (A by-product of the wrinkles was the loss of electrical conductivity across the blanket.) After crinkling, the approximately 4 × 6-ft mylar sheets were layed out flat, with the aluminum side in the same direction, to form 30 layer blankets. The blanket assembly was finished with the addition of the outside layer of black silicone-coated dacron cloth (Fig. 232). The cloth weighed 5.00 ± 0.25 oz/yd.^{2} Neither the reflectance or transmittance characteristics exceeded 6% between wavelengths of 0.3 and 0.8 μ. The black cloth was used to render the spacecraft insensitive to simulator Sun-spectrum differences. Other advantages of the high-emittance black were low surface temperatures, low reflectance, resistance to ultraviolet radiation, and a durable, easy to clean temperature control surface.

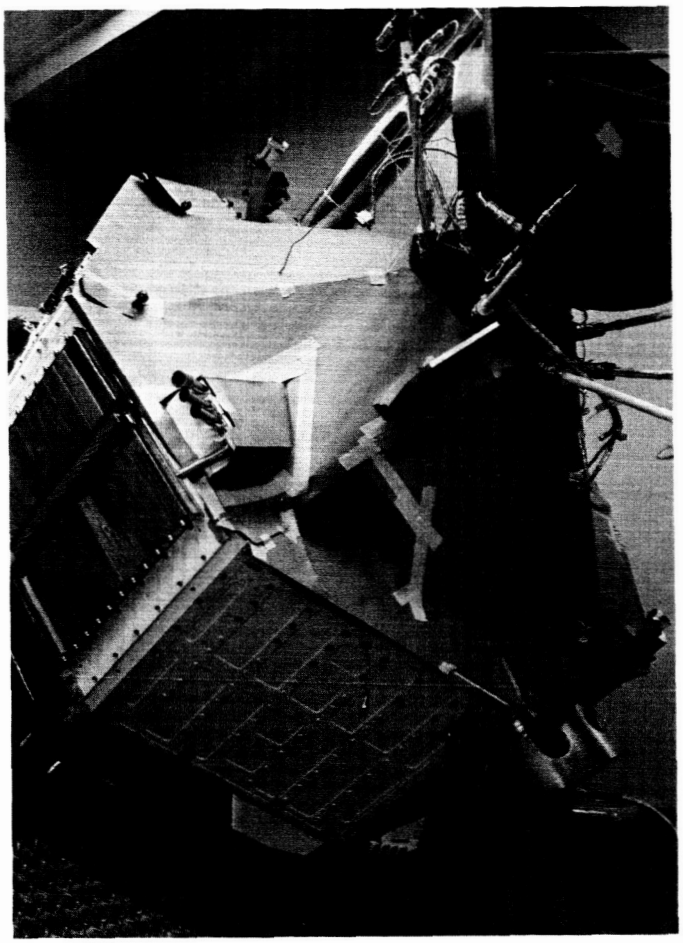


Fig. 231(a). Blanket pattern installed on TCM (top)

Because of material width limits, two such blankets were required to fabricate one complete shield. A razor knife was used to cut the blanket to match the paper pattern. All edges of the blanket were then secured by approximately six machine-sewn sail-type stitches per inch. With the addition of a nylon zipper, velcro strips, and lacing flaps, that phase of the operation was completed. The shield was then fitted to the spacecraft TCM for final positioning of the peripheral attach angles. These prefabricated 0.020-in.-thick polished aluminum angles were hand-sewn to the blanket and, in turn, attached to upper electronic case screws on the final spacecraft assembly. The final inspection of the shield took place on the spacecraft because their flexibility rendered a dimensional inspection meaningless.

b. Retarder shield. The retarder thermal shield was mounted under the high-gain antenna, and formed the top portion of the upper thermal shield. The complexity of the spacecraft structure and assembly procedures contributed to the two-part upper shield. When assembled

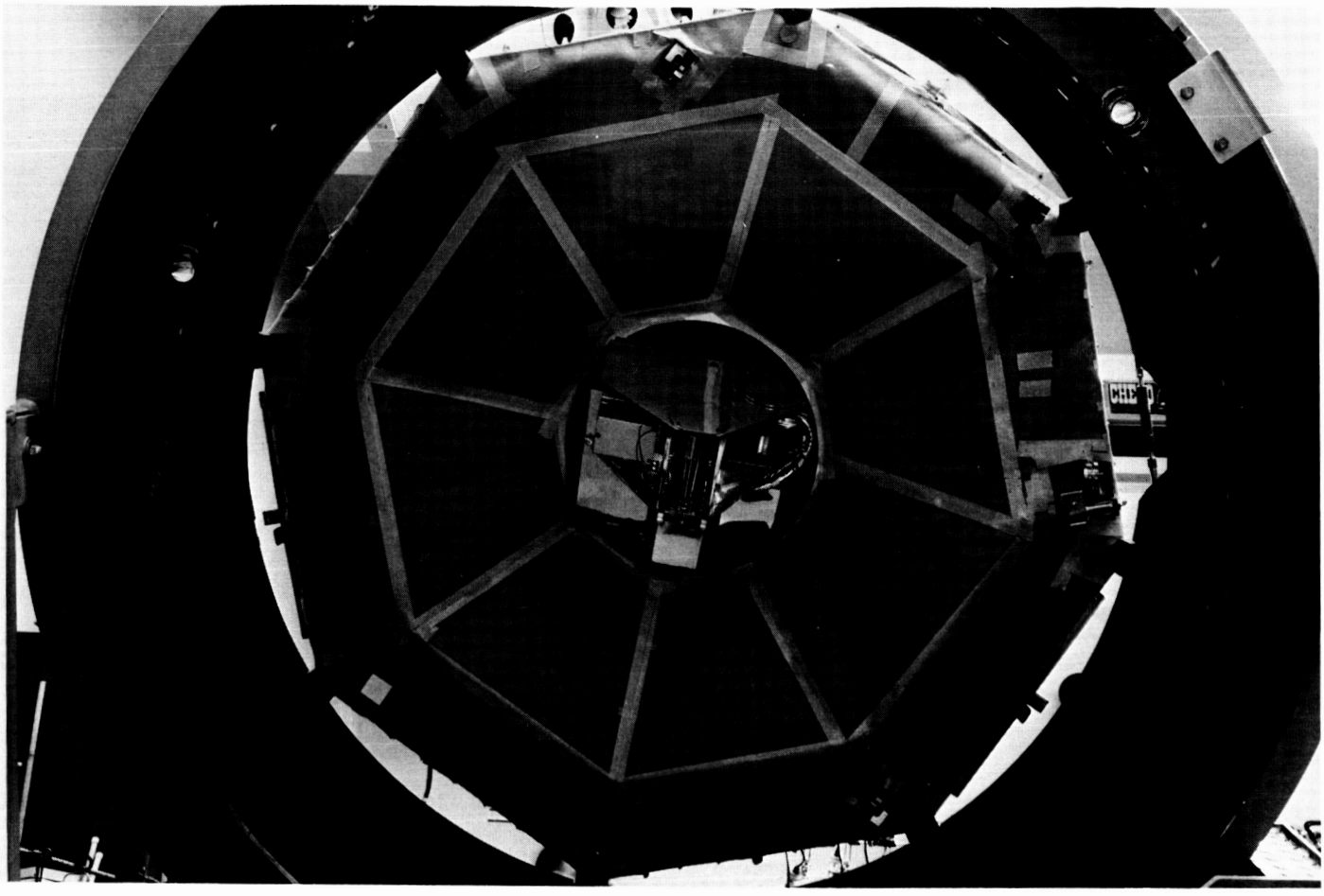


Fig. 231(b). Blanket pattern installed on TCM (bottom)

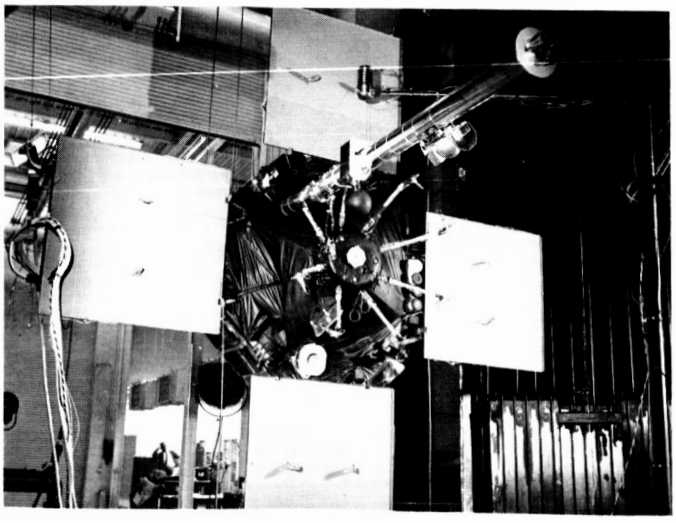


Fig. 232. Upper thermal and retarder shields (TCM)

to the spacecraft, the two shields were joined together by a continuous lacing. The retarder shield construction was exactly the same as the upper blanket: 30 layers of crinkled ¼-mil aluminized mylar plus one exterior layer of black dacron. Although small in size (approximately 24 in. in diameter), the shield contained 18 cutouts for the protruding structure plus eight flaps for lacing (Fig. 233). That presented the first real compromise between the theoretically worthless shield and the practically possible one. The thermal shorts caused by the multitude of holes from sewing were thermally degrading. One point in its favor, however, was the fact that it was shaded by the high-gain antenna and was not subject to direct solar inputs.

c. Lower thermal-shield blanket. The lower thermal-shield blanket covered the bottom of the spacecraft except for the science platform and necessary protrusions

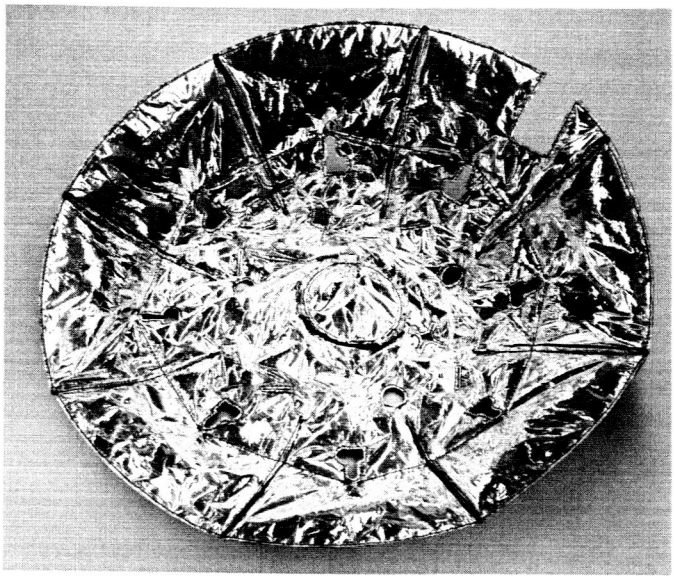


Fig. 233. Retarder shield

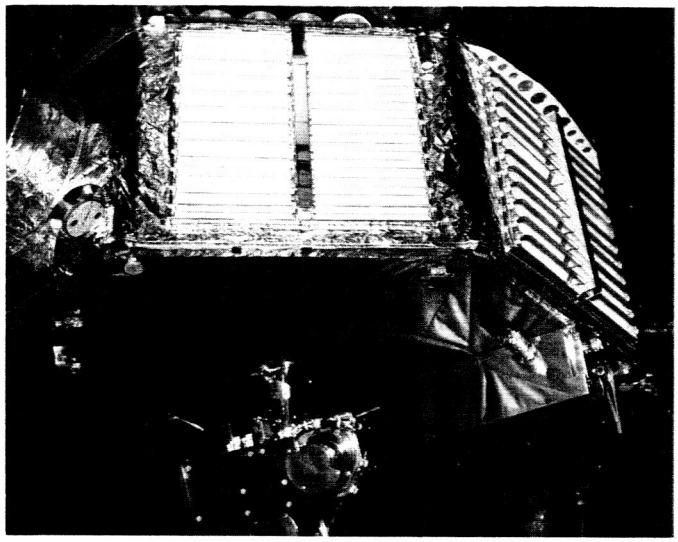


Fig. 234. Lower shield

such as connectors, switches, and Sun sensors. The purpose of the shield was to prevent an excessive loss of heat to the heat sink of space. Its thermal requirements differed from the upper shield because the outer surface remained at a low constant temperature due to its space orientation. Heat losses through the shield were permissible, but constant and known values had to be ensured. Initial indications were that ten layers of mylar plus an outside layer of black dacron would be sufficient. The dacron was used on the exterior because of its durability for the possible exposure to solar radiation during midcourse maneuver. The shield was constructed using the same techniques developed in the upper thermal shield. The peripheral attachments were also 0.020-in. polished aluminum angles sewn to the blanket, which, in turn, were assembled to the spacecraft by lower case screws. In the center of the shield was a large hole for installing it around the planetary science platform (Fig. 234). The perimeter of the hole was secured to the spacecraft H-frame structure which allowed the platform to protrude below the shield. The final inspection was made on the spacecraft TCM.

d. Peripheral shields (case shields). Active louver assemblies were mounted on five cases, and shielding was necessary in the many areas left exposed. The case shields had to be many sizes and shapes in order to insulate the required areas. Their purpose was much the same as that of the lower shield: heat-loss reduction to a low known constant value. Multilayer crinkled aluminized mylar was the material used. The added stiffness of an outside layer of 5-mil mylar facilitated attachment (Fig. 235). Ten layers of ¼-mil mylar and one 5-mil sheet with the mylar side out were sewn together in the same manner as the blankets. Thermally and mechanically, velcro hook and pile nylon appeared to satisfy attachment requirements. The hook portion of the fastener was bonded to the spacecraft, and the pile strip was sewn to the mylar shield. It was possible to dimensionally define and mechanically measure the case shields, and, thus, to ease fabrication and inspection.

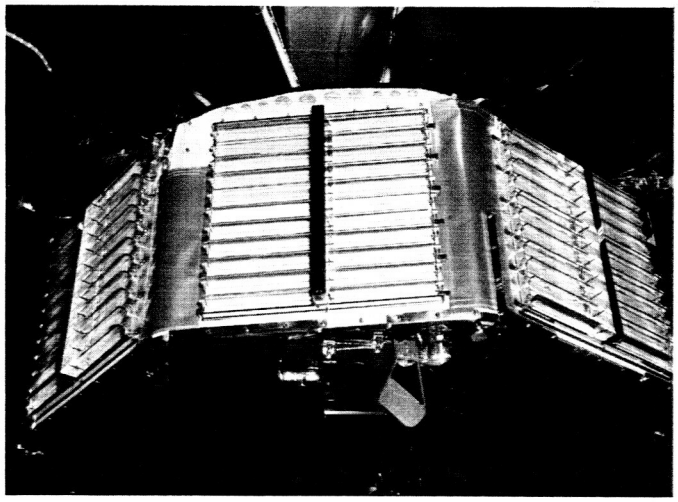


Fig. 235. Case shields

4. TCM Testing

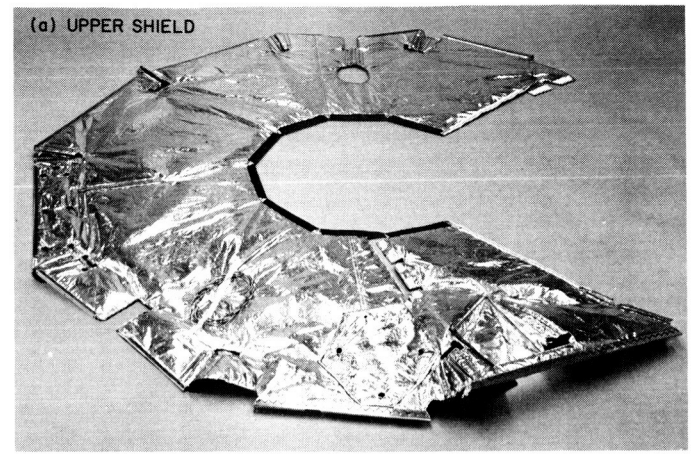
Based on calculations and *Mariner II* experience, the thermal shields were thought to be an adequate thermal control system. The *Mariner* Mars 1964 TCM

simulator tests were the most comprehensive tests in the program. Redesign, fabrication, and installation of new shield components were accomplished on an around-the-clock schedule as the thermal characteristics of the spacecraft and various shielding approaches became known. The conclusion of the first phase of testing confirmed the adequacy of the basic temperature control design. Subsequent tests, comprising ten separate configurations and 35 test modes, were conducted with the spacecraft positioned in three different Sun attitudes. At the completion of the TCM testing in the JPL 25-ft space simulator, an adequate temperature control shielding hardware design had evolved. Numerous mechanical and thermal modifications had been made in search of the desired results. Some of the major shield modifications required during the TCM test and before PTM testing are described below.

a. Upper thermal shield. This shield performed to thermal design expectations but the blanket sustained damage to the inside mylar layer during assembly. A 1-mil sheet of aluminized teflon was added to increase tear resistance shown in Fig. 236 (a). Inadequate venting of the air trapped within the blanket was noted. During the chamber pumpdown, the blanket ballooned because of internal pressure. Groups of ¼-in. diameter holes through ten layers (and staggered in successive layers) provided the necessary venting.

b. Lower thermal shield. Initially, ten layers of mylar with a black dacron exterior was found to be insufficient. Twenty layers of mylar were added, then a low-emittance outside layer of aluminum foil, all without significant change to the shield efficiency. Finally, a twenty-layer mylar shield, with a mylar outside layer, was used with successful thermal results as shown in Fig. 236 (b). The mylar, however, disintegrated during the test in which the shield was exposed to solar radiation. A 1-mil teflon outside layer, which yielded the same thermal results, was added to remedy the situation. Teflon was also added to the inside for tear resistance. Vent holes were added in the same manner as on the upper blanket.

c. Peripheral case shields. Mechanically, these shields assumed many configurations to accommodate the constantly evolving spacecraft power profile. Several methods of securing them were attempted to improve their efficiency. The use of metal clips to attach the side blankets was time consuming and presented undesired thermal-conduction paths. The number of mylar layers



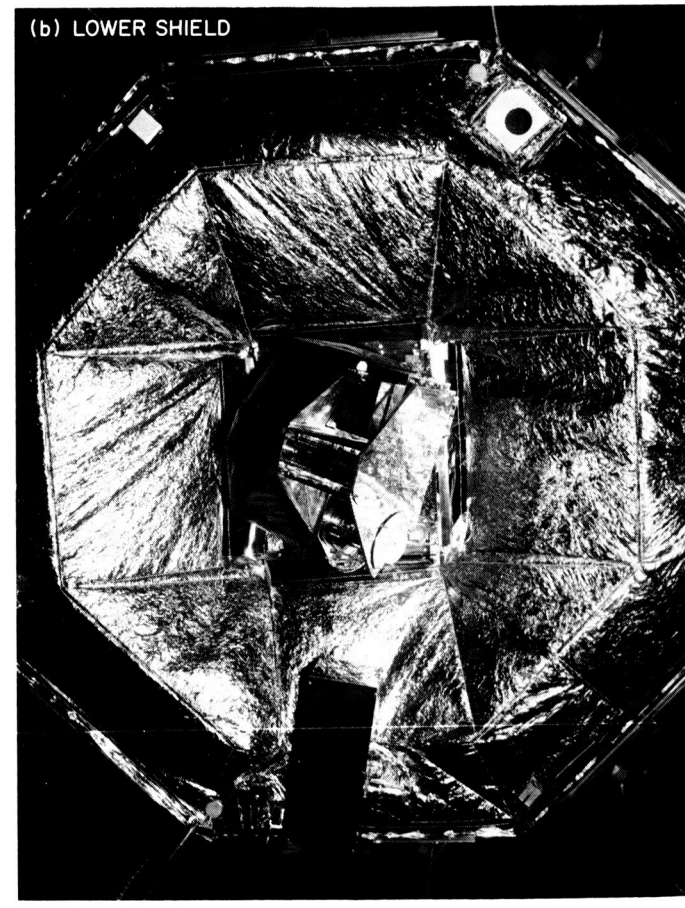


Fig. 236. Improved blanket shielding

and the outside surface emittance experienced several changes before desired results were reached. The final design consisted of metal shields made of 0.012-in.-thick polished aluminum. These shields used existing threaded holes for support, and were spaced approximately 0.30 in. from the surface of the electronic chassis (Fig. 237). The

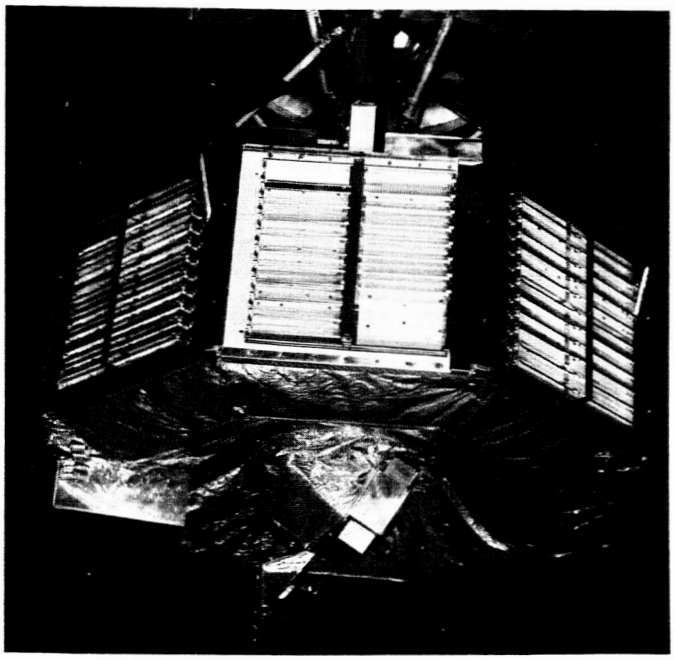


Fig. 237. Louvers and metal case shield

1-lb weight penalty incurred was justified by the mechanical simplicity and thermal repeatability of the design.

d. Planetary science shield. During the TCM simulator tests, the temperatures on the scan platform were below the minimum desired for operating limits at Mars. The uncertainty of the conduction and radiation paths required a more positive control. A turret-type redesign was necessary to form a radiant coupling between the platform and the warmer bus cavity. A multilayer mylar shield of the same construction as the lower blanket was added to the platform. The platform shield joined the lower shield with a thermal labyrinth seal that allowed platform rotation (Fig. 238 and 239). Surface finishes within the shielded area on the platform were painted a high-emittance black to aid the radiant coupling.

5. PTM Testing

All modifications that resulted from the TCM simulator tests were incorporated in the PTM. Prior to acceptance, all hardware had been structurally qualified on the STM. Minor revisions to the case shields were required during the PTM simulator tests. These changes, concerning exposed octagon side areas, were made by relocating case shields. These substitutions prompted a redesign of the case shields that allowed multiple combinations of basic side-shield components to be used wherever required. The origin of mylar flakes discovered on the spacecraft throughout the tests was traced to blanket edges. Subsequent blankets were heat-cut with a wedge-shaped soldering iron tip at 750 and 1000°F. At the conclusion of PTM testing, a flight-type acceptable temperature control shielding system was completed.

6. Flight Spacecraft Simulator Tests

The first flight spacecraft thermal tests revealed that further modifications were necessary due to internal power-profile changes. One louver assembly was added and one was relocated to another bay. Case shields were also relocated to accommodate the new configuration. The universal design of the case shields permitted repositioning without redesign.

Sun shades were added to the top of the octagon structure to minimize reflected stray light interference with the Canopus sensor. These shields modified the upper thermal blanket and resulted in large solar inputs being conducted into the bus.

Inspection of the thermal shields after the system of the tests revealed several problems. The upper thermal blanket had outgassed excessively, the dacron thread used for sewing had shrunk, exposed mylar edges had flaked because of ultraviolet exposure, and system cabling had permanently deformed the shield. Any or all of these items could be detrimental to the flight performance. Before concluding the thermal control tests, a new top blanket with black dacron bound edges was installed to prevent and contain mylar flaking. System cabling was removed and extreme caution was taken in routing the thermal test cabling.

The test was resumed and completed with successful results. The upper thermal shield shrank but caused no adverse effects. Outgassing occurred, and the spacecraft was cleaned without incident. The upper shield was considered flight acceptable as the result of ample time in the simulator, which ensured maximum shrinkage and outgassing. Subsequent tests on flight vehicles used the flight upper shield during the thermal portion only, avoiding the possibility of damage because of the additional cabling. Spare upper blankets not used in the simulator were subjected to thermal–vacuum cleaning in separate tests. This treatment consisted of installing the shield on a bus structure in a 6 × 7-ft vacuum chamber. The blanket was then heated by 250-w infrared lamps (Fig. 240) to 300°F, and cured for 24 hr at 3×10^{-5} torr. The blanket materials were successfully outgassed and preshrunk.

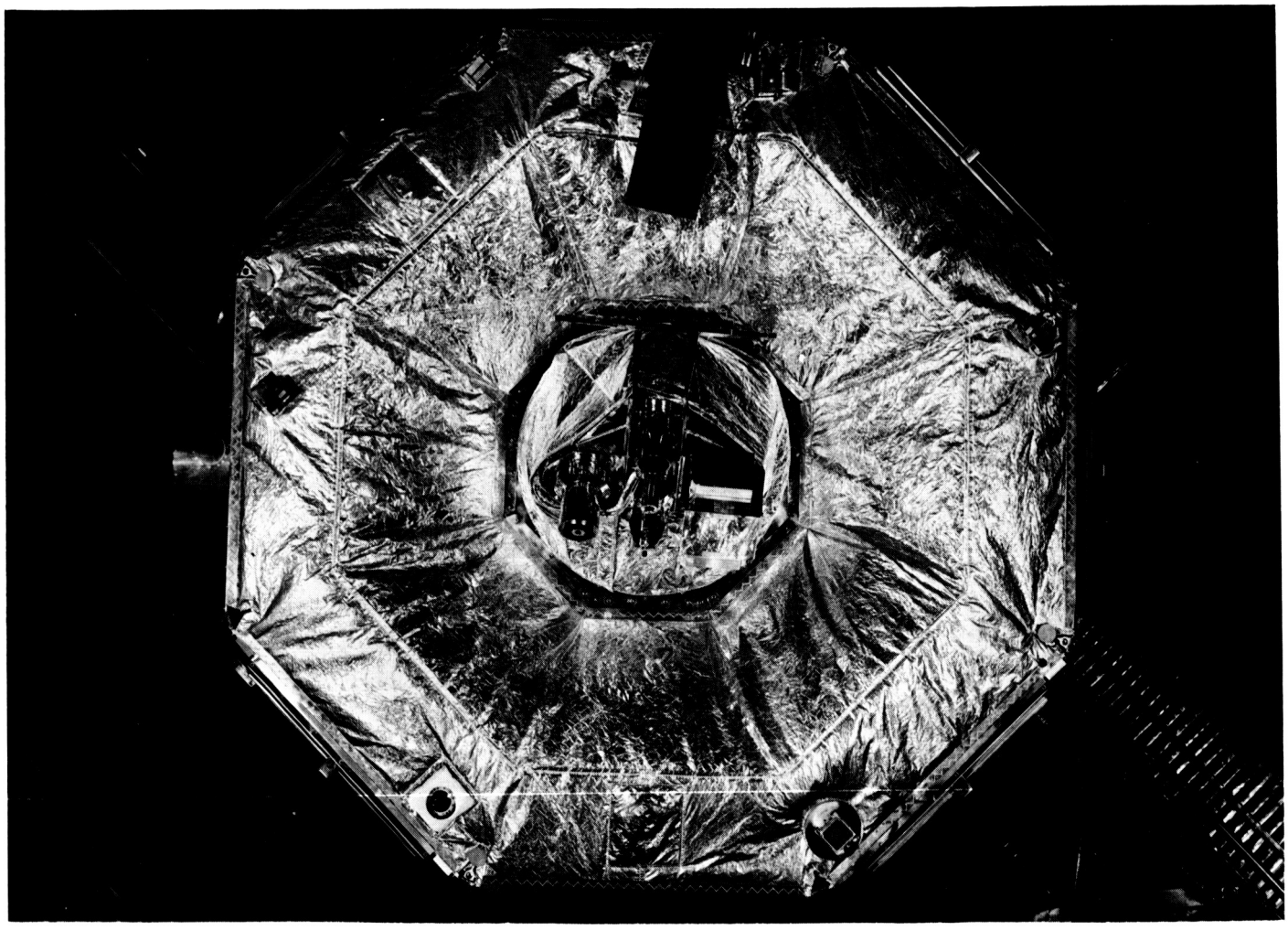


Fig. 238. Lower shield (platform turret)

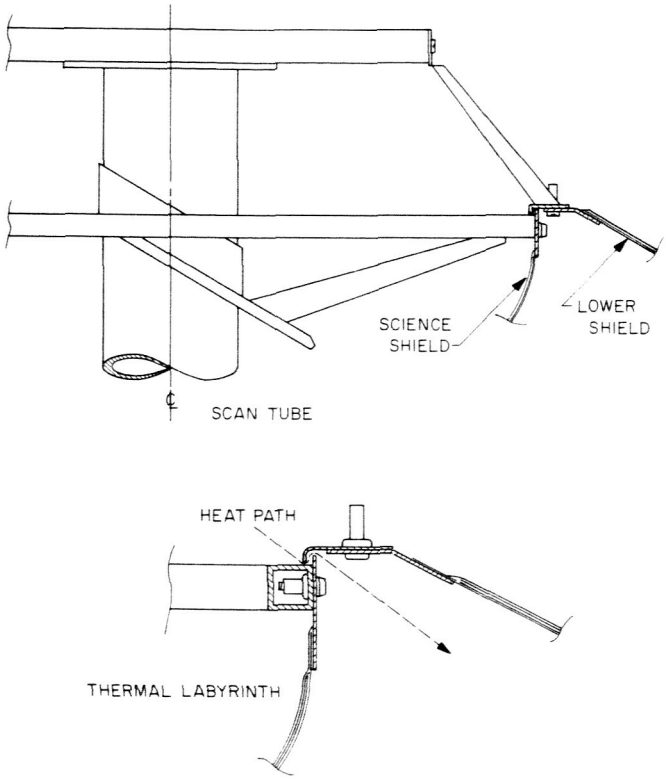


Fig. 239. Turret labyrinth seal

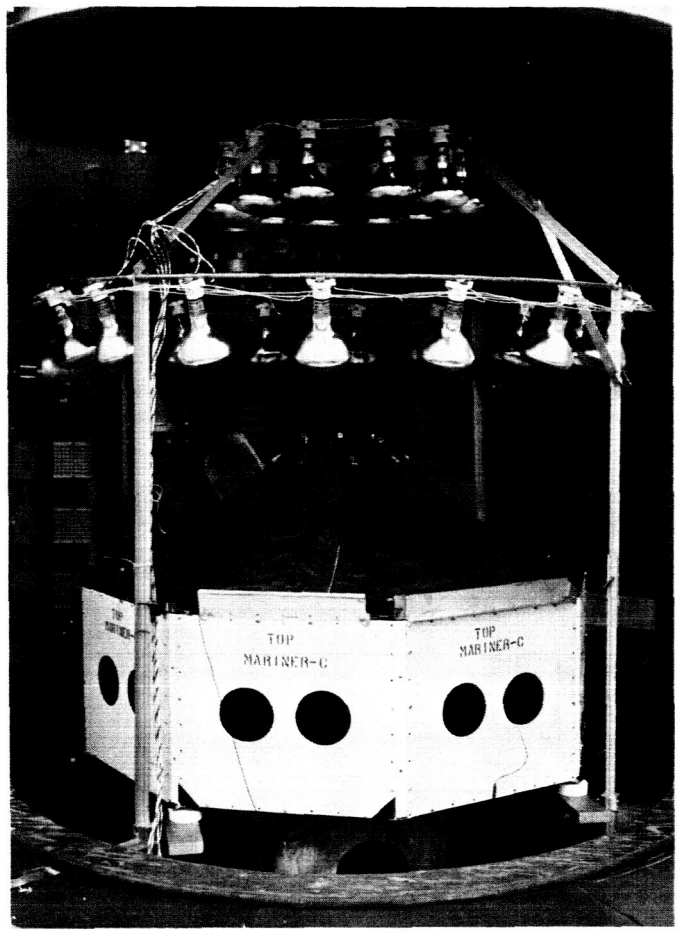


Fig. 240. Thermal–vacuum cleaning of upper thermal shield

C. *Louvers*

1. Functional Description

The purpose of the temperature control louvers is to provide an active means of controlling the spacecraft thermal environment by varying the effective emittance of the non-Sun-oriented surfaces of the spacecraft. The requirement for active control was established early in the program when it was determined that completely passive techniques could not account for the fluctuations in internal power dissipated and the change in solar intensity. As the spacecraft definition progressed, it became clear that the degree of active control necessary was dependent on the constantly changing internal power profile, and that an optimum balance of passive and active control could not have been established until late in the design phase. The resultant philosophy was to establish a single louver assembly design and to provide an adequate mounting interface with each electronic chassis. The final decision as to which electronic assemblies would require active control could have been made late in the program with a minimum effect on the system.

Based on *Mariner II* experience, louvers were selected as the active control technique with defined operating temperatures of 55°F (fully closed) to 85°F (fully open). Acceptable performance limits for the defined operating area were set at 7-w maximum dissipation at an average temperature of 50°F, to 46-w minimum dissipation at an average temperature of 90°F.

2. Design Implementation

a. General design. As ultimately defined, the *Mariner* Mars 1964 spacecraft has six electronic subassemblies fitted with temperature control louvers (Fig. 241). The louver area on each assembly is 1.4 ft², giving an approximately 8.4 ft² total active control area for the spacecraft. (*Mariner II* carried only 1.25 ft² of louvers.)

A louver assembly consists of 22 louvers driven in pairs by 11 spirally wound bimetallic elements. Separate actuators, rather than a ganged linkage, were chosen to

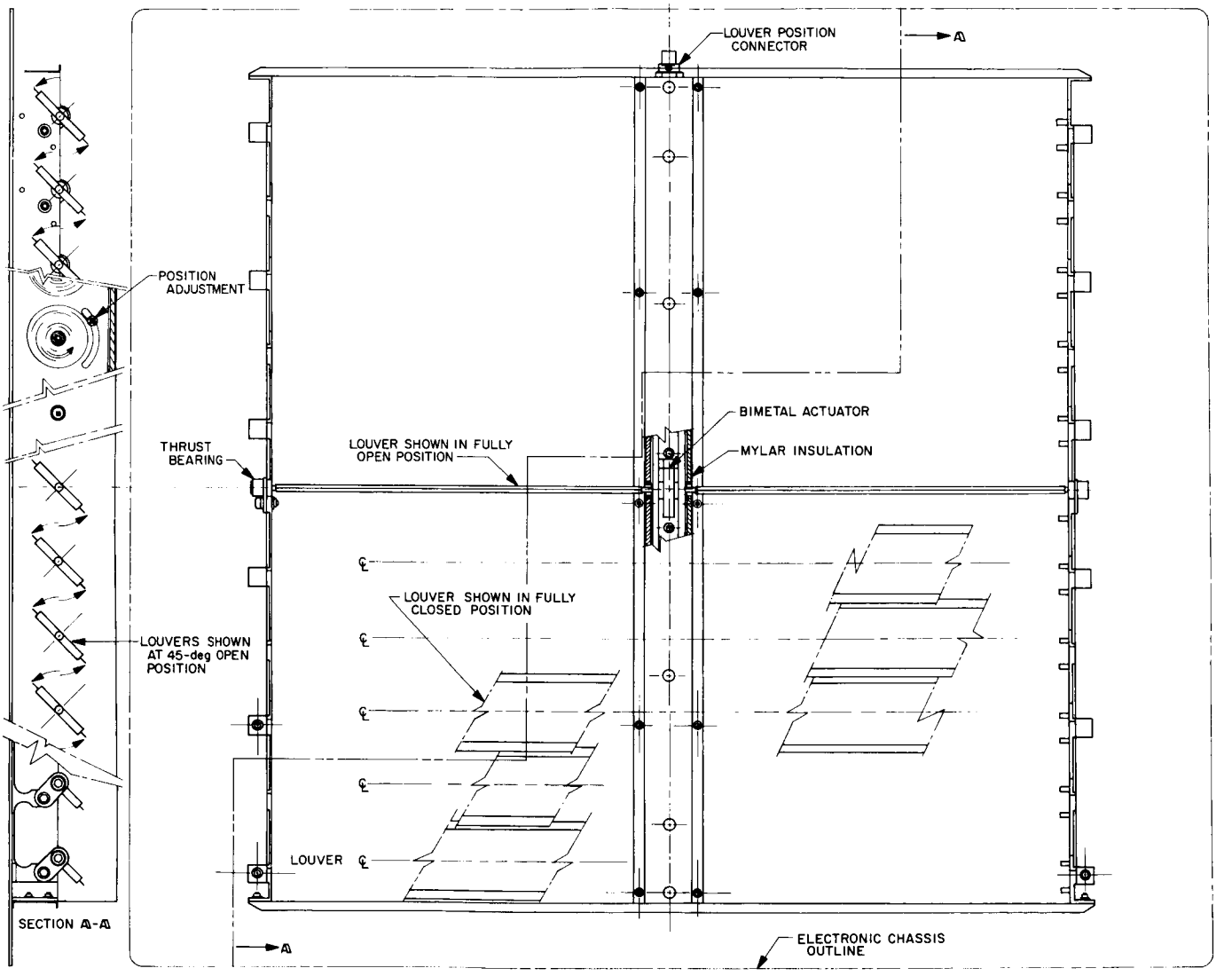


Fig. 241. Assembly view of *Mariner* Mars 1964 louvers

increase the reliability inherent in independent actuation. These driving elements are situated in a housing located down the center of the electronic chassis, and are insulated and shielded to provide radiation coupling to the face temperature of the chassis. The bimetallic actuators are sized to provide 90-deg rotation for 30°F temperature change. Although bearing friction in a zero acceleration field should theoretically be negligible, consideration for free deflection position error, under a reasonably assumed retarding torque, placed a tolerance of ± 5-deg error in position on the design. The resultant error in equilibrium temperature could have easily been ignored.

b. Bearing design. Bearings used as louver pivots consisted of a glass-filled teflon material that is machinable, dimensionally stable, and resistant to changes in friction due to the vacuum environment. The outer bearing housing consisted of the filled teflon sleeve running on a hard-anodized aluminum shaft with adjustable end play being provided by a teflon thrust pad. The inner bearing support consisted of a filled teflon spool, which was also the bimetal actuator anchor running on the hard-anodized bore of the actuator housing. The louvers were fitted with square splined nylon stub shafts that mated with the actuator spool, which thus allowed louver removal without actuator disassembly. The use of hard anodize as a bearing surface against teflon was a decision based on vacuum data, which indicated that unprotected aluminum shafts, when run in conjunction with a teflon bearing, could possibly suffer an increase in friction as the bearing became impregnated with foreign debris. As a further protection against seizure, bearing clearance was allowed to be quite sloppy (0.003 to 0.004 in. in both radial clearance and end play).

c. Structure design. Due to the large number of louvers on each spacecraft, considerable effort was expended to develop a lightweight louver. As a result of analyses and tests, the final configuration consisted of a thin-wall aluminum tube with two 0.005-in.-thick aluminum cover sheets bonded to form a narrow box section. The adhesive used was a high-strength flexible epoxy.

The resonant frequency of a single louver was found to be approximately 400 cps; however, skin thickness could not be reduced below this because of the high probability of damage from the handling necessary. A considerable weight savings was realized in the actuators by using radiation coupling in place of the heavier conduction coupling used in the *Mariner* Venus 1962 design. As a result of this change in philosophy and other weight savings, the *Mariner* Mars 1964 louver assembly weighed approximately 1.02 lb/ft² of active area as compared to the 1.73 lb/ft² for the *Mariner* Venus 1962 design.

d. Position transducer design. As a crude indication of proper louver operation, angular position telemetry was provided on the center louver actuator in the form of a semiconductor strain gauge. To be compatible with the telemetry channel input, a high-gain 500 Ω gauge was bonded to the bimetal element and calibrated to give approximately 80 Ω variation when the bimetal was flexed the equivalent of 90 deg at the shaft. Since these semiconductor gauges are extremely temperature-sensitive, it was necessary to calibrate each assembly in several failure mode louver positions and to correlate the resultant reading with the chassis temperature transducer. The estimated accuracy of the engineering measurement was therefore approximately ± 15 deg.

e. Assembly installation. Due to the fragile nature of the assembly, numerous attaching screws were used to align the louver frame to the electronic chassis. Louver blades were then installed individually when a test or flight buildup was scheduled. This procedure was later altered to incorporate a ground handling protective cover, which was installed on the completed chassis buildup after it was concluded that damage was likely if the louvers were repeatedly handled. Figure 242 shows the louvers installed on the spacecraft.

3. Test Experience

Following the initial development tests to prove the adequacy of the bearing and louver blade design, 41

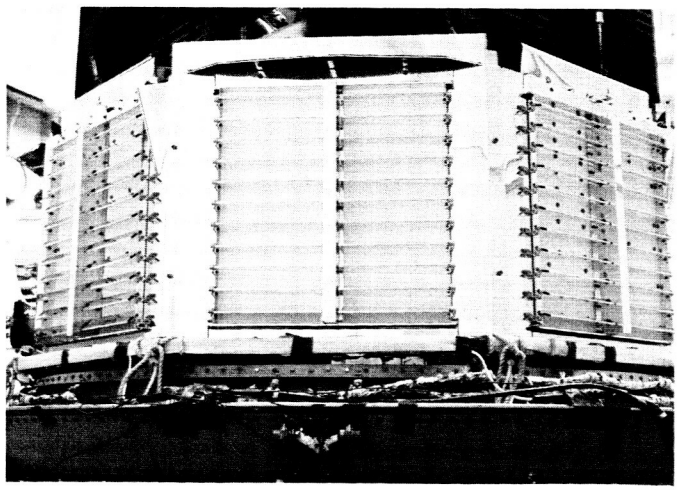


Fig. 242. Louvers installed on spacecraft

louver assemblies were fabricated and subjected to the appropriate type-approval and flight-acceptance tests. No structural failures resulted from any of these tests. Functionally, louver performance was within the specified limits with the measured power dissipation for the TA assembly at 6.9 w at 55°F (fully closed) and 52.6 w at 80°F (fully open).

Later TCM tests indicated that not only were more than the five originally anticipated louver assemblies required, but also the internal power distribution necessitated that four of the six assemblies be recalibrated to be fully closed at 60°F instead of the originally specified 55°F. The standard louver assembly configuration and the adjustable range actuator allowed these changes to be made with no design change or retesting required.

Later verification during vacuum-simulator tests of the flight spacecraft indicated that the redefined quantity and temperature range was satisfactory. The early flight data on *Mariner IV* has confirmed proper operation with the chassis temperature and corresponding louver position telemetry in direct agreement.

D. Surface Finishes and Materials

The overall thermal design and temperature control surface selection approach was basically conservative. Margins for uncertainty in surface property measurements and behavior in space were allowed, both in design and surface selection. Exotic, unproven, irrepairable, and easily damaged materials were not considered for use. For example, vacuum-deposited aluminum has properties somewhat superior to those of polished aluminum surfaces. However, the cost of repair in dollars, schedule, and component reliability in the event of damage, far outweighed the advantages of using vacuum-deposited aluminum. The validity of this conservative philosophy in surface selection was verified during testing when a space simulator incident deposited substantial amounts of oil on the MC-4 spacecraft thermal surfaces. Nearly all of the surfaces involved could have been, and were, adequately cleaned to ensure reliable mission performance.

1. Surface Selection Criteria

The criteria for selecting temperature control coatings included the proper combination of radiative properties and reliable behavior in the space environment as well as satisfactory performance in the terrestrial environment. The latter criterion includes durability and cleanability for handling, behavior in a simulator, and behavior in space as affected by prelaunch conditions. While severe terrestrial conditions were not considered (i.e., long outdoor exposure or salt spray), the problems connected with fabrication, handling, and assembly were real constraints. For example, bare aluminum can generally be used without surface protection, while bare silver, although satisfactory in the space environment, will tarnish in the terrestrial environment. Many surfaces (such as the exterior surface of the chassis) were painted before the installation of components, component testing, spacecraft installation, and final testing. Thus, there was ample opportunity for damage to the temperature control surface or contamination thereof that could result in poor performance in space.

While not a general constraint, response to simulator spectrum mismatch was considered in the design, and was the basis for the selection of rhodium plate instead of gold plate on the attitude control jets.

2. Applications

a. Metals. Bare metals such as aluminum, silver, gold, and rhodium have low solar absorptance, low emittance, and, therefore, behave as thermal isolators in minimizing both the absorbed solar energy and the energy radiated from the vehicle to space. Metallic surfaces other than aluminum (e.g., magnesium, copper, stainless steel) are normally gold-plated to provide either low emittance, corrosion protection, or both. These surfaces can then be painted to increase the absorptance or emittance as required.

In the case of the attitude control jets, a lower emittance was required than was obtainable from bare stainless steel, and it was planned to establish the temperature control design from simulator tests. Therefore, rhodium plating was selected in preference to gold, since it was a thermally grey metal and, therefore, much less sensitive to simulator spectrum mismatch than gold.

b. Conversion coatings. A commercial conversion coating designated Dow 7 was used on machined magnesium parts in which a high emittance was desired or emittance was unimportant to the thermal design. The process was controlled by matching material being coated to a color reference sample known to produce a minimum emittance of approximately 0.70. In addition to this minimum emittance, the conversion coating provided a degree of corrosion protection.

A brush-on conversion coating designated Dow 19 was used for repair and touch-up of remachined areas. Since

the Dow 19 provided a very thin coating, emittance of approximately 0.2 resulted. Its use was limited to situations in which, either by reason of the thermal design requirements or due to the small area ratios involved, this low emittance was not a detriment. The Dow 19 low emittance, and the degree of corrosion protection provided, was used to advantage on the areas adjacent to the spacecraft feet that mated with the *Agena* adapter. A low emittance was desirable to minimize heat loss from those areas.

Instrument design and calibration of the Ionization Chamber required that temperature control be achieved without adding significantly to the particle absorption properties of the sphere. A conversion coating for the stainless-steel ball was used to produce an $\alpha_s \approx 0.90$ and $\varepsilon \approx 0.70$. It permitted satisfactory temperature control without adversely affecting the instrument performance. Because this was a passive conversion coating, the properties produced were extremely sensitive to initial metal surface conditions. In order to provide reproducible uniform properties, the surface was liquid-honed prior to application of the conversion coating.

c. White paints. Faces of the basic chassis, under the louvers, required only a high emittance for cruise conditions. However, it was necessary to minimize the solar load input during pre-Sun acquisition and midcourse maneuver operation. This could have occurred when sunlight fell on the faces of the chassis. Since the maximum exposure time was less than 10 hr, long-term ultraviolet stability was not a prime concern. The original thermal design included the use of an inorganic white paint on the chassis faces. This inorganic paint was primarily developed for ultraviolet stability and had a low solar absorptance and a high emittance. After painting the initial TCM hardware, it became apparent that extreme precautions would be required in order to provide reliable adherence to the large surface areas. Reevaluation of the thermal requirements indicated that an organic paint with a slightly higher solar absorptance and somewhat lower emittance, but with far superior adhesion and durability properties, would perform satisfactorily. This paint was subjected to ultraviolet tests and found also to be suitable in some sunlit applications for the Mars mission spacecraft, including the high-gain antenna feed and the Solar Plasma Probe. The inorganic white paint was used only on the Cosmic Ray Telescope radiator in which the extremely high emittance and low solar absorptance was critical to the instrument operation.

d. Black paints. The back sides of the solar panels were originally painted with a satin-black polyurethane paint, which had been successfully used on both the *Mariner* Venus 1962 and *Ranger* programs. Subsequent problems with stray reflections into the Canopus sensor required that the paint be changed to a gloss black. Since some of the panels had already been painted, they had to be recoated with gloss black in order to provide the required texture.

Most of the internal components of the spacecraft were coated with a flat-black epoxy paint. This material had a high emittance and therefore provided maximum radiation coupling internal to the basic spacecraft structure.

e. Other paints. Metal-filled paints have a solar absorptance to emittance ratio approximately equivalent to that of black paints. However, since both the solar absorptance and emittance metal-filled paints are substantially lower than that of black, thermal transients during an eclipse period are substantially reduced. Since the properties of the paint used were sensitive to handling, the applications were restricted to the areas that could either be adequately protected from damage or readily repaired.

The high-gain antenna presented an interesting temperature control problem. It was necessary to maintain the maximum temperature below the limits of the adhesive used in the honeycomb fabrication and to provide optimum temperature for minimum thermal distortion at planet encounter. The surface coating also had to be able to avoid concentrating reflected solar energy on the antenna feed if the Sun should become incident along the parabolic axis.

A black paint would have produced temperatures in excess of the structural limits of the antenna at launch, and a white paint would have resulted in low temperatures with accompanying thermal distortion at Mars. Poor lateral thermal conduction of the thin-gauge skins eliminated the possibility of a practical mosaic approach. Greys formulated with combinations of white and black pigments were difficult to control in addition to being subject to ultraviolet darkening in space.

It had been reported that chrome oxide pigmented paints have a solar absorptance of approximately 0.70 (the desired value) and are stable to ultraviolet. A special chrome oxide pigmented polyurethane paint was formulated. In addition to the proper radiative properties, a primary criterion for selection was that certain characteristic spectral reflectance properties exist in the 4000 to 6500 A region, particularly in the reflectance peak at 5000 to 5500 A. Ultimately, this material was used on the front face of the high-gain antenna dish as

well as on the omnidirectional antenna ground plane and the Ionization Chamber Sun shade.

f. Shield materials. An initial thermal design constraint was that the outer layer of the upper thermal shield be insensitive to differences between solar and simulator energy distribution, and that it not produce appreciable reflected thermal inputs to other portions of the spacecraft. Since the preliminary design of the spacecraft superstructure required that the upper thermal shield conform to a compound curvature, coated fabrics were not initially seriously considered. Pre-formed black polymeric materials, which could withstand the temperatures produced by an insulated black surface (approximately 260°F), were considered for this application. However, when the superstructure design was finalized and the compound curvature eliminated, a tailored fabric approach to the upper thermal shield became more practical than the pre-formed teflon concept. Samples of a dacron fabric coated with a black-pigmented silicone rubber were obtained and evaluated. It was found that the coated fabric contained substantial amounts of volatile materials, and it was necessary to precondition the material prior to fabrication into thermal shields. Subsequent chamber testing revealed that this preconditioning was not sufficient to completely outgas the material, and additional conditioning was performed on the fabricated shields.

While minimum emittance would have been desirable on the outer layer of the lower thermal shield, the possibility of incident solar energy during maneuver prevented the use of aluminized polymer films with the aluminum side as the external surface. Therefore, it was necessary to provide an outer layer that would have at least a moderate emittance. It was estimated that ½-mil aluminized teflon would have an emittance nearly equal to 0.40 and would be suitable thermally. However, ½-mil film has poor tear resistance and is extremely difficult to handle. Therefore, 1-mil aluminized film with emittance nearly equal to 0.60 was used as a suitable compromise of acceptable physical properties and moderate emittance.

It was originally planned to wrap all cabling external to the basic structure with aluminized mylar strips with the aluminized side out. This configuration resulted in a minimum absorbed solar energy and minimum radiation to space. A fortunate accident occurred when part of the cabling on one of the flight spacecraft was wrapped with the mylar side of the strip out. The ultraviolet radiation in the space simulator resulted in catastrophic disintegration of this material. Further investigation revealed that the tape with the aluminum side out had also been embrittled, which indicated a potential problem in this area. The damage was apparently due to penetration of ultraviolet through discontinuities in the aluminum film. These discontinuities resulted from local damage to the aluminum film during tape application to the spacecraft cabling. As a substitute, aluminum-coated pigmented tedlar appeared to be a logical choice. It was known that tedlar was less sensitive to ultraviolet physical damage than mylar. Commercially available white tedlar contains a pigment that is a strong absorber of ultraviolet. Therefore, any ultraviolet radiation that could penetrate the aluminum coating would be stopped in the very shallow depth of the film and would not be permitted to penetrate and create physical damage at any significant depth. Extensive tests verified the suitability of this solution, which was the one chosen.

E. Absorptivity Standard

1. Background

One of the problems that was recognized with the *Ranger* and *Mariner* Venus 1962 spacecraft designs was the difficulty encountered in interpreting the temperature data that was collected during flight in order to aid in the design of later spacecraft. With the limited number of measurement channels, it was possible to determine only the condition of the spacecraft and to indicate the adequacy of the temperature control subsystem. For example, it was clear that the *Mariner II* flight temperatures were much higher than expected (based on analysis and testing in a space simulator), yet, from the data that was received, it was not possible to actually isolate the cause of the problem. A number of effects or combination of effects could have caused the same observed condition.

In the *Mariner* Mars 1964 design, two steps were taken toward solving the problem. First, a significant increase in the number of temperature measurement channels was made possible by further subcommutating the data encoder. The time interval between data samples was increased considerably, but this was not considered to be a severe compromise because the temperatures during the long cruise to Mars would change very slowly. The second step taken to improve the data reduction capability provided a means of separating the variables associated with the spacecraft temperature. The temperatures depended basically upon three things: (1) the internal power dissipated by the electronics, (2) the amount of

energy radiated to space, and (3) the amount of energy absorbed from solar radiation. There was already a significant number of measurements that would have indicated the status of the various subsystems of the spacecraft and given an indication of how much electrical power was being consumed. The energy emitted from the spacecraft was primarily through the electronic bays and this was regulated by thermostatically actuated louvers. One louver blade of the set on each of three bays was instrumented to telemeter the opening angle, with care taken not to degrade the performance of the individual blades. Based upon ground tests, it would have been possible to estimate the heat radiated to space. From the louver position readings and the electrical power measurements, it was anticipated that the problems associated with these two variables, which might have affected the temperature control subsystem, could be identified.

The solar radiation absorbed was the largest thermal input to the spacecraft temperature control subsystem, particularly the appendage items to the bus, and, unfortunately, was the most difficult to determine. To give a positive measurement of this input, an instrument was designed to measure the energy absorbed by typical surfaces used on the spacecraft. The case of an insulated flat plate in sunlight was selected as being the most useful measurement within the scope of a number of constraints that were imposed. With a sample surface radiatively and conductively removed from the spacecraft, it was possible to isolate the effect of the solar radiation on the temperature control of surfaces.

2. Design Constraints

It was necessary to recognize the relative importance of this instrument, later named the absorptivity standard, in the design of the spacecraft. Although valuable for evaluating the performance of the temperature control subsystem, the absorptivity standard would probably not provide any inflight information that would improve the chance of a mission success. A possible exception to this was the case in which one spacecraft was launched and a temperature control problem was observed before the second spacecraft was launched. However, when considering the difficulty of adjusting anything on the spacecraft during the relatively short launch opportunity, this possibility appeared to be unlikely. With the relative importance on the spacecraft determined to be secondary to mission success, a number of other constraints logically followed. If the absorptivity standard had begun to compete with more such important areas as the temperature control of the spacecraft due to weight, schedule, or manpower requirements, its priority would clearly have been secondary. This priority, in turn, would have demanded that any interface with the spacecraft be minimal. Specifically, no special circuitry was to have been required by the data encoder, no electrical power was to have been used, the weight was to have been limited to approximately 1 lb, and it was generally not to compromise the spacecraft design in any way. In addition, the instrument was required to meet the type-approval, flight-acceptance, and quality-assurance standards required of any flight item.

The encoder constraint dictated that its interface be identical to the other standard temperature measurements. A major problem turned out to be associated with the uncertainties in the standard flight-temperature measurements. An initial investigation of the accuracy required of the temperature measurements precluded any significant absorptivity data. Subsequently, a method was conceived that permitted a limited number of flight-temperature measurements to the precision required. This was accomplished by telemetering the action of a thermostat rather than by a direct measurement of temperature. Within the weight constraint of approximately 1 lb, it was possible to measure the absorptance of four samples. A black sample was included as a measurement of the intensity of the solar radiation and to provide information on the stability of Cat-a-lac black paint after prolonged exposure to the space environment. A sample of the most stable JPL white paint was included because of the rather large uncertainties associated with that type of surface. White surfaces are known to yellow after prolonged exposure to ultraviolet, but the magnitude of such a degradation is not known. A sample painted with aluminum silicon paint was included for similar reasons, and also because it would give an indirect indication of the temperature of the attitude control jets located at the tips of the solar panels. The fourth sample was one of polished aluminum, which was included primarily because of its wide use on the spacecraft as a temperature control surface. It was also included as a verification that the ground test with ultraviolet, proton, and electron bombardment of these surfaces was valid.

3. Detail Design Description

Ideally, each sample surface should have been a flat plate that absorbed solar radiation and emitted radiant energy from the front face only (i.e., perfectly insulated on the edges and the back). The absorptivity standard was designed to isolate the sample surfaces from radiation and conduction influences of the spacecraft. The

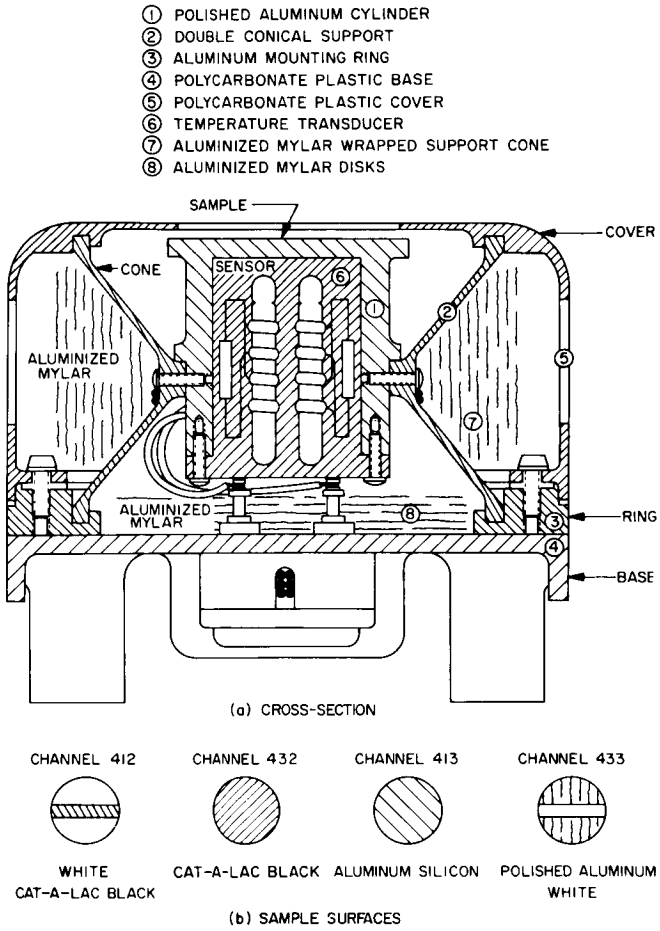


Fig. 243. Absorptivity standard

sample surface in Fig. 243 is located on the end of a polished aluminum cylinder, which encloses the temperature transducer. The sample cylinder was mounted in a double conical support. Resistance to conduction was achieved by providing lightening holes in the cones and fabricating the support from plastic. Lexan, a polycarbonate plastic, was chosen for its high strength and low conductivity. All lexan parts were coated with vapor-deposited aluminum to achieve a low emissivity.

The support cones were sandwiched between the lexan cover and the aluminum mounting ring. The cover served to block radiation (from sources other than the Sun) from reaching the sample. In addition, the lip overhanging the sample surfaces prevented stray and reflected sunlight from reaching the cavity between the sample cylinder and the support. The four sample assemblies were mounted in a row on a lexan base, which, in turn, was located on the spacecraft upper ring structure above Bay I (Fig. 29).

The sunlit areas of the covers and base were painted to give temperatures close to the sample temperatures in order to reduce gradients and, therefore, heat exchange with the sample. To reduce radiation interchange within the sample assemblies, the support cone was wrapped with aluminized mylar, and disks of aluminized mylar were laid on the base. The wires from each sensor were wrapped around the support structure to prevent any heat losses through the wires from originating within the sensor itself.

The temperature sensors were each composed of four mercury thermometers and 13 precision resistors encapsulated in a glass-filled potting compound. Each thermometer had four platinum wires passing through the glass wall to the capillary passage. Each thermometer was pressurized to 200 psi with hydrogen to reduce vibration sensitivity. The outer ends of the platinum wires were connected to rings, to which the circuitry was soldered. A typical sensor circuit is shown in Fig. 244. Combinations of 5, 10, and 15 Ω resistors bridged adjacent rings of each thermometer, and the thermometers were wired in series with a 500 Ω resistor. As the sensor cooled or heated, the mercury in each thermometer receded or advanced, progressively making contact with fewer or more platinum wires. When the mercury thread bridged two wires, it shorted out the connecting resistor. Because the temperature at which the mercury touched or withdrew from a wire was known to 0.1°F, the step

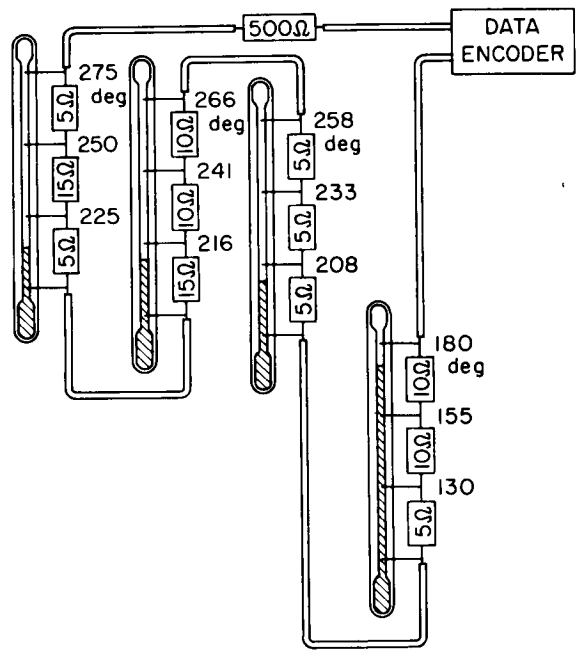


Fig. 244. Typical absorptivity standard sensor circuit

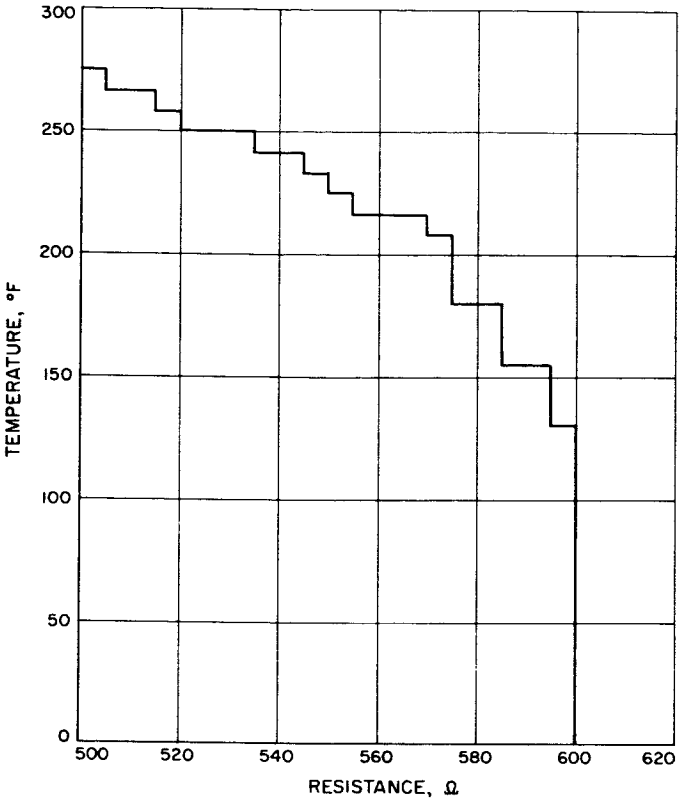


Fig. 245. Sensor signal vs temperature

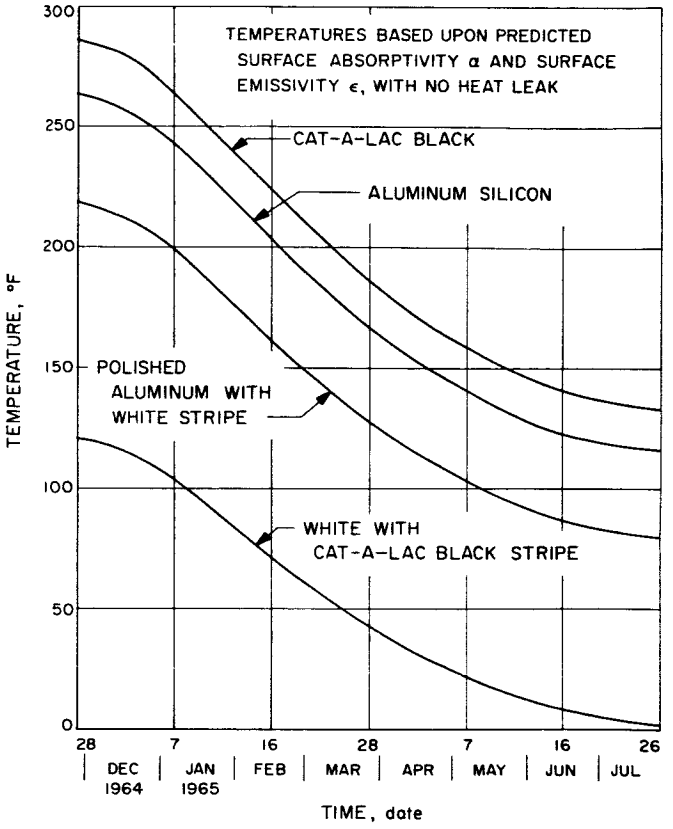


Fig. 246. Predicted temperature history of ideal flat plate samples

change in resistance of the sensor signaled a specific temperature. With three such steps per thermometer, a total of 12 temperature points per sensor was provided (Fig. 245). The total resistance range of each sensor was 500 to 600 Ω, which was compatible with the data encoder constraint.

The four samples, as mounted on the absorptivity standard, are shown in Fig. 243. A black stripe was added to the white sample to raise the temperature sufficiently to prevent freezing of the mercury in the thermometers as the spacecraft receded from the Sun. A white stripe was added to the polished aluminum to decrease the sample temperature at the Earth solar intensity to a level compatible with the polycarbonate plastic. The predicted temperature histories for ideal flat plate samples are shown in Fig. 246.

4. Early Flight Results

The data up to the midcourse maneuver demonstrated that the absorptivity standard on *Mariner IV* was performing properly. All data numbers seen following launch and during midcourse were of nominal values and in the proper order. Two data points were seen during the steady-state cruise between launch and midcourse. The white sample warmed up one data step, although the solar intensity was decreasing. This was indicative of an increase in the solar absorptance of the white paint, and was substantiated when the polished aluminum sample also warmed one data step. The degradation of its white stripe more than offset the decrease in solar radiation intensity.

XVII. SPACECRAFT SUBSYSTEMS: ELECTRONIC PACKAGING AND CABLING

A. Packaging Design

The packaging program objectives were to develop a structurally efficient, compact, and highly flexible design for the spacecraft electronic equipment, and, in addition, to develop techniques for mounting and interconnecting electronic components to provide the capability of surviving the rigors of launch and flight environments.

The structural efficiency in electronic packaging was obtained through an integrated design. Electronic equipment subchassis provided mounting and interconnecting planes for the electronic components and stiffened the electronic assembly chassis. The electronic assemblies, together with the spacecraft frame, formed a rigid octagonal electronic equipment compartment.

The electronic-equipment design flexibility was obtained through standardized assembly and subassembly configurations. The electronic subassemblies were of standard profile, which allowed them to be located in any assembly of the electronic equipment compartment. The spacecraft packaging layout is shown in Fig. 247 and 248. Thus, with profile established, the subassembly and subsystem packaging design proceeded independently of final location in the spacecraft. Different packaging techniques or different cordwood module and component sizes were readily accommodated by varying the subassembly width.

B. Subassembly Development

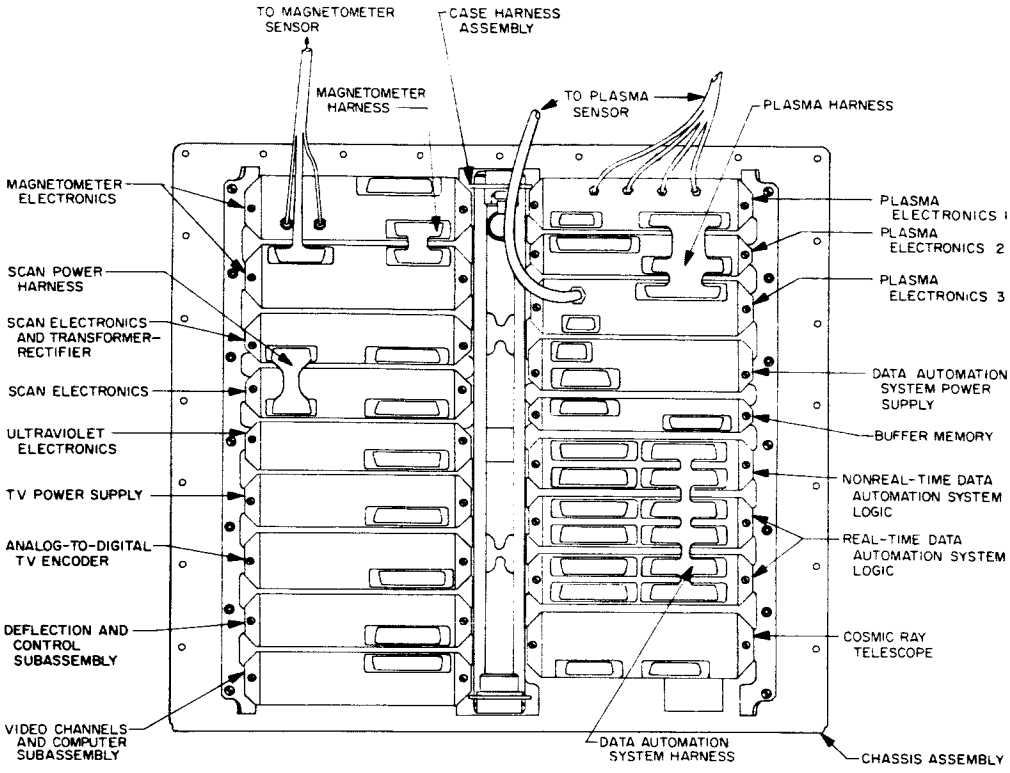
Within the above packaging constraints, two types of basic electronic subassemblies were considered. Each had the same basic subchassis structure but differed in interconnecting cabling technique. One type (used on *Ranger* and *Mariner* Venus 1962) required a flexible cable harness to the subassemblies for electrical interconnections. The other type (developed for *Mariner A* and *Mariner B*) had the interconnect harness fixed to the assembly chassis and the subassemblies plugged into the chassis cable assembly. The plug-in technique was favored because it would have eliminated the need for flexing the cables and ensured straight mating of connectors through guide pins. However, the requirement to use as much equipment designed for the *Mariner* Venus 1962 spacecraft as possible led to the final selection of the *Mariner II* type subassembly construction, as shown in Fig. 249. Although this figure shows components on printed wiring boards, the cordwood packaging techniques were readily adapted to the same basic configuration.

C. Electronic Assembly and Chassis Development

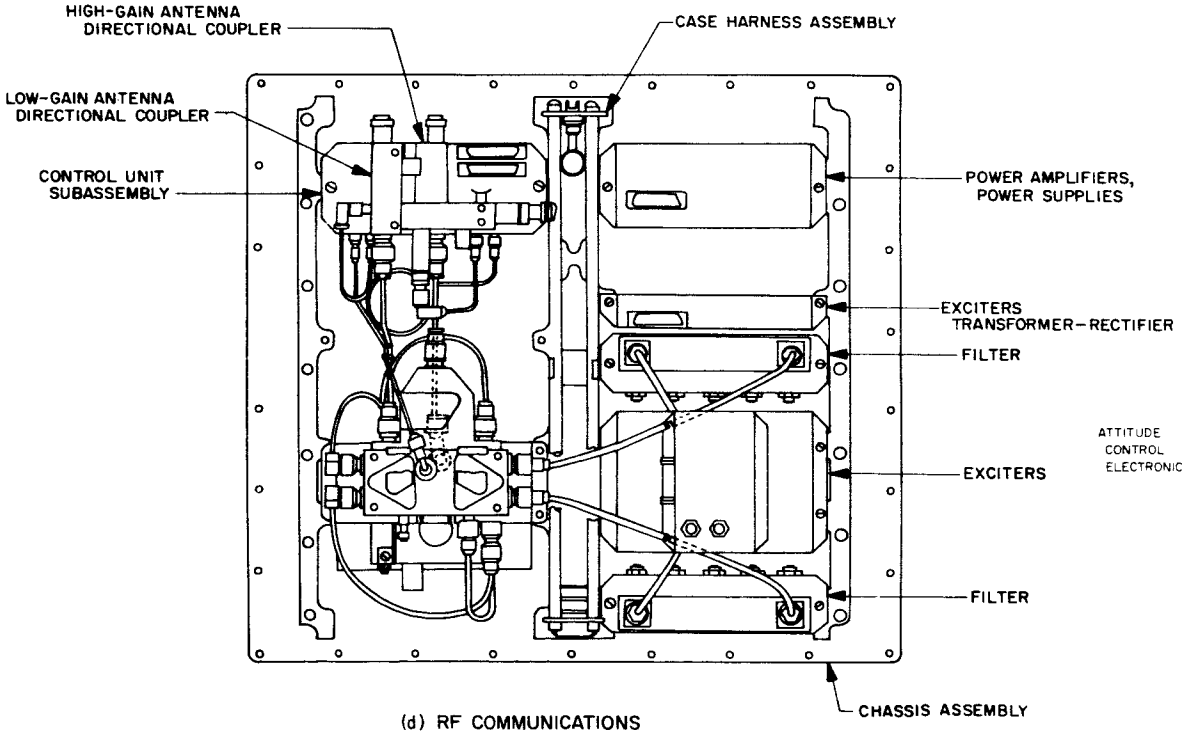
In previous spacecraft, the electronic subassemblies were mounted as gussets in a pan-shaped assembly chassis and then bolted to the spacecraft on a single mating surface. In *Mariner* Mars 1964 spacecraft, further structural integration of electronic subassemblies was accomplished by using open-ended chassis, which improved the structural efficiency by eliminating redundant structures. The assemblies were placed inside the frame and were bolted to the frame on external peripheral and internal mounting flanges.

During the early spacecraft development, magnesium and aluminum chassis were evaluated in two center-section configurations: the T-section and the flight box-section. The first vibration tests were conducted on a rigid fixture (Fig. 250) to evaluate the relative advantages of these materials and configurations, and to determine the chassis wall thicknesses. The test results indicated that the rigid vibration fixture provided such an overriding support to the chassis that the various chassis geometry and materials made little difference in the vibration responses within the subassemblies. Schedule requirements forced a conservative design selection of the 0.100-in.-thick wall magnesium center box-section configuration.

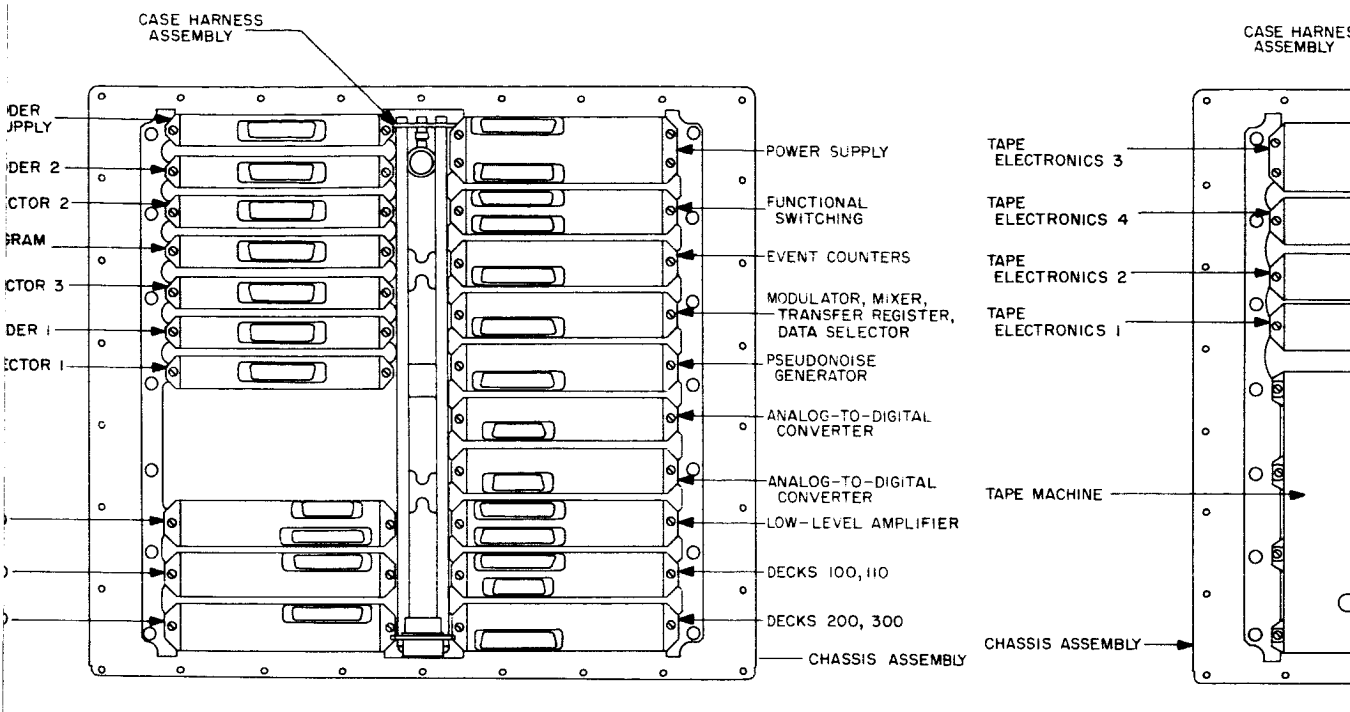
A new fixture was fabricated using spacecraft structural rings and simulating the stiffness of half of the octagonal electronic-equipment compartment. In this fixture, tests were continued to determine the effects of chassis lightening. In successive steps, the base wall thickness was reduced in local areas to 0.050 in., the mounting flanges were radiused around the fastener attach points, and holes were added to the four webs, which reduced the chassis weight by 19%. The lightened chassis is shown in Fig. 251. Repeated tests showed only small changes in acceleration levels at resonance between the light and heavy chassis. These tests indicated that some of the material remaining was not needed, but further lightening was restricted by machinability and fragility in handling. Observations were made (by means of a stroboscopic light) during the tests, and acceleration measurements were taken. The results indicated that the vibration environment within the subassemblies was



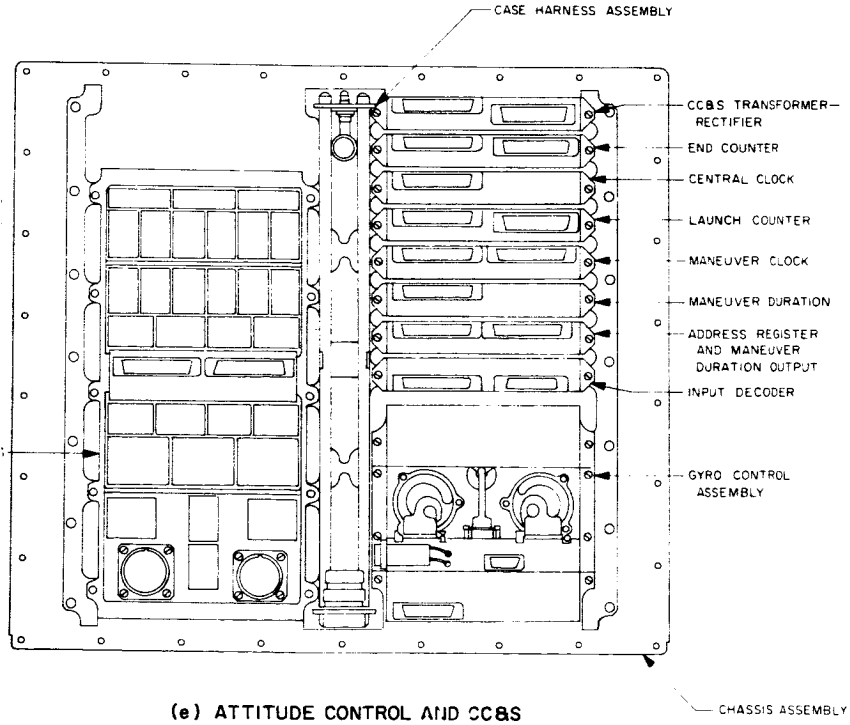
(a) SCIENTIFIC EQUIPMENT ELECTRONICS ASSEMBLY



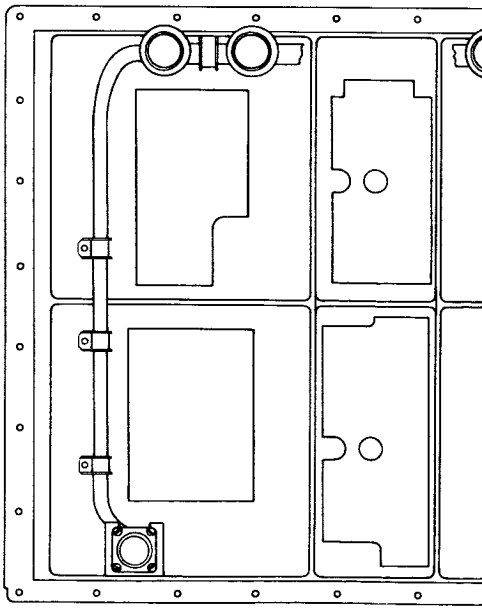
(d) RF COMMUNICATIONS ELECTRONICS ASSEMBLY



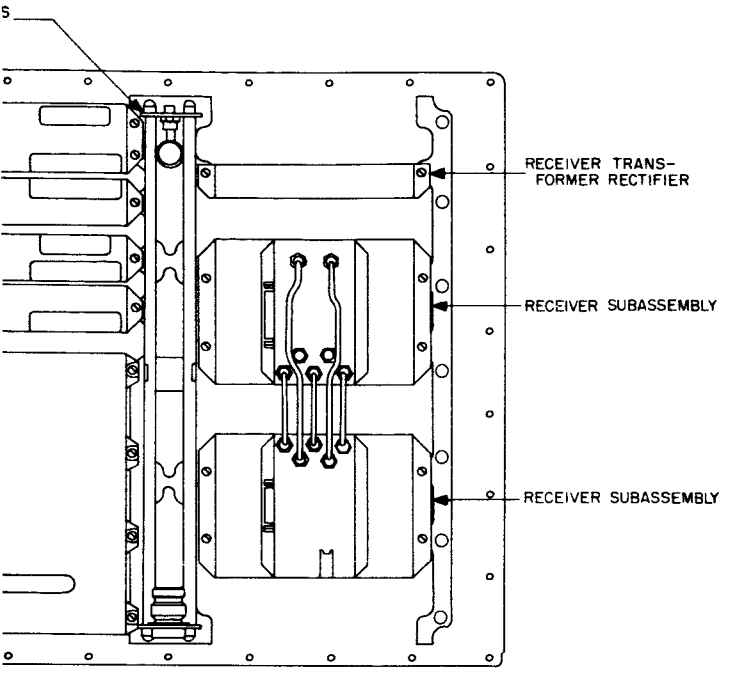
(b) DATA ENCODER AND COMMAND ELECTRONICS ASSEMBLY



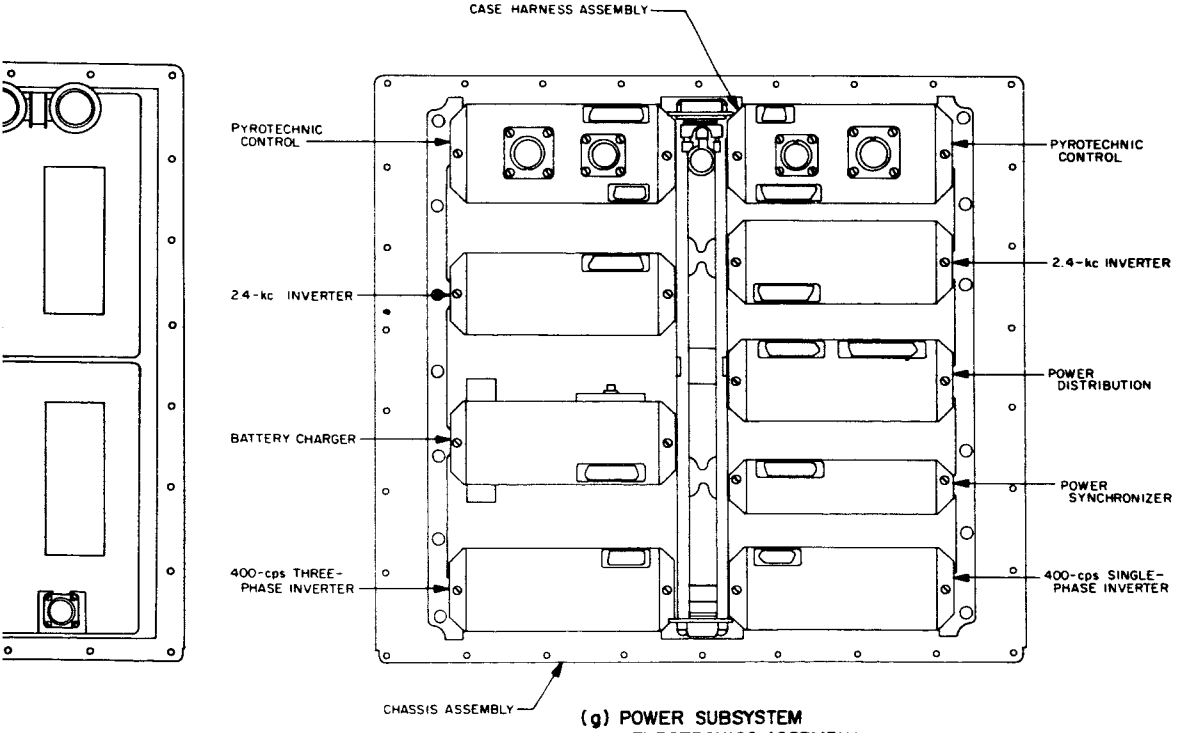
(e) ATTITUDE CONTROL AND CC&S ELECTRONICS ASSEMBLY



(f) POWER REGULATOR ELECTRONICS ASSEMBLY



(c) RECEIVER AND TAPE MACHINE ELECTRONICS ASSEMBLY



(g) POWER SUBSYSTEM ELECTRONICS ASSEMBLY

Fig. 247. Subsystem electronic packaging

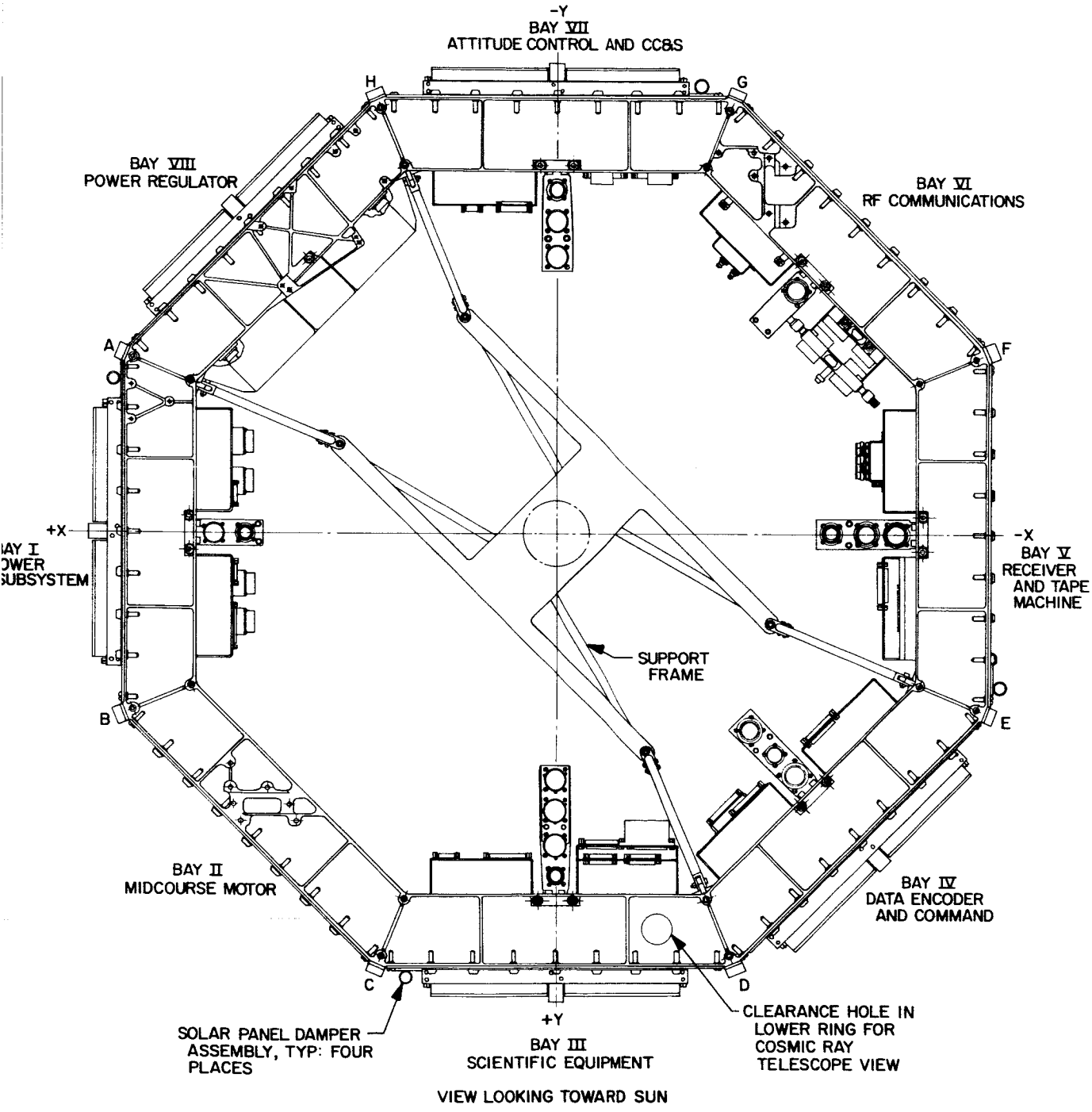


Fig. 248. Spacecraft electronic packaging viewed toward Sun

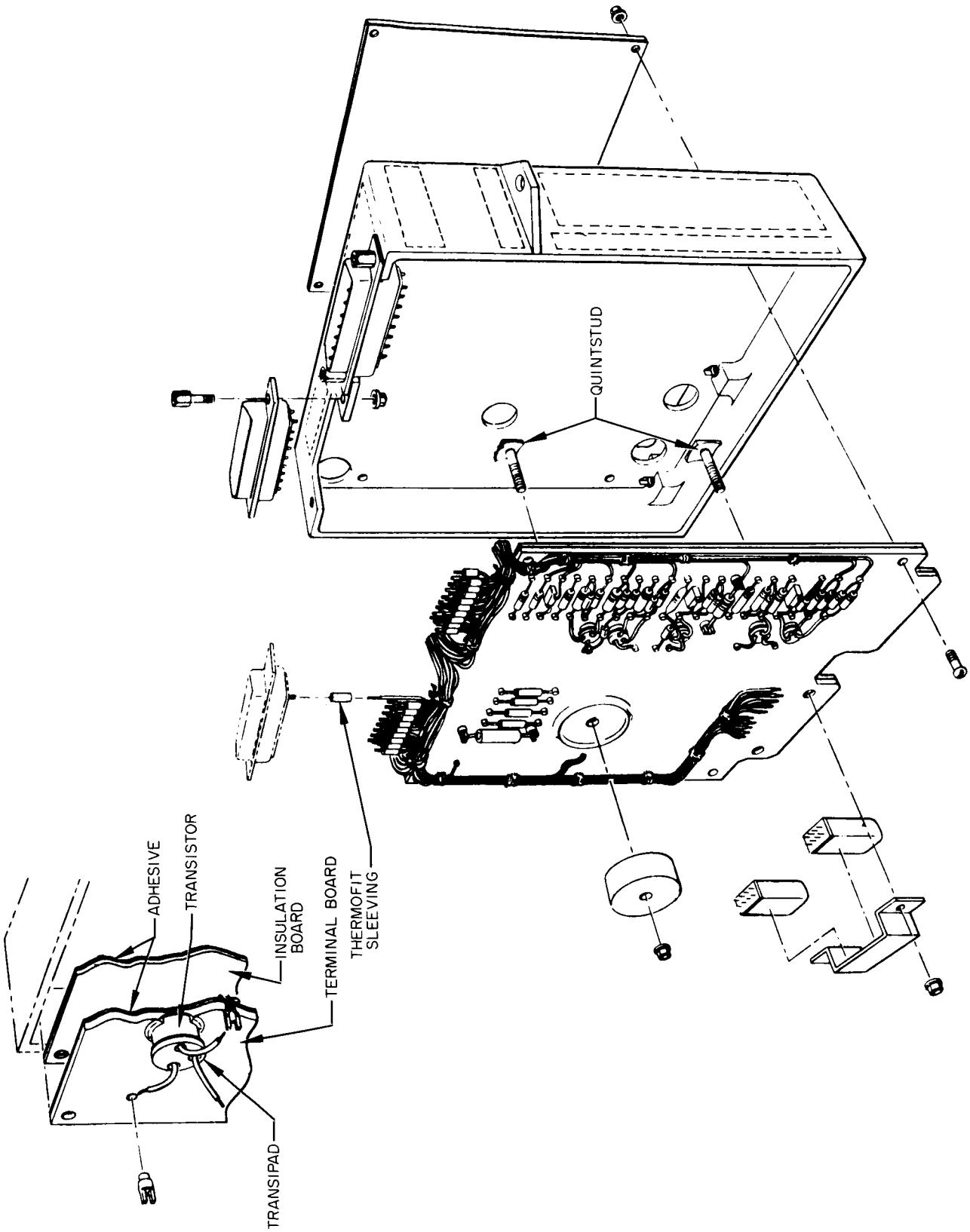


Fig. 249. Typical *Mariner* Mars 1964 subassembly

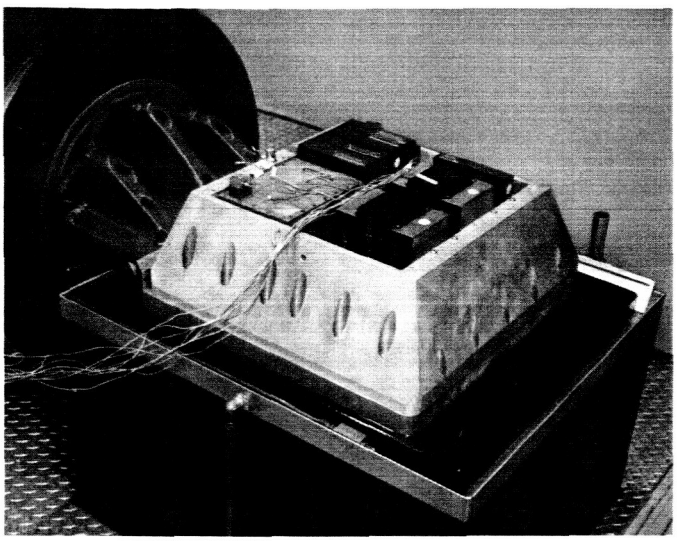


Fig. 250. Prototype assembly in block vibration test fixture

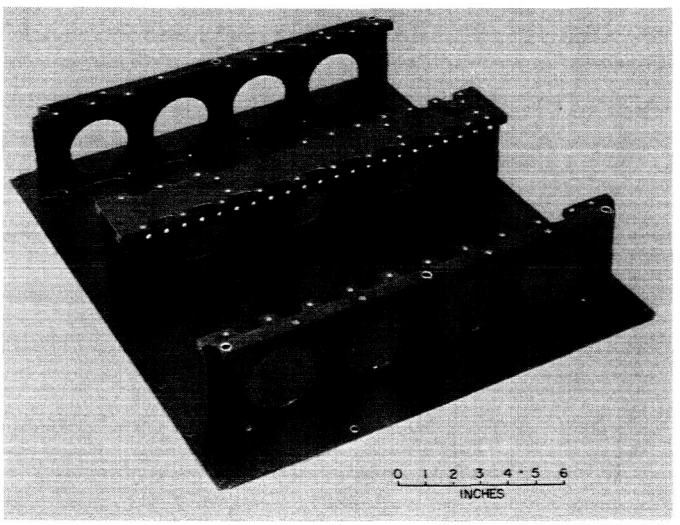


Fig. 251. *Mariner* Mars 1964 assembly chassis

compatible with the components and packaging techniques used. The final chassis design was subsequently qualified on the complete spacecraft structural tests.

The average weight of the *Mariner* Mars 1964 chassis was 4.25 lb compared to the 4.51-lb average *Mariner* Venus 1962 chassis. However, the *Mariner* Mars 1964 chassis were 37% larger than the *Mariner* Venus 1962 chassis and, thus, were nearly 30% lighter in construction.

D. Electronic Equipment Integration

The spacecraft electronic equipment was packaged inside the 15-in.-wide and 16½-in.-high openings in the octagon structure. The spacecraft midcourse motor was placed in Bay II. The spacecraft subsystems were located in the remaining seven bays as a result of the following considerations:

1. Subsystems were to be confined to a single assembly for ease of handling, checkout, and qualification testing
2. Subsystems with a large number of interconnections between them were to be in the closest proximity to reduce cable lengths
3. Subassemblies with high power dissipation were to be distributed to obtain spacecraft temperature control within specified limits
4. Subsystems were to be located so that the spacecraft CG was within the limits of midcourse motor alignment capability
5. Special sensor requirements were to be met (such as an unobstructed view of the Sun for the solar plasma sensor)

The final configuration (Fig. 248) was a result of several studies to obtain an optimum condition. The midcourse motor was located in Bay II. The radio equipment was located in Bay VI to place the radio electronics as close as possible to the two spacecraft antennas and reduce RF losses in the cables. The receiver did not fit in Bay VI, and, therefore, was located in half of the adjacent bay, Bay V. The attitude control gyros required alignment with the spacecraft principal axis. Of the four choices, Bay VII provided the most satisfactory position for the gyros and attitude control electronics because of the added advantage of proximity to the Canopus sensor, located under adjacent Bay VIII. Bay III was well suited for the science electronics since it provided a good location for the solar plasma sensor to be pointed at the Sun. Juggling of the remaining subsystems per the previously mentioned requirements placed the CC&S and attitude control systems in Bay VII, the data encoder and command subsystems in Bay IV, and the video tape recorder in the remaining half of Bay V. The power subsystem required two bays for heat dissipation. Thus, the booster regulator was specially designed to fit the outside area of Bay VIII, and the battery was located inside the bay where a more uniform temperature environment was available. The remaining power conversion equipment was then located in Bay I next to the battery and booster regulator.

E. Packaging Techniques

Insofar as it was practical, electronic equipment was packaged on standard-shape subassemblies. However, a large variety of packaging techniques was required to accommodate different types of circuits using many types of components. In addition, the vendors who participated in the design and fabrication of *Mariner* equipment had different capabilities and experiences in electronic packaging. Electronic equipment packaged at JPL is described here in detail.

1. Planar Packaging

The planar packaging technique used printed wiring boards with bifurcated terminals for component mounting and interconnecting. This offered design flexibility and ease of component replacement. It was also suitable for components differing greatly in size, such as power supplies. It is virtually impossible to package large components together with small components in cordwood configuration. The packaging of a typical power inverter is shown in Fig. 252. The planar packaging technique allowed for direct heat sinking of power components, as was necessary for the booster regulator. Here, power transistors and rectifiers were directly mounted to the metallic structure close to the external radiating surface. This planar packaging was adopted for all power equipment, the Ionization Chamber, the TV and scan electronics, and the CC&S.

2. Hybrid Packaging

The planar packaging technique was also used in conjunction with welded cordwood modules. Repetitive circuits, such as flip-flops and gates, were packaged in three-dimensional modules and then mounted on printed wiring boards. Figure 253 shows a typical hybrid subassembly in which higher density packaging was obtained, and some flexibility advantages of planar packaging were retained. Hybrid packaging was used for the TV encoder, the magnetometer electronics, the data encoder, and the video electronics.

3. Welded NRT DAS Packaging

The NRT DAS logic was originally designed to use pellet components. During fabrication, however, some difficulties were encountered with pellet components and with the processes used. A new packaging design was undertaken using standard components and known fabrication techniques.

The original pellet NRT DAS was packaged in a 6 × 7-in. subchassis, 1.7 in. wide. A review of the available space in the science equipment subassembly showed that the subchassis width could be increased to 2.34 in.

At the onset, it was recognized that the component interconnection was the major problem to be solved. A geometric analysis of the logic diagram, module sizes,

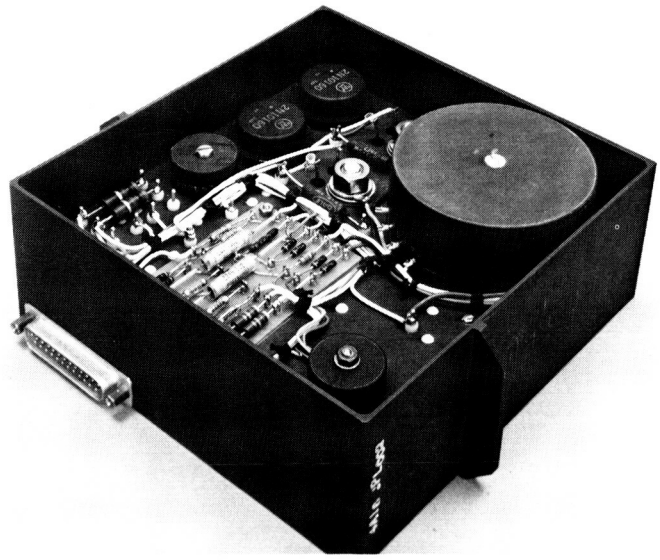


Fig. 252. Typical power inverter packaging

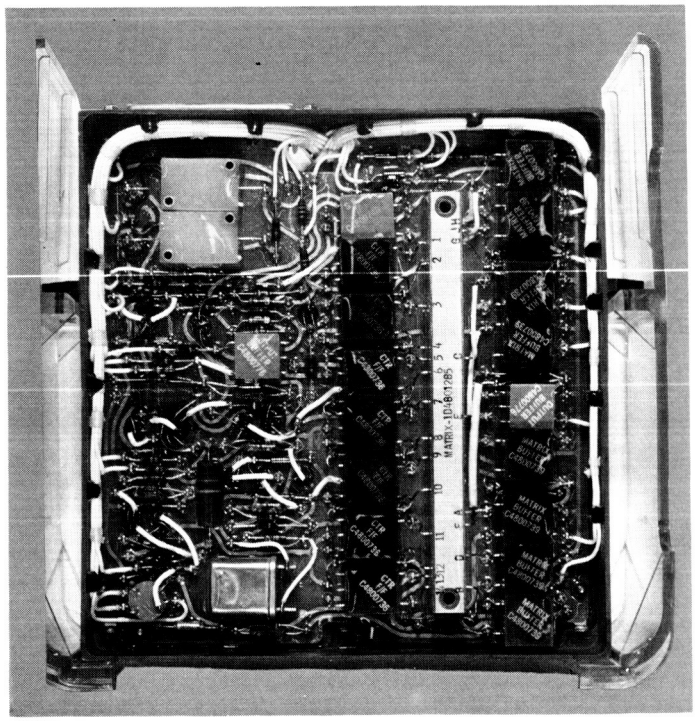


Fig. 253. Hybrid packaging of the TV encoder

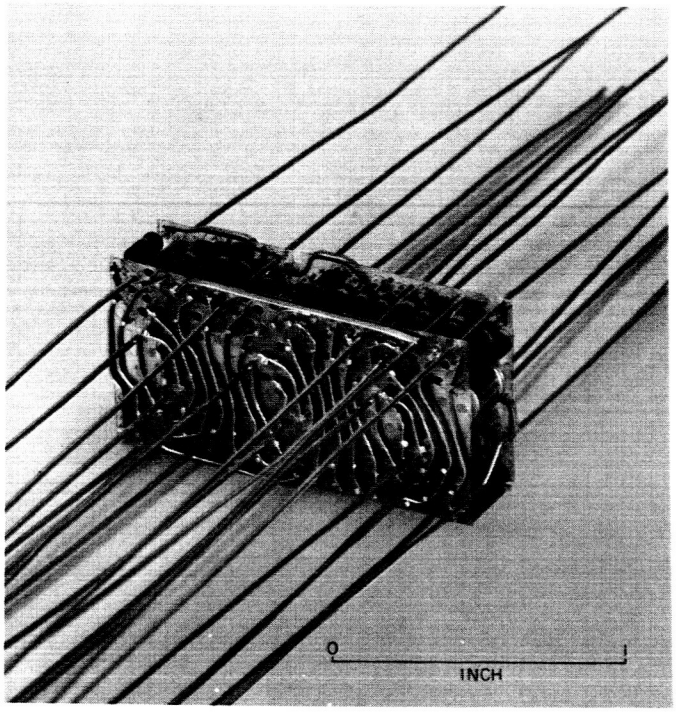


Fig. 254. Typical welded NRT DAS module

and subchassis configuration showed that three levels of interconnection would be desirable:

1. Welded-ribbon component interconnection to form cordwood modules
2. Welded-ribbon intermodular connection to form sticks
3. Soldered-wire interstick and connector interconnection to form the subassembly

Each module was designed independently to a minimum size with the use of one layer of interconnecting ribbon. To accomplish this, the output leads were positioned at random but brought outside the module on both sides. Figure 254 shows a typical module prior to embedment.

With 24 leads randomly positioned on each side of some of the modules, the difficult encapsulation problem was solved by using two 0.015-in.-thick predrilled epoxy glass headers for each module. These headers provided lead positioning and photographically printed lead identification, and functioned as sides for encapsulation.

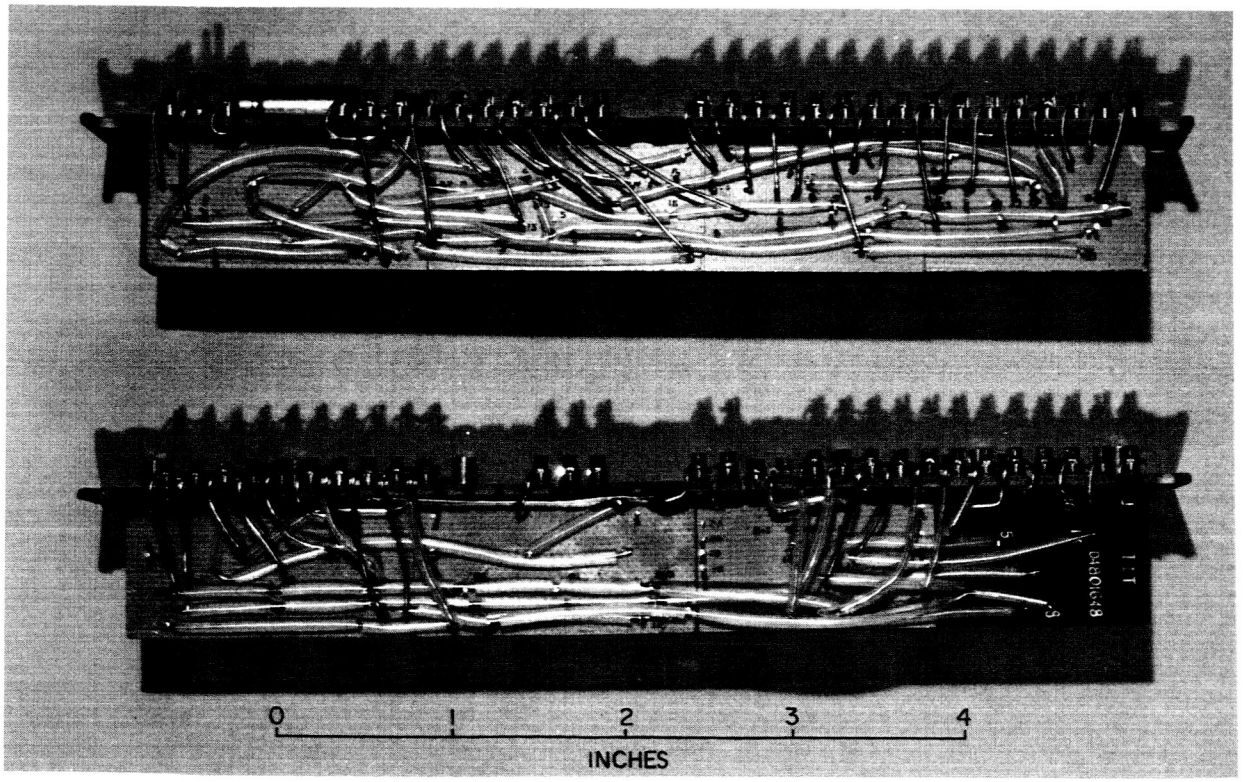


Fig. 255. Typical welded sticks

Figure 255 illustrates two typical stick assemblies. The intermodule interconnections were made by welded ribbon on both sides, and the outgoing paths were brought up to the nearest bifurcated terminals on the stick terminal board. This design featured soldered joints for terminating connector wiring and made it possible to add components on the terminal board. Figure 256 shows the interconnection of sticks and Fig. 257 a sectional view of the completed assembly.

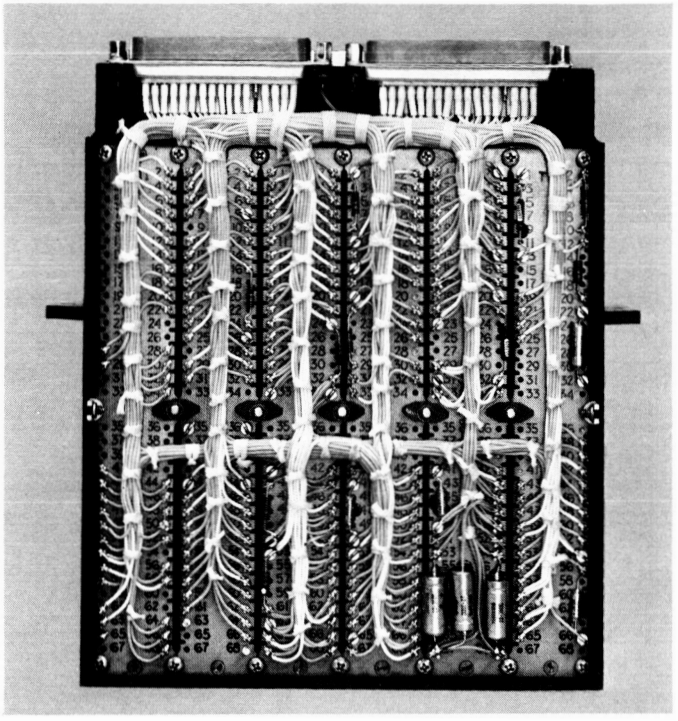


Fig. 256. NRT DAS subassembly

With the described packaging, an assembly of some 2400 pellet components was replaced with a cordwood configuration using standard components, with a penalty of 15% increase in weight and 35% in volume.

4. Receiver and Exciter Packaging

Figure 81 shows the two assemblies containing the radio equipment, in which special packaging was used. This special packaging is typical of RF applications in which geometrical shapes are of functional importance.

Figure 258 illustrates the style of packaging used in the receivers and exciters. Components were typically mounted on T-sections and then bolted in RF-sealed compartments.

5. Other Packaging Techniques

The spacecraft command subsystem was packaged in welded cordwood modules that were mounted in a

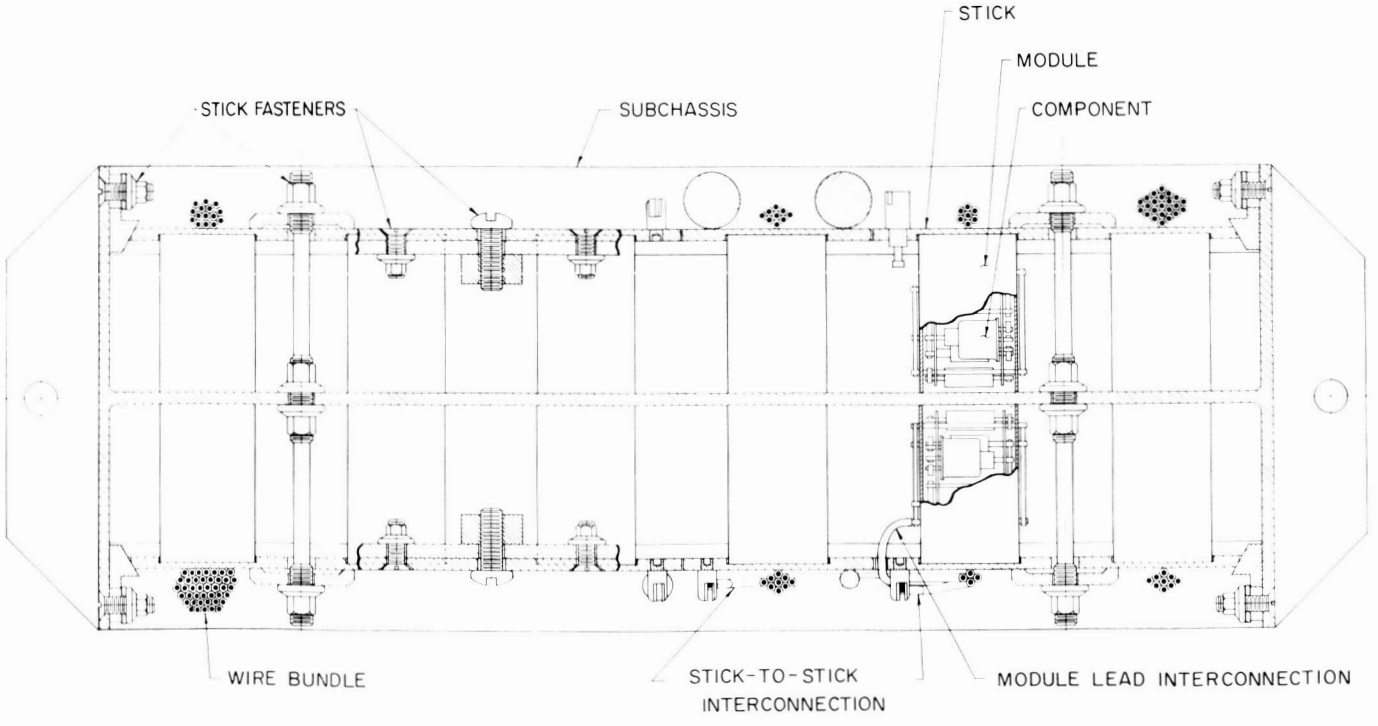


Fig. 257. Subassembly sectional view

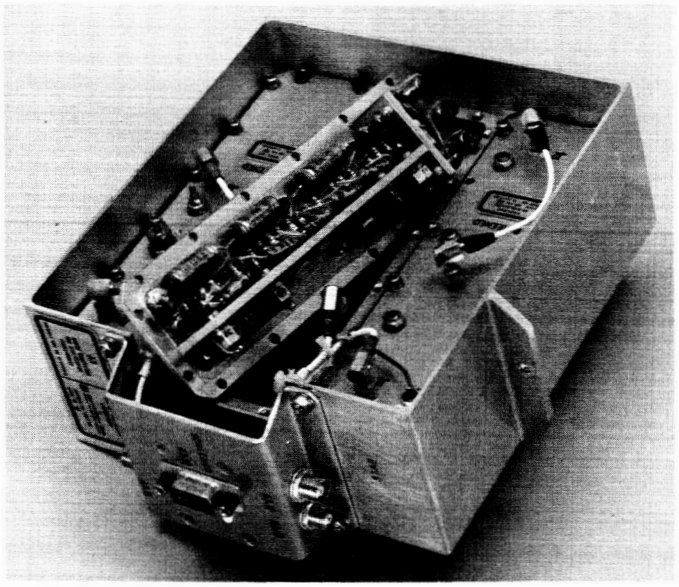


Fig. 258. Typical RF packaging

checkerboard configuration to one of a pair of printed wiring boards. The other printed wiring board of the pair contained the alternate checkerboard configuration. This sandwich was then mounted in the standard type subchassis as shown in Fig. 259.

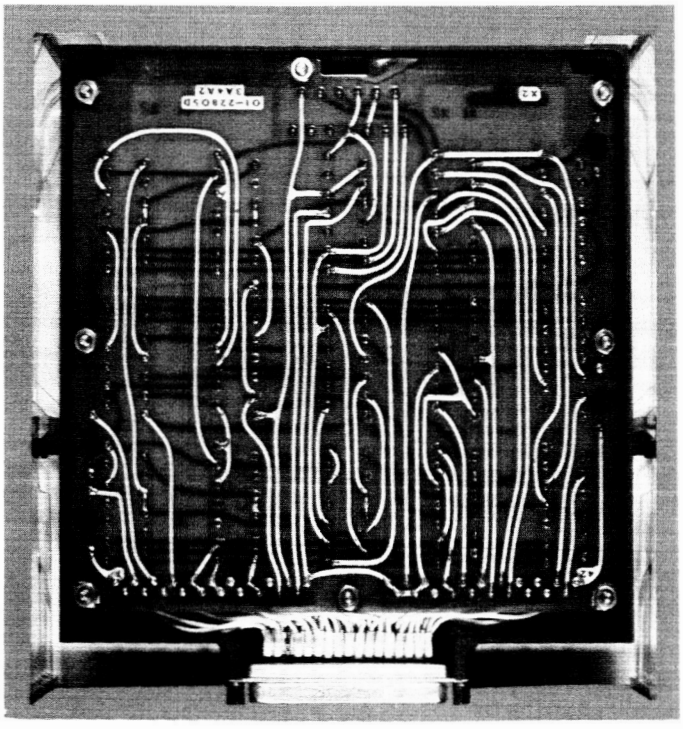


Fig. 259. Command subassembly

The attitude control subsystem also used welded cordwood modules, but was interconnected by a multilayer printed wiring board. The attitude control electronics used a standard-shaped subchassis that was larger than normal, because of a desire to keep the electronics in one subassembly. Soldered three-dimensional modular (cordwood) packaging was used in the Cosmic Ray Telescope (Fig. 260). The plasma electronics subassembly used plated-through-hole circuit boards into which formed leads of component parts were soldered. Here, also, flat miniature transistor and diode leads were soldered directly to the printed conductors.

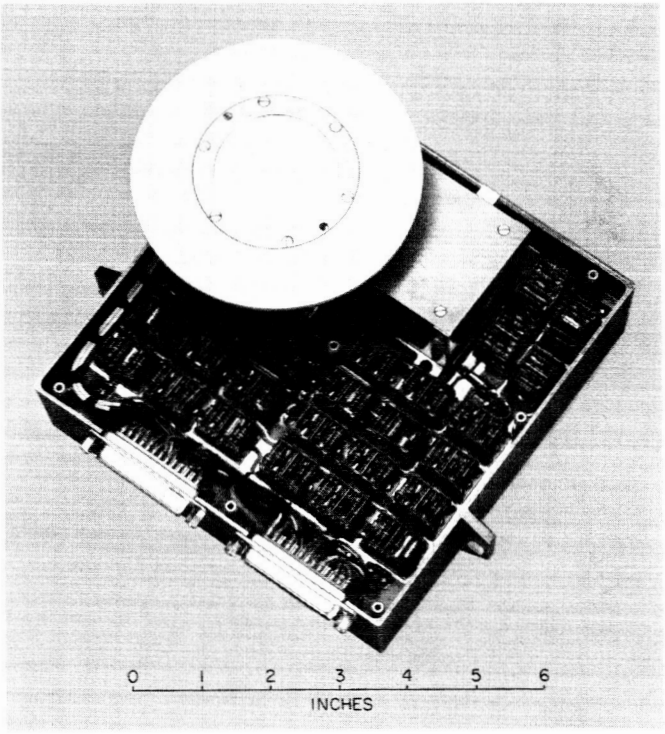


Fig. 260. Soldered-cordwood packaging in the Cosmic Ray Telescope

F. Science Instrument Packaging

Two primary considerations influenced the packaging and geometry of the science instruments:

1. The size and direction of sensitivity of the sensing element
2. The direction, alignment, geometry, and clearances of the attachment to the spacecraft

The Helium Magnetometer electronics and optics were mounted on either side of a sphere containing the magnetic coils. The Ionization Chamber electronics were

packaged on an I-section, U-shaped chassis that supported the electronics on printed wiring boards. The electronics were located on each side of the I-section. The U-shaped chassis held the two sensors in optimum orientation and distributed the instrument weight around the cylindrical low-gain antenna mast.

The Cosmic Dust Detector 50-in.^{2} sensor plate was attached to the detector electronics chassis. The location selected was above the superstructure holding the high-gain antenna. The instrument chassis and associated electronics were designed to attach directly to the superstructure legs. The Trapped Radiation Detector sensors were mounted to a box-shaped chassis that contained the instrument electronics. The Solar Plasma Probe sensor was a cup with screens at various voltages. The instrument electronics were packaged in the Bay III chassis. The Cosmic Ray Telescope was mounted on a standard subassembly at the base of the Bay III chassis. The sensor looked aft through a hole in the lower octagon structure ring. The planetary scan subsystem consists of a lens and optical sensor joined to a small preamplifier chassis at the platform mounting flange. The packaging of the preamplifier electronics was accomplished with the use of printed wiring boards.

G. TV Camera Packaging Development

Prototype television camera packaging is shown in a sectional view in Fig. 261. The vidicon tube, solidly supported inside the chassis with two end clamps, was completely surrounded by electronic printed wiring boards. The electronics section was fastened rigidly to the optical section at a flanged mounting surface.

This initial hard-mount design for mounting the TV vidicon tube was based on past experiences with *Ranger* tubes and on the expected spacecraft environments. When the TV camera failed to pass an increased level type-approval test, a thorough investigation of the problem was pursued. The goals of the investigation were: (1) to determine the destructive frequencies of the vidicon tube and how it failed, and (2) to determine the vibration environment of the tube in the camera and how the environment could be improved.

1. Tube Failure Investigation

A unity gain vibration fixture was used to grip the tube solidly but to still allow photographic access. The test results indicated that: (1) there was a wide variation in the vibration response characteristics in both *Ranger*- and *Mariner*-type tubes from tube to tube, (2) the ruggedized *Mariner*-type tube construction was mechanically superior to the *Ranger* type, and (3) the resonant frequency range of the ruggedized *Mariner* tube was 400 to 700 cps.

2. Tube Environment and Mounting Investigation

Concurrently with the tube failure investigation efforts, the tube mounting designs were analyzed and tested. To obtain realistic test results, an accurate structural mockup of the vidicon camera chassis was built from flight-type hardware. Acceleration measurements were made in three planes at the tube face, the tube socket, and the chassis. Three types of tube mountings were analyzed: the prototype hard-mount, a teflon O-ring, and an experimental soft-mount. Test results are plotted in Fig. 262.

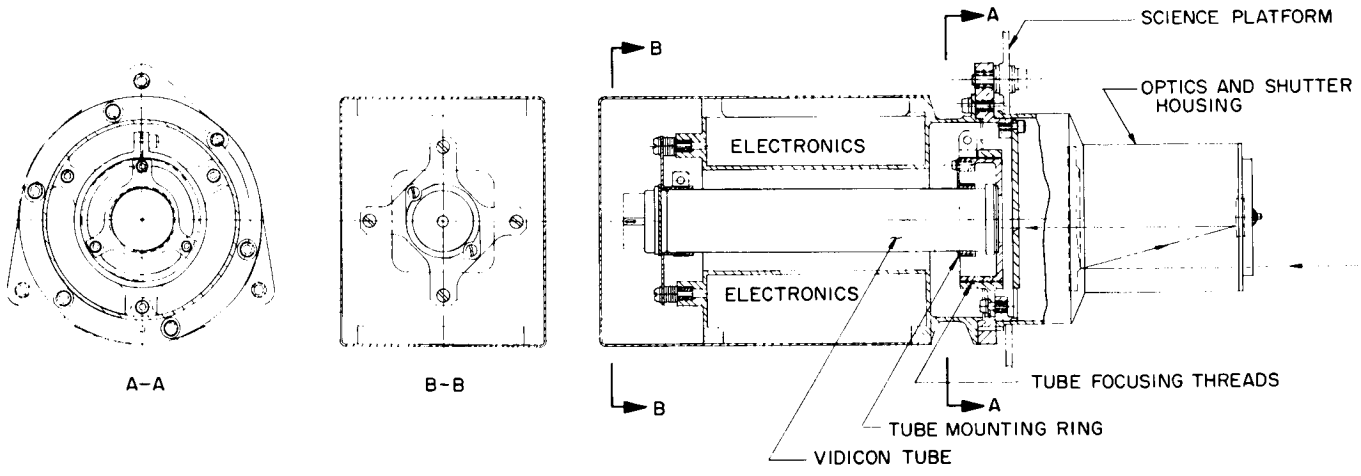


Fig. 261. Television camera section view

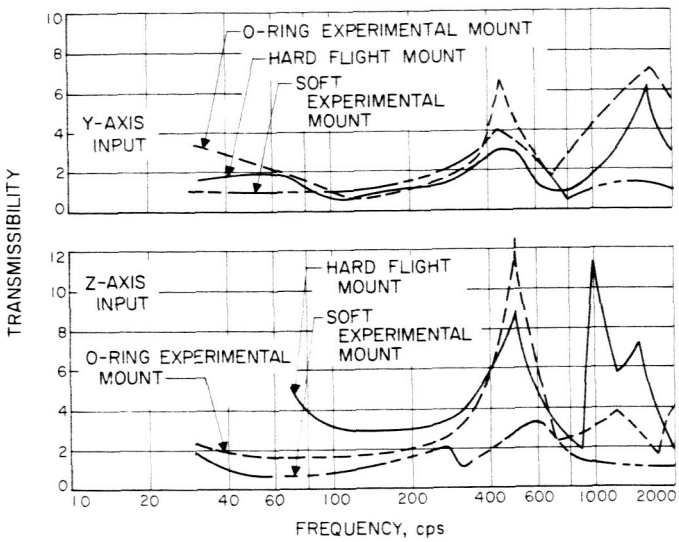


Fig. 262. Comparison of tube mounts tested on hard fixture

It was suspected that the damaging 400- to 500-cps resonance experienced by the hard-mount was actually introduced by the test fixture, since a hard-mounted tube had successfully passed complete spacecraft TA vibration tests. This emphasized the need for testing the available hard-mounted tube configuration to realistic spacecraft levels to prove the adequacy of the design, while simultaneously developing a soft-mounted configuration.

3. Test Fixtures and Test Methods

The first tests were conducted in the TA block test fixture. For further tests, a special fixture was built to hold the science platform (Fig. 263). The stability of the fixture preserved the science platform vibration isolation features and allowed control of the vibration input to be moved from the vibration table to the platform itself, which then allowed the platform to be vibrated in a manner closely simulating the actual spacecraft environment. During the tests, it became necessary, however, to limit excessive cross coupling with a special peak control circuit. This technique provided a more realistic sinusoidal vibration simulation and resulted in drastic reduction of response at the tube socket. Typical Z-axis response is shown in Fig. 264. Control of noise levels in a similar manner was difficult due to the inability to control cross coupling.

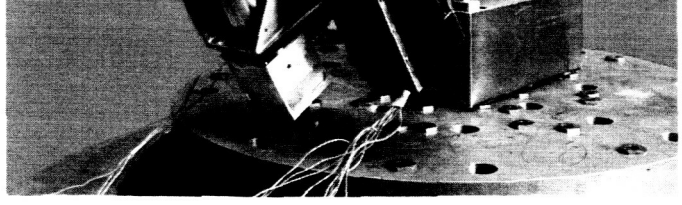


Fig. 263. Television special test fixture

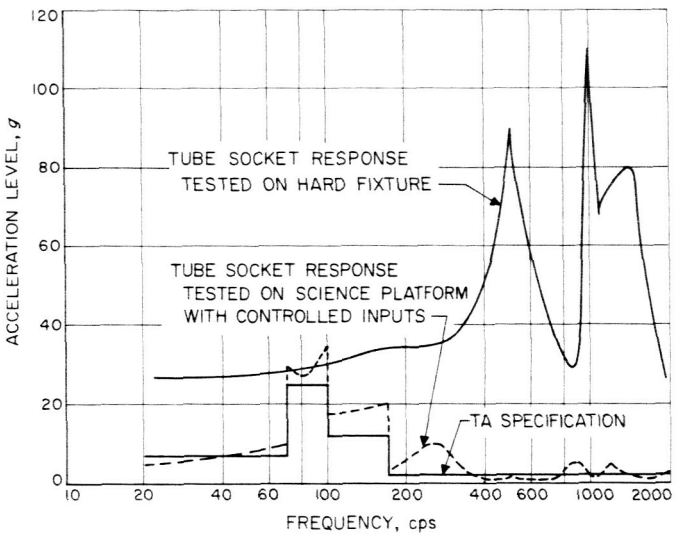


Fig. 264. Spacecraft Z-axis responses on TV tube

At that time, a ruggedized tube in a new soft-mount successfully passed the TA sinusoidal and noise tests in the more severe environment of the block test fixture. The mounting method was developed through a parallel effort, and consisted of two compressed foam plastic supports and a spring system that seated the tube face on the focusing ring. Figure 265 shows the flight configuration.

This investigation led to the following conclusions:

1. Block-style or rigid vibration test fixtures, although easy to use at times, introduce very high gains that are not representative of flight environments.
2. The ruggedized *Mariner* tube construction was found to be superior to the original tube, and was adopted for flight.
3. The original hard-mounted tube design was satisfactory but required difficult testing procedures.

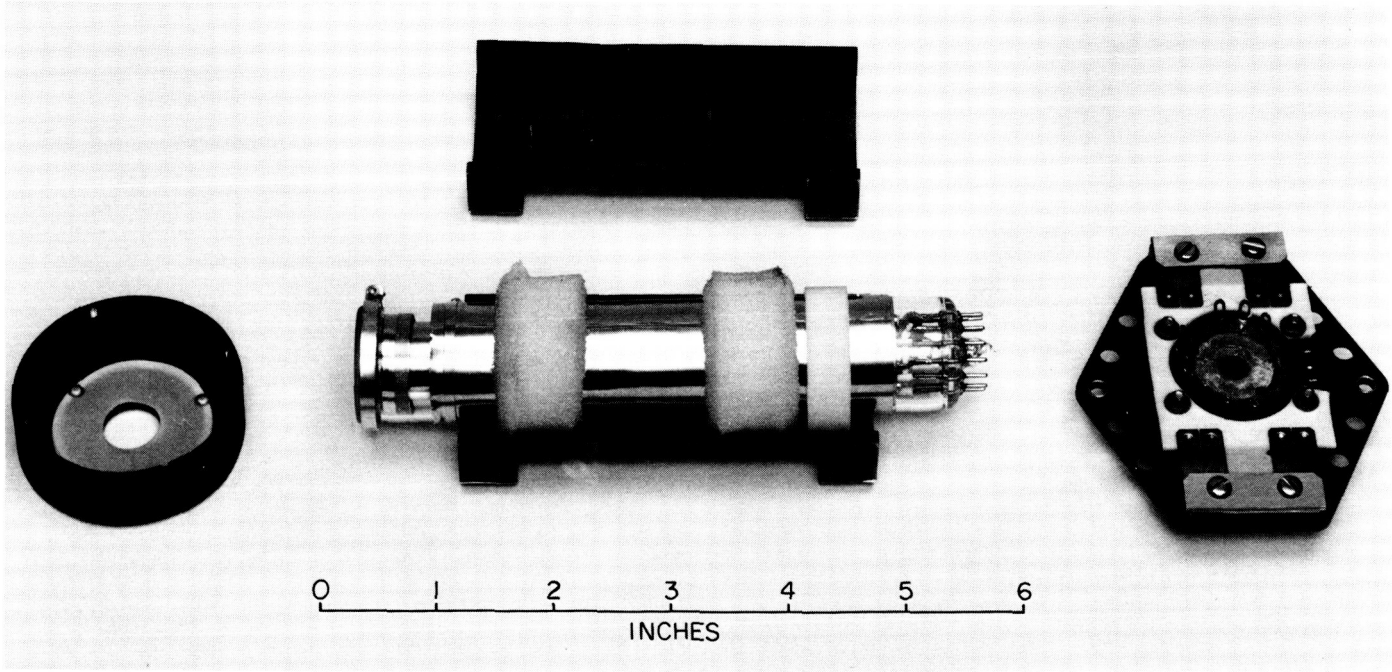


Fig. 265. Television tube soft mount

4. The new soft-mount provided better overall safety margins.

H. Electronic Equipment Handling, Storing, and Shipping

To protect the electronic subassemblies and thermal control surfaces during fabrication and bench testing, polycarbonate plastic frame pairs were attached to the sides of each subchassis (Fig. 253). For additional protection in storage or shipment, moisture and dust proof plastic containers were provided. Figure 266 illustrates how the subassembly, with the protective frames attached, was placed in the container on top of a retainer. For protection of electronic equipment during assembly and bench testing, hard anodized aluminum fixtures were provided. In addition, these fixtures held the chassis in accurate alignment during the installation of the subassemblies. The chassis attached to the fixture at the existing spacecraft mounting points and supported the cable harnesses.

Protection of assemblies in storage and shipment was provided by a tough double-plastic container, shown in Fig. 267. The inner box was made to accommodate the assembly handling fixture, and rested inside the outer container on plastic-foam blocks. The shock protection provided by the container was tested to limit the shock to less than 27 g to the handling fixture during a 30-in. drop test. The containers featured a moisture and dust seal, space for a desiccant bag, a humidity indicator, and an automatic pressure-relief valve. The boxes were painted white to reduce the heat absorption from exposure to direct sunlight.

I. Spacecraft Cabling

1. Design Concept

The functional requirement of the electrical wiring system was to electrically interconnect the spacecraft assemblies and subassemblies. The primary design objective was to perform this function with maximum reliability using materials and techniques that resulted in minimum size and weight. Electrical design considerations included control of magnetic and electrostatic interference, voltage drops, and undesired power losses. Mechanical aspects were also considered. These included: conductor and insulation strength, adequate harness support, accessibility during construction, and capability for rework.

The basic design of *Mariner* Mars 1964 cabling was a derivation of the *Ranger* and *Mariner* Venus 1962 spacecraft. Shielded or twisted wires and separate routing of

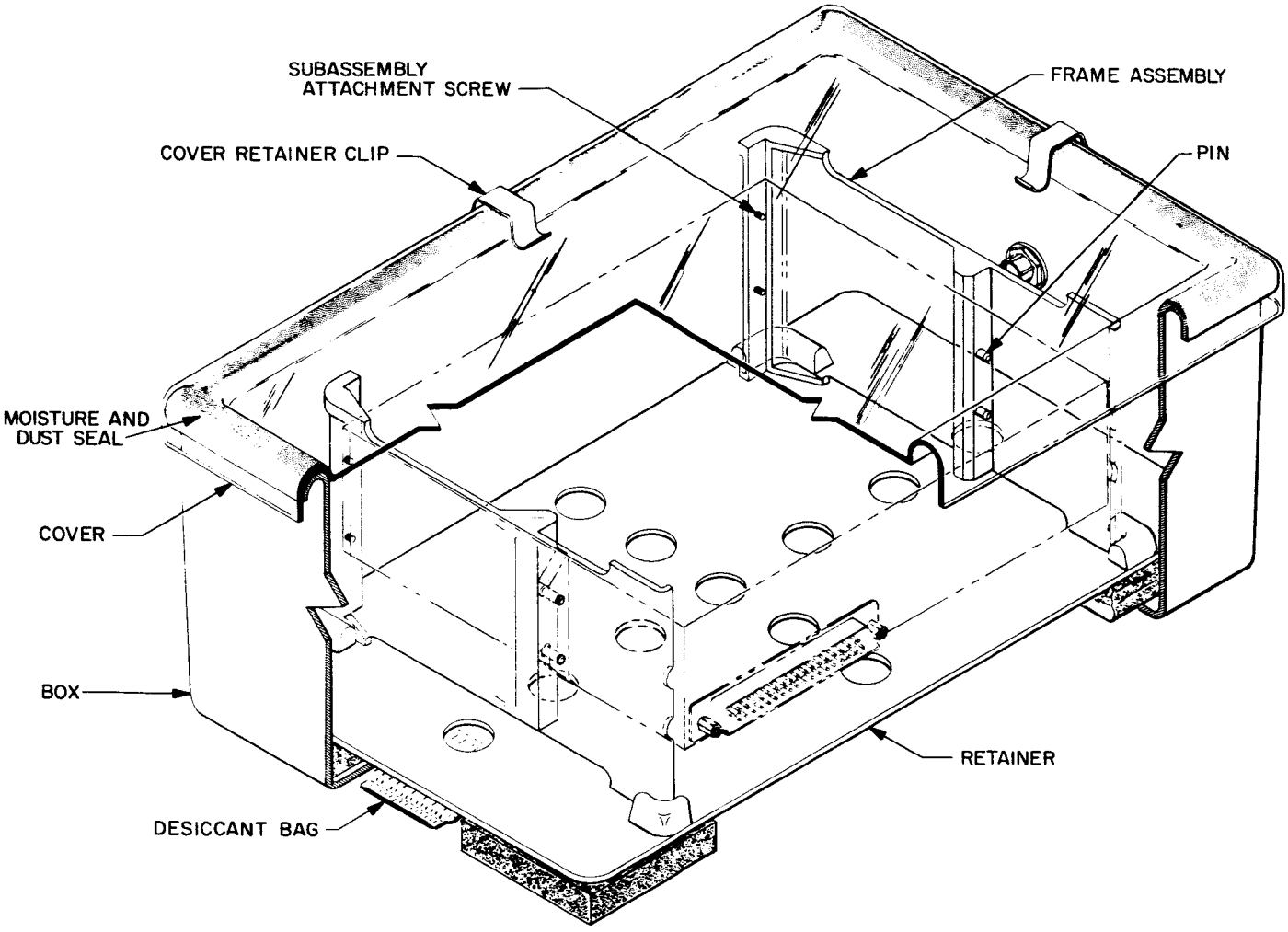


Fig. 266. Subassembly handling and storage container

clean and noisy signal wires were used to satisfy spacecraft electrical and magnetic field requirements. The system consists of three major types of harnesses:

1. Case harnesses were used to electrically interconnect the subassemblies of each subsystem, connect the subsystems into the spacecraft system (ring) harnesses, and provide access for subsystem and system test. A typical case harness (Fig. 268) consisted of a main wire bundle (trunk) from which breakouts were routed to connect to the subassemblies with modified Cannon D type connectors. The harness trunk was supported by a tubular bracket and end-plate assembly that mounted to the center of the chassis. Pigtails from the top of the case harness connected to an upper ring harness with modified Bendix PT-type connectors. Connectors of the same type were hard-mounted in the lower end plate to accept pigtails from the lower ring harness and checkout cables from the operational support equipment.

2. The upper ring harness consisted of a support structure (trough) in which two separate harnesses were mounted. One of these was mounted in the bottom of the trough and used to distribute power to the spacecraft subsystems. The other harness, which interconnected all the spacecraft subsystems, was further broken down into two main bundles secured as far as possible from the power harness and crossing it at right angles to provide maximum signal separation. All of the connectors on this harness were hard-mounted except four pigtails to the solar panels and three to the Cosmic Dust Detector,

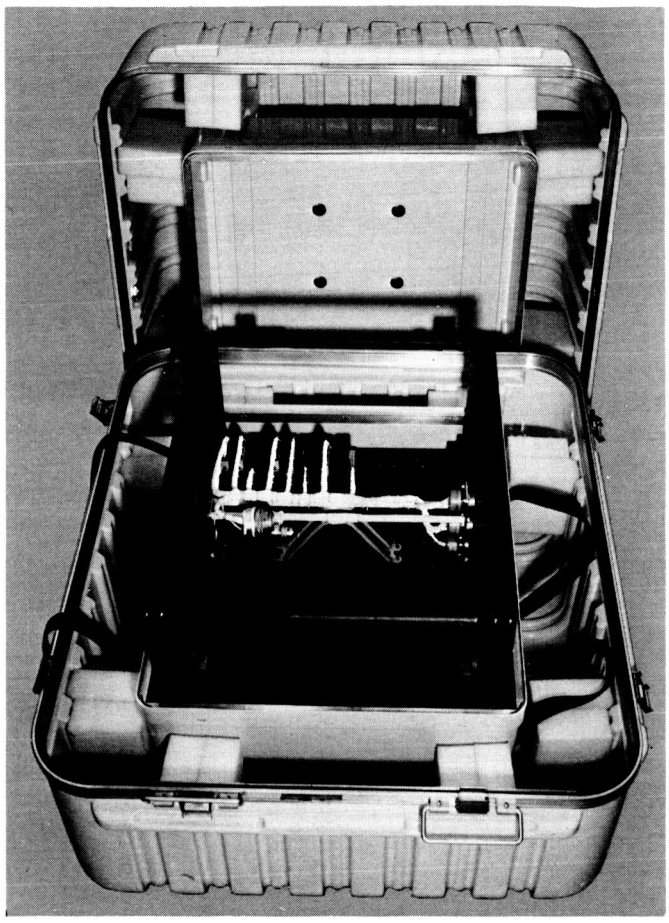


Fig. 267. Assembly shipping container

Trapped Radiation Detector, and absorptivity standard. The lower ring harness was mounted along the inner periphery of the lower portion of the spacecraft bus, and consisted primarily of attitude control subsystem functions and interconnections to the umbilical and inflight connectors. Figure 269 shows the upper and lower ring harnesses mounted on the spacecraft.

3. A number of small miscellaneous harnesses were used to interconnect such outlying items on the spacecraft as science instruments, pyrotechnic devices, gas valves, and the postinjection propulsion system. Each harness in this category was given individual consideration to ensure that it was mounted and protected in such a way that any unique operational requirements could be met. Wires to the scan platform instruments, for instance, were routed down the center of the platform support tube in a loose, flexible bundle to allow them to twist during rotation of the platform.

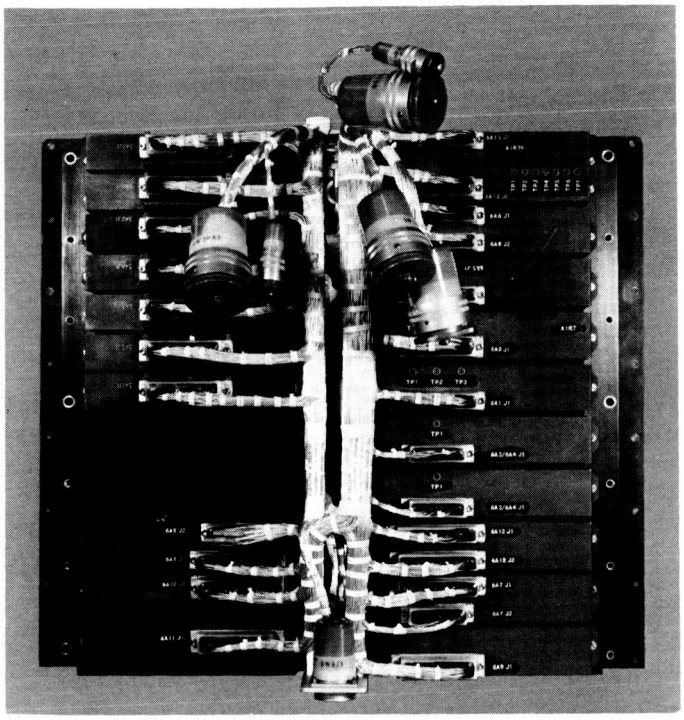


Fig. 268. Bay IV data encoder and command harness

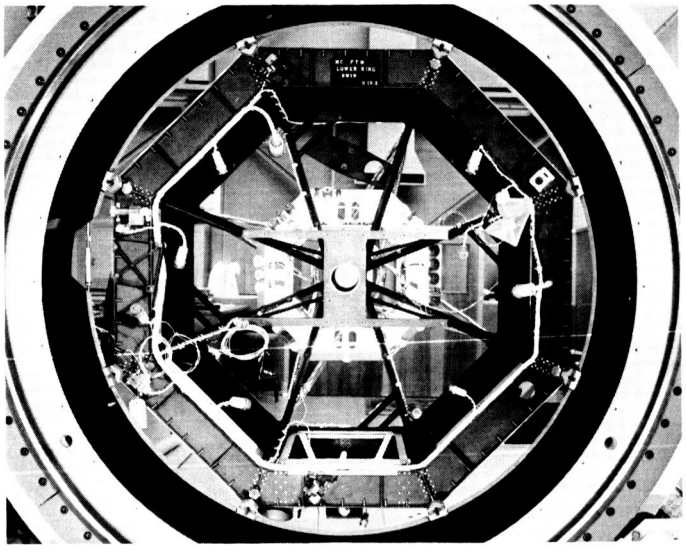


Fig. 269. Upper and lower ring harnesses

2. Materials

The wire used was based on a JPL specification, with deviations to provide for bondability, tighter tolerances on insulation wall thickness, and different conductor characteristics. The insulation consisted of three layers of 0.0003-in. polytetrafluoroethylene, helically wrapped and fused around the basic conductor.

Two types of potting compound were used. The Bendix connectors were potted with a polyurethane compound. In order to maintain the self-aligning characteristics (pin/socket float) of the Cannon D type connectors, a two-layer potting process was used. The connector solder cups were first covered with a relatively soft silicone compound, and the remainder of the potting cup was filled with the harder polyurethane to provide support for the wire bundle.

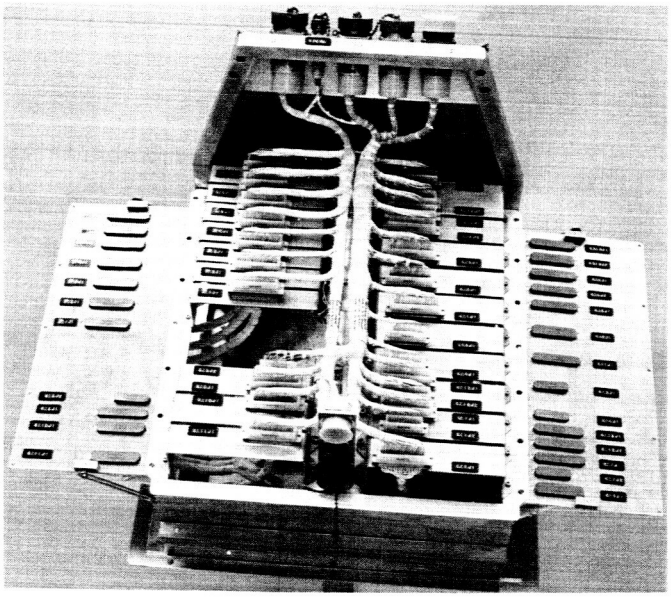


Fig. 270. Fabrication fixture, Bay IV data encoder and command harness

The remainder of the materials used for insulating splices and tying and supporting wire bundles were chosen for their ability to perform their function with a minimum of outgassing and degradation due to environment. Nylon, teflon, dacron, and certain types of silicone and thermofit sleeving were used in various applications.

3. Fabrication

Each case harness was fabricated on a three-dimensional fixture. Fixture connectors simulating the subassembly connectors were back-wired to connectors mounted on the sides of the case mockups. Connections within the fabricated harness were confirmed by "buzzing" from the soldered wire to the appropriate connector pin (or socket) on the side of the mockup. This configuration eliminated the need for unplugging and probing flight connectors during harness assembly and QA test. The connectors of the fabricated harnesses were also

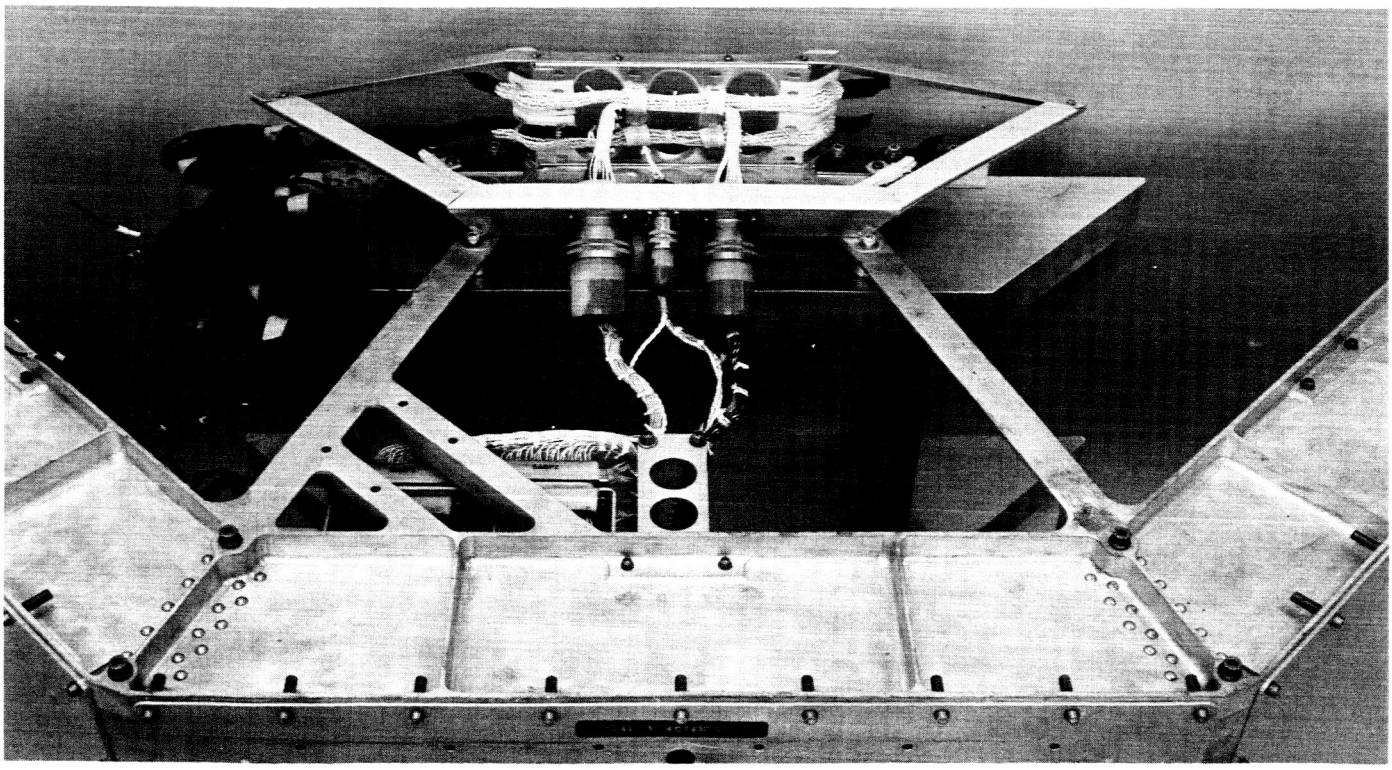


Fig. 271. Upper ring harness fabrication fixture and completed upper ring harness

potted while mounted on this fixture. A typical case harness fabrication fixture is shown in Fig. 270.

The upper ring harnesses were fabricated in the flight trough structures, thus eliminating any necessity for handling the unsupported harness. The flight trough was mounted on a flat plate with spacers and feed-through connectors located to determine the length of the few pigtails involved. This fixture, with a completed upper ring harness, is shown in Fig. 271.

Because no removable flight support was designed for the lower ring, this harness was fabricated on a three-dimensional fixture with feedthrough connectors located at all the interfaces to permit inspection and continuity checks without disconnecting the flight connectors. This fixture and a support stand with swiveling head, typical of that used with all fabrication fixtures, are shown in Fig. 272.

All miscellaneous harnesses were fabricated on a full scale mockup of the spacecraft, some items of which were removed for the required access. These harnesses were then removed and installed on the flight hardware.

4. Test

A preliminary type-approval vibration test on a typical case harness and its support structure was completed successfully before any case harness fabrication was begun. Impact, vibration, and thermal shock tests were also conducted on a case harness of medium complexity before potting. No mechanical failures occurred in any of these tests.

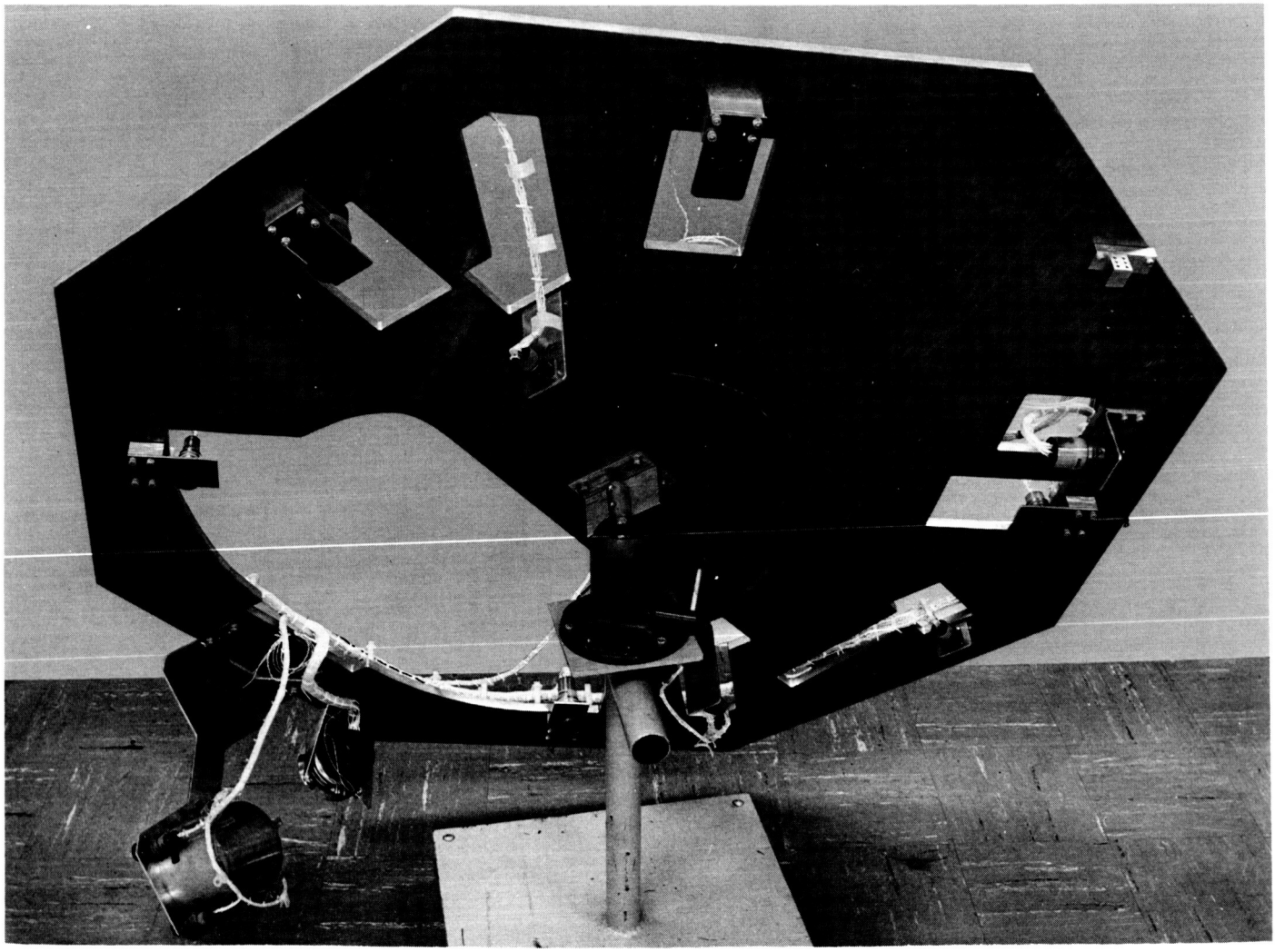


Fig. 272. Lower ring harness fabrication fixture and adjustable support stand

A complete set of representative ring and case harnesses was provided to the STM spacecraft. These harnesses were fabricated and inspected to flight standards and were reinspected during, and subsequent to, completion of the STM test program. In addition, flight quality and configuration case harnesses were furnished to all systems but the science subsystem for use during type-approval tests of subsystem electronics.

XVIII. SPACECRAFT SUBSYSTEMS: SCIENCE

A. General Description

The *Mariner* Mars 1964 science subsystem consists of scientific instruments and ancillaries selected to meet the mission objectives. All of the instruments, except the television, are capable of making measurements during the cruise portion of the flight; they are programmed to gather interplanetary data concerning the solar plasma, micrometeorites, magnetic fields, and energetic particle distribution in space. The experiments to be conducted with the instruments in Table 57 are under the direction of the principal investigators shown in Table 58. The ancillary equipment consists of the data automation subsystem, the planetary scan subsystem, and the narrow angle Mars gate.

Some of the ground rules established for the science subsystem were generated by the Project Office, and others were required by the JPL Space Sciences Division in order to control the design and development of the

Table 57. *Mariner* Mars 1964 science instruments and ancillaries

Description	Spacecraft unit number	Weight lb	Power w	Look angle	Purpose	Number of sensors	Output data
Instruments							
Cosmic Ray Telescope	21	2.58	0.598	30 deg half-angle cone along + Z axis	To detect and measure trapped corpuscular radiation in the vicinity of Mars. To measure the flux and energy of alpha particles and protons as a function of position and time in interplanetary space.	One sensor, three detectors in telescope	Digital
Cosmic Dust Detector	24	2.10	0.201	22 × 22 cm plate perpendicular to ecliptic in direct and retrograde motion	To make direct measurements of the dust particle momentum and mass distribution in the Earth–Moon, Mars–Deimos–Phobos, and interplanetary regions.	Two	
Trapped Radiation Detector	25	2.20	0.350	Three sensors 70 deg to Sun–probe line, 30 deg half-angle cone One sensor 135 deg to Sun–probe line, −30 deg half-angle cone	To search for magnetically trapped particles in the vicinity of Mars and, if found, make a preliminary estimate of their distribution, energy spectra, and identity. To monitor solar cosmic rays and energetic electrons in interplanetary space to determine their angular distribution, energy spectra, and time history.	Four	
Ionization Chamber	26	2.71	0.460	Omnidirectional (except as shadowed by bus)	To detect and measure the average omnidirectional flux of corpuscular radiation in regions between Earth and Mars. To measure the average specific ionization attributable to this flux. To measure the omnidirectional flux and specific ionization of charged particles that may be trapped in the vicinity of Mars.	Two	

Table 57. *Mariner* Mars 1964 instruments and ancillaries (Cont'd)

Description	Spacecraft unit number	Weight lb	Power w	Look angle	Purpose	Number of sensors	Output data
Instruments							
Solar Plasma Probe	32	6.41[a]	2.65 average, 2.90 peak	30 deg half-angle cone, 10 deg from Sun – probe line	To measure the spectral distribution, flux density, and time history of the positively charged solar plasma traveling outward from the Sun and to correlate these measurements with those from the Helium Magnetometer.	One (three sections)	Pulse width
Helium Magnetometer	33	7.50	7.30	One sensor along spacecraft Z axis, one sensor along Y axis, one sensor along X axis	To investigate the existence of a Mars planetary field and determine its characteristics as a function of direction, magnitude, multipolarity, and orientation with respect to the planetary rotational axis. To investigate the interaction between planetary and interplanetary magnetic fields. To measure the magnitude and direction of the steady and slowly varying components of the interplanetary magnetic field and to determine its variation with heliographic latitude and longitude.	One	Pulse width
Television	36	11.28[a]	8.0	1.05 × 1.05 deg	To make preliminary topographic reconnaissance of portions of the surface of Mars. To attain an improved knowledge of areas of possible living matter. To obtain additional data on the Mars surface reflectivities so that the design of future systems will be enhanced.	One sensor, 2 alternate color filters	Digital, pulse width sequenced
Ancillaries							
Data automation system	20	11.91[a]	6.5 average during cruise; 5.6 average during encounter; 8.0 peak during encounter	Not applicable	To provide the sequencing, processing, storage, buffering, and encoding necessary to realize the optimum scientific value of each instrument. To perform certain engineering measurements in addition to those made by the spacecraft data encoder.	None	See Data Automation System, paragraph J
Planetary scan subsystem	31	5.65[a]	4.65 (2.4 kc), 2.81 (400 cps)	119.7 deg in cone, 180-deg scan width	To point the TV sensors at a point on the planet that is dependent upon the bisector of radiation and the trajectory of the spacecraft.	One	Pulse width
Narrow angle Mars gate	7MG1	0.20[a]	Included in DAS power requirement (~0)	2.5 × 1.5 deg	To trigger the DAS into the TV sequencing mode, as a backup to the TV planet-in-view sensing function.	One	None

[a]Measured values, no cabling harnesses included.

Table 58. *Mariner* Mars 1964 principal investigators

Instrument	Principal investigator	Affiliation
Cosmic Ray Telescope	J. Simpson	University of Chicago
Cosmic Dust Detector	M. Alexander	Goddard Space Flight Center
Trapped Radiation Detector	J. Van Allen	State University of Iowa
Ionization Chamber	H. Neher	California Institute of Technology
Solar Plasma Probe	H. Bridge	Massachusetts Institute of Technology
Helium Magnetometer	E. Smith	Jet Propulsion Laboratory
Television	R. Leighton	California Institute of Technology

subsystem. The more significant of these ground rules were:

1. Redundancy had to be included so that a failure of the scan subsystem to start wide-angle scanning or to stop scanning after acquisition could not abort the mission.
2. The science subsystem had to be capable of an operating test on the launch pad prior to liftoff.
3. All scientific data taken during the encounter period had to be stored and played back to Earth as many times as practicable after encounter. In addition, selected measurements required for engineering evaluation of the instruments or data interpretation had to be added to the encounter mode data and sent back in real time by the telemetry subsystem.
4. All science flight equipment had to undergo a component part screening program.
5. The Helium Magnetometer had to be located as far as possible from likely sources of permanent or slowly varying (< 10 cps) magnetic fields.
6. Complete spare units had to be provided for the planetary scan, data automation, and television subsystems. Selected spares were optional for the remainder of the science subsystem.
7. A complete science subsystem test had to be accomplished before delivery to SAF.

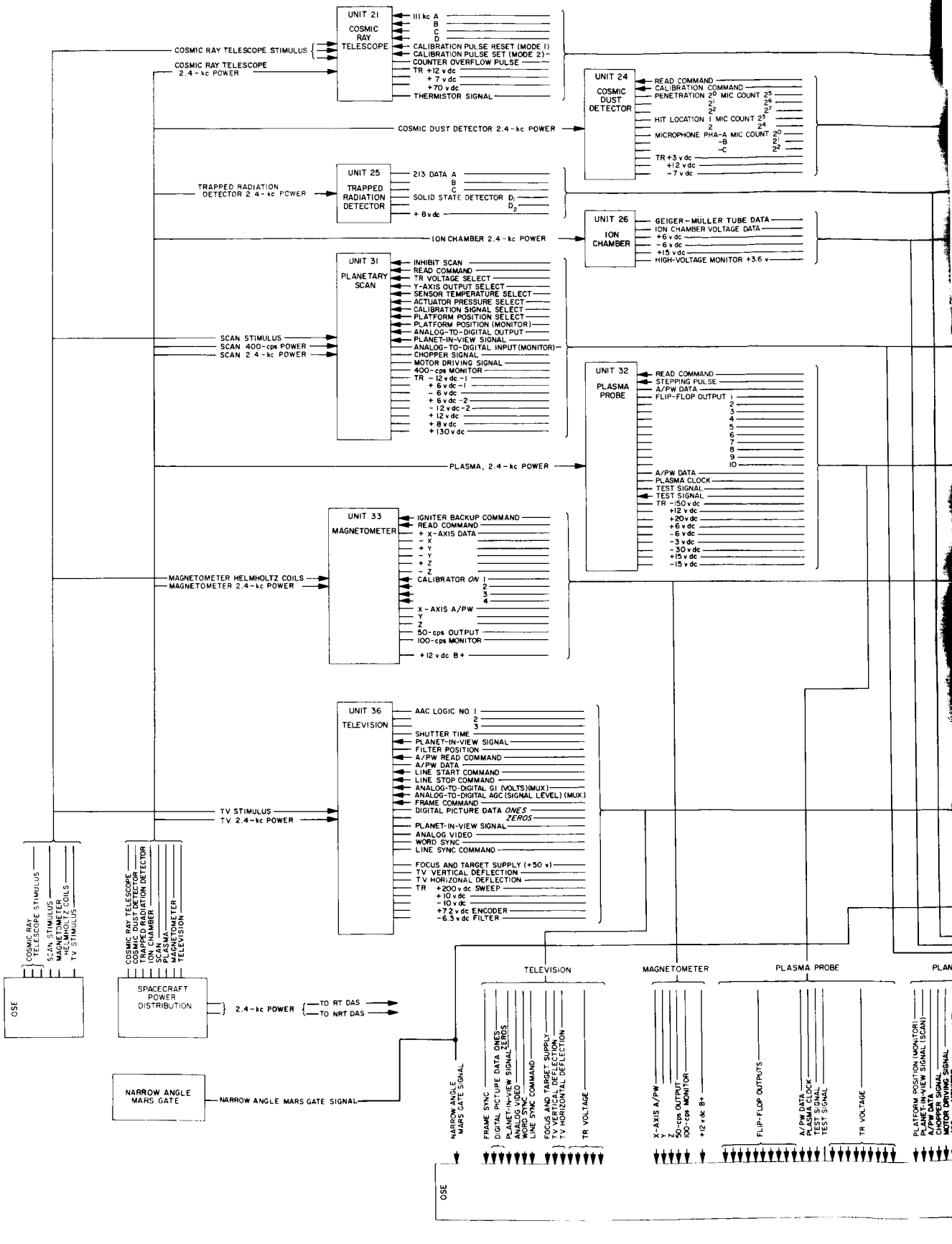
A functional block diagram of the science subsystem is shown in Fig. 273. The spacecraft was launched in Data Mode 2 with the science subsystem deenergized. When the spacecraft separated from the *Agena* launch vehicle, the cruise or real-time data automation system and the interplanetary instruments were energized. The format of the DAS output during Data Mode 2 is shown in Fig. 274 (a). In spacecraft Data Mode 1, no science data were transmitted, although the RT DAS continued to sample the instruments.

The initiation of the encounter mode by either the CC&S MT-7 command or the data encoder DC-25 command accomplishes the following:

1. The television, NRT data automation subsystem, narrow angle Mars gate, planetary scan subsystem, and tape recorder are energized.
2. The NRT DAS sequences the TV, but does not issue start/stop commands to the tape recorder.
3. The protective cover is removed from the TV, NAMG, and PSS sensors. The scan platform moves through 180-deg arcs until the planet is acquired. An output from the PSS through the DAS to the data encoder initiates Data Mode 3. The real-time format for spacecraft Data Mode 3 is illustrated in Fig. 274 (b). The PSS then tracks the planet to ensure that the platform continues to point at the bisector of brightness defining the location of Mars.

When the edge of the lighted disk comes into view of either the television or narrow angle Mars gate, the DAS tape-recorder start circuitry is enabled. The DAS waits until the beginning of the next standard sequence to start the recording cycle. All science data acquired during encounter are stored in the spacecraft tape recorder. The measurements made by the RT DAS are sent back via the telemetry channel and are transferred to the NRT DAS for storage. Scan platform motion is inhibited during the science encounter (picture sequence) mode.

The science encounter mode and spacecraft Data Mode 3 are terminated when the second end-of-tape signal occurs. A backup stop-recording circuit is also included in the DAS. This circuit is set after 18 pictures and reset after 22 pictures have been taken. The reset function activates the "switch to Data Mode 2" command to the data encoder in exactly the same fashion as in the second end-of-tape signal. The spacecraft stays in Data Mode 2 until either a MT-8 or DC-26 command cause the encounter instruments and the NRT DAS to be deenergized.


UNIT 21
COSMIC RAY TELESCOPE
111 kc A
B
C
D
CALIBRATION PULSE RESET (MODE 1)
CALIBRATION PULSE SET (MODE 2)
COUNTER OVERFLOW PULSE
TR +12 v dc
+7 v dc
+70 v dc
THERMISTOR SIGNAL
COSMIC RAY TELESCOPE STIMULUS
COSMIC RAY TELESCOPE 2.4-kc POWER
UNIT 24
COSMIC DUST DETECTOR
READ COMMAND
CALIBRATION COMMAND
PENETRATION MIC COUNT
HIT LOCATION MIC COUNT
MICROPHONE PHA-A MIC COUNT
-B
-C
TR +3 v dc
+12 v dc
-7 v dc
COSMIC DUST DETECTOR 2.4-kc POWER
UNIT 25
TRAPPED RADIATION DETECTOR
213 DATA A
B
C
SOLID STATE DETECTOR D1
D2
+8 v dc
TRAPPED RADIATION DETECTOR 2.4-kc POWER
UNIT 26
ION CHAMBER
GEIGER-MÜLLER TUBE DATA
ION CHAMBER VOLTAGE DATA
+6 v dc
-6 v dc
+15 v dc
HIGH-VOLTAGE MONITOR +3.6 v
ION CHAMBER 2.4-kc POWER
UNIT 31
PLANETARY SCAN
INHIBIT SCAN
READ COMMAND
TR VOLTAGE SELECT
Y-AXIS OUTPUT SELECT
SENSOR TEMPERATURE SELECT
ACTUATOR PRESSURE SELECT
CALIBRATION SIGNAL SELECT
PLATFORM POSITION SELECT
PLATFORM POSITION (MONITOR)
ANALOG-TO-DIGITAL OUTPUT
PLANET-IN-VIEW SIGNAL
ANALOG-TO-DIGITAL INPUT (MONITOR)
CHOPPER SIGNAL
MOTOR DRIVING SIGNAL
400-cps MONITOR
TR -12 v dc -1
+6 v dc -1
-6 v dc
+6 v dc -2
-12 v dc -2
+12 v dc
+8 v dc
+130 v dc
SCAN STIMULUS
SCAN 400-cps POWER
SCAN 2.4-kc POWER
UNIT 32
PLASMA PROBE
READ COMMAND
STEPPING PULSE
A/PW DATA
FLIP-FLOP OUTPUT
A/PW DATA
PLASMA CLOCK
TEST SIGNAL
TEST SIGNAL
TR -150 v dc
+12 v dc
+20 v dc
+6 v dc
-6 v dc
-3 v dc
-30 v dc
+15 v dc
-15 v dc
PLASMA, 2.4-kc POWER
UNIT 33
MAGNETOMETER
IGNITER BACKUP COMMAND
READ COMMAND
+X-AXIS DATA
-X
+Y
-Y
+Z
-Z
CALIBRATOR ON
X-AXIS A/PW
Y
Z
50-cps OUTPUT
100-cps MONITOR
+12 v dc B+
MAGNETOMETER HELMHOLTZ COILS
MAGNETOMETER 2.4-kc POWER
UNIT 36
TELEVISION
AAC LOGIC NO.
SHUTTER TIME
PLANET-IN-VIEW SIGNAL
FILTER POSITION
A/PW READ COMMAND
A/PW DATA
LINE START COMMAND
LINE STOP COMMAND
ANALOG-TO-DIGITAL G1 (VOLTS) (MUX)
ANALOG-TO-DIGITAL AGC (SIGNAL LEVEL) (MUX)
FRAME COMMAND
DIGITAL PICTURE DATA ONES
ZEROS
PLANET-IN-VIEW SIGNAL
ANALOG VIDEO
WORD SYNC
LINE SYNC COMMAND
FOCUS AND TARGET SUPPLY (+50 v)
TV VERTICAL DEFLECTION
TV HORIZONAL DEFLECTION
TR +200 v dc SWEEP
+10 v dc
-10 v dc
+72 v dc ENCODER
-6.3 v dc FILTER
TV STIMULUS
TV 2.4-kc POWER
OSE
COSMIC RAY TELESCOPE STIMULUS
SCAN STIMULUS
MAGNETOMETER HELMHOLTZ COILS
TV STIMULUS
COSMIC RAY TELESCOPE
COSMIC DUST DETECTOR
TRAPPED RADIATION DETECTOR
ION CHAMBER
SCAN
PLASMA
MAGNETOMETER
TELEVISION
SPACECRAFT POWER DISTRIBUTION
2.4-kc POWER
TO RT DAS
TO NRT DAS
NARROW ANGLE MARS GATE
NARROW ANGLE MARS GATE SIGNAL
TELEVISION
MAGNETOMETER
PLASMA PROBE
NARROW ANGLE MARS GATE SIGNAL
FRAME SYNC
DIGITAL PICTURE DATA ONES
ZEROS
PLANET-IN-VIEW SIGNAL
ANALOG VIDEO
WORD SYNC
LINE SYNC COMMAND
FOCUS AND TARGET SUPPLY
TV VERTICAL DEFLECTION
TV HORIZONTAL DEFLECTION
TR VOLTAGE
X-AXIS A/PW
Y
50-cps OUTPUT
100-cps MONITOR
+12 v dc B+
FLIP-FLOP OUTPUTS
A/PW DATA
PLASMA CLOCK
TEST SIGNAL
TEST SIGNAL
TR VOLTAGE
PLATFORM POSITION (MONITOR)
PLANET-IN-VIEW SIGNAL (SCAN)
PLASMA
CHOPPER SIGNAL
MOTOR DRIVING SIGNAL
OSE

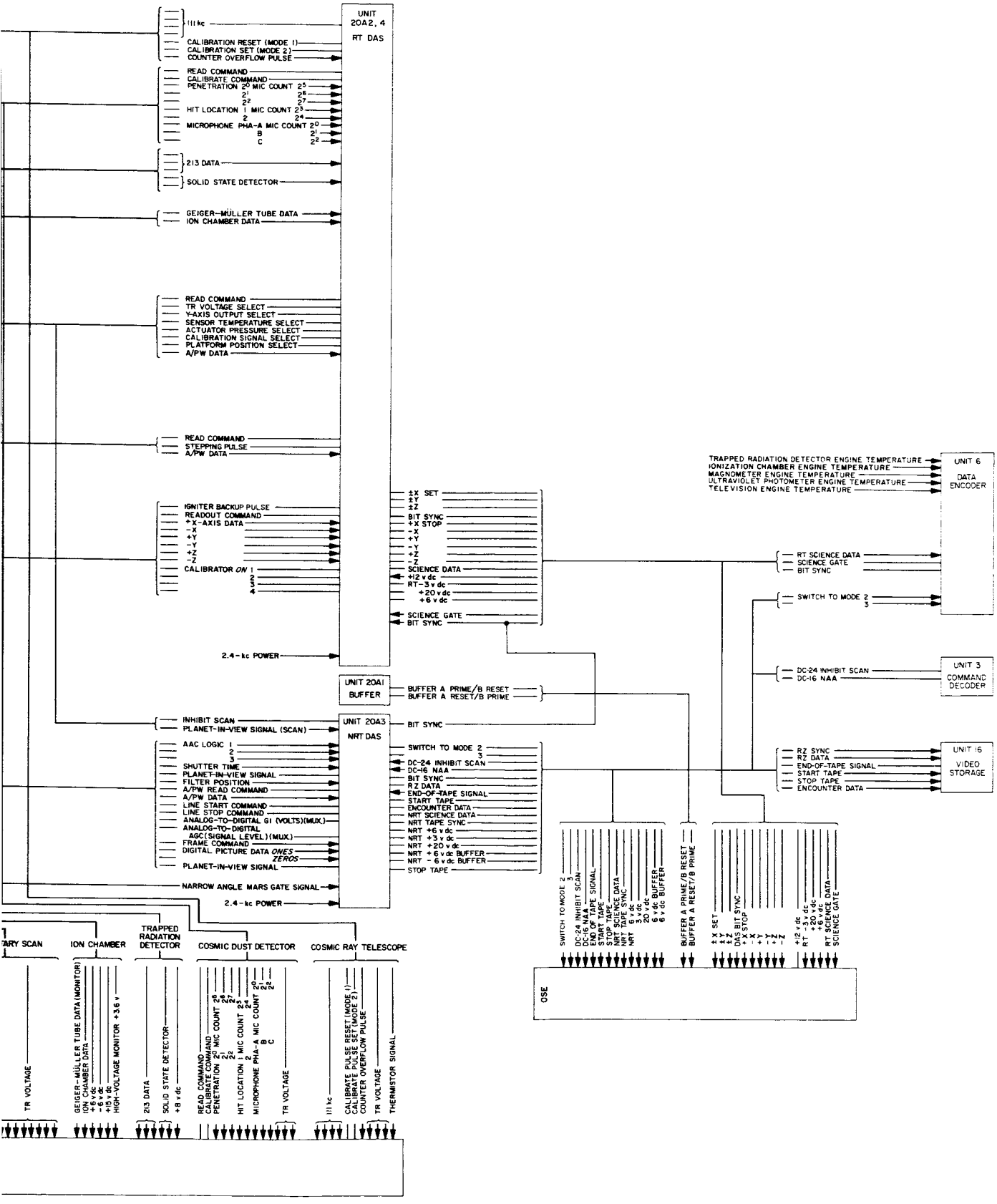


Fig. 273. *Mariner* Mars 1964 science subsystem functional block diagram

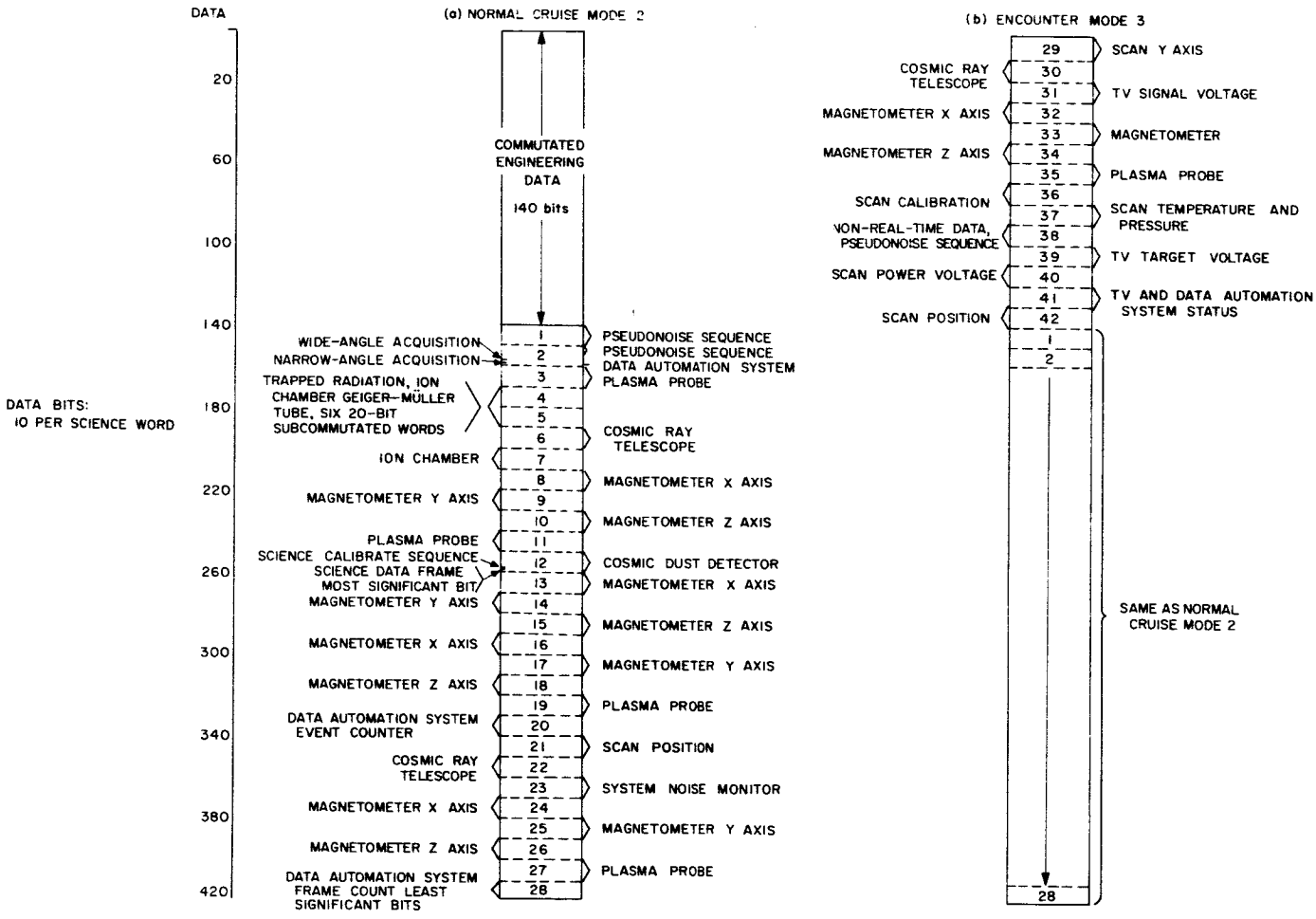


Fig. 274. Science subsystem real-time data format

The playback of stored science data is initiated by either a CC&S or a ground command. The science subsystem is deenergized, Data Mode 4 is initiated, and the stored data are transmitted to Earth. The pictures are transmitted individually; between each picture the data encoder is switched to Data Mode 1 so that engineering telemetry can be transmitted and the condition of the spacecraft evaluated. No new data are obtained during Data Mode 4, but the spacecraft reverts to Data Mode 2 upon completion of picture playback.

B. Cosmic Ray Telescope

1. Experimental Objectives

The Cosmic Ray Telescope (Fig. 275) was designed to measure (1) absolute and relative flux levels, and (2) energy spectra of the two main components of primary cosmic radiation (protons and ionized helium) that occur in the energy range from 1 to 180 Mev per nucleon. In addition, the telescope should identify helium ions having energies in excess of 180 Mev per nucleon and electrons in a low-efficiency fashion over a small range of energies. The specific aims of these measurements are directed towards the determination of fluxes in both interplanetary space and the vicinity of Mars. These aims include: (1) measurement of the radial gradient of the low-energy cosmic ray intensity in the inner solar system between 1 and 1.5 AU; (2) measurement of the ratio of low-energy protons and helium ions as a function of radial distance from the Sun; (3) the search for trapped protons and electrons at Mars; (4) the search for shock-front accelerated electrons near Earth and Mars; (5) the study of the time dependence, composition, and spectra of solar-flare particles in interplanetary space; (6) the search for a persistent solar contribution to the low-energy proton spectrum at solar minimum; and (7) the comparison of results with the Geiger–Müller counters and the Ionization Chamber to determine whether high-energy electrons are present.

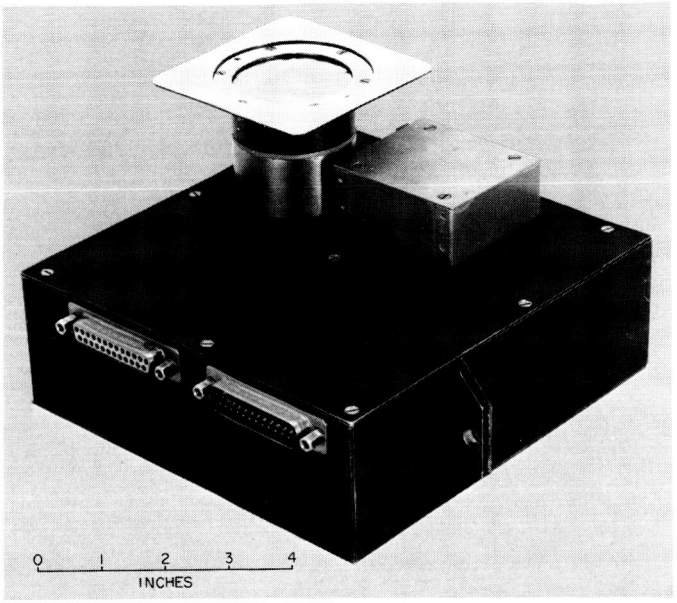
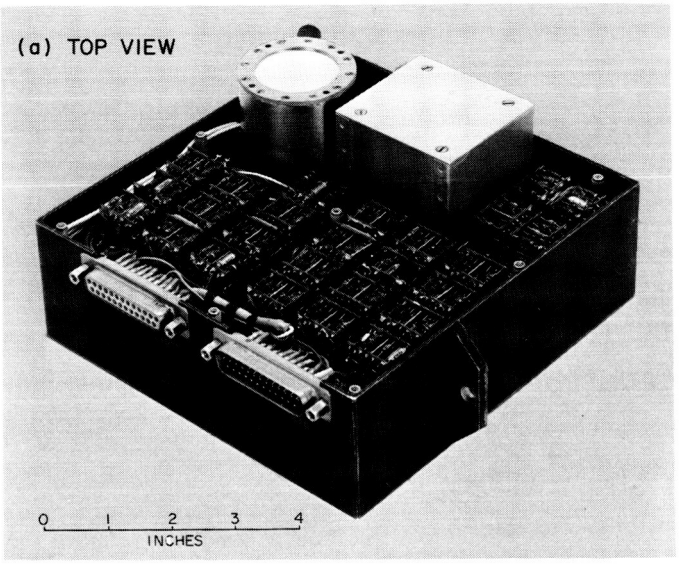


Fig. 275. *Mariner* Mars 1964 Cosmic Ray Telescope



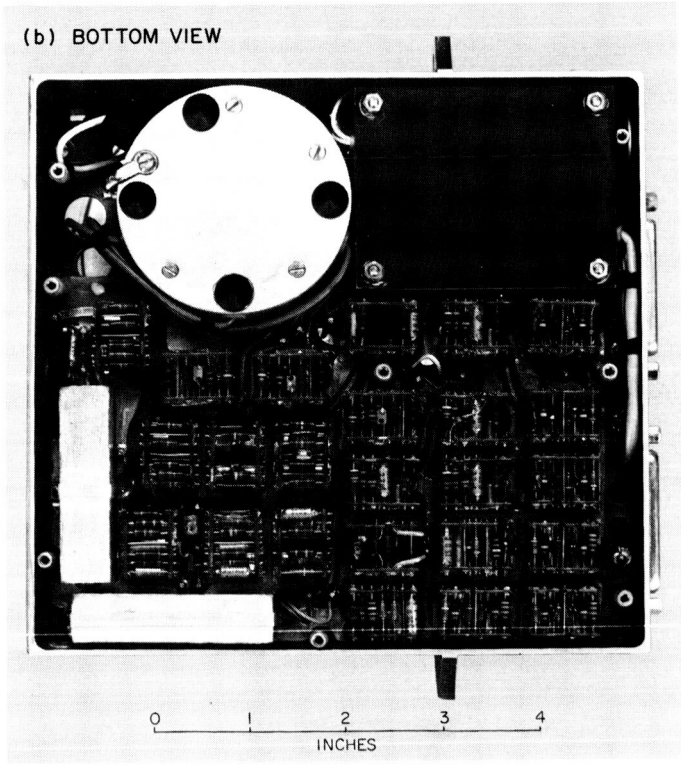


Fig. 276. Cosmic Ray Telescope

2. Description

a. Physical description. The Cosmic Ray Telescope weighs 2.58 lb and draws 598 mw of power. The electronics are contained in a standard JPL chassis 2 in. in depth with a center web. The majority of the electronic components were built into soldered cordwood submodules as shown in Fig. 276 (a) and 276 (b). These modules were inserted into "mother-boards" that fit on each side of the chassis. Each unit contains 1180 electronic components. The telescope, which is fastened to the center web, contains three gold silicon surface barrier detectors labeled D_1, D_2, and D_3 (Fig. 277). The look angle is a cone with a 30-deg half-angle from the axis of the telescope. The telescope looks out of the bottom of the spacecraft in the antisolar direction. Attached to the telescope through the bottom ring of the spacecraft is a temperature fin designed to prevent the detectors from exceeding 50°C in case the telescope looks directly at the Sun. The stack of preamplifiers in their shielded can are positioned next to the telescope (Fig. 275). On the other side of the module next to the back end of the telescope is the power converter shown in Fig. 276 (a).

b. Functional description. The three gold silicon detectors are arranged with absorbers between the first and second and the second and third detectors, as shown in Fig. 277. When any energetic charged particle passes through matter, it loses energy through ionization. When such a particle passes through a solid-state detector, it creates a number of electron-hole pairs that are swept out of the silicon before recombination can occur by an electric field created by a bias voltage. A charge thus produced in any detector is deposited at the input of a charge-sensitive preamplifier, where it is converted to a voltage pulse that is directly proportional to the amount of charge produced in the detector and, hence, to the energy lost by the particle. Figure 278 is the functional block diagram for the instrument. The amplifiers

are connected to pulse height discriminators D_1, D_1', D_2, D_3, and D_3'. Except for D_3', these discriminators produce pulses only if the input to them exceeds a level corresponding to an energy loss of 210 kev. The threshold of D_3' is 420 kev. In addition, the amplifier associated with detector D_1 is connected to a height-to-time converter that sorts pulses corresponding to energy losses between 210 kev and 5.2 Mev into 128 channels.

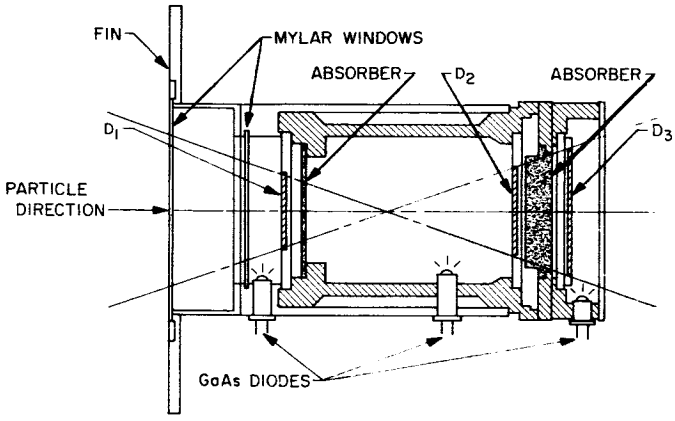
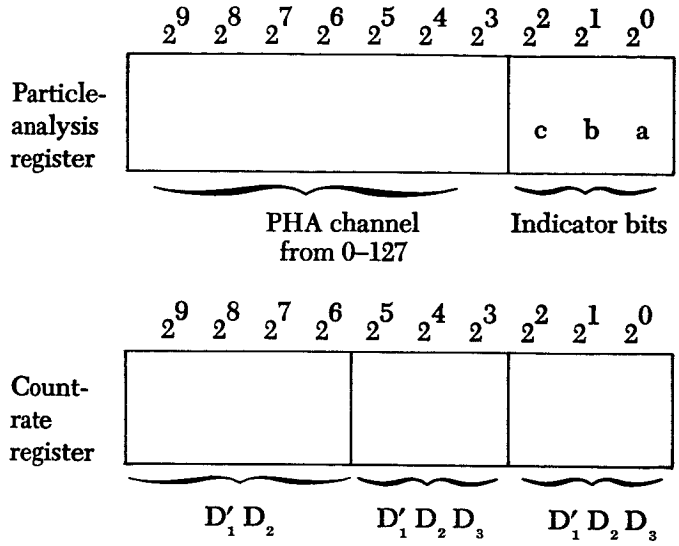


Fig. 277. Cosmic Ray Telescope, cutaway view

The discriminators are connected to the coincidence and anticoincidence logic circuits. These logic circuits are then connected to two 10-bit registers as shown below:



The first register (words A and C) reads out the pulse-height-analyzer channel number (0–127) and the three indicator bits a, b, and c. Bit "a" is a *one* if there is one

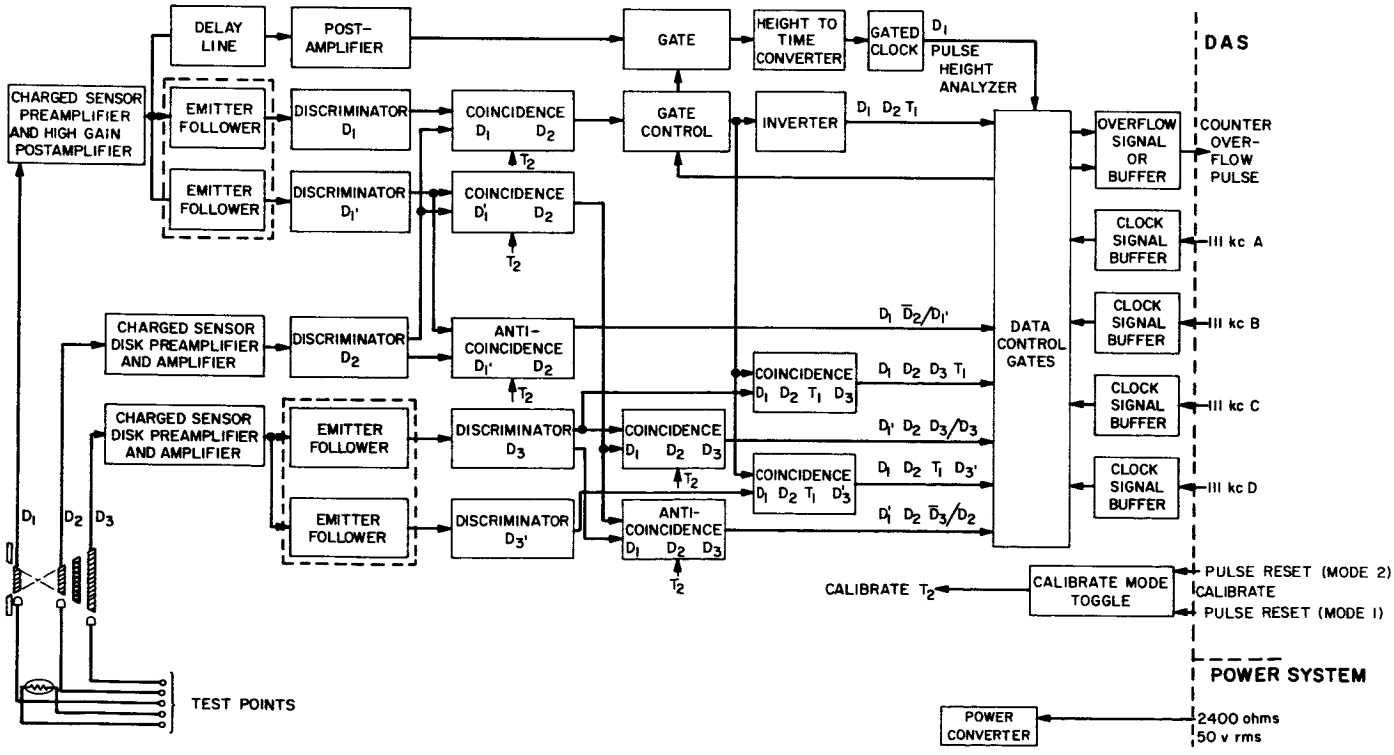


Fig. 278. Cosmic Ray Telescope functional block diagram

or more $D'_1 D_2 \overline{D}_3$ events between readouts. Bits "b" and "c" are *one* if D_3 and/or D'_3 are hit, respectively, in coincidence with the analyzed event. In the rate words (B and D), three bits are allotted for the $D'_1 D_2 D_3$, three bits for the $D'_1 D_2 D_3$, and four bits for the $D'_1 D_2$ events. These data outputs are shown below:

1. Pulse height number from 0–128, plus range indications
2. Three coincidence counting rates: $D_1 D_2$ protons and helium 0.8 Mev per nucleon–30 Mev per nucleon; $D_1 D_2 \overline{D}_3$ protons and helium ions 15–70 Mev per nucleon; and $D_1 D_2 D_3$ protons 70–170 Mev per nucleon, and helium 70 Mev per nucleon

The registers are read out alternately by the data automation system. To accomplish this, the DAS adds pulses to the register at 111 kc until the register overflows and then counts the number required to produce an overflow. The complement of this number is the actual reading in the register. The registers are cleared after each readout.

3. Design Evolution

The design of the Cosmic Ray Telescope was based on that of the units flown on the *IMP* and *OGO* satellites. Because of the limited amount of weight and volume allowed for the instruments on the *Mariner* Mars 1964 spacecraft, this instrument was much smaller than those flown on other satellites. This made the deletion of some of the readout binaries and one of the two telescopes used on *OGO* necessary.

On August 21, 1963, a design review was held in Chicago to evaluate the electronic circuits, and to determine the expected performance, accuracy, and stability of the instrument. From a composite of various laboratory results and theoretical calculations, it was determined that the estimated window drift (rate data) would be 13 to 23%, and that the estimated stability of energy analysis would be 14%. These results were based, in part, upon thermally induced variations occurring between a high temperature of 75°C and low temperatures between −20 and −45°C.

Changes were made in the original circuits, and other circuits were added as the instrument was assembled and tested. These new circuits were needed because of incompatibility in electronic circuits built for the Cosmic Ray Telescope. Other circuits and components were changed to obtain proper wave shapes and to adjust the timing needed between circuit pulses. Some of these changes were:

1. A Zener diode was added as a limiter to prevent overflow of the HTC.
2. A Zener diode was added to the output of the D_2 preamplifier to prevent saturation of the discriminator.
3. A capacitor was added to the coincidence and anticoincidence circuits to prevent feedthrough.
4. An inverter circuit was added.

After the first two instruments were built and the remaining instruments were in various stages of construction, it was determined that the four bits that comprise the D_1 rate would not produce meaningful data. This was discovered when the telescope flown on the *IMP* produced higher D_1 rates than anticipated. To compensate for the high D_1 rate, two binaries that prescaled the $D_1 D_2 \overline{D}_3$ indicator bit were rewired to prescale the D_1 rate. This, in effect, divided the D_1 rate by a factor of 4.

One other change to the telescope came about because of the detectors. In an operating condition, the temperature of the detectors cannot exceed 50°C. If the detectors had been unprotected, this temperature could have been surpassed during the spacecraft's tumbling after liftoff or during the midcourse maneuver when the telescope might have been required to look directly into the Sun. A temperature fin, which extended the barrel of the telescope by ¾ in. (Fig. 275), was added to the telescope. At the end of the barrel extension an aluminized mylar window covered the opening; an aluminized mylar window also covered the end of the telescope. This created a tube ¾ in. long fastened to the end of the telescope, with an aluminized mylar window at each end of the tube to reflect the sunlight. The end of the tube flared outward into a temperature fin, forming a flat square surface painted white to minimize heating. This temperature fin was expected to keep the detectors below 40°C regardless of the spacecraft orientation.

4. Fabrication

a. Techniques. The Cosmic Ray Telescope was contained in a standard JPL module 2 in. wide, with the telescope and amplifier housing protruding approximately 1 in. The circuitry comprising the electronics is assembled into soldered cordwood submodules, which are inserted into a mother-board containing the printed circuits that make the interconnections between them.

The Cosmic Ray Telescope contained two of these mother-boards, one on each side of the main module. The power converter and the preamplifier stack were shielded and fastened separately to the center web. The telescope barrel containing the three detectors was also fastened to the center web.

The use of cordwood submodules permitted high-density packaging of components, but also had some disadvantages. Whenever it became necessary to investigate a problem in an instrument, the task was made difficult because of the inaccessibility of test points. If a component needed replacement at the bottom of a submodule, all the components above it had to be removed, or the submodule had to be removed from the mother-board (a process requiring several hours because of the cabling connections).

5. Test Experience

The instruments were environmentally tested in accordance with JPL specifications. The operation of the telescope was determined by measurements made in three separate modes: normal, calibrate, and programmed.

a. Type-approval testing. There were two failures during the vibration testing of the TA instrument. The first failure was caused by a large filter capacitor in the power converter that broke loose during the second plane of vibration. The capacitor broke loose because the potting was not strong enough to hold the large components in place. Another potting was then used to hold the capacitor and other large components. During the next vibration test, the large components held securely but the D_2 shielded amplifier cable broke. This cable was repositioned and secured with potting, and no problems were encountered during the final vibration test.

Several thermal–vacuum tests of the TA unit were required. One condition that made the testing of this instrument difficult was that, although the temperature for the TA test was 75°C, the temperature of the telescope could not be allowed to go above 50°C (the critical temperature for the detectors). An attempt was made to keep the telescope cool by using a cold plate in contact with the temperature fin. This maintained a cool temperature for the telescope, but the plate caused noise problems with the instrument. In fact, a battery-operated thermocouple connected to the telescope caused enough noise to preclude obtaining intelligible data. It was decided that the approach of trying to keep the telescope below 50°C and yet testing the electronics at 75°C was impractical. Consequently, the TA test temperature was reduced to 50°C.

The first thermal–vacuum test failed because of a noisy instrument. The next three failures were caused by faulty OSE. The last three attempts were unsuccessful because of detector failures. The remainder of the environmental tests (radio-frequency interference, low-frequency vibration, acceleration, and shock) were passed with no problems.

b. Flight-acceptance testing. Not too many problems were encountered during the FA testing because of the experience gained from the TA tests and because the FA tests were less rigorous. The FA test problems occurred in the SN/MC-1 and SN/MC-3 instruments.[8] The SN/MC-1 instrument had a D_1 detector failure, which probably resulted from a mechanical strain on the detector. The mechanical strain was caused either by a screw forced against the detector or because the housing clearance of the detector was insufficient and the housing, as a result, produced a strain on the detector during the thermal–vacuum test. After the detector housing was remachined and the D_1 detector replaced, the SN/MC-1 unit passed the thermal–vacuum test.

During the thermal–vacuum test of the SN/MC-3 unit, data words A and C were lost. This malfunction did not recur.

c. System testing. Problems were encountered during the system testing of the telescope instruments. Some of the testing difficulties attributed to the telescope were later ascribed to OSE problems. It was found that the telescope could not be put into calibration by the DAS calibration pulse. This problem was solved by reversing the calibration leads in the telescope.

Several of the instruments had noise problems on the spacecraft. The SN/MC-4 unit, for instance, worked on the bench, but on the spacecraft the rate words overflowed their registers. A screw was added to one side of the back cover, which greatly improved the instrument when it was on the bench, but the data still overflowed when the unit was tested on the spacecraft.

[8] Throughout this section, the letters SN are prefixed to subassembly serial numbers to distinguish them from spacecraft serial numbers.

C. Cosmic Dust Detector

1. Experimental Objectives

Knowledge concerning the origin, composition, and dynamic properties of the cloud of dust particles surrounding the Sun is fundamental to the study of the solar system. Until this decade, information concerning the physical and dynamic characteristics of dust particles in space came from a variety of ground-based experiments. Meteor observations using visual, photographic, and radar techniques produced measurements of the mass, velocity, density, and composition of individual meteoroids colliding with the Earth's atmosphere. These studies were limited to particle masses greater than 10^{-4} g until radar observations of particles with limiting masses of approximately 10^{-6} g were reported. For particles with masses less than 10^{-6} g, photometric observations of the Zodiacal light, solar corona, and sky radiance have represented the major optical techniques used to obtain measurements of the sizes and dynamics of dust particles near the Earth and in deep space. Composition, age, and gross accretion rates of meteoroidal and dust-particle material have been obtained from analysis of collections of remnants of these particles surviving passage through the Earth's atmosphere. These collection studies included dust particles with masses as low as 10^{-10} g.

The direct study of the physical and dynamic properties of dust particles in space with masses between 10^{-13} to 10^{-6} g started with the measurements from dust particle experiments on various rockets, satellites, and space probes. The *Mariner* Mars 1964 dust particle instrument was designed to make continuous measurements of the flux of such particles near Earth, through interplanetary space, and in the vicinity of Mars.

2. Description

a. Physical description. The Cosmic Dust Detector is shown in Fig. 279. The plate, seen in a vertical position, is the bi-directional sensor; it measures 22 × 22 cm, and weighs 0.5 lb. The sensor was mounted to the electronics chassis, which weighs 1.6 lb and draws 201 mw of 2.4-kc power. The unit was mounted on the struts above the main spacecraft bus, between Bays III and IV, with only the sensor protruding above the upper thermal blanket. During flight, the normal of the sensor plate was parallel to the ecliptic.

Temperature control of the instrument was passive, and was monitored indirectly throughout the flight. Figure 29 indicates the mounting of the instrument on the spacecraft.

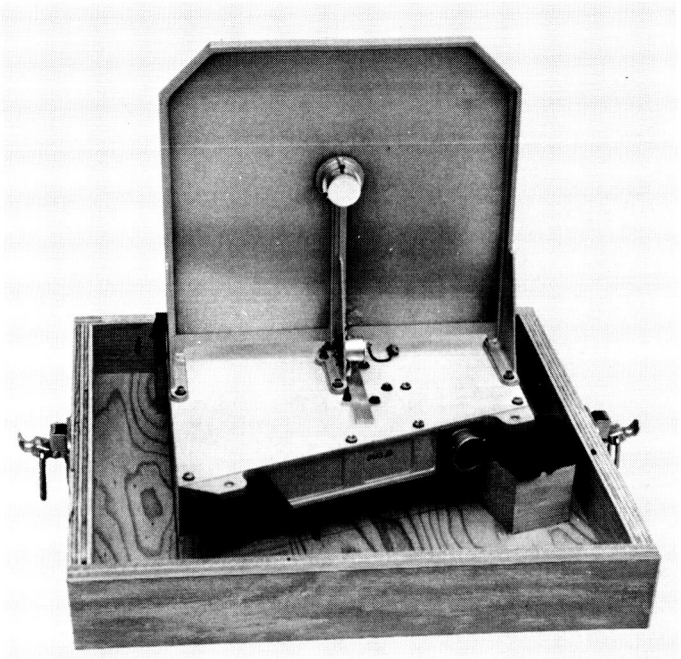


Fig. 279. *Mariner* Mars 1964 Cosmic Dust Detector

Each unit contains 707 electronic components, of which 187 are transistors or diodes.

b. Functional description. The sensor is an aluminum impact plate, 0.030 in. thick, with a crystal acoustical transducer (microphone) bonded to one side. This impact plate was coated on both sides with a nonconducting material. A thin film of aluminum was then deposited over the dielectric. The impact plate/dielectric/aluminum film combination formed a penetration detection capacitor. When a static potential was connected across the capacitors through a limiting resistor, a particle penetrating the dielectric would produce a voltage pulse across the limiting resistor. The films are greater than an order of magnitude more sensitive than the microphone, so their primary function is to indicate the direction of the impacting particle, and to detect particle hits below the microphone threshold.

The instrument memory consists of two 8-bit registers (Fig. 280): the first is for the accumulation of microphone hits and is never reset to zero; the second consists of three bits of film data, two bits of directional data, and three bits of PHA data. The second register is the microphone and film data register and is reset after each readout. The data in the two eight-bit registers are parallel-dumped, on command, into the DAS in an alternating sequence (every other data frame).

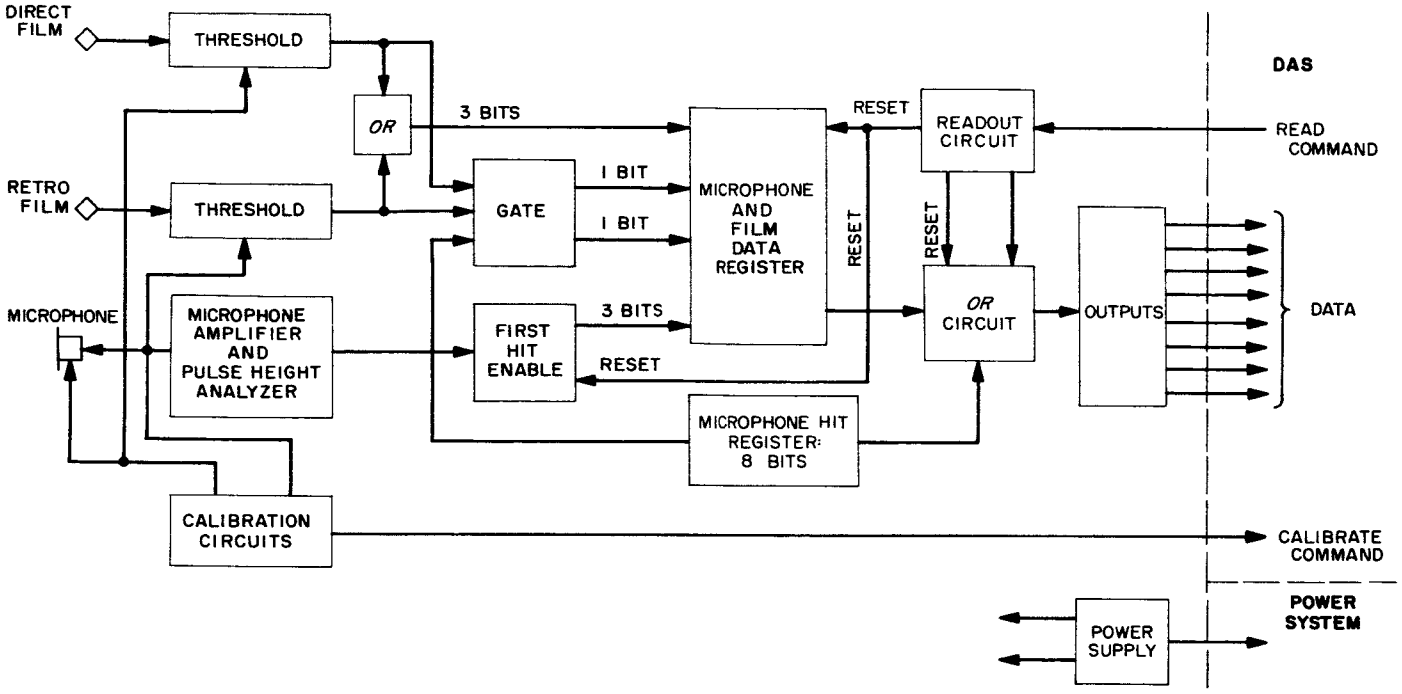


Fig. 280. Cosmic Dust Detector functional block diagram

The instrument calibration consisted of three procedures. In the first, the momentum sensitivity of the microphone and penetration detectors of a prototype instrument were determined using a hypervelocity particle gun. In the second, the sensitivity of the microphone was again measured as a function of the momentum of falling beads (non-hypervelocity calibration), and a correlation between these results and those of the first was established. The pulse-height analyzers of the flight model instruments were then calibrated using the non-hypervelocity methods. (The microphone PHA was designed with a nominal threshold of 10^{-5} dyne-sec and a logarithmic scale covering up to 3×10^{-4} dyne-sec in seven discrete levels.) In the third, the probability of false hits due to inflight spacecraft operational events was determined by monitoring the instrument output through the telemetry link during a long-term quiet test in which the spacecraft was continuously operated in cruise mode for 24 to 48 hr. During that period, the spacecraft inflight mechanical functions were exercised to determine instrument sensitivity to acoustical shocks and vibrations.

The instrument PHA was calibrated in flight by means of the acoustical transducer mounted on the sensor structure. Upon receipt of a calibrate command from the DAS (every 23⅔ hr at 8⅓ bps), the transducer imparted a mechanical shock to the impact plate, producing an output from the microphone.

There were two levels of calibrate signal amplitude. They were generated in the instrument electronics, and alternately pulsed the acoustical transducer on DAS calibrate commands. One level produced a PHA binary readout of 6, and the alternate level produced a binary readout of 3. In each case, a microphone count was stored in the eight-bit accumulator register.

The calibrate command also energized the film circuitry, alternating between the two sides. The resultant output of the calibrate command was a film hit, particle direction, a PHA signal indicated in the microphone and film data register, and a microphone hit stored in the accumulator register.

3. Procurement

The Cosmic Dust Detector was furnished by NASA's Goddard Space Flight Center.

4. Fabrication

The Cosmic Dust Detector electronics were fabricated under contract to Goddard Space Flight Center. Welded modular construction was used in the fabrication of the unit, with a welded matrix configuration for interconnecting wiring.

The penetration sensor assembly was fabricated at NASA's Goddard Space Flight Center. The sensor and electronics package were mated before delivery to JPL.

5. Test Experience

The TA level testing of the Cosmic Dust Detector was completed with no problems in December 1963. During FA and system testing, problems were detected that required changes in the instrument. During FA testing, it was found that the calibrate transducer mounted on the center rib of the sensor was not producing the correct PHA output. This was the result of a changing acoustical impedance between the calibrate transducer and the transducer bonded to the sensor. It became necessary, therefore, to delete this transducer from the instrument. The calibrate pulse then directly activated a transducer bonded to the sensor plate.

Acoustical type hits (no film or direction indication) were noted during system testing, which revealed a need for more mechanical isolation between the spacecraft and the instrument. This was done, and, in a test involving the MC-1 spacecraft, an acoustical attenuation of greater than 100 db between the spacecraft and the instrument was measured.

The sensor capacitor exhibited noisy operation during the system testing of the MC-1 spacecraft. The static voltage across the capacitor was reduced and the film thickness on the plate was changed. Two film preamplifiers were added to the film circuitry to reduce the input impedance and to increase the system response time.

D. Trapped Radiation Detector

1. Experimental Objectives

Energetic particle measurements were to be made during the *Mariner* Mars 1964 cruise period and during Mars encounter. Due to the varying distance of the spacecraft from the Sun and the long flight time of the mission, much helpful information could be obtained in particular areas of interest. The Trapped Radiation Detector was designed to:

1. Monitor solar cosmic rays and energetic electrons in interplanetary space, and study their angular distribution, energy spectra, and time histories
2. Search for magnetically trapped particles in the vicinity of Mars, and make preliminary determinations as to their spatial distribution, energy spectra, and identities
3. Provide further information on the densities and temporal changes of the Van Allen radiation belt during ascent from Earth to the interplanetary medium.

2. Description

a. Physical description. As seen in Fig. 281, there are four sensors mounted on a magnesium chassis. The exterior volume of the chassis is approximately 83 $in.^3$ (5.5 × 4.9 × 3.1 in.).

The detectors are the solid-state detector D_1 and D_2, and the Geiger–Müller tubes A, B, and C. The chassis contains the Geiger–Müller tube electronics, the power supply, and the electronics for the solid-state detector (D_1 D_2). The D_1 D_2 detector electronics are contained in a separate shielded chassis within the main chassis. The total weight of the instrument is 2.2 lb, and it draws approximately 350 mw of 2.4-kc power. The instrument is located atop the bus at Bay IV, midway between the −X and +Y axes of the spacecraft as shown in Fig. 29. Temperature control of the unit is passive, and is monitored by means of a thermal transducer contained within the instrument. Each instrument contains 290 electronic components.

b. Functional description. Detectors A, B and C are Geiger–Müller end-window counters, which measure the total number of charged particles passing through their sensitive volumes. The sensitive volume of each tube is shielded so that low-energy particles can enter only by passing through the window at the end of each tube. Only higher-energy particles can penetrate from other directions. If an allowance were made for non-directional counting of higher-energy particles, a directional measurement could be made of the low-energy particles.

Detectors A and B. The windows of detectors A and B are covered by approximately 1.4 mg/cm^2 of mica, and admit electrons $\geq$ 40 kev and protons $\geq$ 500 kev. A shield defines the angle through which particles can enter the window; this look angle is 60 deg, and lies along an axis that is 135 deg to the Sun–probe line for detector A, and 70 deg to the Sun–probe line for detector B. (The Sun–probe line is in the Z-axis plane in Fig. 29.) A visor was incorporated at the end of the tube housing to protect the detectors from direct sunlight during cruise.

Detector C. An aluminum foil of 19 mg/cm^2 was placed over the 1.4 mg/cm^2 of mica on the C detector

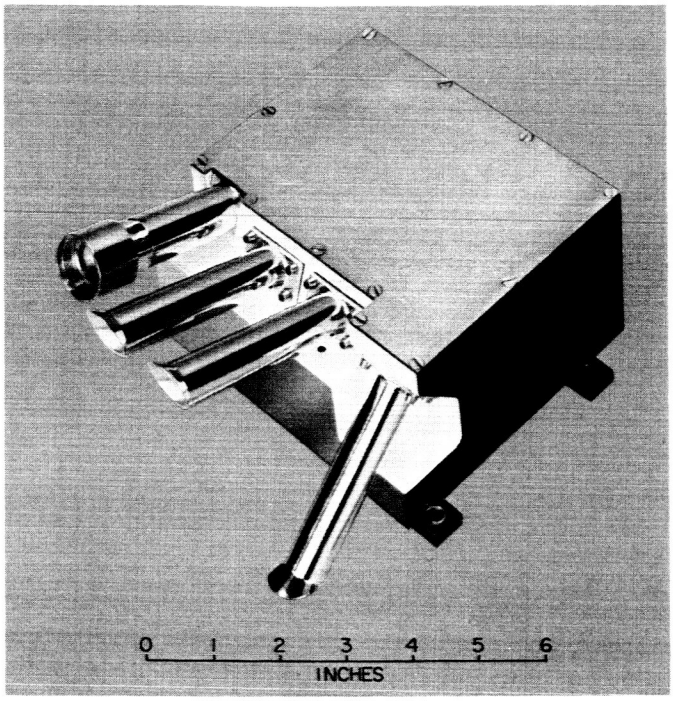


Fig. 281. *Mariner* Mars 1964 Trapped Radiation Detector

window. This extended the energy threshold of the detector to admit electrons $\geq$ 70 kev and protons $\geq$ 900 kev. The look angle of 60 deg for detector C was along an axis 70 deg to the Sun–probe line. The shield configuration was the same as the configuration on detectors A and B (Fig. 281). The Geiger–Müller counter outputs were shaped for use in the data automation system by saturating current amplifiers (Fig. 282).

Detector D. Detector D is a silicon surface barrier diode, with a thickness of 35 μ, that was covered with a nickel foil equivalent to 0.242 mg/cm^2 air to make it light-tight. This detector is essentially insensitive to electrons of any energy. Through amplitude discrimination, two levels of proton detection are possible:

D_1 = 0.5 to 11.0 Mev

D_2 = 0.9 kev to 4.0 Mev

The look angle of detector D is 60 deg and lies along an axis 70 deg to the Sun–probe line (Fig. 29).

The solid-state detector output (Fig. 282) is fed into a linear charge-sensitive amplifier (preamplifier) that is followed by a series of voltage-sensitive amplifiers (postamplifiers). The output of the second postamplifier is fed in parallel to two more amplifiers having different voltage gains. The outputs of these amplifiers are, in turn, sent to two identical amplitude discriminators having a common reference supply. The ratio of the energy discrimination levels is set by the ratio of the amplifier gains. The reference supply is temperature-compensated to keep the discrimination level constant. Table 59 summarizes the counting rates of the detectors.

Table 59. Trapped Radiation Detector counting rates

Detector	Shielding, in.	Energy for penetration $E >$ Mev	Dynamic range and counting rates, cm/sec
A	0.032 magnesium 0.020 teflon	Electrons $\geq$ 0.04 Protons $\geq$ 0.50	0.1 to 50,000 0.1 to 50,000
B	0.032 magnesium 0.020 teflon	Electrons $\geq$ 0.04 Protons $\geq$ 0.50	0.1 to 50,000 0.1 to 50,000
C	0.032 magnesium 0.020 teflon	Electrons $\geq$ 0.07 Protons $\geq$ 0.90	0.1 to 50,000 0.1 to 50,000
D_1	—	Protons 0.50 to 11.0	45,000
D_2	—	Protons 0.90 to 4.0	45,000

3. Procurement

The design and fabrication of the instrument was assigned to the State University of Iowa. Electronic components used in the fabrication of the circuitry, with the exception of the power supply, were purchased and screened under JPL cognizance.

Two major problems were evidenced in the procurement of parts, which caused a delay in the fabrication schedule. The first was the delay in obtaining screened parts for delivery to the fabricator. The second was the unavailability of flight-quality Geiger–Müller tubes and solid-state detectors.

4. Fabrication

Soldered cordwood modules, which were proved reliable throughout the testing and inflight phases of the program, were used in the fabrication of the unit.

5. Test Experience

The major source of concern during the testing was in the area of the solid-state detector. Failures in this area were caused initially by defective detector grounding bonds. Since the detector was contained in a Micro-Dot connector, the ground bond to the connector

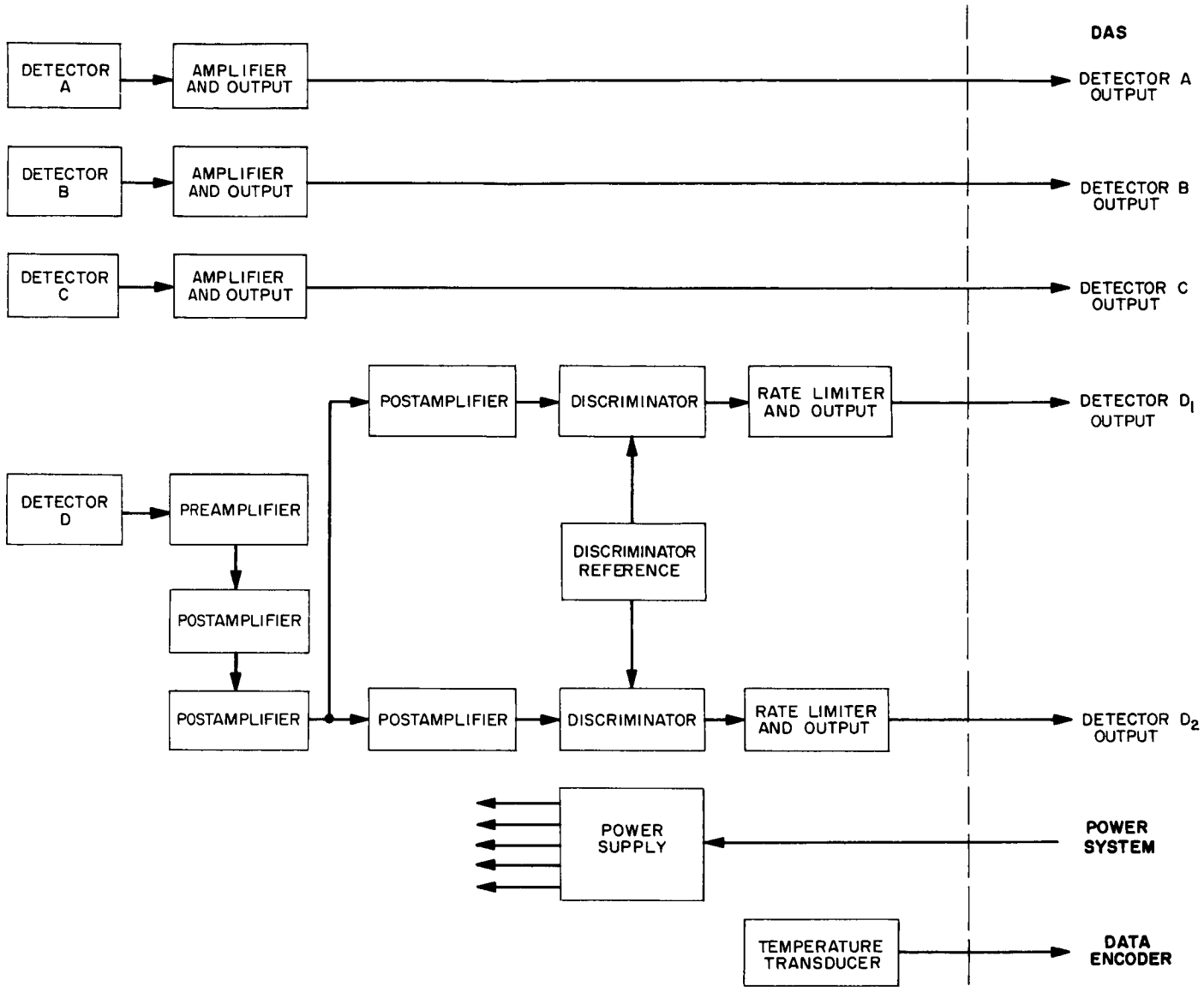


Fig. 282. Trapped Radiation Detector functional block diagram

case was critical. The use of a conductive epoxy to strengthen this bond eliminated the problem, and no subsequent failures occurred.

Malfunction of the 25-ft space simulator during testing of the SN/MC-4 unit may have caused detectors A and C to drift about 20 to 30%. This failure was attributed to a malfunction of the voltage regulator tubes associated with these detectors. Whether or not the chamber malfunction caused this failure has not been determined. Subsequent testing verified that a filter capacitor placed across the voltage regulator tubes did stop the fluctuation in counting rates. The change was incorporated on the SN/MC-4 unit only.

E. Ionization Chamber

1. Experimental Objectives

In recent years, considerable emphasis has been placed upon determining the energy distribution and the time variation of charged particles in the region that extends from the Earth's surface to the boundary of the magnetosphere. With the advent of unmanned interplanetary exploration, the opportunity was presented to extend the

range of interest beyond the magnetosphere into interplanetary space, and even into regions of close proximity to various planets.

Among the many and varied instruments used for making useful measurements regarding charged particles in space are the ionization chamber and the Geiger–Müller counter. A particularly stable type of integrating ionization chamber was first developed in 1953. A modification of this instrument adapted it and a suitable Geiger–Müller tube for use on the *Mariner* Mars 1964 spacecraft.

The Ionization Chamber experiment on this mission was designed to investigate (1) the dependence of the intensity of ionizing radiation in space upon distance from the Sun; (2) the temporal variations of the ionizing radiation and their correlation with measurements of the magnetic field and plasma flux at the spacecraft and with solar-terrestrial disturbances; and (3) the intensity and extent of magnetically trapped radiation around Mars.

2. Description

a. Physical description. The instrument package consists of four main items: (1) the Ionization Chamber, (2) a Geiger–Müller tube, (3) electronic circuitry comprising the power supply, amplifiers, and pulse shapers, and (4) the chassis to which the foregoing three items are mounted. The overall dimensions of the 2.7-lb assembly are 13.4 × 9.8 × 5.0 in. The assembled system is shown in Fig. 283. The instrument requires less than 500 mw of 2.4-kc 50-v-rms power for its operation. Each instrument contains 197 electronic components, of which 60 are diodes and transistors.

The Ionization Chamber consists of a 5-in.-diameter 0.010-in.-thick steel shell, which houses the fused-quartz electrometer system. The shell interior was evacuated at bakeout temperatures (400°C) and then filled with argon gas to a pressure of 4 atm. A black-oxide coating applied to the exterior provides the desired thermal emissivity.

The other sensor consists of a commercially available tube encased in a steel cylinder 0.83 in. in diameter by 5.0 in. long with a wall thickness of 0.008 in. End caps cushion the tube within the cylinder, and shock-mount the fragile tube in proper position. The external surface is also oxide-coated for thermal considerations.

The power supply and the data conditioning circuitry were fabricated on four printed circuit boards. All circuit components were mounted on one side of laminated-

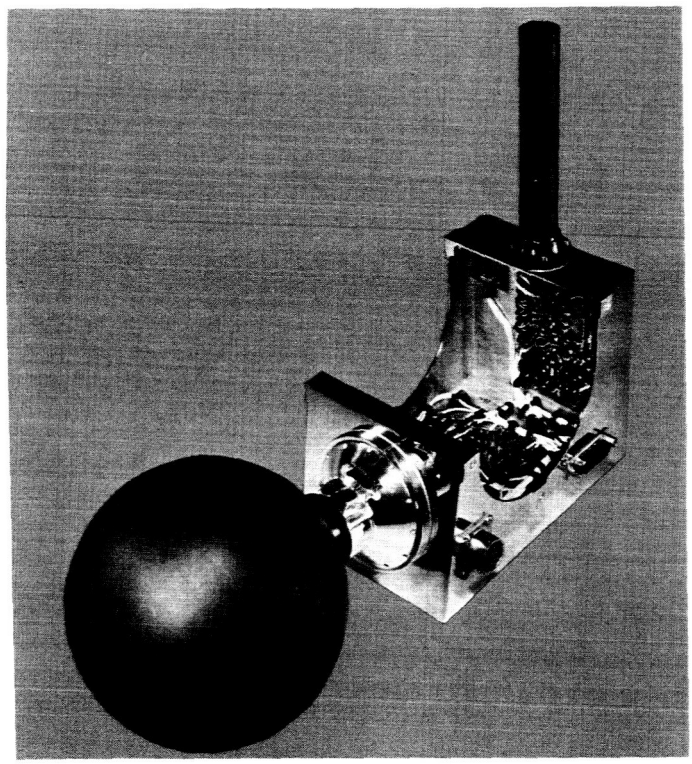


Fig. 283. *Mariner* Mars 1964 Ionization Chamber

epoxy circuit boards and soldered to gold-plated forked terminals. A conformal coating of epoxy covered the components and circuit board and, thus, provided protection against shorting, moisture corrosion, and electrical leakage. An insulating board was bonded to the back of each circuit board and the boards were held to the instrument chassis by screws and an epoxy bonding material. A typical circuit board mounted on the chassis is illustrated in Fig. 284.

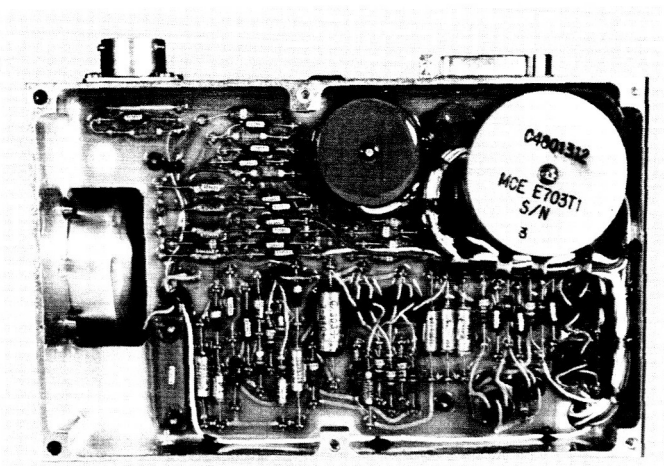


Fig. 284. Typical Ionization Chamber circuit board

The instrument chassis was machined from a solid block of magnesium alloy. The chassis surface was gold-plated to provide proper thermal emissivity. The Ionization Chamber and the Geiger–Müller tube were bolted to the chassis at right angles to each other as shown in Fig. 283. This unorthodox configuration contained a semicircular cutout that allowed the instrument to be mounted to the cylindrical antenna mast approximately 36 in. above the spacecraft bus. The instrument was mounted between two flanges on the mast structure, and was attached to these flanges by means of six screws with insulating inserts.

Two connectors on the instrument chassis provided for (1) input power to the instrument, output signals to telemetry, and a connection to spacecraft ground; and (2) monitor voltages and signals to the operational support equipment.

b. Functional description. The Ionization Chamber consists of a stainless-steel sphere filled with argon gas. A quartz electrometer is housed within the sphere and consists of a quartz collector rod and a thin quartz fiber, which is separated from the rod by approximately 0.02 in. The collector is coated with Aquadag and the fiber is coated with a thin film of metal. Although the collector is electrically isolated from the fiber and sphere, it is normally positively charged. This charge is produced by a positive 310-vdc potential on the fiber, which induces a negative image charge on the Aquadag surface of the collector near it. As a result of this image charge, the fiber is attracted to the collector and momentarily contacts it. During contact, electrons pass from the collector to the fiber. When the electron exchange is completed, the fiber springs back to its normal position leaving the rod positively charged to 310 v.

When ionizing particles penetrate the sphere, the gas within the chamber becomes ionized. The resulting positive ions are attracted to the grounded sphere, and the electrons are attracted to the collector and tend to neutralize its positive charge. When the collector charge is sufficiently neutralized, the image charge attains sufficient magnitude and the fiber is pulled to the collector and finally contacts it. A surge of electrons passes from the collector to the fiber and through a load resistor. This current pulse is amplified, shaped, and presented to the DAS as shown in Fig. 285. Each output represents a fixed amount of charge collected from the gas. Thus, the interval between pulses is inversely proportional to the ionization rate.

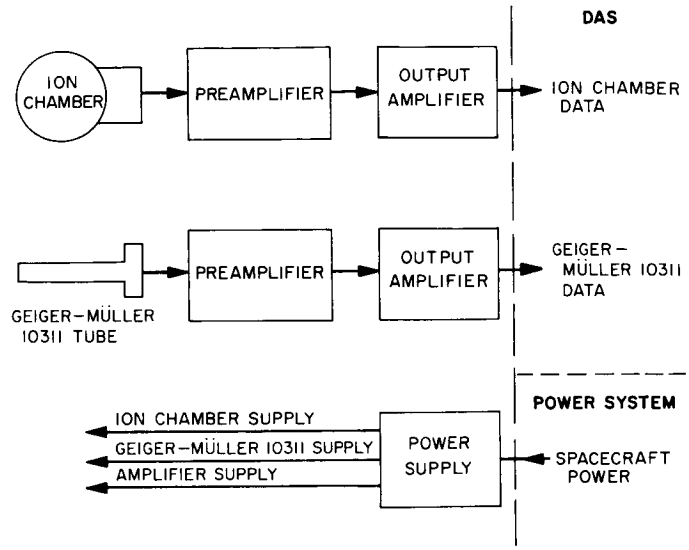


Fig. 285. Ionization Chamber functional block diagram

The Geiger–Müller sensor is comprised of a glass tube encased in a stainless-steel cylinder. The anode consists of a tungsten wire stretched along the axis of the tube, and the cathode consists of a thin, transparent conductive coating on the inner glass wall. Approximately 900 v are maintained between the electrodes. Charged particles, which penetrate both the steel shield and the glass wall and enter into the sensitive volume of the tube, ionize the gas molecules. The high electric field between the anode and the electrode accelerates the dissociated ions and electrons. The electrons accelerate rapidly because of their low mass, and ionize other gas molecules. The ultimate result of the avalanche effect produced between the electrodes is a momentary current flow through an appropriate load resistor. The resultant pulse is amplified, shaped, and delivered to the DAS as shown in Fig. 285. One output pulse is generated for each charged particle that penetrates the shield and enters the sensitive region of the tube. Thus, the pulse rate is directly proportional to the radiation flux.

Through a judicious choice of Geiger–Müller tube shield thickness, both the Ionization Chamber and the tube detect particles of the same energy. Electrons of energy greater than 0.5 Mev, protons of energy greater than 10 Mev, and alpha particles of energy greater than 40 Mev are capable of penetrating the walls of either detector. Both sensors have omnidirectional sensitivity. The Ionization Chamber measures the average rate of ionization, and the Geiger–Müller tube measures the omnidirectional flux of energetic particles.

3. Design Evolution

The concept of the Ionization Chamber was not unique with the *Mariner* Mars 1964 program; it evolved from previous satellite and spacecraft programs, the most recent of which was the *Mariner* Venus 1962 mission. *Mariner II* carried detectors almost identical to those of *Mariner IV*, only in a different physical configuration. Minor circuit modifications and repackaging of the detectors to conform to the Mars spacecraft constraints were performed at JPL, where electronic breadboards were built and tested (all other units were fabricated by subcontractors).

Design reviews, conducted by both JPL and the subcontractors, resulted in a few minor engineering change requests early in the prototype development stages. Such requests included changing the subchassis from aluminum to a magnesium alloy with special heat conductive properties, and changing the proposed method of Ion Chamber mounting to conform more closely to configurations already proven. Other changes were found necessary later in the environmental testing program, and the resultant rework was performed at JPL.

4. Procurement

The fabrication of the Ionization Chamber units was subcontracted in June 1963. These units included the thermal control model, prototype TA model, proof test model, three flight units, and one set of selected spare components. Delivery of the final flight unit to JPL occurred in February 1964.

5. Fabrication

Fabrication proceeded smoothly with one exception: the screened electronic components, which were to have been provided by JPL under the terms of the contract, were not available in sufficient selection and quantity early enough in the program to prevent a schedule slippage of the first units delivered.

A quality control program was established by the subcontractor in accordance with JPL requirements. As a result of this program, a quality control plan was completed and approved before flight hardware fabrication. The quality control plan included a flow chart covering all phases of assembly, test, and inspection from initial receipt of raw materials to delivery of completed units to JPL.

Inspection of the first circuit boards assembled revealed that component leads had been bent to provide strain relief before the component was soldered to the terminals. Past experience had indicated that such treatment enhanced, rather than inhibited, the possibility of component failure. Due to the scarcity of the screened components involved, and out of deference to the delivery schedule, it was decided to accept the component mounting technique in the one unit concerned, originally designated as the TA unit. However, this unit was redesignated as the PTM in order to allow TA tests to be performed on a unit identical to the flight unit.

Although 90% of the fabrication work was performed by a subcontractor, the California Institute of Technology coated the quartz collector and fiber before final assembly and testing of the instrument.

6. Test Experience

In addition to acceptance tests performed on delivery, TA tests, FA tests, and system tests were performed.

Type-approval tests on the TA unit were completed in January 1964. No failures were observed during TA testing of the unit, although a previous arcing failure during an FA thermal–vacuum test had indicated the necessity for adding a bleeder resistor to the power supply. Flight acceptance of the last flight unit was performed in March 1964. Extensive environmental testing was also performed, and, in addition, all units were given extensive calibration tests. (Calibration tests included monitoring sensor outputs under instrument exposure to standard X-ray and Co^{60} irradiation in a controlled environment, as well as periodic checks of the instrument response to standard Co^{60} sources in a fixed position aboard each spacecraft.) The last of these calibrations was performed at the AFETR facility shortly before the launch of *Mariner IV*.

F. Solar Plasma Probe

1. Experimental Objectives

The Plasma Probe experiment was designed to determine the positive-ion flux density in the range of 5×10^{-5} to 5×10^{-9} particles/cm^2 sec in the energy spectrum between 30 ev and 10 kev. The instrument was also intended to measure the directional characteristics of the plasma flux within a 30-deg half-angle cone centered 10 deg off the Sun–probe line along its temporal and spatial variations. The physical state of the plasma is intimately related to that of the magnetic field, and it was considered necessary to compare measurements made by the Solar Plasma Probe to those made by the Helium Magnetometer.

2. Description

a. Physical description. The Plasma Probe is shown in Fig. 286. The sensor is a Faraday cup mounted on the upper spacecraft superstructure above Bay III, with its receiving aperture center line tilted 10 deg from the Sun–probe line. (The mounting arrangement is shown in Fig. 29.)

The instrument sensor consisted of a cup-like shell and a number of enclosed electrodes. Originally, the shell was in two parts (a cylindrical wall and a circular back plate); both pieces were gold-plated magnesium. The wall cylinder section included an outer flange for mounting to the spacecraft, and inner flanges for grid support. The outer and shield grids operated at ground potential and were mounted directly to the flanges; the modulator and suppressor grids were electrically isolated from the shell by stand-offs. The variable modulator voltage and suppressor bias of −150 v entered through connectors on the outside of the wall. All grids were constructed of tungsten wire mesh. The three collector electrodes, mounted to the inside of the back plate, were 120-deg sectors, each separated from its neighbors by 1/16 in. Connectors on the outside of the back plate, in addition to carrying the collector signals to the preamplifiers, allowed direct electrical access to the collectors for test purposes. The probe was 4½ in. in depth and 6 in. in outside diameter (excluding the mounting flange), and the front cover had a 2½-in.-diameter viewing aperture.

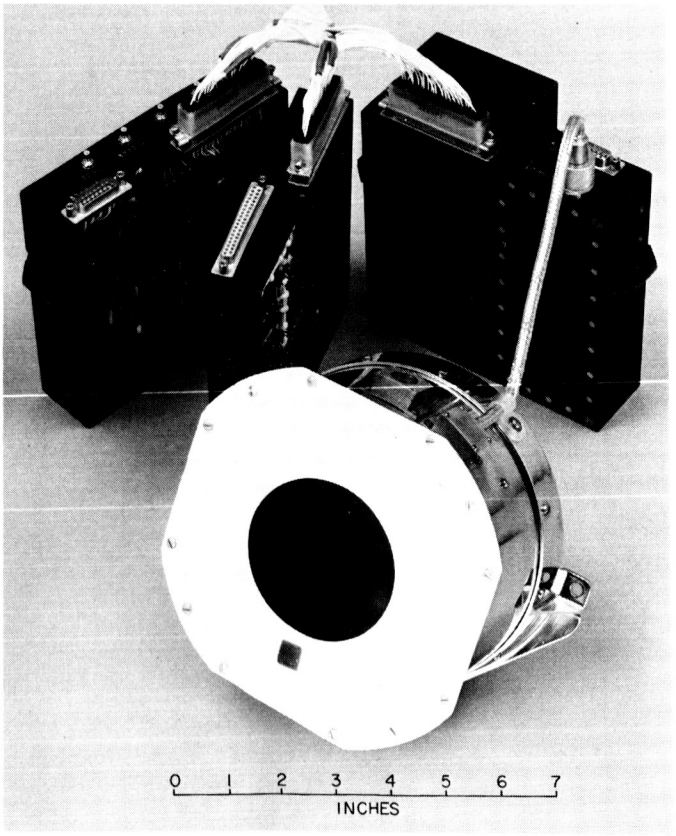


Fig. 286. *Mariner* Mars 1964 Solar Plasma Probe

The three electronic modules were mounted in spacecraft Bay III just below the sensor. The composition of these modules is shown in Table 60. The instrument contained 1300 electronic components, of which 618 were either diodes or transistors.

Table 60. Description of Plasma Probe electronics modules

Module	Surface	Circuit designation	Description
32A2	Lower	Preamplifier	Preamplifiers, analog gates, sum amplifier
	Upper	Signal processor	Remainder of measurement chain through analog-to-pulse-width converter; test signal and standard signal generators
32A3	Lower	Digital No. 1	Interface multivibrators, program and collector counters, sequence flip-flop, window-counter trigger circuit
	Upper	Digital No. 2	Window counter, window power control, bookkeeping circuits including diamond, enable gate for both diamonds
32A4	Lower[a]	Power converter	
	Upper	High-voltage modulator	Window power control output amplifier, synchronization multivibrator and flip-flop, modulator through output transistors and associated gates
		High-voltage rectifier	Modulator output transformer, dc multiplier, bleeder/divider

[a]The high-voltage monitor amplifier was mounted on a shield between the modulator and rectifier circuit boards. The −30 v storage capacitor was attached above module 32A4.

b. Functional description. The functional block diagram of the Plasma Probe is shown in Fig. 287. Figure 288 shows a top and sectioned view of the sensor. The plasma (positive ions, electrons, and light) enters the cup through grid 1, which is maintained at cup-shell potential. A square wave voltage on grid 2 modulates

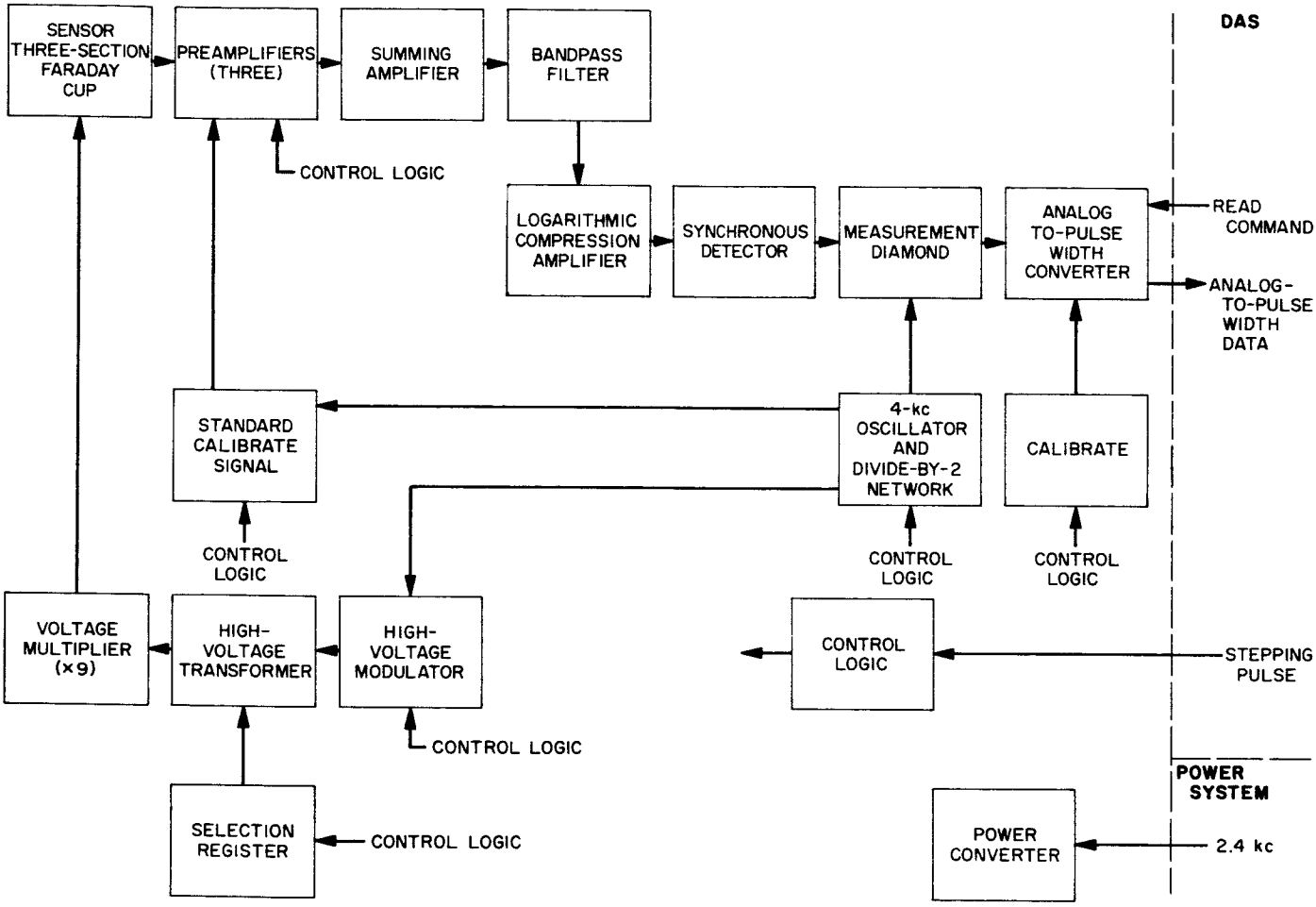


Fig. 287. Solar Plasma Probe functional block diagram

the incoming charged particles. Grid 3 is kept at cup-shell potential to serve as an electrostatic shield between the modulating grid and the collectors. Grid 4 is held negative, with respect to the collectors, and acts as a suppressor grid.

The collector is divided into three sections. From an analysis of the relative signal amplitudes of individual segments (Fig. 289), direction is determined unambiguously within a broad solid angle of circular cross section centered at the cup normal. Reverse photoelectric current, generated by light reflected from the collector onto the back of the suppressor grid, is overcome by modulating the positive-ion current without modulating the reverse photocurrent, and then detecting the ac component of the collector outputs.

The collector outputs are amplified by the three preamplifiers (Fig. 287) and sent to a set of three gates. In the "all collector" mode, the outputs are summed to a single ac signal and fed to a bandpass filter peaked at the synchronization frequency. In the "sequential-collector" mode, the individual outputs are selectively fed to the filter. The in–out transfer function of the compression amplifier closely approximates a logarithmic response over the four-decade dynamic range of the signal from the filter. The synchronous detector demodulated the signal from the compression amplifier, and the output of the synchronous detector is stored on an analog diamond circuit. The analog-to-pulse-width converter is connected across the diamond, and samples the voltage there on a format fixed by the data automation system. The sampling of the system through a cycle is shown in Table 61.

The high-voltage level and mode switching are accomplished through the instrument's control logic by using the DAS stepping pulse as a clock. The plasma output is

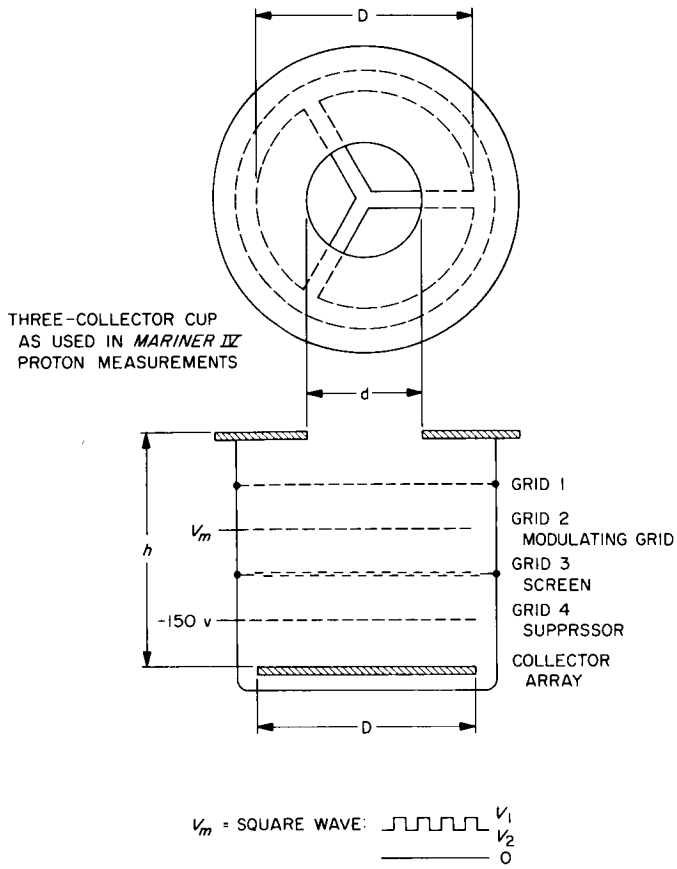


Fig. 288. Solar Plasma Probe sensor, top and sectioned view

Table 61. Plasma Probe voltage sampling format

Step	Mode	Voltage level
1 to 16	All collector	1–16 sequentially
17 to 19	Sequential collector (2, 3, 1)	1
20 to 22	↓	2
23 to 25	↓	3
26 to 28	↓	4
29 to 31	↓	5
32 to 34	↓	6
35 to 37	↓	7
38 to 40	↓	8
41 to 43	↓	9
44 to 46	↓	10
47 to 49	↓	11
50 to 52	↓	12
53 to 55	↓	13
56 to 58	↓	14
59 to 61	↓	15
62 to 64	↓	16
65	Preamplifier 2	1
66	Preamplifier 3	↓
67	Preamplifier 1	↓
68	Set	↓
69	High voltage	↓
70	Temperature	↓
71	Marker	↓
72	Reset	↓

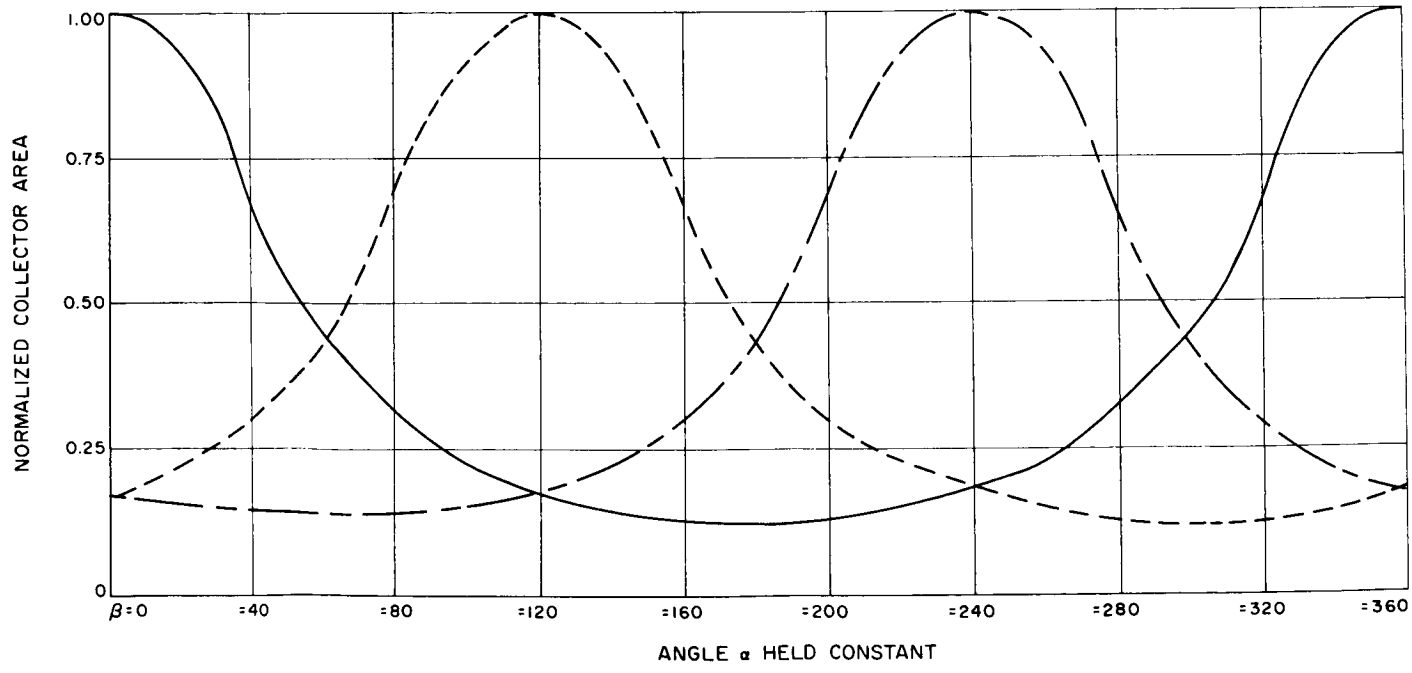


Fig. 289. Individual collector response

sampled in DAS words 3, 11, 19, 27, and 35. In spacecraft Data Mode 2, the instrument receives four stepping pulses, and in Data Mode 3 it receives five stepping pulses; thus, 18 frames are sampled before a Plasma Probe cycle is completed in Data Mode 2, and 14.5 frames are required in Data Mode 3. Step pulses are issued two DAS words prior to readout, and the analog-to-pulse-width conversion occurs one word prior to readout.

3. Procurement

The Solar Plasma Probe was furnished to JPL by MIT. The electronic modules were fabricated under subcontract from MIT, and the primary design of the instrument was accomplished by the MIT Lincoln Laboratories under JPL and GSFC contracts for *Mariner A* and *B*, *Explorer X*, *IMP*, and *OGO*. The instrument sensor was designed and built in the Laboratory for Nuclear Sciences at MIT.

Under the direction of MIT, the electronic components were procured by the subcontractor using JPL-approved screening specifications as procurement specifications. Each vendor screened his own products before delivering the accepted items to the prime subcontractor for Plasma Probe fabrication. In the interest of maintaining a schedule and promoting reliability, the screening of key items was performed with subcontractor QA personnel in constant attendance.

The power supplies were purchased by MIT from another vendor and supplied to the Plasma Probe subcontractor as an assembled circuit board. All power supply transformers and chokes were fabricated by this other vendor and were not screened. On October 29, 1963, schedule difficulties forced JPL to waive the requirement for 100% screening and to leave it to the discretion of the instrument supplier. However, all electronic components (except for a few resistors in SN/MC-5) were screened in the flight units.

4. Fabrication

The following waivers were required so that the Plasma Probe could be built within a reasonable weight and volume.

1. Use of TO-51 encased transistors. The reliability of these units proved to be no better than predicted. of the 26 problem/failure reports listed as component failures, 13 were due to TO-51 transistors. Furthermore, it was discovered that many of the transistors were not hermetically sealed. When a vacuum environment was used in conformally coating the PTM, many transistors became impregnated with the conformal coating. Subsequent coating was performed without the aid of a vacuum, although the impregnation itself was never established as a cause of failure.
2. Use of less reliable resistors. Reliability had to be sacrificed for packaging considerations. Three out of the remaining 13 problem/failure reports listed these resistors as causes of failures.
3. Use of plated-through-hole printed circuit boards, as opposed to fork terminal construction, in order to save space.

5. Test Experience

During the seventh day of the TA thermal–vacuum test, the power transformer developed a short. The combination of vacuum, heat, electrical stress, and potting voids caused an insulation breakdown between two windings. As a result of the failure, the following changes were made: (1) the location of one winding was changed; (2) the internal construction was redesigned to permit more thorough impregnation; (3) the potting technique was changed; and (4) the potting compound was changed. The last change afforded post-fabrication inspection. The power supply vendor did not possess a heated vacuum chamber, but did achieve void-free potting by alternating the in-process units between a hot oven and an unheated vacuum chamber.

During the FA vacuum test of the MC-3 spacecraft, the Plasma Probe produced sufficient periodic electrical noise to interfere with the Spacecraft System operation. The noise, apparently produced by arcing in the sensor, caused concern that spacecraft operation would be jeopardized during flight. After an intensified effort, it was learned that the cup tended to arc for periods up to 2 hr after evacuation. The arcing was caused by outgassing due to air trapped behind the silicon rubber insulators, and disappeared when the silicon rubber was replaced with Kel-F.

G. *Helium Magnetometer*

1. Experimental Objectives

The reasons for making magnetic-field measurements during the Mars mission are:

1. To establish whether a planetary field exists, and to determine the characteristics of the field (magnitude, direction, multipolarity, and orientation relative to the planetary rotational axis)

2. To investigate the nature of the boundary between planetary and interplanetary magnetic fields
3. To measure the magnitude and direction of the steady and slowly varying components of the interplanetary magnetic field, and to determine its variation with heliographic latitude and longitude

To meet the experimental goals, the magnetometer had to have the following operational characteristics:

1. Three outputs proportional to the three mutually perpendicular components of the magnetic field, with a sensitivity threshold of ≤ 0.25
2. A frequency response of 1 cps maximum
3. A dynamic range (0 to 1 cps) of $\pm$ 360 γ
4. A nine-bit conversion, plus one sign bit
5. A known zero offset less than 1 γ
6. Calibration capability to apply fields of +40, +80, −40 and −80 γ at the sensor (1 γ = 10^{-5} gauss)

2. Description

a. Physical description. Figure 290 shows the Magnetometer sensor and electronic modules. The module on the left contains the Magnetometer power supply, ignition logic, RF power supply, and analog-to-pulse-width converters. The module on the right contains the basic signal chain circuitry and ancillaries. The spherical portion of the sensor is the Helmholtz coil housing. The sensor weighs 1.25 lb, and the two modules together weigh 5.0 lb. The average power input to the instrument is 7 w. Each instrument contains 805 electronic components of which 183 are either transistors or diodes.

b. Functional description. Figures 291 and 292 show the Helium Magnetometer sensor schematic and system functional block diagram. The physical principle underlying the operation of the Magnetometer involves the transparency of a plasma of metastable helium atoms to a beam of resonant radiation at 1.083 μ wavelength, and the dependency of this transparency on magnetic fields. A set of Helmholtz coils are used to produce a rotating magnetic-field vector in the plasma contained in the absorption cell, and a lead sulfide detector senses the modulation of the light beam. Any asymmetry in the resultant magnetic field (vector sum of the sweep plus ambient field) causes asymmetry in the light modulation. With a sweep vector of constant amplitude and angular frequency, external dc fields cause a component in the modulation at the frequency of the sweep vector. This phenomenon was phase-dependent on the direction of the field with respect to the light axis. In the absence of external fields, the modulation of the light beam is at twice the frequency of the sweep vector. Any fundamental component caused by an ambient field is amplified by the system electronics and synchronously demodulated. The demodulated signal is integrated, amplified, and fed back as current to the sensor coil system

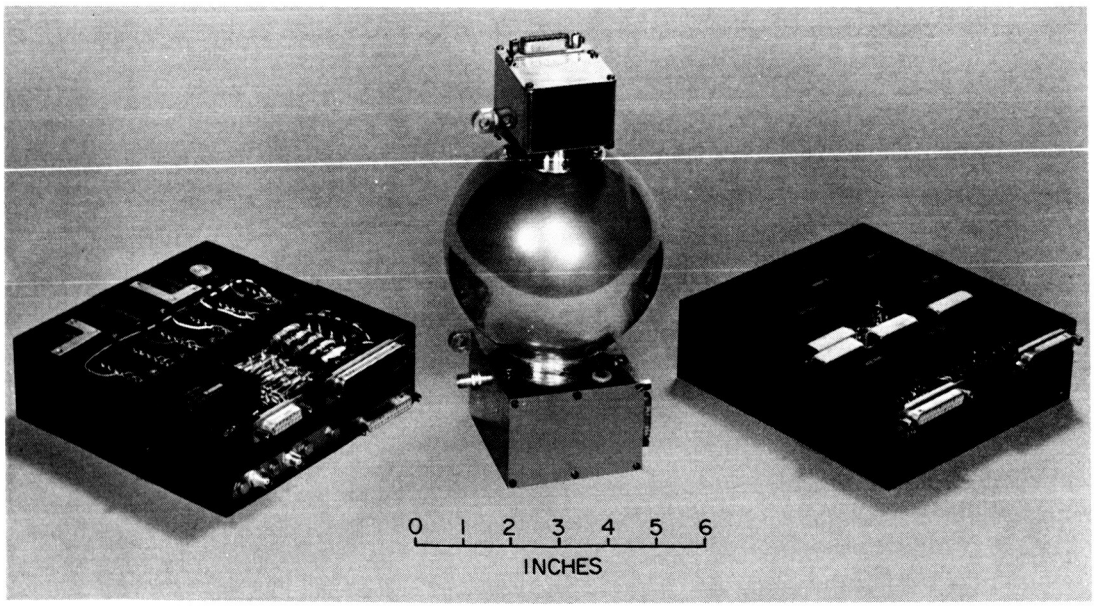


Fig. 290. Helium Magnetometer sensor and electronics modules

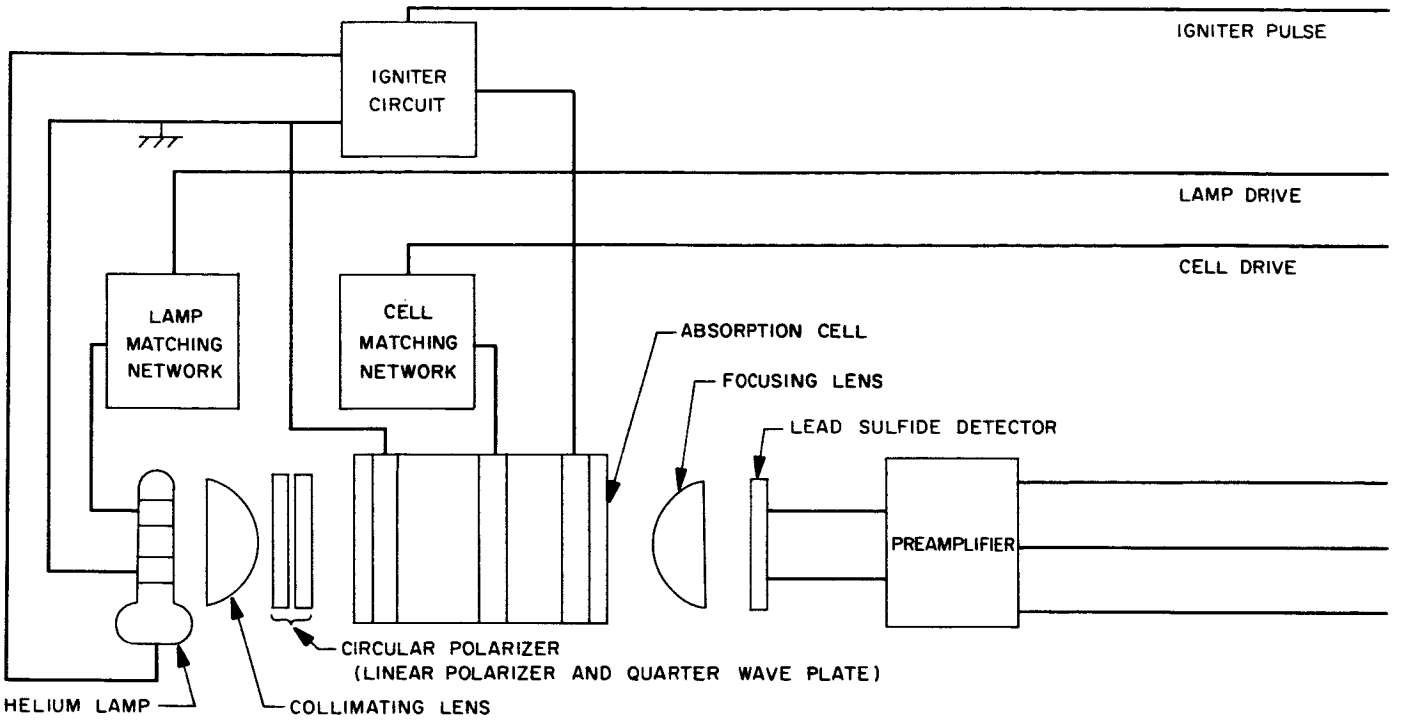


Fig. 291. Helium Magnetometer sensor schematic

to null out the external field. The voltage output of the system is directly proportional to the magnetic-field component being nulled out. The sweep vector is commutated between the X–Z plane (Z being the light axis) and the Y–Z plane to accomplish three-axis operation.

Radio-frequency power maintains a discharge in the lamp to provide a source of the resonant radiation and a glow discharge in the cell to generate the metastable helium atoms. The igniter system is used only to initiate the discharge.

3. Design Evolution

a. Design reviews. Extensive testing was performed on the Magnetometer breadboard by JPL personnel to determine the capability of the instrument to meet the operational design performance requirements. The packaging design was reviewed to determine whether or not the hardware would comply with the reliability requirements for the project. Evaluation of the design analysis and breadboard testing of the instrument resulted in a number of JPL-originated design changes in circuit, optical, thermal, electronic packaging, and mechanical design.

The original sensor design used plastics in both the optical system and the packaging design. Because of the deleterious effect of vacuum on plastics, and because of the poor heat distribution afforded, the sensor was redesigned using materials with compatible mechanical, thermal, and optical properties acceptable for space application.

The results of the circuit design reviews and breadboard testing led to circuit modifications and redesigns to correct the following problems:

1. Low sensor preamplifier input impedance
2. Inadequate system null stability
3. Excessive use of decoupling networks
4. Questionable reliability of igniter operation
5. Sweep vector asymmetry
6. RF oscillator instability
7. RF power matching crosstalk
8. Inadequate recurrent surge, turn-on transient, and short-circuit protection in the power supply
9. Pick-up and groundloops

The effect of the design changes was an overall reduction in electronic components and an order-of-magnitude decrease in system offset.

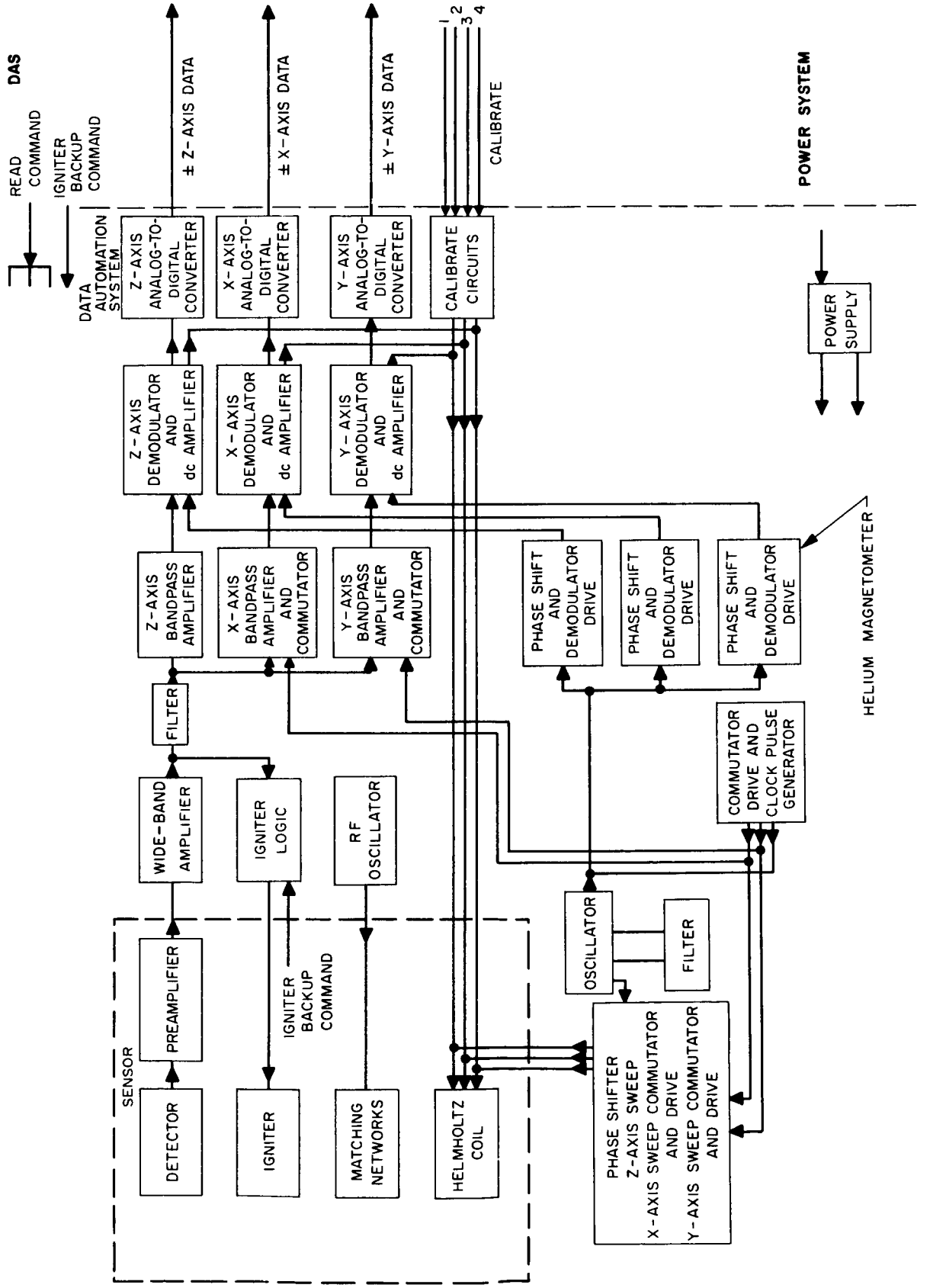


Fig. 292. Helium Magnetometer functional block diagram

b. Modifications of hardware from vendor. Several significant design changes were incorporated on vendor-supplied hardware subsequent to its receipt at JPL. These changes were prompted mainly by problems encountered during unit and system testing. These modifications were:

1. The RF matching networks in the sensor were modified and relayed out to reduce RF interference and increase RF efficiency.
2. A thermal shield was added to the sensor to reduce the predicted Earth-to-Mars temperature drop.
3. The helium lamps and cells were redesigned to extend their lifetimes. The lamps were modified to increase the helium reservoir, and were filled to a higher pressure. (Stabilization burn-in was incorporated as a fabrication technique.) The lamp mounting in the sensor was modified to minimize local heating. The cells were modified by a large increase in helium pressure, a change in sealing techniques, and an increase in glass thickness. Both lamps and cells were tested after fabrication to ensure low leak rates. A change of pressure of 30 to 50% could have been tolerated. The measured mechanical leaks were found to be less than 2% per year.
4. The lamp and cell igniter circuit was modified to increase the ignition potential from 1000 to 1600 v. This modification was made to extend the lifetime of the lamp and cell because their ignition potential increased as they aged.
5. The power supply was modified to increase filtering against power-line variations. This change was required to eliminate interference during spacecraft operation whenever power was applied to the encounter instruments.

4. Procurement

The Magnetometer was fabricated for JPL by a subcontractor. Such items as the analog-to-pulse-width converters, all optical components, and certain special-purpose devices (including nonmagnetic transistors for the ignition circuitry) were supplied to the subcontractor by JPL.

5. Fabrication

The majority of the packaging is centered around welded-cordwood modular construction. Exceptions to this are the power supply, which is of normal two-dimensional construction, and the sensor. The sensor package is hybrid by the nature of the components used. The sensor mechanical structure is shown in Fig. 293. The preamplifier is soldered cordwood, and the igniter circuitry is two-dimensional. All sensor components are nonmagnetic.

The most significant problem encountered during manufacture of the Magnetometer was quality control in the electronic welding process. This difficulty resulted from a difference in quality standards for welding between the vendor and JPL specifications. The problem was resolved by training operators to set up and employ weld schedules consistent with JPL standards.

Another problem encountered after fabrication was rework of the sensors to install new lamps and cells and to modify the RF matching networks. The sensors were serially fabricated and some components were bonded down over screws.

6. Test Experience

Environmental testing was performed in accordance with JPL specifications. All TA and FA level testing was completed without failure. The thermal–vacuum portion of both FA and TA tests was performed in a special thermal–vacuum chamber equipped with a magnetic shield, and the instrument performance was monitored in a low magnetic field. All environmental testing and instrument calibration was supported by a test console to monitor instrument functions using simulated data automation system and power system interfaces.

During systems testing, the ambient magnetic field at the magnetometer sensor location was maintained near a null through the use of a Helmholtz coil placed around

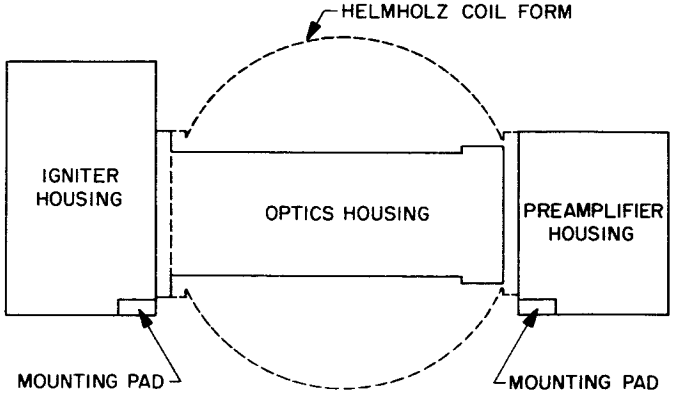


Fig. 293. Helium Magnetometer sensor mechanical structure

the sensor. The Helmholtz coil current was controlled from the science OSE. One significant problem was discovered during system testing. When NRT power was on, there were large power-line transients at 8⅓ cps while the buffer memory cores were being reset. The magnetometer outputs are derived from 25- and 50-cps signals from the sensor. The harmonics of 8⅓ cps transients were not sufficiently filtered in the power supply, and they beat with the 25- and 50-cps signals in the signal chain, causing very low frequency signals at the magnetometer output equivalent to 30 γ field disturbances. To eliminate the problem, modifications were made in the power supplies to incorporate additional filtering.

H. Television Subsystem

1. Experimental Objectives

The purpose of the television subsystem is to make preliminary topographic reconnaissance of portions of the surface of Mars; to attain an improved knowledge of areas of possible living matter through photographs; and to attain additional knowledge of Mars surface reflectivities to aid the design of future, more detailed photographic missions.

2. Description

a. Physical description. Of the six subassemblies contained in the television subsystem, two (the optics and the camera head) are joined together and located on the scan platform of the spacecraft. The other four subassemblies, comprising the bulk of the electronics, are contained in standard *Mariner* subchassis and located in spacecraft Bay III.

In each subassembly, the electronic components were mounted on fiberglass printed circuit boards. Printed circuit wiring was used throughout the subassemblies. Wherever similarities in circuitry made it possible, encapsulated welded electronic modules were used to conserve volume and weight.

The television subsystem is comprised of six electronic subassemblies, as follows:

1. The optics subassembly, which contains the beryllium Cassegrain mirrored telescope with shutter and stray-light shield (Fig. 294).

2. The camera-head subassembly, which contains the vidicon tube, the tuned preamplifier, the 100-kc oscillator, filtering circuits, and distribution circuits.

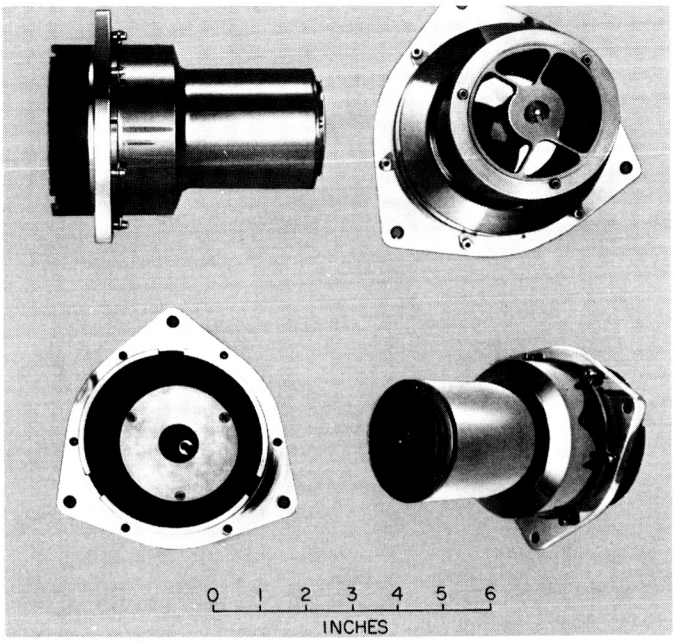


Fig. 294. Beryllium cassegrain mirrored telescope

The electronic circuits are located in separate compartments around the vidicon tube, and are electrostatically shielded from each other.

3. The video channels and computer subassembly, which contain all video channel functions, gain-control computer circuitry, planet acquisition camera control and computer circuitry, the frame control logic and control logic gates of the camera control logic functions.

4. The deflection and control subassembly, containing all the sweep functions, the G1 control and shutter control circuitry, and the DAS command logic and divide-by-25 logic control circuitry.

5. The TV encoder subassembly.

6. The transformer–rectifier power supply subassembly.

Each TV subsystem instrument contains 2036 electronic components and weighs 11.3 lb. The power consumption is 8.0 w.

b. Functional description. The television subsystem consists of a single camera using a narrow angle telescope. The camera is a shuttered system that uses a slow-scan vidicon capable of storing an image with negligible degradation for a 24-sec frame time. The subsystem was designed to take and encode two-color TV pictures upon receipt of frame and line start signals from the DAS.

The photo image is focused onto the vidicon photoconductive target by the optical assembly. The exposure time is controlled by the shutter. The output signal from the vidicon tube is the electrical video signal. This video signal is amplified and the amount of amplification is controlled to provide an output video signal within a specified voltage range. The signal amplitude is sampled and measured to provide an indication of when the planet is in view. A computer in the subsystem performs these functions of gain control and signal amplitude measuring. The analog video signal is then converted into a digital form for processing in the DAS and storage in the tape recorder. A functional block diagram of the system is shown in Fig. 295. The subsystem is divided into eight functional parts.

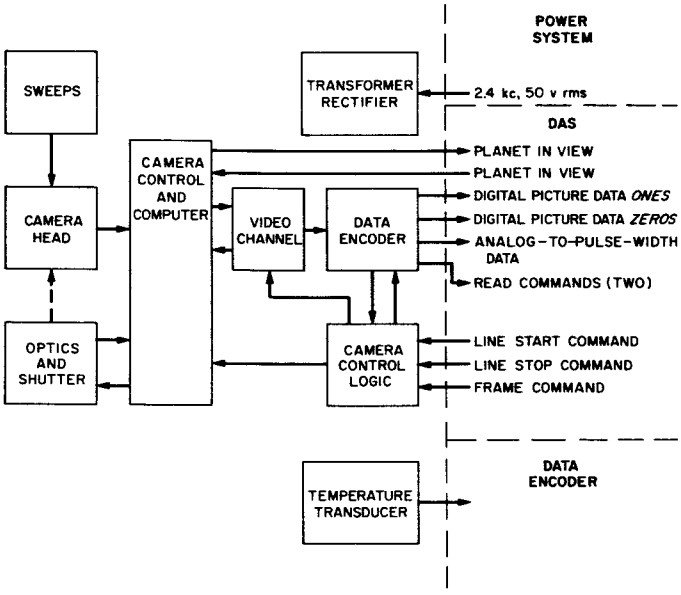


Fig. 295. Television subsystem functional block diagram

Optics and shutter. The optics and shutter comprise the mechanical assembly of the telescope and the shutter/filter. The telescope is an $f/8$ Cassegrain with a 12-in. effective focal length and a 1.05 × 1.05-deg field of view. The shutter is a rotating disc type, with a filter introduced into the light path by the application of a current pulse.

Camera head. The camera head contains the vidicon tube, preamplifier, 110-kc oscillator, and filtering and distribution circuits. The vidicon tube is the photosensor that provides the electrical video signal. The 110-kc oscillator provides vidicon beam modulation, which serves as a carrier for amplitude-modulated video information. The video signal is amplified by the tuned preamplifier.

Sweeps. Deflection of the vidicon beam is controlled by the horizontal and vertical sweep circuits and the 4-kc oscillator. The sweep circuits provide the voltages necessary for horizontal and vertical deflection of the vidicon beam both during picture readout and when the vidicon target is being erased and primed for the next picture.

Camera control and computer. The gain control computer, shutter control, G1 control, and planet acquisition circuits are contained in the camera control and computer. These circuits perform simple computer operations and provide control of functions that affect the TV subsystem operation and dynamic range. Control of shutter time, video gain, vidicon beam current, and planet acquisition sensing are performed by this circuitry.

Camera control logic. The camera control logic consists of the external DAS command logic, divide-by-25 logic control, frame control logic, and control logic gates. These circuits provide logic control of all camera timing functions such as shutter, picture readout, target erase and prime, and other switching functions.

Video channel. The video channel provides amplification, demodulation, and direct current clamping of the video signal. The video channel consists of an RF amplifier, a detector, and a video output amplifier.

Analog-to-digital conversion. Analog-to-digital conversion of the TV picture data is accomplished with PCM conversion to six bits per picture element. These data are clocked out to the DAS at 83,333 bps. The data output conditioner, accumulator and shift register, analog-to-digital comparator and gates, 1-Mc clock and gate, ramp generator, matrix, matrix buffers, programmer, and OSE buffers perform this function. In addition, analog-to-pulse-width conversions are performed on certain critical TV performance data. The line-synchronization circuit reconstructs line-synchronization information for the camera control logic.

Transformer–rectifier power supply. The power supply transforms the 2.4-kc square wave power, with appropriate regulation, into the voltages necessary to operate the entire TV subsystem.

The television subsystem provides several outputs:

1. PCM 83.3-kc data to the DAS: this is the digitized video data.
2. Planet-in-view signal to the DAS: this signal indicates that the subsystem has received sufficient illumination from a source or has received a planet-in-view command from the DAS.
3. Multiplexed data: this is an analog-to-digital pulse-width conversion for two critical TV parameters, signal voltage level and G1 readout voltage.
4. Digital status data: five digital bits are parallel-decoupled to indicate the status of the video gain control circuitry, color filter position, and shutter exposure time.

3. Design Evolution

The *Mariner* Mars 1964 television subsystem evolved from the design of the two-camera subsystem of the *Mariner B* spacecraft. Most of the circuits used in the Mars spacecraft TV subsystem were basically identical to the *Mariner B* design. Timing differences brought about some changes in the logic circuitry, which primarily involved changing the interconnections between counting units and gates. The major areas of change that evolved during the design and testing phases of the *Mariner* Mars 1964 Project are discussed in the following paragraphs.

a. Vidicon tube. With a 24-sec frame time proposed, the camera tube that was selected for the television subsystem had to be capable of slow-scan readout and of storing an image with negligible degradation for the time allotted. Light weight, ruggedness, small size, and simplicity of design were the requirements that led to the selection of an electrostatic vidicon tube. The photoconductor target material chosen for the vidicon was an antimony compound or ASOS material, which had been developed during the *Ranger* program. One of the producers of slow-scan vidicons had experienced considerable difficulty in manufacturing ASOS surfaces to *Ranger* specifications. As a result, a new target material based on a selenium compound was developed, which was claimed by its manufacturer to have easier reproducibility and the ability to withstand high temperatures. To verify performance, two vidicons were manufactured, in accordance with *Mariner* Mars camera tube specifications, and delivered to JPL for evaluation.

Apart from the new target material, this vidicon had electrical characteristics generally similar to previous tubes supplied for the *Mariner* program. However, some desirable improvements (dictated by experience with *Mariner B* TV subsystem) were incorporated.

The most significant characteristic of this new tube and its target material was its ability to erase stored signals without the use of erase lamps as required for the ASOS tubes. This characteristic eliminated an entire circuit, reduced the power requirements, and simplified operation. The new target material also had improved sensitivity and operating characteristics over a wider range of temperatures than the ASOS surface. This temperature characteristic eliminated the need for a temperature stabilization circuit that had been designed for the *Mariner B* TV subsystem.

As design and testing of the subsystem continued, tests of the first series of tubes with the new target material revealed that saturation became evident at illumination levels greater than 0.045 ft-cd-sec. As applied to the *Mariner* Mars 1964 TV camera, this would have necessitated a reduction in the illumination supplied by the optical system, and nullified any advantages gained by the improvement in sensitivity. Therefore, steps were taken to combine the feature of improved sensitivity with a wider dynamic range. This was accomplished by a modification in the processing of the photosensitive face plate. The result was an increase in the saturation level to 0.25 ft-cd-sec with a possible further increase in sensitivity. The process required additional intermediate steps in the treatment of the vacuum-deposited photosensitive layer. While this altered process added more steps to the preparation of the photosensitive target and a possible reduction in the yield of acceptable vidicons, it was felt that the improved performance justified the change.

Delays in implementing the vibration environmental evaluations of the flight-type vidicon tube were due, in part, to uncertainties in the knowledge of the *Mariner* spacecraft structural reactions to a vibration input. Because of the location of the TV camera on the scan platform and because of the need for all subassemblies to be extremely lightweight, complete spacecraft structural testing was required to determine the magnitude of any spacecraft resonances that would significantly affect the vidicon. As a result of the *Mariner* STM tests, the type-approval specifications for the TV camera were changed. Vibration testing of the vidicon indicated that it was marginal and could not be relied upon to meet the *Mariner* TA requirements. Therefore, a change was made to a still more ruggedized electrostatic version of the vidicon that had recently been developed for fast-scan TV rocketry applications.

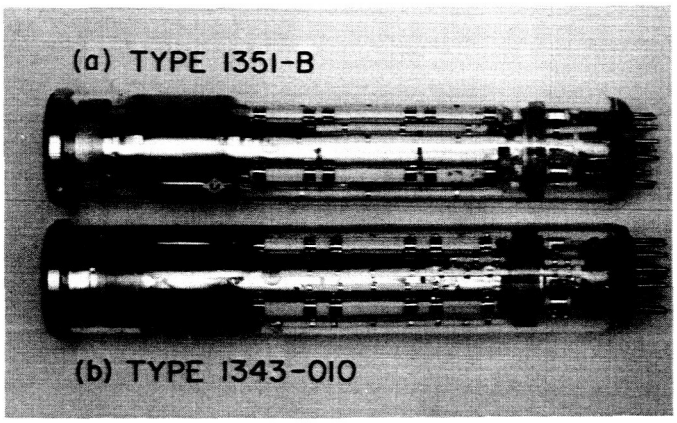


Fig. 296. Electrostatic vidicon mechanical construction

The mechanical construction of the electrostatic vidicon is illustrated in Fig. 296. The original ruggedized vidicon is shown in Fig. 296(a) and the structurally modified unit developed to meet the more stringent specifications is shown in Fig. 296(b). A major problem during vibration testing was the relationship of the vidicon electrode assembly to the glass walls. Some flexibility was required during the glass-scaling processes to prevent glass fracture. This flexibility was obtained by close-knit wire-mesh spacers placed fore and aft of the electrode assembly. While the welded construction ensured axial stability of the electrodes, radial flexing with high radial accelerations tended to cause vidicon failure. When this occurred, the electrode assembly was crushed and distorted against the glass walls, and fractures of the interconnecting leads were made possible. The improved, modified vidicon represented an effort by JPL and the manufacturer to maximize structural strength within the basic limitations of the electrode assembly structural design. Changes that were recommended included increased welding of the supports and an improved lead arrangement, particularly the G2 lead, which had consistently fractured during vibration testing.

The combination of the new target material and the improved ruggedized tube resulted in the final flight vidicon tubes that met all requirements.

b. Vidicon tube mechanical mounting. The mounting of the vidicon tube in the camera head chassis was critical. The face plate of the vidicon had to be maintained at a specified distance from the optics for optical focus. The centering of the vidicon had to be maintained so that the small area of the vidicon face plate that was electrically scanned was the area on which the optical image was focused.

The initial mounting method consisted of clamping the tube near the front and the back with teflon O-rings. In addition, the tube was held in axial compression against a front mounting surface by a spring arrangement acting through the tube socket. The subchassis was joined to the optics subassembly through three screws and two large threaded rings. The camera head chassis broke away from the optics subassembly during a TA preliminary test using the vibration specifications in existence at that time; the vidicon tube, however, was not damaged.

A redesign of the connections between the camera head subchassis and the optics was undertaken. Manufacturing problems had been encountered with the mechanical parts used in the tube mounting; therefore, a new design of tube mounting as well as the subchassis was undertaken. This design required that a ring be bonded onto the vidicon tube near the face plate. (In this hard-mounted method, the front part of the tube is securely fastened to the front mounting surface, and the back part of the tube is also securely, but not as rigidly, held in place.) It was with this type of mounting that the original vidicon first failed TA vibration tests.

Vibration tests had indicated that a hard-mounted modified vidicon in a fixture of unity-gain would pass the camera TA specifications. However, there was less assurance that it would pass specifications when the same tube was hard-mounted in a resonant configuration; i.e., with the camera head mounted where the acceleration could be amplified several times because of camera-head structural resonances. While the hard-mounted modified vidicon in the camera head aboard the PTM spacecraft survived the spacecraft environmental test, the same vidicon in the camera head was unable to survive the more severe TA specified tests at the subassembly level.

To provide a higher level of confidence in the TV camera operation by ensuring performance at the TA assembly testing level, the tube suspension in the camera head was changed from a hard-mount to a radially flexing mount (soft-mount). This technique is illustrated in Fig. 297. Two cylindrical polyurethane foam dampers supported the tube radially. A spring-loaded centering device assisted the foam in centering the tube optically. The tube was constrained axially by the flat spring-loaded tube socket, and teflon bearing surfaces permitted the tube to slide freely in the radial direction. The axial socket pressure and the mechanical centering device provided additional assurance of correct tube alignment in the event of any deterioration of the foam in space.

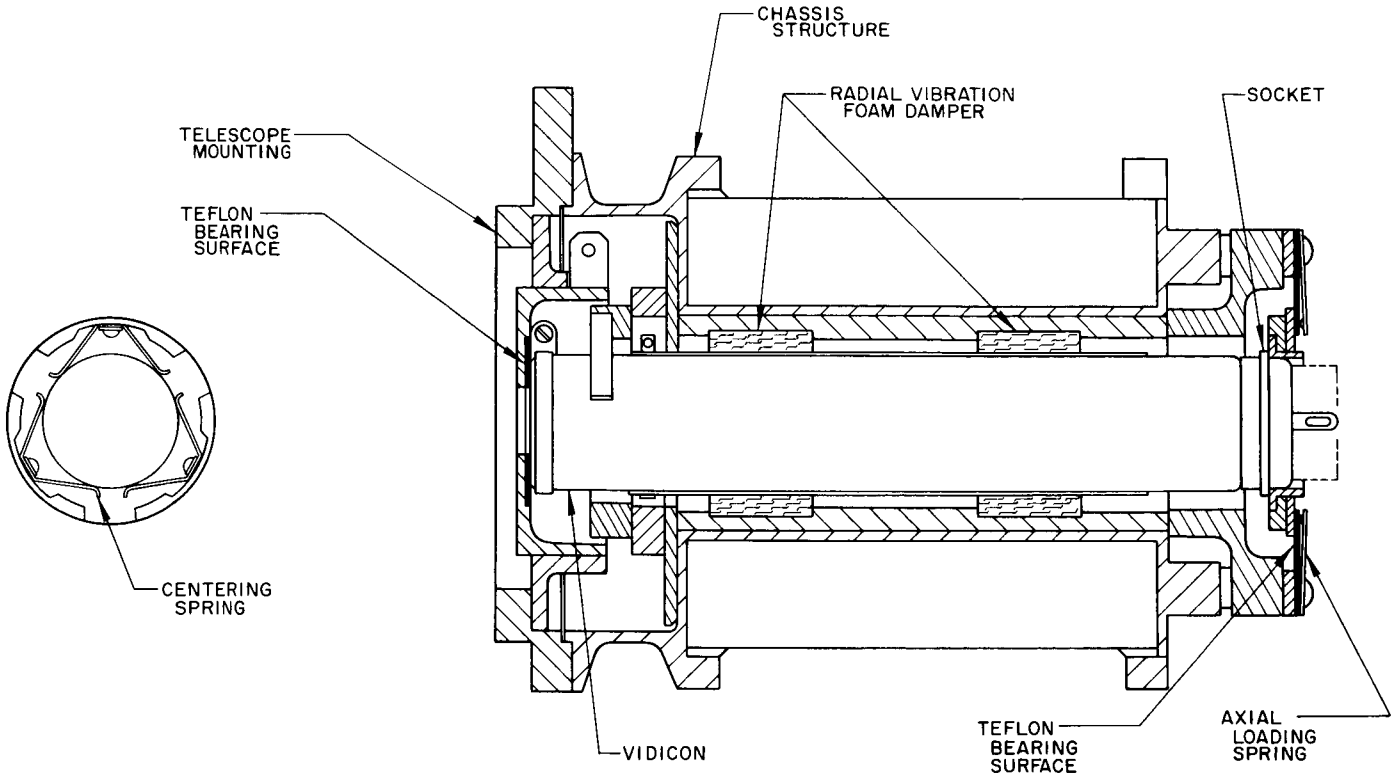


Fig. 297. Vidicon tube mechanical mounting, soft mount

With the tube mounted in the camera head, triaxial accelerometers indicated that the gain was less than 2 over a 25- to 2000-cps range. No problems were experienced passing TA requirements for the camera head subassembly with this arrangement. Optical centering was well within the specified tolerances after vibration.

c. Shutter. The shutter designed for the *Mariner B* TV camera was a rotary blade shutter in which the length of a single electrical pulse controlled the exposure time. For the *Mariner* Mars 1964 subsystem, design weight and power restraints imposed a shutter exposure time of 200 msec. A shorter shutter exposure time requires faster (larger and heavier) optics. A two-pulse drive was chosen for the *Mariner* Mars system, as opposed to the single-pulse drive of the *Mariner B* design. In a two-pulse system, the exposure is timed by the electrical interval between pulses. In a single-pulse system, the exposure can be controlled by a mechanical delay. For a 200-msec exposure, a mechanically timed system was no longer feasible, but an electrically timed one-pulse system, similar to the *Mariner B* shutter, would greatly increase the solenoid energy requirements. Since the then current capacitor weight for a 25-msec solenoid pulse was 0.3 lb, any increase in pulse length would have completely nullified the weight saved in the optical system.

During TA thermal–vacuum testing, a shutter stopped operating. The problem was found to be thermally induced binding between a teflon sleeve bearing and the steel shaft. The use of teflon bearings was discontinued.

As the testing of the TV subsystems continued, it became evident that some parts of the shutter mechanism were subject to excessive wear. Electrofilm was used on the parts that would come into contact with each other, although even that would have worn after approximately 5000 cycles and resulted in a possible cold-weld in space at the points of metal-to-metal contact where the electrofilm had worn off. To improve this situation, solenoids with nylon balls (rather than electrofilmed steel balls) and a nylatron spool bushing at the interface of the solenoid to the shutter linkage were tried. The shutter operation with the new parts was marginal because the new solenoids gave a lower output torque than the former solenoids. The nylatron spool feature, however, was found to be quite desirable.

Because time limitations prevented a new solenoid design, the decision was made to (1) rebuild the flight shutters with solenoids of the original design, (2) replace the link that adjoins the solenoid and is subject to wear, and (3) install the nylatron spool bushing between the link slot and the solenoid pin. To limit the number of cycles on the rebuilt shutters, and thereby reduce the chances of wear and cold-weld in space, the replacement of the shutters did not occur until just before the final system test of the spacecraft at Cape Kennedy.

d. Shutter control. As previously discussed, a two-pulse shutter control rather than the one-pulse control was required. A circuit to control the timing between shutter pulses (exposure time) was required. The circuit had to be capable of switching to either 80 or 200 msec. In addition, a circuit for controlling the shutter pulse width was required to ensure that the shutter solenoid received sufficient electrical power.

As testing reached the point at which the shutters started to fail due to wear, it was observed that the shutters would open but would fail to close. A measurement of the shutter drive pulses revealed that the magnitude of the close-shutter current pulse was somewhat less than that of the open pulse, resulting in a 20% drop in torque in the drive mechanism. A review of the circuitry revealed an alternate charging path through a diode that permitted some of the charge of the close-pulse capacitor to recharge the then depleted open-pulse capacitor. The diode was used to provide a charging path for the second capacitor, but it was found that the second capacitor could be charged through a transistor that becomes reverse-biased during the charging time. With the diode removed, the current pulses were almost identical and provided equal power to the shutter solenoid.

e. Gain control computer. After the scientific requirements were established, it became apparent that the television subsystem would have to cover a wide range of illumination: bright at the subsolar region of Mars and dark at the terminator. To cover this range, the video gain would have to be fairly low so that high-light video wouldn't saturate the amplifiers or the encoder. However, if the video gain were low, the pictures taken of the dark areas would have been useless because of the lack of contrast.

A simple computer was designed to control four levels of video gain. With the gain set high, four different attenuation circuits could be switched in the video signal chain. The video signal level would be sampled and, if the level were greater than 6 v, the next higher attenuation would be used. The computer was designed to raise the gain after a "red" exposure, but it could reduce the gain after any exposure.

Due to uncertainties in the expected amount of Mars illumination, an additional safety factor was incorporated into the subsystem. Prior to planetary encounter, the camera will be in the "photometer" mode. In that mode, the vidicon beam current is larger than required for a normal picture. This high beam current creates sufficient charge at the target surface to prevent distortion by excessive illumination. When the scene brightness is greater than 900 ft-L, the video signal will be large enough to cause the computer to issue a logic command to the shutter control circuit to switch to fast-shutter exposure time. The shutter control circuit will switch to slow exposure time when the scene brightness decreases significantly. The vidicon beam current will be reduced to the normal amount after planet acquisition is achieved. This computer greatly extends the dynamic range of the TV subsystem in providing the capability to take both good high-light and good low-light pictures.

f. Planet-in-view circuit. It became a requirement of the mission to have the television subsystem provide a backup planet acquisition indication. To meet this requirement, a planet-in-view circuit was designed. This circuit samples the video signal level and provides commands when the signal level exceeds a certain reference voltage for a specified period of time. One of these commands unlocks the computer and causes the G1 control to switch the vidicon beam current to normal. The other command gates on an oscillator that sends a continuous signal to the DAS. The planet-in-view signal issued by the DAS bypasses the signal level sensing circuit and causes the commands to be issued.

During subsystem testing, this circuit was found to be too sensitive and a refinement had to be made to prevent a premature planet-in-view signal. The first six scan lines were shorted out so that the shutter microswitch pulses, which occasionally appeared in the video signal, could not initiate a planet-in-view signal.

4. Procurement

There were several areas of difficulty experienced in procuring the television subsystem. Some of these areas are described below.

a. Components. The television subsystem contained 2033 electronic components, all of which were to be

screened before installation in the flight subsystem. Numerous delays were encountered in this process. Some delays resulted from the lack of procurement policies geared to schedule commitments; others resulted from inadequate realization of the schedule requirements by those responsible for screening, stocking, or handling components, and from poor feedback concerning failure rates, lead-times, or deliveries of components. Still other delays were the result of an inadequate review of the screening specifications by all cognizant personnel.

These problems resulted in serious schedule delays and increased costs due to work stoppages at two vendors because JPL could not deliver the screened components on schedule.

b. Transformers and chokes. The transformers and chokes were designed to meet special requirements not specified as "off-the-shelf" items. Preliminary designs of these transformers and chokes were made at JPL, and prototype items were fabricated at JPL. A subcontractor was chosen who was able to produce transformers and chokes superior to the prototype items and specifications. Some problems did develop with the large high-voltage power supply transformer, but these problems were rapidly solved and new transformer units were supplied quickly.

A coupling transformer and an oscillator choke were built and supplied by another subcontractor. These components were to be used in the preamplifier and 110-kc oscillator, and required special care in design. Several different designs were tried before the final ferrite high-Q, cup-core design was chosen. The same material from the same manufacturing batch had to be used for the cores of both the transformer and the choke for temperature stabilization. Unfortunately, the high-Q response dropped somewhat when the items were encapsulated, and it became necessary, because of noise pickup, to shield the transformer.

Two coils per subsystem were required for the purpose of exciting reed relay switches. These coils were built to a JPL specification that had been written for a different instrument. During the fabrication of a subassembly of the TV subsystem, it was found that the lead wires would pull out of the coil body while they were being stripped of insulation. This led to a major redesign of the attachment of the lead wires to the coil.

c. Shutter parts. The various shutter parts (i.e., linkages, wheel-latches) were made in a precision machine shop under the supervision of JPL inspectors. The parts were then shipped to JPL and assembled. The switches were purchased from a vendor and were modified versions of an off-the-shelf item.

Four types of solenoids for the shutter were purchased from another vendor. The first type was characterized by an electrofilm coating, steel balls, a teflon coil insulation and coil wrap, and resistance-welded lead attachment to the coil. However, a second type was purchased because the electrofilm wore off and the lead attachment caused some difficulties.

This type consisted of teflon overall coating, soldered lead attachment, steel balls, teflon coil insulation and coil wrap, and a teflon bearing. The teflon coating on the ball races caused trouble, and the teflon bearing bound at certain temperatures. The soldered lead attachments were also a problem.

The third type had nylon balls, another electrofilm overall coating, a bronze bearing, and ML insulated wire. Terminals were used instead of lead wires. This solenoid type failed because of low torque.

The fourth type had steel balls, the same overall electrofilm coating as the third unit, teflon coil insulation and coil wrap, a bronze bearing, and a resistance welding and soldering lead attachment. This type of solenoid worked well until after 30,000 cycles, at which point the bearing became gritty. Solenoids of this type were retrofitted at Cape Kennedy.

d. Telescope. The prototype telescopes were manufactured by a third subcontractor. The parts for the flight units were made at the vendor's precision machine shop, source-inspected by JPL QA, and sent to JPL. At JPL the parts were reinspected and then sent to a fourth subcontractor for assembly. The fourth subcontractor also manufactured the optical mirrors. All of the flight telescopes were delivered ahead of schedule.

e. Vidicon. The first vidicons started out with an ASOS target material. The modified vidicons featured a selenium compound target material. Three tubes with the new-type selenium compound target material were supplied by the manufacturer. Based on the results of the best tube of the three, a specification for slow-scan vidicons, which would meet the *Mariner* Mars 1964 requirement, was submitted to the manufacturer.

After the tube failure in TA vibration testing, this manufacturer supplied a vidicon that had been developed for TV rocketry applications. The new tubes

proved satisfactory and became the final flight-type tubes. Retrofitting of these tubes into the flight TV subsystems occurred in June and July of 1964.

5. Fabrication

Four television subassemblies using electronic welded cordwood modules were fabricated by a subcontractor. The camera head subassembly was fabricated by JPL, and all subassembly testing was performed by JPL.

6. Test Experience

a. Television subassembly and subsystem testing. Each subassembly received preliminary testing prior to being assembled into the subsystem. The subassembly testing consisted of individual circuit operation, installation of trimming components, temperature testing, and telemetry point calibrations as required.

Subsystem assembly and testing consisted of operating the entire subsystem by (1) setting adjustable potentials for optimum camera performance; (2) aligning vidicon sweep; (3) sizing the vidicon raster; and (4) untwisting the vidicon sweep format. Upon successful completion of this operation, the subsystem was given flight-acceptance or type-approval testing.

b. SN/MC-1 prototype television subsystem. For FA and TA testing, the TV subsystem was divided into two units. One unit was the camera head and optics, and the other unit was the electronic circuitry. The camera head unit was tested to the levels specified for assemblies under 10 lb. The electronics unit was installed in a large *Mariner* chassis filled with other simulated science subassemblies, and tested to the levels specified for assemblies over 10 lb. Only the electronics unit of the SN/MC-1 subsystem was vibration-tested because the prototype camera head, which had failed during TA vibration testing, was slated to be replaced by a second prototype camera head of a new mechanical design. This second unit was intended to be retrofitted into the SN/MC-1 subsystem at a later date.

The thermal–vacuum portion of the FA testing was started in November 1964. The thermal–vacuum test was interrupted by a failure in the encoder subassembly, which was due to a defective welded electronic module. The testing was resumed, but only a marginal picture was obtained at the lower limit of the temperature cycle because of bit errors in the encoder. Satisfactory results were obtained at the high-temperature portion of the test. The high voltage transformer in the power supply failed just after the completion of thermal–vacuum testing. An analysis of the faulty transformer showed that a redesign of the construction technique was required.

Post-test engineering calibrations agreed with the pre-test data. These data were taken as a short-form calibration to provide a base line from which to make quantitative judgments on the effects of environmental testing on the TV subsystem.

The SN/MC-1 TV subsystem was delivered to the science STC for checkout with the other science subassemblies before delivery to SAF. Fabrication and subassembly testing on the prototype retrofit camera head was completed, and the subsystem was returned from SAF in January 1964 for retrofitting. The subsystem was reassembled, tested, and re-delivered to SAF. Inspection, FA testing, and conformal coating of the camera head were waived by the Spacecraft Systems Manager because of the urgency of the schedule.

Initial spacecraft testing was hampered by interface difficulties with the DAS and the OSE, although continued testing resolved these difficulties. A failure occurred in the camera head due to the shorting of two transistors. The circuit was carefully analyzed and a minor design change was made.

Two problems were encountered with the SN/MC-1 subsystem. In the first, the vidicon tube became overexposed from an improper light concentration and caused an erroneous planet acquisition signal to be initiated by the subsystem. The vidicon tube spot caused by the overexposure of light was erased by a special procedure. The planet-in-view circuitry was slightly redesigned to increase the light integration time and eliminate small bright-spot sensitivity. A special turn-off procedure was made part of spacecraft testing to prevent the camera from being turned off in an open-shutter condition. In the second problem, excessive bit errors in the DAS output TV data occurred, which were found to be caused by a missing capacitor in the TV encoder. The missing capacitor was also determined to be the cause of the bit-error problem during FA thermal–vacuum testing. Television subsystem operation was normal in all PTM spacecraft testing after that time.

Pre-test calibrations were made and type-approval testing was performed in accordance with JPL specifications. Type-approval testing included dynamic and static magnetic-field tests, RF interference tests, shock and static acceleration tests, thermal shock tests, a bench

handling test, explosive atmosphere and humidity tests, thermal–vacuum tests, and vibration tests.

During the vibration tests, a failure occurred in the camera head and the vidicon tube was found to be damaged. The vidicon tube was replaced and another vibration test was conducted, with the result that another vidicon tube was damaged. The prototype camera head was then used for numerous vibration tests to aid in the testing of new type vidicons and to develop a new mounting method. A new soft-mounting tube method was installed in the prototype camera head, and a new type of ruggedized vidicon tube was used for the final vibration test, which was successful with these modifications.

During the TA thermal–vacuum testing, a shutter failure occurred that was caused by a thermally induced binding between a teflon sleeve bearing and the steel shaft of the solenoid. The use of a teflon bearing was discontinued, and a new solenoid was installed in the shutter.

The camera head unit was installed aboard the STM spacecraft, which was then tested to greater-than-expected launch vibration levels. The prototype subsystem operated normally after the test.

Type-approval RF interference tests were conducted on the SN/MC-1 subsystem. After a week of testing, the shutter operated marginally because of excessive wear on the link, which required reworking. (This shutter was the same one used on the camera head during the tube mount testing and developmental program.)

A transistor failure occurred after the TA shock test. The cause of the failure was determined to be a defective component and was not directly traceable to the shock test. No failures occurred when the shock test was repeated. The TA thermal shock test on the camera-head unit completed the TA testing program. The SN/MC-1 subsystem was then prepared for life testing.

c. SN/MC-2 television subsystem. There were no problems encountered in the flight-acceptance tests, and the post-test engineering calibrations indicated normal TV subsystem performance. The TV subsystem operated normally during the first system test of the MC-2 spacecraft, except that it could not be induced into a fast shutter operation. The problem was caused by a low output voltage from the TV power supply. The subsystem was removed from the spacecraft and bench-tested. Operation was normal after the TV power supply was adjusted and the subsystem was returned to SAF.

The retrofitted camera head underwent FA vibration testing and thermal–vacuum testing, after which the entire subsystem was delivered to SAF and installed aboard the MC-3 spacecraft. The TV subsystem operated normally, except that two black lines appeared through the middle of each picture. This black line problem was caused by white spots or tube blemishes in the vidicon black-mask area, which caused the subsystem to lose black clamp.

The SN/MC-2 subsystem was installed on the MC-4 spacecraft, and operated normally during the first system test, except for the same two black lines that had appeared previously. The TV subsystem was removed from the spacecraft, the vidicon tube was replaced, and the black line problem ended.

The SN/MC-2 subsystem was calibrated and designated as a flight spare. It was shipped to Cape Kennedy and installed aboard the MC-3 spacecraft while the SN/MC-4 subsystem was receiving a shutter retrofit and calibration. All operations were normal. A calibration verification test was performed, after which the shutter was replaced with a rebuilt flight shutter and the final calibration was performed.

d. SN/MC-3 television subsystem. No problems were encountered during FA testing of this subsystem and the post-test engineering calibrations indicated normal operation.

The SN/MC-3 subsystem was delivered to the science STC, and random transistor failure occurred during checkout. The transistor was replaced and there was no recurrence of the problem. The subsystem was then delivered to SAF and installed aboard the MC-3 spacecraft.

Subsystem testing aboard the MC-3 spacecraft showed that the subsystem could not be induced into a fast shutter condition because of a low TV power supply voltage. (This same condition had occurred on the SN/MC-2 subsystem.) The TV subsystem operated normally during the first two system tests of the MC-3 spacecraft. The fast shutter problem had not been corrected, but the cause was known. Poor data was received from the first system test, which was due to OSE problems. The data from the second system test showed black words at the end of each line. Tests performed a month later showed that the problem was caused by the OSE.

The subsystem was removed from the spacecraft for camera-head retrofit and engineering change request updating. The FA vibration tests and thermal–vacuum tests were performed on the camera head after it was retrofitted. The fast shutter problem was eliminated by adjustment of the power supply. The subsystem was then delivered to SAF and re-installed on the MC-3 spacecraft for vibration testing; TV subsystem operation was normal during the verification tests.

During the pre-vacuum verification test, the black word problem appeared again in the TV data and the subsystem was removed from the spacecraft. Calibration of the SN/MC-3 subsystem was performed, and there was no recurrence of the black words at the end of each line. The subsystem was then installed aboard the MC-4 spacecraft. The subsystem operated normally during all testing of the MC-4 spacecraft at JPL, which included vibration testing, system testing, and thermal–vacuum testing in the space simulator.

The SN/MC-3 subsystem remained aboard the MC-4 spacecraft when it was shipped to the Cape in September 1964. The performance was normal during the first AFETR system tests of the spacecraft. The TV was removed from the spacecraft for shutter retrofit and calibration, and was then reinstalled on the MC-4 spacecraft where it performed normally for the last two system tests held at Cape Kennedy.

e. SN/MC-4 television subsystem. There were no problems encountered during the FA testing of this TV subsystem, and post-test engineering calibrations confirmed normal operation. The subsystem was delivered to SAF and then returned for a power margin test. (It had received the camera-head retrofit before it was delivered to SAF.) During thermal–vacuum testing, the vidicon tube originally installed displayed a defocusing condition at low temperatures. Due to a shortage of vidicon tubes at that time, it was decided to leave the tube in the subsystem until a more satisfactory replacement was received and tested.

The subsystem was delivered to SAF and installed aboard the MC-3 spacecraft, but did not operate aboard the spacecraft. It was removed from the spacecraft and bench-checked, but no abnormalities could be found. It was then installed aboard the MC-4 spacecraft where it operated properly.

The SN/MC-4 subsystem was then removed from the MC-4 spacecraft for a vidicon tube replacement. The new tube was installed and, during bench testing, the subsystem operation became intermittent and finally quit. A bad microswitch in the shutter was found to have been shorting the 10 v to the signal common. The nonoperating conditions duplicated those conditions aboard the MC-3 spacecraft when the subsystem had failed to operate. The switch was replaced and the design changed to prevent this from happening again.

The subsystem was installed on the MC-3 spacecraft. The data from the first pre-simulator verification test with this subsystem showed black words at the end of each line. The problem was isolated to be the OSE and good data was finally obtained. Because of time shortages, the subsystem remained aboard the MC-3 spacecraft throughout the space-simulator tests and all subsystem operations were normal. Good operation of the subsystem was noted during the final JPL system test of the MC-3 spacecraft. The SN/MC-4 TV subsystem was shipped with the spacecraft to Cape Kennedy.

The TV subsystem was removed from the spacecraft as soon as it reached the Cape and a thermal calibration was performed. (This testing had been bypassed when the subsystem was installed aboard the MC-3 spacecraft.) No further vacuum testing was required since the subsystem had already been vacuum-tested extensively in the space simulator.

Subsystem operation was normal during the first AFETR system test. The subsystem was removed from the spacecraft for shutter retrofitting and calibration. The vidicon saturated during the calibration because of an error in the illumination intensity when the subsystem was first assembled and tested, and it was necessary to change filters in the shutter to correct the condition. The new filters gave the subsystem the greatest color separation of any of the TV subsystems. The final AFETR calibration was then performed and the subsystem was installed on the MC-2 spacecraft.

The operation of the SN/MC-4 TV subsystem was flawless during all final operations before launch. These operations included the final system test and the ESF electrical tests. The SN/MC-4 TV subsystem was launched on the MC-2 spacecraft.

f. SN/MC-5 television subsystem. This subsystem was built with the new vidicon mount configuration. No problems were encountered in the FA tests, and post-test engineering calibration verified proper operation of the subsystem.

The subsystem was delivered to SAF and installed aboard the MC-2 spacecraft. Subsystem operation was normal during the second system test of the MC-2 spacecraft. The camera head unit was removed from the spacecraft for the purpose of a shutter retrofit. The camera head was returned to SAF, and a special test was performed to verify proper operation of the subsystem with the new shutter. The video data appeared to be anomalous and shutter operation sounded irregular. The entire subsystem was removed from the spacecraft and bench-checked. It was found that the shutter would not operate properly with the new nylon ball solenoid. The shutter was reworked and the former solenoid reinstalled, after which proper operation of the subsystem was verified.

The SN/MC-5 subsystem was reinstalled on the MC-2 spacecraft, and underwent thermal–vacuum testing in the space simulator. All subsystem operations were normal. Some very small white spots were noticed on the pictures taken with no illumination and maximum gain. These spots were blemishes common to all the vidicon tubes. The subsystem operation was also normal during the verification tests of spacecraft vibration.

The subsystem operation was completely normal throughout the final system test on the MC-2 spacecraft, and it was shipped with the spacecraft to Cape Kennedy.

A system test, ESF electrical test, and on-pad checks were held at Cape Kennedy. Proper subsystem operation was observed during all these different tests. The subsystem was then removed from the MC-2 spacecraft for calibration and shutter retrofitting.

The error in calibration light intensity was discovered during final calibration, and the gain of the subsystem had to be adjusted accordingly. The subsystem was then returned to the spacecraft.

During the AFETR final system test, the TV subsystem performed normally until the fast shutter test. The subsystem could not be induced into fast shutter. The change of the subsystem gain had raised the fast shutter threshold to a level just above the vidicon saturation. The threshold level was lowered by a simple trimpot adjustment that was made with the subsystem aboard the spacecraft. Because the threshold point was just slightly above the saturation level and only a very small adjustment brought the subsystem back to normal, a decision was made to lower the fast shutter threshold levels on all of the TV subsystems. The trimpot was, therefore, adjusted again. Another test of the SN/MC-5 TV subsystem aboard the spacecraft was held and the operation was entirely satisfactory.

The SN/MC-5 TV subsystem operation was flawless during the final testing, which included ESF electrical tests, dummy on-pad checks, and on-pad tests. The SN/MC-5 TV subsystem was launched aboard the MC-3 spacecraft.

I. Planetary Scan Subsystem

The planetary scan subsystem was the ancillary to the science subsystem used to acquire and track the planet Mars during the period immediately preceding the television picture-taking sequence.

1. Description

a. Physical description. The subsystem is composed of two electronic modules, a sensor assembly, and a drive motor. All elements of the subsystem, except the motor, are shown in Fig. 298. The center assembly contains the preamplifiers, optics, and detector, and is mounted on the planetary scan platform. The assembly on the left contains the power supply and motor drive electronics, and the assembly on the right contains electronics. The two electronic modules are mounted in electronics Bay III. The subsystem weighs 5.65 lb and draws 4.65 w of 2.4-kc, 50-rms power, and 2.81 w of 400-cps, 28-v-rms power. The instrument contains 512 electronic parts of which 141 are either transistors or diodes.

b. Functional description. The subsystem is designed to scan 180 deg in the process of searching for the planet. The scanning provides motion in one direction while the moving spacecraft provides motion perpendicular to

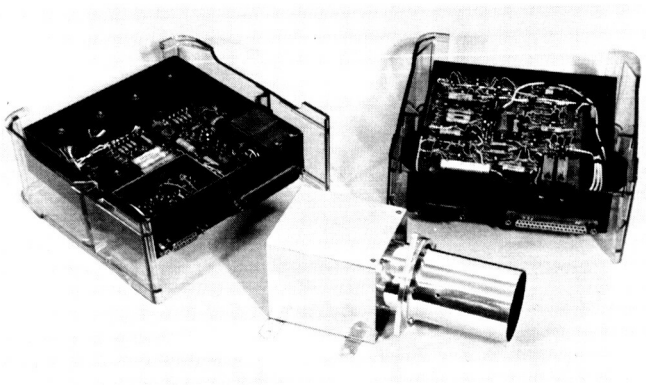


Fig. 298. *Mariner* Mars 1964 planetary scan subsystem

the scanning plane. Limit-switch action produces signals that reverse the direction of motion at the end of each 180-deg sweep. When the planet comes into the field of view of the sensor, which is an optical system with a 25-deg field of view, the subsystem will switch to planet tracking operation and the signal will be processed so that the desired portion of the planet is used as nulling plane for the servo system. This is called wide angle acquisition. A 400-cps motor is used for searching and tracking. To indicate that the planet has been acquired, a 2.4-kc signal is routed to the data automation system for processing. Upon receiving a scan-inhibit command from the DAS, the scanning or tracking motion ceases.

Based on the mission requirements, the following design objectives were established: (1) an operating range of 9000 to 70,000 km from Mars; (2) planet tracking accuracy of $\pm$ 1 deg plus 1% of the planet angular diameter; and (3) operating temperature range of -40 to $+80$°C. The searching and tracking speed of the motor assembly is ½ deg/sec with an output torque of 30 in.-lb, and was chosen to satisfy the subsystem's required dynamic responses and mechanical loading. A shaft-position potentiometer, linear within 0.2%, indicates the scan-platform position.

To accommodate the subsystem performance evaluation during tests and in flight, six channels of data are time-multiplexed and converted to a pulse width prior to delivery to the data automation system for digitization.

To obtain a scan subsystem with a high probability of accomplishing its mission, the following major guidelines were established in the subsystem design:

1. Simplification of design by the incorporation of devices with a minimum number of components consistent with the design requirements
2. Performance of positive logical decisions and identification prior to each critical operational execution
3. Incorporation of subsystem redundancies to improve the subsystem's reliability

A functional block diagram of the scan subsystem is shown in Fig. 299. When the subsystem is energized, a signal from a one-shot multivibrator circuit presets all logic circuits, and the subsystem enters the planet-searching mode of operation. This is accomplished by placing a positive dc voltage at the output of the X-axis filter through the use of the searching driver. This voltage is then phase-detected with a reference signal derived from the 400-cps motor driving signal shifted 90 deg in phase. The phase-detected signal, after amplification, is used to drive the motor. Upon completion of each 180-deg search, the motor reverses its drive by sequence of:

1. Planet-searching logic, which is reset by a wave-shaped and noise-filtered signal initiated by the limit switching action
2. A dc voltage of the proper polarity, which is applied to the output of the X-axis filter by the searching driver
3. The dc voltage, which is phase-detected, amplified, and applied to the motor as directional drive signal

A radiation detector is used to detect the presence and location of the planet. When the planet is in view of the detector, a pair of dc signals will be generated, the magnitudes and polarities of which will depend on the amount of energy received and the location of the planet. The X-axis output is used as the error signal for planet tracking, while the Y-axis output determines the angular position of the planet with respect to the detector mount. Both signals are modulated by a pair of photomodulators prior to amplification by the preamplifiers and amplifiers. A pair of synchronous detectors is used to demodulate these amplified ac signals before filtering.

The X-axis signal at the output of the preamplifier is sampled by the planet-in-view logic, where noise filtering and signal verification are performed. A planet-in-view signal is sent for the purpose of changing the spacecraft data mode to the data automation system for processing, and, at the same time, the subsystem is changed from the searching to the tracking mode of operation by inhibition of the searching driver's output. The X-axis signal is then used as the servo error signal to track the planet. The motor driving and directional control perform identical functions while in either the tracking or searching mode.

The filtered Y-axis output signal is amplified and converted from a bipolar to a unipolar signal. This signal, the platform position, and signals required for the subsystem performance evaluations are time-multiplexed and analog-to-pulse-width converted and sent to the data automation system for processing.

To prevent a false planet acquisition, a dc signal of sufficient magnitude for motor actuation is applied to the output of the X-axis filter, and is used to drive the motor in a fixed direction. Upon actuation of a limit switch, the

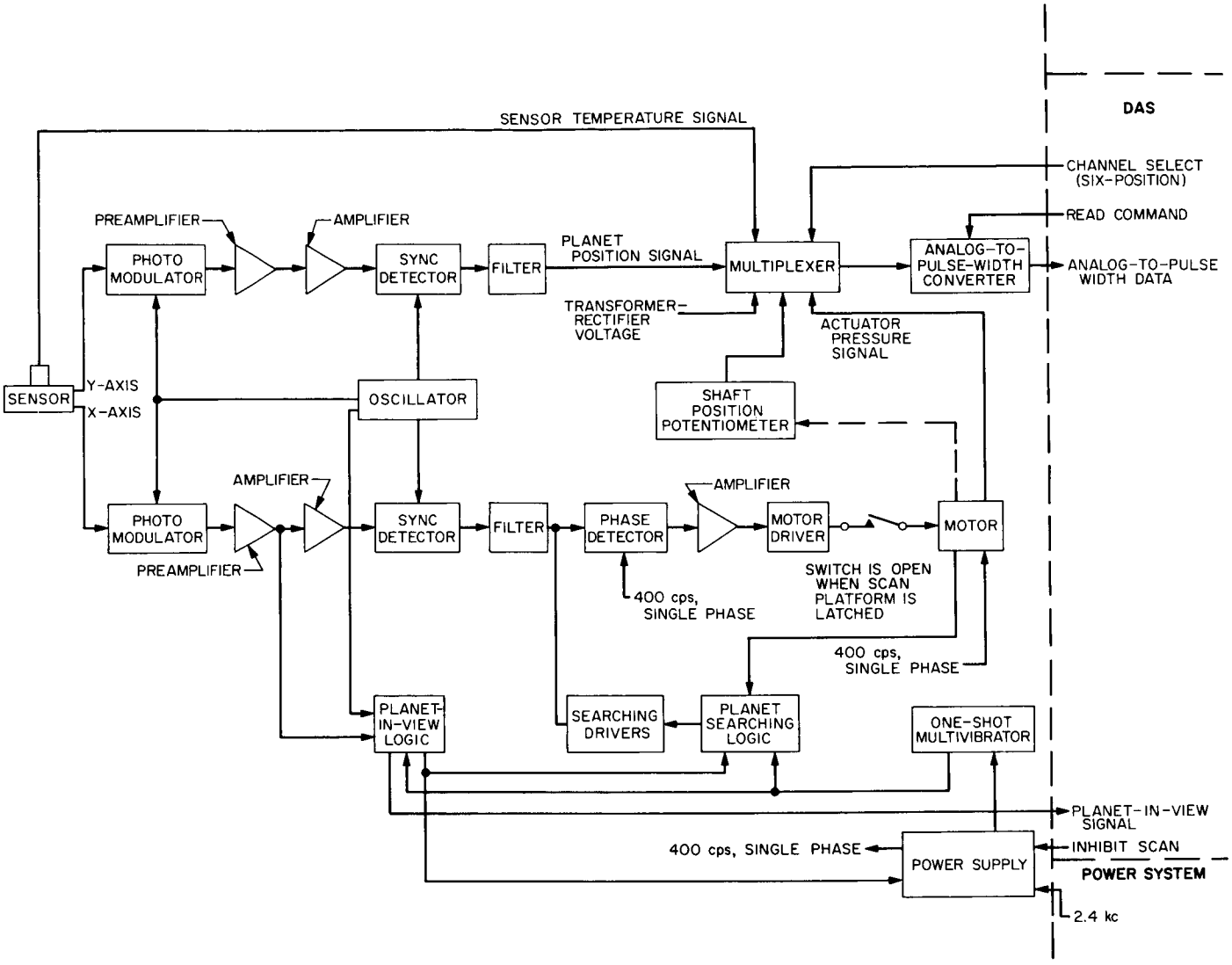


Fig. 299. Planetary scan subsystem functional block diagram

subsystem is capable of switching back to the searching mode if there is no output from the sensor X-axis.

2. Design Evolution

The concept of planetary scan was originated on the *Mariner A* and *Mariner B* programs, during which the system logic was developed to provide step scans across the planet upon command from the data automation system. These systems were designed to operate in a spacecraft in which weight and power could be amply allocated to the system. To obtain a system having the weight and power consumption compatible with the *Mariner* Mars 1964 requirements, a new system was developed (Ref. 29). This system was designed to scan across the surface of the planet at the radiation bisector of the planet and above and below the bisector in a triangular pattern. This scan pattern was later eliminated and the sensor output was offset so that a desired portion of the planet surface in the southern region was selected as the nulling plane for the scan servo subsystem.

Two additional changes were made during the mission planning stages. A fiber optics system (Ref. 30) was originally designed as a part of assembly 31A1, but had to be deleted because of problems encountered in the fabrication of the fiber cone (Ref. 31). A backup optical design was initiated and successfully completed. The problems with the earlier fiber optical system were later eliminated by the manufacturer.

The second problem was of the same nature as the first. The sensor in the original design could not be reproduced by the manufacturer in the quantity or with the characteristics necessary to establish it as a reliable

component. A second manufacturer was able to produce a sensor of adequate sensitivity and stability. (Ref. 32 and 33.)

3. Procurement

Whenever possible, all electronics and mechanical components of the planetary scan subsystem were procured by JPL, screened, and tested before delivery to the various manufacturers for subassembly fabrication.

The subassemblies fabricated by the various manufacturers were mechanically inspected and assembled at JPL to form the units of the subsystem prior to electrical testing.

A number of problems were experienced during the procurement of electronic components that resulted in slippages in the flight hardware completion schedule. These delays were partly due to the relatively long lead time required for the manufacturing of the highly reliable components and the delays in the delivery because of priority. These difficulties were relieved by the establishment of the level of priority required for partial shipment and through the assistance of other NASA agencies.

4. Fabrication

A total of 501 electronic components were required for the fabrication of each subsystem. Wherever possible, components having a history of high reliability were chosen, tested, and screened in accordance with existing specifications. Components designed and constructed for performing special tasks were also tested and screened to specifications written for that purpose. Since the subsystem required various techniques for development and fabrication (e.g., detector and optical fabrication, module and electronic packaging), components and assemblies were fabricated by manufacturers specializing in their respective fields.

A number of problems were experienced in the fabrication of the detector. The p–n junction was formed by diffusing boron atoms into the top layer of the n-type silicon bulk material to form a p layer. Evaluation of the fabricated detectors indicated that the response was not uniform across the surface. This was believed to be due to nonuniform distribution of impurities. The impurity density gradient towards the junction was also believed to be nonuniform across the surface, thus producing an irregular drift field affecting the speed of the minority carriers toward the junction. In addition, the detector had a fragile structure, which made mechanical mounting difficult. This fragility was thought to have been caused by excessive thermal stresses during fabrication while the silicon was being cooled too rapidly. Various techniques of fabrication were developed to overcome these difficulties. Detectors, which were fabricated by the technique of diffusing impurities more uniformly across the surface and cooled in a closely controlled temperature environment, had a response that was fairly uniform. To obtain detectors of an even higher quality, units having superior characteristics were selected from those fabricated with a yield of approximately 15%.

To conserve power, switching coil and magnetically operated reed switches were used as the commutating elements for the data multiplexing. The coil was constructed so that an electrically insulated metal spool was used to contain the wire-wound coil with the spool as a part of the shield. Signal leads were shorted to the grounding shield when the unit was operating at high temperature because of the differences in the temperature coefficient of expansion of the various parts. The switching coils were then modified to use a removable spool, thus enabling sufficient insulation to be placed between the coil and the grounding shield.

To conserve weight, volume, and power consumption without sacrificing reliability, thin-film microcircuit networks were used in the searching, tracking, and planet-in-view logic circuits. These semiconductor networks, along with the other logic electronic components, were packaged in welded modules in order to take advantage of their physical configuration and small dimensions. Module No. 1 had dimensions of 1.20 × 0.57 × 0.40 in. and contained five flip-flops, two NOR gates, two resistors, and two capacitors. Module No. 2 was 1.50 × 0.47 × 0.43 in. and consisted of four flip-flops, four NOR gates, five diodes, and three resistors.

5. Test Experience

Test procedures were established and tests were performed to verify the subsystem design, capability, and performance under simulated flight environments. Upon completion of the mechanical testing, all units were carefully inspected for possible mechanical damage. The thermal–vacuum tests were divided into a number of test cycles, each consisting of a complete operational sequence in the type-approval and flight-acceptance testing.

The subsystem successfully passed all tests and the performance was within the limits specified. The following problems were encountered.

During the first cycle of the thermal–vacuum test of the type-approval subsystem, two scan reversals were observed that did not actuate the limit switches. These occurrences were determined to have been caused by transient noise introduced by monitor switching of the test equipment. The switching functions were minimized and no subsequent occurrences were observed during the second part of the test. Noise isolation was later incorporated into test equipment to keep these external interferences to a minimum.

Bench evaluation of the subsystem performance upon completion of the flight-acceptance tests indicated that the sensitivity of the detector incorporated in the SN/MC-4 unit was unstable and had decreased. Since these tests were used to verify the ultimate detector stability, the detector was replaced and all applicable portions of the tests were repeated.

A 140-msec interruption of the planet-in-view signal was experienced during a spacecraft system test using the subsystem SN/MC-3 unit. Extensive analysis and tests were made to determine the cause of this behavior, but no conclusive test evidence was secured to indicate any subsystem operational abnormality. Investigations were subsequently initiated attempting to locate the cause external to the subsystem, again without results.

J. Data Automation Subsystem

The data automation subsystem is the nerve center of the science subsystem. It has to supply the synchronizing, controlling, sampling, formatting, converting, buffering, and encoding of data from the science instruments or their ancillaries. In addition, it provides a central terminal for the issuance and receipt of commands to or from other spacecraft subsystems.

The DAS is divided into two functionally and physically separate units: the real-time DAS and the non-real-time DAS. The entire DAS subsystem (Fig. 300) consists of: (1) the RT DAS, packaged in two 1½ × 6 × 7-in. chassis; (2) the NRT DAS, packaged in one 2 × 6 × 7-in. chassis; (3) two identical 1320-bit core buffer memories, which are used in conjunction with the NRT DAS and are housed in one 1 × 6 × 6-in. chassis; and (4) two electrically separate ac-to-dc power converters (one for the RT DAS and one for the buffers and NRT DAS) both of which are packaged in one 1½ × 6 × 6-in. chassis.

1. Functional Description of the Real-time DAS

A functional block diagram of the RT DAS is shown in Fig. 301. Its primary purpose is to gather data samples from the science instruments and arrange them in a format suitable for real-time transmission by the telemetry link. The RT DAS performs the basic functions of analog-to-digital conversion, pulse-rate conversions, event timing, and digital data transfers.

The real-time DAS has three basic modes of operation: cruise, cruise-calibrate, and encounter. During the cruise mode of operation, the real-time DAS shares the telemetry channel, and is synchronized with the engineering

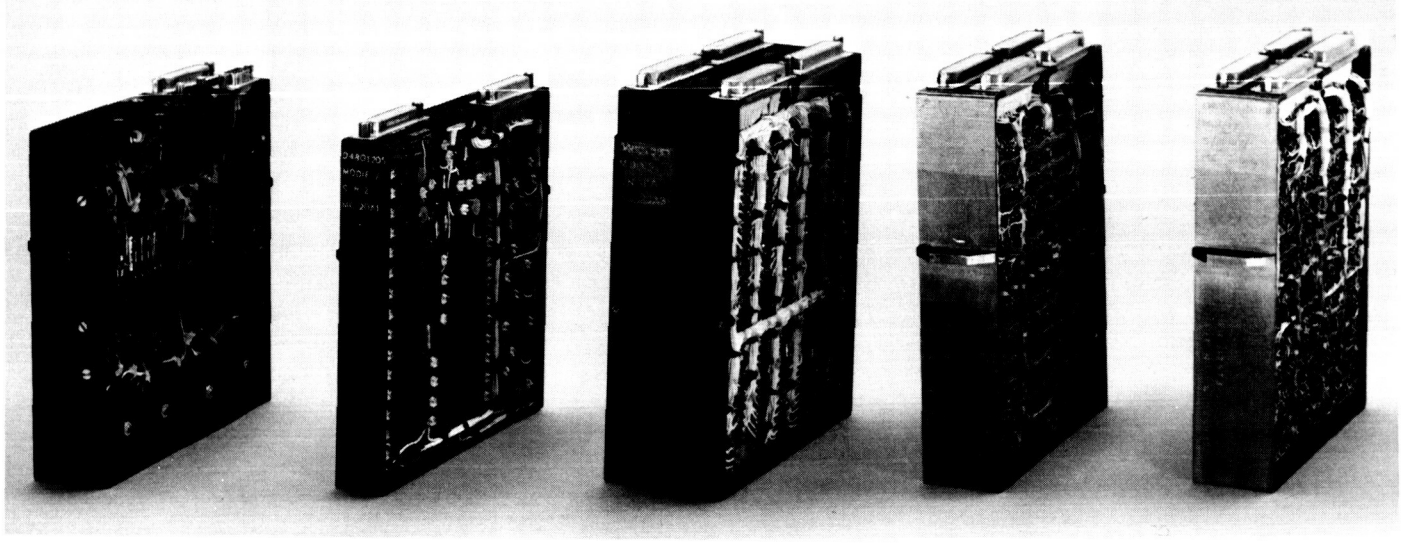


Fig. 300. Data automation system subassemblies

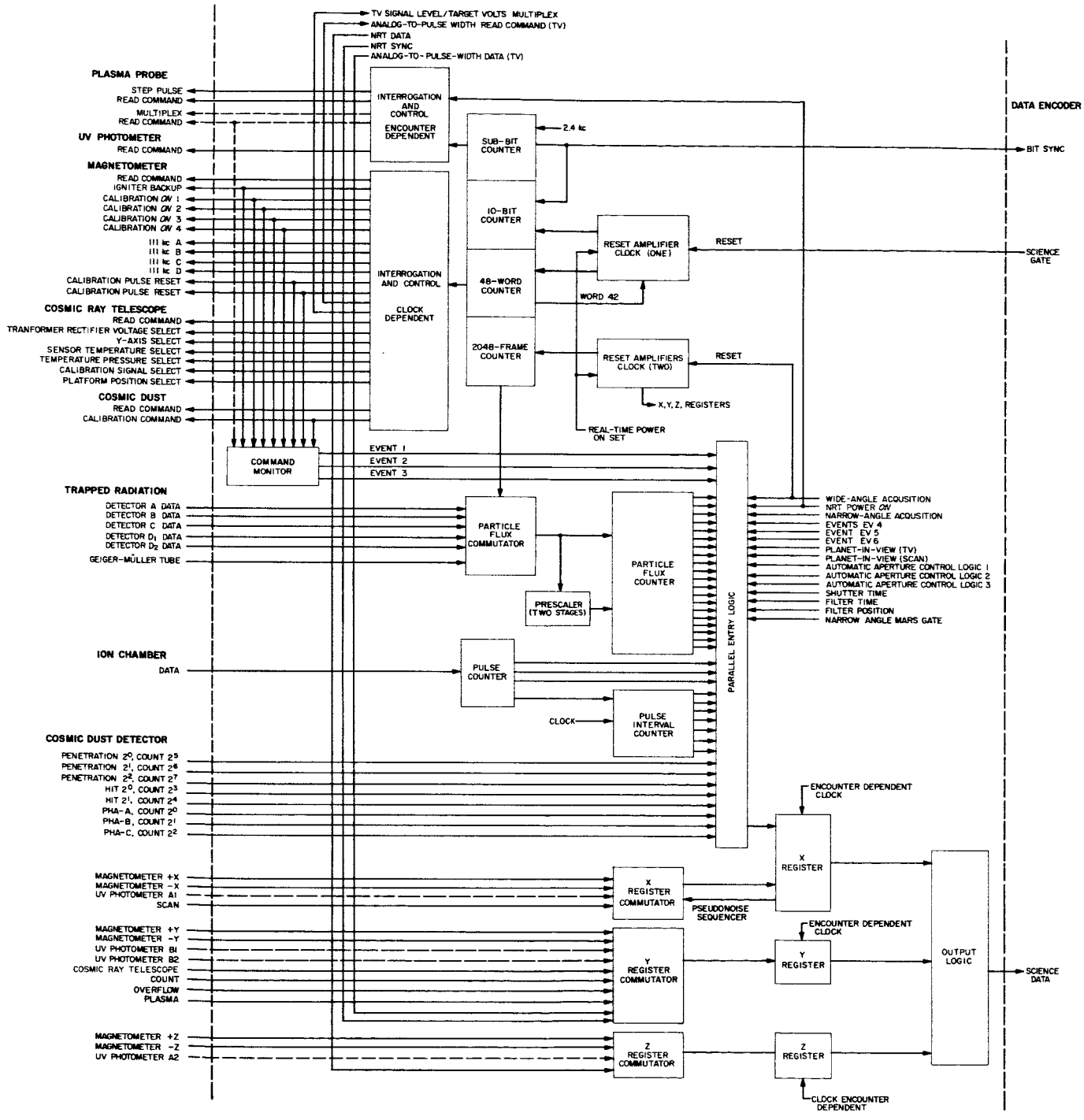


Fig. 301. Real-time DAS functional block diagram

data by a science gate signal from the data encoder at the start of each data frame. In this mode, 280 bits out of the 420-bit RT DAS frame are used by the data encoder for science. The remaining 140 bits are commutated by the data encoder through 100 engineering measurements.

The calibrate mode exercises the inflight calibration circuits in some of the instruments. This mode is activated at 7.17- or 28.67-hr intervals, depending upon the spacecraft bit rate. The format does not change during this mode of operation. The Cosmic Ray Telescope calibrate mode consists of a 128-frame sequence. During

the 24-frame magnetometer calibrate mode, a sequence of four commands is generated by the RT DAS. A single start command is used to calibrate the Cosmic Dust Detector.

The encounter mode, when enabled through the initiation of Data Mode 3, adds the 140 bits normally used by the data encoder from engineering measurements to the RT DAS output.

a. Format. The data format of the real-time system is shown in Fig. 302. Although the science data words are of various fixed lengths (from 1 to 20 bits), the DAS word length is 10 bits. There are 28 words (280 bits) in the Data Mode 2 (cruise) format and 42 words in the Data Mode 3 (encounter) format of which 10 are encounter-oriented. The RT DAS is mechanized in such a fashion that it always operates as though it were in Data Mode 3. Dormant encounter instruments are sampled through Data Mode 2 even though the telemetry data encoder does not accept these 14 words. In this manner, the DAS format is not changed for Data Mode 3; it is merely expanded by appending the 14 encounter-oriented words. During Data Mode 2, the DAS format contains 39 measurements; in Data Mode 3, 61 measurements are made.

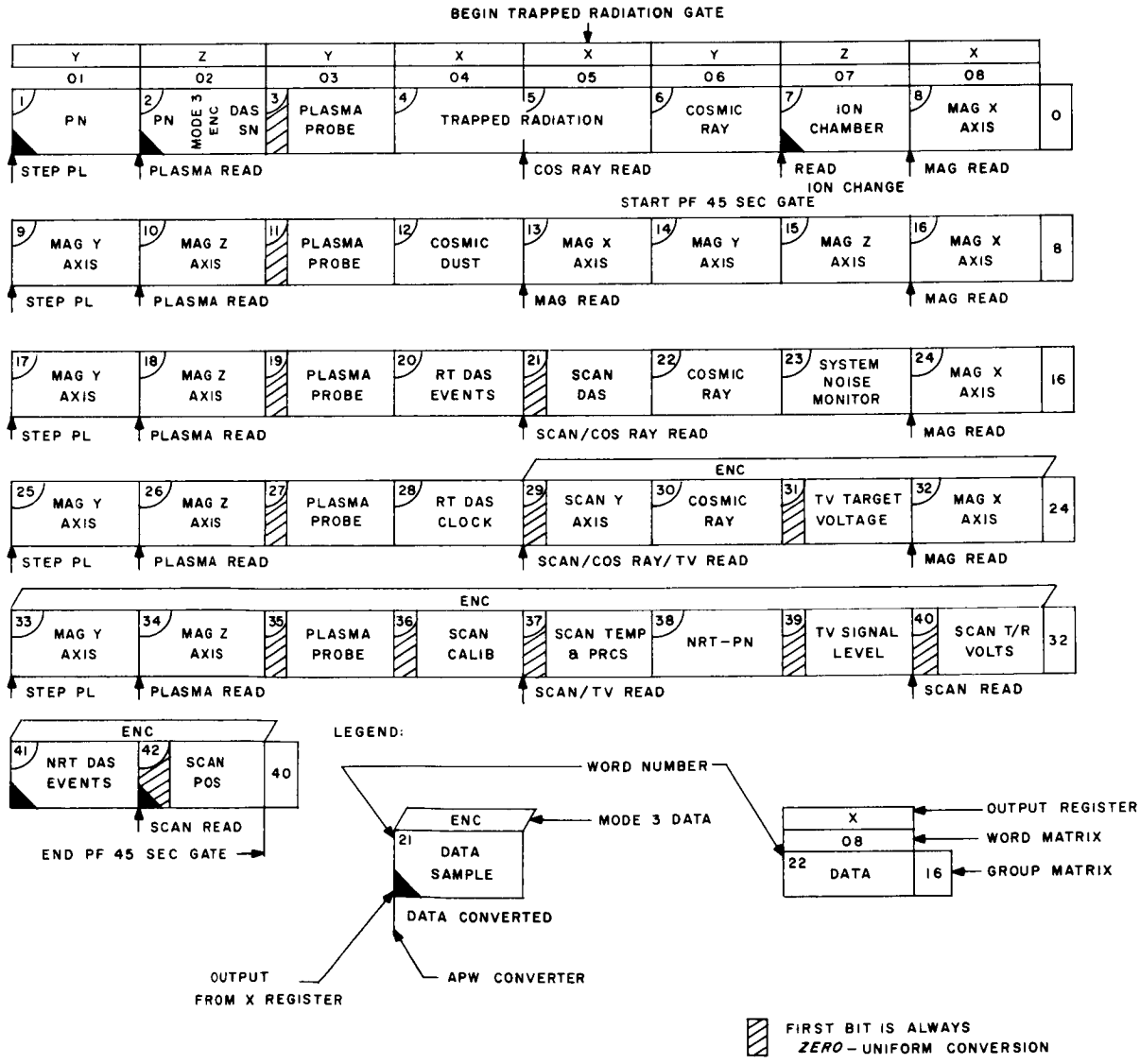


Fig. 302. Real-time DAS word format

The RT DAS contains three output-counter shift registers (X, Y, and Z). These registers and their operation during each data frame are shown at the top of the data-word column of Fig. 302. They enable the DAS to make analog conversions of the three axes in the magnetometer simultaneously, thereby eliminating the correlation ambiguities inherent in making successive samples of the three axes.

Since the RT DAS is synchronized to the telemetry bit rate, a change in the bit rate will only compress or expand the time scale of the DAS format. Every word and bit that can otherwise be spared is used (as indicated in Table 62) to give as much information about the status of the science subsystem as possible. Each frame of RT science data contains approximately 42 bits that are known or are predictable *a priori* in Data Mode 2; an additional 27 bits are added in Data Mode 3. The known bits include: (1) 15 bits of pseudonoise sequence for the identification of science data; (2) 3 bits of DAS serial number to preclude any ambiguity if more than one spacecraft is being tracked, and to furnish each system with a distinguishable mark for the purpose of test history; (3) 11 bits of frame number to identify each frame uniquely for recurring periods of 28⅔ hr; (4) 13 sign bits that are always *zero* because of unipolar analog conversions; and (5) 43 bits for continually monitoring the internal status of DAS functions and events, and for measuring predictable events in science instruments.

b. Data handling. The data handling accomplished by the RT DAS consists of complementary count conversions, interval and pulse counting, parallel data acquisition, and analog-to-digital conversions.

Complementary count. In an instrument containing its own count accumulator (the Cosmic Ray Telescope), the complement of the binary number in the accumulator is read out by the DAS. This is done in a manner similar to the way the DAS handles analog signals through the

Table 62. *Mariner* Mars 1964 DAS real-time format details

Word	Bit	Data
2	1[a]	Pseudonoise sequence
	2	Pseudonoise sequence
	3	Pseudonoise sequence
	4	Pseudonoise sequence
	5	Pseudonoise sequence
	6	Wide-angle acquisition
	7	Narrow-angle acquisition
	8	DAS serial number
	9	DAS serial number
	10	DAS serial number
12	1[a]	Cosmic dust
	2	Cosmic dust
	3	Cosmic dust
	4	Cosmic dust
	5	Cosmic dust
	6	Cosmic dust
	7	Cosmic dust
	8	Cosmic dust
	9	Magnetometer calibrate
	10	DAS frame number [a]
20	1[a]	Magnetometer calibrate 1
	2	Magnetometer calibrate 2
	3	Magnetometer calibrate 3
	4	Magnetometer calibrate 4
	5	Planet-in-view (Mars gate)
	6	Planet-in-view (scan)
	7	NRT power on
	8	Cosmic ray calibrate
	9	Magnetometer ignition
	10	Cosmic dust commutator
23		System noise monitor
28	1[a]	DAS frame number
	2	DAS frame number
	3	DAS frame number
	4	DAS frame number
	5	DAS frame number
	6	DAS frame number
	7	DAS frame number
	8	DAS frame number
	9	DAS frame number
	10	DAS frame number
38		10 bits of NRT pseudonoise sequence from buffer output
41	1[a]	TV shutter time
	2	TV automatic aperture control 3
	3	TV automatic aperture control 2
	4	TV automatic aperture control 1
	5	TV planet-in-view
	6	TV filter position
	7	Inhibit scan
	8	End-of-tape marker/TV frame start
	9	Tape start/stop
	10	Cosmic dust commutator

[a]Most significant bit.

analog-to-pulse-width converters. The DAS sends a burst of 111-kc pulses to the instrument for a maximum interval of 11.5 msec. These pulses enter the instrument count accumulator in parallel with the data input and are simultaneously counted by the DAS. When the counter in the instrument overflows, an inhibit signal is sent to the DAS; the DAS, in turn, stops counting and sending pulses to the instrument. The binary number in the DAS register is *one* plus the *one's* complement of the original number in the instrument accumulator.

Count rates. If an instrument having one or more random count-rate outputs does not have its own count accumulators, this function is performed by the DAS. There are six such inputs to the *Mariner* Mars 1964 DAS. These count-rate inputs from the energetic particle detectors are commutated so that four inputs are read once every eight frames and two inputs are read once every four frames. They are sampled for approximately 45 sec at 8⅓ bps, and for one-fourth of this period at the 33⅓ bps telemetry rate. A single, 20-stage counter is available for these inputs. When a *one* appears in the twentieth stage, two stages of prescaling are added to the count, although they are not read out since their use is indicated by the twentieth bit. Twenty bits are read out each frame for the count-rate data inputs.

Interval and pulse counting. The Ionization Chamber data are encoded in a different manner from the data of any other instrument; the Ionization Chamber pulses are counted continuously by the DAS and are encoded in two different ways. At a fixed point in each frame, the 10-stage ion-pulse interval counter is reset and six stages of the counter begin counting pulses having a 1.2-sec period (at the 33⅓ bps telemetry rate, the time interval is 0.3 sec). When the first ion pulse occurs, it inhibits the 6-bit time count for the remainder of that frame; it is also counted in a three-stage counter, thereby giving the time from the last reset to the first pulse and the total number of pulses in that frame. When 7 pulses have been received in one frame, the 6-bit time portion of the register is reset to zero. When 8 pulses are received, the tenth stage is set to indicate that the remaining 9 bits then represent a straight binary count of accumulated pulses; the tenth stage remains a *one* for the remainder of the frame. The register will overflow upon receipt of 511 pulses.

Parallel data. When it is not required that registers in an instrument be cleared upon readout, or when only a few bits are to be read, the DAS performs a parallel bit transfer. This is done for the Cosmic Dust Detector and the television subsystems. The Cosmic Dust Detector has two 8-bit registers that are sampled during alternate frames. The TV subsystem has 5 bits of status information (shutter time, filter position, planet-in-view, and automatic aperture control 1, 2, 3) which is read once each frame during Data Mode 3.

Analog-to-digital conversions. The use of an analog-to-pulse-width converter can improve analog-to-digital conversions in systems in which physical separation of the analog source and the digital converter is a necessity. In such systems, the transmission of analog signals from one part of the system to the other may result in errors in measurement due to noise interference.

When a measurement is to be made, a read command is initiated by the DAS and sent to the instrument. An analog-voltage-to-pulse-width converter in the instrument generates a rectangle whose length is proportional to the magnitude of the voltage being measured. The trailing edge of the rectangle is shaped and sent to the DAS.

Coincident with the generation of the read command, a gate is opened allowing a known clock frequency to be counted in a DAS register. When the delayed signal is returned by the instrument, the gate is closed and the state of the counter represents the analog voltage.

2. Functional Description of NRT DAS

The primary functions performed by the NRT DAS (Fig. 303) were to:

1. Provide logical control of the encounter sequence
2. Control the television and video storage subsystem operation during encounter
3. Format, identify, and buffer the television data before transferring it to the video storage subsystem
4. Provide logical control of real-time data transferred from the RT DAS to the tape recorder

The NRT DAS has three basic operational modes: reset, cycle, and record.

a. Reset mode. The reset mode is listed among the operating modes even though it represents an essentially nonoperative condition of the NRT DAS. The reset mode is in effect until the dc supply voltages have stabilized at their proper levels after the application of 2.4-kc power to the power supply unit. The 2.4-kc power is

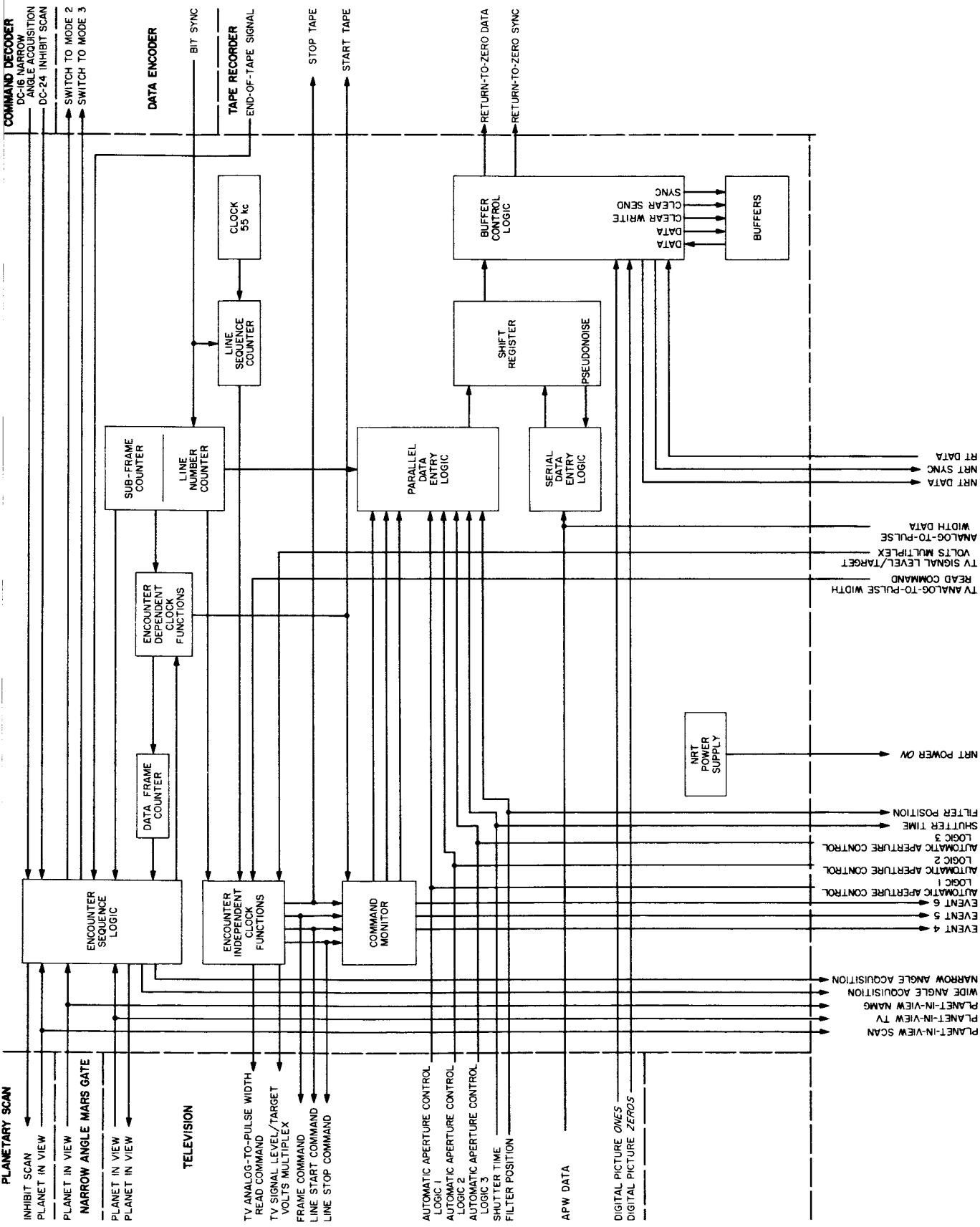


Fig. 303. NRT DAS functional block diagram

switched to the DAS by the CC&S or by ground command. During the application of power, critical control functions have to be maintained in an *off* condition.

b. Cycle mode. During the cycle mode, which becomes effective when dc voltages are developed, the NRT system performs all of its normal data sampling functions. The TV pictures are commanded and data samples are taken and stored in the core buffers. During this time, however, tape start commands are not generated, and data are not recorded on magnetic tape.

The cycle mode was a system requirement, since the television subsystem required certain control signals from the DAS to synchronize its logic. The scan subsystem detects the planet during the cycle mode and produces the wide-angle acquisition signal. The wide-angle acquisition signal is routed to the data encoder and to the RT DAS to initiate Data Mode 3. The NRT system reenters the cycle mode at the end of the record mode and remains in this condition until power is removed from the system.

c. Record mode. The record mode is enabled when the planet comes into the field of view of either the TV vidicon or the narrow-angle Mars sensor. The record mode is also enabled by ground command DC-16. During the record mode, data are acquired as shown in Fig. 304, which is a gross timing diagram of the NRT encounter data frame. During the 144-sec encounter data frame, two TV pictures are taken and recorded during subframes zero and two. A TV picture contains a 200 × 200 element matrix of discrete points, and 24.12 sec are required to read, identify, and record the data. An additional TV picture, indicated by the dotted line, is shuttered but not recorded. The phase of the subframe counter, which is cycling continuously during the cycle mode, is an additional condition for the entry of the system into the record mode. The record mode, therefore, is entered in such a way that only complete encounter data frames are recorded on tape.

An encounter data frame produces 401 data blocks of approximately 1280 bits (one line) each. The number of spare bits in each data block is a function of the stability of the 10.7-kc oscillator. During subframes zero and two, TV and real-time data are multiplexed between the two buffers. One block of data is generated every 120 msec (the TV line rate and the encounter real-time telemetry rate).

The NRT system is capable of handling 1200 bits of TV information, and of making one analog-to-digital conversion of 10 bits and a number of parallel digital transfers in the 120-msec line interval.

The record mode is terminated when the second end-of-tape loop signal occurs in the tape recorder. A backup signal from the DAS can also terminate the record mode when 22 TV pictures have been commanded.

3. Physical Description

The flight configuration of the DAS (excepting the interconnect harness) is shown in Fig. 300. The system is composed of these five subassemblies plus nine ancillary analog-to-pulse-width converters, which are located in the science instruments.

Subassembly 20A1, the NRT-DAS buffers, contains two physically and electrically identical 1320-bit-serial, sequentially-addressed core memories or buffers. The average weight of these subassemblies is 1.25 lb.

The non-real-time subsystem was packaged on one subassembly, which contains 52 welded cordwood modules and weighs approximately 3.25 lb.

The real-time subsystem was packaged in two subassemblies, and is composed of 86 pellet-component modules, 11 transformer modules, and 1 crystal module. The two subassemblies weigh approximately 2.8 lb and 2.6 lb each.

One subassembly contains two independent power supplies: one for the NRT DAS subassembly and buffers, and one for the two RT DAS subassemblies. The complete power supply weighs 2 lb. When energized, the NRT DAS draws 5.6 w of 2.4-kc, 50-v-rms power. The RT DAS uses 6.5 w of 2.4-kc, 50-v-rms power. The DAS contains 11,130 components, including 961 transistors, 3520 diodes, and 2640 cores (for the buffer storage).

4. Design Evolution

The initial design envisioned a science subsystem that relied upon synchronization and interrogation signals from the data encoder, and upon switching and control functions from the central computer and sequencer. The data conditioning required for each instrument was to be accomplished in the instrument.

It soon became apparent that the functions necessary to properly operate the science instruments could not

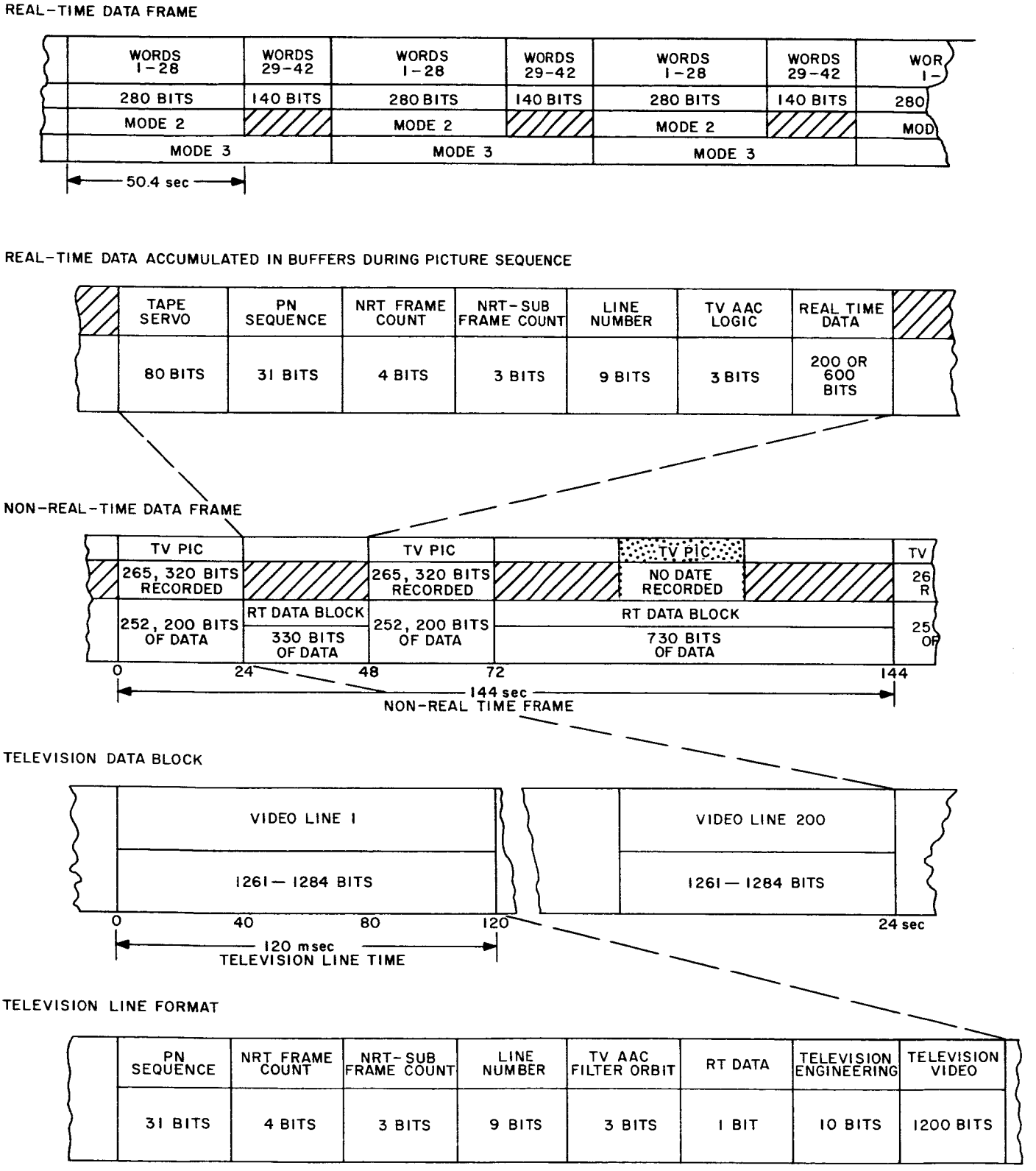


Fig. 304. NRT DAS word format

be supplied from either the data encoder or the central computer and sequencer. In addition, it was decided that the handling of the digital output of the TV data would be done by a science data automation system, but that the video data would be digitized within the TV subsystem itself.

As the number of instruments increased from five to nine, the complexity of the DAS increased from simple data conditioning to that of data sequencing, buffering, converting, and controlling. With a growth in the requirements placed upon it by the instruments and the spacecraft, the DAS design had to be modified in the following manner:

1. The tape recorder was made into a separate subsystem (video storage subsystem).
2. The DAS was split into two separate sections: (a) the NRT DAS, comprising the control logic for the encounter instruments and the buffers; and (b) the RT DAS, comprising the real-time control logic.
3. The power supply was split into two completely separate parts, one for the RT DAS and one for the NRT DAS. The NRT DAS power supply is energized only during the period that the encounter instruments are operating.
4. The DAS format was changed to incorporate new instruments, which necessitated changes in both the design and the interfaces of the DAS.

In March 1963, a NASA Headquarters' review resulted in another modification to the science subsystem; some instruments were removed and new ones were added. These changes forced another redesign of the RT DAS, which occurred after the DAS design was to have been frozen; as a result, the actual design freeze could not be made until May 15, 1963.

After the first PTM spacecraft system test, a number of modifications were made to the DAS to enhance the performance of the science subsystem and the spacecraft. These were:

1. Isolation of bit synchronization between RT and NRT DAS to prevent one from interfering with the other
2. Increase of DAS output pulse margins to the instruments
3. Modification of event registers to use NRT power-on as the set function
4. Improvement of narrow-angle-acquisition interface isolation with the RT DAS, through the use of an isolation amplifier, to prevent a false indication of planet acquisition
5. Modification of the logic to prevent spurious pulse output at NRT power-on and power-off
6. Modification of NAMG interface circuits to prevent shorted or open connections between the NAMG and the DAS from causing false planet acquisition
7. Reduction of high-speed flip-flop loading
8. Increase of high-speed flip-flop margins
9. Elimination of four high-speed flip-flops
10. Modification of the output of the DAS to be "data" instead of "not data"
11. Decrease of capacitive loading and isolation of some RT DAS functions from those in the NRT DAS
12. Addition of event register outputs to the OSE
13. A decision to revert the NRT DAS to welded cordwood construction rather than pellet construction

The removal of the ultraviolet photometer in July 1964 resulted in elimination of the encounter-dependent function of the RT DAS format. This was accomplished by shifting a few wires in the gating circuits, and was considered to be only a minor change.

5. Procurement

The building of the main DAS, consisting of the RT and NRT logic subassemblies, was subcontracted. The contract included the logical design of the complete DAS, the integration of the buffers and power supplies into it, parts screening, and field service at JPL and Cape Kennedy

The power supply subassembly was designed, developed, and fabricated to the DAS power supply design specification. The screened electronic components were furnished to the subcontractor by JPL.

A contract was awarded to a separate firm for the purposes of: (1) investigating the packaging techniques, manufacturing, testing, and quality-assurance procedures and component screening criteria in relation to the pellet components being used in the system; (2) investigating and evaluating manufacturing and testing procedures and the quality assurance program of the suppliers furnishing

pellet-type components; and (3) recommending methods for increasing the reliability of the components and the system.

The analog-to-pulse-width converters were fabricated under a fixed price contract. The design and development of these modules was accomplished at JPL. A contract for a pelletized converter was cancelled in July 1963 because of serious component interconnection problems. A welded version of the NRT DAS was subcontracted in December 1963.

6. Fabrication

a. Real-time DAS subassemblies. The RT DAS logic was fabricated from pellet modules. The term module, as it is used here, refers to pelletized (resistors, capacitors, and diodes) and miniaturized (TO-47 cased transistors) components assembled into a unit capable of performing discrete logic functions. Two module configurations used 1.4 × 0.9 × 0.275 for storage elements and 1.4 × 0.7 × 0.275 for decision elements. Each module was composed of two envelopes, which were not necessarily complete in themselves. An assembly-level diagram is shown in Fig. 305. In terms of circuits, there are three non-exclusive categories: interface, storage (e.g., flip-flops), and logic gates. These circuits were packaged one or more per pellet envelope. Two envelopes were assembled and formed a circuit module containing one or more complete circuits. Logical significance was lost at the stick level and did not reappear below the final assembly level. A typical envelope is shown in Fig. 306. (The screening serial numbers are clearly seen on the tops of the transistor cases.) Figure 307 shows an assembly of five modules into a stick. Figure 308 shows one side of a tray (JPL module or blivit) interconnected and wired to a pair of connectors and ready for checkout as a unit.

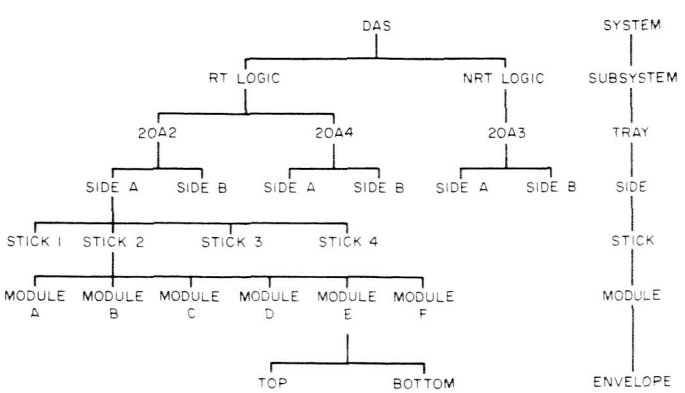


Fig. 305. Real-time logic assembly tree

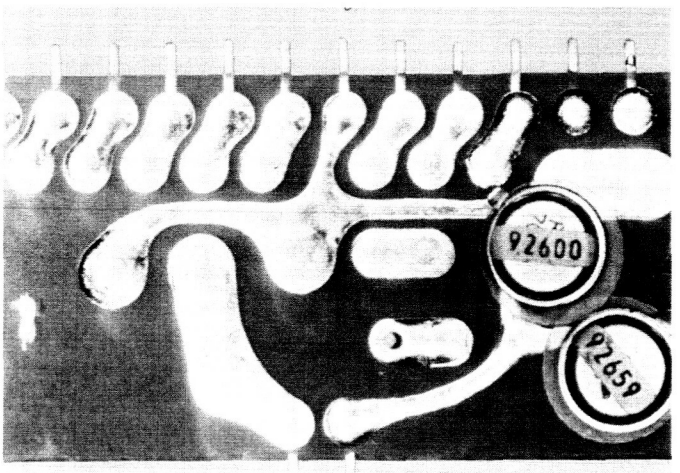


Fig. 306. Assembled data automation system envelope

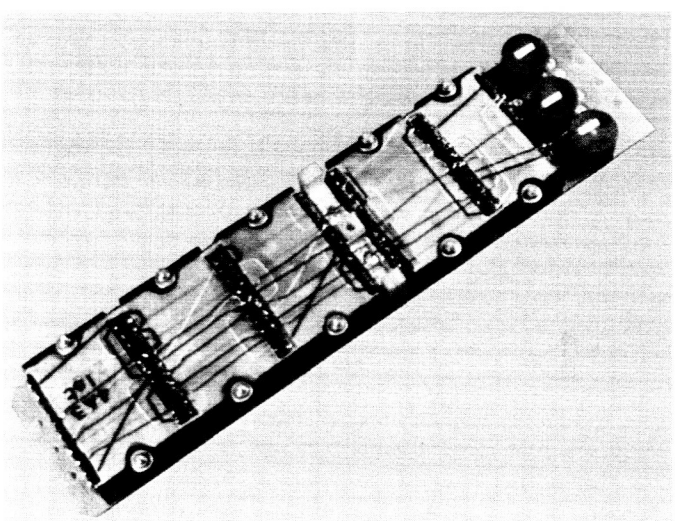


Fig. 307. DAS logic stick

Parts screening. In accordance with *Mariner* Mars 1964 mission requirements, a program was established by which all components (pellet and conventional) were screened, burned-in, and identified at the subcontractor's facility. The program had numerous shortcomings, but, in view of the scope of the undertaking, it had to be considered highly successful. One-quarter million components were screened, most of which were too small to be handled without mechanical aids.

Screening and burn-in specifications were prepared by the subcontractor for all components not on the JPL Preferred Parts List. These specifications were subsequently reviewed, modified, and approved by JPL.

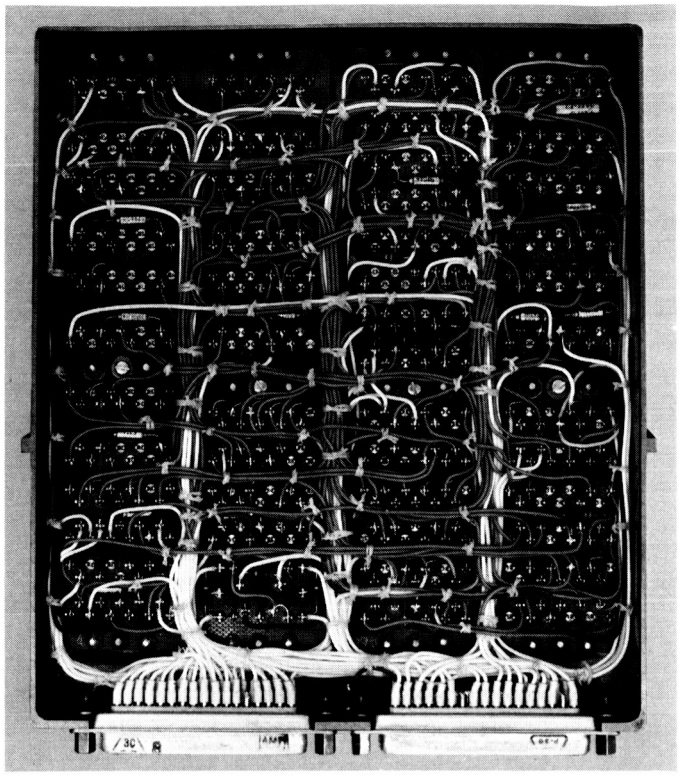


Fig. 308. One side of a DAS logic tray

Mechanical inspection procedures for pellet components were based on envelope fabrication requirements. These specifications included:

1. Finish of contact surfaces
2. Parallelism of contact surfaces
3. Thickness
4. Diameter
5. Non-contamination and uniformity of pellet edges (to prevent bridging or shorting)
6. Cracks or delamination of ceramic materials
7. Contact seal for pellet diodes

A final review of the rejection rates of pellet components indicated that the majority of pellet rejects occurred during initial mechanical inspection.

Envelope assembly. Envelope assembly was performed in an area separated from normal production activity. Qualified components were received from the burn-in area with IBM cards containing component type, serial number, manufacturer, and value. A sheet of 3-mil glass epoxy was cut to size and drilled to accept components and leads in the correct location for each type of envelope. The leads were then inserted into a silicone-rubber holding block.

Locating pins were set in a mold and used as registration and holding points during molding and subsequent operations. To start the assembly procedure, the locating film was placed over the locating pins of one-half of the mold. The leads in their silicone blocks were inserted into the mold; the components were inserted in their appropriate locations in the glass-epoxy film, and these locations were recorded by circuit nomenclature on the component IBM cards along with the envelope serial number (originated at that point). The components were handled only by means of vacuum tweezers, and the assemblers were required to wear white gloves or finger cots when hand-touching or holding the mold. A visual inspection was performed to ensure correct component insertion and location. The mold was closed with its mating half, and its bottom and side seams were sealed to prevent leakage of the epoxy. The mold was then closed and placed in an oven for preheating. The potting resin was weighed and preheated. It was then degassed under vacuum, the catalyst added and mixed, and poured into a lead toothpaste tube and again degassed. A compound mixture report was prepared showing proportions used, duration of preheat and degassing, and other pertinent data. The epoxy was then injected into the mold from the tube, using minimal pressure, until epoxy was observed in the reservoirs. The filled mold was placed in an oven and cured for 1 hr at 140°F.

The mold was removed from the oven, opened, and the excess material removed. The epoxy was not yet fully cured and was still flexible enough to permit handling without fear of fracturing the substrate. The envelope was inspected with a microscope at 16 to 20 magnification, and any epoxy over the component end-caps was carefully removed. Small pin-hole voids were repaired by injecting them with epoxy from hypodermic syringes. The substrate was given a final cure in an oven at 140°F for 1 hr to gain the full physical properties of the epoxy. Following this, the components were tested individually to ensure that diode polarity and resistor values were correct.

Meanwhile, "masks" were prepared. (A mask is a stencil with an open area representing the interconnection pattern required for the circuit in the envelope.) The mask was etched from sheet brass, using standard photolithographic techniques. The mask was applied to the substrate so that it was in intimate physical contact with

the surface of the substrate. The conductor and component areas were then cleaned and prepared for the vacuum deposition process. The substrates were placed in a holding fixture that had a capacity of six active circuits, a dummy substrate with sample components for destructive testing, and a monitoring glass slide for checking deposition uniformity and thickness.

Deposition of the circuitry was performed in a specially built vacuum-deposition chamber. To start the deposition process, the bell jar was evacuated and flushed with helium. Glow discharge in the helium atmosphere was performed at approximately 1.5 kv and 30 ma for 5 min. At the end of that time, the system was pumped down to less than 10^{-5} torr. At that point, a thin flash of nichrome was evaporated from a tungsten filament. This was followed by evaporation of a preweighed charge of copper and then by a coating of tin indium from molybdenum boats. The electrical resistance of the deposit on the glass side was tracked during deposition to ensure that preestablished maximums were not exceeded. The resistance value was converted to a thickness reading for control purposes. Nichrome was used as a base coat to enhance adhesion of the deposited material to the substrate. The copper layer was used to conduct and to build up a material thickness for subsequent operations. The tin-indium deposit uniformly pre-tinned the material before soldering.

When the substrates were removed from the bell jar, the masks were removed from the dummy and it was subjected to a deposit adhesion and soldering test. The acceptance of the active circuits was predicated upon the outcome of these tests.

Due to low temperature constraints, a 50–50 tin-indium solder was used for soldering transistors onto the envelope. This alloy has a melting point of 117°C and soldering was performed at 130°C. Fountain soldering was used because the solder can be protected from contamination by an oil bath. The envelope was fluxed and immediately soldered. The flux and oil were cleaned from the envelope, and the solder was inspected under a microscope for cleanliness, granulation, non-wetting, and adhesion. When this inspection was completed, the transistors were inserted and hand-soldered in place. The envelope was then encapsulated to protect the circuitry from handling and environmental hazards. The encapsulant was transparent with a low-dielectric constant for minimum effect on circuit characteristics. The circuit was subjected to an electrical inspection and marked according to its circuit use.

Two envelopes were joined together to make a module. Up to seven modules could then be mounted onto an epoxy glass stick, and four sticks were assembled together in half of a tray.

b. Buffers. Each buffer subassembly was fabricated on two identical printed circuit boards using two-dimensional packaging. This packaging was unconventional in that the component density was far greater than normal. Figure 309 shows the prototype buffer.

A JPL inspection revealed that some of the buffer pulse transformer leads were straight and possibly taut on one of the board assemblies. It was felt that straight or taut wires could lead to a reliability problem. There was no known method available by which the evaluation of the exact state of the leads could be made, nor could they be reworked without damage to the unit. The board in question was deemed unflightworthy. In order to avoid the risk this board represented, a new board was purchased to be installed in the flight buffer. The questionable board was used for an advanced JPL study project.

c. Non-real-time DAS. The NRT DAS was originally fabricated from pellet components in the same manner described for the RT DAS. The discovery of the resistor problem, together with the general shortage of pellet components, and the particular shortage of diodes, resulted in a decision to produce welded cordwood NRT DAS flight units.

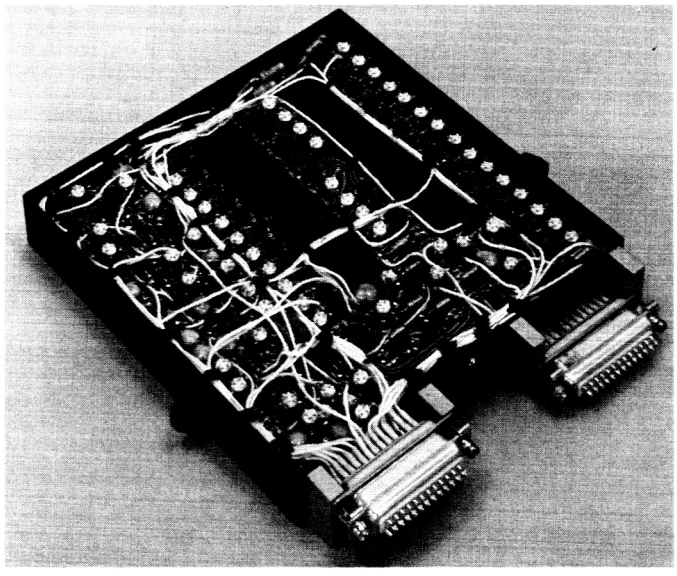


Fig. 309. Data automation system prototype buffer

The welded NRT DAS used the same basic circuit design as the pellet NRT DAS. However, the unit was completely repackaged by JPL to ensure that it would fit into the spacecraft. The welded NRT DAS used miniaturized standard components assembled into modules. These modules were assembled together to form a stick, and the sticks were interconnected by means of a welded matrix. Interstick connections, as well as plug-to-stick connections, were made by means of a preassembled harness. An assembled welded NRT DAS is shown in Fig. 310.

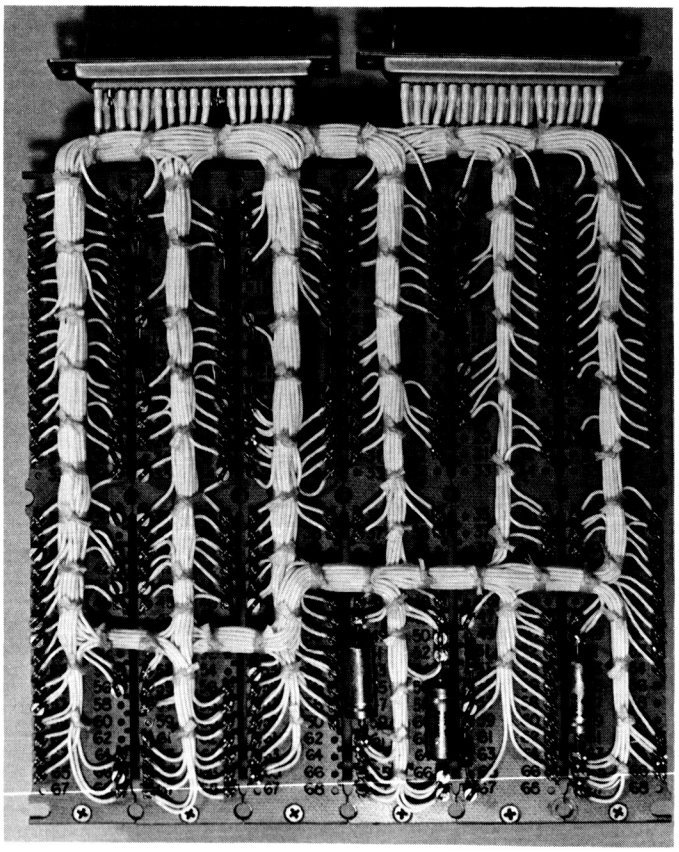


Fig. 310. Assembled and welded non-real-time data automation system

7. Test Experience

Of the 40 problem/failure reports written against the main logic of the DAS, 21 were detected while the subsystem was installed on a spacecraft. Of these, 13 were not failures, but resulted from a defect in some other subsystem or from a lack of understanding of the DAS operation. Of the remaining eight only two were written against flight units installed on flight spacecraft.

All of the buffer memories passed TA and FA tests without any failures. There were 17 failure reports written, and of these, 13 were written at the vendor's facility for defects discovered during manufacturing or predelivery testing. The remainder were detected and corrected before environmental testing was completed at JPL. No failure occurred after delivery of the hardware to SAF.

The buffer design specification called out the original version of the JPL specification. Revisions A and B of this specification called for the TA thermal–vacuum test to be performed at 75°C instead of at the 65°C level. The margin problem that resulted from this change was caused by a shift with temperature of the switch core thresholds. The subcontractor was able to circumvent the problem by providing a varying half-select current amplitude as a function of temperature. This was accomplished by replacing the fixed select amplifier current limiting resistor with one that had a temperature coefficient of resistance of 1300 ppm.

All of the DAS power supplies passed TA and FA tests without failure. An engineering change request was approved in April 1964 to modify the 2.4-kc timing interface between the power supply and the real-time DAS. The deficiency in the original interface was apparent only at TA temperatures when an otherwise unnoticed ringing on the 2.4-kc pulse moved into the logic threshold. No failures occurred after delivery of the units to SAF.

All welded NRT units passed the FA and TA environmental testing. During TA vibration testing, however, several wires were broken and individual strands were fractured. The soldered interconnect used in the welded subassembly was significantly different in design from that used in the pellet subassembly. The welded NRT DAS wires were bound in large bundles traversing the length of the sticks, while the pellet unit wires formed a mat over the sticks. The pellet systems had been subjected to vibration testing without the benefit of stycasting of the cable ties or of conformal coating. After using a stycast on the cable ties and conformally coating the subassembly, no more trouble was experienced in TA testing. There were, however, some pre-SAF testing failures in bench testing these units. During the bench testing, it was discovered that after completion of the encounter sequence and the subsequent switch to Data Mode 2, the first stage of the data frame counter would continue to count, although the balance of the counter was properly inhibited. The difficulty was traced to a

missing weld of the inhibit signal line to the first stage of the counter. After the weld was completed, normal operation was observed.

Initial checkout revealed that the circuit preventing issue of scan inhibit and switch to Data Mode 2 signals was inoperative. This circuit function was derived from the fall time of the 6- and 20-v power supplies. In repackaging the NRT DAS for welded construction, the capacitors on these lines had been increased. The effect on 6- and 20-v fall times was sufficient to preclude the normal circuit operation. When the original capacitance values were used, normal operation was observed.

The frequency of the 10.7-kc buffer clock was found to vary by more than 20% as the unit was taken through the flight-acceptance temperature range. The instability was traced to the oscillator frequency-determining capacitor. A temperature-dependent Cerifill capacitor had been specified (in error) during the design of the welded modules. Substitution of a temperature-stable Corning glass capacitor reduced the drift, through the type-approval temperature range, to less than 0.3%. No failures occurred after delivery of this equipment to SAF.

K. Narrow Angle Mars Gate

The NAMG is located on the planetary scan platform of the spacecraft. It provides an acquisition signal to the data automation system when Mars enters its field of view. The signal causes initiation of the science planetary encounter sequence.

During a normal encounter, the planetary platform scanning stops and the wide-angle planet sensor causes the platform to be tracking Mars when the NAMG acquisition signal occurs. If there is a malfunction in the wide-angle planet sensor or if the miss distance is too great for proper tracking, the NAMG can still provide an acquisition signal as it scans across the planet, which will stop the scanning motion and hopefully permit a limited amount of planetary science data to be obtained.

By May 1963, it had been decided to proceed with the design of an NAMG to be incorporated on the planetary scan platform. The NAMG would provide the narrow-angle acquisition signal. The schedule called for delivery of an unqualified proof test model by August 1963. The first fully qualified flight unit was delivered to the spacecraft assembly facility in November 1963, less than 6 months before the project officially began.

The requirements imposed on the NAMG design were many and varied; it had to meet all the environmental requirements for *Mariner* type-approval and flight-acceptance tests. In addition, a severe vibration specification was added because of resonance of the scan platform structure upon which the NAMG is mounted, and the general *Mariner* Mars 1964 requirements of low magnetic field and long lifetime also had to be met. The specific NAMG requirements that were established are given in Table 63.

1. Design Evolution

Almost immediately upon initiation of the development of the NAMG, it was decided to proceed with a design that took the form of a cylinder with a simple lens and baffle in front of a cadmium sulfide photoconductive cell, a field stop to define the field of view, and a

Table 63. Specific NAMG requirements

Category	Requirements
Size	1-in. in diameter by 4-in. long
Weight	Less than 0.2 lb
Power	Less than 65 mw
Field of view	A rectangle 2.5 (in a direction perpendicular to the scan motion) by 1.5 deg
Stray light	Rejection of sunlight more than 22 deg off axis
Output	13 ±3 vdc (acquired) 0.5 ±0.5 vdc (unacquired)
Output rise time upon acquisition	Less than 20 μsec
Sensitivity acquired	Object completely within the field of view and having a color temperature of 3500°K and an illuminance greater than 0.01 ft-cd
	Object completely filling the field of view and having a surface brightness greater than 30 ft-L
Not acquired	Object completely within the field of view and having a color temperature of 3500°K and less than 0.0005 ft-cd illuminance
	Object completely filling the field of view and having a surface brightness less than 1.5 ft-L
Alignment	Line of sight to the center of the field of view to be perpendicular to the mounting surface within 0.25 deg
Temperature	Operation to be within specifications between −30 and +55°C; operation to be within all specifications except for sensitivity between −30 and +100°C

simple electronics package in the back. The cylinder was to be mounted by a flange and electrically connected to the spacecraft by soldering a three-wire cable to three terminals on the back of the NAMG. It was also decided to combine the cadmium sulfide cell, electronics, and terminals into one welded package. This integrated module concept was adopted, but because of the short schedule, a soldered cordwood module was developed as a parallel effort.

The first layouts of the electronics module showed that the NAMG would have to be somewhat larger than had been anticipated, about 1 in. in diameter. Since the space was available, the 1-in. diameter was extended the entire length of the unit to provide better structural rigidity and to greatly improve the stray-light baffling.

Calculations showed that the aberrations involved in the use of a single-element lens would be tolerable and a simple piano-convex lens of 1.5-in. focal length and 0.5-in. diameter was used. Calculations also showed that the NAMG could operate even with the lens omitted, but the ability of an optical system to provide a sharply defined field of view, a substantial reduction in the inherent time lag of cadmium sulfide cells, and a much larger safety margin to the sensitivity requirements gave ample justification for the use of a lens. The lens used was the longest focal length and the largest diameter that could fit in the package and still allow room for the electronics and the stray-light baffling.

The baffling was knife-edged, just large enough to clear the field of view at the front of the NAMG, and sharp-threaded on the inside of the tube at as large a diameter and thread pitch as was structurally permissible. The interior of the NAMG was completely black-anodized. These steps together with the field stop in the focal plane were effective enough to permit rejection of the Sun at 22 deg off axis.

The field of view chosen was a rectangle 1.5 by 2.5 deg in a direction perpendicular to the platform scanning direction. Figures 311 and 312 show the typical encounter geometry. The rectangular field of view gives an earlier acquisition and requires less encroachment into the field of view by the planet than an elliptical shape would. The long dimension was chosen to give overlap during the scanning motion, so that the planet could be acquired at any miss distance that would provide enough signal. The short dimension was chosen to give a considerable safety margin for triggering the NAMG, and to give a shape that closely matched the sensitive area of

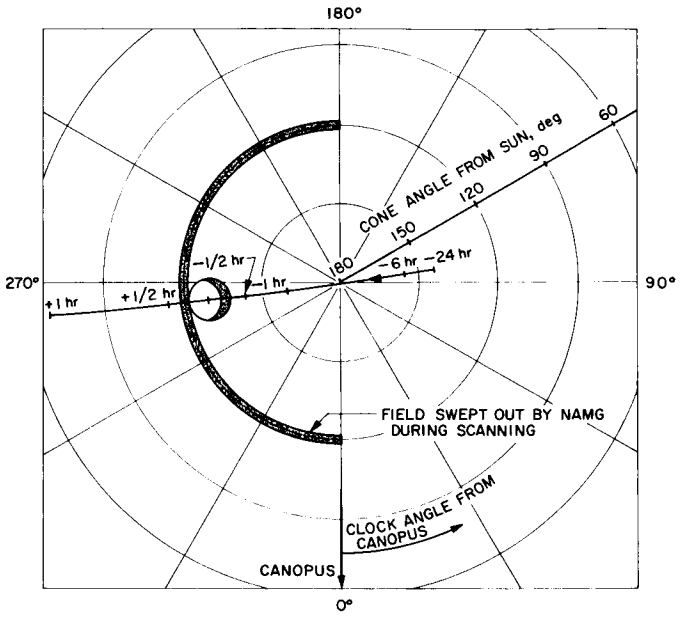


Fig. 311. Typical trajectory encounter geometry

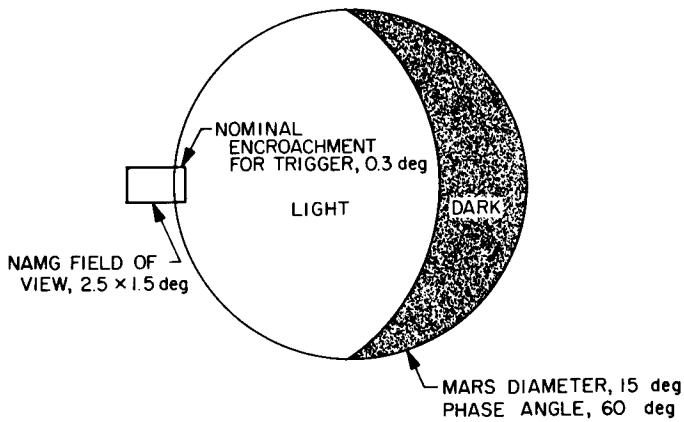


Fig. 312. Nominal encounter geometry

the cadmium sulfide photoconductor. The photoconductive cell was placed far enough behind the field stop to permit the light entering the aperture to diffuse over most of the sensitive area, thus minimizing any effects that might be caused by the photoconductive pattern.

The cadmium sulfide cell itself consumed a large portion of the development effort. Questions arose concerning the stability of the cells as a function of time and temperature, the quality control of the cells, what effect a leak in the hermetic seal might have, and how to weld the cells into the module. Considerable effort was spent

on screening and selecting cells. No time was available to delve into source quality control and inspection, and reliance had to be placed on a very thorough visual inspection plus electrical measurements before and after temperature cycles. Complete answers on cell stability and vacuum effects are still not available, but the safety factors that were built into the NAMG were far larger than the variations that have been observed.

The welded electronics module encountered problems with weld schedules and with the potting mold. The difficulties were of a minor nature, however, and the elimination of interconnections inside the NAMG resulted in a boost in reliability as well as in easy interchangeability of electronics. The circuitry used operates satisfactorily with a very wide range of component variations and uses a minimum number of components. Although the originally specified load required current from the NAMG only in the *off* condition, the electronics proved to be sufficiently adaptable to be used without change in the final configuration that required current only in the *on* condition.

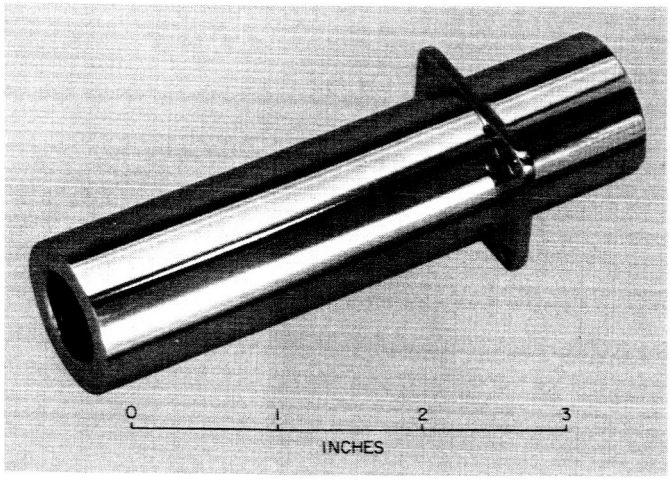


Fig. 313. Narrow angle Mars gate

The final NAMG design is shown in Fig. 313 through 317. The mechanical assembly had a total of 10 parts, and the electronics module contained some 9 electronic components and 28 total pieces of all kinds.

2. Test Experience

Since the actual operating conditions were inaccessible, the testing program for the NAMG used two different simulators. Simulator I was a large, well collimated, well calibrated source used as the primary reference. It provided a 0.5-deg diameter planet that was corrected to approximately 3500°K color temperature to match Mars, and was variable in intensity over the range of interest. Simulator II was a very small, uncollimated, and portable source that could be used under confined conditions and during environmental tests. The color temperature was uncontrolled and the intensity was calibrated against Simulator I before and after each use.

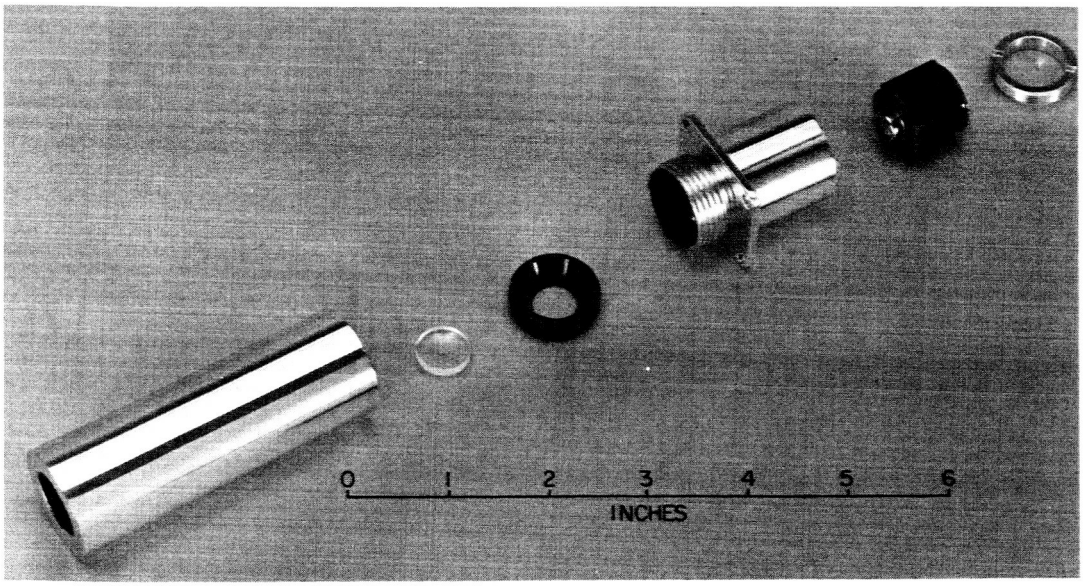


Fig. 314. Exploded view of narrow angle Mars gate

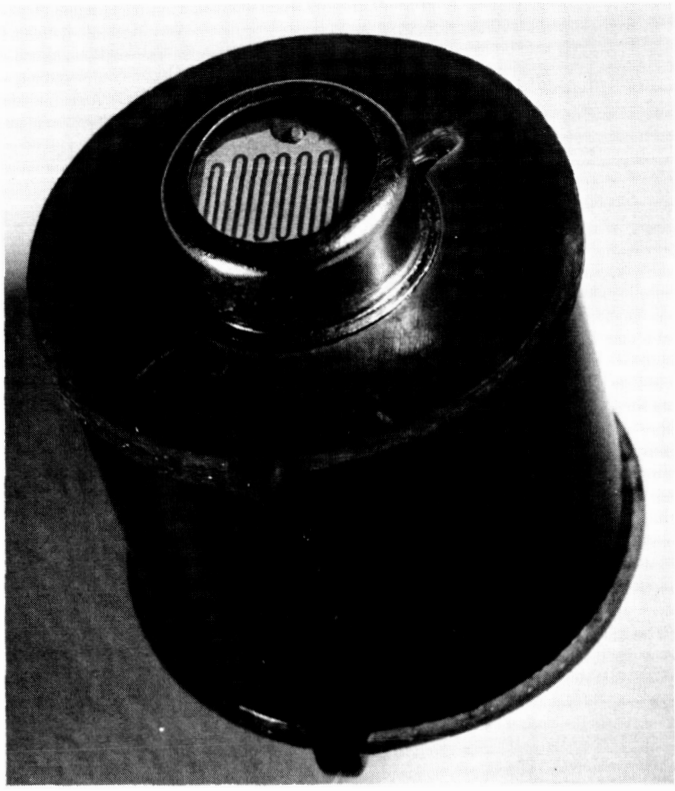


Fig. 315. Electronics module

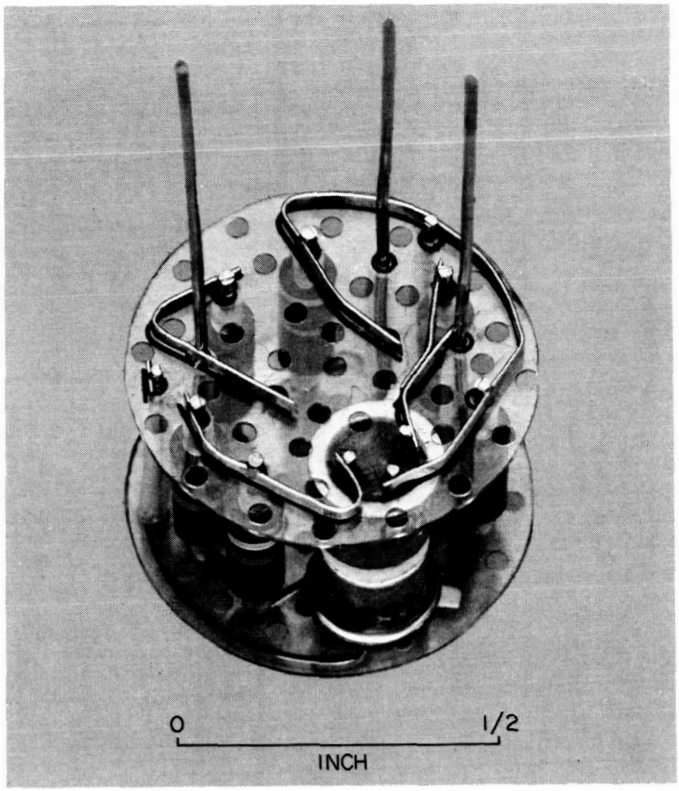


Fig. 316. Interior of electronics module

No difficulty was encountered during type-approval testing except during thermal–vacuum tests, when it became apparent that prolonged exposure to high temperature would increase the sensitivity beyond the specified limits. Special tests were run to determine whether the sensitivity leveled off or continually increased as a function of time. The sensitivity leveled off at a value outside the original specification but close enough that it would not in any way jeopardize the mission. Long-term tests subsequently have verified the leveling off, and the new specification reflects a wider sensitivity range to allow for this temperature problem.

Flight-acceptance tests were performed without incident on the four flight units. The complete FA testing for each unit took about one week. Magnetic tests conducted before and after vibration on the TA unit and after vibration on all FA units were all well within specification.

After completion of the type-approval testing, the TA unit was placed on an accelerated life test to observe the long term operating behavior and to discover any unexpected failure modes. The life test was run at 167°F,

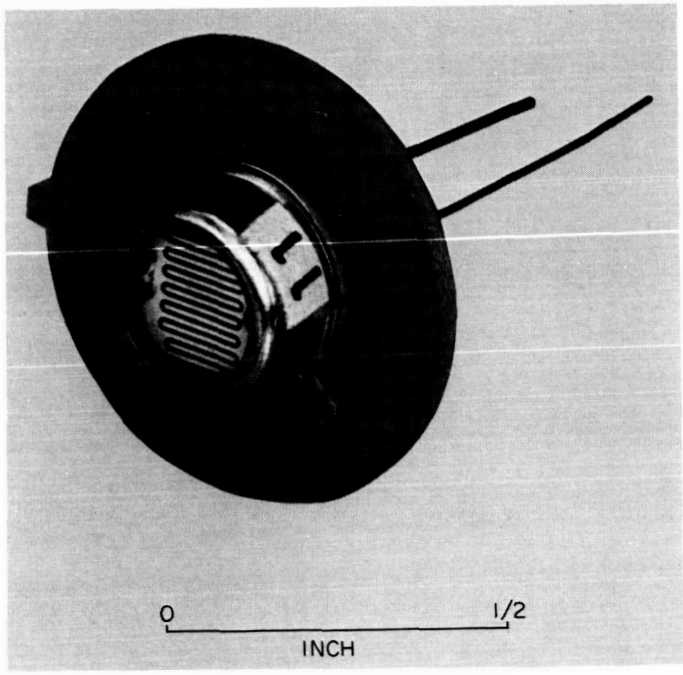


Fig. 317. Photosensitive cell in header

since previous experience had indicated that high temperatures provide the worst environment for cadmium sulfide photoconductive cells. The life test unit had normal power applied at all times and was run through a simulated encounter sequence every 100 to 200 hr.

After an increase of about 3 to 1 during the first 300 hr of the life test, the sensitivity remained relatively constant for more than 8000 hr. The unit operated correctly at every simulated encounter.

A number of a special tests were performed to determine whether an unforeseen problem might exist, and, if so, what solutions would be possible. One such problem was the moons of Mars entering the field of view and causing premature turn-on of the NAMG. One of these special tests showed that the NAMG could withstand micrometeorite frosting of 90% of the lens and still perform adequately.

3. Flight Experience

During the flight of *Mariner III*, when it became apparent that the shroud had probably failed to separate from the spacecraft, encounter science was commanded *on* in an effort to learn more about the spacecraft. Immediately, the NAMG gave an acquisition signal.

Sun illumination of any portion of the lower thermal shield, even with the science cover closed, would certainly have caused an acquisition signal. Since the probability was about 50% that the Sun was illuminating the thermal shield, this afforded the most likely explanation of the narrow angle acquisition that occurred.

On *Mariner IV*, the NAMG performed no function during the flight prior to the midcourse maneuver. The NAMG was operating correctly at the OSE prelaunch checkout, and presumably will perform its function at encounter.

XIX. SPACECRAFT OPERATIONAL SUPPORT EQUIPMENT

The basic goal of the spacecraft OSE was to provide a tool capable of verifying the design and flight readiness of the PTM and flight spacecraft. To accomplish this objective, the OSE was mechanized so that it was capable of exercising the spacecraft through all of its standard and backup modes of operation. The OSE had to be sufficiently flexible to adapt to nonstandard conditions, and had to be capable of supporting troubleshooting necessary to locate failures down to the provisioned spare level. To minimize troubleshooting time, the OSE was structured so that it could differentiate between OSE and spacecraft problems.

The OSE includes those elements (both electrical and mechanical) necessary to support subsystem, system, and launch readiness testing of the PTM and flight spacecraft. It is divided into three distinct categories: system test complex equipment, launch complex equipment, and mechanical support equipment.

The STC was designed to control, to stimulate, and to evaluate and support the testing of the spacecraft. The LCE was designed to support the spacecraft prelaunch operation and to verify the final flight readiness of the spacecraft, with particular emphasis on prelaunch readiness tests and on the countdown operation during the on-pad period when the spacecraft was mounted on the launch vehicle.

A. System Management Tools

To ensure the logical and controlled development of the needs and requirements of the OSE, several management tools were used to guide and gauge the growth of the OSE development from its conception through fabrication, delivery, modification, maintenance, and operation. The basic means used to control this effort were: (1) The *Mariner C* OSE Design Specification Book, (2) The *Mariner C* OSE Circuit Data Sheet, (3) The *Mariner C* Operational Support Equipment Design Preparation and Delivery Schedule, (4) The *Mariner C* OSE STC block diagram, (5) problem/failure reports, and (6) engineering change request design control.

The concept of using a system test complex for the evaluation of spacecraft was first used by JPL for the *Ranger* program. To match and complement the advancing spacecraft technology, the OSE was also forced to grow at a rapid rate. The task assigned to the OSE designers was that of generating equipment that could support a test and evaluation program with precision, flexibility, and reliability. To meet these requirements, several new control or management tools were brought into play for the first time.

The OSE Design Specification Book paralleled the Spacecraft Design Specification Book and was the basic accurate and most current description of the operational support equipment described in engineering language at the system level for all *Mariner* OSE. In application, this publication was used to establish the design of the OSE at system and subsystem levels, and to disseminate changes in the OSE as they occurred. The publication contained design criteria, design characteristics and restraints, and functional specifications. The OSE suppliers and supporting technical divisions were responsible for providing functional specifications covering their equipment. Included in this publication were documents covering layouts of the system test complex as it was used in the various test areas, interface definitions between subsystems, cable lists, and block diagrams of special test configurations that were available for evaluation of the various subsystems.

The circuit data sheets were the control documents that defined the circuits and their respective signals interfacing between two subsystems or routed via system-supplied cables and/or J-boxes. The computer data subsystem interface sheet covered three discrete groups of equipment. The first group consisted of the circuits that interface between individual subsystems within a typical system test complex (e.g., radio to command). The second group consisted of the circuits that interface with peripheral equipment (e.g., printers). The third group consisted of interfaces that involved the computer data system (e.g., science to computer). Although the computer data system was considered to be an advanced development for the *Mariner* program, it represented the largest single interface in the STC.

Each circuit data sheet contained a maximum of eight circuit descriptions diagramming (for each interface) the OSE subsystem end circuits; interconnecting features were included as necessary. Design of the OSE subsystems proceeded on the assumption that other subsystems and the overall system environment were as reflected in the circuit descriptions. Change in a particular interface end circuit or wiring was coordinated and established by

modifications of the circuit description. The completeness and stability of the circuit descriptions were useful quantitative indicators of design status.

A cabling block diagram was used as an aid in determining the physical interfaces between OSE subsystems, between the OSE subsystems and the spacecraft, and between the OSE subsystems and the auxiliary support equipment. This diagram was also extensively used in determining such things as cable-connector assignment, cable length, and the physical location of each subsystem in the STC. The block diagram illustrated the OSE STC area, which remained essentially constant for the whole test program, and indicated the spacecraft cabling configurations as they applied to the three main test areas (SAF, the environmental test laboratory, and the space-simulator facility) to which the spacecraft was transported for system and environmental testing.

The JPL Quality Assurance and Reliability Office established and monitored the quality of the OSE. Failure reporting on the OSE began with its delivery to SAF. Problem/failure reports were used to monitor and control the direction and type of fixes employed, and permitted the OSE integration engineer to keep abreast of the operation, and enabled him to spot potential trouble areas.

The design of the *Mariner* OSE was frozen on May 1, 1964, and the design was then brought under control of the engineering change request system. The need to make changes was usually a result of hardware reviews, prototype testing, interface incompatibility, or component failure.

Each engineering change request contained a functional description of the proposed change, and was sufficiently detailed that the performance, schedule, cost, and effective implications of the proposed change could be determined.

B. Facilities

During the test and evaluation program, the spacecraft was exposed to different environments that simulated launch and flight conditions. For the *Mariner* Mars 1964 program, three basic JPL and three AFETR environmental facilities were used.

1. JPL Facilities

a. Spacecraft assembly facility. The spacecraft and STC were first assembled and tested at SAF, where all hardware assembled into a spacecraft and/or an STC were brought together for the first time. The high bay area is maintained in a clean condition, with positive-pressure air conditioning and dust and humidity control. The facility includes a pit for conducting hazardous operations, a 10-ton bridge crane with a 35-ft hook height, and ample 400- and 60-cps power to support the testing of three spacecraft simultaneously.

b. Spacecraft environmental facilities. To verify that the PTM and flight spacecraft could operate satisfactorily after exposure to FA vibration levels (determined from those expected of the *Atlas D* and *Agena D* during the boost phase), the spacecraft was vibrated in the roll axis and in two lateral axes. Before and after each axis of vibration, a system verification test was performed using the STC. During vibration, the spacecraft performance was monitored via an RF telemetry link. Vibration testing was performed in the spacecraft environmental facilities using a vibration exciter with a 30,000-lb vector force rating, a granite oil table, and a horizontal test fixture for vibration in all three spacecraft axes. Other environmental laboratory equipment includes acoustic chambers, shock equipment, centrifuges, and climatic test facilities such as temperature, salt, fog, and explosive-atmosphere chambers.

c. Space-simulator facilities. There were two primary reasons for subjecting the spacecraft to the vacuum and thermal environments of the space simulator: (1) to establish the functional integrity of the spacecraft operating in a simulated space environment, and (2) to perform a final verification of the ability of the temperature control subsystem to maintain spacecraft temperatures within design limits. Because of the extended duration of the Mars flight, it was possible to test only certain portions of the flight sequence in real time; the less dynamic parts of the pseudo flight were fast-stepped.

The space-simulator facility houses a 25-ft diameter, 40-ft-high simulator chamber. This chamber uses liquid nitrogen cold walls as a heat sink and collimated mercury xenon arc lamps for solar radiation simulation. The chamber can be evacuated to approximately 10^{-6} mm Hg.

2. AFETR Facilities

Spacecraft test operations at Cape Kennedy were conducted in the spacecraft checkout facility (Hangar AO), in the explosive safe facility, and at the launch complex. These test areas were used to confirm that the spacecraft

survived shipment in operating condition; that all systems were functioning properly; that the spacecraft was compatible with the Test Range, the launch-vehicle, and the launch-complex equipment; and that the spacecraft was ready for commitment to launch.

a. Spacecraft checkout facility. Hangar AO is the principal JPL facility at Cape Kennedy. A complete system test complex was installed in this facility to provide a detailed checkout of the spacecraft before launch operations; some of this equipment was also used during launch operations. The operations center and communication center are also housed in this hangar.

b. Explosive safe facility. The explosion-proof facility, in which hazardous operations on the spacecraft were performed, is located in a remote area. Two buildings of framed, reinforced concrete pilasters and corrugated walls constitute the permanent installation. The sterilization and assembly laboratory has an air lock and three 5-ton explosive-proof bridge cranes with 35-ft hook height. The propellant laboratory has reinforced concrete walls and a 10-ton, 30-ft-hook-height traveling crane. Instrumentation facilities and offices are located in trailers. The ESF was used for final preparation of the spacecraft before it was transported to the launch complex; this preparation included installation of the pyrotechnic squib and midcourse motor and loading of the liquid propellant. Hazardous testing and adjustments were performed in this area just prior to launch operations.

c. Launch complex. During a spacecraft launch operation, certain monitoring and control equipment is installed in the launch complex. The LCE includes a control console in the blockhouse for controlling spacecraft power, a commutator, a central computer and sequencer, and the capability for hard-wire monitoring of power, gyros, and telemetry while the spacecraft is on the launch pad. The LCE also includes antennas installed on the umbilical tower.

The spacecraft monitor and control equipment is housed in a blockhouse console connected to the spacecraft by means of a long-line multiconductor cabling and an umbilical connector. Test personnel monitored and controlled the spacecraft during prelaunch operations from this area.

Spacecraft control equipment, such as power supplies and signal conditioning units, are located in the launch pad building and on the umbilical tower. This equipment was controlled from the blockhouse during launch operations. Parabolic antennas are located on both the service and umbilical towers to provide an RF link between the launch pad, Hangar AO, and the DSIF areas.

C. System Test Complex

The system test complex (Fig. 318) consists of about 45 racks of operational support equipment capable of evaluating and troubleshooting the spacecraft on both the subsystem and system levels.

The STC is composed of several groups of OSE. The first group is the direct counterpart of the spacecraft flight subsystem, and contains such units as the radio, command, power, CC&S, data encoder, attitude control, pyrotechnics, tape recorder, and science subsystems. The function of the STC equipment is to: (1) differentiate between spacecraft and OSE failures; (2) exercise and/or stimulate the OSE subsystems to simulate flight-type operation; (3) monitor and evaluate the OSE subsystems during subsystem and system tests; (4) provide self power for subsystem test and evaluation; and (5) provide the necessary input, stimulus, and output loading required for spacecraft subsystem test and troubleshooting.

The second group of OSE in the STC completes the command and telemetry group. Two prime OSE subsystems perform this operation: the ground command subsystem, which sends commands to the spacecraft; and the ground telemetry subsystem, which demodulates, decommutates, distributes, and prints out the telemetry data.

The third group consists of support items: the central recorder, the central timing system, the power distribution system, the telemetry processing system, and the telemetry TTY encoder.

The fourth group, the computer data system, consists of a medium-sized general purpose computer and a data input system.

In addition to the equipment enumerated above, there was also some ancillary equipment, which included system cabling, special adapter cables, isolation devices, J-boxes, stimulus boxes, break-in and break-out boxes, and the spacecraft simulator.

The STC was laid out in a rectangular pattern, with the subsystem test consoles forming the periphery. To facilitate the handling of both intersubsystem and spacecraft cables, the whole complex was staged on a raised floor. The spacecraft was mounted on a universal-ring

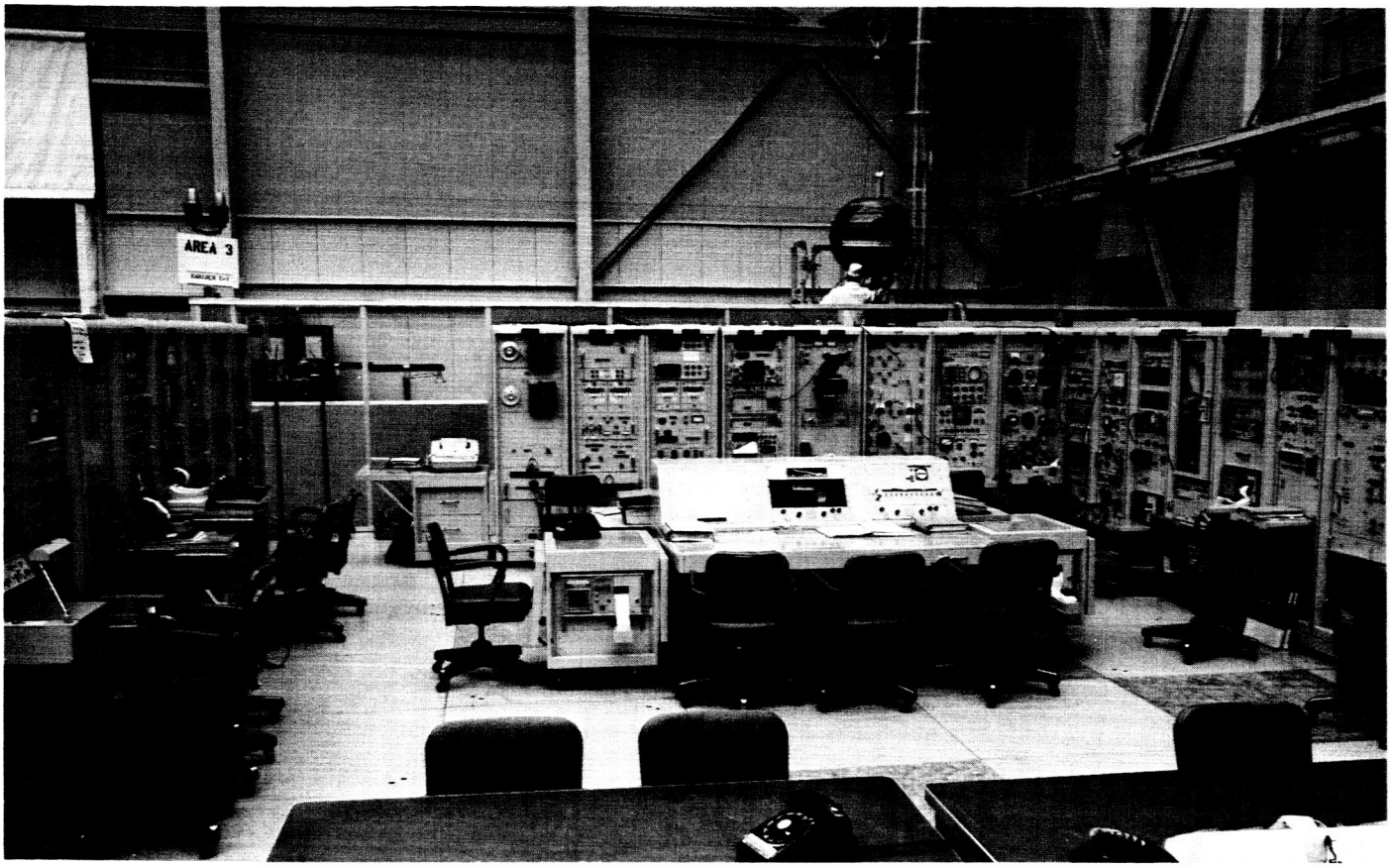


Fig. 318. System test complex

holding fixture for structural rigidity, which, in turn, was secured to a positioning fixture required for assembly and articulation during testing.

1. Basic Capabilities

a. Power. Each OSE subsystem has the capability of providing power to its corresponding spacecraft subsystem when basic spacecraft power is not available and for troubleshooting and evaluation purposes. The OSE subsystem provides this independent power operation by means of special cables plugged directly into the appropriate spacecraft subsystem in lieu of the ring harness. The input power has the same characteristics as that normally supplied to the spacecraft subsystem from the spacecraft power supply.

b. Power monitoring. Each OSE subsystem is capable of monitoring its transformer–rectifier outputs. The selection of the outputs is monitored to provide maximum information on spacecraft subsystem performance. Monitoring of the transformer–rectifier is accomplished by the use of meters having an accuracy of 2% or better, full scale. Facilities, such as oscilloscopes and recorders, are also provided on front panels of the OSE for additional monitoring.

c. Subsystem interface simulation. Each OSE subsystem has the capability of independently simulating the output loading and the inputs, which the spacecraft subsystem would experience during spacecraft operation, so that the spacecraft subsystem can be operated independently of the rest of the spacecraft and of the system test complex.

d. Running time. Each OSE subsystem records, on an elapsed-time meter, the running time of its respective spacecraft subassemblies. The instrumentation of this parameter is accomplished by monitoring an output of the individual transformer–rectifier unit. (The measurement is independent of the operation of the OSE.)

e. Subsystem monitoring. Each OSE subsystem is mechanized so that all commands, controls, and/or stimuli that are applied to the spacecraft are brought out on connectors and the back of the OSE for monitoring by the computer data system.

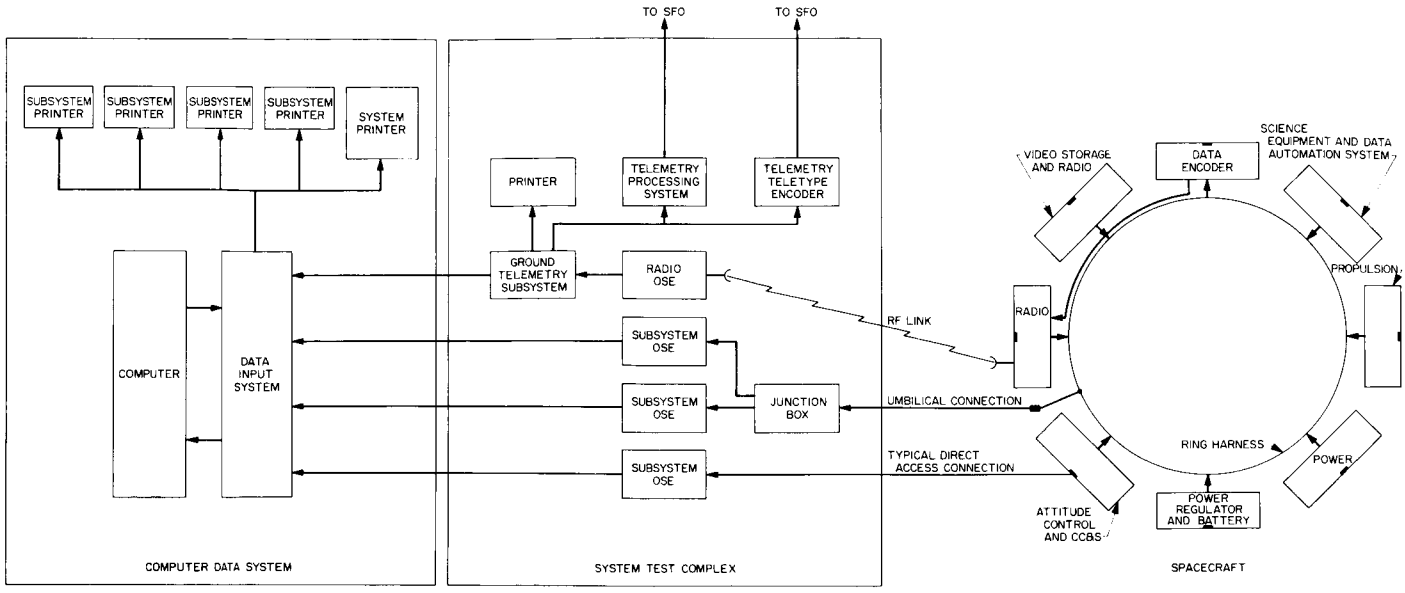


Fig. 319. System test complex configuration at SAF

f. Self-check capability. Each OSE subsystem is mechanized to have either an automatic or a manual self-check mode. Redundant checks, such as push-to-check lights, are used in some areas.

2. Functional Description

The system test complex is used in essentially the same configuration at both SAF and at the spacecraft checkout facility (Hangar AO). Figure 319 is a block diagram of the configuration at SAF. The STC makes contact with the spacecraft in three ways: (1) through the separation and the umbilical connectors, which provide an interface with the entire spacecraft system, (2) through the RF link, and (3) through direct access connections to the individual subsystems of the spacecraft.

System measurements are made through the umbilical connection. The signals are brought out to the J-box where they are separated and fed to the appropriate OSE subsystem. Direct access connections to the individual spacecraft subsystems provide for direct measurements of the subsystems as individual pieces of equipment. Connections are made directly to the appropriate OSE subsystems in the STC. The RF link between the spacecraft radio subsystem and the radio OSE provides a method for measuring spacecraft telemetry parameters. The RF connection can be either a hard-line connection or an actual RF link.

In addition to monitoring such performance parameters as voltages, currents, and waveforms, the individual OSE subsystems provide stimuli to the spacecraft and measure the response of the spacecraft to the stimuli. One of the unique features of the *Mariner* STC is the use of a Univac 1218 computer for processing the test data. As illustrated in Fig. 319, the computer data system is isolated from the spacecraft so that it does not affect the circuits between the spacecraft and the STC. The use of the computer data system provides three basic advantages:

1. The computer prints out the data in readily usable engineering numerical values, whereas the STC data is printed in data numbers.

2. Limits can be set on the computer and, if the incoming signals exceed these limits, the computer sets up an alarm that alerts the equipment operators.

3. The computer operates in a data suppression mode in which repetitive data are not printed out. The only data that are printed represent a change.

The computer data subsystem consists of the computer, the data input subsystem, a system printer, and several subsystem printers. The signals received by the individual OSE subsystems are fed to the data input system, which converts them to a form acceptable to the computer. The output from the computer is also fed to the data input system, which then feeds the information to the system and subsystem printers for printout.

The spacecraft telemetry data are received by the radio OSE and are, in turn, fed to the GTS. The ground telemetry subsystem demodulates and decommutates the telemetry signal and provides digital and bit-synchronous information to the data input subsystem, the telemetry processing subsystem, the telemetry encoder, and a printer programmer. The telemetry processing subsystem and telemetry encoder provide inputs to the SFOF, where the data can also be processed and monitored. The GTS, telemetry processing subsystem, telemetry encoder, and printer programmer are equivalents of the equipment provided in the DSIF stations for receiving and processing actual spacecraft telemetry information during flight.

The system test complex was used at SAF during spacecraft assembly and system tests; portions of the STC were also used in the environmental testing areas to monitor the spacecraft during the environmental tests. The STC equipment was physically moved from SAF to the environmental area, as required for tests. The computer remained at SAF and was connected to the STC equipment by a long run cable. During vibration tests, the STC was connected to the spacecraft through the umbilical connector (the connection was broken during the actual vibration periods). In the space simulator, the STC was connected to the spacecraft by the umbilical connector and by a limited number of direct access connections.

3. Electrical Characteristics

All elements of the OSE operate from a 105/125-v, 60-cps, single-phase, three-wire power source and/or from 120/208-v, 400-cps, three-phase, four-wire power sources.

Each rack or group of racks has appropriate overload protective devices. The ac power distribution lines are protected from noise and from the transient effects of power switching normally performed by subsystem OSE. This protection takes the form of isolation introduced at the power input terminals of each subsystem, and is accomplished by the use of a triple- or quadruple-shield isolation transformer.

Electrical connections from the OSE to the spacecraft do not influence the operation of the spacecraft because all circuits in the OSE, which interface with the spacecraft, have circuit returns that are isolated from the OSE chassis ground.

4. Calibration Program

As a result of the need to keep the OSE measurement indications correct, a total of more than 500 calibrations were accomplished on the *Mariner* OSE from December 1963 to October 1964. As instruments were added to the calibration program, they were established in a recall system at suitable intervals. This schedule continued, with minor modifications, through final tests at JPL prior to shipment of the OSE to Cape Kennedy where one final calibration was made prior to prelaunch checkout (to ensure that out-of-calibration conditions did not result from direct or peripheral effects of the cross-country transportation).

To provide as much assurance as possible of accurate and comparable calibrations at JPL and at Cape Kennedy, it was recommended that common documents be used as calibration procedures by each vendor. Accordingly, abbreviated calibration procedures were developed. These documents were used for final calibrations at JPL, and for the subsequent calibrations at Cape Kennedy.

The AFETR calibration was performed as a concentrated program in a mobile laboratory at the JPL site in early September 1964, and was supplemented by a special amplifier calibration in mid-October.

The effectiveness of the program was evidenced by the fact that when the instruments were submitted for successive recalibrations, there was a progressive increase in the number that were found to be still within tolerance. All of the equipment was calibrated to a known base line (traceable to the National Bureau of Standards) and was thoroughly compatible in calibration to equipment of other commercial and government installations.

5. Radio Subsystem OSE

The radio subsystem OSE (Fig. 320) was used to test the complete radio subsystem, from the initial subsystem preacceptance tests through the ETL, SAF, and Cape Kennedy tests. Figure 321 is a functional block diagram of the radio subsystem OSE.

The radio subsystem OSE is the basic tool for evaluating the spacecraft receiver performance, the spacecraft command capability over the RF link, and the S-band phase-locked-loop receiver at 2298 Mc. It also furnishes a means of demodulating the spacecraft telemetry signal from the RF carrier for the recovery of data by the ground telemetry subsystem. In addition, the RF OSE is

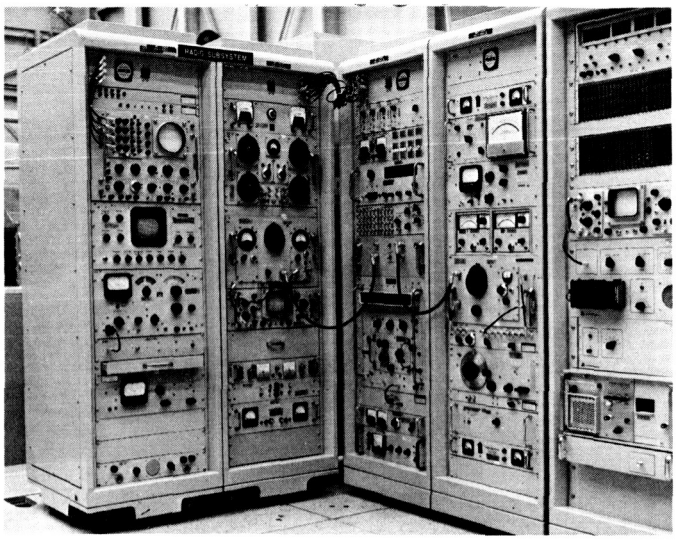


Fig. 320. Radio subsystem OSE

the access source to the spacecraft radio subsystem test points for measuring, monitoring, and recording spacecraft RF power and frequencies, for spacecraft receiver and transmitter functions, for spacecraft TR and dc-to-dc converter voltages and currents, and for monitoring the operating mode of the radio subsystem and its reaction to spacecraft and OSE-simulated commands. The OSE is also mechanized to support the turn-around ranging system.

The radio subsystem OSE represents a significant departure from the L-band radio OSE used on *Ranger* and *Mariner* Venus 1962 spacecraft. It is more compact, using four tall (6-ft) racks rather than the eight short racks used in the L-band OSE. The S-band OSE uses a greater quantity of solid-state components and has several switching panels that reduce external cabling and provide greater speed and ease of monitoring and recording spacecraft OSE functions. The radio S-band OSE proved to be extremely reliable in supporting the testing and evaluation of the spacecraft's radio subsystem.

6. Flight Command Subsystem OSE

The flight command OSE test console is designed to test the spacecraft flight command subsystem in all possible modes of operation. All tests necessary to determine the functional integrity of the spacecraft flight command subsystem can be performed by the OSE. The test console can generate any command word, modulate the word into the *Mariner* Mars phase shift keyer format, check the flight for proper response, and print the results. All tests on the spacecraft flight command subsystem can be performed either automatically or manually. The flight unit digital response is measured both quantitatively and qualitatively.

The test console is divided into the operational support equipment test console and the data logger console. The OSE test console is designed to perform all tests that can be made when the flight command subsystem is at SAF. The data logger console connects to the OSE test console and allows the performance of laboratory-type tests. A functional block diagram of the flight command OSE is shown in Fig. 322.

a. SAF test. The primary purpose of the OSE test console in SAF testing was to monitor (and simulate if desired) the spacecraft flight command subsystem for proper operation while it was in the spacecraft. The OSE test console connected through a 120-ft cable to the test points in the airborne unit, and could operate in one of the three following modes (Mode 2 being the normal mode).

Mode 1. The OSE test console generates the command words, modulates the bits, generates synchronization and sends this signal to the RF OSE for transmission to the spacecraft. The OSE test console then monitors the airborne flight command subsystem and records any errors.

Mode 2. The OSE test console only monitors the test points. The commands are generated by the ground command system. The GCS is identical to the units located at all DSIF stations that are used to send commands to the spacecraft.

Mode 3. The OSE test console receives the command words from the GCS and compares them to the proper response from the spacecraft flight command subsystem.

b. Bench test. The bench test of the spacecraft flight command subsystem checks out the system in its entirety. A bench test chassis allows the operator to put the flight unit in any type of environmental chamber and conduct complete tests.

Two types of tests can be performed on the airborne subsystem when bench testing: (1) a test of the command decoder, and (2) a test of the command detector. Special tests that can be performed in the bench test are: (1) detector correlation, (2) detector bandwidth, (3) word start error, and (4) bit error.

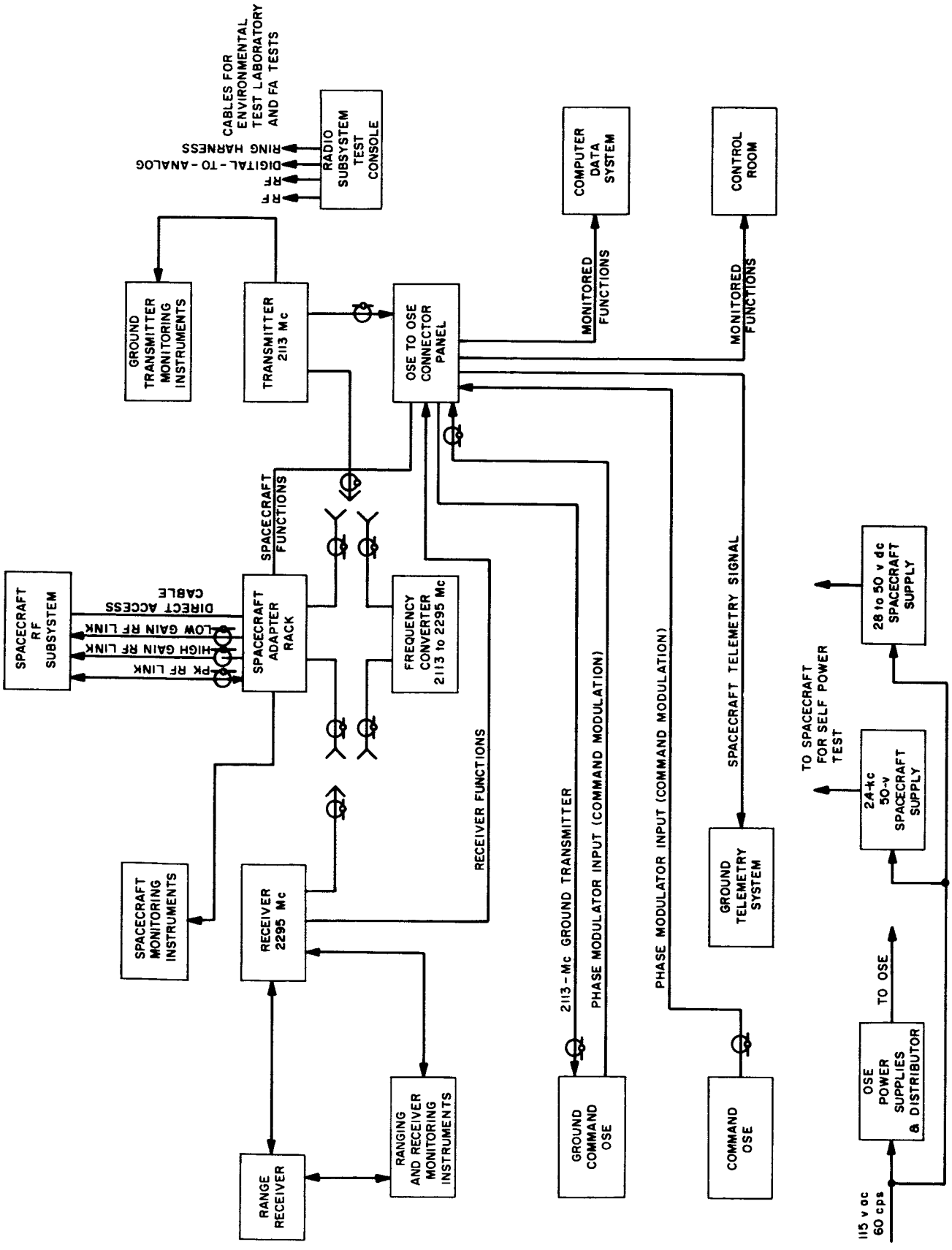


Fig. 321. Radio subsystem OSE functional block diagram

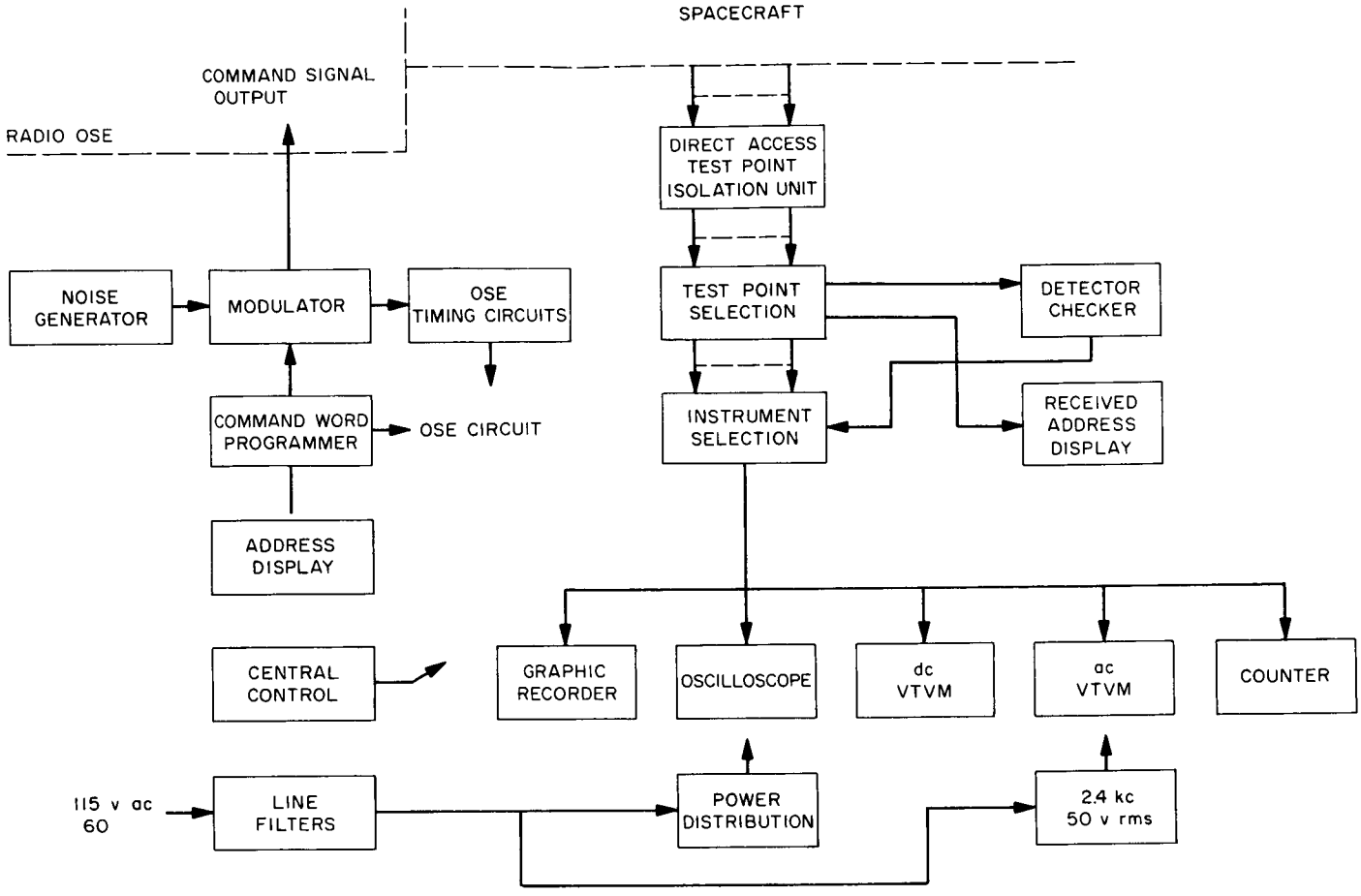


Fig. 322. Flight command subsystem OSE functional block diagram

c. Functional element test. The functional elements of the spacecraft flight command subsystem are the command detector, the command decoder, and the transformer–rectifier unit. The command decoder and command detector are checked in the same manner as in the procedure for bench testing, but with only the proper outputs monitored (and the others ignored). The transformer–rectifier unit is tested by loading it with either maximum or minimum loads and observing the power-in, power-out, regulation, and ripple displayed on the oscilloscope. The power-in and power-out can be measured on any of the functional subassemblies.

d. Data logging test. The data logger automatically selects one of the output lines on the spacecraft flight command subassembly and measures the pulses on this line for rise time, crest time, fall time, saturation voltage, and leakage. This test is accomplished in conjunction with a digital voltmeter and a 10-Mc time interval meter. The data logger selects the correct input line by monitoring the transmitted word generated in the OSE test console. After recognition of the address line, the data logger operates completely asynchronously from the other units of the test console.

e. Life test. The configuration of the life test is the same as that for bench testing. During the life test, a series of measurements is made on the flight equipment. One of the modes for these measurements is the "data logging" mode, which exercises each isolated switch at least three times and measures its five parameters. The remainder of the measurements exercise such modes as (1) detector out-of-lock/decoder inhibited; (2) detector in-lock/decoder inhibited; (3) standby (commands issued); and (4) VCO input grounded.

f. Conclusion. The flight command subsystem OSE provides a manual or automatic test program for testing the spacecraft command subsystem. It interfaces with the ground telemetry system and with the ground command

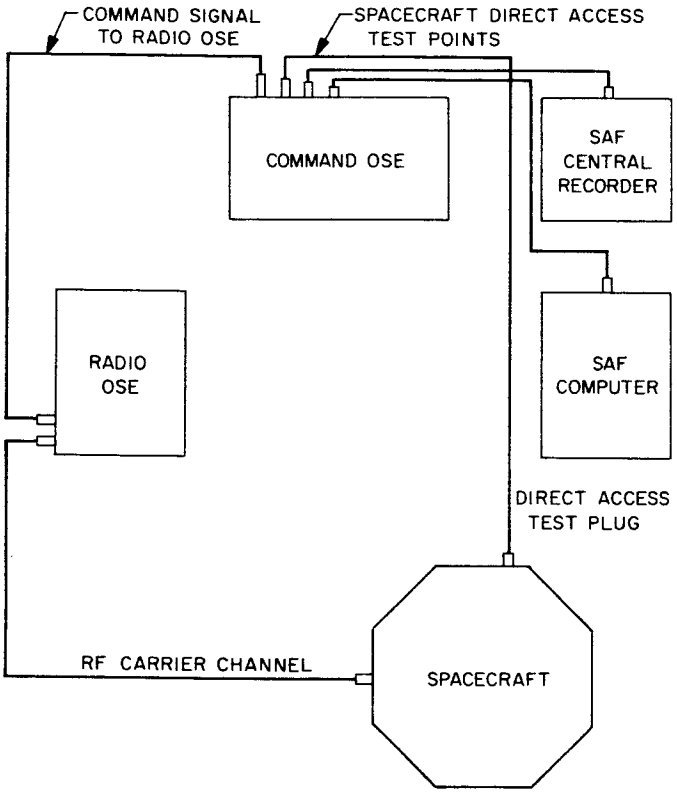


Fig. 323. Flight command subsystem OSE interfaces during spacecraft testing

subsystem (Fig. 323). The OSE generates all signals and programmable commands required by the airborne subsystem (or its individual assemblies) to receive, decode, and continuously monitor outputs from the flight command subsystem. In addition, it can be used (at SAF) to send commands to the spacecraft.

7. Ground Command Subsystem OSE

The primary function of the GCS is to biphase-modulate a command word that is encoded and then transmitted via the RF link to the spacecraft. The command word in the *Mariner* Mars 1964 program is a 26-bit binary word, which may fall into one of two general categories: the direct command or the quantitative command. There are 29 DC commands and one three-part QC command. Each DC command instructs the spacecraft to perform a specific function. The QC command is used for midcourse correction only, and programs the spacecraft to roll, pitch, or burn the thrust motor command. In addition to programming the function to be performed, the QC command supplies information pertaining to the length of time the command is to remain operative.

The intermediate link between ground command and flight command is the radio subsystem. The ground radio subsystem, located at the DSIF stations, phase-modulates the S-band carrier with the information received from the ground command subsystem.

The GCS sends a command to the spacecraft radio subsystem through the radio subsystem OSE. The return signal from the spacecraft is received by the radio subsystem OSE and fed to the GCS. During an operation, the GCS continually monitors the spacecraft-transmitted signal for command synchronization and for data bits during transmission. The GCS receives the spacecraft-transmitted signal from the radio subsystem OSE, detects it (with a detector similar to the flight detector), and compares the detected signal with the command signal that was originally sent to the spacecraft. If any discrepancy is noted between the two signals, the GCS inhibits the transmission of the command information to the radio subsystem OSE transmitter. This loss of modulation causes the spacecraft flight command subsystem to lose lock, which, in turn, inhibits the processing of the command at the spacecraft.

a. Modes of operation. The ground command subsystem operates in three modes. In one of the modes, the GCS sends a command word to the spacecraft. In another, it operates in a verify mode, in which it is able to simulate transmission of a word. During this mode of operation, the subsystem performs exactly the same functions as it does during transmission, except that the word is not sent to the radio subsystem. The GCS performs a complete self-check of all of its functions when operating in the verify mode. In the third mode of operation, the GCS checks the paper tape (received over TTY lines) that contains the command word.

During a typical operation, the QC command is sent from SFOF over TTY lines to the DSIF station, and the information is then relayed to the spacecraft. In order to detect errors prior to transmission, the same command word is sent over the TTY lines three times. The GCS checks the word, verifies the word format, checks each of the three words against each other, and punches the command word on paper tape. If the word is valid, it is then processed by the GCS, which goes through a verify cycle to check its own operation before finally transmitting the word to the spacecraft.

b. System description. The GCS consists of three separate subsystems: the control and verify subsystem, the modulator subsystem, and the detector subsystem. When

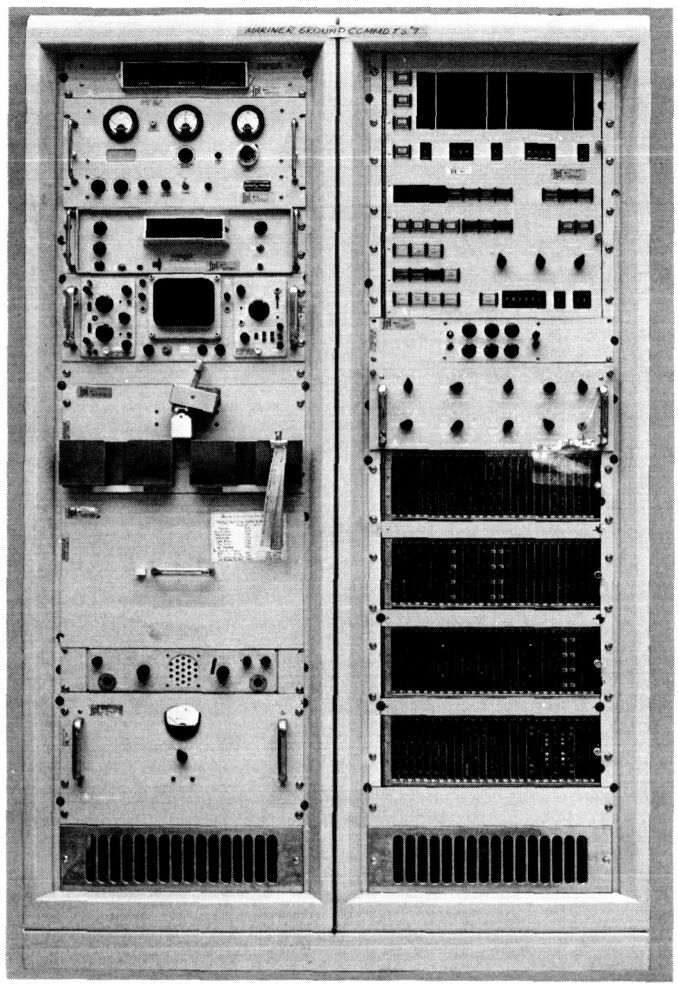


Fig. 324. Ground command subsystem OSE

integrated, they form a complete system (Fig. 324) that continually tests for errors during operation.

Control and verify subsystem. The control and verify subsystem uses a solid-state negative true logic system, the major function of which is to sequence and verify the various system operations. All system functions are sequenced by the program control counter, which consists of an eight-position shift register that is enabled by any one of eight separate AND gates. The position of the bit in the shift register determines the operation to be performed. As soon as the system completes an operation, the bit is clocked to the next position in the shift register by enabling the proper AND gate. This operation is repeated until the GCS has completed its cycle, which takes approximately 56 sec.

To ensure reliability, the GCS employs error detection circuitry to verify many of its functions. It also has the capability of ensuring proper operation of its error detection circuitry. Any one of six error detection circuits may be checked by selecting the desired circuit on the GCS console and reading a predetermined program tape. Several of the important checks performed are: verifying that operations are sequenced in the prescribed manner; ensuring that the GCS modulator and detector are in synchronization; and making a bit-for-bit check of the information sent to the spacecraft during transmission.

During normal operation, the signal sent to the radio subsystem is inhibited if an error is detected; however, in case of an emergency, the system is capable of being operated by manually overriding the error circuitry, or by using the emergency mode. When in the emergency mode, no checks are performed and the word is transmitted by circuitry not used during normal operation.

Modulator subsystem. The purpose of the GCS modulator subsystem is to biphase-modulate the subcarrier with the 26-bit binary command word. This is accomplished by using a phase shift keyer that maintains a reference phase of a coherent sine wave for a binary *zero*, but which shifts its phase by 180 deg for a binary *one*. The modulator consists of four units: the phase shift keyer, the PN generator, a binary counter that produces a frequency defined as $2\ f_s$, and a modulo-two adder.

In order to use phase shift keying techniques, it is necessary to establish phase coherence or synchronization between the modulator and the detector. Synchronization is established by using two PN generators, one at the GCS modulator, and the other at the spacecraft flight command detector. When the two PN generators emanate the exact code permutation, they are in phase with respect to each other and phase coherence is established. At that point, the spacecraft PN generator is in lock with the GCS PN generator and is capable of following the ground PN generator within a predetermined frequency and phase deviation. To achieve lock between ground and the spacecraft within a reasonable length of time, it is necessary to offset the clock frequency of the ground command PN generator, with respect to the spacecraft PN generator, by a relatively small amount.

The ground command PN generator consists of a shift register that uses modulo-two feedback to create a pseudonoise code that repeats itself once every second. The PN generator clock frequency $2\ f_s$ is derived from a variable oscillator and a binary counter, which acts as a divider. Initial lock acquisition is achieved by decreasing the oscillator frequency, and thereby decreasing the $2\ f_s$

frequency. Since 2 f_s is the clock for the PN generator, the 2 f_s offset causes the GCS PN generator to drift with respect to the spacecraft generator. The 2 f_s offset chosen is slow enough to allow lockup when correlation exists between the two PN generators, and, at the same time, to ensure that lockup occur within a 6-min interval. In the modulator, the PN code and 2 f_s are half-added to produce PN + 2 f_s, which is used by the spacecraft to establish synchronization. The data portion of the word is phase-modulated by forming a sine wave from a square wave.

The sine wave is then sent to the phase shift keyer, which is keyed by the word bit. With 0 v (binary *zero*) applied, the phase shift keyer maintains the phase of the input sine wave. With −6 v (binary *one*) applied, the phase shift keyer shifts the sine wave by 180 deg. The data and synchronizing portions of the word are then added to produce the output of the modulator.

Detection. The GCS detector is used to demodulate the command word sent by the radio subsystem, and to ensure that the information sent by the GCS is the same as that transmitted by the radio subsystem. The GCS detector also simulates the flight command detector, thereby providing a means of checking system operation before sending a word to the spacecraft. The detector uses an S-band phase-locked-loop receiver to demodulate the RF signal. After the RF carrier signal is detected, the submodulated portion of the signal is received by the GCS detection circuitry, which uses the same principles as the modulator: a phase shift keyer, a 2 f_s generator, a PN generator, and a modulo-two adder. The incoming signal passes through the phase shift keyer, a sine-wave shaper, and a bandpass filter, and a coherent sine wave is produced. Once established, this frequency is used as one of the voltage controls to the VCO, which provides the input to a divider that, in turn, produces 2 f_s (the clock frequency for the PN generator). After synchronization is established between the modulator and detector PN generators, the original command word may be reconstructed. The detector PN code and detector 2 f_s are half-added and put through an inverter to produce $\overline{PN' + 2f_s'}$, where prime denotes that the signal is derived from the detector. This signal is then linearly added to the modulator signal. Since the phase of the cosine wave is determined by the binary bit transmitted by the GCS, a comparison may readily be made between the GCS modulator output and the GCS detector output.

Displays. The time-of-day display in the upper left-hand corner of the console is internally wired to the control logic. By selecting the automatic operating mode, the GCS automatically sends a command word, which is initiated when the time of day is equal to the timed-start thumb-wheel setting. The displays on the left side of the console are the input and output signal strengths of the S-band receiver, a counter, which displays multiples of the f_s frequency, and an oscilloscope.

In the upper right-hand corner of the console, the 26-bit command is displayed in octal form. The word is displayed three times, and each display corresponds to the particular register that is used at different intervals during operation. The vehicle subcarrier displays indicate whether the telemetry data received from the spacecraft are good, questionable, or bad. It also indicates whether or not the spacecraft and GCS are in synchronization and displays the offset from the 2 f_s frequency. The remaining displays are self-evident, and relate to such functions as power turn-on, mode of operation, and word in process.

8. Power Subsystem OSE

The power subsystem OSE (Fig. 325) provides power monitoring and control to support the spacecraft power subsystem through test operations consisting of: initial power application, power subsystem evaluation, spacecraft system tests, environmental testing, and a final integrated system test (just before the unit was transported to the launch pad). A functional block diagram of the subsystem OSE is shown in Fig. 326. The power subsystem is mechanized to be remotely controlled from other elements of the OSE, such as the CC&S OSE.

The CC&S OSE is capable of preventing spacecraft power from being applied unless hold current and relay position interlocks are satisfied. Once spacecraft power is applied, these two interlocks may be removed to allow the issuance of CC&S commands without losing spacecraft power. If CC&S OSE power is lost, external power is turned off by the power subsystem OSE.

System test sets and an adapter rack were provided for use in laboratory and FA testing. The system test set simulates spacecraft voltages and loads monitored and controlled by the OSE. A transfer assembly, on command from the control panel, selects between the spacecraft and self-test assembly. The test set is capable of automatic self-test before or during any operation with the spacecraft or power subsystem. The maximum duration of this automatic sequence is 90 sec, and, on successful completion, it assures that the monitor, recording, and

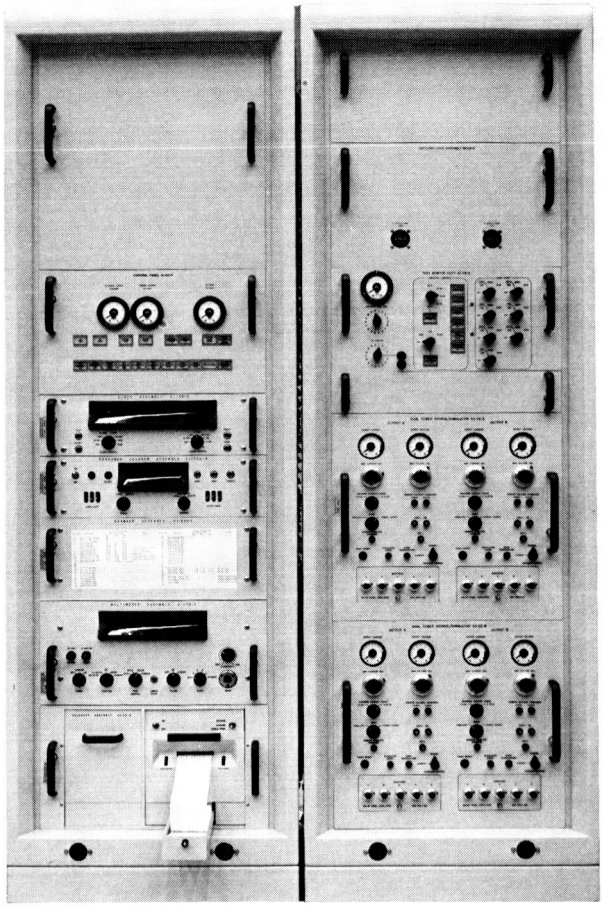


Fig. 325. Power subsystem OSE

power control functions of the OSE are operating within the required tolerances. Because all self-test simulation is self-contained, no external equipment is necessary to complete the self-test.

The power subsystem OSE incorporates all the elements of power, monitor, and control necessary to provide detailed subsystem analysis and records required to support the spacecraft power subsystem in the laboratory and system test areas. In addition, it provides simulation of interfaces that the flight equipment (when in the spacecraft) normally encounters with other spacecraft subsystems.

The power subsystem OSE design logically divides the equipment into two groups: one group consists of the monitoring and operator control area, and the other group consists of the various power supplies, simulators, and associated logic and switching networks. The major assemblies in each group are given in Table 64.

Table 64. Power subsystem OSE major assemblies

Category	Equipment
Group 1	Transfer assembly
	Control panel
	Self-test assembly
	Automatic data acquisition and recording subsystem
	Transformer–rectifier monitor assembly
Group 2	Test monitor assembly
	Switching logic assembly
	Auxiliary power supply assembly
	Dual power source/simulator

a. Transfer assembly. On command, the transfer assembly selects either the self-test assembly or the spacecraft functions. It is interlocked so that it cannot apply power to the spacecraft during an OSE self test. Also, if a self test is performed on the OSE during an operation with the spacecraft, power is not removed from the spacecraft. All external functions pass through the transfer assembly so that a logical selection between the self-test or operate modes can be made. The tolerance detector circuit cards are located in this assembly. These circuit cards make up a system of primary continuous monitors to detect malfunctions in the spacecraft power subsystem. The output of these detectors is a *fail* indication on the operator control panel. By separate control, the operator may elect to have the *fail* indication latch or not. During automatic self test, the detectors are required to respond to signals that are both in tolerance and are marginally out of tolerance. If, and only if, all test conditions are satisfied for all detectors, a single self-test *complete* indication is given.

b. Control panel. The control panel assembly provides the operator with controls to place the spacecraft power subsystem and/or OSE into the desired mode. All primary indications affecting the operation and state of the flight and power OSE are displayed. The operator may conduct an OSE self test, a test in conjunction with the spacecraft power subsystem, or both. Controls available to the operator include:

1. Spacecraft switching to external or internal power
2. Simulated solar panel power
3. OSE self-test (automatic upon initiation)
4. OSE operate (transfer to spacecraft)
5. Battery charger enable (allows automatic operation of the OSE charging circuits)
6. *Fail* indication latch set

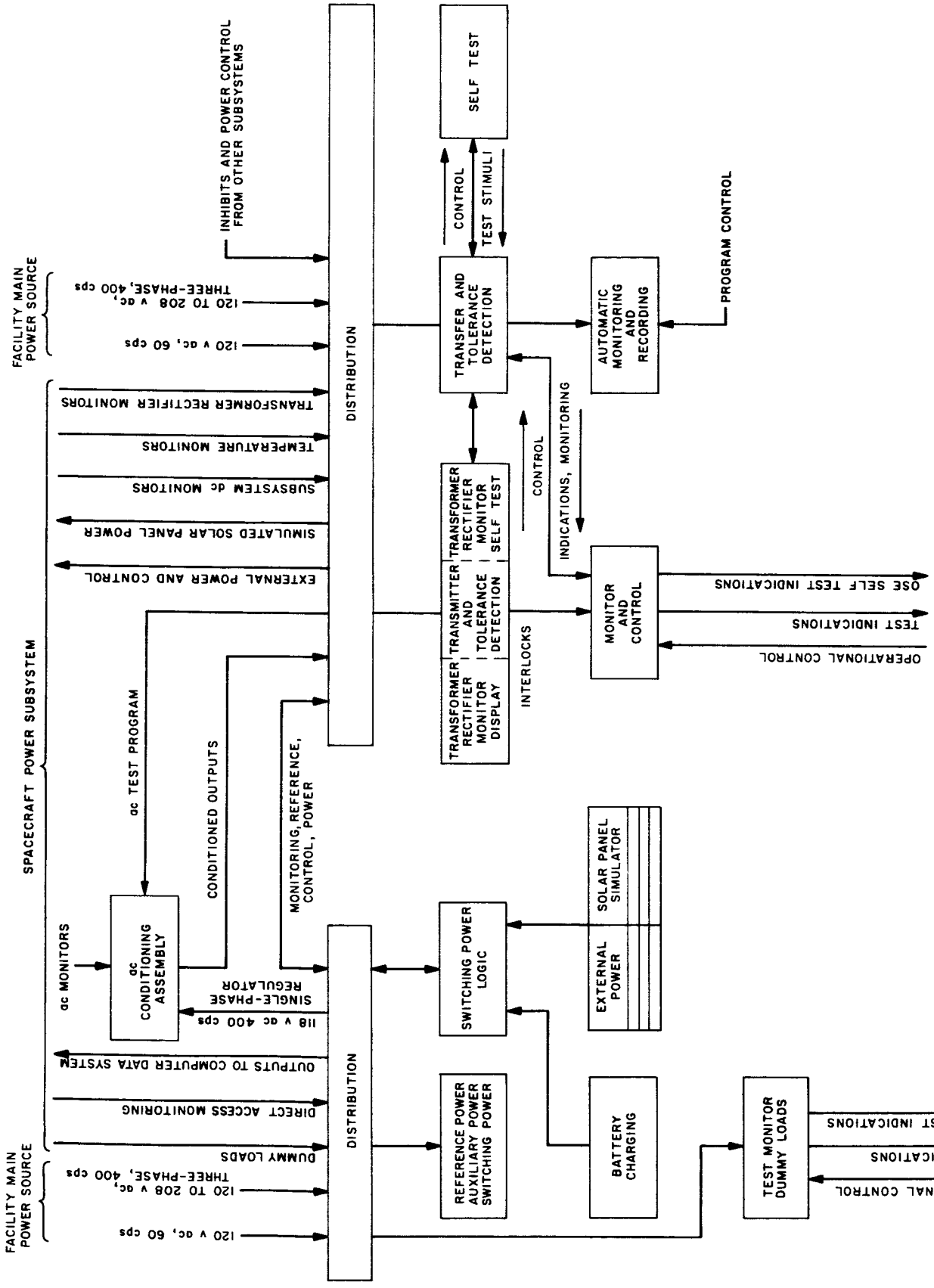


Fig. 326. Power subsystem OSE functional block diagram

7. Manual charge initiate

Monitoring displayed on the control panel includes:

1. Current supplied to the spacecraft from the OSE
2. Spacecraft primary system voltage
3. Spacecraft battery voltage
4. Positive indications for each of the controls listed above
5. An out-of-tolerance indication for the following primary monitors (either high or low)
   Battery voltage
   Battery temperature
   Booster regulator voltage (two units)
   Booster regulator temperature (two units)
   Inverter voltage 50 vac 2.4 kc (two units)
   Inverter voltage 28 vac 400 cps
   Inverter voltage A 26 vac 400 cps
   Inverter voltage B 26 vac 400 cps
   Inverter voltage C 26 vac 400 cps
6. An indication that the external power is above the upper tolerance limit (which also prevents switching to external power from either the *off* mode or the internal power mode)
7. An indication that a remote power control interlock is in effect, which prevents application of spacecraft power
8. Positive indications that OSE self-test is complete; that battery charging is required, and that battery charging from the OSE is taking place

c. Self-test assembly. The self-test assembly provides simulation for all spacecraft power functions monitored or controlled by the power OSE. Its test routine is commanded automatically from the control panel assembly upon transfer to OSE test. During automatic self test, all monitors and tolerance detectors are required to respond to marginal conditions.

d. Automatic digital monitoring and recording subsystem. Four assemblies make up the automatic digital monitoring and recording portion of the OSE. This subsystem is capable of fully automatic, semiautomatic, or manual operation at the discretion of the operator. The monitors are visually presented and permanently recorded on printed tape. Channels are available for 200 inputs, which may include ac, dc, and resistance measurements. It is automatically controlled in self test by the control panel to provide a printed record of the OSE during this mode. A clock assembly is included to provide timed automatic scans at prescribed intervals without an operator, for overnight use, or during extended life tests. Each time an automatic scanning cycle is initiated, the clock assembly records the time on the permanent record.

e. Transformer–rectifier monitor assembly. The TR monitor assembly is provided in the power OSE as a gathering point for data from power subsystems supplied by attitude control, CC&S, and space science experiments. These data inputs are filtered, where required, and distributed to the data monitoring subsystem for display and/or recording.

f. Test monitor assembly. The test monitor assembly is a special test assembly included in the OSE to provide direct access to all applicable spacecraft functions (whether simulated or real) for purposes of fault finding, analog recording, or manual testing. In addition, it houses dummy loads for the spacecraft power subsystem, and switching controls for simulating spacecraft commands that normally originate in the CC&S attitude control or command decoder subsystems.

g. Switching logic assembly. The switching logic assembly provides necessary control, logic, and protection for application of external power, solar panel simulated power, and battery charging.

h. Auxiliary power supply assembly. The auxiliary power supply assembly houses auxiliary, switching, and precision reference power supplies required by the spacecraft power subsystem and the OSE. All external functions leaving the OSE are short-circuit-protected so that a failure in the spacecraft or associated equipment does not destroy cabling.

i. Dual power-source/solar panel simulator. Two assemblies are used to provide four separate isolated outputs for simulated solar panel power. These units serve both as the simulators and as a constant-voltage power supply for external power and/or battery simulation. The main regulator is controlled from a voltage reference source or from a function generator, which provides the mode desired.

The power simulator developed for the *Mariner* Mars 1964 OSE met the requirements of a portable, maintainable field-test unit. It was designed to combine

requirements of both solar panel power simulation and external/internal power simulation into a single unit in order to eliminate redundant functions, simplify operation, reduce size and weight, improve reliability, and reduce costs for the same quality of construction, components, and power capability.

To adequately simulate the flight solar panel power configuration, it was required that four electrically isolated power sources be used. For this reason, each simulator contains two independent units. Two such assemblies are located in secondary power OSE to provide the required four simulated solar panel power inputs and (by changing modes) one external power source to the spacecraft power subsystem.

9. Central Computer and Sequencer OSE

Operational support equipment for the central computer and sequencer consists of five main assemblies:

1. Blockhouse assembly
2. Blockhouse power supply assembly
3. System assembly
4. System power supply assembly
5. Logic-panel assembly

These assemblies are used in three basic configurations: laboratory testing, system testing, and launch-mode testing. In the laboratory-testing configuration, the full capability of the OSE is used (all five assemblies), plus a signal conditioning assembly, and a preset counter and printer to fully monitor and exercise the CC&S through a complete simulated flight sequence. This configuration includes monitoring the CC&S outputs that normally interface with other portions of the spacecraft through a special set of systems cables. The normal OSE/CC&S interfaces are monitored through the umbilical cable and direct access cables. The direct access cables are connected from the OSE to the CC&S through the signal conditioning assembly. The CC&S OSE is illustrated in Fig. 327.

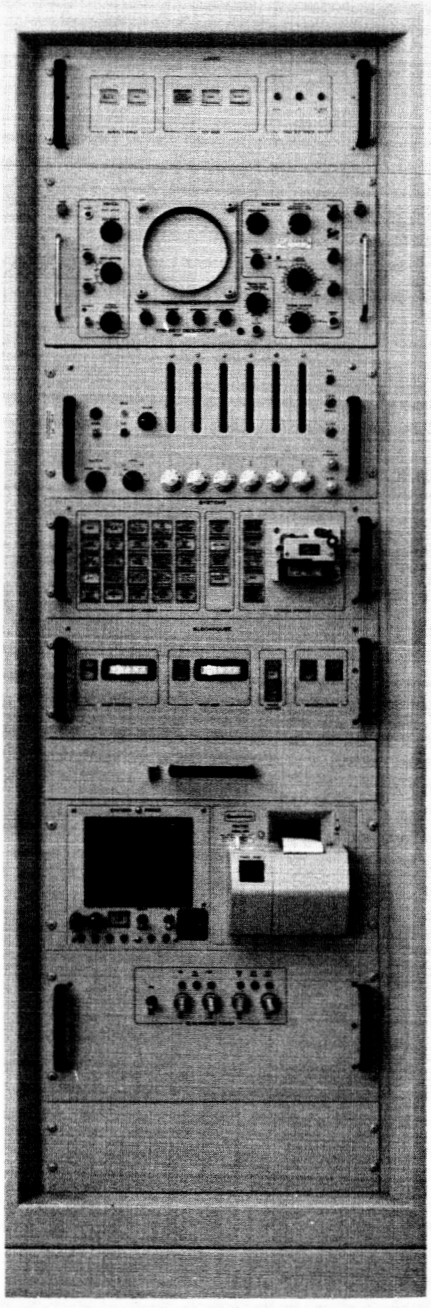


Fig. 327. Central computer and sequencer OSE

In the system testing configuration, the CC&S is installed in its normal position in the spacecraft and monitored by the OSE only through the signal conditioning assembly and umbilical cable. The system power supply assembly, which normally provides power to the CC&S, is not used in this mode because the CC&S is powered from the spacecraft power subsystem; the blockhouse assembly, blockhouse power supply assembly, system assembly, logic assembly, printer, and counter are used instead.

In the launch mode testing configuration, the CC&S is installed in the spacecraft and is ready for flight. The CC&S launch complex equipment monitors the CC&S

through the umbilical cable and uses only the blockhouse assembly, blockhouse power supply assembly and preset counter in this mode.

a. Blockhouse assembly. All preflight preparation and testing is accomplished using the blockhouse assembly. The blockhouse assembly performs or monitors the following functions:

1. Inhibit counters
2. Relay hold
3. Clear counters
4. Encounter update or master timer speedup
5. Encounter update or master timer speedup verify
6. Relay position indication
7. CC&S *clear* indication
8. CC&S OSE/power OSE interlock

b. Blockhouse power supply assembly. The blockhouse power supply assembly provides the following dc voltages to the blockhouse, system, logic-panel, and system power supply assemblies:

+28 vdc

−28 vdc

+31 vdc isolated for relay hold

−28 vdc isolated for relay hold

c. System assembly. The primary purpose of the system assembly is to operate and monitor the CC&S during system testing of the spacecraft. It forms an integral part of the laboratory-testing configuration, but is not used in the launch-mode configuration. The following functions are monitored or controlled in the system assembly:

1. Spacecraft commands
2. Launch and maneuver speedup
3. 1 pps internal check
4. Master timer speedup
5. Midcourse maneuver control
6. *Agena D* relay clamp

d. System power supply assembly. Input power to the CC&S is 2.4-kc 50-vac-rms square wave. In the absence of spacecraft power, input power is supplied by the OSE (during laboratory and subsystem testing only) and is controlled by a switch on the front panel of the system power supply assembly. This interface is monitored at all times, and, if the voltage increases by 10% above nominal or 15% below nominal for a period of 15 msec or greater, the interface is automatically open-circuited and a no-go signal issued.

e. Logic-panel assembly. The logic panel automatically sequences and monitors the CC&S through its entire flight sequence in the laboratory and subsystem configuration. Sequencing of the CC&S is accomplished by remotely controlling the manual functions found in the system and blockhouse assemblies. A coded printout cycle, initiated by this assembly whenever any CC&S output event occurs, gives CC&S time and event information. The monitoring and printout capability of the logic assembly may be used in a manual rather than an automatic mode. Monitoring of CC&S events that occur during a spacecraft systems test is performed in the manual mode.

f. Periphery equipment. Periphery equipment for the CC&S OSE consists of:

1. The CC&S simulator
2. The CC&S spacecraft substitution box
3. The computer data system J-box

CC&S simulator. The CC&S simulator (Fig. 328) is a portable test instrument capable of functionally qualifying the CC&S OSE. The design of the simulator was

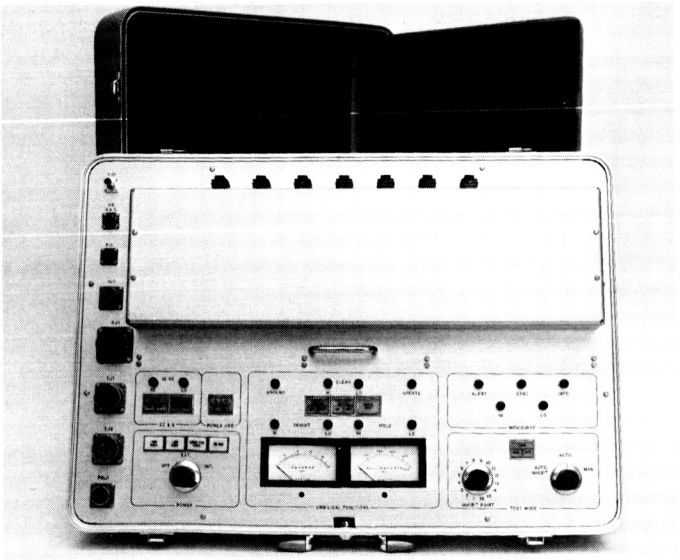


Fig. 328. CC&S simulator

accomplished to satisfy the need for a portable test instrument in three primary program test areas: OSE fabrication; spacecraft test operations; at Cape Kennedy. In OSE fabrication, the simulator was used to assist in qualifying every OSE interface at either the connector inputs to the OSE or at the spacecraft end points of all OSE cabling. In addition, the simulator was used to automatically cycle the OSE on a continuous basis thus allowing an adequate number of operational hours to be accumulated by the OSE before being used with an actual CC&S. In spacecraft test operations, the simulator was used to verify the operational readiness of the OSE before its participation in any test operation. At Cape Kennedy before launch-complex spacecraft test operations, the simulator was used to qualify all CC&S umbilical signal lines.

The CC&S simulator is packaged in an all-weather aluminum industrial carrying case and weighs approximately 37 lb. All connectors, controls, and meters are located internally for maximum protection.

CC&S spacecraft substitution box. The CC&S spacecraft substitution box (Fig. 329) was designed to replace the CC&S for initial cabling checks on a new system test complex.

The substitution box is also used in place of the CC&S to vary the 38.4-kc signal, as desired, either above or below nominal during special spacecraft tests. In addition, it can be used if the CC&S is not available for some reason, or if troubleshooting is being performed on some other subsystem in the spacecraft. The box derives its power from the CC&S OSE cabling, and the only auxiliary equipment needed is a counter to calibrate the 38.4-kc power synchronization.

Computer data subsystem J-box. The computer data subsystem J-box was designed to provide buffering between the subsystem and certain CC&S OSE interfaces.

The computer data subsystem monitors the state of all CC&S relays and the following functions at all times during a system test: relay hold, inhibit counters, CC&S 1 pps, CC&S transformer–rectifier voltages, RF load, parity check, clear counters, encounter update and verify, and relay position indicator.

The J-box is powered from the CC&S OSE and requires no auxiliary equipment. Its use in a system test

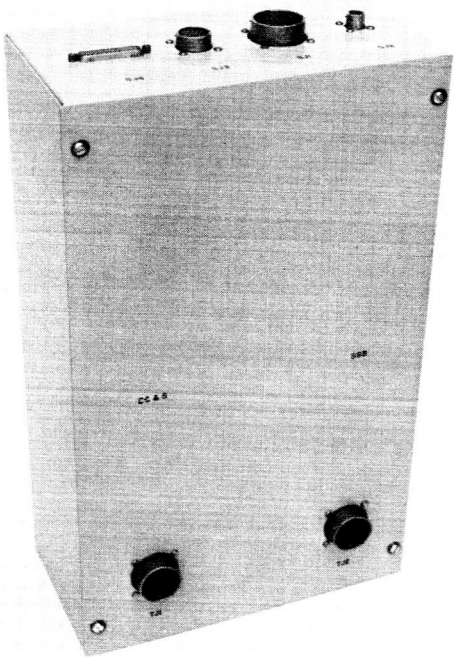


Fig. 329. CC&S spacecraft substitution box

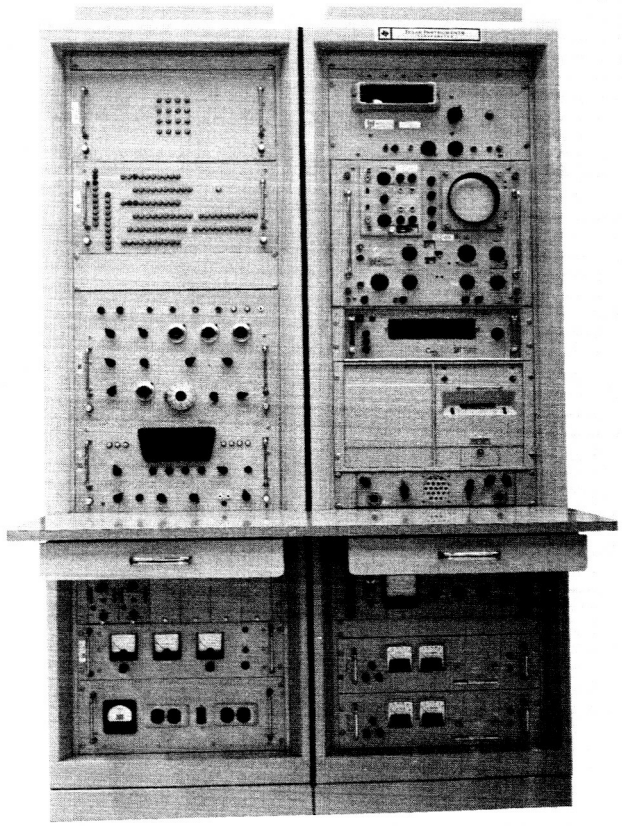


Fig. 330. Data encoder OSE

is entirely optional, and it is never used in conjunction with launch-complex equipment.

10. Data Encoder Subsystem OSE

The *Mariner* Mars 1964 data encoder subsystem OSE (Fig. 330) is a 100-channel time-multiplexed PCM encoder. Commutated analog data are digitized and serially mixed with synchronization information to form a composite telemetry signal output that modulates the spacecraft transmitter. The data encoder OSE was designed to provide two separate, but related, capabilities. The first capability is performing complete tests and calibrations on the data encoder at the subsystem level. The second capability is to monitor and perform, in conjunction with the STC, all possible data encoder operations consistent with complete spacecraft testing. The data encoder OSE is housed in a standard two-bay 6-ft rack.

a. Subsystem test operation. A data encoder subsystem test essentially consists of verifying proper commutator operation and accurate processing of all telemetry inputs, exercising all mode command interfaces, and confirming correct composite telemetry signal output. To accomplish this, the STC mechanization (Fig. 331) includes a commutator, analog telemetry input simulator, a command simulator, a composite signal demodulator, and various data display devices.

The commutator consists of a series of counters that sequence in the same manner as the spacecraft encoder's commutator. It is synchronized to the spacecraft encoder by the commutator deck synchronization signals received from the spacecraft encoder clock that drives both units. Once synchronized, the OSE commutator free-runs, and comparison of OSE and spacecraft encoder synchronization times determines the spacecraft

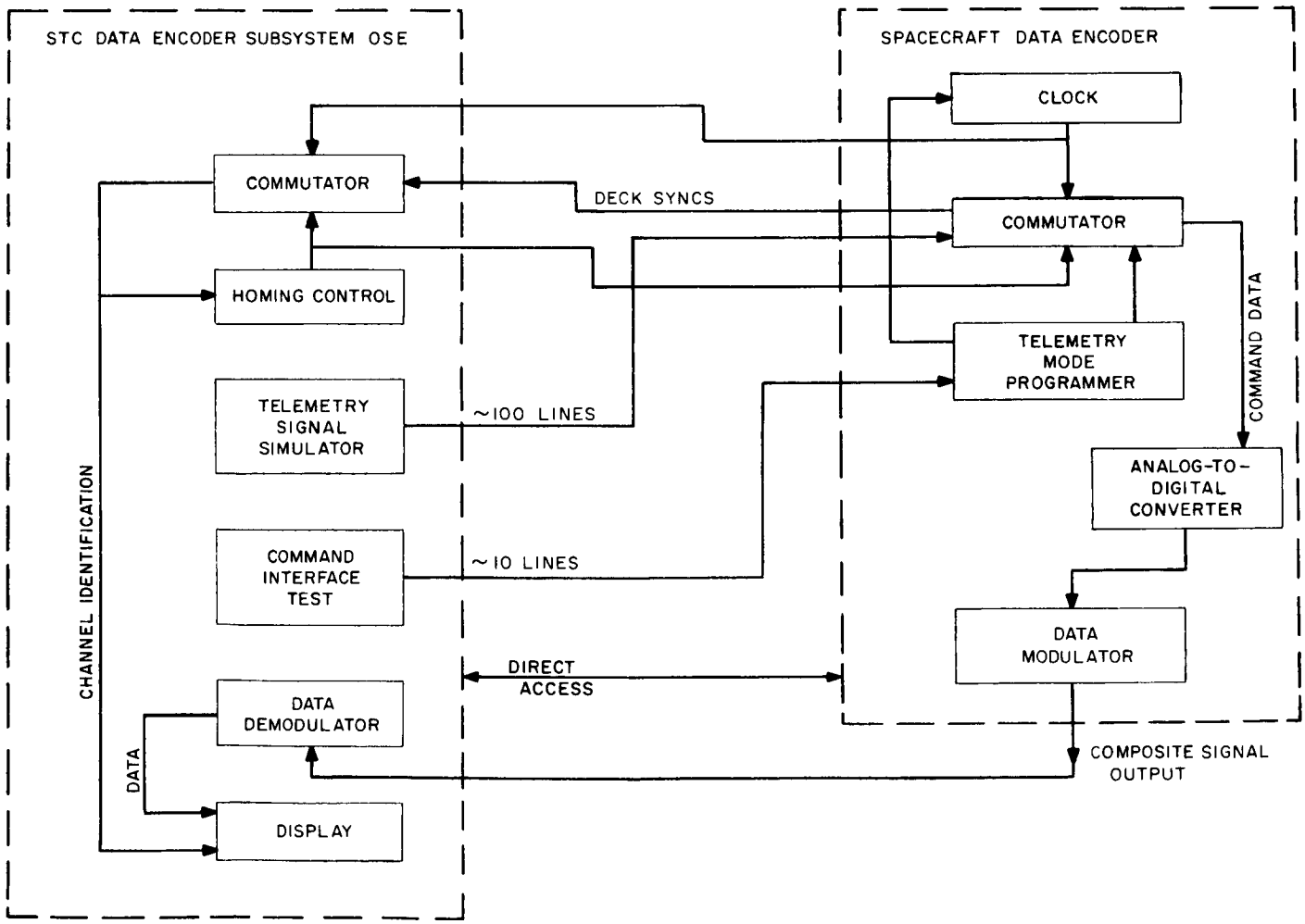


Fig. 331. Data encoder OSE functional block diagram

encoder commutator performance. The analog signal source provides precision inputs to all the spacecraft telemetry input lines of the spacecraft encoder. These inputs (resistor, voltage, and digital) allow proper check-out and calibration of the encoder's signal processing and analog-to-digital conversion. The command simulator exercises all the spacecraft command mode inputs to the encoder, such as Data Modes 1, 2, 3, 4, and bit rate change. Evaluation of the encoder's performance is based on the output data encoded and printed by the composite signal demodulator and display devices.

In addition, the equipment has homing capability, which reduces the test time considerably. In the homing mode, an OSE clock is substituted for the encoder clock, operating both commutators at high speed. When the desired channel is reached, the clock and commutators stop and that channel is interrogated continuously.

b. System test operation. When the data encoder is assembled in the spacecraft, the STC, as part of the spacecraft system test complex, monitors the encoder's performance. In this configuration, the STC operates in much the same manner as in subsystem tests. Deck synchronization and composite signal outputs are received from the encoder, and homing capability is preserved via the spacecraft's umbilical connector. The telemetry signal and command simulators are not used since these inputs are replaced by actual spacecraft functions. However, command capability is still maintained by means of the direct-access functions. As the name implies, the direct-access functions are cabled directly between the OSE and the encoder, without being channeled through any intervening test complex or spacecraft cabling. In addition, the STC contains several isolated buffers to send encoder status functions and signals to other units in the test complex.

c. Performance evaluation. The data encoder OSE operated effectively throughout the *Mariner* Mars 1964 test program. The only significant problem observed was the unusual susceptibility to noise of the OSE/spacecraft interface circuits, especially in the long lines used in the launch configuration. It is recommended that on future programs such noise-immune circuits as low-impedance integrating decision circuits be used on these interfaces, both in the encoder and in the OSE.

11. Attitude Control Subsystem OSE

The attitude control subsystem OSE consists of the system test set and the launch-complex set.

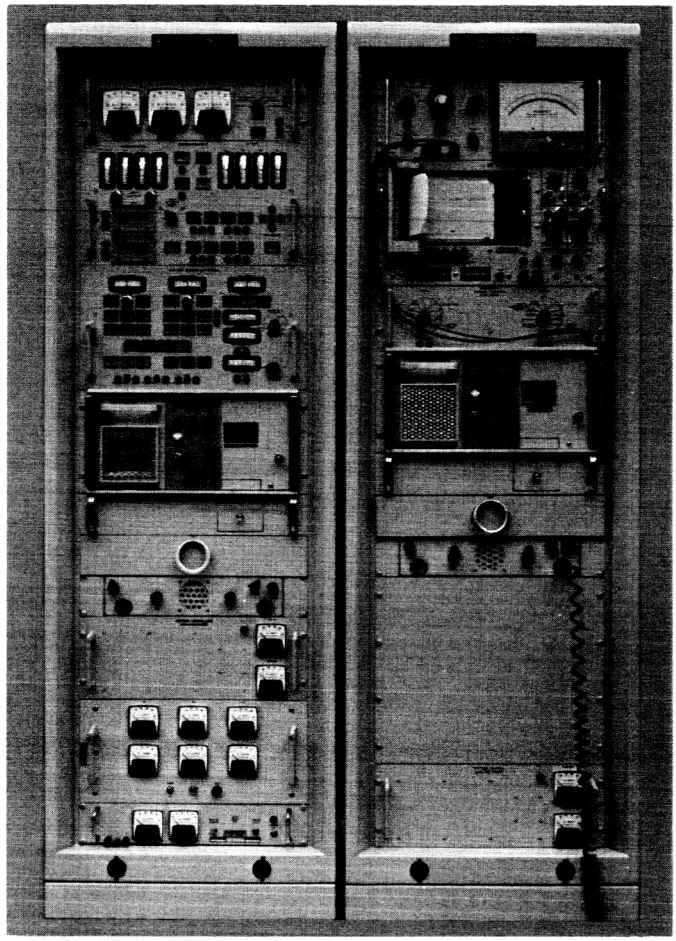


Fig. 332. Attitude control OSE system test set

a. System test set. The system test set (Fig. 332) is capable of testing and evaluating the attitude control subsystem, during spacecraft system and subsystem tests, in conjunction with the spacecraft subsystem interfaces. All monitoring, test, and control devices in the system test set are provided with self-test capability at the test console. These self-test features do not detract from the normal operation of the OSE and do not react with the flight equipment. A functional block diagram is shown in Fig. 333.

Direct inputs. Voltage monitoring of the pitch, yaw, and roll gyro amplifiers verifies midcourse maneuver phasing, rate control of position changes, and operating conditions of the gyros using heading errors. The monitoring is performed by the gyro monitor panel assembly. Due to the relatively high resistive isolation in the gyro amplifier test outputs, a line amplifier assembly located in the J-box is used through which all three signals pass.

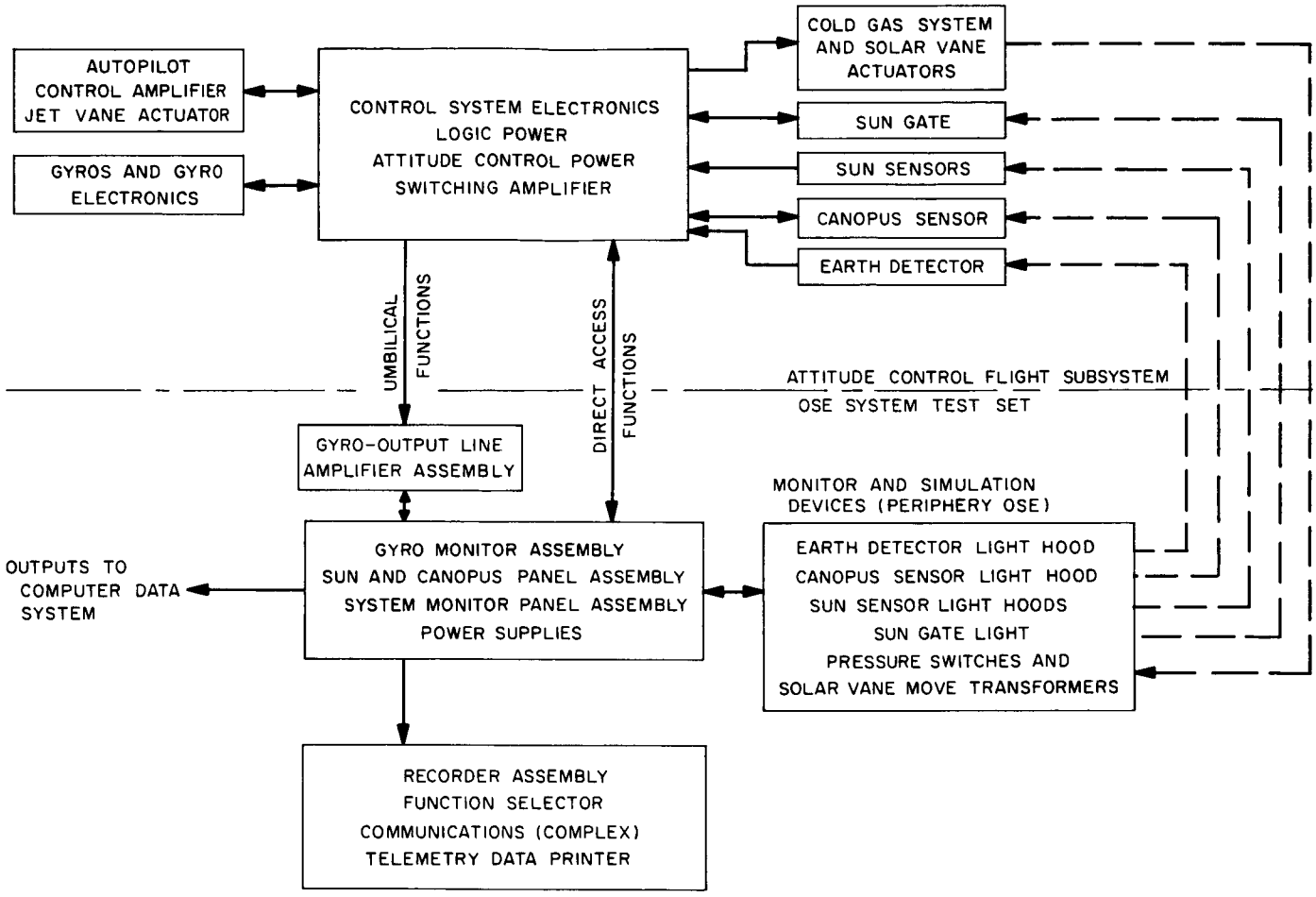


Fig. 333. Attitude control OSE system test set functional block diagram

Voltage tolerance detectors are used to verify correct levels of the following transformer–rectifier units:

±26 v logic power

±26 v attitude control

+25 v Canopus sensor power

±35 v gyro power

The outputs of the Canopus sensor are checked by the Sun and Canopus acquisition panel assembly using several methods:

1. The brightness (intensity) output voltage to the telemetry circuits is displayed in analog form on a panel meter.
2. The Canopus cone-angle voltage is monitored and displayed on a panel meter. The reading corresponds to the electrical setting of the Canopus sensor field of view, and is compared to the OSE position stimulus.
3. The roll error signal is presented on a panel meter.
4. The acquisition signal is detected and is used to operate a panel indicator.

The pitch and yaw position error signals to the telemetry circuits are indicated by panel meters at the system test set and represent the inputs to the pitch and yaw switching amplifiers. The roll error indication is the roll switching amplifier input. These three monitors are used to check the trip points of the three switching amplifiers. The roll rate command signals (magnetometer calibration and roll search) are also indicated on the roll position error meter. The voltages derived from the four jet vane position potentiometers in the actuator assembly are presented on panel meters of the system analysis panel assembly and are compensated to reflect the angle of rotation. These voltages are used to verify the autopilot phasing and operation with respect to the attitude control subsystem. The Earth detector telemetry signal is

level-detected to indicate normal operation when properly stimulated. A microswitch actuated by the Canopus sensor Sun-shutter solenoid activates an indicator at the system test set.

Indirect inputs. A pneumatic system of pressure switches, bleed orifices, and check valves is used to detect the operation of the spacecraft control gas valves used for pitch, yaw, and roll stabilization. This pressure switch system verifies the valve operations by indicators at the system test set.

Prior to the *Mariner* Mars 1964 program, all space-simulation tests on completed spacecraft were performed with the attitude control gas subsystem disconnected or capped, because a sudden change in gas pressure in the chamber due to operating a number of gas valves might have caused excessive changes in chamber pressure. A pressure-switch monitoring system was used for the first time on the PTM that permitted testing of the attitude control subsystem without breaking any connectors or capping the gas system. The advantages of this technique are twofold: the integrity of the attitude control subsystem as a whole is maintained and the solar vane actuators are allowed to operate in the normal manner, since they depend on the operation of the gas systems.

Twelve gas valves are used on the spacecraft to control its attitude. The valves are located at the ends of the solar panels in the following configuration: four valves on the +X panel, four valves on the −X panel, two valves on the +Y panel, and two valves on the −Y panel. The system for monitoring the operation of one gas valve at atmospheric pressure is shown in schematic form in Fig. 334. When the gas valve operates, the gas flows through the check valve and operates the pressure switch. Gas is continually bled to atmosphere through the orifice so that the pressure switch will reflect the absence of pressure soon after the gas valve is shut off.

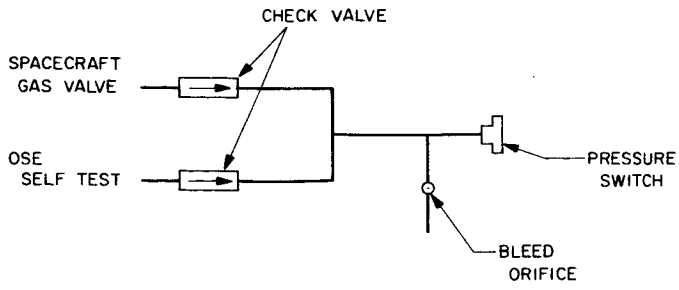


Fig. 334. Gas-valve monitor system for use at atmospheric pressure

The other check valve provides an inlet for self-test pressure to operate the pressure switch, and isolates the self-test pressure source from the flight gas valves. The system in Fig. 334 is used for each gas valve, and manifold blocks are machined in such a way that the check valves, pressure switches, and bleed orifice components are inserted into the blocks and the check valves are connected to the gas valves.

The system used in the vacuum chamber is a modification of the atmospheric-type system. The result is illustrated in Fig. 335, which shows the configuration of the bleed orifices of all four pressure-switch assemblies. The pressure-switch bleed orifice assemblies are connected together and brought out of the chamber to a reservoir tank and vacuum pump. This pump creates a vacuum that approximates the one seen by the pressure switch. Therefore, when a gas valve operates, the pressure actuates the pressure switch and the external vacuum pump extracts the gas passing through the bleed orifice. The external vacuum pump is not started until the chamber pressure is down to a reasonable vacuum or the pressure switches will be reverse-pressurized and damage will result.

The self-test check valves are connected together and brought out of the chamber in a manner depicted in

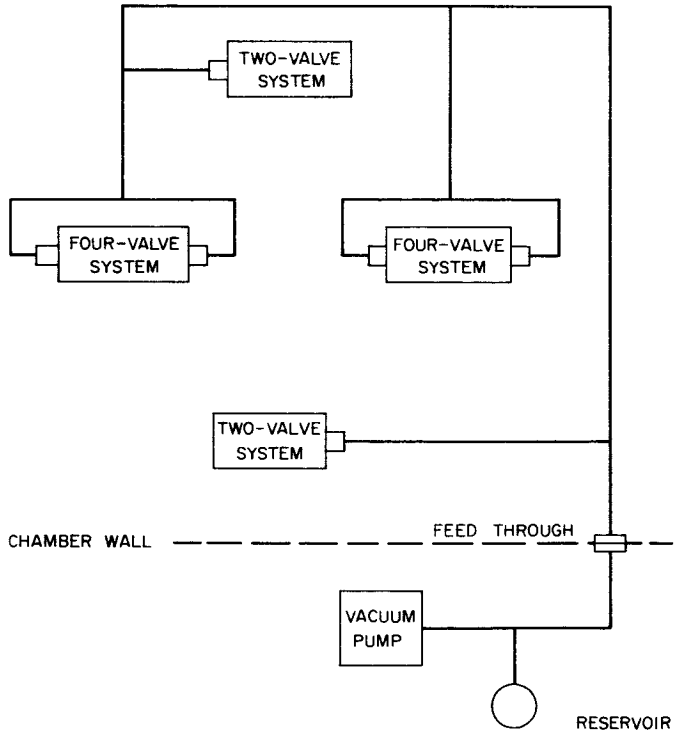


Fig. 335. Gas-valve monitor for vacuum-chamber testing

Fig. 335. A dry-nitrogen pressure source was connected to this line so that the pressure switches could be tested in the event of the loss of gas-valve indications. All of the pressure switches are actuated simultaneously.

Movement of each of the four solar vane actuators, as a function of the gas-valve actuations, is detected by a linear transducer. A steel slug is flexibly connected to a point near the solar vane thermal actuator. When the solar vane actuator is stepped, the slug is moved into or out of a linear transducer assembly that produces an output corresponding to the movement of the slug. These outputs are displayed on panel meters at the system test set. The attitude control switching amplifier is forced to switch at a rate no greater than 1 pps by the injection of an error signal slightly larger than the deadband switch point. The error signal is obtained by controlling the illumination of the cruise Sun sensors and by using the derived rate feedback as the shutoff signal. The solar vane electronics force the solar vane to step +0.01 deg for every pulse from a counterclockwise gas jet. A pulse from a clockwise gas jet results in a −0.01 deg step. Monitoring of this action is accomplished by totalizing the number of clockwise and counterclockwise gas-jet actuations algebraically until a count of 100 is registered. At that time, the switching amplifier forcing function is removed, and the solar vane net movement is read on the solar vane meter monitors. Since 100 pulses are monitored, a difference of 1 deg should be noted on the solar vane meters.

Direct outputs. Provision is made at the system test set to operate the autopilot power relay when it is desired to actuate the autopilot subsystem separately from the normal midcourse maneuver sequence.

Comprehensive analysis of the rate and position gyro system is accomplished by using a dynamic rebalance loop in the system test set. This rebalance loop simulates the dynamics of the spacecraft. With this capability, the gyros are less susceptible to damage, and long duration turns become attainable. As the gyro senses an error rate, an out-of-phase voltage appears at the gyro power-amplifier output; e.g., a plus voltage for a counterclockwise error rate. The voltage amplitude is directly proportional to the error rate, and exceeds the switching-amplifier rate threshold at approximately 0.02 deg/sec in the roll channel and 0.07 deg/sec in the pitch and yaw channels.

Supposing a counterclockwise error rate, operation of this system is as follows. Exceeding the switching-amplifier rate threshold activates a clockwise valve; the OSE pressure switch senses nitrogen flow and applies an integrator input in phase with the gyro-amplifier output. This input is integrated according to a spacecraft acceleration constant and supplies a torquer current (rebalance current) out of phase with the gyro-amplifier torquer current. As torquer current is reduced to the value corresponding to the switching-amplifier lower-limit rate threshold, the clockwise valve turns off and grounds the integrator input. The gyro-amplifier output remains at the switching-amplifier lower-limit rate threshold for a constant error rate and/or until integrator decay of sufficient magnitude occurs, which reduces the torquer rebalance current. This cycle continues until spacecraft motion is stopped. Any change in the direction of rate reverses the sequence.

During commanded turns (midcourse maneuver), the operation sequence is basically the same, with the exceptions that (1) the current to be balanced out is the turn command current triggered by the CC&S, and (2) a position storage capacitor is inserted in the gyro loop. The integrator balances the three gyro loops and holds the gyro gimbal system at a relatively constant position, thereby reducing the chances of possible damage to the gyro from such causes as sudden disturbances to the spacecraft while the gyro loop is saturated.

The attitude control OSE provides certain subsystem analog and status functions to the computer data system for redundant monitoring, recording, and time correlation with other spacecraft events. In this way, a complete record of the operation of the attitude control subsystem as a portion of the total spacecraft during a system test was provided. In addition, a special subroutine was used to dynamically verify the performance of the autopilot and jet vane control.

Indirect outputs. The system test set periphery equipment consists of seven light hoods to stimulate sensors in the attitude control subsystem. Four light hoods stimulate the sixteen Sun sensors used for Sun acquisition and Sun-line orientation. One light hood provides a collimated source to operate the two Sun-gate sensors. Another light hood simulates the star Canopus and provides roll error signals and acquisition signal level testing of the Canopus sensor. Fifteen light sources are required in this hood to provide clockwise, counterclockwise, and null stimuli for five separate cone angles. Also housed in this light hood is a high-intensity source to actuate the Sun shutter electronics that protect the optics of the sensor. The last light hood is used to test the Earth detector, which aids in verifying Canopus acquisition by

acknowledging the geometric presence of Earth during the early part of the flight path.

b. Launch-complex set. The attitude control launch-complex set consists of the gyro monitor panel assembly, identical to the unit in the system test set, a voltmeter, and the gyro line amplifier assembly with associated power supply. Provision was made at the panel assembly to electrically bypass the line amplifiers in the event of a critical failure late in a launch attempt. These units provide continuous monitoring of the gyro outputs from spacecraft power turn-on to liftoff and precision measurement capability for comparing gyro heading data.

Self-test signals originating in the gyro monitor panel assembly are sent to the line amplifiers during the proper test mode. The performance of the amplifiers is then displayed on the panel meters.

12. Pyrotechnic Subsystem OSE

The pyrotechnic subsystem OSE has three basic support roles: subsystem evaluation, system testing, and launch operations. The functions that were required to support both system testing and the launch operations were built into one panel and identical units were used in both support areas.

During the subsystem and system test and evaluation portions of the program, the pyrotechnic OSE provided the following capabilities:

1. Testing of the spacecraft squibs by determining, both before and after sending a fire squib command, if the squibs had actually fired.
2. Monitoring of the voltage on the capacitor banks in the different pyrotechnic control subassemblies.
3. Giving a visual indication (by lights) of the position of the different squib-firing relays. These circuits were continually monitored to determine if any unscheduled squib-firing commands had been issued.
4. Giving visual indication of the position of the midcourse inhibit and transfer relays.
5. Generating a permanent record of each squib-firing pulse (current), on a high-speed, direct-writing oscillograph.
6. Recording, via an elapsed time indicator, the exact length of time that power was applied to the spacecraft pyrotechnic control units. A secondary function is giving a visual indication of the arming (power *on*) of each pyrotechnic control unit.
7. Providing 2.4-kc power (used in the absence of the spacecraft power) in support of subsystem evaluation of the spacecraft pyrotechnic subsystem.

For the launch operation, the pyrotechnic OSE was required to monitor the following umbilical functions:

1. The position of the pyrotechnic fail-safe relay
2. The position of the solar panel or scan platform pinpuller

Another tool used in the pyrotechnic area is the field test kit. The field test kit (Fig. 336) is a self-powered portable instrument used (1) to determine the condition of the spacecraft pyrotechnic subsystem before and after the installation of squibs or squib simulators, and (2) to verify that the subsystem is flight-ready after final spacecraft flight preparation in the explosive safe area. The instrument:

1. Determines the voltage charge on capacitor banks within the pyrotechnic control units
2. Discharges capacitor banks if a charge exists
3. Determines that all squib firing lines are continuous and are not shorted or grounded
4. Accurately measures the resistance of each squib and squib firing line

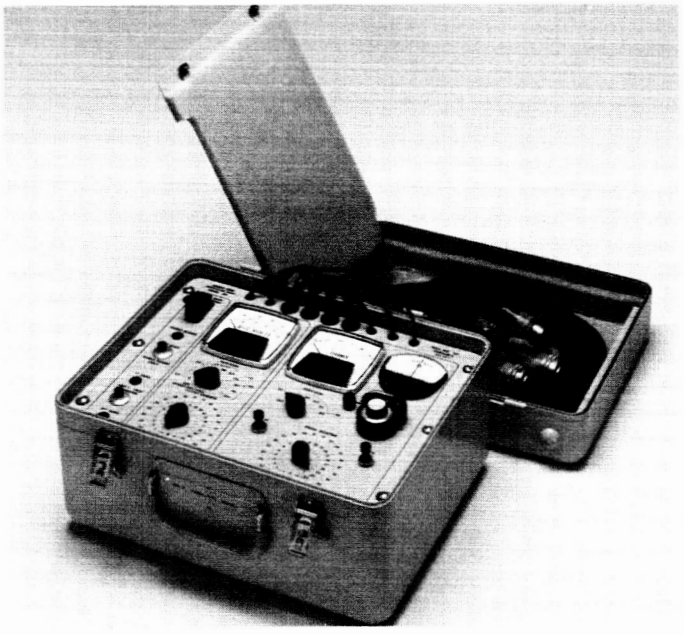


Fig. 336. Field test kit

5. Indicates the position of propulsion transfer relays within the pyrotechnic control units
6. Indicates the position of propulsion inhibit relays within the pyrotechnic control units
7. Indicates the presence (if any) of potential existing in the output of the pyrotechnic control units
8. Self-tests circuitry for battery condition, meter, and indicator integrity

13. Video Storage Subsystem OSE

The video storage subsystem OSE was used to stimulate and monitor the VSS while it was installed on the spacecraft during system test operations, during FA and TA testing, during final acceptance testing at the vendors, and during various bench-testing operations.

The video storage subsystem OSE capability includes supplying 2.4-kc power, 400-cps single-phase power, and 400-cps three-phase power. The picture-recording sequence is simulated by the DAS sequence simulator. Length of picture, period of bit synchronization without data, and the length of pause between pictures is variable. Data are obtained in the form of a seven-bit digital word with the *one*, *zero* pattern selected by toggle switches.

In the system-test configuration, the OSE generates subsystem control functions and monitors various subsystem parameters through the umbilical and direct-access cables. Isolation of the spacecraft is attained by using transformer-coupled circuitry, isolation amplifiers, and isolated power supplies.

The VSS OSE is contained in a dual-bay rack (Fig. 337). The following commercial test equipment is incorporated: an oscilloscope with differential preamplifiers, a frequency counter, a digital voltmeter, a galvanometer control panel, and a 2.4-kc power supply. The OSE used in the VSS bench-test configuration and in special testing contains an rms voltmeter and an audio oscillator.

Four running-time meters are provided. These meters indicate (1) the elapsed time that the VSS subsystem was powered, (2) the time that the record motor was running, (3) the time that the playback motor was running, and (4) the time that the OSE was energized.

Outputs are fed from the OSE to the computer data system, which monitors OSE indications of track status and record *on/off* status. A special program is available from the computer data system to use the integrator monitor signal for an indication of in-synchronization playback. The integrator monitor function is available at the central recorder so that it can be recorded during the playback mode.

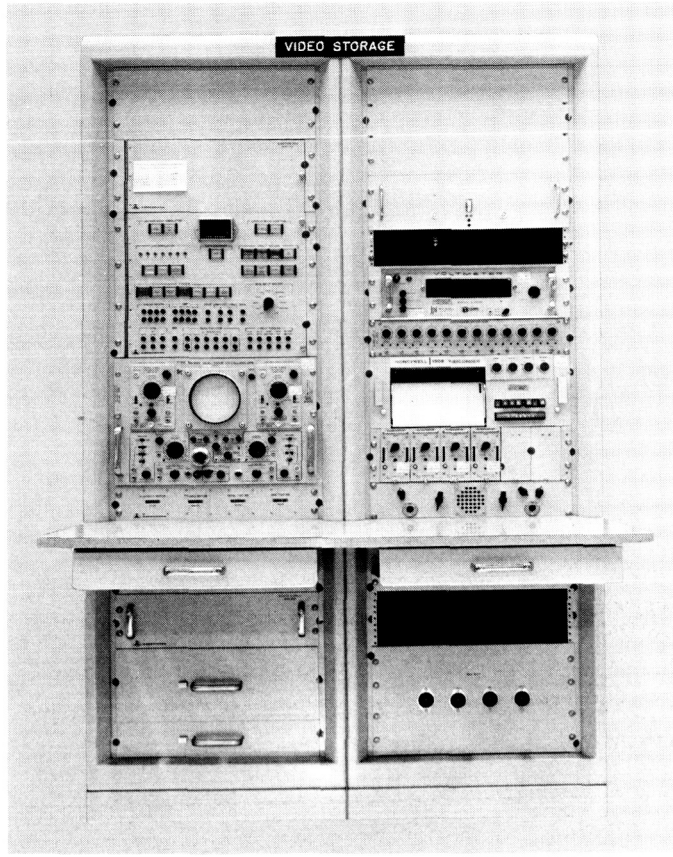


Fig. 337. Video storage subsystem OSE

14. Science Subsystem OSE

The science subsystem OSE includes all the nonflight hardware used to test the science subsystem. The basic requirements for the science OSE are:

1. To supply power and spacecraft conditioning signals to the science subsystem in lieu of the Spacecraft System
2. To stimulate the flight instruments with flight- or bench-test type inputs
3. To operate and monitor the science subsystem flight instruments without the DAS
4. To monitor and record the flight-instrument power-supply output voltages

5. To monitor and record the output of the flight instruments, including the DAS
6. To monitor and record the outputs of the DAS either directly or through the spacecraft telemetry link
7. To compare the digital output of the DAS with the analog or digital outputs of the flight instruments
8. To record the discrete events occurring within the science subsystem

In describing the science OSE (Fig. 338), the isolation box may be considered as the OSE interface with the spacecraft, and the remainder of the system may be divided into three areas: instrument monitoring and stimulation, DAS monitoring, and the PDP-4 computer interface. The isolation box is mounted on the spacecraft mounting fixture; it contains terminal boards for routing signals and printed circuit boards that afford isolation, signal conditioning, and cable-driving capabilities to the system.

The first area of the OSE consists of the equipment used to power, stimulate, and monitor all of the scientific instruments except the DAS. The 2.4-kc and 400-cps power is generated by the power supply, with the 2.4-kc input adjustable in both amplitude and rise time.

The instrument stimulators fall into four categories: radioactive sources, internal stimulators housed within the OSE, stimulators separate from the integral OSE system, and the spacecraft platform cover stimulus lights. The radioactive sources are supplied by the instrument cognizant engineers for the Ionization Chamber, Trapped Radiation Detector, and Cosmic Ray Telescope instruments. The sources have holders that are mounted either to the associated instrument or to the spacecraft. The internal stimulators are controlled by the OSE operators. They include three test currents for the Solar Plasma Probe, and the pulses for the Cosmic Ray Telescope and the Cosmic Dust Detector. The external stimuli consist of light sources for the planetary scan, the subsystem TV collimator and target, and the Magnetometer Helmholtz coil system that is used to null out the Earth's field at the Magnetometer. The Helmholtz coils may also be used to induce 60 γ offsets along each Magnetometer axis.

The platform stimulus lamps are mounted in the scan-platform cover. The lamps are mounted in front of the TV vidicon, the planetary scan sensor, and the narrow-angle Mars gate. The launch checkout equipment stimulus control chassis contains variable power supplies and control logic for the stimulus lamps. Power to the stimulus lamps is provided through the umbilical cable from this chassis to the spacecraft.

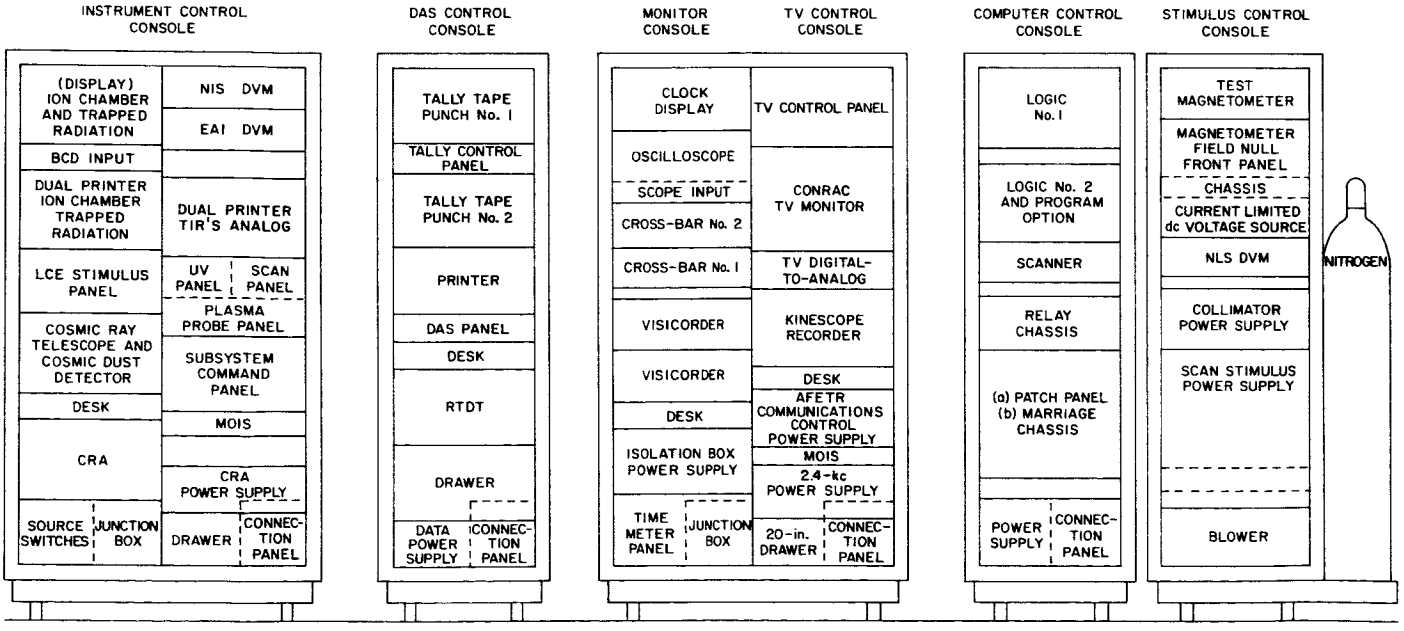


Fig. 338. Science OSE

The OSE is capable of measuring the five types of signals originating in the science instruments. All functions, except discrete DAS events, are routed through crossbar selectors so that each signal can be monitored by a digital voltmeter, an oscilloscope, or both. All analog signals and instrument power-supply voltages are monitored on a digital voltmeter and recorded on a printer. Pulse intervals are measured in the interval counter, and the values are recorded on a printer. The Ionization Chamber data are expressed as a function of the time between successive pulses; the interval counter mentioned above measures the time and records between pulses. Six Geiger–Müller tubes (five in the Trapped Radiation Detector and one in the Ionization Chamber) transmit serial pulse trains to the OSE. These pulses are counted in the count-rate accumulator and are printed out at 1-min intervals. Pulses from the Cosmic Ray Telescope are counted and recorded. The Cosmic Dust Detector output is monitored by a series of lights that check the state of two of eight bit registers.

A visicorder is used to record discrete events from the DAS; these signals are level shifts. A second visicorder is used to measure and record the position of the scan platform.

Four sources of television data are available from the isolation box: analog video, TV digital 83.3 kc, DAS digital 10.7 kc, and DAS digital from the umbilical cable. The TV control panel contains monitoring lights that indicate the status and type of data being received; it also has switching capabilities for selecting the desired data to be monitored. All digital data go to the TV digital-to-analog converter. All analog data are displayed on a television monitor and recorded on 35-mm film by a kinescope recorder. The 10.7-kc digital data are processed by an external computer.

The DAS control console houses the equipment for formatting, displaying, and recording the DAS data output. The DAS control panel selects either hard-line data from the science isolation box or data from the ground telemetry station; it can also select the real-time bits that are stripped from the 10.7-kc digital television data by the TV control panel. The selected data are sent to the real-time data translator where they are transformed from a digital to an octal format. The output of the data translator is sent to three data printers for display. These displays can be compared with the direct instrument outputs as printed out by other parts of the OSE already described. For permanent records, the data from the translator are put on a paper punch.

The computer control console was designed to provide signal conditioning for a PDP-4 computer under advanced development of the science OSE. The computer control console could be connected to the spacecraft in place of the instrument control consoles. The flight instruments' performance (except the TV) could then be analyzed by the PDP-4 computer. Schedule time did not permit a test of this configuration or preparation of programs for it. Instead, the PDP-4 computer control system was adapted for computer analysis of the 83.3-kc digital TV data because the flight TV data program was not yet available.

Each of the three sets of science OSE was tested prior to its delivery to the spacecraft operations facility. The initial science OSE testing was completed using nonflight instruments. Not all of the features of the OSE were fully used; however, all of the concepts embodied in the systems were verified to the extent that the schedule permitted.

The science OSE performed as designed and proved extremely versatile and conveniently adaptable to the many test modes required (including environmental testing and launch operations).

15. Computer Data System

The system testing of all *Mariner* Mars 1964 spacecraft was aided by the use of a real-time on-line automatic data system that provided for the acquisition, processing, printout, and recording of test data. One of the most important functions of this system was the suppression of redundant telemetry and analog data samples so that only significant data were printed out during test operations. The system-test operators and data analysts were thus relieved of the task of assessing reams of inconsequential data.

A block diagram of the computer data system is shown in Fig. 339. The input data acquisition capabilities of the system are as follows: (1) bit-serial PCM telemetry data from either data encoder OSE or ground telemetry OSE (up to three data streams simultaneously); (2) 176 analog data channels, including 80 submultiplexed channels, from the spacecraft direct-access or umbilical connectors (via the OSE); (3) 144 status or *on–off* type signal channels from the spacecraft and OSE; (4) 96 event channels, including 16 transient detectors, from the spacecraft and OSE; (5) digital video signals at either 10.7-bps DAS buffer rate, or 8⅓-bps video-storage playback rate; (6) 10 counter registers; (7) a real-time clock; and (8) a spacecraft (CC&S) clock.

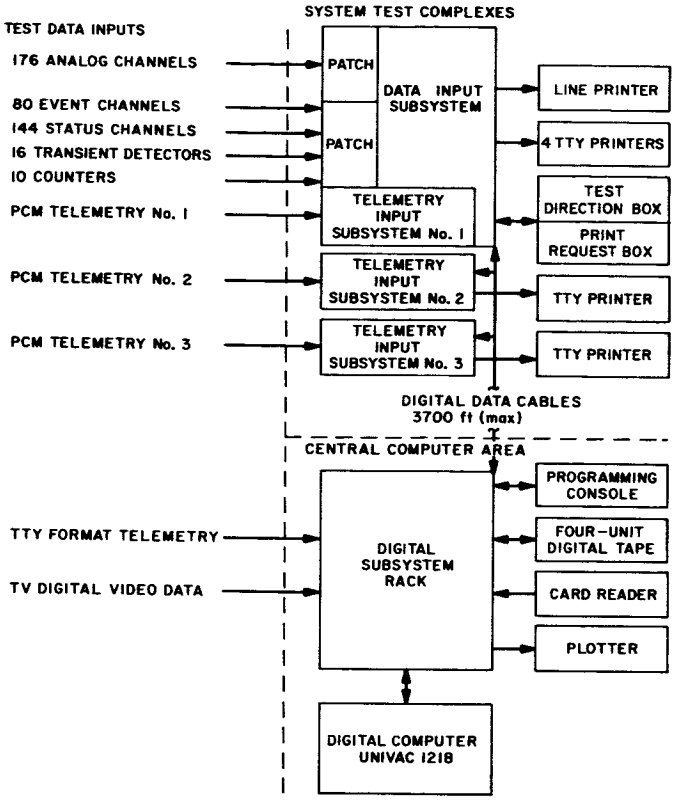


Fig. 339. Computer data system block diagram

All types of incoming data are formatted and recorded on digital magnetic tape prior to processing or editing to permit subsequent non-real-time analysis either on the system computer or off-line on the IBM 7094 computer.

The real-time data processing and display functions consist of: (1) computer decommutation of PCM telemetry; (2) raw-data limit testing; (3) data compression (comparison of each telemetry or analog data sample to its corresponding previous value to suppress printout, unless the sample value has changed by more than a preset tolerance); (4) scan control of the analog multiplexer; (5) conversion of data to engineering units; (6) message formatting, and identification of all types of printed data with 9-digit English-language titles; (7) identification and printout of status changes, event occurrences, clock and counter readings; and (8) printouts of specific classes of data at the test director's request. Non-real-time processing provides for recalculation of recorded test data, selective tabulation of data derived from the different spacecraft subsystems, and data plotting.

A reproduction of a typical page of line printer telemetry data is shown in Fig. 340. The upper left-hand section identifies test step number, and shows spacecraft command, status, events and counter data, as well as analog data if they are being acquired. The upper right-hand section shows about 6 min of engineering telemetry data output in the data compression format. All time tags are 1-msec precision, enabling the determination of the stimulus event, as opposed to the response event, in case of doubt. Data shown are in engineering units, including a signal exponent to indicate the location of the decimal point.

The printout shown was generated at the test director's request; it is the latest available reading of all engineering telemetry channels, and illustrates one of several request printout options that are available.

The Univac 1218 computer and the associated control console and magnetic tape units are shown in Fig. 341. One of the racks contains clocks, displays, and logic for communications with the data input system, as well as a programming console, a card reader, and a plotter. The data input system and data printers (Fig. 342) are located in the STC. Control signals, such as special printout requests, enter the system from the test director's console located in the test complex. The main data printer displays all messages and data generated by the system. Six teleprinters are used to display subsets of the total engineering and science data to the representatives of the various spacecraft subsystems.

The flow chart for the real-time program (Fig. 343) shows the main soft-ware features of the system. During the system test and postlaunch period from February 1 to November 30, 1964, the computer data system was operated 3730 hr, or 51% of the total hours available. The down-time was 10% of the total operating time, and the down-time during the periods of requested test support was 1.7%.

16. Telemetry Teletype Encoder

The telemetry teletype encoder was designed and constructed by the DSIF for use on both the *Mariner* and *Ranger* programs. Its primary use is in a typical DSIF tracking station as a means of applying telemetry data to teletype lines for near-real-time transmission of the telemetry data to the SFOF at JPL. Its use in the spacecraft system tests, environmental tests, and launch tests was also primarily the same as in a tracking station. This enabled the SFOF and all associated operations personnel to become familiar with (1) spacecraft operations in virtually all possible phases before flight, and (2) interfaces nearly identical to those that would be encountered in the actual flight.

```
     MC-4    S/C AND STC VERIFICATION TEST (ETR)                    NOVEMBER 10 1964          PAGE 021

14.23.13.500 GCD XMIT  ON   00000  000  0000

                                                                 14.23.16.945 BAT DRAIN   3682-3  3207-3
                                                                 14.23.20.515 EARTH DET   3378-3  7324-3
                                                                 14.23.20.935 SYS PWR     1390-1  1340-1
14.23.21.018 STEP NO 176
14.23.23.500 CMD EVENT ON   00000  000  0000
                                                                 14.23.26.605 EV CH 3/4   0502    0501
                                                                 14.23.29.545 EXCIT PWR   2845-2  2747-2
14.23.39.262 GRND CMND    DC08          6 652 0 0000 0
14.23.39.494 GCD XMIT  OFF  00000  000  0000
                                                                 14.23.48.655 PSL I RAD   9593-4  8400-4
                                                                 14.23.48.865 L ANT PWR   8300-2  7100-2
                                                                 14.23.57.055 BATTERY E   3748-2  3774-2
                                                                 14.24.22.466 BAY 3 LP    4757-2  4460-2
                                                                 14.24.29.816 CHAM PRES   6471-2  5999-2
14.24.51.382 PLASMA T1 ON   00000  000  0000
                                                                 14.25.04.466 BAY 4 TMP   7356-2  7160-2
                                                                 14.25.42.266 BAY 5 TMP   7533-2  7336-2
                                                                 14.25.46.466 X OSC TMP   7965-2  7669-2
                                                                 14.26.11.667 X/-Y TEMP   7291-2  7094-2
                                                                 14.26.24.267 BAY 6 TMP   8171-2  7975-2
                                                                 14.26.28.467 BAY 1 LP    1000-1  9701-2
                                                                 14.26.29.517 EARTH DET  -5673-4  3378-3
14.26.35.457 GCD XMIT  ON   00000  000  0000
14.26.45.457 CMD EVENT ON   00000  000  0000
                                                                 14.26.46.737 PSL OUT E   3637-2  3684-2
                                                                 14.26.46.947 BAT DRAIN   3999-3  3682-3
                                                                 14.26.48.207 EV CH 3/4   0503    0502
                                                                 14.26.50.937 SYS PWR     1500-1  1370-1
14.27.01.219 GRND CMND    DC28          6 662 0 0000 0
14.27.01.452 GCD XMIT  OFF  00000  000  0000
                                                                 14.27.06.267 BAY 7 LP    1039-1  1014-1
                                                                 14.27.10.467 BAY 7 TMP   7814-2  7616-2
                                                                 14.27.14.457 B/RS IN I   2818-3  2742-3
                                                                 14.27.16.137 PSL OUT E   3519-2  3637-2
                                                                 14.27.27.057 BATTERY E   3616-2  3748-2
                                                                 14.27.27.267 BAT CHG I   4814-6 -2949-5
                                                                 14.27.28.947 BAT DRAIN   4158-3  3999-3
                                                                 14.29.58.259 CAV/HELIX   9300-2  7400-2

14.30.13.288  REQUEST  E/TM/1  LAD  EU
  HIGH SYNC  DECK 20X  DECK 21X  AGC CORSE  CMD VCO F  PTCH GYRO  YAW GYRO  ROLL GYRO  CANOP INT  PSL OUT E
    0000+0     3100-2    5000-2    -1142-1    0000+0     1601-6     2200-6     2240-6     4600-2     3519-2
  DECK 22X   RCVR SPE  PITCH POS  YAW POS    R POS/SCH  EV CH 1/2  EV CH 3/4  CHAM PRES  PIP N2 PR  FUEL PRES
    3200-2     6199-2    6400-2    6300-2     3700-3     1070-1     5030-1     6235-2     5693-1     3307-2
  MED SYNC   ADC/PNG    DECK 30X  B/RS IN I  PSL I RAD  BR1 OUT I  BATTERY E  2.4 E OUT  X/-Y PSI   -X/Y PSI
    0000+0     4700-2    0000+0    2818-3     9991-4     1500-3     3616-2     5064-2     1462+0     9701-1
  LO DRIVE   DK 40/41X  DK 42/43X  H ANT PWR  L ANT PWR  AGC FINE   BAT CHG I  FUEL TEMP  X/-Y TEMP  -X/Y TEMP
    8358-4     0000+0    0000+0    8000-3     8300-2    -1233-1     4814-6     1483-1     7291-2     7234-2
  CCS E TME  BR2 OUT I  SP 4A1 I  SP 4A5 I  SP 4A3 I  SP 4A7 I  BAT DRAIN  2.4 OUT I  OXDZR PSI  EXCIT PWR
    3024-2     1656-6    1301-5    1113-5     7795-6     1113-5     4158-3     1349-3     1222-1     2845-2
  CAV/HELIX  EXC -25V   EXC -15V  CONE ANG.  TAPE PSI  SV POS +X  SV POS -X  SV POS +Y  SV POS -Y  CC/S +28V
    9300-2    -2488-2   -1510-2    0000+0     2129-2    -2913-2    3069-2     4127-2    -3578-2     2774-2
  SYS PWR    BAY 1 TMP  BAY 3 TMP  T403       BAY 5 TMP  BAY 6 TMP  BAY 7 LP   BAY 8 TMP  PIP N2 TP  SP4A1 TMP
    1510-1     7822-2    7294-2    8500-2     7533-2     8171-2     1039-1     6100-2     1476-1     7474-2
  CANOP TMP  S ACT TMP  ABS STD 1  ABS STD 2  SCI COVER  STD CEL I  RES CEL I  STD CEL E  TV TEMP    ION C TMP
    8400-2     7622-2    9700-2    1260-1     9200-2     2031-2     4022-2     6269-1     8300-2     7196-2
  TEMP REF   BAY 2 TMP  BAY 3 LP  BAY 4 TMP  X OSC TMP  BAY 1 LP  BAY 7 TMP  T427       BATT TEMP  SP4A5 TMP
    6400-2     1481-1    4757-2    7356-2     7965-2     1000-1     7814-2     7900-2     7365-2     7590-2
  L RNG TMP  U RNG TMP  ABS STD 3  ABS STD 4  UP SHLD T  LO SHLD T  TAPE TEMP  T437       TRD TEMP   MAG TEMP
    7682-2     7497-2    1260-1    1260-1     2990-1    -8810-3     7271-2     7189-2     5200-2     7379-2
  P SUN SEN  Y SUN SEN  EARTH DET  BAD        BAD        BAD        BAD        BAD        BAD        BAD
    1829-4     1152-4   -5673-4    0000+0     0000+0     0000+0     0000+0     0000+0     0000+0     0000+0
```

Fig. 340. Typical line printer telemetry data



Fig. 341. Univac 1218 computer and associated control console and magnetic tape units

In the *Mariner* Mars 1964 case, the encoder receives as its inputs telemetry data from the ground telemetry subsystem and time data from the central timing subsystem, both situated in the system test complex. The encoder then formats the telemetry data into equivalent teletype characters and inserts the time information at regular 5-min intervals.

The telemetry encoder synchronizes with the incoming data in Data Modes 1 and 2 in much the same way as the synchronizing information to present a TTY page print. The data printout is interrupted every 5 min to print a line that includes the DSIF station identification and the time (day, hour, minute, second).

During high bit rate (33⅓ bps) telemetering, the information rate of one TTY line is sufficient to transmit all the data in near-real time; therefore, two TTY lines are used in which the encoder drives two paper-tape punches. The paper-tape outputs of the two punches feed the two transmitter distributors at the input to each line. The data are then sent over the lines to the SFOF to be used in real-time analyses and to be used by the SFOF computing system for decommutation.

17. Central Timing System

A study was conducted to determine how the *Mariner* OSE could best be mechanized. This study indicated

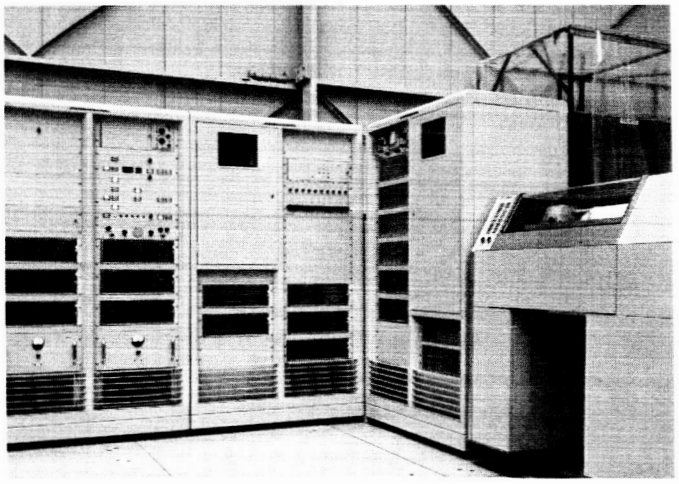


Fig. 342. Data input system

the need for a common time reference for the entire system test complex. The system provided to carry out this function was called the central timing system. To be functional, such a system had to be able to support the OSE in any area in which tests might be performed. The system was one in which timing signals were distributed to a repeater known as the timing isolation unit. The STC and LCE each had one such unit. This unit also drove several remote display units. The basic system used the NASA 36-bit time code. The heart of the system was the central timing generator, which could be either synchronized from a central timing source or left free-running. When used at JPL, the synchronization source was provided by the JPL Standards Laboratory. For AFETR operations, time synchronization was AMR-BR19, BRIG-B code. Under certain conditions of testing, data were recorded on tape and played back for a more thorough analysis. The timing isolation unit was compatible with the output of the time code recorded by the ground telemetry subsystem. By changing the timing isolation unit cables coming from the central time code generator to the time recorded on the GTS tape, the timing on the complex was in synchronization.

18. Central Recorder

The central recorder (Fig. 344) maintained a constant monitor on functions of the spacecraft and OSE operations during a subsystem or system test. The record from the central recorder made it possible to correlate all operations of the system test procedure with spacecraft functions and time.

The central recorder was also used as a visual monitor for normal operation system tests. The record was useful

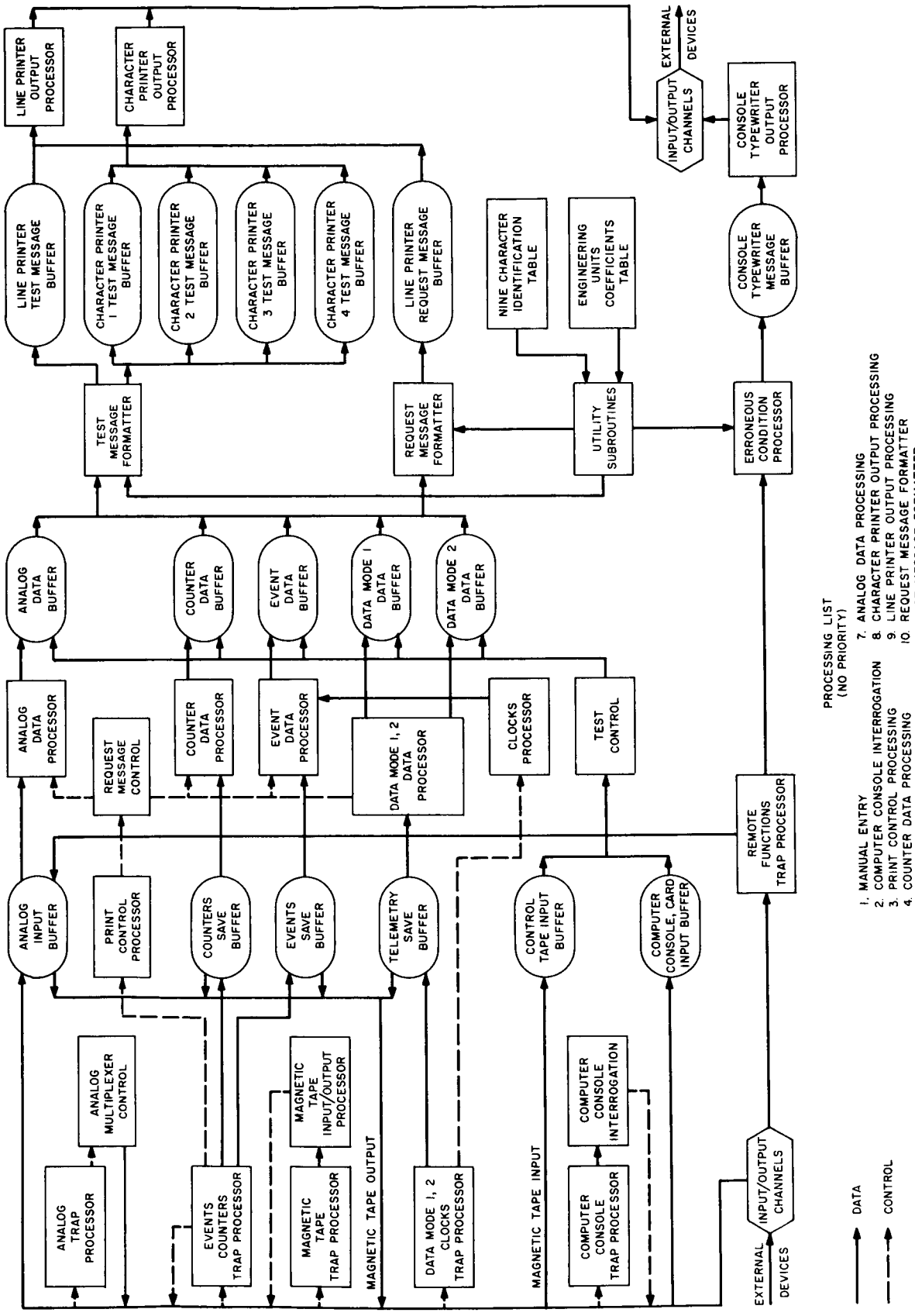


Fig. 343. Computer data system real-time program flow chart

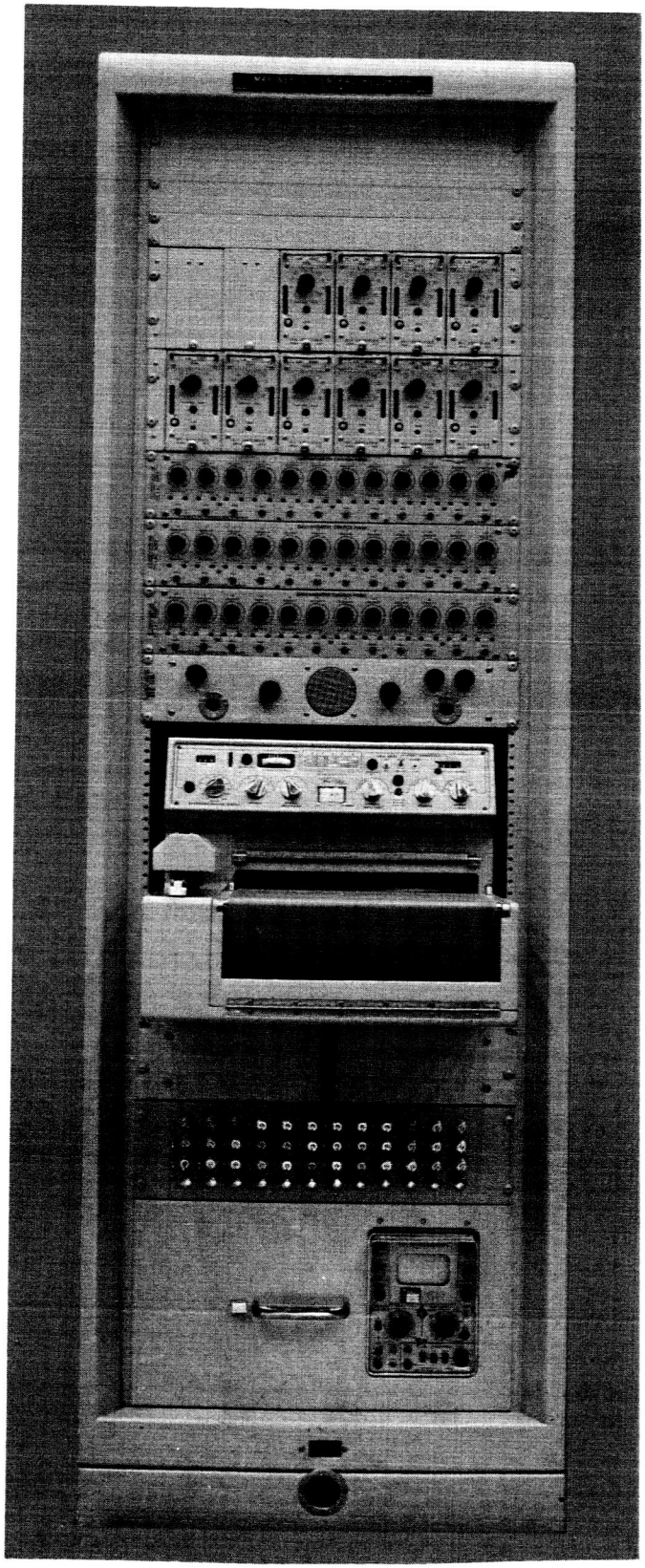


Fig. 344. Central recorder assembly

in postoperational evaluations, and was stored for later comparison with other similar tests.

The amplifiers in the central recorder provided amplification of low-level signals or circuit isolation, or both, as necessary for proper operation of the galvanometers in the central recorder. The central recorder consists of the following major elements:

1. One recorder, which has a 50-channel capacity on a 12-in.-wide 350-ft-long direct-print paper, can be fixed to make the record permanent, if desired.
2. A maximum of 50 galvanometers.
3. Four galvanometer control panels of 12 channels each.
4. Six amplifiers in a single module. These amplifiers are wide-band (0 to 10-kc) differential dc amplifiers.

The central recorder was usually turned on at least 30 min before the start of a system test. This was necessary to load the recorder with recording paper, to allow the mercury-vapor lamp to come up to its normal operating temperature, and to permit the operator to check his incoming signals for their proper deflection. At a normal paper speed of 0.07 in./sec, the recorder could run continuously for 16 hr.

19. Ground Telemetry Subsystem

a. Function. The ground telemetry subsystem (Fig. 345) OSE is to the system test complex what the DSIF and SFOF are to the data handlers and analysts during the actual flight of the mission.

The GTS OSE accepts the spacecraft's composite telemetry signal from the data encoder via a hard wire, from the radio subsystem OSE, or from the GTS OSE tape recorder; the signal is then routed to the data demodulator. The demodulator separates the composite signal into its two channels of synchronization and data recovery. A phase-locked loop is employed by the demodulator to ensure that the demodulator clock is not only at the same frequency but also has the same phase as the spacecraft clock. Once the demodulator's phase-locked loop has been locked, the demodulator begins to compare its locally generated pseudorandom code to the spacecraft preudorandom code recovered from the synchronization channel of the composite telemetry signal; this comparison is made by integrating the output of a phase detector and sampling the output level of the integrator. Once the two pseudorandom codes are correlated,

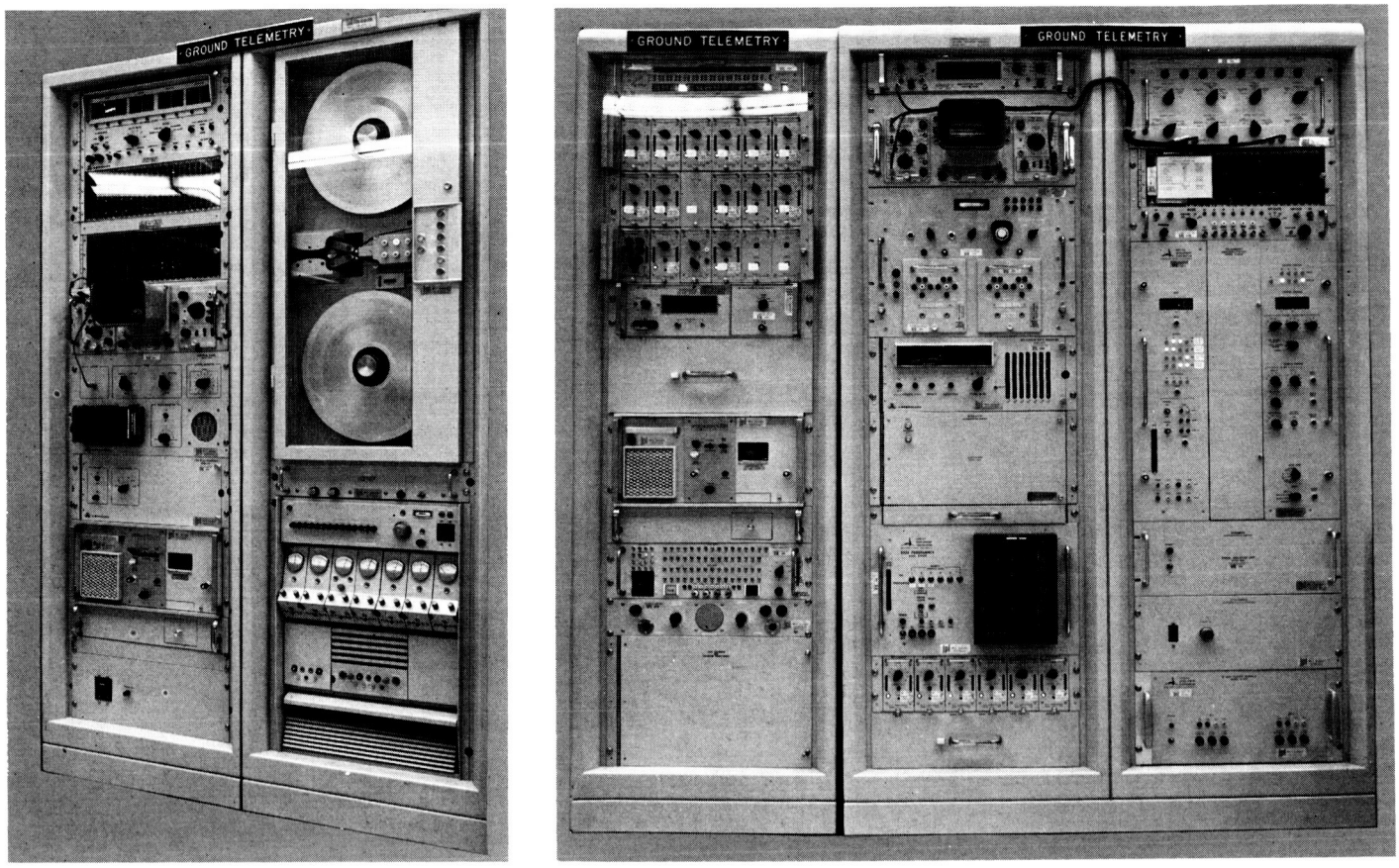


Fig. 345. Ground telemetry subsystem assembly

the demodulator begins to produce bit-synchronizing signals identifying each data bit, and word-synchronizing signals, which are seven-bits long, identifying each telemetry word. In the data channel, the data portion at the composite signal is routed to a phase detector, the output of which is integrated over one-bit time. The output of the integrator serves as the steering pulse for the data flip-flop, which is toggled by bit-synchronizing signals. Thus, the demodulator accepts a composite telemetry signal and, from that, produces digital data, bit-synchronizing signals, and word-synchronizing signals. Data, bit-synchronizing signals, and word-synchronizing signals are routed to the several users, and are also further processed by the GTS.

In the OSE, data, bit- and word-synchronizing signals, as well as the original composite signal are routed to the tape recorder for permanent recording. Data, bit- and word-synchronizing signals are also routed to the data decommutator, in which the serial data are grouped into seven-bit words, and each word is identified with the proper data-encoder channel address. The decommutator is able to properly identify each word by synchronizing itself with the data-encoder commutator; the synchronization is accomplished by detection of a unique synchronizing word located at the beginning of each rate frame. Also, the decommutator generates digital synchronization status signals so that the data users may be aware of the validity of the data.

From the decommutator binary coded decimal data, measurement commands (address signals), read commands, and synchronization status signals are routed to the printer programmer. In addition to the decommutator information, the printer programmer also receives time information including hours, minutes, and seconds. The digital printers accept the information from the printer programmer and provide a printed record of the channel address and its decimal data number with a time tag in hours, minutes, and seconds.

In the normal mode of operation, the GTS receives the NASA 36-bit time code signal from the central timing generator through a timing isolation unit. The GTS time

code translator/generator then translates from this signal the NASA 28-bit dc-level shift code and binary-coded decimal time including days, hours, minutes, and seconds. Whenever the central timing generator becomes inoperative, the GTS translator/generator is switched to the generate mode and it supplies time to the timing isolation unit to distribute to the rest of the STC equipment.

The GTS OSE also has a ground instrumentation facility that consists of 13 Inter-Range Instrumentation Group FM channels, which are recorded on one track of the OSE tape recorder. The VCO's are modulated by critical spacecraft signals and by spacecraft OSE signals; thus, a record of the spacecraft's performance is obtained that adds much greater detail to the information obtainable from the composite telemetry signal. Since the GTS OSE interfaces with almost every other subsystem in the STC, complete isolation is maintained between the GTS and all other subsystems.

b. Design evaluation relative to Mariner *Venus 1962.* The major differences between the GTS OSE of the *Mariner* Mars 1964 project and the *Mariner* Venus 1962 project are: (1) the data demodulator was modified for automatic synchronous acquisition, which reduced the maximum time for demodulator lockup from hours (for *Mariner* Venus) to 4 min (for *Mariner* Mars); (2) the data decommutator was modified to decommutate data for all spacecraft telemetry modes; (3) the encoder simulator was modified to provide digital outputs (i.e., data, bit-, and word-synchronizing signals) thereby allowing the decommutator to be checked without depending on the demodulator; (4) a more reliable digital printer was used; (5) a magnetic tape recorder was made an integral part of the GTS OSE; and (6) the switching unit functions were extended to include even the critical signals; i.e., the composite telemetry signal, which allowed the switching from one source to another without ever dropping demodulator lock (thus, there was no interruption of data to the complex).

c. System performance. Although several problems of a repetitious nature were encountered with the GTS digital printers during the initial months of the STC checkout, these problems were corrected and the printers were proven reliable. Evaluation of the entire GTS OSE revealed that the system was well designed, fabricated, and tested. A total of six engineering change requirements incorporated more desirable changes to the GTS system, and, excluding the many printer problems, relatively few failures occurred in the three sets of GTS OSE during the 5500 hr of accumulated checkout times.

20. Telemetry Processing Subsystem OSE

The overall function of the telemetry processing subsystem OSE is to enable IBM format (digital) recording of the *Mariner* spacecraft television signals. To facilitate a performance check of the various spacecraft subsystems involved in taking, storing, and transmitting the TV pictures, several access points along the signal flow path are brought out for recording. These access points are:

1. The 10.7-kc DAS output
2. The 8⅓-bps tape output
3. The 8⅓-bps ground telemetry OSE output

The TPS OSE isolates all signals and reformats them for transmission onto a pair of coaxial cables. The actual IBM format recording is done on either the Univac 1218 digital computer (part of the computer data subsystem) or an IBM digital translator in the telemetry processing station. While the spacecraft was at JPL for testing, recording was performed at the telemetry processing station; but while it was at AFETR, all recording was performed on the Univac 1218 computer. A program was written for the IBM 7094 so that the IBM-format-recorded TV data could be printed out in tabular form or made into 35-mm slides by the link video film recorder.

D. Launch Complex Equipment

The LCE for the *Mariner* Mars 1964 program consisted essentially of six racks of equipment: two located in the launch pad building immediately beneath the umbilical tower, and four located in the blockhouse. These six racks contained selected elements of most of the subsystems represented in the STC that were required to support the launch operations. In many instances, parallel equipment was available to support the operations in Hangar AO. Many electrical modifications were made to this equipment so that it could operate in the long lines and the high noise levels encountered at the launch complex.

The purpose of the LCE was to set the spacecraft in the launch mode after it was mated to the launch vehicle. Figure 346 is a block diagram of the OSE configuration at both Hangar AO and the explosive safe facility at Cape Kennedy. During spacecraft testing at the explosive safe facility, the spacecraft was connected to the system test complex for monitoring purposes through the RF link only. A connection was made through the umbilical connector to the dummy run trailer, which contained similar equipment to the LCE. When the

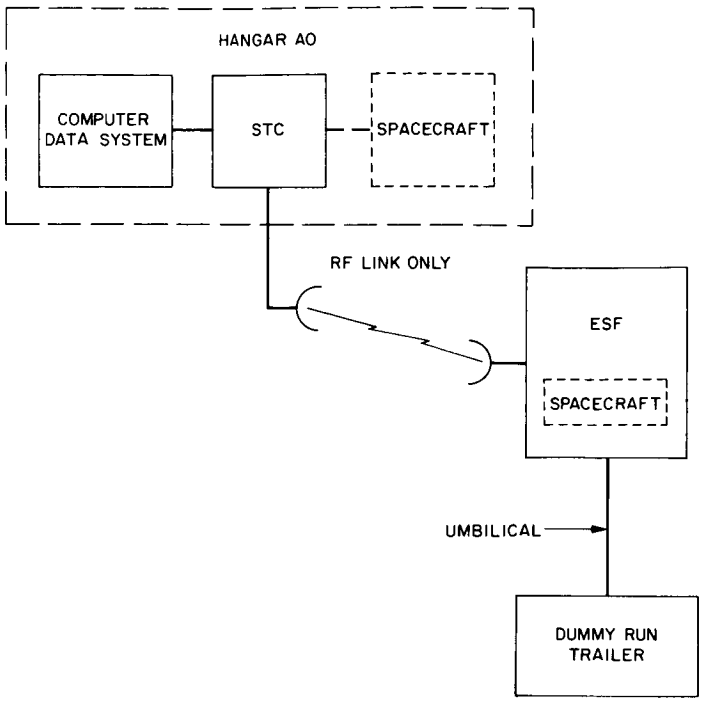


Fig. 346. OSE configuration at Hangar AO and ESF

spacecraft was moved to the launch complex, it was connected to the OSE in the configuration shown in Fig. 347. The parasitic antenna on the shroud provided a means for connecting the spacecraft to the STC through the RF link, using either the antenna on the service tower or the antenna on the umbilical tower. A hard-line RF connection was also made through the umbilical tower and was routed through the launch pad building and the blockhouse to the STC at Hangar AO.

The equipment located in the launch pad building consisted of science OSE, launch support power, and line-driver amplifiers (required because of the long-line cables between the launch pad building and the blockhouse). The blockhouse equipment consisted primarily of power control, data encoder, attitude control, and CC&S OSE subsystems.

1. Launch Support Power OSE

The launch support power OSE (Fig. 348) incorporated those elements of power, monitoring, and control necessary to support the spacecraft power subsystem during the prelaunch operation in the launch complex.

The equipment furnished the basic monitoring and controlling features provided in the system test set, but reflected the constraints and design considerations imposed by the launch operation and site. No automatic data monitoring and recording was provided. The launch control set was distributed over three areas: the blockhouse, the launch pad building, and the umbilical tower.

a. Control panel. The control panel was housed in the blockhouse console and provided the same operator interface as the system test counterpart except that:

1. The control function of solar panel power simulation was not present
2. Recorder electronics *off* control was provided
3. No direct access functions were included

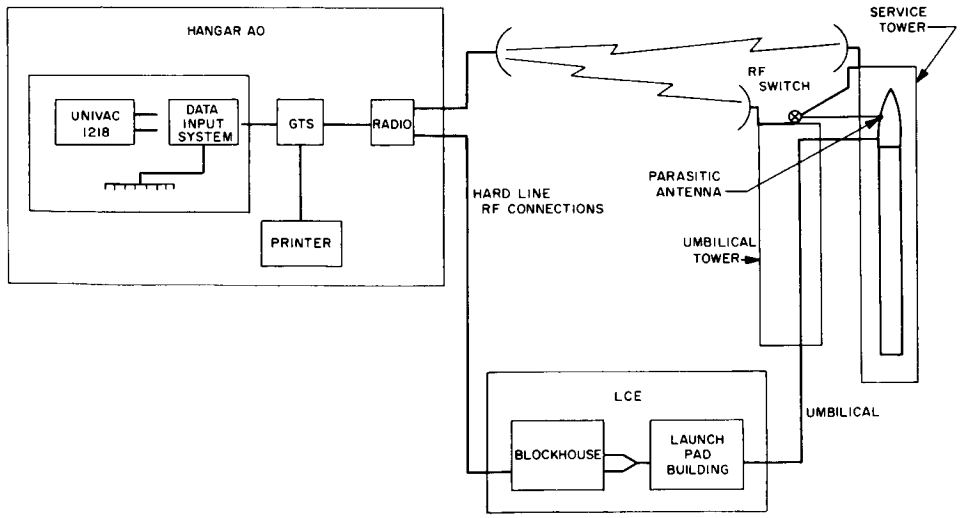


Fig. 347. OSE configuration at launch complex

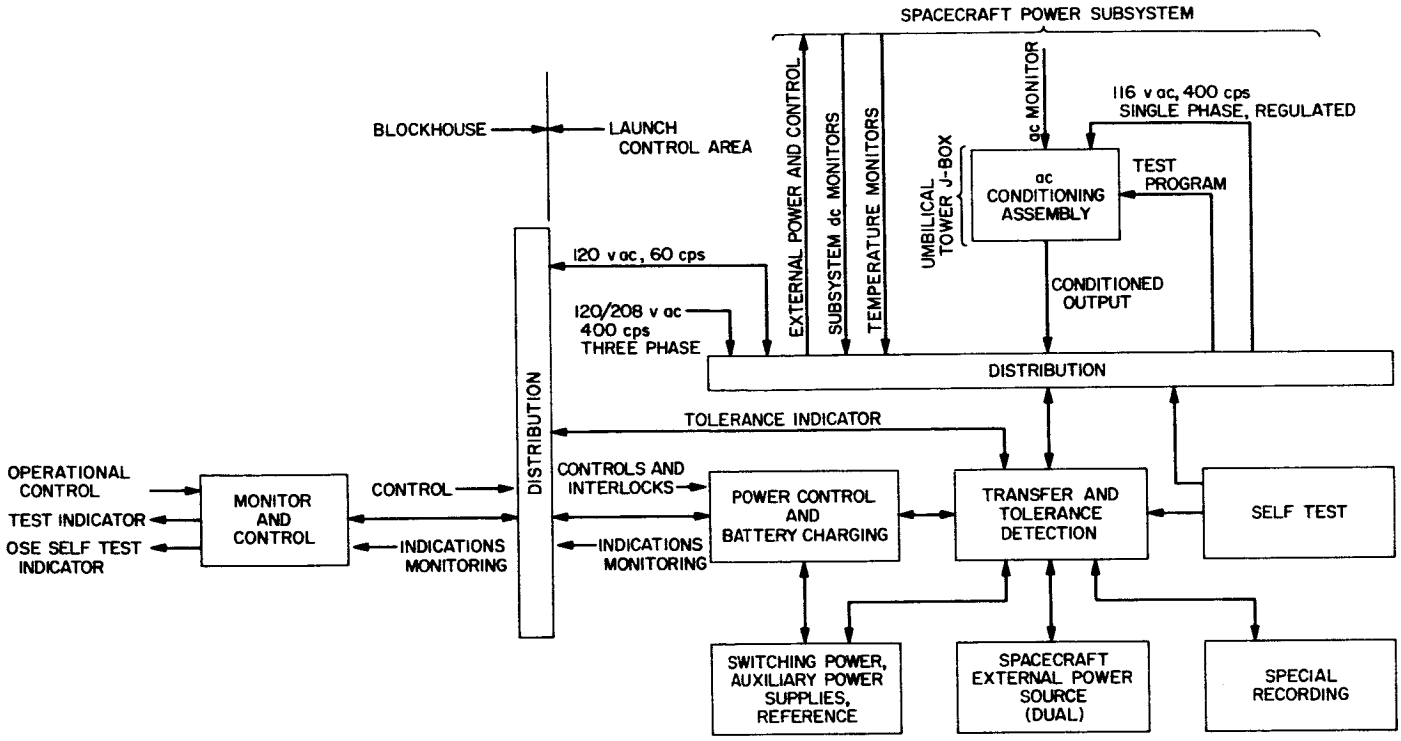


Fig. 348. Launch support power OSE functional block diagram

b. Power monitor and control console. This console, located in the launch pad building, contained the major portion of the LCE. The equipment contained in the power monitor and control console consisted of:

1. Auxiliary power supply assembly, which provided the same features as the system test set auxiliary power supply assembly.
2. Transfer assembly, which provided the same features as the system test set transfer assembly.
3. Self-test assembly, which provided the same features as the system test set self-test assembly.
4. Power control assembly, which provided the necessary control logic and protection for application of external power and battery charging.
5. Dual power source simulator, which served as the adjustable, constant-voltage, current-limited power supply for external power.
6. Power distribution assembly, which was essentially the junction point for distribution of ac power within the LCE. The assembly housed the 60-cps isolation transformer and the 400-cps, single-phase regulator assembly. Metering was provided both for the three-phase and the regulated 400-cps power.
7. The ac conditioner assembly, which was identical to the system test set assembly and was installed in the umbilical tower J-box.

c. Alternating current conditioner assembly. This assembly, contained within the umbilical tower J-box, housed the ac-to-dc conditioner circuits, associated dc power supplies, and the operate/test transfer circuits required for self-test. The assembly was powered from the 120-v, 400-cps regulated source within the power OSE, and was tested as part of the power OSE self-test routine.

The complex waveforms of the spacecraft ac power and the various configurations of OSE test cabling presented transmission problems that made direct monitoring of the pertinent ac voltages unsatisfactory.

The approach used in the *Mariner* Mars 1964 power OSE to reduce transmission problems applied signal conversion or conditioning as close to the spacecraft power system as was permissible. The ac conditioner monitored the spacecraft ac power system voltages, and produced dc output voltages that were directly proportional to the rms value of the monitored ac voltages. These dc voltages were sent to the power OSE monitoring assemblies, where they were monitored continuously

by the tolerance detectors and were periodically sampled by the automatic data monitoring system.

Using conditioners between the spacecraft and OSE monitors required the extension of the power OSE self-test and transfer functions to the conditioner circuits. Power to operate the conditioners also had to be supplied. One of the six conditioner channels is represented in block diagram form in Fig. 349. The ac signal from the spacecraft was connected through a low-capacitance, low-thermal-coefficient cable to the monitor input of the conditioner assembly, and was then connected through the *operate* (or normal) position of the transfer relay to the input of the signal conditioner. The dc output of the conditioner was connected through the power OSE/umbilical J-box cable run to the power OSE monitor circuits. This cable also carried the *test* and *operate* transfer commands to the conditioner circuits and the *test* and *operate* verifying indications back to the OSE. The dc power for the signal conditioner was provided by the transformer-rectifier supply contained within the conditioner assembly. This supply was powered from the regulated 400-cps source within the power OSE through a separate cable. Another cable from the power OSE brought self-test inputs to the conditioner by way of the *test* position of the conditioner transfer relay. The *function* command from the transfer relay was used to program the conditioners, as required, to accept a clipped sine wave as a test voltage.

The conditioner self-test was initiated by the power OSE monitor's test function and was integrated with that function to transfer the ac conditioner's inputs from spacecraft voltages to test voltages that originated in the power OSE self-test assembly. The high, low, and normal test voltages applied to the conditioners substituted for the spacecraft voltage waveforms and, in conjunction with the tolerance detector test logic circuits, provided a check on the performance of the conditioner circuits. In addition, the automatic data monitoring system could be used to display and compare the self-test voltages.

The conditioner assembly housing, was a cast aluminum box, with removable top and bottom cover plates

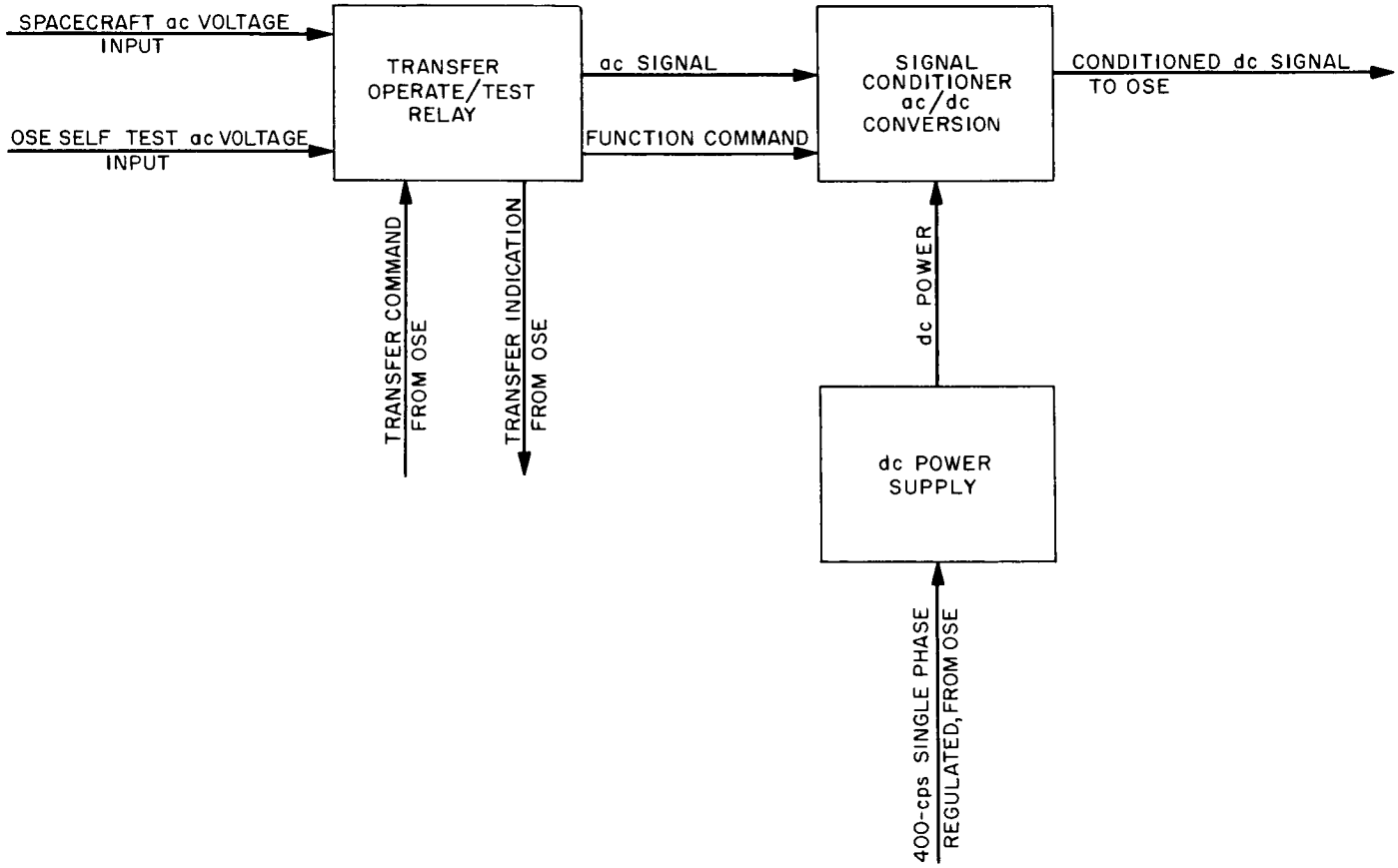


Fig. 349. Typical ac signal conditioning channel block diagram

and gasket seals. Within the housing, all active circuit components were mounted on ten plug-in printed circuit cards of which there were six ac conditioners, two dc power supplies, and two transfer relay assemblies. These cards were held in the sockets by retainer brackets fastened to the top cover plate. A plate recessed in the top face of the housing held 22 test points that permitted monitoring the internal input and output voltages of the conditioner cards.

The conditioner assembly measured approximately 9 in. long, 9 in. wide, 7 in. deep, and weighed approximately 7 lb.

2. LCE Electrical System

The LCE electrical system provided monitoring and control of the spacecraft while it was on the launch pad, and supported certain required prelaunch operations.

The monitoring functions included power and operating criteria not available through telemetry; the control functions included power changeover (external to internal) and certain command functions. Prelaunch operational support included verification of spacecraft flight-ready status by both umbilical and RF monitoring.

3. Delivery and Evaluation

The bulk of the LCE was delivered to SAF in subsystem component form. After complete assembly and checkout using a spacecraft simulator, the LCE was connected to the operational spacecraft and was used during a dummy run operation that verified both the LCE and the spacecraft for prelaunch testing. The LCE and spacecraft were subsequently shipped to Cape Kennedy where the LCE was installed and checked out at the launch complex.

Additional LCE (similarly checked out) was used in support of other testing (e.g., vibration space chamber, explosive safe area), and was housed in a dummy run trailer.

Certain items required only at the Cape (such as power supplies, adapter cables, J-boxes, test coordinator consoles, remote control panels) were sent directly there for installation and checkout, ahead of the majority of the equipment.

Most LCE underwent in-process as well as final inspection at the component level. In addition, an inspection was made of the assembled consoles and dummy run test setup to eliminate last minute inconsistencies and poor workmanship. Operational difficulties were reported as failure reports.

4. Special Equipment

The most critical item of special equipment used as part of the LCE was the spacecraft simulator. The function of the spacecraft simulator was to test the launch complex facility, including the LCE, the launch pad equipment, the blockhouse installation areas, and the umbilical connector interface on the spacecraft. It was the electrical counterpart of the spacecraft, simplified to make it a portable piece of test equipment; it could be carried and operated by one man. The waterproof case was 18 in. wide, 17½ in. high, and 11 in. deep. Cables stored in a compartment located in the lid brought the total weight of the unit to 25 lb. Power voltage sources were independently variable, a capability which was nonexistent in either the spacecraft or other test equipment.

A form of the air-half umbilical receptacle, which was accessible under a hinged door in the case, was mounted in the simulator. To facilitate mounting, the funnel housing was removed. Power connectors and test points were provided under a door on the opposite side of the simulator.

The catenary umbilical launch complex cable could be connected to the simulator, and all OSE functions and operations could be performed as if a spacecraft were being tested. The simulator checked the operation of the cabling and its wire conductivity, the umbilical-tower J-box and amplifier, and the signal condition and operation of each of the OSE subsystems. Calibration adjustments on equipment could be made from signal sources within the simulator.

Other special equipment included: (1) isolation transformer assemblies, which were designed to isolate the individual OSE subsystems from each other as well as from line noise; and (2) line regulators with noise filters, which were designed for such areas as the umbilical tower to minimize the effects of surge transients and noise on the signal conditioning equipment located in that area.

5. Problems and Limitations

A major problem involved in the design of the LCE was the coordination of inputs from a great variety of sources. The unique configuration of the spacecraft system resulted in the final spacecraft configuration (and

subsequently the final LCE configuration) being determined only just before the LCE was needed to support the spacecraft tests.

With the activation of LC 13 for spacecraft use, consideration was given to improving the design of the cable link between the spacecraft and the first JPL equipment interface (umbilical-tower J-box). Although the total cable length between the spacecraft and the umbilical tower J-box was increased from 50 to approximately 87 ft by the new routing of these cables, several advantages were realized and most of the disadvantages were eliminated by a change in individual cable design. The original LC 12 installation required the use of a special cable retractor that pulled the 50-ft catenary (boom) cables clear of the retracting boom during launch. The advantages gained were: (1) a minimum cable length (50 ft) and (2) an installation using the fewest interfaces. The new installation used 75-ft cables permanently routed down the boom (although still replaceable). The added length and extra boom plate interface was compensated for by designing the cables with adequate low-resistance lines for external power and charging functions (no splices), and by including special low-capacitance wiring for critical functions. The remaining link to the spacecraft consisted of a catenary cable approximately 12 ft long, which incorporated all special program requirements between the spacecraft and the boom plate.

The requirement for extensive signal conditioning and amplification of spacecraft signals, and the relatively severe environmental penalties imposed by the umbilical-tower location of the JPL umbilical-tower J-box resulted in a requirement for extensive expansion of the video pair installation at each complex. Six video pair lines were permanently installed between the umbilical tower (JPL J-box area) and the launch pad OSE area (launch-pad-building launch-control shelter in LC 12 and launch pad building first stage vehicle room in LC 13). Also, six lines were installed between the launch complex OSE area and the launch pad building on each complex, where connection could be made to existing terminations of the permanently installed video pair lines routed through the complexes.

In addition to the remote control of JPL-supplied 400-cps generators (as formerly provided for the *Mariner* Venus 1962 Project on LC 12), additional remote control of 60-cps power was provided to support the JPL equipment located on the umbilical tower and in the launch pad OSE. The control panels for these circuits were located in each blockhouse.

E. Mechanical Support Equipment

1. Ground Handling Equipment

The spacecraft ground handling equipment was used during the spacecraft assembly, testing, and handling phases of the program. Because of the nature of the spacecraft design, the ground-handling equipment was highly integrated and optimized on *Mariner* Mars 1964. Experience gained on previous spacecraft programs was applied to the ground-handling equipment design to achieve a system that would maximize operational simplicity and allow safe access to the spacecraft components during all phases of the operations. Special attention was paid to the height of spacecraft equipment. The need for climbing above or crawling under the spacecraft was reduced if not entirely eliminated.

The attention to similar details in the ground handling equipment area significantly contributed to the speed, ease, and safety with which the spacecraft assembly, testing, and handling operations were accomplished.

The following characteristics were considered in the design of the mechanical ground handling equipment:

1. The spacecraft structure relied on the ground handling equipment to provide stiff structural support during ground tests. This stiffness was necessary to maintain the structural alignments and to eliminate unnecessary movement when the spacecraft was at rest during electrical tests.
2. The equipment had to be designed to allow personnel to work with and around it safely and efficiently. To eliminate any personnel or equipment hazards as a result of handling-equipment failures, all the equipment was designed with a safety factor of 5 or greater on ultimate strength, or 3.75 based on yield strength, whichever was greater. In addition, a hazard safety factor of 2 g was applied to these safety factors for all equipment subjected to dynamic loads.
3. The equipment was composed of as few parts as possible. Since floor space was at a premium, the equipment was designed to perform multiple functions. The hardware had to be capable of easy compliance with spacecraft changes and improvements.
4. All handling equipment that might be in the vicinity of the spacecraft had to be capable of being kept clean to prevent contaminating the spacecraft.
5. The hardware had to be made quickly and inexpensively. Development efforts were minimized and

the best available commercial parts were used whenever possible.

The ground handling equipment designed and built for *Mariner* consisted of a universal support ring, spacecraft positioner, dolly, universal ring spacer, transport trailer, hoisting equipment, shipping container and covers, and a purging-control assembly.

a. Universal support ring. The universal support ring (Fig. 350) consisted of a machined ring forging approximately 5 ft in diameter and 12 in. high. This unit supported the spacecraft octagon in approximately the same manner when it was being moved as when it was mated to the booster adapter. The center portion of the U-ring was open to allow access to the spacecraft. The spacecraft rested on eight points on the stable U-ring that were used to restrain the spacecraft base plane and shear lips dimensionally. The spacecraft was mated to the U-ring during most of the tests and operations.

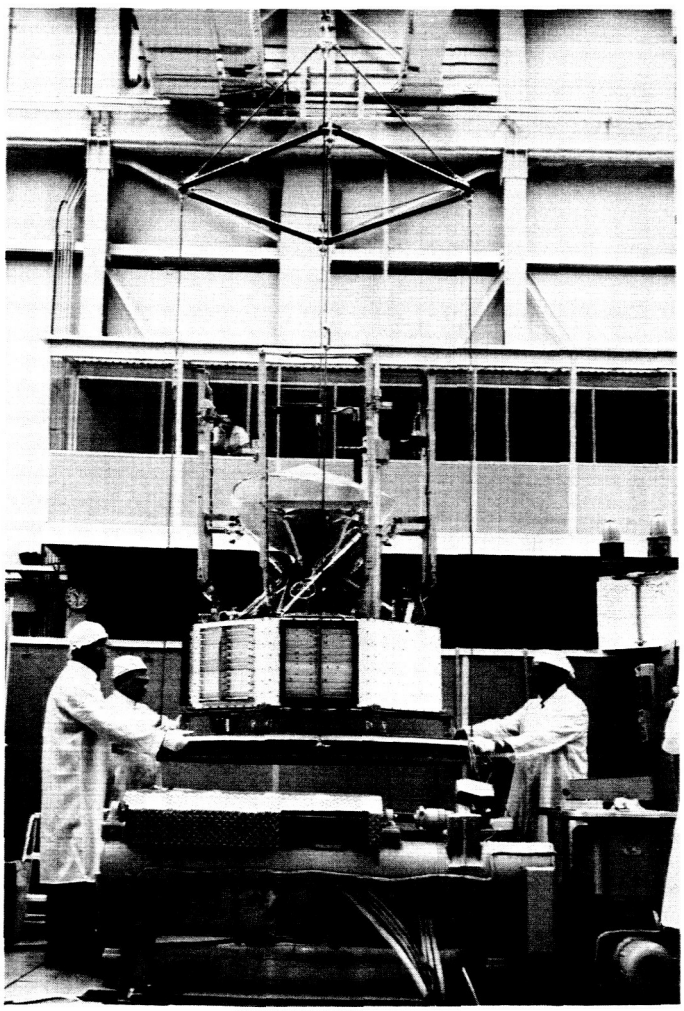


Fig. 350. Universal support ring and hoisting equipment

The universal ring incorporated the following features:

1. A cable that clamped shoes over the spacecraft–U-ring feet. The cable was tensioned by a turnbuckle. The shoes were mounted to the U-ring by a spring-loaded member, which released the shoes when the cable tension was relaxed.
2. Four lifting eyes for the attachment of hoisting cables.
3. Two sponge-rubber pad surfaces: one for sealing the upper shipping-container can, and the other for sealing the lower shipping-cover diaphragm. The sealing surfaces were located inboard of the hoisting eyes. This allowed the spacecraft to be hoisted while in an encapsulated condition.
4. A purging access fitting was provided between the two container sealing surfaces to allow the nitrogen purging hoses to be connected when the shipping cover was in place.
5. Tapped holes were provided on the inside surface of the ring for mounting science-equipment test hardware used during spacecraft electrical tests.
6. Three sockets, spaced 120 deg apart, were provided for the installation of two different sets of support legs. One set, approximately 2 ft long, was used when working access to the base of the spacecraft was required and the spacecraft positioner was unavailable. The other set of legs, about 3 in. long, was used to attach the U-ring to the spacer, dolly, or transport trailer.
7. Four mounting brackets were provided on the outboard side of the U-ring for attaching it to the spacecraft positioner.

b. Spacecraft positioner. The positioner consisted of a steel base frame and the necessary power, control, and drive hardware for tilting and turning the spacecraft. The positioner weighed 5000 lb and was used for the system-test operations and to orient the spacecraft in the most desirable equipment-access position. The tilting axis was capable of placing the spacecraft at a convenient working height at any roll-axis position between the vertical and the horizontal. Figure 351 shows the spacecraft on the positioner in a near-horizontal attitude. The rotational drive was capable of turning the spacecraft 350 deg about the roll axis. The U-ring was bolted

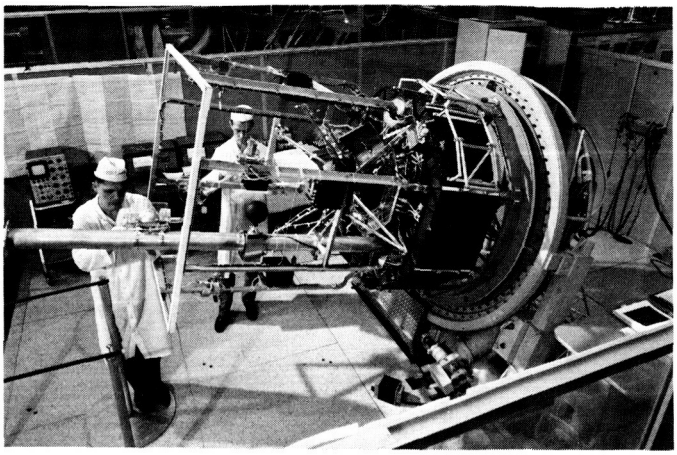


Fig. 351. Spacecraft attitude on positioner

to the turntable ring, which was open to allow equipment access. As many as six technicians could work on the spacecraft at the same time without interfering with each other.

c. Dolly. The dolly consisted of a circular channel, about 5 ft in diameter, to which the three U-ring support legs attached. Four swiveled casters were bolted to the bottom of the dolly; each dolly caster was equipped with a brake. The dolly was used for moving the spacecraft about any shop area. The flight adapter and its ground handling support ring could also be mounted to the dolly.

d. Spacer. A triangular spacer was built to raise the spacecraft, when it was mounted on the dolly, to an optimum working height. It attached to the dolly or trailer in the same manner the U-ring did.

e. Transport trailers. The transport trailer was used for intershop or interarea spacecraft transport. The flight spacecraft were mounted on these trailers when they were shipped in electronics vans (Fig. 352). The flight adapter, encapsulated spacecraft, and shroud were mounted on the transport trailers and towed to the pad by pickup truck. The trailers were constructed of aluminum frame covered with an aluminum flooring. The wheel base was 87 in. had a tread width of 74 in. and had a road clearance of only 7 in. The trailer was high enough to clear the ramp when it was loaded in the shipping van, but low enough to allow the spacecraft to be loaded into low-overhead clearance vans and to provide access to the spacecraft during the final assembly and shroud mating operations.

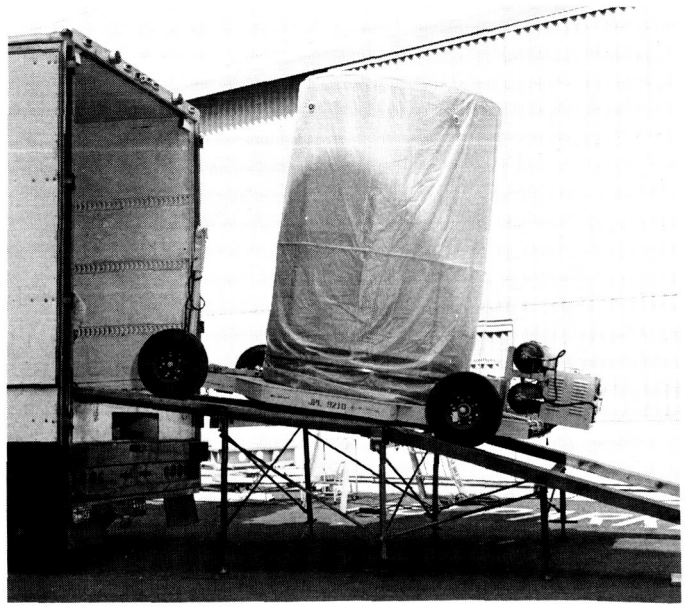


Fig. 352. Spacecraft mounted on transport trailer for shipment

Maximum maneuverability was obtained by the use of a special front end that allowed the wheels to be turned ±85 deg. Special storage containers and racks for supporting nitrogen purge tanks were mounted on the back of the trailer. The purging box was mounted on the back of the trailer during transport. There were no trailer springs; the "soft ride" was dependent on low-pressure standard automobile tires.

f. Hoisting equipment. The hoisting equipment (Fig. 350) consisted of a flexible spreader frame that held four cables out from the lifting hook. Four easily removable cables were attached to the spreader frame. The flexible frame ensured constant tension in each of the four lifting cables. Late in the program, a plastic sheet was mounted to the frame to catch any debris that might fall from the hoist drive or trolley system. Occasionally, because of short crane heights, a set of special, short hoist cables had to be used to lift the spacecraft.

g. Shipping containers. When the spacecraft was moved around JPL or Cape Kennedy, or shipped across country, special shipping-container hardware was required. This hardware consisted of a diaphragm to lower the spacecraft, a perforated cylinder, a perforated cylinder extension, a top cover diaphragm, and a shipping bag.

The lower diaphragm was used to seal off the bottom of the spacecraft. It was made of a heavy sheet of vinyl material, and was attached to a ring that was bolted to

the inner base of the U-ring. A seal was provided by a rubber gasket.

The perforated cylinder was mounted over the spacecraft. It bolted to a flange on the U-ring and was perforated to allow the spacecraft–cylinder clearances to be viewed as the cylinder was lowered. It also kept the shipping bag from touching the spacecraft. It was used when the spacecraft was shipped with the solar panels and low-gain antenna removed. Shipping van internal heights did not permit the spacecraft to be shipped completely assembled. Lifting hooks were provided at the base to allow the cylinder and shipping cover to be easily lifted.

The perforated cylinder extension was also constructed of perforated aluminum. It was bolted to the top of the perforated cylinder, and afforded protection to the completely assembled spacecraft.

The top cover diaphragm bolted to either the perforated cylinder, if the spacecraft was shipped by van, or to the cylinder extension, if the complete spacecraft was moved or stored. It was fabricated from aluminum and protected the top of the spacecraft. It also supported the shipping bag, and acted as a baffle when purging gas was introduced through the top.

The shipping bag was fabricated from thick translucent vinyl plastic, and fit over the perforated cylinder and cylinder extension. When the spacecraft was shipped in a van and the extension removed, the excess bag material was gathered and taped to the top diaphragm. A purging opening was provided at the top of the bag. The bag was sealed at the base against a rubber gasket around the U-ring and was squeezed against the seal by a tension band.

h. Purging-control assembly. A special purging-control assembly was used to purge the spacecraft when it was either under the shipping bag or flight shroud. The purging assembly accepted high-pressure nitrogen gas and contained a filter, a pressure regulator, a valve, a flow meter that could read flow rates between 2 and 200 ft^3/min, a humidity indicator, and an outlet pressure gauge that measured pressure in the spacecraft cavity.

2. Magnetometer Mapping Fixture

The Magnetometer test fixture was used to support the complete spacecraft, less solar panels, when the spacecraft magnetic field was mapped. It was a massive device

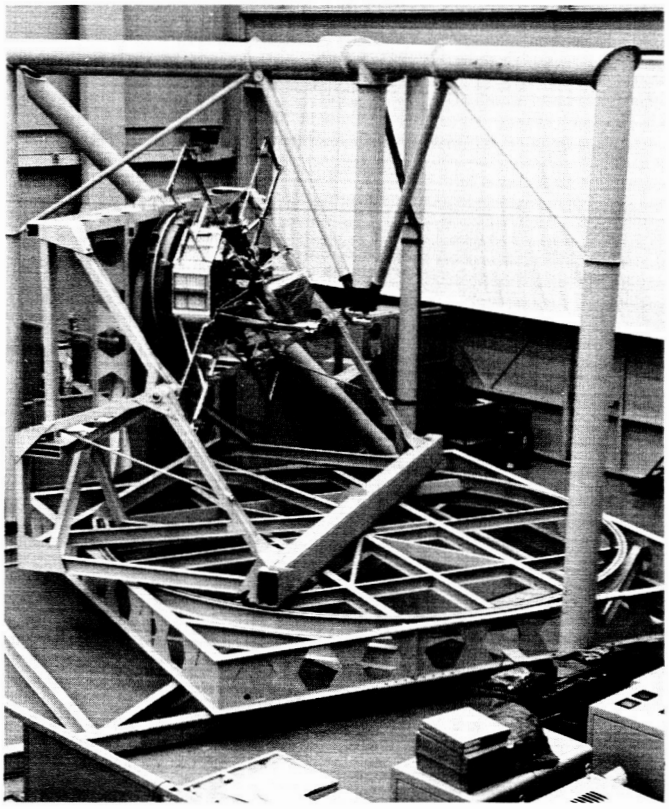


Fig. 353. Magnetometer mapping fixture

(Fig. 353) to accommodate rotation of the complete spacecraft around the flight Magnetometer location and transverse movement under a test magnetometer probe. The test fixture was fabricated from lightweight, nonmagnetic aluminum.

a. Design description. The Magnetometer test probe support consisted of a 20-ft-high by 20-ft-wide stiff tripod assembly, which accurately located the test probe at the flight Magnetometer sensor location. It was fabricated from large-diameter thin-wall aluminum tubing. A horizontal test fixture contained a turntable capable of rotating the spacecraft about an axis through the probe and normal to the ground. Since the magnetometer sensor was located near the top of the spacecraft, this turntable was necessarily large to meet the rotation criteria. The test fixture was fabricated from aluminum I-beams and channels. A vertical turntable was mounted on the horizontal turntable. The spacecraft was mounted to the vertical turntable by the U-ring. The rotational axis was displaced from the spacecraft roll axis to allow the spacecraft to be rotated about an axis through the sensor probe and parallel to the ground. The vertical turntable was gimballed to allow the spacecraft

to be mated in the normal attitude. Seventy feet of track was provided, which allowed the horizontal turntable and spacecraft to be translated under the probe sensor.

b. Design features. The fixture allowed the spacecraft to be rotated and displaced about any axis through the magnetometer sensor. The structure was light enough that all operations could be done manually. It was portable enough that it could be assembled or disassembled within a day and stowed in two large moving vans.

This lightweight rigid structure was achieved through the use of aircraft jig practice backed up by conservative stress analysis. The total deflections were less than 0.125 in., and the displacements were repeatable to within 0.010 in.

XX. ENVIRONMENTAL AND LIFE TESTS

The information presented in this section covers the environmental type-approval, flight-acceptance, and special developmental tests performed at both the system and subsystem levels. The information presented is sketchy compared to the wealth of data available from the 30 to 40 full-scale tests and some 1675 subsystem tests. A short discussion about an individual test in this section represents the condensation of a detailed test report averaging 200 to 300 pages long.

Any adequate discussion of the environmental testing program requires the inclusion of failure information. The fact that these tests could uncover weaknesses in both the design and fabrication of the equipment, so that these weaknesses could be, in most cases, eliminated or reduced prior to flight, indicates that the test program performed a vital function and contributed significantly to the success of the mission.

The report is necessarily critical of the complete test program, the object being to uncover faults and weaknesses in its planning, reporting, and implementation. It is not intended to detract from the success of the undertaking; it is intended to present an assessment of the adequacy of the environmental test program and to point toward the obvious steps that would benefit future spacecraft programs.

Spanning more than 2 years of spacecraft development, the testing program represents a significant stride in the Laboratory's progress in spacecraft development. Experience was acquired in the use of the type-approval test to detect potentially damaging problems. Unlike *Mariner* Venus 1962, the *Mariner* Mars 1964 program was geared to the type-approval test. Analyses of the problems uncovered and the success of *Mariner IV* indicate the soundness of this philosophy. A summary of the system-level environmental test program problems and innovations is shown in Table 65.

The environmental test program was established by a Project Office requirement for flight acceptance testing of all PTM, flight, and spare spacecraft equipment, and type-approval testing of one complete set of prototype spacecraft equipment. All equipment was required to pass the tests before being considered acceptable for flight. Establishment of the criteria for acceptance in these test programs was the responsibility of the Spacecraft System Manager. The TA and FA tests, with separate and distinct functions, are considered to be the principal and formal test program of the *Mariner* Mars 1964 Project. The type approval environmental tests were intended to verify designs. They were intentionally severe to compensate for material and fabrication differences in flight hardware. The flight acceptance environmental tests were intended to be as severe as the expected flight conditions and to define certification of readiness for flight. It was assumed that when a prototype survived the TA testing, the flight hardware, which was constructed to the same design, would be capable of performing its mission.

Table 65. System-level environmental test problems and innovations

Problem	Test	
	TA	FA
Interface problems resolved through system environmental tests	3	3
Piece-part changes that should have been detected at assembly level	1	2
Failures in structure or piece-parts that could only be detected at system level	3	1
Changes indicating need for closer monitoring of major systems	1	2

In general, assembly TA testing provided qualification against environments that were independent of the spacecraft, such as humidity, static acceleration, and explosive atmosphere. However, the assembly and system designs required further qualification against such spacecraft interacted environments as shock, vibration, thermal–vacuum conditions, and environmental RF radiation. In the selection of these tests, emphasis was placed on environmental interactions rather than on performance interactions. Protection against performance interactions was provided by the assembly-level performance test, in which the assembly was monitored against specification requirements, and by assembly and subassembly margin testing. In addition to providing design qualification, the PTM tests (and assorted system-level mockup tests) provided environmental data to increase the confidence in the adequacy of assembly-level tests and to identify deficiencies.

The assembly-level FA tests were limited to two environments in which equipment operation could be evaluated and that could be simulated in a well controlled manner. Passage of the FA tests demonstrated the ability of the equipment to perform satisfactorily in these selected environments at levels at least as severe as flight. This information together with the performance tests and inspection results provided implicit evidence that the FA equipment was similar to the TA equipment and thus capable of performing in all environments.

In accordance with the project policies and requirements, environmental requirements in the form of system and subsystem general specifications for TA and FA tests were established at an early date in the program. Each cognizant hardware division then performed its testing in accordance with a specific environmental test specification and in a manner consistent with the intent of the general environmental specification and the appropriateness for each item. This approved test specification or a waiver was required prior to the performance of any formal environmental test. The complete test program covered such wide and diverse environments as vibration, shock, EMI, temperature cycling and extremes, humidity, explosive atmosphere and magnetic field effects.

Emphasis is placed on deficient environmental tests, problems, failure trends, and oversights. The inclusion of failure information in this document is indicative of the adequacy of the environmental testing program. Wherever possible, the relation between a failure and an environmental test is pointed out. However, when viewed in relation to the scope of the total program, these data represent a high quality of performance for both the hardware and the test operations.

The limited number of problems encountered during spacecraft flight acceptance testing and the successful launch and midcourse maneuver of *Mariner IV* attest to the adequacy of the system-level TA and subsystem-level TA and FA testing. A total of 83 design changes was documented as a result of assembly-level tests. Of these, 39 originated at the TA level, 14 at the FA level, and 30 during other environmental tests. The majority of the changes instituted during FA-level testing were due to schedule slips, which necessitated running FA tests prior to or concurrently with TA tests. On an ideal schedule, the TA testing would have demonstrated the need for the design change before flight hardware was fabricated. A performance comparison between subsystem TA and FA vibration tests in the two most critical environments (vibration and thermal–vacuum) is given in Table 66.

Table 66. Assembly-level vibration vs thermal–vacuum performance

Test	Environment								Overall failure rate, %
	Vibration				Thermal–vacuum				
	No. of tests	Pass	Fail	Failure rate, %	No. of tests	Pass	Fail	Failure rate, %	
TA	244	214	30	12.3	95	76	19	20.0	14.5
FA	538	512	26	4.8	310	282	28	9.0	6.3

The fact that the overall subsystem FA failure rate was less than one half the failure rate of the more severe TA environment points out the effectiveness of the TA testing and its ability to uncover flaws or the need for design changes or improvements.

The failure rate on the flight configuration subsystems was less than 3% after deleting failures of parts that were eliminated by retrofit or the incorporation of engineering change requests. This would have been the expected failure rate if TA testing had been completed prior to the start of the FA testing. It is also noted that preacceptance screening was effective in reducing part failures.

The environmental test program definitely effected an improvement in the design and quality of the equipment flown. The trend of improvement between TA and FA testing is evidenced by the reduction in failure rate shown in Table 66. The improvement in equipment quality can more readily be seen by comparison of the number of failures encountered in subsystem testing with those encountered in system testing. (Over half of the assemblies tested were later subjected to FA system-level environmental tests.) The improvement is even more striking when it is realized that only three of the 16 failures in system-level tests appear to have been amenable to detection at the assembly level. The remainder were associated with environmental interactions or ancillary equipment unsuitable for assembly tests.

In the area of magnetics control, the limitations of a tight schedule and the use of hardware developed in previous spacecraft programs, such as *Ranger* and *Mariner* Venus 1962, made it impractical to substitute nonmagnetic items for the reliability of the tested and tried hardware. Since magnetics control efforts were rather new, there was a period of evolution and development, and a firm program was not established with sufficient lead time to achieve optimum results. Significant

strides have been made in the field of magnetics control, however, and a great deal of knowledge and experience has been acquired. Specifically,

1. Particular magnetic problem areas were identified
2. A materials study was conducted to categorize 147 spacecraft materials into the classifications of magnetic, nonmagnetic, and borderline materials
3. Magnetic shielding materials and techniques were investigated for several particular applications
4. Demagnetization of solar panels was successfully conducted and a limited study of this technique made

The importance of completing TA environmental testing early in a project cannot be overemphasized. Accomplishing required design revisions prior to FA testing saves expensive retrofit and retesting, and allows increased environmental exposure of flight hardware. Design changes originating as a result of FA test problems sometimes paralleled identical problems arising in a concurrent TA test. This occurred, for example, in the DAS and in the Cosmic Dust Detector.

During the TA testing program for subsystems, no failures were experienced in the following tests:

1. Bench handling
2. Transportation vibration
3. Static acceleration
4. Package drop
5. Explosive atmosphere

Each of these tests will be reviewed on future programs with a view to deleting them or to limiting them to specific hardware items whose testing may be expected to yield meaningful results. Elimination of these tests could permit more time and care to be devoted to the test areas that have demonstrated a failure pattern.

There were no subsystem humidity test failures after the maximum humidity was reduced from 95 to 75% by an amendment to the general specification. However, some of the original failures might have occurred at the lower humidity levels, since the failed modules had defective conformal coating. It appears desirable, therefore, to retain this test for future programs, since it has shown the capacity to sort out design weaknesses and workmanship defects. Some thought, however, should be given to the use of a modified humidity test for flight acceptance.

The *Mariner* Mars 1964 spacecraft equipment was subjected to an orderly and conservative environmental test program. Clearly defined general testing requirements enabled attention to be focused on potentially damaging problems, and contributed to the timely accomplishment of the test program. Satisfactory completion of the testing activity permitted Project Office management to approach the launch with confidence in the environmental integrity of the spacecraft.

From the data accumulated in this program, a number of conclusions (or observations) can be drawn:

1. Many categories (or types) of the TA environmental tests caused no failures. This provided a strong implication that if a unit passed certain key environmental tests, it would pass all tests. Complex wave vibration and thermal–vacuum were the key tests. It is reasonable to assume that a minimum TA environmental test program for *Mariner* could have deleted all the handling environments, explosive atmosphere, and static acceleration tests and still have produced quality hardware, provided operational restraints such as shipping containers and conformal coating were substituted. Dropping all tests but thermal–vacuum and vibration is not advocated; however, it is suggested that by purposefully structuring key tests and acknowledging operational constraints, it seems reasonable to discontinue less productive tests.
2. The shock test resulted in three failures, all of which were latching relay malfunctions. (There were no relay malfunctions during vibration.) Although this represented a small failure rate, it indicated possible fragility of latching relays in a shock environment. Although the mechanism of failure was not fully understood, it appeared to be related to workmanship. Lengthy tests were run on a large number of samples to determine if the relays continually degraded with repetitive shocks; a few failed initially, but it was not until about the forty-fifth test that consistent failures occurred, at which time the entire sampling began to show degradation.
3. Of the 55 FA test failures, 14 resulted in redesign. Ten of these 14 tests had not been preceded by TA testing. Four failures were identical on each of the 4 flight units of one subsystem. The nature of the failure was very subtle, and it was felt that the same anomaly should have been seen during the TA

testing. Discounting these 4 FA failures, all 10 of the FA environmental test failures that resulted in redesign had one thing in common: TA testing had not yet occurred.

4. Vacuum tubes (specifically photomultiplier and vidicon) represented a vulnerable vibration soft-spot. Neither of the final *Mariner* fixes (ruggedizing in one application, isolating in the other) would have been difficult in the initial design, had every vacuum tube application been viewed from the very outset as a vibration problem amenable to solution.
5. The 13 workmanship errors detected during TA environmental testing indicate the need for a pre-type-approval test.
6. The failures detected during system level environmental testing illustrate certain unavoidable deficiencies in the assembly-level testing: some units (such as spacecraft cabling) are not amenable to assembly-level tests; subsystem environmental interactions cannot be simulated nor controlled; and degradations can occur between assembly-level flight acceptance and final incorporation into a spacecraft. System-level testing is the only solution for such problems.

A. System-level Environmental Tests

The philosophy used to establish the *Mariner* Mars 1964 environmental test requirements was that the system configuration provide the only true mechanical, thermal, and electrical environment and interactions for the various spacecraft equipment. Due to the state-of-the-art in estimating the effects of various inputs on a highly complex system such as *Mariner*, and in order to ascertain subsystem influences and, thus, to fortify assembly-level test requirements, there was an unavoidable requirement for an early system test. In general, the static environments, such as thermal soak and linear acceleration, were independent of assembly-level testing and could be readily achieved on the subsystem level. However, the dynamic environments (such as vibration, thermal–vacuum, and RFI-produced environmental interactions) were quite dependent upon the response characteristics of the total vehicle, and were, therefore, best achieved at the system level.

The system-level test requirements for *Mariner* were based on the established JPL policy of setting flight-acceptance test levels at the 95-percentile values of the flight environment, and the type-approval tests at a more severe level (in excess of the 99-percentile value), so that definition of the environment was possible. For example, the FA vibration spectra were established from *Ranger* data by generously enveloping the 95-percentile level in 50-cps bands. Test duration was set equal to the time that the wideband vibration level was within 10 db of the maximum. Such a test obviously involves a more severe environment than would be encountered on any one flight; however, experience has indicated that there is usually one peak in the power spectral density from a flight measurement that is within 3 db of the test level constructed in this manner. A detailed discussion of the method of estimating the expected launch dynamic environment is reported in Ref. 34.

Type-approval testing at the system level was performed on the PTM. The program consisted of full-scale vibration, shock, acoustic, space-simulation and thermal–vacuum, and EMI tests. Flight-acceptance testing was performed on each of the flight-quality spacecraft (MC-2, MC-3, and MC-4) for such environments as vibration, thermal–vacuum, and EMI.

Magnetics evaluation was not performed at the system level. Procedures were developed, however, for mapping the spacecraft with the solar panels removed and for mapping the individual solar panels. The information gained in these mappings was used primarily in interpreting the data furnished by the flight magnetometer and not to satisfy an environmental requirement. Some attempt was made to estimate the total spacecraft field from the fields of the various assemblies and to correlate this resultant field with the results of the mappings described above. It is expected that requirements for future magnetometer-carrying spacecraft will contain restraints for magnetics evaluation on the system level as well as on the assembly or subassembly level.

1. System-level TA Testing

The purpose of the system-level TA environmental testing (demonstrating design adequacy of the vehicle in its most representative test configuration) was logically achieved by evaluating the expected environment and then prescribing tests that were a practical compromise between realism and economy. The qualification tests proved the design adequacy, and demonstrated (with a margin) a minimum level of equipment capability. To compensate for the statistical limitations of the small number of samples, and to provide insurance in the location of faults and inadequacies, the imposed test conditions were, by selection, more severe than the operational conditions. They were not, however, intended to be so severe as to exceed reasonable safety limits or to excite unrealistic failure modes. The system-level test requirements for *Mariner* are given in Table 67.

Table 67. System-level environmental test requirements

Test	TA level	FA level
Space Simulator		
Part I: System validation for launch through encounter and playback	10 days at 10^{-5} mm Hg (or less)	250 hr at 10^{-5} mm Hg (or less)
Part II: Temperature control verification	108 hr at 30 to 134 w Simulated solar intensity	134 hr at 30 to 134 w Simulated solar intensity
Sinusoidal vibration	Roll axis 5 to 15 cps, 1.5 g rms for 1.6 min 15 to 450 cps, 1.5 g rms for 4.8 min 450 to 800 cps, 5.0 g rms for 0.8 min 800 to 2000 cps, 10.0 g rms for 1.3 min Reverse sweep (from 2000 to 5 cps)	Roll axis 20 to 200 to 20 cps, 0.5 g rms for 3¼ min Two lateral axes 20 to 200 to 20 cps, 0.5 g rms for 3¼ min per axis
	Three lateral axes 5 to 150 cps, 0.75 g rms for 4.9 min 150 to 450 cps, 1.25 g rms for 1.5 min 450 to 800 cps, 5.00 g rms for 0.8 min 800 to 2000 cps, 10.00 g rms for 1.3 min Reverse sweep (from 2000 to 5 cps)	Not Applicable
Noise vibration	Roll axis and three lateral axes Shaped spectra, 18.1 g rms overall 550 to 2000 cps, 0.2 g^2/cps for 3.0 min 3 db/octave roll-off below 550 cps	Roll axis and two lateral axes Shaped spectra, 10.7 g rms overall 550 to 2000 cps, 0.07 g^2/cps for 1.0 min 3 db/octave roll-off below 550 cps
Torsional vibration	Two 69 cps pulses, 205 rad/sec^2 for 0.14 sec 20 to 150 to 20 cps, 12.86 rad/sec^2 for 6.0 min 50 to 150 to 50 cps, 154 rad/sec^2 for 11.0 min	Not Applicable
Acoustic	Approximately 142 db shaped spectrum for 90 sec	
Shock	Shroud V-band release firing Spacecraft separation and V-band release firing All spacecraft pyrotechnics fired	All spacecraft pyrotechnics fired
Electromagnetic interference (RF susceptibility)	Launch complex RF *Agena* telemetry RF C-band beacon	Launch complex RF *Agena* telemetry RF C-band beacon

a. Dynamic tests. The objective of the dynamic testing was to demonstrate the integrity of the spacecraft for the deleterious effects of the launch dynamic environment. An attempt was made to follow a consistent instrumentation schedule throughout the series of dynamic tests.

Vibration tests. The PTM was subjected to sinusoidal vibration excitation along its roll axis Z, and along each of three lateral axes, X, XY Bay II, and XY Bay VIII, at frequencies between 5 and 2000 cps for a total of about 17 min per axis (Fig. 354). The selection of three specific lateral axes was based on an assessment of the critical geometric orientations of spacecraft internal components to ensure excitation of these elements in their maximum response modes. The test levels are shown in Table 68.

Table 68. Vibration test levels

Frequency cps	Frequency sweep time min	Acceleration amplitude, g rms	
		Roll axis	Lateral axes
5 to 15	1.6	1.5	0.75
15 to 150	3.5	1.5	0.75
150 to 450	4.8	1.5	1.25
450 to 800	0.8	5.0	5.0
800 to 2000	1.3	10.0	10.0

The frequency sweep rate for sinusoidal vibration tests was 1 min per octave.

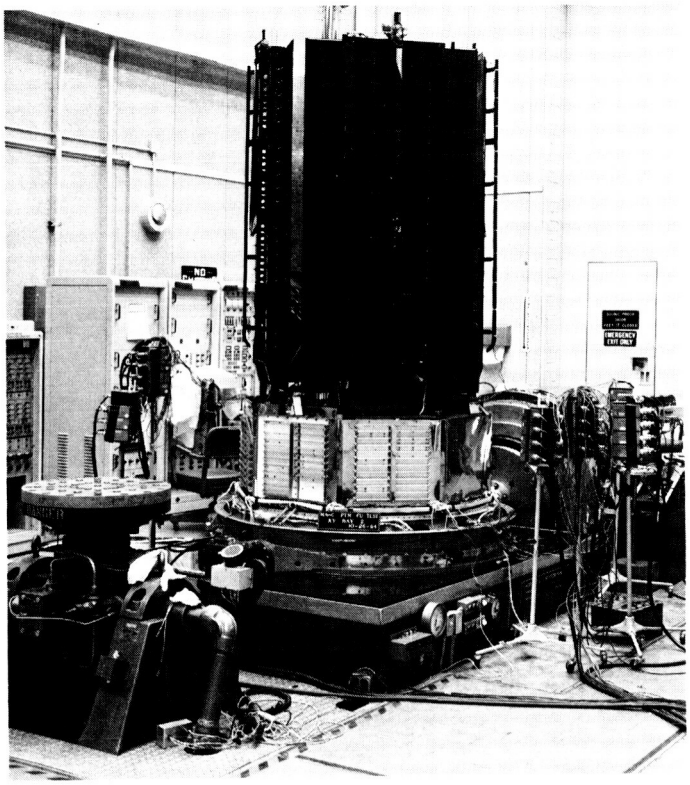


Fig. 354. PTM subjected to lateral vibration testing

Following each period of sinusoidal excitation, the spacecraft was subjected to random noise vibration for 3 min per axis. The test, which consisted of a programmed sequence of bandlimited Gaussian noise, was executed by means of a magnetic tape recording. Type-approval and FA noise spectra are illustrated in Fig. 355. Some 39 data points were monitored during the series of vibration tests. As evidence of testing adequacy, Fig. 356 through 358 present the input control and a response measurement from a typical test.

After completion of linear sinusoidal and random vibration, the spacecraft was subjected to a torsional sweep sine wave excitation and a transient sine wave

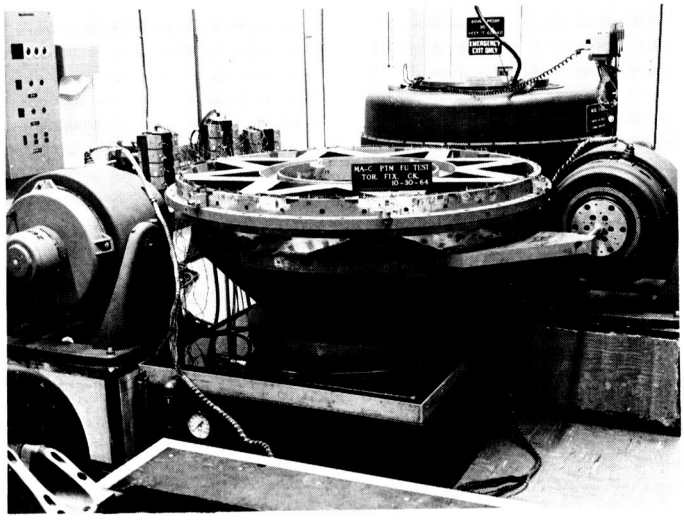


Fig. 356. PTM torsion test setup before installation of spacecraft adapter

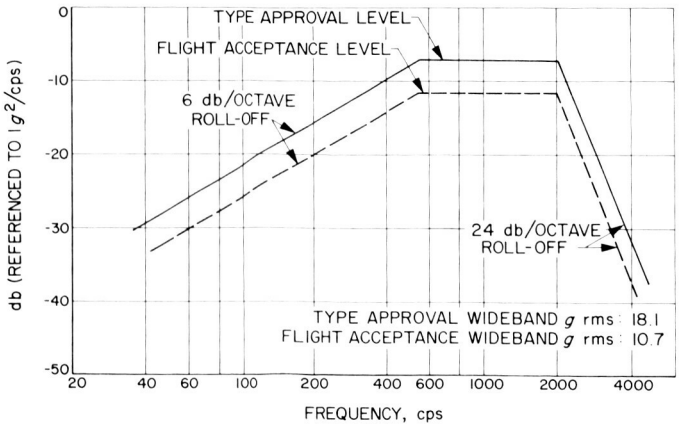


Fig. 355. TA and FA random noise spectra

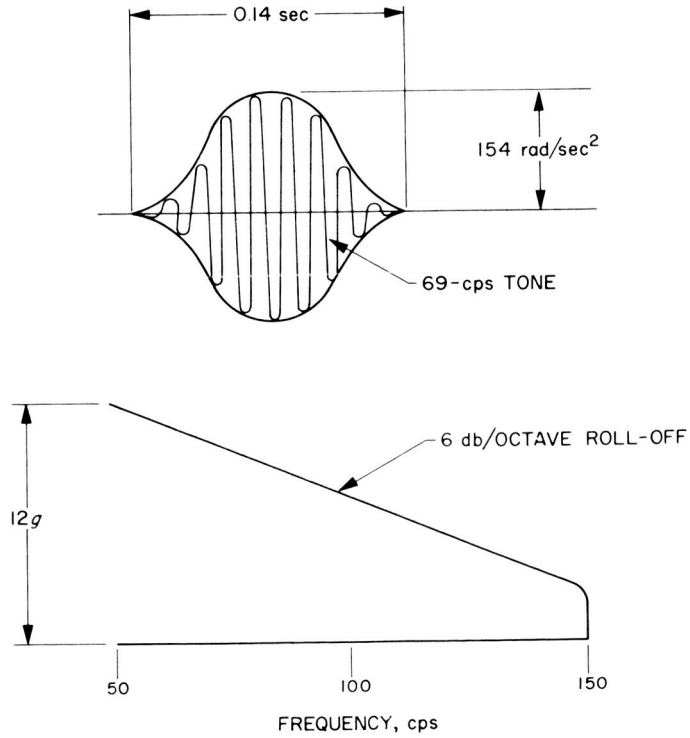


Fig. 357. PTM swept torsional spectrum

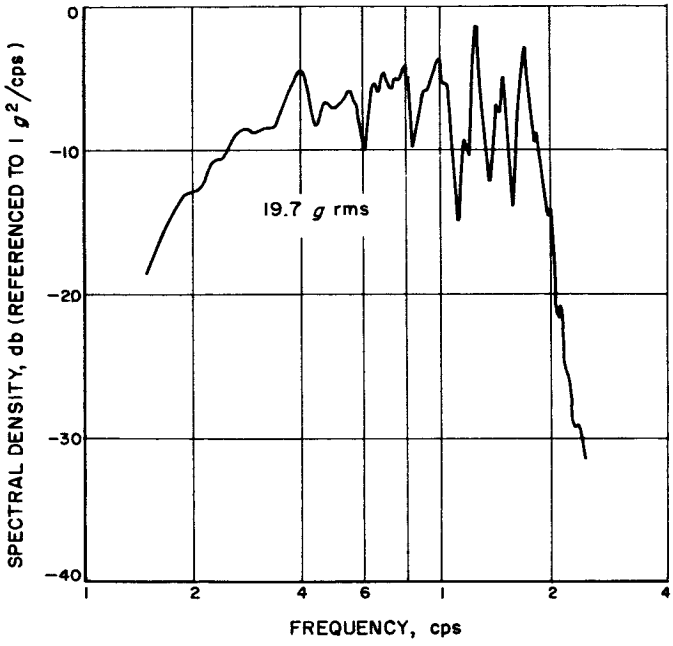


Fig. 358. Typical input spectrum, PTM roll axis noise test

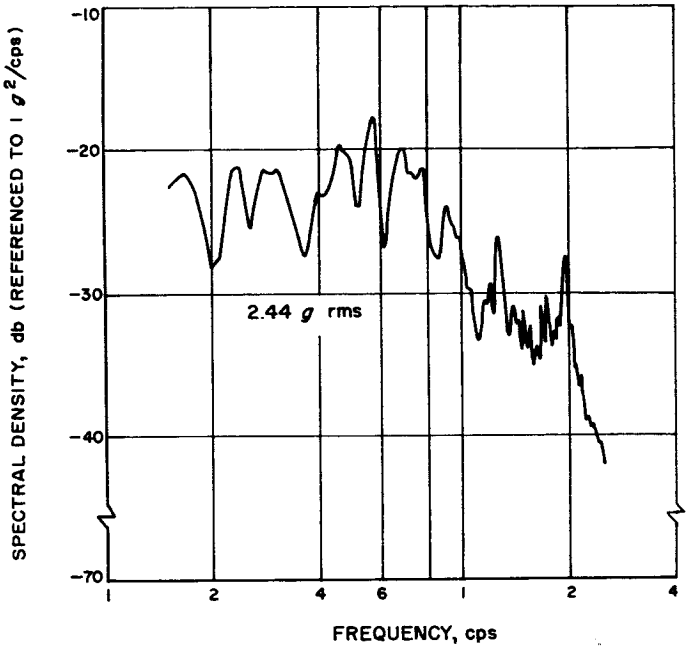


Fig. 359. Typical response spectra, spacecraft flight transducer to PTM roll axis noise test

pulse input about its roll axis, in accordance with the schedule shown in Table 69. These tests were intended to demonstrate integrity for the staging torsional transients and to determine the torsional impedance of the vehicle (Fig. 359 and 360).

Due to some problems encountered in the first series of PTM tests, and in order to demonstrate a high level of confidence that the flight vehicles were unaffected by testing anomalies experienced during their FA tests, a retest was scheduled. However, due to test facility and

Table 69. Roll axis sine-wave inputs

Frequency, cps	Frequency sweep time	Angular acceleration rad/sec²	Remarks
69	0.14 sec	205	Amplitude modulated tone
20 to 150 to 20	3.0 min	12.86	Torsional sweep
50 to 150	5.5 sec	154	Rolled-off spectrum— 6 db/octave
150 to 50	5.5 sec	154	Rolled-off spectrum— 6 db/octave
69	0.14 sec	205	Amplitude modulated tone

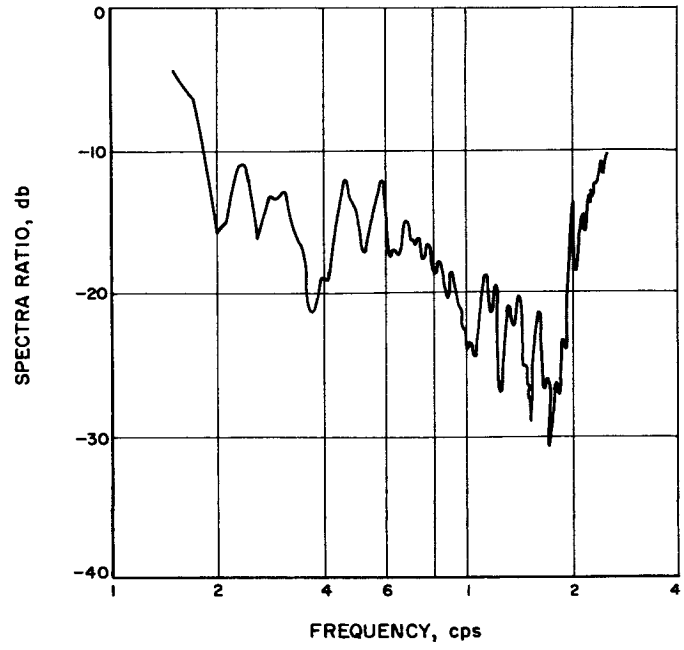


Fig. 360. Spectra ratio, response of spacecraft flight transducer to PTM roll axis noise spectrum

scheduling problems, only a limited portion of the overall test objectives was realized.

A failure of the planetary scan subsystem platform cover occurred during noise vibration of the PTM in the

Bay VIII XY axis. This failure was due to improper installation of the threaded inserts in the honeycomb plate and to understrength rod-end supports. These failures were corrected by improved quality control during fabrication of the honeycomb plate and by a structural strengthening of the mounting studs.

The Canopus sensor also experienced failure as a result of these tests, partly due to the improper use of the thermal/electrical isolation stand-off washers in the buildup but largely due to a design inadequacy. Nevertheless, the prototype spacecraft satisfactorily withstood the imposed vibration environments.

Shock tests. Shock testing of the PTM was performed in order to verify the integrity of the spacecraft for the environment produced by the firing of pyrotechnic devices and V-bands onboard the spacecraft. The following tests were performed:

1. Shroud V-band release
2. Spacecraft V-band release
3. Spacecraft solar panel release
4. Spacecraft science platform release

The spacecraft was maintained in the launch configuration for these tests. Pyrotechnics were fired in chronological order corresponding to the sequence encountered in flight.

The PTM was not affected by shock. The most severe shocks occurred during the spacecraft V-band release. A maximum response of 160 g (peak) at the spacecraft flight position accelerometer was measured. Some responses on the spacecraft feet were higher than 160 g (peak); however, these did not have direct correlation with spacecraft components and were not unexpected because of the proximity of the V-band. Low-frequency ring-out due to the release of the stored energy in the deformed structure associated with the V-band tensioning was also detected.

Each principal subsystem in the spacecraft was tested to the TA specification on the shock table, which is shown in Fig. 361. Although subsystem responses due to this input were not monitored, the following method was used to correlate test levels and the actual PTM pyrotechnic firings.

Assuming a subsystem to have a critical damping ratio of 0.025 ($Q = 20$), a conservative estimate of its response

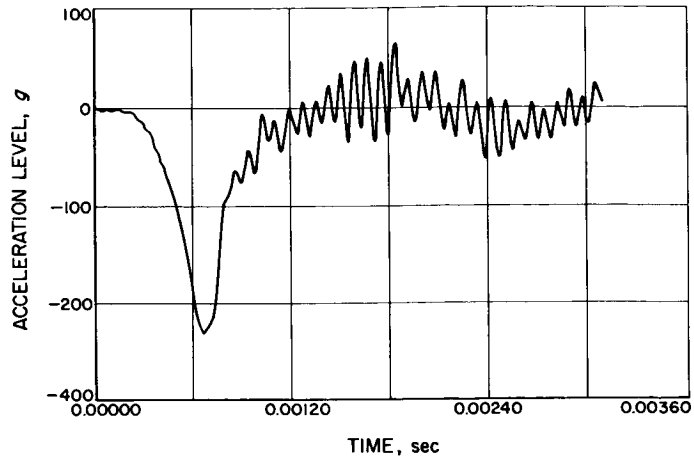


Fig. 361. Type approval shock table input

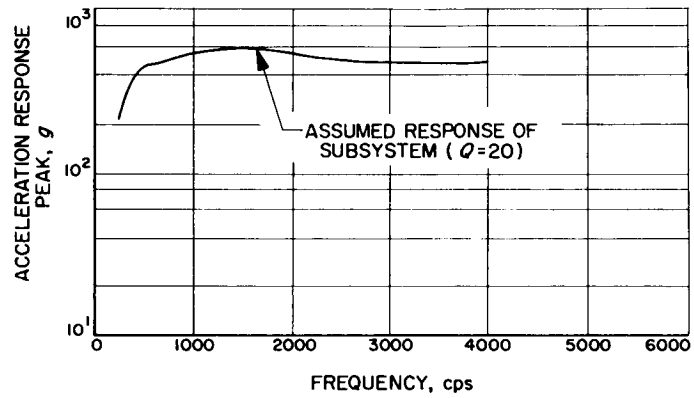


Fig. 362. Shock spectrum of type approval transient

to the TA shock would be approximately 1.5 times the input magnitude, and a maximum shock spectrum magnitude of 580 g (peak) would occur (Fig. 362). This shock spectrum was then compared with shock spectra from the pyrotechnic shock test. The pyrotechnic shock spectrum for a typical assembly (attitude control electronics) was shown to be conservatively enveloped by the TA shock spectrum upon examination of the relative differences in magnitudes (Fig. 363).

Acoustic test. The PTM spacecraft was exposed to 90 sec of reverberant-field wide-band Gaussian acoustic noise shaped to conform to the spectrum shown in Fig. 364. During the test, a 0.3-amp fuse in the CC&S failed. This failure was attributed to a turn-on power overshoot in the CC&S transformer. No other anomalies were noted. The acoustic tests confirmed the capability of the vehicle to survive the expected environment associated with the launch phase.

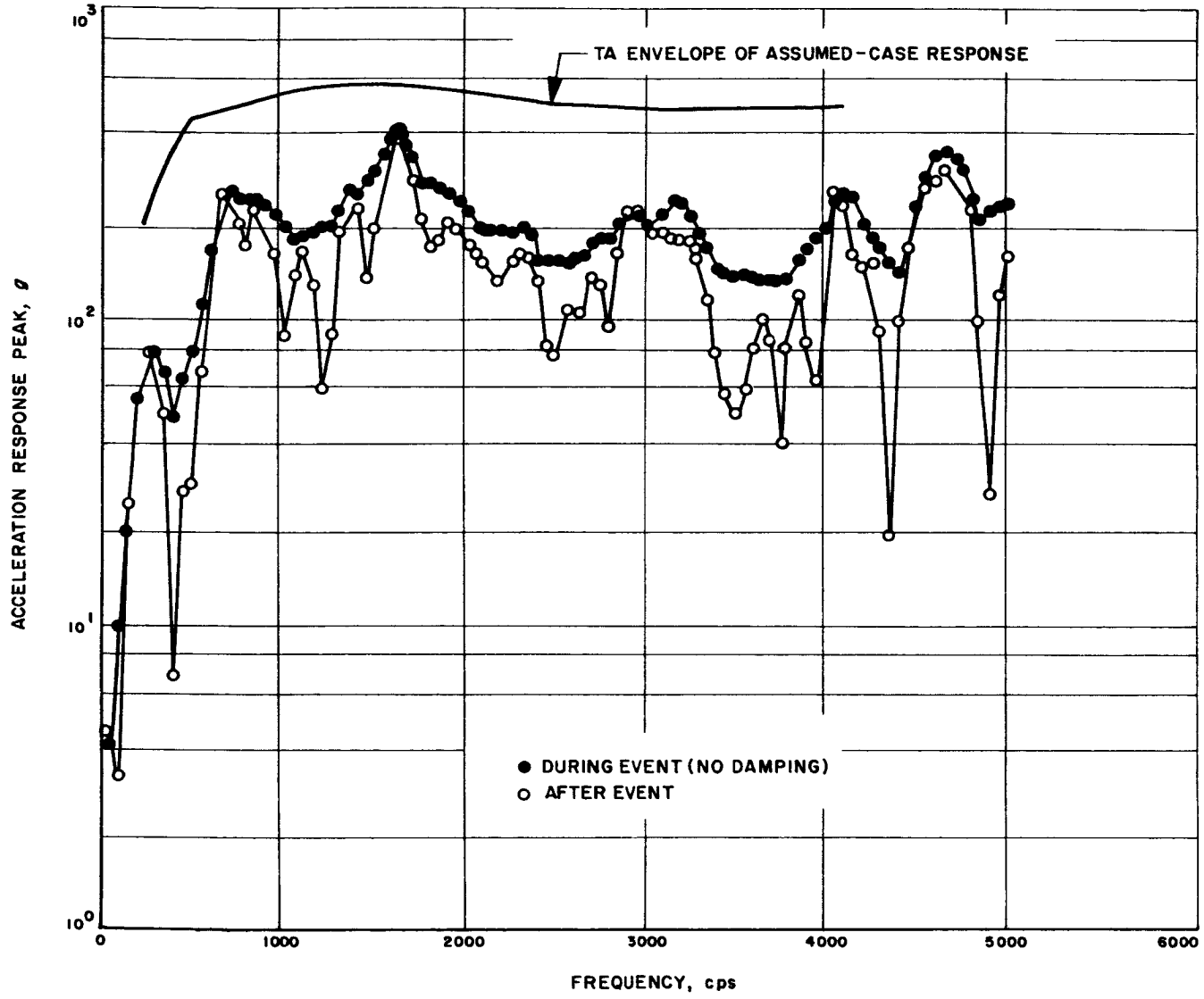


Fig. 363. Typical shock spectrum, X-direction accelerometer, PTM V-band firing

b. Space simulator/thermal–vacuum tests. To demonstrate the integrity of the *Mariner* vehicle for the unique space vacuum environment, tests were performed at the system level on the PTM and on each flight-quality spacecraft.

The PTM was tested in the JPL 25-ft space simulator to simulated launch-pressure profiles and specific thermal environments associated with the various flight modes (launch, midcourse maneuver, cruise, and encounter) for approximately 250 hours. These tests demonstrated adequate design of the spacecraft for the thermal environment, and all the components aboard the spacecraft operated within the allowable temperature limits. Some minor changes to the thermal shield configuration were made at the conclusion of the test in order to optimize flight temperatures. The long period of satisfactory operation in this extreme environment increased confidence in the *Mariner* capability to function as designed in the space environment.

The space simulator test began in March 1964. During the test, the steady-state values of chamber temperature and pressure were $-270 \pm 5°F$ and 10^{-6} mm Hg, respectively. The test was successful in spite of some minor problems. The spacecraft was operated for approximately 250 hours. The equipment that had been previously tested and was operating before the space-simulator test, performed in the same way in the solar–vacuum environment. Equipment without prior test experience (the radio

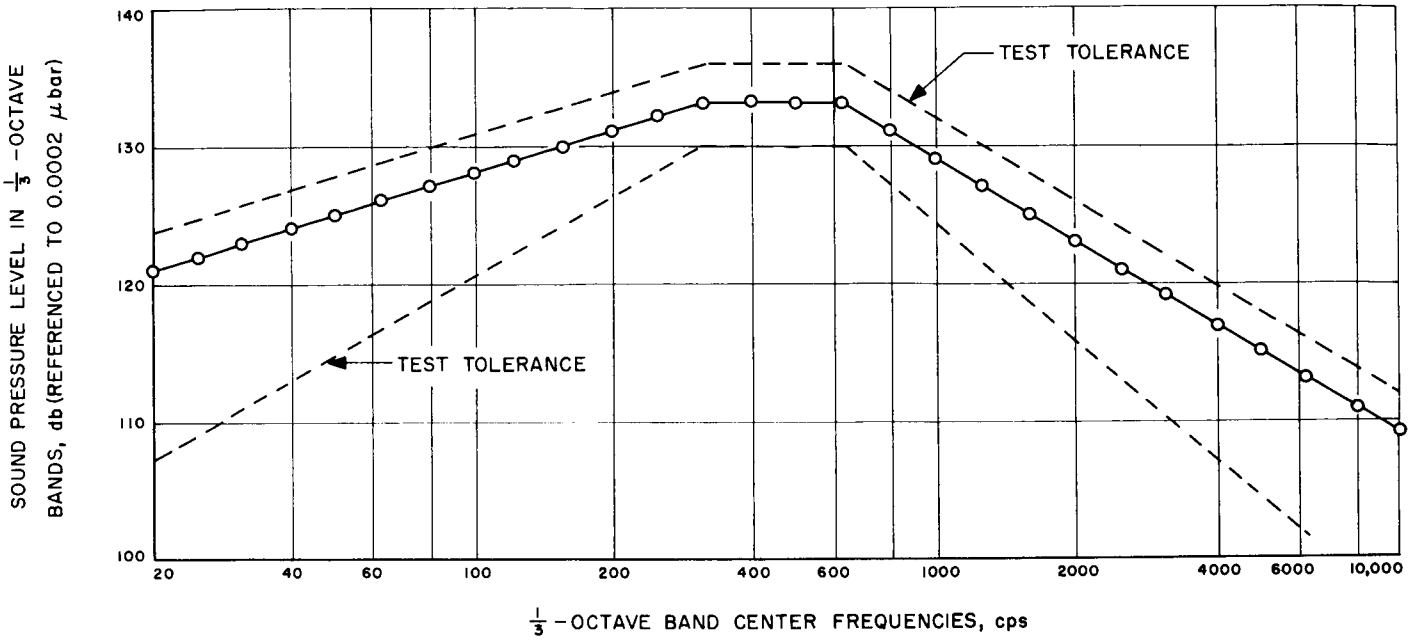


Fig. 364. Acoustic noise spectrum

and the attitude control solar vane system) were observed to malfunction in the chamber. Nevertheless, the long period of operation in the extreme environments increased confidence in the ability of the spacecraft to function as designed.

Because of the thermal configuration changes to the spacecraft between the system test and the thermal test, the effect of test cables on spacecraft performance could not be evaluated in this test series.

c. EMI tests. Although considerable shielded-room subsystem tests were performed, the greater part of the EMI effort was on system-level testing. Among the tests performed on the Spacecraft System was an RF simulation test. This test subjected the spacecraft to an RF environment that simulated (with a margin) the calculated or measured RF levels from onboard launch vehicle sources and AFETR ground sources (such as radar) that participate in a spacecraft launch. This test was intended to ensure that the spacecraft, including pyrotechnics, was not adversely affected by the presence of the RF environment, and to ensure that cognizant operating personnel became acquainted with the characteristics of any interference. These tests helped to eliminate confusion and delays in the operations at AFETR.

Another test was performed to evaluate the effects of electrical transients induced at the spacecraft umbilical and separation connectors. This test was intended to determine the sensitivity of the spacecraft connector leads to transients that might be encountered during the launch phase. High-voltage tests were conducted on both the STM and PTM spacecraft to determine the effect of generation and ultimate discharge of electrostatic charge from the surface of a launch vehicle. Tests of this nature had been performed on *Ranger* spacecraft and were repeated to determine how the results could be applied to the *Mariner* Mars 1964 program.

To ensure that the S-band communications receiver onboard the spacecraft would not have its sensitivity degraded by the presence of RF noise in its receiver bandpass, a series of measurements were made during the space simulator tests. These tests, performed on both the PTM and the flight spacecraft, were made to determine that no interfering RF noise levels would be contributed by any spacecraft subsystem. It was discovered on the PTM that the attitude control gas valves and the gyros emitted noise bursts in excess of desired levels. Additional tests were requested to determine how this noise might interfere with the receiver operation during the spacecraft's Mars encounter.

Other tests covered conducted noise on OSE power cables and electrical transient effects. The complete objective of the transient test was not met due to transistor failures in the data encoder under 20-v impressed transients. The desired full level transient was 75 v. The

conducted noise test was intended to determine which OSE consoles were "noisy" and would require additional filtering or isolation transformers. The objectives of this test were not fully realized because of limited test time on the system test complex.

RF simulation tests. Two RF simulation tests were performed on the PTM spacecraft. These were a system RF simulation test and a launch countdown and dummy run test with live pyrotechnics.

The PTM was subjected to a simulated RF environment during the system test. Interference was noted on the radio OSE precision coupler power readout and on some low-level channels of the data encoder. It was determined that the *Agena D* telemetry simulator was the cause of the interference. A subsequent test performed the same day determined that interference to the data encoder channels was reduced when the simulation power density level was decreased. The precision coupler interference (a power reading displacement) was eliminated by the replacement of a coaxial cable on the spacecraft. The *Agena D* telemetry simulation level was reduced for flight spacecraft.

The AFETR RF simulation sources were provided for the PTM simulated precountdown and countdown tests. For these tests, *Agena D* flight-type antennas were used for the simulated telemetry signal and the C-band beacon signal. A flight-type C-band beacon was used in these tests. In addition, a 100-w RF level at the transmitter frequency was radiated from the omnidirectional antenna. No interference to any spacecraft subsystem, including pyrotechnics, was observed during these tests. Radio-frequency power levels at selected squib locations were measured to determine the general magnitude of the levels. A minimum safety margin of 27 db, with the EMI simulation sources and with the S-band 10-w transmitter on, was determined in this test for one of the squib locations measured.

In the live squib simulation test, the usual simulation sources were used. The effects on results using the onboard pulse beacons included:

1. *Agena* C-band beacon. An actual flight-type beacon was used with a flight-type antenna mounted on the *Agena* forward-section adapter. Although characteristics peculiar to such flight equipment were provided for, the RF power level for this source did not exceed the expected flight level. Any RF-level safety margin from this source would have been a result of RF reflections from within the SAF pit walls back to the spacecraft.

2. Guidance pulse track beacon. This source was simulated with a CW RF generator. The simulated RF power density level exceeded the calculated average power level but not the peak level.

3. FPS-16 radar transmitter. This source was simulated with a CW generator. This power density also exceeded the calculated average value but not the peak power level. However, including shroud attenuation effects, an adequate safety margin for peak levels existed.

The effect of peak power levels on spacecraft pyrotechnics is an unknown factor. Results obtained during the simulation of the two flight pulse beacons and the FPS-16 radar provided only a marginal indication of spacecraft capability. It has been proposed for future applications that an RF simulation with live squibs be performed using peak power levels to specifically determine that no hazard exists. Table 70 lists the RF levels used for the simulation tests.

S-band RF noise tests. To determine that the spacecraft communications system would not be degraded by broadband RF noise contributed by science or other subsystems on the spacecraft, a series of measurements were made with *Mariner* Mars 1964 vehicles in the space-simulator chamber. Acceptable RF noise levels were defined for the spacecraft receiver transmitter and image frequencies, and for the OSE test receiver frequency. In order to measure the actual noise levels at the receiver frequency, an S-band receiver with a low noise figure was fabricated. Components for this system were assembled from design drawings for flight equipment. The receiver low noise was obtained by using a low-noise parametric amplifier. A military-type receiver with adjustable bandpass filters (with one down to a 100 cps bandwidth) was incorporated in the system. A significant feature of the receiver system was a predetection recording-frequency translating circuit. Magnetic tape recordings were made during space simulator tests for subsequent analysis.

Table 71 summarizes the permissible noise levels and the noise receiver equipment sensitivity that was available for measurements.

Table 71 also indicates that additional sensitivity was required of the test equipment. The receiver listed for

Table 70. RF simulation levels and test margins

Simulated transmitter	1 Frequency Mc	2 Calculated power density dbm/m²	3 Specification power density[a] dbm/m²	4 MC-1 actual test level[b] dbm/m²	5 MC-1 actual test margin[c] db	6 MC-2, 3, 4 actual test level dbm/m²	7 MC-2, 3, 4 actual test margin[d] db	8 Shroud attenuation at particular frequency db
Offboard sources								
Atlas Azusa Mark II transmitter	5060	18.3	26	28.6	45	28.6	45	35
FPS-16 radar transmitter	5690	14.6 average 52.5 peak	22	20[e]	49 average 11.5 peak	20	49 average 11.5 peak	44
Command destruct transmitter	Classified	− 3.0	4	4	35	4.1	35	28
Atlas guidance pulse subsystem ground transmitter	Classified	−18.5 average 13.7 peak	18	28	82 average 49 peak	28	82 average 49 peak	35
Atlas guidance rate subsystem ground transmitter	Classified	7.8	18	18	45	18	45	35
Onboard sources								
Atlas telemetry No. 1	229.9	− 8.7	− 2	1.2	10	1.2	10	0
Atlas Azusa transponder	5000	−13.3	19	16.2[e]	30	16.2	30	
Atlas guidance pulse subsystem transponder	Classified	− 8.9 average 23.4 peak	− 1	1.3	10 −22	1.3	10 −22	
Atlas guidance rate subsystem transponder	Classified	−12.4	− 5	− 1.2	11	− 1.2	11	
Agena D telemetry	244.3	19	36	36	Not determined	25	6	
Agena D transponder (CW)	5765	−18.1	17	14.7	Not determined	14.7	33	
Agena D transponder (pulse)	5765	1.5	40	51.2	Not determined	51.2	50	

[a]Specified power density levels based on RF launch environment at LC 12 calculated for *Ranger*.

[b]Values determined from simulation equipment settings used for *Ranger* tests.

[c]Column 4 minus Column 2 plus Column 8.

[d]Column 6 minus Column 2 plus Column 8.

[e]Within 3 db of specification level.

making the 2295-Mc OSE measurement is a standard field-intensity meter. A low-noise-level receiver is required for this measurement.

Umbilical and separation connector transient test. This test was intended to determine the sensitivity of the umbilical separation connector circuitry of the PTM to electrical transients while in the launch mode. The test was halted when it was only one-third completed because of transistor failures in the data encoder caused by 20-v transients. The battery voltage monitor fuse was blown by 75-v transients. It is highly desirable that this test become a requirement for future missions.

Conducted noise from OSE. Considerable data were collected during this test before it was determined that the instrumentation was being saturated with the 60-cps voltage. A filter was devised that was not optimum. A sharper filter will be required for future programs and tests. Because of scheduling problems and the unsatisfactory quality of the data, this test was not completed.

High-voltage tests. It had been suggested that the generation and ultimate discharge of large amounts of electrostatic charge from the surface of a rocket-propelled vehicle could act as a failure mechanism on the spacecraft. Analysis of this phenomenon indicated that because

Table 71. EMI receiver equipment sensitivity and requirements

Measurement	Frequency, Mc	Permissible noise levels	EMI estimated receiver sensitivity with coaxial cables
Spacecraft	2116	−161.22 dbm in 20 cps bandwidth	−151.3 dbm (100 cps bandwidth) +7.6 db cable loss = −143.7 dbm (100 cps bandwidth)
	2017 (image)	−111.22 dbm in 20 cps bandwidth	−142 dbm (100 cps bandwidth) +7 db cable loss = −135 dbm (100 cps bandwidth)
	2295	13.9 dbm in 12 cps bandwidth	−87 dbm (5 Mc bandwidth) +8 db cable loss = −79 dbm (5 Mc bandwidth)
OSE	2295	−159.8 dbm in 20 cps bandwidth	−87 dbm (5 Mc bandwidth)

the aerodynamic shrouds used to protect the spacecraft during launch were not perfect Faraday cages, charges would be induced on spacecraft circuit elements by the accumulation of charge on the shroud exterior. Because of the difference in time constants between the shroud and the spacecraft element relative to the same external reference, the voltage induced on the spacecraft element might not be able to follow rapid voltage changes on the shroud. Thus elements interior to the shroud could be subjected to voltages with respect to the shroud (spacecraft ground).

The test on the STM allowed the preliminary gathering of empirical data necessary for extrapolation of the results of the *Ranger* Block III high-voltage test to cover the *Mariner* Mars 1964 spacecraft. The tests indicated that the *Mariner* shroud was approximately as good a shield against static discharge phenomena as was the *Ranger* shroud. The discharge-induced transients measured were within an order of magnitude of those measured under similar conditions for the *Ranger* spacecraft.

The tests on the PTM indicated that the spacecraft was not susceptible to high-voltage discharging from the shroud for breakdown potentials of up to 150 kv. In addition, the squibs used for the midcourse motor firing and for the solar panel pinpuller were not susceptible to the voltage discharges.

2. System-level FA Testing

Flight-acceptance environmental testing at the system level was performed to certify flight worthiness and to demonstrate the capability of each spacecraft to withstand environments from initial fabrication through launch and injection to the encounter phase. The tests consisted largely of vibration, space-simulation, and certain EMI analysis-type tests. The input levels were those estimated to be the actual operational environmental conditions. System-level FA testing was conducted on each flight-quality spacecraft (MC-2, MC-3, and MC-4).

a. Dynamic tests. Each flight-quality spacecraft was subjected to a series of vibration tests including both low-frequency sine sweeps and random noise. These tests were an attempt to simulate the deleterious effects of the vibration and acoustic field that accompanies *Atlas/Agena* operations from launch to injection.

While comparable in severity to the expected environment, the imposed test levels were considered to be mild enough to avoid fatigue or a reduced life expectancy of the vehicle, yet severe enough to detect spacecraft assembly errors and subsystem early life failures. The vehicles were not subjected to such other types of dynamic testing as torsion or shock, since it had been previously demonstrated in the PTM tests that those environments were adequately covered by the three-axis vibration tests.

Each spacecraft was shaken in the roll axis and in two lateral axes (Fig. 365). Before and after each axis of vibration, a system verification test was performed, using only the umbilical cable and the special Canopus sensor and Sun sensor test cables from the STC. Before vibration of the spacecraft and upon completion of the system verification test, the spacecraft was conditioned for the launch mode, was transferred to internal power, and all external cables were disconnected.

During vibration, spacecraft performance was monitored via the RF telemetry link. After each axis of vibration, the umbilical and special test cables were reconnected and another system verification test was performed to determine the spacecraft condition.

Each spacecraft was attached firmly and securely to the vibration exciter by the vibration test fixture. A typical vibration test schedule for the flight spacecraft

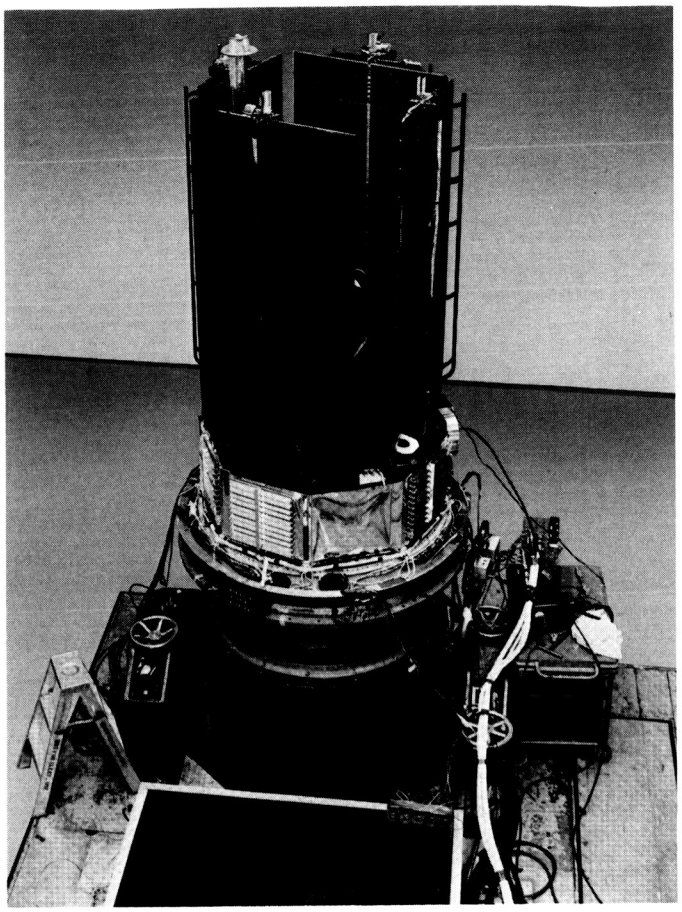


Fig. 365. Test setup, MC-4 FA vibration test, Z axis

Table 72. MC-2 vibration test run schedule

Run No.	Axis	Test type	Frequency range, cps	Specified level g rms	Duration sec
1	XY[a]	Pretest integrity, sine sweep	40 to 200	0.354	68
2	XY[a]	Noise equalization	150 to 2200	0.5	120
3	XY[a]	Equalization verification	150 to 2200	0.5	120
4	XY[a]	Equalization verification	Shaped noise	5.6	8
5	XY[a]	FA noise	Shaped noise	10.7	60
6	XY[a]	FA low-frequency sine sweep	200 to 20 to 200	0.5	196
7	XY[b]	Noise equalization	150 to 2200	0.5	120
8	XY[b]	Equalization verification	150 to 2200	0.5	120
9	XY[b]	Equalization verification	Shaped noise	5.6	8
10	XY[b]	FA noise	Shaped noise	10.7	60
11	XY[b]	FA low-frequency sine sweep	200 to 20 to 200	0.5	196
12	Z	Noise equalization	150 to 2200	0.5	120
13	Z	Equalization verification	150 to 2200	0.5	120
14	Z	Equalization verification	Shaped noise	5.6	8
15	Z	FA noise	Shaped noise	10.7	60
16	Z	FA low-frequency sine sweep	200 to 20 to 200	1.0	196

[a]Bay II.

[b]Bay VIII.

NOTE: The shaped-noise spectrum for equalization verification and FA-level runs was a spectrum with the specified PSD level flat from 550 to 2000 cps and rolled off at a rate of 6 db/octave below 550 cps and 24 db/octave or greater above 2000 cps. Power-spectrum density levels were 0.07 g^2/cps for FA and 0.02 g^2/cps for equalization noise runs. Sweep rates for all sine-wave tests were ½ min/octave band.

is given in Table 72. The pretest integrity of the spacecraft was determined by an examination of the results of a low-level sine sweep in the first axis of vibration. The examination consisted of comparing the behavior of the scan platform with similar results from the previous PTM and STM vibration tests.

In order to develop the proper and complete dynamic characteristics of the flight spacecraft, the PTM PIPS was installed in place of the flight unit. Its fuel tank was filled with 21.5 lb of distilled water and pressurized to 150 psi; its nitrogen tank was unpressurized. The flight jet-vane actuator assembly was used with the PTM PIPS. Flight-acceptance vibration testing of the flight PIPS assembly was conducted independently of flight spacecraft testing.

Test levels. Each spacecraft was subjected to noise vibration along two lateral axes and the roll axis for a duration of 60 sec per axis. Each test was executed by means of a magnetic tape recording, and consisted of a programmed sequence of Gaussian noise with a spectrum of 0.07 g^2/cps from 550 to 2000 cps (rolled off at 6 db/octave below 550 cps and at 24 db/octave above 2000 cps). The wideband rms value was 10.7 g rms. In addition, each vehicle was subjected to sinusoidal vibration along each of the three axes at frequencies between 20 and 200 cps. The input level was 0.5 g rms for the lateral axes tests, and was 1.0 g rms for the roll axis test. Prior to each noise test, a standard technique of equalization was accomplished with low-level sine-wave inputs. As a check of the test input levels and to ensure adequate equalization and protection from overtesting, an intermediate-level noise vibration test was conducted prior to the full-level FA test. This test was 8 sec in

duration, and used the same spectrum as the FA test but with an rms value of 5.6 g.

The FA noise excitation levels compared with the TA levels in the following manner: (1) the test duration per axis was 60 sec (or ⅓ that of the PTM); (2) the wideband rms value was 10.7 g rms (or 18.7 for the PTM), (3) both tests had comparably shaped spectra (flat from 550 to 2000 cps with a 24 db/octave roll-off above 2000 cps and a 6 db/octave roll-off below 550 cps). The power density spectrum level in the flat range was 0.2 g^2/cps for the PTM and 0.07 g^2/cps for the FA test. This was a margin of approximately 4.5 db.

Test technique. Control for all vibration tests was obtained through six appropriately mounted accelerometers, which were located on the vibration exciter fixture very near the adapter bolt circle, equally spaced around its circumference and sensitive to acceleration in the direction of motion.

Low-frequency control (20 to 200 cps) was accomplished using the peak selection reading of the six accelerometers. High-frequency sine-wave (150 to 2000 cps) and random-noise control was accomplished by using the quadratic mean of the six accelerometers.

Limiting of the shear force imparted to the adapter/vibration exciter fixture was a requirement for the control of these tests. The force suppression levels for the FA vibration test series were:

$$\text{Lateral axes} = 4500 \pm 5\% \text{ lb}$$

$$\text{Roll axis} = 6500 \pm 5\% \text{ lb}$$

The input amplitudes were never suppressed since the maximum force levels observed during the tests on any vehicle were:

$$\text{Lateral axes} = 1700 \text{ lb at } 70 \text{ cps}$$

$$\text{Roll axis} = 2800 \text{ lb at } 45 \text{ to } 80 \text{ cps}$$

Equalization of the vehicles for the random-noise tests in all axes was accomplished with low-level sine-wave inputs. With the vibration exciter control system on servo, and with control exercised by the quadratic-mean circuit, plots were made of the voltage required to hold the sweeping sine-wave input at 0.50 g rms. The sweep was performed at a logarithmic rate of 0.50 min/octave from 150 to 2200 cps. The system was then equalized through the use of peak-notch filters and the graphic equalizer. When the trial equalization was complete, a verification sine sweep was run. The resulting plot was then compared with the equalization plots from the corresponding PTM tests. Equalization was at least as good as the PTM and the final plots were generally flat within ±2.0 db, although occasional peak notches of up to 4 db were noted. In several instances the verification runs indicated inadequate equalization of the system. Additional trial equalizations were then performed, which produced satisfactory results.

A number of selected data points were recorded on a direct-writing oscillograph during each test so that the environmental requirements project representative could monitor the input reference and the behavior of the spacecraft in real time. All input-reference test data were reduced as quickly as possible in order to minimize the need for repeating tests. System verification test data were thoroughly evaluated after each vibration to ensure that the spacecraft was in the proper condition for the next run. Generally, each spacecraft satisfactorily withstood the imposed vibration. The ring harness trough assembly was observed to experience a structural failure at the conclusion of the MC-3 spacecraft tests, although it was not directly attributable to vibration. In addition, there were considerable difficulties with the flight instrumentation system. It is also noted that a number of facility-induced anomalies occurred, none of which, however, caused any significant difficulty. A comparison of the actual FA noise environments for each spacecraft is given in Table 73. (The desired wideband level was 10.7 g rms.) These tests demonstrated the readiness of each vehicle for launch.

b. Space-simulation thermal–vacuum tests. Space-simulation tests were conducted on the MC-2, MC-3, and MC-4 vehicles in the 25-ft space simulator (Fig. 230) from March through November 1964. The objectives of the tests were:

1. To establish the functional integrity of a spacecraft operating in a simulated space environment

Table 73. Comparison of spacecraft FA noise test levels

Axis	Spacecraft		
	MC-2	MC-3	MC-4
XY[a]	10.8	10.8	11.0
XY[b]	10.8	8.7	11.6
Z	11.9	14.6	12.6

[a]Bay II.
[b]Bay VIII.

2. To perform a final verification of the ability of the temperature control subsystem to maintain spacecraft temperatures within design limits
3. To verify that spacecraft performance in a simulated space environment was not affected by test cables

The first objective was accomplished by performing a spacecraft system test. This test consisted of operating the spacecraft in a space environment simulating the Mars mission. The environment included a solar source of varying intensity with cold vacuum chamber walls (Fig. 366). The second objective was met in a similar manner, except that (1) the spacecraft was subjected to greater extremes of temperature than specified, (2) the test was of a shorter duration (usually lasting until steady-state conditions were met in the various modes), and (3) fewer telemetry cables were used. The third objective was determined by a comparison of the first two objectives.

The simulated solar-radiation source was a lamp array of 133, 2½-kw mercury xenon lamps. The light beam was projected in such a way as to permit off-axis tests. The heat sink of deep space was simulated by the liquid-nitrogen-filled black panels lining the walls and the bottom of the chamber. A vacuum pressure of 10^{-6} mm Hg was achieved in a three-phase operation. The operational sequence stepped the pressure down using wind-tunnel compressors and mechanical and diffusion pumps.

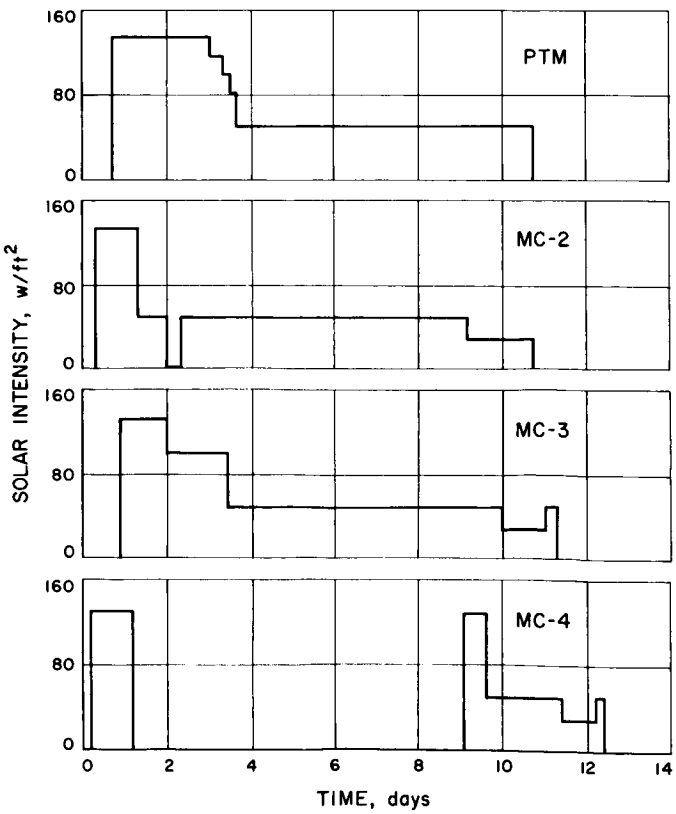


Fig. 366. Space-simulator system test, solar intensity history

The following items are possible sources of error in the test data:

1. The solar-radiation source, although simulating the intensity of the Sun, could not simulate its spectrum
2. The simulated collimation angle was different from that of the Sun
3. Effects of chamber re-reflectance, thermal gradients, and extraneous radiation are undefined
4. The actual launch pressure profiles could not be simulated (Fig. 367).

MC-2. The MC-2 spacecraft was subjected to space-simulation testing during July 1964. During the system portion of the test, a general overall spacecraft bus temperature increase over the PTM was noticed. Slight thermal modifications to the bus produced the desired temperatures. A comparison of temperatures between the system test and the thermal test indicated that the effect of OSE cables was to cool the spacecraft a few degrees.

MC-3. The MC-3 spacecraft was subjected to thermal–vacuum testing during August 1964. During the test, a leak in the attitude control subsystem and a loss of spacecraft power control caused an increase in chamber pressure. In general, the spacecraft operated within the desired temperature ranges.

MC-4. During September 1964, the MC-4 spacecraft was subjected to environmental testing in the space simulator. The spacecraft experienced a rise in chamber pressure during the space-simulation test. The pressure rise occurred during an attempt to restart one of two blowers that operate in parallel downstream of the ten diffusion pumps and upstream of the mechanical pumps. When a control valve was opened, the diffusion pumps surged and the chamber pressure increased to 100μ because of the in-rush of trapped air from the idle pump. The diffusion pump beaters shut off automatically, and the isolation valves between these pumps and the chamber closed automatically, but not before some

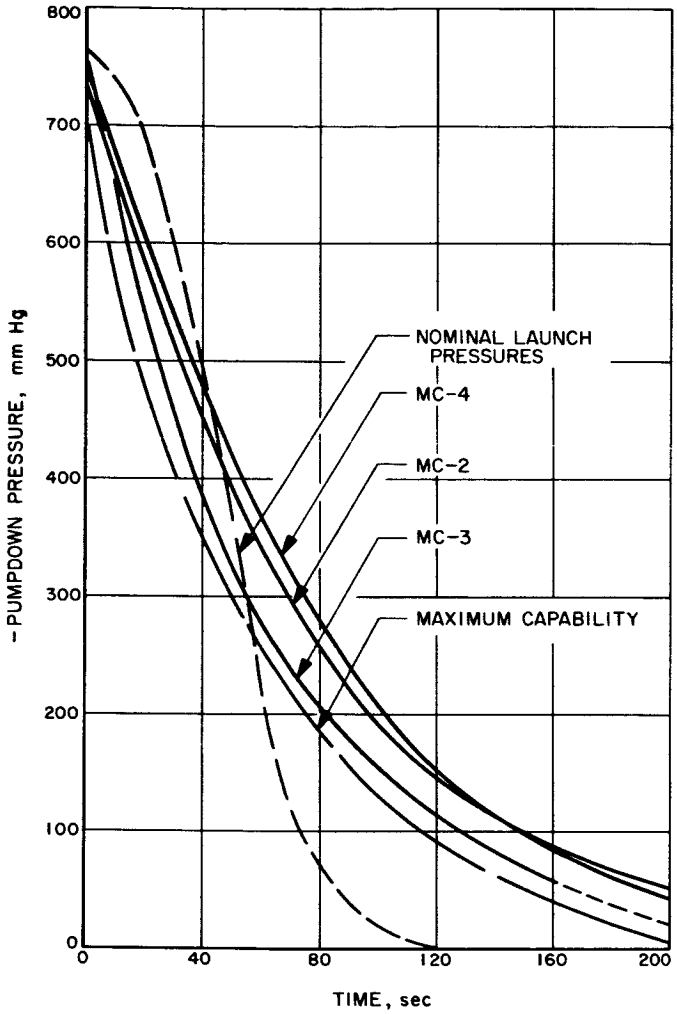


Fig. 367. Comparison of simulated launch pressure profiles to maximum simulated pumpdown capability and to *Mariner* Mars 1964 launch pressures

oil and air had entered the chamber permitting spacecraft arcing. It was determined after considerable analysis that this anomaly had no significant effect on the spacecraft.

c. EMI RF simulation tests. The flight spacecraft were subjected to an RF simulation test to verify that all spacecraft systems would not receive interference in the RF environment present at the launch complex. The RF power density levels used on flight spacecraft were the same as on the PTM, except for the *Agena* telemetry simulated source.

These tests were performed according to the FA environmental test specification (RF levels and calculated test margins are listed in Table 70).

On the MC-2 spacecraft, the cosmic dust collector noted penetration effects with the RF sources on. No other interferences were noted. Schedule limitation precluded further investigation of the problem.

One failure occurred on the RF simulation equipment in this series of tests. The traveling-wave-tube amplifier used for the *Atlas* guidance pulse and rate subsystems failed as the test began. The amplifier was bypassed and the resulting power level was approximately 0 dbm/m² for both systems. The level required in the procedure was 18 dbm/m².

During the RF simulation test of the MC-3 spacecraft, the following disturbances were noted:

1. When the *Atlas* guidance pulse subsystem transmitter was turned on, the cosmic dust experiment experienced a slightly noisy reset line. This disturbance was not seen on the data and it cleared up after a few minutes.

2. The precision coupler RF power monitor in the OSE showed a 0.1-db increase in power when the *Agena* telemetry source was turned on.

3. The data encoder reported a one-count discrepancy in the low-level channels.

Because of the limited spacecraft test time available, the disturbance was not investigated further.

On the MC-4 spacecraft, the data encoder reported a one-count discrepancy with the RF simulation sources on. No other subsystems noted interference. The data encoder interference was not investigated further due to limited test time.

B. Subsystem Environmental Tests

Type-approval and flight-acceptance testing of all *Mariner* Mars 1964 spacecraft subsystems was a Project Office requirement. Environmental specifications were released, which precisely specified the procedure for establishing the test environment. These specifications were inadequate by themselves, however, for two reasons. First, such documents could not possibly have specified the functional tests necessary to determine acceptance or rejection. Second, with such a large complex spacecraft, it would have been difficult to write one general specification entirely applicable to each item on the spacecraft. For these reasons, each cognizant hardware engineer covered the testing of his particular hardware in an appropriate specification detailing the necessary functional tests, acceptance criteria, and deviations from the basic environmental specifications.

Before being released, these test specifications were reviewed to ensure that the environmental test program specified was appropriate to the particular piece of hardware.

Two types of subsystem environmental tests were performed during the development of the project. Type approval environmental tests were intended to verify designs. They were intentionally severe to compensate for material and fabrication differences in flight hardware. Flight acceptance environmental tests were intended to be as severe as the expected environment and to define certification of readiness for flight. All flight equipment was subjected to FA testing. The assembly-level FA tests were limited to two environments in which equipment operation could be evaluated, and which could be simulated in a well controlled manner. Passage of the FA tests demonstrated the ability of the hardware to perform satisfactorily in the selected environments at levels at least as severe as flight. This information combined with inspection and performance testing results provided implicit evidence that the FA equipment was similar to the TA equipment and, thus, capable of performing in all environments.

A summary of the subsystem environmental test requirements and the results of the program are given in Tables 74 and 75. The types of problems or failures encountered are shown in Table 76.

Table 74. Assembly-level environmental test requirements

Test	TA test level	FA test level
Bench handling	Free-fall corner drop	Not applicable
Drop test	Height variable to weight	↓
Transportation vibration	1.3 g, 2 to 35 cps 3.0 g, 35 to 48 cps 5.0 g, 48 to 500 cps	↓
Explosive atmosphere	Fuel and air during assembly operations	↓
Humidity	75% humidity and varied temperature	↓
Shock	5 to 200 g, 0.7 ± 0.2 msec pulses, 3 axes	↓
Static acceleration	± 14 g, 3 axes for 5 min	↓
Vibration low frequency (all assemblies)	1 to 4.4 cps 4.4 to 15 cps, 3 g peak for 3 min	↓
Complex wave (assemblies ≥ 10 lb)	16.4 g rms noise for 90 sec 5.0 g rms noise 2.0 g rms sine, 15 to 40 cps 9.0 g rms sine, 40 to 250 cps 4.5 g rms sine, 250 to 2000 cps[a] for 600 sec	9.0 g rms noise for 6 sec 3.0 g rms noise 1.5 g rms sine, 15 to 40 cps 6.0 g rms sine, 40 to 250 cps 3.0 g rms sine, 250 to 2000 cps[b] for 200 sec 9.0 g rms noise for 6 sec
Thermal–vacuum	−10°C for 4 hr 75°C for 12 days 10^{-4} mm Hg	0°C for 2 hr 55°C for 40 hr 10^{-4} mm Hg
Thermal shock (for external assemblies)	+75 to −46°C	Not applicable

[a]9.0 g for assemblies ≤ 10 lb.
[b]6.0 g for assemblies ≤ 10 lb.

Table 75. Subsystem environmental test summary

Environment	Number of subsystems in test	Number of tests	Number of failures	Failures %
TA tests				
Bench handling	22	39	0	0
Package drop	25	39	0	0
Transportation vibration	27	85	0	0
Humidity	31	51	5[a]	10.2
Explosive atmosphere	18	19	0	0
Shock	49	116	3	2.6
Acceleration	46	89	0	0
Low-frequency vibration	51	90	6	6.7
Complex-wave vibration	54	154	24	15.6
Thermal–vacuum	50	95	19	20.0
Thermal shock	56	28	1	3.6
Total		805	58	7.2 (average)
FA tests				
Thermal–vacuum	41	310	28	9.80
Complex-wave vibration	49	538	26	4.8
Temperature	2	21	1	4.76
Total		869	55	6.33 (average)
Overall Total		1674	113	6.86

[a]All failures at 95% relative humidity.

Table 76. Classification of subsystem environmental test problems or failures

Failure classification	TA testing	FA testing	Bench, system, and vendor testing	Total
Design change required	39	14	30	83
Component failure	14	19	26	59
Workmanship	13	12	9	34
Operator error	7	9	8	24
OSE failure	8	8	8	24
Miscellaneous and undefined	6	4	6	16
Total	87	66	87	240

1. Subsystem TA Environmental Testing

Design adequacy of the *Mariner* Mars 1964 subsystems and assemblies was verified by type-approval testing. Ten test environments were defined for the normal encounter sequence from fabrication through flight. Although not a project requirement, this was the preferred sequence for conducting the type-approval test program. All tests were not appropriate for each item; therefore, applicable tests were specified by the unit test specification.

Some of the tests were based on military or aerospace requirements. The conditions from the military specifications were readily determined to be more severe than those encountered by the spacecraft equipment, but this severity generally posed no problem for the majority of the equipment. In cases in which equipment was not compatible with these tests, special handling procedures were established and the test requirements were waived. Other environmental test requirements were based on spacecraft design information, experience, or special studies. The thermal–vacuum test requirements for the assemblies were based on experience and on design data. (The temperature test range has been used for JPL spacecraft projects with only minor changes since *Explorer 1*.) The thermal design of the spacecraft provided a temperature environment well within this range for all inboard parts of the spacecraft. Outboard parts such as the solar panels and antennas required special testing, which was beyond the scope of the general specification but was completely defined in the environmental test specification for those assemblies. The capability of the *Mariner* Mars 1964 spacecraft to provide a satisfactory thermal environment was verified in the system-level space simulator tests.

Certain tests such as vibration and shock required special analyses. Although the basic tests for the assemblies and spacecraft are summarized in the following paragraphs, a number of additional tests were performed on selected assemblies as a result of continual study of the test environment. Three of the specified tests were designed to verify the capability of each unit to withstand the shock and vibration stresses imposed during handling, packaging, and shipment. Three tests were performed to simulate the environment encountered by the spacecraft during final launch preparation and countdown. The shock, static acceleration, vibration, temperature, and thermal shock tests simulated the environment encountered by the spacecraft during launch and flight; the equipment was expected to function according to its design intent throughout the tests.

*a. **Bench handling of subassemblies.*** Each subassembly, without protective packaging, was dropped on a 2-in.-thick fir bench or table at a 45-deg inclination, with at least one point of the assembly in contact with the table prior to drop. Six drops from six different positions constituted the test. Upon completion of the test, the assembly was energized, and, after a sufficient warmup period, satisfactory operation was verified.

*b. **Drop test.*** The assembly or subassembly, with protective packaging, was dropped onto a concrete floor. The configuration for this test (assembly or subassembly) was representative of the configuration in which a commercial carrier would have handled the item. The height, as specified, was measured from the floor to the point of the package nearest the floor; the package was dropped on any of its corners, edges, or surfaces. Six such drops, landing on six different corners or edges, constituted the test. Upon completion of the test, the assembly was tested for satisfactory operation.

*c. **Transportation vibration.*** The transportation vibration test was conducted to study the effects encountered by a component when it was shipped by such standard means as aircraft (turbojet or propeller-driven), rail, ship, or truck. The test severity was designed to ensure an adequate test simulation level in the event that the transportation history and transportation vibration levels were either uncontrolled or unknown. In specific instances, the shipping package was used as part of the test setup.

*d. **Explosive atmosphere test.*** This test was conducted to ensure that the assemblies would operate in an explosive atmosphere environment, which occurs as a result of

launch vehicle fueling operations, without igniting the atmosphere.

e. Humidity test. The objective of this test was to ensure that the assemblies were capable of operating in a humid environment. While the spacecraft could normally be expected to be operating only in a controlled atmosphere prior to launch, the remote possibility existed of encountering humid conditions during handling and/or prior to launch.

f. Shock. The shock tests verified integrity for the environment associated with the firing of pyrotechnics.

g. Static acceleration. Each assembly was subjected to a static acceleration of ± 14 g in three orthogonal directions, one direction parallel to the axis of thrust, for 5 min. The assembly was required to operate in the launch mode during the test.

h. Vibration. The low-frequency and complex-wave vibration tests simulated the deleterious effects of structural excitation and acoustic coupling during booster operation (e.g., midcourse maneuver circuitry), which was not required to function within tolerance during these tests, but which was required to survive them (i.e., the assembly was required to operate in accordance with its test specification without any repair or adjustment following the test).

1. The low-frequency vibration testing subjected each assembly to sinusoidal vibration between 1 and 15 cps in each of three orthogonal directions.
2. The complex-wave vibration tests, consisting of a sequence of band-limited Gaussian noise and combined noise and sinusoidal vibration, were programmed by means of a magnetic tape recording. Tests were conducted in each of three orthogonal directions.

i. Space-flight temperature tests. These tests were designed to verify that assemblies would perform satisfactorily with a safety margin in a combined thermal–vacuum environment. The margin was incorporated as a design-verification tool to accelerate aging and to account for uncertainties in the thermal environment. The tolerances of input–output quantities designed into a particular assembly were verified at the low- and high-temperature extremes of this test. The tolerances were maintained, and the varied input–output parameters were specified in the unit vacuum with a duration of 4 hr at low temperature (nominally $-10°C$), and 12 days at high temperature (nominally 75°C). Temperatures were modified by unit test specification in accordance with the TCM testing results.

j. Thermal shock tests. External assemblies were subjected to a thermal shock test to ensure their capability to withstand thermal shock during a change in spacecraft attitude or when the spacecraft entered the Earth's shadow.

k. RF interference tests. Conducted and radiated interference and susceptibility tests were performed when necessary to ensure against interference with other assemblies on the spacecraft, or against vulnerability to interference from launch-area ground RF sources.

Radio-frequency interference tests were performed on the following selected spacecraft subsystems: the science experiments, the narrow angle Mars gate, the CC&S, communications, and the squib-firing assembly. The significant problem during these tests was the difficulty encountered in separating the support equipment RF noise from that of the modules under test.

2. Subsystem FA Environmental Testing

Qualification of *Mariner* Mars 1964 subsystems and assemblies for flight was accomplished using a prescribed test schedule. The general FA specification also established the environmental limits to which components and subassemblies were exposed before delivery to SAF (preacceptance testing). Unit test specifications were generated by each subsystem cognizant engineering group, which specified the performance parameters to be met during and after exposure to environmental stress. Deviations from the requirements of the general specifications, the exact configuration of the unit during test, and the schedule of operations to verify performance were incorporated into the unit test specifications.

A summary of the environmental tests used in the flight-acceptance series is given in Table 77.

Table 77. FA environmental test recapitulation

Environment	Number of tests	Passed	Failed	Failed, %
Vibration	538	512	26	4.83
Thermal–vacuum	310	282	28	9.00
Temperature	21	20	1	4.76
Total	869	814	55	6.33 (average)

a. Vibration tests. Each flight unit was subjected to noise and sinusoidal vibration. Levels and durations were less severe than those employed in TA testing, but somewhat higher than the expected flight level. Equipment that did not operate during booster operation (e.g., midcourse maneuver circuitry) was not required to function within tolerance during these tests, but it was required to survive them. For example, the assembly could not experience problems during vibration that would be detrimental to the Spacecraft System, but it had to be capable of operation in accordance with its test specification without any repair or adjustment resulting from the test.

b. Thermal–vacuum tests. These tests were designed to verify that assemblies would perform satisfactorily in a combined thermal–vacuum environment. The test levels were somewhat more severe than expected flight conditions; a margin of safety that was incorporated to compensate for uncertainties in the thermal environment and to precipitate failure from fabrication weaknesses.

The test consisted of satisfactory operation (per the unit test specification) for 2 hr at 0°C and for 40 hr at 55°C. (Some of the external assemblies had estimated operating temperatures below 0°C, and the test requirements were modified accordingly for those assemblies.)

3. Magnetics

Essentially all magnetics environmental testing was conducted on the assembly or subassembly level. The *Mariner* Mars 1964 was the first JPL program in which a definite effort was made at magnetics control. The *Mariner* Venus 1962 program had highlighted the need for such an effort, and had initiated several study programs of the various problems in magnetics control. From these studies, the first general magnetics specification was developed. Since the magnetics effort was new, one of the main tasks required was to disseminate proper magnetics control information to the hardware personnel before design began.

All TA, PTM, and flight spacecraft equipment was to be examined for its magnetic quality against the magnetics specification to ensure to the greatest possible extent meaningful magnetometer measurements. To satisfy the requirements for environmental testing and to incorporate revised magnetics design restraints that were more definitive, a project-oriented specification was issued. This specification for the first time included the specific requirements described in the following paragraphs for magnetics test scheduling and documentation.

a. Magnetics test sequence. All *Mariner* Mars 1964 type-approval and flight hardware was evaluated for magnetic fields in the following sequence:

1. Type-approval hardware. All type-approval units were evaluated for static (permanent) magnetic fields and dynamic (electrically energized) magnetic fields before type-approval vibration testing. All type-approval units were evaluated for static magnetic fields following type-approval vibration testing.

2. Flight hardware. All flight hardware was evaluated for static (permanent) magnetic fields following flight-acceptance vibration testing.

b. Magnetics evaluation certification. All magnetics tests performed were documented in the manner appropriate to the hardware classification. Type-approval hardware evaluation was recorded on the environmental test results summary report, and the flight hardware evaluation was properly recorded on the SAF delivery certification report.

This specification was the culmination of a lengthy review of various magnetics control efforts, magnetics evaluation of spacecraft materials and subassemblies, and repeated attempts to define adequate magnetics design restraints consistent with the steadily progressing state of the art. Magnetics control efforts, however, received a low priority in view of other severe design requirements. There was a reluctance to deviate from proven design in order to search for suitable nonmagnetic substitutes in the face of the higher priority requirements for reliability, performance, and meeting the launch schedule. Since much of the design of *Mariner* Mars 1964 equipment had been carried over from the *Ranger* and *Mariner* Venus 1962 projects, a great deal of effort was directed at working with cognizant engineers to define the magnetics requirements, the problems involved, and possible improvements and techniques available.

To assist in these efforts, a special study was contracted to determine the magnetic properties of spacecraft components. Incident to this study, a handbook was compiled of terms, formulas, units, and measuring methods pertaining to the properties of magnetics. This handbook was distributed throughout the Laboratory and was of great value in generating a greater awareness and interest in the magnetics control problem. An additional result of the contracted study was a plan for an integrated program for further development of magnetics

control, including a more sophisticated field-prediction technique.

Magnetic mapping of *Mariner* Mars 1964 assemblies and subassemblies was begun in August 1963. The mapping information was summarized in two documents. The first document defined the assembly or subassembly mapped, its serial number, the field at 3 ft, the field at the spacecraft flight magnetometer location, and recommended corrective action, if necessary. The second document was extracted from the first, and defined only those assemblies that exceeded the magnetics design restraints. These two summaries were updated and reissued at frequent intervals. By August 1964, 1908 mappings had been performed on *Mariner* Mars 1964 assemblies, subassemblies, and piece-parts. Many subassemblies were mapped more than once under different conditions, such as before and after vibration tests, with power applied, and occasionally after an engineering change had been made.

The tight time schedule for this program and the stress placed on reliability reduced the possibility of investigating corrective measures when the magnetics design restraints were exceeded. Corrective action was performed when it did not delay schedules or influence reliability. Generally this action consisted of replacing a magnetic material with a nonmagnetic material, providing a limited amount of magnetic shielding, or, as in the case of the solar panels, demagnetizing. The most significant achievement in the magnetics control effort was the ability to successfully deperm the solar panels, so that their effect at the spacecraft flight magnetometer was negligible. This reduced the spacecraft field at the magnetometer about 70%. The panels were depermed from a field of about 30 γ to less than 1 γ at the sensor, using a pair of 7-ft diameter deperming coils developed for that purpose.

The construction of these coils in a very short period was in itself a significant achievement. The large coils were conceived, designed, and constructed within 2 months. They were designed to produce a 100-gauss alternating field along their axes at 1/20 cps, so that voltages induced in spacecraft circuits by this field would not damage the spacecraft. Because of the uncertainty in such a large scale operation, and due to insufficient time to thoroughly investigate the necessary techniques and precautions in deperming a spacecraft, it was decided not to attempt deperming of the spacecraft bus but to concentrate all effort towards the solar panels. In view of this decision and the lack of experience at 1/20 cps, circuit components were hastily assembled to tune and operate the coils at 60 cps. Using a 230 v, 60-cps ac input, it was possible to generate a field of about 22 gauss along the coil axis. Subsequent tests with the TA solar panels indicated that 10 gauss for 10 min with a gradual decrease at the end was sufficient to deperm the panels. The coils were then dismantled, shipped to Cape Kennedy and reassembled in order to deperm the flight solar panels before the scheduled spacecraft launchings. The stability of the solar panels following this deperming remains an uncertainty. Study programs are planned to investigate the stability question and to study deperming of the spacecraft bus.

About 60% of all *Mariner* Mars 1964 hardware produced was evaluated magnetically. Table 78 gives the estimated percentage for each of the *Mariner* Mars 1964 spacecraft.

Table 78. Magnetics evaluation of *Mariner* Mars 1964 hardware

Spacecraft or assembly	Hardware magnetically evaluated, %
TA	50
MC-1	90
MC-2	90
MC-3	60
MC-4	20

Of the 1908 assemblies mapped, more than 140 exceeded the magnetics restraints imposed by the specifications. Piece-parts that particularly resulted in excessive fields were relays, shafts and bearings, solenoid cores, permanent magnets in the gyros, the traveling-wave tube, stainless-steel springs in the pressure regulators, torque motors, bimetal spirals in temperature control devices, modules with welded nickel ribbon buses, and kovar bus bars on the solar panels. The particular assemblies with large fields were the CC&S subsystem, the attitude control subsystem (due to the use of a large number of relays), and the DAS logic assemblies with their welded modules. The DAS logic assemblies were very unstable as a result of vibration testing. Except for the permanent magnet in the attitude control subsystem, the vibration testing affected the magnetics stability of all the above magnetic components to some extent.

In spite of the necessity for a large number of waivers on the magnetics design restraints, the resultant magnetic

fields of the two flight spacecraft launched in November 1964 were relatively low. A direct comparison of the total spacecraft fields between *Mariner* Venus and *Mariner* Mars is meaningless due to the greater complexity, number of subsystems, and increased requirements placed on the *Mariner* Mars mission. Although the total *Mariner* Mars field was about twice that of *Mariner* Venus, the field associated with *Mariner* Mars appears to be considerably more stable. With the spacecraft solar panels depermed, the magnetic fields at the magnetometer sensor were determined to be:

	H_X	H_Y	H_Z
MC-2	2.5γ	21.0γ	17.4γ
MC-3	5γ	11.5γ	30.1γ

A considerable amount of work remains to be done in order to achieve magnetically clean spacecraft. Significant improvements were made by the *Mariner* Mars 1964 Project and greater confidence was acquired in magnetics control efforts.

4. Life Testing

The ultimate aim of any life test is to gain information about the operating characteristics of given equipment as a function of time, and, as a result, to be able to estimate the useful life of the equipment. Traditionally, the concept of a life test is based on statistical considerations and is commonly applied to the testing of relatively inexpensive and readily available hardware.

Such an approach to the *Mariner* Mars 1964 life test program was not practical, since the unit cost severely limited the number of samples that could be chosen. In addition, the length of the mission also presented a severe problem in the design of a statistically meaningful life test, since large samples and long test times would be required to generate data for even the simplest of reliability analyses.

However, it was still more than desirable to discover the time-dependent operating characteristics of the *Mariner* Mars 1964 hardware. Therefore, a life test based on more practical considerations was defined in the decision to limit the life test objectives to the following:

1. The analysis of such effects as the degradation of performance as a function of time, the critical failure modes, and the influence of the assorted test environments on these effects
2. To support, whenever necessary, the diagnosis of inflight problems
3. To provide, whenever possible, indication of the nature and extent of the likely deterioration of flight hardware

The use of the life test program in obtaining estimates of the life expectancy of the *Mariner* Mars spacecraft was inadequate because:

1. The specific units assigned to the life test were the type-approval units, which had just completed the extensive environmental test program designed for them. This factor prohibits their being considered a representative sample of the flight hardware, and a "sample of one" is a poor statistical representation.
2. The individual subsystems tested underwent a wide assortment of environmental conditions ranging from simulated flight and ambient laboratory conditions to extensive temperature cycling. Such variations in environmental stresses are difficult to assess statistically.

The principal outputs of the life test will be the analysis of performance degradation and of the critical failure modes, and the effect of the assorted environments on these areas. From this viewpoint, the use of accelerated environmental conditions is acceptable and appears desirable. An uneventful life test will yield little useful information. However, if at the completion of the tests the critical failure modes and performance degradation characteristics become known, and if the mechanisms contributing to these effects are understood, estimates of the useful life of the hardware under normal operating conditions may be made by a comparison of the life test data with other significant information.

Periodic estimates are being made of the mean time between failures for the various units using the life-test data, and data from all the other tests performed on the TA and similar units.

A life test at the subsystem level was established as a part of the project policies and requirements, and all active spacecraft subsystems and components were governed by this requirement. The type-approval units were assigned for use in the life test and were required to be made available for this purpose immediately following TA testing.

Preliminary life test plans were generated and distributed to the JPL division Project Representatives and the

cognizant personnel. This preliminary plan was essentially a list of the equipment to be subjected to life testing, with comments relative to the gross effort. Following this, a definitive test philosophy for performing life tests of TA assemblies, a set of ground rules based on that philosophy, and a set of life-test plans for the individual subsystems and assemblies was generated in the form of a planning document. Included in this document was a summary of the type of environments to which the various units were to be subjected and the availability of the various facilities for performing the life tests. A description of the life tests is given in Table 79, and a summary of the failures encountered is given in Table 80. After *Mariner IV* encounter, additional data will be reported that will amplify and extend the work being performed in this area.

5. Miscellaneous Subsystem Environmental Tests

a. CC&S fuse acoustic. As a result of the *Mariner* PTM acoustic testing, a failure was observed in the 3/10 amp fuse in the CC&S subsystem. To determine if the failure was the result of excessive acoustic excitation, two separate items were subjected to a 142-db reverberant acoustic field for a period of 90 sec. The fuses were checked before and after the excitation and no failures were noted, and, on the basis of this, the fuses were certified to be adequate for use in the *Mariner* mission.

b. Cosmic Ray Telescope acoustic test. As a result of problems experienced with the Cosmic Ray Telescope, the acoustic susceptibility of the telescope thermal-fin mylar window was investigated. The assembled Cosmic

Table 79. *Mariner* Mars 1964 life tests

Subsystem	Reference designation	Unit serial number	Date life test started	Operating hours			Remarks
				Before life test	From start of test to 2/15/65	Total	
Cosmic Dust Detector	24A1	TA	NA	1524	NA	NA	Life testing, including temperature cycling from −20 to 75°C in vacuum, to be performed by the experimenter.
Ionization Chamber	26A1	111	10/16/64	790	3051	3841	Instrument operating in vacuum of 10^{-5} torr at ambient temperature.
Cosmic Ray Telescope	21A1	TA	NT	NT	NT	NT	Unit not subjected to life tests.
Trapped Radiation Detector	25A1	TA	10/16/64	1313	3192	4505	Unit operated in temperature chamber and subjected to temperature cycling.
Helium Magnetometer	33A1	2	10/12/64	756	2874	3650	Sensors housed in magnetic shield in vacuum and operated at 30°C for first 2000 hr, and then controlled at initial temperature (20°C) of flight sensor. Electronics operated at 40°C throughout the test.
	33A2	2	↓	756	2874	3630	
	33A3	0		691	2874	3565	
Solar Plasma Probe	32A1–32A4	MC-0	12/16/64	NA	NA	NA	Unit operated at 33°C in vacuum. Test performed at MIT.
DAS	20A1	2	12/23/64	1040	1060	2100	Units operated in ambient temperature and pressure environment.
	20A2	MC-7	2/12/65	1330	70	1400	
	20A3	TA	12/23/64	840	1060	1900	
	20A4	MC-7	2/12/65	1330	70	1400	
	20A5	3	12/23/64	1040	1060	2100	
Planetary scan subsystem	31A1–31A3	TA	8/24/64	531	1969	2500	Unit operated in 25°C and 10^{-3} torr environment.
Television	C36	MC-TAM	8/4/64	525	1055	1580	Unit operated in 70°F and ambient pressure environment.
Data encoder	6A1–6A13	1	1/7/64	NA	9521	NA	Ambient temperature and pressure environment.
		3	7/10/64	1494	5131	6625	Ambient pressure and 167°F environment.

NOTE: NA Not available
NT Not tested

Table 79. (Cont'd)

Subsystem	Reference designation	Unit serial number	Date life test started	Operating hours			Remarks
				Before life test	From start of test to 2/15/65	Total	
Command subsystem	3A1–3A7	2	7/9/64	1500	5130	6630	Ambient pressure and 167°F environment.
Radio subsystem	2	MC-0	1/27/64	1450	456	1906	Flight temperature and 10^{-6} torr environment.
Tape machine	16A1–16A5	2	8/4/64	1305	4680	5985	Nonoperating life test at flight temperature and 10^{-6} torr.
Power subsystem	4A8–4A13, 4A15–4A18	02	8/17/64	675	4640	5315	Unit operated in flight mode in vacuum and subjected to temperature cycling from −10 to +75°C.
Battery	4A14	6	2/11/64	0	6540	6540	Units subjected to life test simulating flight conditions. Each unit operated under different temperatures ranging from 50 to 100°F, with one unit following the flight temperature profile.
		7	2/11/64	0	2112	2112	
		8	8/19/64	0	4320	4320	
		9	5/1/64	0	5496	5496	
		10	11/28/64	0	1896	1896	
Attitude control electronics	7A1	002	6/15/64	354	5872	6226	Unit operated in 167°F and atmospheric pressure environment.
Sun sensors	7PS6	2	6/15/64	NA	6150	NA	Unit operated in 75°F and atmospheric pressure environment.
Earth detector	7ED6	2	5/12/64	380	6360	6740	Unit operated in 75°F and atmospheric pressure environment.
Canopus sensor	7CS8	004	12/18/64	424	1750	2174	Units operated in 70°F and atmospheric pressure environment.
		103	12/3/64	540	1437	1977	
Narrow angle Mars gate	7HG1	011	5/12/64	400	6775	7175	Unit operated in 75°F and atmospheric pressure environment.
Solar pressure control assembly	7PC	8	10/5/64	0	3840	3840	
Jet vane actuators	7JV1	2, 4, 7, 32	8/24/64	0	4800	4800	
Attitude control gyros	7A2	012	4/1/64	NA	6800	NA	Unit operated for 1038 hr at 165°F and 10^{-6} torr. Additional operations at ambient temperature and pressure.
CC&S	5A	MC-TA	4/1/64	537	5815	6352	Unit operated at temperature from 14 to 167°F and atmospheric pressure.
Scan actuator and support	31A4	C111	11/9/64	NA	NA	NA	Unit to be operated at nominal cooling shroud temperature of −131°F and 10^{-5} torr.
Dampers, retarder, and timer	8111	C126, C104, C132	11/9/64	NA	2426	NA	Units stored at 131°F and 10^{-5} torr.
Science cover latch actuator	31M2	C4, C-prototype	11/9/64	NA	NA	NA	Units operated cyclically at 55°C and 10^{-5} torr.
Pyrotechnic control subsystem	8A1, 8A2	1003, 1004	8/31/64	430	4544	4974	Cyclically activated and stored at 135 to 155°F and 15×10^{-3} torr.
PIPS	10A	003	2/10/64	NA	NA	NA	Flight-type system, filled and pressurized to flight levels, was stored at temperatures ranging from 80 to 120°F and 1 atm. Unit removed and fired on 3/12/64 and 6/11/64. Life test completed after 323 days of storage.

NOTE: NA Not available
NT Not tested

Table 80. Failures encountered during life tests

Unit	Operating time	Nature of failure	Remarks	Unit	Operating time	Nature of failure	Remarks
Tape recorder	NA	Lower than specified reset level of the integrator monitor signal	The operation of the system remained unchanged. Detailed analysis of the problem was performed at the conclusion of the test.	CC&S	2700 hr	Broken wire in the end counter magnetic module	Failure was apparently due to extensive stressing of the wire during TA shock and vibration tests combined with temperature cycling during life test.
	NA	High bit-error rate	The error rate of the VSS was acceptable from a *Mariner* Mars 1964 mission standpoint. To correct this problem would have required a redesign of the unit and was not attempted.	Science cover latch actuator	NA	Indication of solenoid plunger movement not received at brush recorder	Solenoid was within tolerance. Microswitch used for end-of-stroke indication was found to be out of adjustment. The switch was part of the test setup.
Battery	1370 hr	Broken plate leads in No. 3 cell	A high-current test prior to life test identified cell No. 3 as being nonuniform. This test was added to the FA test sequence to detect any defect in flight batteries.	Postinjection propulsion system	2 months	Pressure transducer failed	All flight systems used redesigned transducers in which this type of failure could not occur.
	5496 hr	End of life	Both units were operating at the elevated temperature of 100°F.	Planetary scan	1061 hr	Unit failed to track	The 180°F neon lamps were damaged when unit was used with new subsystem checkout equipment. Lamps were replaced and testing continued.
Canopus sensor (flight spare)	190 hr	Short in OSE resulted in damaged Canopus sensor components	Damaged components were replaced.	Television	NA	Shutter failure occurred 9/4/64[a]	The failure was due to mechanical wear of the shutter from excessive number of operations. This was an expected failure.

[a]The wearout mode on the shutter was in the solenoid bearing, which became gritty and caused the solenoid to lose net torque output.
NOTE: NA Not available

Ray Telescope TA unit was suspended in the 930-ft^3 reverberation chamber and subjected to 90 sec of 142-db shaped acoustic noise. The unit was subsequently disassembled and inspected. No failures were detected.

c. Tape deck acoustic test. The purpose of this test was to verify the adequacy of the spacecraft tape-transport vibration-isolation system when it was subjected to acoustic excitation. The tape-transport case, having the flight-type vibration-isolation system and mass simulated components, was suspended in the 930-ft^3 reverberation chamber by elastic cord, and subjected to 90 sec of 142-db acoustic noise.

The vibration levels, recorded by three orthogonal accelerometers in the case, were of low magnitude and well within the vibration-test requirements.

d. Solar Plasma Probe acoustic test. To investigate the acoustic susceptibility of the Solar Plasma Probe, the TA unit was subjected to 90 sec of an 142-db acoustic field. The unit was subsequently inspected and no failures were detected.

e. Solar panel pinpuller shock test. To determine the effects of explosive pinpuller firing on the *Mariner* Mars solar panels, a pinpuller shock test was performed. A solar panel was mounted vertically by its hinges and actuator fittings. The panel was fitted with two pinpullers and a number of accelerometers. As a result of the firing of the squibs, it was established that the effects on the panel were similar to those experienced during the *Mariner II* flight to Venus. These tests demonstrated that the *Mariner* Mars 1964 solar panels would not be significantly affected by the transients associated with the firing of the pinpullers.

f. Vidicon tube support material evaluation. To determine the effects of the thermal–vacuum environments on the mechanical properties of the vidicon-tube support

material, a series of tests were performed. The first set of tests consisted of subjecting a simple single-degree-of-freedom system to a low-frequency sine sweep (1-*g*-rms input, 10 to 2000 cps), using the vidicon support material as the elastic medium, to determine the natural frequency of the system and its peak response. Following this vibration test, the material itself was subjected to an FA thermal–vacuum test, which consisted of a soak in a vacuum of 10^{-6} mm Hg at 32°F for 2 hr and at 131°F for 40 hr. At the conclusion of the FA thermal–vacuum test, the system was again mounted on the vibration exciter, subjected to the same vibration test, and then subjected to another thermal–vacuum test using the TA levels. This last test consisted of a soak in a vacuum at 10^{-6} mm Hg at 14°F for 4 hr and at 167°F for 12 days. At the conclusion of the test the unit was again subjected to the sine-sweep vibration test.

The response plots for the test system are shown in Fig. 368. It is evident from a comparison of the curve obtained before the FA thermal–vacuum test with that obtained afterwards that the environment resulted in a slight increase in both the resonant frequency and the peak-amplitude response. Larger changes in resonant frequency were noted after subjecting the unit to the TA level thermal–vacuum test, but not with an accompanying corresponding increase in acceleration amplitude.

A tendency of the polyurethane to outgas in the vacuum was observed. Approximately 3 g in 70 were outgassed as a result of this environment. (The outgassing was an indication of the effects noted in the vibration response, considering the fact that changes in the mechanical properties of the material existed as a result of the environment.) The testing was performed at such a late date in the program that the significance of the outgassing and the changing mechanical properties could not be translated into direct effects on the vidicon camera, although, on the basis of the specific results, it appeared that the performance would not be seriously degraded.

6. Analysis of Subsystem Environmental Tests

The small quantity of subsystem problems during system-level flight-acceptance testing attests to the adequacy of subsystem qualification and acceptance testing. It is probable that some environmental levels in the type-approval test schedule could have been lowered for selected items of hardware without detracting from the purpose of these tests. The overall failure rate of 7.2% in TA testing was diluted even further by the inclusion of 271 tests (32% of total) in environments of dubious use for design evaluation.

A total of 83 design changes were documented as a result of problems encountered during environmental testing. Of the 83 changes, 39 originated at the TA level, 14 at the FA level, and 30 during bench, system, or vendor environmental tests. The majority of the changes instituted during FA level testing were due to schedule slips, which necessitated running FA tests prior to, or concurrently with, TA tests. On an ideal schedule, the TA testing would have demonstrated the need for the design change before flight hardware was fabricated. A performance comparison between TA and FA tests in the two most critical environments (vibration and thermal–vacuum) is presented in Table 66.

Experience acquired during the *Mariner* environmental testing program indicates the advisability of limiting outside, or vendor, testing to those facilities that have been thoroughly screened and approved by cognizant representatives of engineering and quality assurance. Thorough indoctrination of vendor personnel in applicable test specifications, standard operating procedures, and reporting systems is a further prerequisite to reliable test performance and data from vendor sources.

The severe environmental exposure during the TA test program revealed several design and component weaknesses that required redesign or substitution of less vulnerable components. Some representative examples are:

1. Encapsulated pellet resistors in the RT DAS were temperature-sensitive and changed value rapidly at the high TA temperature of 75°C. A redesign incorporated glass-coated pellet resistors.
2. The original television vidicon tube could not survive TA-level vibration. A highly ruggedized tube and soft-mounting solved this problem. The camera also encountered a low temperature problem necessitating redesign of the shutter solenoid bearing.
3. The radio subsystem's original dual-cavity-amplifier power supply lost voltage regulation at the upper TA temperature. This problem was resolved by a redesign using a hybrid (cavity and TWT) amplifier.
4. A redesigned transformer was incorporated in the Solar Plasma Probe power converter after failure of the original design during TA thermal–vacuum testing. A number of other changes were incorporated into the instrument, but time did not permit deletion of the T0-51 package transistors that constituted the most consistent problem area.

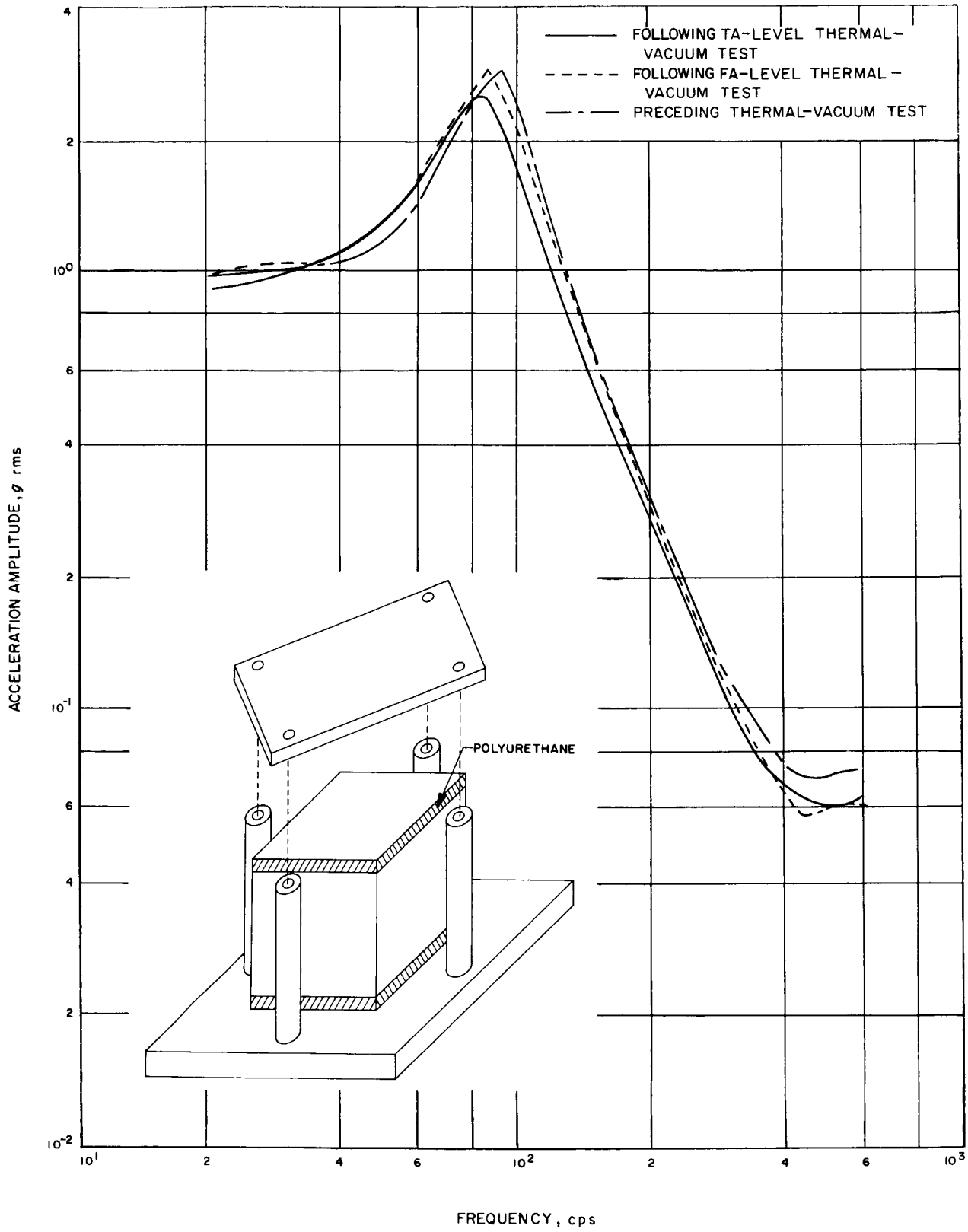


Fig. 368. Test setup and response curves of vidicon-tube support-material evaluation test

5. The Canopus sensor image-dissector tube experienced failure in vibration similar to the TV vidicon, until a ruggedized tube was developed.
6. A number of structural elements, including the solar panels, required modification after STM or PTM vibration testing failures.
7. A number of electronic part failures were observed during TA testing. Most of these are considered to have resulted from infant mortality since no failures were observed in the several instances after part replacement. Preacceptance screening was effective in reducing part failures to a minimum during the testing of flight hardware.

Documentation of all waivers or deviations from specification test requirements was a project requirement. The greatest percentage of waivers appeared in the areas in which the least informative environments (in the area of design evaluation) were a requirement; i.e., transportation vibration, explosive atmosphere, package drop, and static acceleration. Transportation handling and humidity testing were waived on the basis that the subsystems involved would not see these environments. The remaining waivers were minor variations in procedure or permission to proceed with testing prior to release of an approved unit test specification.

C. Miscellaneous Qualification and Developmental Testing

During the *Mariner* Mars 1964 program, many special developmental and qualification tests were conducted to prove the feasibility and adequacy of the spacecraft mechanical hardware. In addition to the PTM, four test spaceframe structures were fabricated. These were:

1. The structural test model, which was composed of mass and structural simulations of all spacecraft components including electrical cables. The STM was used primarily for the structural qualification tests of the basic structure.
2. The temperature control model, which was composed of thermal mockups of all critical spacecraft items. All external surfaces and thermal shields were flight equivalent. Electrical resistors were mounted on unweighed electrical component mockups. The TCM was used primarily for the first series of space-simulator tests.
3. The developmental test model, which was a structural simulation of the flight spacecraft structure. It was composed of mass mockups of all structurally critical spacecraft items. It was primarily used for LMSC structural vibration qualification tests. It could also have been used as a backup qualification structure in the event of an STM structural failure.
4. The extra test model, which was composed of a basic octagon structure ballasted to the proper boost weight and moment of inertia. It was used for LMSC *Agena*/spacecraft separation tests and other interface tests.

These prototypes were used in most of the mechanical tests. The developmental spaceframe schedule (Fig. 369) contained a summary of the test spaceframe use.

In addition to the spaceframe tests, many developmental tests using prototype and test hardware were performed. These tests were used to confirm analyses, to verify problem solutions, and to gather critical information essential to project success.

1. Spacecraft Structural Tests

Three basic tests were conducted on the composite STM spacecraft: a static test, an initial vibration test, and a final vibration test.

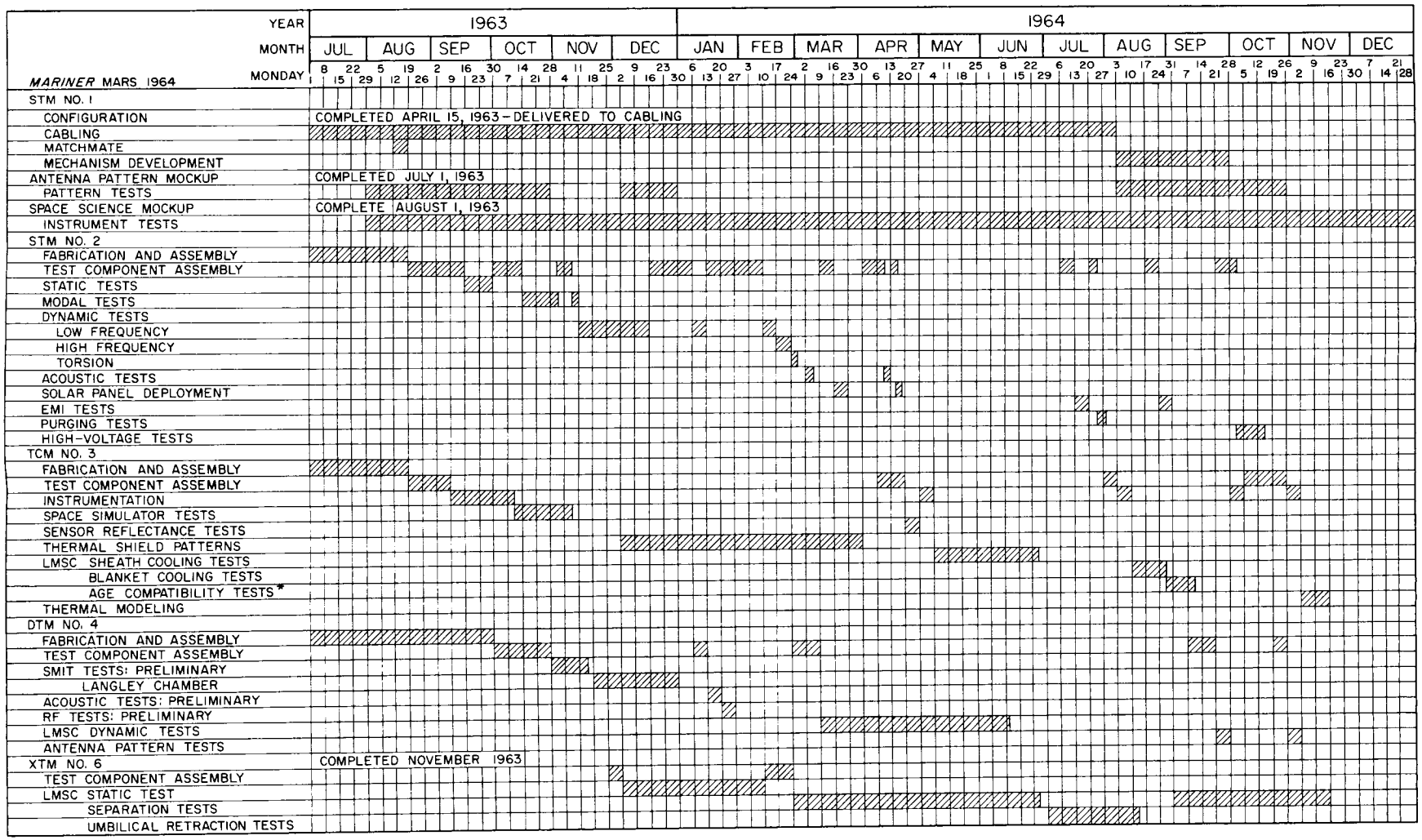
a. Static test. The objective of the static test was to demonstrate the structural integrity of the spacecraft/adapter interface at an early date in the program. The tests were conducted in two phases.

Phase I. Phase I consisted of a V-band/spacecraft lower structure proof test. This test demonstrated the capability of the spacecraft/adapter interface and spacecraft lower structure to support the loads induced by the V-band.

Phase II. Phase II consisted of an ultimate shear and overturning moment static test. This test demonstrated the structural integrity of the primary structure, adapter, and separation system to sustain the design load environment.

A secondary objective of the test program was to establish the stiffness characteristics of the spacecraft adapter. Of major concern was the character of the radial stiffness and its influence on matchmating or separation.

The test vehicle subjected to both Phase I and Phase II was the complete basic octagon structure with electronic assemblies installed and a structural LMSC spacecraft adapter. The solar panels, low-gain antenna, high-gain antenna, and superstructure were not included. The midcourse motor was simulated by the use of a substructure



* AUTOMATIC GROUND EQUIPMENT

Fig. 369. Developmental spaceframe schedule

and a simulated PIPS thrust plate. A simulated central torque tube, the upper and lower bearings, and a split bearing cap simulated the science platform. The LMSC adapter included only the primary adapter structure and the spacecraft ejection springs.

Figure 370 shows the general setup and fixtures used in Phase II. The STM adapter test specimen was oriented in the static test jig so that loads could be applied in any of five lateral directions. Loads were applied to the specimen through a 10,000-lb-capacity hydraulic jack and the special loading plate attached to the top of the bus. Load monitoring was accomplished through a 5000-lb-capacity load cell. A detailed mechanical inspection was performed on the adapter prior to its installation on the STM.

The critical load condition to which the Phase I test was performed was a nominal V-band strap tension of 2600 lb and an overtest to 125% of the nominal load (3250 lb). The critical environmental load condition to which the Phase II test was performed was a limit load of 4 g lateral and 1 g axial. These loads were applied at the spacecraft boost configuration CG (22.50 in. above the separation plane and 1.50 in. off the spacecraft roll axis). Load-level magnitudes were:

	Limit loads	*Ultimate loads (125% of limit load)*
Lateral	2280 lb	2850 lb
Axial	570 lb	570
Overturning moment	51,000 in./lb	63,500 in./lb

In addition to the loads defined, a 2600-lb design preload existed in the V-band strap as well as an 80-lb ejection spring force in each of four springs. These preloads were both limit and ultimate values in the tests.

The instrumentation for both test phases consisted almost entirely of strain gauges widely dispersed throughout the spacecraft and adapter. The strain gauges used in these tests were foil gauges. Data from sources other than strain gauges were obtained from linear potentiometers, thermocouples, force links, and the load cells. An automated digital readout data system was used to collect all of the information and to permit rapid raw-data reduction for computer programming. Accuracy of the instrumentation system was estimated to be ±5%.

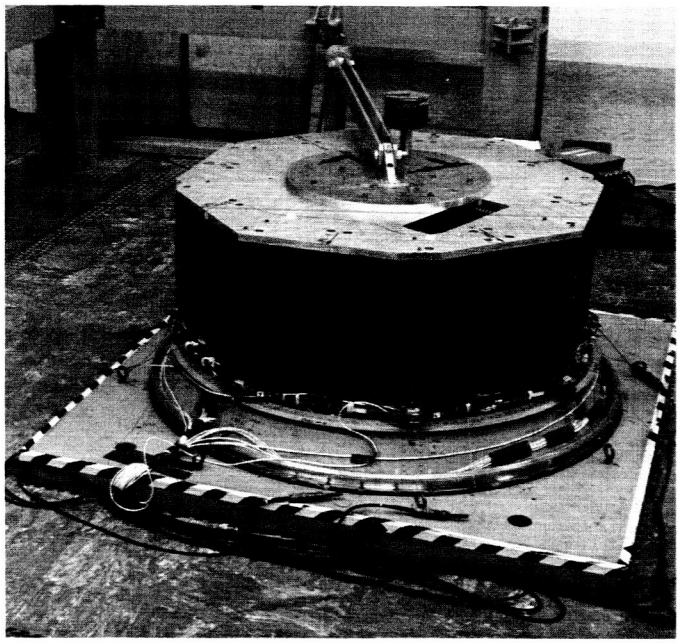


Fig. 370. Static test setup

These tests demonstrated the capability and integrity of the spacecraft lower bus structure, adapter, and separation joint to readily support the stresses and deformation induced by the V-band and the design load environment. An evaluation of the on-site test data, a visual inspection of the vehicle after the tests, and subsequent assessment of the pertinent strain gauge data indicated that the structure sustained the ultimate load conditions without permanent set, excessive stresses, or damage.

b. Initial spacecraft structural-vibration test. Developmental vibration testing of the structural test model was conducted in December 1963, and was concluded because of a structural failure of a substandard solar panel structure. Qualification vibration testing of a modified and more complete STM was conducted in February 1964. The objectives of this test were to determine:

1. The dynamic response characteristics of the STM for input loads
2. The adequacy of the primary structure and the structural components when subjected to structural qualification dynamic loads
3. The adequacy of the environmental vibration specification on the spacecraft, particularly in the low-frequency range

The STM was mounted on the *Mariner/Agena D* adapter, which, in turn, was mounted to the appropriate

vibration fixture for torsional excitation, for excitation parallel to the roll axis, and for excitation in two other orthogonal directions. A typical test setup is shown in Fig. 371. Sinusoidal excitation from 5 to 35 cps was accomplished with an electrohydraulic vibration exciter. Electromechanical vibration exciters were used for excitation of frequencies above 35 cps. All vibration testing was conducted at the JPL environmental test laboratory.

For the low-frequency (5 to 150 cps) structural developmental and type-approval testing, peak control was used because of tighter maximum load control. For the high-frequency (150 to 2000 cps) and complex-wave portion of the test, quadratic-mean control was used because input of this type is more symbolic of equal energy distribution. Six control accelerometers were equally spaced on the diameter of the vibration exciter fixture at the adapter/vibration fixture interface.

Input and response acceleration was measured with piezoelectric-type accelerometers. Dynamic strain in the test structure was measured with strain gauges. The strain gauges on the solar panel dampers were wired and calibrated to read load directly. All measurements were recorded on magnetic tape. Detailed instrumentation location was given in instrumentation data sheets. Dynamic deflection of the solar panel tips was measured photographically with a high-speed movie camera synchronized with strobe lights. A grid pattern was superimposed on the film by means of a split-image technique, thereby providing direct visual measurement of the solar panel tip excursions. Tension in the V-band was monitored and recorded before and after each forced-vibration test.

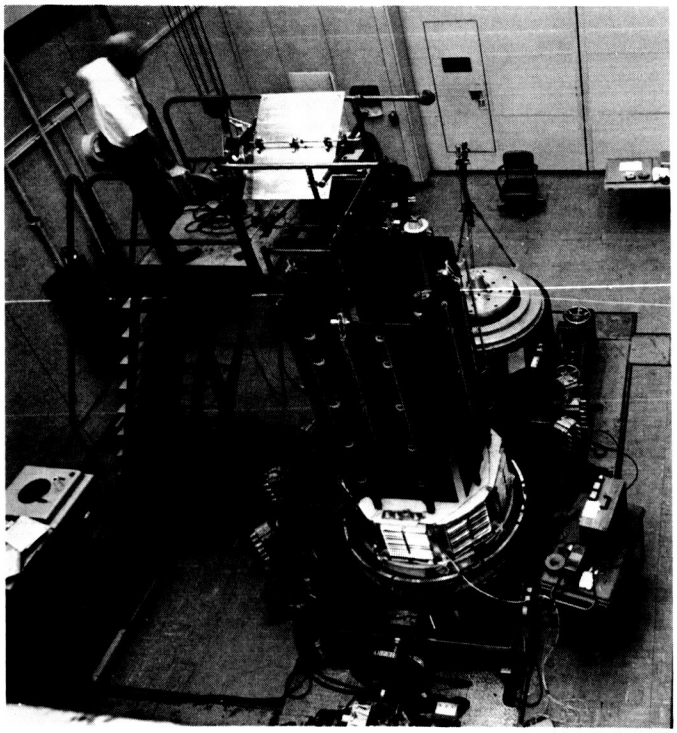


Fig. 371. Overall STM vibration test setup

Structural qualification vibration loads were applied to the STM. Low-level sinusoidal sweeps were made prior to each TA test. The response of pertinent parts of the test structure was evaluated from direct-write plots before running the test at full level.

The initial STM developmental vibration tests were to determine response data and to perform preliminary qualification tests on various structural elements. The interpretation of the test data was complicated by the strongly nonlinear behavior exhibited by several elements of the spacecraft. This was particularly evident in: (1) the solar panel boost dampers; (2) the bladder fuel sloshing in the PIPS; (3) the backlash in the scan-platform bearings when the friction load was overcome.

Reduced response information for the PIPS propellant tank during the most critical Z-axis low-frequency test showed that the resonant peak occurred at 108 cps. This appeared only on the unfiltered plot, which indicated that an input at 108 cps excites a response at a different frequency (54 cps). The PIPS successfully completed the test.

Response information for the high-gain antenna is shown in Fig. 372. Additional response information was obtained for the Canopus sensor, the science platform,

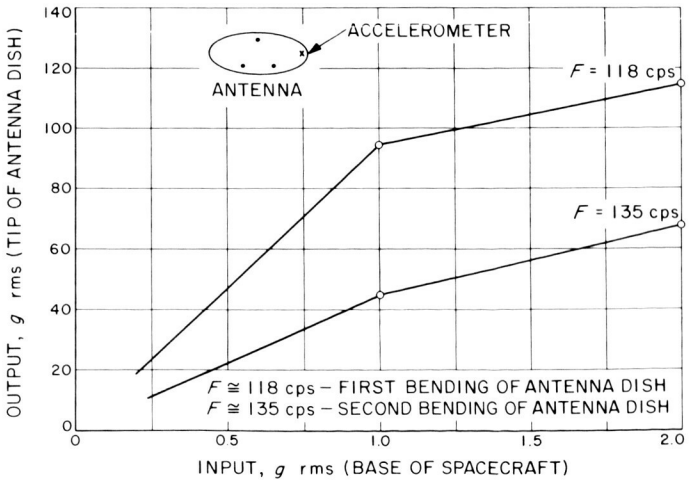


Fig. 372. High-gain antenna structural response

and the adapter. These data were used to check the analysis of the structural elements and to provide the basis for the determination of improved component-vibration specifications.

The STM successfully demonstrated its ability to withstand structural qualification vibration loads with the exception of a few high-frequency failures of some spot welds on the upper cable trough. These were attributed to poor fabrication control.

c. Final spacecraft structural vibration test. A complete series of tests was conducted on the STM after several hardware modifications. This test qualified most of the structural hardware. The test was a repeat of the preliminary vibration test. The test objectives were:

1. To obtain additional structural response information with respect to the design changes in the spacecraft structural elements, and to acquire further data on the relationship between structural response and pressure in the midcourse motor propellant tank.

2. To improve confidence in the modified test specifications of critical components relative to the STM environment. Specifically, better transducer coverage was used in critical areas and actual hardware was included in place of mockups to give a more realistic and informative picture of the response of the TV and Canopus sensor.

3. To qualify the complete structure, including those items that were modified or added after the preliminary test.

The test setup, instrumentation, and loads were essentially the same as for the initial spacecraft structural-vibration test. The interpretation of the test data indicated that the dynamic response characteristics of the *Mariner* spacecraft were very similar to the results obtained during the preliminary test, except for the fully pressurized condition of the PIPS fuel tank.

The structural response characteristics of the propulsion system were extremely sensitive to propellant tank pressure. There was dynamic coupling between the propulsion system and other spacecraft elements, so that in some modes the response of the entire spacecraft was a function of propellant tank pressure. For maximum propellant tank pressure, the most critical Z-axis low-frequency test data indicated a higher dynamic response for a comparable input level.

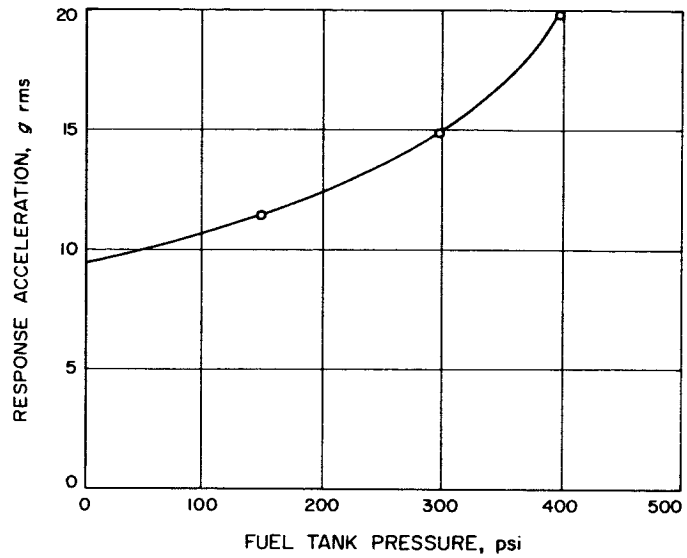


Fig. 373. PIPS total vector response as a function of tank pressure

Figure 373 illustrates the total vector response of the PIPS fuel tank for various fuel tank pressures due to a type-approval level vibration input to the spacecraft. Excitation to the spacecraft was 2.0 *g* in the axial direction; the frequency of the fundamental mode was 55 cps. These phenomena are characteristic of dynamic fluid motion in a bladdered tank.

Because of the damper nonlinearity, different response characteristics were observed in the upsweeps and downsweeps. These test results confirm the adequacy of the solar panel damper vibration test specification and design.

Sufficient vibration testing of the STM was performed to demonstrate the structural integrity of the test vehicle subjected to the most severe test conditions.

The following failures occurred during the testing:

1. A solar vane deployment mechanism bracket (rejected flight hardware), which had undergone previous STM testing, failed during lateral low-frequency vibration. It was replaced for the remaining tests, and the failure was attributed to fatigue.

2. The omnidirectional antenna support bracket, which had undergone previous STM testing without damage, developed a crack through the bracket and doubler during axial low-frequency vibration. A doubled bracket was installed for the axial high-pressure tests.

3. Inspection of the STM following the test sequence revealed several failures at the tie-down locations of the upper cable trough. These failures were attributed to improper fabrication methods that were accentuated by fatigue.

Aside from the fatigue failures noted above, the STM successfully withstood structural qualification vibration loads in the most critical test configuration. A supplementary test was conducted late in the program to verify the adequacy of the revised and additional hardware that were fabricated late in the program.

Several improvements were incorporated in the *Mariner* Mars dynamic test program over previous test programs. A special load control circuit was developed for the STM tests by the environmental test laboratory. The unique features of this control circuit were its capability of controlling the acceleration input to the test structure from six discrete control points, and automatically switching to a constant magnitude force control if the maximum vibration exciter output force exceeded a preset value. Using the six point acceleration control, two different methods of acceleration monitoring were used:

1. Peak control, which, instantaneously sensing the outputs of all six control accelerometers simultaneously, selects and controls from the transducer with the maximum output signal

2. Quadratic-mean control, which controls from the dc signal obtained from the square root of the sum of the squares of all six transducer signals

2. STM Testing

a. Basic structure static test. The structure for this static test (Fig. 370), which was composed of the STM basic octagon structure, STM ballasted electronic chassis, attitude control gas-bottle support structure, and PIPS support structure, was mounted on the *Mariner/Agena D* adapter, which, in turn, was bolted to a rigid foundation. The test specimen was oriented in a static test jig so that loads could be applied in any of five lateral directions to the spacecraft roll axis. Loads were applied with hydraulic jacks to the specimen through a loading fixture. Test loads were monitored on load cells.

Instrumentation in all phases of the test consisted almost entirely of strain gauges widely dispersed on the spacecraft and adapter. The strain gauge outputs were recorded on punched-paper tape storage for computer programming.

This test demonstrated the capability of the spacecraft basic structure, adapter, and separation joint to support the stresses and deformations induced by the V-band and by loads in excess of the design load environment.

b. Vibration qualification test. The structural test model was mounted on the *Mariner/Agena D* adapter, which, in turn, was mounted to the appropriate vibration fixture for torsional excitation, for excitation parallel to the spacecraft roll axis, and for excitation in two other orthogonal directions. Electrohydraulic vibration exciters were used for low-frequency sinusoidal excitation below 35 cps, and electromechanical vibration exciters were used for higher-frequency harmonic and random noise testing. Input and response acceleration was measured with piezoelectric-type accelerometers, and dynamic strain was measured with strain gauges. All instrument measurements were recorded on magnetic tape for ease of data reduction.

The interpretation of the test data was complicated by the strongly nonlinear behavior exhibited by several elements of the spacecraft. This was particularly evident in the solar panel boost dampers, the bladder fuel sloshing in the PIPS, and the backlash in the scan platform bearings when the frictional load was overcome.

c. Modal survey. The complete structural test model, in which point dampers were replaced with solid links, was mounted on the *Mariner/Agena D* adapter, which, in turn, was mounted to a rigid foundation (Fig. 374).

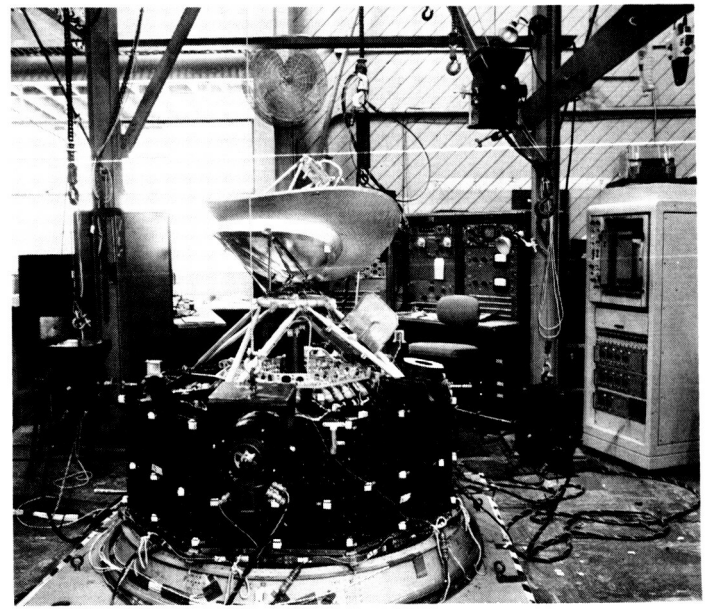


Fig. 374. Modal survey test setup

Excitation necessary to stimulate the normal modes of the test structure was provided by several small portable electromechanical vibration exciters. Frequencies and mode shapes of the test model were measured with small movable accelerometers.

An estimate of structural damping was derived from logarithmic decrements for the well defined modes. No well defined normal modes exhibiting gross vehicle motion were excited below 150 cps; however, the normal modes involving the motion of structural assemblies were surveyed. These mode shapes and damping were used for iteration of the structural analyses.

d. Acoustic tests. The objectives of the STM acoustic tests were (1) to subject the STM spacecraft to the PTM-type test in preparation for testing the PTM, and (2) to measure the acoustic transmission loss of the flight-type shroud.

The STM configuration for the pre-PTM acoustic test was identical to that of the PTM acoustic test. The spacecraft was placed in the JPL 930-ft^3 reverberation chamber on an isolated dolly and subjected to a 142-db reverberant acoustic field. The STM configuration for the flight-type shroud transmission loss test was identical to that of the DTM acoustic test. The spacecraft was encapsulated in the shroud and mounted to a 3-ft portion of the *Agena D* forward equipment.

The shroud acoustic transmission characteristics differed widely from those measured during the DTM test. The differences were partly due to the difference in shroud design and partly due to the sensitivity of the setup configuration on the results.

e. EMI group tests. The STM was used for three EMI group tests. In the first test, the STM was used in the measurement of the shroud attenuation to a broad range of frequencies. The second test was to determine the RF coupling into the spacecraft from the *Agena* telemetry and C-band beacon systems. The third test was a high-voltage test to investigate the breakdown of accumulated charge on a spacecraft shroud.

The objective of the shroud attenuation measurements was to examine the RF shielding characteristics of the flight model shroud in the frequency range of 10 to 10,000 Mc. These data were necessary for evaluation of the susceptibility to RF fields of the flight-configuration spacecraft.

It was found that the shroud offered a nominal RF attenuation of 35 db across a frequency range of 100 to 10,000 Mc. Below 100 Mc, a resonant-cavity effect within the shroud cavity became apparent. The insertion of the STM spacecraft mockup caused a shift in the frequencies at which resonances appeared, as compared to the earlier shroud attenuation test that did not use a spacecraft model.

In the RF simulation test of the PTM during the system test performed in February 1964, it was discovered that the data encoder and the OSE precision coupler power readout were susceptible to the *Agena* telemetry RF power-density level. The value that was used for this test had been established from levels derived from *Ranger* tests. After the interference was noted there was doubt that the level taken from the *Ranger* tests was applicable to a *Mariner* Mars 1964 configuration. The difficulty in calculating this level was caused by the unknown near-field effects of the RF energy coupled into the spacecraft from the *Agena* antenna. The test was run to establish a simulation level that would be applicable to the configuration of the *Mariner* and the *Agena* forward section. It was decided that the RF level contributed by the *Agena* C-band beacon would also be determined in this test.

As a result of the test, the *Mariner* Mars 1964 RF power-density level from the *Agena* telemetry source was determined to be +19 dbm/m^2. The level for the C-band beacon was determined to be approximately +1.5 dbm/m^2 peak pulse power and −28 dbm/m^2 average power. It was determined that the *Agena* telemetry Yagi simulation antenna should be in a horizontal position, and that the C-band beacon simulation horn antenna should provide vertical polarization. These antenna orientations were used in all EMI simulation tests. The reduced *Agena* telemetry RF level was used in flight spacecraft tests; the C-band beacon RF level was left unchanged.

f. Low-speed (handling) impact tests. During Cape Kennedy operations with the MC-3 spacecraft, a number of hoisting cranes malfunctioned during normal operations such as (1) mating of the spacecraft to its work fixture (U-ring); (2) lowering of the shroud onto the adapter; and (3) lowering the spacecraft protective cover onto the U-ring while the spacecraft was installed. The net result of these malfunctions was that the spacecraft experienced abnormal impact transients of unknown magnitudes. Measurements of the actual crane lowering

speeds were made, which resulted in reasonable estimates of the most severe impact velocities.

To demonstrate integrity of the flight spacecraft for these events, the structural test model was subjected to a set of low-speed impacts onto a U-ring in the environmental test laboratory. It was estimated that of all the instances of malfunctioning cranes, the most damaging would have been the direct impact of the spacecraft onto the U-ring. For this reason, the other incidents were not simulated. The tests performed on the STM consisted of nine controlled impacts of the spacecraft onto the U-ring. Four impacts were conducted at approximately 0.8 in./sec vertical sinking speed and five impacts at approximately 2.4 in./sec. An estimate of the impact speed experienced at Cape Kennedy was 2.25 in./sec.

The STM was instrumented with approximately 30 accelerometers in locations similar to those employed on earlier PTM shock tests (V-band, pyrotechnic firings). The data from these accelerometers were recorded on tape for each run and were analyzed using both high-speed oscillograph playbacks and shock spectra. High-speed motion pictures were also taken during each impact.

The suspected configuration of the STM for each impact was such that spacecraft feet A and H were approximately $\frac{5}{8}$ in. lower than feet D and E, which were opposite them.

An evaluation of the data indicated that the most severe impact was experienced during the fourth test at 2.4 in./sec, at which time the STM impacted the U-ring with the spacecraft feet somewhat off-center relative to the U-ring feet. The data on the accelerometers of interest indicated that the transient experienced was less severe than similar transients experienced by the PTM during the pyrotechnic firings. The spacecraft flight transducer recorded a maximum transient response of 17 g (zero-to-peak), compared to 155 g (zero-to-peak) from V-band release, with comparable frequency spectra. On the basis of the test performed, it was concluded that of the incidents experienced at AFETR none was as severe as the shock due to V-band release. Since the spacecraft design had been demonstrated to be compatible with that particular environment, there was no reason to believe that the MC-3 vehicle was degraded by these incidents.

g. Shroud cavity purging tests. To provide proper environmental control for the spacecraft during prelaunch operations, a dry-nitrogen purge was provided for the spacecraft when it was encapsulated by the shroud or storage container. The test objective was to demonstrate the capability of the purge system to adequately purge the spacecraft when it was encapsulated by the shroud.

The test procedure was to purge the shroud cavity using the portable purge control unit until a low dew point (between -15 and $+10°$F) was achieved at the lower shroud system purge fitting. At that time, the purge was stopped and the increase in dew point was monitored for a period varying from 5 to 25 hr.

Gas leakage through the test shroud prevented a high enough pressure buildup under the shroud to permit use of the dew-point indicator on the portable purge control unit. However, it was possible to consistently maintain a dew point less than $+15°$F for periods greater than 5 hr after the purge had been stopped even with the excessive shroud leakage.

h. Solar panel deployment tests. The objective of this series of tests was to observe the solar panel actuation system, including the solar panel release with "live" squibs and the opening and latching sequence. Although each subsystem had been tested individually, it was thought that a complete system test would be advantageous.

The STM was mounted on the spacecraft positioner, and oriented so that the roll axis was horizontal (Fig. 375). Two panels were mounted on opposite sides of the octagon with their hinge axes vertical. The other two panels were not used because of the difficulty in simulating a zero acceleration condition.

In the first tests, the deployment system did not function properly, although the pyrotechnics worked as designed; subsequent tests eliminated the pyrotechnics. The deployment problem was simply that the panel deployment spring torques did not equal the sum of the resisting torques. Each element was performing to its specified requirements, but the problem was the incompatibility of the requirements rather than substandard operation of any unit. The retarder was reworked (the rewind spring replaced with a ball detent) and the solar panels spring torques increased to 40.0 in.-lb over the original 25.0 in.-lb. A complete second series of tests was performed successfully on the STM.

Tests were also performed without the central retarder in the system and the results indicated a high probability of success if the cruise dampers and latches were redesigned. Hardware was designed and fabricated, and tests

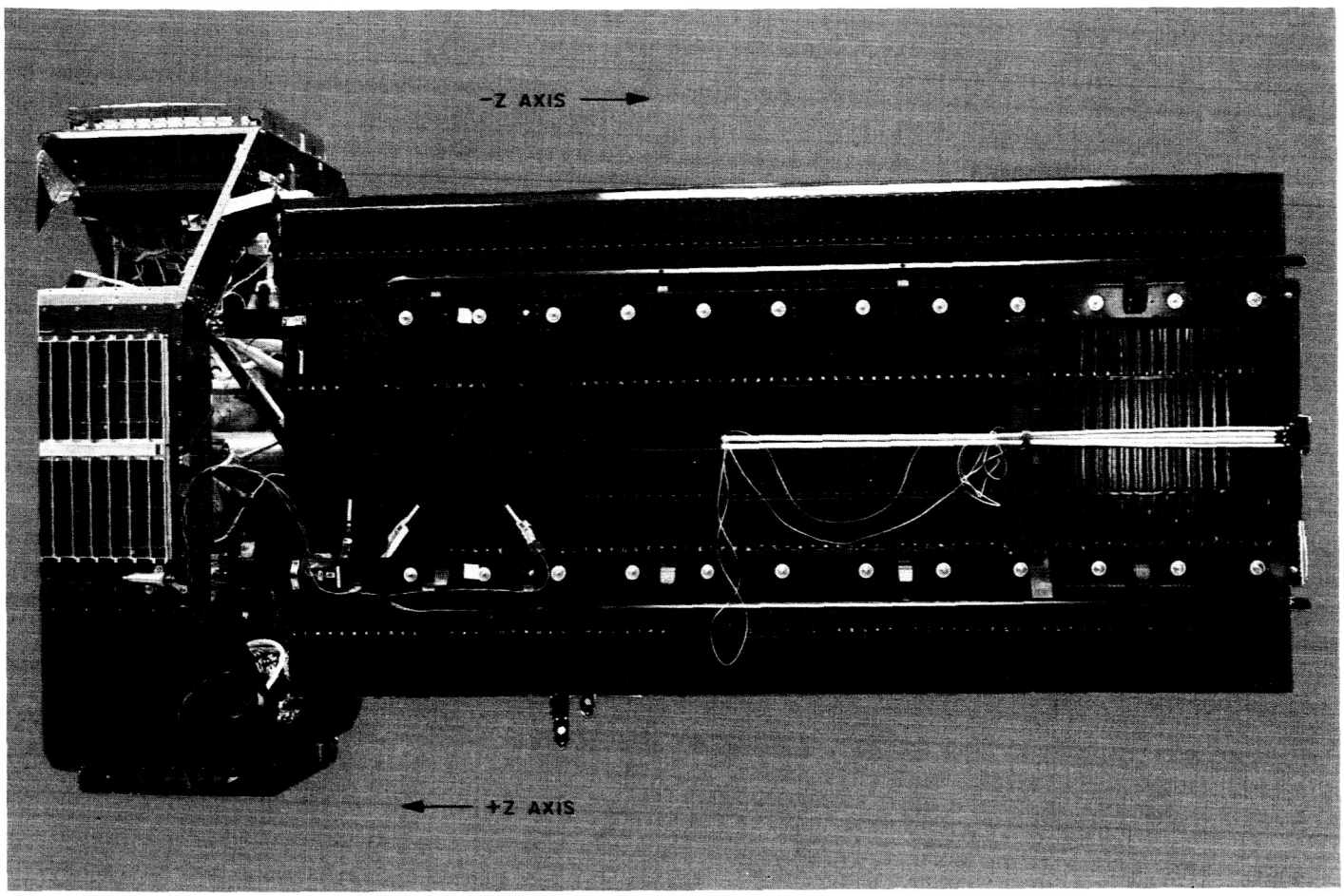


Fig. 375. Solar panel deployment test setup, solar panels undeployed

were initiated on a special mount (not the STM) to prove the design concept. This design became the prime system with the retarded system acting as a backup.

Over 33 detailed functional qualification tests of the free-fall deployment system were conducted. The test series investigated the several deployment system parameters as well as the structural response of the solar panels for a range of significant spacecraft and deployment system conditions. These conditions involved such variables as abnormally high spacecraft pitch/yaw separation rates and/or malfunctioning deployment springs.

i. Scan platform bearings. The ability of the scan platform to provide a reasonable environment for the instruments during boost was the subject of some concern prior to testing of the STM spacecraft. Dynamic gains through the bus structure, across the bearings, and into the cantilevered mount were not thoroughly understood from analysis because of the nonlinear response of bearing clearance.

However, vibration testing indicated that bearing clearance was not a large contributor to the overall gain of the system but, in fact, provided a certain degree of attenuation at higher frequencies. No failures in the platform structure occurred during any series of tests, and it was concluded that a satisfactory environment was achieved for the science instruments.

Inspection of the sleeve scan bearings after completion of the first series of STM type-approval tests indicated only a slight change in appearance to that of a well-burnished bearing, an accompanying increase in radial clearance of 0.001 in., and no increase in end play.

3. TCM Testing

a. Space simulator test. The objectives of the temperature control model test program were:

1. To verify the adequacy of the basic thermal-design philosophy

2. To empirically establish (in conjunction with analysis) spacecraft surface preparation and thermal-shield configuration commensurate with required temperatures and temperature ranges for all anticipated flight conditions
3. To investigate thermal perturbations on the spacecraft resulting from the midcourse maneuver

Temperature control model testing was performed in the 25-ft space simulator at JPL. The TCM was physically supported by cables within the chamber test volume. Solar simulation was provided by mercury zenon lamps and an associated optical system. Light intensity was regulated by a thermopile monitor located above the TCM. During the test, the vacuum chamber was maintained at a pressure less than 10^{-5} mm Hg. Pressure within the bus cavity was monitored by a vacuum gauge and ran only slightly higher than the chamber. The liquid-nitrogen-cooled shroud within the chamber was held near −270°F. Temperature measurements were taken by 175 Chromel–Constantan thermocouples. Electrical resistance heaters, in lieu of electronic equipment, were used on the TCM to provide heat. Heaters were also used in some areas to simulate solar heating.

Ten separate tests, comprised of 35 test modes, were conducted with the TCM in three different Sun attitudes and at Earth and Mars solar intensities. Changes were made after each test as required by the measured temperature distribution.

At the completion of the TCM testing, temperatures were within tolerance for all flight modes. In addition, adequate margins were provided to allow for uncertainties. It was anticipated that the flight spacecraft would be thermally identical to the TCM. However, changes to the spacecraft after the TCM tests resulted in spacecraft temperature changes. These, in turn, required modification of the louver locations and of the thermal-shield design. The final flight thermal configuration was based on flight-spacecraft space simulator data.

b. Stray-light reflectance tests. It was essential that the spacecraft attitude control optical sensors not be affected by stray reflected light. The Canopus sensor and Earth detector were the two sensors most likely to be susceptible to scattered light. The geometry of the spacecraft and the sensors' locations was such that nothing could physically block the sensor or detector field of view. However, it was possible for stray reflected sunlight outside the field of view to enter the sensor baffle cavities and impair the sensors' performance.

A test was conducted using developmental solar panels and solar vanes to determine the effect of stray light on the Canopus sensor. This test was performed in the celestial simulator facility using a carbon-arc lamp as a light source. Light intensities were measured with a visual response detector (spectra spot meter). Results from the test confirmed the existence of the stray light problem and the fact that further exploration with a complete spacecraft would be required to resolve it.

After reviewing the configuration requirements and spacecraft schedules, the temperature control model was chosen for the initial spacecraft reflectance tests for the following reasons:

1. It represented the external configuration and surface finishes required for a meaningful test.
2. It was a full scale model built with flight-type hardware (less, primarily, the internal electronics).
3. Its weight was about half that of the flight spacecraft.

Spacecraft preparation for this test included Sun shades and finishes necessary to eliminate stray light reflections as determined from engineering layouts. Because of uncertainties in the area of temperature control shield hardware, several different configurations were included in the test plan, specifically the use of louvers or polished shields in prime areas of concern. Final inspection of the spacecraft on the fixture included checking the deployed position of panels, vanes, dampers, correct exterior cabling, clamps, plumbing, shades, and thermal shield installation. The geometry of the spacecraft and sensors' locations indicated that only two solar panels and the hardware adjacent to the sensors' positions could affect their operation. In this respect, only two solar panels were used and little concern was given to the area 180 deg from the sensors' look angles.

The handling and positioning problems were much the same for the TCM as for a flight spacecraft. Lifting and positioning techniques had been previously developed, but an adequate spacecraft mounting fixture for this test had to be procured. Hanging the spacecraft by cables was ruled out because of limited overhead crane capability and the potential disturbances caused by the air conditioning in the building. A triangularly shaped three-wheeled dolly of geometry within the shadow of the spacecraft was found to meet the requirements. This method of support allowed simple positioning of the spacecraft to accommodate the Sun source. Figure 376 shows the PTM test configuration; the TCM test setup

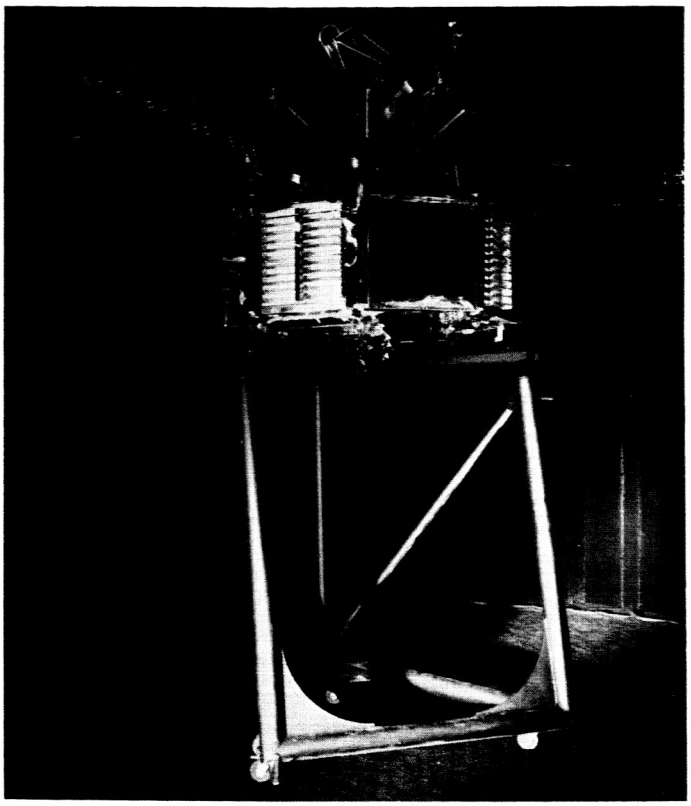


Fig. 376. Spacecraft setup for stray light reflectance test

was identical. The area around the Canopus sensor was accessible for positioning a camera or photometer and for a visual inspection from the sensors' location.

The first part of the test consisted of moving the spacecraft under the simulated Sun to illuminate a portion at a time until the entire area in question had been visually inspected for stray light. Because the human eye is very sensitive to light, it was a good instrument to use for initial problem area definition. This portion of the test uncovered obvious unacceptable light sources, which delayed the use of a more exact photometer reading until hardware corrections could be made. The use of photographs to document findings was helpful in designing the fixes that were necessary.

In subsequent tests on the TCM, and finally on the PTM, photometric measurements of the illumination on the Canopus sensor and Earth detector yielded satisfactory results. These results indicated a safety factor of 5 for the Canopus sensor after light source corrections for color and intensity.

The reflectance tests proved to be necessary for the assurance of proper operation of light-sensitive sensors. Although seemingly isolated from this type of interference on the spacecraft, engineering layouts fell short of predicting primary and secondary reflected light sources. Known light-reflecting capabilities of individual parts were of little value when they were joined in the final assembly of the spacecraft. The individual components formed a complexity of surfaces that were complementary in forming the stray-light problem. The results yielded conclusive evidence of the necessity for testing and the need for a more subjective look at sensor design and location for future spacecraft configurations.

c. Prelaunch spacecraft cooling tests. The prelaunch cooling system reduced spacecraft temperatures to acceptable limits at the time of launch. The system used for the *Mariner* Mars 1964 program consisted of a cooling blanket placed over the shroud through which cold air was forced. The spacecraft cavity was cooled by conduction through the shroud.

The cooling system tests, performed at the LMSC test facility at Moffett Field, used an air conditioning system similar to that used at the Cape, a test shroud and adapter, and the complete TCM spacecraft. Two series of tests were performed. The first series of tests was performed using a styrofoam cooling sheath in lieu of the cooling blanket. The tests were repeated with the cooling blanket replacing the cooling sheath.

The test results indicated a marginally acceptable capability to keep the ambient gas temperature under the shroud to between the required 40 to 65°F at launch with a specified inlet air temperature.

d. Solar pressure vane thermal tests. This test series was performed in order to determine the preinjection thermal–vacuum environment effects on a folded vane. A TCM solar panel was fitted with solar vane hardware and placed in the space simulator with the back side of the panel facing the Sun. The panel temperature was maintained at 240°F to duplicate actual parking orbit conditions. The simulator was then returned to ambient conditions and opened. The vane partially opened, but some of the ¼-mil mylar had bonded together where the dacron "scrim" had been placed. (Scrim is a 2 × 2-in. pattern of dacron thread bonded to the mylar to prevent the propagation of tears.)

A second test was performed on this same vane. The vane was refolded and placed alone in the 6 × 7-ft vertical vacuum chamber. No solar simulation was used but the internal shroud temperature was held at 240°F

for several hours. The chamber was returned to ambient conditions and opened. The vane would not open this second time when released. Again the adhesive had bonded the mylar together. It was noted, however, that the mylar did not bond in the immediate area of the framework; the framework was thermally sluggish and it held the mylar temperature below the softening temperature of the adhesive.

With the results of these tests, it was decided to eliminate the scrim and use thicker mylar, which also eliminated the troublesome adhesive problem. Tear tests were performed on various samples of mylar to determine the proper thickness. It was found that 1-mil unscrimmed mylar had essentially the same resistance to tearing as the ¼-mil scrimmed mylar. In these tests, a tear was started by cutting into the mylar with scissors. A force gauge was then used to determine the amount of force required to propagate the tear.

A second vane was recovered with 1-mil mylar and refolded. The vane was placed in the 6 × 7-ft vertical vacuum chamber with the chamber shroud temperature at 240°F. The vane was released but did not open. Visual inspection revealed that the mylar had melted slightly at that temperature and stuck to itself. It also appeared that the mylar had shrunk in area by about 10%.

At that point, it was decided that mylar would not be an appropriate material, at least on the panel pointed at the Sun during the parking orbit (Bay III). Teflon, because of its better resistance to heat, was placed on the Bay III vane. In addition, it was folded so that the teflon side rather than the aluminized side faced outward. A high-emissivity surface would also reduce the vane temperature.

Testing of this vane in the vacuum chamber at 240°F indicated it would open properly. Mylar was retained for the other three vanes, because of the black back-side requirement imposed by the Canopus sensor. All of the vanes, however, were folded like the teflon vane so that the high-emissivity surface was exposed. In this type of folded configuration and with their position on the spacecraft away from the Sun during the parking orbit, the maximum expected temperature was 200°F. Tests were again performed in the vacuum chamber on this configuration with a shroud temperature of 200°F. No problems were encountered with the vane opening.

The last thermal–vacuum test was performed to ascertain the effect of the all-metal shroud on the vanes. The inner lining of the metal shroud reached a temperature of about 400°F because of the aerodynamic heating on the outside skin. A test was performed in which a folded vane was held 3.0 in. above a flat aluminum plate in the 30-in. horizontal vacuum chamber. The plate was heated to 450°F and held there for 30 min; the rest of the internal shroud was at ambient conditions. After the test, the vane opened properly.

4. DTM Testing

a. Simulated midcourse interaction test. Early in the design of the *Mariner* Mars 1964 spacecraft, it became apparent that the complicated structural and geometric relationships between the spacecraft and its autopilot system made accurate analysis of their interactions very difficult. Complete analysis would have required more man hours of work than were available, so it was suggested that a test be performed to verify proper autopilot operation. This autopilot verification test series had to be completed long before the PTM spacecraft was available, so that any autopilot problems discovered could be solved and the hardware modified in time for the build-up of flight spacecraft. Two corollary objectives of the test series were: (1) determination of allowable variations in the damping coefficient of the solar panel cruise dampers, and (2) determination of the heat pulse from the midcourse motor firing.

The test series was approved and then executed using the DTM which was mass-ballasted to simulate flight moments of inertia and center of gravity, and which had a prototype autopilot, a gyroscope package, a motor firing pyrotechnics package, and a midcourse motor mounted in the bus.

The test required that the spacecraft be suspended in a large vacuum chamber in such a manner that it simulate the six degrees of dynamic freedom it would have floating in space. The spacecraft, suspended in that way, was then commanded to execute a midcourse motor firing. The resultant behavior of the spacecraft and autopilot were monitored via camera coverage and hard-lined oscillograph readout.

One of the main difficulties in executing this test was suspending the spacecraft in such a way that its six degrees of rigid body freedom were unrestricted. The suspension system developed was composed of an on-spacecraft gimbal system, permitting two degrees of rotational freedom, and a long pendulum, which allowed the third degree of rotational freedom and two degrees

of translational freedom. The third degree of translational freedom (vertical rise) was provided by a counterweight and pulley system, which was isolated from spacecraft structural resonances by a very soft spring in the pendulum cable. One final problem in the design of the spacecraft suspension was that of arresting the spacecraft's flight after it had been allowed to accelerate freely through the 30-ft stroke of the suspension system. This problem was solved by constructing the suspension counterweight of long chain sections. Thus, as the spacecraft neared the ceiling of the vacuum chamber, the counterweight chain would begin to pile up on the chamber floor, lightening itself, absorbing energy, and stopping the spacecraft's flight.

This test required the use of a very large vacuum chamber; the 60-ft diameter spherical chamber at Langley Research Center, Virginia, was the most desirable. The spherical tank provided plenty of room for lateral swinging of the spacecraft and also provided a desirable geometry for the installation of a rocket blast diffuser (Fig. 377). This diffuser (after some developmental modifications in early firings) efficiently reduced the high Mach number flow from the motor nozzle to a gentle backflow out of the diffuser and along the walls of the vacuum chamber. Proper design of this diffuser was extremely important in preventing the gas swirl in the chamber from creating undesirable disturbing torques that would act on the spacecraft.

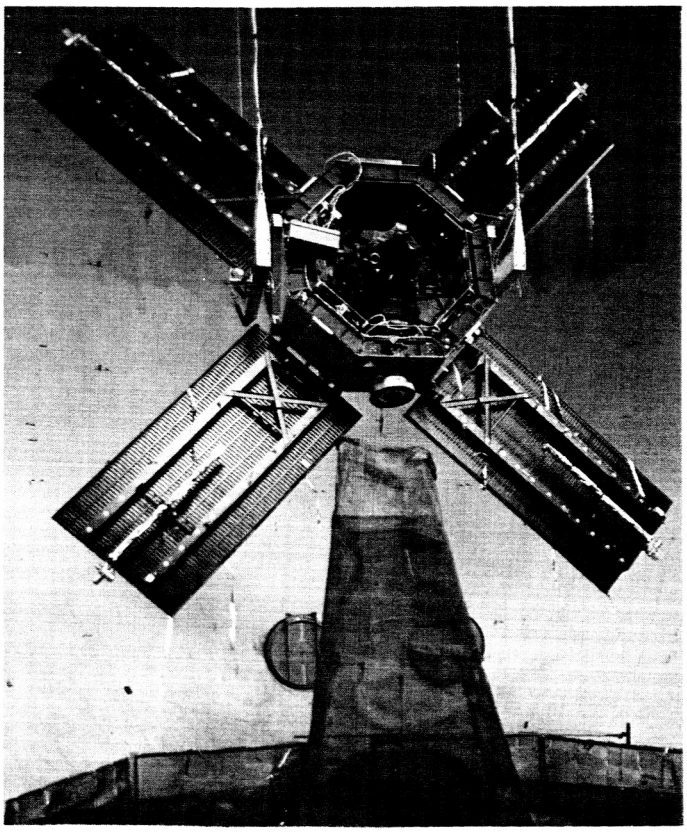


Fig. 377. Simulated midcourse interaction test blast diffuser

The results indicated that the autopilot system could control the spacecraft during the propulsion sequence.

b. Acoustic test. The two objectives of the DTM acoustic test were (1) to determine the responses of selected spacecraft locations when subjected to a high-level acoustic field, and (2) to measure the shroud acoustic-transmission loss.

The DTM spacecraft was attached to a flight-type adapter, encapsulated in a shroud, and mounted to a 3-ft portion of the *Agena D* forward section. The equipment was then subjected to a 142-db acoustic field. Equipment degradation noted as a result of the imposed acoustic field consisted of:

1. Blistering of paint on high-gain antenna dish
2. Rupture of aluminum-foil membranes on Bay II (PIPS) shield
3. Shroud shredded debris shaken loose

c. LMSC combined vibration test. Vibration tests of the shroud, adapter, and spacecraft system were conducted at LMSC with the objective of demonstrating structural integrity of the shroud and shroud/spacecraft interface hardware, and to obtain measurements of interface clearances at critical locations. In addition, the first few normal vibration modes of the system were evaluated.

The test vehicle consisted of the complete DTM spacecraft, a test shroud and adapter, spacecraft and shroud V-bands, and an *Agena* forward midbody. A series of sinusoidal excitations were used to satisfy the test objectives.

As a result of these tests, it was concluded that the shroud/spacecraft system was qualified to withstand the maximum flight dynamic loads. All critical clearances were determined to be adequate. However, a quantitative determination of clearances was largely unsuccessful due to problems in the clearance measurement system. Also, a detailed determination of the normal modes of the system could not be made because of test system inadequacies.

d. Antenna pattern tests. Antenna pattern tests were conducted to confirm adequacy of the spacecraft high- and low-gain antenna RF patterns. These patterns had to be known for different spacecraft configurations and attitudes.

Mockup pattern test. The initial tests were performed using a full scale aluminum spacecraft mockup. It duplicated the exterior spacecraft envelope to within $\pm\frac{1}{2}$ in. The mockup included accurate antenna mounting dimensions and simulated all RF reflective surfaces. Structurally, the mockup had to withstand winds up to 40 mph, and generally rougher handling than a flight spacecraft.

The test range was composed of a 22-ft-high fiberglass tower on which the mockup spacecraft was mounted with the roll axis parallel to the ground. A shelter approximately 100 yards from the tower housed the controls for rotating the tower and instrumentation recording equipment; 3300 ft away from the tower was a 10-ft diameter dish antenna used to illuminate the spacecraft with RF energy.

A crane with a 35-ft boom height was used to lift the mockup spacecraft to the top of the tower. Once the spacecraft was secured on the tower, the four solar panel mockups and the antennas were installed. The tower was leveled within 0.1 deg by a precision bubble level. The spacecraft high-gain antenna was aimed at the remote dish by a theodolite, which, in turn, indexed the tower for repositioning. Using the index points found previously, the spacecraft was rotated in clock and azimuth angles while illuminated by the remote dish. A digital antenna pattern recorder continuously recorded on magnetic tape the signal levels at different spacecraft orientations.

Satisfactory preliminary antenna pattern information was recorded from this test. However, further testing on a flight-type antenna system was required. Later tests verified that a more representative spacecraft geometry was required for determining final pattern profiles.

DTM pattern tests. The DTM spaceframe was used for final antenna pattern tests. The sequence of operation was much the same as for the mockup vehicle pattern tests, except for the spacecraft handling operation. The preparation of the spacecraft included removing all internal components for weight reduction, addition of simulated solar vanes, science experiments, and temperature control louvers. The use of flight-type solar panels dictated that wind-load calculations heavily influence the design of the spaceframe support structure. The more delicate nature of this prototype spacecraft made it mandatory to revise the scheme used in assembly on the tower. The spacecraft was completely assembled on a stand near the tower and then lifted from the stand in a horizontal position by a 35-ft crane. With the solar panels in their deployed position, the complete spacecraft was then lifted and secured to the tower (Fig. 378). Alignment of the spacecraft to the remote antenna was aided by a telescopic sight mounted directly to the spacecraft. To safeguard the vehicle and to obtain more accurate data, a wind velocity meter was installed. Testing was stopped and the spacecraft was reoriented to a more favorable position in high winds.

Pattern tests of this type were compulsory because the RF antenna patterns were affected by the spacecraft configuration. Full-scale accurate mockups gave the most conclusive results because of uncertainties in electrical scaling of a spacecraft. The most successful patterns were taken at night, when RF interference and

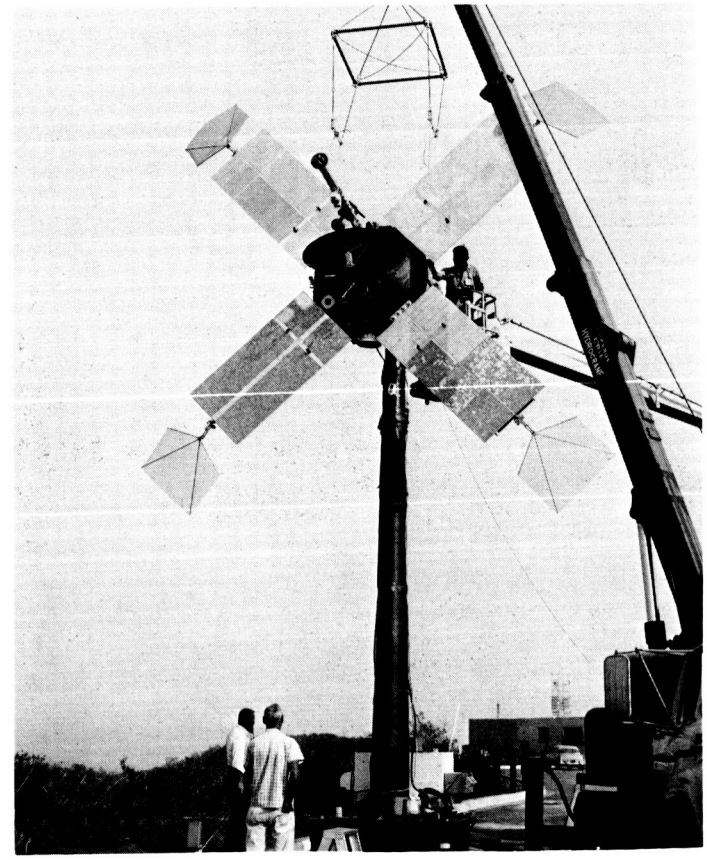


Fig. 378. DTM mounted to antenna range tower

winds were low. The temperature environment was also more stable at night.

5. XTM Testing

a. LMSC adapter/spacecraft static test. A series of tests were performed at LMSC to provide data for structural evaluation and to qualify the spacecraft adapter under critical flight-loading and ground-handling conditions. In addition, the spacecraft V-band was released at the end of the test series to demonstrate its postload separation capabilities. The test vehicle consisted of mounting the XTM spaceframe to a test adapter by a spacecraft V-band. The adapter was bolted to an *Agena* forward midbody that was mounted on a rigid foundation.

The test vehicle sustained all required loads with no evidence of failure or damage. The postload V-band separation appeared normal.

The spacecraft structure was qualified in a similar series of tests performed at JPL using the STM spacecraft. For a future program, these two tests might easily be combined.

b. LMSC spacecraft separation tests. A *Mariner* Mars spacecraft was separated in simulated flight from its *Agena D* boost vehicle following injection. The spacecraft was clamped to the *Agena* adapter at its eight feet by means of a V-band, which, at separation, was released by two pyrotechnic cutting devices. Differential separation velocity was then imparted to the spacecraft by the release of stored energy in four spring mechanisms attached to the adapter.

The spacecraft separation tests were performed to demonstrate the functional operation of the separation system and to determine the effects on the spacecraft of various unbalanced separation forces. Testing was conducted by Lockheed at its Burbank Flight Test Facility using the JPL-provided separation test model, the XTM, and an LMSC-provided *Agena* adapter. The XTM was ballasted to simulate inertial properties of the flight vehicle to within 10% and to position the center of gravity at the forward end of the restrictive envelope on the nominal roll axis. The configuration of the test model is shown in Fig. 379.

Test setup. Nominal separation occurred parallel to Earth to eliminate gravitational effects. The test vehicle was suspended by a system designed to allow it six degrees of freedom. Support was provided by a single vertical pendulum, 65 ft in length, whose projection passed through the spacecraft center of gravity. A soft spring (rate under 10 lb/in.) was installed at the top of the pendulum so that vertical translation of the spacecraft CG could be obtained. The spacecraft was attached to the pendulum through a yoke that made a "parallelograming" four-bar linkage. The yoke picked up the spacecraft at adjustable pivot points that were attached to the top of the XTM octagon at longerons A and E. These points were adjusted so that a line through them parallel to the floor passed through the spacecraft CG. Bearings were installed at all pivot points to give the spacecraft free rotation in pitch, yaw, and roll. The *Agena* adapter was bolted to a vertically rigid strong back. The spacecraft was mated to the adapter, which moved it 4 in. longitudinally from a free hanging condition, and then ejected parallel to the floor using the pendulum tension as the compensating force opposing gravity.

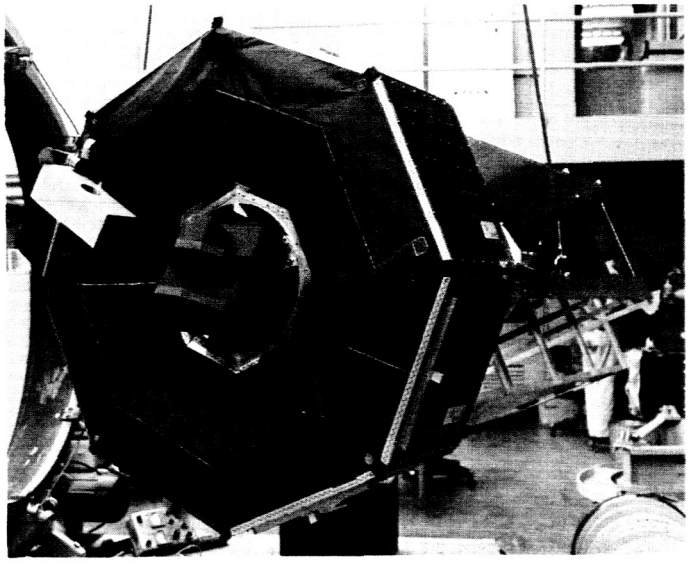


Fig. 379. XTM separation test model configuration

To record the spacecraft motions as it separated through the first 6 in. of travel, a special four camera data system was used. The cameras were bolted independently to the floor and arranged in a plane parallel to the floor at 90-deg angles to each other. Each lens was marked with cross hairs so the camera setup would serve as the stationary reference frame. The cameras were aimed at 6 × 8-in. cross-hatched targets mounted on the spacecraft roll axis forward and aft and on both sides of the CG at the suspension yoke pivot points (on both ends of the test pitch axis). The cameras were synchronized so that target position vs time could be related between cameras. The 400 frame/sec photographic record from these cameras provided the attitude history of the spacecraft as it separated from the adapter. Three cameras

operating at 1000 frames/sec were set up to view the V-band release characteristics. A single overall documentation camera operated at 24 frames/sec.

The four data films for each test were read on a special machine. Then, using a 7094 computer system, the raw data were transformed into spacecraft attitude vs time relationships for longitudinal, lateral, and vertical displacements, and pitch, yaw, and roll rotations. Using computerized techniques, the attitude histories were differentiated with time to obtain three linear velocities and three rotational rates.

As an expedient means of obtaining approximate spacecraft angular rates, a Fairchild rate gyro was used. The gyro was mounted to the top of the octagon near the spacecraft CG, and was monitored through a hard line using a visicorder and oscillograph. The flight separation monitor system (three linear potentiometers mounted unsymmetrically near three of the four separation springs) was included in the tests. The separation spring, which was not accompanied by a potentiometer, was adjusted to compensate for the lack of the instruments' spring force. This was also done on the flight system. Displacement-time history was taken from these instruments.

Test results. Nine test phases were run, which provided meaningful data on separation mechanics. Each phase included three to six separations. Parameters affecting the separation dynamics were varied in each phase. These parameters were spacecraft CG offset, spring rate, spring stroke, spring misalignment, and number of pyrotechnic bolts fired. When the parameters were varied from nominal, the adjustments were made to give additive effects in the yaw mode. Pitch rates induced by these adjustments were, in all cases, less than the accuracy of the data system and were neglected.

Table 81 lists test conditions and results for each phase of testing. In some cases, anomalies in the setup or adjustments forced a modification of the rates by digital simulation techniques to match the specified test conditions.

An error analysis showed that the error from the data gathering and reduction system was less than or equal to the following 3 σ values with 94.5% confidence:

1. Tip-off rate = 0.336 deg/sec
2. Velocity = 0.394 in./sec

The three high-speed cameras viewing the V-band release showed that in several instances the V-band, wildly gyrating because of the release of its own stored strain energy, returned and struck the separating spacecraft. During early test phases, V-band restraint was provided by eight slack lanyards at the clamping shoes. In Phases 7, 8, and 9, the lanyards were replaced by Bungee cord. This fix proved unsatisfactory, since the V-band in several instances struck the spacecraft. Additional tests beyond Phase 9 were run to develop a restraint system that would ensure spacecraft safety. Separation data were taken on the first six of these tests. These tests provided a restraint system composed of slack lanyards and non-preloaded springs replacing the Bungee cord. Three of these tests were performed with two bolts firing, and three were performed with one bolt firing. During the single bolt tests, the V-band again struck the vehicle.

Table 81. Spacecraft separation test conditions and results

Test conditions					Test results		
Phase	CG offset	Spring rate	Stroke	Spring misalignment	V-band bolts fired	Tip-off rate deg/sec	Test velocity in./sec
1	0.0	NA[a]	NA[a]	NA[a]	2	0.2	~1.0
2	0.0	Nominal	Nominal	Nominal	2	0.2	25.9
3	0.0	Nominal	Nominal	Nominal	1	0.2	26.0
4	0.0	Nominal	Nominal	~3 deg	2	1.1	26.2
5	0.0	Nominal	±0.030 in.	Nominal	2	0.3	25.6
6	0.0	Max/min	Nominal	Nominal	2	0.4	25.9
7	1.125	Nominal	Nominal	Nominal	2	1.5	25.4
8	1.125	Max/min	±0.030 in.	~1 deg	2	1.9	25.6
9	1.125	Max/min	±0.030 in.	~1 deg	1	1.9	25.5

[a]Not applicable since springs were absent. Test was to determine V-band effects on separation.

A concentrated effort to devise a satisfactory restraint mechanism began, and more tests were performed with full photographic coverage of the V-band. No separation data were taken during these tests. A satisfactory system of 12 preloaded springs and taut lanyards (a set at each of the eight shoes, and a set on each side of both pyrotechnic release mechanisms) evolved.

Conclusions. The separation tests demonstrated that the system performed as expected and that under maximum tolerance conditions, spacecraft tipoff rates would

be below the required 3 deg/sec. The test results, combined with the LMSC separation analysis (predictions from which were in extremely close agreement with test results), gave an expected maximum tip-off rate for the flight spacecraft of 1.5 deg/sec. This value was based on the CG position reported by JPL, *Agena* postinjection limit cycle rate, and maximum installation procedural tolerances. This was a worst-on-worst condition to which the CG offset contributed 70%. Results also predicted that the absolute velocity increment to the spacecraft at separation was 22.4 in./sec, with a velocity relative to the *Agena* of 31.0 in./sec.

Linear velocity measurements from the three linear potentiometers differed from the photographic measurements by a maximum of 3.2 in./sec low. This indicated that the potentiometers had a large error band, and that predictions for a nominal separation were qualitatively more accurate than flight telemetered potentiometer data. Rate gyro data, not as accurate as photographic data, were useful for quick information.

The series of separation tests pointed out, and later solved, the V-band release dynamics problem.

6. Launch Vehicle Interface Tests

a. Shroud wind-tunnel test. The purposes of the shroud wind-tunnel test were to evaluate the effects of the static and fluctuating pressures on the stability of the spacecraft shroud, and to obtain fluctuating pressure data to be used for spacecraft transonic high-frequency vibration prediction efforts by JPL. The tests were performed on a 1/10-scale model of the spacecraft (over-the-nose) shroud/*Agena D* vehicle in the 8 × 6-ft transonic wind tunnel at the NASA Lewis Research Center. The investigation covered the Mach number range of from 0.56 to 2.0 for angles of attack of 0, ±3, and ±6 deg.

b. Launch vehicle shroud contamination. There were two general sources of the contamination associated with the launch vehicle: that associated with the construction byproducts in the shroud system, and that associated with retro-maneuver combustion products.

Contamination from the shroud system appeared to be amenable to elimination. During various dynamic tests using prototype and engineering model shrouds, contamination in the form of metal chips and shavings fell from the shroud onto the spacecraft. For example, during the acoustic test of the DTM with the shroud, a lot of debris fell from the shroud onto the DTM. During another test, a flight configuration shroud was exposed to an acoustic sound field of about 155 db and, again, a lot of debris fell from the shroud onto the spacecraft. Following this test, it was proposed that a program be instituted for acoustic cleaning of shrouds prior to launch.

Other sources of shroud system contamination were: (1) combustion process byproducts escaping from the shroud separation system; and (2) particulate matter jarred loose by the shroud separation. Numerous Fastex films have been made of separation-system firings without obtaining visual evidence that gas escapes from these units. The shroud V-band was observed to occasionally strike various bracketry that probably knocked chips loose. However, a restraining system was devised to ensure that nothing would impact the structure during retraction.

The second major source of contaminants was combustion products from the retro system. The *Atlas* retro system was examined in this respect, and it was concluded that less than 2×10^{-6} lb of gas particles per square inch would pass along the area of the spacecraft. It was concluded that the problem of contamination from the process previously mentioned requires further study.

c. Shroud acoustic test. The objectives of the shroud acoustic tests were (1) to evaluate the effects of an acoustic field and shroud V-band separation shock on RF paint adhesion, and (2) to determine if acoustic vibrations and V-band separation shock would cause the RF finish to release contaminating particles.

The test specimen consisted of a complete flight shroud system, including the transition section, fastened to an acoustic termination board and diaphragm support fixture. Simulated lenses were provided at the spacecraft lens locations and the shroud cavity was covered to catch falling particles. The equipment was subjected to the acoustic field generated by firing a Bell Model 8247 rocket motor. The reference acoustic sound pressure level outside the shroud was 155.2 db (Re: 2×10^{-4} μbar).

No damage was incurred due to firing of the V-band pyrotechnics. However, the JPL contamination requirements for maximum allowable particle size were not met; but the Project Office accepted the situation as being a minimum risk to the mission.

d. RF attenuation test of shroud EM 476. The objective of this test was to determine the RF shielding properties of the shroud in a range of frequencies from 100 to 10,000 Mc. The shielding provided by the shroud was

used in evaluating the effects to the spacecraft subsystems when the vehicle was in a flight configuration exposed to RF fields at the Cape. The average attenuation between 200 and 2000 Mc was found to be approximately 30 db. Between 2000 and 10,000 Mc it was approximately 37 db. Below 200 Mc the attenuation fell rapidly to a minimum measured value of 1 db at 100 Mc.

e. Solar panel shroud impact simulation test. When the *Agena* shroud system was changed from the clam shell to the over-the-nose configuration, extensive analysis and tests were conducted to verify that the spacecraft would survive shroud impacts. These impacts could occur if the shroud were ejected in a non-standard manner. Because of the small clearances between the solar panels and the ejecting shroud, spring-mounted guide rails were attached to the solar panels.

The two main test objectives were (1) to obtain design data for the protective guide rails to be installed on the solar panels, and (2) once the guide rails were designed, to show that the solar panel/damper superstructure system could survive the loads imposed by shroud impacts at different stations and velocities.

Four tests were conducted. During the first two tests, an impact mode was assumed in which the aft end of the shroud would strike an intermediate point on the guide rail. The third test used a newly designed guide rail. The final test, using impact information supplied by LMSC, used two solar panel structures, four boost dampers, and a superstructure. The final test setup is shown in Fig. 47. The testing verified that the design was adequate and that the solar panel guide rail system would survive a shroud impact.

7. Other Developmental/Qualification Testing

a. EMI support of AFETR operations. Measurements were made at the Cape to verify that the S-band spacecraft communications system would not be subjected to any interfering RF levels during the launch operations. This effort was considered of particular significance, since it was the first time that the S-band system had been used on a JPL spacecraft, and the first time such a system had undergone tests at Cape Kennedy. The survey period was determined by launch-complex availability, by noise-measurement participation at JPL on backup spacecraft, and by the final repackaging of the EMI receiver.

No interfering noise levels or discrete spectral components were observed at the spacecraft receiver frequencies $\pm$ 63.4 kc using a receiver with a sensitivity of -151.4 dbm in a 100 cps bandwidth. Measurements were made prior to and during the combined system test.

In addition to the noise measurements, standard field intensity meters covering a wide frequency range (150 kc to 10,000 Mc) were shipped to the JPL station to be available in the event that RF interference occurred on any of the systems. (No interference occurred.)

b. RF noise survey of the 25-ft space-simulator chamber. During the PTM space-simulator tests, one telemetry channel exhibited an unexplained offset. The RF noise emitted by the space-chamber mercury xenon lights and/or RF output from the chamber iris servo control were considered to be possible causes of the telemetry disturbance. A noise survey was made from a frequency of 150 kc to 2240 Mc with standard field intensity meters. No noise was observed to be emitted from the iris control. The lights did emit noise below a frequency of 40 Mc. The greatest noise level observed was induced by the antenna and was 92 db above a bandwidth of 1 μv/Mc and below a frequency of 2 Mc. No noise was observed at frequencies above 40 Mc, including frequencies in the vicinity of 2116 Mc.

c. Damped-structure feasibility tests. Because of the location of the solar panels on the *Mariner* Mars 1964 spacecraft, it appeared that the panels would have to withstand more vibration than the *Mariner* Venus 1962 panels did, although the additional panel area per spacecraft pound led to an unbearable penalty in overall spacecraft weight. These "facts of life" resulted in the use of an unconventional damped-strut support system, which protected the panels from vibration and allowed a very significant reduction in weight. The proposal of this approach was based on some experimental work done in August 1962, in which the damped-strut control of *Mariner* Venus 1962 panels and structure was achieved. (The success of those tests also led to the use of damped solar panels on the *Ranger* Block III program.)

Damped panels did not lend themselves to simple analysis, so it was necessary to build and test a prototype lightweight solar panel and damper system. The design was verified with a 10-*g* (0-peak) sinusoidal vibration test swept through all panel resonances up to 200 cps. The test panel's ratio of total panel weight to panel structural weight was 2.5 to 1, whereas the same ratio for the flight panels was only about 2.1 to 1. Thus, the test panels had a higher loading per pound of structure than the flight panels did, although no structural problems occurred.

Concurrent with the development of the solar panel damped support system, another use of the heavily damped structural concept was investigated. In this case, not only weight but also space limitations required a very tall, slender structure for the low-gain antenna support. This structure, 7 ft tall and 4 in. in diameter, supported by conventional techniques would have developed tip excursions in excess of 10 in. during spacecraft vibration qualification, and would have induced excessive loads into the spacecraft upper structure. A damped support system was proposed for the control of this slender structure, and subsequent testing indicated that the damped support system would reduce the structure's loads and excursions by a factor of more than 20. The tests were conducted on a thin-walled aluminum tube controlled by previously described concentric tube dampers. A test series studying the variation of damping coefficient revealed that the structure's resonant behavior was rather insensitive to variations in damping.

From these tests, it was concluded that the use of damped structures on the *Mariner* Mars 1964 spacecraft would result in large savings of structural weight, and would allow the use of a desirable, lightweight, slender, low-gain antenna support structure. Applications on future spacecraft would appear to be equally attractive.

d. Electronic packaging development testing. After having established the basic concept and design of the electronic packaging, decisions had to be made about the details of the basic electronic chassis design. The choices were (1) center section geometry (box vs T), (2) web thicknesses (0.100 vs 0.070 in.), and (3) material (magnesium vs aluminum).

To compile comparative data about the various options, several chassis were fabricated with the above features, mounted in a rigid vibration fixture, and vibrated in three planes at an input sweep of 3 *g* from 20 to 1500 cps.

Results of the first series of tests (in one plane) showed approximately the same resonant frequency (about 280 cps) and the same gain at resonance (about 25) for three types of box section chassis: 0.070 in. web aluminum, 0.070 in. web magnesium, 0.100 in. web magnesium. It was concluded that the fixture introduced fictitious resonances of such strength that a true evaluation of the different chassis configurations was not possible.

Because of the lack of development time, it was decided to proceed with the conservative 0.100 web magnesium box section chassis configuration for all prototype chassis, and to run additional tests later with these prototype chassis in a more realistic fixture before ordering flight chassis. This would not only check the adequacy of the chassis design, but would also afford the opportunity of evaluating means of lightening the design.

A new chassis test fixture was fabricated using some flight-rejected structural rings to form a three-bay section of the octagonal bus. This fixture (Fig. 380) was intended to approximate the stiffness of the members of the spacecraft to which the chassis were attached.

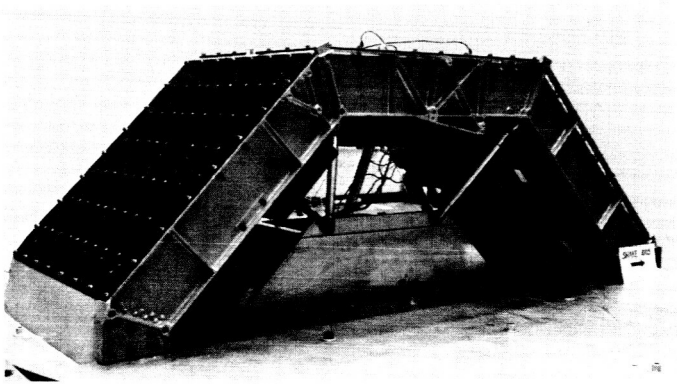


Fig. 380. Three-bay electronics chassis vibration fixture

Tests were conducted with original prototype chassis (0.100-in. web magnesium box section), some "as is" and some lightened with holes and scallops in the box section and side rails and with recesses in the web. The input level was a 1 *g* sine sweep from 20 to 1500 cps.

The results of these tests were somewhat inconsistent, but showed minor increases in acceleration levels and small decreases in resonant frequency between heavy and lightened chassis. It was concluded that the basic mounting geometry, rather than the amount of material in the web and box sections, provided the primary stiffness (subchassis attached to chassis and chassis attached to spacecraft structure). As a result of these tests, lightened chassis were selected for flight, and a weight savings of 6 lb was realized.

e. Preliminary matchmate tests. Preliminary matchmate tests were performed in order to ensure that mechanical compatibility existed between the spacecraft and launch vehicle interface hardware provided by LMSC. These tests were performed each time new hardware configurations were mated for the first time. Two of the early tests, using test hardware, are described below.

First, a mockup spacecraft was mated to a test adapter furnished by LMSC. Since many detailed hardware items were missing from both the spacecraft and adapter, the test demonstrated only gross procedural, design, and dimensional compatibility problems. As a result of this test, certain critical spacecraft/adapter mating surfaces on the adapter were reworked and plans were made for a second test.

During the second preliminary matchmate test, the STM spacecraft was mated to the reworked adapter. The test setup is shown in Fig. 381. During this test, one additional spacecraft/adapter mating surface (foot F) was reworked. Again, certain procedural, design, and interference problems were experienced and recommendations for their solution were presented to the proper agencies.

Each of these tests brought out several problems that could not easily have been found without a physical mating of hardware. Such tests, performed early in the program, were an extremely valuable design tool.

f. Solar pressure vane deployment tests. The purpose of this test was to open a folded solar vane to ascertain the effects that the opening impact of the solar vane framework would have on the mylar covering.

A mockup solar panel was placed in the 7 × 14-ft horizontal vacuum chamber. The plane of the panel was horizontal with the cell side upward. A mockup attitude control gas jet and a solar vane actuator were attached to the end of the panel. A complete set of solar vane hardware was then attached to the panel, and a special solenoid release was incorporated to release the vane. The vane was released and observed, while opening, with two Millikan cameras operating at 500 frames/sec. The open vane traveled to the deployed position but failed to stay there because of the 1 g field. The high-speed photography indicated that the vane unfolding operation was rather violent, as expected, but visual inspection of the vane revealed no tearing or other physical damage to the mylar covering.

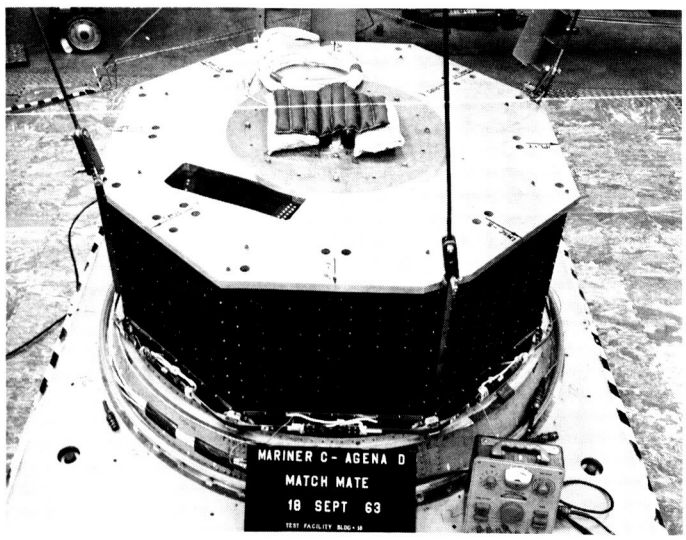


Fig. 381. Preliminary matchmate test setup

A second series of deployment tests were performed in a vacuum chamber to determine the reliability of the new folding technique, and the ability of the unfolding vane to clear the newly installed solar panel guide rails. A mockup panel with rails and solar vane hardware was mounted in the 6 × 7-ft vertical vacuum chamber. The plane of the panel was vertical, with the panel hinge axis at the top. The panel was then rotated around its hinge axis so that the vane CG was vertically aligned over the vane deployment axis; thus, while the vane was unfolding, the gravity effects tending to pull the vane away from the panel were minimized. The chamber shroud temperature was maintained at ambient, but the chamber pressure was reduced. Several runs were made and the vane unfolded properly each time and cleared the solar panel guide rails by 2.0-in. minimum. Millikan cameras were again used to observe the effects.

g. Solar vane actuator impact tests. The purpose of these tests was to determine the effect that the vane deployment impact load would have on the solar vane actuator.

A flight-type solar vane actuator and a set of solar vane hardware were installed on a mockup solar panel. The mylar was removed from the vane to reduce air drag; string was tied from tube to tube of the vane framework so that it would assume the same configuration when released as the mylar-covered vane. The hinge axis of the vane deployment mechanism was oriented vertically to reduce gravity effects. The vane was released and allowed to both unfold and deploy. The operation was as expected; a rotation of 2 to 3 deg of the bimetal element in the solar vane actuator was noted as the vane hit the limit stop, but this small angular movement was not considered a problem.

A second test was performed using the solar vane as a pendulum. A panel with solar vane hardware was oriented with the panel hinge axis horizontal. The vane deployment spring was removed and the panel rotated around its hinge axis until a position was obtained in

which the vane, when released, would swing out as a pendulum and just touch the limit stop. The vane deployment spring was then reinserted and the test repeated. The gravity effects were compensated for by the panel position so the spring would impart additional energy to the vane to duplicate the actual impact. The results were essentially the same as the previous test with a 2 to 3 deg rotation of the bimetal element observed.

As a result of the unusually high solar vane positions indicated after the launch of *Mariner IV*, a third test was performed. Realizing that the first test probably included some friction effects due to side loading on the bearings, a vane actuator was set up with the vane deployment axis horizontal. The deployment spring was removed and the vane allowed to hang freely. The mount for the solar vane actuator was then rotated about the vane deployment axis until the free-hanging vane just touched the limit stop on the bimetal element. The vane was then used as a pendulum and pulled back and released. The amount of pullback was calculated so that the angular velocity of the vane at impact duplicated actual inflight deployment conditions. This test was similar to the second test except that gravity was used to supply the impact velocity. (It was intended to reduce the effects of gravity in the second test and to use the actual spring to supply the velocity over and above the gravity effects.) In these tests, however, the bimetal actuator moved approximately 10 to 15 deg, which was in close agreement with flight data. A pointer, attached to the motor gearhead shaft, indicated that most of the motion was a result of bimetal insulator coupling slipping on the shaft.

h. High-gain antenna and Canopus sensor temperature control test. The test objective for the Canopus sensor was to demonstrate the feasibility of the thermal design and survival capability of the sensor during a worst-case maneuver. The high-gain antenna test was intended to reveal any focusing of sunlight on the feed, which would result in the feed overheating.

An octagonal frame simulated the spacecraft lower ring. The Canopus sensor was mounted to this frame, as was a multiple-layer mylar heat shield. This simulated the sensor thermal interface with the spacecraft. The frame was fitted with heaters so its temperature could be controlled to match expected spacecraft temperatures. The high-gain antenna assembly was mounted to the top of the frame along with another multiple-layer mylar heat shield. This simulated the thermal antenna/spacecraft interface. The entire apparatus was suspended in the 25-ft solar simulator so that it could be rotated to allow sunlight to fall on either the antenna or the sensor. Figure 382 shows the test apparatus in the simulator.

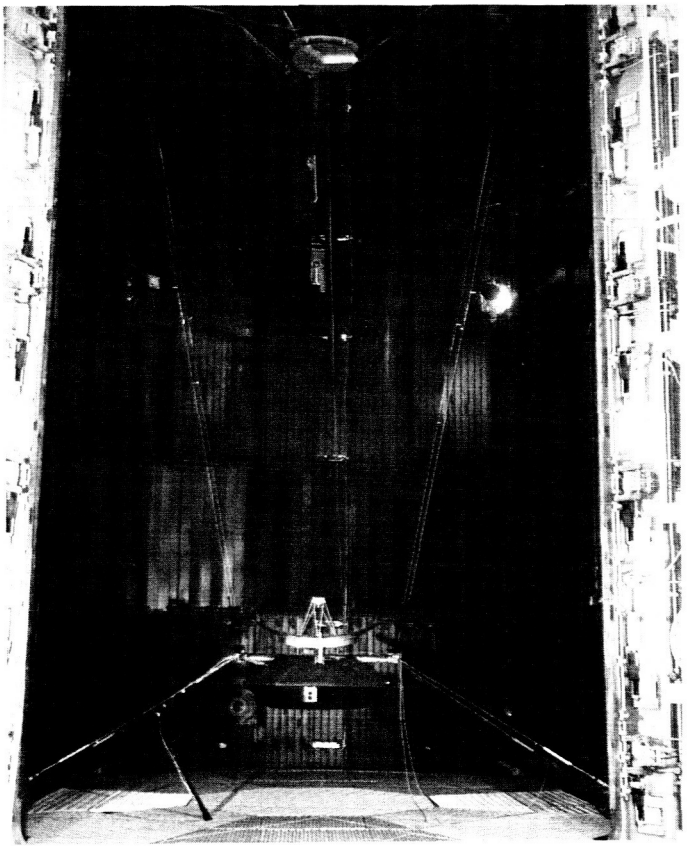


Fig. 382. High-gain antenna and Canopus sensor temperature control test

Tests were performed to simulate Earth cruise, Mars cruise, and a worst-case midcourse maneuver for the sensor. The tests simulated only a worst-case maneuver for the antenna.

The Canopus sensor reached steady-state temperatures of 18°F in the Mars condition and 36°F in the Earth condition. During midcourse maneuver, it did not exceed 75°F. These results verified the feasibility of the thermal design, and no changes were recommended. As the spacecraft developed, it was found that the lower shield configuration used during this test was not correct. In addition, a redefinition of the upper temperature limit of the sensor during short transient heating periods permitted a more desirable metal-to-metal mounting of the sensor. This mounting was verified to be acceptable in subsequent thermal tests using the TCM.

The high-gain antenna feed did not exceed 70°F. This was well below its maximum allowable temperature of

150°F. The test showed no significant sunlight focusing on the feed, and therefore no special provisions or maneuver orientation restrictions were required.

i. High-gain antenna thermal–vibration test. During analysis of the boost environment at the high-gain antenna, it was discovered that considerable aerodynamic heating of the antenna reflector would occur during the *Agena* burns. This heating would lead to some structural weakening of the bonded reflector and would present the possibility that the vibration levels experienced during *Agena* burns might significantly weaken the antenna.

A thermal–vibration antenna test was performed to verify that this condition would not degrade the antenna structure (Fig. 383). A bank of heat lamps provided the required 220°F temperature and a special magnetic tape was tailored to provide a vibration environment equivalent to the *Agena* burn. The vibration testing simulated transient impulses by the input of exponentially decaying sinusoids, and then again by the input of rapidly swept sinusoids. These two types of inputs were analytically tailored to produce the same structural response of the antenna, and the results of the two types of tests were compared to determine the similarity between the laboratory results and the analytical predictions. The laboratory results revealed only moderate agreement between the antenna's structural response to the swept-sine and the decaying-sine transients, although the antenna easily passed both tests.

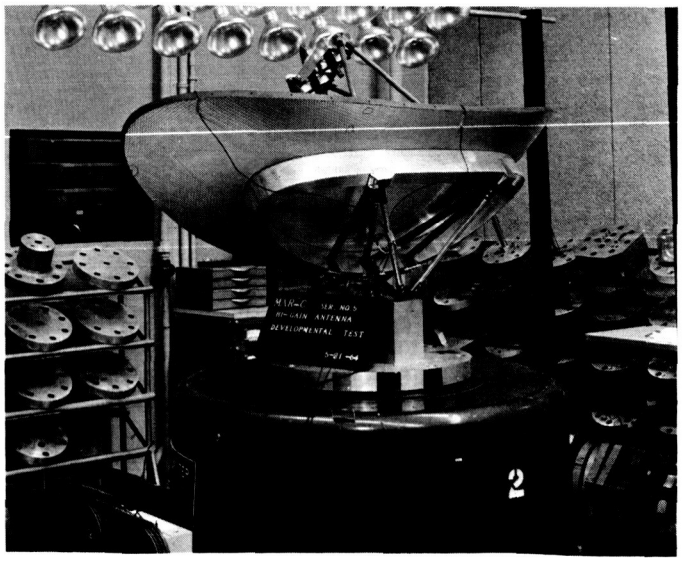


Fig. 383. High-gain antenna thermal–vibration test

It was concluded that further refinement of the transient testing technique was needed to achieve accurate transient waveforms in the test laboratory. Further development of the transient technique would be worthwhile because it more closely approximates vibrational environments experienced during boost. The standard test techniques using swept sinusoids generally result in considerable overtesting of any particular structure. This is because a large safety factor must be used in establishing a swept sinusoid equivalence to a transient impulse unless detailed knowledge of the particular structure to be tested is available. In general, no such detailed knowledge is available when test specifications are established. As a result, spacecraft structures are considerably heavier than the boost environment requires. The large structural weight that could be saved by developing accurate transient testing techniques justifies their development.

j. Thermal-shield outgassing test. Thermal-shield outgassing tests were performed using both black dacron material and a complete shield blanket.

Black dacron material. The outgassing of spacecraft organic materials, when exposed to space environment, increased the chances of degrading the optical sensor and thermal control surface performance. To minimize the possibilities of outgassing, the black dacron outer-layer material was pretreated in a vacuum chamber prior to the blanket-shield fabrication.

Knowing the existence of the outgassing tendencies and quantities from previous tests, a program of thermal–vacuum cleaning was undertaken. A vacuum chamber 4 ft in diameter by 5 ft long and equipped with cold-wall capability, two 16-in. diffusion pumps with liquid-nitrogen cold traps, and the capability of 2×10^{-7} torr was used. An aluminum oven approximately $36 \times 18 \times 54$ in. (Fig. 384) was built to house the material in the chamber. Strip-type resistance heaters, which lined the walls of the oven, were capable of heating the black dacron material to 300°F and the nylon shield components to 200°F. Five thermocouples were installed to monitor temperatures.

Thirty-foot lengths of the material were draped on rods in the oven in a manner to allow volatiles to escape through holes at either end of the oven. Precision-weighed reference samples were placed at critical positions in the oven. The chamber pressure was lowered to approximately 3×10^{-5} torr, and the chamber walls stabilized at 70°F prior to turning on the heat. The 24-hr

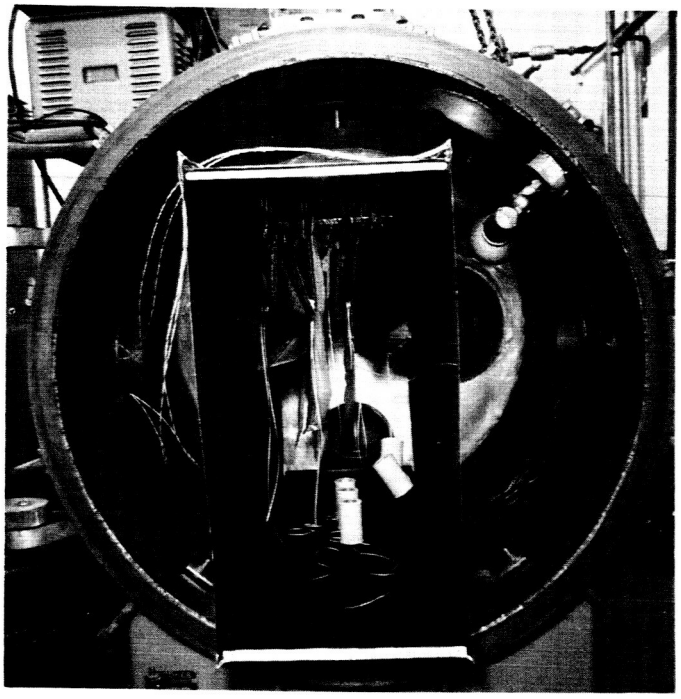


Fig. 384. Thermal shield material outgassing test setup

outgassing test then began. Because of material outgassing, the desired vacuum was not reached until approximately the last 6 hr of the test.

The reference samples that were in the oven were reweighed and checked for their weight loss. These figures generally compared with prior tests. The black dacron cloth for thermal-blanket construction was marginally outgassed because of the quantity of material in the chamber and the resulting temperature gradient.

Complete shield blanket. The first space-simulator test on a flight spacecraft revealed that the upper thermal shield outgassed excessively. This test also revealed that the dacron thread, which had not been pretreated, shrank and exposed the edges of the mylar inner layers to sunlight. It was concluded that the edges of the blanket should be bound and that the individual shield blankets should be subjected to a separate thermal-vacuum treatment to outgas the shield materials and stitching, in addition to preshrinking the assembled blankets.

A bell-type vacuum chamber 6 ft in diameter and 7 ft high with liquid-nitrogen cold walls was used. The DTM bus (Fig. 385) structure was used to support the thermal shield. Two banks of 250-w infrared heat lamps were installed above the spacecraft for uniform heating. Six thermocouples and the flight temperature transducer

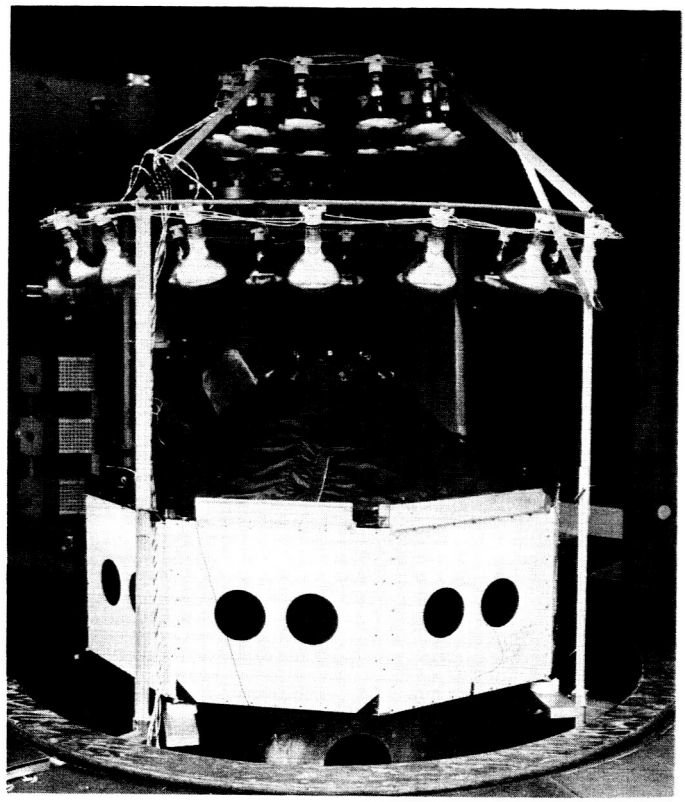


Fig. 385. Thermal shield blanket outgassing test setup

were set up for continuous monitoring by a recorder. The thermal blanket was weighed and then installed on the structure in a flight-type manner.

The chamber pressure was lowered and the upper cooling shroud was cooled to −70°F before the heat lamps were turned on. The upper cooling shroud was intended to trap the outgassing products so they would not contaminate the chamber pumping system. After the temperatures and vacuum stabilized at 300°F and 3×10^{-5} torr, the 24-hr duration test began. After the blanket was removed from the chamber, it was reweighed and inspected.

Thread shrinkage occurred without any apparent damage to the shield blanket. Oil condensation on the chamber walls and reduced blanket weight supported the success of the treatment.

k. Thermal shield blanket ballooning test. During the shield outgassing and shrinkage tests, it was noted that the thermal blanket ballooned when it was exposed to fast decompression. (This phenomenon was noted earlier on TCM testing, and resulted in the incorporation of vent

holes in the blankets.) A series of tests were conducted on the upper and lower blankets to verify that the ballooning would not result in blanket structural failure or interfere with the functions of other spacecraft components.

The upper thermal shield blankets were mounted in a flight configuration on the DTM bus structure. A geometric mockup of the Cosmic Dust Detector was mounted on the superstructure. The bus structure was placed in the 6-ft chamber, and the chamber pumped down at rates comparable to the boost pressure decay. At the completion of the first test, the structure was turned over and the operation repeated using the lower shield. The total duration of each test was approximately 3 min. During that time, the chamber pressure was reduced at the rate shown in Fig. 386. Photographs were taken through a chamber porthole to record the blanket behavior (Fig. 387).

These tests verified the adequacy of the blanket interlayer-venting provisions in the upper and lower shields. They also confirmed the shield structural adequacy and the nonexistence of interferences with other spacecraft hardware.

l. Solar panel space-simulator tests. There were three objectives of these tests:

1. To determine appropriate temperature control surface treatments for the attitude control jet assembly and the solar vane actuator
2. To investigate temperature gradients in the solar panel structure
3. To verify the solar vane survival under worst-case launch heating

A flight-type solar panel structure, including attitude control jets and solar vane assembly, was suspended horizontally in the 25-ft solar simulator as shown in Fig. 388. Because of the uncertainty in the simulated-sunlight spectrum, the panel face was painted black and a correction was made for the difference between solar-cell absorptivity and black-paint absorptivity. The absorptivity apparatus was placed on the panel about 2 ft from the end. Thermocouples were used to measure temperature.

Tests were conducted at Earth intensity (134 w/ft^2), Mars intensity (51 w/ft^2), and without lights. One test was run with the panel inverted and the solar vane folded

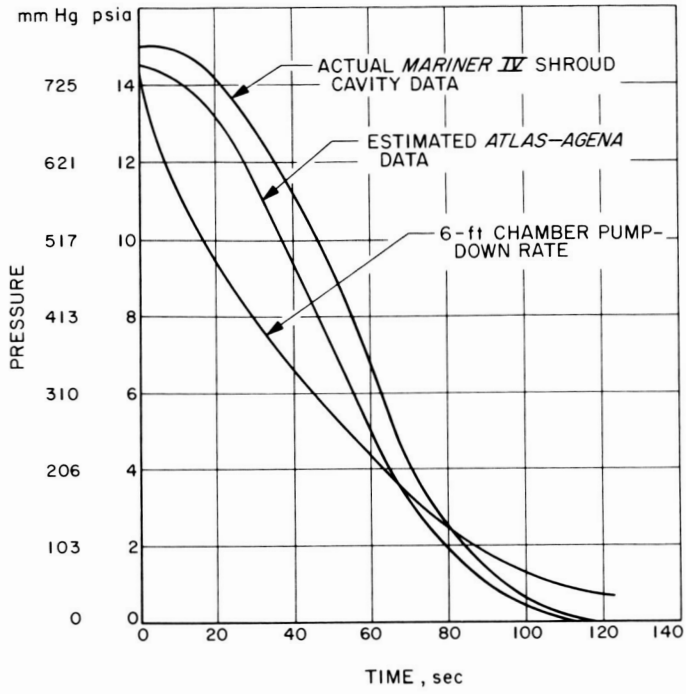


Fig. 386. Boost environment spacecraft cavity pressure decay curves

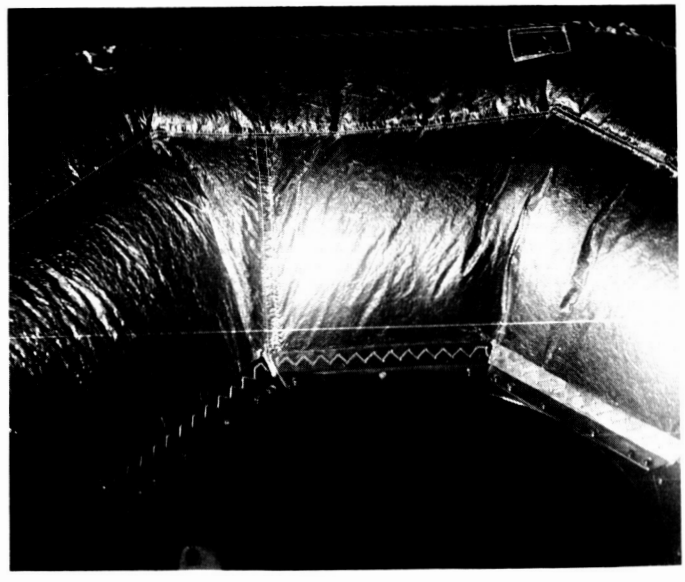


Fig. 387. Ballooned lower thermal blanket

in the launch configuration to determine heating effects on the vane.

The results for each test objective were:

1. Combinations of painted and metallic surfaces provided temperatures well within operating limits for

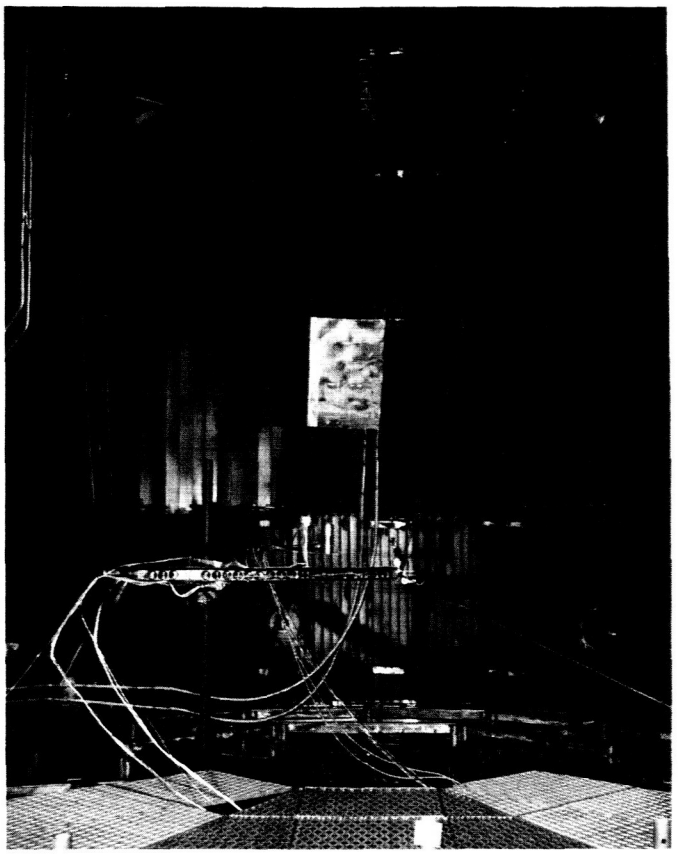


Fig. 388. Solar panel space-simulator test setup

the solar vane and attitude control jet assemblies: solar vane electronics, 140°F at Earth and 0°F at Mars; attitude control jets, 150°F at Earth and 5°F at Mars.

2. Lateral gradients of 20°F existed in the panel because of edge effects and because the spar acted as a cooling fin. There was a negligible temperature drop between the solar cells and the panel surface. Expected flight temperatures were 150°F at Earth and 15°F at Mars.

3. Shrinking and permanent wrinkling of the solar vane could have occurred during worst-case launch heating. Vane changes were made to ensure launch-heating survival.

m. Solar panel transporter test. The solar panels were shipped in four-wheeled transport trailers that could be towed by standard vehicles. The trailers were used as shipping containers when moving the panels on or off the Laboratory. The trailers and suspensions were designed to isolate the panels from all significant road shocks. Because of the particular function and character of the trailer shipping container, a special dynamic road-qualification test was conducted. An instrumented type-approval solar panel was mounted in its transport trailer and towed to the Table Mountain Solar Test Site and across the Mohave Desert. Vibration and shock data were measured enroute.

Data analysis and solar tests conducted between and after the test showed no panel electrical or structural degradation. The stresses and loads experienced by the panel were less than the flight panel would experience during the flight-acceptance vibration testing.

n. Low-gain antenna extreme temperature test. An extreme temperature test was performed on the low-gain TA antenna (Fig. 389). The experiment demonstrated that no significant electrical changes were necessary because of the extreme temperatures the antenna would experience during a midcourse maneuver. Because of an oversight, no minimum secondary control surface temperatures were specified. As a result, the ground-plane temperature fell short of its predicted 220°F, reaching a value of only 208°F. Despite this lower temperature it

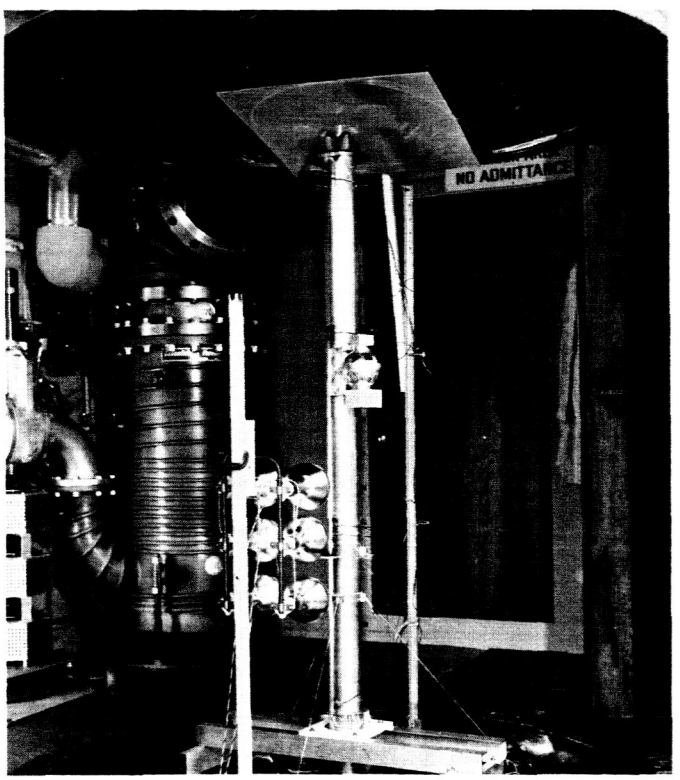


Fig. 389. Low-gain antenna extreme temperature test setup

was demonstrated in the test that (1) the materials of the ground plane and aperture (aluminum) achieved 360°F, (2) the bonding material between the ground plane and the circular waveguide was tested to 240°F, (3) the aperture radome and Epon 901 bonding material had surface temperatures up to 250°F, and (4) the nylon screws had surface temperatures up to 930°F.

Based on the experimental evidence and a comparison of pre-test and post-test data, the subjection of the low-gain antenna to the extreme transient temperatures indicated an insignificant effect on the antenna's electrical performance during a midcourse maneuver.

o. Electronic-assembly shipping container. In December 1963 during transportation handling and vibration testing of the *Mariner* battery, the electronic-assembly shipping container experienced a catastrophic failure. Subsequently, a series of vibration tests were conducted with simulated electronic cases to evaluate the shipping container. Initial tests revealed failures due to poor bonding of the urethane isolators. A second series of tests also resulted in failure of the isolator bond. During this second test series, acceleration monitoring of the simulated electronic case recorded spikes considerably above acceptance levels for flight hardware.

The shipping container was then modified. It subsequently survived a transportation-vibration test performed at JPL and a package drop conducted by the vendor. During the transportation-vibration tests, spikes in excess of specification levels were experienced at its resonant frequencies. However, the cognizant engineer considered these to be within acceptable levels. Subsequently, all containers were retrofitted or replaced by the improved configuration.

p. Solar panel structural developmental tests. The weight limitations of the *Mariner* Mars 1964 program required a radical departure from past solar panel structural designs. The reliable heavier *Ranger* and *Mariner* Venus 1962 panel structures had to be abandoned in favor of a new structure approximately half the weight per surface area. This significant structural weight reduction required that a considerable development program be undertaken to demonstrate the structural flight worthiness.

Early attention was directed to the radically different substrate (transverse corrugations) portion of the panel and its effect upon the installed solar cells. Because of the unique all-bonded construction, additional tests were directed to the development of proper and reasonable manufacturing acceptance criteria. Before production of flight hardware began, a full series of informal preliminary tests defined the areas in this new design that required rework and further development.

Some important preliminary developmental tests of the system were:

1. *Acoustic test of substrate samples.* This test showed the critical sensitivity of spot-welded construction to acoustic energy. Based upon these results, spot-welding was abandoned and replaced with an all-bonded substrate construction.
2. *Skin-buckling tests.* This test showed the importance of continuous bonds and established acceptance/rejection bond-void criteria for the manufacturer.
3. *Solar-cell and substrate flexural tests.* A series of tests were conducted to determine the buckling characteristics of the critical unsupported substrate back corrugation flats. Flexural static tests were conducted, followed by dynamic flexural tests. These tests developed a relationship between static and dynamic buckling criteria. The dynamic stress required to cause buckling was 1.6 times the equivalent static stress for this particular configuration. Using a test setup similar to the dynamic buckling tests, low-cycle fatigue studies were also performed upon the substrate corrugations.

The purpose of the final developmental qualification test was to determine the ability of the panel to survive *Mariner* vibration environment without degradation. A second purpose of this test was to determine the frequency response characteristics of the solar panels, as supported upon discrete dampers in the spacecraft configuration. The input levels to the test were rather carefully developed, from preliminary STM data, to envelope panel responses for the most critical STM test conditions. The panel successfully passed the qualification test sequence and demonstrated structural adequacy for flight purposes. Subsequent tests to failure vividly illustrated the lack of excessive (unnecessary) margins of safety. At 112% of ultimate vibratory load, functionally noncritical cracks developed in the substrate corrugations.

D. Special Problems

During the course of the project development, a number of significant problems arose that warranted special attention. These problems were of such scope and magnitude as to jeopardize the success of the mission, and

were therefore subjected to a thorough study under a maximum effort. Three of the problems were the direct result of the inability of certain hardware to survive the imposed environments.

1. Canopus Sensor

On the PTM vehicle, a flight-like sensor was subjected to the TA vibration test series, at the conclusion of which it was determined that the sensor was inoperable. The Canopus sensor used in the PTM tests employed the "original" tube design in which a butt-weld existed in the wires from the dynode structure at the glass-to-metal seal in the aft end of the image dissector tube. The failure mode observed was breakage of the anode wire through the butt weld. It was later established that this tube model had experienced a similar failure during component TA testing, and, therefore, the occurrence of a failure during PTM vibration was not surprising.

An improved version of the tube was subjected to a series of tests in normal subsystem TA configuration with adjusted test levels, but it was unable to survive the second plane of vibration. These adjusted test levels were based on information gathered from the PTM tests. The failure mode was the same experienced previously: that of breakage of the anode wire at the glass-to-metal seal.

Subsequent examination of the data available from this test revealed that the unit experienced gains much larger than expected based on experience gained during tests performed on the prototype unit. Since the TA unit differed from the prototype in only two respects (i.e., the prototype unit had an instrumented mockup of the image dissector tube and was mounted to the vibration fixture with stand-off washers), it was decided to perform another series of tests to discover which of the two major differences contributed to the unexpected gains. The results of these tests indicated that hard-mounting the unit on the vibration fixture resulted in an increase of gains in a frequency range critical to the sensor.

It was decided that the TA vibration levels, generated as a result of the preceding work, were still subject to question and that further testing was called for. Provisions were made to mount a Canopus sensor on the PTM and to subject the entire assembly to the PTM vibration levels. In essence, the spacecraft was to be used as an elaborate vibration fixture with all instrumentation and performance testing being performed on the Canopus sensor. The test was to have two objectives: to determine inputs to the Canopus sensor for assembly-level TA and FA environmental testing, and to qualify an actual Canopus sensor at the PTM vibration test levels.

Two "improved T" (thick wire) tubes were subjected to the new test. One performed satisfactorily after the test, but the other failed after one plane of noise at about 12 *g* rms (slightly higher than normal TA). During this same period, the cognizant hardware division was pursuing development of a rugged version of the image dissector tube, since it presented the only clear path toward a substantial vibration margin for the sensor. In view of the schedule, it was decided to forego further study of the problem until such time as the flight hardware could be retrofitted with the rugged version. This was accomplished prior to launch with substantial confidence, since a sensor with the ruggedized tube satisfactorily passed normal assembly-level type approval.

Possibly the most important factor derived from this environmental problem reaffirmed that vacuum tubes are highly susceptible to vibration damage and require special consideration.

2. Vidicon Camera

Unlike the Canopus sensor problem, the TV satisfactorily survived the PTM TA vibration tests. In the initial design, based on past experience with *Ranger* tubes, the tube was hard-mounted inside the camera. The first indication of a significant problem was when the camera failed to survive the *Mariner* component TA vibration test. Immediately, a study was undertaken to determine (1) the destructive frequencies of the vidicon tube and mode of failure, and (2) the vibration environment of the tube in the camera and how this environment could be improved. A unity-gain tube holding fixture was used for vibration tests on the *Ranger*-type and ruggedized *Mariner* tubes.

The tubes were subjected to a 3 min, 16.4-*g*-rms random noise, and to a 9 *g* sine wave with a 5 min sweep from 20 to 500 cps, a 1.75 min sweep from 500 to 1000 to 500 cps, and a 1.25 min sweep from 1000 to 2000 to 1000 cps. The tube was functionally tested after each test.

The results obtained indicated that: (1) there was a wide variation in the vibration response for both *Ranger*- and *Mariner*-type tubes from tube to tube; (2) the ruggedized *Mariner*-type tube construction was mechanically superior to the *Ranger* type; (3) the critical frequency range of the ruggedized *Mariner* tube was 400 to 700 cps; (4) failures occurred in the weld joints and conductor leads.

A structural mockup of the vidicon camera chassis was constructed from flight-type hardware. Hard-mounting of the tube and several softer tube-mounting designs were tested. The three tube mountings tested were: (1) the hard-mount, (2) the O-ring mount, in which the tube was supported at each end with two teflon O-rings, and (3) an experimental soft-mount in which the tube was suspended by a resilient potting material.

The results of these tests indicated that the experimental soft-mount provided the maximum tube protection, and that the damaging 400 to 500 cps resonance experienced by the hard-mount design was actually a characteristic of the block-style test fixture.

A new soft-mounted tube passed the TA tests in the more severe environment of the block-style test fixture. As a result, and because of the tube malfunction due to the high-frequency cross-axis response problem on the flexible fixture, further testing was discontinued and the new soft-mount design was adopted for the flight configuration.

3. LMSC Instrumentation System

During FA vibration testing of the MC-3 spacecraft, the first time the flight vibration and acoustic instrumentation was subjected to system-level environmental testing, the flight microphone displayed a totally unacceptable behavior. It appeared to have a very high sensitivity to vibration, and its mounting configuration, at the point at which it was attached to a highly resonant bracket, made it quite impossible to determine if the character of the response it was measuring was either vibratory or acoustic in nature.

This argument was easily substantiated since a laboratory reference microphone was suspended in close proximity to the flight microphone and it yielded indications of a significant acoustic noise field accompanying the imposed FA random vibration.

The flight microphone was initially set on the high-gain position, the zero reference calibrations of which were 124, 144, and 154 db. Tape speed was 30 in./sec, giving a frequency response of from direct current to 5 kc. Calibration was accomplished using a pistonphone calibrator. During the first test, at approximately 85 to 100 cps, the waveform of the microphone broke up and went into full band oscillation. At that time also, a wander of the zero reference level was observed at a rate of approximately direct current to 2 cps.

It was subsequently determined that the low-frequency drift was due to the sensing of local pressure fluctuations from the room air conditioning.

The same problem occurred during the vibration tests performed on the MC-2 spacecraft, although a different microphone and amplifier system were used.

In an attempt to solve the vibration problem surrounding the flight microphone, the installation of the microphone was modified for the test series with the MC-4 spacecraft. Instead of hard-mounting to the resonant bracket (as had been done previously), some degree of isolation was now obtained by inserting sheets of 0.060-in.-thick silicon rubber between the microphone and the bracket and the nut and the bracket.

The MC-4 spacecraft was subjected to the vibration test series, and the behavior of the microphone was characteristic of the behavior previously observed on MC-2 and MC-3, in that the direct current drift was still present. An analysis of the information obtained from the microphone during the noise tests also indicated that the bracket modifications were not particularly beneficial to the collection of data.

In view of the schedule and the problems encountered, the microphone was dropped from the mission in favor of a new vibration transducer mounted at the adapter/*Agena* interface. This change permitted use of the high-frequency telemetry channel vacated by the microphone, and provided the first JPL opportunity to obtain inflight simultaneous vibration data on the spacecraft and at the spacecraft/*Agena* interface.

4. Summary

Although each of these problems was significant at the time of its discovery, all of them were solved.

Attempts at modifying the normal component TA test levels and test technique were made to solve both the Canopus sensor and vidicon tube problems, but the actual solutions were obtained by design improvements. In the case of the Canopus sensor, the tube was modified by internal structural stiffening. The vidicon solution was obtained by vibration isolation. This reaffirms the fact that the best approach to the solution of environmental-type problem areas is to improve the design rather than to change the test requirements.

XXI. SYSTEM TESTS

System testing of the *Mariner* Mars spacecraft took many different forms, but in all cases the purpose was to test the spacecraft as a complete system. The system tests differed from the assembly-level environmental tests in that the spacecraft was tested for its actual operation as an integrated system.

The intersubsystem tests usually initiated system testing and differed from the system tests in that the spacecraft was not completely assembled electrically and was not necessarily operated in any semblance of the flight sequence. The intersubsystem tests were performed at SAF only during the initial spacecraft buildup; they were not required at Cape Kennedy because the spacecraft had been completely assembled and subsystem-tested at SAF before shipment.

Similar system tests were performed both at Cape Kennedy and at JPL, and differed only in minor detail because of the difference in facilities. Other tests such as the ESF test and the on-pad functional tests, which had been simulated by dummy runs at JPL, were performed only at the Cape. The test sequence was highly dependent on the availability of test facilities and equipment; however, general principles were usually followed:

1. A system test always followed assembly and subsystem checkout, to verify the functional integrity of the spacecraft.
2. A system test always preceded the shipment of and followed the arrival of the spacecraft at Cape Kennedy.
3. The last system test was performed before final commitment of the spacecraft to the launch pad. After this test, no flight equipment could be removed or connectors disconnected.
4. The weight and CG, free mode, matchmate, dummy run, and vibration tests were always grouped together, because the spacecraft had to be assembled in the full flight configuration during these tests.
5. The magnetic mapping test was usually performed during or after a system test while the spacecraft was still in an electrically complete configuration.

The system tests exercised the spacecraft through the flight sequence from launch to picture playback in all primary and backup modes. For example, several encounter sequences were performed with some using CC&S commands and others using ground commands. System tests were performed several times on each *Mariner* spacecraft, at both JPL and Cape Kennedy. All of these tests were essentially identical, except for minor changes caused by the normal evolution of the procedure.

The "combined system test" was the overall name given to the preliminary Cape Kennedy on-pad tests. These tests were performed on the launch vehicle and on the spacecraft. The spacecraft portion of the combined system test included:

1. Spacecraft/launch complex functional tests
2. Calibration of the RF links between the spacecraft, the blockhouse, and Hangar AO
3. Countdown Part 1 and Countdown Part 2
4. Cooling
5. J-FACT
6. Simulated launch
7. RF interference
8. Umbilical release and cooling blanket retraction

The flight-acceptance composite tests performed at Cape Kennedy were a part of the combined system test. The *Atlas*, *Agena*, and spacecraft interfaces were verified by J-FACT, which was primarily concerned with the postlaunch interfaces between the *Atlas* and the *Agena*. Spacecraft participation in J-FACT ended essentially at launch when the spacecraft umbilical was pulled. The Countdown Part 2 portion of the launch countdown dummy run was an exact simulation of the actual launch day countdown. During SAF testing and during the first series of tests at Cape Kennedy, live pyrotechnics were not installed and the PIPS was not fueled. Except for these differences, the countdown was performed as if the spacecraft were actually going to be launched. The PTM spacecraft was used to verify the compatibility of the SFOF and DSIF with the *Mariner* spacecraft.

A. PTM System Testing

1. Test Description

The PTM spacecraft was used for flight spacecraft design verification. It was subjected to a variety of tests

in order to verify spacecraft design and performance. Many of the tests were performed at more severe environmental levels than would normally be expected in flight. In general, when PTM testing revealed the need for a design change, the change was incorporated and tested on the PTM before being included in the flight spacecraft.

The primary objective of PTM testing was to determine the degree to which the assembled spacecraft met the design criteria and restraints in both ambient and simulated flight environments. Four categories of supplementary objectives had to be fulfilled in order to attain the primary objective; these are given in Table 82. Table 83 lists the tests performed on the PTM and describes the objectives and acceptance criteria of each test.

2. Test Chronology

On November 1, 1963, PTM assembly began at SAF. Installation and checkout of related facility support equipment and operational support equipment progressed concurrently.

The PTM was used for design verification of the flight spacecraft that were assembled at SAF in early 1964. This prototype of the final flight spacecraft was scheduled to be subjected to a variety of tests (many at more severe environmental levels than would normally be encountered in flight) in order to verify spacecraft design and performance.

Detailed test procedures were released just before the performance of each test on the PTM. Testing of the PTM provided the means of validating the test procedures for use on the flight spacecraft. All problems or failures that occurred during testing were recorded on problem/failure reports.

During the assembly period (November 1 through December 18, 1963), a controlled disassembly and inspection of all PTM equipment as-delivered was performed. This inspection uncovered some discrepancies that, in most instances, were corrected. As a result, the PTM was assembled to the electrical test configuration (without solar panels, solar pressure vanes, thermal shields, or temperature control louvers), and very few major mechanical or electrical interface problems occurred. The assembly was completed on schedule; however, because of variances in hardware delivery to SAF, the actual sequence of installation of the individual subassemblies differed somewhat from the optimum installation sequence, and non-flight-equivalent equipment was used as a temporary substitute in many instances when PTM hardware was not available.

Table 82. Supplementary objectives of PTM system testing

Category	Objectives
Interface compatibility and system performance	To demonstrate that the subsystems exhibited nominal performance characteristics.
	To demonstrate that the spacecraft would perform all logic functions for a normal flight sequence in all appropriate operational modes.
	To verify that all system analog signals were within tolerance and remained in tolerance throughout the test program.
	To establish that the input threshold of digital circuits had an adequate margin above the spacecraft noise level and an adequate margin below the input signal level.
	To verify that each subsystem met the requirements of its functional specification and design specification.
Parameter variation and failure mode	To demonstrate that, as various failures were induced in the primary function, the backup circuits and redundant paths performed as intended.
	To verify that none of the backup circuitry or redundant paths, when in their quiescent modes, interfered with the proper operation of their primary function.
	To determine the effect on the Spacecraft System of certain selected failure modes, and to develop possible corrective procedures.
	To evaluate system performance characteristics during a planned series of parameter variations at extremes of tolerance.
	To determine design safety margins by varying parameters outside the specified limits.
Environmental performance	To demonstrate that the Spacecraft System would perform to specification during and after subjection to prelaunch, boost, and injection environments.
	To demonstrate operability of the Spacecraft System under a simulated space environment.
Miscellaneous	To determine if the signals exhibited excessive long-term drift rates, even though they remained in tolerance.
	To determine failure rates within the time available.
	To develop and verify the system test procedures for such functions as flight readiness testing, data acquisition and processing, and communications.
	To develop a testing procedure and to train operations personnel.

Table 83. PTM test objectives and acceptance criteria

Category	Objectives
Mechanical assembly operation	To assemble all components of the PTM structure, superstructure, mounting bracketry, cables, electronic cases, and antennas for verification of the mechanical design and alignments.
System test complex and facility support equipment test	To assemble and test the STC and its related flight support equipment (without a spacecraft) to verify their complete readiness to support the *Mariner* system test effort. The STC and facility support equipment could not violate the grounding philosophy dictated by the spacecraft and OSE design specifications. There had to be a minimum of 2 MΩ in which infinite resistance was specified. All interfaces had to be correct in design and operation.
System test complex/ spacecraft ground integrity test	To verify that the grounding techniques of the spacecraft and STC conformed to JPL specifications (that no unknown ground loops were present in the spacecraft and none were introduced when the STC was connected to the spacecraft).
Initial power application	To safely apply and distribute spacecraft electrical power to a newly assembled spacecraft, and verify that the power met the applicable specifications. If new assemblies had to be substituted at any time after the completion of initial power application, the portion of the procedure involving the hardware to be substituted had to be performed again before the circuitry was incorporated into the Spacecraft System.
Subsystem tests	To evaluate the performance of each subsystem while operating with spacecraft power.
Intersubsystem tests	To minimize the chance of equipment damage caused by improper interfacing. All interfaces had to agree with the circuit data sheets and function per design specification. To functionally test all interfaces between subsystems and verify their agreement with the circuit data sheets. If new assemblies had to be substituted at any time after the completion of these tests, the portion of the procedure involving the hardware to be substituted had to be performed again before the circuitry was incorporated into the Spacecraft System. To make a preliminary determination of any possible effects the subsystem might have on the system environment. No major interactions, except those specifically designed into the spacecraft, could exist between spacecraft subsystems.
Telemetry channel calibration	To verify (and correct, if necessary) calibration curves for all telemetry channels. System calibration and monitoring had to guarantee that the stability and accuracy of each telemetry channel were within design specification tolerance.
System tests	To establish the functional integrity of the spacecraft within the constraints imposed by testing operations and the Earth environment. All subsystems had to operate per functional specification. (All instances of anomalous performance had to be completely documented, thoroughly investigated, and appropriate disposition made.)
Parameter variation tests	To determine the effects on spacecraft behavior of controlled variations in selected system parameters.
Magnetic mapping of spacecraft and solar panels	To measure the magnetic fields produced at the Magnetometer sensor by current flow in the various spacecraft subsystems and spacecraft harnesses. Sufficient data had to be obtained to accurately determine the magnetic characteristics of the spacecraft. To determine the components of the permanent magnetic field of the spacecraft and of the coefficients of induction for an external magnetic field at the location of the Magnetometer sensor.
Weight and CG measurement	To accurately determine the actual weight and CG of the spacecraft (cruise configuration), and to adjust the PIPS thrust axis to the spacecraft CG.
Matchmate to *Agena* adapter and shroud	To prove the mechanical and electrical interface compatibility between the spacecraft and the *Agena* adapter and shroud.
Dummy run tests[a]	To verify the compatibility of the LCE with the spacecraft. To evolve and test the procedures to be used for the actual launch.
Free-mode test	To demonstrate the correct operation of the spacecraft on solar power without any electrical connection to support equipment. To verify the functional integrity of the spacecraft in the absence of any support equipment electrical connections.

[a]Simulated precountdown, simulated countdown, and live pyrotechnics test.

Table 83. (Cont'd)

Category	Objectives	Category	Objectives
Simulated midcourse interaction test	To verify that the autopilot subsystem is capable of maintaining and controlling spacecraft attitude during the burning of the PIPS motor, and to verify that the dynamic properties of the spacecraft structure do not have a harmful effect on autopilot performance.	EMI tests	To determine the RF susceptibility of spacecraft and OSE when subjected to an RF environment similar to that expected at the Cape. Spacecraft performance could not be degraded when the spacecraft was irradiated by RF sources simulating all known AFETR sources.
Space-simulator tests	Part 1. To establish the functional integrity of the spacecraft while operating in a simulated space environment. Part 2. To verify the design of the temperature control subsystem.		To determine the contribution from spacecraft subsystems to the RF level that might degrade the performance of the spacecraft receiver. Power absorbed had to be low enough to guarantee that pyrotechnics would not fire.
Vibration tests	To verify that the spacecraft could operate satisfactorily during and after exposure to acoustic and vibration levels higher than those expected during the boost phase from the *Atlas* and the *Agena*.		To measure the RF susceptibility and power absorption of the pyrotechnics subsystem. The levels measured had to be low enough to prevent intrasubsystem interference. To measure the RF noise levels of the STC and the conducted interference of the OSE power cables.
SFOF/DSIF/ spacecraft compatibility test	To achieve early compatibility verification among system elements of the SFOF, DSIF, and the spacecraft. The SFOF and DSIF had to be capable of performing to spacecraft and mission requirements, since this test was their responsibility.	Test support for MC-2, MC-3, MC-4	To perform detailed investigations and probings of all problems encountered during the test program of the flight spacecraft, including the flight test.
Failure-mode tests and logic circuit test	To investigate the effects on the overall system of selected failures that could not be easily analyzed otherwise. All spacecraft behavior under abnormal conditions had to be completely understood. Sufficient data had to be obtained to permit the SPAC director to exercise his team under nonstandard conditions.	Flight-spares system qualification on PTM	To verify that the spare electronic equipment functioned normally in the Spacecraft System environment. Flight spares had to operate in the system for at least 100 hr. Spares qualified on MC-4 had to undergo at least 100 hr of space-simulator testing and pass vibration tests at FA levels.

The system test complex and its related facility support equipment were installed and tested during the spacecraft assembly period. By December 13, 1963, the following tests of the STC and facility support equipment had been satisfactorily completed:

1. Cabling continuity
2. STC ground integrity
3. Initial application of power to the STC
4. Self-test of each spacecraft subsystem OSE
5. Testing of the interfaces between components of the OSE
6. Measurement of the EMI produced by each item of OSE and facility support equipment on the STC

The initial application of spacecraft power (as opposed to OSE power) to each of the spacecraft subsystems was begun on December 19 and satisfactorily completed on December 24, 1963. Photographs were taken of the various voltage and current waveforms for comparison with photographs previously taken during launch-type testing in the laboratory.

The PTM subsystem interface test was performed during the period of December 30, 1963 through January 10, 1964. In this test, all interfaces between subsystems were open-circuit and closed-circuit checked using extensive instrumentation. Most of the interfaces checked out normally and compared favorably with the circuit data sheets.

The last of the interface testing was completed on January 10, 1964.[9] The telemetry interface checkout was successful and showed only minor problems. The science and video storage interface checkouts revealed some

[9]The remainder of the tests were performed in 1964.

problems associated with the start and end-of-tape signals in various modes noted. This system interface, however, did include playback of lines of TV data to the ground telemetry subsystem, which provided preliminary confidence that the total TV data link was operable.

A special test performed on the attitude control subsystem included investigation of noise and its effects on the autopilot. This test was based on results of the SMIT performed at Langley Research Center using the STM spacecraft. A successful pyrotechnics subsystem test was performed on January 14.

System Test 1, prelaunch to postencounter phase, was performed on January 16. The general results of the test were encouraging and indicated that the spacecraft performed functionally to specification.

The postencounter portion of System Test 1 was performed to check out the backup modes at encounter and to play back one picture from the video storage subsystem. The telemetry processing station was "on line" during the entire test, and information was printed out on both the line and character printers.

The concept of computer monitoring of spacecraft operations was demonstrated to be feasible, and the effort to make the system completely operational and more useful before the start of flight spacecraft testing was increased.

Parameter variation tests were started on January 27. The first part of the tests consisted of varying the booster-regulator output to a lower-than-nominal value and observing the spacecraft characteristics. The preliminary results indicated that the spacecraft worked normally around 49 vdc, and exhibited various subsystem abnormalities when the booster went below this level. Some of the difficulties experienced were:

1. The data encoder bit rate went from the normal 8⅓ to a 5 bps value due to shift in spacecraft reference frequency.
2. The science DAS went out of synchronization.
3. The radio subsystem could not be locked up.

The second part of the test consisted of:

1. Setting the booster to a higher-than-nominal value of 58 v
2. Varying the synchronizer frequency to 36.9 kc from a nominal 38.4 kc
3. Setting the synchronizer frequency to 39.9 kc

A thermal control power survey was conducted to determine and verify the power dissipation figures used in the design. Fifty power measurements were made, and the results of the survey indicated that the data obtained compared closely with the design data.

A thorough survey was performed to determine the status of the outstanding engineering change requests. Arrangements were made to release all equipment so that the changes could be incorporated and tested before delivery to SAF.

Before the attitude control gas subsystems were returned to SAF, a leak test was performed. During the test, it was discovered that the low-pressure side had severe leaks. These leaks were fixed and the system was pressurized and checked at flight value.

The primary requisite for performing the second system test was to test the complete spacecraft with all known deficiencies removed and with all the latest engineering changes incorporated.

A preliminary checkout of the spacecraft was performed on February 21 in order to test the many changes that had been incorporated in the spacecraft equipment. Problems in the power area and the computer data system were later resolved.

System Test 2 was performed during the period February 24 to February 26. The major problem experienced during the system test was an abnormal encounter sequence, which probably resulted from a supersaturated spot on the TV vidicon tube.

A partial reset of the data encoder event counters was noted. This problem was associated with the power subsystem (OSE) scanning. The EMI group radiated the spacecraft with all known onboard and offboard sources. The only interference noted was with the *Agena* telemetry 242.3-Mc signal. There was an apparent 10-db increase in the radio subsystem telemetry channel power readout from the precision coupler. Tests confirmed that the pickup was being induced by a coaxial cable in the precision coupler link. The data encoder experienced interference on the low-level signals.

Permanent magnetic field mapping was performed on the spacecraft upon completion of System Test 2 using a specially designed fixture (Fig. 390 and 391). Preliminary reports indicated that a 50 γ field was present at the sensor due to the permanent magnetic field of the spacecraft. The sources of this field were not located.

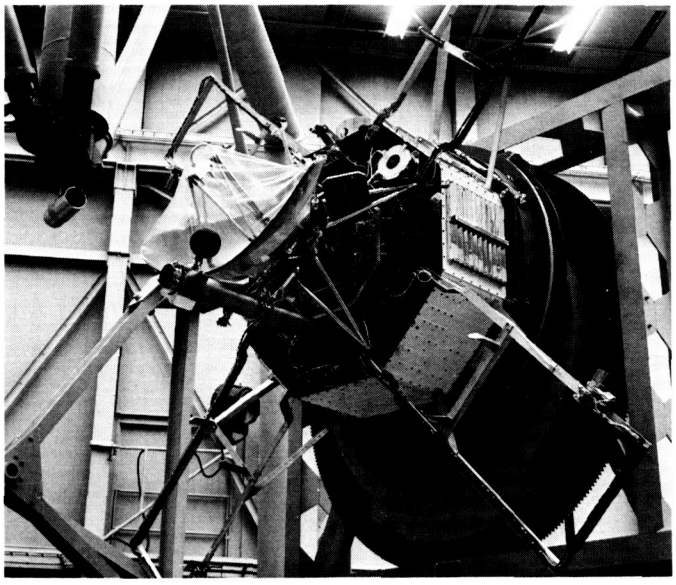


Fig. 390. Spacecraft in position for magnetic mapping test

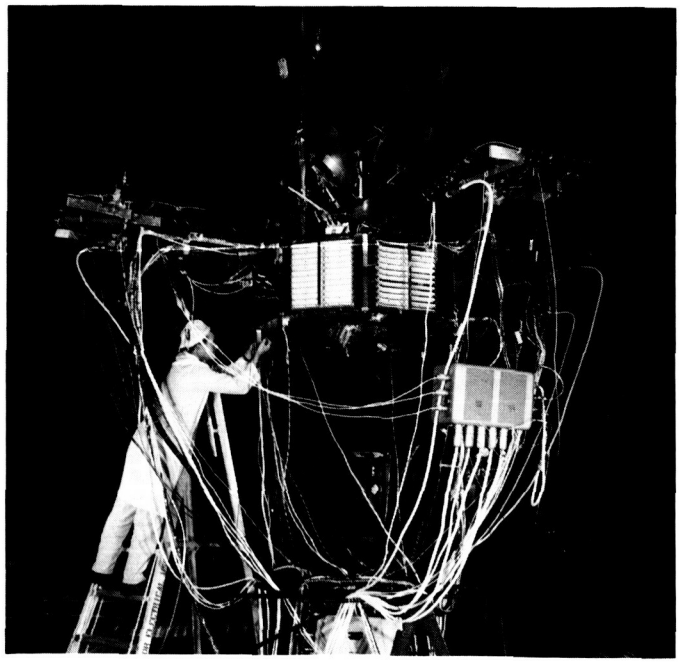


Fig. 391. Spacecraft preparation for space-simulator testing

Upon completion of the magnetic mapping, the spacecraft was prepared for the space simulator. The thermocouples, solar panel stubs, attitude control special gas manifolds, and thermal shields were installed. The spacecraft was delivered to the space simulator and suspended in the chamber on March 4 (Fig. 391). The system verification test was performed between March 5 and 7, when the chamber doors were closed and the evacuation started.

During the system verification test, numerous problems were encountered with the new testing configuration. Difficulty was experienced in obtaining the narrow angle Mars acquisition via the narrow angle Mars gate and by DC-16. Since a normal science encounter sequence could be attained using the TV planet-in-view signal, it was decided to go into the space-simulator test.

The solar pressure vane actuators could not be driven in both directions. The effect of gravity was determined to be the cause, and it was decided to proceed with the test even though only unidirectional drive was available.

The first part of the space-simulator test started on March 7. This test established the functional integrity of the spacecraft while operating in a simulated flight environment. Throughout the 10-day operation of the spacecraft, the radio subsystem did not perform normally with either of the two power amplifiers. The problem was apparently caused by the lack of a thermal path for the cavity baseplates. The CC&S OSE (including special function boxes) caused several anomalies that resulted in the CC&S commands being issued at abnormal times.

The attitude control Sun sensor stimulus lamps failed, and the only valves that could be actuated were the positive yaw and roll jets. This failure was due to an improper design that did not permit the stimulus lamp heat to be carried off by conduction. The Cosmic Dust Detector accumulators showed some spurious counts. Despite some difficulty in the video storage subsystem area during the encounter record sequence, the test objective was not invalidated. The TV picture data was played back satisfactorily.

On March 17, the formal space-simulator test was completed and, on March 18, the chamber door was opened and the postvacuum test performed. After the test the spacecraft was returned to SAF.

On March 19, disassembly was started to allow incorporation of outstanding engineering change requests. The

spacecraft was reassembled and prepared for vibration. All nuts and bolts were torqued to their specified values, and 40 instrumentation accelerometers were mounted throughout the spacecraft.

On March 28, the spacecraft was transported to the vibration facility. On March 30, the TV optics and electronics were sent to the TV laboratory for incorporation of a vidicon tube. Power was applied to the spacecraft and a system verification was performed. At that time, it was discovered that only one solar pressure vane actuator worked properly; all the others malfunctioned completely or in part. The verification test was completed on March 30. On March 31, the spacecraft was installed on the *Agena* adapter and then mounted on the vibration fixture. The remaining events of the vibration test were completed between April 1 and 6.

The spacecraft was excited in torsional, roll, and lateral axes, and subjected to acoustic vibration. The spacecraft passed all axes of vibration except for these principal discrepancies:

1. The science cover latch mechanism tore loose from its honeycomb structure during the first lateral (X-axis) vibration. The cover was repaired and reinstalled in time for the roll-axis vibration.
2. The Canopus sensor failed during vibration on one of the axes. This failure was discovered during the last verification test on April 6.

The spacecraft was returned to SAF on April 7 and preparations were started for the second portion of the space-simulator test. The instrumentation accelerometers were removed for this test. The spacecraft was weighed on April 10 and a CG determination was made. The total spacecraft weight was approximately 576 lb.

On April 18, a system verification test was performed outside the JPL space simulator. On April 19, the PTM was suspended in the space simulator and a thermal control test was begun. The primary purpose of this test was to verify the design of the temperature control subsystem. In addition to testing the spacecraft in the new minimum cable configuration, a major change was made to the thermal shields installed on the spacecraft. These shields were changed primarily to reduce weight. The chamber was pumped down on April 22, and the thermal control test was completed on April 24. The test was satisfactory and the preliminary results indicated no problems.

On April 25, the spacecraft was prepared for magnetic mapping. The spacecraft was mapped on April 25 and 26 in order to establish what, if any, effects the strong magnetic fields from the vibration tables had on the spacecraft magnetics.

The *Agena* matchmate test was started on April 27 and was completed satisfactorily on April 30. On May 2, precountdown checks were started which were designed primarily to check out the compatibility of the launch complex equipment with the spacecraft and to evolve the procedures that would be used for the launch complex activities. The simulated precountdown took approximately 6 hr to complete, and all systems functioned normally. The spacecraft was radiated with electromagnetic radiation throughout the test. Preliminary results showed that the spacecraft was unaffected by offboard and onboard sources while it was in the launch configuration with the shroud on. The spacecraft low-gain antenna radiated 100 w of S-band power, and the results indicated that there was no danger of the squibs being activated by this relatively high-powered RF environment.

Two simulated countdowns were performed on May 5. The first countdown was a short one in which the spacecraft was conditioned into the launch mode, and evaluation was limited essentially to the observation of the telemetry signals. The second countdown exercised the spacecraft extensively by using all of the umbilical and RF command links. All subsystems performed as designed.

The pyrotechnic shock test was performed on May 6 and 7. The test consisted of activating the pyrotechnic devices, which release the shroud V-band and the spacecraft V-band, as well as the spacecraft pyrotechnics, which release the solar panels and planetary scan platform. The results indicated that the spacecraft could survive these environments without difficulty, although pellets flew when the shroud V-band was released. (It was not known at that time whether the pellets could penetrate the shroud and damage the spacecraft.)

The PTM was prepared for SMIT operations from May 11 through May 14. The SMIT operations were started on May 15 and were concluded successfully on May 22.

On May 23, the PTM spacecraft was prepared for an investigation of the anomalous behavior experienced during the encounter phase of the thermal control test. After extensive testing in the space simulator with special cabling and circuitry, the problem was isolated to the ultraviolet photometer.

On May 28, the PTM was returned to SAF and was connected to the LCE to determine if the LCE performed normally after the major cleanup, which followed PTM simulated precountdowns and countdowns. All equipment performed normally. Except for a few minor modifications that were to be incorporated, the LCE was essentially ready for shipment to Cape Kennedy.

The PTM was prepared for vibration on June 2 and 3 and was then moved to the environmental facility. The spacecraft was vibrated in the X–Y axis and no visual damage was observed. On June 4, the spacecraft was vibrated in the Z axis, after which it was returned to SAF. The results of this vibration test showed that the Canopus sensor with the heavy-gauge wire tube was able to survive the vibration environment.

By June 5, the spacecraft had been updated and all outstanding engineering change requests were incorporated, the most significant of which were:

1. Hybrid radio subsystem
2. DC-22, DC-28, and DC-29 circuitry, and the appropriate harness changes
3. Extensive changes in the power subsystem, including the booster switchover circuitry modifications, that changed the time constant from 10 to 3 sec and the level of switching to 48 v
4. New absorptivity standard
5. New transformer in the onboard CC&S relay hold module, which subsequently operated normally on the first try.

On June 12, a special noise investigation began. The noise between various signal grounds and the spacecraft ground was measured and documented. The data encoder susceptibility to half-phase resets and loss of synchronization in the lower decks was established when the power subsystem was put into and out of boost mode. The known ground loops were interrupted to determine their effect on the data encoder behavior. However, the breaking of the ground loops did not eliminate the synchronization and half-phase resets. The half-phase resets were not considered a major problem.

On June 13, one-half of the gas subsystem was removed from the spacecraft for repair of a leak that had developed in the bellows. It was estimated that the flexible joint was actuated approximately 65 times. The system was not stress-relieved, so the problem might also have been associated with handling.

On June 15, a series of investigations were conducted to determine if the effects of the noise due to ultraviolet photometer high-voltage breakdown could be prevented from disturbing the spacecraft circuitry. The results of these tests indicated that, by appropriate filtering on all lines going to the ultraviolet photometer or by isolating the photometer cabling, the effects of high-voltage breakdown could be eliminated.

On June 16, the non-real-time welded DAS type-approval unit was installed, and the compatibility test between the SFOF and the spacecraft was started. The first day of testing consisted of going through the launch mode and the Sun and Canopus acquisition modes twice; no spacecraft failures occurred. On June 17, two midcourse maneuvers were performed. The first maneuver was aborted by SPAC. At the end of that day's test, an inadvertent DC-25 (encounter science on) command was issued to the spacecraft. The SFOF test director chose to proceed with this nonstandard operation to exercise the SFOF, SSAC, and SPAC Groups and the data system. Full recovery from the nonstandard operation was obtained within 1 hr.

On June 18, the spacecraft was exercised through two encounter modes and one playback mode. All spacecraft functions were normal. The SFOF/spacecraft compatibility test was concluded on June 19. The spacecraft was then placed in the cruise mode and the command matrix was tested for SFOF familiarization. The spacecraft operated normally.

A spacecraft logic circuit test was performed from June 23 to June 25 to examine in detail the performance of the onboard spacecraft logic concerned with monitoring, switching, and inhibiting functions. Satisfactory results were obtained.

On June 25, the free-mode test procedure was followed while the spacecraft was connected to the STC with all direct-access cables. The purpose of the test was to obtain a basis for comparison of free-mode and cable-mode testing. The spacecraft was then prepared for the free-mode test. This preparation consisted mainly of installing the traveling wave tube amplifier in the radio subsystem.

The results of the free-mode test established the compatibility of the solar panels and the spacecraft, the

ability of the spacecraft to give valid data even though connected to direct-access cables, and the adequacy of the onboard circuitry to operate in a sharing mode with the battery and on full solar power. The test was considered very successful and demonstrated that the transients affecting radio power amplifier and exciter switching, data encoder half-phase resets, and data encoder deck skipping were also present when there were no connections to the OSE.

On June 29, the free-mode configuration was again established to permit the magnetometer personnel an opportunity of seeing the current-field changes in this configuration. A special coil was used to take the magnetometer sensor out of saturation; the initial results indicated that the current field was insignificant.

From June 30 through July 7, the transfer of radio power amplifiers and exciters, the data encoder half-phase resets, and the deck skipping phenomena that occurred with power transients were investigated. Prior to the investigation, the abnormal behavior of the radio and data encoder occurred in an unpredictable fashion. In certain spacecraft modes, the transient would occur at certain times, but could never be repeated consistently during investigation periods. The investigation during that period established a repeatable method of obtaining abnormal indications in the radio and data encoder subsystems: placing the spacecraft in a share mode between solar power and battery power at a very precise level and then releasing the boost-mode inhibit at the power OSE. Having established such a control, the investigation was centered around observing the DC-7 (change power amplifiers) command and the DC-8 (change exciters) command lines. This investigation showed that radio switching originated in the command isolation-pulse switch. Corrective action was taken to lower the resistance of the 10-v power-supply load resistor to the command circuitry from 220 to 1 Ω, which, in turn, desensitized the response of the isolation-pulse switch to transients.

The data encoder investigation showed that the half-phase reset was originating in the spacecraft harness. The corrective action taken involved disabling the OSE reset line at the data encoder module.

The deck skip phenomena could not be isolated to a single circuit and were probably the result of cumulative pickup in cable harnessing in general. The removal of any cable-harness function from the data encoder caused the data encoder's deck-skipping susceptibility to decrease, but no one line by itself showed the same effect. Major design changes were required to remove this effect, and the problem was not considered serious enough to require such action.

Between July 8 and 10, the half-phase reset, radio subsystem switching, and design changes were verified. The incorporated changes seemed to eliminate the problems associated with power transients.

A parameter variation test was started on July 10 after the installation of 60-v Zener diodes on the output of the booster-regulator in the power subsystem. This test was a rerun of a test conducted on the PTM much earlier in the program. Its objective was to establish whether the margins of operation increased as a result of the changes incorporated in the power subsystem. The test consisted of varying the dc input to the 2.4-kc inverters (normally furnished by the booster-regulator), and varying the 38.4-kc synchronizer frequency (normally furnished by the CC&S). The spacecraft was operated through five modes of parameter variation, and, in all cases, above-normal spacecraft functions were observed up through but not including encounter. During encounter, the video storage, DAS, and TV subsystems would not operate properly at these limits.

The Canopus sensor operated normally in all of these tests, as well as on the backup 38.4-kc isolator in the power subsystem and on the free-running mode of the power subsystem.

Video storage and encounter science subsystems were run through a special test at $\pm 2\%$ frequency variations. Performance of all subsystems was normal. Video storage also worked well when recording at $+2\%$ and playing back at -2%.

The PTM was inactive during much of the MC-4 buildup and test. Immediately preceding the launch of *Mariner III*, the PTM spacecraft was put in a full flight-support configuration and connected to its STC.

During the launch and postlaunch phases, various effects of the apparent nonseparation of the shroud from the *Mariner III* spacecraft were simulated. These included operation of the system at low bus voltage, interaction between attitude control gas-valve operation and the Magnetometer (in the "panels up" configuration), and spacecraft free-mode operation during daylight hours (also in the "panels up" configuration).

During preparation for a vibration test, the spacecraft receiver had difficulty locking to the ground test transmitter (the AGC readout indicated a displacement from the normal no-signal condition, and telemetry AGC indicated an input signal whether the test transmitter was on or off). It was found during testing of the radio that an internal lock condition could occur when the ranging receiver was on. It was decided to modify the countdown procedure to delete the use of the ranging receiver in the transponder during launch.

Additional tests were conducted to help resolve some spacecraft behavior characteristics observed during the *Mariner III* flight.

During a system verification test that occurred after *Mariner IV* was launched, a midcourse maneuver was conducted to confirm OSE and spacecraft ability to perform the maneuver and provide practice for the SFOF operations team. A test on December 3 verified that the SFOF tapes for the MC-3 midcourse maneuver commands were of proper duration and polarity.

A special test was performed to determine why the spacecraft lost Canopus after DC-27 was sent. Various power-change transients and roll error values were used in an effort to knock the Canopus sensor out of track. The Canopus sensor did not lose lock at any time.

On December 11, a plasma probe test was conducted to observe the effects of the noise due to high-voltage arc on the science DAS and data encoder. The science DAS lost synchronization and the data encoder skipped on the 200-deck segment of the commutator. Neither radio nor attitude control subsystem was affected.

B. Flight Spacecraft System Testing

1. Test Description

The primary objective of the flight spacecraft test plan was to provide two fully-qualified spacecraft for the first day of the available launch period of the 1964 Mars mission. Table 84 lists the tests performed on the flight spacecraft and describes the objectives and acceptance criteria of each test.

To meet the primary objective, the total assembly and test time (approximately 7 months) was apportioned on the basis of the following considerations:

1. The testing was not to verify design, as in the case of the PTM, but rather to verify that the equipment operated normally. The testing was primarily concerned with qualification, and used the test data obtained from the PTM as a standard against which to check flight spacecraft performance.

2. The flight spacecraft acceptance criteria were: (a) the spacecraft operate for 250 hr in a solar-vacuum environment without any major failures. (A major failure was defined as one that would prohibit the successful completion of the mission; e.g., a power failure would be considered major, whereas a temperature transducer failure would be considered minor.) (b) The spacecraft could be shipped to AFETR only upon successful completion of the final system test at JPL. (A successful system test was defined as one in which no major misoperation occurred.)

3. The flight system spares had to be qualified in a system environment before incorporation on MC-2 or MC-3 spacecraft. The minimum system qualification time for any subsystem was 100 hr.[10] The PTM and the MC-4 spacecraft were used to qualify the flight spares.

4. The same methodical and cautious initial power application and intersubsystem tests were performed on the flight spacecraft as were performed on the PTM.

5. Since only one spacecraft had been tested before the flight spacecraft test plan, verification tests were performed on all subsystems to ensure that their outputs were within specification and compared closely to the PTM; e.g., a parameter variation test was performed on the flight spacecraft, and the overall effects were studied and compared to the results obtained from the PTM test. However, the limits of any variation were restricted to the tolerance boundaries.

6. The environmental tests, both vibration and space simulation, were scheduled to be performed as close to the shipping time as possible. The object was to give maximum assurance that the equipment committed to the mission was the equipment used to meet the qualifications stated in (1).

7. The testing ensured compatibility of the spacecraft and all other elements used in the Mars mission. The Space Flight Operations System did not undergo formal testing with the flight spacecraft as it did

[10] Total test time (subsystem and system) was 400 hr minimum.

Table 84. Flight spacecraft test objectives and acceptance criteria

Category	Objectives
Mechanical assembly operations	To assemble a flight spacecraft for verification of the mechanical design and alignments.
STC and facility support equipment test	To assemble and test the STC and its related facility support equipment (without a spacecraft) in order to verify their complete readiness to support the system test effort. The STC and facility support equipment could not violate the grounding philosophy dictated by the spacecraft and OSE design specifications. There had to be a minimum of 2 MΩ where infinite resistance was specified. All interfaces had to be correct in design and operation.
STC/spacecraft ground integrity test	To verify that the grounding techniques of the spacecraft and STC conformed to JPL specifications (i.e., that no unknown ground loops were present in the spacecraft and were not introduced when the STC was connected to the spacecraft).
Initial power application	To safely apply and distribute spacecraft electrical power to a newly assembled spacecraft, in order to verify that the power met the applicable specifications. If new assemblies had to be substituted at any time after the completion of initial power application, the portion of the procedure involving the hardware to be substituted had to be performed again before the circuitry was incorporated into the Spacecraft System.
Subsystem tests	To evaluate the performance of each subsystem while operating with spacecraft power.
Intersubsystem tests	To minimize the chance of equipment damage caused by improper interfacing. All interfaces had to agree with the circuit data sheets and function per design specification. To functionally test all interfaces between subsystems and to verify their agreement with the circuit data sheets. If new assemblies had to be substituted at any time after the completion of the intersubsystem tests, the portion of the procedure involving the hardware to be substituted had to be performed again before the circuitry was incorporated into the Spacecraft System. To make preliminary determination of any possible effects the subsystems might have on the system environment. No major interactions, except those specifically designed into the spacecraft, could exist between spacecraft subsystems.
System test	To establish the functional integrity of the spacecraft within the constraints imposed by testing operations and the Earth environment. All subsystems had to operate per functional specification. (All instances of anomalous performance had to be completely documented, thoroughly investigated, and appropriate disposition made.)
Telemetry channel calibration	To verify (and correct, if necessary) calibration curves for all telemetry channels before the final system test. The accuracy of each telemetry channel had to be within the design specification tolerances.
Matchmate and *Agena* adapter and shroud	To establish early compatibility between the spacecraft and the *Agena* adapters and shrouds.
Dummy run tests (simulated pre-countdown and simulated countdown)	To verify the compatibility of the LCE with the flight spacecraft. To verify the procedures to be used for the actual countdown. To train personnel for the actual countdown.
EMI tests	To determine the RF susceptibility of spacecraft and OSE when subjected to an RF environment similar to that expected at Cape Kennedy To determine the contribution to spacecraft subsystems to the RF level that might degrade the performance of the spacecraft receiver. Spurious noise levels could not exceed the tolerances established in JPL specifications.
Space – simulator tests	Part 1. To establish the functional integrity of the spacecraft while operating in a simulated space environment. Part 2. To perform a final verification of the ability of the temperature control subsystem to maintain spacecraft temperatures within design limitations. To verify that spacecraft performance in a simulated space environment was not affected by test cables.
Vibration tests	To verify that the spacecraft could operate satisfactorily during and after exposure to FA vibration levels (determined from those expected from the *Atlas* and *Agena* during the boost phase).
CG measurement	To accurately determine the actual weight and CG of the spacecraft (cruise configuration), and to adjust the PIPS thrust axis to the spacecraft CG.

Table 84. (Cont'd)

Category	Objectives
Free-mode test	To demonstrate the correct operation of the spacecraft on solar power, without any electrical connection to support equipment. To verify the functional integrity of the spacecraft in the absence of any support equipment electrical connections. Sufficient telemetry data had to be obtained to verify the correct operation of the power subsystem in the system environment using solar power. To establish initial compatibility among the solar panels, their cabling, and the spacecraft. To verify that the STC and associated cabling do not affect spacecraft data readouts.
Magnetic mapping of spacecraft and solar panels	To measure the magnetic fields produced at the Magnetometer sensor by current flow in the various spacecraft subsystems. To determine the components of the permanent magnetic field of the spacecraft and of the coefficients of induction for an external magnetic field at the location of the Magnetometer sensor.
Final inspection and system test	To prepare the spacecraft for launch and to establish that it was fully acceptable for flight. All inspection discrepancies had to be resolved, and all change requests had to be verified as having been incorporated.
Preparation for and shipment to Cape Kennedy	To prepare the STC, spacecraft, and supporting spares and equipment for shipment to the Cape. The suspension and cooling capabilities of the vans used to move the equipment had to be certified.
OSE arrival, examination, and assembly at Cape Kennedy	To determine, by means of a visual inspection and temperature and vibration records, that the spacecraft and the OSE had not been damaged or exposed to any adverse environment in shipment.
Mechanical preparation at Hangar AO and ESF	To complete the mechanical activity required to mate the spacecraft with the launch vehicle. During the first launch complex activities, the test procedure had to be checked out as to its adequacy to ensure that the spacecraft was properly prepared for launch.
Electrical test at ESF	To establish that the spacecraft was ready for the launch complex testing activities.
Move to launch complex and test	To verify that all control, power, and monitor circuitry performed as designed, including the LCE, long lines, and spacecraft circuitry.
Combined system test (J-FACT portion)	To ensure and demonstrate a working compatibility of the spacecraft boosters, launch complex, AFETR, and all supporting agencies involved during launch attempts, thereby maximizing the probability of successful launch during the mission-unique small launch period.
Combined system test[a]	To simulate the launch countdown exactly (except for *Agena* fueling).
Verification of science calibrations	To perform final laboratory-type calibrations of science instruments.
Final system acceptance test	To permit a detailed examination and verification of the spacecraft readiness for flight.
Final mechanical and electrical preparation for flight	To complete the mechanical and electrical preparation necessary for certification of the spacecraft for flight with such items as test hardware and protective covers removed.
Final launch vehicle/spacecraft mating and countdown	To perform final verification that all control circuitry, data links, personnel, and procedures checked out satisfactorily, and that the spacecraft was ready to enter the launch countdown.

[a] Simulated launch portion.

with the PTM, but spacecraft data were made available to SFO upon request. Compatibility tests between the spacecraft, LCE, *Agena* shroud and adapter, launch complex, and supporting personnel were performed at various times during the overall test program. The test plan was designed to allow sufficient time for correction of any incompatibilities.

2. *Mariner III* Test Chronology

Mechanical assembly of *Mariner III* started April 7. The gas subsystem was delivered to SAF on May 2. The solar pressure vane actuators required extensive rework before they could be accepted. The actuators were installed on the spacecraft but difficulty was experienced in fitting the gas subsystem to the spacecraft structure.

Although this problem was resolved, when a flight-type solar panel was used to determine any mechanical problems in installing the tubing on the panel, it was discovered that the dimensions of half of the gas subsystem did not permit a proper assembly. One-half of the gas subsystem was removed and sent back for rework, after which it was returned to SAF to be reinstalled.

By May 21, subsystem, ground integrity, and interfacing tests were completed. System Test 1 began on May 22 and was completed on May 27. The test was very successful and only minor problems were encountered.

The attitude control leak test was performed from May 28 through June 1. Preliminary results showed that some torquing had to be performed after detection of a large leak; the leak rate after such corrective action was satisfactory. After completion of the attitude control leak test, the problems noted on System Test 1 were investigated.

A noise investigation was performed, and the data encoder OSE was found to have an oscilloscope improperly terminated. The removal of the ground cleared up the noise.

An investigation was also performed on the updating of the Canopus cone angle with the CC&S master timer commands. It was established that the time interval necessary between sequential commands is 3 sec, and that the problem encountered in system testing with the insertion of the updates was caused by insufficient time between sequential commands.

On June 3, the DAS/Cosmic Ray Telescope interface problem was investigated, and the OSE was found to have been partially responsible for the difficulty. A TV encounter sequence check was performed, and a normal TV fast shutter was obtained. On June 3, the video-storage subsystem was replaced with a flight spare. This was the first step in cycling out the flight tape machines for servicing to meet the less than 500 tape passes required before launch. (The requirement was later reduced to 200 passes.)

On June 5, preparation was started for the first *Agena* matchmate test, which consisted of mating the spacecraft with the *Agena* flight adapter and shroud. Upon completion of the test, the spacecraft was placed in the SAF pit area for the simulated precountdown and countdown.

The simulated precountdown was started on June 12, and the simulated countdown was started on June 13. Any problems experienced during precountdown would have delayed the launch. The countdown was very successful. The procedures and personnel were checked out satisfactorily, and the actual countdown procedure was finalized.

The cooling sheath was found to be unnecessary during the dummy run in the air-conditioned building. However, personnel were familiarized with the installation of the sheath, and time studies were requested for the mating and demating of the sheath.

On June 15 and 16, a matchmate test with the spare adapter and shroud was performed. Some problems in procedures and hardware were discovered. There was an unacceptable amount of RF leakage in the shroud, and several items had to be sealed to permit effective spacecraft purging. In addition, the *Agena* adapter in-flight disconnector was rotated from the proper position, the spacecraft V-band safety straps came in contact with the temperature control louvers, the SIT bracket was found to be too close to the spacecraft thermal shield, and the transporter hardware boxes interfered with the shroud guide-rail system.

On June 17, updating operations on the spacecraft began by which all engineering change requests were incorporated. The attitude control gas subsystem was installed on June 25. Tedlar cable wrapping replaced much of the mylar cable wrapping, and power cases I and VIII were installed on June 29. Proof test model cases V and VI were installed in preparation for System Test 2 conducted from July 2 through July 4. Inasmuch as the radio cases were held up in the subsystem area due to difficulties in FA qualification, it was decided to proceed with the system test using the PTM radio subsystem. This action was taken to ensure that the remainder of the spacecraft was operating normally so that time would not be lost because of other problems.

System Test 2 was performed in two parts: Part 1 (on July 2 and 3) consisted primarily of engineering exercises; Part 2 (on July 3 and 4) consisted of cruise science calibration, radio checks, a normal encounter, playback of one picture and a two-line scan of all other pictures, and a cruise science statistical data quiet test. The spacecraft was in a flight configuration except for a nonflight non-real-time DAS. The overall system test results were satisfactory.

The TV subsystem camera head assembly was removed upon completion of the system test for inclusion of a new shutter mechanism. Cases V and VI were returned to the PTM, and the PIPS was returned to the laboratory for substructure modification.

Flight radio cases V and VI were delivered and installed on the spacecraft. The TWT amplifier failed shortly after power was applied. While awaiting resolution of the problem, telemetry calibrations were performed on the receiver and cavity power amplifier. The damaged TWT was removed after it was found that there was a circuit problem related to the power supply in the warmup mode.

A new TV subsystem shutter and filter combination was installed to eliminate the potential of cold weld, and a verification test was performed. The new mechanism was found to be marginal, and a decision was made to replace the new shutter with one of the original types that had performed normally in the past.

On July 11, the PTM TWT was installed on *Mariner III*, and a bleeder resistor was incorporated to prevent charge buildup on the collector. The TV subsystem camera head assembly was reinstalled, and the spacecraft was delivered to the space simulator on July 11 to begin electrical testing. The spacecraft was suspended in the chamber and all direct-access cables were installed. On July 12, spacecraft power was turned on, and a system verification test was performed. Two planet encounters were run with playbacks and postencounter cruise phase operations. After all difficulties experienced during the system verification test were resolved, the chamber door was closed, spacecraft power was turned on, and the chamber was evacuated. The operation was satisfactory until July 15, when it was discovered that the Canopus sensor was not operating properly. Since it was believed that the high-voltage circuitry of the sensor had failed, atmospheric conditions were returned, and a test to verify the cause of the failure was performed. The spacecraft power was then turned off and the Canopus sensor removed. The TA sensor was installed, and a verification test was performed satisfactorily. A vacuum was then established, and RF power was turned up. The test sequence was resumed with the midcourse maneuver on July 16 and 17; the CC&S MT-1 through MT-6 commands were checked out satisfactorily.

On July 17, the Geiger–Müller 10311 tube output was found to be erratic. In addition, the radio exciters switched during turn-off of the gyros (which had previously occurred during the CC&S MT-1 through MT-6 command exercise). The Magnetometer Z axis came out of saturation several times during the early part of the operation. The question was whether the magnitude of the Earth's field, as seen by the Magnetometer Z-axis sensor, went to a low value or whether the instrument partially failed during these periods. The test was completed July 24 after a total of 244 hr in vacuum. The chamber was opened and magnetic mapping of the space simulator was performed.

Mariner III was then prepared for the thermal control and minimum-cables portions of the simulator test. When the spacecraft temperature was recorded on July 27 at 10°F higher than it had been on the PTM, the chamber was opened and new temperature control hardware was installed. The test was resumed and completed on July 30 with only minor incidents, and with the temperature values remaining at the desired levels.

Because trouble arose in *Mariner IV* vibration testing, the *Mariner III* schedule was changed to accommodate magnetic mapping, weight and CG, and free-mode tests prior to vibration. Following mapping and weight exercises, the free-mode test was performed on August 6. The only difficulty in the test occurred when solar intensity dropped so low that the spacecraft power subsystem went into the battery boost mode. The vibration tests were run from August 7 to August 9 without incident. After a system verification test, in which switching trouble was experienced with the data encoder and radio exciters, a final inspection was performed from August 11 to August 15.

Part 1 of the final system test (System Test 3) was completed on August 16 without problems. Part 2, on August 17 and 18, revealed some trouble in radio OSE calibrations, which was corrected. Six encounter sequences were performed successfully, including video playback, cruise science quiet test, and calibration.

Mariner III was prepared for shipment in flight configuration except for the real-time DAS, the Canopus sensor, the Ionization Chamber, the attitude control gas subsystem flight nozzles, the TV shutter, the solar panels, the Sun shutter, and the solar pressure vane and attitude control electronics. The spacecraft arrived at Cape Kennedy on August 28.

Following a system verification test, AFETR System Test 1 was completed on September 4. The picture playback and cruise science calibration were particularly

successful. The spacecraft was then committed to mechanical preparation for movement to the launch complex. Operations were concluded on September 8.

After several delays due to hurricanes, the *Atlas* was finally erected on LC 13 on September 14, and *Mariner III* was rescheduled for removal to the pad on September 18, following completion of matchmate at ESF.

During the erection of *Atlas* 289D, a stretch sling failed. Although the launch vehicles were not damaged, B-FACT was delayed two days to allow further investigation of the failure.

The *Mariner III* electrical tests were completed successfully, the flight shroud was installed, and the RF checks were good. The spacecraft was moved to the pad and mated to the *Agena*. Power and functional tests started on September 19; difficulty experienced in the blockhouse with data-encoder and science functions was later corrected.

Part 1 of the countdown was completed on September 21 after approximately 8 hr of testing. Problems with the data encoder did not stop the test. Part 2 of the countdown was completed on September 23, and, in a real situation, the operation would have resulted in launch.

A very successful J-FACT was run on September 25, with excellent support from all personnel and procedures. Because of problems associated with the first part of the countdown, Part 1 was repeated on September 27 with only one anomaly: the umbilical lanyard did not retract. This problem was later resolved.

After the shroud and adapter were removed, weight and CG measurements were made. The preliminary weight was set at 575 lb. The spacecraft was then partially disassembled and moved to ESF for an attitude control leak test.

Following magnetic mapping, science calibrations were successfully reverified. The mapping showed values of 20 γ horizontal, 20 γ vertical, and 28 γ in the total field measured at the magnetometer sensor. These values varied somewhat from the previous JPL survey, but the deviation was not considered critical.

The final system test, AFETR System Test 2, was completed on October 13 after 86.2 hr of testing operations. A cruise science quiet test was run on the same day. Following final electrical reverification on October 14, all spacecraft systems were pronounced "go" in the post-test critique, and the spacecraft was released for final mechanical flight preparations.

The spacecraft was moved to ESF on October 21. During mate with the *Agena* adapter, a problem developed with the shroud umbilical door. An investigation produced a satisfactory fix for the door latch.

Final mechanical flight preparations were completed at ESF on October 26, and the spacecraft was moved to the pad and mated with the *Agena* the next day. The spacecraft on-pad functional test was completed without problems. Part 1 of the countdown was uneventful except for the radio subsystem switching from cavity to TWT amplifier as a result of a power transient.

A near-perfect J-FACT was completed on October 31; the only incident was a 40-min hold for a live launch on a nearby pad. Only minor variations were permitted from an actual launch countdown procedure.

On November 1, *Mariner III* was ready on LC 13 for the first firing attempt, scheduled for 17:45 GMT, November 4. The launch scheduled for November 4 was delayed one day to allow more time to analyze an *Agena* velocity meter relay problem and to further review the downrange S-band instrumentation status.

After considering these two outstanding items, a "go" was issued and the spacecraft was launched at 19:22:04.920 GMT, November 5. The spacecraft experienced no difficulty in the countdown or during the holds. The shroud failed to eject properly and, therefore, the spacecraft was unable to extend its solar panels. The spacecraft was tracked until battery power was exhausted.

In an effort to determine the probable failure mechanism of the *Mariner III* spacecraft, a test shroud was placed in a vacuum chamber. Catastrophic shroud ruptures developed when heat and vacuum were applied simultaneously. Further investigation was conducted by LMSC and a program was begun to eliminate the possibility of shroud failure during the *Mariner IV* flight test. Several meetings were held at Cape Kennedy to review the analysis of the shroud failure, the possible corrections, and the related effects to the schedule. The meetings yielded further evidence that the honeycomb in the shroud definitely could have delaminated as a result of entrapped air. Consequently, a metal shroud was designed and fabricated by LMSC for *Mariner IV*.

Table 85. Comparative system test schedules, *Mariner III* and *Mariner IV*

Operation	Date, 1964	
	Mariner III	*Mariner IV*
Mechanical assembly	April 9 to May 19	April 24 to June 9
Initial power application	April 27 to May 16	April 29 to May 7
Subsystem and intersubsystem tests	May 11 to 20	April 30 to June 4
System Test 1	May 21 to 28	June 5 to 6
Telemetry calibrations	April 28 to May 29	June 8 to 12
Matchmate to Agena adapter and shroud	June 8 to 16	June 13 to 18
Simulated precountdown	June 12	June 18
Simulated countdown	June 13	June 19
Equipment updating	June 17 to July 1	July 2 to 16
System Test 2	July 2 to 4	June 25 to 27
Preparation for space-simulator test, Part 1	July 6 to 13	August 9 to 13
Space-simulator test, Part 1	July 14 to 24	August 13 to 24
Preparation for space-simulator test, Part 2	July 24 to 26	August 24 to 26
Space-simulator test, Part 2	July 26 to 30	August 26 to 29
Preparation for vibration test	July 31 to August 4	July 27 to August 3
Vibration test	August 7 to 10	August 3 to 6
Weight and CG measurement	August 6	August 6
Magnetic mapping	August 4	July 26
Free-mode test	August 6	August 8
Final inspection	August 11 to 14	August 30 to September 2
System Test 3	August 15 to 18	July 22 to 24
Preparation for shipment to Cape Kennedy	August 19 to 22	September 7 to 10
Shipment to Cape Kennedy	August 23	September 11
Arrival, inspection, and assembly at Cape Kennedy	August 28 to 31	September 14 to 17
AFETR System Test 1	August 31 to September 4	September 18 to 22
Mechanical preparation at Hangar AO	September 5 to 10	September 23 to 25
Mechanical preparation at ESF	September 10	Not applicable
Matchmate to Agena adapter and shroud	September 14 to 16	September 26 to October 6
Electrical test at ESF	September 11 to 19	September 30 to October 9
Spacecraft moved to launch complex	September 19	October 10
On-pad functional test	September 19 to 22	October 10
RF link calibration	September 19	October 12
Cooling test	September 19	October 13 to 14
Simulated countdown, Part 1	September 21 to 22	October 13
Simulated countdown, Part 2	September 23	October 14
J-FACT	September 25	Not applicable
Simulated countdown, Part 1	September 24	October 13
Simulated launch with RF interference	September 28	Not applicable
Umbilical release and cooling blanket removal test	September 29	Not applicable
Spacecraft demated from launch vehicle	September 29	October 15
Attitude control quantitative leak test	October 1 to 5	October 2 to 5
Verification of science calibrations	September 30 to October 6	October 19 to 20
Magnetic mapping	October 6	October 16 to 17
AFETR System Test 2	October 7 to 14	October 17 to 23
Mechanical preparation at Hangar AO	October 15 to 20	October 23 to 26
Mechanical preparation at ESF	October 21 to 23	October 27 to 28
Matchmate to Agena adapter and shroud	October 22	October 28
ESF electrical test	October 23 to 26	October 29 to 30
Spacecraft moved to launch complex	October 26	October 31
On-pad functional test	October 27 to 28	November 2
J-FACT	October 29	Not applicable
Simulated launch	November 2	Not applicable
Countdown, Part 1	November 3	November 26
Launch	November 5	November 27 to 28

3. *Mariner IV* Test Chronology

A comparative schedule of the *Mariner III* and *Mariner IV* system test operations is shown in Table 85. Mechanical assembly of *Mariner IV* started April 9 and progressed very slowly because of late hardware deliveries. Radio subsystem Cases V and VI were delivered and installed, and a subsystem test was performed. The gas subsystem, ultraviolet photometer, attitude control subsystem, PIPS, Cosmic Ray Telescope, and temperature control louver frames were installed. Attitude control, radio, and science ultraviolet photometer subsystem tests were performed, and the spacecraft was then prepared for system testing.

System Test 1 was performed on June 5 and 6. Many problems were encountered during this test, in which the main objective was to obtain a brief survey of the overall spacecraft.

Between June 8 and 13, the spacecraft was prepared for *Agena* matchmate testing. The formal matchmate test was performed with the spare *Agena* adapter and shroud from June 13 to 15.

By June 17, the spacecraft was mated with the flight adapter and shroud and the spacecraft was prepared for a precountdown. The results of the matchmate tests were comparable to those obtained with *Mariner III*.

The simulated precountdown test was started June 18. The following difficulties were experienced:

1. The two coaxial connectors to the catenary were reversed, and fixing them caused some time delay.
2. The Cosmic Dust Detector did not reset.
3. The plasma data had higher values than usual.
4. The science TV OSE digital-to-analog converter caused TV picture noise spots and was replaced by a spare.
5. The TV stimulus lamps were not bright enough, and a DC-16 (narrow-angle acquisition) command had to be used.

On June 19, the simulated countdown was successfully performed. The only problem was the receipt of four events in the data encoder registers that were caused by some power transients, which did not cause any holds.

The test team went through the complete normal launch exercise, including some typical types of holds from the booster and range areas. The spacecraft would have been launched in a real countdown.

From June 20 to 24, problems experienced during System Test 1 were investigated. In addition, some hardware changes were incorporated, mainly in the science area. Difficulties experienced with the science OSE (including the Magnetometer, science isolation box, scan position indicator, and the TV) during the System Test 1 were investigated and subsequently corrected.

System Test 2 was performed from June 25 to 27. All flight hardware was installed on the spacecraft except for the Canopus sensor, radio subsystem (two cavity amplifiers), prototype Magnetometer, prototype science cover, and prototype Cosmic Dust Detector. The only problems experienced during the test were:

1. The radio had a low power output, which was known prior to the test.
2. The Cosmic Dust Detector was not evaluated, since the instrument was a TA unit.
3. The magnetometer operated normally except for Z-axis dropout of null during quiet periods, and did not have the capability of the 60 γ nulling steps incorporated in the OSE.
4. The TV could not be put into fast shutter with the science cover TV stimulus lamps, and five words were lost at the end of each picture line. The *Mariner III* TV data also showed the loss of the last two lines of each picture, but this was not considered a serious problem.

During this system test, as well as during the *Mariner III* System Test 2, the spacecraft radiated off the high-gain antenna. A special piece of flexible coaxial cable was used instead of the normal rigid cable, since the latter could not be easily disconnected from the radio case.

On June 29, the spacecraft equipment was released for incorporation of engineering change requests, calibration, and all other outstanding work. The original schedule called for completion of the updating period by July 2, but it was not until July 16 that sufficient equipment was returned to start electrical testing. The gas subsystem, released for modification, was returned

July 13. On July 17, power was applied to the spacecraft and the power subsystem was calibrated. The checks indicated that the TV subsystem was not performing properly. The problem, which seemed to be in the TV 10-v supply, was investigated. On July 18, the electrical test continued and normal operation was recorded on all subsystems including the science subsystem and its OSE. The power subsystem completed its telemetry calibrations on July 18.

System Test 3 was performed July 23 to 25. It was essentially successful except for a jerky motion on the planetary scan platform, difficulty with the narrow angle Mars gate, and a faulty TV target. The spacecraft went immediately into magnetic mapping (Fig. 390), in which values recorded were on the order of 30 to 40 γ.

Many problems were encountered during vibration tests, particularly while installing the flight solar panels. The spacecraft was run through a vibration test on August 5 with only minor problems.

A verification test was followed by weight and CG determination in full flight configuration, except for the PIPS motor. A free-mode test on August 8 was uneventful except for certain noncritical anomalies in the radio subsystem. Several problems were encountered during the system verification test that preceded the space-simulator operations: some of the coaxial cables failed; an Earth ground connection was damaged; a power OSE connector was faulty; and trouble developed in the TV subsystem. After resolution of all problems, the chamber was pumped down and the test was conducted from August 13 to 24 (Fig. 391). Principal problems were noted in the attitude control vacuum system, the solar-pressure vanes, Plasma Probe high-voltage power, and the Cosmic Ray Telescope. Operation of the scan platform appeared smooth.

Following the satisfactory completion of System Test 4 at SAF, the *Mariner IV* spacecraft was prepared for shipment to Cape Kennedy. The convoy departed for the Cape on September 7 and arrived on September 14.

A visual inspection of the spacecraft after unpacking showed no damage to the spacecraft other than loosening of certain bolts and attaching hardware associated with the attitude control gas lines. The system test complex was installed and, after calibration of the spacecraft TV camera head and electronics, Part 1 of AFETR System Test 1 was started on September 18.

System Test 1 was completed on September 22. The following problems were encountered: failure of the Sun gate OSE lamp; TV OSE control panel difficulties; and the fact that the Ionization Chamber had to be removed for incorporation of an engineering change request. Electrical tests, with the shroud on and off, were concluded on September 22, and the spacecraft was released for preliminary matchmate preparation. The *Agena* matchmate operations were completed on September 28, in less time than matchmate on *Mariner III*. The ESF electrical tests were then performed, along with the attitude control leak test. On October 7, spacecraft science equipment was removed for laboratory calibration verification.

A second matchmate with the *Agena* adapter was accomplished on October 8. *Mariner IV* was then moved to LC 12 and mated to the *Agena*.

Part 1 of the countdown was completed on October 31. Several problems were detected and resolved with the LCE, but the spacecraft experienced no difficulty. On November 3, spacecraft power was turned on and no problems with the spacecraft or OSE were detected.

Due to the shroud failure of *Mariner III*, the *Mariner IV* spacecraft was demated from the *Agena* on November 6 and moved to ESF. The shroud was removed and shipped to LMSC, but the spacecraft was not demated from the *Agena* adapter. The spacecraft/*Agena* adapter combination was then placed under protective cover, and constant dry-nitrogen purge was maintained.

Complete launch pad checkouts were performed on LC 12 to support the new launch date of November 27. All of the blockhouse equipment and remote lines to Hangar AO were functioning normally. The spacecraft simulator was used to check the ESF electrical test complex before making connections to the spacecraft. The only difficulty was in obtaining a good hard-line link for the TV data back to Hangar AO.

The new all-metal shroud arrived on November 22 and was prepared for installation at ESF. The shroud was installed on November 23, and 95% surface contact was measured, eliminating the necessity for any scrapping of the adapter. The separation spring alignment was verified and no realignments were necessary. Separation spring stroke and preload were measured, adjustments were made, and the shroud was mated for the final time. The shroud V-band torquing was completed on November 24 without incident.

During the shroud dry-nitrogen leak test, the leak rate was found to be excessive. Adjustments were made on

the umbilical door and, in addition to obtaining complete latching for all door positions, an excellent pressure seal was obtained. Final electrical checks were made at the ESF, and the spacecraft was moved to the launch pad and mated with the *Agena* on November 24.

On November 25, the cooling blanket was installed and voltage/no-voltage checks were made on the umbilical cable before connecting it to the spacecraft. Spacecraft power was turned on and countdown Part 1 was started, with the objective of performing the most detailed spacecraft verification permitted within the limits of the launch complex environment. The only problem encountered was with launch complex RF cabling, which was easily resolved.

On November 27, the spacecraft joined the launch countdown at L − 220 min. The launch effort was terminated at L − 60 min because of a problem in the STC S-band radio subsystem. Troubleshooting and data analysis of the S-band problem continued after the countdown was terminated. Based on the results of exhaustive testing, worst-case analysis, and range scheduling, the second launch attempt was scheduled for November 28 at 14:22 GMT.

The spacecraft countdown started at L − 230 min. The spacecraft was placed on external power at 09:32 GMT, and was successfully launched at 14:22:01.309 GMT, November 28. There were no unscheduled holds.

4. MC-4 Test Chronology

The MC-4 spacecraft was assembled from the flight spares and was maintained as a field backup for *Mariner III* and *Mariner IV*. As a result, much hardware exchange occurred between System Test 1 and vibration tests; e.g., Plasma Probe, Ionization Chamber, planetary scan platform. The spacecraft was shipped to Cape Kennedy following JPL operations, and a limited series of system-type tests were performed.

On July 22, mechanical buildup at JPL had proceeded to a point at which the first electrical tests could be started; these tests included power, data encoder, pyrotechnics, attitude control, flight command, and CC&S subsystem checks. Mechanical assembly continued concurrently with these tests, and was completed on August 11.

Intersubsystem tests, except for radio Cases V and VI, were performed from July 28 to July 30. The attitude control gas subsystem was installed, and by July 31 most of the science equipment was on the spacecraft. Science interface and subsystem tests were then performed.

The subsystem tests and interface checks were completed, and the spacecraft was then prepared for system tests, which took place from August 12 to August 14. Problems were experienced with power amplifier and radio exciter switching, a defective connection in the scan platform, and varying receiver local oscillator drive. Despite other minor discrepancies, the system test was considered very successful.

The start of MC-4 vibration testing was delayed to allow the incorporation of additional equipment, and the first verification test was run on August 20 without incident. A special Magnetometer test was performed to determine the cause of Magnetometer interference from the TV subsystem during the final *Mariner III* test (System Test 3). The results indicated that when the Magnetometer transformer–rectifier was powered by a separate supply, the interference was removed.

The first lateral axis of vibration was performed on August 22; the second axis of lateral vibration and the Z-axis vibration followed on August 23. A failure in the pyrotechnic arming switch was the only problem experienced with the tests and a spare was installed.

Weight and CG determinations were made, and System Test 2 was run between August 26 and 28 without major problems. The spacecraft was then prepared for space-simulator tests, preceded by a system verification test. During the simulator test, the facility lost vacuum while the spacecraft was operating in a critical mode. This caused oil to spray over the spacecraft, which affected the Ionization Chamber, radio, CC&S, and Cosmic Dust Detector.

The MC-4 spacecraft was disassembled and the hardware was inspected and retested. By September 9, the spacecraft reassembly was completed, and it was prepared for retest in the space simulator. The verification test was performed with only minor anomalies on September 11. The space-simulator test, completed on September 15, took place without major problems. The spacecraft was then subjected to a satisfactory thermal control test, after which it was shipped to Cape Kennedy, where it arrived on September 29.

Assembly of the spacecraft was completed by October 2. All MC-4 test operations were performed by members of the flight spacecraft test teams on a noninterference

basis. The system verification test yielded only minor OSE problems, and the OSE System Test 1 was completed successfully on October 6.

The spacecraft was then disassembled for final inspection. The MC-4 spacecraft, unlike *Mariner III* and *Mariner IV*, did not undergo final inspection at JPL. Disassembly was followed by a detailed system verification test, and the spacecraft was placed in standby, except for isolated special tests. The spacecraft was maintained and tested at the Cape so that it would comprise a set of flightworthy spares and be a backup to *Mariner IV*.

An attitude control leak test was performed on the spacecraft at ESF between October 28 and November 2. After completion of the leak test, the spacecraft was returned to Hangar AO and all missing hardware was installed. The spacecraft was put in a ready state to support any investigation during the launch or postlaunch operations of *Mariner III*.

After the launch of *Mariner III*, MC-4 was placed in a full flight configuration to maximize the probability of meeting the launch period constraint for *Mariner IV*. On November 10, the spacecraft power was turned on and a system verification test was performed. The only difficulty experienced was with the Cosmic Ray Telescope. Alignment checks were performed on the TV subsystem and scan platform. Science calibrations were completed on November 12. The Trapped Radiation Detector, Ionization Chamber, Solar Plasma Probe, and Helium Magnetometer checks were also performed at that time.

During the period November 13 to November 17, Part 1 of the system test, which included the magnetic current loop measurements, was performed. On November 18, magnetic mapping was performed. The final system test was completed on November 17 with only minor problems experienced. Magnetic current loop tests were conducted on November 17; all measurements were within tolerance.

Final mechanical preparations were completed on November 20. Two updated TA solar panels were inspected, sunlight-tested, and assembled to the spacecraft. The final mechanical buildup was completed on November 24, and was followed by weight and CG measurements. The spacecraft was mounted on its transporter with a protective cover and prepared for removal to ESF if necessary.

XXII. QUALITY ASSURANCE AND RELIABILITY

The *Mariner* quality assurance and reliability program applied proven reliability techniques to monitor and control the quality and reliability aspects of the test and flight spacecraft. The significant activities of the quality assurance effort were: (1) selection of procurement sources (vendor surveys); (2) contractor source inspection; (3) receiving inspection; (4) failure and deficiency feedback; (5) examination and inspection (procedures); (6) control of nonconforming material; (7) data reporting and corrective action; and (8) inspection, measurement, and test equipment. The significant activities of the reliability effort were: (1) reliability prediction and estimation; (2) failure mode, effect, and critical analyses; (3) design review; (4) failure reporting and correction; (5) standardization of design practices; (6) parts and materials program; and (7) subcontractor and supplier control.

A. The Quality Assurance Program

The quality assurance program, as developed and implemented for the *Mariner* Mars 1964 mission, was a direct and effective result of the *Mariner* project policy and requirements document. Table 86 lists the major operations performed under the quality assurance program.

1. Organization

Figure 392 illustrates the quality assurance organization at JPL. One senior staff member of the Quality Assurance and Reliability Section was assigned as the representative to the *Mariner* project, and one senior quality assurance engineer was assigned to each technical division. The cognizant QA engineer had direct supervisory responsibility for a permanently assigned group of inspectors, the number of which depended on the workload.

This organization enabled the QA personnel to become acquainted with the cognizant engineers and the particular idiosyncrasies of various hardware and packaging concepts early in the project. It also improved communications between technical divisions, improved problem reaction time, and facilitated the training of inspection personnel in that their learning curve would closely parallel the design, development, manufacture, and test of the flight hardware. Another significant advantage of this approach was the knowledge gained of the methods, manufacturing systems, and inspecting systems of the vendors used by the individual technical divisions.

Table 86. Major operations performed under the quality assurance program

Operation	Purpose
Quality assurance surveys	To ensure that the vendor was capable of producing a reliable quality product.
Procurement documentation review	To review such documents as contracts, and purchase orders for inclusion of quality assurance requirements.
Contractor quality assurance requirements	To recommend quality requirements for inclusion in contract.
Contract negotiations	To interpret and clarify quality assurance requirements to JPL personnel and proposed vendors.
Contractor indoctrination	To indoctrinate contractors on JPL level of workmanship and specifications.
Quality assurance plan	To approve contractor's QA plan.
Parts screening	To perform screening activity at JPL and to monitor it at contractor's facility.
Failure reporting	To report failures at JPL and at contractor's facility.
Methods review	To review quality assurance procedures for conformance to JPL specifications before fabrication of prototypes.
Prototype in-process inspection and indoctrination	To determine specification discrepancies, processes, and workmanship by careful monitoring.
Prototype review	To approve prototype unit prior to fabrication of first flight unit. To document and resolve workmanship deficiencies.
Review of contractor quality program	To ensure compliance with contractor's quality assurance plan.
JPL in-process inspection	To establish predetermined mandatory inspection points and JPL flow charts and to originate QA instructions.
Test verification	To monitor specific test operations.
Final inspection	To perform final inspection at contractor's facility before submission to JPL.
SAF certification	To perform documentation review and reinspection cycle before acceptance at SAF.
SAF–AFETR operation	To perform continual quality surveillance from SAF operations through launch.

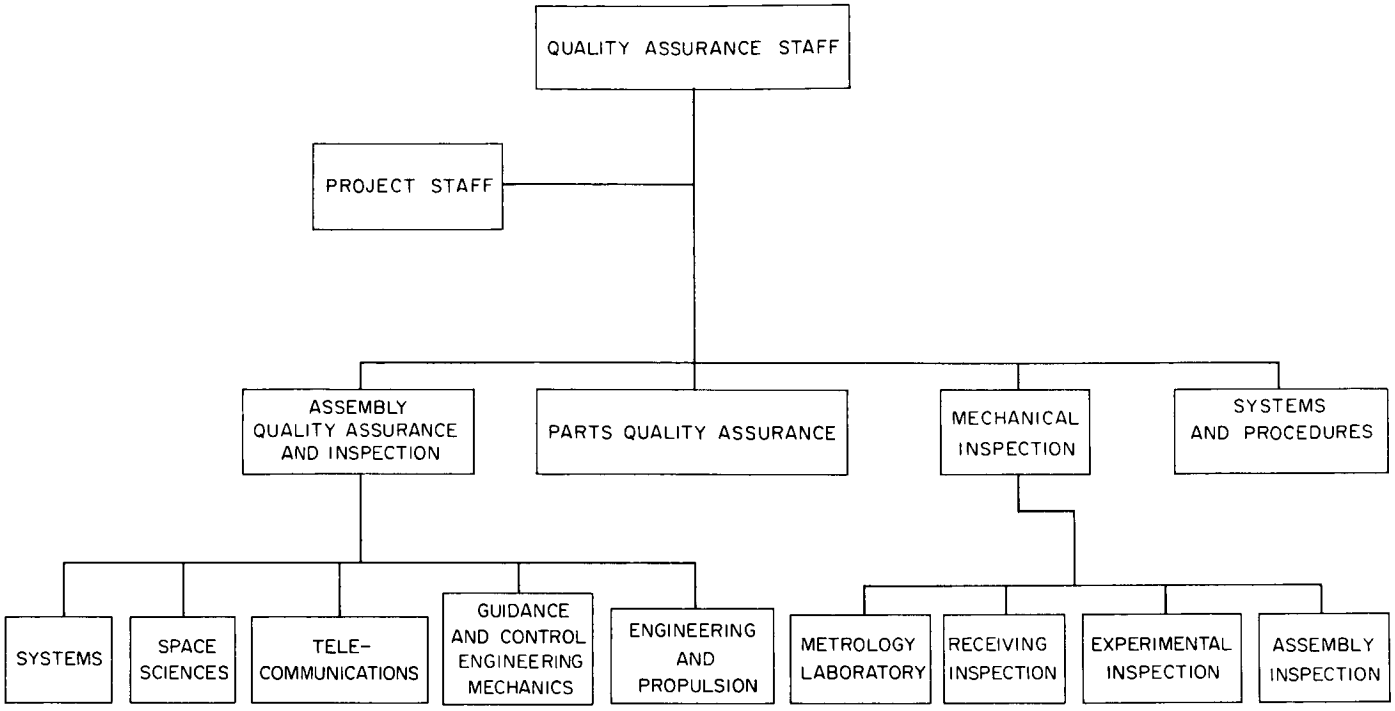


Fig. 392. Quality assurance organization

Repeated visits by QA inspectors to the suppliers' facilities, in close communication with the cognizant engineers and under the supervision of the responsible QA engineer, soon enabled QA personnel to pinpoint weaknesses and strong points in the suppliers' system; and more effective assistance was given to the supplier in correcting or eliminating defect-causing areas. Resident inspectors, monitored by visits of the responsible QA engineers, were assigned to suppliers as needed, the number of which was determined by the volume of work, criticality of operation, and quality capability of the particular manufacturer. This constant and continual contact with the supplier resulted in a more rapid indoctrination of the vendor in JPL methods and standards, and made the manufacturer aware of the quality level sought.

The divisional and field operation was supported by the parts quality assurance group (responsible for component screening) and by the mechanical inspection group. A QA engineer and a supervisor, together with mechanical and spacecraft inspectors, were assigned to SAF. They were independent of SAF, acted as redundant toll gate inspectors, and performed an additional auditing function. All hardware delivered to SAF and installed or removed from the spacecraft was controlled and reinspected by this independent group, and the effort allowed an evaluation of the quality efforts of the individual technical divisions.

A personnel staff of 40 was assigned full time to cover the hardware quality assurance engineering and in-process inspection. This number did not include the personnel used, as required, in the mechanical inspection, metrology, parts screening, failure reporting, or systems and procedures areas.

2. Systems and Procedures

The purpose of the Systems and Procedures Group was to unify and standardize procedures and forms, and to generate a basic policy for quality assurance. The efforts of this group on the *Mariner* Mars program were directed to vendor surveys, quality assurance procedures, and quality assurance instructions.

a. Quality assurance procedures. The Quality assurance procedures were Laboratory-wide policy documents that delineated the guidelines to be followed in all areas of quality assurance.

b. Quality assurance instructions. The Quality Assurance Instructions document was an in-process inspection

"tool." It was a hardware-oriented document that resulted from the quality assurance plan and the flow plan, both of which were submitted by the supplier. These plans were approved by the cognizant technical and quality assurance engineers, after which the Quality Assurance Instructions document was written and released by the JPL QA Systems and Procedures Group. Over 100 individual QA instructions and flow plans were released for use on *Mariner* Mars hardware.

c. Vendor surveys. The quality assurance vendor survey was performed by personnel of the QA Systems and Procedures Group. The survey was used to measure the vendors' capability to control the quality level of the hardware, and was conducted independently of the technical division personnel but at their request. This independent survey enabled the procurement, technical, and QA personnel to use its results as another factor in determining the caliber of the supplier. Approximately 200 vendor surveys were performed in conjunction with the *Mariner* Mars project.

3. Parts Screening Program

The purpose of the screening program was to provide parts as free as possible from latent defects and incipient failure. The screening program was divided into two areas. Major suppliers set up and administered their own parts programs after approval of their plans and specifications by the cognizant technical personnel and the JPL reliability staff. In addition, a screening effort was expended at JPL, which involved the assignment of 28 Parts QA personnel. Figure 393 illustrates the operational sequence of the *Mariner* parts screening program.

The JPL reliability staff prepared 59 Hi-Rel specifications, accepted 4 Hi-Rel specifications from other sources for use by JPL, prepared 63 procurement specifications for parts rated "preferred," and prepared 361 screening specifications for commercial grade parts. Application of these specifications to *Mariner* Mars 1964 components resulted in the following statistics:

1. The total number of electronic piece-part types was 484
2. The number of preferred or Hi-Rel parts by type was 133
3. The number of types not preferred or Hi-Rel was 351

A survey showed that 27.5% of the part types were rated preferred or Hi-Rel, and that the number of preferred or Hi-Rel parts comprised 53.5% of the total number of parts used.

In the period from June 1, 1963 to June 1, 1964, approximately 190,000 parts were screened at JPL, and sample inspections were made of 60,000 Hi-Rel parts for stores. The screening was broken down according to the following averages:

1. 87.1% of the TA parts were screened
2. 82.0% of the PTM parts were screened
3. 97.0% of the flight parts were screened

Since a program of this kind at no time upgrades parts, but only measures the ability of a particular component to survive a defined environment (in an effort to eliminate the infant failure portion of the reliability curve), measurement of the results in increased spacecraft reliability is difficult. The nature of a spacecraft program makes it impossible to draw a data line and to measure extended mean time to failure or spacecraft life, but a review of the small number of failures during test at both JPL and Cape Kennedy demonstrates the worth of the parts effort and contributes significantly to a higher degree of confidence in achieving mission success.

4. In-process Inspection

In-process inspection was a project requirement; all spacecraft hardware was to be inspected while it was in the process of fabrication or rework. This inspection was the most important single action taken in the control and measurement of the quality level of the spacecraft hardware. The Quality Assurance Instructions document, containing the flow plan, was the basic guideline document used during the inspection; it determined the "who, what, where, when, and how" of the inspection and acceptance procedure for individual pieces of hardware.

Acceptance criteria were listed in the Quality Assurance Instructions document for each inspection point. The document specified points and types of inspection for both vendor and JPL quality assurance personnel. The finalization of the document resulted in 1500 specified JPL inspection points during the in-process phase of hardware manufacture, plus 256 specified final inspection points by JPL. A typical flow plan is illustrated in Fig. 394.

Documented history of spacecraft hardware was a major responsibility of the QA organization; all inspections performed were documented, and copies were forwarded

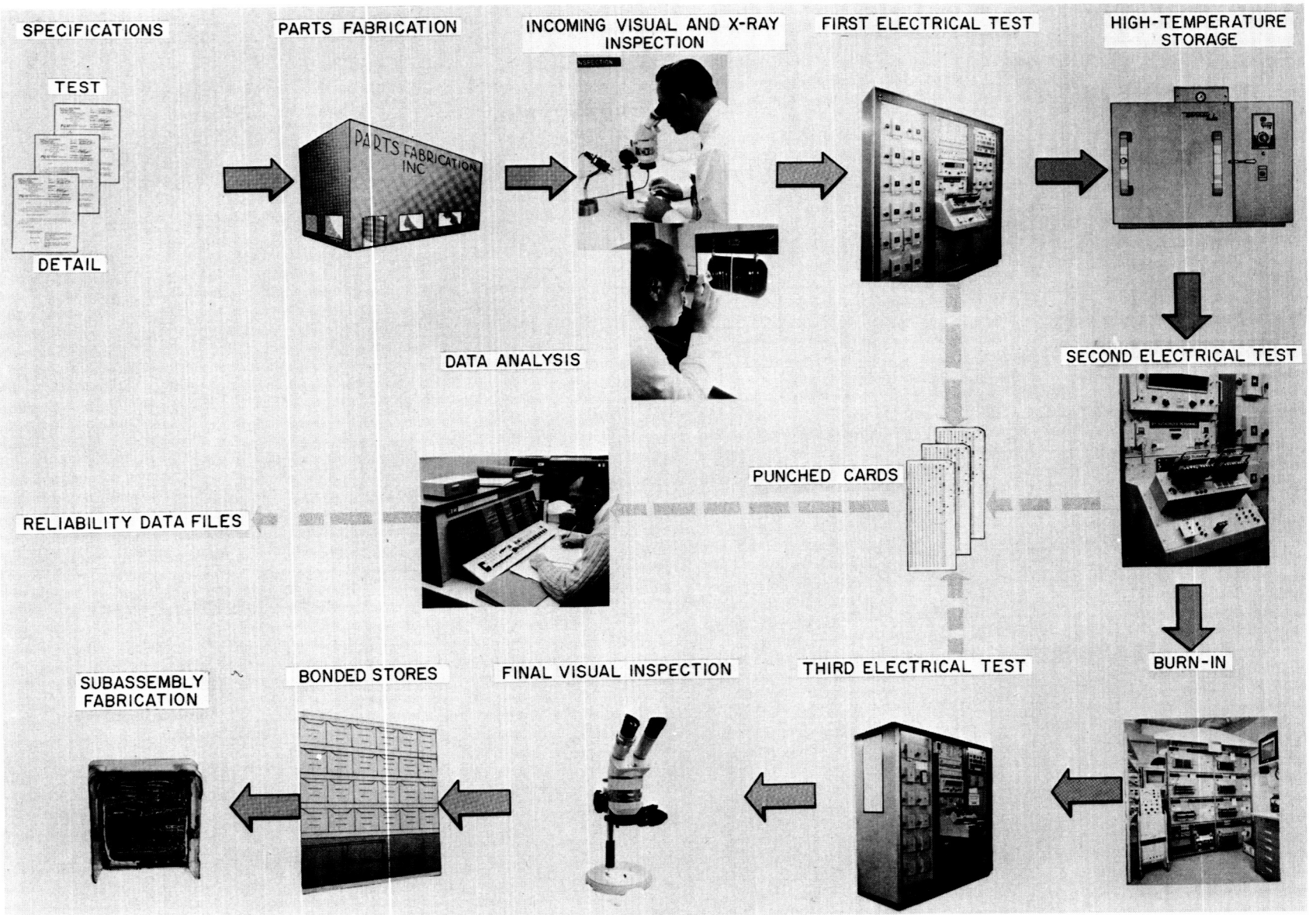


Fig. 393. *Mariner* Mars 1964 parts screening program

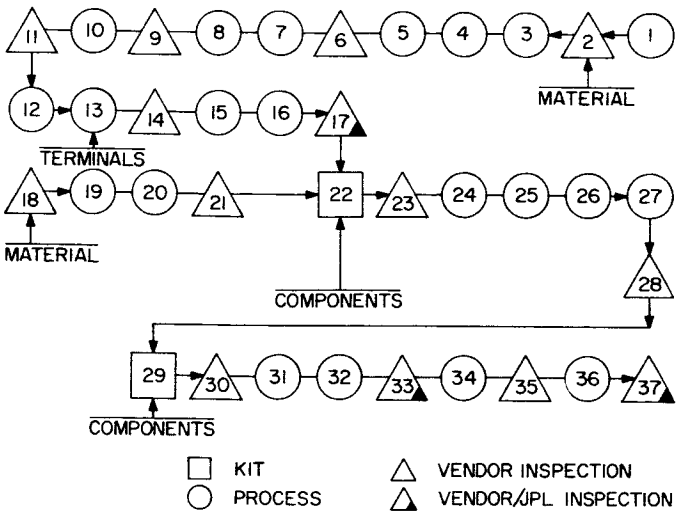


CHART NO.	OPERATION
1	MAKE NEGATIVE OF DRAWING
2	INSPECT NEGATIVE AND MATERIAL
3	SHEAR MATERIAL
4	CLEAN BOARD AND PRINT
5	ETCH BOARD
6	INSPECT
7	DRILL
8	ROUTE
9	INSPECT
10	PLATE CIRCUITRY
11	INSPECT
12	IDENTIFY
13	INSTALL TERMINALS
14	INSPECT
15	SOLDER TERMINALS
16	CLEAN
17	INSPECT
18	INSPECT MATERIAL
19	SHEAR, ROUTE, DRILL
20	IDENTIFY
21	INSPECT
22	SET UP KIT
23	INSPECT
24	BOND BOARDS
25	BOND TRANSISTOR
26	CLEAN BOARDS
27	CURE
28	INSPECT
29	SET UP KIT
30	INSPECT
31	INSTALL COMPONENTS AND SOLDER
32	INSTALL COMPONENTS AND SOLDER
33	INSPECT
34	BOND CAPACITOR
35	INSPECT
36	CLEAN
37	INSPECT

Fig. 394. Typical quality assurance flow plan

to a central documentation center. An audit of the documentation center revealed that the predetermined controlled inspections of the QA instructions resulted in the performance of 25,400 inspections of hardware. (These did not include mechanical or component inspections at the parts level.) The documentation center also housed photographs of each subsystem at the time of its delivery to SAF. The documents contained in the central documentation center include Quality Assurance Instructions, Material Review Board reports, SAF certifications, SAF removal and recertifications, environmental test result summaries, hardware disposition logs, and spacecraft status logs. This documentation, filed by serialized subsystem and spacecraft number, formed a history of each spacecraft and its integral parts.

5. Spacecraft Equipment Certification at SAF

Each technical division was required to certify the quality and flight worthiness of its hardware before its admittance into SAF. The SAF certification process, through verification, inspection, and documentation, traced the history of the hardware being submitted and confirmed and substantiated its condition upon receipt. The certification process consisted of a documentation review, inspection, color photographs of the hardware, disposition of any open items, and sign-off by the cognizant engineer and the QA engineer. Figure 395 shows a typical subassembly or assembly flow sequence through SAF.

This operation was permanently staffed with one QA engineer as supervisor and two mechanical inspectors (one mechanical and one spacecraft inspector per spacecraft, including the PTM spacecraft). The permanent assignment of inspectors to a particular spacecraft from initial buildup through JPL tests and Cape Kennedy prelaunch tests enabled the inspectors to (1) be thoroughly familiarized with the spacecraft and (2) maintain continuity of history and documentation as subsystems were interchanged between *Mariner* Mars spacecraft. The documentation package submitted for review with the hardware verified that:

1. The FA testing was satisfactorily accomplished and the proper documentation completed.
2. Records existed covering in-process and final hardware inspections, or, in the case of deviations, records of such deviations as a result of Material Review Board action.
3. All engineering change requests of record were implemented on the hardware before its delivery.
4. Confirmation existed of measured results in the following areas: weights, power consumption and accumulated running time, magnetic field mapping, and radioactive source identification.
5. Design documentation was released.

UPON RECEIPT OF HARDWARE, ALL REQUIRED DOCUMENTS SUPPORTING HARDWARE ARE REVIEWED

HARDWARE INSPECTION AS REFERENCED PER APPLICABLE QUALITY ASSURANCE INSTRUCTIONS

SIX CATEGORIES IN ROUTING HARDWARE
(a) HOLD: WAITING FOR INSPECTION
(b) ACCEPTED: ROUTE TO SPACECRAFT
(c) ACCEPTED: ROUTE TO STOCK
(d) REJECTED AT SAF: ROUTE TO DIVISION OR TO VENDOR
(e) REMOVAL OF DISCREPANT HARDWARE FROM SAF
(f) HARDWARE RESUBMITTED TO SAF

ALL HARDWARE PHOTOGRAPHED PRIOR TO ITS INSTALLATION ON THE SPACECRAFT.
HARDWARE IDENTIFIED AND STORED: STATUS OF HARDWARE MAINTAINED ON HARDWARE DISPOSITION LOG

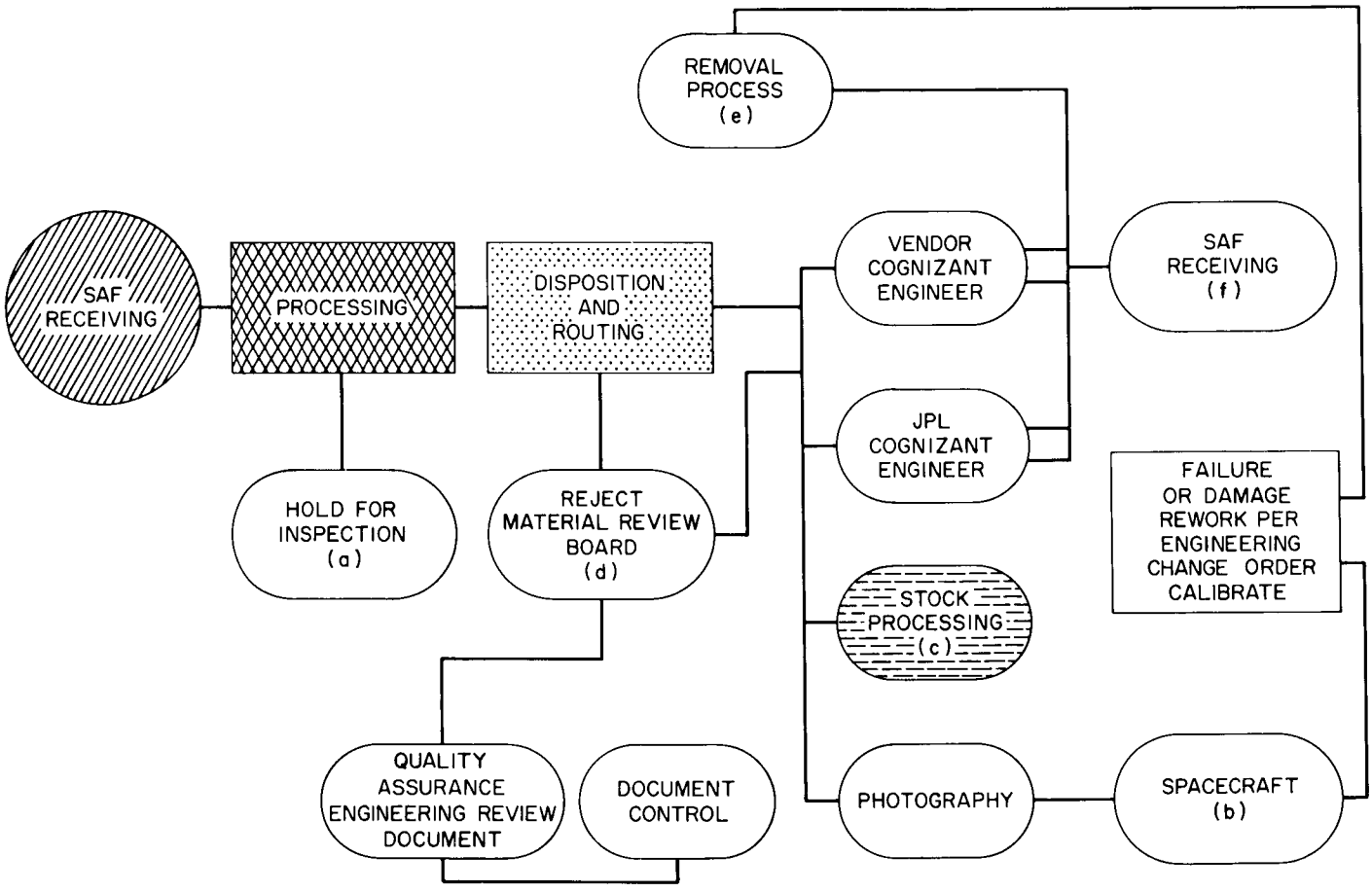


Fig. 395. Typical flow of assemblies and subassemblies through SAF

6. Spacecraft Shipment to Cape Kennedy

The cognizant spacecraft inspectors monitored packing of all spacecraft and support hardware for shipment. A QA supervisor, three mechanical inspectors, and three spacecraft inspectors were assigned to Cape Kennedy to provide proper QA coverage at the launch site. A controlled-access stockroom was set up at the Cape and all movement of hardware to or from it was monitored by quality control. All packages were sealed with "tamper-proof" seals and were opened only under an inspector's surveillance. As spacecraft arrived, all pieces of hardware were inspected for shipment and humidity damage, and the accelerometers were checked. After acceptance, complete control of all hardware and around-the-clock surveillance of the spacecraft were imposed. All movement of hardware to or from the spacecraft was documented and spacecraft status logs were issued after each major event. These controls continued up to the time of launch.

The postlaunch QA effort consisted of monitoring proper storage of the MC-4 spacecraft and flight spares. A significant effort was made in preparing final spacecraft status logs.

B. The Reliability Program

1. Reliability Audit

In recognition of the stringent demands imposed by the length of the Mars mission, the reliability responsibilities for the project were organizationally disseminated into several groups, such as the design sections, the subcontractors, and the *Mariner* Mars 1964 Project Office. In order to maintain a central cognizance over the total project reliability activity, a reliability monitoring group was formed. The main tasks performed by this group were: surveillance and coordination, including attendance at design reviews; development and maintenance of the problem/failure reporting system; continuous audit of the reliability status of the hardware; and monitoring of the information flow between the subsystem fabrication groups, the subsystem and system test complexes, the space flight operations area, the launch vehicle area, and system management.

2. Problem/Failure Reporting

The JPL problem and failure reporting system for the *Ranger* and *Mariner* Venus projects provided a closed-loop system that allowed for effective collection, distribution, analysis, and corrective action of all reported anomalies. Since the Mars spacecraft did not involve the quantities of hardware and paperwork usually associated with a full-scale production program, the decision was made to keep the reporting system on a more personal manual level rather than to automate the paper flow. This became an effective method of keeping failure reporting on a responsible technical working level for analysis and corrective action by allowing anyone to originate a report who believed a problem or failure existed. The problem/failure report was used to record failures and problems occurring during type approval testing and/or flight acceptance testing of the PTM, the flight systems, and the flight spares; and during bench testing of subassemblies, assemblies, and subsystems commencing with the first application of power. These reports were written at JPL and at Cape Kennedy during the *Mariner IV* flight. The reports were written on the flight spacecraft from telemetry data monitored at SFOF. (A record of inflight anomalies is considered especially useful in planning for future programs, both in a hardware sense and in a procedural sense.) A typical problem/failure report is shown in Fig. 396. Figure 397 shows the quantity of these reports versus calendar time and project development. There were nearly 1500 problem/failure reports written on tests, flight performance, and operational support equipment throughout the *Mariner* Mars program.

The actual mechanization of the problem/failure reporting system hinged on the relationship between each subsystem's cognizant engineer (who had the responsibility for analysis and corrective action on each report), the section manager, and the spacecraft project engineer, who had final authority for evaluating the significance of the analysis and corrective action before problem/failure report closeout. This interaction enabled each cognizant engineer to determine the amount of corrective action needed on his subsystem, such as having parts failure analysis performed or starting a design change action to modify the design of the subsystem. At the same time, the cognizant engineer's section manager was aware, through his sign-off responsibility, of the problems or failures occurring on the subsystems under his control. In making a final sign-off, the spacecraft project engineer incorporated his knowledge of the overall Spacecraft System and how each individual problem/failure report, failure analysis, or design change might affect the total Spacecraft System.

3. Environmental Testing

Although environmental testing on the Mars spacecraft was performed and supported by a separate test group, it was an integral part of the reliability program. The two classes of reliability-oriented tests of most significance performed on the *Mariner* Mars equipment were the TA and the FA tests. These tests were performed on both the subsystem and system levels on flight configuration hardware.

The combination of these two levels of environmental testing proved very successful, especially in the indication and elimination of design deficiencies and quality problems. In all, there were 805 subsystem TA tests and 846 subsystem FA tests performed on the *Mariner* hardware.

4. Reliability Prediction and Failure Mode Analysis

A reliability prediction and failure mode assessment of the *Mariner* Mars spacecraft was made in 1963. Most of the design changes recommended concerned increasing subsystem reliability through redundancy. The techniques

☒ Flight (S/C Ser. No._____) ☒ **PROBLEM / ☐ FAILURE REPORT** №
☐ OSE (Complex Ser. No._____)

1. PROJECT ☐ Ranger ☒ Mariner ☐ Other_____ | 2. PROBLEM/FAILURE DATE 3-8-64 | 3. LOG NO.

	A) REFERENCE DESIGNATIONS	B) NOMENCLATURE	C) SERIAL NUMBER	D) OPERATING TIME
4. SUB-SYSTEM	Power - 04	Power Subsystem		
5. ASSEMBLY	4A8	Power Regulator	06	3 hrs
6. SUB-ASSEMBLY				

7. REPORTING LOCATION ☒ JPL Sec. 342 ☐ Vendor_____ ☐ SAF ☐ ETR Other_____

8. PROBLEM/FAILURE NOTED DURING ☒ Bench Testing ☐ In-Process Testing ☐ TA Testing ☐ FA Testing ☐ Systems Testing ☒ Specific Environment Room Ambient ☐ Other_____ | INITIAL DISTRIBUTION DATE

I

9. DESCRIPTION OF PROBLEM/FAILURE

During bench testing it was observed that at 48 VDC input and 40 ohm load, the output voltage oscillated at 60 cps with a 1 volt p-p amplitude. For heavier loading of the booster or for higher or lower input voltages, the oscillation did not occur. The oscillation was present in both the main booster and the maneuver booster.

Originator Frank F. Baran Date 5-26-64 Cognizant Engineer Frank H. Wright

10. VERIFICATION & ANALYSIS

Experimental and theoretical investigations showed that the phase and gain margins were marginal. For a unit constructed with nominal parameter components, the phase margin was 10 degrees and the gain margin 6 db at 48 VDC input. With a buildup of component tolerances it was possible for oscillations to occur.

II

11. CAUSE OF PROBLEM/FAILURE ☒ Design ☐ Piece Part Failure ☐ Operator Error ☐ Damage (Mishandling) ☐ Adjustment ☐ Workmanship ☐ Manufacturing ☐ O.S.E. Failure ☒ Other Component Tolerance Buildup

12. FOLLOW-UP ASSIGNMENT ☒ Cognizant Engineer ☐ Design Review ☐ Vendor_____ ☐ Components Evaluation Group ☐ Material Review Board ☐ Quality Assurance ☐ Other_____

13. PART DATA

A) PIECE PART NAME & NUMBER	B) SERIAL NO.	C) CIRCUIT DESIG.	D) MANUFACTURER	E) DEFECT	F) PRI.	G) SEC.

PERSON COMPLETING SECTION II Signature_____ Date_____

14. CORRECTIVE ACTION TAKEN

Changes were made in the feedback loop that increased the phase margin to 40 degrees and the gain margin to 26 db. These changes were incorporated into 4A8 S/N 06 and the unit became stable. They were also incorporated into all other flight units per ECR 7438.

III

15. DISPOSITION ☒ Reworked ☒ Redesigned ☐ Readjusted ☐ Scrapped ☐ Other_____

16. EFFECTIVITY ☐ This Unit ☒ All Units ☐ Other_____ ECR No. 7438

Signature Cognizant Engineer s/ Frank H. Wright Sec. 153 Date 7-15-4 | Signature Cognizant Sec. Chief s/ F. A. Paul

IV

17. REVIEW CONCURRENCE Reliability Coordinator s/ T. P. Samuels Date 7-16-4 Spacecraft Project Engineer s/ John Casani Date 7-15-4

18. CLASSIFICATION ☒ Critical ☐ Non-Critical

V

19. STANDARD & SPECIAL DISTRIBUTION

P/FR RELIABILITY STAFF JPL 1846 OCT 64

Fig. 396. Typical problem/failure report

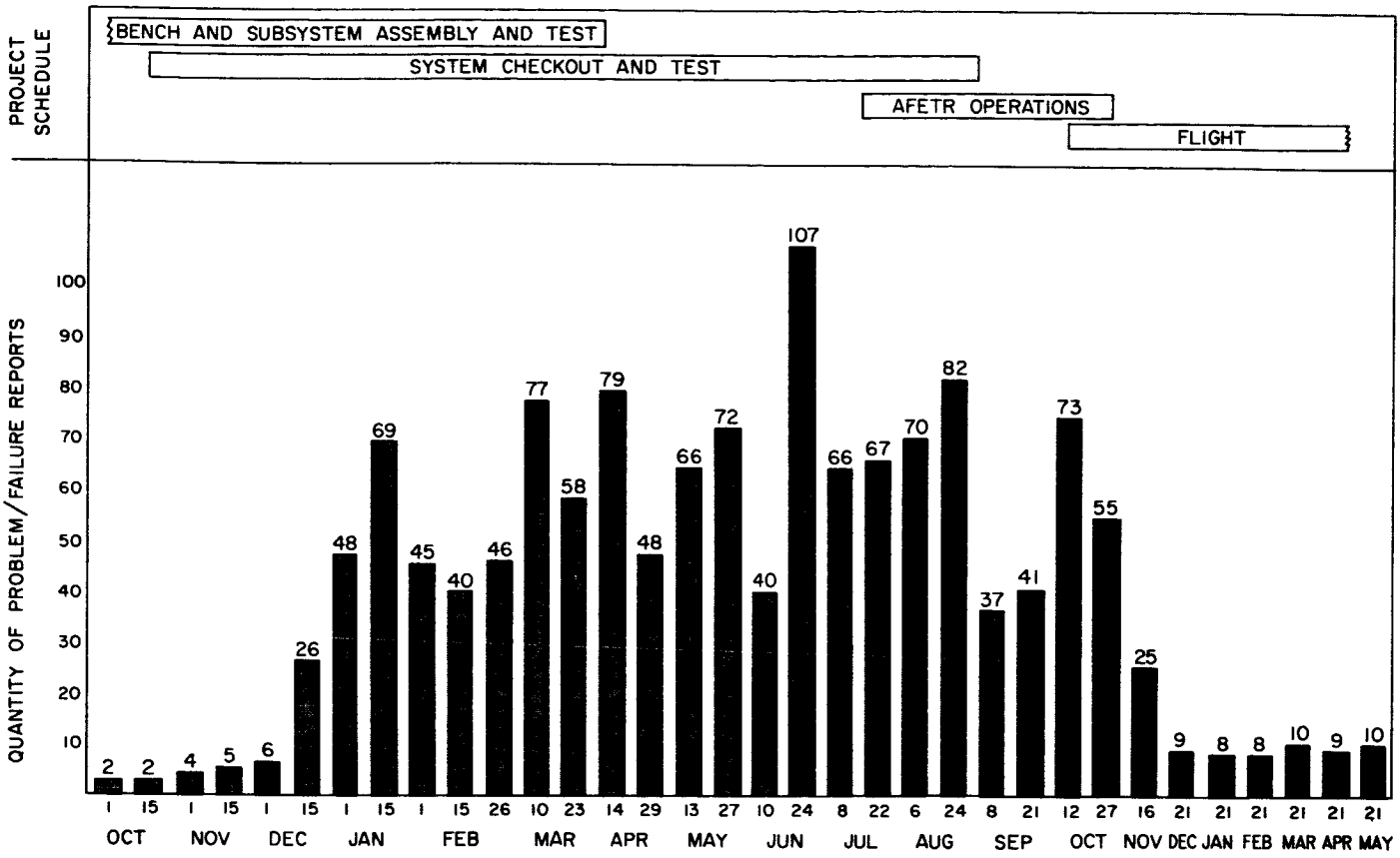


Fig. 397. Problem/failure quantity breakdown

used in modeling the assessment were conventional, and employed the functional block diagram method of analysis. The assessment covered typical failure modes and design interfaces, and gave success probabilities for each functional unit.

5. Design Review

Design reviews of the major *Mariner* Mars spacecraft subsystems began in the spring of 1963. These reviews were performed on hardware designed and fabricated both at JPL and by prime hardware subcontractors, and were conducted by a spacecraft review board. The board was headed by the Spacecraft System Manager and was composed of parts personnel, packaging and cabling personnel, reliability and quality assurance personnel, subsystem section managers, system design personnel, and other members of the *Mariner* Mars 1964 Project considered to have knowledge valuable to the design review activity. The procedure was to have cognizant technical personnel conduct a review on their subsystem before the Design Review Board, with special attention given to the subsystem designs and their consistency with subsystem interfaces, using such typical techniques as check lists and circuit analyses. Design was frozen and put under formal design change control early in 1964.

6. Parts Screening

The screening program was based on individual parts screening specifications used by JPL and its subcontractors. During the program, approximately 350,000 parts were screened. The general process involved burn-in and parameter drift screening, although some parts experienced a more sophisticated screening environment. Normal burn-in included about 168 hr at the manufacturers' rated conditions for each part. Drift screening involved taking each part and testing it under normal conditions against rigid allowable drift tolerance parameters, which were determined from parts qualification data. Evidence of the value of the parts screening program exists in the successful elimination of large numbers of marginal parts, and, hopefully, in the failure-free operation of most of the *Mariner IV* equipment during the many months of cruise operation.

The original requirement for 100% parts screening on PTM and TA hardware was waived, and the requirement for 100% screening on flight equipment was relaxed. Each division was to perform screening on a best-effort basis, and a minimum achievement of 85% screening parts was considered to be an acceptable value.

7. Failure Analyses

Parts failure analyses were performed on approximately 110 individual parts at JPL during the course of the *Mariner* Mars program. Failure analyses were also conducted at the plants of major subsystem subcontractors. The intent of these analyses was to determine the physical mechanisms resulting in specific parts problems and/or failures. Appropriate steps could then be taken to eliminate the parts problems at their origins, with the understandable goal of increasing system reliability. Such a wide variety of electronic part types and associated problems were encountered during the program, that an even greater variety in methods and techniques of failure investigation was required. For example, a typical laboratory investigation of a failed transistor included thorough electrical characterization at several temperatures, hermetic seal tests, analysis of gases within the case, electron microprobe analysis of certain metallic materials, and metallurgical sectioning to examine internal structure (all of which required the talents of specialists in electronics as well as in the fields of chemistry, metallurgy, and physics).

The *Mariner* Mars program made use of the JPL Preferred Parts List, which tabulates the parts applicable to all electronic equipment supplied by subcontractors and fabricated at JPL, and includes high-reliability parts, preferred parts, and OSE parts. Each category of electronic parts had to meet the appropriate processing, quality assurance, and reliability requirements outlined in the 487 *Mariner* Mars parts specifications.

Table 87 lists the parts distribution on the spacecraft subsystems. All of the major types of electronic and electromagnetic parts are listed, excluding such parts as solar cells and connectors.

Table 87. Distribution of electronic and electromagnetic parts throughout the *Mariner* Mars spacecraft subsystems

Subsystem	Capacitors	Diodes	Resistors	Transistors	Other[a]	Subsystem totals
Attitude control	280	349	573	121	74	1397
Cabling	2	0	3	0	0	5
CC&S	255	734	1058	266	261	2574
Command	406	791	1195	345	50	2787
Cosmic Dust Detector	148	70	365	117	21	721
Cosmic Ray Telescope	257	256	480	193	10	1196
Data automation system	917	4382	4374	1210	2844	13727
Data encoder	1614	1475	3316	915	93	7413
Ionization Chamber	69	41	212	20	19	361
Helium Magnetometer	208	79	390	101	24	802
Planetary scan subsystem	82	96	212	65	47	502
Solar Plasma Probe	137	375	528	241	9	1290
Power	125	228	359	121	68	901
Pyrotechnics	30	44	102	2	30	208
Radio	413	227	633	123	175	1571
Television	366	413	942	254	28	2003
Trapped Radiation Detector	59	40	135	39	10	283
Video storage subsystem	202	295	730	215	37	1479
Total subsystem components	5570	9895	15607	4348	3800	39220

[a]Included in this column are inductors, relays, transformers, cores, controlled rectifiers and switches, crystals, thermistors, fuses, transducers, sensitors, and tubes. Connectors are not included.

NOTE: These numbers are based on preliminary information from the JPL Quality Assurance and Reliability Division.

8. Postlaunch Reliability Analysis

Reliability analysis work is being performed on testing and failure data collected from both ground-based activities and the flight spacecraft during the flight of *Mariner IV*. These studies are intended to supply information that will be of value in the establishing the reliability of future JPL space efforts.

XXIII. SPACE FLIGHT OPERATIONS SYSTEM

The Space Flight Operations System is a combination of the Earth-based (1) mission-independent facilities and personnel of the DSN and of AFETR and (2) the mission-oriented equipment, personnel, and procedures required to direct and evaluate the space flight operations of the *Mariner* Mars mission. To accomplish its tasks, the SFO System uses the capabilities of the DSN in a configuration suitable for achieving the requirements of the mission. The primary objective of the SFO System is to track the spacecraft, evaluate the tracking and telemetry data, process and disseminate the data, determine appropriate commands to be sent to the spacecraft, and provide proper command execution.

A second objective of the SFO is to evaluate and compare spacecraft and tracking information with information obtained from ground observations during the flight. A third objective is to provide information and experience on space flight operations and mission performance for use in future mission planning. Documentation supporting the SFO System is shown in Fig. 398.

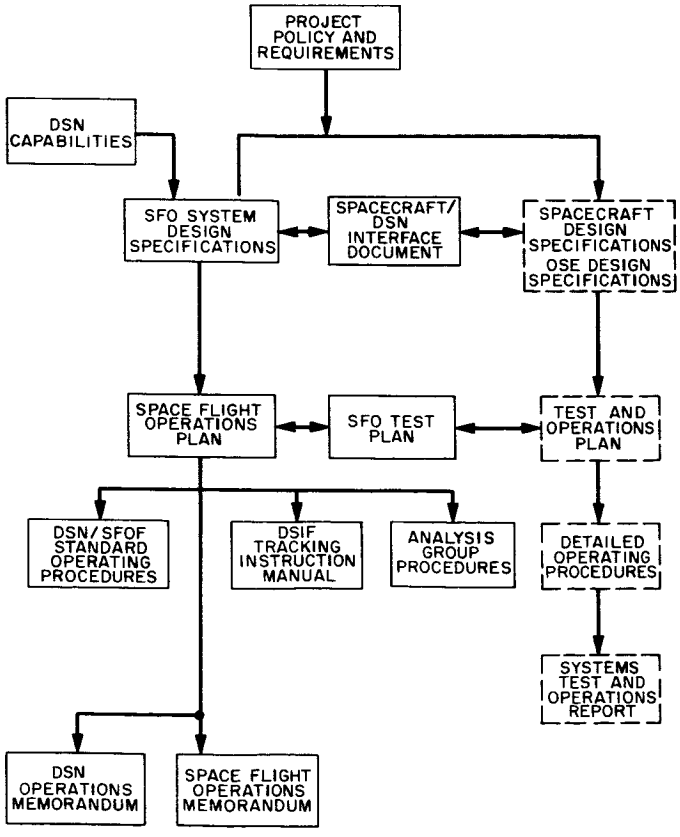


Fig. 398. Space flight operations documentation plan

In addition to the DSN equipment used by the SFO System, a certain amount of equipment is required that is peculiar to the operations of the *Mariner* Mars mission. Mission-dependent equipment includes such items as the ground telemetry system demodulator, the ground telemetry system decommutator, and the video film recorder.

A. Organization

The basic organization of the SFO System is shown in Fig. 399. The overall operational organization of the SFO is illustrated in Fig. 400. The *Mariner* Mars SFO System organization is, in many instances, distinct from the mission-independent organization of the SFOF. In some capacities, the functions of such mission-dependent personnel as the Data Processing Project Engineer and such mission-independent personnel as the Communications Coordinator of the SFOF converge and are integrated. Figure 401 charts the basic SFOF organization responsible for controlling and monitoring SFOF functions for the *Mariner* Mars mission.

The SFO System works on a three-shift, 24-hr day basis from launch to the end of the mission. During normal cruise phase operations, monitoring is performed by a minimum staff; during such high activity phases of the mission as operational tests, launch, midcourse maneuver, and encounter, the space flight operations functions are performed by a full complement of personnel.

1. SFO System Design

The SFO System design team was organized to formulate the SFO System design and to provide the plans, procedures, and tests required for the preparation and execution of the flight. The activities of the team were coordinated by the Space Flight Operations Director. The team consisted of: (1) the DSIF Operations Manager, (2) the SFOF Operations Manager, (3) the Data Processing Project Engineer, (4) the Communications Coordinator, (5) the FPAC Director, (6) the SPAC Director, and (7) the SSAC Director. The required design characteristics of the SFO System were to include.

1. The capability to determine the trajectory and perform the necessary corrections to the trajectory.
2. The capability to receive, record, and interpret telemetry data continuously for the duration of the flight, so as to monitor the spacecraft performance,

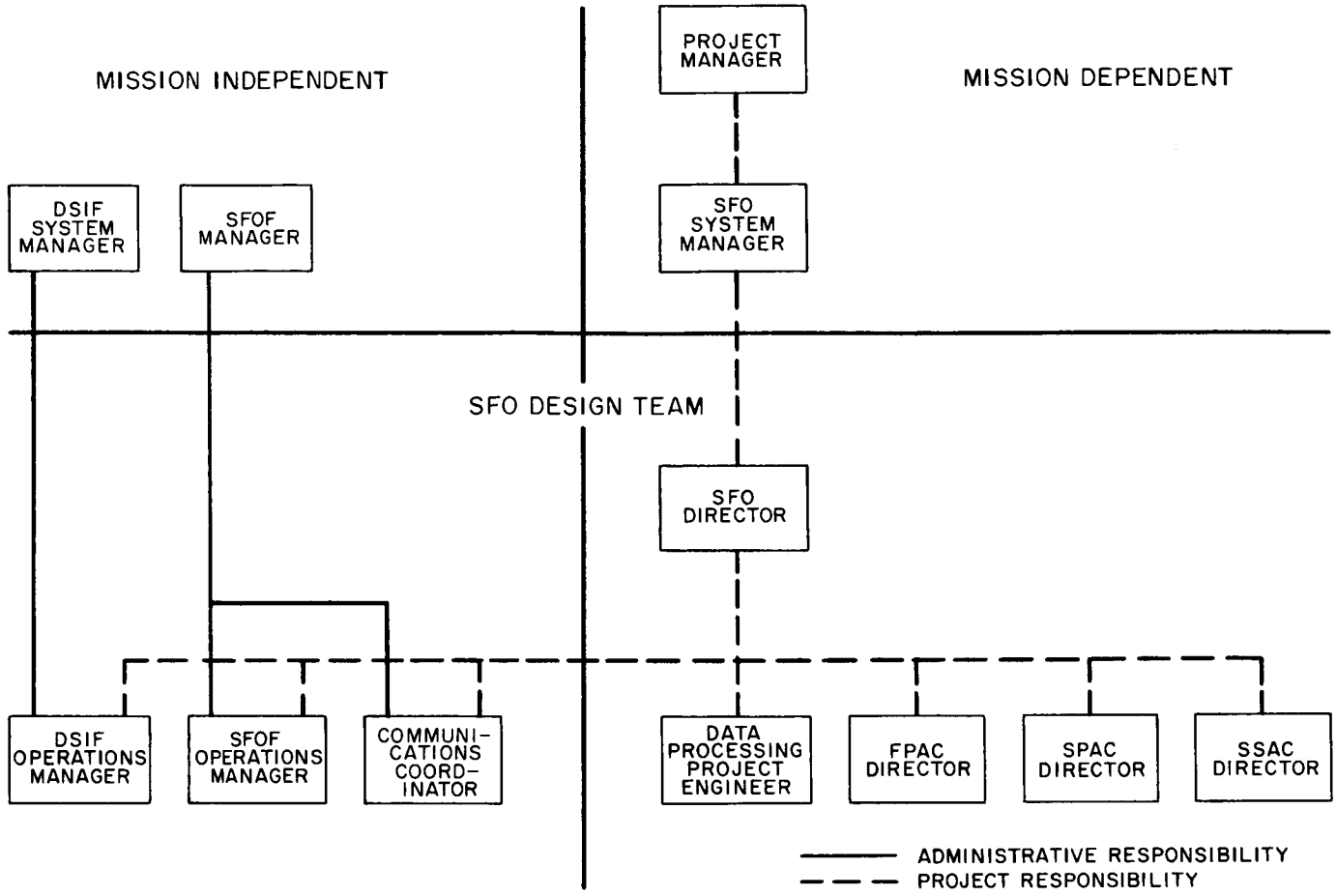


Fig. 399. Space flight operations prelaunch planning and design organization

detect any alarm conditions, and perform any necessary command functions.

3. The capability to describe spacecraft position and science sensor orientation in a variety of coordinate systems; in particular, to generate at Mars a variety of geometrical relationships between the instrument sensors and the planet.

4. The use of facilities and equipment of the SFOF.

5. Sufficient communications between JPL and the DSIF to simultaneously obtain telemetry from two spacecraft and tracking data from one spacecraft from each of the prime DSIF stations.

6. Sufficient data processing facilities and programs to perform the functions of spacecraft monitoring, trajectory determination and possible trajectory corrections, and spacecraft and scientific analysis.

2. Technical Analysis Groups

The technical analysis groups assist in the definition of the standard mission, recommend courses of action during nonstandard events in order to optimize the value of the mission, and perform the intragroups and intergroup technical liaison required to achieve these objectives.

a. Flight Path Analysis and Command Group. It is the responsibility of FPAC to use the tracking and pertinent telemetry data to obtain the best estimate of the actual trajectory of the spacecraft and, supported by the DSIF, to interpret the data supplied by the tracking stations. It is also the responsibility of this group to generate the spacecraft commands affecting the flight path, using the support of SPAC and SSAC to the degree required. Included in FPAC functions are computing, maneuver analysis, orbit determination, tracking data analysis, and trajectory calculation.

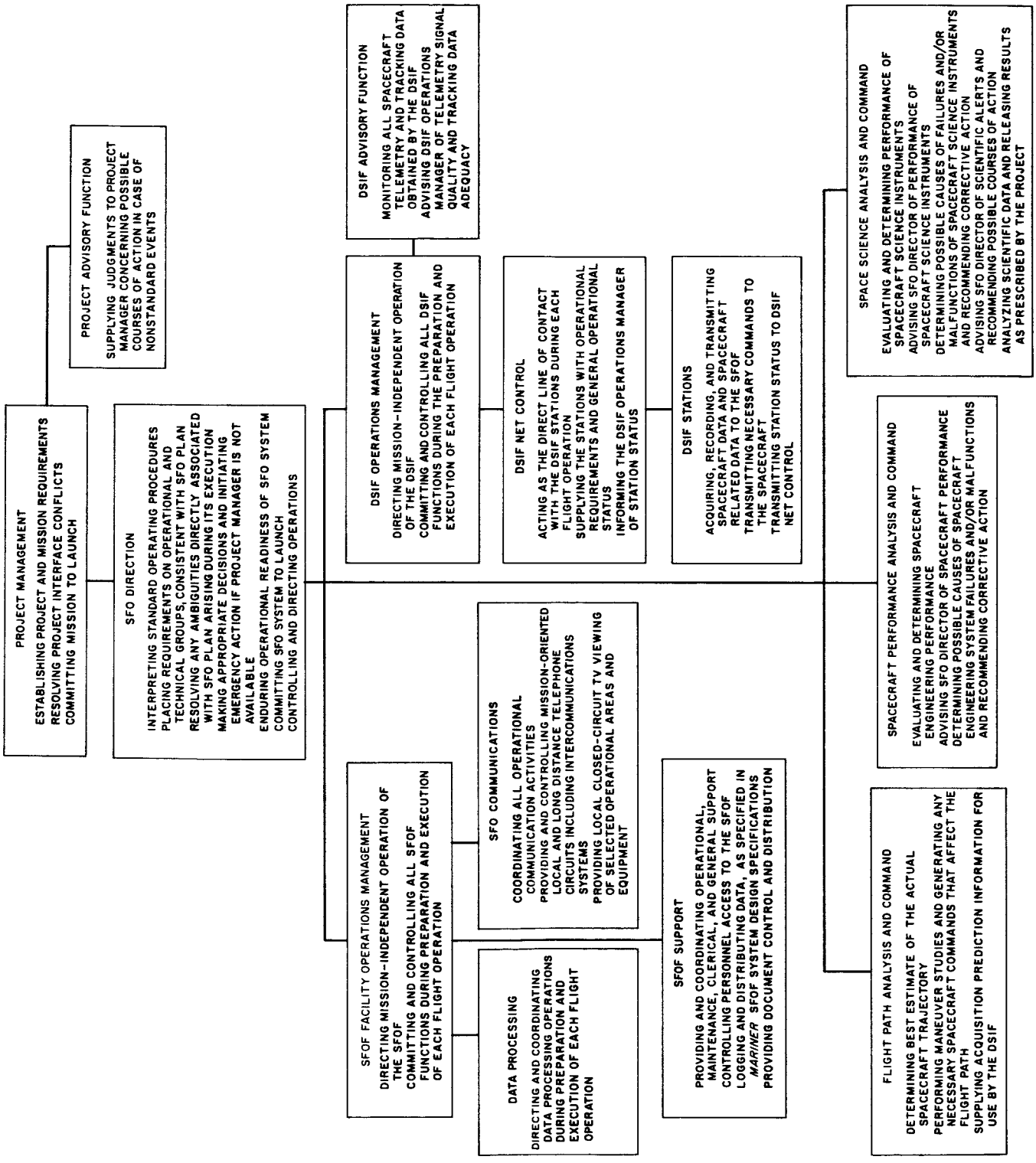


Fig. 400. SFO operational organization

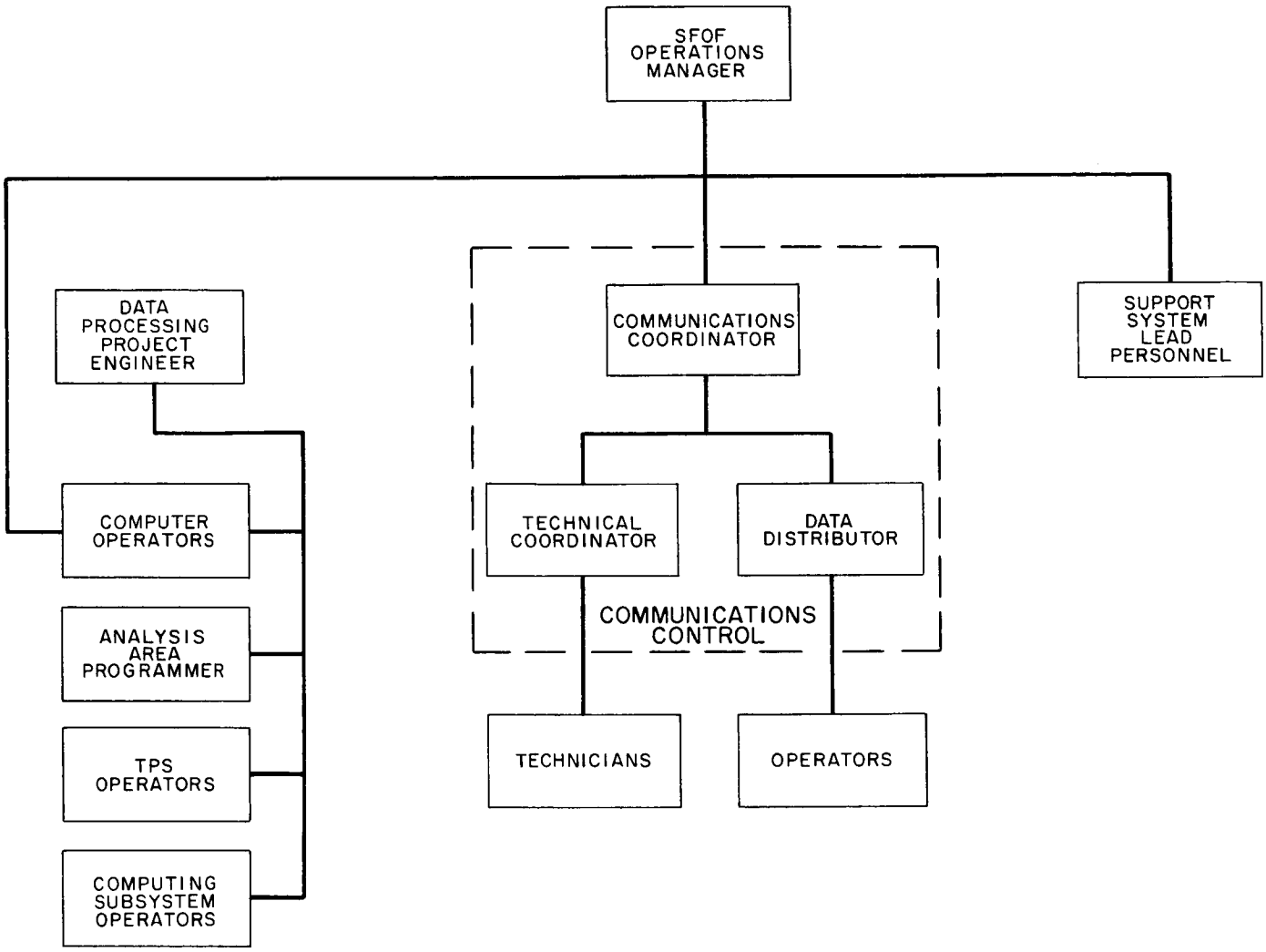


Fig. 401. Space flight operations organization for *Mariner* Mars 1964

b. Spacecraft Performance Analysis and Command Group. It is the responsibility of SPAC to determine the spacecraft performance and to recommend spacecraft commands as determined by the engineering behavior and performance of the spacecraft required for mission success. Included in SPAC functions are engineering mechanics (such as monitoring of spacecraft temperature, pyrotechnics, scan actuator, and science cover) and propulsion analysis.

c. Space Science Analysis and Command Group. It is the responsibility of SSAC to: (1) represent the experimenters in the mission operation; (2) examine and analyze, to the extent necessary, the data from the spacecraft science instruments and any other sources in order to inform the SFO Director of the status of the science instruments and to recommend appropriate action to improve the scientific worth of the mission; and (3) control the flow of, and the mathematical operations performed on, the data pertinent to the experiments during the interval between data acquisition and data transmission to the appropriate scientists.

3. Data Processing

The computing subsystem, which provides the on-line data processing, display, and command/control functions to the data processing subsystem, consists of two parallel multicomputer systems. Each multicomputer system consists of an IBM 7040 input/output processor, an IBM 7288 multiplexer, an IBM 7094 main processor, and two IBM 1301 disc files.

Teletype data received at the SFOF are entered directly into the IBM 7288 multiplexer. The raw telemetry data,

which have been received via microwave or phone line (high-speed data), are preprocessed in the telemetry processing station and then fed into the IBM 7288.

The IBM 7288 multiplexer acquires data from all sources, and converts the data to format for entry into the data processing system. The processing phase includes data identification, conversion to engineering units, data alarm monitoring, and conversion to the proper format for printing and plotting. Data are stored in disc files for later recovery and processing by the data processing subsystem. Storage includes data files for immediate processing during the operational phase and permanent files that allow retrieval of data for subsequent analysis and processing. Data are distributed to the user groups in forms of plots and tabulations. Selected parameters are also distributed for status display.

In the preliminary processing, the telemetry data are decommutated, the channels are identified, and the data samples are time-tagged and compared to preset limits. If the data deviates from the preset limits, the cognizant user area is notified. The spacecraft telemetry alarm is a mission-dependent capability.

B. Computer Programs

The function of the *Mariner* computer programs is to provide the required data in the proper format in the areas of flight path analysis, telemetry monitoring, spacecraft performance analysis, science analysis, command generation, and, also, for mission evaluation, control, and operational information.

Basic space flight data processing programs are those programs necessary to accept and log incoming data, to monitor spacecraft telemetry and tracking data, and to perform alarm functions in real time. Analysis programs consist of two categories: real-time analysis programs and non-real-time analysis programs.

The real-time analysis programs are necessary to determine and analyze the performance of the spacecraft, and are required for the evaluation of science experiments in near-real time and the diagnosis of the flight path in near-real time.

Non-real-time analysis programs are unnecessary to the actual space flight operation but complement the detailed analyses. This category includes the programs that determine physical constants and locations from the tracking data and that perform detailed analyses and reconstructions of video data. These programs are not used in the normal course of space flight operations. Input from non-real-time analysis programs into the real-time analysis programs may be used, provided such input, or a substitution of parameters, is deemed necessary and appropriate to the fulfillment of mission objectives.

The mission-dependent programs identify, decommutate, time-tag, edit, and format incoming data. They exist in both the IBM 7040 and the 7094 computers, each of which operates on raw data. The 7040 performs alarm monitoring functions on raw data in real time. A description of some of the computer programs used by the SFO System is given in Table 88.

C. SFO System Checkout

The checkout of the SFO System included tests required to bring the system to operational readiness and the criteria required to determine system readiness. A series of spacecraft operational compatibility tests and operational tests were performed. The two series of tests established were designed to demonstrate the compatibility between a spacecraft and the SFO System, and to demonstrate the operational readiness of the SFO System. The communications network of the SFO System, both during the tests and during the launch of *Mariner III* and *Mariner IV*, is shown in Fig. 402. The test schedule is shown in Fig. 403.

1. Spacecraft Operational Compatibility Tests

A series of spacecraft operational compatibility tests was conducted before launch and before the spacecraft was shipped to Cape Kennedy. Magnetic tapes and/or on-line data from flight spacecraft were used to simulate standard operations for these tests. In addition, the prototype spacecraft or magnetic tapes of data were used to simulate nonstandard conditions. The primary objective of these tests was to ensure that the ground-based facilities were compatible with the spacecraft; that they were capable of processing telemetry received from the spacecraft; and that they were capable of transmitting commands to the spacecraft.

a. Spacecraft/DSIF SAF/SFOF Operational Compatibility tests. Three types of tests were used to verify the status and compatibility of the spacecraft with the DSIF, AFETR, and SFOF operations to be used during the mission: (1) non-real-time tests, (2) real-time tests, and (3) real-time closed-loop tests.

Table 88. SFO computer program description

Type of program	Designation	Title	Description
SPAC	VPIM	Variable Parameter Input Program	Loads and stores the coefficients required for the conversion of raw data to engineering units.
	AGCM	Station AGC Prediction Program	Plots the predicted station AGC for a given pass using the DSIF station pretrack calibration.
	SIPM	Star Identification Program	Generates star maps indicating the positions of the stars with relation to the spacecraft at various times during flight.
	SSDM	Suppressed Data Program	Decommutates the engineering data and converts the raw data values to engineering units. Also incorporates data suppression so that only changing data are displayed.
FPAC	TDP-ODG	———	Edits tracking data from the disc and generates a data table for use by the ODP.
	ODP	Orbit Determination Program	Determines the spacecraft orbit from tracking data. Also generates predictions for the tracking stations.
	TRAJX	Trajectory Program	Determines the trajectory from the initial injection conditions.
	MCIM	Midcourse Program	Determines the maneuver parameters necessary to correct the trajectory for the desired encounter conditions.
System	MACE (IBM 7044)	*Mariner* Editor Program	Decommutates *Mariner* data and supplies data to the print, plot, and conversion subroutines in real time.
	JPEDIT (IBM 7094)	*Mariner* Dependent Editor Program	Decommutates *Mariner* data and writes a special data table on the disc for use by the *Mariner* user programs. Also processes 7044 log tapes, and generates a tape containing digital spacecraft video data (Data Mode 4).
Science	DSTM	Cosmic Dust Program	Lists the accumulative counter data and the hit analysis data derived from the cosmic dust experiment. Contains a suppressed data option to display only the changing data.
	MAGM	Magnetometer Analysis Program	Carries print and plot portions. Converts raw data to scientific units. Transforms magnetic vectors from the spacecraft coordinate system to the celestial coordinate system. Determines the total magnetic vector, and performs averaging of data over convenient periods of time.
	CRTM	Cosmic Ray Telescope Analysis Program	Decommutates data transmitted by the Cosmic Ray Telescope, and, using averaging techniques, provides particle rate and flux summaries. Contains print and plot portions.
	PLAM	Solar Plasma Analysis Program	Decommutates data transmitted by the Solar Plasma Probe and its ancillaries (i.e., temperature, power). Resultant data indicate the solar plasma spectrum during each instrument analysis cycle. Contains print and plot portions.
	RADM	Trapped Radiation Detector Analysis Program	Decommutates data according to the given detector being sampled. Averages these data, and provides particle rate and flux summaries. Contains a print and plot portion.
	IOCM	Ionization Chamber Analysis Program	Determines ionization level detected by the Ionization Chamber, and, from that, determines the particle rate and flux.
	DAS 1 DAS 2 DAS 3	DAS Scan Programs	Analyze the scan data while the scan platform is scanning, and predict scan position for a given future time. Compute the time for transmission of a command to stop the scan platform at a given position.

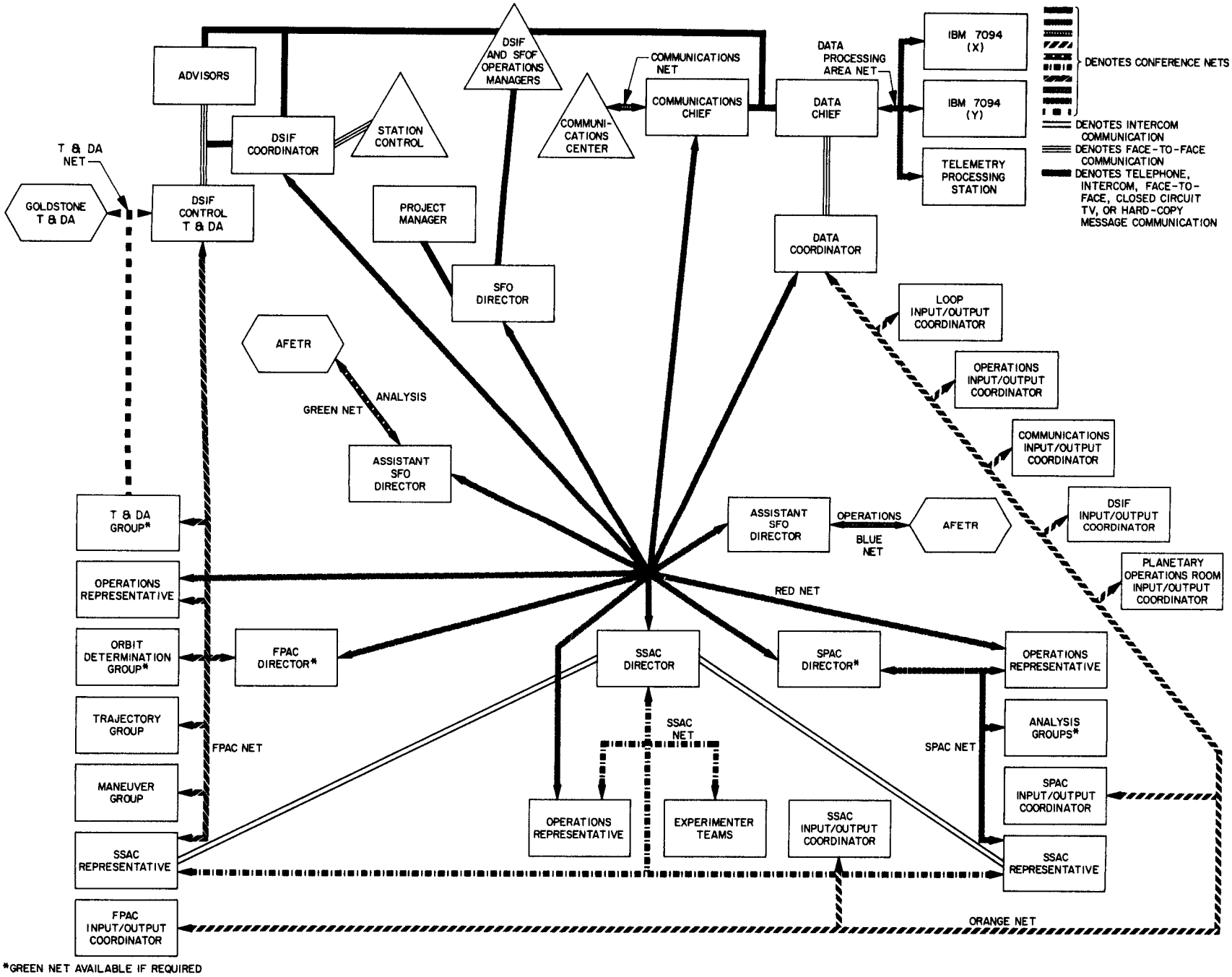


Fig. 402. SFO System communications network

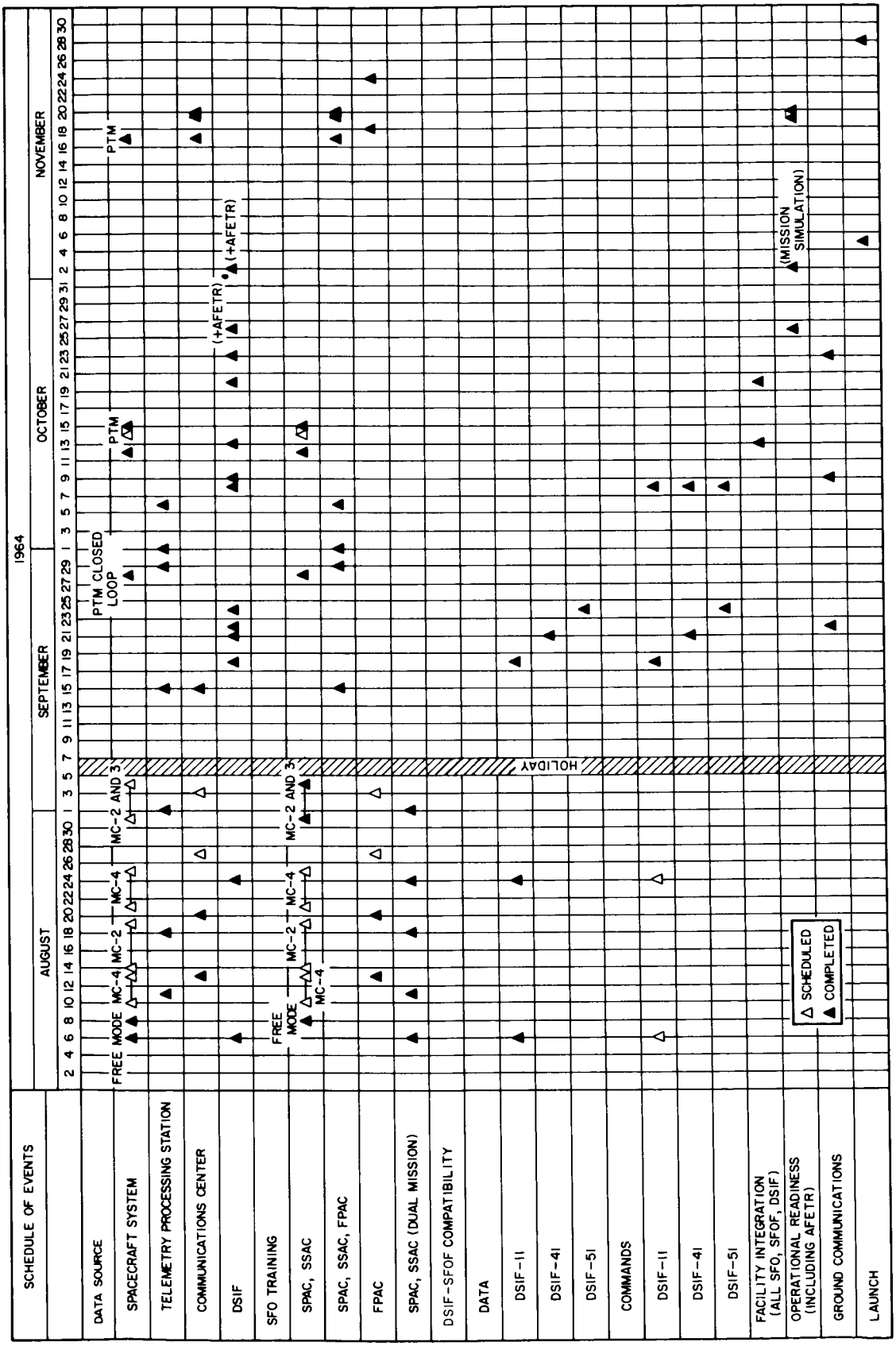


Fig. 403. SFO System test schedule

b. Non-real-time tests. System tests were conducted using the entire *Mariner* spacecraft. The spacecraft, which was monitored by the STC, transmitted telemetry data in real time to the DSIF ground telemetry subsystem located in the STC. The GTS received and processed the data and produced a TTY paper tape record of the spacecraft telemetry according to a defined format.

On a non-real-time basis, the TTY paper tape record of the spacecraft telemetry was hand carried from the STC (at SAF) to the SFOF for processing by the data processing subsystem. The data processing subsystem, using the SPAC and SSAC IBM 7040 basic telemetry computer programs, processed the spacecraft telemetry data via the TTY paper tape input. Video data were processed by the IBM 7094, the Link film recorder, and the JPL photography laboratory.

These tests were accomplished in conjunction with the computer program checkout efforts and during program integration into the SFOF programming subsystem. The use of the spacecraft-generated data during this period ensured compatibility of spacecraft data with the programming subsystem. Due to the length of the time period involved in this effort, periodic demonstrations of the data processing were held for the analysis area directors and the SFO Director.

c. Real-time tests. These tests were conducted during *Mariner* PTM and flight spacecraft system tests on a noninterference basis with SAF. The spacecraft, which was monitored by the STC, transmitted telemetry data in real time to the DSIF ground telemetry subsystem located in the STC. The TTY encoder output (TTY paper tape and/or high-speed data) was transmitted to the SFOF data processing subsystem in real time via the SFOF communications system.

The SFOF, using the data processing subsystem and the SPAC and SSAC IBM 7040 and 7094 telemetry programs, received, processed, and displayed (by means of the various types of output devices) the spacecraft telemetry data being received in real time. The IBM 7040 monitored the tests throughout the entire SAF test period, and was used periodically to drive the display devices located in the SFOF. At various intervals, the data recorded on the IBM 7040 were processed in the 7094, and bulk output was obtained for examination by the technical analysis groups. Video data were processed by the IBM 7094, the film recorder, and the JPL photography laboratory.

No formal test sequences were used during these tests because they were used mainly as a source of real-time spacecraft data for hardware and programming compatibility and for output capability checkout.

d. SFOF IBM 7040/7094 program demonstrations. This group of demonstrations exercised all of the available user programs, both in the IBM 7040 and in the 7094. Many of the user programs were not ready at launch time. The demonstrations acquainted the users (SPAC, SSAC, and FPAC) with the program capabilities and restraints. The analysis area personnel exercised all of their programs at designated times using the spacecraft data or simulated tracking data, depending upon the program.

e. Real-time closed-loop tests. The real-time closed-loop tests were conducted on the PTM spacecraft. The loop tests were conducted in accordance with the procedures and sequence of events established by the SFO Director. A voice line was established and maintained between the SFO Director and the Spacecraft Test Director for coordination of the test.

The PTM was operated through discrete portions of the flight in corresponding blocks of time; these blocks covered the spacecraft events from L − 30 min through planet postencounter. The spacecraft was operated in each of two data rates (33⅓ or 8⅓ bps) and in each of the four data modes:

1. Data Mode 1, which is engineering data only
2. Data Mode 2, which is engineering and science data
3. Data Mode 3, which is science data only (used at encounter)
4. Data Mode 4, which is TV picture playback

The data processing subsystem in the SFOF received, processed, and displayed the telemetry data in real time. These data were then analyzed by SPAC and SSAC personnel. All spacecraft commands were used during the tests to verify their validity and the validity of the spacecraft's reactions.

Four days were required to complete a real-time closed-loop test. A test was divided into four parts, each requiring one day (approximately 8 hr) of spacecraft operations.

Part I exercised the spacecraft through the periods from L − 30 min to L + 1 hr, and from Canopus acquisition − 30 min, to Canopus acquisition + 30 min. All spacecraft commands pertinent to those time phases of space flight were transmitted to the spacecraft.

Part II exercised the spacecraft through the period of M − 30 min to M + 3 hr. During that time, all spacecraft commands pertinent to the midcourse maneuver were transmitted to the spacecraft.

Part III exercised the spacecraft through E − 2 hr to E + 1 hr. During that time, all spacecraft commands pertinent to encounter were transmitted to the spacecraft.

Part IV was the playback of the spacecraft video information recorded on the spacecraft tape recorder. One picture was played back and required approximately 8 hr of spacecraft operation. Video data were processed by the IBM 7094, the Link film recorder, and the JPL photography laboratory in order to produce hard-copy pictures.

2. Operational Tests

A series of operational tests were conducted before launch, which did not involve the flight spacecraft or the PTM. The primary objective of these tests was to ensure that all elements of the SFO System, including technical and operational personnel, were prepared to support the spacecraft after launch. Criteria were established for the evaluation of the tests conducted; the satisfaction of these criteria proved the readiness of the SFO System to support the mission.

These tests indoctrinated and exercised the SFO System operational and technical personnel in the systems and procedures to be used for the mission. The DSN provided support to SFO during these system tests.

a. SFO training tests. There were seven SFO training tests, each of which used the SFOF equipment and facilities for approximately 10 hr. The procedures and sequence of events for each test were established by the SFO Director.

The data (tracking, telemetry, and station messages) for the SFO training tests simulated discrete portions of the flight in corresponding blocks of time; these blocks covered the spacecraft events from L − 30 min to planet postencounter. The data for the training tests were used to exercise the data processing subsystem in both the prime and backup modes.

The SFOF telemetry processing station simulated the DSIF stations during the internal SFO training tests. The data package for each test was given to the cognizant communications engineer with the procedure and sequence of events for the transmission of the data to the SFOF data processing subsystem.

The data processing subsystem received, processed, and displayed the incoming tracking and telemetry data and station messages for analysis and action by the appropriate SFO personnel (SPAC, SSAC, and FPAC) in real time. Appropriate commands, as required by the sequence of events or as indicated by the data being received, were prepared for simulated transmission in real time to the DSIF. The commands were prepared in accordance with the procedures delineated in the SFOP.

b. Facility integration tests. There were two facility integration tests. The duration of each was approximately 24 hr, and the procedures and sequence of events for each test were established by the SFO Director.

The spacecraft tracking and telemetry data for the facility integration tests simulated a mission in the same manner as in the SFO training tests. The data were generated to activate the DSIF station equipment and systems to the greatest extent possible.

The DSIF stations participated by routing the simulated spacecraft tracking and telemetry data through the station equipment and systems, and transmitting the data to the SFOF via the communications system. The data were transmitted in accordance with the procedures and sequence of events delineated in the TIM. The DSIF stations received and acknowledged receipt of the spacecraft commands and tracking predictions in accordance with procedures delineated in the TIM. The DSIF stations executed the spacecraft commands and verified the execution times in accordance with the procedures established in the TIM.

The SFOF participation consisted of receiving, processing, and displaying the incoming tracking and telemetry data in real time. The SFO personnel within the SFOF analyzed the data and took appropriate action as required. The SFOF also prepared and transmitted spacecraft commands, prediction data, and station messages in real time to the appropriate DSIF stations in accordance with the established procedures.

c. SFO operational readiness tests. There were two operational readiness tests. The duration of the first was approximately 72 hr; the duration of the second was approximately 24 hr. The procedures for these tests were delineated in the SFOP.

The spacecraft tracking and telemetry data for the operational readiness tests were generated to simulate the mission in the same manner as in the SFO training tests. The data for the tests were generated to activate and exercise the DSIF station equipment and systems to the greatest extent possible.

Participation of AFETR in the tests (approximately 6 hr for each test) included: simulating and providing *Atlas/Agena* booster launch countdown and boost-phase flight events through injection; simulating and providing AFETR tracking data; calculating the parking orbit, transfer orbit and orbital elements, injection criteria, and the DSIF look angles; and transmitting all these data to the SFOF via the communications system.

Participation of the spacecraft checkout facility in the tests (approximately 6 hr for each test) included: providing simulated prelaunch and launch spacecraft telemetry data; providing launch countdown status and spacecraft flight events through the injection phase; transmitting these data and information to the SFOF via the communications system.

The DSIF Goldstone, Woomera, and Johannesburg stations participated in the tests by processing the simulated spacecraft tracking and telemetry data through the station equipment and systems, and transmitting the data to the SFOF via the communications system in accordance with established procedures and sequence of events. The stations also received and acknowledged receipt of the spacecraft commands and tracking predictions in accordance with established procedures, in addition to executing the spacecraft commands and verifying the execution times, also in accordance with established procedures.

The DSN/SFOF participated in the testing by processing tracking and telemetry data. During this phase of SFO operational readiness testing, the DSN provided space and equipment for the tests in the SFOF for the actual functions to be performed by members of the *Mariner* project groups.

Tracking data. The SFOF responded to the incoming data from AFETR and the DSIF stations in real time. The tracking data from AFETR were processed, and spacecraft tracking look angles and prediction data were transmitted to the appropriate DSIF stations in accordance with established procedures. The tracking data from the DSIF stations were processed to establish the orbit of the spacecraft, and additional prediction data were then transmitted to the appropriate DSIF stations. The tracking data established the orbit of the spacecraft and determined the requirements for the midcourse correction. Midcourse maneuver commands were prepared and transmitted to the appropriate DSIF station for simulated transmission to the spacecraft.

Telemetry data. The spacecraft telemetry data were processed and analyzed in real time. Backup commands that might be required because of spacecraft onboard malfunctions were prepared in the SFOF and transmitted to the appropriate DSIF station for simulated transmission to the spacecraft. The SFOF monitored and displayed the incoming tracking and telemetry data and reported the status of the mission.

D. Mariner Mars 1964 Mission Summary

1. *Mariner III* Summary

Mariner III was launched from AFETR LC 13 at 19:22:04.920 GMT, November 5. Approximately 60 min after launch, and as a result of analysis of engineering telemetry data, SPAC reported that the solar panels were not deployed and that the spacecraft was still on battery power. When it became apparent that there was no solar power and that the spacecraft attitude control subsystem was not functioning properly, a decision was made to send a command to the spacecraft to turn off the gyros before the launch counter ran out in order to back up the CC&S L-1 and L-2 events and conserve battery power. This would extend the life of the spacecraft and would give additional time for any possible corrective action.

Subsequent to turn-off of the gyros, both engineering and science telemetry data gave indications that the spacecraft had not become attitude-stabilized, denoting that either the *Agena* or the shroud had not separated from the spacecraft. Separation velocity was calculated by LMSC as approximately 28 in./sec (a factor that was approximately normal with the shroud on); both the oxygen depletion and the C_3 value further verified that the shroud was still on the spacecraft. The FPAC group reported *Agena* tracking data that showed the *Agena* retromaneuver had occurred, indicating that the *Agena* was not attached to the spacecraft.

It was decided to perform a maneuver that might shake the spacecraft free of the *Agena* or shroud. Because of command equipment malfunctions at Woomera, however, the emergency maneuver sequence was not completed. A second maneuver was attempted from the Johannesburg station. The maneuver command series was sent and stored in the spacecraft. The execution of the maneuver was not verified, however, since the last telemetry reception from the spacecraft occurred prior to the time of maneuver start.

a. Description of space flight operations. *Mariner III* space flight operations began at 10:37:00 GMT (L − 295 min), November 5, 1964, when communication was established between SFOF in Pasadena and AFETR.

The spacecraft checkout facility acquired the spacecraft in two-way lock at 14:06:00, went to one-way lock prior to launch, and remained in lock until 19:24:33. During that period, the facility provided spacecraft telemetry to the SFOF.

Launch occurred at 19:22:04.920, and, at 19:25:00, data were received at Bermuda. At 19:27:00, the transmission of Bermuda data were interrupted and Antigua data were transmitted until 19:35:00.

Elements of injection conditions of the parking orbit were received from AFETR at 19:36:00, and elements of injection conditions of the transfer orbit, based on the actual parking orbit and the nominal second burn, were transmitted from AFETR 6 min later. The launch azimuth was verified as 102.9 deg by AFETR at 19:42:00. Woomera acknowledged receipt of look angles from AFETR at 19:43:00, and Woomera acknowledged predicts from the SFOF at 19:46:00.

The FPAC group announced that the spacecraft would enter the Earth's shadow at 19:44:44 and would leave the Earth's shadow at 20:05:40. The FPAC group announced further that separation would occur at 19:58:22; that Johannesburg rise would occur at 19:53:04; that Johannesburg set would occur at 20:01:04; and that Woomera rise would occur at 20:07:04.

All systems appeared to be functioning properly during the initial phase of the flight. At approximately L + 60 min, SPAC personnel confirmed that the science instruments were on, but that there was no indication of solar panel power. The spacecraft was declared to be in a nonstandard mode. Analysis of the Pretoria data produced a C_3 of 4.04 km^2/sec^2 rather than the C_3 of 10.4 required to inject the spacecraft into a Mars trajectory. However, since the epoch corresponding to that calculation was in error by 5 hr, it was decided that nominal DSIF acquisition predictions would be used until the anomaly could be solved.

At that time, the AFETR analysis net had been set up to make recommendations between the Project Manager at Cape Kennedy and the SFO Director and Analysis Area Directors at the SFOF in Pasadena.

The DC-15 command was sent at 23:06:02, and power data indicated the gyros were off at 23:12:09. The purpose of the DC-15 was to turn off the gyros for power conservation, to back up deployment of the solar panels, and to effect turn-on of the attitude control subsystem. A decision was made to transmit a DC-25 followed by a DC-26 command in order to determine whether the scan platform would move; this would presumably have determined whether the *Agena* was still attached to the spacecraft. The DC-25 command was transmitted at 23:21:30 and verified at 23:23:00. Data revealed little or no scan platform movement and almost immediate wide- and narrow-angle acquisition. The use of this command failed to verify whether or not the *Agena* was attached to the spacecraft. The DC-26 command was transmitted at 23:29:05 and verified at 23:30:00. This command was supposed to turn off planet and cruise science and the battery charger, and thereby reduce the consumption of spacecraft power. Science instruments were verified as being off at 23:32:00.

The maneuver command began with the transmission of QC 1-1 at 23:51:58. The command detector was out of lock and the command was retransmitted at 00:00:00 in the emergency mode. The tracking station was requested to use the emergency command mode of the command system so that commands could be transmitted in one-fifth the normal time and would not be inhibited. The QC 1-2 command was sent at 00:01:30; QC 1-3 was transmitted at 00:03:45; DC-27 was sent at 00:05:00 to start the maneuver and was confirmed at 00:07:00; and DC-29 was transmitted at 00:08:00. The DC-13 command was transmitted at 00:14:00 to shut off the gyros, and was confirmed at 00:15:00 by the presence of Mode 2 data; DC-1 was transmitted at 00:38:41.

At 01:09:00, SPAC reported a normal pitch turn duration, and, at 01:29:00, the roll turn was verified as being of normal duration. No pitch or roll motion was expected nor was any observed, since the maneuver was inhibited and the gyros were shut off. It was planned

to transmit DC-14 at 01:40:00 to uninhibit the maneuver sequence and allow the motor to burn. The command system at Woomera failed prior to the scheduled transmission of DC-14 and, as a result, no motor burn occurred.

At 01:44:00, command transmission was changed from Woomera to Johannesburg, which was instructed to reduce its transmitter power from 10 to 1 kw. At the time Johannesburg was in command lock, at 10:12:00, SPAC estimated the spacecraft life as 2 hr, 13 min.

At 02:29:00, DC-28 was loaded in the GCS, and was transmitted at 02:37:25 to turn on the battery charger and turn off 2.4-kc power to the VSS.

Another QC 1-1 command was transmitted at 03:28:03 and verified at 03:28:43; QC 1-2 was transmitted at 03:30:25, and QC 1-3 at 03:32:35. A DC-27 command was sent at 03:35:27; DC-14 was sent at 03:45:00 and verified at 03:45:22; DC-19 was transmitted to turn off the gyros at 03:45:55 and was verified at 03:46:17.

The motor burn was calculated to start at 05:19:27; and estimated battery life was to end at 04:05:55. No verification of the maneuver was possible.

b. Performance analysis. Some difficulty in properly evaluating the performance of the *Mariner III* spacecraft was encountered as a result of various aspects of the flight. This was partly attributable to gaps in the telemetered data during the early portion of the flight, and partly due to the apparently nonstandard environment that existed. No obvious spacecraft design errors were discernible from the spacecraft's performance. Most subsystems operated quite normally; those that did not experienced anomalies of a type that indicated either a greater noise sensitivity than expected on the basis of test experience or a much more severe environment than anticipated. Since most of the evidence indicated that the aerodynamic fairing remained with the spacecraft throughout the flight, the severe environment assumption appears to be the more reasonable explanation.

The various engineering subsystems were classified in the following manner: those that operated normally; those that cannot be properly evaluated because of interference with the spacecraft operation by the aerodynamic fairing; and those that experienced anomalies that may or may not have been induced by the environment to which the spacecraft was exposed both before and after injection.

Of the anomalies experienced, not all are fully understood. A malfunction in the radio subsystem was most serious because it is not known whether it was induced by the conditions resulting from failure of the protective aerodynamic fairing to clear the spacecraft. Another anomaly occurred between L + 78 and L + 204 sec when the low-deck commutator skipped from position 423 to position 425. The occurrence of a single, low-rate deck skip is not common. This deck skip was not readily explicable, since no electrical transient of the type that cause deck skips is known to have occurred during this interval. (It may be relevant that this interval brackets an abnormal vibrational shock noted at L + 103 sec.) A pressure increase at about L + 104 sec was detected on the shroud cavity pressure transducer, an event that may also be related to the deck skip. The monitoring of any abnormal spacecraft activity at L + 103 sec was not possible because that telemetry data frame was being commutated through the *zero* science position of the frame.

The spacecraft incurred some physical damage prior to L + 463 sec, at which time the −X solar vane telemetry channel was sampled for the first time. This sampling indicated that the potentiometer wiper arm had either been driven completely beyond its normal limiting position in the opposite direction, away from the normal launch position, or that it had sustained a short. At L + 589 sec, the +Y solar vane telemetry measurement showed that the potentiometer wiper arm had either been driven completely beyond its normal limiting position in the opposite direction, away from the normal launch position, or that it had sustained an electrical open circuit. Later in the flight, this telemetry measurement indicated a shift in the potentiometer position, or a partial circuit closure once more. Since the change was not abrupt, it was surmised that the physical motion of the potentiometer wiper arm must have been the cause of the shift in telemetry reading.

Perhaps related to the solar vane damage is the fact that the positive yaw valves may have been rendered inoperative during the preseparation phase. The Magnetometer data indicated that the positive yaw valves had not been firing, which seemed to be corroborated by the analysis of the attitude control gas consumption rates. The Magnetometer could sense changes of approximately 300 γ in the magnetic flux with a periodicity corresponding to the anticipated solenoid activation for gas jet firing under the flight conditions existing. This could have been possible only because of the close proximity of the gas jet assemblies to the Magnetometer.

Such proximity could have existed if the panels had not been permitted to deploy fully.

The SPAC engineers are confident that solar panel deployment was not impaired by failure of the pyrotechnics to fire the squibs. The firing command, which also activates circuits to fire the solar panel pinpuller squibs, was undoubtedly issued since the scan platform was unlatched. Both pyrotechnic channels provided current at least to some of the squibs because the proper event register readings were observed to substantiate this fact.

The spacecraft performed as would have been expected with the aerodynamic fairing on it. The excessive expenditure of attitude control gas had no effect on spacecraft rates. Even with the solar panels undeployed, the gas jet orientation was designed so that as long as both valves fired to provide a certain torque to the spacecraft, the couple to produce this torque would exist even though the couple would be severely reduced from its nominal value when the panels were fully deployed.

For a time during the flight it appeared that one of the solar panels might have deployed. This appearance was due to an event register No. 3 indication in the first decodable data received from Woomera, which matched that expected for normal panel deployment. Additional information was deciphered after the spacecraft stopped transmitting showing that one of the events had not occurred by L + 52 min. This was considerably past the normal time for solar panel deployment via the SIT command, which is nominally issued at separation plus 180 sec. At L + 53 min, the CC&S L-1 launch command was issued to provide the backup solar panel deployment/scan platform unlatch signal. It is probable that the event in register No. 3 was due to the L-1 command causing current to be passed through one or more shorted squibs in pyrotechnic channel B, although occurrence of shorted squibs is not too unusual. (Tests showed that 20% of the squibs of this configuration fired, short at ignition due to the combustion products and the bridgewires within the cartridge.)

Little doubt remains as to whether the aerodynamic shroud remained with the spacecraft or was ejected. Much effort was expended analyzing spacecraft data to verify that the shroud was not ejected.

Based on analyses of data and/or photographs of the flight, the following arguments are presented to support the theory that the shroud remained on the spacecraft:

1. Motion pictures taken from Melbourne at L + 80 sec showed objects approximately 10 in. in diameter, which initially appeared next to the shroud, appearing in the area of the *Agena* later on.
2. Photographs taken from Vero Beach at L + 101.9 sec showed what may possibly have been shroud fragments.
3. The *Atlas* rate gyros detected a pitch (down $\pm 22\frac{1}{2}$ deg) at L + 103.1 sec, which corresponded to the application of a 30- to 50-lb load for 10 msec through the spacecraft CG and normal to the vehicle roll axis. This initial downward pulse was followed by ringing at the second bending mode (12 cps) of the vehicle, which could be explained by material being blown from the bottom shroud surface and adhering to the spacecraft.
4. Approximately 0.23 sec after the start of the *Agena* first burn, an impact occurred; a second impact occurred 0.1 sec later, and a third 0.8 sec later. Each succeeding shock was of increasing magnitude. The data appeared to indicate that impact between the shroud and the *Agena* or spacecraft occurred several times during that period.
5. Injection energy corresponded very closely to the energy that would have been achieved had the shroud not been ejected.
6. Oxidizer depletion occurred during the *Agena* second burn. With the indicated nominal *Agena* engine performance, this could have occurred if an additional mass of significant size had been present throughout both burns.
7. The Magnetometer detected magnetic fluxes with the periodicity of the gas valves being actuated. These could only have been sensed if the solenoids were near the Magnetometer.
8. No bona fide cosmic dust hits were observed.
9. The received power level showed up to 20-db variation in a few seconds rather than the 2 to 4 db predicted from the nominal antenna pattern. Large rapid variations, similar to those observed in the received signal level, could have been caused by interference patterns between the parasitic antenna on the shroud and the distorted pattern from the low-gain antenna.
10. The solar panels showed no sign of illumination, i.e., no current was drawn from them. Solar panel deployment events were not seen.

11. The Sun sensors appeared to have a broad null region, greater than 180 deg. This would have been impossible unless the primary Sun sensors, mounted on top of the octagon, had not been illuminated and the acquisition Sun sensors, mounted at the bottom of the octagon, had been partially shaded.

12. The Sun gate sensor, with its 10-deg field of view, gave no telemetry indication.

13. The antenna pattern was of sufficiently fine structure to permit variations of 12 to 16 db to be seen every few seconds, whereas the expected variations were 2 to 4 db over the same time interval.

14. The solar panel temperature, sampled every 4.2 sec in Data Mode 1, measured an approximately constant −30°F. These measurements were made on opposite solar panels, and more extreme variations between them would be expected (approximately a 50°F difference) if sunlight had been shining on the spacecraft. In addition, the measured temperature in sunlight would have been much higher.

15. The Trapped Radiation Detector and Ionization Chamber showed low-energy particle intensities, 100 times less than would be expected in that region of space. It must be concluded that the field of view of the sensors was definitely obstructed. This would indicate that the shroud was at least as low as the top of the octagon.

16. Earth detector readings made when the gyros were off indicated an illumination level that could only have been a reflection from the fairing; this level could not have represented direct illumination of the cell.

17. In general, temperatures measured at points above the top of the octagon were lower than expected. The temperature sensors would nominally have been exposed to the Sun; they were designed to dissipate solar input in accordance with variations in temperature control. Obviously, no solar input was present.

The spacecraft responded properly to all commands transmitted to it. Actually, 17 commands were sent (11 direct commands and 6 quantitative commands). The 6 quantitative commands were the duration commands for pitch, roll, and motor burn for the two maneuvers attempted. The direct commands were DC-1, DC-13, DC-14, DC-15, DC-19, DC-25, DC-26, two DC-27's, DC-28, and DC-29. This represents about one-third of all the available commands.

Deck skips, observed at various times during the flight, occurred primarily at times when the power on the spacecraft was being switched; similar situations had been noted during system testing. In addition to the low deck skip, a severe transient struck the spacecraft at 22:48:00. It reset the 60-word counter in the data encoder during a science frame and consequently reset the high-rate deck to the telemetry channel 100 synchronization word. The Plasma Probe was noted as skipping 61 steps in its cycle at approximately the same time, and the Cosmic Dust Detector recorded two film penetrations (one on each side of the plate) also at about the same time. There are no explanations for these anomalies.

An incremental step of telemetry channel 220 from a digital number of 20 to a digital number of 21 was noted when the gyros went off at 23:10:04 with the transmission of DC-15. Gyro power transients have been known to cause deck skips, but this phenomenon occurred for the first time.

2. *Mariner IV* Summary

Mariner IV was launched from AFETR LC 12 at 14:22:01.309, November 28, with an inertial launch azimuth of 90.5 deg East of North. After liftoff, the booster rolled to an azimuth of 91.4 deg and performed a programmed pitch maneuver until booster cutoff. During sustainer and vernier stages, adjustments in vehicle attitude and engine cutoff times were commanded, as required, by the ground guidance computer to adjust the attitude and velocity at *Atlas* vernier engine cutoff.

After *Atlas/Agena* separation, there was a short coast period before the first ignition of the *Agena*. At a preset value of sensed velocity increase, the *Agena* engine was cut off. At that time, the *Agena*/spacecraft combination was coasting in a nearly circular parking orbit in a southeasterly direction at an altitude of 188 km and an inertial speed of 7.80 km/sec.

After a parking orbit coast time of 40.87 min, which was determined by the ground guidance computer and transmitted to the *Agena* during the *Atlas* vernier stage, a second ignition of the *Agena* occurred. The *Agena* was cut off with the *Agena*/spacecraft combination in a nominal Earth–Mars transfer orbit 96 sec after the second ignition.

Injection (second *Agena* cutoff) occurred at 15:04:27.2 over the Indian Ocean at a geocentric latitude of −26.25

deg and a geocentric longitude of +68.82 deg. The *Agena*/spacecraft combination was at an altitude of 197.2 km and was traveling at an inertial speed of 11.443 km/sec. At 15:05:50.2, the *Agena*/spacecraft entered the Earth's shadow. The *Agena* separated from the spacecraft 1 min, 18 sec later. At 15:17:34.8, *Mariner IV* left the Earth's shadow after being in the shadow for a total of 11 min, 44 sec. Within an hour after injection, the spacecraft was receding from Earth in an almost radial direction with decreasing speed. This reduced the geocentric angular rate of the spacecraft (in inertial coordinates) until the angular rate of the Earth's rotation exceeded that of the spacecraft.

The CC&S L-1 event (deploy solar panels and unlatch scan platform) occurred at 15:15:05. The CC&S L-2 event (turn on attitude control) occurred at 15:19:02, which was 0.691 sec off the nominal time for the event. Event readings indicated the proper step in event register No. 2. Sun acquisition was completed at 15:31:04, and was confirmed by a step-up in event register No. 4.

The deployment of the solar panels and the beginning of Sun acquisition occurred on time following *Agena*/spacecraft separation. Sun acquisition was completed by 15:31:04.

The pyrotechnics operated normally at separation. Both channels were armed and all expected indications for solar panel deployment and scan platform unlatch were received, which indicated proper operation of the pinpullers. Pyrotechnic current indications were also seen at the CC&S L-1 event, which was not considered abnormal since pinpullers have a possibility of shorting after they have been fired. Telemetry indicated that the VSS launch mode was turned off on time.

Deck skips and resets were observed between 16:59:00 and 17:22:35, although performance before and after that time was nominal. During that period, the encoder saw 7 high-rate resets, 17 medium-rate skips and resets, and 15 low-rate skips and resets. All data observed during this 23-min period looked good with no significant change to any of the engineering measurements. The cause of this anomaly has not been determined.

The CC&S L-3 event (initiate Canopus acquisition) occurred on time at 06:59:01, November 29, and an object was acquired at 07:10:03. The L-3 event was confirmed by an event register No. 2 indication. (The event registers then read 1754.) The start of the Canopus acquisition sequence was at a clock angle of 60 deg with Canopus as reference. The object acquired was at a clock angle of 119 deg (in the vicinity of Markab). The next object acquired was the star Alderamin at a clock angle of 115 deg.

The gyros came on again at 13:12:57 and roll search was started. The gyros went off at 13:29:20, and the star Regulus was acquired at a clock angle of 279 deg. Since the first cyclic pulse occurred on time at 16:59:10, November 29, it was decided to transmit the necessary radio commands for Canopus acquisition after Goldstone acquired the spacecraft on November 30.

The first DC-21 command was transmitted at 09:13:00 November 30, and was verified at 09:13:55. Roll search started and continued until the gyros went off at 09:20:52. The star acquired was tentatively identified as Naos. A second DC-21 command was not transmitted until 10:45:00 because of science calibrations. The second DC-21 resulted in a roll search of short duration. The object reacquired was either the same object or a new object identified as Gamma Velorum.

A third DC-21 was transmitted at 10:57:09; gyros came on and roll search was started. An object was acquired at 10:59:26. The gyros went off at 11:02:47, and the expected saturated Earth detector reading was observed. The object acquired was determined to be Canopus by the light intensity observed by the Canopus sensor and by the saturated condition of the Earth detector.

All temperatures were near stabilization with the exception of those at Bays I, VII, and VIII, which ran hotter than equilibrium because of the activity of the gyros during the Canopus acquisition sequence. Temperatures were about eight degrees lower than anticipated, but were well within the tolerance allowed. Several of the temperatures were considerably cooler than expected: the Magnetometer was 20°F cooler, the Ionization Chamber was 30°F cooler, and the solar panels were 15°F cooler. Even with the lower temperatures, it is expected that all subsystems will remain within operating limits through the encounter phase.

The data acquisition system cruise calibrate sequences occurred on time. At 13:42:00, approximately 3 hr after Canopus acquisition, a transient was observed on the spacecraft roll channel. Cross-coupling effects were also

noted on pitch and yaw channels. The transient did not cause loss of acquisition and its effects gradually diminished. The cause of the transient is unknown.

On December 1, the spacecraft temperatures were fully stabilized. All temperatures were within operating ranges. The propulsion system appeared normal with no evidence of leakage. Attitude control gas consumption was detected. At 10:10:00 December 2, the spacecraft roll axis momentarily dropped lock on Canopus and the gyros came on. Canopus was reacquired almost immediately and the gyros went off after their minimum run time. The first solar vane movement was detected on the +X vane at 04:48:00 December 2.

The *Mariner IV* trajectory correction maneuver scheduled for December 4 was inhibited by ground command. The sequence of planned maneuver events was followed through receipt of DC-27 by the spacecraft. Almost immediately after the spacecraft responded to DC-27, Canopus acquisition was lost and a roll search was begun. A successful maneuver requires that roll and pitch stabilization be maintained by star lock and Sun lock until the time of the maneuver pitch turn. The maneuver was inhibited by a DC-13 at 14:47:13 December 4, after Canopus lock was lost. Sun lock remained stable during that period. The maneuver clock continued to run, which is normal after DC-13, and issued the maneuver events at the proper times. No spacecraft reaction occurred, which is proper following a DC-13 command.

The spacecraft continued to roll until 14:52:00, when the first object was acquired. The DC-21 commands were transmitted at 15:22:00, 15:32:00, and 16:02:00, and short-duration roll searches occurred for each DC-21.

It was decided to discontinue the attempt to acquire Canopus during the Goldstone pass since little time remained in the Goldstone view period.

Woomera acquired the spacecraft at 14:15:19 December 4. At 21:53:45, DSIF Net Control advised Woomera that command procedures were to start for the acquisition of Canopus. Command modulation was turned on at 22:14:30, and telemetry channel 104 indicated command loop in lock at 22:24:25. The first DC-21 command was transmitted at 22:40:00. Two more DC-21 commands were transmitted to the spacecraft, which resulted in Regulus acquisition being confirmed at 23:33:14. Three additional DC-21 commands were transmitted to the spacecraft, and, at 23:59:22, the acquisition of Canopus was confirmed.

The second attempt to perform the midcourse maneuver occurred on December 5, when it was successfully completed at 16:44:00.

XXIV. SYSTEMS ANALYSIS AND MISSION PLANNING

In this Section, the term systems analysis covers the activities of defining a standard set of flight paths to a planet, the analysis of correction maneuvers to the standard flight path, and the operational determination of the actual flight path from radio tracking data.

The term mission planning covers those activities concerned with analyzing mission trade-offs, such as launch constraint analysis, range safety waiver requests, models of mission-success probability, studies of planet-contamination probability, and launch period and launch window planning.

A. Mission Planning

1. Studies of Impact Probability

To protect Mars from possible contamination by viable organisms from Earth, the National Aeronautics and Space Administration set the policy that any unsterilized spacecraft launched to Mars must have less than a 10^{-4} probability of accidental impact with the planet. The efforts and analyses carried out to ensure that the probability of accidental impact by the *Mariner* spacecraft or the *Agena* is less than 10^{-4} are described briefly here. A more detailed analysis and explanation is contained in Ref. 35.

The *Mariner III* spacecraft was to be aimed at launch to send the spacecraft to the nominal aiming point. Expected dispersions in the injection conditions, however, would require a trajectory correction maneuver. The maneuver would attempt to place the spacecraft on a trajectory passing through the nominal aiming point. If the initial correction failed to achieve an acceptable planetary encounter, a second maneuver would be available. It was obvious that following injection and one or both trajectory corrections there would be a finite possibility of having attained an impact trajectory by accident. Following injection, the *Agena* would perform a yaw maneuver and would fire a solid retro-rocket in order to ensure that the *Agena* stage would have the less than 10^{-4} probability of impacting the planet.

The *Mariner IV* mission profile differed from the *Mariner III* profile in one important aspect. The spacecraft was to be aimed at launch to pass sufficiently away from the planet that the probability of impact at injection would be less than 10^{-4}. This would allow for the removal of the *Agena* retro-rocket, with a subsequent increase in energy from the launch vehicle due to the decreased weight, and a lengthening of the launch period by about 4 days.

The overall probability of the spacecraft or *Agena* or both impacting the planet was the sum of eleven probabilities (Fig. 404). In order to compute the individual probabilities, the following assumptions were made:

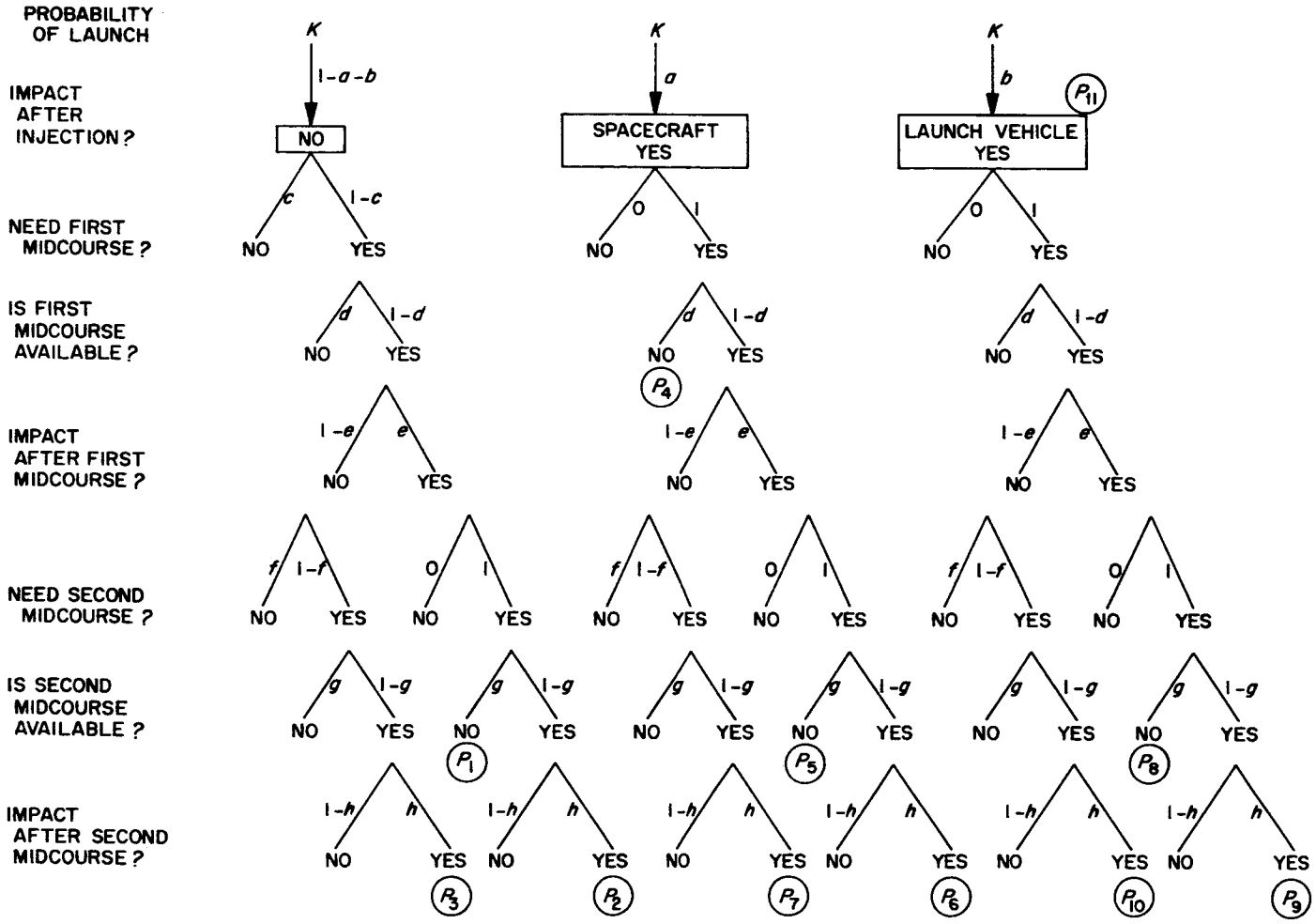
1. The probability of the spacecraft or the *Agena* impacting the planet at injection (before retro on the *Agena*), without a biased trajectory, was 2×10^{-3}. This figure was found by mapping the injection dispersions given by the covariance matrix of injection errors to the planet, and by integrating over the planet capture radius.

2. The probability of the *Agena* impacting the planet after the retro-maneuver was 10^{-5}. This figure was found by multiplying the probability of impact before retro by the probability of an unsuccessful retro-maneuver.

3. If nominal nonbiased trajectories were used, the probability of requiring a midcourse correction to the trajectory, even though the spacecraft was not on an impacting trajectory, was 0.98. This figure was found by mapping the injection dispersions to the planet and integrating over the area in which an acceptable encounter occurred.

4. The probability of requiring a midcourse correction if the trajectories were biased was 1.0.

5. The probability that the spacecraft would be able to perform a midcourse correction, if one were required, was 0.97. This figure was derived from the assumption that the probability of the spacecraft being operable at injection was 0.98, and the probability of a successful motor burn, given an operable spacecraft, was 0.99. The probability of a successful second maneuver was 0.96 or 0.95. This figure was found by multiplying the probability of a successful first maneuver by the probability of the spacecraft surviving the time span between first and second maneuver. The time span between maneuvers was assumed to be 2 weeks maximum if the first maneuver resulted in impact, and 6 weeks



NO BIAS *AGENA* RETRO

$a = 0.002$

$b = 10^{-5}$

NO RETRO YES BIAS

$a = 0.9 \times 10^{-4}$

$b = 10^{-4}$

$c = 0.02$

$d = 0.02$

$e = 10^{-4}$

$f = 0.90$

$g = 0.03$

$h = 10^{-4}$

$k = 0.74$

$P_1 = (1-a-b)(1-c)(1-d)(e)(g)$

$P_2 = P_1\left(\frac{1-g}{g}\right)(h)$

$P_3 = P_1\left(\frac{1-e}{eg}\right)(1-f)(1-g)(h)$

$P_4 = (a)(b)$

$P_5 = (a)(1-d)(e)(g)$

$P_6 = P_5\left(\frac{1-g}{g}\right)(h)$

$P_7 = (a)(1-d)(1-e)(1-f)(1-g)(h)$

$P_8 = (b)(1-d)(e)(g)$

$P_9 = P_8\left(\frac{1-g}{g}\right)(h)$

$P_{10} = (b)(1-d)(1-e)(1-f)(1-g)(h)$

$P_{11} = b$

$P\left(\begin{smallmatrix}\text{SPACECRAFT}\\ \text{LAUNCH VEHICLE}\end{smallmatrix}\ \begin{smallmatrix}\text{YES}\\ \text{NO}\end{smallmatrix}\right) = K\sum_{i=1}^{7} P_i$

$P\left(\begin{smallmatrix}\text{LAUNCH VEHICLE}\\ \text{SPACECRAFT}\end{smallmatrix}\ \begin{smallmatrix}\text{YES}\\ \text{NO}\end{smallmatrix}\right) = KP_{11}$

$P\,(\text{BOTH YES}) = K\sum_{i=8}^{10} P_i$

$P\,(\text{ANY IMPACT}) = K\sum_{i=1}^{11} P_i$

	RETRO (10^9)	BIAS (10^9)
P_1	2875.0	2881.0
P_2	9.296	9.315
P_3	9295.0	9314.0
P_4	40,000.0	1800.0
P_5	5.88	0.2646
P_6	0.01901	0.00086
P_7	19.01	0.85545
P_8	0.0294	0.294
P_9	0.000095	0.00095
P_{10}	0.09505	0.9505
P_{11}	10,000.0	100,000.0
	RETRO (10^4)	BIAS (10^4)
$P\left(\begin{smallmatrix}\text{SPACECRAFT}\\ \text{LAUNCH VEHICLE}\end{smallmatrix}\ \begin{smallmatrix}\text{YES}\\ \text{NO}\end{smallmatrix}\right)$	0.386	0.1036
$P\left(\begin{smallmatrix}\text{LAUNCH VEHICLE}\\ \text{SPACECRAFT}\end{smallmatrix}\ \begin{smallmatrix}\text{YES}\\ \text{NO}\end{smallmatrix}\right)$	0.074	0.74
$P\,(\text{BOTH YES})$	0.0000092	0.000092
$P\,(\text{ANY IMPACT})$	0.460	0.844

Fig. 404. Model for computing the probability of planetary impact

maximum if the first maneuver did not result in impact. The difference in time resulted in the difference in probability.

6. The probability of requiring a second maneuver was 0.10. This was found by computing statistically the size of the first maneuver as a result of the injection dispersions. The dispersions in executing this maneuver were given by the covariance of execution errors, and were then mapped to the planet and integrated over the region of acceptable planetary encounter.

7. The probability of impact following a maneuver was, at most, 10^{-5}. This probability was found by mapping the dispersions from the execution of the midcourse maneuver to the planet and integrating them over the planet capture area. This quantity was highly sensitive to the size of the maneuver and the miss distance to be corrected.

8. The probability of a successful launch was assumed to be 0.74. By using the assumptions in the model shown in Fig. 404, the eleven individual probabilities could be computed from the above estimates, and the total probability of planet impact was computed to be approximately 0.9×10^{-4}.

In addition to the possibility of contaminating Mars by accidental impact, the planet might also be contaminated by viable particles expelled from the spacecraft as it passed the planet. These particles would come from the gas expelled by the attitude control jets, the gases expelled by the midcourse motor, and the outgassing from the spacecraft.

Particles outgassed from the spacecraft would have a negligible probability of contaminating the planet for two reasons. First, since the temperature of the spacecraft would be highest during the early phase of flight, it was expected that what little outgassing did occur would take place at that time, subjecting the particles to months of ultraviolet radiation. Also, the ratio of area to mass of the particles outgassed would be from 10^3 to 10^6 times that of the spacecraft, and, hence, the effect on the trajectory of the particles due to solar pressure would be proportionately larger than on that of the spacecraft. The spacecraft nominally would be perturbed about 20,000 km off course by solar pressure. Even if the particles survived the ultraviolet environment, they, too, would undoubtedly be perturbed by solar pressure considerably off an impact course.

It was estimated that the probability of viable organisms being expelled from the midcourse rocket motor was essentially negligible because of the extremely high temperature environment the particles must survive. Even if a viable organism survived, it would then have to travel at least 200 days through space to encounter Mars, since the midcourse maneuver would occur within the first few days of the mission. During that time, the particles would be exposed to continuous ultraviolet radiation with a high probability of destruction. In addition, the particle trajectory would be radically different from the spacecraft trajectory.

The question of the probability of viable organisms in the attitude control gas impacting the planet was somewhat more complex, since the gas jets might operate in the close vicinity of the planet. In that event, a small amount of the gas might impact the atmosphere of Mars if there were no further perturbations. However, four considerations were involved in that determination:

1. The control gases would leave the spacecraft with a relative velocity of 0.7 km/sec, which implies that they would follow a considerably different flight path than that of the spacecraft.

2. The flight time to the planet would be measured in days or hundreds of days except for those particles expelled near the planet, and it was reasonable to expect that the interplanetary environment would destroy any viable organisms except those emitted very near the planet.

3. With the solar sail control system functioning, the number of attitude control jet actuations was expected to be reduced almost to zero, except during maneuvers; thus the amount of gas expelled was expected to be very small.

4. The effect of solar pressure on the emitted particles would be 10^3 to 10^6 times greater than on the spacecraft. Particles emitted anywhere but very near the planet would be blown far away from the planet. It was considered highly unlikely that any viable organisms emitted prior to a few days before encounter would enter the Mars atmosphere.

A further study was made to estimate the probability that particles ejected near the planet would impact it. It was assumed that viable particles would be expelled at constant velocity and would be uniformly distributed in an exhaust cone about the jet-nozzle axes. It was also assumed that only one out of every thousand organisms

in the attitude control subsystem would be expelled during that period because (1) the control jets would, in all likelihood, not be operating due to the solar sails, and (2) some would already have been expelled during the flight. Assuming a 15,000-km miss distance, the number of particles n to enter the planet's atmosphere was computed to be

$$n = 0.26 \times 10^{-8} N$$

where N is the assumed number of viable organisms in the system.

The filtering system in the attitude control subsystem would keep it extremely clean but not sterile; some viable organisms would exist. (To estimate the number closely was difficult.) The U. S. Army Biological Laboratories in Fort Detrick, Maryland, reported that it found white, gram-positive rods and some yellow, gram-positive cocci in bottled nitrogen. The maximum number of colonies found (in the three commercially filled tanks tested) in 16 lb of nitrogen was 12. The spacecraft gas tanks were assembled and filled in ultra-clean rooms, under conditions much cleaner than those used for manufacturing and filling the commercial bottles. There was, therefore, no reason to believe that the spacecraft tanks were any more contaminated than the commercial tanks. On that basis, the two 2½-lb spacecraft tanks contained approximately four viable organisms.

All attitude control nitrogen from the spacecraft tanks had to pass through two filters in series. Each filter was efficient enough to prevent less than one 0.3 μ particle in 100,000 from passing through it. Laboratory experience at Fort Detrick and at the Communicable Disease Center of the Public Health Service indicated less than one failure in 100 of these filters. Thus, the probability of ejection of a single viable microorganism from the nitrogen attitude control jets equalled the number of available microorganisms times the composite probability of failure of the two filters in series, or 4×10^{-4}. Substituting this value of N for the number of viable organisms expelled by the attitude control subsystem yielded a composite probability of impact on Mars by a viable organism of less than 10^{-12}.

In summary, it can be stated with considerable assurance that outgassing, particle ejection from the midcourse motor, and particle ejection from the attitude control jets have a negligible probability of impacting and contaminating Mars.

2. Launch Constraints Analysis

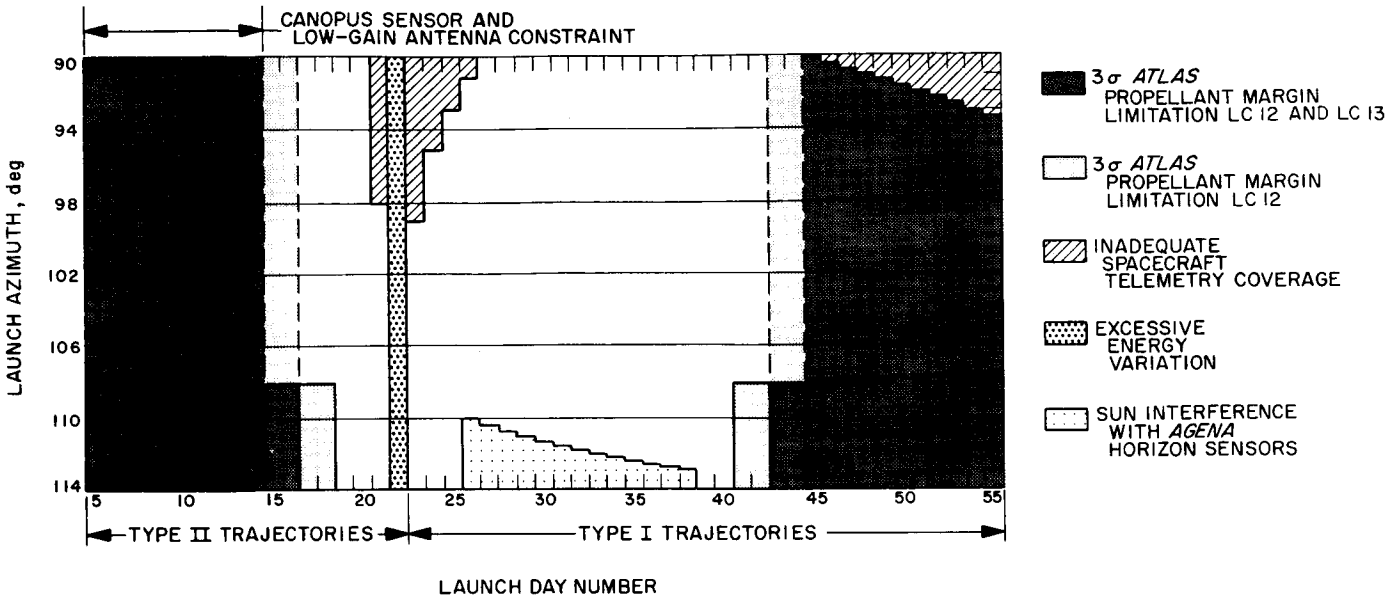
The purpose of the launch constraints analysis was to define all the constraints affecting the launch of *Mariner III* and *Mariner IV* brought about by the Spacecraft System, Launch Vehicle System, Space Flight Operations System, and the Deep Space Network System.

A summary chart of the launch constraints resulting from a preliminary analysis is presented in Fig. 405. There appeared to be no constraints imposed by the spacecraft system other than the one due to the Canopus sensor and low-gain antenna operational characteristics. These characteristics indicated that any launch day prior to day 15 was unfavorable. (For security reasons, the launch period was considered in terms of day numbers, with October 21, 1964 as day 1.)

Performance of the Launch Vehicle System limited the launch period to day 5 through day 55. A preliminary analysis indicated, however, that, if the requirement for 3 σ propellant margins were to be honored, the launch period would have to be constrained to days 15 through 44 for the *Atlas* 289D/*Agena* 6931 launch vehicle combination on LC 13, and to days 17 through 42 for the *Atlas* 288D/*Agena* 6932 launch vehicle combination on LC 12. Launch day 22 was eliminated from the launch period for several reasons.

If the requirement for 3 σ propellant margins in the *Atlas D* were to be honored, then the launch windows on days 15 and 16 would have to be truncated at a launch azimuth of 108 deg, which made the azimuths from 108 to 114 deg unavailable for launching. The other known constraint that was imposed by the *Atlas D* on the launch windows was the maximum permissible cold-soak time after liquid oxygen loading began. It appeared that launch window durations of at least 2 hr would be available. The maximum acceptable LOX topping time was established to be at least 3 hr.

The *Agena D* restart timer was not capable of accommodating variations of more than 810 sec in parking orbit coast time within a given launch day. For that reason, it was not always possible to use the full launch azimuth corridor between 90 and 114 deg, which was particularly true on launch days when injection occurred downrange. Also, the restart timer had a limited capability of supporting a launch period of more than 4 days, because the *Agena D* timer could only use a maximum of four "patch plugs." (These plugs provided the gross



NOTES:

(1) TELEMETRY COVERAGE CONSTRAINTS WERE BASED ON JPL-ASSUMED AFETR SHIP LOCATIONS WITH REALISTIC RANGE RESTRICTIONS; THEY WERE NOT BASED ON AFETR COMMITTED COVERAGE

(2) TRACKING AND TELEMETRY COVERAGE PLAN WAS BASED ON TWO SHIPS POSITIONED IN THE INDIAN OCEAN AND ONE SHIP IN THE SOUTH ATLANTIC.

(3) TEN MINUTE LOCKUP TIME ON SPACECRAFT TELEMETRY (S-BAND) WAS ASSUMED FOR WOOMERA DSIF TO SHOW WORST POSSIBLE CASE. (CLASS I REQUIREMENTS WERE BASED ON A LOCKUP TIME OF 2 min.)

Fig. 405. Preliminary summary launch constraints for *Mariner* Mars 1964

variations in parking orbit coast time necessary to support a second burn.) It was anticipated that for the *Mariner III* and *IV* launch period, a few days at most would have their launch windows slightly truncated.

It was required that the *Agena D* be removed and revalidated after 28 days on the launch pad if it had not been mated, or after 15 days if it had been mated. The revalidation would require about 6 days if it had not been mated and 10 days if it had been.

The *Agena* horizon sensors could respond improperly to cloud masses within their field of view; cold clouds in the vicinity of the ascent trajectory could induce error signals in the *Agena* guidance system, since the sensors interpret the coldness of the clouds as the coldness coming from space. The reported cold-cloud formation was put into a computer program to determine the amount of midcourse maneuver required to correct for trajectory errors induced by the cold clouds. It turned out that for both *Mariner III* and *Mariner IV*, the largest midcourse maneuver required for this effect was only about 10 m/sec, as compared to the total available midcourse maneuver capability of 87 m/sec. Thus, the cold clouds did not create a constraint to the launch windows.

The *Agena D* horizon sensors would not function properly if the Sun was in their field of view. In the preliminary analysis, a constraint resulting from such a problem had been established to begin on day 26 at a launch azimuth of 110 deg (Fig. 405). This constraint decreased to a launch azimuth of 113 deg on day 39 when the restriction ended.

Adverse weather conditions could have resulted in a launch hold. Such conditions were:

1. Excessive surface winds and/or excessive wind shear.
2. Excessive clouds or excessive rain in the line-of-sight path to the *Atlas*. These clouds could cause excessive attenuation of the guidance signal. Maximum tolerable precipitation at the launch site, as well as minimum ceilings, could further restrict the launch.

The SFO System imposed no constraint. The minimum turnaround time between launches of 2 days permitted the SFO System personnel to support both launches on a continuous basis.

The following DSN communication links had to be operating satisfactorily prior to launch:

1. A voice line and a TTY line from the SFOF to the JPL Operations Center at Cape Kennedy.
2. Communications between Cape Kennedy and Antigua (or alternate), and communications between Cape Kennedy and the tracking station(s) providing the post-second-burn tracking data.
3. TTY line(s) between the SFOF and the mandatory DSIF station(s).

The determination of tracking- and telemetry-coverage inadequacies was complicated by numerous operational considerations:

1. Positioning of range instrumentation ships, scheduled to support *Mariner* launches, so as to optimize the coverage capability throughout the launch period.
2. Assessment of the coverage capabilities of the range instrumentation ships for support to satisfy the Class I metric and telemetry requirements (i.e., the rss error in the estimate of miss components could not exceed 2250 km at I + 5 days).
3. Analysis of station-peculiar coverage constraints such as horizon masks, antenna constraints, lockup time requirements, atmospheric refraction.
4. Ascertainment of realistic station coverages. (This involved continuously reviewing the requirements placed upon AFETR and monitoring the responses to these requirements.)
5. Interfacing of the GSFC stations located at Bermuda and Carnarvon with AFETR stations in support of requirements for tracking coverage.
6. Interfacing of AFETR with the DSN.

Included in Fig. 405 are the launch window constraints due to inadequate Class I telemetry coverage as determined by the preliminary launch constraints analysis. The information shown was based on assumed AFETR range instrumentation ship locations and not on AFETR-committed tracking and telemetry coverage. It was also based on the assumption that it would take 10 min for Woomera to lock up on the spacecraft telemetry signal at S-band frequency.

Figure 405 shows no constraints due to a lack of tracking coverage. The launch windows on the days in the vicinity of day 22 and on the days following day 45 were truncated as a result of the lack of continuous spacecraft telemetry coverage after separation. Day 22 was completely eliminated by the telemetry coverage constraint.

A constraint that resulted from the inability to realistically deliver and analyze the AFETR tracking and telemetry data much before 36 hr dictated that at least one launch window (or one launch day) should elapse between launch attempts.

As a result of the number of days comprising the *Mariner* launch period, it was expeditious to form day groupings for the purpose of analyzing the tracking- and telemetry-coverage capabilities of AFETR and of the DSN. This had little effect on the analysis, since the ascent trajectories changed very little from one day to the next. The launch period was divided into 9-day groupings, with a particular day designated for each grouping to be used for the analysis.

On September 17, 1964, AFETR committed the range instrumentation ship Twin Falls for tracking and for launch vehicle and spacecraft telemetry reception support. The Sword Knot was committed for the reception of launch vehicle and spacecraft telemetry, and the Coastal Crusader was committed for launch vehicle telemetry reception. The Twin Falls and the Sword Knot were located in the Indian Ocean and the Coastal Crusader was located in the South Atlantic.

The locations of the range instrumentation ships specified by AFETR, with the appropriate slant range capabilities for telemetry reception, were included in the station view period computer program. The output of that program indicated the ship view capabilities for every 3 deg of launch azimuth from 90 to 114 deg. The tracking-coverage capabilities of the Twin Falls was not programmed, since it was horizon-limited for tracking and since there appeared to be more than sufficient tracking coverage of Class I requirements. The output from the station view period computer program was subsequently inserted into the plotting program and processed to produce coverages plotted on Earth maps and on view-period graphs. In addition to programming ship coverages, the AFETR and DSN land stations were also run

through the station view period computer program with a 0-deg elevation constraint. The task then remained to compare the land- and ship-station coverages with the coverage requirements to detect inadequacies in the coverage of the Class I requirements. In order to facilitate that effort, the available and required coverages were plotted on view-period graphs and Earth maps. A view-period graph is shown in Fig. 406 and an Earth map is shown in Fig. 407.

Upon receipt of the committed coverage of the Class I tracking and telemetry requirements, a comparison was made of the AFETR commitments with the coverages shown in the view-period graphs and Earth track maps generated at JPL. It was found that there was a close agreement, which provided a cross check on the AFETR commitments.

The final launch window designs are presented in Fig. 408, which is a photograph of the launch constraints board that was maintained in the JPL Operations Center at Cape Kennedy.

The available launch windows were kept current by a continuing analysis of changes to old constraints or by the creation of new ones and a revision of the launch windows as required. This process continued up until launch of the *Mariner III* and *Mariner IV*.

3. Range Safety Waiver Request

Before the launch of *Mariner III*, AFETR had permitted launches between launch azimuths of 93 and 111 deg to minimize the hazard to populated areas below the launch vehicle ascent path. However, because of the difficulty involved in accomplishing the Mars mission for the first time, it was necessary to maximize the probability of getting two successful launches during the 1964 launch opportunity, since another launch opportunity would not occur again until 1966. One of the ways to increase the probability of launching two vehicles was to maximize the size of the launch windows, thus maximizing the launch corridor. A written request was sent to AFETR Range Safety asking for a launch corridor from 90 to 114 deg. A waiver was granted that authorized a launch corridor for *Mariner* Mars spacecraft from 90 to 114 deg.

4. Model of Mission-success Probability

A mathematical model was evolved to determine the probability of obtaining various combinations of the *Mariner* Mars 1964 mission objectives. The model assumed that the mission and spacecraft could be divided into independent, functional blocks whose series and parallel combination comprised the total mission. Various parameters, which defined the independent functional blocks stochastically, were then introduced and the results were presented as functions of these parameters. The following assumptions were made:

1. The probability of a launch on any day of the launch period was established at 0.3.
2. The probability of a successful injection was set at 0.74.
3. A value of 0.98 was estimated to be the probability of the spacecraft being operable at injection.
4. For the time period during transit, the ratio of failure rates of components stored aboard the spacecraft to operational failure rates was estimated to be 0.
5. The ratio of probable component failure rates (as estimated by an analysis firm) to the failure rates for *Mariner II* was estimated to be 0.19.
6. The launch delay between the first and second launches was due to failure in the first launch.

Based on the above assumptions, the following probabilities for mission success were calculated:

1. The probability of obtaining at least one set of 3-month cruise data out of two programmed launches was 0.86.
2. The probability of obtaining at least one occultation, television, or fields and particles success out of two programmed launches was 0.81.
3. The probability of obtaining at least one occultation, television, or fields and particles success out of two programmed launches (given that one spacecraft was functioning properly at injection) was 0.80.
4. The probability of obtaining at least one occultation, television, or fields and particles success out of two programmed launches (given that both spacecraft were functioning properly at injection) was 0.96.
5. The probability of obtaining at least one set of occultation, television, and fields and particles successes out of two programmed launches was 0.49.

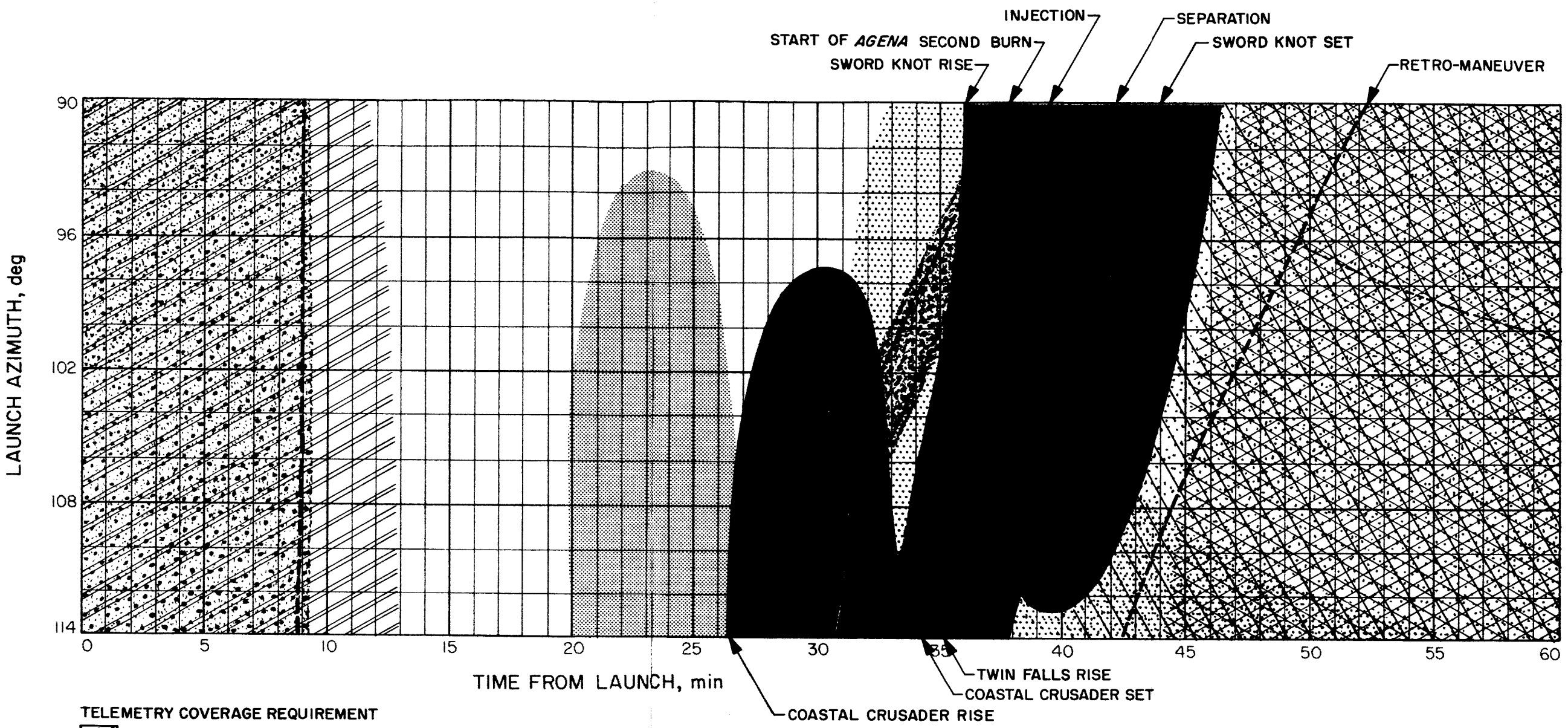


Fig. 406. AFETR and DSIF station view periods for Group I launch period

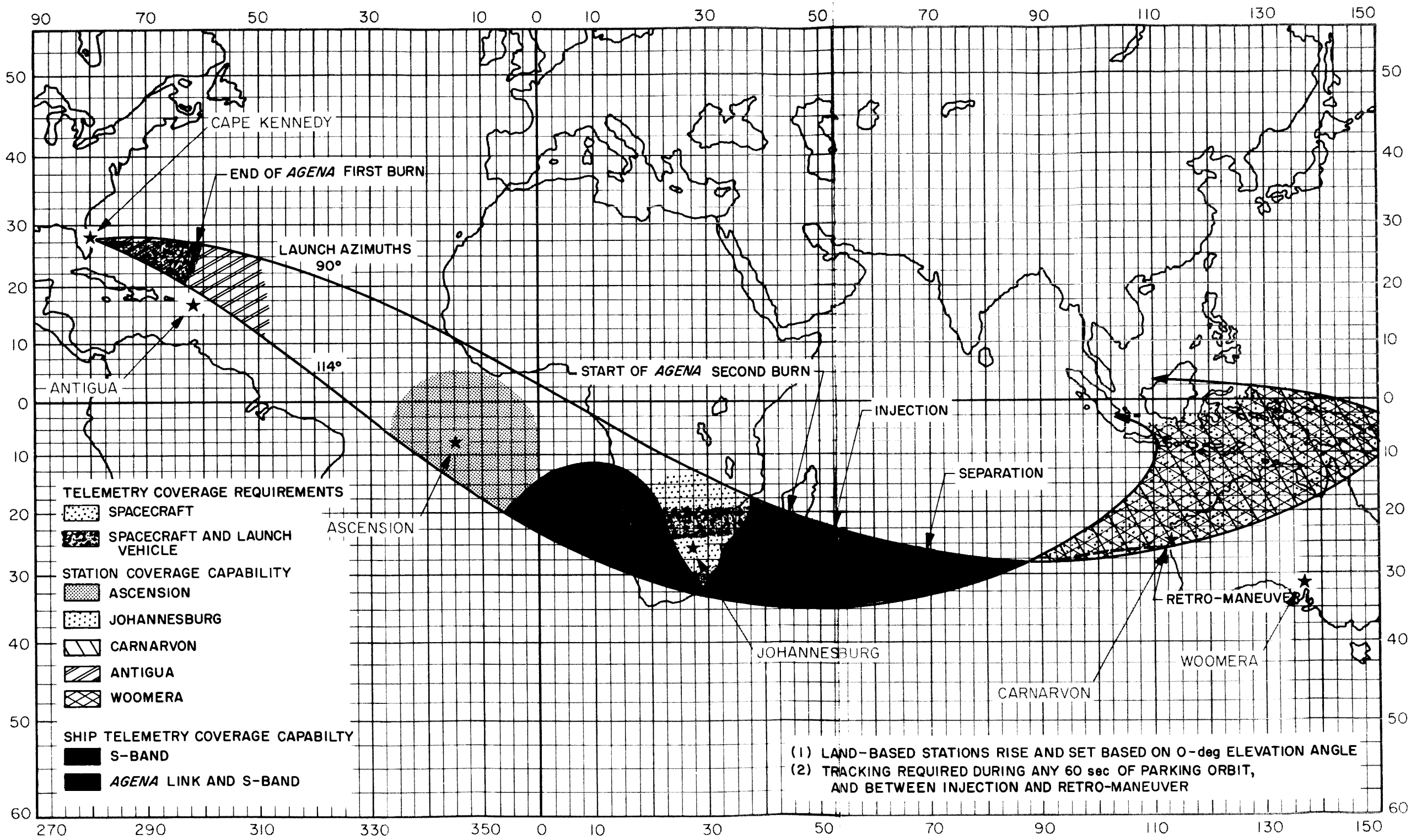
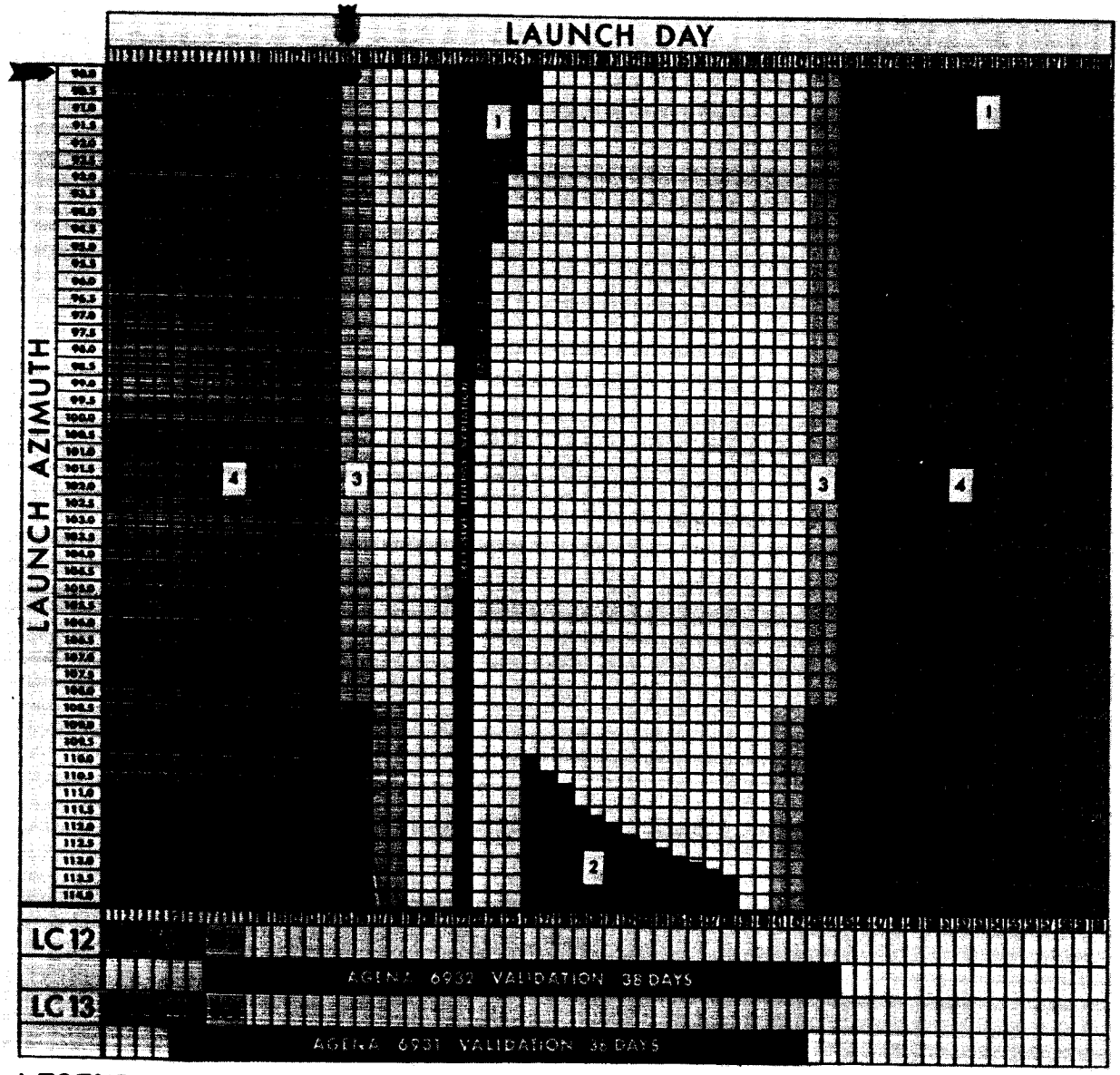


Fig. 407. Class I tracking and telemetry coverage for Group I launch period



LEGEND

(1) LACK OF CONTINUOUS SPACECRAFT TELEMETRY COVERAGE

(2) SUN INTERFERENCE WITH *AGENA* HORIZON SENSOR

(3) LAUNCH VEHICLE PROPELLANT RESERVES LESS THAN 3σ LC 12

(4) LAUNCH VEHICLE PROPELLANT RESERVES LESS THAN 3σ LC 12 AND LC 13

Fig. 408. *Mariner* Mars 1964 launch constraints

5. Tracking and Performance Panel Activities

a. 36-hr data-return plan. Included in the *Mariner* Mars 1964 mission objectives was the requirement to launch two spacecraft during the launch period. The two launchings were to take place as close as 48 hr apart. This close scheduling required early engineering evaluation of the first launch before full commitment of the second launch. To meet the need for early engineering evaluation of the first launch, it was necessary to perform a launch vehicle trajectory and subsystem performance analysis covering the period from liftoff through *Agena* retro-maneuver. It was further determined that, in order to be able to deliver a complete evaluation of the first launch to the mission director in time for a second launch 48 hr later, the necessary data from the AFETR downrange stations had to be delivered to Cape Kennedy within 36 hr of the first launch.

Since this requirement would not have been satisfied by the application of the usual data-return capabilities, a 36-hr data-return plan was devised by the Air Force by which especially dispatched aircraft were supplied downrange for the pickup and delivery of the necessary data. The plan specified that one C-130 aircraft was to be located at Antigua, two were to be located at Ascension Island, two at Mauritius, and one C-135 jet transport was to be located at the Jan Smuts Airport in Johannesburg. A C-130 was to pick up the data from the Coastal Crusader in the South Atlantic and deliver them to Ascension Island; the second C-130 would then fly the Coastal Crusader data and the Ascension Island data to Cape Kennedy. Data from the two ships in the Indian Ocean were to be taken first to Mauritius, then to the airport in Johannesburg, and subsequently flown to Cape Kennedy by the C-135.

b. Telemetry reader station. Since the fastest responsible delivery time of data from Johannesburg and from the two range ships in the Indian Ocean was about 36 hr, the analysis personnel at the Cape would be hard-pressed to analyze all the launch vehicle telemetry data in time for a 48-hr second launch attempt. In consideration of this difficulty, a telemetry reader station was established at Pretoria. Implementation of the reader station required that the data be displayed on oscillograph-type recorders for subsequent examination by launch vehicle engineers, specifically at the Pretoria station, for analysis of the telemetry data. There was a voice line available from Pretoria to Cape Kennedy for reporting the findings of this analysis.

c. AFETR S-band system. An S-band system was installed on the Twin Falls, the Sword Knot, and the Coastal Crusader. In addition, S-band systems were installed at Pretoria and Ascension Island.

These locations of the AFETR S-band systems were in operation for *Mariner III*. However, since, for various reasons, the S-band systems did not meet the mission requirements for the *Mariner III* flight, the number of stations capable of receiving S-band telemetry was reduced in order to double up equipment at the sites that did have this capability. As a result, the Pretoria station and the Sword Knot and Twin Falls ships had two receivers.

An RF compatibility test was conducted between the spacecraft transponder and the Cape Kennedy S-band system at Hangar AO. Two complete RF links were used in conjunction with the OSE. This test proved the compatibility of the S-band system with the spacecraft transponder.

d. Support by GSFC tracking stations at Bermuda and Carnarvon, Australia. Goddard Space Flight Center was requested to support the *Mariner* flights by providing tracking coverage at Bermuda and Carnarvon during the near-Earth phase of the mission. Bermuda coverage was requested because the position of the station enabled better tracking coverage for the early launch azimuths than such AFETR stations as Antigua. Carnarvon coverage was requested since injection was over the Indian Ocean, and that station had the advantage of providing coverage of Class I tracking requirements.

6. Operations Optimization

a. Delay of Agena *retro-maneuver.* A request was submitted to LeRC for a delay in the *Mariner* Mars 1964 *Agena* retro-maneuver for as long as practical within the *Agena* vehicle capability. The request was made in order to facilitate acquisition and tracking of the spacecraft in a critical phase of its trajectory. During appreciable portions of the launch windows, support of the Class I tracking requirement for 60 sec of *Agena* tracking between injection and retro-maneuver was dependent upon ship support. Because tracking data from land stations are of higher quality than data from tracking ships, it was desirable to obtain as much land-station tracking as possible. If the *Agena* retro-maneuver was delayed until at least 330 sec after separation, then Carnarvon would have the opportunity to provide at least 60 sec of post-retro-maneuver tracking data. In addition to providing land-station-quality tracking data, Carnarvon could

also be very useful in resolving discrepancies between other tracking stations, as well as act as a vital backup to the Woomera DSIF site.

In view of these considerations, LeRC rescheduled the *Agena* retro-maneuver from 200 sec after separation to 600 sec after separation. (This determination was based on the *Agena* vehicle capability.)

b.* Atlas *booster steering program. It was determined that a capability for *Atlas* booster steering would increase the probability of mission success, although such a capability could not result in the violation of any of the flight constraints. The constraints that had to be considered were the inflight bending moments, guidance, aerodynamic heating, and booster package staging. The bending moment and guidance constraints limited steering during earlier times of flight, whereas the staging and aerodynamic heating constraints dictated steering as soon as possible.

Based on the above constraints, steering was enabled about 100 sec after launch, and allowed steering commands from 100 to 110 sec. A preselected steering rate of 0.28 deg/sec was chosen, with a deadband corresponding to a 1.5 σ dispersion of the trajectories from their prescribed nominal. This steering maneuver was sufficient to correct 3 σ dispersed trajectories to 1.5 σ.

c. Auxiliary sustainer engine cutoff. A study to determine the effect of ASCO was performed by LMSC on *Mariner* Mars mission objectives in the event that the *Atlas* guidance failed. The results indicated that without a backup on the start–restart timer, which determined when *Agena* second burn would start, the mission objectives could not be satisfied in most cases with or without ASCO. In fact, for the 3 σ depressed case, an impact would result with ASCO, whereas without it the lowest parking orbit altitude obtained would be 62 nm. It was, therefore, decided to delete ASCO from the mission, since it did not help achieve the mission flyby objectives and could cause an impact prior to *Agena* second burn.

d. Simulated-launch and operational-readiness combined test. The simulated-launch and operational-readiness test was originally planned to be completely separate tests. The simulated launch involved the full countdown sequence of events up to L − 18 sec. The operational-readiness test was to begin after a simulated launch. However, in the actual launch, the prelaunch and postlaunch operations would be tied together at various interfaces, and it was felt that these interfaces should be simulated as closely as possible. As a result, the two tests were combined into one.

7. Mission Analysis of *Mariner III*

It has been fairly well established that the shroud did not eject from the *Mariner III* spacecraft. The nonstandard events that occurred early in the flight and that confirm this conclusion were as follows:

1. There was no change in the RF signal strength when the shroud should have been ejected.
2. *Agena* first burn was about 2 sec too long.
3. During *Agena* second burn, the oxidizer was depleted 1½ sec before the nominal cutoff.
4. The spacecraft separated from the *Agena* stage at a rate determined to be 28 in./sec, instead of at the designed rate of 32 in./sec.
5. The transfer orbit energy was substantially reduced.

The conclusions derived from these nonstandard events were:

1. The shroud was somewhat opaque to RF signals, which should have caused the signal to increase when the shroud was ejected.
2. Because it was still carrying the load of the 300-lb shroud, the *Agena* stage was required to consume more propellant (that is, burn longer) in order to attain the required parking orbit injection velocity.
3. Since much more propellant was consumed during *Agena* first burn than the nominal design called for, the oxidizer was depleted even before the nominal cutoff on second burn was reached.
4. The mechanism used for separating the spacecraft from the *Agena* stage was a system of compressed springs. The spacecraft separation rate was slower than expected, which indicated that there was more mass associated with the separation than only that of the spacecraft.
5. Since oxidizer depletion occurred during *Agena* second burn, the lower energy orbit was to be expected.

B. Trajectory Design

1. History and Analysis

The final standard trajectories used for the *Mariner* Mars 1964 mission were selected only after several itera-

tions between available trajectories and possible spacecraft designs. Parametric studies of the relationship between flight time, launch date, and injection energy were conducted to reveal acceptable launch intervals and trajectory characteristics. Upon gathering all physical limitations and determining the spacecraft subsystem constraints that were to be placed upon the flight path, the *Mariner* trajectories were then selected and computed precisely using a multiple-body computer program.

a. Parametric study of Mars trajectories for the 1964 launch opportunity. Approximately every 25 months, the injection energy required to effect a ballistic transfer from Earth to Mars becomes a minimum. To obtain the largest possible payload weight from the *Atlas/Agena* boost vehicle, it was necessary to launch near this period in 1964. Results of the trajectory studies are illustrated in Fig. 409 and 410. Two sets of closed contours representing two types of trajectories are presented. Type

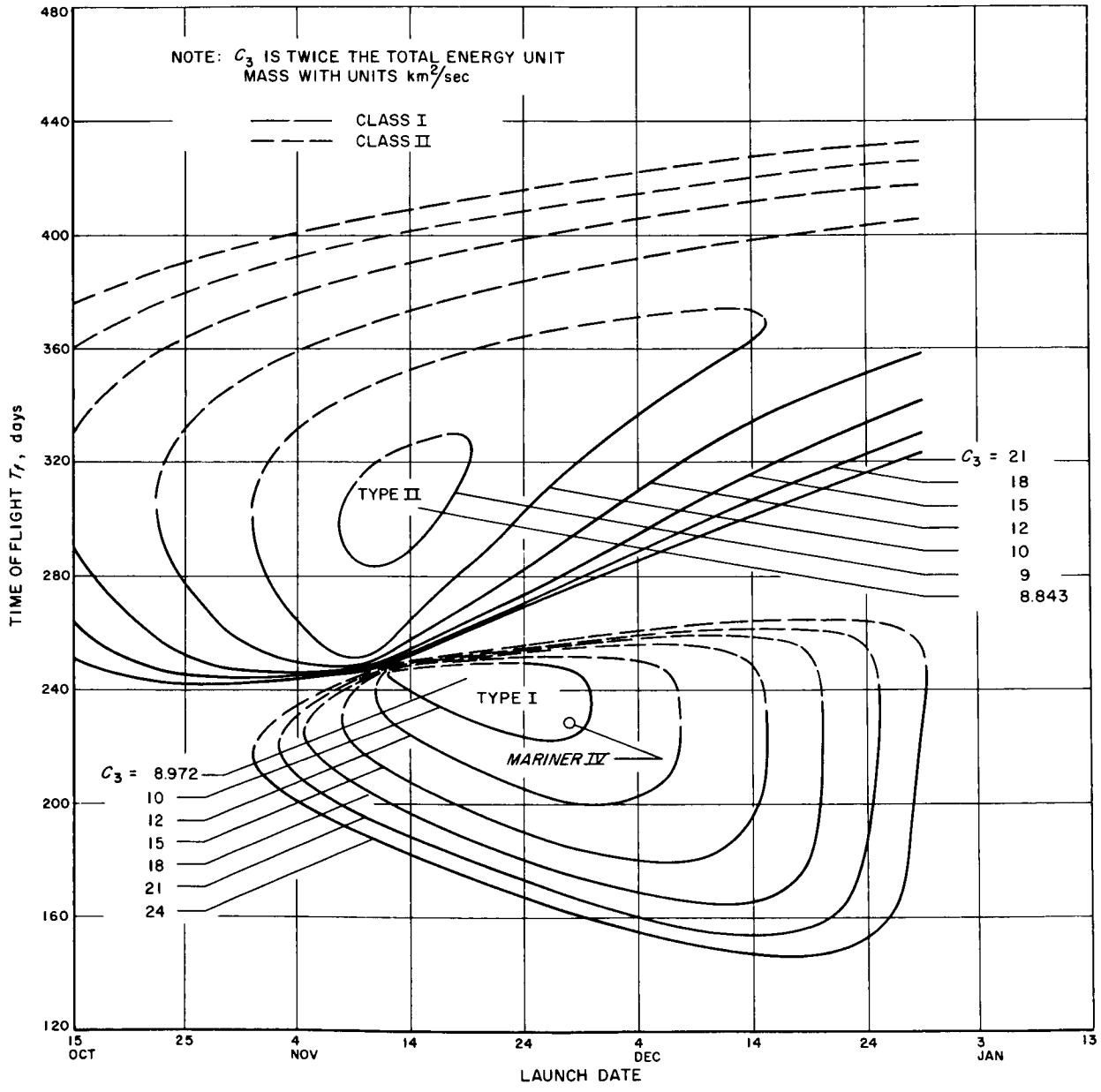


Fig. 409. Time of flight vs launch date

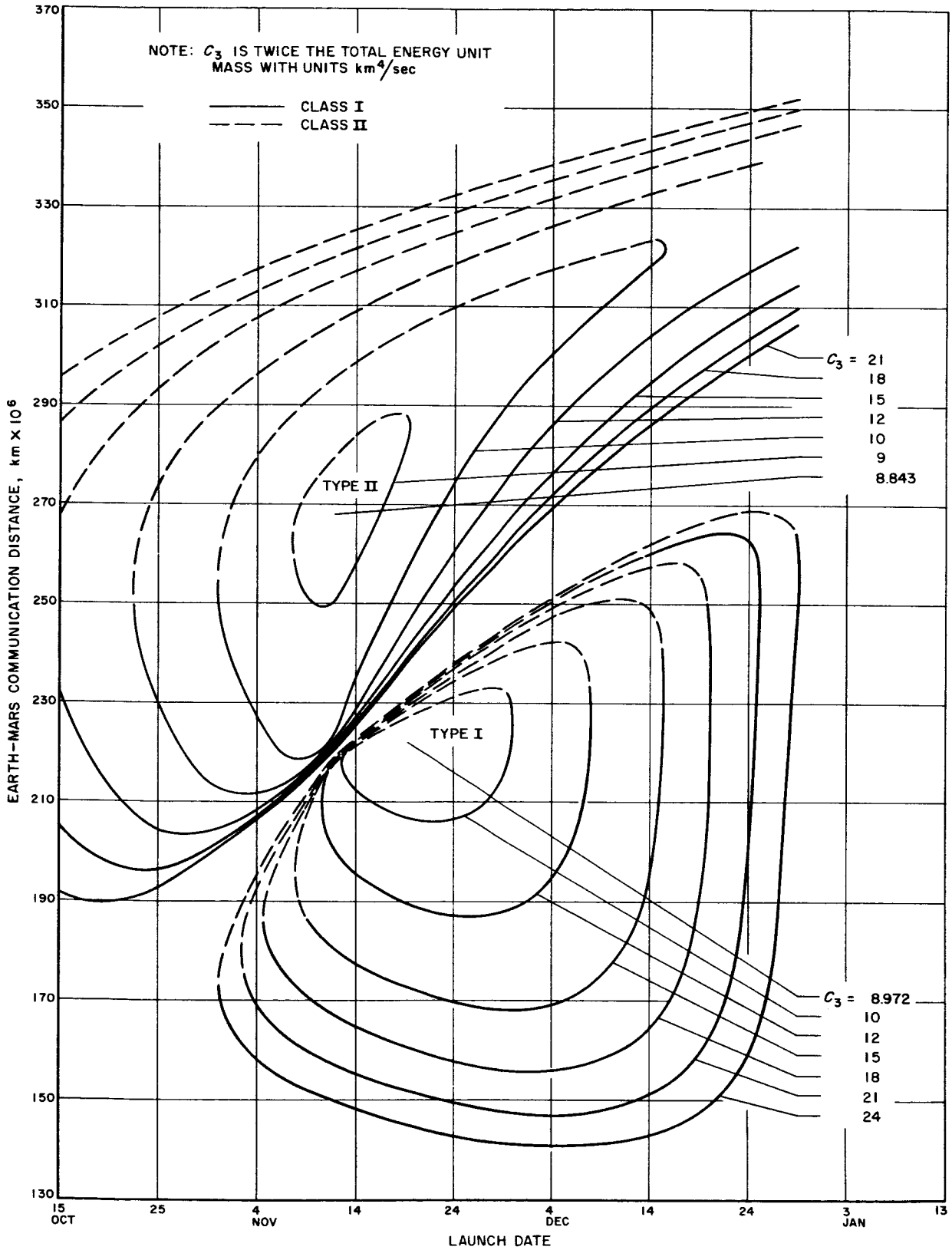


Fig. 410. Earth–Mars communication distance vs launch date

I trajectories are characterized by a heliocentric transfer angle less than 180 deg from launch to encounter. For Type II trajectories, the total transfer angle lies between 180 and 360 deg. It is worthwhile to note the following important properties of these trajectories:

1. Type II trajectories have longer flight times and communication distances at encounter.
2. For a given injection energy C_3 and launch date, up to four different trajectories are available.
3. For each of the trajectory types, there was a minimum energy transfer for each launch date, and absolute minimums occurred on November 19 for Type I (T_F = 228 days, C_3 = 8.972 km²/sec²) and on November 14 for Type II (T_F = 334 days, C_3 = 8.843 km²/sec²).
4. For a given energy above the absolute minimum, there is a corresponding launch interval or permissible firing period.

A more detailed description of the parametric study is given in Ref. 36.

b. Major mission objectives and ground rules. Certain basic mission objectives and ground rules were established to serve as a starting point in the trajectory selection and spacecraft design philosophy. Six of the major factors that proved decisive in the preliminary trajectory design were:

1. Obtaining scientific data during a close flyby to the planet Mars and transmitting these data back to Earth.
2. Using the *Atlas/Agena* launch vehicle and a 100-nm circular parking orbit.
3. Two spacecraft launchings with at least a 2-day arrival-date separation.
4. Launch from two separate Cape Kennedy launch pads with a maximum launch azimuth spread from 90 to 114 deg East of true North.
5. Attitude-stabilized spacecraft using the Sun and Canopus as reference bodies.
6. The maximum allowable Earth–spacecraft communication distance was approximated to be 250 million kilometers.

c. Overall trajectory design. The overall trajectory design involved parameters connected with the acceptance of Type II transfers, the selection of arrival dates, the firing period, and the selection of the aiming point and arrival time.

Acceptance of Type II transfers. To increase the probability of launching two spacecraft, a launch period composed of both Type I and Type II transfers was selected to provide a maximum number of launch days. Inspection of Fig. 409 and 410 reveals that the energy contours for both Type I and Type II transfers provided overlapping flight times and communication distances at encounter. In essence, this meant that there was almost a continuous transition in the trajectory characteristics when going from Type II to Type I transfers. This eliminated complications arising from large variations in angular relationships and distances between the spacecraft and various celestial bodies when switching trajectory types during the launch period.

Selection of arrival dates. After closely observing and checking all the Type I and Type II transfers, a decision was made to use trajectories with small variations in arrival date. Since the relative positions of Earth, Mars, and the Sun were fixed for a given arrival date, the selection of constant-arrival-date trajectories allowed the use of a fixed high-gain antenna. These trajectories also permitted the use of a fixed aiming point because of the relatively constant spacecraft approach direction and speeds, which imposed less stringent design requirements on both the planetary scan subsystem and the science experiments.

The use of a single arrival date, however, was not allowable because of the requirement of at least a 2-day separation between the Mars encounter of each spacecraft. The arrival dates selected were July 17 and 19, 1965 for the Type II trajectories, and July 15 and 17, 1965 for the Type I trajectories. These arrival dates resulted in transfers that were near minimum energy for each launch date, and ensured that a maximum firing period would be available once the spacecraft was built and once the maximum injection energy attainable by the *Atlas/Agena*/spacecraft combination was calculated.

The communication distances at encounter for these arrival dates varied from 216.3 to 220.4 million kilometers, with the 250-million-kilometer maximum to be reached approximately 25 days past encounter. This allowed sufficient time for two complete transmissions of the television picture data.

Firing period. Since there is a direct relationship between injection energy achievable from a given booster

and the weight of a spacecraft, a trade-off between firing period and spacecraft weight existed. A design goal of 575 lb for the spacecraft was finally established, which resulted in a firing period of approximately 27 days. By decreasing the performance reserves of the launch vehicle and removing the *Agena* command destruct system and retro-rocket, the launch period could have been extended to about 36 days.[11] Figure 411 plots the required injection energy C_3 versus launch date for the selected arrival dates, and depicts the increasing energy requirements as the launch period is lengthened.

Subsequent to spacecraft completion and establishment of the injection energy available for the allotted launch vehicles, a decision was made to schedule the first spacecraft launch on November 4, 1964. It was also decided that only one spacecraft was to be launched during the Type II firing period. Therefore, only one arrival date was required; the date chosen was July 17, 1965. However, for launch vehicle performance reasons, an arrival date of July 17 was not acceptable for launch on November 10, 1964 (Type II). Therefore, July 19 was selected as the arrival date for that launch day. Since it was possible for two launches to occur during the Type I launch period, the two arrival dates previously mentioned were selected. The launch- and arrival-date planning is illustrated in Fig. 412.

Aiming-point and arrival-time selection. Along with the selection of trajectories based upon the major constraints already enumerated studies had to be conducted to determine the region near Mars that would be the most desirable for flyby. The selection of this region

[11]Removal of the command destruct system and *Agena* retro-rocket was to be considered only in the event that it was impossible to launch both spacecraft during the nominal launch period. Permission to remove the command destruct system had to be obtained from NASA and permission to remove the *Agena* retro-rocket had to be obtained from AFETR.

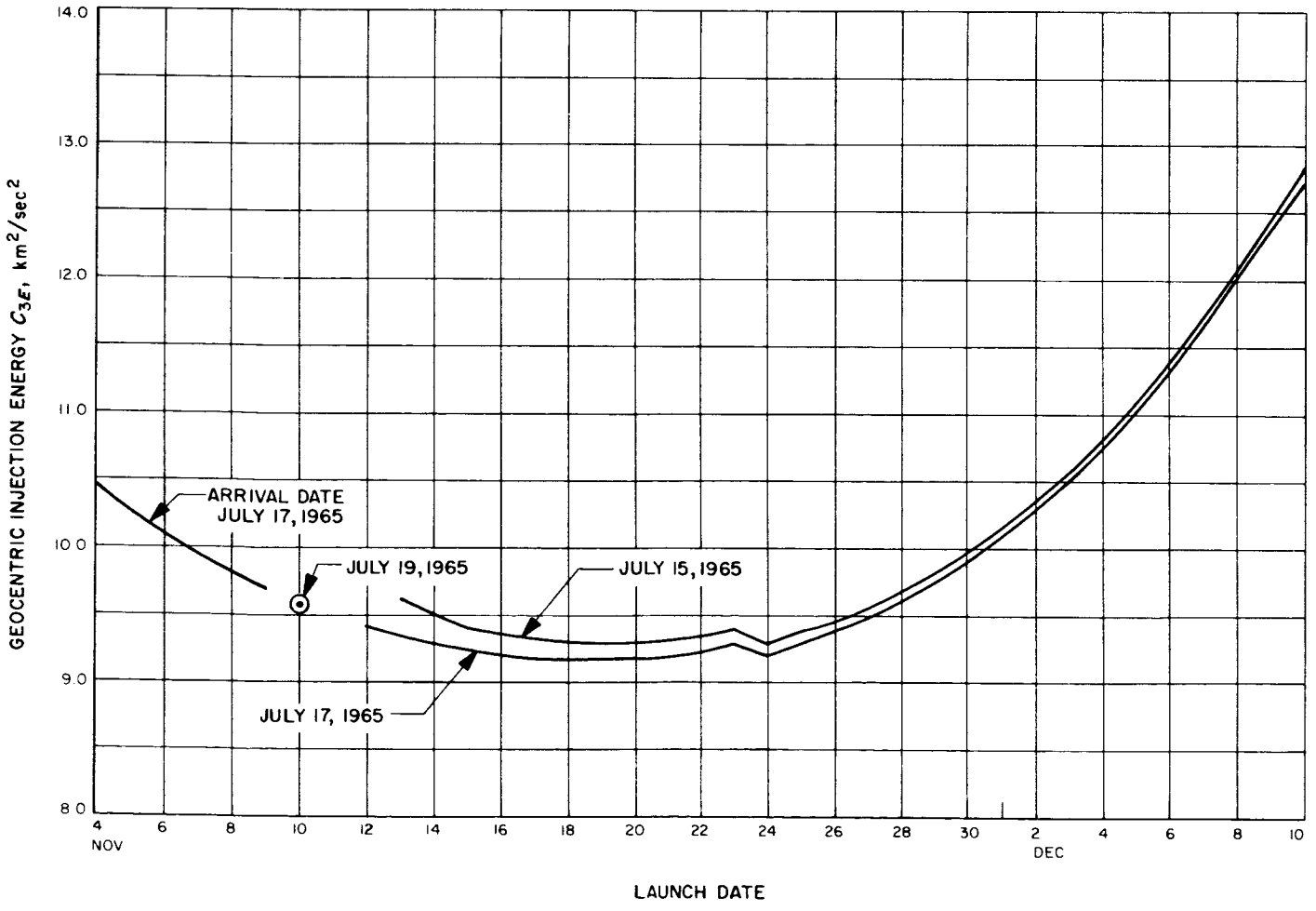


Fig. 411. Geocentric injection energy C_{3E} vs launch date

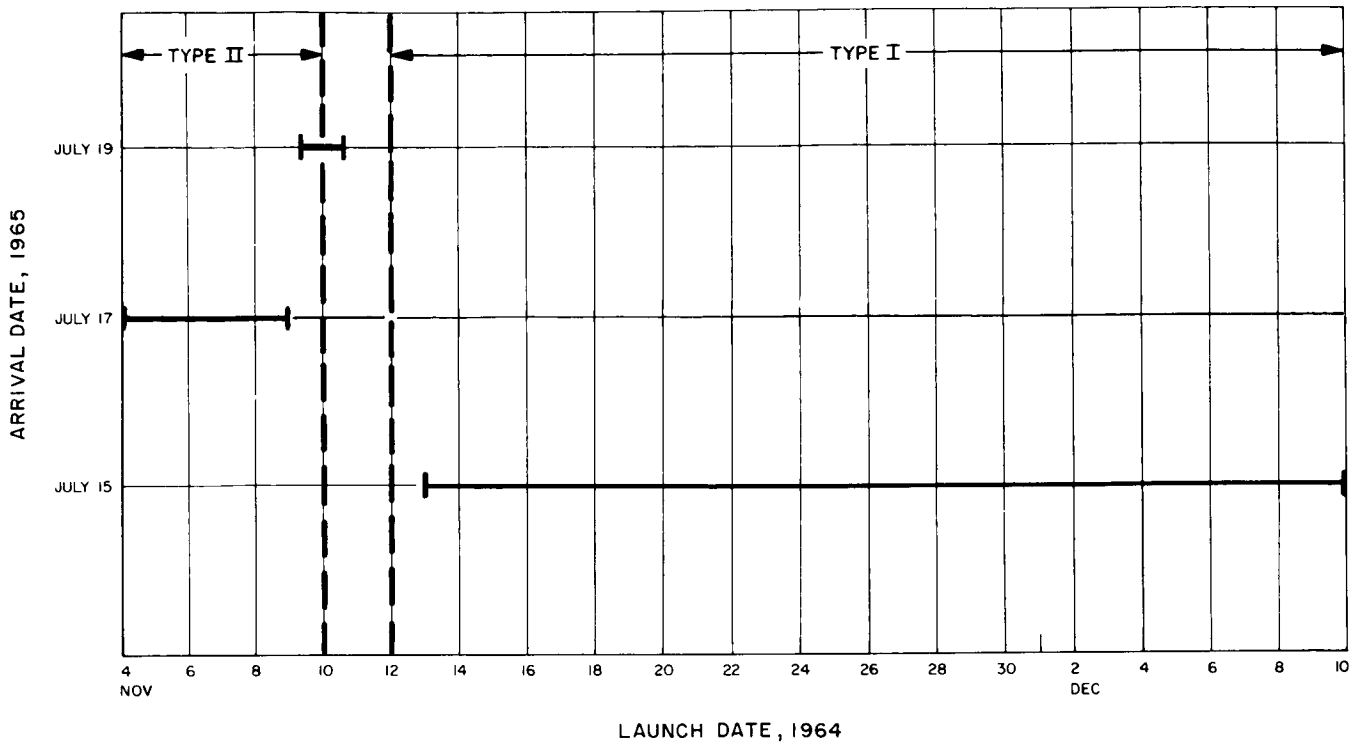


Fig. 412. Arrival date vs launch date

(aiming point) was governed by a number of constraints imposed by the spacecraft design and by planet-science considerations. The more important constraints were:

1. The Sun–probe–near limb of Mars angle had to be greater than 0 deg during the entire encounter phase. This was necessary because the Sun would be used for a power source and as a reference body for the attitude control subsystem.

2. No part of Mars or its moons could fall within a region ± 26 deg in clock angle and 92 ± 36 deg in cone angle during the encounter phase. This constraint ensured that the Canopus sensor would not have bodies other than Canopus within its field of view. An equivalent statement of this constraint is that the Canopus–probe–near limb of Mars angle had to be greater than 36 deg during the entire encounter phase.

3. It was desirable that the spacecraft pass the planet within 40,000 km of the surface, since the various fields and particles experiments aboard the spacecraft required a close enough pass to yield maximum scientific return. Also, the pass had to be close enough to achieve the desired picture resolution from the television system.

4. The aiming point had to lie between 0 and 90 deg from the **T** axis in the **T–R** plane. This plane, which is useful in describing the aiming-zone characteristics for a target body, is defined as being normal to the incoming asymptote of the spacecraft approach hyperbola. Vector **T** is a unit vector parallel to the ecliptic plane and **R** is normal to **T**. The first-quadrant constraint on the aiming point was necessary to ensure that the planet would fall within the field of view of the planetary scan subsystem and to provide a picture trace across a desirable region of the planet.

5. The Earth–probe–near limb of Mars angle had to be less than 0 deg sometime during the encounter phase. This would enable the spacecraft to pass behind Mars as seen from the Earth, so that the occultation experiment could be performed to determine the characteristics of the Mars atmosphere.

6. The probability of the spacecraft impacting Mars had to be less than 10^{-4}.

The aiming point was specified in the **T–R** plane by a vector **B** directed from the center of Mars to the point at which the incoming asymptote pierced the **T–R** plane.

It was usually specified either by its two components $\mathbf{B}\cdot\mathbf{T}$ and $\mathbf{B}\cdot\mathbf{R}$ or by its magnitude **B** and polar angle θ measured from **T** to **R**. A typical **T–R** plane plot is shown in Fig. 413. In this figure, the SPM = 0 deg contour has the property that any aiming point **B** lying inside this contour would result in a planet pass such that the first constraint would be violated. Similarly, the region labeled CPM = 36 deg would result in violation of the second constraint. In order to satisfy the fifth constraint, the aiming point had to lie within the region labeled EPM = 0 deg. The region labeled IMP = 10^{-4} had to be avoided to satisfy the sixth constraint.

After careful consideration of the above constraints, aiming points were selected to lie on the center line of the Earth occultation contour with an encounter parameter magnitude **B** = 12,000 km. Since the center line varied slightly with trajectory type and arrival date, the aiming point had to change slightly also. The final aiming points selected in the preflight analysis are listed in Table 89.

Table 89. Selected aiming points

Trajectory type	Arrival date, 1965	θ, deg
I	July 15	60
I	July 17	70
II	July 17	80
II	July 19	80

One further consideration in the preflight trajectory planning was the selection of the precise arrival time. This arrival time had to be chosen so that the spacecraft would be in view of the Goldstone tracking station during the encounter sequence. Since the television sequence was designed to occur before closest approach, the arrival time (defined as the time of closest approach to Mars) was taken to be 1 hr past the middle of the Goldstone view period. The nominal times for the various arrival dates were:

Arrival date, 1965	Arrival time, GMT
July 15	01:48:00
July 17	01:44:00
July 19	01:40:00

2. Mission Targeting

After considering all constraints, final precision trajectories were computed and a final trajectory document was published updating the preliminary trajectory report. A targeting criteria specification was also prepared for the boost vehicle contractor for his use in preparing firing tables. These tables required a detailed simulation of the *Atlas/Agena* ascent trajectory to determine the proper guidance and control settings. Also, the launch and parking orbit coast times were computed to yield arrival conditions at Mars as specified. The tables were computed for a 90- to 114-deg launch azimuth interval. The daily firing window was about 3 hr, with injection locations confined to a region of about 10.5 deg in latitude and 69.6 deg in longitude over an area slightly West of South Africa and extending into the Indian Ocean. Parking orbit coast times ranged from 19.1 to 34.6 min, depending upon the launch date and launch azimuth.

3. *Mariner IV* Biasing

In view of the delayed launching of *Mariner IV*, removal of the *Agena* retrorocket was requested. The weight reduction in the *Agena* resulting from the removal of the retrorocket allowed an increase in available injection energy C_3 which provided a few extra days of launch period. Since the retrorocket was required to achieve a less than 10^{-4} probability of the *Agena* impacting Mars, a decision was made to bias the nominal aiming point at Mars. This biasing consisted of two parts:

1. The yaw bias, which could be anticipated before launch, consisted of an error in the yaw orientation of the *Agena* at the start of the second burn. The error, caused by an ullage control system torque during the parking orbit, was expected to reach 1 deg.

2. It was found that a reduction in injection velocity introduced a bias in the aiming point at Mars that complemented the effect of the built-in yaw bias. A 3 m/sec injection-velocity decrease was selected in order to yield a launch aiming point that would satisfy the 10^{-4} constraint. This aiming point resulted from the combined effects of both the injection velocity and yaw biases.

4. Flight Results

a. Launch phase. The launch of *Mariner IV* occurred at an inertial launch azimuth of 90.5 deg East of North. After liftoff, the booster rolled to an azimuth of 91.4 deg and performed a programmed pitch maneuver until booster cutoff. During the sustainer and vernier stages, adjustments in vehicle attitude and engine cutoff times

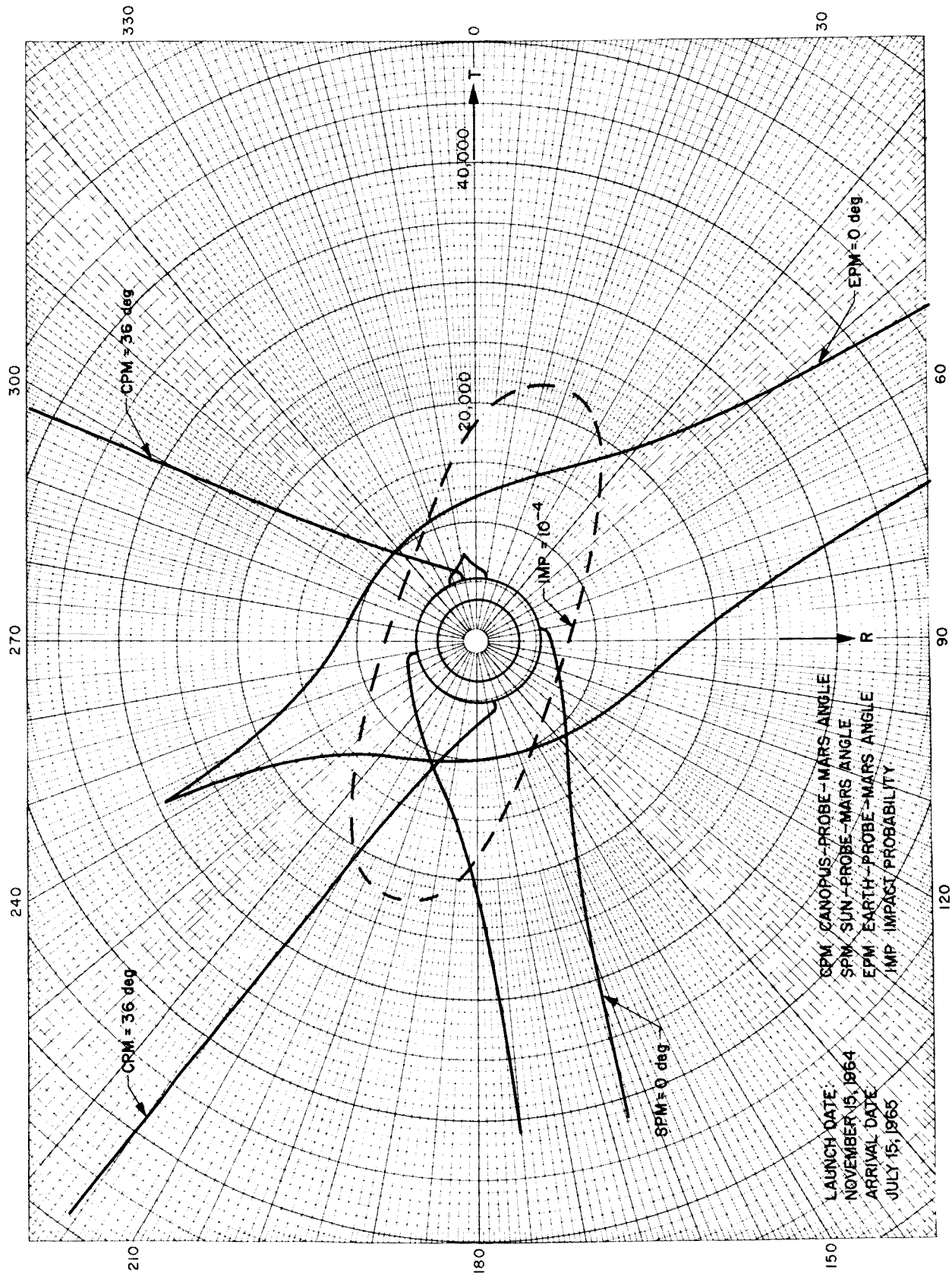


Fig. 413. Aiming point and constraint regions for Type I launch and July 15, 1965 arrival

were commanded, as required, by the ground guidance computer to adjust the attitude and velocity at *Atlas* vernier engine cutoff.

After *Atlas/Agena* separation, there was a short coast period before the first ignition of the *Agena* engine. At a preset value of sensed velocity increase, the *Agena* engine was cut off. At that time, the *Agena/*spacecraft combination was coasting in a nearly circular parking orbit in a southeasterly direction at an altitude of 188 km and an inertial speed of 7.80 km/sec.

After a parking-orbit coast time of 32 min, 14 sec, determined by the ground guidance computer and transmitted to the *Agena* during the *Atlas* vernier stage, a second ignition of the *Agena* occurred. The *Agena* was cut off 96 sec later, with the *Agena/*spacecraft combination in a nominal Earth–Mars transfer orbit.

The launch-phase ascent-trajectory profile is illustrated in Fig. 414, and a sequence of events from launch to acquisition of Canopus is shown in Fig. 415.

b. Premidcourse cruise phase. Injection (second *Agena* cutoff) occurred at 15:04:27.7 GMT over the Indian Ocean at a geocentric latitude of −26.25 deg and a geocentric longitude of 68.82 deg. The *Agena/*spacecraft combination was at an altitude of 197.2 km traveling at an inertial speed of 11.443 km/sec. At 1 min, 23 sec after injection, the *Agena/*spacecraft entered the Earth's shadow. The *Agena* separated from the spacecraft 1 min, 18 sec later. At 15:17:34.8 GMT, *Mariner IV* left the Earth's shadow after being in the shadow for 11 min, 44 sec. Within an hour after injection, the spacecraft was receding from Earth in almost a radial direction with decreasing speed. This reduced the geocentric angular rate of the spacecraft (in inertial coordinates) until the angular rate of the Earth's rotation exceeded that of the spacecraft. This phenomenon is illustrated in Fig. 416. Also shown in this figure is the tracking-station coverage and the locations of the various spacecraft events.

Tracking data gathered and analyzed before the midcourse maneuver indicated that, without a correction, the spacecraft would pass the upper leading edge of Mars at a closest approach distance of 252,800 km. Closest approach would have occurred at 01:25:11 GMT on July 17, 1965. In order to alter the trajectory to pass through the selected aiming region centered at approximately 10,000 km from the center of Mars, a midcourse velocity of 16.70 m/sec was required. (The maximum capability was 87 m/sec.)

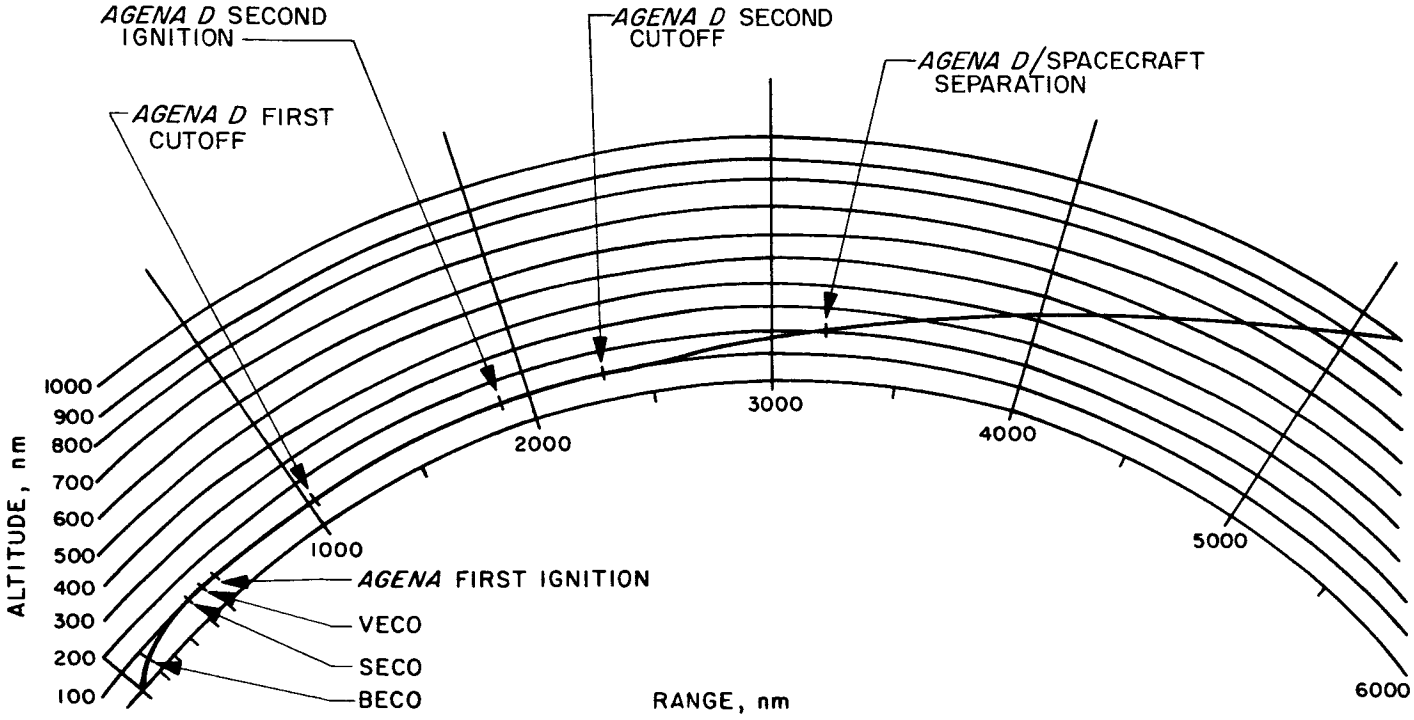


Fig. 414. Ascent trajectory profile

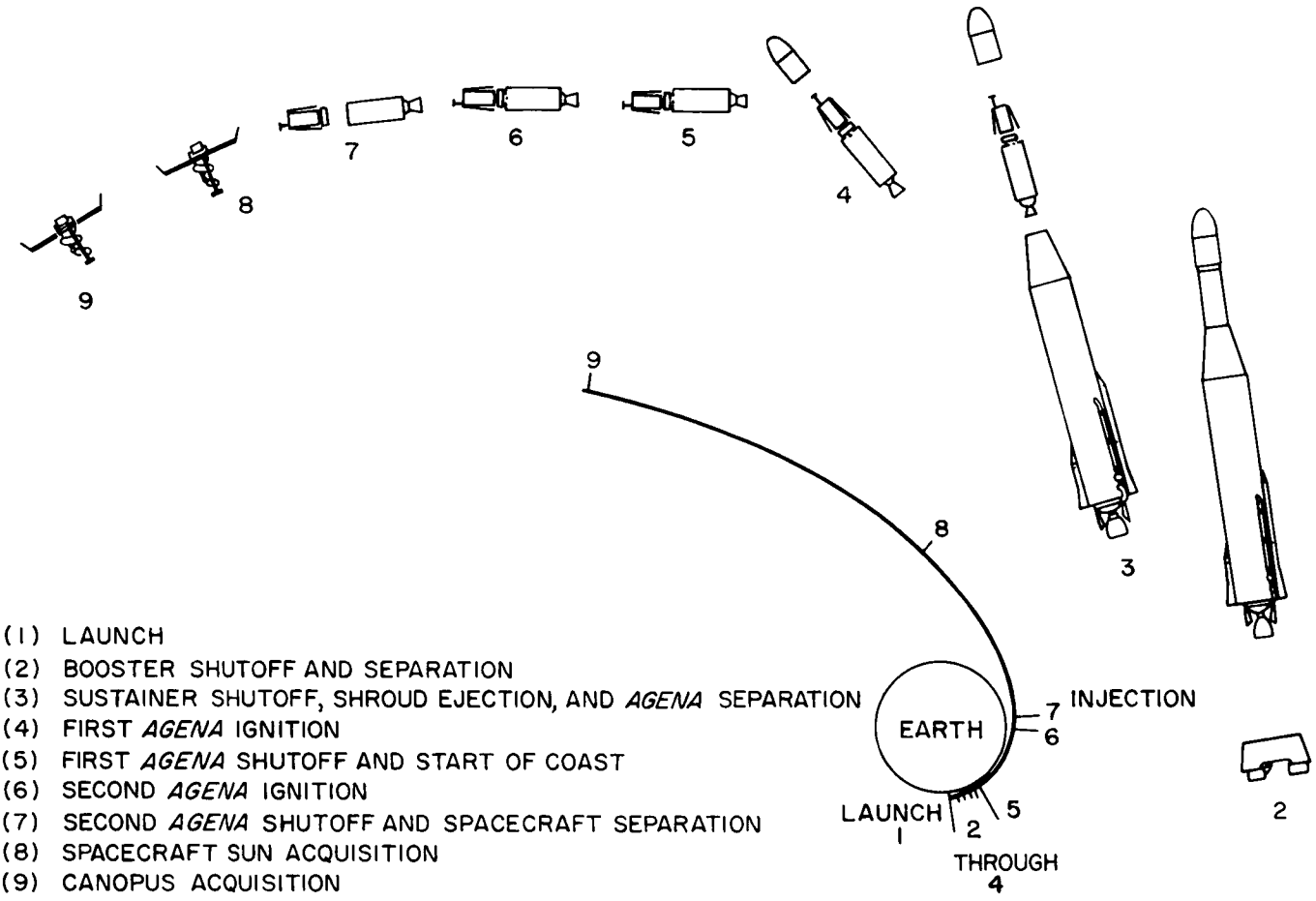


Fig. 415. Sequence of events to Canopus acquisition

In addition to altering the distance of closest approach, the correction was also selected to change the arrival time to 01:46:00 GMT on July 15, 1965, thus allowing preset commands to properly activate various subsystems at encounter. The midcourse motor was ignited at 16:09:25 GMT on December 5, 1964, at which time the spacecraft was at a geocentric distance of 2,022,400 km moving at an inertial speed of 3.139 km/sec relative to Earth. Preliminary analysis of tracking data received during and after the motor burn indicated that the maneuver was performed properly. Injection and encounter conditions for the premidcourse orbit used to determine the midcourse maneuver are given in Table 90.

c. Postmidcourse cruise phase. During the month following the midcourse maneuver, several redeterminations of the *Mariner IV* orbit were completed. The encounter conditions resulting from these computations are illustrated on a **T–R** plane perpendicular to the incoming asymptote at Mars in Fig. 417. The figure shows the occultation regions, the aiming point, and the *a priori* postmidcourse execution error dispersion ellipse. Also shown is a contour that encloses the desired aiming region; all four of the postmidcourse orbits lie well within this contour.

The postmidcourse heliocentric trajectory projected on the ecliptic plane is illustrated in Fig. 418, which includes the orbits of Earth and Mars. The positions of the spacecraft and the planets are depicted at 30-day intervals from launch to encounter. The postmidcourse trajectory characteristics are given in Table 91. The close flyby of the planet will result in a heliocentric energy C_3 increase of 33.25 km²/sec². Also, since the spacecraft will pass underneath the planet, the inclination of the heliocentric trajectory plane will change by 3.1 deg. In the process of such a plane change, the longitude of the descending node will be increased by approximately 180 deg. Important trajectory parameters at encounter are given in Table 92.

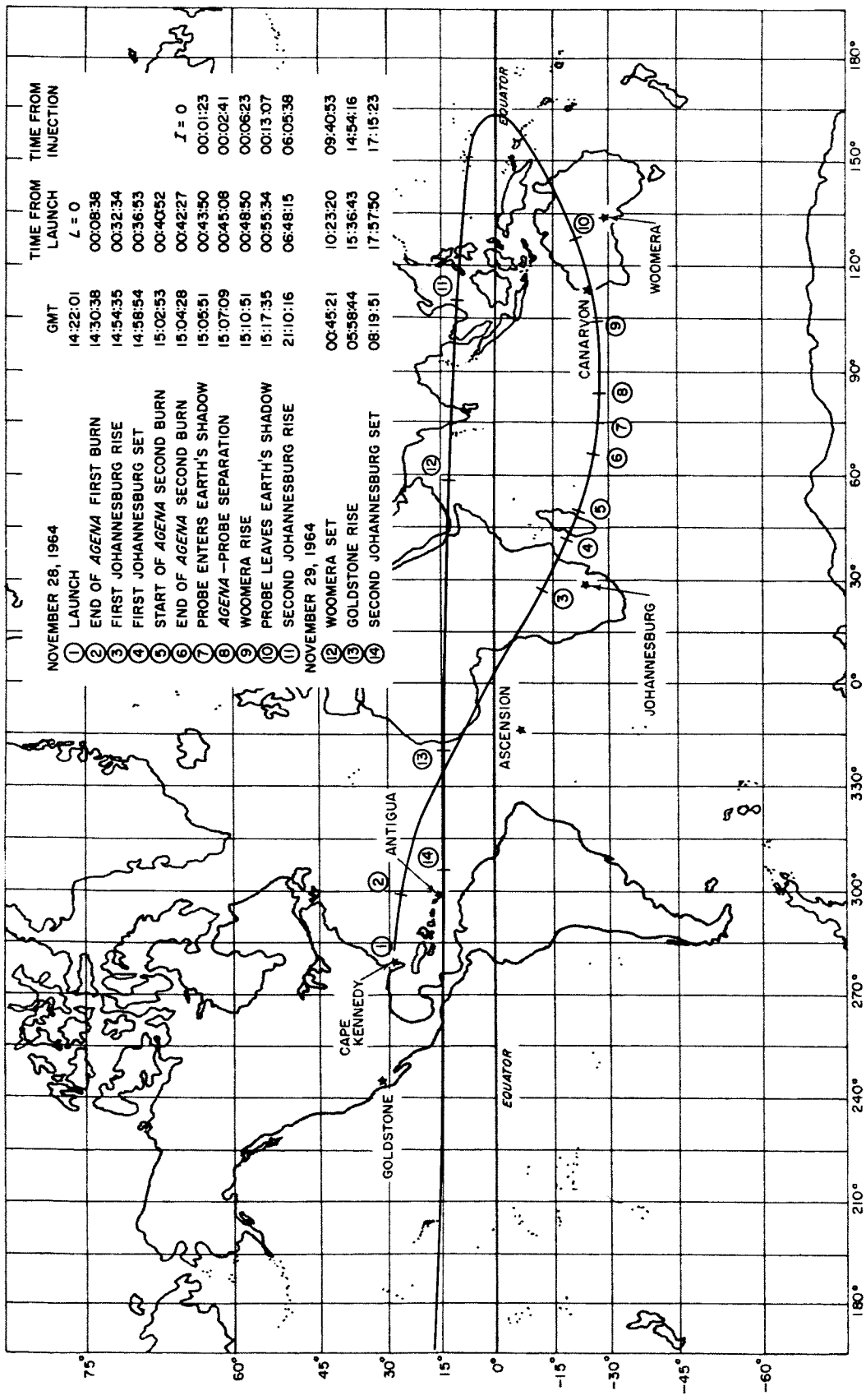


Fig. 416. Earth track of *Mariner IV* trajectory

Table 90. Orbit used for determination of the *Mariner IV* midcourse maneuver

Initial conditions[a]		Heliocentric orbital elements		Trajectory characteristics at encounter	
Earth-fixed spherical coordinates	Inertial Cartesian coordinates	Element	Value	Characteristic	Value
R = 6872.9573 km	X = 5668.2509 km	Semimajor axis a, km	191,275,000	Time of flight, days	230.4628
ϕ = −28.130141 deg	Y = 2146.6407 km	Eccentricity e	0.2289	Time of closest approach July 17, 1965, GMT	01:28:15
θ = 86.212637 deg	Z = −3240.4334 km	Inclination i, deg	0.1347	Target parameter magnitude $\lvert \mathbf{B} \rvert$, km	255,535
V = 10.775777 km/sec	$\dot{X}$ = −1.8839630 km/sec	Longitude of ascending node Ω, deg	68.724	Component of **B** along **T** axis $\mathbf{B} \cdot \mathbf{T}$, km	−224,582
Γ = 13.165104 deg	$\dot{Y}$ = 10.978611 km/sec	Argument of perihelion ω, deg	352.37	Component of **B** along **R** axis $\mathbf{B} \cdot \mathbf{R}$, km	−121,906
σ = 90.439744 deg	$\dot{Z}$ = 1.2281457 km/sec	Time of flight T_F, days	528.076	Altitude of closest approach to Mars, km	249,853
		Perihelion radius r_p, km	147,486,000	Sun–probe distance at encounter, km	232,241,000
		Aphelion radius r_a, km	235,064,000	Earth–probe distance at encounter, km	218,318,000
		Vis-viva energy C_3, km²/sec²	−693.838	Hyperbolic approach speed at Mars, km/sec	4.3085

[a]Epoch: November 28, 1964, 15:07:27 GMT.

Table 91. *Mariner IV* postmidcourse orbit

Heliocentric orbital elements	Pre-encounter	Postencounter
Semimajor axis a, km	191,567,000	201,224,000
Eccentricity e	0.2301	0.1686
Inclination i, deg	0.1290	2.9786
Longitude of ascending node Ω, deg	68.481	226.899
Argument of perihelion ω, deg	352.71	200.17
Time of flight T_F, days	529.285	569.804
Perihelion radius r_p, km	147,495,000	167,293,000
Aphelion radius r_a, km	235,640,000	235,154,000
Vis-viva energy C_3, km²/sec²	−692.781	−659.536

Table 92. Trajectory characteristics at encounter

Characteristic	Value
Time of flight T_F, days	228.4486
Time of closest approach, July 15, 1965, GMT	01:08:03
Target parameter magnitude $\lvert \mathbf{B} \rvert$, km	14,034
Component of **B** along **T** axis $\mathbf{B} \cdot \mathbf{T}$, km	7,068.8
Component of **B** along **R** axis $\mathbf{B} \cdot \mathbf{R}$, km	12,123.4
Altitude of closest approach to Mars, km	8,613
Sun–probe distance at encounter, km	232,502,000
Earth–probe distance at encounter, km	216,310,000
Hyperbolic approach speed at Mars, km/sec	4.4028

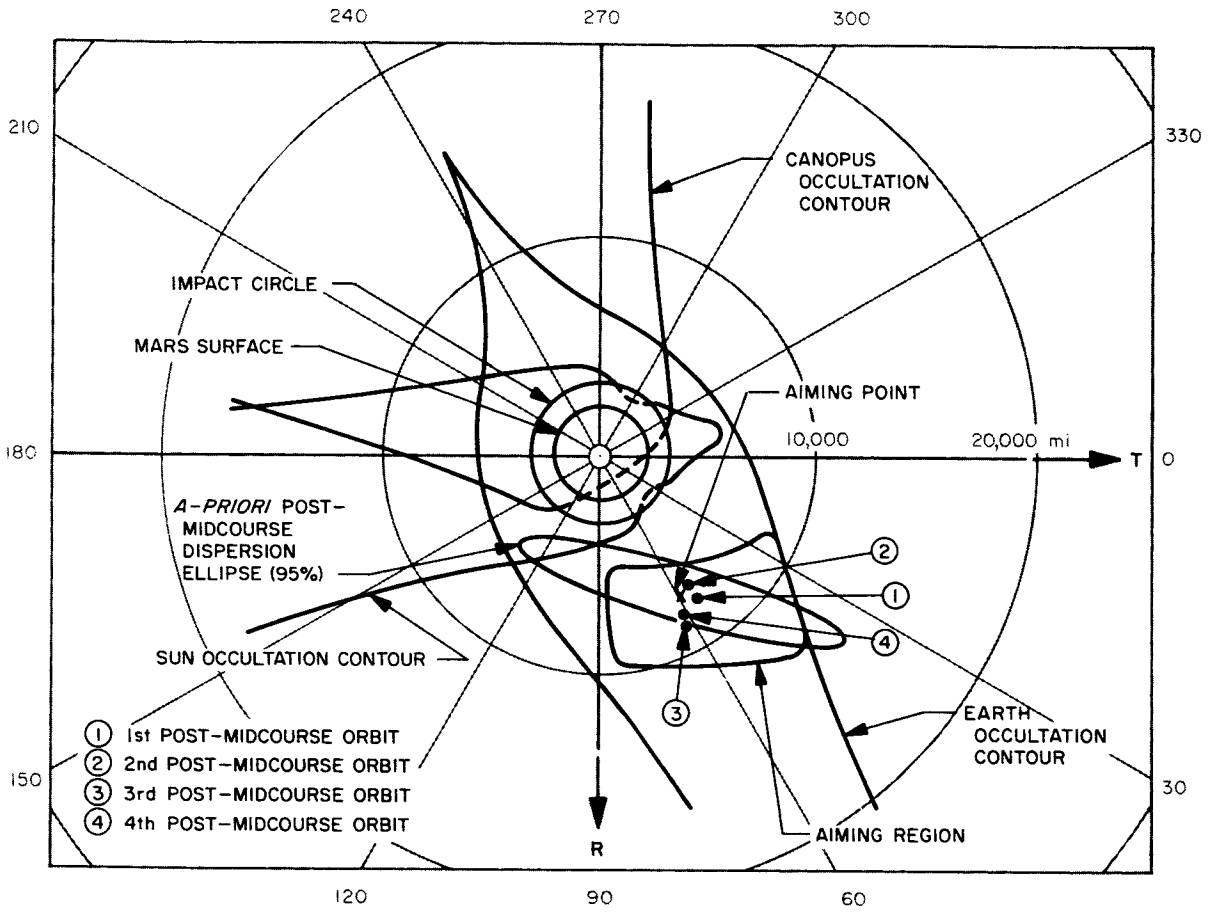


Fig. 417. *Mariner IV* aiming zone and constraint region

The trajectory data provided correspond to the fourth postmidcourse orbit shown in Fig. 417. Plots of the Earth–probe distance, Sun–probe distance, and Earth cone (Earth–probe–Sun) angle as functions of time from launch are presented in Fig. 419 through 421.

C. Guidance Analysis

1. Preflight Analysis and Characteristics of *Mariner* Mars Guidance

The control of *Mariner* Mars target-arrival parameter components $\mathbf{B}\cdot\mathbf{T}$, $\mathbf{B}\cdot\mathbf{R}$, and the time of flight T_F was important for several reasons including: control of flyby distance, look angles, and illumination for science instruments; correct timing of automatic encounter sequences; and adequate DSIF view periods at encounter. The task of the launch vehicle was to inject the spacecraft into a trajectory having the required arrival parameters; however, because of normally occurring guidance uncertainties, the initial trajectory parameters were not acceptable. Radio tracking data received after injection were used to determine the initial trajectory and to compute a velocity increment that, when added to the spacecraft velocity vector, would correct the trajectory parameters. This maneuver was called the midcourse correction maneuver. For *Mariner IV*, the addition of the velocity increment was achieved by commanding the spacecraft to turn in succession about its pitch and roll axes until the small onboard rocket motor was pointed in the proper direction. The motor was then commanded to burn for a specified length of time. Normal performance variations in the spacecraft guidance equipment and rocket motor resulted in errors in the velocity increment, which caused a residual error in the arrival parameters.

The information in Table 93 and the dotted ellipses in Fig. 422 describe the dispersion (in the target coordinates $M = \mathbf{B}\cdot\mathbf{R}$, $\mathbf{B}\cdot\mathbf{T}$, T_F) at the aiming point for the Mars flyby due to random injection errors (Ref. 37).

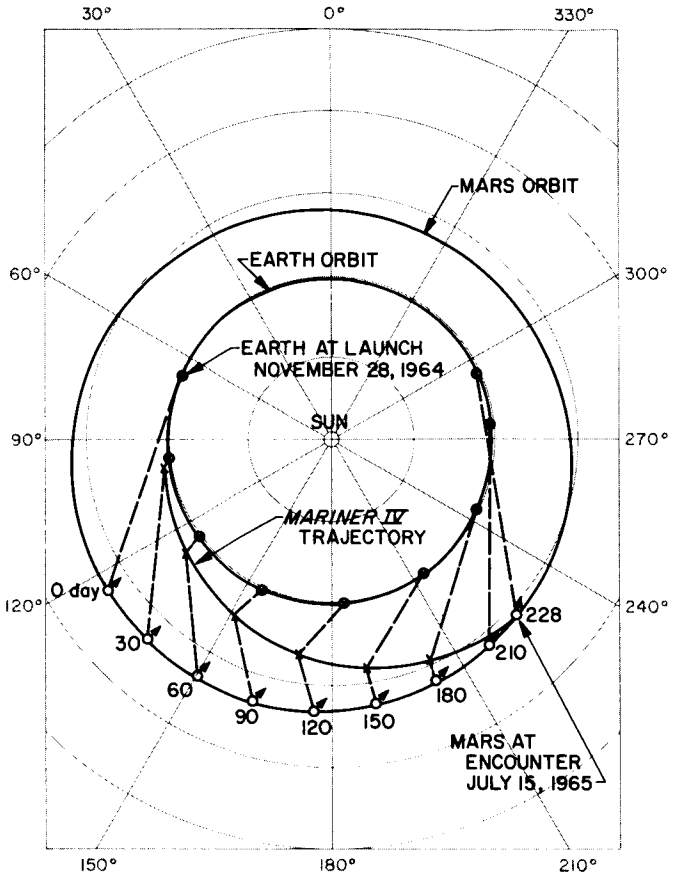


Fig. 418. *Mariner IV* trajectory

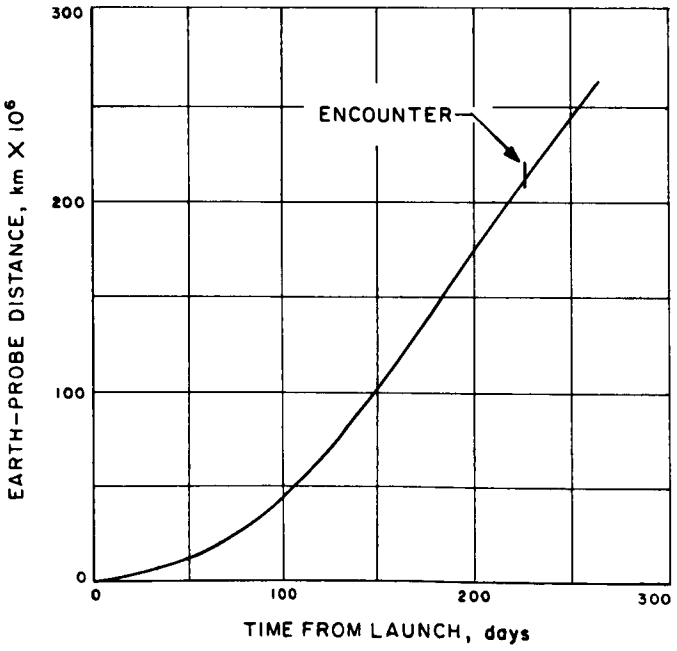


Fig. 419. Earth–probe distance vs time from launch

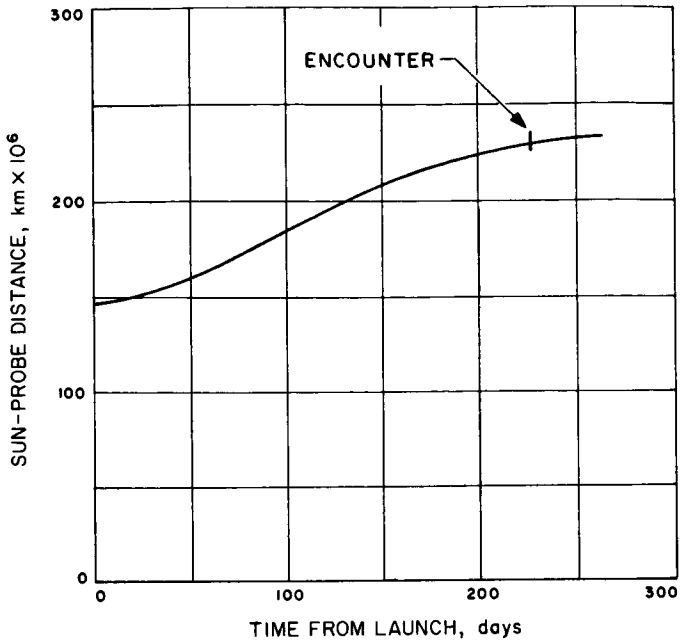


Fig. 420. Sun–probe distance vs time from launch

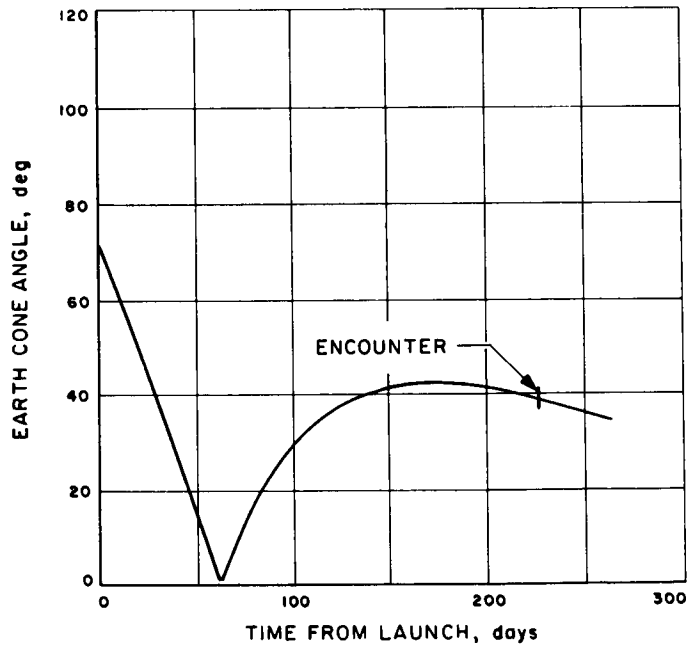


Fig. 421. Earth cone angle vs time from launch

The midcourse maneuver velocity increment had two components: one in the critical plane and one in the noncritical direction (Fig. 423). The velocity gradients of the two spatial miss components λ_1 and λ_2 define the so-called critical plane, and, since the component V in the direction N perpendicular to this plane will not

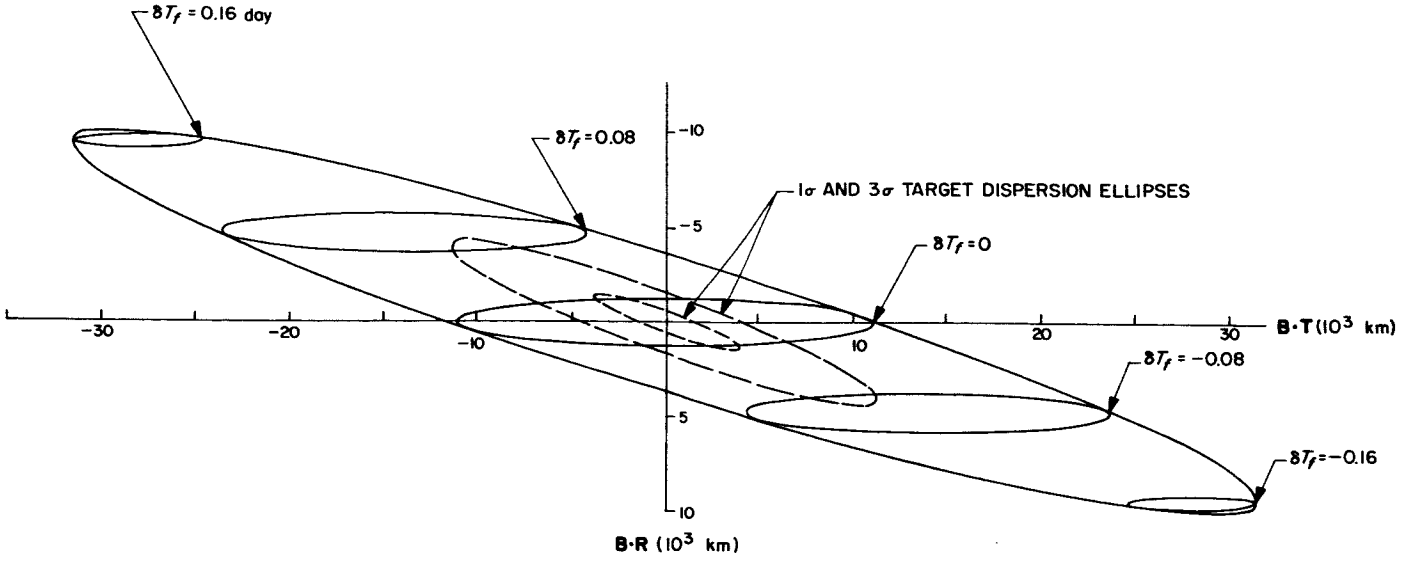


Fig. 422. Type I capability ellipses at 5 days from injection

Table 93. Trajectory characteristics and 1σ dispersions due to injection errors

Trajectory type	Launch date	Flight time T_f days	Injection dispersion		
			Ellipse semimajor axis km	Ellipse semiminor axis km	δT_f days
I	November 15, 1964	243	245,014	30,956	2.095
II	November 10, 1964	250	222,860	30,269	1.848

affect the spatial miss, N defines the noncritical direction. Figure 423 shows the orientation of a critical coordinate system (u_1, u_2, u_3).

To find the velocity (and thus the fuel) requirements for the *Mariner* Mars maneuver, the rms velocity magnitude for the full maneuver and the rms magnitude of the critical maneuver were computed. The proposed 60 m/sec fuel capability for the spacecraft was more than sufficient to correct 99% of the spatial target deviation if the critical plane maneuver were made any time on or after the first day past injection. For the Type I trajectory, the 60 m/sec midcourse capability would be more than enough to correct the spatial miss and the time of flight if it were executed at any time on or after the first day past injection. The tentative execution time for the midcourse maneuver was the fifth day past injection, although it could be executed any time between the second and fourteenth days.

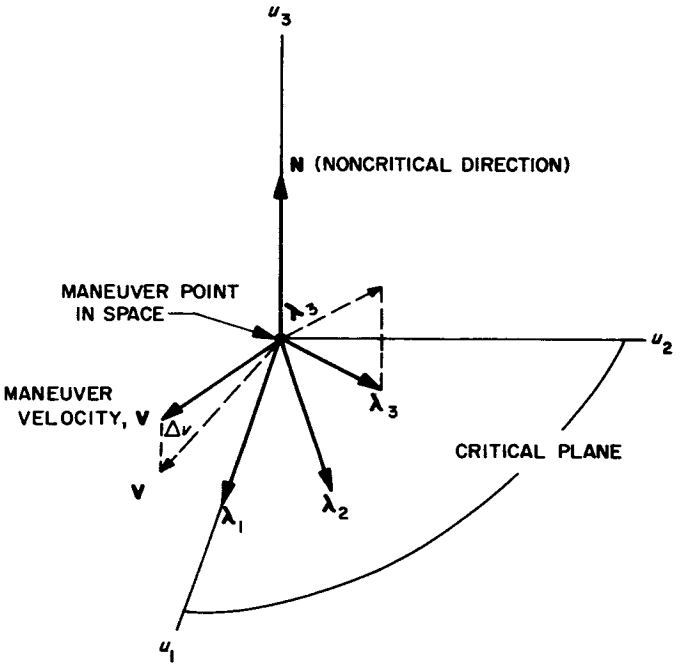


Fig. 423. Critical coordinate system

The problem of the velocity capability was also approached from the opposite standpoint; that is, how much spatial miss could be corrected with a 1 m/sec velocity increment.

The unit sphere containing all velocity vectors of 1 m/sec and less at a midcourse point on the trajectory maps is converted into an ellipsoid of correctable target

coordinates whose projection on the **R–T** plane is the so-called "capability ellipse." Figure 422 shows the capability ellipses for a typical Type I trajectory for a maneuver at 5 days after injection. The outer ellipses contain all the possible misses that could be corrected with a 1 m/sec midcourse capability if the maneuver were made in the critical plane. The set of smaller ellipses encloses areas in which the miss might be corrected and the flight time varied by the amount specified with the 1 m/sec maneuver. For instance, the small ellipse whose center is at the origin encloses the set of all misses that might be nulled without changing the uncorrected time of flight. Superimposed on each figure are the 1 σ and 3 σ target dispersion ellipses due to injection errors.

Because of tolerances in the components of the spacecraft guidance system, the midcourse maneuver would have some errors, and, thus, the miss at the target would not be totally nulled. The specifications for maneuver performance were that the uncertainty in orbit determination should contribute less than 2250-km-rss miss, and that a 15 m/sec maneuver execution error should contribute less than 4070-km-rss miss at the target. The rss of these two values is 4650 km. Time-of-flight errors were highly correlated with spatial errors, and 4650-km-rss miss was correlated with an error of 30 min rss in flight time.

2. Midcourse Maneuver Operations Program

a. Nature of the program. The maneuver capability existed in order to allow the trajectory to be altered so that scientific data might be obtained by measurements performed near Mars.

The *Mariner* Mars midcourse maneuver operations program had two primary purposes:

1. To perform calculations that would enable the operations personnel to select the most advantageous maneuver once the orbit achieved by the spacecraft was known. The spacecraft could be used to gather significant scientific information even if it followed a trajectory very different from the nominal one.

2. To code the commands that were to be transmitted to the spacecraft and that would cause it to perform the desired maneuver. The midcourse maneuver would require three 26-bit stored quantitative commands, which would be sent to the spacecraft and stored until the real-time direct command was sent that would initiate the sequence.

The computation of the maneuver had to allow for a variety of practical constraints imposed by the limitations of the spacecraft. The program accordingly contained two types of subprograms. The first subprogram called for a set of drivers for the trajectory program, which could be used to explore the different classes of trajectories available to the spacecraft after a maneuver, with specialized output relevant to the operational situation. The second subprogram included decision routines that also used the trajectory program and that were used to compute and code the desired maneuvers. These subprograms were written as separate loops to be compatible with the SFOF monitor system.

b. Constraints. There were two types of constraints involved in the midcourse maneuver operations program:

1. Absolute constraints that had to be satisfied for a physically realizable maneuver (i.e., a velocity that would not require more fuel than was actually in the tank).

2. Other constraints that would increase the value of the mission by their satisfaction but that would not abort the mission if they were violated. These were: maintenance of two-way lock through the low-gain antenna during the entire maneuver sequence; and performance of the maneuver over a DSIF station with command capability.

Making the spacecraft pass through the desired aiming zone at the desired time could have been considered an additional constraint, although this was the ultimate purpose of the midcourse operations program. Figure 424 shows the aiming zones best suited for the science experiments. Table 94 shows the relative values of each zone.

The arrival time was chosen to satisfy the following conditions:

1. That the Goldstone station be locked up 3½ hr before narrow-angle acquisition, assuming that it will take approximately 1 hr after spacecraft rise to lock it up

2. That the spacecraft enter the occultation region at least 1 hr prior to the Goldstone set

3. That the Goldstone station also be available, if possible, when the spacecraft emerges from the occultation region

Other nonstandard constraints could have been imposed. For example, if one spacecraft bay were operating

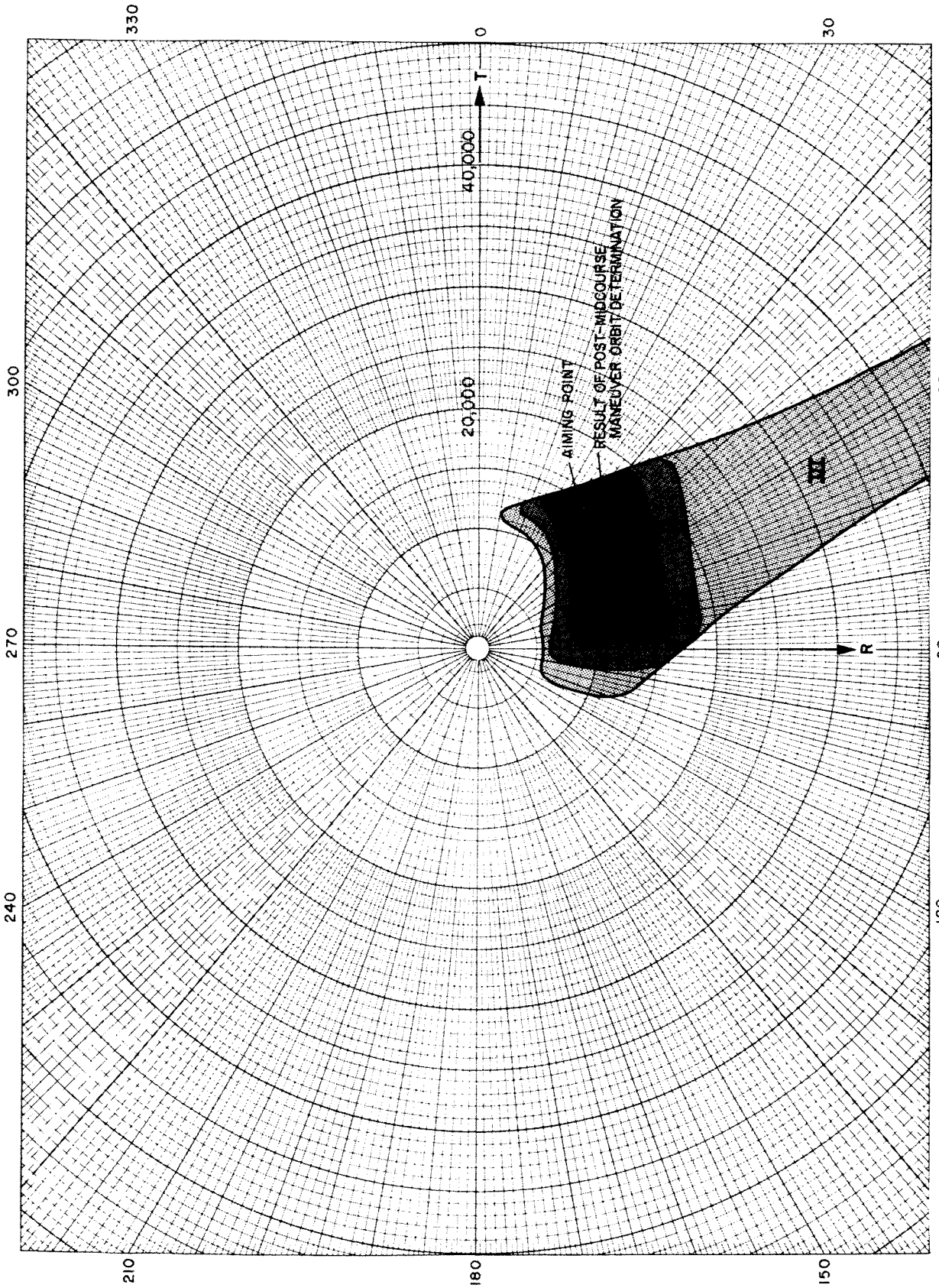


Fig. 424. Typical maneuver regions I, II, and III for Type I launch and July 15, 1965 arrival

Table 94. Aiming zone values

Item	Zone		
	I	II	III
Value of occultation and TV experiment	≥0.7	≥0.8	≥0.6
Value of fields and particles experiment	≥0.25	≥0.5	—
If trajectory passes through zone	Make no maneuver	Make no maneuver	Make first maneuver Do not make second maneuver
If trajectory does not pass through zone	Make first maneuver	Make first or second maneuver	Make first or second maneuver

hotter than anticipated, the maneuver could be constrained so that the angle of sunshine incidence would not be greater than some specified value on that bay during the entire maneuver sequence.

Figure 425 shows the constraints that operationally determined the time at which to make the maneuver. These were:

1. Canopus acquisition and orbit determination would require at least two days.

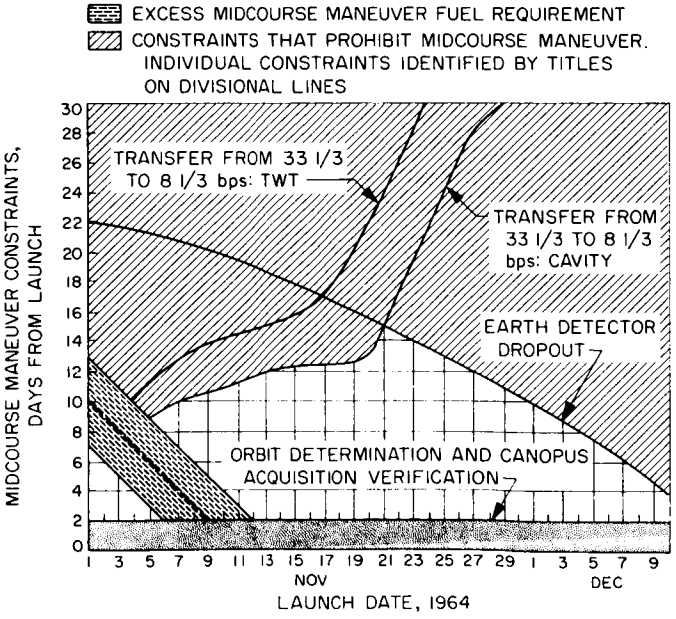


Fig. 425. Midcourse maneuver constraints

2. For Type II trajectories, the maneuver would be made either before or after the band of times around November 10 that require a large velocity.

3. The maneuver would be made early enough that the Earth detector could verify Canopus reacquisition, and that high-bit-rate telemetry transmission would still be possible.

c. Program operation. There were three types of input to drive the midcourse maneuver operations program:

1. Results of the orbit determination program
2. Spacecraft parameters that defined the spacecraft geometry and status
3. Control parameters, such as desired aiming conditions

Figure 426 is a functional block diagram of the *Mariner* Mars maneuver operations program. There are seven independent blocks that were programmed separately. All of these blocks, with the exception of numbers 3 and 4, required the use of the space trajectory program as a subroutine.

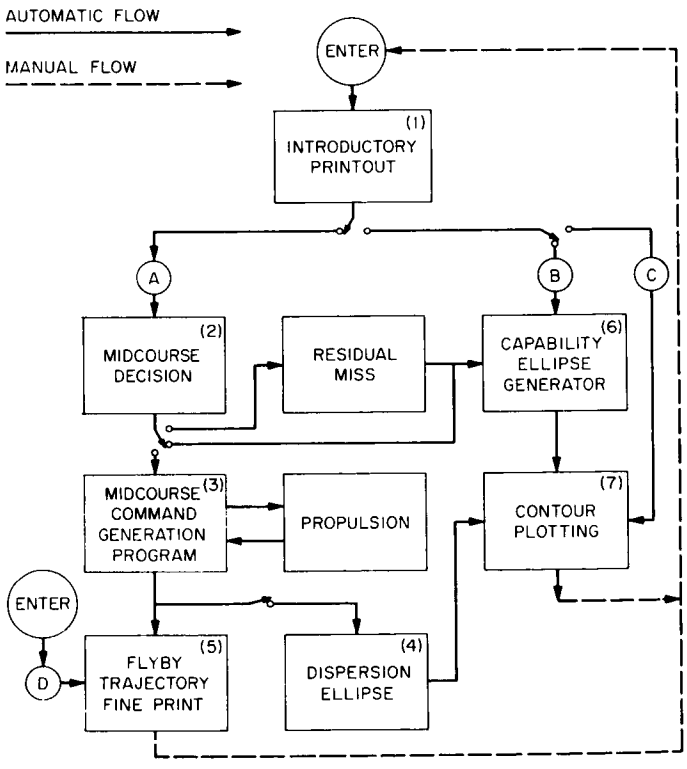


Fig. 426. *Mariner* Mars midcourse maneuver operations program functional block diagram

Functional blocks 1, 2, 3, and 5 were required for both standard operation (i.e., it was possible to put the spacecraft on a trajectory that would pass near the nominal aiming point at a satisfactory time) and nonstandard operation (i.e., it was not possible to put the spacecraft on a trajectory that would pass near the nominal aiming point at a satisfactory time). Functional blocks 4, 6, and 7 were designed to assist in making operational decisions during nonstandard operating conditions. Brief descriptions of each operational block are given below.

Introductory printout. The information required on the introductory printout described the orbit determination and gave an initial estimate of the quality of the orbit obtained. Input quantities from the orbit determination program were used to obtain an initial estimate of the miss distance and time-of-flight error that existed between the best-fit trajectory and the nominal aiming point.

Midcourse decision program. The purpose of the midcourse decision program was to calculate the required velocity increment subject to various constraints. The constraints that were evaluated were: (1) the propulsion constraint, (2) the time-of-flight constraint, and (3) the low-gain antenna constraint. The propulsion and time-of-flight constraints were defined to be absolute. If it were not possible to reach the **B • R, B • T** location requested without violating an absolute constraint, the midcourse decision program would then print a simple statement to that effect and proceed with the mission capability study. If it were possible to reach the location requested without violating an absolute constraint, the output of the midcourse decision program would be fed directly to the midcourse command generation program. If the low-gain antenna constraint were violated, some of the telemetry data during the midcourse maneuver could be lost. Figure 427 is a block diagram of the decision program logic.

The output from the midcourse decision program fell into three groups. The first group specified the trajectory conditions (i.e., position, velocity, and time) at which the midcourse rocket motor would ignite. The second group was a set of brief statements that would be printed out if called for by the decision sequence that formulated the midcourse maneuver. The third group contained detailed numerical information related to the test for the antenna constraint.

Midcourse command generation program. The purpose of the command generation program was to convert the velocity vector correction determined in the midcourse decision program into three commands expressed in binary form and adjusted to a form usable by the CC&S. The pitch and roll turn times were computed by dividing the required turns by the turn rates. The burn time was computed in a subroutine that accepted the velocity magnitude and pertinent spacecraft telemetry data as input. This was necessary since the motor would be turned off by a timed command rather than by an integrating accelerometer and the commands would be transmitted via TTY. The midcourse command generation program also calculated a noise moment matrix of midcourse execution errors and performed a complete trajectory error analysis.

Dispersion ellipse program. A set of dispersion ellipses could be computed from the covariance matrix of errors in the orbit. The maneuver program mapped the dispersions to the target and calculated the dispersion ellipses. (The ellipses could be plotted to the same scale that was used in the plots of the general constraints.)

Flyby trajectory fine print program. The purpose of the flyby trajectory fine print program was to obtain a special printout on individual trajectories that would provide the capability to choose a trajectory intelligently in both standard and nonstandard situations. The printout was obtained by running the trajectory program from the midcourse point past closest approach. Many additional calculations were required that were not provided in the trajectory program.

Capability ellipse generator. The capability ellipse generator provided the maximum capability ellipse in the **R–T** plane, assuming that maximum maneuvers would be applied in the critical plane. If there were insufficient fuel to null the spatial miss and acceptable flight time, the minimum residual miss associated with acceptable flight time would be computed.

Contour plotting program. The purpose of the contour plotting program was to aid in the evaluation of various spacecraft and trajectory constraints as they pertained to various areas of interest in the **R–T** plane. This program was primarily an aid in selecting new aiming points in nonstandard situations. The option to tabulate the plotted quantities was also available.

3. Flight Results

a. Orbit determination. The premidcourse orbit determination resulted in the terminal conditions in Table 95, which gives the desired terminal conditions and those

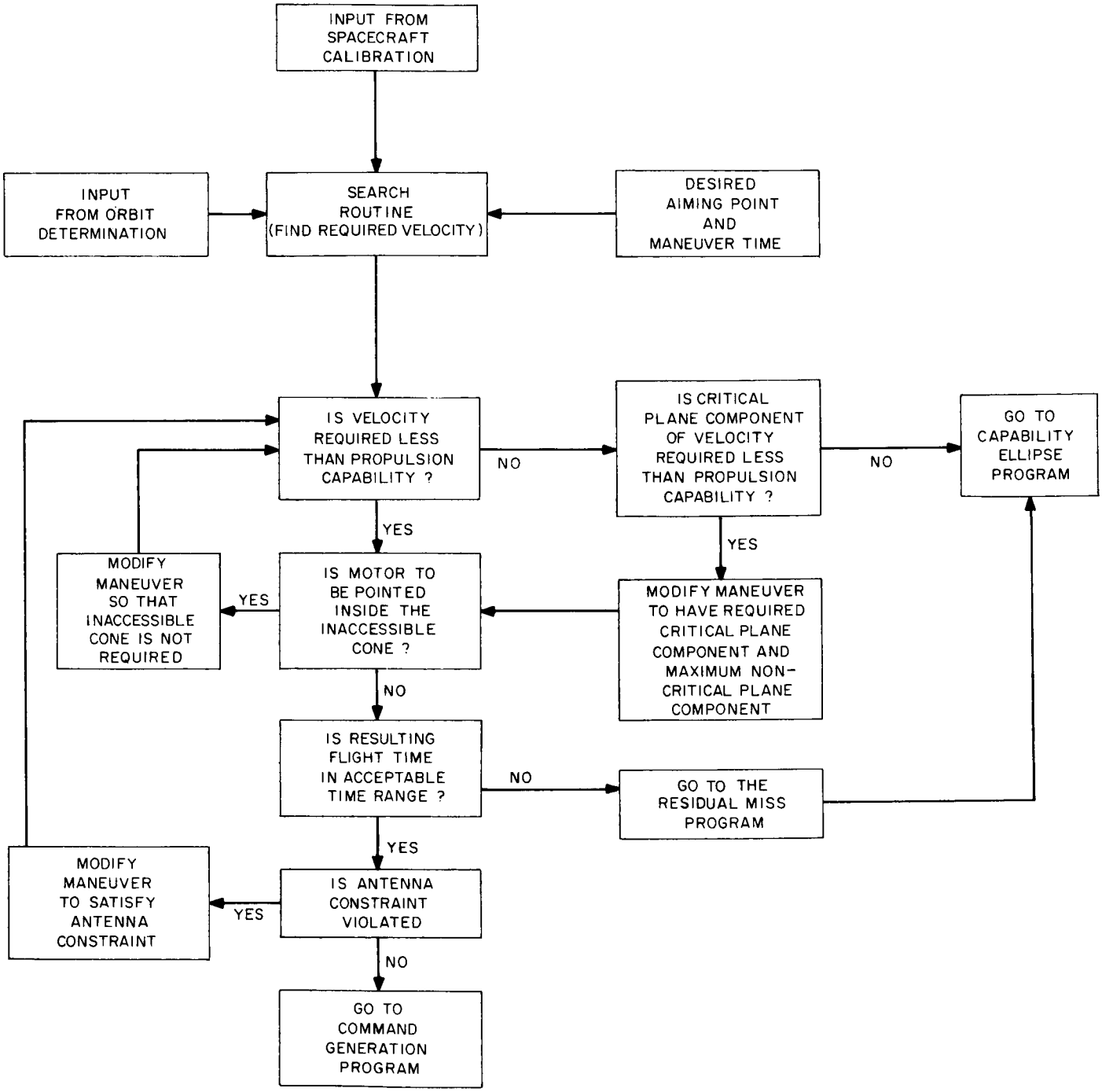


Fig. 427. Decision program logic diagram

Table 95. Terminal conditions

Parameter	Premidcourse	Desired[a]	Postmidcourse[b]
B • R, km	−121,700	10,390	12,303
B • T, km	−224,503	6000	7411
Time of closest approach, GMT	7/17/65 01:27:09	7/15/65 01:48:44	7/15/65 01:03:45

[a]See Fig. 424. Zone II for allowable spatial tolerances. Flight-time tolerances were taken to be from 3 hr earlier to 2 hr later than the time listed as desired.

[b]From orbit determination computer program with tracking data through 1/23/65.

achieved according to the postmidcourse orbit determination available.

The required maneuver was computed as a function of the time in which it was executed. Results of these computations for every day of an entire week showed that all the constraints could be satisfied and that the magnitude of the maneuver was slowly decreasing as a function of time. Figure 428 illustrates this effect.

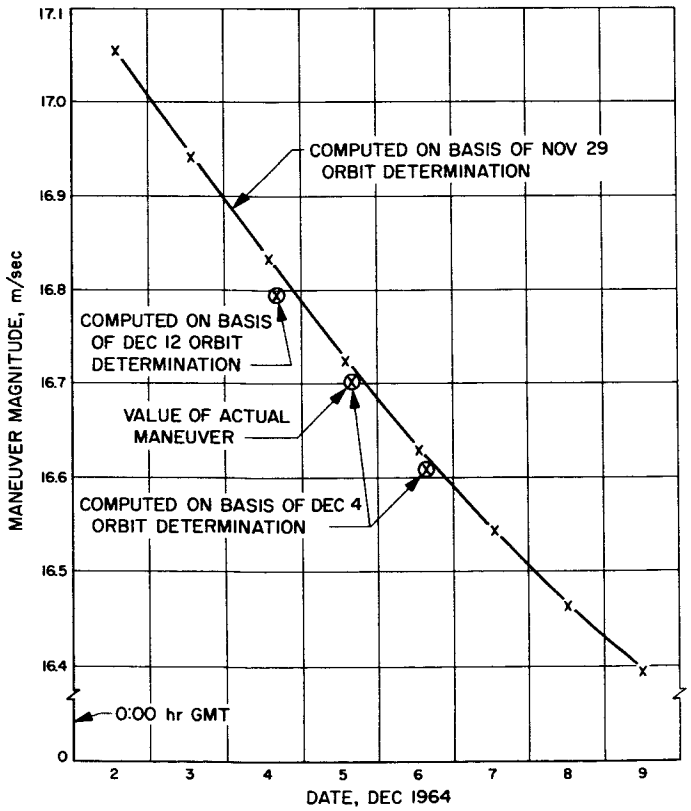


Fig. 428. Midcourse maneuver performance time vs magnitude

b. Maneuver execution. During the maneuver sequence, various telemetry outputs were very carefully monitored. The first maneuver attempt on Friday, December 4 was inhibited when the Canopus sensor initiated a roll search after the command to execute the maneuver was transmitted. It was noted that the spacecraft was at the very edge of its roll limit cycle when the command was sent. It was decided to try and send the DC-27 command at a time when the spacecraft would be roughly at the center of its roll limit cycle. On December 5, the maneuver was transmitted 10 min, 35 sec earlier than the time for which it had actually been computed in order to have the spacecraft in the center of its roll limit cycle. The effect of transmitting the maneuver that much earlier was to move the aiming point approximately 115 km away from the nominal aiming point in the +T direction.

The commanded pitch, roll, and burn sequence was not precisely the same as the computed values due to the necessity of quantizing the commands. Table 96 lists both computed and commanded quantities, as well as the estimates of the actual values and the standard deviations of those estimates.

The postmidcourse orbit determination showed that a second maneuver would not be needed. The estimate of the actual maneuver was computed by taking the difference in velocities between the premidcourse and postmidcourse orbits at the nominal time of motor shutoff.

Table 96. Maneuver parameters

Category	Pitch turn deg	Roll turn deg	Velocity magnitude m/sec
Computed	−39.23	156.08	16.705
Commanded	−39.16	156.06	16.699
Estimated[a]	−39.47	156.71	17.072
Standard deviation of estimate	1.03	0.088	0.059
Estimated execution error	− 0.31	+0.65	+0.37
A priori standard deviation[b]	0.69	0.69	0.14

[a]From orbit determination computer program with tracking through 1/23/65.

[b]From execution error analysis.

The position of the spacecraft during the motor burn actually changed slightly, but by such a small amount compared to the uncertainties in position that it could be ignored.

To estimate the turn magnitudes, the turns required to point the motor opposite to the estimated velocity direction were computed. The initial spacecraft coordinates were referenced to the Sun direction (controlling pitch and yaw) and the Canopus direction (controlling roll). From telemetry readouts, the spacecraft went into the inertial control mode with the positions in the three limit cycles as listed in Table 97. It was from these initial conditions that the pitch and roll turns in the "estimated" category in Table 96 were computed.

To obtain the best possible estimate of the actual midcourse maneuver, it would be necessary to have a consistent pair of premidcourse and postmidcourse orbit determinations. This is due to the fact that the orbit determination program estimates various other parameters in addition to position and velocity of the spacecraft. For example, if the premidcourse and postmidcourse orbit determinations converge to slightly different values of the estimated mass of the Earth, these two orbits will be inconsistent. When all the flight data have been collected, the two orbits will be forced into consistency by using the results of the premidcourse orbit as *a priori* information for the postmidcourse orbit, and the results of the postmidcourse orbit as *a priori* information for the premidcourse orbit through several iterations until the two orbits are consistent. This process, however, represents a large block of computer time and will not be attempted until all the tracking data have been collected.

Table 97. Three limit cycle positions

Direction	Position in limit cycle deg	Range of limit cycle deg
Pitch	−0.29	±0.50
Yaw	+0.29	±0.50
Roll	−0.12	±0.25

D. Orbit Determination

Part of the FPAC team responsibility is to support all JPL space flight missions by performing three primary functions:

1. As quickly as possible after launch, it computes an accurate estimate of the spacecraft orbit so that, if necessary, a midcourse maneuver can be computed and performed.

2. After a maneuver has been performed, it computes an estimate of the new trajectory into which the spacecraft has been placed. For the *Mariner IV* mission, this estimate will determine whether a second maneuver must be performed, and will allow the remainder of the mission to be controlled in a way that should provide the maximum probable return from the science experiments. Throughout the cruise and encounter portions of the flight, the orbital estimate will be updated repeatedly as new tracking data are received.

3. Throughout a mission, it provides the tracking stations with antenna pointing predictions and transmitter frequencies for maintaining radio contact with the spacecraft.

In addition to these inflight functions, three more functions are of importance to the *Mariner* Mars project:

1. By performing orbit determination accuracy and capability studies, preflight mission planning contributions are made.

2. Through reduction and analysis of tracking data, the DSIF is aided in advancing the state of the art in tracking and communications equipment.

3. Through careful postflight analysis of tracking data, contributions are made to the planning of future missions and to the scientific community in general by improving man's knowledge of the values of physical constants and tracking station locations.

1. Orbit Determination Methods and Tools

a. Tracking data. One of the first requirements of precise orbit determination is a source of accurate tracking data. These data can include almost any kind of measurement that in some way describes the position or velocity of the spacecraft at some point along its trajectory. The most important measurements made by the tracking stations are of angles and of two-way doppler.

Angular measurements of the spacecraft's position (right ascension and declination) are valuable primarily during the very early portion of a flight when the orbit is poorly known and the trajectory geometry is changing

rapidly. After a few hours of flight, the spacecraft reaches an asymptote and repeated measurements of the slowly changing angles are no longer valuable.

Two-way doppler measurements are of more continual value during flight. When a narrow bandwidth radio signal of known frequency is transmitted to the spacecraft, the motion of the spacecraft with respect to the transmitting station causes the signal to be received at a slightly lower frequency (the well known doppler effect). The signal is retransmitted by the spacecraft and returns to the station after having received an additional frequency shift on the downward leg of its trip. The received signal is compared to the one transmitted to determine the total doppler shift, which provides a measure of the radial velocity (range rate) of the spacecraft with respect to the station.

In practice, the magnitude of the doppler shift is not recorded instantaneously; instead, the cycles of the doppler tone are continuously counted and periodically read out. The difference between two successive counter readings is the total phase shift or range change over the elapsed time between readouts. Dividing this quantity by the counting time gives a measurement of the average doppler shift or range rate over that period. The time between counter readouts is variable; it may be set at from 1 to 60 sec. The allowable time between readouts is determined by how rapidly the spacecraft range rate is changing. Since counter readout is nondestructive, the continuous doppler count can often be maintained for as long as several hours. Thus, in the heliocentric portion of the flight when the range rate is changing very slowly, range differences may be formed over periods of from 10 to 15 min rather than between every readout. This procedure, known as doppler compression, is used both to improve data accuracy and to decrease data reduction time.

The two-way doppler system that has been developed by the DSIF is probably the most accurate source of spacecraft tracking data in existence. It uses extremely precise rubidium frequency standards (stable to about 1 part in 10^{11} over long and short periods of time), and can provide low-noise, unbiased tracking data from a spacecraft that is transmitting at a power of 10 w from a range of over 100 million kilometers. When short count times (less than 3 min) are used, the major source of error is the inability of the doppler counter to respond to phase shifts of less than one-half cycle. The difference between any two counter readings, therefore, can be in error by that much. At a count time of 60 sec, this amounts to an unbiased noise source with a standard deviation of about 0.02 cm/sec. As the count time is increased, the one-half-cycle error takes on a smaller cycles-per-second value, and, at count times greater than 600 sec, other noise sources with a standard deviation as low as one-fourth that size become dominant.

b. Computational method. An estimate of the spacecraft's orbit is computed from the tracking data by means of a weighted least-squares fitting technique. Briefly, the problem is to compute, by means of a least-squares fitting technique, a theoretical spacecraft trajectory that best fits the observations of the true trajectory. Since the free space trajectory must obey a known deterministic set of equations of motion, the problem reduces to one of finding a set of trajectory initial conditions. Thus, the independent variables that specify a spacecraft trajectory, and whose effects can be seen in the tracking data, consist not only of the initial spacecraft position and velocity but also include the masses of the various gravitating bodies, the lunar and planetary ephemeris scaling factors, and the reflectivity of the spacecraft (since its trajectory is perturbed by the force of the impinging sunlight). It is because the effects of these parameters can be accurately measured by doppler tracking that the determination of a spacecraft's orbit can frequently produce values of physical constants that are far more accurate than those available from other methods.

Although the direct result of the least-squares fit to the tracking data is the set of trajectory initial conditions, the parameters that are of most interest are the target conditions that result from integrating the trajectory forward to its point of closest approach to Mars. These conditions could consist of the spacecraft's areocentric spherical or Cartesian coordinates at the time of closest approach; however, they are more often expressed in what is called the **B** plane system, defined in Fig. 429.

The least-squares orbit computation also produces an estimate of the orbit accuracy. This is a function of the way in which the data are weighted and of the *a priori* uncertainties that are attached to the physical constants and station locations. The accuracy estimate appears in the form of standard deviations on the estimated parameters. These deviations can also be mapped to the target time to show uncertainties in the **B** plane, and are expressed in terms of the semimajor axis, semiminor axis, and orientation angle of the 1 σ dispersion ellipse in the plane.

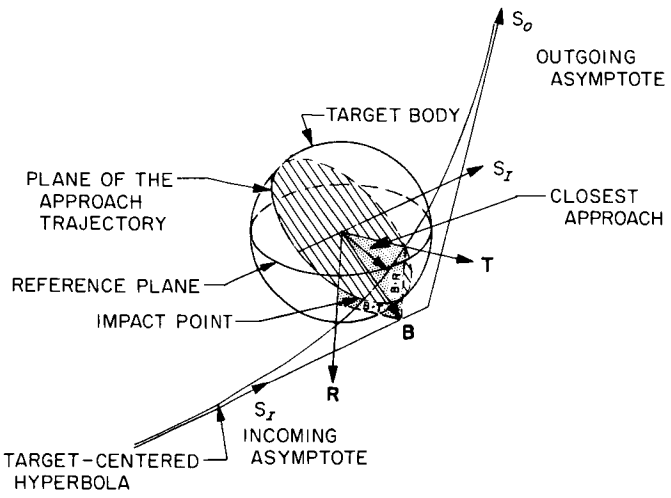


Fig. 429. Definition of B·T, B·R system

c. Data weighting. In classical least-squares fitting, each data point is given a weight that indicates the assumed variance on the point. Thus, measurements that are considered more accurate exert a stronger influence on the estimate. The variances are presumed to be uncorrelated in time. Errors are assumed to arise from several different sources, among which are:

1. Granularity of the doppler counter
2. Drift of the rubidium frequency standard
3. Refraction, stemming from an incorrect model of the Earth's atmosphere
4. Computations, such as roundoff in the trajectory integration

During real-time operations, the data variances are arbitrarily increased to cover the possibility of unpredictable errors such as the use of bad data, spurious forces from attitude control jets, and computer program input errors. During the *Mariner IV* flight, two-way doppler is being given an effective standard deviation of 0.03 m/sec for a sample rate of 60 sec, even though the observed noise on the data is nearly two orders of magnitude smaller.

2. Accuracy Requirements and Preflight Studies

The orbit determination accuracy required for the *Mariner* Mars mission was separated into three classes, which were defined as follows:

1. Class I requirements were those necessary to ensure the accomplishment of primary mission objectives. They were mandatory requirements, which, if not met, would result in a decision not to launch.
2. Class II requirements were those necessary to accomplish all stated mission objectives. They represented the desired performance, but their violation would not constitute grounds for holding the launch.
3. Class III requirements represented the ultimate in desired performance.

In order to determine whether the accuracy requirements could be met, statistical accuracy studies were performed using simulated data from selected representative trajectories.

a. Launch phase requirements and studies. The original *Mariner* Mars orbit determination accuracy requirements were:

1. For Class I, the rss error in the estimate of miss components could not exceed 5000 km at I + 5 days. An early orbit had to be determined shortly after injection.
2. For Class II, the rss error in the estimate of miss components could not exceed 5000 km at I + 2 days.
3. For Class III, the rss error in the estimate of miss components could not exceed 500 km at I + 2 days.

These requirements referred only to the early, premaneuver portion of the flight. It was during this time, of course, that an accurate orbit was most important, since it was needed for the computation of the midcourse maneuver. Because the *Mariner* Mars spacecraft are capable of performing two maneuvers, it was also important that the orbit be redetermined within a reasonable time after the execution of the first maneuver.

Orbit determination accuracy is primarily a function of four parameters:

1. The trajectory geometry that determines how well the effects of various orbit parameters can be measured by the tracking data
2. The assumed error in the estimates of universal and spacecraft constants
3. The effective data noise

4. The amount of available tracking data, and the tracking pattern (e.g., data taken near launch or encounter might be more valuable than those recorded during cruise)

The first *Mariner* Mars 1964 orbit accuracy study began late in 1963. It demonstrated in every case considered that the semimajor axis of the **B** plane dispersion ellipse after 5 days of tracking was less than half that specified by the Class I requirement. After 2 days of tracking, only three cases had semimajor axes greater than half the Class II requirement. The results demonstrated the value of near-Earth tracking in that, for nearly every case, the loss of an early Woomera pass had a more serious effect on the probable orbit accuracy than did the loss of a full 48 hr of data later in the flight.

During the first half of 1964, consideration was given to including the occultation experiment among the primary objectives of the mission. It was felt that in order to ensure adequate probability of success for this experiment, miss-parameter dispersions had to be limited to approximately 4650 km. Since the only other significant source of target error (maneuver execution errors) had a magnitude of about 4070 km, orbit determination dispersions would have to be less than 2250 km at the time of the maneuver (nominally 5 days after launch). The accuracy study had shown that this figure could be attained. Based on this and other considerations, the occultation experiment was adopted and the orbit determination accuracy requirements were revised as follows:

1. For Class I, the rss error in the estimate of miss components could not exceed 2250 km at I + 5 days. An early orbit had to be determined shortly after injection.

2. For Class II, the rss error in the estimate of miss components could not exceed 2250 km at I + 2 days.

3. For Class III, the rss error in the estimate of miss components could not exceed 400 km at I + 5 days.

During the Spring and Summer of 1964, two additional studies of the premaneuver portion of the flight were made. In the first, an intensive study of two representative trajectories was performed. Its purpose was to provide a detailed analysis of the relative effects of the various error sources that corrupt orbit accuracy. Among the significant results of this study were:

1. Orbit uncertainties would be only moderately affected by changes in data weighting.

2. For an early launch date, the major source of error would be uncertainties in station locations. For a later launch date, uncertainty in the solar pressure force would be the primary error source.

3. Uncertainties in the Earth's gravitational constant and in the astronomical unit would contribute a neglible amount to the orbit uncertainty.

The second study was an attempt to look at probable orbit determination accuracies for every day in the launch period. This was done using conic approximations to the true trajectories; therefore, the results were probably not accurate to better than 10%. The purpose of the study was to ascertain whether there were any portions of the launch period during which orbit determination capability would be significantly poorer than that demonstrated in the original study. Results of the study produced the following information: (1) there was no launch date on which the Class I accuracy requirements could not be met; (2) there was a steady increase in orbit determination capability as later launch dates were used; and (3) an apparent discontinuity near November 11 was related to the transition from Type II to Type I trajectories. The generally unusual behavior of trajectories launched on November 11 later caused that date to be eliminated from the launch period.

b. Cruise studies. Several studies of the cruise phase of the Mars mission were performed to learn (1) how soon orbit determination errors would be small enough to permit a second maneuver, if it were required; (2) how knowledge of the miss parameters could improve through the long heliocentric portion of the flight; and (3) how accurately physical constants and station locations could be determined. These studies resulted in a knowledge of some facts concerning the tracking of the *Mariner IV* spacecraft during the heliocentric portion of its flight:

1. Only two-way doppler tracking would be needed; angular data would be of no value.

2. Following a maneuver performed from 3 to 10 days after launch, 3 to 5 days of tracking would reduce the semimajor axis of the dispersion ellipse to less than 2000 km.

3. Tracking the spacecraft for a few hours once or twice per week from a single station would result in the same orbit accuracy as continuous tracking.

4. After 60 to 90 days of tracking, solar pressure forces would be well enough known to be a negligible source of error. After that time, the semimajor axis would remain relatively constant from 300 to 500 km until shortly before encounter.

5. Tracking through the heliocentric phase could provide an estimate of the astronomical unit with a standard deviation of less than 500 km.

c. Encounter studies. Many studies have been made of the encounter portion of a *Mariner* Mars flight, some of which are still underway and will continue until shortly before *Mariner IV* encounter. The important results obtained through midcourse maneuver are summarized below.

With data up to 6 hr before the time of closest approach to Mars included in the orbit estimate, the semimajor axis is not significantly smaller than its cruise value (300 to 500 km). Adding data through the time of closest approach decreases its value to about 25 km. When 2 more hours of data are added, a value of approximately 0.5 km results, which is not substantially improved by any further addition of data.

In order to support the occultation experiment, the best value of the ground transmitter frequency must be predicted in real time for rapid acquisition of the spacecraft upon its emergence from behind Mars. It should be possible to make this real-time prediction with orbit errors of less than 2 parts in 10^9. This figure is at least an order of magnitude smaller than predicted errors from other sources.

In order to successfully support the occultation experiment, it is necessary that the spacecraft's range rate near the time of occultation be estimated as accurately as possible. During postlaunch analysis, it was possible to limit errors in this estimate to less than 0.001 m/sec. This figure is more than an order of magnitude smaller than the predicted effects of the model of the thinnest Mars atmosphere.

Current estimates of the uncertainty in the mass of Mars vary from 0.1 to 2%. Reduction of encounter phase tracking data will reduce this uncertainty to 0.001%, at the most.

3. Computer Program Development

Extensive postflight reduction of the tracking data gathered during the *Mariner II* flight past Venus has resulted in estimates of the miss parameters for that mission that are probably in error by no more than 10 km. Thus, it is possible to compare these final estimates with the values that were predicted at various times during the flight, and, thereby, to evaluate the errors in the real-time orbit computations of *Mariner IV*.

The *Mariner* Venus program could estimate only the initial position and velocity of the spacecraft. It could not correct errors in the values of physical constants and station locations, and did not consider these error sources in its computation of miss parameter uncertainties. The *Mariner* Mars program estimated, and treated as error sources, the values of 66 different parameters (up to 20 at one time).

The *Mariner II* trajectory was seriously perturbed by forces from uncoupled attitude control jets, and the ground computer program did not include these forces in its equations of motion. Although the spacecraft for the *Mariner* Mars mission were designed to eliminate such forces, they were included in the equations of motion of the IBM 7094 computer program, which estimates their magnitudes.

The two remaining major error sources that are not accounted for in the *Mariner* Mars computer program are computer round-off and errors in the planetary ephemerides. A new version of the program, which will use double precision arithmetic and estimate orbital elements of the Earth and the target body, will be available for postflight analyses. (During the flight, these error sources will be statistically accounted for by means of effective data weightings.) Other significant limitations arise from uncertainties in the values of the astronomical unit, the mass of Mars, and the ephemerides of the Earth and Mars. Once the necessary program corrections have been made, careful postflight analysis of the data should produce major improvements in the knowledge of all of these quantities. These improvements should leave only such unpredictable and unusual forces as micrometeorite impacts and attitude control gas leaks normal to the Earth–spacecraft line of sight as error sources during the cruise and encounter portions of future planetary flights. Accuracy during the near-Earth portion of such flights will continue to be limited by the accuracy of the ground measurement of spacecraft area and reflectivity properties.

4. Real-time Space Flight Operations

a. Functional description. During the first few hours of a mission, the primary function of orbit determination

is the computation of tracking predictions. These predictions are necessary to enable the DSIF stations to establish and maintain contact with the spacecraft Because of their great importance, a highly redundant system of checks and recomputations has been established to minimize the probability of transmitting incorrect predictions.

Several weeks before a launch, predictions based on a nominal boost phase are generated for equally spaced (3 deg) launch azimuths covering every day of the launch period. These are delivered to the tracking stations to provide a backup in case of a communications outage during the launch. Then, when the prelaunch countdown reaches L − 5 min, predictions based on a nominal boost phase at the predicted launch time are generated. In case there is a hold during the last 5 min, the computation is restarted. This set of predictions is transmitted to the stations either if the actual launch azimuth differs significantly from all those included in the nominal set or if, for some other reason, they appear to be more accurate.

The first data obtained after launch result from tracking the launch vehicle as it coasts in parking orbit. These data are collected by AFETR stations and are processed at Cape Kennedy to provide an estimate of the initial conditions of the parking orbit. A nominal second burn is assumed, and transfer orbit predictions are generated. These are transmitted to the SFOF for comparison with the prelaunch nominal predictions, and from there are passed on to the DSIF stations at Johannesburg, South Africa, and Woomera, Australia. In addition, the initial conditions from the AFETR orbit computation and the raw data are also transmitted to the SFOF for checking and recomputation.

Once the second vehicle burn has occurred, the booster is again tracked by AFETR and the data are processed at the Cape to provide an estimate of the transfer orbit. (Although the launch vehicle's orbit differs from the spacecraft's after separation, the difference remains small long enough that predictions based on the *Agena* orbit can be used to acquire the spacecraft signal.) The procedure used during the parking orbit is then repeated, and predictions, initial conditions, and raw data are sent to the SFOF for checking and recomputation.

Once a DSIF station has acquired the spacecraft signal, the tracking data are transmitted to the SFOF and processed to provide a more accurate orbit and a better set of predictions. Until enough data have accumulated, combined fits to AFETR and DSIF data can be made. Once it appears that a reasonably good orbit has been determined, predictions for the next several hours of flight are computed and transmitted. The primary task then becomes the determination of the most accurate orbit possible for use in the computation of the midcourse maneuver.

b. Mariner III operations. Orbit determination for the *Mariner III* launch began at L − 5 min with the computation of nominal tracking predictions. Holds in the countdown caused the computation to be restarted twice. Operations then proceded as scheduled through the parking orbit phase of the flight. The trajectory initial conditions computed at Cape Kennedy and at the SFOF and the predictions generated from them appeared to be near nominal.

The first indication that the spacecraft trajectory might be nonstandard came at L + 45 min. The orbital elements of the escape trajectory computed at Cape Kennedy included a value of $C_3 = 4.08$ km²/sec², whereas the nominal value was 10.4 km²/sec². However, the epoch time associated with the trajectory initial conditions was in error by 5 hr, indicating a possible error in computations. When the elements were retransmitted at L + 50 min, the epoch time was nominal but the value of C_3 remained nonstandard. An independent reduction of the data used in the Cape Kennedy orbit computation was completed at the SFOF at L + 53 min. The results of the SFOF computations were in good agreement with Cape Kennedy conditions and indicated $C_3 = 4.04$ km²/sec².

Since both the SFOF and Cape Kennedy orbit computations had used only data from the Pretoria station, the possibility that the data were biased still existed. Woomera had not been able to maintain a solid lock on the spacecraft signal, and had not provided enough data to permit an independent orbit computation based on DSIF tracking. However, a fit to data gathered by the Sword Knot tracking ship agreed with the SFOF and Cape Kennedy results and confirmed the nonstandard nature of the trajectory.

At L + 176 min, Woomera established two-way lock with the spacecraft. Twenty minutes later, an orbit computation using two-way doppler angles was begun from that station. The initial conditions obtained were in good agreement with those obtained from the fits to AFETR data; a C_3 value of 4.06 km²/sec² was indicated.

This orbit was used to generate tracking predictions that were used during the remainder of the flight.

During the remainder of the operations, a number of orbit computations were made using various combinations of data from AFETR stations at Pretoria, Carnarvon, and on the tracking ships, and from DSIF stations at Woomera and Johannesburg. All results were consistent and indicated that the spacecraft would miss Mars by about 67 million kilometers, with closest approach occurring on April 15, 1965. Reduction of data obtained by tracking the *Agena* after the nominal time of the retro-maneuver indicated that the maneuver had occurred, and verified that the *Agena* had separated from the spacecraft. After tracking was terminated, predictions for the next 5 days were generated so that a search for the spacecraft signal could be maintained.

c. Mariner IV operations. With few exceptions, orbit determination operations in support of *Mariner IV* were entirely nominal and proceeded as scheduled. The major points of interest can be summarized as follows:

1. The reduction of AFETR data and the generation of tracking predictions proceeded as scheduled from launch through signal acquisition by Woomera. All results were near nominal.

2. The first fit to DSIF data indicated a near-standard trajectory with a correctable miss.

3. All subsequent orbit computations were consistent with the original fit, and by L + 16 hr, the computed miss parameters had converged to nearly constant values.

4. The orbit used for the computation of the aborted December 4 maneuver included data through L + 4 days and had a semimajor axis of approximately 1100 km.

5. The orbit used for the computation of the December 5 maneuver included data through L + 6 days and had a semimajor axis of 1080 km.

Throughout the premaneuver portion of the flight, the quality of the tracking data was excellent. Two-way coverage was nearly continuous, and, with the exception of isolated points, no bad data were detected. No inconsistencies between the three DSIF stations being used were discovered.

Of the few anomalous events that occurred, three are described here. First, uncertainties in target miss parameters could not be computed between L + 3 days and L + 6 days because of a computer program error. The error was isolated and corrected before the computation of the final premaneuver orbit. Second, the estimate of forces due to solar radiation pressure was consistently higher than the preflight estimate. It was discovered later that this anomaly was caused by incorrect positioning of the solar vanes during solar panel deployment. Since the error was not discovered until after the maneuver had been performed, an error of approximately 1000 km was introduced in the postmaneuver miss distance. Third, reduction of *Agena* data indicated a premaneuver miss distance about 150,000 km greater than that obtained from fits to spacecraft data. This problem has not been entirely resolved, but the difference can probably be attributed to the velocity increment produced by the spring separation of the spacecraft from the *Agena*.

XXV. TRACKING AND DATA ACQUISITION SYSTEM

The technical activities of the DSN, AFETR, and GSFC in support of the *Mariner* Mars 1964 mission are described in this Section. The tracking and telemetry coverage discussed are concerned with only the prelaunch activities and flight operations up to and including the midcourse maneuver.

Tracking and telemetry coverage for the *Mariner* Mars 1964 mission is provided by the DSN and by AFETR. In addition to this primary coverage, GSFC provided backup coverage for *Agena*-booster tracking and telemetry requirements.

The AFETR tracking and telemetry facilities were used to provide coverage during the *Atlas* and *Agena* flight portions of the mission. The three basic pre-injection requirements for near-real-time data were DSIF initial acquisition predictions, orbital elements of the parking orbit, and the initial estimate of spacecraft injection conditions. The five areas of the AFETR support plan are: (1) metric data from launch to 5000 ft, (2) engineering sequential data, (3) telemetry data, (4) communications support, and (5) data processing support.

The AFETR station names and number designations, the GSFC support facilities, and the DSIF stations in the *Mariner* Mars mission are given in Table 98.

Backup C-band radar tracking coverage was provided by GSFC at the Bermuda and Carnarvon stations of the Manned Space Flight Network. Bermuda covered the early *Agena* period of flight and Carnarvon provided support during the post-*Agena* retro period. The Space Tracking and Data Acquisition Network station at Tananarive provided FM/FM telemetry coverage of the *Agena*. Bermuda recorded telemetry data on the *Atlas* link (229.9 Mc) and the *Agena* link (244.3 Mc). Carnarvon recorded telemetry data on the 244.3-Mc *Agena* link only.

The DSN consists of the DSIF stations, interstation communications, and the mission-independent portions of the SFOF. The DSIF support function consisted of obtaining angular position, doppler, and telemetry data from the spacecraft during the postinjection phase of the mission. The three primary DSIF stations committed to the mission were Pioneer, Goldstone, California (DSIF-11), Woomera, Australia (DSIF-41), and Johannesburg, South Africa (DSIF-51).

Table 98. T&DA support facilities: *Mariner* Mars 1964 near-Earth trajectory phase

Facility	Number
Air Force Eastern Test Range	
Patrick Air Force Base, Florida	0.18
Cape Kennedy, Florida	1
	1.16
Grand Bahama Island, Bahama Is.	3
	3.16
San Salvador, Bahama Is.	5.16
Grand Turk, British West Indies	7.18
Ascension Island	12
	12.16
Pretoria, South Africa	13
Merritt Island	19.18
Antigua, British West Indies	91
	91.18
Melbourne Beach, Florida	None
Vero Beach, Florida	None
Williams Point, Florida	1.2
Cocoa Beach, Florida	None
Range instrumentation ships	
Twin Falls	1886
Sword Knot	1852
Coastal Crusader	1851
NASA/GSFC Manned Space Flight Network	
Bermuda	None
Carnarvon, Wales	None
NASA/GSFC Satellite Tracking and Data Acquisition Network	
Tananarive, Malagasy Republic	None
NASA/JPL Deep Space Network	
Deep Space Instrumentation Facility	
Goldstone Pioneer, Goldstone, California	DSIF-11
Woomera, Australia	DSIF-41
Johannesburg, South Africa	DSIF-51

A. Tracking and Data Acquisition Requirements

The T&DA requirements were divided into two categories: (1) tracking and telemetry coverage requirements placed upon AFETR, GSFC, and JPL/DSN; and (2) the technical data and support required by the tracking and telemetry facilities. These requirements were originated by both LeRC and JPL for the purpose of obtaining flight system performance data, look-angle calculation

data, and launch vehicle post-retro-maneuver orbit determination data. The look-angle calculation data were used as an acquisition aid by the tracking stations. Requirements based on range safety considerations were originated by AFETR.

1. Development and Classification of Requirements

The tracking coverage requirements were developed in the following manner:

1. The mission requirements stated that the spacecraft must pass Mars at the desired aiming point, at the desired time, within a certain accuracy tolerance.

2. A midcourse maneuver was to be used, if necessary, to correct trajectory errors at injection.

3. Therefore, a requirement for orbit determination accuracy prior to the midcourse maneuver was imposed so that the maneuver could meet the mission accuracy requirements at encounter.

4. The tracking coverage, data interval, and data accuracy requirements were then placed on AFETR and the DSN in support of the orbit determination accuracy requirements.

The telemetry coverage requirements for the *Mariner* Mars 1964 mission were developed in much the same manner.

2. Launch Vehicle Tracking Requirements Placed on AFETR

The requirement was placed on AFETR to provide tracking coverage of the launch vehicle that would satisfy four specific needs; i.e., range safety, launch vehicle performance evaluation (Table 99), AFETR look angle calculations, and launch vehicle post-retro-maneuver orbit determination (Table 100).

3. *Agena* Booster Tracking Requirements Placed on GSFC

The Tracking and Data Systems Directorate of the Goddard Space Flight Center was given the responsibility of providing backup C-band radar support at the Bermuda and Carnarvon stations during the tracking and data acquisition of the *Agena*. The radar and telemetry facilities of the MSFN stations at Bermuda and Carnarvon were designated as the support stations for the mission. The Tananarive station, which is operated by the Space Tracking and Data Acquisition Network, provided FM/FM telemetry coverage of the *Agena*.

4. Mission Requirements for Tracking Placed on AFETR

The mission requirements for tracking coverage resulted from the need to calculate DSIF look angles as an acquisition aid and the need for raw data to contribute to the accuracy and reliability of the spacecraft orbit determination process. The C-band beacon was to be tracked by AFETR in the *Agena* stage. (There was no requirement for AFETR tracking of the spacecraft.) Until separation, the orbits of spacecraft and *Agena D* would be the same. At separation, a relative velocity of about 2 ft/sec would be imparted to the spacecraft by the separation system springs; this, however, would not alter the total momentum. Since this separation velocity was small, AFETR tracking of the *Agena D* stage both before and after separation would be very valuable in determining the spacecraft orbit and in checking other tracking systems. Even after the retro-maneuver of the *Agena D* stage (several minutes after separation), tracking information would be helpful during the flight.

The processing of AFETR raw data after injection into the transfer orbit was involved with, and conditional upon, the telemetry identification of certain events. The relative weighting of the different AFETR data types (e.g., range and angles with respect to DSIF data) was a task requiring more information than what was available to AFETR; hence, it was important that the raw data be supplied. Requirements placed by JPL stated that the *Agena D* orbit be determined by AFETR and that raw tracking data be furnished to JPL during launch. Raw data are defined as azimuth, elevation, and range points that have not been altered by smoothing or weighting. One exception to this definition was exhibited by the desirability of correcting the tracking ships' raw data for the motion of the ships. However, the tracking ships' range data are valuable even if the motion factor of the ships has not been eliminated from the data.

5. Mission Requirements for Tracking Placed on the DSN

Requirements were placed on the DSN for the DSIF to track the spacecraft enabling it, in turn, to supply the raw tracking data for the determination of spacecraft orbits. These spacecraft orbits were necessary for generating prediction messages and for calculating the required midcourse maneuver.

Table 99. Launch vehicle tracking coverage required of AFETR (LeRC requirements)

Data required[a]	Interval	Class I[b]	Class II	Class III	Purpose and remarks
Metric launch data					
Position x, y, z	0 to 2000 ft	±2 ft	±½ ft	None	Required for overall evaluation of stage performance or gross malfunction analysis. Also required for analysis of vehicle roll and pitch performance.
Velocity V_x, V_y, V_z, V_r	0 to 2000 ft	±2 ft/sec	±½ ft		
Acceleration A_x, A_y, A_z, A_r	0 to 2000 ft	±1 ft/sec^2	±½ ft/sec^2		
Position x, y, z	2000 to 5000 ft	±10 ft	±1 ft		Optical position data reference to bottom horizontal *Agena* paint pattern line.
Velocity V_x, V_y, V_z, V_r	↓	±5 ft/sec	±½ ft/sec		
Acceleration A_x, A_y, A_z, A_r	↓	±2 ft/sec^2	±½ ft/sec^2		Continuous tracking required.
Position x, y, z	5000 to 100,000 ft	±10 ft	±2 ft		10/sec required; 5/sec acceptable from theodolites.[c]
Velocity V_x, V_y, V_z, V_r	5000 to 100,000 ft	±10 ft/sec	±5 ft/sec		
Acceleration A_x, A_y, A_z, A_r	5000 to 100,000 ft	±10 ft/sec^2	±5 ft/sec^2		
Position x, y, z	100,000 ft through VECO +1 sec to *Atlas/Agena* separation	±500 ft	±250 ft		Evaluation of *Atlas* and *Agena* guidance and control system performance. Continuous tracking required. Joint GD/C–LMSC requirement.
Velocity V_x, V_y, V_z, V_r	↓	±10 ft/sec	±5 ft/sec		Joint GD/C–LMSC requirement.
Acceleration A_x, A_y, A_z, A_r	↓	±10 ft/sec^2	±5 ft/sec^2		Joint GD/C–LMSC requirement.
Radar polar coordinate data, corrected azimuth, elevation and slant range	Launch to *Atlas/Agena* separation	±500 ft	±250 ft		LMSC requirement.
Position and velocity data	L +20 sec until *Atlas* VECO +50 sec		Best available	↓	GE requirement.
Metric midcourse data					
Position x, y, z	*Atlas/Agena* separation through first burn cutoff +60 sec	±10,000 ft	±1000 ft	±200 ft	To determine parking orbit injection conditions and to enable trajectory analysis.
Velocity V_x, V_y, V_z, V_r	↓	±200 ft/sec	±20 ft/sec	±2 ft/sec	LMSC requirements.
Radar polar coordinate data, corrected azimuth, elevation, and slant range	↓	±10,000 ft	±1000 ft	±200 ft	
H	↓	±10,000 ft	±1000 ft	±200 ft	
Metric orbital and space data					
Position x, y, z	*Agena* second-burn ignition −10 sec to second-burn cutoff		±10,000 ft	±1000 ft	*Agena* restart and powered flight, to determine injection conditions and vehicle performance.

[a]10 points/sec.

[b]Class I, II, and III requirements are discussed in Section XXIV.

[c]Events are used to determine intervals as they vary with the mission (LMSC requirements).

Table 99. (Cont'd)

Data required[a]	Interval	Class I[b]	Class II	Class III	Purpose and remarks
		Metric orbital and space data			
Velocity V_x, V_y, V_z, V_r	Agena second-burn ignition −10 sec to second-burn cutoff		±200 ft/sec	±20 ft/sec	LMSC requirements.
Radar polar coordinate data, corrected azimuth, elevation, and slant range			±10,000 ft	±1000 ft	
H	↓	±10,000 ft	±1000 ft	±200 ft	
Position x, y, z	Agena second-burn cutoff to retro-maneuver	±10,000 ft	±1000 ft	±200 ft	Final stage vehicle mission trajectory, to determine injection conditions and vehicle performance.
Velocity V_x, V_y, V_z, V_r	It is mandatory that any 60 sec of continuous tracking data be obtained during this interval	±200 ft/sec	±20 ft/sec	±2 ft/sec	Track of the second stage for as long as possible after retro-maneuver (not to exceed 3 hr after injection) was desirable to support secondary test objectives. This requirement for post-retro-maneuver was allowed to constrain the possible firing window that might otherwise have been available.
Radar polar coordinate data, corrected azimuth, elevation, and slant range	↓	±10,000 ft	±1000 ft	±200 ft	
H		±10,000 ft	±1000 ft	±200 ft	

Table 100. Launch vehicle tracking coverage required of AFETR (JPL requirements)

Data required[a]	Amount of data required data point/min			Accuracy of data required		
	Class I	Class II	Class III	Class I	Class II	Class III
Range, m	2	10	10	1000	10	1
Azimuth elevation, deg	2	10	10	0.5	0.02	0.005

NOTE: Requirements for raw data delivery to JPL/AFETR were: no later than L +1 hr for Class I data; and near-real time (within 2 min of the event) for Class II data.

[a]These data were required for each of the following events:

1. First *Agena D* burnout to first *Agena D* burnout +60 sec (Class I)
2. First *Agena D* cutoff to first *Agena D* cutoff +180 sec (Class II)
3. First *Agena D* cutoff to second *Agena D* ignition (Class III)
4. Any continuous 60 sec between injection and *Agena D* retro (Class I)
5. Injection to injection +2 hr (Class II)
6. Injection to loss of track (Class III)

Table 101. JPL requirements for *Mariner* Mars 1964 spacecraft tracking coverage by the DSN

Class	Orbit determination accuracy requirements
I	At injection +5 days, the rms error in the estimate of miss components could not exceed 2250 km. An early orbit had to be determined shortly after injection.
II	At injection +2 days, the rms error in the estimate of miss components could not exceed 2250 km.
III	At injection +5 days, the rms error in the estimate of miss components could not exceed 400 km.

First, an early orbit of the spacecraft had to be determined to allow calculation of look angles for subsequent tracking. In general, the DSIF initial acquisitions were performed with the aid of (1) preflight prediction data graphs or tabulations, and (2) inflight prediction messages based on the actual orbit as determined by AFETR. Subsequent acquisitions were made with prediction messages based on orbits calculated to satisfy the need for a final premidcourse maneuver orbit (Table 101).

Second, a final premidcourse maneuver orbit of the spacecraft had to be determined with sufficient accuracy to permit a midcourse maneuver to be made within the accuracy requirements.

Under normal conditions, the mission objectives could be realized with a single maneuver; however, a backup

maneuver was provided in case any of the errors listed above were excessive.

Raw tracking data in the form of two- and three-way doppler and antenna pointing angles would be provided by the DSIF for orbit determination. These data would contain noise resulting from correlations in the data, variations in refraction correction, oscillator drift, cycle-count drops and transmitter variations, to name a few causes. Therefore, it was necessary to specify the amount of noise that could be expected, so that the *a priori* orbit determination capability could be predicted as the launch azimuth and launch days were varied.

The estimates of the data noise expected are given in Table 102. These data were used to establish the data weightings that determined the orbit determination accuracy capability.

6. Telemetry Coverage Requirements

Requirements for coverage of the spacecraft telemetry through the spacecraft S-band or *Agena D* links were placed on AFETR and on the DSN. A requirement for backup telemetry support was placed on GSFC. The requirements placed on AFETR for coverage of the launch vehicle telemetry are described below.

a. Requirements placed on AFETR. An evaluation made by LeRC of the *Atlas D/Agena D* performance resulted in a requirement that the launch vehicle's telemetry systems be tracked during certain phases of the flight. In addition, AFETR range safety required launch vehicle telemetry data during the boost phase. The requirements are given in Table 103.

The spacecraft telemetry could be received by a station equipped for S-band and also a station designed to receive *Agena D* telemetry. The spacecraft transmitter would be continuously radiating from liftoff, and the telemetry signal would modulate the 98-kc subcarrier of the *Agena D* telemetry system. Both links would be exploited by AFETR to satisfy the spacecraft telemetry coverage summarized in Table 104.

Table 102. DSIF tracking data accuracy

System noise	Two-way doppler (1σ)[a] cps	Angles (1σ)[a] deg	Time synchronization (1 day after data are taken) sec	Absolute transmitter frequency stability over 1-min interval
Expected noise for S-band system	0.01	0.02	0.001	1×10^{-11}
Expected noise for L- to S-band conversion system	0.01	0.02	0.002 (Longer than S-band because L- to S-band stations are overseas)	3×10^{-11}

NOTE: High-frequency noise is 1 sample/min; two-way doppler data counted over 1 min.

[a] 1σ is a figure of accuracy.

Table 103. AFETR launch vehicle telemetry coverage (LeRC requirements)

Class	Requirements
I	During prelaunch calibrations on internal and external power. From L −2 min to *Agena D* first cutoff +25 sec. From *Agena D* second ignition −18 sec to *Agena D* second cutoff +20 sec. From *Agena D*/spacecraft separation −10 sec to continuous DSIF view +2 min.
II	During prelaunch calibrations on internal and external power. Continuous coverage from L −2 min to *Agena D* rocket ignition +1 min.
III	Same as for Class II.

Table 104. AFETR spacecraft telemetry coverage (JPL requirements)

Class	Requirements
I	During prelaunch calibrations. From launch to *Agena D* first cutoff +25 sec. From *Agena D* second ignition −8 sec to *Agena D* second cutoff +20 sec. From *Agena D*/spacecraft separation −10 sec to continuous DSIF view +2 min.
II	From launch to continuous DSIF view +10 min.
III	Same as Class II.

NOTES: Continuous DSIF view begins on all launch days for most launch azimuths at Johannesburg first-rise (0-deg elevation angle).
Continuous DSIF view always begins no later than Woomera first-pass rise (0-deg elevation angle).
Continuous DSIF view always begins between injection and injection + 15 min, depending on launch day and launch azimuth.
The spacecraft telemetry data were transmitted via the *Agena D* link and the spacecraft link before *Agena*/spacecraft separation. Coverage of either link before separation in support of spacecraft telemetry coverage requirements was satisfactory.

The requirements for data return for analyses were that data from the first launch *(Mariner III)* be returned and evaluated in 36 hr to support the second launch *(Mariner IV)* as soon as 48 hr after the first launch.

b. Requirements placed on GSFC. Telemetry coverage requirements placed on GSFC consisted of:

1. Telemetry data gathered at the participating stations for the life of the *Agena* telemetry transmitter via one telemetry link
2. Certain real-time readouts
3. Magnetic tape recordings, direct-write recordings, and telemetry operator's logs
4. Oscillograph recordings at Carnarvon.

c. Requirements placed on the DSN. The DSN was required to obtain spacecraft telemetry coverage beginning at Woomera rise + 2 min. Requirements were also placed on DSIF-51 to cover portions of the flight between launch and Woomera rise. The DSN capabilities during this early period would be used when possible, in harmony with the AFETR facilities. The majority of support during this early phase would be provided by AFETR. Data would be delivered to the SFOF by TTY for analysis.

B. Support and Facilities

1. AFETR Support

Following launch of each spacecraft, extensive use was made of the tracking and telemetry facilities at AFETR (Fig. 430) in support of the mission. Two basic requirements for AFETR near-real-time data that existed during the pre-injection phase of the mission were:

1. Initial acquisition data for the DSIF
2. An initial estimate of the spacecraft injection conditions

In general, the AFETR T&DA support plan consisted of the areas discussed in the following paragraphs.

a. Metric data. From launch to 5000-ft altitude, metric data were obtained by Cape Kennedy strip film camera sites. Primary coverage from about 5000 ft to BECO was provided by C-band radar at Cape Kennedy, Patrick Air Force Base, and Grand Bahama Island. Additional metric coverage was provided from the cinetheodolite system at the Cape, which operated at 5 samples/sec. This system was committed on a visibility-permitting basis from about 1000- to 90,000-ft altitude. Midcourse metric data from BECO through *Agena* first-burn cutoff were provided by radar at Cape Kennedy, Grand Bahama, San Salvador, Grand Turk, Bermuda, and Antigua. *Agena* second-burn coverage was provided by Pretoria radar and by range instrumentation ships. The tracking ships RIS 1886, Twin Falls (Uniform); RIS 1851, Coastal Crusader (Whiskey); and RIS 1852, Sword Knot (Yankee) supported that portion of the mission.

b. Engineering sequential data. Launch engineering sequential coverage was provided by 16-, 35-, and 70-mm fixed cameras at Cape Kennedy, Williams Point, Cocoa Beach, Patrick Air Force Base, Melbourne, and Vero Beach. All image-to-frame ratios were generally as requested by the project requirements.

c. Telemetry data. Telemetry coverage to radio horizon was provided by the receiving and recording stations at Cape Kennedy, Grand Bahama, San Salvador, Antigua, Ascension Island, Pretoria, and the three range instrumentation ships.

d. Support instrumentation. Most of the communications support instrumentation provided for the mission was at Cape Kennedy. All Florida mainland instrumentation sites were linked by TTY and voice lines. A subcable through Antigua connected downrange stations with Cape Kennedy. Existing VHF and HF radio links tied the ships and aircraft to land stations. Connection with the radar sites at Johannesburg and Ascension Island were made via TTY and voice circuits. Metric, engineering sequential, and telemetry data were all recorded against coded time. All major AFETR stations supporting the program used standard 17-digit modified binary codes. Time correlation between Cape Kennedy, Antigua, and Ascension was ± 5 msec. Instrumentation summary charts are presented in Table 105.

e. Data processing. Data recorded on film, strip charts, and tapes were reduced and processed at Patrick Air Force Base. Telemetry data were duplicated and processed at Cape Kennedy.

2. GSFC Support

a. Station coverage. Backup C-band radar tracking and data acquisition coverage were provided by GFSC at the Bermuda and Carnarvon stations of the MSFN. Bermuda covered the early *Agena* flight and Carnarvon provided support during the post-*Agena* retro period. The STADAN station at Tananarive provided FM/FM telemetry coverage of the *Agena*. Bermuda recorded

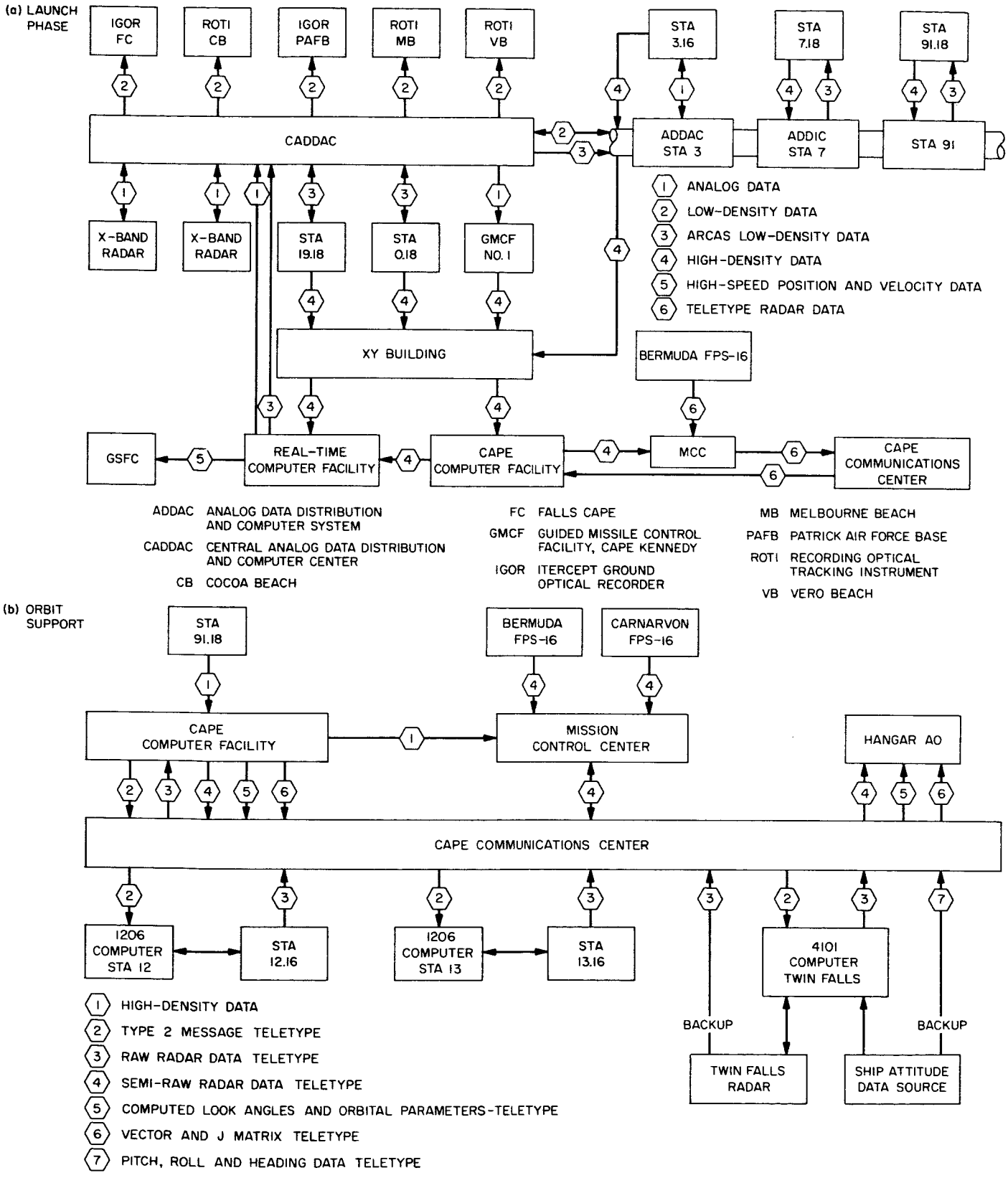


Fig. 430. Tracking facilities supporting *Mariner* Mars 1964 at Cape Kennedy

Table 105. AFETR instrumentation summary for *Mariner* Mars 1964

Location	Instrumentation	Use
Cape Kennedy Merritt Island Launch Area	Cinetheodolites	Metric data
	C-band radar	Metric data, range safety
	Fixed-camera system (strip film camera and RC-5)	Metric data
	LC cameras (16, 35, and 70 mm)	Engineering sequential data
	Telemetry Pulse amplitude modulation/FM/FM (VHF) 2 links FM/PM (S-band) 1 link	Internal data
	Command destruct	Range safety
	Wire sky screen	Range safety
	TV sky screen	Range safety
	Telemetry electronic sky screen	Range safety
	L-band radar (AN/FPS-8)	Range safety
	High-resolution radar tracker (X-band radar)	Range safety
	IBM 7094 computer	Range safety
	Intercept ground optical recorder (35- and 70-mm cameras)	Engineering sequential data
Williams Point	Intercept ground optical recorder (35- and 70-mm cameras)	Engineering sequential data
Cocoa Beach	Cinetheodolite	Metric data
	Recording optical tracking instrument (70-mm cameras)	Engineering sequential data
Patrick Air Force Base	Cinetheodolites	Metric data
	C-band radar (AN/FPQ-6)	Metric data, range safety
	Intercept ground optical recorder (35- and 70-mm cameras)	Engineering sequential data
Melbourne	Recording optical tracking instrument (70-mm cameras)	Engineering sequential data
Vero Beach	Recording optical tracking instrument (70-mm cameras)	Engineering sequential data
Grand Bahama Island	C-band radar	Metric data
	Telemetry Pulse amplitude modulation/FM/FM (VHF) 2 links	Internal data
	Command destruct	Range safety
San Salvador	C-band radar (AN/FPS-16)	Metric data
	Command destruct	Range safety
Grand Turk Island	Command destruct	Range safety
	C-band radar (AN/TPQ-18)	Metric data
Antigua	C-band radar (AN/FPQ-6)	Metric data, range safety
	Telemetry Pulse amplitude modulation/FM/FM (VHF) 2 links	Internal data
	Command destruct	Range safety

Table 105. (Cont'd)

Location	Instrumentation	Use
Ascension Island	C-band radar (AN/FPS-16)	Metric data
	Telemetry FM/FM (VHF) 1 link FM/PM (S-band) 1 link	Internal data
Bermuda	C-band radar	Contingent on committment by NASA
Pretoria	C-band radar (AN/MPS-25)	Metric data
	Telemetry FM/FM (VHF) 1 link FM/PM (S-band) 1 link	Internal data
RIS Twin Falls (T-AGM-11)	C-band radar	Metric data
	Telemetry FM/FM (VHF) 1 link FM/PM (S-band) 1 link	Internal data
RIS Sword Knot (T-AGM-13) RIS Coastal Crusader	Telemetry FM/PM (S-band) 1 link FM/FM (VHF) 1 link	Internal data
Aircraft	Range user equipment	GE guidance system calibration
	None	Return of data

telemetry data on the *Atlas* link (229.9 Mc) and the *Agena* link (244.3 Mc). Carnarvon recorded telemetry data on the 244.3-Mc *Agena* link only. The network configuration committed to support of the mission is shown below:

Station	*FM telemetry*	*C-band radar*	*SCAMA*	*Teletype*
Mission Control Center	X		X	X
Bermuda	X	X	X	X
Carnarvon	X	X	X	X
Tananarive	X		X	X
Kano[12]			X	X

b. Computer support. The Data Operations Branch was responsible for all mission computing and coordinating tasks required by GSFC. During the prelaunch countdown, all the tracking stations supporting the mission participated in the CADFISS[13] roll call to ensure valid radar data flow capability. Launch trajectory data were supplied to the GSFC computers by the AFETR complex. Events were passed to the GSFC Operations Director from the mission controller at the MCC. Approximately 1 week before launch, nominal pointing data were transmitted to the participating stations. During the transmitting lifetime of the vehicle, GSFC computers updated and displayed the data as required. In addition, acquisition messages were generated and transmitted to the participating stations. Radar data from Bermuda and Carnarvon were reformatted into standard 38-character *Gemini* format and transmitted to AFETR in near-real time.

c. Acquisition aids. The acquisition aids provided pointing information to the radar and telemetry RF inputs during the life of the onboard telemetry transmitter.

d. Radar coverage. The Bermuda and Carnarvon radar of the Goddard MSFN provided a portion of the

[12]Required as a communications relay point for Tananarive.

[13]Computer and data flow integrated subsystem test.

C-band radar tracking of the *Mariner III* and *Mariner IV Agena* booster vehicles. Communications between the AFETR radar controller and the remote sites were established over the Goddard conference loop and the DOD tie lines. Bermuda exercised standard phasing techniques as directed by the AFETR Radar Controller. As the downrange radar source, Carnarvon was responsible for phasing with Twin Falls and Pretoria during acquisition. Pretoria and Twin Falls used 80-pulse recurrence frequency 1,024,000-yd separation, but neither was equipped with identification coders.

e. Telemetry coverage. The GSFC coverage for the *Agena* booster was provided by Bermuda, Carnarvon, and Tananarive, all of which received and recorded the telemetry signal. Limited real-time readouts were provided by Carnarvon. Two receivers each were used by the three stations for telemetry reception. The oscillograph was set up at Carnarvon only to record Inter-range Instrumentation Group channel 14 in order to display velocimeter information with a minimum galvanometer deflection of 3 in. Recording speed was 8 in./sec. The recorder speed used to record signal strength was 10 mm/sec. Signals were recorded on 1-in. 14-track magnetic tape at Bermuda and Carnarvon and on ½-in. 7-track tape at Tananarive at a speed of 60 in./sec with a 100-kc reference.

f. NASA ground communications. Participating stations used existing full-time voice, teletype, and high-speed data circuits. Part-time circuits were not committed for the mission. During countdown, launch, and parking-orbit phases, the GSFC Communications Center and all participating stations were fully activated. Mandatory communication coverage periods during prelaunch were called up by the communication manager as required by the network controller. The communication links to all participating stations are indicated in Fig. 431. No critical coverage was required during the mission; however, special coverage was called on the voice, TTY, and HSD circuits from Cape Kennedy, Goddard, and Bermuda during the launch phase. The following communication circuits were designated for use during the mission:

Site	*Routing indicator*	*Voice*	*TTY*	*HSD*
Bermuda	GBDA	X	X	X
Mission Control Center	GMCC	X	X	X
Goddard Space Flight Center	GSPA	X	X	X
Carnarvon	ACRO	X	X	
Tananarive	LTAN	X	X	

The subswitching centers at London, Honolulu, and Adelaide were committed to support as required. Kano was used as a communications relay point for Tananarive.

g. Support arrangement. The MCC at Cape Kennedy was used for control of the GSFC support during the mission. No special modifications were required for the support of the mission. However, Tananarive was not operational as of launch and certain local modifications were implemented to ensure support.

h. Special data-handling requirement. In support of the 36-hr data-return plan, the Tananarive station had to deliver the telemetry tape from *Mariner III* to the Jan Smuts Airport in Johannesburg within 15 hr after launch. (If two copies of the tape were available, the time would be extended 2 hr.) The Tananarive station director was to inform the network controller via SCAMA when the tape had left the station and the estimated time of arrival at Pretoria, and the Project Office was to inform the Pretoria station of that time.

3. DSN Support

The *Mariner* Mars 1964 mission DSN T&DA support consisted of providing the facilities, equipment, and personnel necessary to meet the space flight operations requirements of the project.

a. DSIF mission support. The DSIF stations committed to support of the mission by the DSN are to obtain angular position, doppler, and telemetry data from the spacecraft during the postinjection phase of the flight. Ranging-data capability, in addition to two-way doppler, is available at DSIF-11 only. The DSIF also sends ground-computed commands in accordance with the procedures outlined in the *Mariner* Mars TIM. The spacecraft checkout facility at Cape Kennedy provided telemetry coverage from launch to local horizon.

Data obtained by the DSIF are transmitted to the SFOF in real time or near-real time by TTY and HSD circuits. In addition, the same data are recorded on magnetic tape at each DSIF station and dispatched to JPL by airmail.

DSIF stations. The following stations were designated the primary DSS for the *Mariner* Mars 1964 mission:

1. DSIF-11, Pioneer Station, Goldstone, California
2. DSIF-41, Woomera, Australia
3. DSIF-51, Johannesburg, South Africa

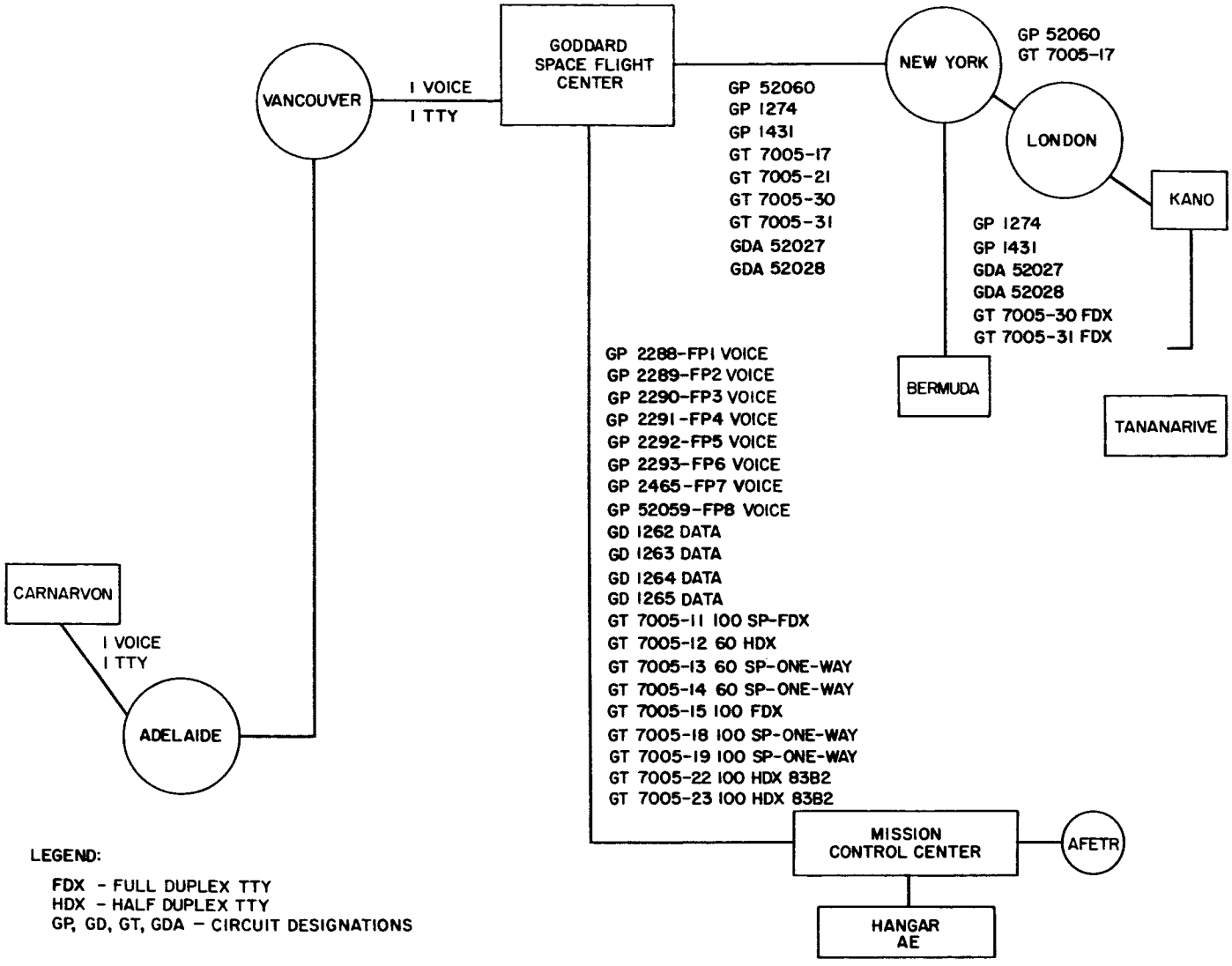


Fig. 431. Network communications configuration

The following stations were designated as the backup DSS for the mission:

1. DSIF-13, Venus Station, Goldstone, California (after April 1, 1965)

2. DSIF-42, Tidbinbilla, Australia (after February 1, 1965)

The L- to S-band conversion system has been used at DSIF-41 and DSIF-51 during the mission. The telemetry system and angle tracking are compatible with either the L- to S-band conversion system or the GSDS S-band system. However, there is a significant difference in the doppler format: use of the ranging subsystem is not possible with the L- to S-band conversion receiver.

One of the *Mariner* Mars 1964 Project requirements was for dual spacecraft coverage. Thus, the DSIF stations incorporated the capability of simultaneously transmitting near-real-time data from one spacecraft while recording and storing telemetry data from a second spacecraft for subsequent transmission to JPL.

Woomera was designated as the primary station for the early part of the flight. Tidbinbilla was scheduled to back up Woomera if dual spacecraft coverage was required, at which time, depending upon its operational

Table 106. DSIF characteristics and capabilities for *Mariner* Mars 1964

Item	Goldstone Pioneer DSIF-11 GSDS S-band[a]	Goldstone Venus DSIF-13	Woomera DSIF-41 L- to S-band conversion kit	Tidbinbilla DSIF-42 GSDS S-band	Johannesburg DSIF-51 L- to S-band conversion kit
Receiver capability	Two	None	One	Two	One
85-ft parabolic antenna mount	Polar (HA-Dec)	Equatorial (Az-El)	Polar (HA-Dec)	Polar (HA-Dec)	Polar (HA-Dec)
Maximum angular rate (both axes), deg/sec	0.7	1	0.7	0.7	0.7
Receiving antenna gain, db	53.0 ±1	Not applicable	53.0 ±1	53.0 ±1	53.0 ±1
Transmitting antenna gain, db	51.0 ±1	53.0 ±0.5	51.0 ±1	51.0 ±1	51.0 ±1
Antenna beamwidth, deg	~0.4	~0.4	~0.4	~0.4	~0.4
Typical system temperature, °K	60	Not applicable	60	60	60
Transmitter power, kw	10	100	10	10	10
Data transmission (via TTY)					
Angles	Real time	None	Real time	Real time	Real time
Doppler	Real time	None[b]	Real time	Real time	Real time
Ranging (to 800,000 km)	Real time	None	None	Real time	None
Telemetry	Real and near-real time	None	Real and near-real time	Real and near-real time	Real and near-real time
Demodulated telemetry	Dual channel	None	Single channel	Dual channel	Single channel
Command capability	Yes	Yes	Yes	Yes	Yes
Data-pack air shipment time to JPL, days	1	1	7	6	5

[a]Capability differences between L- to S-band conversion kit stations and GSDS S-band stations: no ranging, doppler format, single receiver.

[b]Coherent two-way doppler when operating at 100 kw with Pioneer station.

readiness, it would become the primary station if the DSN were overloaded.

Dual spacecraft coverage at DSIF-51 was to be provided by means of the L- to S-band conversion system covering one spacecraft and either a portable telemetry package or a modified angle channel of the S-band receiver covering the other spacecraft.

The parameters and capabilities of each DSIF station are given in Table 106. The operational frequency assignments are listed in Table 107. Approximately 2 hr are required to change the operating frequency at a station. Compatible telecommunications modes are listed in Table 108. Operational block diagrams of the stations are presented in Fig. 432 through 434. Ground operational modes are listed in Table 109.

The sample-rate capability for acquisition and prediction information required by the DSIF is described in Table 110. Station reports are periodically transmitted by each DSIF station to the SFOF.

Table 107. Operational frequency assignments during flight

Channel	Receive, Mc	Transmit, Mc
21	2297.592593	2115.699846
22	2297.962963	2216.040895
23	2298.333333	2116.381944
24	2298.703704	2216.722994

DSIF coverage. Three prime stations were assigned to meet the requirements placed on the DSIF by the *Mariner* Mars project. Any change in assignment had to be coordinated between the DSIF Operations Manager and the *Mariner* Mars 1964 Space Flight Operations Director so that no decrease in coverage would result from a change in prime stations.

Table 108. Compatible telecommunications modes

	One-way doppler	Two-way doppler	Two-way noncoherent doppler	Angle tracking	Ranging	Command	Telemetering
One-way doppler				X			X
Two-way doppler				X	X	X	X
Two-way noncoherent doppler				X[a]		X	X[a]
Angle tracking	X	X	X[a]		X	X	X
Ranging		X		X			X[b]
Command		X		X			X
Telemetering	X	X	X[a]	X	X[b]	X	

[a]Only at receiving station.

[b]Simultaneous operation not yet demonstrated.

Table 109. Ground modes

Mode	Transmit/receive (first digit)[a]	Antenna/microwave (second digit)[a]
1	One-way doppler (receive only)	SCM maser
2	Two-way, one station (transmit/receive)	SCM paramp
3	Two-way, two stations noncoherent (receive only)	SCM mixer
4	Two-way, two stations coherent (receive only with reference signal from transmit station)	SAA paramp
5	Receive only. No doppler	SAA mixer

[a]EXAMPLE: In ground mode 21, one station is transmitting to spacecraft and receiving two-way doppler using the SCM maser.

NOTE: Telemetry is available in all receive modes except zero.

Table 110. Acquisition and prediction information for DSIF stations

Time, min.	Origin	Station	Sample rate and amount
L +22	Impact predictor building	51, 59	1 sample/2 min, station rise to station rise +24 min
L +25	Impact predictor building	41	1 sample/2 min, station rise to station rise +24 min
L +30	Impact predictor building	41, 51	1 sample/5 min, station rise to station rise +100 min
L +100	Cape communications control	41, 51	1 sample/5 min, L +90 min to L +4 hr
L +220	Cape communications control	41, 51	1 sample/5 min, L +4 hr to L +10 hr
L +520	Cape communications control	11, 41, 51	1 sample/5 min, L +9 hr to L +30 hr
L +1440	Cape communications control	11, 41, 51	1 sample/5 min, L +26 hr to L +10 days

The DSIF provides coverage equivalent to 24 station hours/day for the duration of the flight. During injection and midcourse maneuver, additional coverage was provided by the prime stations up to the full view period of each station. (During the critical portions of other missions, the DSIF may not be able to provide full 24-hr/day coverage of the *Mariner IV*. The amount of reduced coverage will be negotiated between the DSIF Operations Manager and the *Mariner* Mars 1964 Space Flight Operations Director.)

DSIF station tracking reports. Tracking reports are submitted during a tracking period (1) every 30 min from launch to midcourse maneuver, and (2) at 1-hr intervals after midcourse maneuver.

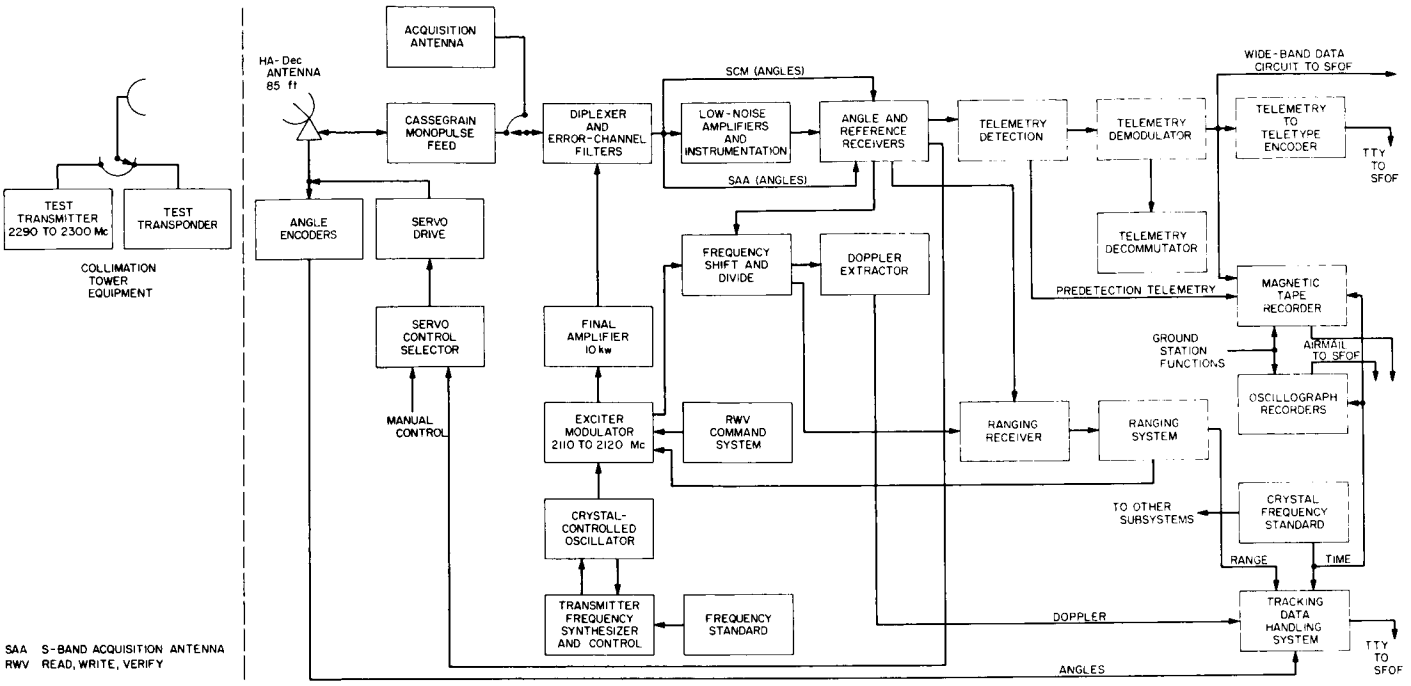


Fig. 432. *Mariner* Mars 1964 typical deep space station (S-band)

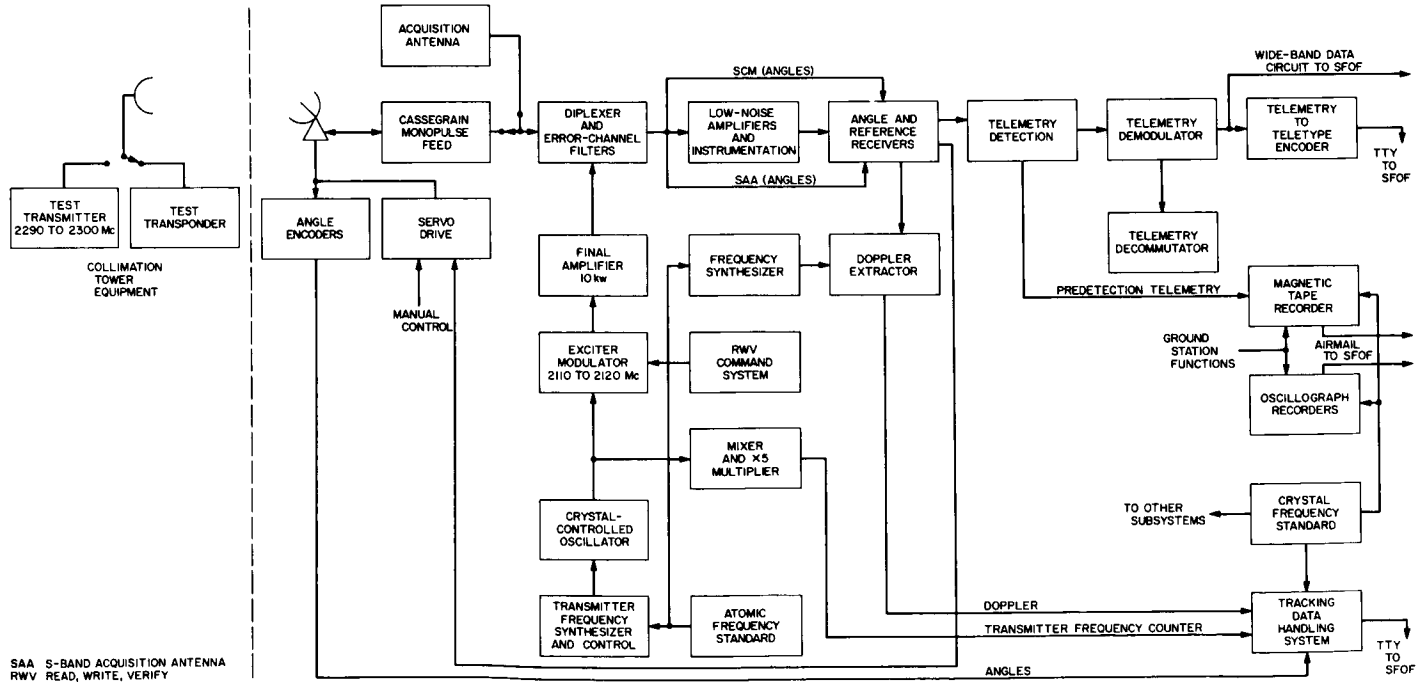


Fig. 433. *Mariner* Mars 1964 typical deep space station (L- to S-band conversion)

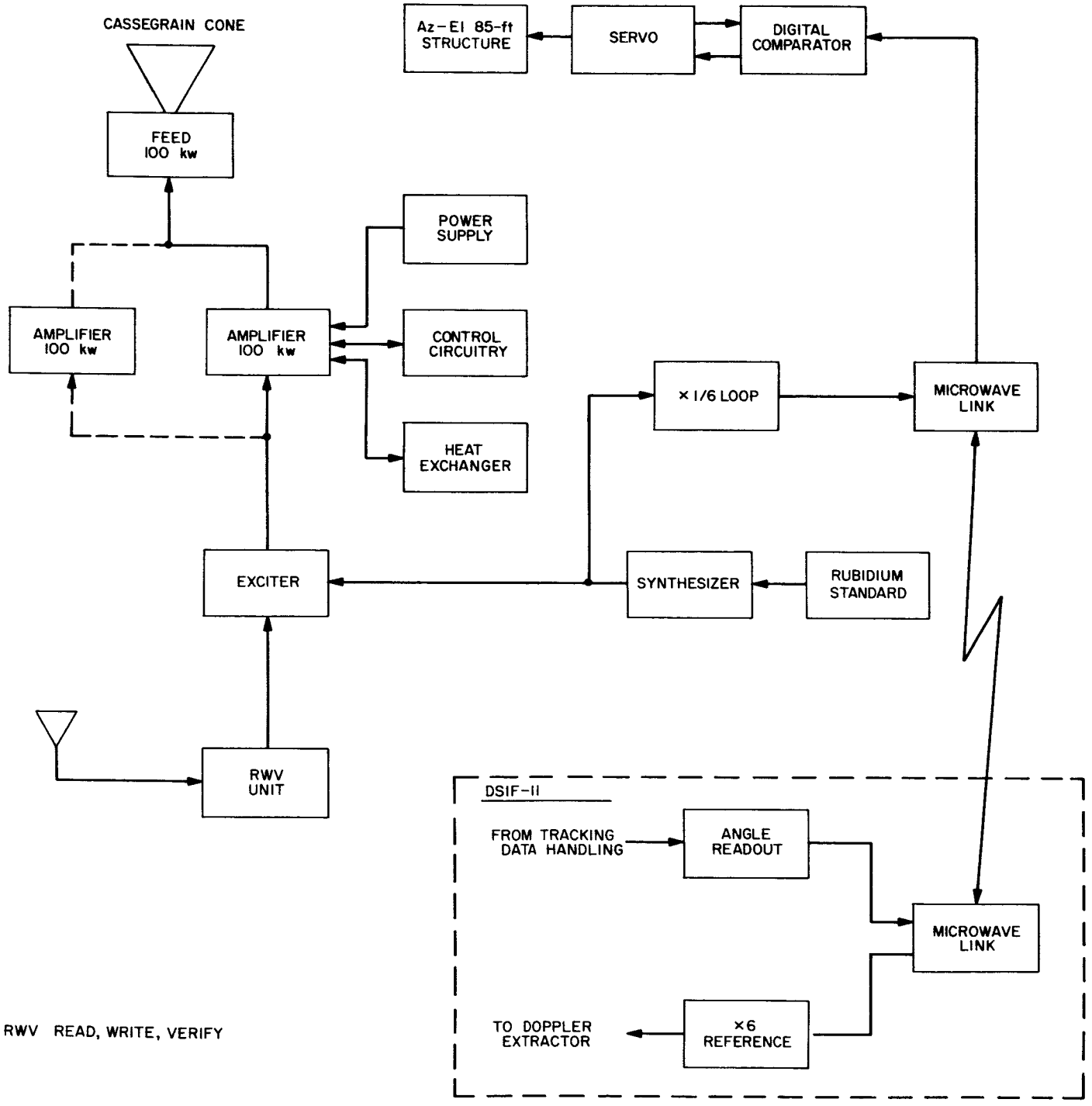


Fig. 434. Goldstone Venus station, DSIF-13 (100-kw transmitter)

Each tracking report is identified with the launch-referenced time (e.g., L + 60 min), and contains the following information:

1. XXP1: last five digits of T × VCO frequency (10-sec count), GMT, and the day of the year every 5 min throughout the period covered by the report

2. Start and/or end time of the ground station tracking mode and actual GMT, and the spacecraft telemetry mode

3. The average signal level in dbm and AGC volts, any variation about this level, and the GMT of the signal level reading

4. The telemetry condition (e.g., in-lock or out-of-lock condition) of each channel

5. The transmitter power and the transmitter *on* and *off* times

6. Sequence of significant events; e.g., (a) time of acquisition, (b) time of loss of signal, (c) time of significant changes in the tracking system (i.e., receiver and servo bandwidth changes), (d) time of abrupt frequency shifts, (e) time of changes in signal level corresponding to spacecraft events or commands, (f) time of command transmission, (g) time of verification of command transmission, and (h) equipment failures and time of occurrence

b. DSN/SFOF mission support. The DSN provided the *Mariner* Mars mission with areas in the SFOF for preflight planning and testing and for execution of the mission. The DSN also provided the technical and operational control areas, operational communications, and the data processing within the SFOF required to support the mission space flight operations.

SFOF coverage. The DSN supplies support coverage in the SFOF for the operational functions of the mission; the support began 1 week before the first flight and will extend throughout the mission. Technical coverage is varied in accordance with mission needs; technical monitoring coverage is essentially the same as operational coverage. Detailed coverage plans for the various groups are presented in the Space Flight Operations Plan document.

Operations and control areas in the SFOF. All mission flight operations, direction, and control originate in the SFOF. The DSN provided the areas required for the *Mariner* Mars mission within the existing SFOF building during the *Mariner III* flight and during launch, midcourse maneuver, and post-maneuver cruise phase of *Mariner IV*. Upon completion of the west wing of the SFOF building in January 1965, the *Mariner* project was provided with additional space in a mission support area, which serves as the control point during both the low-activity cruise phases and the high-activity maneuver and encounter phases of the flight. During the high-activity phases, each technical area has a representative located in the mission support area. Each representative informs the SFOD of his activity and informs the personnel in his analysis area of any other activities that might affect spacecraft performance.

Technical areas. The DSN provides the technical areas in the SFOF for the analysis and evaluation of mission data. These areas include the Flight Path Analysis Area, the Spacecraft Performance Analysis Area, and the Space Science Analysis Area. In addition, a spacecraft model room, located in the Spacecraft Performance and Analysis Area, is provided. Computer inquiry stations (input/output) and status displays are available in the technical areas. These technical areas, supervised by an area director, are operated according to procedures outlined in the Space Flight Operations Plan.

Operational communications. The operational communications system, which is controlled from the Communications Center in the SFOF, provides two basic functions for the *Mariner* Mars mission. In the first, it controls the connection of the various operational and technical areas to each other and to external networks. In the second, it routes information in both directions between the DSIF stations and AFETR and the appropriate areas in the SFOF.

Communication lines between the various DSIF stations and the SFOF are shown in Fig. 435 along with AFETR communication facilities. Although the figure indicates that the high-speed data lines are available, their use should be on an engineering basis only since the reliability and error rates have not been established and their operation is not fully qualified.

Data processing. The amount of data processing required for Mars spacecraft varies as a function of the spacecraft activity. However, it is a mission requirement that full data processing be available 30 min after a request is made by the SFOD or his designated representative.

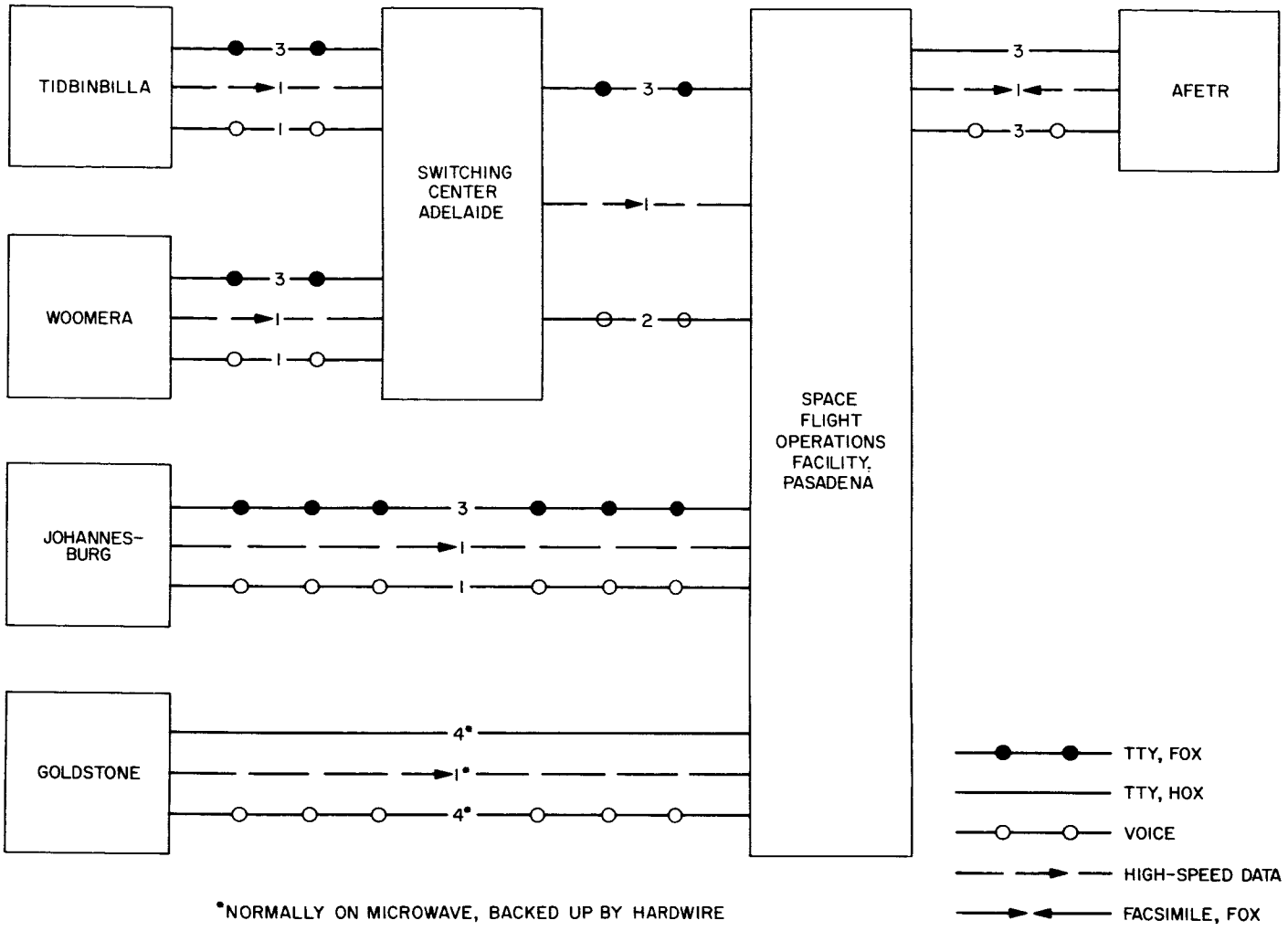


Fig. 435. Communication lines (DSN)

c. Data flow and processing. The various types of data processing available in the SFOF are discussed below. The data flow paths to, from, and within the AFETR, DSIF, and certain areas of the SFOF facilities supporting the *Mariner* Mars mission are presented. Also discussed are data flow, raw data flow, the data processing subsystem, and data processing hardware, configurations, and controls. (The mode of data processing used at any given time is primarily dictated by the standard sequence of events.) The *Mariner* Mars mission is concerned with real-time and non-real-time data.

Real-time data. The nature of *Mariner* Mars space flight operations makes real-time data flow of primary concern. Control of this flow and of data processing is necessary so that the proper data are received and processed at the proper intervals. These data are received in real or near-real time via hard-line or radio communication link and are entered automatically in the DPS. The data are operated on by the processing subsystem and are displayed on-line in the user areas as rapidly as operational priorities and user programs permit. Data are classified as real time if they are transmitted via microwave, phone line, or teletype within 5 min (in the case of Goldstone) or 10 min (in the case of other DSS) from time of receipt at the tracking station. If buffered in a link (including the DPS) for more than 5 min but less than 30 min, data are classified as near-real time.

Non-real-time data. Data received by the DPS either in the form of magnetic tape recordings or of delayed transmission from a communications link (more than 30 min after receipt of data at the DSIF station) are classified as NRT data. The main characteristic of these data is that their processing is delayed and the results are prepared off-line from the DPS. There is no necessity for a

feedback path from the analysis area or for very rapid throughput and display. Data from all of the sources are entered directly or by magnetic tape into either of the two available IBM 7040's, which perform the same input functions on both non-real-time and real-time data, but which record the collected and formatted input data on magnetic tape only. These tapes are then batch-processed on the 7094 at prescheduled intervals, and magnetic tapes are generated to drive the off-line display devices.

The complete data flow to, within, and from the SFOF is shown in Fig. 436 through 438. The flow from the SFOF is comprised of acquisition and tracking information as well as commands for the DSIF, general status information, and spacecraft performance data. The incoming data circuits are routed through the SFOF Communications Center to the IBM 7288 for processing by the IBM 7040. These data are also made available on teletype machines and closed-circuit TV in the user areas.

Data processing subsystem. The mathematical processing of incoming data constitutes the major effort in data handling in the SFOF. The type of incoming data (whether telemetry or tracking) and the ultimate users determine the type of computation required. The principal groups using spacecraft or spacecraft-related data and the type of data each group uses are listed below. It is the responsibility of these groups to interpret, analyze, and evaluate their cognizant type of data.

Group	*Type of data*
SPAC	Engineering telemetry
SSAC	Science telemetry
FPAC	Tracking
DSIF Net Control	DSIF status
Mission and Operations Control	Summary of all data and their status

The DSN DPS provides three services in support of the above-mentioned operations. In the first, the following data are fed into the 7040: all data from teletype, phone lines, microwave channels, and the TPS; also, all

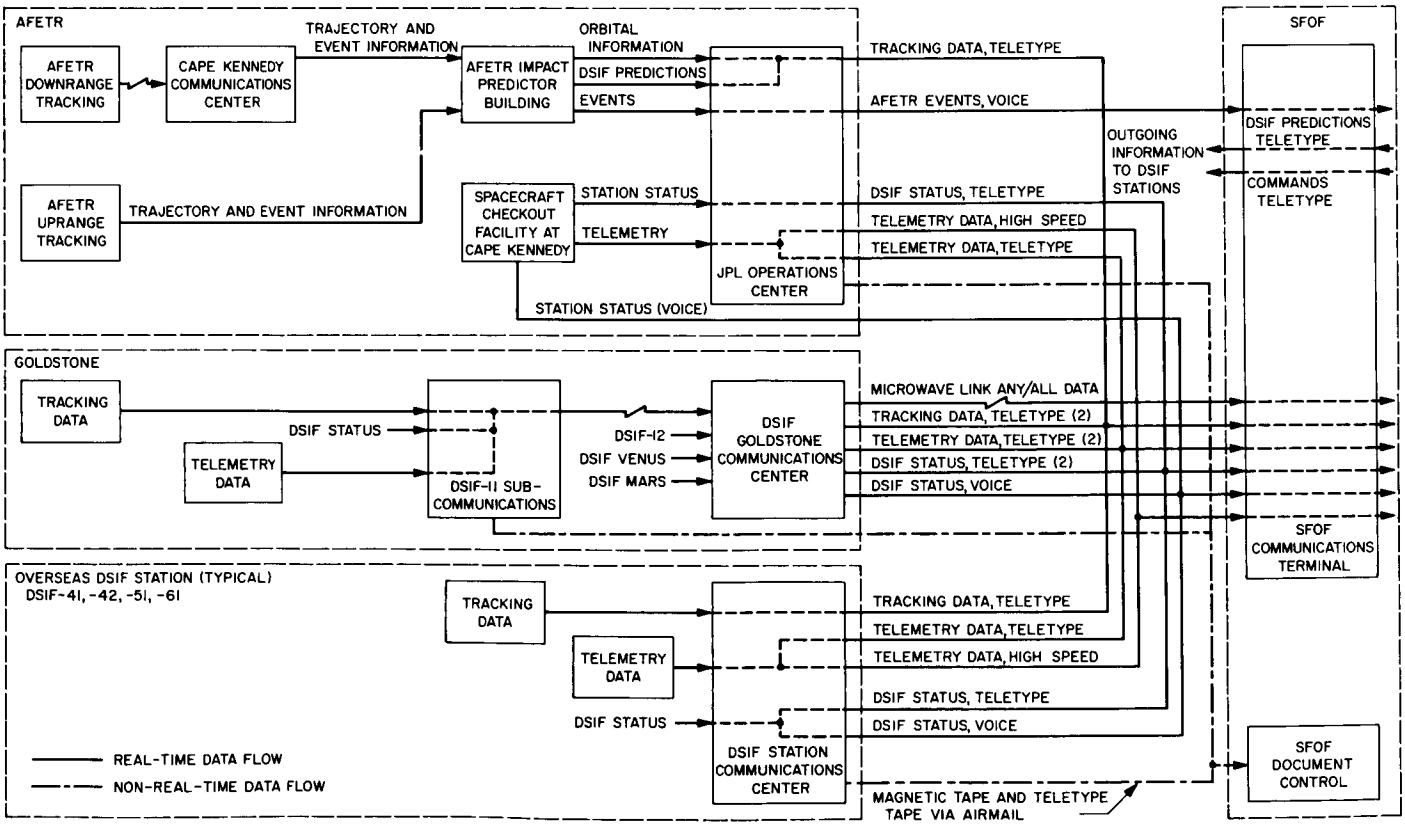


Fig. 436. Data flow from AFETR and DSIF stations to the SFOF

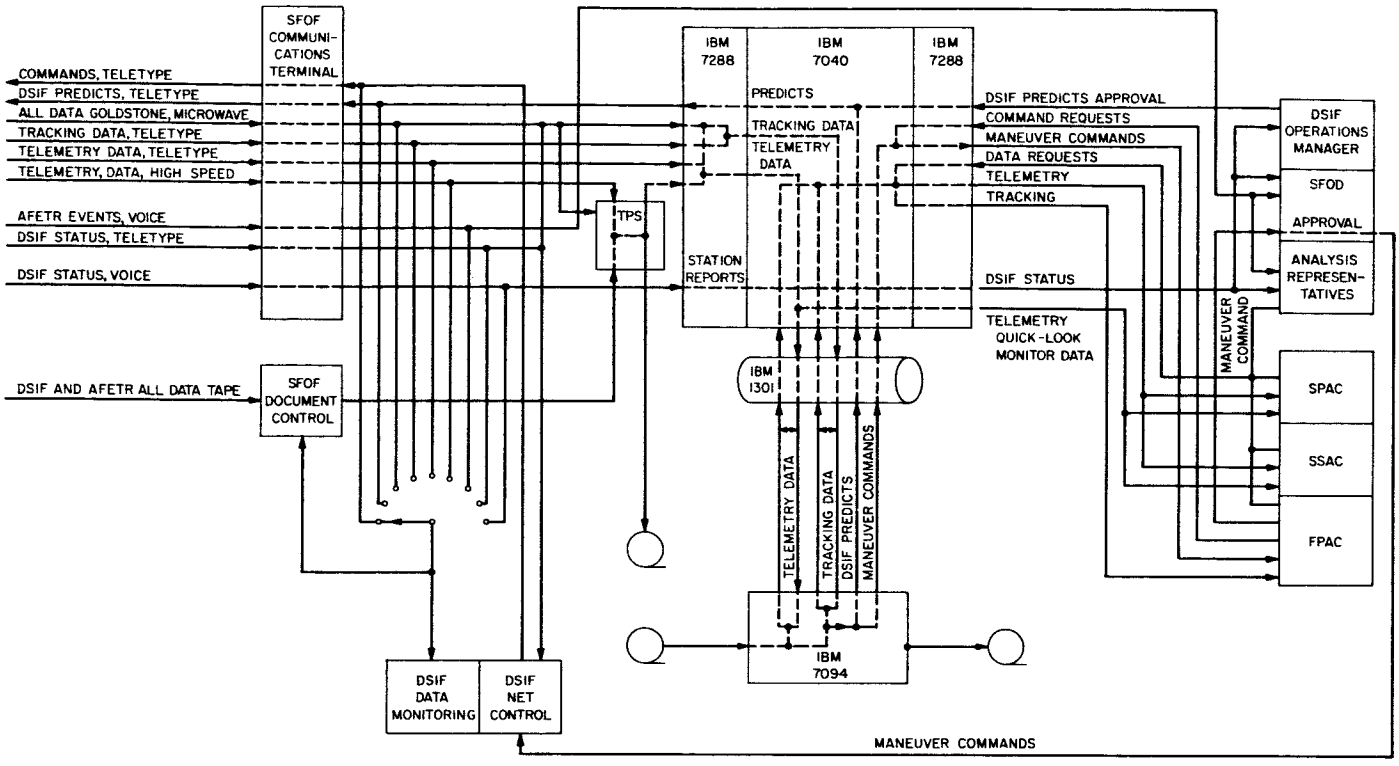


Fig. 437. Complete data flow within the SFOF

requests, parameters, and data from the user areas (Fig. 439) via the inquiry station or the card readers. The inputs are identified and separated by spacecraft number and type of data; these types include tracking, telemetry, and administrative data. All incoming data are written on raw data tape in a sequential mode with proper identification to allow separation and processing in the 7094 in non-real time. If overlaps occur in DSIF coverage and two stations send identical telemetry data to the SFOF, the choice of transmission to be inserted in the 7040 is determined through the data processing control console. The transmission from the rejected station is recorded but is not available for further real-time processing.

In the second, the 7094 complex performs functions in both on-line and off-line modes. By means of the computer complex, the raw data table is sorted into a master data table for analysis routines. From these routines, final reduced data prints and plots of all data are generated for the IBM Disc File Complex, the IBM 1401, and the SC 4020. Through the 7094, telemetry data from the TPS and raw data tapes recorded by the 7040 are processed, and the midcourse maneuver commands and DSIF predictions are computed and generated for transmission to the individual DSIF stations.

In the third, the TPS (Fig. 440) is used to convert telemetry data received in analog, digital, or composite subcarrier form to a format compatible with a 7288 high-speed subchannel and with 7094-compatible magnetic tape. The conversion process is accomplished either in real time using the HSD communications system or in non-real time using data recorded on magnetic tapes.

During the most critical portions of the mission, it is possible to provide parallel processing through the TPS, which also provides a backup capability in the event of prime TPS failure. Each TPS is equipped with two parallel output buffers that feed subchannels into two different 7288's. In the event of prime 7040 failure, the two parallel output buffers enable the backup 7040 to be switched into the prime position without disturbing the data flow.

The TPS operates in four different modes:

1. Mode I is the dual-thread mode. When the computer subsystem is operating in a backed-up mode (Modes I, IIA, or IIIA), the TPS provides dual-thread processing (Fig. 441) of the data inputs and a simultaneous output from each processing path.

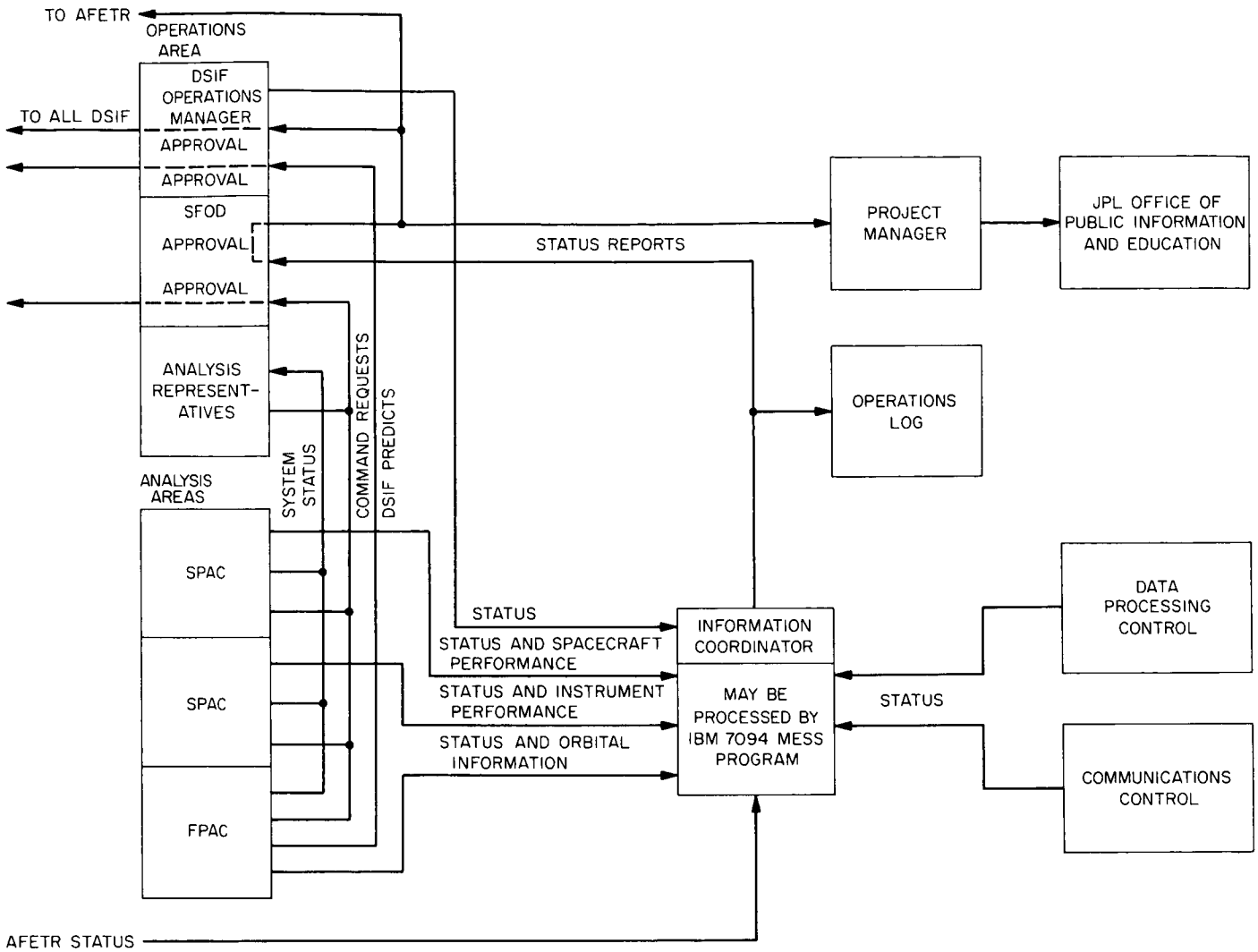


Fig. 438. Complete data flow from the SFOF

Each of these outputs is patched to a different 7040 complex.

2. Mode II is the single-thread mode. When the computer subsystem is operating in a non-backed-up mode (Modes IIB, IIIB, or IV), the TPS provides single-thread (Fig. 441) processing of the data inputs and provides one output for the mission.
3. Mode III is data logging. When the TPS is not sending high-speed data directly to the 7040's, the data are logged in one or more of the methods described in Table 111.
4. Mode IV is analog tape playback. Analog tapes recorded at the DSIF stations and in the SFOF are processed in the manner described in Table 111.

Table 111. Data logging and processing capabilities

Mode	High-speed line input	FR 1400 recording	IBM compatible recording	Strip-chart recording	High-speed output to IBM 7040
I	X	X	X	X	X
II	X	X	X	X	X
III	X	X	X	X	None
IV	None	None	X	X	None

Data processing control. Flight status and data type determine the DPS mode of operation and the control program used.

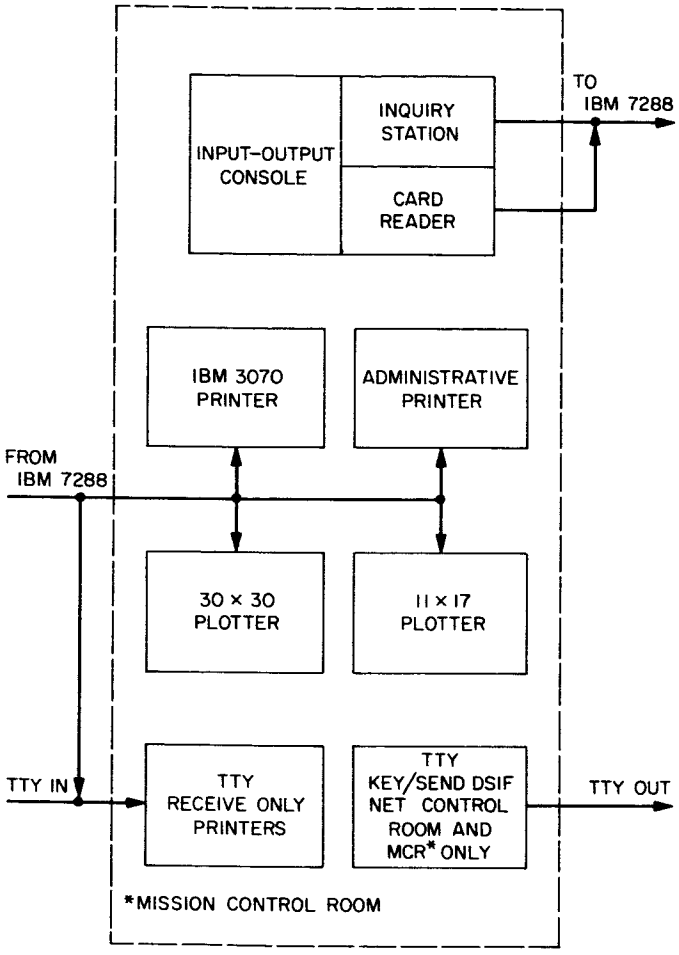


Fig. 439. Typical user area equipment

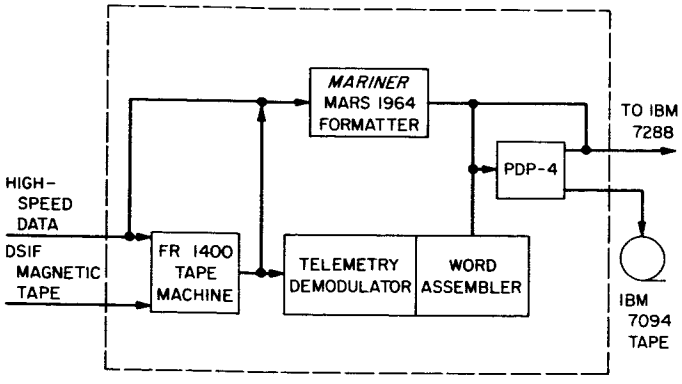
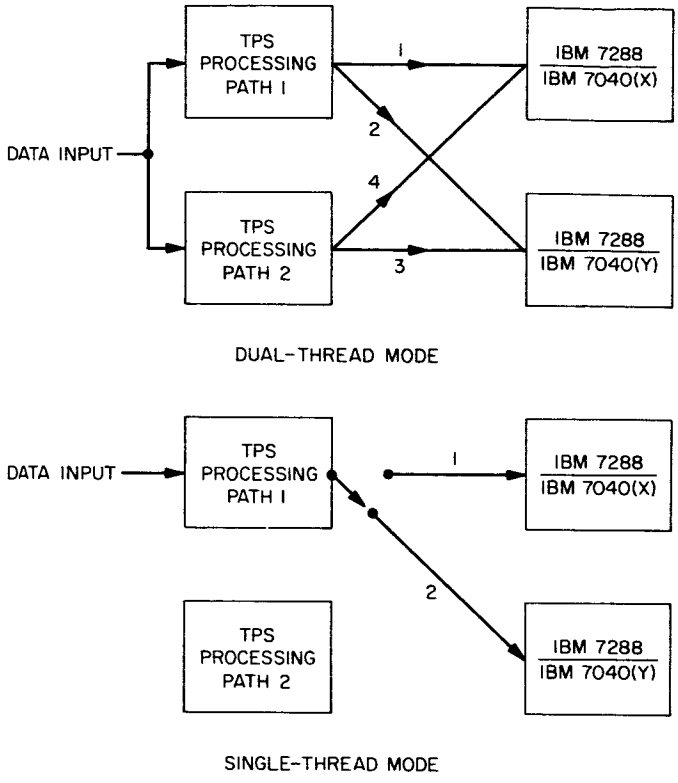


Fig. 440. Telemetry processing subsystem

The DPS has six operational modes (given in Table 112). These modes provide different data throughput and failure recovery times as required for various mission conditions. The flow of data through the DPS is controlled from the data processing control console. All switching



NOTE: TPS OUTPUT PATHS 1 AND 3 ARE NORMAL OUTPUT CABLE PATCHES. OUTPUT PATHS 2 AND 4 CAN BE PATCHED ALSO IF REQUIRED.

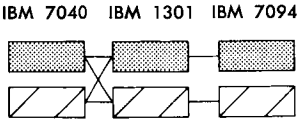
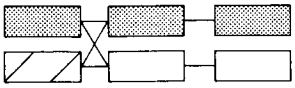
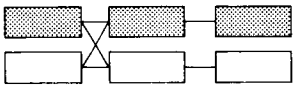
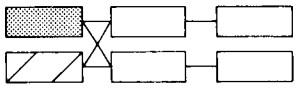
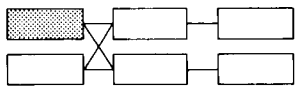
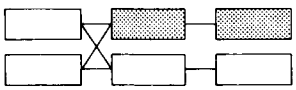
Fig. 441. Single- and dual-thread TPS processing modes

of computer subsystem and input/output equipment, as well as the control of the computer program priorities, is initiated from this console. Control functions at the control console are based on equipment performance and on operational requirements specified by the SFOD. The seven user areas in the SFOF contain computer input/output equipment. These areas perform data analysis and/or command control functions in the data processing subsystem.

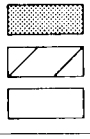
The *Mariner* Mars mission-dependent data processing programs are divided into three categories:

1. Real-time operational monitoring and processing programs that include all 7040 computer programs.
2. Near-real-time operational space flight analysis programs that are processed in the 7094 computer for operational flight path analysis and spacecraft and science instrument performance analysis.
3. Non-real-time space flight analysis and research programs that have multiple options and functions.

Table 112. Operational modes of the data processing subsystem

Mode	Equipment configuration	Data processing paths	Uses
I		Two complete real-time parallel processing paths using two each 7040's, 1301's, and 7094's. Failure recovery time: immediate.	This mode is designed for use in the most critical portions of a mission when the quickest reaction time of the SFOF is required. Mode I takes maximum advantage of the redundancy built into the system and affords shortest recovery time in the event of failure.
IIA		One complete real-time processing path with 7040 backup only. The 7040 failure recovery time: immediate. The 7094 failure recovery time: 30 min maximum.	This mode of operation incorporates the 7040 backup feature described in the Mode I configuration. However, there is no backup available for the Disc and 7094 Complexes.
IIB		One complete real-time processing path with no backup. The 7040 failure recovery time: 5 to 50 min. The 7094 failure recovery time: 30 min maximum.	In this mode, one complete subsystem (a 7040, a Disc File Complex, and a 7094) is assigned to the mission. No backup of input or processing is assigned.
IIIA		Real-time processing by two parallel 7040's only. Data for 7094 processing are batched.	This mode is used when the throughput time achieved in either Mode IIA or Mode IIB is not required. In this mode, all 7094 processing is performed on a batch basis. As in Mode IIA, all data from remote sites are flowing in parallel to both 7040's. The active 7040 is used to provide real-time outputs for user areas and to prepare tapes for 7094 input. The standby 7040 is used to log all input data on magnetic tape for use in recovery in the event of a failure requiring the standby 7040 to become active. Recovery, in the event of an on-line 7040 Complex failure, will take a maximum of 10 sec. The standby 7040 is also used for testing failing external devices.
IIIB		Real-time processing by one 7040 only, with no backup. Data for 7094 processing are batched.	This mode is similar to Mode IIIA with the exception that the second 7040 is not in standby mode and is not available for test purposes. This mode provides the same operational capability as Mode IIIA, but failure recovery time may be significantly longer. In the event of a 7040 failure, recovery may, as in Mode IIB, take up to 1 hr.
IV		Noncritical, non-real-time 7094 disc processing of batched data. Output is via IBM 1403 and SC 4020.	This mode is a non-real-time mode that involves only the 7094 or 7094 disc operation. All operation in this mode consists of batch-processing previously collected data. Because of the noncritical nature of the mode, failures are significant only in that they cause operation to be suspended until recovery is accomplished. Processing is at pre-specified intervals in Mode IV and output is via the SC 4020 and the IBM 1403 printers.

Key



Primary data processing path for two spacecraft

Backup data processing path for same two spacecraft

Available for processing data from additional spacecraft

The 7094 computer programs are controlled by a percentage time-sharing scheme (Fig. 442). The percentages are fixed by the SFOD and are based on user preflight requests and the standard sequence of events.

A detailed description of the operation of the 7040 and 7094 control programs can be found in the Programming Standards for SFOF User Programs document.

C. Operational Readiness Testing

The operational readiness tests verified the design of certain portions of the SFO System, their operational compatibility, and the operational compatibility of the spacecraft/SFO system. The tests also provided operational training in certain areas of the SFO System. Test procedures followed three phases.

1. Phase I: Facility Internal Tests

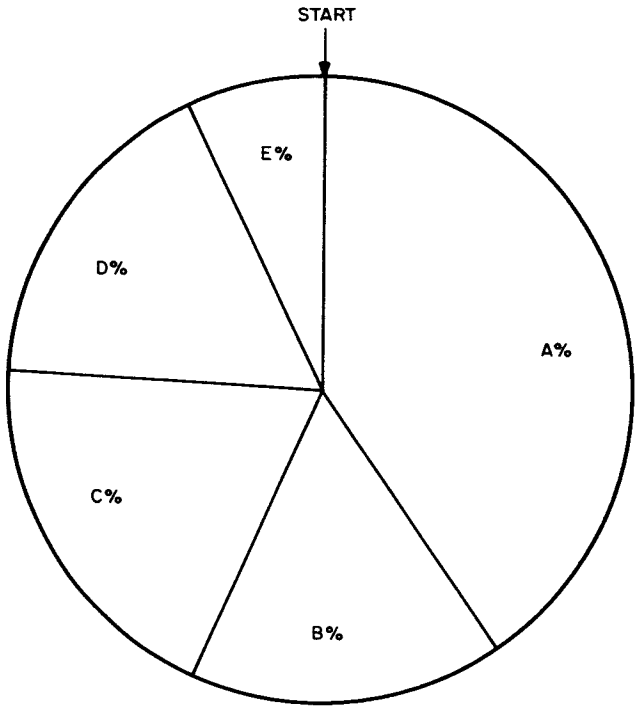
The tests in this phase were intended to verify the design and internal compatibility within AFETR, the DSIF, and the SFOF (independently of each other) in much the same manner as the spacecraft prototype system and subsystem design tests were intended to verify the design and internal compatibility of the spacecraft.

a. DSIF internal tests. These tests served to verify the operational status of the DSIF systems used during the mission as required by the Space Flight Operations Plan. The plan and procedures required for the DSIF internal tests were the responsibility of the DSIF Operations Manager.

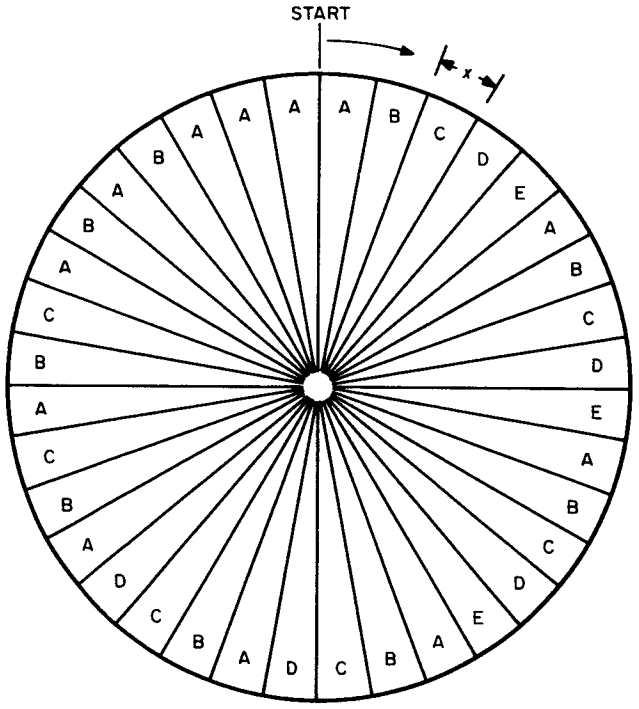
b. AFETR internal tests. These tests served to verify the operational status of the AFETR facilities and systems to be used during the mission as delineated in the Project Requirements Document. The plan and procedures for the AFETR internal tests were the responsibility of the AFETR manager of operations control.

c. SFOF internal tests. These tests verified the operational status of the SFOF systems used during the mission as required by the Space Flight Operations Plan. The plan and procedures required to accomplish the SFOF internal tests were the responsibility of the SFOF Operations Manager.

d. SFOF familiarization. A series of lectures and demonstrations were presented, which were designed to familiarize the *Mariner* Mars 1964 operations personnel with the SFOF.



a. ALLOWABLE PROGRAM RUN TIME IN PER CENT OF SOME ARBITRARY TOTAL CYCLE TIME



b. PROGRAM RUN SEQUENCE; x = FIXED EXECUTION INTERVAL OF EACH PROGRAM

Fig. 442. IBM 7094 processing control scheme

2. Phase II: Spacecraft–operations Compatibility Tests

The spacecraft/operations compatibility tests verified the design and operational compatibility between the spacecraft and the SFO System.

a. Spacecraft/DSIF/SFOF operations compatibility tests. These tests are discussed in Section XXIII.

b. Spacecraft/DSIF operations compatibility tests. Three tests were performed to verify the operational status and compatibility of the spacecraft with the DSIF station equipment used during the mission. These tests were conducted and controlled in accordance with the schedule and procedures established by the DSIF Operations Manager.

RF up-link test. The RF up-link test used the facilities and equipment at the DSIF Pioneer station. The DSIF transmitter was operated to:

1. Demonstrate the GCS with the 10-kw transmitter
2. Verify modulation indexes of the 10-kw transmitter
3. Verify spacecraft lock stability with the GCS command modulation turn-on
4. Verify bit-to-bit correspondence of GCS inputs with decoder output (not as an error-rate check)
5. Verify command transmission at various spacecraft receiver signal levels and frequency offsets
6. Verify command lock through the spacecraft telemetry
7. Verify polarity requirements
8. Determine lockup periods as a function of signal level
9. Demonstrate the use and necessity of the bass boost network for command-system lockup (false locks) at high signal strengths

RF down-link test. The RF down-link test also used the facilities and equipment at the DSIF Pioneer station. The DSIF station receiving equipment and data system was operated to:

1. Demonstrate real-time decommutator readouts such as SPE, AGC, and command verify telemetry from the spacecraft transponder
2. Determine demodulator and decommutator lockup periods as a function of signal level and bit rate (Rate 1 and Rate 2 lock)
3. Determine relative system thresholds for both carrier and subcarrier
4. Verify bit error rate at a given signal-to-noise ratio
5. Verify polarity compatibility for the complete system (e.g., receiver-to-demodulator, demodulator-to-TTY encoder)
6. Demonstrate use of bass boost to compensate for ground receiver response with various receiver signal strengths

Ranging and doppler systems compatibility test. This compatibility test used the facilities and equipment at DSIF-11 and DSIF-13. For the ranging system, the test included lockup period demonstration, mutual interference measurements with command telemetry functions, and system thresholds. For the doppler system, the test included verification of lockup periods at various doppler frequency change rates $\dot{f}$, verification of maximum in-lock $\dot{f}$, determination of maximum permissible amplitude rates of up-links and down-links, and determination of two-way thresholds. A compatibility test between the two stations included measurements of doppler jitter due to microwave link, verification of lockup times, and two-site two-way operations (loop test).

c. DSIF/SFOF compatibility test. This test was repeated three times for three different DSIF stations. The test established the compatibility of the DSIF stations tested with the SFOF using *Mariner* Mars 1964 data and commands. The test consisted of *Mariner* telemetry input to the DSIF S-band receiver, which was then converted by the *Mariner* demodulator and TTY encoder. The resultant data were forwarded to the SFOF where they were compared with the original data. Commands were transmitted to the DSIF via TTY or high-speed data lines and then transmitted to the spacecraft by the station and verified by the GCS.

3. Phase III: Operational Tests

Phase III tests indoctrinated and exercised the SFO System operational and technical personnel in the systems and procedures to be used for the mission. The DSN provided support to the SFO System during the Phase III system tests.

D. Tracking Operations

1. *Mariner III* Tracking Summary

After a 1-day delay in the launch attempt of the *Mariner III*, the spacecraft was launched on an azimuth

of 102.9 deg from Cape Kennedy on November 5, 1964, at 19:22:04.920 GMT[14] (11:22 a.m. PST). Preliminary analyses of launch vehicle trajectory data, sequence of flight events, and Launch Vehicle System data indicated that the flight performance of the first stage (*Atlas* 289D) was nominal. The *Agena* 6931 first burn was about 1.5 sec longer than nominal, and the second-burn shutdown was at a lower-than-desired velocity. The *Agena*/ spacecraft combination was successfully placed into a parking orbit with an apogee of 100 nm, a perigee of 100 nm, and an inclination of 30.6 deg during the initial *Agena* burn period.

At liftoff, *Mariner III* was tracked by Station 1 and Station 0.18. The spacecraft monitoring station acquired the spacecraft in two-way lock at 14:06:00 and went to one-way lock before launch; it remained in lock until 19:24:33 (L + 2 min 28:08 sec). While it was in lock, the monitoring station provided spacecraft telemetry to the SFOF. The Mark I event was confirmed at 19:24:18.6, and the Mark II event at 19:24:21.4, with the signal level at −135 dbm during the monitoring station view period. Bermuda also tracked the vehicle during that time period (19:25) and sent data to JPL. At 19:27, the Antigua station began sending tracking data to JPL and the Bermuda data were interrupted. The Antigua data ended at 19:35.

Confirmation of Mark III through VII events was logged at 19:32. These events occurred as follows: Mark III at 19:27:07.2, Mark IV at 19:27:25.2, Mark V at 19:27:27.35, Mark VI at 19:27:29.52, and Mark VII at 19:28:19.52. Data from Ascension Island were first received at 19:44, and the quality appeared good. Pretoria acquired the spacecraft at 19:54 and began transmitting data. The Mark X event (injection) was observed during Pretoria tracking at 19:55:41.15.

Johannesburg acquired the spacecraft signal in one-way RF lock at 19:54:45, at a received level of −142 dbm, and maintained lock until 19:55:52 using the S-band acquisition aid antenna. Because of the 16-deg beamwidth, DSIF-51 was able to achieve RF lock while the spacecraft was still in Earth orbit and was exceeding the angular-rate capability of the 85-ft antenna. At 20:01, the Twin Falls tracking ship acquired the signal and sent data until the MSFC participating station at Carnarvon acquired at 20:05 and transmitted data. Twin Falls finally lost track at 20:13.

[14]All time is given in GMT unless otherwise stated.

Woomera acquired the spacecraft on the horizon at 20:08:04, and, following standard procedures, switched from the acquisition aid antenna to the automatic tracking antenna at 20:10:29 with the received signal level at − 141 dbm. After approximately 30 sec, the antenna lost the spacecraft, and the receiver dropped RF lock at 20:11:08. For the next 90 min, DSIF-41 had considerable difficulty in acquiring RF lock with the spacecraft. The two major problems in acquisition were: (1) the transmitted power from the spacecraft was 10- to 15-db too low, and (2) the predictions being used by the station (L − 5 min nominals) were in error because of the nonstandard trajectory. The effects of these two problems and of the servo problems occurring late in the countdown made correct interpretation of various indications difficult. Had these indications been correctly interpreted, an earlier acquisition might have resulted. At approximately 21:41, Woomera acquired the spacecraft with the SCM/maser configuration, and tracked satisfactorily for the duration of the view period. Times for Mark IX, XI, XII, and XIII events were confirmed as follows: Mark IX at 19:54:05.95, Mark XI and XII at 19:58:22.9, and Mark XIII at 20:08:25.8.

At 20:17, the SSAC Group at SFOF reported a preliminary indication that the spacecraft science instruments had been turned on. The Carnarvon data ended at 20:25, at which time the uncorrected data from the Twin Falls ship were resumed. The end of raw data from AFETR was recorded at 21:08.

At 21:27, the first indication of nonstandard spacecraft performance was reported by the SPAC Group: the spacecraft was still operating on battery power without benefit of solar panel power. The spacecraft was then declared to be in a nonstandard mode. Analysis of the Pretoria data produced a C_3 of 4.04 rather than the C_3 of 10.4 required to inject the spacecraft into a Mars trajectory. However, since the epoch corresponding to this calculation was in error by 5 hr, it was decided to use the nominal DSIF acquisition predictions until the anomaly could be solved.

Woomera was requested to go into two-way lock at 22:02:00. The station reported two-way command lock at 22:34:00. The command detector was in and out of lock so often that the station was directed to send the commands whenever they were in lock during the command transmissions. At 22:58:00, the transmitter power was reduced to 1 kw. A DC-15 command was transmitted at 23:06:02. Power data indicated that the gyros were off at 23:12:09. The DC-15 was sent in order to turn off

the gyros for power conservation, back up deployment of the solar panels, and effect turn-on of the attitude control subsystem. It was decided to transmit a DC-25 followed by a DC-26 in order to determine whether the scan platform could move; this would presumably have determined whether the *Agena* was still attached to the spacecraft. The DC-25 command was sent at 23:21:30 and verified at 23:23:00. Data revealed little or no scan platform movement and almost immediate wide angle and narrow angle acquisition. The DC-26 command was sent at 23:29:05 and was verified at 23:30:00. It turned off planet and cruise science and the battery charger, and it reduced the consumption of spacecraft power. Science instruments were verified as being off at 23:32:00.

Subsequent to turn-off of the gyros, both engineering and science telemetry data indicated that the spacecraft had not become attitude-stabilized, denoting that either the *Agena* or the shroud was still on the spacecraft. Further analysis indicated, however, that the *Agena* had separated, but that the shroud was still attached to the spacecraft. It was decided to perform a maneuver that might shake the spacecraft free of the shroud. Because of command equipment malfunctions at DSIF-41, however, the emergency maneuver sequence was not completed.

At 01:44:00, command transmission was changed from DSIF-41 to DSIF-51. Johannesburg was instructed to reduce its transmitter power from 10 kw to 1 kw; the station was in command lock at 02:12:00. At that time, SPAC estimated the spacecraft life as 2 hr 13 min (04:23:00). A second maneuver was attempted from Johannesburg. The maneuver command series was sent and stored in the spacecraft. The execution of the maneuver was not verified, however, since the last telemetry reception from the spacecraft occurred before the maneuver start. Before telemetry data ended at 04:05:15.5, they showed a steady drop of power from the spacecraft battery. The spacecraft was acquired by DSIF-51 at 00:01:38, and track was maintained until 04:06:24, when it was lost.

When a detailed analysis was performed to determine the failure mode, it was concluded that the first speculation that the shroud did not completely jettison had been correct. Further JPL investigation indicated that the shroud, a lightweight fiberglass laminated honeycomb structure, may have failed when exposed to the combined thermal–vacuum environment.

2. *Mariner III* T&DA Support Summary

a. Optics coverage. There were 15 metric, 32 engineering sequential, and 33 documentary cameras committed to the *Mariner III* launch. All metric and documentary cameras and 29 of the engineering sequential cameras were operating at liftoff.

b. Radar coverage. Eleven radar stations provided radar tracking data during the *Mariner III* launch. Continuous radar coverage was maintained from L + 0 to L + 1554 sec. There was a gap in the coverage from L + 1554 to L + 1872 sec, but it was resumed at L + 1872 and maintained to L + 2218 sec, and from L + 2278 to L + 2396 sec. The tracking coverage provided by individual radar stations and the range instrumentation ships is summarized in Table 113.

c. Telemetry coverage. Continuous telemetry coverage was maintained from L − 484 through L + 788 sec. Following a gap from L + 788 to L + 1101 sec, additional coverage was maintained from L + 1101 to L + 3698 sec. A summary of coverage by land stations and shipboard instrumentation is presented in Table 114.

d. Vehicle instrumentation. The telemetry signal quality was excellent with the following coverage times for usable signal:

Station	*Time, L + sec*
Hangar AE (Cape Kennedy)	471
Tel 2 (Cape Kennedy)	490
Antigua	790

3. *Mariner IV* Tracking Summary

Following a 1-day delay in the launch attempt because of an RF anomaly in the spacecraft communications subsystem, *Mariner IV* was launched on an azimuth of 91.4 deg East of true North from Cape Kennedy on Saturday, November 28, 1964, at 14:22:01.309 (6:22 a.m. PST). A preliminary analysis of launch vehicle trajectory data, real-time data, flight events, and Launch Vehicle System data indicates that first- and second-stage launch vehicle flight performance, including spacecraft separation, was excellent. The *Agena* and the spacecraft were successfully placed in a parking orbit with an apogee of 99.7 nm, a perigee of 93 nm, and an inclination of 28.3 deg during the initial *Agena* burn period.

Table 113. Summary of *Mariner III* radar tracking coverage

Station	Mode	Automatic track time, L +sec	Estimated reducible data, L +sec
Cape Kennedy (1.16)	Skin tracking	8 to 65	8 to 299
	Beacon tracking	65 to 299	Not applicable
Patrick Air Force Base (0.18)	Beacon tracking	8 to 467	8 to 467
Merritt Island Launch Area (19.18)	Skin tracking	16 to 103	16 to 408
	Beacon tracking	103 to 410	422 to 449
	Beacon tracking	422 to 449	Not applicable
X-band radar 1.1 (Cape Kennedy)	TV	0 to 1.5	Not applicable
	Intermediate range	1.5 to 38	
	Skin tracking	38 to 130	
1.2 (Cape Kennedy)	TV	0 to 2	Not applicable
	Intermediate range	2 to 38	
	Skin tracking	38 to 130	
Grand Bahama Island	Beacon tracking	63 to 386	Not applicable
San Salvador	Beacon tracking	132 to 572	Not applicable
Grand Turk	Beacon tracking	193 to 696	193 to 696
Antigua	Beacon tracking	392 to 768	392 to 719
Ascension Island	Beacon tracking	601 to 1554	632 to 1503
Pretoria	Beacon tracking	1872 to 2218	1883 to 2218
		2278 to 2396	2278 to 2360
RIS Twin Falls	Beacon tracking	2268 to 2338	2292 to 2338
		2378 to 4129	2380 to 2528
		4168 to 5019	2858 to 3076
			3117 to 3321
			3376 to 3572
			3732 to 3842
			3900 to 4127

After a predetermined coast period, the *Agena* was restarted and injected the spacecraft into its planned Mars transfer orbit. The launch and near-Earth trajectory portion of the mission completed to midcourse are considered highly successful. The following paragraphs give a capsule summary of mission tracking operations.

At liftoff, AFETR Station 1 and the DSIF spacecraft monitoring station locked on the spacecraft. Patrick Air Force Base acquired the spacecraft some 14 sec later and began sending trajectory data to Cape Kennedy. At that point, the trajectory was reported as nominal. The Mark I event was confirmed at 14:24:14.52, and the Mark II event was confirmed at 14:24:17.4. Bermuda began tracking at

Table 114. Summary of *Mariner III* telemetry coverage

Station	Frequency, Mc	Usable coverage L +sec
Tel 2 (Cape Kennedy)	229.9	−484 to +480
	244.3	−484 to +475
Grand Bahama Island	229.9	46 to 521
	244.3	25 to 518
Antigua	244.3	300 to 788
Ascension Island	244.3	1101 to 1625
Pretoria	244.3	1837 to 2447
RIS Coastal Crusader	244.3	1609 to 1982
RIS Sword Knot	244.3	2090 to 3698
RIS Twin Falls	244.3	2234 to 3149

14:25 and data appeared good. Cape Kennedy confirmed the Mark events as follows: Mark III at 14:27:00.4, Mark IV at 14:27:18.9, Mark V at 14:27:20.9, Mark VI at 14:27:23.1, Mark VII at 14:28:13.8, and Mark VIII at 14:30:38.6.

Antigua acquired *Mariner IV* at 14:35 and began sending data that ended at 14:36. At 14:38, Bermuda data were back on the line. Grand Turk began transmitting data at 14:43, and, at that time, the flight trajectory was reported as nominal. At 14:55, the suitcase telemetry station at Ft. Dauphine, Republic of Malagesy, locked on the spacecraft and maintained lock until 14:59. The Pretoria tracking station acquired the spacecraft at 14:58 and sent tracking data until loss of track at 15:02. At that time, RIS Twin Falls acquired the spacecraft, and AFETR began sending corrected ships' tracking data at 15:06. The Mark IX event was confirmed by AFETR at 15:02:50; the Mark X event (injection) was confirmed at 15:04:27.4.

At 15:10:48, Woomera acquired the spacecraft in the lock mode and reported a signal level of −120 dbm. The signal level reported by DSIF-41 at 15:14:00 was −87 dbm. The Mark XI event was confirmed by Cape Kennedy at 15:07:08.6, and Mark XII was confirmed at 15:07:10.1.

The spacecraft RF power was reported by JPL to be up at 15:12:42. At that time the spacecraft science experiments were also reported good. The start of Sun acquisition by the spacecraft was reported at 15:23, and 1 min later, at 15:24, the spacecraft was on solar power. Sun acquisition and two-way lock were confirmed at 15:31. At 15:35, the DSN Manager reported the signal level at

DSIF-41 as −90 dbm, and the near-Earth trajectory phase of the mission was considered successfully covered. Woomera continued tracking with normal received signal and good two-way tracking data being obtained through the end of its view period on November 29 at 00:46:56.

Johannesburg acquired the spacecraft at 21:31:40 on November 28. A normal spacecraft signal and good tracking data were received through December 1, and two-way lock was successfully transferred between DSIF stations; DSIF tracking periods through December 1 are shown in Table 115.

The deep space stations (DSIF-11, 41, and 51) continued to track the spacecraft successfully without incident through December 3. Cruise science calibration occurred on time the entire flight period. Except for a few minor ground communications problems (high-speed data and voice links) that were corrected, the DSN tracking operation proceeded smoothly. The midcourse maneuver was tentatively scheduled for the time on December 4 when both Goldstone and Woomera were viewing the spacecraft; motor burn was scheduled to take place at approximately 16:15. The tracking periods for this immediate time frame are shown in Table 116. The scheduled maneuver sequence was followed through receipt of DC-27 (Initiate Midcourse Maneuver) by the spacecraft. After the spacecraft responded to the Goldstone transmission of DC-27, Canopus acquisition was lost and a roll search began. Since a successful maneuver requires that roll and pitch stabilization be maintained by Sun lock and star lock until the time of the maneuver-initiated pitch turn, and since conditions were nonstandard and the time remaining in the Goldstone view period was limited, the maneuver was inhibited by a DC-13 (Maneuver Command Inhibit) at 14:48. Sun lock remained stable during that time. The spacecraft continued to roll until 14:52, when the first object was acquired. Ground commands for roll override (DC-21) were transmitted at 15:22, 15:32, and 16:02 and short-duration roll searches occurred for each DC-21 sent. Subsequently, Canopus acquisition and midcourse maneuver were then anticipated for December 5. The DSIF station tracking periods for that time frame are presented in Table 117.

Tracking activities of the DSN immediately before and after the inhibited midcourse maneuver proceeded without incident. Several two-way tracking transfers were effected during that period between the DSIF stations; the received spacecraft signal was normal; and good two-way tracking data were obtained. Some minor difficulties

Table 115. DSIF station tracking periods through December 1, 1964

Station	Acquisition		End of track	
	Time, GMT	Date, 1964	Time, GMT	Date, 1964
41	15:10:48	November 28	00:45:56	November 29
51	21:31:40	November 28	08:04:27	
11	06:41:41	November 29	18:26:20	
41	14:20:56		01:01:19	November 30
51	22:09:15		08:07:40	
11	06:40:10	November 30	18:30:45	
41	14:26:25		00:58:40	December 1
51	21:54:40		08:07:55	
11	06:38:11	December 1	18:29:28	
41	14:22:27		00:57:45	December 2
51	21:48:29		08:06:33	December 2

Table 116. DSIF station tracking periods for anticipated midcourse maneuver

Station	Acquisition		End of track	
	Time, GMT	Date, 1964	Time, GMT	Date, 1964
11	06:38:40	December 2	18:27:00	December 2
41	14:33:20		00:21:00	December 3
51	21:49:25		08:00:32	
11	06:34:48	December 3	18:23:33	
41	14:16:24		00:51:15	December 4
51	21:43:30		07:57:50	
11	06:32:27	December 4	18:20:06	

Table 117. DSIF station tracking periods for midcourse maneuver attempt

Station	Acquisition		End of track	
	Time, GMT	Date, 1964	Time, GMT	Date, 1964
41	14:15:19	December 4	00:46:36	December 5
51	21:39:13	December 4	07:54:30	
11	06:27:42	December 5	18:16:16	
41	14:10:00	December 5	00:43:00	December 6

were experienced with the high-speed data from Goldstone to the SFOF but they were resolved. During that time frame, DSIF-11 reported receiving signal strengths of −143 dbm, and DSIF-41 reported receiving signal strengths of −139 dbm. Several doppler sample-rate experiments were performed at DSIF-11 during the same period.

On December 5, the day chosen for the actual midcourse maneuver, DSIF-11 reported the receiver, demodulator, decommutator, and TTY encoder in lock, and a signal of −143 dbm was received at 06:44. Two-way lock with the spacecraft was reported by the station at 07:00:30. At 12:35:48, command modulation was reported turned on, and the command system was in lock at 12:41:41. Goldstone reported all stations and systems "go" at 13:03, and QC 1-1, the initial command of the midcourse maneuver sequence, was initiated at 13:05:00. The spacecraft commands along with the transmitted and verified times are presented in Table 118.

The midcourse maneuver was successfully completed at 16:54:57 on December 5. Motor ignition occurred at 16:09:19 and lasted 20 sec, 48 counts, until 16:09:39. All spacecraft maneuver events were performed successfully and at the nominal times. Woomera acted as backup to Goldstone and tracked the spacecraft while DSIF-11 sent the midcourse commands. Canopus was reacquired after the completed Sun acquisition sequence by transmitting one DC-21 (roll override) to the spacecraft to overcome the first Canopus sensor lock on the star Gamma-Vega. At the completion of the midcourse maneuver, the DSN support of the *Mariner* Mars 1964 mission was considered to have been successful.

4. *Mariner IV* T&DA Support Summary

a. Optic coverage. There were 15 metric, 32 engineering sequential, and 8 documentary cameras committed to the *Mariner IV* launch at AFETR Station 1. All of the cameras were operating at liftoff.

b. Radar coverage. A total of nine land-based radar stations and three range instrumentation ships provided tracking coverage during the flight. Continuous coverage was obtained from L + 0 to L + 704 sec. A summary of the radar coverage provided by the individual stations is shown in Table 119.

c. Telemetry coverage. Continuous telemetry coverage was provided from L − 420 to L + 728 sec. A summary of the coverage is provided in Table 120.

Table 118. Spacecraft commands for midcourse maneuver

Command	Transmission time, GMT	Verified time, GMT
QC 1-1	13:05:00	13:06:15
QC 1-2	13:10:00	13:10:55
QC 1-3	13:15:00	13:15:55
DC-29	13:45:00	13:45:54
DC-14	14:05:00	14:05:54
DC-27	14:25:00	14:25:54
DC-13	15:03:00 (loaded and ready in GCS)	16:31:00 (removed from GCS)
DC-21	16:52:00	16:52:54

Table 119. Summary of *Mariner IV* radar coverage

Station	Mode	Automatic track time, L + sec	Estimated reducible data, L + sec
Patrick Air Force Base	Beacon tracking	14 to 487	14 to 438
Cape Kennedy (1.16)	Skin tracking	11 to 73	11 to 73
	Beacon tracking	78 to 298	78 to 298
Mod IV 1.1 (Cape Kennedy)	TV	0 to 2	Not applicable
	Intermediate range	2 to 74	
	Skin tracking	74 to 130	
1.2 (Cape Kennedy)	TV	0 to 2	Not applicable
	Intermediate range	2 to 72	
	Skin tracking	72 to 129	
Merritt Island Launch Area	Beacon tracking	0 to 6	0 to 3
	Skin tracking	14 to 90	14 to 452
	Beacon tracking	90 to 478	
Grand Bahama Island		61 to 399	61 to 399
San Salvador		141 to 561	Not applicable
Grand Turk		171 to 174	Not applicable
		201 to 239	201 to 239
		261 to 275	288 to 600
		288 to 600	
Antigua		401 to 704	401 to 640
RIS Sword Knot		Limited commitment	2201 to 2428
RIS Twin Falls		Limited commitment	None

Table 120. Summary of *Mariner IV* telemetry coverage

Station	Frequency, Mc	Usable coverage L + sec
Tel 2 (Cape Kennedy)	229.9	−420 to +500
(1)	244.3	−420 to +500
Grand Bahama Island	229.9	25 to 513
(3)	244.3	25 to 513
Antigua (91)	244.3	343 to 728

d. Vehicle instrumentation. The telemetry signal quality was excellent with the following coverage times for usable signal:

Station	*Time, L + sec*
Hangar AE (Cape Kennedy)	477
Tel 2 (Cape Kennedy)	500
Antigua	719

E. Performance Evaluation Summary

Tracking performance and associated problem areas recognized during the early portion of the mission and summarized briefly in this section were extracted primarily from minutes of the *Mariner* T&DA support critique conducted after each launch.

1. *Mariner III* T&DA Performance Evaluation

a. AFETR metric and VHF telemetry support. No significant problems were reported by AFETR representatives in providing the required metric and VHF telemetry support of the *Mariner III* flight.

b. AFETR S-band support. An attempt to evaluate S-band performance of the four AFETR stations was complicated by the reported shroud failure. Collapse of the shroud before its ejection from the spacecraft led to speculation that the antenna pattern was deformed. Therefore, it was impossible to predict the spacecraft antenna pattern with certainty. The span of time during which the stations could receive the S-band signal was doppler-limited due to receiver capability, but, during the possible receive time, the actual received signal strength was not known with sufficient certainty to indicate why the coverage was limited to the extent observed.

Coastal Crusader (Whiskey). The S-band signal should have been visible on the Coastal Crusader for approximately 5.5 min, with doppler acquisition at +50 kc and tracking to −50 kc. Postlaunch tests showed that the actual capability with the receiver used at that location should have been limited to acquisition from +2 to −75 kc, a frequency range that would have limited the receive time to 3 min as the spacecraft was receding from the site. With a spacecraft transmitter power of 1 w and an antenna gain of 0 db, the maximum received signal strength at the input to the S-band preamplifier at that site should have been −115 dbm. (With a receiver sensitivity of −140 dbm, a signal strength margin of 25 db exists.) With the spacecraft antenna pattern undistorted from what was predicted, the actual gain would have been from −5 db to −20 db for the aspect angles existing for the Coastal Crusader during the possible receive time. Any significant distortion or "skew" in the antenna pattern could have reduced the signal to the marginal level indicated.

RIS Sword Knot (Yankee). A situation similar to the Coastal Crusader existed on the Sword Knot for the doppler frequency acquisition capability of the S-band receiver. The signal should have been acquired from +0.9 to −71 kc, or for approximately 3 min as the spacecraft was receding from the site. The same signal considerations as noted in the case of the Coastal Crusader were encountered, with the additional complication that the spacecraft had separated from the *Agena* launch vehicle. Therefore, the exact orientation of the antenna was unknown.

Station 13 (Pretoria). The doppler frequency range at Station 13 was limited to acquisition from +18 to −54 kc. The signal was within that range for 25 sec. With the high elevation angle of 81 deg, the maximum signal level should have been approximately −100 dbm. The maximum signal level indicated at the site was −108 dbm. The signal apparently passed through the receiver frequency range so rapidly that the receiver operator was not able to tune the receiver to within 2.5 kc of the received frequency to obtain a receiver beat note.

RIS Twin Falls. The doppler frequency range on the Twin Falls was limited to acquisition from +31 to −46 kc. With the high elevation angle at that location and with the ship's large antenna system, the Twin Falls had a 20-db-greater signal margin than any of the other stations. Even so, the received signal fluctuations were great enough to cause minor dropouts on the initial track (up to the antenna elevation limits) and major dropouts as the spacecraft receded from the site. The large signal fluctuations are believed to have been created by the spacecraft, since the independent antenna systems on the Twin Falls (the broadband and the S-band antenna) reported the same signal fluctuations.

c. MSFN T&DA support. The MSFN was designated as the lead division within GSFC to provide the T&DA support of the *Mariner III* flight. The MSFN stations providing this support were Bermuda, Carnarvon, and Tananarive. Telemetry through *Agena* separation and metric support for range safety were provided by Bermuda. The VHF telemetry and FPS-16 radar support were provided by Carnarvon. Only VHF telemetry support was provided at Tananarive.

A minor problem was experienced in operational readiness at Tananarive due to the schedule on which the station was made operational. In addition, communications to Tananarive were interrupted more than was desirable.

None of the minor problems experienced was sufficiently serious to degrade the support provided. Although some difficulty was encountered in getting valid pointing data to Carnarvon, the station acquired the *Agena* by means of acquisition aids.

d. NASA communications support. Goddard Space Flight Center representatives reported that no serious communications problems were experienced in supporting the *Mariner III* mission. Special coverage was provided by the common carriers during launch. Some concern was voiced over the reliability and quality of the voice and TTY communications with the Johannesburg station. Problems existed in providing clear instructions to the station due to the intermittent outages of the voice lines. Since the reliability of the TTY appeared greater than that of the voice lines, it was suggested that adequate operational procedures be developed using the TTY as the prime method of communicating operational instructions to the stations.

e. DSN support. The three DSIF stations supporting *Mariner III* were located at Goldstone, Johannesburg, and Woomera. The project requirement for standard Woomera operation on the first pass was that the station acquire and maintain the spacecraft in one-way lock for 80 min before going to two-way lock in order to optimize reception of maximum valid telemetry data.

Woomera L − 7 min hold and S-band acquisition antenna problem. Prior to launch, when Woomera was working on the near collimation tower, it was found that in hour angle the antenna drove right through boresight and failed to snap on. At that point, the station was declared red and the servo system was rebalanced, after which successful, although rather sluggish, snap-ons were achieved. Similar checks were made on the far collimation tower with satisfactory results. The station was then declared green (even though the early failure to snap on was not fully understood), because it was felt that the aided track mode of manually nulling the S-band acquisition antenna errors would give adequate backup. While this was true for the signal levels expected (above −130 dbm), it was not true for the signal levels (below −140 dbm) actually received from *Mariner III*.

The primary reason for the delayed acquisition was a failure of the servo system when it was operated in the S-band acquisition aid mode. A significant factor in the delay was the unexpected low and fluctuating *Mariner III* signal level. The problem was traced to the S-band acquisition antenna isometric amplifier in the servo system. Under large error conditions, including noisy conditions associated with low signal levels, the amplifier would "hang up" in an out-of-balance condition. This resulted in the system driving off at full rate during signal levels below −140 dbm. With large misalignments at any signal level, the system would fail to acquire because of the time constant associated with release from the out-of-balance condition.

Investigation of the amplifier problem revealed that the output voltage-limiting Zener diodes were connected from output to ground rather than from output to the input of the stage. The placement of these diodes had caused the amplifier to be overdriven and, therefore, slow to recover. Placement of the diodes across the amplifier merely limits the output without overdriving the amplifier. The problem was resolved by eliminating the amplifier. In addition to removing the hang-up problem, this solution also simplified the setting up process, since it made one less dc amplifier to balance and it removed the polarity reversal introduced by the isometric amplifier. Reconnection of the diodes causing the problem was not accomplished because of the limited time between launches, and because the system performed satisfactorily with the amplifier removed. The station was later modified to the standard configuration.

Considerable difficulty was also experienced in maintaining RF lock with the spacecraft after initial acquisition due to the nonstandard trajectory and the use of L − 5 min nominal predictions. Postflight analysis showed these predicts to be out of nominal by about 1 deg in declination and 7 deg in hour angle. Use of

AFETR predicts was precluded when it was found that they contained a 5-hr epoch error from computer garble. The SFO Director advised DSIF-41 to use the nominal preflight predictions until the anomaly could be solved. When the second run of AFETR predictions was made available for use, Woomera had already achieved RF lock on the spacecraft.

Woomera and Johannesburg GCS problems. Considerable difficulties were experienced with GCS operation during the flight. These difficulties were a result of equipment design errors and procedural problems not anticipated before launch. A light on the GCS panel, showing command loop lock, received a wrong polarity voltage from the ground telemetry system because of a wiring error, and erroneously indicated to the GCS operator that the system was out of lock. Since the in-lock indication voltage was received from the telemetry decommutator, it was concluded that the command system was in lock and plans were made to proceed with command transmission. The next procedure was to normalize the GCS frequency offset, but, because the frequency was incorrectly adjusted too rapidly, the command loop lock was dropped. When the drop was resolved, the command loop was locked up and commands were transmitted. While a DC-14 command was being transmitted, the loop dropped lock again and it appeared as if the last spare amplifier had failed, so command operations were transferred to DSIF-51. It was later determined that the amplifier had saturated but had not failed (a condition that had also been noticed during Spacecraft System tests before launch).

Quality of Woomera tracking data. Trouble developed in the Woomera doppler tracking system 10- and 1-cps frequency synthesizer adapters at L − 48 hr. Two more synthesizers were installed in parallel with the original units, and no further trouble was experienced. The station configuration was then arranged to use the additional synthesizers as prime equipment and the original synthesizers as backup.

It was reported that good doppler data were received from Woomera between 22:08 and 01:34 GMT. Based on *Ranger* experience, 0.01-cps noise was expected; 0.033-cps noise was experienced. A two-cycle bias apparently existed in the doppler counters, although the discrepancy could have been in the trajectory (likely under the circumstances). An intermittent power supply in the transmitter doppler section was actually suspected. The discrepancy occurred at the same time that the station attempted two-way lock. This hardware was repaired before launch of the *Mariner IV*.

Quality of Woomera and Johannesburg telemetry data. Less than 20% of the first 90 min of Woomera tracking contained useful data. This performance was due to the characteristics of the spacecraft signal, the use of poor angle predictions, and a partially failed spacecraft transponder. After DSIF-41 acquired at 21:44, good data were received until 03:44, partly because the establishment of two-way lock resulted in bypassing the failed portion of the spacecraft transponder and partly because of the subsequent signal increase. All data received at Johannesburg were good from acquisition to loss of signal at 04:08. The ground telemetry and recording subsystems at both stations performed satisfactorily.

Suitcase telemetry operation at Fort Dauphine and Johannesburg. The beamwidth of the antenna for the suitcase telemetry operation was approximately 15 deg, and the spacecraft stayed within the beam for approximately 2 min. The system temperature was 1200°K; 2 B_{Lo} was 80 cps; and the tracking threshold was −150 db. The tape recorder was capable of recording 20 min of data on two 4-in. tapes.

The suitcase telemetry system was designed for an expected performance of nominal trajectory with acquisition at 900 nm at a signal level of −121 to −122 dbm. The only available comparison, since Fort Dauphine did not acquire any data, is with the DSIF acquisition aid, which had an 8-db advantage over the suitcase telemetry system. Based on this comparison, the suitcase telemetry should have received a signal level of −142 to −143 dbm, which is just at threshold for aural acquisition.

SFOF and 36-hr data return operations. The 36-hr data return operations functioned as designed. There were no major problems associated with the SFOF function.

f. Performance summary. The overall T&DA support for the *Mariner III* mission was satisfactory, and all major commitments were fulfilled. Tracking and telemetry coverage was virtually uninterrupted from liftoff at 19:22:04 on November 5 to 04:05:55 on November 6, when the last audible signals were issued from the spacecraft. Sufficient information was recovered from the flight for a detailed failure analysis, which disclosed the cause of the failure, and for consequent determination of remedial action to be taken in future missions.

2. *Mariner IV* T&DA Performance Evaluation

a. AFETR support.

San Salvador. Tracking data were lost from L + 239 to L + 288 sec due to an undetermined problem with San Salvador equipment. When the spacecraft reached 520-nm slant range, the track was lost. This range was the upper end of an interference zone extending from 504 to 520 nm. When the spacecraft was abeam of the station, it was reacquired. The interference zones present between slant range intervals caused no further problems as the spacecraft was tracked at increasing range. Loss of track was believed to have been caused by a malfunction in the logic circuitry of the digital range machine.

Pretoria. The maximum spacecraft time above the horizon, as viewed from Station 13, was 4 min with a maximum elevation of 2.5 deg. Receiver No. 1 acquired the signal at the horizon, and receiver No. 2 acquired it at its maximum positive tuning capability; both receivers tracked to the horizon. The reported signal fluctuations were probably caused by multipath propagation phenomena at the low elevation angles.

RIS Sword Knot (Yankee). There was an apparent offset of approximately 30 sec on the Sword Knot in the horizon times predicted and those reported by the other stations. This offset reflected the error in the predictions and in using a launch azimuth of 90 deg instead of the actual 91.4-deg azimuth. Receiver No. 1 acquired at the horizon and tracked through the maximum elevation of 25.5 deg to approximately 13 deg above the horizon. Receiver No. 2 acquired the signal 30 sec after receiver No. 1 acquired it and lost the signal 23 sec before No. 1 did. There are two possible causes for loss of the S-band signal at that high an elevation angle: one could be from a drop in signal strength below the receiver threshold; and the other could be from an excess in the receiver doppler capability.

To investigate the signal strength that should have existed, the same slant range and spacecraft parameters predicted earlier were used. The power transmitted was 1 w with a 0-db gain antenna, and the receiving antenna had an effective gain of 16 db. With the range of 3.2×10^6 ft existing at the time, the received signal level should have been approximately −114 dbm. The spacecraft antenna pattern indicated that, because of the aspect angle existing at that time, the signal level received at the ship could have dropped 20 db below the value obtained using the above parameters. The manual tracking antenna could not have been accurately positioned with that signal level, since it is well below the minimum discernible level of the pan scope of −115 dbm.

The possibility of exceeding the receiver doppler limits was based upon information received from the Sword Knot as a result of prelaunch tests. The doppler offset measured before launch had apparently shifted so that the doppler acquisition ranges were from +74 to −28 kc for receiver No. 1 and from +55 to −48 kc for receiver No. 2; this gave a system capability of acquisition at +74 kc and of tracking to −60 kc. No effort was made to change the crystals before launch, since any area restricted by the lessened capability was covered by the overlapping of adjacent stations.

Loss of receiver lock was indicated on the Sword Knot by complete loss of signal. At the time of receiver signal loss, the pan scope would have given no signal indication, and, if the receiver lost lock because of exceeding the doppler limits, there would have been no receiver signal strength (AGC voltage) indication. However, for receiver No. 2 to have lost the signal first, there must have been a difference in the two receiver sensitivities.

RIS Twin Falls. To clarify the evaluation of the Twin Falls' S-band performance, the receiving system capability is reviewed here. A tracking receiver and a data receiver were connected by means of multicouplers to S-band preamplifiers and to down converters driven by right-hand circular and left-hand circular antenna outputs. The tracking receiver outputs to the tracking electronics were at a frequency of 20 Mc. The interference frequency amplifier in the tracking electronics had a predetection bandwidth of 1 Mc, which gave a tracking sensitivity of −110 dbm with the 4-db noise figure of the S-band system.

The data receivers had a predetection bandwidth of 2.5 kc, which gave an effective receiver input noise level of −136 dbm. Laboratory tests made with a transmitter modulated in the same manner as the *Mariner* Mars spacecraft transmitter have indicated that the data receiver will lock to signal levels as low as −144 dbm below the receiver noise level. The sensitivity (of the same type of spectrum display used on the Twin Falls) was measured and found to be −115 dbm. It was determined that the signal strength predicted during the required Class I coverage was actually well above the minimum signal levels required for the S-band receiver system. (Note that the spacecraft signal level was increased from 1 to 10 w at approximately L + 45.1 min.) With a plotted range and using antenna gains of 0 db for the spacecraft

and +35 db for the ship, the signal level was always in excess of −99 dbm. The data receivers were offset in frequency to provide optimum coverage of the anticipated doppler frequency shift. Data receiver SN/107 had a frequency acquisition range from +91.2 to −13.7 kc, and was connected to the left-hand circular antenna channel. Data receiver SN/113 had a frequency acquisition range from +41.2 to −64.5 kc (hold in range to −78 kc), and was connected to the right-hand circular antenna channel.

Based upon the above information, two possibilities arose for not receiving data part of the time. First, the spacecraft antenna was designed for right-hand circular polarization. The input to the left-hand circular channel of the S-band antenna would be attenuated below that predicted, but no measurements were made on that component of the spacecraft-radiated signal. With signal margins for the data receiver greater than 40 db and for the tracking receiver greater than 15 db, this effect would probably not have completely prevented signal acquisition in the left-hand circular receiver channel. Second, no receiver lock would have been achieved by transferring data receiver SN/107 to the broadband antenna from L + 3030 to L + 3210 sec, since the negative doppler shift of the S-band signal was outside of the receiver's capability at that time. The signal frequency would have been within the frequency range of the spectrum display unit connected to the receiver, but the signal level was too low when using the broadband antenna to be detected at the slant range existing during that time period. With a transmitting antenna gain of 0 db, a receiving antenna gain of 16 db, a spacecraft S-band power output of 10 w on a range of from 5.1 to 7.0 × 10^6 yards, the signal level would have been between −118 and −120 dbm.

Testing by the ship's personnel upon completion of the ship's tracking operation turned up a problem with the tracking receivers. Operation in the crystal-controlled mode caused the antenna carrier relay to lock up with no receiver input present. Hence, the receiver was operated in the AFC mode. (This same problem had existed when the system was delivered.) In the AFC mode, the receiver was designed to lock to (and cause the tracking receiver first local oscillator to follow) any change in the input frequency. When no signal was present in the receiver, the first local oscillator was offset in frequency because of the imbalance in the discriminator. Both tracking receivers on the Twin Falls were measured and found to have a large frequency offset. The receiver that was in the right-hand circular channel was offset 598 kc above the nominal frequency. The offset in the left-hand circular channel was sensitive to the IF gain setting. When the IF gain was set to the nominal value for the mission, the offset was 300 kc above nominal. Original measurements indicated that the receiver was also offset 590 kc above nominal. Increasing the IF gain setting could reduce the offset to 100 kc above nominal. The discriminators were exchanged between the receivers, and the frequency sensitivity with gain was noted in the left-hand circular channel, which indicated that the phenomenon was a function of the discriminator characteristic. The procedure for setting up the tracking receiver was to use the crystal-controlled mode to tune the first local oscillator and the pre-selector to exactly the input frequency. A signal received at the receiver input (e.g., 395 Mc) would be mixed with the first local oscillator (in this case, 425 Mc) in the first mixer to produce a 30-Mc signal, which had a predetection bandwidth of approximately 1 Mc, that would be provided to the antenna automatic-tracking electronics. In the tracking receiver, the 30-Mc signal was fed to a second mixer that was also driven with a 40-Mc second local oscillator tunable ±250-kc signal in the second IF amplifier. The second IF amplifier had a 1-Mc bandwidth filter. In the crystal-controlled mode of operation, the AFC voltage from the discriminator was disconnected from the first local oscillator. When the receiver was switched to the AFC mode of operation, the first local oscillator would remain at 425 Mc if the discriminator were perfectly balanced. To relax the requirement for a perfect discriminator, AFC modes of operation are normally used after a signal has been acquired in the crystal-controlled mode, or gated frequency sweep is used to overcome the discriminator offset during signal acquisition. With a 598-kc offset in the first local oscillator, the received signal would have been 98 kc outside of the tracking electronics and second IF amplifier passbands.

Even with these problems in the AFC mode of operation, this system could have worked if the ship's personnel had been advised of the problems and instructed in the corrective action necessary. With the second local oscillator tuned to 40 Mc, the received signal would also be outside of the 1-Mc passband in the second IF amplifier. Decreasing the second local oscillator frequency 100 kc or more would put the received signal within the passband of the second IF amplifier. The output of the discriminator would correct the frequency of the first local oscillator, and, with this AFC loop closed, would center the signal in the 30-Mc IF. The offset at 30 Mc would be approximately equivalent to the second local oscillator offset.

With the setup existing for the *Mariner IV* launch, there was a more than equal chance that the automatic tracking receiver system would not have a chance to function. The manual frequency control of the second local oscillator would have had to be offset in the proper direction.

Even without the automatic tracking capability, the data receivers should have locked to the spacecraft signal as long as the S-band antenna was slaved to the C-band radar and the *Agena* vehicle and the spacecraft were close together. This condition existed until the *Agena* retro-maneuver was performed long after the end of Class I requirements. Tests performed with a test aircraft indicated that the maximum boresight error existing between the radar and telemetry antennas was 0.4 deg. This was well within the 3-db beamwidth of 2.5 deg. Since no search mode was initiated during this slave to the radar, the degradation to the received signal should have been approximately a 1.2-db amplitude modulation at the 30-cps conical scan rate. During the time the circular scan mode was in use, the received signal would have had superimposed upon the conical scan modulation an amplitude modulation of approximately 4.6 db, at a rate of 2.3 cps. During the ± 5 deg sector scan, approximately one 400-msec pulse should have been received every 2.1 sec. It was possible during the last scan mode for the data receiver to have been tuned through the spacecraft frequency when there was an absence of signal. If this had been the only scan mode used, it could explain the loss of signal part of the time, but not for the entire search period. A blip-scan ratio might have existed that could have also degraded the pan-scope presentation; the exact amount has not been evaluated.

Another factor in the possible loss of S-band signal strength concerns the spacecraft antenna pattern. After separation at L + 45.1 min, the tumble could easily have caused 30-db nulls in the anticipated signal strength. Determining the actual null periods is virtually impossible with the information available.

No single reason was found for the Twin Falls having received no S-band data in the entire 10-min Class I period, or in the subsequent time period when acquisition should have been possible. Examination of the tracking and data receivers upon their return to Patrick Air Force Base may reveal additional information to help resolve the problem. It was concluded with reasonable certainty that the tracking receivers were operating outside of the frequency acquisition range, and that there was evidently a combined frequency and space search problem with the data receivers that was not successfully solved within the tracking period.

b. MSFN support. The MSFN stations providing T&DA support for the mission were Bermuda, Carnarvon, and Tananarive. Telemetry through *Agena*/spacecraft separation, metric support, and range safety were provided by Bermuda; VHF telemetry and FPQ-6 radar support were provided by Carnarvon. Only VHF telemetry support was provided at Tananarive.

Bermuda. The FPS-16 angle system at Bermuda was in a red condition for 10 min as the result of a short circuited -150 vdc bus in the elevation equalizer and switching unit. Support of the computer and data flow integrated subsystem test was delayed until 10:52 GMT. The test was subsequently very well coordinated with voice cues.

In addition to the angle system problem, an ADRAN *n*th-time tracking gate problem developed at 13:50, which was quickly traced to the line carrying interference-region switching information to the event recorder. The line was disconnected and the trouble cleared 1 min later. Interference-region switching information did not appear on Channel 7 of the event recorder during the *Mariner IV* flight.

Both acquisition aids provided good tracking and an excellent signal. Acquisition aid No. 1 encountered one brief burst of interference that pulled the antenna off track 15 to 20 deg, but it reacquired track within 3 sec and tracked smoothly the rest of the pass. Acquisition aid No. 2 also experienced a short burst of interference that caused the system to lose track momentarily. No reasons for the interference were readily apparent.

Carnarvon. Acquisition aid No. 1 at Carnarvon experienced multipath reception at elevation angles up to 14 deg. Tracking was very good with good signal strength. Tracking was deliberately broken at 16:01:30. Acquisition aid No. 2 had poor signal strength because of multipath reception, but the signal strength increased rapidly and tracking became very good in all respects. Tracking was deliberately broken at 16:01:30, after completion of the required commitments.

Tananarive. Before the launch of *Mariner III*, a 20-db attenuator pad was inserted between the preamplifier and the multiplex input at Tananarive, because, without the presence of a signal, a 100-μv noise

level was indicated on the receiver signal strength meter. After insertion of the 20-db pad, the noise level decreased to approximately 10 μv.

c. NASA communications system support. Communications support for the flight was generally good. Although some circuit outages existed, at no time did it appear that the mission was in jeopardy due to faulty communications.

A complete power failure occurred at the South African DSIF-51 radio terminal transmitter site (Olifantsfontein) approximately 50 min after liftoff. When the main (commercial) power failed, an automatic cutover switch did not actuate the auxiliary power supply. Investigation showed that the cutover switch was not properly adjusted. This failure left the Johannesburg station without communications for approximately 45 min. Fortunately, the failure occurred when the spacecraft was not within the view period of the station. Communications were restored to DSIF-51 before the next view period.

d. DSN support.

Launch pass at Johannesburg. During the launch pass at Johannesburg, the station obtained one-way lock for 3 sec (starting at 14:57:10). The predicted angles used for the acquisition attempt were obtained from the L − 5 min predicts. Comparison of the predictions with the actual angles of the antenna position obtained from the tracking data revealed that the predicted flight path varied from 12 deg to 1 deg below the local horizon mask and 13 deg to 0 deg below the antenna limit stops. The spacecraft was below the horizon throughout the entire pass. The short one-way RF acquisition occurred when the actual and predicted declination angle difference became less than 2 deg. The predicted values should have been within 1 deg of the true angles in both hour angle and declination.

VCO frequency error during initial Woomera to Johannesburg transfer. In preparation for the initial first-pass transfer from DSIF-41 to DSIF-51, the frequency X_{AI} of the incoming station transmitter VCO was calculated by the SFOF. The equation used to calculate this frequency was designed to provide a ground transmitter VCO frequency that would reach the spacecraft transponder at the zero SPE voltage point, which would give the station the best frequency to achieve instantaneous two-way lock with the spacecraft. In calculating X_{AI}, a value of +44 cps instead of −44 cps was used in the equation. The effect of this error was to set the incoming station transmitter VCO 88 cps higher than its correct value for instant lock. When the incoming station (Johannesburg) switched its transmitter on, both ground receivers dropped lock. Woomera subsequently relocked one way, and Johannesburg was instructed to search ±10 cps about its VCO frequency in an effort to lock the up-link. This was not successful and DSIF-51 was instructed to switch off its transmitter and lock up one way because of the requirement to receive telemetered space science calibrations. At that time, it was discovered that due to a misunderstanding of instructions the DSIF-51 transmitter was on 10 kw on the SCM instead of on the required S-band acquisition. Both Woomera and Johannesburg were instructed to remain in one-way lock.

At the end of the science calibration period, Woomera turned on its transmitter and went into two-way lock. Johannesburg was provided with the corrected X_{AI} frequency and modified to transmit through the S-band acquisition antenna, and a smooth transfer between stations was effected. Subsequently, control was successfully passed back to Woomera and again back to Johannesburg at approximately 30-min intervals to provide orbit comparison data to the T&DA System.

Suitcase telemetry station at Madagascar. The spacecraft was acquired by this suitcase telemetry station approximately 2 min before it was expected to rise, and was tracked for approximately 2½ min. The signal was maximized at approximately 4 deg from the initial pointing angle, and the doppler shift was as expected. Signal strength at acquisition was −120 dbm. No trouble was experienced in following the spacecraft, using only the remote AGC meter on the antenna as a pointing guide. The change of bias potentiometer setting to compensate for the change in doppler was accomplished. However, a large static phase error was built up during the time interval in which the operator tried to check the performance of the recorder. Shortly after that, the doppler rate became quite high (indicating it was probably the point of closest approach) and a dropout occurred. The signal was reacquired, but was soon lost again and was not reacquired.

Playback of the tape indicated a severe change in signal wave shape as a function of the static phase error. This was due to the change from the center point of the slope of the telemetry detector, which caused the detector to be nonlinear. Reduction of the data indicated that the demodulator had no problem in locking on the signal; however, acquisition of synchronization sometimes took almost a minute. One time point was quickly defined on

the tape (the 1600 mark of WWVH) but no other points during the time of data recording were readily discernible.

Suitcase telemetry station at Johannesburg. The spacecraft was acquired almost on the horizon and was tracked for approximately 3½ min from this station. At that time, the ground antenna was pointing toward a null of the spacecraft antenna and the signal was too weak to maintain lock.

This suitcase telemetry station tape had three time marks, each a minute apart, but were garbled and very difficult to read. More care should be exercised in future time labeling, and the use of separate tracks for time and voice messages is important.

e. Phase termination. The first Goldstone pass was uneventful; the spacecraft was acquired near the horizon and two-way lock was effected almost immediately. Tracking and data acquisition proceeded routinely thereafter.

XXVI. PROBLEMS AND RECOMMENDATIONS

This Section describes some of the typical problems encountered during the development of the *Mariner* Mars 1964 Project, and presents recommendations that should alleviate such difficulties. To an extent, many of the possibilities for improvement were recognized at the time, but irrevocable launch data precluded application of the remedial action. The experience gained during the project, however, may well be used to advantage on other similar space programs. For this reason, the recommendations are made with a view to facilitating the design and development of future systems, and may help to avoid the pitfalls or expedient measures that were encountered by the *Mariner* program. The problems and recommendations pertaining to the overall *Mariner* Mars 1964 Project (from a management point of view) are not included in this volume. It is felt that such comments should include the entire *Mariner* Mars 1964 flight, and will more appropriately appear in a later volume of the project report.

A. Launch Vehicle System

An example of launch vehicle schedule problems was the unavailability of complete interface hardware for use in PTM matchmate tests. The shroud system was incomplete due to unavailability of certain adapter mounted hardware. Similarly, the three flight shroud systems matchmated with the two flight spacecraft before shipment to Cape Kennedy did not incorporate hardware qualified for flight in all respects. Flight-hardware shortages were most numerous in the area of adapter and V-band instrumentation, although shortages in shroud system handling equipment were chronic right up to prelaunch operations.

Project requirements included certain mission trade-off studies. One of these was the generation of a plan for the return of launch vehicle diagnostic telemetry and S-band spacecraft telemetry data (transmitted via the *Agena* telemeter) within 36 hr, and for the evaluation of launch vehicle tracking and telemetry data as rapidly as possible. A more timely initiation of such a study would have permitted its evolution by an iterative process, which is essential to all complex problems involving inputs and constraints from interfacing organizations. A plan for rapid data return was generated late in the program, the value of which was not fully realized until it was demonstrated by the successful diagnosis of the *Mariner III* cause of failure in time to rectify the problem for *Mariner IV*.

The Launch Vehicle System and its mission-peculiar hardware were not tested with the same philosophy as the Spacecraft System because of their very nature and genealogical ties to weapon system vehicles. Weapon system vehicles are developed for large quantity use and to meet mission reliability goals through highly redundant launches. This of course is not possible on space exploration missions, where the number of possible launches is limited. The testing of interface hardware was largely confined to developmental and qualification tests of nonflight hardware using the concept of "qualification through similarity" to qualify flight hardware.

Agreements should be reached in the preparation and sign-off of the project development plan on all known difficult organizational interfaces, and a mechanism should be established for expeditiously resolving any new or additional problems that may arise during the life of a project. In the launch vehicle interface area, the project development plan should typically provide for the establishment of:

1. Regularly scheduled interface working meetings with specific chairmen and commitments to full support of the meetings.
2. Regularly scheduled reviews of the status of the launch vehicle and of the interface hardware development.
3. Working level communication channels, including degree of responsibility to be delegated on each side of the interface.
4. Designated scheduling activities, including assignments of responsibility as to agency. Consideration should be given to method of resolving discrepancies and conflicting schedule constraints.
5. An agreement on the distribution of technical documents. The classes of data that will receive automatic and simultaneous distribution to the agencies named in the agreement should be specified.
6. A plan for the activation and/or support of technical panels set up to handle exchange, discussion, and review of technical information in those areas that are either complex and involve constraints and inputs from interfacing organizations, or that need exposure to informal group discussions before formal documentation and approval. The agency responsible for documenting minutes of the meetings should be designated for each panel.

7. An agreement on the responsibility for preparation of interface documents, and on the extent to which multiple agency signatures are required in each case.
8. An agreement on the participation and support by each agency in all tests of interface hardware including matchmates, dummy run tests, and combined system tests. The agreement should be established to ensure that the proper agencies are represented for each test category (e.g., design verification tests should not be of interest to launch operations personnel, whereas preliminary matchmate of both test and flight hardware would be of great interest to launch base personnel). Participation would provide needed familiarization and training of personnel, and should aid in the refinement of test and operation procedure documents.
9. An agreement on joint participation in the timely development of mission trade-off studies, which are prerequisites to a selection of alternative or optional approaches to attainment of mission objectives.

Contractual requirements should include provisions that ensure proper hand-over of flight hardware from one organization to another. Appropriate launch base personnel should participate in matchmate tests, combined systems tests, DD-250 buy-offs, and the preparation of operations and procedure documents that guide prelaunch checkout and test activities.

If the concept of qualification by similarity continues as an accepted principle in any phase of Spacecraft System development, rigorous quality control procedures should be required, which recognize the reduction in confidence accompanying any hardware not subjected to flight acceptance testing.

It is suggested that incentive contracts contain performance and schedule incentives appropriate to the importance of these parameters to planetary mission success.

B. Spacecraft System

1. Octagon Structure

The following problems were encountered during the design and fabrication of the basic structure:

1. The science payload change near the end of the preliminary design phase required that the secondary structure be completely redesigned. Although the changes were incorporated without significantly compromising the final design, they did increase the costs and delayed the development structure deliveries.
2. The schedule was severely jeopardized by the late delivery of the forging billets from the vendor. Only through the use of premium time during the machining operations were the assembly schedules met.
3. The problems encountered in using titanium fasteners complicated the assembly sequence. Ultimately all the problems (galling, contamination, and nut locking torque) were satisfactorily resolved, but only with considerable detailed effort.
4. Several parts were damaged during the application of the surface treatment and were scrapped. The etching process removed more material than allowable, rendering the parts structurally unsound.
5. The surface treatment was found to be primarily a surface preparation treatment for later coating applications. The surface protection afforded by this treatment was minimal; corrosion was noted on several parts that were not kept in an environmentally controlled area.

For the same or a similar structure to be built in the future, the following recommendations are made:

1. Large forgings for machinings should be ordered as soon as the design has progressed to the point at which the gross shapes and dimensions have been defined. Special attention should be paid to the forged-billet material properties. Extensive use of coupon material tests is recommended.
2. The magnesium components should be treated with material that will provide more corrosion protection.
3. The design approach of minimizing the post-assembly machining operations should be continued. There were pay-offs attributable to such a design approach.
4. Press nuts or equivalent female fasteners should be used in all hard-mounted applications.
5. The flight structure and mechanical ground equipment should be designed concurrently. Design and operational simplicity were achieved by this approach.

2. Spacecraft Superstructure

The major problems associated with superstructure fabrication were dimensional control during tube forming and weld quality and part distortion during welding.

a. Tube forming. Tube forming problems were encountered in the fabrication of both the ring half-sections and the strut tubes. Problems with forming the half-sections included controlling the wall thickness and the outside and inside diameter of the formed ring. Wall thickness was controlled by starting with ⅛-in. wall material, drawing it to a nonuniform wall thickness (thin on one side, thick on the other), and forming the half-ring with a short radius on the thin-wall side of the tube. In this way, the material on the thin side was compressed and thickened while the thick side was stretched. The bend radius of the ring segments was controlled by forming it over a machined block. However, some half-sections were delivered with an undersized bend radius. These segments were clamped to a fixture of proper diameter, heated to 450°F, and allowed to cool on the fixture. This procedure was repeated until the part was of the proper dimensions.

The main problem associated with fabrication of the strut tube was swaging the tube end without developing cracks in the internal surface of the reduced section. A one-step swaging process would not produce satisfactory parts, so an acceptable two-step process was developed.

b. Welding. Obtaining finished parts of acceptable weld quality was the most difficult and persistent problem. Since welding of thin-gauge aluminum structures is essentially an art, this problem was attacked mainly by a cut-and-try process based upon fabrication and engineering experience. Once a procedure producing nearly acceptable welds was evolved, it was followed religiously and reiterated until the part was acceptable or was rendered useless by the production of more defects or unacceptable distortions.

The technique as finally developed consisted of: using the same top-quality welder for the fabrication of all parts; using a shielding gas with a low dew point and checking the dew point at the torch regularly; preheating the parts to be welded in a controlled and repeatable fashion; cleaning and maintaining clean parts, particularly in the areas to be welded; and rigidly controlling the welding procedure. This technique, although seldom producing an acceptable part on the first attempt, did produce remarkably good parts for the complexity of the joints involved. Generally, the parts had to be reworked four or five times before they were acceptable.

Part distortion was minimized by controlling the weld procedure. All welding was accomplished by first tack-welding the parts together in a fixture, and then finish-welding them in the free state. If the parts were constrained, thermal stresses from the welding heat would cause local yielding and, upon cooling, distortion. This problem was minimized by sizing the fixture to allow for welding shrinkage and by allowing the parts to expand during welding and return very nearly to the desired dimensions when cool. Dimensional uncertainties were allowed for by providing extra material in the areas that were to be machined to final critical dimensions.

3. Boost Dampers

The problems encountered in the damper development program can be broken into two groups: epoxy bonding, and filling techniques. An epoxy bonding problem was discovered with the first set of dampers that were assembled using the bonding technique. The problem, which was a failure of the same joint on each of three dampers, was traced to an incorrect etching technique on the aluminum piston. A consultation with the manufacturer of the epoxy resulted in a procedure being used throughout the remainder of the program with no failures or further problems.

The most bothersome problem was that of uniformly filling the dampers. The method of filling consisted of coating the piston with a thick layer of silicone fluid, wetting the inside of the cylinder with the silicone, and inserting the piston into the cylinder. It was found that to obtain consistency in loading, the piston had to be inserted at a steady rate of less than 0.25 in./hr. At that rate it took over 2 days to fill a damper. Even then, about 20% of the dampers had to be refilled to meet specification performance. When the filling operation was accelerated, the reject rate became intolerably high. Due to the limited time and manpower available, a more satisfying filling method was not developed, although it seems that there is no technical reason that a better method cannot be found. It is not unlikely that a more uniform filling technique would also help solve the thermal–vacuum test difficulties.

Recommendations concerning boost damper development are:

1. Use on future spacecraft whenever the need for a damped-structure concept exists
2. A more uniform filling technique
3. A damping fluid with a small apparent viscosity change as a function of shear rate
4. In some applications, it would be desirable to replace the O-ring seals with a bellow-type seal

5. The existing design, with only very minor changes, is suitable for use on a system that must be heat-sterilized and/or gas-sterilized

From the feasibility studies of damped structures made early in the program, it was determined that their use for the *Mariner* Mars spacecraft would result in large savings of structural weight. Continued investigation in this area makes the application of damped structures to future spacecraft seem equally as attractive.

4. Solar Panel Deployment System and Solar Panel Cruise Dampers

a. Solar panel deployment system. One of the major problems encountered with the solar panel deployment system was the installation of the spring arbor assembly to the spacecraft. The difficulty in installation led to the scrapping of one of the first spring designs, the negator leaf springs.

Another problem in the solar panel deployment area was the method of attaching the clock spring inner coil to the arbor. The arbor had to have a 0.250-in. diameter hole through it and be able to slip inside the inner coil (about 0.375-in. diameter), which left a wall thickness of 0.062 in. At first it was thought that the inner coil and arbor outside surface could be made square to provide the torque-carrying capability. It was found, however, that Elgiloy could not be used in this application, since it cannot be formed over an arbor less than ten times the material thickness (the material used was 0.025 in. thick). Different materials were investigated, which could be formed over a smaller arbor, but the alternate materials were either magnetic or lacked the ultimate strength necessary. The method of attachment finally decided upon was the use of a hole through the first coil and a pin in the arbor. Since the arbor wall thickness was only 0.062 in., the pin could not be pressed in but had to be machined as an integral part of the arbor (a rather expensive proposition).

The use of an early complete solar panel deployment system test cannot be overemphasized. Although each subsystem performed nominally, gross problems were encountered when all the components were tied together.

The use of a free-fall panel-deployment system is strongly recommended for future missions. In such a system, the weight is reduced and the reliability increased. The successful performance of a free-fall system on *Mariner IV* adds additional confidence to such an approach.

b. Cruise dampers. The major problem encountered in the cruise damper subsystem development was the design of a latch that would meet all the necessary functional requirements. These requirements were low engaging force, high retraction force, zero backlash, ease of operation, light weight, nonmagnetic characteristics, and functional simplicity. However, an additional requirement was imposed that latching motion could not take place tangent to the arc of motion. This requirement resulted from having started the cruise damper system design after the solar panel structure and bus structures had been designed and were being fabricated. By that time, it was too late to make basic changes in the design of the solar panel and bus structures. As a result, the Mark I latch assembly was subject to very stringent adjustment requirements for proper operation, and subsequent operational difficulties were encountered. The redesign required for the Mark II damper system and the new shroud envelope permitted the latch to be designed to a more reasonable set of requirements that resulted in a trouble-free Mark II latch.

Considerable manufacturing difficulty was experienced by the vendor that gold-plated the Mark I cruise damper. The body of the damper was plated on the outside and coated on the inside. The vendor scrapped 10 damper bodies before developing the proper technique. The difficulty was the primary reason for using aluminum for the damper body of the Mark II design, since the Mark II dampers were fabricated on a schedule that could not allow parts to be scrapped.

The most important recommendation that can be made for the cruise damper is an early start on any problem with the interfaces to enable changing them while there is still time. Specifically, the areas that need particular attention are the dynamic requirements and the geometric interfaces.

With regard to the dynamic requirements, it is most probable that the requirements for accuracy of frequency and damping matching between panels were more stringent than necessary. Based on the SMIT results, it is felt that the original requirements were tighter than necessary, as were the final requirements. Unfortunately, however, this area was hard to define precisely until tests were run, when the hardware was already built. An early effort should be made to analytically predict the system response, and, thereby, to obtain reasonable requirements that can be verified by testing.

A desirable simplification of the system would be to eliminate the latch. It can be shown that the latch is not necessary from a dynamic standpoint, although it may be desirable from a ground-operational standpoint. The latches and dampers on *Mariner* Mars spacecraft were not designed to hold the panels in a 1 *g* field, although that would have been desirable during the spacecraft assembly operations; however, the weight restrictions did not permit the feature to be included in the design.

5. Science Platform

a. Actuator. One of the problems encountered during fabrication of the actuator was porosity in the magnesium gear housings. Even though all the housings were machined from the same piece of raw material, two of the fourteen units would not hold pressure for extended periods of time, and, hence, were used as special test units. In addition to the porosity problem, difficulty was experienced in getting an acceptable protective coating on the magnesium gear housings and covers. The majority of the first units delivered were rejected for faulty coatings, that could be removed with the thumb nail.

Some difficulty was also experienced in the fabrication of the clutch plates because of the nickel and chrome plating, which deposited heavily on the sharp edges of the parts and prevented good surface contact between the clutch surfaces. These plates were rejected and refinished by grinding to the correct dimensions following plating.

b. Science cover. Fabrication of the aluminum honeycomb plate, originally thought to be a straightforward process, became involved with a series of problems that resulted in a costly loss of development time. For the most part, the problems resulted from fabrication difficulties experienced by the vendor, which were not caught during inspection. However, a few problems were the direct result of the honeycomb design defects that were uncovered during the fabrication and test procedure. As a result, a decision to use aluminum honeycomb in the future should be tempered by a more thorough study of the application and of the fabrication methods used.

During initial vibration tests of the science cover assembly (both as a separate unit and as assembled on a complete test vehicle), catastrophic failure occurred when the latch attachment fittings in the cover plate pulled through. Upon inspection, it was noted that core fill and insert bonding had not been applied as specified. An example of this failure is illustrated in Fig. 443. Additional quality control measures were introduced to ensure proper fabrication. As a backup, minor changes were incorporated in the attach fittings and support structure to provide a safety margin on the load-carrying capability of the inserts.

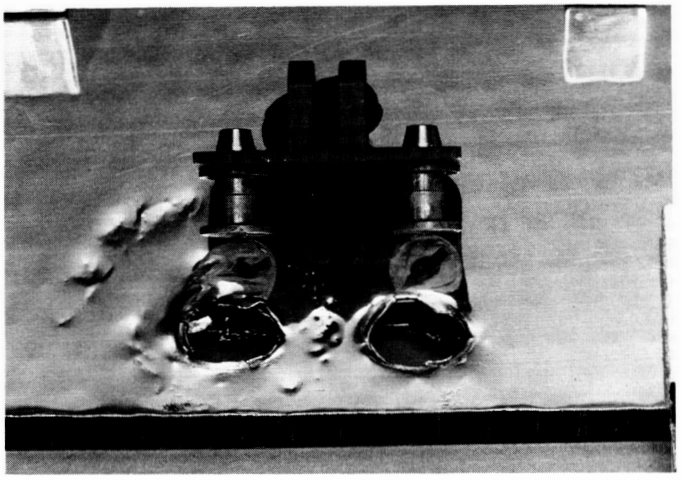


Fig. 443. Science cover honeycomb insert failure

One improvement incorporated for the second set of covers consisted of changing to a higher temperature adhesive. It was felt that this was necessary after checking the possible transient solar heat input during midcourse maneuver. The revised adhesive curing procedure resulted in an internal pressure capable of producing the skin delamination illustrated in Fig. 444. Judging from the location of the damaged area, it appeared that the insert fill adhesive was outgassing at a sufficiently high rate during cure that the pressure could not be adequately vented through the perforated core. After some revision in the method of heat application, this problem was resolved.

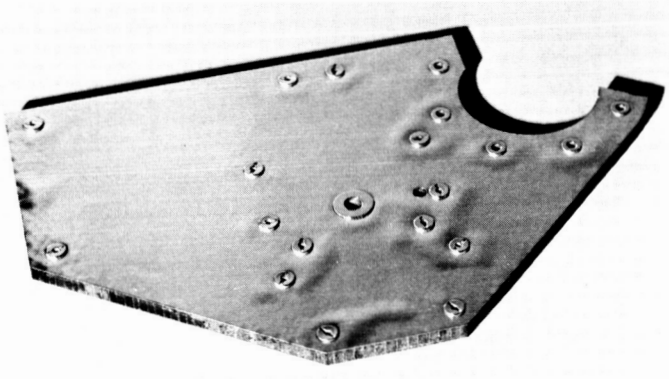


Fig. 444. Science cover skin delamination

A final problem, discovered late in the schedule, was the result of a routine check for entrapped volatiles that could possibly outgas and contaminate the science optics. The first cover plate subjected to the thermal–vacuum cycle outgassed in sufficient quantity to form droplets on the condensation plate. Analysis of the condensate revealed that it was a hydrocarbon, which was traced to inadequate control of cleanliness during the fabrication process. The existing cover plates were removed from the flight hardware assemblies and subjected to a number of thermal–vacuum outgassing cycles. The procedure was repeated until no measurable loss of weight in the cover plate was evident.

Problems that arose during the design and qualification of the cover were basically the result of schedule. The science cover still has much room for improvement, both in concept and in detail. The lack of definition of the cover interface requirements resulted in an unavoidable compromise, which clearly lacked any semblance of structural optimization. As a by-product of the design, further consideration should be given to the possible problems and anticipated advantages of honeycomb fabrication.

6. Solar Panel Structure

While bonded construction has many potential advantages, its greatest defect is that no extant inspection technique can adequately verify its physical characteristics by non-destructive means. The problems encountered point out the need for rapid, non-destructive gauging techniques in soft metals less than about 0.008 in. thick.

Tight fabrication process control by cognizant engineering personnel is a necessity. Where manufacturing personnel reassignments occurred during the program, the quality of hardware deteriorated rapidly. Handling damage was a daily occurrence. Man, rather than the qualification test environments, proved to be the biggest source of damage. Additional training of personnel cannot be expected to reduce the nature of this problem, since most of the damage to the panels was inflicted by skillful, well-trained, careful technicians assigned specifically to panel work. It is recommended that, on any similar future programs, realistic handling problems be considered; skin thickness should be no less than 0.006 to 0.008 in. to adequately resist typical handling damage. It is also recommended that early engineering control be set up over all fabrication practices and parameters that affect vital performance features. In addition, it is recommended that QA organizations have the tools, staff, and knowledge to continuously monitor these critical parameters.

Specific hardware improvements for a planar, Sun-oriented solar cell array are:

1. Modular structure for repairs and logistic reasons.
2. Dielectric, nonmetallic skins, with conventional metallic corrugations.
3. Design tempered with repeated qualification test requirements as well as flight environmental requirements. This would lead in a follow-on design to the use of steel or titanium hinge bearings, steel inserts, and structural fasteners in all areas exercised in test sequences and operations.
4. Improved shear capability of the corrugated substrate by reducing the size of or eliminating the lightening holes in the regions of shear transfer to spars.

C. *Radio Subsystem*

1. Green Corrosion

After in-process inspections, the T-section modules of the radio subsystem were subjected to electrical and thermal tests. Following these tests, a final inspection revealed green-colored foreign matter under the sleeving in areas not accessible for cleaning. It appeared as if the material resulted from copper corrosion brought about by entrapment of the still active flux between the wire and the sleeving, which prevented the ionizing media from evaporating. In evaluating the problem, flux was applied to the entire length of a wire, and the wire lost only 0.21% copper by weight. (Actually, the corrosive residue was about the size of a typewritten period.) From the results of the evaluation, it was reasonable to assume that the parts in question would be acceptable and the amount of corrosion insignificant.

2. Capacitor Problems

The discovery of loose gold flakes in certain types of capacitors provided the explanation for several previously unexplained momentary signal and power losses during system testing of the transponder. The flaking was the result of rotation of the rotor. Most of the power losses occurred in multiplier modules that required far more tuning than the average module. A Hi-Rel version of the capacitor was installed in a retrofit program, which solved the problem.

3. Varactor Diode

A few varactor diode failures that occurred in the screening program were attributed to junction problems,

which resulted from the amalgamation of gold and aluminum. The connection was believed to contribute to circuit losses, and, in some cases, to the circuit opening. However, since failures occurred only during the screening process, screening tests were considered adequate to detect the problem.

4. Uniformity of Modules

As a transponder was inspected, a number of discrepancies were noted that were classified as missing parts, wiring errors, incomplete schematics, and generally poor workmanship. Each module was corrected by the manufacturer during retrofit of the capacitors by performing a detailed inspection just before seal-in. This inspection was made by the engineer who was familiar with both the modules and the drawings. Each module was inspected against its schematic for component values, against an assembly drawing for completeness, and against a photograph for parts replacement. Each component on the assembly drawing was marked with yellow pencil to verify the presence of the part in the module. Any component additions or changes were marked in red. This documentation became part of the record on each flight transponder.

5. RF Filter

During one of the first bench verification tests performed on the system, exciter noise at the receiver frequency appeared at a level that would reduce receiver threshold. The problem was solved by placing an RF filter at the output of each exciter. The filter was designed with a rejection band centered at the received frequency. This type of design provided about 100 db of rejection at the received frequency with less than 0.2-db insertion loss at the transmitted frequency.

6. Load Isolator

Variations in load VSWR caused detuning of the exciter output stage. The problem was solved by placing a ferrite load isolator at the output of each exciter.

7. Receiver and Exciter Power Supplies

During one of the first system tests performed on the PTM, the transponder was being seriously affected by a low-frequency ripple appearing on the 50-v-rms, 2.4-kc spacecraft power supply. From the measurements made, the data showed that VCO and ranging channel modules were most susceptible to this ripple, but results from other tests performed indicated that other modules were also being affected. A redesign effort was begun on the transponder power supplies. A series regulator was added to the output voltage lines. The additional filtering provided by the regulator solved the problem.

8. Power Amplifier and Power Supply

Two single RF amplifiers combined to form a dual power amplifier and two single power supplies combined to form a dual power supply were evaluated for their potential as the transmitter power amplifier stage. The investigation led to the conclusion that the initial amplifier design would not fulfill the mission lifetime requirements. Efforts were immediately started to develop another amplifier source. A power supply program was started concurrently to produce flight acceptable units satisfying the voltage requirements of the amplifiers.

Tube life expectancy was the major problem. Close contact with the tube manufacturer was established early in the program to explore the possibilities of extending tube life. The main life-shortening factor was the evaporation rate of solid materials from the cathode surface, which led to gradual clogging of the grid holes. Actual cathode life was far in excess of 10,000 hr, but grid clogging led to gradual changes in tube characteristics. Operation with reduced filament voltage and correspondingly reduced cathode temperature was found to be the most effective way to increase tube life. Especially selected and processed tubes were supplied directly by the factory. These tubes could be operated with 5-v filaments. Life tests were started immediately. An attempt to predict life expectancy from the data proved inconclusive. About that time, a backup tube was showing promise of having a longer life with essentially the same RF performance characteristics. In the meantime, exploratory investigations were being conducted with TWT amplifiers, which had already logged considerable life-test data that was lacking with both of the other tube types.

In conjunction with the RF amplifier effort, the power supply program was carried through to successful completion for both the TWT amplifier and the triode cavity amplifier. Efficiency of better than 80% was attained within the allotted size and weight constraints established for the program.

9. Ranging Channel

During a regular test performed on the PTM, the system receiver indicated a received signal whether the ground transmitter was turned on or off. Investigation of other systems confirmed the results observed with the

PTM. Further analysis revealed that the receiver lock problem was caused by a signal coming from the ×30 frequency multiplier and reaching the receiver by an oscillatory loop formed through the energized ranging channel. The signal was of spurious origin and was caused by a parasitic oscillation in an amplifier stage of the multiplier. The parasitic oscillation was believed to have been caused by an excessively long lead on a particular bypass capacitor. Reworking the module to provide a more effective bypass by shortening the capacitor lead eliminated the cause.

Since closing of the receiver–transmitter oscillatory loop required that the ranging channel be on (even though this was not the primary cause of failure), false receiver lock was avoided by not turning the ranging channel on. On flight units, flight schedules did not permit reworking the modules, so the decision was made to launch and fly with the ranging channel off.

10. Antennas

a. Low-gain antenna.

Squint of peak of beam. Squinting of the beam at its peak was caused by the unsymmetrical TM_{01} mode adding with the desired dominant circularly polarized Te_{11} mode. It was blamed on poor test range quality and alignment inaccuracies, and was not discovered until during the first test of the first flight-type antenna.

The solution was to suppress propagation of the unwanted mode in the crimped transition section with a series of seven ¼-in.-diameter wire loops protruding into the waveguide along each of the four internal transition ridges.

Excessive ripple on the main lobe. Excessive ripple was measured during the first full scale test of the low-gain antenna on the spacecraft. It was caused by large left-hand circularly-polarized back-lobe reflection off the spacecraft bus. To solve the problem, two rows of eight parasitic elements were added below the circular ground plane. These elements reflected back radiation from a controlled point, and actually improved the forward lobe radiation characteristics.

Extreme temperature environment. As a result of solar-simulator tests, it was predicted that the low-gain antenna waveguide could heat to as much as 300° F during maneuver and non-Sun aligned periods. A special type-approval test was conducted to prove that the antenna could survive under these conditions. No problems were experienced as a result of the test; if a problem had been encountered at that point, it is assumed that temperature control paint would have been an acceptable solution. However, the problem points up the necessity for early solar simulation tests of exposed critical items such as antennas.

b. High-gain antenna. A crack in the rear skin outside the elliptical support beam was caused by a higher-than-expected amplification factor. It was solved by bonding a full doubler in the weak area. Since externally mounted appendages will usually see amplified inputs relative to the predicted booster induced input at the separation plane, it is recommended that the earliest first test of the composite structural test model spacecraft take high priority at the outset of the final design phase.

11. General Recommendations

Pyramiding of specifications should be avoided; complete specification review should be made at the start of a program. This should be accomplished before any manufacturing begins, so that all parties concerned are aware of their obligations and can attempt to eliminate misunderstandings or misinterpretations of specifications.

The use of flow charts and travelers should be continued to ensure proper and adequate inspection. Particular inspection items should be specified in related documents.

Permanent QA & Reliability inspectors should be assigned to a project, so that they become thoroughly familiar with contractual requirements, problem areas, and equipment. Many errors occur during the initial fabrication of a spacecraft that require corrective action and solutions. Valuable experience is lost when inspectors are changed.

Inspection responsibilities should be increased to include configuration inspection of parts placement and values to ensure uniformity of modules.

More extensive use should be made of colored photographs as an aid in inspecting configurations; and more extensive use should be made of detailed check lists and process sheets.

More stringent procedures should be established for rework and inspection of failures occurring in preliminary module testing.

D. Power Subsystem

1. Power Regulators

The main booster-regulator failure-sensing circuitry detects either high- or low-voltage failure. To prevent triggering by noise, the response of this circuitry must be slow. To prevent excessive overvoltage for short times, Zener diodes were added to the output of the main booster regulator, which suggests a better failure detection method: overvoltage should be detected by means of sensing the current through the Zener diodes.

Replacement of the motor-driven switch that transfers the spacecraft from external ground power to internal battery power should also be investigated. This could be done with semiconductors or a hybrid circuit using a small relay and transistors to eliminate junction drops. The existing switch is heavy and also has a high magnetic field.

2. Power Synchronizer

The *Mariner* Mars power synchronizer has a 38.4-kc input signal, and has square-wave outputs of 2.4-kc, single-phase 400 cps and three-phase 400 cps. There is an internal 38.4-kc oscillator that functions if the input signal is not present. The highest synchronized frequency used on the spacecraft is 2.4 kc. Therefore, the primary frequency reference could be in this package, and could be 4.8 kc to yield a symmetrical 2.4-kc square wave. The backup oscillator could also be 4.8 kc. This would reduce the number of flip-flops in the countdown and, therefore, would also increase reliability.

The synchronizer flip-flops are composed of discrete parts. The use of microminiaturized flip-flops should be investigated, since they may improve reliability and facilitate manufacture by reducing the number of solder connections.

In the *Mariner* Mars 1964 configuration, if the power synchronizer fails, the 2.4-kc inverter will continue to operate. The three-phase inverter will not function, however, because it requires a driving signal. However, if the three-phase logic were to use the 2.4-kc inverter output as a clock, the three-phase 400-cps inverter would operate with a failed synchronizer.

3. Battery Charger

The *Mariner* Mars battery charger has two modes of operation: charge at 15 w maximum, and boost at 40 w. The boost mode prevents operation from the battery if sufficient solar power is available. With the proper selection of battery and solar panel voltage, the boost function can perhaps be eliminated. If elimination of the boost function is not possible, it is recommended that two separate circuits be used for boost and charge. The boost requirement of 40-w maximum output makes the charge mode operation inefficient and necessitates a more complex circuit than needed.

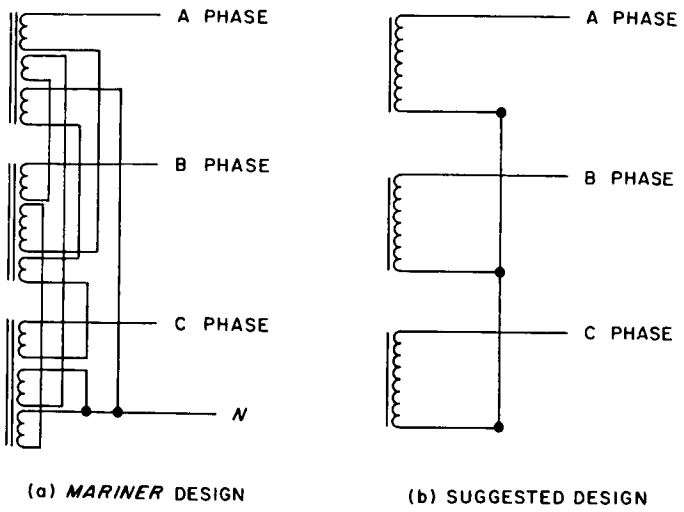


Fig. 445. Power system output transformer connections

4. Output Transformer

The load on the three-phase 400-cps inverter is connected in a floating neutral Y configuration. With this load, the two transformer connections give the same signals. The recommended scheme (Fig. 445) has fewer windings and interconnections, and should be considered for future designs.

5. Battery

Improvement in life and reliability of the type of battery used on *Mariner* Mars spacecraft should be attempted by further work in the following areas:

1. Prevention of plate movement during vibration, which endangers the plate tabs or wires and could tear the separator.
2. Reduction of position sensitivity, which will improve battery life on Earth and reduce the number of system test batteries required.
3. Improvement in the separator system, since it is usually the first component to fail in a battery cell, would benefit all silver electrode batteries.

6. Flight Converter Fabrication

A number of problems were encountered during the fabrication and testing of the flight converter equipment.

One of the most urgent problems in the early stages of fabrication was the availability of screened or JPL Hi-Rel component parts. In general, the procurement time for JPL Hi-Rel parts made it faster to screen commercial components at the vendor's facility. The screening program was a source of new problems. The vendor did not have adequate facilities either in quality or quantity until well into the screening schedule; the screening procedures written by the vendor were, in many cases, not measuring what was desired, or not measuring it correctly. The design changes such as standardization of components caused problems because of poor overall scheduling or because of demands for increased quantities of components above the limited capacity of the vendor. The JPL screening specifications were untried in many cases or were not clear in what measurement was required or the conditions under which a measurement was to be made. A large number of screening specification and procedure changes were made as a result. A high component attrition rate was experienced in the screening process, which caused considerable reprocurement and rescreening. A nominal attrition rate was expected, since unselected commercial parts were being screened; however, a very high rate was observed. This increase over the nominal expected rate was caused by two factors: specification errors that overstressed the components, and the vendor's procedural errors that overstressed the components. The screening program operated satisfactorily after the initial problems were solved. The components screened at the vendor's facility and used in the flight electrical converters proved to be generally superior to the high-reliability components, and a much higher confidence level existed in them.

The fabrication process was a source of numerous problems. In general, the problems fell into several categories, with considerable overlap in many cases: (1) design changes, (2) rework, (3) scheduling and material availability, and (4) planning changes.

Approximately 315 design changes were made to the conversion equipment before and during the fabrication process. These changes varied from simple drawing corrections to extensive hardware changes, and caused significant rework. The changes resulted from circuit deficiencies found during tests and incompatibilities with other spacecraft subsystems, and were made to correct drawing errors and many electronics packaging errors. Nearly every design change affected one or more of the other general categories mentioned above.

E. CC&S Subsystem

The following recommendations, listed in order of importance, would improve the existing *Mariner* Mars 1964 CC&S subsystem, although the accomplishment of these improvements would require a complete redesign of the CC&S:

1. Reduction of component density to eliminate "stacking," and provision of specified 3/16-in. body-to-terminal lead lengths

2. Elimination of back-side printed circuit wiring

3. Redesign of packaging and potting techniques of magnetic shift registers and counters

4. Provision of proper spacing for subassembly harnessing

5. Replacement of shift registers with units having wider margins and not requiring sensistor temperature compensation

6. Redesign of input decoder subassembly to reduce complexity

7. Redesign of magnetic counters to increase margins so that initial test time is reduced and the need for optimization of adjustments is eliminated

F. Data Encoder Subsystem

Some purely hardware problems were experienced during manufacturing of the data encoder units. One, which resulted in a 3-week delay in delivery, was a discovery by X-ray inspection of subchassis connectors that voids were present in the connector-pin solder cups. It was found that, in order to meet the specification for appearance of the pins, the heat applied to the pins was kept at a minimum, which caused the voids. Because of the possibility that the joints might fail under vibration, it was decided to rework all connectors, using another soldering process.

Other problems were encountered in component handling and module encapsulation. Since some components were very susceptible to handling breakage, all the parts were coated with an epoxy compound upon receipt from the vendor. The major problem in module encapsulation was inconsistency of the encapsulating material between lots. The solution to the problem was simply to take sufficient time and care in the encapsulating process.

System testing of the data encoder with the entire spacecraft disclosed two problems. Both of these problems were due to excessive noise transients in the Spacecraft System that were unanticipated and, therefore, not thoroughly guarded against in the data encoder design. The first problem was the fact that the event counters were being reset by these noise transients. The problem was solved by deleting the reset capability of the counters by cutting the reset line in the encoder. Since the capability to reset the event counters was only a convenience for ground testing, deleting the capability did not detract in any way from the operation of the data encoder.

The second problem was deck skipping, whereby the commutator would skip one or several channels in a commutating sequence. The majority of these instances was due to the premature firing of the synchronizer circuits in the commutator. The skips were always correlated with severe power transients or high-voltage arcing on the spacecraft. Since the problem would occur only a few times during the mission, and since correcting the problem would require redesign and retrofit, jeopardizing the spacecraft schedule, it was decided not to correct the problem.

The following recommendations for improvement are based on a *Mariner* Mars type spacecraft, and, therefore, include items that could be improved on the present data encoder design without changing the data encoder interfaces with the rest of the spacecraft.

The most obvious improvement to the data encoder would be to eliminate the deck skip problem. This would require redesign of the synchronizer and clock driver circuits.

Several analog circuits in the present design have been in use for some time on *Mariner A*, *B*, and Venus programs. These circuits, such as the comparator isolation amplifier and low level amplifier, should be investigated from the standpoint of modification to use new devices. There is a great possibility that updating these circuits would result in a simplification that would improve their performance and increase their reliability.

All circuits should be investigated with the purpose of eliminating the use of parts that do not appear on the JPL Preferred Parts List.

Dipped case capacitors in open circuitry should be replaced with molded case capacitors. The dipped case units have been found to be extremely fragile. Ceramic capacitors in the low level amplifier should be replaced with glass capacitors to eliminate the piezoelectric effect under vibration.

On the system level, the commutator layout should be redesigned to achieve a better signal distribution. For example, the present system has 70 analog channels supercommutated through Output Switch 10, and only 16 analog channels supercommutated through Output Switch 11.

The commutator and the channel assignment should be studied to use the telemetry channel more efficiently and to maximize the probability of success for each measurement. This implies assigning relative priorities for each measurement, determining a realistic sample rate for each measurement, and assigning the channels accordingly.

To use the telemetry channel more efficiently, a separate commutator deck should be used for measurements pertaining only to midcourse maneuvers. Another telemetry mode would be created to switch this deck into the commutation sequence during such maneuvers.

To increase reliability of the system, another study should be made to use any increase in weight allocation for redundancy. For very little increase in weight, resulting in a fairly significant increase in reliability, redundancy techniques could be applied to the supercommutation and subcommutation switches.

G. Attitude Control Subsystem

1. Gyro Control Assembly

For future designs of gyro systems with operational requirements similar to those of the *Mariner* Mars spacecraft, the primary recommendations are:

1. Much tighter quality control on the manufacturer of the inertial instruments. It is suggested that a permanent QA representative be present at the manufacturer's facility during all critical assembly operations.

2. A method of proving that the quality control measures involved at the vendor's plant are really effective, such as a JPL-controlled tear-down of selected inertial sensors from various manufacturing lots.

3. An effective lot quality control program in which all instruments that are part of the lot from which

the tear-down sample was picked will be rejected if the sample is found to be contaminated.

4. Much longer lead time for the procurement of truly Hi-Rel components.

5. When welded circuits are involved, stringent quality control measures should be placed on the component lead material from the time the type of component is selected.

6. Extremely high density in welded module components should be avoided. Some loss of reliability is involved because the module is difficult to assemble and handle.

7. Transformer–rectifier assemblies should not be encapsulated with high-gain regulators. A minor but annoying problem exists in the command current regulator of the *Mariner* Mars gyro control subassembly, which is caused by spike coupling and pickup from the transformer–rectifier to the input circuits of the current regulator. The result is a small priority error at the regulator output. This error was not discovered until it was too late in the schedule to make any design changes on the module.

2. Solar Pressure Vanes

It is recommended that a non-foldable vane be used on future flights. With a non-foldable vane, the covering could be more easily installed and a lighter configuration would result.

The amount of attitude control gas being carried on future missions can probably be reduced, since the ability of the vanes to balance solar pressures has been demonstrated on *Mariner IV*. Although the vanes have not damped the spacecraft oscillations, the balancing of solar pressure alone has resulted in a significant savings in gas.

3. Canopus Sensor

The star sensor developed for roll control of *Mariner IV* has been a significant step forward in the state of the art of attitude control devices. Inflight stability has been excellent, and has allowed a reevaluation of short- and long-term photocathode and electron-multiplier stabilities. Power consumption of under 1 w and a total transistor count of under 15 are possible in second generation sensors of this type. If desired, a reduction of bandwidth in the brightness control loop can decrease flat background response by a factor of 10 or more.

Inflight commands available on *Mariner IV* include a brightness gate override command, which allows a means for the rejection of bright particles during flight. Future spacecraft, however, must provide for satisfactory control system operation in the presence of such particles making use of onboard logic. A means of effecting this may be through the use of a time constant increase and upper brightness gate inhibit when roll acquisition is complete. Dirt particle rejection, resulting from the use of a color recognition technique, should be avoided because of the increased sensor complexity and the uncertain surface condition of the interfering dirt particles.

4. Earth Detector

For future missions, it is recommended that the Earth detector have a telemetry channel of its own during the initial 20 days of the mission. This would allow a much better estimate to be made of roll position.

5. Sun Gate and Sun Sensors

It is recommended that a photodetector with a metal enclosure and a transparent window be evaluated for future applications of the Sun gate and sensors. This would simplify construction and assembly of the sensors, and would permit a reduction in weight by eliminating the suspension of the glass enclosure by elastomer components.

6. Sun Shutter

The Sun shutter assembly aboard *Mariner IV* has performed satisfactorily, and has a high probability of completing a successful mission. For future applications, however, it is recommended that several other approaches be considered:

1. If a mechanically actuated shutter is desired, a solenoid design with fewer parts and that does not present formidable lubrication problems should be used.

2. A smaller and lighter actuator requiring less power could be used if the shutter were positioned between the sensor lens and the image dissector tube face. Extreme caution should be exercised, however, to prevent contamination of the lens system, which could result in false sensor output signals.

3. A solid-state optical shutter, using glass that darkens when exposed to light and clears when intense light is removed, should be investigated. None of the glass now available appears adequate in response time or attenuation.

4. A device similar to (3), except that the opaque effect is caused by an electrochemical reaction rather than by an inherent characteristic of the glass, should also be investigated.
5. The star image in one axis should be defocused to spread the Sun energy over a larger area to prevent damage to the image dissector tube.

H. Propulsion Subsystem

Although the CG measurement and motor alignment operations of the *Mariner* Mars spacecraft were very successful, as illustrated by the preciseness of the midcourse maneuver on *Mariner IV*, several problems arose during the program. The occurrence of these problems leads to the following recommendations for future programs.

Early in the preliminary mechanical design, the method of measuring weight and CG and of adjusting the motor should be thoroughly considered. In the *Mariner* Mars program, the design of the propulsion system's thrust plate had been frozen before the mounting and adjustment methods were chosen. Although a satisfactory substructure design was evolved, mounting the motor directly to the spacecraft could have resulted in a lighter-weight structure.

An extensive study to determine the constraints that limit the adjustment capability of the motor should be performed early in the program. The adjustment capability determines the nominal CG envelope, which should be as large as possible. The substructure flown on *Mariner* Mars is a second generation design. Its adjustment capability is approximately double that of the original design. No other changes had to be made to increase the capability, since the additional translational space already existed. Redesign of the substructure was required because analytical CG determinations showed that the CG fell outside the adjustment capability of the first substructure.

A conservative vernier adjustment capability should be estimated early in the design stage to increase the allowable CG envelope and to determine the magnitude of allowable offsets. The method of vernier adjustments was developed late in the program, primarily because the original functional requirement, which required that the CG be within 10 mrad of the motor center line, was too restrictive. It could not account for all possible shifts and errors. Because corrections could be applied directly to the maneuver turns for known offsets, the accuracy of the maneuver could be increased and the functional requirement restrictions relaxed. This method essentially eliminated the need to reposition the motor just before launch. It is recommended that the maneuver turn adjustment capability be recognized early in the design and used.

The major source of error contributing to the 2.5-mrad pointing uncertainty from CG measurements was load cell inaccuracy. This inaccuracy was minimized by taking the average of reactions as measured by three instruments. However, more accurate load cells should be designed and used in future programs.

I. Pyrotechnic Subsystem

1. Pyrotechnic Firing Units

Recommended improvements of the pyrotechnic firing units on subsequent *Mariner* Mars type spacecraft are:

1. Elimination of the inhibit PIPS motor function from the pyrotechnic units, which can, and should, be performed by the spacecraft CC&S.
2. Change of the circuitry supplying current to the science cover solenoid to provide a step current function rather than a short duration current pulse.
3. Reduction of the weight and volume of storage capacitors through further product improvement.
4. Improvement and expansion of telemetry instrumentation circuitry within the units to obtain more definitive telemetry data.
5. Reduction of volume and weight of present units through the use of smaller lightweight components, and through the incorporation of more advanced packaging techniques. It is estimated that volume and weight could be reduced by 25%.
6. Relocation or improvement of the access ability of the firing unit direct-access and firing-line output connectors. The present configuration, after final spacecraft buildup, does not permit the performance of final no-voltage checks or of safety operations without the possibility of damaging fragile solar panels.
7. Development of specialized separation arming switches.
8. Development of reusable squib simulators.

2. Pyrotechnic Arming Switch

Several problems were encountered during the design and development evolution of the PAS. One problem

area was the basic switch unit itself. Since it was highly desirable to use a hermetically sealed switch, the selection was immediately narrowed to two switches. One switch showed a susceptibility to being triggered by reduced ambient pressures, and its use was eliminated. The basic problem with both switches, however, was that the total actuator arm travel was about 0.010 in. The use of a leaf spring actuator amplified the travel to roughly 0.080 to 0.100 in. For this application, a 0.500-in. travel would be desirable to eliminate the need for close tolerances between the spacecraft and the adapter. In order to live with the small amount of travel, the arresting pad on the *Agena* was made adjustable and go/no-go gauges were made to ensure the proper adjustment after the spacecraft and adapter were mated.

The travel could be increased by using a switch with more travel and/or a leaf spring with more deflection per given load. As for a better leaf spring, one easy way to obtain more deflection is by using a material with a lower Young's modulus. Beryllium copper is fairly low at 18×10^6 psi. Fiberglass, however, has high stress capability with an elastic modulus on the order of 6×10^6 psi.

These changes would make the system simpler and less prone to mistakes in adjustments. However, the present design performed quite well with a minimum of problems. The PAS and attitude control turn-on of both *Mariner III* and *Mariner IV* was accomplished as designed.

Another problem encountered in the basic switch area was that one of the microswitches in the PTM unit wore out because of an excessive number of actuations. Although the switch would still function, the point at which the switch triggered changed drastically. Apparently, the switch wobble frame seal has a fatigue life, and actuation beyond that point causes erratic operation. Attempts to readjust the switch closing position produced only temporary results.

3. Separation-initiated Timer

The problems encountered during the developmental program, with the exception of handling damage, in no case resulted in improper functioning of the assembly. Therefore, it might be concluded that the SIT achieved its design goals by providing the required flight switching sequence. However, the following improvements would have been worthwhile had time allowed:

1. Replacement of the silicon rubber volume compensator with a gas-filled metal bellow to eliminate the possibility of high-pressure seal leakage.
2. Incorporation of a temperature-compensating orifice to improve timing temperature dependency.
3. Qualification of an extended overtravel microswitch to allow less critical switch adjustment and a simplified recocking procedure.

J. Video Storage Subsystem

1. Electronic Design Changes

a. Record head driver. Head current rise time is an important factor to be considered in recording over previously recorded tape. Current rise time as great as 15% of one NRZ bit width has little if any effect on playback signal parameters, provided that the recording is made on an erased or uniformly biased tape. However, the current rise time must usually be less than about 5% of NRZ bit width in order to record over previously recorded data. Insufficient rise time results in the old magnetization reacting with the new and causing playback signal distortion, amplitude modulation, and an apparent time shift in the pulses with respect to one another. The problem is not affected appreciably by the peak level of head current as long as the current is sufficient to erase a previously recorded tape completely. However, it would be advantageous to reduce the peak current level slightly in order to lessen residual dc erasure effects. This would yield a slight increase and better uniformity in the playback signal amplitude.

b. Differential amplifier. Because of performance deficiencies that arose during the testing of the *Mariner* Mars flight electronic modules, it seems propitious to improve the dc balance of the amplifier. Temperature effects are rather excessive and may be improved by tighter control of transistor betas. The silicon alloy transistors presently used exhibit a tendency to increase beta when repeatedly subjected to high temperatures. A possible solution might be to change the transistors to a silicon planar type, for instance. In addition, resistor R10 should be mounted external to the amplifier module. This method of mounting would allow amplifier balancing adjustments to be made after potting. Also, the method currently used to mount external resistors should be modified to one that is not as susceptible to shorts between the mounting stud and the case, and to one in which there is no possibility of melting the stud solder joint while attaching external components.

c. Channel change circuits. These circuits use a capacitor energy storage bank employed in a standard relay steering circuit. They have the disadvantage that on short relay drive pulses the relay can hang-up in a neutral state in which the steering center arm does not make contact with either of the two energy storage contacts. In this configuration, the circuit becomes inoperative. These circuits should be replaced by circuits that are not susceptible to relay hang-up such as the one used for rate change commands in the flight data encoder. If the encoder circuit were adopted, the relay driver design should be redesigned to eliminate the high-temperature leakage problem it now has.

d. Peak detector. A change in the operating threshold of the peak detector appears to be desirable. The extant design requires a minimum playback signal level of approximately 5.5-v peak to peak to operate. In the present system, playback signal levels can and occasionally do drop close to this point. Marginal operation of the peak detector has been alleviated somewhat by increasing amplifier gain, thereby boosting signal levels. Gain adjustment to account for tolerance buildup and channel-to-channel balance is an acceptable corrective measure, but should not be used in future systems to correct for an inherent design flaw.

One approach would be to completely redesign the peak detector and the rest of the data restoration circuitry and, where necessary, use a concept that is not as sensitive to varying pulse rise times and amplitudes. Most of the problems associated with this circuitry stem from the fact that standard logic circuits were used in this application when custom designed circuits would have been a much better and simpler solution.

e. Differential preamplifier. Some consideration should be given to extending the high-frequency limit of the pass band, because there may be some slight degradation of the playback signal resulting from attenuation of higher frequency components.

f. Count two and stop circuit. Several malfunctions occurred during VSS testing in noisy environments. These malfunctions pointed out a weakness in the standard logic group currently used, which was designed to operate from fast rise time pulses. This is not a desirable characteristic for flip-flops that are used in control circuits in which the flip-flops are only triggered once every few minutes. There is a definite need for a low speed flip-flop that is not susceptible to false triggering on noise spikes. The present count-two flip-flops should be replaced by circuits that are not as susceptible to noise.

In addition, the count-two circuit should be relayed out so that it is entirely within one subchassis. With the present layout, noise spikes are picked up in the wiring harness, causing false counts.

g. End-of-tape sensor circuit. This circuit and its sensor proved during testing to be the most troublesome design deficiency in the *Mariner* recorder system. The defect in the operation of the circuit is that the circuit puts out multiple pulses during the playback mode while a slightly dirty foil is passing under the sensor. In addition, the circuit produces a false count on power turn-on and turn-off.

A completely different approach at sensing the end of tape should be employed on future programs, such as using an optical sensor that operates from a reliable light source. This approach should not be adopted until the important effects of tape debris on optical sensors have been thoroughly investigated.

A second approach that presently shows merit is triggering the end-of-tape sensing circuitry with the leading edge of the conductive foil and inhibiting any future firings for a long period of time (35 sec). This approach would cure the multiple track change problem but would not correct the turn-off pulse problem. The circuit, if used, should be redesigned to eliminate the false pulse.

2. Mechanical Design Changes

a. Main assembly. Flat washers underneath the cover mounting screws should be replaced by two flat peripheral steel bands. One band on each cover would prevent the kind of deformation caused by the washers becoming indented in the surface of the covers.

b. Spring wiper assembly. A possibility exists of the felt pad "taking a set" with time. The spring wiper arm should have a lower spring rate to maintain a more constant pressure adjustment as the pad compresses. There is also the possibility of the pressure distribution across the tape becoming unequal as the pad accumulates debris from the tape coatings, which could lead to poor contact of the foil and sensor and, also, to poor tape tracking. A bifurcated arm would be more desirable from this standpoint. Contact may further be improved by forming an arc on the portion of the spring to which the pad is bonded.

c. Capstan assemblies. Dimensional stability of the parts can be improved by requiring that the individual parts be temperature-cycled and that the temperature limits be extended.

Consideration should be given to applying a rough chrome frosting to the portion of the capstan shaft in contact with the tape, which should permit reduced pressure belt tension and result in reduced head wear.

With the present design, once the final grinding of the capstan is done, no parts can be removed without disturbing the capstan shaft runout. This means that the clutch cannot be worked on, which sometimes becomes necessary, and it also means that the assembly has to be completely removed from the transport to replace the capstan coupling belt. The belt could be replaced more easily if the flywheel were removed without upsetting the runout. The assembly can be redesigned in such a way as to lock the main bearings, shaft, and housing in a single unit without involving the pulleys, flywheel, and clutch, all of which can be mounted independently.

From time to time during testing, playback jitter has shown up intermittently in one or more units. Causes for the jitter are complex and interrelated and are not easily separated. An approach that would eliminate a possible source of jitter is increasing the pulling force exerted on the tape by the capstans, which would involve several steps: increasing tape wrap angle on the capstans, increasing capstan diameter, increasing coupling pulley diameters, and using a heavier cross-section coupling belt.

d. Sense guide assembly. End-of-tape sensing malfunctions have occurred on several occasions as the conductive foil accumulates a coating of tape debris. Useful life before failure may be extended by changing to a multiple slip-ring contact arrangement instead of the present two-ring arrangement. Consideration should be given to replacing the sensing function with a photoelectric device.

e. Connector assembly. Tests should be made to determine whether the connector plate can be replaced with a gold- or nickel-plated magnesium piece to which a standard hermetic connector can be soft-soldered. This would result in a weight and cost saving if it proved feasible. Tests should include measurements of leakage rate after exposures to vibration, shock, temperature cycling, and thermal shock.

The pins of this connector are necessarily rigid because of the hermetic seal. The mating connector in the case harness is potted rigid also, which has resulted in damage to the transport connector. The mating case harness connector pins should be redesigned to allow some freedom of movement.

f. Pressure transducer. This component contains a wire-wound resistance element. Resolution of the transducer is limited by this element to between 0.1 and 0.2 psia. The purpose of the transducer is to indicate, by pressure readings taken at widely spaced intervals, whether the recorder seals are leaking. Interpretation of such measurements has been hampered by the poor resolution of the device. A replacement should be sought, which has a continuous film resistance element. Emphasis should be placed on resolution and repeatability; accuracy of calibration and linearity are of lesser importance.

g. Shock mount. The shock mount as presently specified is the insert from a standard vibration isolator that was selected on the basis of resonant frequency measurements. In the future, special mounts should be procured using a nonstandard mounting stud designed to reduce the possibility of the attaching hardware coming loose. One possible configuration would be to tap all the way through the stud, countersinking the end normally hidden from view, and run a flat head screw through to replace the present male threaded stud. The double nut and lockwire arrangement should be retained.

h. Electronic packaging. The electronic subchassis packaging should be thoroughly reviewed. The present scheme does not lend itself to repair or rework. In fact, several of the present flight subchassis have been damaged due to necessary repair and rework during fabrication and unit testing. A packaging scheme offering more ease of module replacement should be employed.

i. Component reliability. The design of all of the recorder circuits should be reviewed to determine where reliability improvements can be achieved by replacing the present components with Hi-Rel parts. This review should include the use of integrated circuits.

j. Shield grounds. The grounding scheme used on the Mars spacecraft should be changed so that all shield grounds are attached to chassis ground and terminated at the signal source. This change would remove much of the noise that is presently in the system.

K. Temperature Control Subsystem

The Mars spacecraft clearly demonstrate the need for initial thermal design flexibility to accommodate later changes in spacecraft design and thermal requirements. Early provisions should be made for changes in the amount and placement of louvers, modifications to shields, paint pattern changes, and other changes to thermal control hardware. A frozen thermal design at the completion of TCM testing would have been catastrophic to the *Mariner* Mars spacecraft.

Realistic thermal test scheduling is important in obtaining adequate temperature control. Future programs would benefit from scheduling TCM tests in two phases: a preliminary "roughing in" series followed by a finalizing sequence. The interval between phases could then be used for making flightworthy modifications to the TCM and for updating thermal requirements. With a single prolonged series of TCM tests, there is inadequate time between tests to fully understand the data secured.

Spacecraft thermal design requires a basis in test environment as well as in space environment. Many potential test errors (such as those associated with the solar-simulator spectrum and collimation) were avoided by a judicious thermal design. Consideration should also be given to the necessity of testing electronic components in their flight configuration without the influence of ground support equipment.

Thermal testing of each flight spacecraft is recommended. Some variation in thermal characteristics among the various *Mariner* spacecraft did exist, and temperature tests provided a continuous check throughout the program for unsuspected thermal changes caused by seemingly minor spacecraft modifications.

A continuing need exists to make electronics designers aware of the inherent limitations of spacecraft thermal control, particularly for components external to the bus. Temperature control complexity is directly related to temperature sensitivity, and can often be minimized by proper circuit design.

Further developmental effort is required in the following areas:

1. Development of a flightworthy stable white paint
2. Optimization of radiation heat shields
3. Development of compact, lightweight, active thermal control devices for small packages

Ground handling problems should be considered in thermal design. Lightweight thermal hardware (such as louvers and thermal shields) should be easily replaced. Surface coatings should be durable and cleanable.

1. Thermal Shields

The materials used in thermal shield fabrication should be thoroughly tested for adaptation to space environment prior to use. Finished assemblies should also be subjected to space and launch environment tests such as outgassing, and launch pressure decay.

The tailored approach to blanket fabrication achieved desired results only after an accurate spacecraft was available for patterns. This method also defined the shielding requirements in terms of handling and final button-up procedures. Thermal control shields are generally fragile in construction and surface qualities. Fabrication, handling, installation, and cleaning must be performed by highly trained technicians.

Although aluminized mylar and teflon were used exclusively and successfully on the Mars spacecraft, new materials should also be considered for future applications.

2. Louvers

The *Mariner* Mars 1964 louver design evolved to a near optimum status from the standpoint of weight, reliable operation, and ease of handling. It may be possible to improve the thermal performance of the louvers by using larger louvers per actuator as on *OGO*. Larger louvers would reduce the heat losses due to mechanical clearance gaps that radiate like black-body cavities. They would also, however, degrade the temperature control design flexibility because larger louvers make it more difficult to reduce thermal gradients resulting from uneven power distribution.

To use the *Mariner* Mars design in its present form, three minor revisions should be incorporated: (1) changing the chassis mounting hole location and the number of attachments (to allow the complete assembly to be removed to discourage mishandling); (2) changing to a newly introduced, nonmagnetic bimetallic material for the actuators; and (3) improving the louver position-monitoring transducer design.

3. Finishes and Materials

While durability was a consideration in selecting the thermal control finish, a reasonable degree of handling

and transport protection was also important. Therefore, a requirement was established that adequate containers be provided for all parts, not only for the protection of thermal control finishes but also for the protection of the structural and functional components of the assemblies. Such a requirement should be a rigidly enforced policy for any future projects.

Several incidents of poor coating adhesion to the substrate occurred during the *Mariner* Mars program. In most cases, the defect was traceable to inadequate surface cleaning prior to paint application. While cleaning procedures were adequate for most components, the major culprit was unexpected and undetected surface contaminants, particularly in the form of silicones from previous processing or testing. Since the normal surface preparation techniques such as grit-blasting or chemical etching are not permissible, a reliable means of detecting surface contamination would be highly desirable for future programs.

A paint control system was established at the beginning of the program. Each can or batch of paint was assigned a project lot number and the radiative properties of each lot were measured. Detailed process and inspection records were maintained for each prototype and flight part painted. In addition, the records maintained include many other details such as paint-film thickness (for each coat applied as well as for final thickness), paint viscosity, and surface preparation. While much of the information recorded might be unnecessary after the mission is completed, the records were invaluable for the instances during the program in which questions or problems arose. A similar system would be highly desirable for future programs.

The eddy current device used to determine the paint thickness proved to be a highly useful tool. It provided a means for ensuring that the minimum thickness for optimum radiative properties was achieved. It also provided a guide to the technicians applying the paint for maintaining uniformity over the entire part surface. A device to furnish similar thickness information on coatings should be mandatory on any future programs.

A problem was encountered in maintaining uniformity and reproducibility of the coating for magnesium. In order to ensure satisfactory properties for thermal performance, it was necessary to restrict the application of the coating to a single vendor. In addition to the problem with radiative properties, the coating did not provide as much corrosion protection as was desirable. For these reasons, it is recommended that, for future programs, the desirability of using anodic protective coatings for magnesium be more thoroughly investigated. The thickness and, therefore, the emittance can be more accurately controlled with this type of coating by maintaining the proper combination of temperature, time, and application voltage.

The metal-filled paint used for the *Mariner* Mars program had undesirable physical properties and was sensitive to handling damage, but, since such damage was controllable and/or repairable, it was acceptable for the spacecraft. It is recommended for future programs that a metal-filled paint system be developed that is more suitable for overall use, since the properties of this type of paint are frequently desirable and sometimes mandatory in spacecraft thermal design.

There still exists the need for a white coating that is stable to space ultraviolet and possesses satisfactory engineering properties for Earth environmental handling and reliable adhesion. Although the inorganic paint had satisfactory ultraviolet stability, its use was restricted to areas in which the requirements for optical properties and ultraviolet stability justified the precautions necessary to ensure adequate adherence and maintenance of cleanliness. A relatively stable organic white coating has been developed, which shows strong promise as a practical engineering material. (Unfortunately, however, it had not been sufficiently developed and tested for consideration during the *Mariner* Mars program.) As the technology of stable white coating development continues to advance, other coating systems may be proven and become available that can be used on future programs. Each application must be considered in the light of its requirements, limitations, and constraints. There exists no such thing as a universal thermal control coating.

Some work is being done with tape-type thermal control surfaces. This approach has several advantages to offer, including more thorough and reliable quality control, better thickness control, and, therefore, better weight estimating and weight control of the vehicle, simple and rapid repair procedures, and the capability of using a wider variety of material systems within the constraints of coating curve temperatures. The major disadvantage of the approach lies in the question of the reliability of the surface adhesion, including not only the problem of the adhesion loss but also the potential problem of expansion of entrapped gases after launch that might cause a greenhouse effect. The application of tapes to spacecraft compound curvatures presents another real limitation.

As a result of the compromises required in the design of the lower thermal shield, a multilayer insulation material capable of withstanding extreme temperatures would be highly desirable.

L. Spacecraft Harnessing

Deviations from standard items specified for wire and connectors caused difficulty in obtaining reliable components during early stages of procurement. This was due in part to the necessary use of new and untried processes and materials, and in part to vendor production and QA inadequacies in fabrication and qualification of the new product. Problems with the modified Bendix PT-type connector, for instance, were eventually minimized and the electrical performance of the flight connector was adequate and reliable.

The Cannon D type connector, however, continued to exhibit a number of problems. These problems ranged from high susceptibility to contamination to loss of pin/socket continuity because of inadequate spring retention due to burrs and poor spring properties. In spite of tight QA control of these connectors and continued engineering liaison in attempts to improve reliability, the connectors were, at best, marginal. Flightworthy connectors were obtained only by using tests to verify adequate contact separation force in each connector socket during final spacecraft prelaunch inspections, and by using especially designed sleeves to repair marginal connectors that could not be replaced because of their location or a time limitation. Efforts to improve the reliability of these connectors by improvements in the present design, by improvements in vendor quality control, or by evaluation of alternate vendors should be continued.

During the early stages of the *Mariner* project, consideration was given to the use of a thin-walled wire insulation of fluorinated ethylene propylene, dip-coated with a polyamide film, for a possible saving in wire weight of about 15%. This wire was not used, however, because of unpredictable and unexplainable cracking and peeling that occurred on the coating during and after harness fabrication.

Early procurements of the wire used on the *Mariner* Mars flight spacecraft also contained such flaws as pin holes in insulation, poorly sintered insulation, lack of bondability, and some mechanical deficiencies. These repetitive wire defects led ultimately to 100% inspection of all wire for insulation breakdown, proper bondability, and necessary mechanical properties. A faster, more sensitive cable checker would improve in-process inspection of cables.

Installation and operational features of two areas of the spacecraft cabling could be improved by some changes in the design of the lower ring harness and the case harness support structure. The problem with the case harness support structure occurred in instances in which two subsystems shared the same electronic chassis, and, therefore, the two subsystem case harnesses were assembled onto the same support structure. The two harnesses could not be separated for bench test of the subsystem without removing one of the harnesses from the support structure, an operation that required such complete disassembly of the harness that total electrical and mechanical reinspection was recommended before reuse of the harness. If current concepts of separate bench tests of each subsystem are continued, the case harness support bracket should be fabricated to allow for separation of the two halves in order to make possible the removal of either harness without disturbing the other.

Some problems were encountered in the installation of the lower ring harness because of difficulties in getting the harness onto the spacecraft without twisting or distorting the breakouts away from their original locations. At best, this caused interferences and possible strain on the conductors. A problem such as this generally occurs to a much lesser degree with all outlying harnesses on the spacecraft, which makes it difficult to guarantee that all harnesses are mounted similarly or, in fact, adequately. The problem of handling during installation combined with the handling during testing and transportation was harder on the cabling than the functional environment. For instance, most conductor sizes and insulation thicknesses are designed not for electrical requirements but for the mechanical strength required to withstand handling. The handling and installation of the lower ring harness could have been improved by the use of a support and hard-mounted connectors where possible.

M. Science Subsystem

1. Cosmic Ray Telescope

Two major problems with the Cosmic Ray Telescope were grounding difficulties and noise in the instrument. Considerable time was spent with each instrument in reducing noise to a level low enough not to affect the data output of the instruments. Although several of the instruments are still plagued with this problem, the

two instruments used on the flight spacecraft were satisfactory at launch.

When the MC-5 instrument was inspected, a green and black deposit had formed between circuits and around the ends of soldered components on the printed circuit boards of some of the submodules. It was found that the substance was the catalyst from the potting compound, which had been improperly mixed. The catalyst was examined and it was decided that, although it is a partial conductor of electricity, it would not attack the printed circuitry or the solder. The discoloration came from organic substances. The instrument was cleaned with alcohol, but, because the laboratory report indicated that there could be pockets of catalyst trapped under the potting, the unit was rejected as a flight instrument until it could be determined if any further reactions would take place.

2. Cosmic Dust Detector

In future *Mariner* Mars type flights, three areas of Cosmic Dust Detector operation should be updated:

1. Having Cosmic Dust Detector power turn-on coincidental with spacecraft power turn-on. This would eliminate the possibility of sensor hits, with no power on the unit, that could cause the sensor capacitor to short.
2. A method of activating the sensor during the inflight calibration sequence so that the films could be monitored during flight. (Only the film circuitry is checked during inflight calibration sequences).
3. A provision for non-hypervelocity calibration of the microphone while the instrument is on the spacecraft. The dropping of selected beads at various points on the spacecraft would give better resolution as to direct sensor hits and particle size of hits occurring on other spacecraft areas during flight.

3. Trapped Radiation Detector

Future *Mariner* Mars type flights would benefit from the use of an indexed source and source holder on the Trapped Radiation Detector. Positioning of the source in the holder was a problem throughout subsystem and system testing.

4. Ionization Chamber

System tests of the Ionization Chamber under simulated space environment revealed two specific problems that were considered serious in that they were discovered very late in the testing schedule, and they indicated a necessity to rework every unit.

The first problem occurred during the vacuum tests of the MC-2 spacecraft in the space simulator. Excessive and erratic Geiger–Müller tube rates were observed. The trouble was traced to a venting problem at the base of the tube. Local geometry allowed air to become trapped in a small pocket near the tube base. The slowly escaping gas allowed areas of partial pressure to form in the vicinity of the tube leads, which caused them to arc when the unit was subjected to hard vacuum conditions and high voltage (900 v). This problem was remedied by adequately venting the tube base.

The second problem occurred during the MC-4 spacecraft tests in the space simulator. It was noted that at low temperatures the instrument would not resume operation when power was reapplied after the instrument had been deenergized. It was determined that the power converter oscillator would not break into oscillation at temperatures below approximately −22°C. Although nominal mission constraints had not required such rigorous starting capability, it was deemed advisable to safeguard against some unforeseen eventuality. The value of the resistor that provides bias to the oscillator transistor was changed on all units. Current tests on typical circuitry indicate a starting capability as low as −55°C.

Another problem that plagued the Ionization Chamber as well as virtually all systems early in the program was the acquisition of screened electronic components. Sufficient screened components were not available on a time scale consistent with instrument fabrication and delivery schedules. It is recommended that future programs thoroughly investigate this problem. An early and accurate definition of the magnitude and scope of the screening effort should be made mandatory. Furthermore, adequate support of the screening operation early in the program is imperative in order to allow sufficient lead time. Consideration should also be given to the question of whether the personnel responsible for component screening should report to line management or to project management.

Problems encountered in environmental testing and system testing indicate that more emphasis should be placed on additional safeguards for ensuring that test equipment failures cannot damage flight instruments. For example, thermostatically controlled ovens failed and exceeded critical temperature limits during testing, and vacuum systems leaked pressure (and oil) under power failures and overheated during water pressure

failures. All such failures damaged or jeopardized flight equipment because of inadequate safeguarding devices and alarm systems. Failures of this type caused considerable concern and required rework of flight instruments late in the program.

Certain radiation-measuring instruments required that radioactive sources be temporarily placed aboard the spacecraft for calibration purposes. On future programs, it is urged that steps be taken to provide that the source detector geometry be absolutely repeatable for successive calibrations. This includes ensuring that (1) there is a unique source for each spacecraft, (2) the source can be secured in the source holder in a single unique position, and (3) the source holder can be mounted to the spacecraft at a unique location and in a unique orientation. Such uniqueness of geometry will minimize the opportunity for human error in the calibration procedures.

5. Solar Plasma Probe

The following problems arose during fabrication of the Solar Plasma Probe:

1. It was not possible to approve the printed circuit board layout before artwork was started, because it was drafted directly from the schematics and the step of assembly layout drawings was omitted.

2. A design problem was indicated when a high-voltage transformer failed during screening. The bobbin design was changed and additional insulation was included to prevent breakdown between the secondary winding and the core.

3. The screening rejection rate on the high-voltage diodes exceeded 50% by a considerable amount. Although there was some question about the screening procedures, it was felt that the diodes themselves were at fault. Two other vendors were considered, but preliminary tests indicated that there was no advantage to be gained in changing vendors.

4. Upon delivery of the PTM, it was found that the peak power demand from the spacecraft was excessive and that an energy storage capacitor (1500 μf, 45 v) would have to be added. Since there was no more room inside the instrument package, it was placed externally on the connector face of module 32A4.

In the event of Plasma Probe redesign, it is recommended that the high-voltage section be made an integral part of the cup. This would eliminate the troublesome high-voltage cable connector assembly and the arcs that resulted when the assembly was placed on the spacecraft.

The use of certain resistors should be eliminated in this subsystem because of the excessive number of early failures attributed to them and because of the lack of supply sources. Some resistors are not built with an adequate safety margin. Slight overstressing of these components, particularly the lower values, caused them to increase in value. Typical cases include: 177 Ω resistors increasing to 1700 Ω; 5.1 k to 120 kΩ; and 5.1 k to 20 kΩ.

6. Helium Magnetometer

The *Mariner* Mars mission marks the first time a low-field helium magnetometer has been used in space. During the development of the instrument, numerous improvements and simplifications were suggested but they could not be qualified in time for application to the flight hardware. Work is now being performed on an advanced helium magnetometer, and considerable reduction in weight and power requirements is feasible for future missions. Any other improvements in instrument performance and increased reliability should, naturally, also be incorporated on future flight instruments.

The basic approach used in system testing of the Mars Magnetometer was sound, but some sophistication of the techniques used would allow earlier detection of system problems. A real-time plot of the digital outputs should be available in conjunction with analog plots for this purpose. If the Magnetometer were mounted on a boom and were remote from the spacecraft, a flux tank could be used in place of the Helmholtz coil, which would enable a reduction in steady and fluctuating fields without requiring elaborate support electronics.

7. Television Subsystem

Two areas of the television subsystem are felt in need of appropriate recommendations. One area pertains to the items that would affect the camera system design, mechanization, and testing before delivery to the spacecraft; and the other area relates the camera system to the spacecraft and to the overall program in general.

a. Camera system. Assuming that an identical or similar camera system was to be built again, the following

hardware and software should be given further consideration:

1. Shutter/shutter circuit interface
2. Component derating
3. Reduction in the number of part types
4. Camera head mechanical design
5. Circuit layout to facilitate testing
6. A better match between the analog video range and the digital video range
7. Formal subassembly test procedures to ensure uniformity in testing of flight units

b. Project interface. It is recommended that two additional pieces of hardware be included to be ready when either the prototype or the engineering model is ready. These additional units should essentially be subsystem simulators with actual end circuits or interface circuits. The design of these end circuits should be frozen at the time of delivery. One of the instrument simulators should support OSE checkout and the other should support the DAS. If circuit, timing, or signal characteristic changes became necessary, an engineering change request type of document would be generated and signed by the cognizant engineers affected.

The science project engineer should be made aware of areas in which components or assemblies are particularly sensitive to environmental conditions. He should then push for early decisions regarding the specific environmental test levels.

Problems and failures that involve two or more subsystems in the science subsystem should be assigned to the science project engineer until the problem or failure has been isolated to a specific subsystem.

Redesign should be performed so that collimator alignment during system testing is easier. Collimator capability in the space chamber would also be very desirable.

8. Planetary Scan Subsystem

The maximum range at which the *Mariner IV* planetary scan subsystem is capable of detecting and tracking a planet is primarily dependent upon whether the planet can be distinguished from the noise appearing with the signal. Based on this design, the amount of energy incident at the detector and available to produce the planet signal is limited by the effective aperture area of the optical system. A planetary tracker has been designed to overcome this difficulty; it has a higher signal-to-noise ratio because of its larger effective receiving cross section. This tracker, with an instantaneous field of view of 180 deg, is capable of eliminating the need for the planet searching operation. Preliminary performance evaluations of an engineering model indicate that it is possible to increase the operating range by several orders of magnitude over that of the system used on *Mariner IV*. It is known that the space background noise received by the tracker is a function of its instantaneous field of view; however, the possibility of eliminating the planet searching electronics and obtaining an increase in signal-to-noise ratio is worthy of consideration.

The neon lamps used in the photomodulator posed mounting problems because of their fragile envelopes. Radiation emitting semiconductor devices have been developed that can be used in place of the lamps. At present, however, construction techniques of these devices are such that the amount of radiation emitted is small, and a large amount of energy is lost through radiation scattering over 2π sterad. To reduce this loss, a small fiber bundle can be used as an energy coupling medium between the device and the photoconductor with the photoconducting material deposited directly on one end of the bundle.

The tracking accuracy is a function of the time constant and, hence, of the "dead zone" of the system. The use of a simply constructed ac motor, having a relatively large time constant, produces a wider deadband of operation. For a subsystem in which higher tracking accuracy is desired, a digital motor and the required control electronics could be incorporated. This would also make it possible to program the position of the planetary instruments.

9. Narrow Angle Mars Gate

The NAMG was developed, fabricated, and flight-qualified in less than 6 months. This was possible primarily because very large safety margins could be built into the performance characteristics of the NAMG, which in turn, permitted the numerous small changes that occurred in the spacecraft system to be accommodated without changes in the NAMG.

Future uses of an NAMG could benefit materially from several changes. First, a connector should be incorporated into the electronics module to avoid the problems that occurred from repeated soldering to the terminals and from the shorting of cable shields due to

limited clearance. Second, development and use of a high temperature burn-in on the photoconductive cells would allow a reduction of the sensitivity tolerance range that had to be allowed on *Mariner*, and would also permit better screening of these parts. Third, an earlier definition of the interface requirements would avoid the confusion, extra components, and interconnections that occurred on *Mariner* due to the many changes in the interfaces.

10. Data Automation Subsystem

Vacuum deposition is used to provide the required conductive interconnections between the pellet components in the envelope. Three problems were encountered in ensuring interconnection adhesion, pattern definition, and solderability of the deposition. These processes were completely interdependent and required simultaneous solution.

The first step was to define adhesion by means of a standardized tape test. The tape test was originally a tool of diagnosis, but later proved invaluable as a process control. Once properly defined and recognized, good adhesion was shown to be primarily a matter of cleanliness. The required cleanliness could only be obtained by vapor-blasting. The vapor blast produced a second-order improvement in adhesion as a result of surface roughening. Cleaning by means of solvents and vapor degreasing were tried, but without success, apparently because these methods failed to attack metallic oxides on the component surfaces.

The pattern definition problem was minimized by establishing the envelope position with reference to the source of deposition material and by ensuring that this position was maintained.

The original deposited interconnection material was copper followed by gold. When dip-soldering was used in an attempt to strengthen the deposited material, problems developed in wetting the deposited material to get the proper thickness of solder and in amalgamation of the deposited material by the solder. These problems were minimized through the use of:

1. A vacuum deposition of tin-indium solder for "pretinning"
2. A nearly eutectic solder and careful temperature control
3. Activated fluxes
4. Fountain soldering equipment to provide agitation, dispersion of flux, and air bubbles, and to provide uniform temperatures
5. Vacuum storage and lapsed time requirements to prevent oxidation and/or contamination of the vacuum-deposited surface before soldering
6. Nichrome instead of copper as the base material

There were several problems encountered with the molding process. Epoxy adhered to the surface of the teflon mold due to etching of the surface by the epoxy stripper. (The force required to separate the mold and remove the envelope sometimes resulted in fracturing it.) Epoxy would creep over the pellet end caps and the module leads. The solution to the problem consisted of lining the mold cavity faces with a teflon tape having a pressure-sensitive adhesive backing. The tape was replaced after each operation, which eliminated the surface-destruction/mold-release problem. The teflon-tape-lined mold provided an interference fit with all pellet components. However, the soft adhesive backing provided a fluid flow situation and allowed the mold to adapt to all component heights without undue pressure on any single component.

There were problems early in the program with the deposition masks. The original masks were too thin and material was deposited on areas other than those desired. This problem was eliminated by using double-etched masks of thicker material. A second mask problem developed due to adherence of deposition material to the mask. This was overcome by coating each mask with a plastic aerosol spray that was later removed with solvents.

In soldering the transistors to the envelopes, shorts occurred between transistor leads, and solder flow under the transistor caused shorts between circuits. These problems were solved by bonding glass-epoxy washers to the transistor cans with an epoxy that covered the transistor seal and formed fillets to the can and the insulating washers.

When the DAS type-approval unit failed, most of the resistors in the instrument showed marked decreases in their resistance. In addition, some resistors in modules from the MC-2 logic assemblies also showed marked changes from their original resistances. From an investigation of this problem, two possible resistor degeneration mechanisms (silver migration and silver palladium reduction) were postulated; reasonable evidence supported both theories. There was no evidence by which either

mechanism could be excluded; thus, it was necessary to assume that both were active.

A common denominator for the proposed mechanisms is that both required the presence of amines at the resistor surface. Exclusion of amines from the resistor surface was proposed as a means of defeating both resistor surface mechanisms. Amines can be excluded in three ways:

1. By providing a protective coating for the resistors
2. By ensuring that the entire amine content of the catalyst is reacted
3. By changing to an alternate encapsulant

In order to protect the mission, it was decided to use a welded non-real-time DAS instead of the pellet units. New pellet real-time units were fabricated for flight use in which all three remedial measures were taken. The resistors were glass-coated, precise control of epoxy/amine ratios was instituted, and epoxies requiring less active amine hardeners were used.

If an identical DAS is used in another program, the following recommendations should be considered:

1. An exhaustive analysis should be performed on the interface circuits. Although several quick fixes were made on the prototype model, no worst-case analysis was performed during the program.
2. The high-speed flip-flops are marginal (3 to 5%) when operated simultaneously at high speed and high temperature. They should be redesigned.
3. Signals routed to the OSE and to other elements of the science subsystem should be redesigned to drive them without the use of an external amplifier or line driver.
4. A worst-case analysis of the complete DAS should be undertaken. The outcome of this analysis should be to recommend specific logical mechanization changes.
5. The wiring layout in the modules, particularly the welded non-real-time assembly, caused excessive circuit loading and cross-talk due to distributed capacity. Rerouting of this wiring should be attempted.
6. The module-to-module connections also contributed to circuit loading and cross-talk due to distributed capacitance. This could be corrected by using low impedance drivers between modules and/or shielding critical interconnecting wires.

The mission design was initiated with a simple science payload that gradually grew to be very complex. Each time an instrument is added, deleted, or has its requirements changed, the DAS is affected. In the *Mariner* Mars project, these changes resulted in late deliveries of flight hardware, late discovery of mechanization problems, inadequate pre-SAF testing, and serious funding difficulties.

In any future programs, a requirement should be established that a JPL engineer and a QA engineer be located at the vendor's facility from the awarding of a contract to its conclusion.

N. Operational Support Equipment

1. Radio OSE

The 2298-Mc phase-locked-loop receiver used on the Mars spacecraft has some design limitations: it is a hybrid system, using both tubes and solid state components; it uses bias batteries for frequency control; it is limited in gain, having a threshold of approximately −120 dbm; it requires a module change to provide full frequency coverage (for five spacecraft RF frequencies); it has poor RF isolation, and, in many instances, actually had an RF leakage signal from the spacecraft that was at times only 5 or 10 db down from the input signal. Use of a DSIF equivalent receiver design, which is now available, would provide an all-solid-state receiver that does not use bias batteries; would provide thresholds ranging from −142 to −152 dbm depending on APC loop bandwidth; would have full frequency coverage for all spacecraft frequencies; and would provide approximately 150 db of isolation to RF leakage signals.

The spacecraft RF power monitor gave readings of spacecraft transmitter power output with errors up to $\pm\frac{1}{2}$ db, and other means had to be used to provide a more accurate measurement. This unit should be redesigned. The 2116-Mc test transmitter presently needs a module change to provide full RF coverage. The unit also has limited RF power output. A DSIF equivalent transmitter design, now available, can provide a 150-kw RF output and has full frequency capability.

The points mentioned above for improved performance are the major design improvements. There are, however, several other changes that could be made for future radio OSE in the area of human engineering. These changes are in commercial test gear, in equipment layout, and in a more automated system of monitoring and evaluating spacecraft functions.

2. Video Storage Subsystem OSE

Data logging facilities for bit error and system evaluation should be incorporated into the OSE. This addition would enable rapid system performance analysis.

All test points should be brought to a central switching system (automatic or manual) thereby eliminating the extensive external patching procedure that is presently required.

3. Ground Handling Equipment

The large structural design safety factor was desirable in consideration of the minor changes that occurred after the initial design and of potential handling abuses that the equipment might have been subjected to. However, the factor-of-2 hazard was indiscriminately applied to heavy equipment design. For most objects over 1000 lb in weight, the hazard factor should be reduced on a sliding scale to unity for 4000-lb items.

Particular attention should be paid to the special system test equipment used during these tests. It was found that the ground handling equipment had more interfaces with this equipment than with the spacecraft.

The universal ring was made from a ring forging of aluminum about 6 ft in diameter. It was machined to a final weight of approximately 200 lb. After it was rough-machined, it was oven-annealed to remove internal stresses. It was found that this treatment was inadequate, since the ring crept during the course of the program. The feet that supported the spacecraft were machined to be in a common plane within ± 0.005 in. It was found after a year that the rings had moved as much as 0.012 in. in a 5-ft diameter.

If the additional stability of a four-wheeled dolly is not required, wheels could be mounted directly to the three legs at the base of the U-ring and the dolly eliminated.

The spacecraft positioner became dynamically unstable and easily displaced when the articulated system CG was above the rotation axis. By tightening tolerances, this movement was minimized. One solution to the problem would be to install a counterbalance so the articulated CG would never go over dead center. The counterbalance would consist of a water tank that could be drained when the positioner was transported.

The positioner turntable rotated 350 deg. The usefulness of the positioner would have been increased if the table had been capable of rotating 365 deg.

The spacecraft U-ring should have been attached at three points to the ground surface on the positioner turntable ball bearing instead of at four hoist-point locations. This surface was not flat or rigid enough to allow the U-ring to be tied down at four locations. As a result, some distortions were introduced into the U-ring.

System test cable troughs or support structures should have been designed into the U-ring spacecraft positioner combination to improve the functional performance and aesthetic appearance of the system test area.

The blue paint that was applied to the ground handling equipment chipped off too easily. During shipment of one of the spacecraft to AFETR, it flaked off and contaminated the spacecraft. Not all of the ground handling equipment should be painted; corrosion resistant, passivated, or plated materials should be used whenever possible. If paints are required, they should be chosen to have high adherence and durability characteristics.

O. *Environmental Tests*

Emphasis is placed here on deficient environmental tests caused by such events as operator induced errors, procedural and inspection inadequacies, and test equipment failures or malfunctions. A large effort was spent in the development of controls and procedures for testing, and many of the controls and procedures implemented were the result of problems uncovered. Typical of these controls in the area of dynamics testing were:

1. Detailed operational procedure and check-off tests for test operators
2. Vibration force limiting and fail-safe provisions
3. Interim tests for environment verification
4. On-site results of PTM and STM testing for diagnostic assessment of the behavior of the flight vehicles
5. Pretest checkouts of such items as fixtures, input control and dump circuits
6. End-to-end calibration of accelerometers and instrumentation systems, and instrumentation installation and calibration procedures

Table 121. Summary of problems encountered during environmental tests

Environment	Problem	Cause
Dynamic	Ionization Chamber vibration overtest	Operator error
	Power subsystem vibration overtest	Facility malfunction
	Solar panel vibration overtest	Operator error
	PTM torsion vibration overtest	Facility malfunction
	Video storage subsystem overtest	Procedural inadequacy
	MC-3 vibration anomalies	Procedural inadequacy, facility malfunction
	MC-4 vibration anomalies	Facility malfunction
Thermal–vacuum	Power subsystem	Inspection and procedural inadequacy
	Plasma Probe cup overtest	Inspection and procedural inadequacy
	Pyrotechnic control unit	Facility malfunction

Table 121 presents a summary of some of the problems encountered during environmental testing. These problems are discussed in more detail in the following paragraphs.

In spite of the controls established, some of the problems could have been easily avoided by the further tightening of maintenance, inspection, and procedural activities; some, however, could not have been avoided. Such items as those considered design deficiencies or oversights are unavoidable in a program as complex as *Mariner* Mars 1964, and should be anticipated in future development activities.

1. Dynamic Environments

Some of the significant problems encountered as a result of dynamic testing originated from both system and subsystem level acoustic, vibration, and shock tests.

a. Ionization Chamber vibration overtest. During the FA vibration test of a flight Ionization Chamber, an overtest of short duration occurred. After the first plane of vibration, it was discovered that some of the bolts in the vibration fixture had only been installed "finger tight." It was estimated that the Ionization Chamber saw an input of 18 *g* rms. To demonstrate that the flight unit was unaffected by the overtest, the TA unit was retested with the same fixture configuration (bolts in finger tight). The overtest condition was repeated in the same frequency spectrum, during the sine sweep, and to the same degree. Based on this test, the conclusion was drawn that the cause of the overtest had been the improperly assembled fixture, and that the TA retest had satisfactorily demonstrated the flight unit to be unharmed by its overtest.

b. Power subsystem vibration overtest. Power subsystem Case 1 was subjected to an overtest during vibration. During the sine sweep, the rms level rose to 21 *g* at approximately 1920 cps on both upsweep and downsweep. Investigation indicated that the fixture was faulty due to a warped slider-plate surface. This test was recorded on an rms strip chart recorder rather than on magnetic tape.

Because of the loose and faulty fixture used as the sine wave excited the resonance of the flaw, a pounding action occurred and a wideband response resulted. Although only rms data were obtained, the overtest is considered to have been a wideband phenomenon consisting of "hash" at all frequencies. However, it is very doubtful that this overtest could have damaged the flight equipment.

c. Solar panel vibration overtest. During FA vibration testing of a solar panel, the panel was erroneously subjected to the *Ranger* FA test specification levels. The panel easily survived the test; however, a tightening of testing and liaison procedures was effected, requiring closer monitoring of environmental tests by the JPL technical division involved.

d. PTM torsion vibration overtest. During the TA torsional vibration tests of the PTM, an overtest of short duration occurred. While performing the fast torsional sine sweep (150 to 50 cps), failure of the torsion test fixture resulted in a "hammering" action that caused high-frequency/high-amplitude inputs to the spacecraft. The failure mode of the fixture was noted by a loosening of the wing connector to the bowl because of faulty inserts, which caused the drive link between the fixture and the vibration exciter to fail.

The specified input to the vehicle was exceeded to the extent that two specific questions were posed: was the input (less the failure effects) near enough to nominal that the test objectives were met, and what were the effects of the other (non-nominal) inputs?

1. *Realization of test objectives.* The test objectives appear to have been met. Figure 446 shows a line

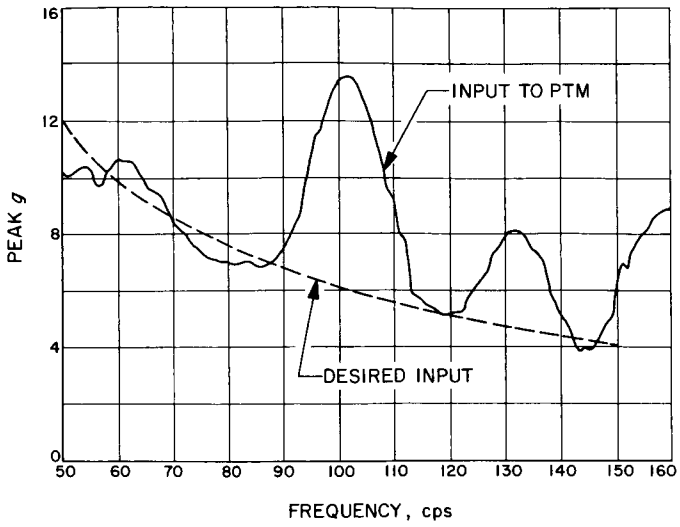


Fig. 446. *Mariner* Mars PTM (line spectrum)

spectrum analysis of a tangential accelerometer with the desired input included. The peaks represent spacecraft and adapter torsional responses that would not be seen at the input to the fixture. A comparison of phase between two opposite tangential accelerometers indicated that the input was indeed torsional in this frequency range.

2. *Effects of non-nominal inputs.* The broken fixture resulted in a hammering that caused high-frequency/high-amplitude inputs to the spacecraft. Figure 447 shows these inputs for the transducer. The inputs are most probably not torsional but rather just "ring-out" of the fixture. The data show the hash that would be expected from the hammering and the well-defined spike at 850 cps that would be expected from a fixture ring-out. Comparing a radial accelerometer and a tangential accelerometer at 1 ft g indicates that the fixture was "breathing" and the open circular top became ellipsoidal. In light of the time history of the run, and with the assumption that similar conditions existed during the first five runs, this condition probably existed for a total of about 2 sec.

The PTM received a low-frequency torsional input that was in excess of the test requirements but not considered to have inflicted any vehicle damage. The torsional test requirements were considered to have been met. The spurious high-frequency hash of the fixture failure was of a relatively high magnitude, but was no more severe than other tests. The spike was extremely severe in amplitude but did no apparent damage.

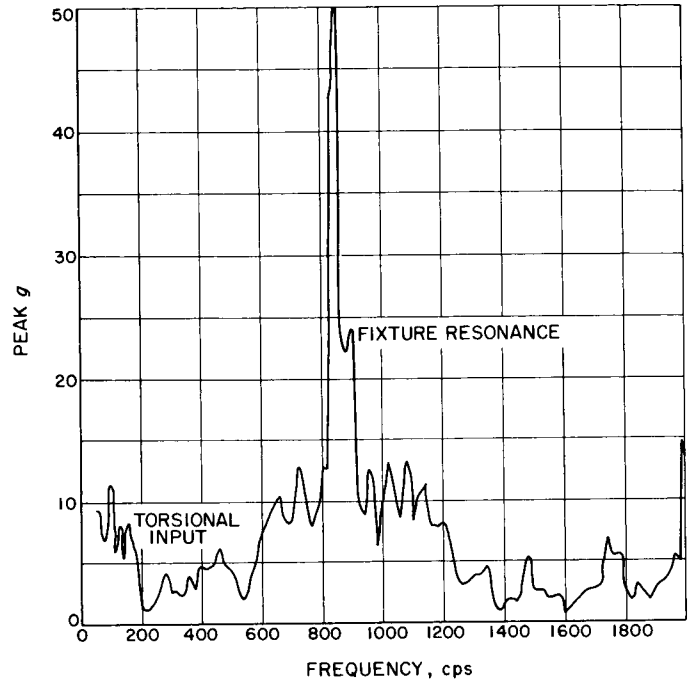


Fig. 447. *Mariner* Mars PTM (test No. 27)

Subsequent retesting of the PTM was accomplished to prove, beyond question, that the vehicle's integrity was adequately demonstrated for torsion.

e. Video storage subsystem overtest. The video storage subsystem was subjected to excessive acceleration shocks during TA testing. The overtest was experienced in the third test plane. The operator did not recalibrate the shock tester before the third plane test. For the test, the shock fixture holding the VSS was turned up on one end. During the first test in the plane, the trace indicating the shock level went off the scale of the instrumentation scope. It was decided to bring the shock level down by changing the initial position of the shock tester sled. During the next test in the plane, the trace stayed on the instrumentation scope but indicated a transmitted shock in excess of 700 g peak to peak. The operator repositioned the sled and conducted another test; the indicated shock acceleration level was 20 to 50 g higher in that test than specified. The fourth and fifth shock tests in the third plane appeared to be normal.

Although the video storage subsystem was apparently not harmed by the anomalous overtest, its occurrence pointed out the need for:

1. Specific operational procedures for shock testing and calibration of shock testers before each testing plane

2. Closer surveillance by JPL Quality Assurance and Reliability personnel to ensure compliance with written procedures

f. MC-3 vibration anomalies. During the low-level noise test in the roll axis and in the first lateral axis, a loud popping noise occurred. The noise was subsequently determined to have been a 2 σ spike (11 g peak) in the tape input spectrum. Such a magnitude is a rather normal occurrence in these tests, since it is possible to obtain occasional levels as high as 15 g peak. However, this particular spike occurred very near the end of the run, when the overall rms level was dropping. It was concluded that the combination of the "falling off" of the overall level coupled with the spike produced a sound characteristic of a tape dropout; hence, the loud "popping" noise. This condition was corrected for the second lateral axis test by effectively erasing the spike from the tape spectrum. There was no evidence to indicate that the environment attendant with this anomaly produced any undesirable effects on the spacecraft.

During the test series, the failure of a booster amplifier in the vibration exciter system generated a spurious input to the vehicle. This input (a sine wave of approximately 1 g rms amplitude at 60 cps for a duration of somewhat less than 15 sec) occurred during the noise calibration portion of the FA test. An examination of the power spectral density plots from the previous tests, indicated that the failing amplifier had been generating 60-cps noise components for some time. It was conservatively estimated that the total environment produced by this testing anomaly was 0.9-g peak at 60 cps for 120 sec. The anomaly subjected the MC-3 vehicle to higher levels than TA levels (PTM lateral levels at 60 cps, although 1-g peak are of significantly shorter duration). This spurious signal is probably the cause of the somewhat lower test levels observed during the XY Bay II axis noise test, since it is presumed that the amplifier was generating 60-cps noise as a significant portion of the calibration level. After the detection of the failure, the amplifier was replaced; hence, there was no effect of the noise signal during the last axis test.

There was no evidence to indicate that the testing anomaly degraded the MC-3 spacecraft. It was planned to retest the PTM to levels and time durations of 60-cps vibration substantially in excess of the imposed testing anomaly, but the plans were not executed before launch.

g. MC-4 vibration anomalies. During the equalization verification sine sweep in the XY Bay II axis, an incident occurred in which the vibration exciter system experienced a momentary instability resulting in loss of servo control. This event occurred about 0.05 sec after the vibration exciter gain had been increased to ½ g rms. The resultant anomaly, although not recorded on magnetic tape (only on direct-write oscillograph), is conservatively estimated to have produced an input to the spacecraft of approximately 1.3 g rms at 150 cps for about 2 sec. This input compares with a PTM lateral input of 1.25 g rms. Although the spacecraft was subjected to a TA-level input at this particular frequency in this axis, subsequent investigation indicated that the structural reliability of the MC-4 vehicle, and specifically the MC-4 solar panels, was considered to be unimpaired as a result of the overtest.

A severe transient occurred during FA testing in the XY Bay II axis approximately 9 sec after the start of the calibration portion of the noise test. Due to the failure of a vacuum tube in the tape playback demodulator circuit, a transient similar to a tape dropout occurred. The transient was repeatable on the tape system in the vibration console and apparently resulted from a particular signal sequence on the tape, since no tape dropout was detectable on other playback systems. The tape system playback amplifier/demodulator was replaced and the noise tape was replayed 12 times through the section in which the transient occurred. No events of signal transient were detected.

The observed transient was analyzed, using shock spectra, and compared to similar shock spectra from spacecraft pyrotechnic, V-band, and shroud V-band release tests (Fig. 448). An examination of the spectra

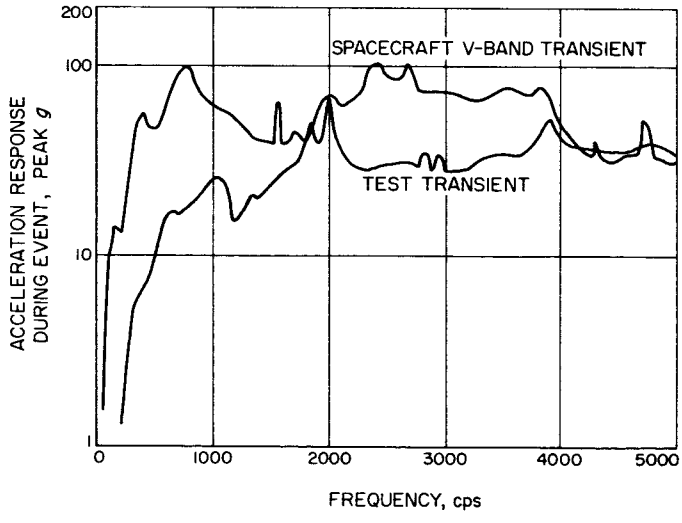


Fig. 448. Comparison of computed shock spectra

indicated that the test anomaly was not as severe as the transient responses due to spacecraft V-band firing. Therefore, it was concluded that the environment produced by the observed transient could be considered insignificant compared to the effects expected from the pyrotechnic events.

No evidence exists currently to indicate that the environments attendant to any of these testing anomalies degraded the MC-4 spacecraft. The vehicle experienced no significant systems test anomalies or mechanical/structural problems.

2. Thermal–vacuum Environments

a. Power subsystem. During the FA thermal–vacuum test of power Case I, the unit was subjected to −30°C for 2 hr. As a result, the chamber cold-wall temperature process was modified. The power subsystem is not known to have experienced any degradation as a result of this environment.

b. Plasma Probe cup overtest. During the FA thermal–vacuum test of the Plasma Probe cup, the high temperature test was erroneously conducted at the standard specification TA temperature of 75°C. The flight worthiness of the cup was not considered to be impaired, since the cup TA test was performed at 125°C.

c. Pyrotechnic control unit thermal–vacuum testing. During TA testing of the pyrotechnic control unit, a significant problem was encountered with the testing facility in its ability to control the temperature environment. The unit had satisfactorily completed the cold-test portion of the thermal–vacuum environment when it was exposed to an anomalous environment in the hot-test portion of the environment.

Approximately 4½ hr after the start of the 12-day high temperature test, the chamber heating valve failed. The valve was repaired with the test unit still in the chamber and the test was restarted. Shortly thereafter, the valve failed again and was replaced. When the test was restarted, temperature was lost again in about 5 hr. The test was begun the third time, and was continued for approximately 5 days at which time temperature control again became erratic. After a fourth try, the test was stopped.

After correcting the problems with the facility, the TA unit was subjected to another 12 days of testing at 167°F and 10^{-4}mm Hg with satisfactory results. At the present time, the TA unit is in life test, having completed some 4000 hr at 145°F and 10^{-5}mm Hg satisfactorily. It appears that the pyrotechnic control subassembly was unaffected by the anomalous test environment.

3. Magnetics

Vibration testing had a significant effect on the magnetic characteristics of the materials used in the spacecraft. Several studies of this problem were made and, as a result, it was found that two of the vibration exciters had sufficient magnetic fields in the area of the object being vibrated to cause magnetic perming of the object during the test. This problem was most evident in the case of the solar panels, which were permed due to flexure of the Kovar bus bars when the panel was vibrated normal to the surface. The solar panels were subsequently depermed following the vibration tests; the deperming resulted in a reduction of the magnetic field to less than 1 γ.

The only solutions to the problem in the absence of nonmagnetic vibrators appear to be (1) a restriction on the use of the offending vibration exciters to test assemblies with magnetic material; (2) the reduction of magnetic material and components in the spacecraft; or (3) a subsequent deperming of the assembly.

4. Other Problems, Overtests, and Anomalies

Tables 122 through 124 present other occurrences experienced during the *Mariner* environmental test program. This listing was compiled from problem/failure reports, test reports, internal reports of the affected JPL technical divisions, and discussions with their appropriate representatives.

5. Recommendations

On the basis of the problems discussed in this section, the following recommendations are proposed.

a. Dynamics. During the testing portion of the *Mariner* Mars project, the vibration requirements were reviewed in terms of the rationale by which the specification levels were established. These levels were based on inflight vibration data observed on *Ranger* flights and on some appropriate wind tunnel tests and auxiliary calculations. The spacecraft acceptance levels were established by generously enveloping the 95 percentile probability level for 50-cps incremental bandwidths; thus, *Mariner* Mars test levels limited to 5% the possibility of exceeding *Ranger* inflight measurements in any particular bandwidth and independent of other bands. Establishment of the TA levels was accomplished by scaling upwards

Table 122. Environmental test equipment or facility malfunction due to operator error and procedural or inspection inadequacy

System or subsystem	Environment	Remarks
Solar vane and solar panel	Vibration	The accelerometer cable connector was loose, causing the servo control system to become unstable during low-frequency vibration. Inspection was tightened.
Data encoder		The FA test tape was run on the TA complex wave vibration test. Procedures were tightened, prohibiting tests with out detail test specification.
Cosmic Ray Telescope		The instrument was not properly secured to the vibration fixture during TA vibration. Screws backed out because of improper torquing.
Radio	Thermal–vacuum	Radio Case V was installed in the chamber backwards and technicians connected the control thermocoupler to the wrong heat exchanger. Audio alarms were installed in all systems, which would indicate a high- or low-temperature condition. Additional installation procedures were released. The installation of test units in vacuum chambers by technical division personnel has been restricted, unless closely monitored by test personnel.
Radio	Thermal–vacuum	Improper installation of thermocouple leads damaged the radio subsystem during FA tests. The problem was partially caused by fatigue of personnel. Detailed procedures were issued.
System cabling		The 25-ft test chamber was opened and exposed to room conditions before the exhaust lines on the contamination plate had reached temperatures above the atmospheric dew point. Therefore, water vapor in the air condensed on the cold surfaces and ran into the feedthrough connector. Thermocouples were placed at the inlet and exhaust lines inside the chamber.
Test equipment		The pressure gauge did not indicate loss of vacuum and the line was opened to the chamber, which caused a pressure rise. The pressure interlock on the vacuum line was being repaired during the test and the line was vented to the atmosphere. The corrective action was to prohibit equipment repairs during the test. A vacuum interlock was installed all STC power.

so that the ratio of the TA to the FA tests was approximately 5 to 3. For the subassemblies, the specifications were altered from those prescribed at the system level to account for the transfer function of the structure.

Uncertainties were encountered because of the following items:

1. At the time of the establishment of the levels, no vibration measurements had been obtained inside any inflight spacecraft. In addition, there was no flight data for the *Mariner* Mars configuration, and analysis indicated that the shroud shape would strongly affect the vibration characteristics.

2. Although the overall rms value of the observed launch vehicle inflight vibration has been quite similar from one flight to another, the spectrum is known to be variable.

3. Testing of the vehicle on the ground is grossly affected by the fixture transfer characteristics that modify the input spectrum.

In consideration of the above uncertainties, it appears necessary that steps to cope with these difficulties be taken in such areas as the following:

1. A large effort should be expended to obtain inflight vibration measurements both from inside the spacecraft and on the launch vehicle. Work in areas such as wind tunnel analysis and acoustical testing of the spacecraft should be emphasized in order to better understand the manner in which the mechanism of vibration is affected and how it is transmitted into and throughout the spacecraft.

2. From a statistical standpoint, a considerably better simulation should be sought. It is known that the inflight vibration is neither periodic nor stationary,

Table 123. Environmental test equipment or facility damage

System or subsystem	Environment	Remarks
Radio	Vibration	The mounting holes in the vibration fixture were not deep enough, and screws bottomed and damaged Case VI. Standards for hole depth and mounting screws were established.
Solar vane actuator		The vibration fixture did not support the output torque assembly as it is supported in flight. The output arm assembly was weakened.
PTM		The high-pressure pump used for lubrication of the bearing on the torsion oil table generated a spurious signal. The test was performed with the pump on low pressure and with the bearing not lubricated. The situation was corrected during checkout before mounting the spacecraft on the test system.
CC&S	Thermal–vacuum	Loss of vacuum in the 25-ft space chamber caused the CC&S to count fast. There was no damage to flight hardware.
Radio		The coolant valve on the vacuum chamber froze open. A heater was installed on the vacuum chamber.
Space simulator		After pumpdown, the chamber door had more leaks than there were clamps available. Chamber pressure was reported to be rising. A high-pressure alarm was not connected, and the test director was not apprised of the potential pressure rise. The door was improved as part of the 25-ft chamber modification and an alarm system was connected.
Canopus sensor		The problem was found to result from a faulty temperature control system.
Radio		During the temperature test of the radio subsystem, a temperature drop from 131 to 32°F was experienced. A faulty relay was found and replaced.
DAS		High vacuum was lost for approximately 20 min due to accidental shutdown of the primary cooling water supply. In no case did the Bell-jar pressure exceed 1×10^{-3}.
Test gear		Oil from the crane dripped on the spacecraft. The crane oil seal leaked. The crane was cleaned and the seals were replaced.
Test equipment		Ground loops occurred between the 25-ft space simulator and the STC as the result of a building contractor error. The OSE feeder transformer neutral was connected to the building ground system.
Test power		A power failure occurred in the vacuum laboratory during the cavity amplifier test. One leg of the 480-v transformer overloaded. Current monitors were installed on all legs of the transformer to balance them.
		A 480-v power failure occurred in the vacuum test area. Maintenance electricians working on the trailer caused a short in the circuit, which was temporarily common to the trailer and to the test area bus. The 480-v circuit was removed from the trailer modification area.

but rather in the grey area of transient, nonstationary processes. Investigations into this problem could possibly develop more realistic and somewhat less conservative simulations and techniques.

3. To compensate for fixture problems, such techniques as multiple vibration systems and flexible fixtures should be studied in order to increase the dimensions in which the vibration testing technique can be controlled.

Function of quality assurance and reliability in environmental testing. The significant problems and overtests previously discussed accent the need for the introduction of QA engineering into the environmental testing program. It would appear that the introduction of the QA function covering the areas below would be quite effective. Documentation monitoring should consist of:

1. Verification of accuracy of test results, summary forms, and reasons for retesting flight hardware
2. Verification of test specifications and applicable waivers, reference designations, and serializations
3. Verification of problem/failure report accuracy
4. Generation of test status and anomaly reports, as required, and of reports on testing that do not comply with applicable specifications and/or waivers

Table 124. Other problems and malfunctions

System or subsystem	Environment	Remarks
Power Case I	Vibration	An error occurred in equalization during FA vibration testing at the vendor's facility.
PTM		Attempts to equalize the vibration system failed. Extensive evaluation of the vibration system revealed an instability of the X-axis drive signal from the sine oscillator to the X–Y recorder and, later, stability problems in the recorder. The booster amplifier generated a spurious beating signal during the equalization sine sweeps and noise calibration portions of the test. The spacecraft was not affected, but test objectives were not realized due to the effect of these problems on the schedule.
CC&S OSE		The magnetic shield used to protect the CC&S from the vibration exciter field during vibration shorted the CC&S 28-v power to the chassis. Insulating material was provided to prevent shorts from the magnetic shield.
Squibs OSE		A test circuit malfunction occurred. Improvements were made in the circuit to eliminate transient responses and to ensure a proper signal to the squibs.
Gyro control assembly OSE	Vibration	During FA vibration testing, the operator tripped over the power cable, which caused a loss of capture on all gyros. The power cables were taped to the floor.
RF exciter OSE	Vibration	The FA test set exciter showed phase spikes during and after vibration of the RF communication assembly. Blower capacity was increased to reduce heating in the FA test set.
Scan subsystem OSE	Thermal–vacuum	Transients were introduced by test equipment during TA high test. These transients caused scan reversals without hitting the limit switches.
Command OSE		Noise "glitches" were induced on cables connecting the OSE and flight subsystem, which caused the OSE to indicate incorrect reception of commands when in the vacuum chamber. The cables were shielded.
MC-4		A thin film of thiolate ester was deposited onto the cold surfaces of the spacecraft and onto the simulator contamination plate during the vacuum system test on MC-4. Most spacecraft polished surfaces were required to be recleaned. The problem was not attributed to the 25-ft space simulator.

Test monitoring should consist of:

1. Verification of the use of the proper equipment, fixtures, and instrumentation for measuring or monitoring the environment
2. Verification of correct procedures for test units, including procedures for proper installation of fixtures and hardware, specifically for dynamic environments
3. Verification of calibration of support instrumentation, stress levels, and the detailed compliance to the applicable test specification
4. Monitoring of an instrumentation calibration program
5. Verification of operating time in a particular environment, specifically failure reporting

Subsystem shock testing. The shock test program for subsystems was performed primarily from the standpoint of producing a certain specified transient. However, in most instances of subsystem testing, it was not known what the specific transfer functions within the individual subassemblies were and what a correlative response characteristic would be. Therefore, it appears desirable to monitor the specific responses of each subsystem during shock tests and at the same position during the full scale tests. This information could then be directly correlated to the environments measured during such events as pyrotechnic firings and separation transients.

Low-frequency transient testing. The laboratory results observed during the high-gain antenna thermal–vibration tests produced only moderate agreement between the antenna structural response to the swept sine and the decaying sine transient. In order to achieve accurate transient waveforms in the laboratory, it appears necessary to require further refinements of the testing technique. Further development of this approach also appears worthwhile since it more closely approximates the thermal–vibration environment during boost.

The technique presently employed for structural integrity demonstration uses swept sinusoids and generally results in overly conservative testing. This is due mainly to: (1) the use of large safety factors to establish the swept sinusoid equivalent for a transient impulse, and (2) a lack of detailed knowledge of the dynamic response characteristics of a particular structure at the time when the test specifications are established. As a result, spacecraft structures appear to be considerably heavier that the boost environment necessitates, and it would appear that large savings could be achieved on future programs by developing the transient testing technique. The corollary to this problem is the development of the tools and techniques necessary to design and analyze for transient loads.

Improved fixture design. To develop more realistic simulations during the ground test program, additional effort should be directed to the study of the fixture problem. Vibration fixtures should be controlled and defined by the normal engineering drawing practice. It appears mandatory that a definition be made, at an early date in the program, of specimen attachment points and the location of hard-mounting points for control accelerometers for all vibration axes on the fixtures. The design of the fixture should reflect attempts at minimization of cross-axis response, with a goal of a maximum response of 1 db below 1000 cps and 3 db between 1 and 2 kc. For specimens with multiple mounting points, the design of the fixture should strive to maintain input acceleration amplitude ratios from point-to-point of ± 3 db below 1000 cps and ± 6 db in the range of 1 to 2 kc. Individual fixtures should be thoroughly evaluated before the testing of any prototype or flight hardware. It is suggested that reasonable dynamic mockups be employed during such an evaluation.

Improved equalization techniques. The present equalization system at JPL uses a long established approach to the problem of equalization techniques; that is, low-level sinusoidal excitation of the system and careful manipulation of several peak/notch filters in the signal path that have adjustable center frequencies, amplitudes, and Q. An attractive solution to the problems associated with this system would possibly be the use of automatic equalization equipment and/or multiple-input vibration exciter systems. This, then, could compensate to some extent for system nonlinearities, structural failures, component malfunctions that change equalization, the elimination of high Q unequalized resonances, and better controlled test inputs. However, before this recommendation can be implemented, considerable in-house work must be accomplished.

Improved shock test techniques. In order to more adequately simulate the staging transients associated with the flight environment, the use of electrodynamic vibration exciters for producing the desired shocks appears attractive for future programs. A prerequisite to the use of these exciters, however, should be a study of the actual staging inputs.

Dynamic modeling of spacecraft. While dynamic modeling was not of particular significance to a program like *Mariner* Mars (largely because of the spacecraft relatively small size and weight) the anticipated size of future spacecraft would indicate that some work should be initiated now on studying the scaling effects of very large complex structures and the testing techniques to be used.

Margin demonstration and/or testing to failure. Due to the present state of the art in estimating vibration environments, and the fact that future programs will be faced with the same problem of prescribing qualification testing levels at early dates with little available information, it appears highly desirable to strive toward a failure test of the prototype vehicle early in the program. Such a test should show just what design margin actually exists. It would be invaluable to know just how much inherent but untested margin there is in a typical design if the need for trade-offs arises late in the program. Such an occasion arose in the *Mariner* Mars program when the shroud configuration and structure were changed without really knowing what effect the change would have on the spacecraft environment. There was a general feeling of safety, which was based on speculation and past history, and the spacecraft/shroud vibration and acoustic tests were completed, although time did not allow rerunning the complex tests. Had the design margin been known at that time, change-over could have been effected more confidently. Weak links in the chain would have been immediately pointed out, and, depending on the margin demonstrated, could have been changed or redesigned at a stage in development when such tasks are easily accomplished.

In consideration of these factors, a demonstration of margin, by a test of failure, appears to be a highly desirable engineering tool.

b. Thermal–vacuum and temperature control. At the completion of the TCM testing, and as a result of tests of the PTM and the flight vehicles, it was noted that the temperatures measured within the spacecraft often necessitated changes to the spacecraft thermal configuration, louvre locations, and thermal shield design. This

type of change (continuous throughout the project) could perhaps have been curtailed if the TCM tests were performed at a very early date and in two phases.

Test phases should consist of a preliminary roughing-in series followed by a finalizing sequence for the demonstration of adequate spacecraft thermal design. The interval between such tests could be used to update the TCM and analyze the data to determine what additional information was needed or desired. The experience of a single prolonged series of tests on *Mariner* resulted in several compromises in thermal design that possibly could be eliminated.

Stray light testing. The stray light reflectance testing proved a necessity for the assurance of the proper operation of the light sensitive sensors. Although seemingly isolated (according to layouts and having information about individual sensor light reflecting capabilities), it became apparent that, when joined together in the final spacecraft assembly, the information at hand fell far short of estimating primary and secondary reflected light sources. The use of the stray light reflectance tests on the *Mariner* Mars program was informative, and its application for future programs should be considered early in the design stage. In addition, these tests yielded conclusive evidence of the necessity for a closer look at both sensor design and location for future configurations.

Launch pressure profile simulation. While pressure decay ratios during the pumpdown process of space simulation testing were reasonable, they were by no means an actual simulation of the launch pressure profile. It is suggested that appropriate steps be taken to produce an adequate, if not more conservative, simulation of the launch pressure profile.

c. Electromagnetic interference. At an early date in the formulation of spacecraft specifications, the electromagnetic requirements should be firmly established. The requirements imposed on the spacecraft should include the EMI practices discussed in the following paragraphs. In general, it is suggested that one of the first tasks should be the generation of EMI design guides. The guideline subjects that could be written are (1) preferred wiring layout, (2) decreasing susceptibility to electrostatic discharge, and (3) RF susceptibility suppression.

Environmental susceptibility test. The primary recommendation to improve the future performance of this test is that it not be attached to other spacecraft tests on a noninterference basis. Sufficient setup, performance, and evaluation time should be allotted for the test.

The RF susceptibility test could be improved by the construction of a test facility in which the simulated RF environment could be repeated with a high degree of confidence. Such a facility is envisioned as being a chamber lined with RF absorbing material. (Reinforcement or cancellation of RF waves cannot be predicted or calculated in a test facility such as SAF.) The spacecraft should be brought to the test facility and placed in the same orientation for each test. The antennas used for the RF simulation should be placed at permanent locations in the chamber and the RF generators should be installed in an adjoining room. The spacecraft support equipment should be set up in a separate room. Safety to operating personnel would also result from the use of such a facility, if the simulation sources were increased in power level.

The simulation equipment used for this test in the future should be capable of providing a realistic environment that would include the peak power levels, repetition rates, pulse widths, and other modulation characteristics.

Transient tests. An RF testing program to demonstrate RF compatibility is recommended for spacecraft and support equipment subsystems. Each spacecraft and support equipment subsystem or unit should also be subjected to a voltage transient test. (Military specifications exist that call out such a test for some military systems.)

To carry out a transient voltage test program, the first phase of the work should be the definition of the transient characteristics. Perhaps a study of the wave shape and amplitude of transients that occur on spacecraft systems should first be studied. Theoretical transient voltage levels occurring during power line switching of spacecraft or launch vehicle circuits, electrostatic discharge, and other possible causes would also help determine the test transient levels.

The second phase of the implementation of the transient test should be the design and/or procurement of transient generating equipment. The third phase of the project should be the actual tests on subsystems after specifications are written defining the points at which the system wiring is to be tested and the test level to which the points are to be subjected. The final phase should involve the corrective action necessary to eliminate susceptibility to the impressed transients. An EMI engineer should participate in the design and review of the corrective action. His participation would be significant

because it would provide the only continuity of the corrective efforts performed on all units. The corrective action should be similar or concurrent with any RF corrective measures.

Electrostatic charge. Guidelines for the design of spacecraft equipment should be established at an early date to avoid problems caused by the breakdown of accumulated charges on a launch vehicle. The guidelines should emphasize integral shielding and no gaps should occur on all circuit elements and/or cable shielding with multiple grounding.

Type-approval tests of a spacecraft system should be performed to demonstrate that voltage discharges will not degrade the performance of spacecraft electronic circuits. A determination of the magnitude of charge buildup and voltage levels on the launch vehicles should be made. This investigation could include the design of experiments to be flown on launch vehicles to determine the various parameters.

Subsystem RF interference tests. It should be required that flight equipment and support equipment be tested for radiated and conducted interference and susceptibility. The RF levels should include those to be encountered at the launch complex and after shroud ejection with a sufficient margin of confidence to ensure that the equipment operates properly. The test program should be performed on early model flight and support electronic equipment. The corrective action taken to eliminate susceptance or radiation should be part of the test program. An EMI engineer should participate in the design of the corrective action. His participation would be significant because it would provide continuity of the corrective efforts on all faulty equipment.

It should be a requirement that all support equipment consoles have RF filters and isolation transformers on the power leads to suppress the RF interference on the test complexes.

Before an RF subsystem interference test program is initiated, the test requirements, test techniques, test equipment, and facilities should be specified and developed.

RF broadband noise and discrete spectral components. It is recommended that the following steps be initiated to determine whether the communications system will be degraded by RF interference originating in spacecraft or support equipment. These steps should be executed early in a spacecraft program.

1. Determination of the permissible noise levels in the receiver and transmitter bandwidths of both the spacecraft and the operational support equipment
2. Determination of what type of noise measurement equipment could best be used to make noise measurements to the limits determined in (1)
3. Development of specifications for test equipment that would be required to measure RF levels at receiver inputs
4. Building or procurement of the noise measurement equipment
5. Writing of test plans with as much detail as possible at an early date

In addition to the noise measurement for the communications system, some spacecraft experiments may also require that certain frequency bands be free of interference. For example, it is possible that a very low frequency experiment requiring low noise levels may be flown on a future spacecraft. A parallel definition of requirements and equipment development may be necessary for special experiments.

It should also be an objective that predetection recording and automatic data processing techniques be incorporated into the measurement equipment. These techniques would help eliminate possible operator error and reduce the required manpower for the tests and data reduction.

d. Magnetics. The following recommendations are made for improving the magnetics control effort on future magnetometer carrying spacecraft.

Timely application of adequate and definitive guidelines for equipment design engineers should be ensured. This may consist of a magnetics handbook, a general design specification, or some other form that relates the magnetics problem to the spacecraft design considerations. It might also include a requirement for a nonmagnetics preferred parts list, or component or subchassis magnetics evaluation:

1. Development of project-oriented magnetics specification including design restraints and criteria with definite quality assurance provisions
2. Inclusion of magnetics as a competing design characteristic in the spacecraft design book

3. Establishment of precise magnetics evaluation procedures based on spacecraft coordinates
4. Inclusion of magnetics evaluation procedures in flow charts and schedules

Very close work with the cognizant engineer and vendors should be maintained in solving hardware magnetics problems. Provision should be made for preliminary mapping during early design stages.

Vibration exciter restrictions should be imposed in vibration testing. Vibration test specifications should define acceptable vibration exciter magnetic field strengths, document the exciter used, and record the actual field at the time of the test.

To facilitate improved magnetics control on future magnetometer carrying spacecraft, study programs in the following areas are recommended:

1. Search for a suitable substitute or redesign of the latching relay
2. Shielding study of mechanical relays
3. Development of a nonmagnetic substitute for Kovar on the solar panel bus bars
4. Development of a substitute for bimetallic magnetic temperature control devices
5. Improvement of techniques of spacecraft magnetic field prediction
6. Development of a nonmagnetic preferred parts list

e. Other recommendations.

Data processing of subsystem test results. In view of the quantity of environmental tests performed on this program, and with an eye toward improved assessment of the specific results obtained, consideration should definitely be given to the use of automated reporting procedures and data processing techniques. The use of the digital computer in the handling, storage, and analysis of such information would be an attribute to a new-generation spacecraft test program.

Reoccurring failure modes and trends, the behavior of similar subsystems and components in multiple environments, and multiple subsystems in single environments are easily extracted parameters from simple computer programs. Frequent scanning of performance could also be obtained without the expenditure of valuable man-hours. For these reasons, it appears highly desirable, if not mandatory, to automate the environmental test reporting program to the fullest extent possible.

Part failure trends. Analysis of problem/failure reports generated during the environmental testing program indicates a number of piece-parts and processes that were vulnerable to the launch and space environment. Some of the more outstanding cases indicating trends of failure are enumerated for the benefit of future projects:

1. Capacitors must be bled before launch to avoid corona effects or arcing at critical altitudes.
2. Ceramic capacitors should not be used for low-level amplification in a vibration environment because of the initiation of piezoelectric action.
3. Non-hermetically sealed capacitors are susceptible to leakage in the space environment.
4. Resistors must be thoroughly screened to determine their ability to maintain a specified resistance through prescribed temperature ranges.
5. Certain types of package transistors and resistors should be avoided in future designs because of their low inherent reliability.
6. Some relays were found to be nonoperational when exposed to shock environments in excess of 100 *g*.
7. Glass (vacuum) tubes constitute a potential major design problem and should be ruggedized and/or soft-mounted.
8. Clearances on high-voltage printed circuits are critical areas to be closely monitored in order to avoid arcing in partial vacuum environments.
9. Voids in potting compounds or conformal coatings are extremely deleterious in a humidity environment. Fabrication processes should employ a high vacuum environment during gelation.
10. Elastomeric components should be degassed by an elevated temperature soak in high vacuum prior to their use.

Test monitoring and documentation. Improved reporting of environmental testing would permit more rapid dissemination of information to the project office and to cognizant technical personnel. This reporting would be best implemented by revised test report forms. All FA and TA tests must be reported in a Test Result Summary, since the total history of an item under test is just as important as the fact that it passed the test. It is also suggested that the Environmental Test Lab reporting forms provide for proper accumulation of the data that

are subsequently to be reported on a Test Results Summary Form.

Completion of TA testing. The importance of completing TA environmental testing early in a project cannot be overemphasized. Accomplishing required design revisions and deleting unsatisfactory subsystems and components prior to FA testing saves expensive retrofit and retesting, and also results in increased environmental exposure of flight hardware. Design changes originating as a result of FA test problems sometimes paralleled identical problems arising in a concurrent TA testing program. Therefore, it is recommended that an attempt be made to complete TA testing at the earliest possible date.

Effectiveness of specific environments. During the TA testing program for subsystems, no failures were experienced in the following tests:

1. Bench handling
2. Transportation vibration
3. Static acceleration
4. Package drop
5. Explosive atmosphere

Each of these tests should be reviewed for future programs with an eye to their deletion or limitation for specific hardware items whose testing may be expected to yield meaningful results. Their elimination could permit more time and care to be devoted to the test areas that demonstrated a failure pattern.

Humidity testing. Results of *Mariner* Mars 1964 subsystem tests disclosed no subsystem humidity test failures after the maximum RH was reduced from 95 to 75% by an amendment to the general specification. However, some of the original failures might have occurred at the lower humidity levels, since the failed modules were found to have defective conformal coatings. It appears desirable to retain and strengthen the humidity test, since it also reveals design weaknesses and some workmanship defects. However, some thought should be given to the use of a modified humidity test for flight acceptance.

Thermal error analysis. As a step in the evolution of improved temperature control and testing, a study could be carried out to analytically predict errors as functions of the various controlling parameters. Such parameters include: uncertainties in emissivity and absorptivity coefficients, variations in internal power, unreproducibility of joint conductivity, and such test facility discrepancies as collimation and spectrum. The output of such a study would have two uses: an input to subsystem thermal test requirements, and an indication of where effort is most efficiently applied in advancing the state of the art.

ABBREVIATION LIST

AAC	automatic aperture control
AD	analog-to-digital
ADC	analog-to-digital converter
AFB	Air Force Base
AFC	automatic frequency control
AFSC/SSD	Air Force System Command/Space Science Division
AFETR	Air Force Eastern Test Range
AGC	automatic gain control
APC	automatic phase control
APW	analog to pulse width
ASCO	auxiliary sustainer engine cutoff
B-FACT	booster flight acceptance combined test
BECO	booster engine cutoff
B/R	booster regulator
CC&S	central computer and sequencer
CD	command decoder
CG	center of gravity
CW	continuous wave
DAS	data automation system
DPS	data processing subsystem
DSIF	Deep Space Instrumentation Facility
DSN	Deep Space Network
DSS	deep space station
DTM	developmental test model
DC	direct radio command
E	time of encounter
ECI	engineering change instruction
EGO	*Eccentric Orbiting Geophysical Observatory*
EMI	electromagnetic interference
ESF	Explosive Safe Facility
FPAC	Flight Path Analysis and Command Group
FA	flight acceptance
FSE	flight support equipment
GCS	ground command subsystem
GD/C	General Dynamics/Convair
GSDS	Goldstone duplicate standard
GSFC	Goddard Space Flight Center
GTS	ground telemetry subsystem

ABBREVIATION LIST (Cont'd)

Hi-Rel	JPL high reliability (parts)
HSD	high speed data
HTC	height-to-time converter
I	time of injection
IF	intermediate frequency
IFM	interfrequency modulation
IMP	*Interplanetary Monitoring Probe*
J-FACT	joint flight acceptance combined test
LO	local oscillator
L	time of launch
LC	launch complex
LeRC	Lewis Research Center
LCE	launch complex equipment
LMSC	Lockheed Missile and Space Center
M	time of midcourse maneuver
MCC	Mission Control Center
MCE	magnetic circuit elements
MSFN	Manned Space Flight Network
MV	multivibrator
MT	internal CC&S command
NAA	narrow angle acquisition
NAMG	narrow angle Mars gate
NASCOM	NASA communications system
NRT	non-real time
NRZ	nonreturn to zero
NASA	National Aeronautics and Space Administration
OGO	*Orbiting Geophysical Observatory*
OSE	operational support equipment
PAS	pyrotechnics arming switch
PCM	pulse code modulated
PHA	pulse height analyzer
PIPS	postinjection propulsion system
PPL	preferred parts list
PRD	program requirements document
PRF	pulse recurrence frequency
PSD	power spectrum density
PS&L	power switch and logic
PSP	program support plan

ABBREVIATION LIST (Cont'd)

PSS	planetary scan subsystem
PTM	proof test model
QA	quality assurance
QC	quantitative command
RT	real time
RT DAS	real time data automation system
RZ	return to zero
SAA	S-band acquisition aid
SAF	Spacecraft Assembly Facility
SCM	S-band monopulse feedhorn and bridge system
SCR	silicon-controlled rectifier
SECO	sustainer engine cutoff
SFO	Space Flight Operations
SFOF	Space Flight Operations Facility
SFOD	Space Flight Operations Director
SIT	separation-initiated timer
SMIT	simulated midcourse interaction test
SPAC	Spacecraft Performance Analysis and Command Group
SPE	static phase error
STADAN	Space Tracking and Data Acquisition Network
STC	system test complex
STM	structural test model
SSAC	Space Science Analysis and Command Group
STL	Space Technology Laboratories
SCAMA	signaling, conferencing, and monitoring arranging
TA	type approval
TCM	temperature control model
T&DA	Tracking and Data Acquisition
TIM	Tracking Instruction Manual
TR	transformer rectifier
TPS	Telemetry Processing Station
TTY	teletypewriter
TWT	traveling wave tube
UNIPAC	Universal Payload Accommodation Capsule
VCO	voltage-controlled oscillator
VECO	vernier engine cutoff
VSWR	voltage standing wave ratio
VSS	video storage subsystem
XTM	extra test model

REFERENCES

1. James, J. N., *The* Mariner R *Project: Progress Report, September 1, 1961–August 31, 1962,* Technical Report No. 32-353, Jet Propulsion Laboratory, Pasadena, Calif., January 1, 1963.

2. Bryden, J. N., Mariner *(Venus '62) Flight Telecommunication System,* Technical Report No. 32-377, Jet Propulsion Laboratory, Pasadena, Calif., January 15, 1963.

3. Neugebauer, M., Anderson, H., Snyder, C., Smith, E. J., *et al., The Mission of* Mariner II: *Preliminary Observations,* Technical Report No. 32-383 (reprinted from *Science,* Vol. 138, December 7, 1962, Vol. 139, January 4, 1963), Jet Propulsion Laboratory, Pasadena, Calif., January 11, 1965.

4. Barnes, F. L., Bollman, W. E., Curkendall, D. W., Thornton, T. H., Jr., Mariner 2 *Flight to Venus,* Technical Report No. 32-395, Jet Propulsion Laboratory, Pasadena, Calif., December 1962.

5. *The* Mariner R *Project: Progress Report—September 1, 1962–January 3, 1963. Volume 1.* Mariner 2 *Flight Report,* Technical Report No. 32-422, Jet Propulsion Laboratory, Pasadena, Calif., July 1, 1963.

6. *The* Mariner R *Project: Progress Report—September 1, 1962–January 3, 1963,* Technical Report No. 32-422, Volume II, Jet Propulsion Laboratory, Pasadena, Calif., July 1, 1963.

7. Costogue, E. N., Mariner *Venus Power-Supply System,* Technical Report No. 32-424, Jet Propulsion Laboratory, Pasadena, Calif., March 30, 1963.

8. Chase, S. C., Kaplan, L. D., Neugebauer, G., Barath, F. T., Smith, E. J., and Jones, D. E., Mariner II: *Preliminary Reports on Measurements of Venus,* Technical Report No. 32-429, Jet Propulsion Laboratory, Pasadena, Calif., March 1963.

9. Jodele, J., Mariner *Spacecraft Packaging,* Technical Report No. 32-451, Jet Propulsion Laboratory, Pasadena, Calif., July 1, 1963.

10. Zoutendyk, J. A., Vondra, R. J., and Smith, A. H., Mariner 2 *Solar Panel Design and Flight Performance,* Technical Report No. 32-455, Jet Propulsion Laboratory, Pasadena, Calif., June 28, 1963.

11. Compiled by H. J. Wheelock; Mariner *Mission to Venus,* Technical Report No. 32-456, Jet Propulsion Laboratory, Pasadena, Calif., July 11, 1963.

12. Anderson, J. D., Null, G. W., and Thornton, C. T., *The Evaluation of Certain Astronomical Constants From the Radio Tracking of* Mariner II, Technical Report No. 32-476, Jet Propulsion Laboratory, Pasadena, Calif., March 1, 1965.

13. Chase, S. C., Kaplan, L. D., and Neugebauer, G., *The* Mariner 2 *Infrared Radiometer Experiment,* Technical Report No. 32-484, Jet Propulsion Laboratory, Pasadena, Calif., November 1963.

14. Snyder, Conway W., Neugebauer, M., and Rao, U. R., *The Solar-Wind Velocity and Its Correlation With Cosmic-Ray Variations and With Solar and Geomagnetic Activity,* Technical Report No. 32-514, Jet Propulsion Laboratory, Pasadena, Calif., October 15, 1963.

REFERENCES (Cont'd)

15. Anderson, H. R., *Ionizing Radiation Measured Between Earth and Venus by* Mariner II, Technical Report No. 32-693, Jet Propulsion Laboratory, Pasadena, Calif., May 15, 1965.

16. Smith, E. J., Davis, L., Coleman, P. J., and Sonett, C. P., *Magnetic Measurements Near Venus,* Technical Report No. 32-732, Jet Propulsion Laboratory, Pasadena, Calif., June 1, 1965.

17. Neugebauer, M., and Snyder, C. W., *Solar-Wind Measurements Near Venus,* Technical Report No. 32-733, Jet Propulsion Laboratory, Pasadena, Calif., June 1, 1965.

18. Neugebauer, M., and Snyder, Conway W., *Preliminary Results From* Mariner II *Solar Plasma Experiment,* Technical Memorandum No. 33-111, Jet Propulsion Laboratory, Pasadena, Calif., November 15, 1962.

19. Lewis, D. W., Gram, M. B., Spehalski, R. J., and Dumas; L. N., *Final Report on* Mariner 2 *Temperature Control,* Technical Memorandum No. 33-140, Jet Propulsion Laboratory, Pasadena, Calif., July 1, 1963.

20. Cherry, W. R., and Zoutendyk, J. A., *The State-of-the-Art in Solar Cell Arrays for Space Electrical Power,* Paper presented at the Third Biennial Aerospace Power Systems Conference, Philadelphia, Pa., September 1–4, 1964, AIAA Paper 64-738, American Institute of Aeronautics and Astronautics, New York, N. Y., 1964.

21. *Qualification Test Report for* Mariner C *Solar Panels and Thermal Test Specimens,* Report No. 63B133, Ryan Aeronautical Company, San Diego, Calif., January 23, 1964.

22. Batchilder, R. R., Wada, B. K., *Stiffness Matrix Structural Analysis,* Technical Memorandum No. 33-75, Jet Propulsion Laboratory, Pasadena, Calif., February 12, 1962.

23. *Structural Characteristics of* Mariner C *Solar Panels,* Report 63B029, Ryan Aeronautical Company, San Diego, Calif., December 20, 1963.

24. Coughey, T. K., "Classical Normal Modes in Damped Linear Dynamic Systems," *Journal of Applied Mechanics,* June 1960, Vol. 27, pp. 269–271.

25. Foss, K. A., "Coordinates which Uncouple the Equations of Motion of Damped Linear Dynamic Systems," *Journal of Applied Mechanics,* September 1958, pp. 361–364.

26. *Qualification Test Report for* Mariner C *Solar Panels and Thermal Test Specimens,* Report No. 63B133, Ryan Aeronautical Company, San Diego, Calif., 1964.

27. Easterling, M. F., *A Long Range Precision Ranging System,* Technical Report No. 32-80, Jet Propulsion Laboratory, Pasadena, Calif., July 10, 1961.

28. Highstrete, B. A., "Ceramic Traveling Wavetubes for Space Vehicles," *Microwave Journal,* January 1964, Vol. 7, pp. 49–57.

29. "Planetary Scan System," in *Space Program Summary No. 37-18, Volume VI,* Jet Propulsion Laboratory, Pasadena, Calif., December 31, 1962, pp. 70–72.

30. "Planetary Scan Subsystem for *Mariner* Mars 1964," in *Space Programs Summary No. 37-21, Volume VI,* Jet Propulsion Laboratory, Pasadena, Calif., June 30, 1963, pp. 75–78.

REFERENCES (Cont'd)

31. Wong, R. Y., *A Fiber Optical System for Space Application,* Technical Report No. 32-646, Jet Propulsion Laboratory, Pasadena, Calif., August 31, 1964.

32. Wong, R. Y., "Carrier Collection and Spectral Response of Radiation Detectors," in *Space Program Summary No. 37-27, Volume IV,* Jet Propulsion Laboratory, Pasadena, Calif., June 30, 1964, pp. 92–97.

33. Wong, R. Y., "Planet-Acquisition-Range Prediction of a Planetary Scan System," in *Space Programs Summary No. 37-28, Volume IV,* Jet Propulsion Laboratory, Pasadena, Calif., August 31, 1964, pp. 101–108.

34. Schiffer, R. A., *Correlation of Launch Vehicle Wind Tunnel Aerodynamic Noise With Flight Vibration Data,* Technical Report No. 32-619, Rev. I, Jet Propulsion Laboratory, Pasadena, Calif., September 15, 1964.

35. Haynes, N. R., and Gordon, H. J., *A Study of the Probability of Depositing Viable Organisms on Mars During the* Mariner *'64 Mission,* Technical Memorandum No. 33-194, Jet Propulsion Laboratory, Pasadena, Calif., October 23, 1964.

36. Clarke, V. C., Jr., Bollman, W. E., Roth, R. Y., and Scholey, W. J., *Design Parameters for Ballistics Interplanetary Trajectories. Part I. One Way Transfers to Mars and Venus,* Technical Report No. 32-77, Part I, Jet Propulsion Laboratory, Pasadena, Calif., January 16, 1963.

37. Warner, M. R., and Nead, M. W., *SPODP—Single Precision Orbit Determination Program,* Technical Memorandum No. 33-204, Jet Propulsion Laboratory, Pasadena, Calif., February 15, 1965.